BACTERIAL SECRETION SYSTEMS

EDITED BY: Ignacio Arechaga and Eric Cascales
PUBLISHED IN: Frontiers in Microbiology

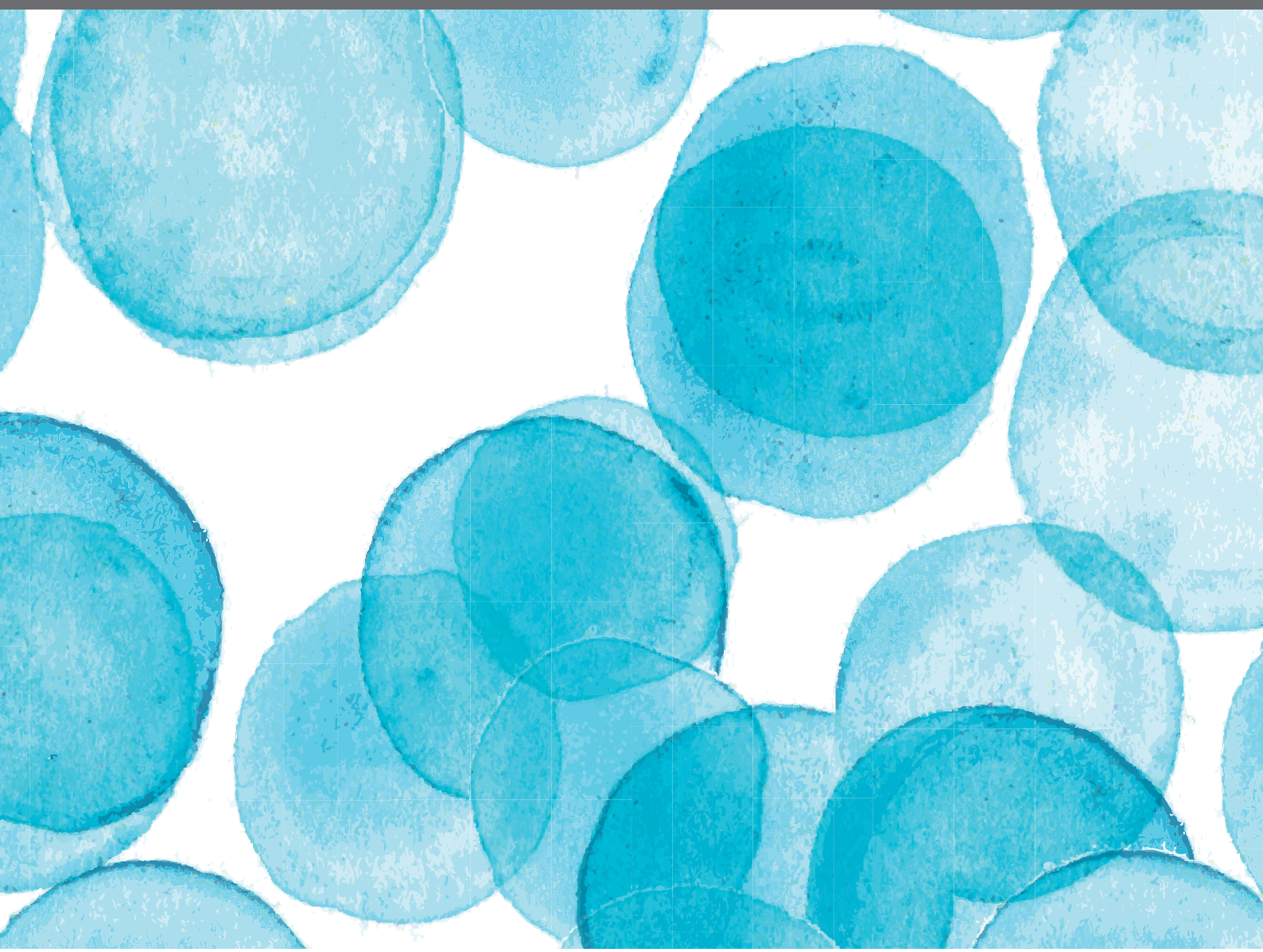

frontiers Research Topics

frontiers

Frontiers eBook Copyright Statement

The copyright in the text of individual articles in this eBook is the property of their respective authors or their respective institutions or funders. The copyright in graphics and images within each article may be subject to copyright of other parties. In both cases this is subject to a license granted to Frontiers.

The compilation of articles constituting this eBook is the property of Frontiers.

Each article within this eBook, and the eBook itself, are published under the most recent version of the Creative Commons CC-BY licence. The version current at the date of publication of this eBook is CC-BY 4.0. If the CC-BY licence is updated, the licence granted by Frontiers is automatically updated to the new version.

When exercising any right under the CC-BY licence, Frontiers must be attributed as the original publisher of the article or eBook, as applicable.

Authors have the responsibility of ensuring that any graphics or other materials which are the property of others may be included in the CC-BY licence, but this should be checked before relying on the CC-BY licence to reproduce those materials. Any copyright notices relating to those materials must be complied with.

Copyright and source acknowledgement notices may not be removed and must be displayed in any copy, derivative work or partial copy which includes the elements in question.

All copyright, and all rights therein, are protected by national and international copyright laws. The above represents a summary only. For further information please read Frontiers' Conditions for Website Use and Copyright Statement, and the applicable CC-BY licence.

ISSN 1664-8714
ISBN 978-2-88963-957-1
DOI 10.3389/978-2-88963-957-1

About Frontiers

Frontiers is more than just an open-access publisher of scholarly articles: it is a pioneering approach to the world of academia, radically improving the way scholarly research is managed. The grand vision of Frontiers is a world where all people have an equal opportunity to seek, share and generate knowledge. Frontiers provides immediate and permanent online open access to all its publications, but this alone is not enough to realize our grand goals.

Frontiers Journal Series

The Frontiers Journal Series is a multi-tier and interdisciplinary set of open-access, online journals, promising a paradigm shift from the current review, selection and dissemination processes in academic publishing. All Frontiers journals are driven by researchers for researchers; therefore, they constitute a service to the scholarly community. At the same time, the Frontiers Journal Series operates on a revolutionary invention, the tiered publishing system, initially addressing specific communities of scholars, and gradually climbing up to broader public understanding, thus serving the interests of the lay society, too.

Dedication to Quality

Each Frontiers article is a landmark of the highest quality, thanks to genuinely collaborative interactions between authors and review editors, who include some of the world's best academicians. Research must be certified by peers before entering a stream of knowledge that may eventually reach the public - and shape society; therefore, Frontiers only applies the most rigorous and unbiased reviews.
Frontiers revolutionizes research publishing by freely delivering the most outstanding research, evaluated with no bias from both the academic and social point of view. By applying the most advanced information technologies, Frontiers is catapulting scholarly publishing into a new generation.

What are Frontiers Research Topics?

Frontiers Research Topics are very popular trademarks of the Frontiers Journals Series: they are collections of at least ten articles, all centered on a particular subject. With their unique mix of varied contributions from Original Research to Review Articles, Frontiers Research Topics unify the most influential researchers, the latest key findings and historical advances in a hot research area! Find out more on how to host your own Frontiers Research Topic or contribute to one as an author by contacting the Frontiers Editorial Office: researchtopics@frontiersin.org

BACTERIAL SECRETION SYSTEMS

Topic Editors:
Ignacio Arechaga, University of Cantabria, Spain
Eric Cascales, Aix-Marseille Université, France

Citation: Arechaga, I., Cascales, E., eds. (2020). Bacterial Secretion Systems. Lausanne: Frontiers Media SA. doi: 10.3389/978-2-88963-957-1

Table of Contents

05 ***Tools and Approaches for Dissecting Protein Bacteriocin Import in Gram-Negative Bacteria***
Iva Atanaskovic and Colin Kleanthous

17 ***Structural and Functional Characterization of the Type Three Secretion System (T3SS) Needle of* Pseudomonas aeruginosa**
Charlotte Lombardi, James Tolchard, Stephanie Bouillot, Luca Signor, Caroline Gebus, David Liebl, Daphna Fenel, Jean-Marie Teulon, Juliane Brock, Birgit Habenstein, Jean-Luc Pellequer, Eric Faudry, Antoine Loquet, Ina Attrée, Andréa Dessen and Viviana Job

32 ***Versatility of the BID Domain: Conserved Function as Type-IV-Secretion-Signal and Secondarily Evolved Effector Functions Within* Bartonella*-Infected Host Cells***
Alexander Wagner, Colin Tittes and Christoph Dehio

39 ***Enterococcal PcfF is a Ribbon-Helix-Helix Protein That Recruits the Relaxase PcfG Through Binding and Bending of the* oriT *Sequence***
Saima Rehman, Yang Grace Li, Andreas Schmitt, Lena Lassinantti, Peter J. Christie and Ronnie P.-A. Berntsson

50 ***Bacteria-Killing Type IV Secretion Systems***
Germán G. Sgro, Gabriel U. Oka, Diorge P. Souza, William Cenens, Ethel Bayer-Santos, Bruno Y. Matsuyama, Natalia F. Bueno, Thiago Rodrigo dos Santos, Cristina E. Alvarez-Martinez, Roberto K. Salinas and Chuck S. Farah

70 ***Regulation of Gram-Positive Conjugation***
Verena Kohler, Walter Keller and Elisabeth Grohmann

83 ***Type V Secretion Systems: An Overview of Passenger Domain Functions***
Ina Meuskens, Athanasios Saragliadis, Jack C. Leo and Dirk Linke

102 ***A Type VI Secretion System Trans-Kingdom Effector is Required for the Delivery of a Novel Antibacterial Toxin in* Pseudomonas aeruginosa**
Benjamin Berni, Chantal Soscia, Sarah Djermoun, Bérengère Ize and Sophie Bleves

116 ***The Dynamic ATP-Driven Mechanism of Bacterial Protein Translocation and the Critical Role of Phospholipids***
Ian Collinson

123 ***Prediction of T4SS Effector Proteins for* Anaplasma phagocytophilum *Using OPT4e, A New Software Tool***
Zhila Esna Ashari, Kelly A. Brayton and Shira L. Broschat

133 ***Confirmed and Potential Roles of Bacterial T6SSs in the Intestinal Ecosystem***
Can Chen, Xiaobing Yang and Xihui Shen

144 ***A Potential Late Stage Intermediate of Twin-Arginine Dependent Protein Translocation in* Escherichia coli**
Hendrik Geise, Eyleen Sabine Heidrich, Christoph Stefan Nikolin, Denise Mehner-Breitfeld and Thomas Brüser

154 ***Distribution, Function and Regulation of Type 6 Secretion Systems of Xanthomonadales***
Ethel Bayer-Santos, Lucas de Moraes Ceseti, Chuck Shaker Farah and Cristina Elisa Alvarez-Martinez

164 ***Baseplate Component TssK and Spatio-Temporal Assembly of T6SS in* Pseudomonas aeruginosa**
David Liebl, Mylène Robert-Genthon, Viviana Job, Valentina Cogoni and Ina Attrée

179 ***Enhancing Recombinant Protein Yields in the* E. coli *Periplasm by Combining Signal Peptide and Production Rate Screening***
Alexandros Karyolaimos, Henry Ampah-Korsah, Tamara Hillenaar, Anna Mestre Borras, Katarzyna Magdalena Dolata, Susanne Sievers, Katharina Riedel, Robert Daniels and Jan-Willem de Gier

190 ***Delivery of the* Pseudomonas aeruginosa *Phospholipase Effectors PldA and PldB in a VgrG- and H2-T6SS-Dependent Manner***
Sarah Wettstadt, Thomas E. Wood, Selina Fecht and Alain Filloux

208 ***Life After Secretion—*Yersinia enterocolitica *Rapidly Toggles Effector Secretion and Can Resume Cell Division in Response to Changing External Conditions***
Bailey Milne-Davies, Carlos Helbig, Stephan Wimmi, Dorothy W. C. Cheng, Nicole Paczia and Andreas Diepold

221 ***Identification of a Contact-Dependent Growth Inhibition (CDI) System That Reduces Biofilm Formation and Host Cell Adhesion of* Acinetobacter baumannii *DSM30011 Strain***
Morgane Roussin, Sedera Rabarioelina, Laurence Cluzeau, Julien Cayron, Christian Lesterlin, Suzana P. Salcedo and Sarah Bigot

235 ***The* Campylobacter jejuni *Type VI Secretion System Enhances the Oxidative Stress Response and Host Colonization***
Janie Liaw, Geunhye Hong, Cadi Davies, Abdi Elmi, Filip Sima, Alexandros Stratakos, Lavinia Stef, Ioan Pet, Abderrahman Hachani, Nicolae Corcionivoschi, Brendan W. Wren, Ozan Gundogdu and Nick Dorrell

247 ***Redundancy and Specificity of Type VI Secretion* vgrG *Loci in Antibacterial Activity of* Agrobacterium tumefaciens *1D1609 Strain***
Mary Nia M. Santos, Shu-Ting Cho, Chih-Feng Wu, Chun-Ju Chang, Chih-Horng Kuo and Erh-Min Lai

262 ***A High-Throughput Interbacterial Competition Screen Identifies ClpAP in Enhancing Recipient Susceptibility to Type VI Secretion System-Mediated Attack by* Agrobacterium tumefaciens**
Hsiao-Han Lin, Manda Yu, Manoj Kumar Sriramoju, Shang-Te Danny Hsu, Chi-Te Liu and Erh-Min Lai

276 ***HpaR, the Repressor of Aromatic Compound Metabolism, Positively Regulates the Expression of T6SS4 to Resist Oxidative Stress in* Yersinia pseudotuberculosis**
Zhuo Wang, Tietao Wang, Rui Cui, Zhenxing Zhang, Keqi Chen, Mengyun Li, Yueyue Hua, Huawei Gu, Lei Xu, Yao Wang, Yantao Yang and Xihui Shen

frontiers in Microbiology

REVIEW
published: 28 March 2019
doi: 10.3389/fmicb.2019.00646

Tools and Approaches for Dissecting Protein Bacteriocin Import in Gram-Negative Bacteria

*Iva Atanaskovic and Colin Kleanthous**

Department of Biochemistry, University of Oxford, Oxford, United Kingdom

Bacteriocins of Gram-negative bacteria are typically multi-domain proteins that target and kill bacteria of the same or closely related species. There is increasing interest in protein bacteriocin import; from a fundamental perspective to understand how folded proteins are imported into bacteria and from an applications perspective as species-specific antibiotics to combat multidrug resistant bacteria. In order to translocate across the cell envelope and cause cell death, protein bacteriocins hijack nutrient uptake pathways. Their import is energized by parasitizing intermembrane protein complexes coupled to the proton motive force, which delivers a toxic domain into the cell. A plethora of genetic, structural, biochemical, and biophysical methods have been applied to find cell envelope components involved in bacteriocin import since their discovery almost a century ago. Here, we review the various approaches that now exist for investigating how protein bacteriocins translocate into Gram-negative bacteria and highlight areas of research that will need methodological innovations to fully understand this process. We also highlight recent studies demonstrating how bacteriocins can be used to probe organization and architecture of the Gram-negative cell envelope itself.

Keywords: bacteriocin, import, Gram-negative bacteria, cell envelope, methods

OPEN ACCESS

Edited by:
Ignacio Arechaga, University of Cantabria, Spain

Reviewed by:
Vasvi Chaudhry, University of Tübingen, Germany
Gerd M. Seibold, University of Ulm, Germany

***Correspondence:**
Colin Kleanthous
colin.kleanthous@bioch.ox.ac.uk

Specialty section:
This article was submitted to Microbial Physiology and Metabolism, a section of the journal Frontiers in Microbiology

Received: *19 December 2018*
Accepted: *14 March 2019*
Published: *28 March 2019*

Citation:
Atanaskovic I and Kleanthous C (2019) Tools and Approaches for Dissecting Protein Bacteriocin Import in Gram-Negative Bacteria. Front. Microbiol. 10:646. doi: 10.3389/fmicb.2019.00646

INTRODUCTION

When exposed to environmental or competition stress bacteria often release proteinaceous toxins called bacteriocins that target and kill neighboring bacteria (Cascales et al., 2007; Cornforth and Foster, 2013). Bacteriocins of Gram-positive bacteria are mostly post-translationally modified peptides with a broad species target range, the best known example being the widely used food preservative nisin. Peptidic bacteriocins have been reviewed extensively (Héchard and Sahl, 2002; Cotter, 2014). The focus of the present review is on protein bacteriocins from Gram-negative bacteria. These are large folded proteins (40–80 kDa) that are composed of multiple domains and tend to have a narrow killing spectrum because of the numerous specific interactions at the cell surface involved in their import. A bacteriocin producer cell is protected from its own bacteriocin by an immunity protein, while sensitive strains lack such protection. These toxins can form pores in the inner membrane, act as nucleases to degrade DNA or RNA in the target cell, or interfere with cell

Abbreviations: CCCP, carbonyl cyanide 3-chlorophenylhydrazone; ColE9, colicin E9; CPA, common polysaccharide antigen; EK, enterokinase; FRAP, Forster recovery after photobleaching; FRET, Forster resonance energy transfer; Im9, ColE9 immunity protein; IM, inner membrane; ITC, isothermal titration calorimetry; LPS, lipopolysaccharide; MMBL, monocot mannose-binding lectin; NMR, nuclear magnetic resonance; NTD, N-terminal domain; OBS, OmpF-binding site; OM, outer membrane; OMP, outer membrane protein; PMF, proton motive force; PPI, protein–protein interactions; SAXS, small-angle X-ray scattering; TIRF, total internal reflection fluorescence.

wall biosynthesis. To do so, protein bacteriocins (hereafter referred to merely as bacteriocins) have to cross a multi-layered cell envelope which is accomplished by parasitizing host proteins involved in nutrient and metabolite trafficking (**Figure 1**).

Bacteriocins have the potential to be developed as much-needed therapeutics to treat multidrug resistant bacterial infections (Cotter, 2014; Behrens et al., 2017). A prerequisite for successfully applying bacteriocins as antimicrobials, however, is to understand how they are imported. Moreover, these import pathways might reveal further processes that could be exploited for newly designed drugs or chimeric bacteriocins with more potent toxicity (Lukacik et al., 2012).

The discovery of new bacteriocins has been accelerated by whole-genome sequencing technologies and implementation of gene mining tools (Jamet and Nassif, 2015; Sharp et al., 2017). While peptide Gram-negative bacteriocins, such as microcins, have been reviewed elsewhere (Duquesne et al., 2007), here we focus on methods used for the study of multidomain protein bacteriocins. The two most explored groups of protein bacteriocins are colicins produced by *Escherichia coli* (Cascales et al., 2007) and pyocins produced by *Pseudomonas aeruginosa* (Ghequire and De Mot, 2014). Nuclease colicins contain an N-terminal translocation domain, a central receptor binding domain, and a C-terminal cytotoxic domain that binds a cognate immunity protein, while in pyocins the location of the translocation and receptor binding domains appears reversed (Michel-Briand and Baysse, 2002). Bacteriocins can be divided into two groups based on the periplasmic energy transducing system they exploit for import. Group A use the Tol–Pal system, which is composed of periplasmic and IM proteins, Pal, TolA, TolB, TolR, TolQ. All but the outer membrane lipoprotein Pal have been documented to be involved in bacteriocin import.

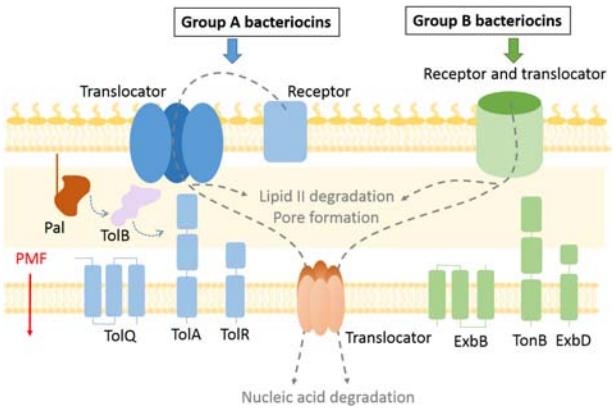

FIGURE 1 | Bacteriocin import pathways. Bacteriocins bind to outer membrane receptors to get imported into the cell. Some bacteriocins (group B) use the receptor protein also as a translocator to cross the outer membrane, while exploiting the TonB system and PMF as an energy source. In case of group A bacteriocins the translocator differs from the receptor protein and the Tol system is used to enter the periplasm. Bacteriocins that degrade lipid II and prevent peptidoglycan recycling remain in the periplasm, while pore forming bacteriocins are inserted in the inner membrane. Nuclease bacteriocins use a distinct protein translocator to cross the inner membrane.

Group B use the Ton system, composed of TonB, ExbB, and ExbD proteins (**Figure 1**). It is likely that all protein bacteriocins fall into these two such groups (Kleanthous, 2010).

Colicin E9 is one of the best understood of the Group A bacteriocins in terms of its translocation mechanism. Import of ColE9 involves assembly of a translocon complex. The OM portion of the translocon includes BtuB, its receptor, its porin translocator OmpF or OmpC, TolB, its periplasmic target, and Im9, its immunity protein. In order to form this OM translocon, ColE9 uses its intrinsically unstructured N-terminus to pass through a porin channel to engage the PMF-coupled Tol–Pal system in the periplasm (Housden et al., 2005). How ColE9 translocates across the OM is not understood, but it is known that the colicin exploits FtsH, the AAA^+ ATPase/protease, to cross the IM. Once inside the cell, the ColE9 DNase causes nonspecific cleavage of double-stranded DNA which results in cell death (Walker et al., 2007). Group B colicins and pyocins pass through Ton-dependent receptors without the involvement of porins. For instance, pyocin S2 binds to a TonB-coupled siderophore receptor FpvAI, and passes through the FpvAI lumen mimicking its cognate ligand (White et al., 2017).

Gram-negative bacteriocins use a variety of pathways and distinct combinations of cell envelope proteins to kill cells, making it challenging to dissect their import mechanisms. Since their discovery, genetic, structural, biochemical, and biophysical approaches have all been deployed to define these pathways often in combination (**Figure 2**). Here, we give an overview of these approaches, pointing out the most recent advancements in the toolkit used for dissecting bacteriocin translocation in Gram-negative bacteria.

PAIRING UP BACTERIOCINS WITH THEIR RECEPTORS

Every bacteriocin begins its journey through the cell envelope by binding to a specific receptor on the bacterial surface. While most bacteriocins bind OM proteins, some use LPS as their primary receptor (Kim et al., 2014; McCaughey et al., 2014, 2016). The specificity of a bacteriocin–receptor interaction narrows down the target range of these toxins. Therefore, pairing up bacteriocins with their receptors is an important first step in applying them as therapeutics (Cotter, 2014). If a sufficient number of bacteriocin receptors are known, a screen for receptor genes in a genome of a pathogen isolated from the site of infection could guide the design of bacteriocin cocktails to specifically eradicate the cause of infection. Additionally, linking a bacteriocin to a receptor of known biological function is the starting point for understanding which import pathway is being hijacked by the toxin.

When searching for a bacteriocin receptor, the first issue to address is its chemical nature. Bacteriocin *neutralization experiments* have often been used to determine if the receptor is within the protein or LPS fraction of the outer membrane (Weltzien and Jesaitis, 1971). If a certain cell fraction contains the receptor, it will bind to a bacteriocin and inhibit its toxic activity, which can be assessed by a plate killing assay (**Figure 2**). Neutralization experiments can also be used to test if a specific

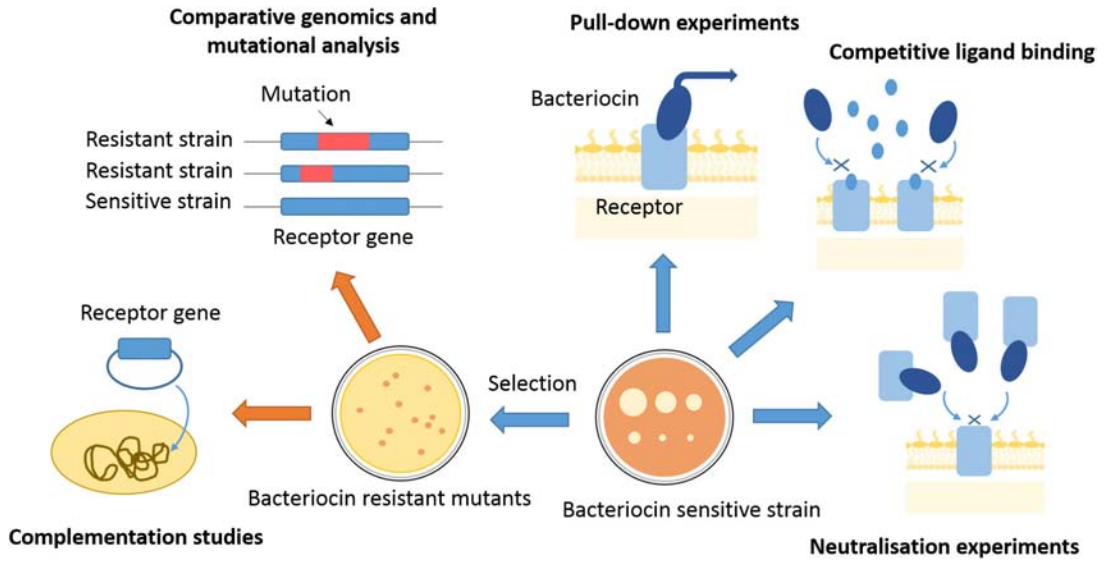

FIGURE 2 | Approaches to finding bacteriocin translocon components. Translocon components can be isolated from membranes of sensitive strains by use of affinity tagged bacteriocins as bait. Competitive ligand binding or bacteriocin binding to a purified translocon component can inhibit bacteriocin activity and give indications about proteins engaged in bacteriocin entry. Bacteriocin-resistant mutants can be selected by use of high bacteriocin concentrations, or generated by transposon mutagenesis. Genomes of resistant mutants can further be analyzed for mutations underlying the resistance phenotype, which can give gene candidates for translocon components. A component of bacteriocin entry has to be further confirmed by complementation studies, where bacteriocin sensitivity is re-established once a resistant mutant is transformed with a gene of interest.

nutrient import pathway is being hijacked by a bacteriocin. If cells are exposed to a bacteriocin in the presence of a nutrient with which it shares its import pathway, competitive binding of the ligand should either inhibit bacteriocin activity or nutrient import. Such experiments were successful in early attempts at receptor discovery. For instance, competitive binding of cyanocobalamin and E-type colicins gave early indications that they all share BtuB as a receptor (Masi et al., 1973). Similarly, such experiments suggested that pyocin S3 and pyoverdine both bind to the ferripyoverdine type II receptor in *P. aeruginosa* (Baysse et al., 1999), and ferredoxin and pectocin M bind to the same ferredoxin receptor in *Pectobacterium artrosepticum* (Grinter et al., 2012).

An alternative approach is one that combines *neutralization assays with cell wall fractionation and protein purification*. OM fractions can be tested for bacteriocin neutralization activity. After singling out the OM fraction with neutralization activity, further analysis by mass spectrometry can identify the receptor. Use of protease inhibitors is important for preventing OM proteases from degrading the bacteriocin, which can be misinterpreted as bacteriocin neutralization. Misinterpretations can also be avoided by co-fractionating OM proteins isolated from a bacteriocin resistant and a bacteriocin sensitive strain, where all OM proteins from each strain have been labeled with two different fluorescent or radioactive labels. Since the resistant mutants should lack the receptor, a fraction with receptor activity should contain only proteins that originate from the sensitive strain (Sabet and Schnaitman, 1973). A limitation of this approach is that receptor concentrations obtained by OM fractionation can often be insufficient to achieve neutralization. This approach is therefore limited to cases where bacteriocin receptors are expressed to high levels or bind the bacteriocin with high affinity.

Instead of testing for neutralization activity, bacteriocin OM receptors can be identified directly by *pull-down experiments*, using a bacteriocin of interest as a bait (**Figure 2**). A bacteriocin should co-elute from the chromatography column with its receptor, where further analysis of the co-eluent by proteolysis and peptide fingerprinting by mass spectrometry can give a receptor candidate. For example, Housden et al. (2005) used a hexahistidine-tagged immunity protein complexed to ColE9 and immobilized on a nickel affinity column to purify components of the ColE9 translocon from OM extracts. These pull-down experiments can be challenging in cases of low-abundance receptors. One way to circumvent this problem is to find receptor overproducers, marked by an increased sensitivity to a bacteriocin of interest (Bowles et al., 1983). Another option is to cultivate cells in conditions that increase bacteriocin sensitivity by inducing receptor expression (Bindereif et al., 1982). Defining growth conditions where a bacteriocin receptor is overexpressed can also give valuable hints about the nature of the receptor. This was the case for several S-type pyocin receptors where it was observed that killing of *P. aeruginosa* was more effective if cultivated in iron-limited conditions (Smith et al., 1992; Sano et al., 1993). This observation indicated that siderophore receptors, which are overexpressed when cells are starved of iron, are involved in import of S-type pyocins. Receptors for pyocins S3, S2, S4, and S5 (Baysse et al., 1999; Denayer et al., 2007; Elfarash et al., 2012, 2014) were all discovered by this route.

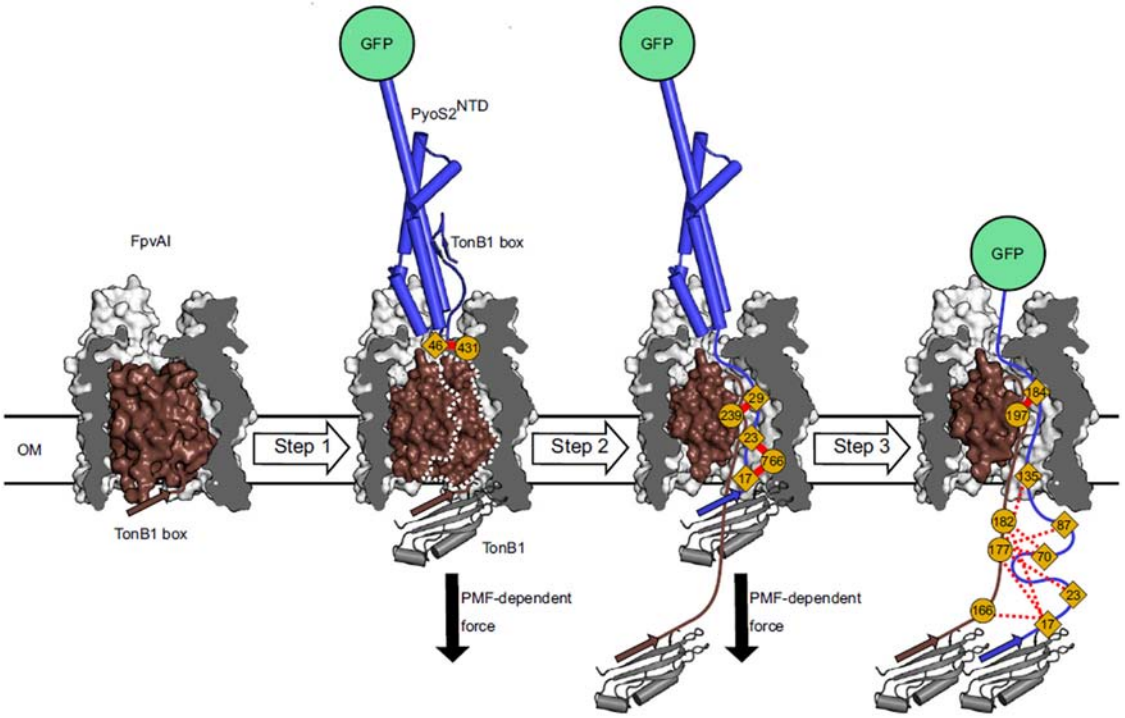

FIGURE 3 | *In vivo* cross-linking strategy developed by White et al. for dissecting the import pathway of pyocin S2 through the FpvAI receptor. Photoactivatable crosslinking data were used to establish a three-step model of translocation. In step 1, pyocin S2 binds to FpvAI and mimics its cognate ligand, ferro-pyoverdine. In step 2, a PMF-dependent mechanical force, applied via the ExbB–ExbD–TonB1 complex in the IM (not shown), drives unfolding of the labile half of the receptor plug domain and the N terminus of pyocin S2 enters the receptor lumen. In step 3, pyocin S2 binds to TonB1 and this interaction drives further passage of the pyocin through the receptor lumen. Complete translocation is blocked by the force-resistant GFP, which enables identification of translocation intermediates and mapping of interactions that govern pyocin S2 cell entry [image taken and used with permission from White et al. (2017), CC BY-NC-ND 4.0].

Another approach for receptor discovery is based on the isolation and characterization of *bacteriocin-resistant mutants*. A resistant mutant can lack a bacteriocin receptor; hence, picking up genetic differences between resistant and sensitive strains can pinpoint the receptor gene (**Figure 2**). When selecting for resistant mutants by use of lethal bacteriocin doses a major challenge is to distinguish between resistant and tolerant strains; only resistant strains bare mutations that specifically alter import machinery components. Therefore, it is always necessary to disregard tolerance by exposure to even higher bacteriocin doses than those used for selection and by checking if a mutant's growth kinetics is affected by the bacteriocin. Finally, resistance can be confirmed by checking if the mutant's OM has lost its bacteriocin binding properties by a neutralization assay or use of a fluorescently labeled bacteriocin to test for cell surface association (**Figure 3**; Rassam et al., 2015; White et al., 2017).

After isolating a resistant mutant, it is possible to compare its OM protein composition with the parental strain. A combination of electrophoresis and mass spectrometry can point out proteins absent in the OM of the resistant strain, but again, this has only been successful in cases where receptor genes are highly expressed (Ohkawa et al., 1980; Baysse et al., 1999). The advent of *whole-genome sequencing and comparative genomics* is now the preferred method of choice. Comparing a mutant's genome with a bacteriocin-sensitive reference strain can pinpoint potential receptor genes (McCaughey et al., 2014). This strategy has been successful in identifying bacteriocin receptors in Gram-positive bacteria (Cotter, 2014). The decreasing cost of DNA sequencing and continuous refinement of bioinformatics tools makes it likely that researchers in the field of Gram-negative bacteriocin import will increasingly turn to whole-genome sequencing. However, comparative genomics still has its limitations especially in the case of bacterial strains with a high rate of spontaneous mutations, where it can be difficult to filter out a mutation associated with bacteriocin resistance.

Receptor genes have also been identified by use of *cosmid libraries*. Genomic fragments from a bacteriocin-sensitive strain can be transformed into a bacteriocin-resistant background. The goal is to identify a fragment that can restore bacteriocin sensitivity and potentially carries a receptor gene (Pilsl et al., 1999; Smajs and Weinstock, 2001). An alternative approach is to construct *a library of transposon mutants* in a strain that is sensitive to the bacteriocin. Sequencing of genomic regions around the transposon insertion site in a resistant mutant can pinpoint genes linked to bacteriocin import (Baysse et al., 1999; de Chial et al., 2003; Elfarash et al., 2014; Ghequire et al., 2017). The power of this approach can be increased with the implementation of high-throughput transposon insertion

sequencing techniques, such as TraDIS (Barquist et al., 2016), since the employment of a dense transposon library can give better genomic coverage and increase the probability of a resistance phenotype being detected. TraDIS has recently been used to show that LPSs bearing O-antigens shield bacteriocin receptors in uropathogenic *E. coli* but that this effect is modulated by growth conditions (Sharp et al., 2019). Nevertheless, if a receptor is an essential gene no transposon mutants will be obtained and a library search will fail to show the receptor. In this case, pull-down experiments or linkage analysis (see below) can be used.

Bacteriocin receptors can also be found by *linkage analysis*, as in the case of S-type pyocin receptors. S pyocins kill *P. aeruginosa* better under iron limiting conditions, which gave indications that their activity might be linked to the pyoverdine import system (Ohkawa et al., 1980; Smith et al., 1992). A collection of *P. aeruginosa* strains was screened for pyocin S2 sensitivity and ferripyoverdine receptor genes typed by multiplex PCR. All S2 sensitive strains had the type I ferripyoverdine *fpvA*I gene, indicating this was the S2 receptor (Denayer et al., 2007). The same approach was used to link pyocin S4 sensitivity to the *fpvAI* receptor gene (Elfarash et al., 2012). Another type of linkage analysis that was successful in bacteriocin receptor discovery was *metabolite analysis*, where pyoverdine production was compared between pyocin S3 resistant and sensitive strains. It was found that pyocin S3 kills only type II pyoverdine producers of *P. aeruginosa*, while type I and III producers were resistant to S3 (Govan, 1978; Baysse et al., 1999). This gave strong indications that pyocin S3 binds to the ferripyoverdine type II receptor, which was confirmed by subsequent studies (de Chial et al., 2003). A future challenge will be implementation of high-throughput linkage approaches, which can be used when there are no initial clues about the import mechanism. This could be achieved through *genome wide association studies*, if both a genome sequence database and a physical strain collection are available. One could then test bacteriocin sensitivity throughout the collection and conduct a gene linkage analysis for a collection of corresponding annotated genomic sequences (Brynildsrud et al., 2016). Genes that are present in a large number of sensitive, but absent in a large number of bacteriocin resistant strains, are then further tested for receptor coding activity. On the other hand, the development of new mass spectrometric approaches in high-throughput metabolomics (Zampieri et al., 2017) could enable full metabolome comparison between bacteriocin resistant and sensitive strains, where metabolites lacking in resistant strains could give hints about import mechanisms being hijacked by the bacteriocin.

The majority of bacteriocin receptors identified to-date are proteins; however, non-proteinaceous receptors have also been identified. Pyocin L1 is a lectin-like bacteriocin produced by *P. aeruginosa*. It consists of tandem MMBL domains and kills cells by targeting the CPA of *P. aeruginosa* LPS, which is predominantly a homopolymer of D-rhamnose. The widespread inclusion of D-rhamnose in the LPS of pseudomonads explains the unusual genus-specific activity of this lectin-like bacteriocin. The discovery of the pyocin L1 saccharide receptor was achieved through a combination of genetics, structural, and biophysical approaches (McCaughey et al., 2014). Alignment of the pyocin L1 protein sequence with other lectin-like bacteriocins revealed the presence of three conserved MMBL sugar-binding domains, giving the first indications that pyocin L1 might bind to polysaccharide rather than to a protein receptor. A *P. aeruginosa* strain sensitive to this pyocin was used to recover resistant mutants, the genome sequences of which showed a deletion in the *wbpZ* gene, which encodes a glycosyltransferase involved in the synthesis of the CPA component of LPS (Rocchetta et al., 1998). Subsequent immunoblotting with a CPA-specific antibody along with transposon insertions in genes *wzt* and *wzm*, which encode the ATP-binding and the membrane components of a CPA dedicated ABC transporter (Lam et al., 2011), confirmed that CPA on the cell surface is required for pyocin L1 killing. Direct binding of pyocin L1 to CPA and D-rhamnose was shown by ITC and NMR spectroscopy. Finally, X-ray crystallography defined the mode of binding of the D-rhamnose receptor to the C-terminal MMBL domain of pyocin L1. This study therefore provides an excellent example how a combination of genomics and mutational analysis combined with biophysics and structural data can identify non-proteinaceous bacteriocin receptors.

In summary, bacteriocin receptors come in many different types and so an equally varied toolkit is needed for their identification (**Figure 2**). Receptors with high expression levels can be pulled-down using a bacteriocin as bait. This might be the only viable approach if the receptor is essential. If non-essential, receptor coding genes can be discovered through isolation of bacteriocin-resistant mutants, either spontaneously generated or induced through transposon mutagenesis. Finally, the future development of high-throughput approaches based on whole-genome sequencing and comparative genomics will alleviate receptor discovery for an ever-growing number of newly identified bacteriocins (Sharp et al., 2017).

IDENTIFYING TRANSLOCON COMPONENTS DOWNSTREAM OF THE RECEPTOR

After binding to a specific receptor, bacteriocins translocate across the OM. The receptor itself can serve as a translocation pore, as for the group B pyocin S2 (White et al., 2017), or another protein can be recruited to the complex to serve as a translocator, as for the group A colicin ColE9 (Housden et al., 2013). Before establishing a translocation model, it is necessary to find all OM and periplasmic components of a bacteriocin's translocon.

Bacteriocin insensitive mutants can be used to find translocon components other than the receptor. Mutant library screens have been particularly useful in this regard. For example, a screen of the Keio collection library for mutants insensitive but still capable of binding colicin S4 showed that *ompF*, *tolA*, *tolB*, *tolQ*, and *tolR* genes are all linked to its translocation. In the same study, it was found that after binding to the receptor OmpW, colicin S4 recruits OmpF and the Tol–Pal system to translocate across the OM (Arnold et al., 2009). A complication of this approach, however, is that *tol* gene knock-outs have altered membrane stability and permeability; deletion of *tolA* in *E. coli* leads

to a pleiotropic phenotype characterized by outer membrane blebbing, release of the periplasmic content, increased sensitivity to cholic acid and SDS, and defective *O*-antigen polymerization (Germon et al., 2001). Indeed, *P. aeruginosa tolQRA* knock-outs are lethal (Wei et al., 2009). Therefore, using *tol* deletion mutants to check if bacteriocin entry is Tol–Pal dependent is not always feasible.

Chimeric bacteriocins have been effectively used to separate the receptor binding and translocation phases of the import process, which can be important for finding translocon components downstream of the receptor. This approach was successfully used to show that colicin Ia uses two copies of the Cir protein for OM translocation – one copy is used as the receptor and the other copy is used for translocation. A chimeric colicin Ia, in which the receptor-binding domain was replaced by that from colicin E3, required BtuB, the colicin E3 receptor, but also a copy of Cir and TonB for its killing activity. This experiment gave indications that one copy of Cir interacts with the receptor-binding domain of colicin Ia to concentrate the protein on the cell surface, while the other copy of Cir interacts with the translocation domain of this colicin so it can pass through the OM and enter the periplasm (Buchanan et al., 2007; Jakes and Finkelstein, 2010). However, direct binding of the Cir translocator with colicin Ia has yet to be demonstrated biochemically. *Receptor bypass* experiments have also been used to find translocon components other than the receptor. In such experiments, the OM is first permeabilized, usually by osmotic shock, so the receptor binding step is bypassed (Thomas and Valvano, 1993). This can be useful when a receptor for a bacteriocin under investigation is not known or when suitable chimeras are not available.

Very little is known about *inner membrane translocation* of Gram-negative bacteriocins. However, mutational analysis successfully identified some IM proteins necessary for transport of nuclease colicins. Walker et al. (2007) used a Δ*ftsH E. coli* strain to show that the toxicity of all nuclease colicins (regardless of their Tol–Pal/Ton dependence) is dependent on FtsH, an inner membrane AAA+ ATPase/protease. This protease cleaves off the DNase domain during import to the cytoplasm (Chauleau et al., 2011; Mora and de Zamaroczy, 2014). In other studies, whole-genome sequencing of an *E. coli* mutant that is insensitive to colicin D gave indications that an inner membrane peptidase LepB is required for cell entry (de Zamaroczy et al., 2001). LepB is a key membrane component of the cellular secretion machinery, which releases secreted proteins into the periplasm by cleaving the inner membrane-bound leader. It was further shown that this protein binds to colicin D and probably directs it to the FtsH protease for cell entry (Mora et al., 2015).

Since IM translocation components are a part of protein translocation systems that are well conserved across different Gram-negative bacteria, it is possible to study the import of bacteriocins from other species using *E. coli* as a model system. The only limitation here is to bypass all the species-specific translocation steps that are mostly localized to the outer membrane. Hence, Mora et al. (2015) used a colicin D/klebicin D hybrid in which the N-terminal import domain of klebicin D was replaced with that of colicin D. Klebicin D targets *Klebsiella* species, but when fused to the receptor binding and the translocation domain of colicin D it can also kill *E. coli* obviating the need for a *Klebsiella* knock-out library. In this way, it was found that klebicin D, like colicin D, uses LepB for import (Mora et al., 2015).

DECONSTRUCTING THE PROTEIN–PROTEIN INTERACTIONS OF BACTERIOCIN TRANSLOCONS

Several approaches can be taken to define binding epitopes and binding induced conformational changes within bacteriocin translocons. PPIs between translocon components have to be first confirmed *in vitro* and *in vivo*. A common approach is *gene complementation* using a bacteriocin-resistant mutant or a bacteriocin-resistant species (Kjos et al., 2014), where the establishment of bacteriocin sensitivity can confirm the involvement of components in bacteriocin import (**Figure 2**). Apart from gene complementation assays, interactions between components can be assessed *in vivo* by *pull-down* experiments. A way to "freeze" the translocon in the assembly phase is by *in vivo* cross-linking (Masi et al., 2007; White et al., 2017) or by a disulphide locked bacteriocin (Housden et al., 2005, 2013). In both cases, a bacteriocin must be able to bind to its receptor and trigger translocon assembly without fully traversing the cell envelope and killing the target cell. Bacteriocin-bound protein complexes can further be extracted from the outer membrane by affinity chromatography using a bacteriocin or its immunity protein as bait. Pulldowns followed by limited proteolysis of the complex, and mass spectrometry of recovered protein fragments, can indicate which binding epitopes are involved in the translocon. For example, Housden et al. (2013) designed a disulphide lock that forms between the TolB-binding epitope of ColE9 and periplasmic TolB following recruitment of OmpF in the OM. A histidine tag on TolB enabled a heptameric assembly of the ColE9–Im9 complex, BtuB, OmpF trimer, and TolB to be purified and analyzed by mass spectrometry. Finally, limited proteolysis, in combination with planar lipid bilayer experiments and native mass spectrometry, demonstrated that within the translocon, ColE9's unstructured N-terminal region passes twice through its bound porin thereby presenting its TolB-binding epitope in a conformationally constrained orientation in the periplasm (Housden et al., 2013).

Calorimetric measurements have also been used extensively in colicin import studies (Housden and Kleanthous, 2011), in particular ITC. ITC parameters can provide evidence of conformational changes within the translocon (Housden et al., 2005). ITC has also been used to determine how a bacteriocin affects existing PPIs within the cell envelope. Changes in the heats of binding in presence of a bacteriocin can indicate if it abolishes or induces a certain PPI. In this way, it has been shown that ColE9 interacts with TolB when entering the periplasm, disrupting the TolB–Pal complex and stimulating formation of a TolA–TolB complex that traverses the periplasm (Bonsor et al., 2009). ITC combined with site-directed mutagenesis can

map translocon-binding sites, as in the case of the ColE9 TolB-binding region. The favorable enthalpy and unfavorable entropy changes associated with ColE9-binding TolB correspond to a disorder-to-order transition that occurs when the intrinsically unstructured region of ColE9 folds and binds TolB (Loftus et al., 2006). In other words, ITC parameters can indicate not only which regions of bacteriocins and their translocon components interact, but also which regions undergo conformational changes and in which phases of the translocation process these conformational changes occur.

Stopped-flow FRET experiments demonstrated how a bacteriocin can remodel PPIs within the cell envelope during import. Papadakos et al. (2012a) used a series of pre-steady-state kinetic experiments utilizing FRET pairs of ColE9 TolB-binding epitope, TolB and Pal, to establish the kinetic basis for competitive recruitment of TolB by ColE9 during which Pal gets displaced from its TolB–Pal complex. Interactions between translocon components have also been investigated using *planar lipid bilayers*. For example, it has been shown that ColE1 occludes TolC channels and that ColE9 occludes OmpF channels in planar lipid bilayers, confirming previous findings that these OMPs are involved in bacteriocin translocation (Zakharov et al., 2004). This approach was also used to identify a TolC box in ColE1 (Zakharov et al., 2016).

ASSEMBLING THE TRANSLOCON

A major challenge in understanding protein bacteriocin import is to assemble their translocons for structural studies where, for the most part, only general import mechanisms have been described (Cascales et al., 2007; Ghequire and De Mot, 2014; McCaughey et al., 2016; White et al., 2017).

Since Gram-negative bacteriocins are large multi-domain proteins, it is thought they must unfold, either partially or completely, in order to translocate across the outer membrane. Introducing *disulphide bonds* to prevent conformational changes in certain regions of a bacteriocin has been a useful approach in delineating such structural changes (Penfold et al., 2004). Similarly, *protease cleavage sites* have been used to probe the accessibility of bacteriocin sequences within a translocon. Zhang et al. (2008) introduced unique EK cleavage sites in a disulphide-locked ColE9 at a number of locations to study the surface accessibility of colicin subdomains shortly after receptor binding. In this experiment, a disulphide-lock within the colicin was used to synchronize translocon assembly; disulfide bond reduction simultaneously triggers initiation of translocation in all bacterial cells. This enabled determination of EK cleavage site accessibility for different regions of the colicin, which gave important insight into the position of ColE9 in the assembled translocon (Zhang et al., 2008).

Studies are beginning to unravel the molecular mechanism(s) by which bacteriocins translocate across the OM. White et al. (2017) developed an *in vivo cross-linking strategy* to map the import of the pyocin S2 NTD through the FpvAI receptor (**Figure 3**). This approach depended on first blocking import of the NTD using a C-terminal GFP. GFP is able to withstand ∼200 pN of force whereas the PMF can only deliver ∼20 pN (Saeger et al., 2012). This strategy allowed the accumulation of translocation intermediates that would otherwise be undetectable by crosslinking. Variants of this GFP fusion were then generated in which benzoylphenylalanine was incorporated at different positions of the NTD using amber suppression and crosslinked following transport into *P. aeruginosa* cells. Detailed mass spectrometric analysis of crosslinked peptides demonstrated that the pyocin not only translocates through FpvAI but that it does so by a process which likely mimics that used by pyoverdine, the natural ligand for FpvAI (White et al., 2017).

An important aspect of nuclease bacteriocin import is the release of the tightly bound immunity protein. All nuclease bacteriocins are produced bound tightly ($K_d \sim 10^{-14}$ M at pH 7 and 25°C) to their immunity protein Papadakos et al. (2012b). The half-life for dissociation for this complex is several days yet killing occurs within minutes. Hence, it has been postulated that an energy transduction path exists that jettisons the immunity protein at the cell surface during import. Zhang et al. (2008) developed a sensitive *fluorescence assay* to investigate immunity release. The assay was based on release of a fluorescently labeled immunity protein into the cell supernatant. Bacteriocin import was synchronized using a disulfide-lock. In this way, fluorescently labeled Im9 was detected in the cell supernatant after the addition of a reducing agent and was dependent on the PMF across the inner membrane (Zhang et al., 2008; Vankemmelbeke et al., 2012), shown subsequently to be linked to global conformational changes within the colicin (Vankemmelbeke et al., 2013). How force might cause immunity dissociation has been investigated by *single molecule atomic force spectroscopy* (Farrance et al., 2013). These studies demonstrated that the ColE9 DNase–Im9 complex is exquisitely sensitive to mechanical deformation at the N-terminus of the nuclease, which could represent pulling into a cell, causing rapid dissociation of the immunity protein.

STRUCTURAL BIOLOGY APPROACHES FOR STUDYING BACTERIOCIN IMPORT

Structural studies are important in gaining a molecular understanding of the bacteriocin translocation process. To-date, there are only a few structures of intact Gram-negative bacteriocins (Wiener et al., 1997; Soelaiman et al., 2001; Helbig et al., 2011; Klein et al., 2016). More informative, in terms of translocation mechanism, are structures of bacteriocins or bacteriocin domains bound to their receptor or a component of the translocon assembly (Kurisu et al., 2003; Loftus et al., 2006; Buchanan et al., 2007; Sharma et al., 2007; Zhang et al., 2009; Housden et al., 2010; White et al., 2017). These structures give information about conformational changes that a bacteriocin induces and shed light on the import mechanism.

Crystallization of bacteriocins can often be challenging due to intrinsically disordered and flexible regions in these proteins. Flexibility can be reduced by deletion of these sequences or by the introduction of intramolecular disulfide bonds (Klein et al., 2016). To complete a structure of a bacteriocin it is often necessary to substitute missing X-ray diffraction data

with results from other experiments. Modeling of data from *analytical ultracentrifugation* (Manon and Ebel, 2010) and *NMR experiments* (Collins et al., 2002; Hecht et al., 2009) can help in filling-in missing parts of a bacteriocin structure. Results from *SAXS* experiments can also be combined with diffraction data; a bacteriocin can be treated as a flexible system, namely by the ensemble optimization method, which enables a distribution of conformations to be included in the final model (Johnson et al., 2017).

Structures of *bacteriocin–receptor and bacteriocin–translocator complexes* are essential to understand bacteriocin import mechanisms. When compared to receptor–cognate ligand complexes, these structures can show to what extent a bacteriocin mimics the ligand (if at all) when traversing the cell envelope. For example, co-crystal structures for E-type colicins bound to the BtuB receptor (ColE2, ColE3) show that the colicins do not mimic the interactions of the ligand and do not induce conformational changes within the globular N-terminal plug domain of BtuB indicative of transport. This contrasts the situation of pyocin S2-NTD bound to its receptor FpvAI where the structure clearly supports a model (validated by crosslinking data) that the pyocin mimics the endogenous ligand, pyoverdine, and transports through the receptor in a TonB-dependent manner (White et al., 2017). For the E colicins (all of which require the Tol complex), entry to the periplasm requires OmpF or OmpC. These porins acts as translocators, which is supported by structures of OmpF in which fragments of E colicins are bound within its lumen (Yamashita et al., 2008; Housden et al., 2010) and by planar lipid bilayer experiments where colicin fragments block ion conductance (Zakharov et al., 2004).

The development of structure–prediction algorithms could broaden the understanding of bacteriocin translocons (Delarue and Koehl, 2018). For instance, protein fold predictions have already been employed in structure determination of a group A colicin translocon component, TolQ (Ovchinnikov et al., 2015). Additionally, future developments in translocon structures will undoubtedly involve cryo-EM methods. It may even be possible to eventually capture a bacteriocin in-transit and use cryo-tomography to map out its interactions within the cell envelope.

VIEWING THE IMPORT PROCESS IN THE CONTEXT OF OUTER MEMBRANE ORGANIZATION

Bacteriocins have become valuable tools with which to investigate spatiotemporal organization in the cell envelope by fluorescence microscopy (Kleanthous et al., 2015). Fluorescently labeled bacteriocins have been used in conjunction with *single particle tracking TIRF microscopy* to show that OMPs display highly restricted mobility in the outer membrane due to the formation of supramolecular assemblies called OMP islands, which also explains the lack of fluorescence recovery for labeled OMPs in FRAP experiments (**Figure 4**). TIRF microscopy of bacteriocin-labeled OMPs has also shown that OMP islands move to the poles as new islands appear in the membrane (Rassam et al., 2015). Even more remarkably, the restricted mobility that is characteristic of OMPs within OMP islands becomes imprinted on inner membrane proteins when the bacteriocin forms its translocon across the two membranes (**Figure 5**; Rassam et al., 2018).

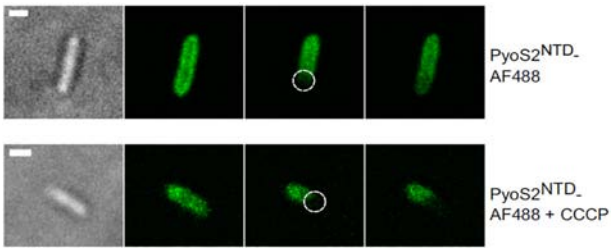

FIGURE 4 | FRAP experiments can be used to show that bacteriocin import is a PMF-dependent process. *P. aeruginosa* PAO1 cells are labeled with pyocin S2 AF488. The bleached region is highlighted (dashed circle). FRAP suggests pyoS2NTD-AF488 has translocated to the periplasm, where it can diffuse laterally. Absence of FRAP observed when cells are treated with 100 μM CCCP indicates that the pyocin remains bound to FpvAI in the OM and that the PMF is necessary for pyocin translocation. Scale bars, 1 μm [image taken and used with permission from White et al. (2017), CC BY-NC-ND 4.0].

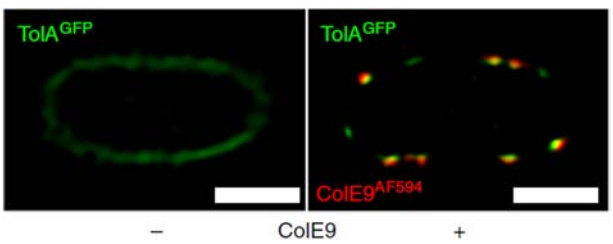

FIGURE 5 | Fluorescently labeled bacteriocins can be used to track outer and inner membrane protein clusters; used by Rassam et al. (2018) to show that bacteriocin-induced clustering of TolA in the IM mirrors that of OMPs in the OM. 2D-SIM z-slice showing significant co-clustering (yellow fluorescence) of GFP-TolA and ColE9AF594 in the IM and OM, respectively. Scale bars, 1 μm [image taken and used with permission from Rassam et al. (2018), CC BY-NC-ND 4.0].

Fluorescently labeled bacteriocins have also been used for dissecting their import mechanism. GFP was deployed by White et al. (2017) to visualize association of pyocin S2 with *P. aeruginosa* cells, block translocation, and trap the pyocin within its receptor, FpvAI, for subsequent crosslinking studies. By switching to an organic dye (AF488), White et al. (2017) demonstrated import of the pyocin S2 domain since in contrast to GFP-labeled protein, fluorescence recovery was observed for AF488-pyocin S2-labeled cells in FRAP experiments. Imported fluorescent protein was also protected against exogenously added protease.

Live cell imaging can also be used to dissect the directionality of PPIs formed between bacteriocins and their translocators. Housden et al. (2018) used a combination of molecular dynamics simulations, fluorescence microscopy, and single channel recording planar lipid bilayer measurements to unambiguously demonstrate from which side of the OM different OBSs of

ColE9 associated with the lumen of the porin. The intrinsically unstructured N-terminal region of ColE9 houses two OBSs (OBS1 and OBS2) that reside within the pores of OmpF and that flank an epitope that binds periplasmic TolB. The studies revealed that OBS2 binds OmpF from the extracellular side, while the interaction of OBS1 occurs from the periplasmic face of OmpF, which ensures constrained presentation of the TolB epitope within the bacterial periplasm (Housden et al., 2018).

THE ENERGETICS AND KINETICS OF BACTERIOCIN IMPORT

The energetics of bacteriocin translocation are still controversial. Indeed, little is known about the energy dependence of individual translocation steps. Since bacteriocins are folded proteins, import is likely to rely on the input of energy, the main source being the PMF generated across the IM. However, some studies suggest that OM translocation is energy independent, as in the case of colicin A (Bourdineaud et al., 1990). Nevertheless, live cell imaging studies are beginning to show the link between PMF, Ton, Tol, and bacteriocin import (White et al., 2017; Rassam et al., 2018).

A way of testing if energy is necessary for a certain phase of bacteriocin import is to disrupt the PMF and then assess import with a suitable assay. Protonic ionophores have been used for this; for example, CCCP was used in FRAP experiments to show that PMF is necessary for import of pyocin S2 (**Figure 4**; White et al., 2017). Disulphide locked colicins and fluorescently labeled immunity proteins have been used to study the energy dependence of immunity protein release (Vankemmelbeke et al., 2012). A sensitive assay for detecting immunity protein release (described above) was used to confirm that both TolB and TolA are necessary for this process in ColE9 import and to define which regions of TolA are engaged. TolA is anchored in the cytoplasmic membrane via a single transmembrane region that interacts to TolQ and TolR and drives a TolA conformational change in response to PMF (Germon et al., 2001). Vankemmelbeke et al. (2009) focused on residue H22 of the TolA IM region that has been previously linked to energy-dependent conformational change of this protein (Larsen et al., 2007). They showed that an alanine mutation of this residue disrupts immunity protein release, which indicated that an energy-dependent conformational change of TolA is essential for nuclease colicin Im9 release at the cell surface. This points to a role for TolA in transducing cellular energy in a manner similar to that described for TonB (Postle and Larsen, 2007), but the mechanism remains unknown. Bonsor et al. (2009) went on to show that it is the contact between TolA and TolB within the periplasm that is the necessary energy-transduction step for nuclease colicin Im release. One model proposes that the rotation of Tol complex transmembrane helices is transduced into a conformational change in TolA that affects its interaction with the TolB–bacteriocin complex and triggers Im protein dissociation (Papadakos et al., 2012). New methodological approaches will be necessary to dissect how the electrochemical potential of the PMF is transduced by the Tol and Ton systems into the mechanical action of bacteriocin import.

Little is known of the kinetics of bacteriocin import beyond the onset of cellular changes these protein toxins induce. Early studies showed that conformational flexibility is a prominent bacteriocin trait, determining the kinetics of import (Duche et al., 1994). Additionally, bacteriocin charge (Walker et al., 2007) and cell envelope properties related to lipid composition are factors that influence the speed of import (Bourdineaud et al., 1990; Walker et al., 2007). In the case of pore forming colicins, measuring cytoplasmic potassium efflux caused by colicin A inner membrane insertion was used to show how inner membrane fluidity influences the kinetics of translocation (Bourdineaud et al., 1990). In the case of nuclease colicins, Walker et al. (2007) observed that inner membrane charge impacts the rate of import. In this study, a strain of *E. coli* in which the level of anionic phospholipids was regulated by isopropyl β-D-thiogalactopyranoside induction was used to show that both inner membrane and bacteriocin charge influence the rate of cell entry. Import kinetics were measured indirectly, through the efficiency of cell killing or DNA damage. Still, little is known about the kinetics of individual translocation steps and how PPIs between translocon components influence the rate of import. Therefore, to understand import kinetics in more detail, methods for direct measurement of individual translocation steps will have to be developed, most likely based on single molecule methods.

FUTURE PERSPECTIVES

As protein bacteriocins begin to be exploited as therapeutics for multidrug-resistant bacteria so our ability to understand their import mechanisms needs to develop (Behrens et al., 2017). Various approaches, ranging from classical biochemical methods to advanced molecular genetics, have been used over the years for translocon component discovery. The development of high-throughput approaches based on whole-genome sequencing and comparative genomics can speed up this process in the future. Calorimetric measurements have been used extensively to identify binding epitopes and to study the nature of interactions between translocon components. Moreover, implementation of various microscopy techniques, channel conductivity measurements, *in vivo* cross-linking, and disulphide locking of bacteriocins have been exploited for determining the directionality of PPIs within the translocon and for identifying entry paths that bacteriocins use when crossing the OM. Finally, *in vivo* imaging of cells bound to fluorescently labeled bacteriocins has enabled visualization of the import process for the first time at single cell level and provided new tools for probing the spatiotemporal organization of the cell envelope.

While substantial knowledge about OM translocation of bacteriocins has been gained over recent years, the IM component of translocation remains to be elucidated. Many questions remain unanswered – which proteins are involved in bacteriocin IM translocation, how is this process energized,

which parts of a bacteriocin are necessary for IM translocation, and which parts enter the cytoplasm. Additionally, a clear link between the OM and IM components of bacteriocin translocons still has to be revealed. For example, are nuclease bacteriocins brought into the periplasm in their entirety before import across the cytoplasmic membrane begins? Finally, the study of bacteriocins in the context of cell envelope organization has breathed new life into bacteriocin research.

AUTHOR CONTRIBUTIONS

IA and CK contributed to the original manuscript and the editorial changes.

FUNDING

IA was funded by the Wellcome Trust Infection, Immunology and Translational Medicine Doctoral Training Centre. CK acknowledges funding from the ERC (OMPorg – 742555), Wellcome Trust (201505/Z/16/Z), MRC (MR/R009937/1), and BBSRC (BB/P009948/1).

ACKNOWLEDGMENTS

The authors would like to thank Ms. Hannah Behrens, Dr. Joanna Szczepaniak, Dr. Nathalie Reichmann, and Dr. Nick Housden for useful discussions and feedback on this manuscript.

REFERENCES

Arnold, T., Zeth, K., and Linke, D. (2009). Structure and function of colicin S4, a colicin with a duplicated receptor-binding domain. *J. Biol. Chem.* 284, 6403–6413. doi: 10.1074/jbc.M808504200

Barquist, L., Mayho, M., Cummins, C., Cain, A. K., Boinett, C. J., Page, A. J., et al. (2016). The TraDIS toolkit: sequencing and analysis for dense transposon mutant libraries. *Bioinformatics* 32, 1109–1111. doi: 10.1093/bioinformatics/btw022

Baysse, C., Meyer, J. M., Plesiat, P., Geoffroy, V., Michel-Briand, Y., and Cornelis, P. (1999). Uptake of pyocin S3 occurs through the outer membrane ferripyoverdine type II receptor of *Pseudomonas aeruginosa*. *J. Bacteriol.* 181, 3849–3851.

Behrens, H. M., Six, A., Walker, D., and Kleanthous, C. (2017). The therapeutic potential of bacteriocins as protein antibiotics. *Emerg. Top. Life Sci.* 1, 65–74. doi: 10.1042/ETLS20160016

Bindereif, A., Volkmar, B., and Klaus, H. (1982). The cloacin receptor of Co1V-bearing *Escherichia coli* is part of the Fe3+-Aerobactin transport system. *J. Bacteriol.* 150, 1472–1475.

Bonsor, D. A., Hecht, O., Vankemmelbeke, M., Sharma, A., Krachler, A. M., Housden, N. G., et al. (2009). Allosteric β-propeller signalling in TolB and its manipulation by translocating colicins. *EMBO J.* 28, 2846–2857. doi: 10.1038/emboj.2009.224

Bourdineaud, J. P., Boulanger, P., Lazdunski, C., and Letellier, L. (1990). In vivo properties of colicin A: channel activity is voltage dependent but translocation may be voltage independent. *Proc. Natl. Acad. Sci. U.S.A.* 87, 1037–1041. doi: 10.1073/pnas.87.3.1037

Bowles, L. K., Miguel, A. G., and Konisky, J. (1983). Purification of the colicin I receptor. *J. Biol. Chem.* 258, 1215–1220.

Brynildsrud, O., Bohlin, J., Scheffer, L., and Eldholm, V. (2016). Rapid scoring of genes in microbial pan-genome-wide association studies with Scoary. *Genome Biol.* 17:238. doi: 10.1186/s13059-016-1108

Buchanan, S. K., Lukacik, P., Grizot, S., Ghirlando, R., Ali, M. M., Barnard, T. J., et al. (2007). Structure of colicin I receptor bound to the R-domain of colicin Ia: implications for protein import. *EMBO J.* 26, 2594–2604. doi: 10.1038/sj.emboj.7601693

Cascales, E., Buchanan, S. K., Duché, D., Kleanthous, C., Lloubès, R., Postle, K., et al. (2007). Colicin biology. *Microbiol. Mol. Biol. Rev.* 71, 158–229. doi: 10.1128/MMBR.00036-06

Chauleau, M., Mora, L., Serba, J., and de Zamaroczy, M. (2011). FtsH-dependent processing of RNase colicins D and E3 means that only the cytotoxic domains are imported into the cytoplasm. *J. Biol. Chem.* 286, 29397–29407. doi: 10.1074/jbc.M111.242354

Collins, E. S., Whittaker, S. B., Tozawa, K., MacDonald, C., Boetzel, R., Penfold, C. N., et al. (2002). Structural dynamics of the membrane translocation domain of colicin E9 and its interaction with TolB. *J. Mol. Biol.* 318, 787–804. doi: 10.1016/S0022-2836(02)00036-0

Cornforth, D. M., and Foster, K. R. (2013). Competition sensing: the social side of bacterial stress responses. *Nat. Rev. Microbiol.* 11, 285–293. doi: 10.1038/nrmicro2977

Cotter, P. D. (2014). An 'Upp'-turn in bacteriocin receptor identification. *Mol. Microbiol.* 92, 1159–1163. doi: 10.1111/mmi.12645

de Chial, M., Ghysels, B., Beatson, S. A., Geoffroy, V., Meyer, J. M., Pattery, T., et al. (2003). Identification of type II and type III pyoverdine receptors from *Pseudomonas aeruginosa*. *Microbiology* 149, 821–831. doi: 10.1099/mic.0.26136-0

de Zamaroczy, M., Mora, L., Lecuyer, A., Géli, V., and Buckingham, R. H. (2001). Cleavage of colicin D is necessary for cell killing and requires the inner membrane peptidase LepB. *Mol. Cell* 8, 159–168. doi: 10.1016/S1097-2765(01)00276-3

Delarue, M., and Koehl, P. (2018). Combined approaches from physics, statistics, and computer science for ab initio protein structure prediction: ex unitate vires (unity is strength)? *F1000Research* 7:F1000FacultyRev-1125. doi: 10.12688/f1000research.14870.1

Denayer, S., Matthijs, S., and Cornelis, P. (2007). Pyocin S2 (Sa) kills *Pseudomonas aeruginosa* strains via the FpvA type I ferripyoverdine receptor. *J. Bacteriol.* 189, 7663–7668. doi: 10.1128/JB.00992-07

Duche, D., Baty, D., Chartier, M., and Letellier, L. (1994). Unfolding of colicin A during its translocation through the *Escherichia coli* envelope as demonstrated by disulfide bond engineering. *J. Biol. Chem.* 269, 24820–24825.

Duquesne, S., Destoumieux-Garzon, D., Peduzzi, J., and Rebuffat, S. (2007). Microcins, gene-encoded antibacterial peptides from enterobacteria. *Nat. Prod. Rep.* 24, 708–734. doi: 10.1039/b516237h

Elfarash, A., Dingemans, J., Ye, L., Hassan, A. A., Craggs, M., Reimmann, C., et al. (2014). Pore-forming pyocin S5 utilizes the FptA ferripyochelin receptor to kill *Pseudomonas aeruginosa*. *Microbiology* 160, 261–269. doi: 10.1099/mic.0.070672-0

Elfarash, A., Wei, Q., and Cornelis, P. (2012). The soluble pyocins S2 and S4 from *Pseudomonas aeruginosa* bind to the same FpvAI receptor. *Microbiologyopen.* 1, 268–275. doi: 10.1002/mbo3.27

Farrance, O. E., Hann, E., Kaminska, R., Housden, N. G., Derrington, S. R., Kleanthous, C., et al. (2013). A force-activated trip switch triggers rapid dissociation of a colicin from its immunity protein. *PLoS Biol.* 11:e1001489. doi: 10.1371/journal.pbio.1001489

Germon, P., Ray, M. C., Vianney, A., and Lazzaroni, J. C. (2001). Energy-dependent conformational change in the TolA protein of *Escherichia coli* involves its N-terminal domain, TolQ, and TolR. *J. Bacteriol.* 183, 4110–4114. doi: 10.1128/JB.183.14.4110-4114.2001

Ghequire, M. G., and De Mot, R. (2014). Ribosomally encoded antibacterial proteins and peptides from *Pseudomonas*. *FEMS Microbiol. Rev.* 38, 523–568. doi: 10.1111/1574-6976.12079

Ghequire, M. G. K., Kemland, L., Anoz-Carbonell, E., Buchanan, S. K., and De Mot, R. (2017). A natural chimeric *Pseudomonas* bacteriocin with novel pore-forming activity parasitizes the ferrichrome transporter. *mBio* 8:e1961-16. doi: 10.1128/mBio.01961-16

Govan, J. R. W. (1978). Pyocin typing of *Pseudomonas aeruginosa*. *Methods Microbiol.* 10, 61–91. doi: 10.1016/S0580-9517(08)70660-3

Grinter, R., Milner, J., and Walker, D. (2012). Ferredoxin containing bacteriocins suggest a novel mechanism of iron uptake in *Pectobacterium* spp. *PLoS One* 7:e33033. doi: 10.1371/journal.pone.0033033

Héchard, Y., and Sahl, H. G. (2002). Mode of action of modified and unmodified bacteriocins from Gram-positive bacteria. *Biochimie* 84, 545–557. doi: 10.1016/S0300-9084(02)01417-7

Hecht, O., Ridley, H., Lakey, J. H., and Moore, G. R. (2009). A common interaction for the entry of colicin N and filamentous phage into *Escherichia coli*. *J. Mol. Biol.* 388, 880–893. doi: 10.1016/j.jmb.2009.03.035

Helbig, S., Patzer, S. I., Schiene-Fischer, C., Zeth, K., and Braun, V. (2011). Activation of colicin M by the FkpA prolyl cis-trans isomerase/chaperone. *J. Biol. Chem.* 286, 6280–6290. doi: 10.1074/jbc.M110.165274

Housden, N. G., Hopper, J. T., Lukoyanova, N., Rodriguez-Larrea, D., Wojdyla, J. A., Klein, A., et al. (2013). Intrinsically disordered protein threads through the bacterial outer-membrane porin OmpF. *Science* 340, 1570–1574. doi: 10.1126/science.1237864

Housden, N. G., and Kleanthous, C. (2011). Thermodynamic dissection of colicin interactions. *Methods Enzymol.* 488, 123–145. doi: 10.1016/B978-0-12-381268-1.00006-9

Housden, N. G., Loftus, S. R., Moore, G. R., James, R., and Kleanthous, C. (2005). Cell entry mechanism of enzymatic bacterial colicins: porin recruitment and the thermodynamics of receptor binding. *Proc. Natl. Acad. Sci. U.S.A.* 102, 13849–13854. doi: 10.1073/pnas.0503567102

Housden, N. G., Rassam, P., Lee, S., Samsudin, F., Kaminska, R., Sharp, C., et al. (2018). Directional porin binding of intrinsically disordered protein sequences promotes colicin epitope display in the bacterial periplasm. *Biochemistry* 57, 4374–4381. doi: 10.1021/acs.biochem.8b00621

Housden, N. G., Wojdyla, J. A., Korczynska, J., Grishkovskaya, I., Kirkpatrick, N., Brzozowski, A. M., et al. (2010). Directed epitope delivery across the *Escherichia coli* outer membrane through the porin OmpF. *Proc. Natl. Acad. Sci. U.S.A.* 107, 21412–21417. doi: 10.1073/pnas.1010780107

Jakes, K. S., and Finkelstein, A. (2010). The colicin Ia receptor, Cir, is also the translocator for colicin Ia. *Mol. Microbiol.* 75, 567–578. doi: 10.1111/j.1365-2958.2009.06966.x

Jamet, A., and Nassif, X. (2015). New players in the toxin field: polymorphic toxin systems in bacteria. *mBio* 6:e285-15. doi: 10.1128/mBio.00285-15

Johnson, C. L., Solovyova, A. S., Hecht, O., Macdonald, C., Waller, H., Grossmann, J. G., et al. (2017). The two-state prehensile tail of the antibacterial toxin colicin N. *Biophys. J.* 113, 1673–1684. doi: 10.1016/j.bpj.2017.08.030

Kim, Y. C., Tarr, A. W., and Penfold, C. N. (2014). Colicin import into *E. coli* cells: a model system for insights into the import mechanisms of bacteriocins. *Biochim. Biophys. Acta.* 1843, 1717–1731. doi: 10.1016/j.bpj.2017.08.030

Kjos, M., Oppegård, C., Diep, D. B., Nes, I. F., Veening, J.-W., Nissen-Meyer, J., et al. (2014). Sensitivity to the two-peptide bacteriocin lactococcin G is dependent on UppP, an enzyme involved in cell-wall synthesis. *Mol. Microbiol.* 92, 1177–1187. doi: 10.1111/mmi.12632

Kleanthous, C. (2010). Swimming against the tide: progress and challenges in our understanding of colicin translocation. *Nat. Rev. Microbiol.* 8, 843–848. doi: 10.1038/nrmicro2454

Kleanthous, C., Rassam, P., and Baumann, C. G. (2015). Protein-protein interactions and the spatiotemporal dynamics of bacterial outer membrane proteins. *Curr. Opin. Struct. Biol.* 35, 109–115. doi: 10.1016/j.sbi.2015.10.007

Klein, A., Wojdyla, J. A., Joshi, A., Josts, I., McCaughey, L. C., Housden, N. G., et al. (2016). Structural and biophysical analysis of nuclease protein antibiotics. *Biochem. J.* 473, 2799–2812. doi: 10.1042/BCJ20160544

Kurisu, G., Zakharov, S. D., Zhalnina, M. V., Bano, S., Eroukova, V. Y., Rokitskaya, T. I., et al. (2003). The structure of BtuB with bound colicin E3 R-domain implies a translocon. *Nat. Struct. Biol.* 10, 948–954. doi: 10.1038/nsb997

Lam, J. S., Taylor, V. L., Islam, S. T., Hao, Y., and Kocincova, D. (2011). Genetic and functional diversity of *Pseudomonas aeruginosa* lipopolysaccharide. *Front. Microbiol.* 2:118. doi: 10.3389/fmicb.2011.00118

Larsen, R. A., Deckert, G. E., Kastead, K. A., Devanathan, S., Keller, K. L., and Postle, K. (2007). His(20) provides the sole functionally significant side chain in the essential TonB transmembrane domain. *J. Bacteriol.* 189, 2825–2833. doi: 10.1128/JB.01925-26

Loftus, S. R., Walker, D., Maté, M. J., Bonsor, D. A., James, R., Moore, G. R., et al. (2006). Competitive recruitment of the periplasmic translocation portal TolB by a natively disordered domain of colicin E9. *Proc. Natl. Acad. Sci. U.S.A.* 103, 12353–12358. doi: 10.1073/pnas.0603433103

Lukacik, P., Barnard, T. J., Keller, P. W., Chaturvedi, K. S., Seddiki, N., Fairman, J. W., et al. (2012). Structural engineering of a phage lysin that targets gram-negative pathogens. *Proc. Natl. Acad. Sci. U.S.A.* 109, 9857–9862. doi: 10.1073/pnas.1203472109

Manon, F., and Ebel, C. (2010). "Analytical ultracentrifugation, a useful tool to probe intrinsically disordered proteins," in *Instrumental Analysis of Intrinsically Disordered Proteins*, eds V. Uversky and S. Longhi (Hoboken, NJ: John Wiley), 433–449.

Masi, D. R., White, J. C., Schnaitman, C. A., and Bradbeer, C. (1973). Transport of vitamin B12 in *Escherichia coli*: common receptor sites for vitamin B12 and the E colicins on the outer membrane of the cell envelope. *J. Bacteriol.* 115, 506–513.

Masi, M., Vuong, P., Humbard, M., Malone, K., and Misra, R. (2007). Initial steps of colicin E1 import across the outer membrane of *Escherichia coli*. *J. Bacteriol.* 189, 2667–2676. doi: 10.1128/JB.01448-06

McCaughey, L. C., Grinter, R., Josts, I., Roszak, A. W., Waløen, K. I., Cogdell, R. J., et al. (2014). Lectin-like bacteriocins from *Pseudomonas* spp. utilise D-rhamnose containing lipopolysaccharide as a cellular receptor. *PLoS Pathog.* 10:e1003898. doi: 10.1371/journal.ppat.1003898

McCaughey, L. C., Josts, I., Grinter, R., White, P., Byron, O., Tucker, N. P., et al. (2016). Discovery, characterization and in vivo activity of pyocin SD2, a protein antibiotic from *Pseudomonas aeruginosa*. *Biochem. J.* 473, 2345–2358. doi: 10.1042/BCJ20160470

Michel-Briand, Y., and Baysse, C. (2002). The pyocins of *Pseudomonas aeruginosa*. *Biochimie* 84, 499–510. doi: 10.1016/S0300-9084(02)01422-0

Mora, L., and de Zamaroczy, M. (2014). In vivo processing of DNase colicins E2 and E7 is required for their import into the cytoplasm of target cells. *PLoS One* 9:e96549. doi: 10.1371/journal.pone.0096549

Mora, L., Moncoq, K., England, P., Oberto, J., and de Zamaroczy, M. (2015). The stable interaction between signal peptidase LepB of *Escherichia coli* and nuclease bacteriocins promotes toxin entry into the cytoplasm. *J. Biol. Chem.* 290, 30783–30796. doi: 10.1074/jbc.M115.691907

Ohkawa, I., Shiga, S., and Kageyama, M. (1980). Effect of iron concentration in the growth medium on the sensitivity of *Pseudomonas aeruginosa* to pyocin S2. *J. Biochem.* 87, 323–331. doi: 10.1093/oxfordjournals.jbchem.a132740

Ovchinnikov, S., Kinch, L., Park, H., Liao, Y., Pei, J., Kim, D. E., et al. (2015). Large-scale determination of previously unsolved protein structures using evolutionary information. *eLife* 4:e09248. doi: 10.7554/eLife.09248

Papadakos, G., Housden, N. G., Lilly, K. J., Kaminska, R., and Kleanthous, C. (2012a). Kinetic basis for the competitive recruitment of TolB by the intrinsically disordered translocation domain of colicin E9. *J. Mol. Biol.* 418, 269–280. doi: 10.1016/j.jmb.2012.01.039

Papadakos, G., Wojdyla, J. A., and Kleanthous, C. (2012b). Nuclease colicins and their immunity proteins. *Q. Rev. Biophys.* 45, 57–103. doi: 10.1017/S0033583511000114

Penfold, C. N., Healy, B., Housden, N. G., Boetzel, R., Vankemmelbeke, M., Moore, G. R., et al. (2004). Flexibility in the receptor-binding domain of the enzymatic colicin E9 is required for toxicity against *Escherichia coli* cells. *J. Bacteriol.* 186, 4520–4527. doi: 10.1128/JB.186.14.4520-4527.2004

Pilsl, H., Smajs, D., and Braun, V. (1999). Characterization of colicin S4 and its receptor, OmpW, a minor protein of the *Escherichia coli* outer membrane. *J. Bacteriol.* 181, 3578–3581.

Postle, K., and Larsen, R. A. (2007). TonB-dependent energy transduction between outer and cytoplasmic membranes. *Biometals* 20, 453–465. doi: 10.1007/s10534-006-9071-76

Rassam, P., Copeland, N. A., Birkholz, O., Tóth, C., Chavent, M., Duncan, A. L., et al. (2015). Supramolecular assemblies underpin turnover of outer membrane proteins in bacteria. *Nature* 523, 333–336. doi: 10.1038/nature14461

Rassam, P., Long, K. R., Kaminska, R., Williams, D. J., Papadakos, G., Baumann, C. G., et al. (2018). Intermembrane crosstalk drives inner-membrane protein organization in *Escherichia coli*. *Nat. Commun.* 9:1082. doi: 10.1038/s41467-018-03521-24

Rocchetta, H. L., Burrows, L. L., Pacan, J. C., and Lam, J. S. (1998). Three rhamnosyltransferases responsible for assembly of the A-band D-rhamnan

polysaccharide in *Pseudomonas aeruginosa*: a fourth transferase, WbpL, is required for the initiation of both A-band and B-band lipopolysaccharide synthesis. *Mol. Microbiol.* 28, 1103–1119. doi: 10.1046/j.1365-2958.1998.00871.x

Sabet, S. F., and Schnaitman, C. A. (1973). Purification and properties of the colicin E3 receptor of *Escherichia coli*. *J. Biol. Chem.* 248, 1797–1806.

Saeger, J., Hytönen, V. P., Klotzsch, E., and Vogel, V. (2012). GFP's mechanical intermediate states. *PLoS One* 7:e46962. doi: 10.1371/journal.pone.0046962

Sano, Y., Kobayashi, M., and Kageyama, M. (1993). Functional domains of S-type pyocins deduced from chimeric molecules. *J. Bacteriol.* 175, 6179–6185. doi: 10.1128/jb.175.19.6179-6185.1993

Sharma, O., Yamashita, E., Zhalnina, M. V., Zakharov, S. D., Datsenko, K. A., Wanner, B. L., et al. (2007). Structure of the complex of the colicin E2 R-domain and its BtuB receptor. The outer membrane colicin translocon. *J. Biol. Chem.* 282, 23163–23170. doi: 10.1074/jbc.M703004200

Sharp, C., Boinett, C., Cain, A., Housden, N., Kumar, S., Turner, K., et al. (2019). O-antigen dependent colicin insensitivity of uropathogenic *Escherichia coli*. *J. Bacteriol.* 201:e00545-18. doi: 10.1128/JB.00545-18

Sharp, C., Bray, J., Housden, N. G., Maiden, M. C. J., and Kleanthous, C. (2017). Diversity and distribution of nuclease bacteriocins in bacterial genomes revealed using hidden markov models. *PLoS Comput. Biol.* 13:e1005652. doi: 10.1371/journal.pcbi.1005652

Smajs, D., and Weinstock, G. M. (2001). The iron- and temperature-regulated cjrBC genes of *Shigella* and enteroinvasive *Escherichia coli* strains code for colicin Js uptake. *J. Bacteriol.* 183, 3958–3966. doi: 10.1128/JB.183.13.3958-3966.2001

Smith, A. W., Hirst, P. H., Hughes, K., Gensberg, K., and Govan, J. R. (1992). The pyocin Sa receptor of *Pseudomonas aeruginosa* is associated with ferripyoverdin uptake. *J. Bacteriol.* 174, 4847–4849. doi: 10.1128/jb.174.14.4847-4849.1992

Soelaiman, S., Jakes, K., Wu, N., Li, C., and Shoham, M. (2001). Crystal structure of colicin E3: implications for cell entry and ribosome inactivation. *Mol. Cell* 8, 1053–1062. doi: 10.1016/S1097-2765(01)00396-3

Thomas, J. A., and Valvano, M. A. (1993). Role of tol genes in cloacin DF13 susceptibility of *Escherichia coli* K-12 strains expressing the cloacin DF13-aerobactin receptor IutA. *J. Bacteriol.* 175, 548–552. doi: 10.1128/jb.175.2.548-552.1993

Vankemmelbeke, M., Housden, N. G., James, R., Kleanthous, C., and Penfold, C. N. (2013). Immunity protein release from a cell-bound nuclease colicin complex requires global conformational rearrangement. *Microbiologyopen* 2, 853–861. doi: 10.1002/mbo3.122

Vankemmelbeke, M., Shea, O. P., James, R., and Penfold, C. N. (2012). Interaction of nuclease colicins with membranes: insertion depth correlates with bilayer perturbation. *PLoS One* 7:e46656. doi: 10.1371/journal.pone.0046656

Vankemmelbeke, M., Zhang, Y., Moore, G. R., Kleanthous, C., Penfold, C. N., and James, R. (2009). Energy-dependent immunity protein release during *tol*-dependent Nuclease Colicin Translocation. *J. Biol. Chem.* 284, 18932–41. doi: 10.1074/jbc.M806149200

Walker, D., Mosbahi, K., Vankemmelbeke, M., James, R., and Kleanthous, C. (2007). The role of electrostatics in colicin nuclease domain translocation into bacterial cells. *J. Biol. Chem.* 282, 31389–31397. doi: 10.1074/jbc.M705883200

Wei, Y., Li, Z., Chen, B., Liang, H., and Duan, K. (2009). Characterization of the orf1-tolQRA operon in *Pseudomonas aeruginosa*. *Microbiol. Immunol.* 53, 309–318. doi: 10.1111/j.1348-0421.2009.00130.x

Weltzien, H. U., and Jesaitis, M. A. (1971). The nature of the cilicin K receptor of *Escherichia coli* Cullen. *J. Exp. Med.* 133, 534–553. doi: 10.1084/jem.133.3.534

White, P., Joshi, A., Rassam, P., Housden, N. G., Kaminska, R., Goult, J. D., et al. (2017). Exploitation of an iron transporter for bacterial protein antibiotic import. *Proc. Natl. Acad. Sci. U.S.A.* 114, 12051–12056. doi: 10.1073/pnas.1713741114

Wiener, M., Freymann, D., Ghosh, P., and Stroud, R. M. (1997). Crystal structure of colicin Ia. *Nature* 385, 461–464. doi: 10.1038/385461a0

Yamashita, E., Zhalnina, M. V., Zakharov, S. D., Sharma, O., and Cramer, W. A. (2008). Crystal structures of the OmpF porin: function in a colicin translocon. *EMBO J.* 27, 2171–2180. doi: 10.1038/emboj.2008.137

Zakharov, S. D., Eroukova, V. Y., Rokitskaya, T. I., Zhalnina, M. V., Sharma, O., Loll, P. J., et al. (2004). Colicin occlusion of OmpF and TolC channels: outer membrane translocons for colicin import. *Biophys. J.* 87, 3901–3911. doi: 10.1529/biophysj.104.046151

Zakharov, S. D., Wang, X. S., and Cramer, W. A. (2016). The colicin E1 TolC-binding conformer: pillar or pore function of TolC in colicin import? *Biochemistry* 55, 5084–5094. doi: 10.1021/acs.biochem.6b00621

Zampieri, M., Sekar, K., Zamboni, N., and Sauer, U. (2017). Frontiers of high-throughput metabolomics. *Curr. Opin. Chem. Biol.* 36, 15–23. doi: 10.1016/j.cbpa.2016.12.006

Zhang, Y., Li, C., Vankemmelbeke, M. N., Bardelang, P., Paoli, M., Penfold, C. N., et al. (2009). The crystal structure of the TolB box of colicin A in complex with TolB reveals important differences in the recruitment of the common TolB translocation portal used by group A colicins. *Mol. Microbiol.* 75, 623–636. doi: 10.1111/j.1365-2958.2009.06808.x

Zhang, Y., Vankemmelbeke, M. N., Holland, L. E., Walker, D. C., James, R., and Penfold, C. N. (2008). Investigating early events in receptor binding and translocation of colicin E9 using synchronized cell killing and proteolytic cleavage. *J. Bacteriol.* 190, 4342–4350. doi: 10.1128/JB.00047-8

Conflict of Interest Statement: The authors declare that the research was conducted in the absence of any commercial or financial relationships that could be construed as a potential conflict of interest.

Copyright © 2019 Atanaskovic and Kleanthous. This is an open-access article distributed under the terms of the Creative Commons Attribution License (CC BY). The use, distribution or reproduction in other forums is permitted, provided the original author(s) and the copyright owner(s) are credited and that the original publication in this journal is cited, in accordance with accepted academic practice. No use, distribution or reproduction is permitted which does not comply with these terms.

frontiers in Microbiology

ORIGINAL RESEARCH
published: 29 March 2019
doi: 10.3389/fmicb.2019.00573

Structural and Functional Characterization of the Type Three Secretion System (T3SS) Needle of *Pseudomonas aeruginosa*

*Charlotte Lombardi[1†], James Tolchard[2†], Stephanie Bouillot[3], Luca Signor[1], Caroline Gebus[3], David Liebl[3‡], Daphna Fenel[1], Jean-Marie Teulon[1], Juliane Brock[1], Birgit Habenstein[2], Jean-Luc Pellequer[1], Eric Faudry[3], Antoine Loquet[2], Ina Attrée[3], Andréa Dessen[1,4] and Viviana Job[1,3]**

[1] Univ. Grenoble Alpes, CEA, CNRS, Institut de Biologie Structurale (IBS), Grenoble, France, [2] Institute of Chemistry and Biology of Membranes and Nanoobjects, Institut Européen de Chimie et Biologie (CBMN), UMR5248 CNRS, University of Bordeaux, Pessac, France, [3] Univ. Grenoble Alpes, Bacterial Pathogenesis and Cellular Responses Group, U1036 INSERM, ERL5261 CNRS, CEA, Grenoble, France, [4] Brazilian Biosciences National Laboratory (LNBio), Centro Nacional de Pesquisa em Energia e Materiais (CNPEM), Campinas, Brazil

The type three secretion system (T3SS) is a macromolecular protein nano-syringe used by different bacterial pathogens to inject effectors into host cells. The extracellular part of the syringe is a needle-like filament formed by the polymerization of a 9-kDa protein whose structure and proper localization on the bacterial surface are key determinants for efficient toxin injection. Here, we combined *in vivo*, *in vitro,* and *in silico* approaches to characterize the *Pseudomonas aeruginosa* T3SS needle and its major component PscF. Using a combination of mutagenesis, phenotypic analyses, immunofluorescence, proteolysis, mass spectrometry, atomic force microscopy, electron microscopy, and molecular modeling, we propose a model of the *P. aeruginosa* needle that exposes the N-terminal region of each PscF monomer toward the outside of the filament, while the core of the fiber is formed by the C-terminal helix. Among mutations introduced into the needle protein PscF, D76A, and P47A/Q54A caused a defect in the assembly of the needle on the bacterial surface, although the double mutant was still cytotoxic on macrophages in a T3SS-dependent manner and formed filamentous structures in *vitro*. These results suggest that the T3SS needle of *P. aeruginosa* displays an architecture that is similar to that of other bacterial needles studied to date and highlight the fact that small, targeted perturbations in needle assembly can inhibit T3SS function. Therefore, the T3SS needle represents an excellent drug target for small molecules acting as virulence blockers that could disrupt pathogenesis of a broad range of bacteria.

Keywords: type III secretion system, *Pseudomonas aeruginosa*, T3SS needle, structure, virulence, immunofluorescence microscopy, mutagenesis

OPEN ACCESS

Edited by:
Ignacio Arechaga, University of Cantabria, Spain

Reviewed by:
Romé Voulhoux, UMR 7255 Laboratoire d'Ingénierie des Systèmes Macromoléculaires (LISM), France
Paul Dean, Teesside University, United Kingdom

***Correspondence:**
Viviana Job
viviana.job@cea.fr

[†] These authors have contributed equally to this work

[‡] Present address:
*David Liebl, Agency for Science, Technology and Research (A*STAR), Singapore, Singapore*

Specialty section:
This article was submitted to Microbial Physiology and Metabolism, a section of the journal Frontiers in Microbiology

Received: *14 December 2018*
Accepted: *05 March 2019*
Published: *29 March 2019*

Citation:
Lombardi C, Tolchard J, Bouillot S, Signor L, Gebus C, Liebl D, Fenel D, Teulon J-M, Brock J, Habenstein B, Pellequer J-L, Faudry E, Loquet A, Attrée I, Dessen A and Job V (2019) Structural and Functional Characterization of the Type Three Secretion System (T3SS) Needle of Pseudomonas aeruginosa. Front. Microbiol. 10:573. doi: 10.3389/fmicb.2019.00573

INTRODUCTION

Bacterial pathogens have developed different strategies to colonize, invade and kill eukaryotic cells. One of the most successful mechanisms involves the use of the type III secretion system (T3SS), a macromolecular complex present on the surface of numerous pathogenic and colonizing species such as *Salmonella*, *Shigella*, *enteropathogenic Escherichia coli* (EPEC), *Yersinia,* and

Pseudomonas spp. (Galán and Collmer, 1999; Galán et al., 2014; Wagner et al., 2018). The T3SS can be described as a multicomponent protein structure consisting of four major constituents: (i) a basal body that anchors the system to the bacterial membranes; (ii) an export apparatus which includes a cytoplasmic sorting platform that selects substrates and provides energy for the secretion process; (iii) a needle filament which protrudes toward the outside of the bacterial surface and serves as a passage for translocator proteins and effectors; and (iv) a translocation pore formed in the eukaryotic cell membrane that allows the entry of virulence effectors into the host cytoplasm.

The basal body and the needle form the so-called needle complex (NC), which represents the core structure of the T3SS. The number of NCs per bacterial cell varies between species. For instance, *Salmonella typhimurium*, assembles between 10 and 100 NCs per cell (Kubori et al., 1998), while only a few NCs were detected on the surface of *Pseudomonas aeruginosa* (Perdu et al., 2015). Notably, the T3SS needle is formed by a single polymerized protein that has been studied in the context of vaccine development against several pathogens (Charro and Mota, 2015; Jneid et al., 2016; Koroleva et al., 2017). It has been shown that immunization with needle proteins induces specific humoral and T cell responses and abrogates bacterial pathogenicity in animal models (Koroleva et al., 2017). In addition, small molecules such as phenoxyacetamide, that are directed against specific residues of the needle protein PscF can inhibit *P. aeruginosa* T3SS secretion (Bowlin et al., 2014) and the same compound also inhibits abscess formation in mice by directly blocking the T3SS (Berube et al., 2017). These results highlight the need for further characterization of molecular aspects and structures of NC assemblies to develop more specific anti-microbial molecules (Izoré et al., 2011).

Formation of the T3SS needle is a spatio-temporally regulated process. Protein monomers of the T3SS needle from different bacterial species have an approximate molecular weight of 9-kDa and display 13% sequence identity and 42% sequence similarity (considering the main human pathogens: *Salmonella, Shigella, P. aeruginosa,* and *Yersinia* sp.) (Kubori et al., 2000; Hoiczyk and Blobel, 2001; Pastor et al., 2005). Prior to secretion and assembly on the bacterial surface the spontaneous assembly of needle monomers in the bacteria cytosol is prevented by binding to two distinct chaperones concomitantly (Quinaud et al., 2005; Sun et al., 2008; Sal-Man et al., 2013), as is also the case for translocator proteins (Job et al., 2010; Discola et al., 2014; Nguyen et al., 2015). High resolution structures of T3SS needle proteins from different bacteria that have been solved to date (Deane et al., 2006; Quinaud et al., 2007; Wang et al., 2007; Sun et al., 2008; Poyraz et al., 2010) by crystallography and solution NMR reveal a similar protein fold composed of a helix-turn-helix motif with two long helices. Furthermore, one notable feature of T3SS needle proteins is an amphipathic C-terminal helix, which is 'trapped' within a hydrophobic concave region of the dual chaperone interface, presumably in order to block self-association (and early polymerization) (Quinaud et al., 2007; Sun et al., 2008). Upon T3SS activation, the needle protein dissociates from its chaperones, binding to the inner rod protein within the basal body (Kuhlen et al., 2018). Polymerization then occurs through addition of 100s of monomers to the distal end of growing needle. Interestingly, some bacteria possess accessory proteins that aid in assembly of the needle filament and accelerate the polymerization process *in vitro,* such as recently reported for *Salmonella typhimurium* (Kato et al., 2018). The final assembled needle in all bacteria is then capped by a tip protein (or soluble translocator), which is absolutely necessary to allow the formation of the translocation pore for the injection of effectors (Matteï et al., 2011; Harmon et al., 2013). During cell contact the specific needle length is essential for proper function yet the exact mechanism of length control still remains controversial (Cornelis, 2006). It has been suggested that a molecular ruler is involved (Kubori et al., 2000; Journet et al., 2003; Wagner et al., 2010; Bergeron et al., 2016), or that needle length is regulated by a precise timing of substrate switching, as suggested by recent mathematical models (Nariya et al., 2016).

The length of a fully assembled T3SS needle varies between bacterial species from 45 to 80 nm (Kubori et al., 1998; Tamano et al., 2000; Pastor et al., 2005; Radics et al., 2014; Park et al., 2018) while the outer and inner diameter range from 5–13 and 2–2.5 nm, respectively (Kubori et al., 2000; Pastor et al., 2005; Poyraz et al., 2010; Fujii et al., 2012; Loquet et al., 2012; Demers et al., 2013; Radics et al., 2014; Hu et al., 2018). Solid-state NMR structures of the T3SS needles of PrgI from *Salmonella* (Loquet et al., 2012) and MxiH from *Shigella* (Demers et al., 2014) indicated a super helical multimeric structure with 5.7 subunits per turn (Loquet et al., 2012) composed of three intermolecular subunit–subunit interfaces, one of which is axial (subunit i to i+11) and two are lateral (subunit i to i+5/6). Interestingly, the orientation of the two aforementioned helices within the needle structure has been the subject of debate (Fujii et al., 2012; Demers et al., 2013, 2014; Verasdonck et al., 2015). The first cryo-electron microscopy studies performed on the *Shigella* T3SS suggested that the C-terminus of each protomer points toward the outside (Deane et al., 2006; Fujii et al., 2012), while studies involving a combination of cryo-EM and solid state NMR indicated that at least in *Salmonella* and *Shigella* T3SS needles have the N-terminus that points toward the outside of the super-helical structure (Demers et al., 2013, 2014; Verasdonck et al., 2015).

In this work we address the architecture of the T3SS needle of *P. aeruginosa* using a combination of mutagenesis followed by phenotypic studies, proteolysis, mass spectrometry (MS), electron and atomic force microscopies (EM and AFM) and molecular modeling. We show that the *P. aeruginosa* T3SS needle monomer PscF has an N-terminal region oriented toward the outside of the filament, while the C-terminal helix of PscF forms the needle core. Using mutagenesis, we found that D76 is essential for needle polymerization as well as its assembly on the bacterial surface, while residues P47 and Q54 are concomitantly dispensable for polymerization but affect needle stability and effector secretion. Our results, analyzed in the context of other published studies, suggest that a common architecture exists between T3SS needles of different bacterial species, which could facilitate the rational design of

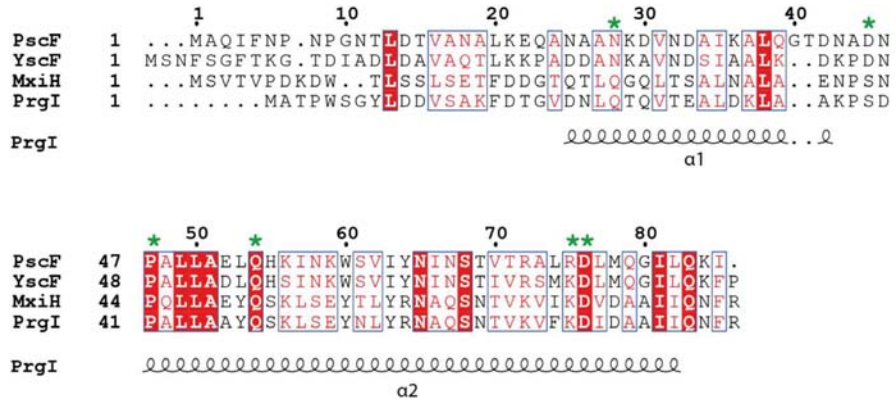

FIGURE 1 | Sequence alignment of needle proteins from different bacteria. PscF from *Pseudomonas aeruginosa*, YscF from *Yersinia* sp., MxiH from *Shigella* sp., PrgI from *Salmonella* sp. The residues mutated in this study are indicated with a green asterisk. Numbers refer to the PscF sequence. Secondary structure elements from the PrgI structure are indicated underneath the sequence alignment. The figure was generated with ESPript, using the new ENDscript server (Robert and Gouet, 2014). Conserved and similar residues are shown in red and blue boxes, respectively.

needle-specific anti-virulence molecules that block or destabilize the T3SS machinery.

RESULTS AND DISCUSSION

Identification of Key Functional Residues of PscF

To uncover the structural elements that are important for the functionality of the T3SS needle in *P. aeruginosa*, we first used a mutagenesis approach coupled to phenotypic studies. We designed seven different PscF point mutants on several bases: conservation of residues between different bacterial species, results obtained in *Shigella flexneri* (Kenjale et al., 2005; Veenendaal et al., 2007), *Yersinia pestis* (Davis and Mecsas, 2007), and *Yersinia pseudotuberculosis* (Torruellas et al., 2005) and predictions/models of PscF fold (**Figure 1**). We generated six single mutants: N28S, D45A, P47A, Q54A, R75A, D76A, and an additional double mutant (P47A/Q54A) whose homologous residues in the *Shigella* needle protein (MxiH-P44A/Q51A) had been shown to be critical for wild-type function (Kenjale et al., 2005; Veenendaal et al., 2007). The D76A mutant had already been studied by our groups and others (Kenjale et al., 2005; Quinaud et al., 2007) and it was further characterized in this study. All mutations were introduced into the pIApG-*pscF* plasmid and transformed into a *P. aeruginosa* clinical isolate CHA strain deleted for the PscF-encoding gene (Δ*pscF*) (Pastor et al., 2005). The cytotoxicity toward macrophages of the Δ*pscF*/*pscF*wt complemented strain had already been reported to be the same as the original CHA strain (Quinaud et al., 2007). We then tested the ability of all complemented strains to infect macrophages measuring the release of the host cytoplasmic enzyme lactate dehydrogenase (LDH) into the supernatant. Most mutant strains killed macrophages with comparable kinetics as the wild-type strain suggesting the existence of a robust core in the protein that can accept local perturbation. However, the two strains carrying PscF-D76A or the double mutant PscF-P47A/Q54A showed significantly attenuated cytotoxicity (with $P < 0.001$) toward macrophages. The *P. aeruginosa* PscF-D76A strain killed only 7.0 ± 1.8% of all cells present in the assay while *P. aeruginosa* PscF-P47A/Q54A strain killed 43.3 ± 6.2% of cells during 3 h of infection. As a comparison, the wild-type *P. aeruginosa* strain killed 87.5 ± 2.8% of all cells during the same period (**Figure 2A**). Both mutations P47A and Q54A alone had no effect on cytotoxicity after 3 h of infection, in agreement with previous observations of hemolysis and invasion in *Shigella* (Kenjale et al., 2005).

To understand the cause of decreased virulence observed with the selected mutants, we first analyzed the expression of the PscF mutants and the secretion profiles of translocator proteins PopB and PcrV in those strains (**Figure 2B**). The T3SS was induced *in vitro* by Ca^{2+} depletion in bacterial cultures, the pellet (containing the entire cell content) and supernatant (containing secreted proteins) were separated by centrifugation and analyzed by Western blotting. All *P. aeruginosa* mutants expressed the different PscF variants (**Figure 2B**), demonstrating that the mutations did not affect the expression of PscF. Analysis of PopB and PcrV in secreted fractions showed reduced levels for the P47A/Q54A strain and a thin band of PopB and no PcrV for the D76A strain, results that are consistent with the decreased cytotoxicity of these two mutants in our macrophage killing assay.

Our results point out that among the conserved residues of the needle protein PscF, D76, P47 and Q54 play essential roles in T3SS functionality, in agreement with other reports on *Shigella flexneri* and *Yersinia pestis* (Kenjale et al., 2005; Torruellas et al., 2005). Interestingly in *Shigella,* the corresponding mutants (MxiH-D73A and P44A/Q51A) secrete Ipa/Ipg proteins constitutively, and are unable to invade epithelial cells and to cause hemolysis (Kenjale et al., 2005; Veenendaal et al., 2007). Other mutations like PscF-R75A in *P. aeruginosa* have no effect on cytotoxicity toward macrophages, while the homologous mutation (MxiH-K72A) in *Shigella* has a significant impact in hemolysis, suggesting a potential different mode of regulation/activation

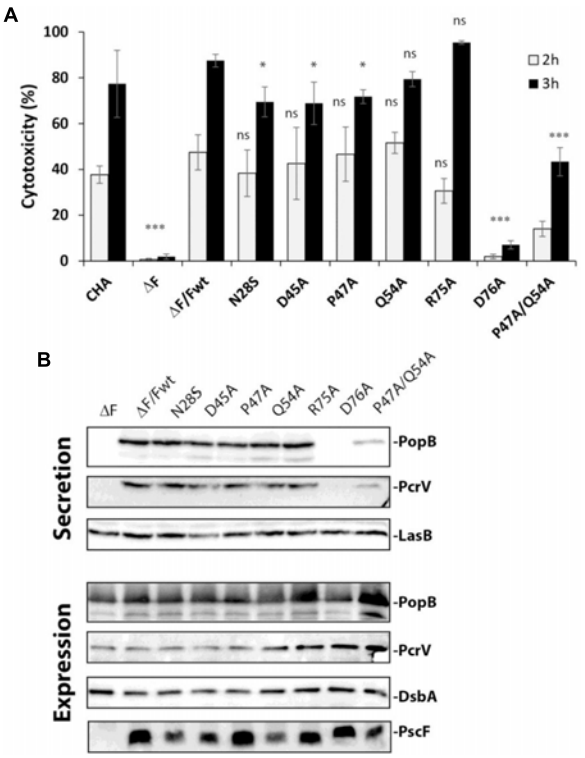

FIGURE 2 | T3SS activity in *Pseudomonas* PscF mutants. **(A)** The cytotoxicity of *P. aeruginosa* strains toward macrophage cells was measured by monitoring LDH release after 2 and 3 h of infection using a multiplicity of infection (MOI) of 5. The PscF deletion mutant (ΔF), D76A, and P47A/Q54A strains show a higher statistical difference at both 2 and 3 h of infection compared to wild-type complemented strain (ΔF/Fwt). LDH measurements were corrected with values corresponding to cells that were not infected; we considered as 100% of cytotoxicity a 1% Triton X-100 treated well. Pairwise differences relative to ΔF/Fwt based on the Tukey test are indicated: ns, non-significant, $***P < 0.001$, $*P < 0.05$. Cytotoxicity of original CHA strain is also reported. **(B)** Western blot of the supernatant (secreted proteins) and total bacteria (expression) fractions after centrifugation were developed with anti-PopB and anti-PcrV antibodies. The expression of PscF variants was confirmed by loading total bacterial extracts on SDS- 15% PAGE. The Western blot was developed using anti-PscF antibodies obtained using a monomeric 6His-PscF (see section "Materials and Methods"). The D76A strain secretes almost no PopB or PcrV while P47A/Q54A secretes less of both translocators as compared to other mutants and the wild-type strain. LasB was used as loading control for the secreted protein, and DsbA as loading control for bacterial expression and as a lysis control for the supernatant (data not shown).

of needle protein polymerization. We thus set out to further understand the specific role of these residues in regards to: (i) proper folding of PscF, (ii) PscF's ability to polymerize and form the needle, (iii) interaction of PscF with the tip translocator protein PcrV, (iv) secretion, localization and abundance of the PscF needle on the bacterial surface.

In vitro Characterization of PscF Needle Mutants

In order to investigate the first two possibilities, i.e., that D76A and P47A/Q54A mutations could affect PscF folding and needle polymerization, we expressed and purified the two PscF mutants in *E. coli* in the absence of their two chaperones PscE and PscG. This allowed the *in vitro* production of filaments, as it was shown in the case of wild-type PscF (Quinaud et al., 2005). Purified PscF wild-type, PscF-D76A and PscF-P47A/Q54A filaments were then analyzed by negative staining electron microscopy (EM) and atomic force microscopy (AFM) (**Figure 3A** and **Supplementary Figure S1**). Both the wild-type and the P47A/Q54A PscF variants formed elongated fibers with outer diameters ranging from 2 to 10 nm indicating that the P47A/Q54A mutation does not prevent the needle polymerization process. The measurement of the diameters of both filaments on EM images suggested a tendency of P47A/Q54A PscF filaments to be slightly thinner than the wild-type ones with a statistically significant difference on diameter size distribution (*t*-test, $P < 0.001$) (**Figure 3B**). The diameter measurements by both EM and AFM thus indicated smaller values than the 8 nm-diameter determined by high resolution methods. This is probably due to a difficulty in identifying the borders of thin needles by EM, and the strong adsorption of the filaments on mica in the AFM experiments, as already found for cylindrical viruses (Godon et al., 2017). The D76A mutant protein could not form filaments suggesting a loss of capacity to polymerize (**Figure 3A**), thus explaining the lack of cytotoxicity of *P. aeruginosa* strains expressing PscF-D76A. On the other hand, in the PscF-P47A/Q54A mutant the 50% decrease in cytotoxicity could be linked to the formation of thinner fibers or could be correlated to a more subtle folding defect of the needle filament.

In order to investigate this last hypothesis we incubated both wild-type and P47A/Q54A PscF needle filaments with trypsin at room temperature and monitored protease digestion for up to 23 h. Samples were taken at different times and analyzed by SDS-PAGE and by liquid chromatography coupled to electrospray ionization mass spectrometry (LC/ESI-MS) (**Figure 3C** and **Table 1**). In our experiments, PscF filaments are a result of the polymerization of a 93-residue monomeric protein that carries a 6His-tag at the C-terminus with an expected mass of 10,218 Da (for the wild-type) and 10,135 Da (for the P47A/Q54A mutant). The SDS-PAGE patterns were apparently similar: both wild-type and P47A/Q54A proteins were surprisingly stable to trypsin digestion, and the full-length protein was also still apparent after 23 h. A major fragment at 6,500 Da (corresponding to fragment Ala37-His93) appeared on SDS-PAGE after 10 min (one asterisk in **Figure 3C**). The kinetics of trypsin cleavage were followed by LC/ESI-MS analysis at different time points (10, 30 min and 6 h of digestion) which allowed precise identification and relative quantification of proteolytic fragments (**Table 1**). All expected trypsin cleavage sites and the fragments identified by LC/ESI-MS are reported in **Figure 3C**. The first trypsin cleavage occurred after Lys21 and Lys36, generating the following three fragments: (Ala2-Lys21), (Ala2-Lys36) and (Ala37-His93). Subsequently, cleavage occurred after Lys56, leading to fragments (Lys37-Lys56) and (Ile57-His93). Moreover, LC/ESI-MS analyses of digested fragments highlighted interesting differences between PscF wild-type and PscF P47A/Q54A needle filaments. Indeed, an additional digested band at a lower molecular mass was visible on SDS-PAGE after 90 min for the wild-type filaments

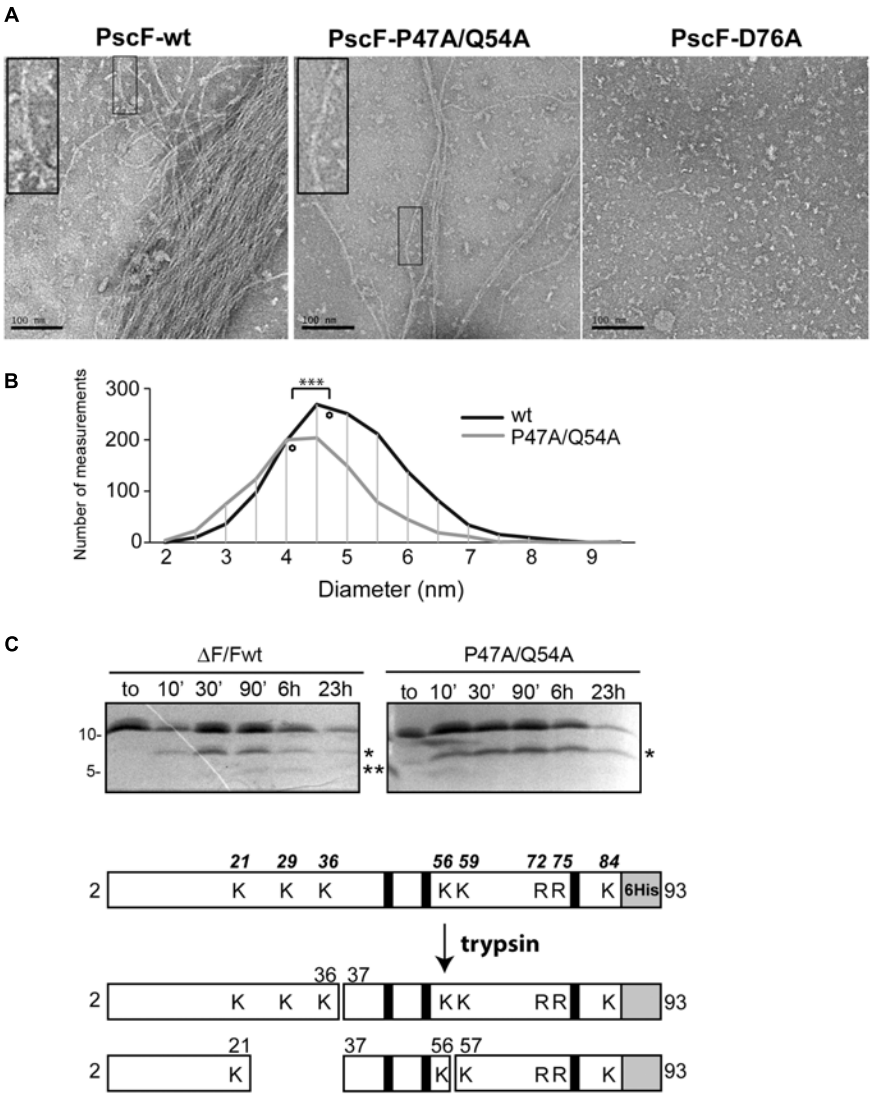

FIGURE 3 | Characterization of PscF wild-type and mutant filaments. **(A)** Negative-staining electron microscopy images of purified PscF wild-type (left panel), PscF P47A/Q54A (middle panel) and PscF D76A (right panel) visualized at the same protein concentration (0.1 mg/ml). Scale bar: 100 nm. **(B)** Diameter distribution of PscF filaments measured on EM images shown in **(A)**. The diamonds represent the average diameter. Wild-type PscF has an average diameter of 4.72 ± 1.02 nm (n = 1390) while PscF P47A/Q54A filaments are thinner with average diameters of 4.15 ± 0.97 nm (n = 986). Statistical analysis: ***$P < 0.001$. **(C)** Trypsin digestion profiles of purified wild-type PscF and P47A/Q54A filaments were analyzed by 16.5% Tris-Tricine and LC/ESI Mass spectrometry. Both proteins are stable with a major cleavage-band at 6.5 kDa (one asterisk) corresponding to fragments 37–93. Only for the wild-type protein is visible a second lower band of 4.5 kDa (residues 57–93) (two asterisks). A scheme of trypsin digestion kinetics determined by MS analysis is reported below, with the corresponding identified fragments. The gray box represents the 6His tag, black lines show the position of D76, P47, and Q54 residues mutated in this study. All trypsin-cleavable sites (lysines, K and arginines, R) are shown with their relative position on the top scheme.

only, corresponding to specific cleavage after Lys56 (two asterisks in **Figure 3C**). This fragment of 4,454 Da (residues Ile57-His93) for the PscF-P47A/Q54A mutant was not visible on SDS-PAGE and detectable only by MS analysis after 6 h in the proteolysis experiment representing 1.1% of the fragment population versus 10.5% in the wild-type PscF at the same time point (**Table 1**). These results suggest that Lys56 is less accessible to proteolysis by trypsin in the PscF-P47A/Q54A filament compared to the PscF wild-type filament. An opposite effect was observed for Lys36, that is more accessible to trypsin cleavage in the PscF-P47A/Q54A filament (with 10.7% of fragment population corresponding to Ala37-His93 with a mass of 6,472 Da) compared to the PscF wild-type filament (with 2.5% of fragment population) (**Table 1** and one asterisk in **Figure 3C**). Therefore, the two filaments are structurally different at least in the region around Lys36 and Lys56.

These results indicate that the P47A/Q54A and wild-type filaments only present a small difference on the outer surface structure (see below). Along with the fact that P47A/Q54A filaments could be slightly thinner, this could explain the

decreased capacities of secretion and cytotoxicity of the strains carrying these mutations. However, one must also consider that the filaments purified form *E. coli* could be structurally distinct from needles assembled within the T3SS apparatus in *P. aeruginosa*.

Needle Visualization on the Surface of *P. aeruginosa* PscF Mutants

In order to further characterize the aforementioned mutations on PscF in a more physiological context, we looked at the localization and/or abundance of the needle on the *P. aeruginosa* surface as well as its interaction with the PcrV tip protein using fluorescence microscopy. We performed immune detection of PscF on fixed cells, using antibodies generated against the PscF native needles (produced during this study) (**Figure 4**). Fixed cells were prepared as described in Section "Materials and Methods" and then separated into two samples: one was incubated with anti-PcrV antibodies (shown in cyan), while the other one was incubated with anti-PscF antibodies (shown in green). In both samples, DNA was stained with SYTO24 (shown in red). The Δ*pscF* and Δ*pcrV* samples were used as negative controls and presented no unspecific labeling with the anti-PcrV antibodies and just weak background with the anti-PscF used at higher concentrations. ΔPscF/PscF-wt and ΔPcrV/PcrV-wt were used as positive controls and showed clearly distinct cell surface-associated fluorescent spots for both proteins all around the bacteria (**Figures 4A,B**). Of note, PcrV could not be detected on the surface of the ΔPscF strain because it only assembles at the tip of the PscF needle. All PscF mutants showed similar patterns of labeling as the positive controls except for the PscF D76A- and P47A/Q54A-expressing strains that showed markedly smaller amounts of PscF and PcrV spots all around their surface (**Figure 4B** and **Supplementary Figure S2**). To eliminate the possibility that the absence of PscF on the *P. aeruginosa* surface was due to a defect in expression of PscF D76A and P47A/Q54A, we repeated the experiment with cells made permeable with Triton X-100 in order to allow the entry of the antibody into the cell. The antibodies directed toward PscF detected the protein in both permeabilized mutant strains (**Supplementary Figure S3**). These data are in agreement with the Western blot results and indicate that PscF mutant proteins were produced within *P. aeruginosa*. Moreover, this experiment showed that D76A and P47A/Q54A mutants have a defect in PscF export and/or assembly onto the bacterial surface.

We then quantified the PscF and PcrV spots per cell using the MicrobeJ plugin (Ducret et al., 2016) of the ImageJ program (Schneider et al., 2012), considering that one spot corresponded to one needle. Between 30 and 40% of wild-type bacterial cells showed one or more PscF spots (up to 6) per cell, with a majority of cells with 1 or 2 spots/cell (**Figure 5B**). Immunolabeling of bacteria expressing PscF D76A showed that only 6.9 ± 1.6% of the counted cells (n = 1713) presented a single visible spot and the P47A/Q54A mutant displayed 8.9 ± 2.4% of the population with 1 or 2 spots per cell (n = 2307). For comparison, the complemented ΔPscF/PscF-wt stain presented 32.8 ± 4.0% of cells with at least one needle (n = 1829) (**Figures 5A,B**) while the negative control ΔPscF strain presented 2.3 ± 1.4% of spots near the bacteria. In all samples, except in D76A and P47A/Q54A, the percentage of cells with PscF and PcrV spots was very similar, indicating that the mutations do not affect binding between the tip protein and the needle. In the case of D76A and P47A/Q54A only 3.2 ± 1.2% (n = 2126) and 5.6 ± 2.5% (n = 2128) of cells presented PcrV spots, respectively, suggesting that the tip/needle interaction is present, but we could not exclude that some D76A and P47A/Q54A needles do not present PcrV at their tip.

These observations explain the absence of cytotoxicity toward macrophages in the case of D76A. Interestingly, although P47A/Q54A mutations affected the number of needles detected,

TABLE 1 | Identification and relative quantifation of PscF (*wt*/mutant) proteolytic fragments by LC/ESI MS.

Proteolysis time	**10 min**		**30 min**		**6 h**	
Theoretical mass (Da) for tryptic fragments of PscF (wt/mutant)	**PscF-WT**	**PscF-P47A/Q54A**	**PscF-WT**	**PscF- P47A/Q54A**	**PscF-WT**	**PscF- P47A/Q54A**
	Measured mass (Da) *(% Area of EIC peaks)*					
2097.09 [(1)] (2-21)	2097.08 *(9.4%)*	2097.09 *(5.6%)*	2097.09 *(18.1%)*	2097.09 *(10.8%)*	2097.08 *(28.1%)*	2097.09 *(30.8%)*
2118.07/2035.03 [(1)] (37-56)	2118.07 *(1.6%)*	2035.02 *(0.2%)*	2118.07 *(3.7%)*	2035.03 *(0.3%)*	2118.07 *(17.6%)*	2035.03 *(3.5%)*
3678.86 [(1)] (2-36)	3678.87 *(7.7%)*	3678.86 *(13.2%)*	3678.85 *(11.4%)*	3678.85 *(12.6%)*	3678.85 *(2.9%)*	3678.85 *(3.9%)*
4454.15 [(2)] (57-93)	4454.36 *(2.6%)*	n.d.	4454.52 *(3.4%)*	n.d.	4454.88 *(10.5%)*	4454.18 *(1.1%)*
6555.45/6472.36 [(2)] (37-93)	6555.63 *(9.4%)*	6472.50 *(9.1%)*	6555.72 *(9.4%)*	6472.55 *(8.5%)*	6555.60 *(2.5%)*	6472.55 *(10.7%)*
10218.47/10135.38 [(3)] (2-93)	10218.67 *(69.3%)*	10135.59 (71.9%)	10218.68 *(54.0%)*	10135.46 *(67.8%)*	10218.80 *(38.5%)*	10135.46 *(49.8%)*

Theoretical mass values for tryptic fragments of PscF (wild-type and P47A/Q54A mutant) are reported in the first column. Both PscFwt and P47A/Q54A mutant were digested with trypsin (trypsin:protein ratio 1:500 w/w) at room temperature. After 10 min, 30 min and 6 h of incubation the samples were analyzed by LC/ESI-MS. The area of the extracted ion chromatogram (EIC) peaks for each fragment were calculated and reported as a percentage of the sum of all fragment (total area of all the peaks). [(1)] monoisotopic mass, [(2)] average mass, [(3)] mass value for the intact undigested protein, missing the methionine at N-termini; n.d., not detected.

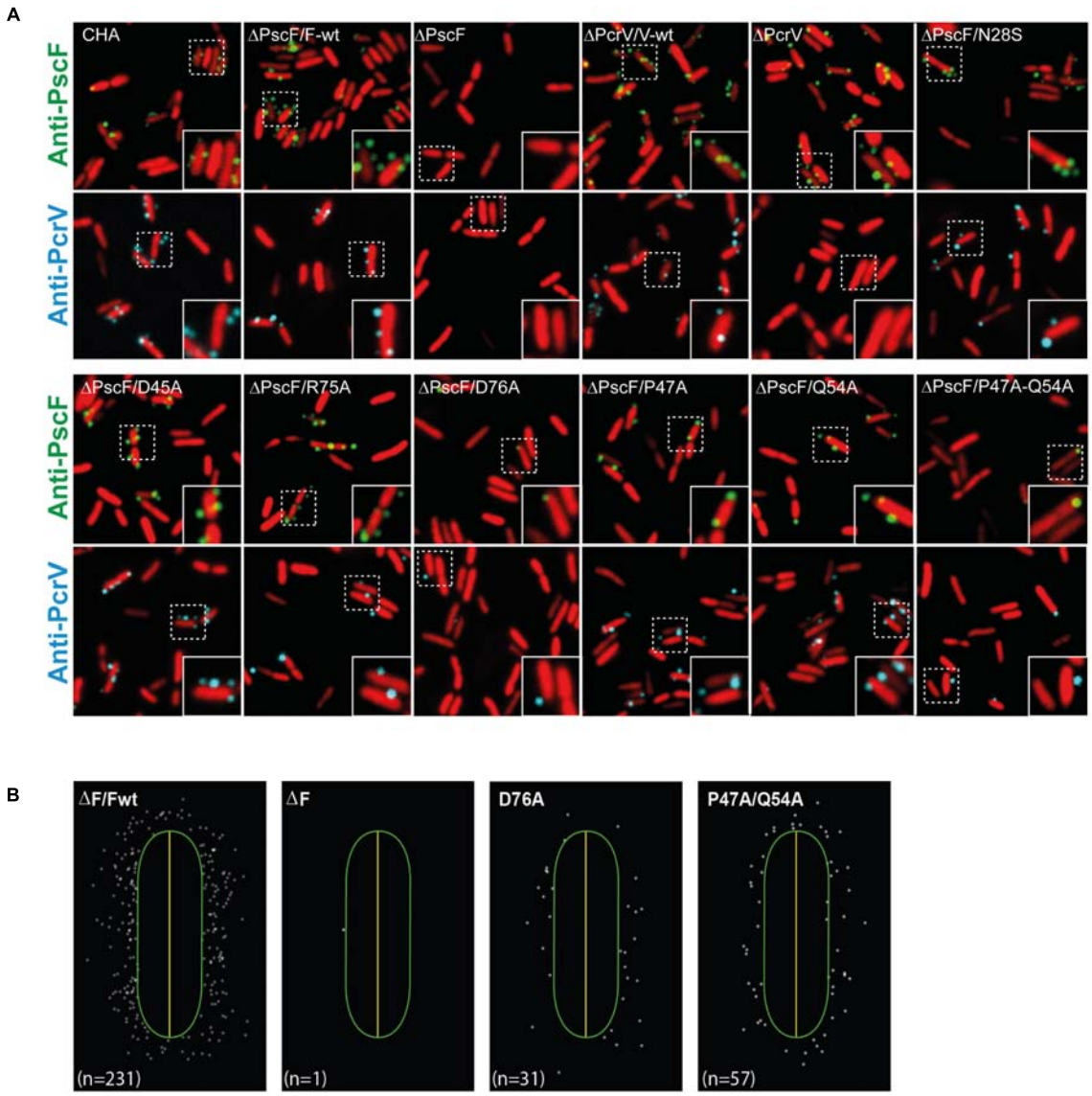

FIGURE 4 | Localization of PscF-needles on the surface of *Pseudomonas aeruginosa*. **(A)** *P. aeruginosa* CHA strain isolated on cystic fibrosis patient depleted for the *pscF* gene (Δ*pscF*) and complemented with pIApG-*pscF* constructs were grown in T3SS-inducing conditions. PscF needles were visualized by immuno fluorescence on fixed bacteria using anti-PscF (in green) or anti-PcrV (in cyan). SYTO24 was used to visualize bacteria (in red). As a negative controls we used *P. aeruginosa* ΔF and ΔV, while ΔF/Fwt and ΔV/Vwt were used as a positive control. Only few PscF and PcrV spots were visible on *P. aeruginosa* strains carrying a PscF-D76A or a PscF-P47A/Q54A. **(B)** MicrobeJ reconstitution of PscF distribution around the bacteria. n = number of spots in the image.

the synthesized needles still allowed injection of toxins, suggesting that the number of needles on the bacterial surface is less crucial than the structure of the needle *per se*. All these data strongly suggest that in *P. aeruginosa* D76A and P47A/Q54A mutants are defective in the *in vivo* needle assembly process while a concomitant instability or defect in the export of PscF through the basal body could not be excluded.

In *Yersinia pestis,* the YscF-D77A variant also shows a defect in the surface exposure of the needle whilst maintaining normal protein expression levels (Torruellas et al., 2005). In contrast, the MxiH-D73A and P44A/Q51A mutants in *Shigella flexneri* were both able to export the needle protein and assemble a NC almost normally (Kenjale et al., 2005; Veenendaal et al., 2007). Furthermore, MxiH-D73A was able to polymerize (Fujii et al., 2012) (unlike PscF-D76A) with no significant structural changes but it lacks the tip complex. Once again, this suggests that the same mutation will cause different effects on the assembly of *Shigella, Yersinia,* and *Pseudomonas* T3SS needles.

Modeling of the *P. aeruginosa* PscF Needle

In order to understand at the molecular level the impact of the D76A and P47A/Q54A mutations, we performed molecular modeling of the *P. aeruginosa* PscF needle, taking advantage of the solid-state NMR structure of the *Salmonella* PrgI needle

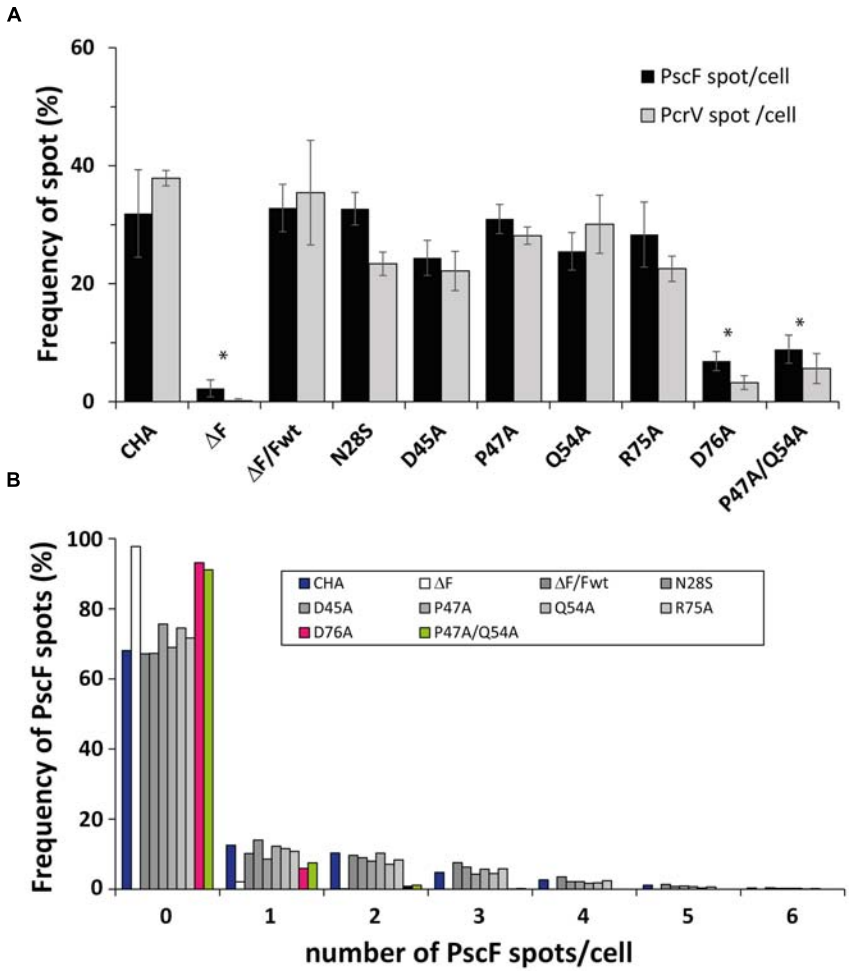

FIGURE 5 | Presence of PscF and PcrV on *Pseudomonas aeruginosa* PscF-mutant strains. **(A)** Images of immunolabeled fixed bacteria in **Figure 4** were analyzed with MicrobeJ to detect and associate each PscF or PcrV spot to only one bacterium. Frequency was considered as the percentage of bacteria with at least one PscF and PcrV spot on the total counted bacteria. About 30–40% of cells had needles with the PcrV tip protein on their surface, with the exception of the D76A strain with only 6.9 ± 1.6% (PscF) and 3.2 ± 1.2% (PcrV), and the P47A/Q54A strain with 8.9 ± 2.4% (PscF) and 5.6 ± 2.5% (PcrV) of cells with spots. **(B)** Distribution of the number of PscF spots/needles per bacterial cell. Between 630 and 2300 individual bacteria were counted. *P. aeruginosa* wild-type and mutant strains had between 1 to 3 PscF spots per cell, except for D76A (in pink) and P47A/Q54A (in green) that presented only one or two spots per cell. Overall comparisons using the Kruskal–Wallis' test indicates significant differences between classes ($P < 0.001$). Pairwise differences relative to wild-type based on Dunn's *post hoc* test are shown: $^*P<0.05$.

(Loquet et al., 2012). We constructed two different models for the PscF needle: one using the protein in the same orientation as PrgI in the filament (i.e., with the C-termini inside and the N-termini outside the needle; that model will be named PscF-forward); and the other one supposing that the PscF protomer is inverted with the N-termini residue inside and the C-termini residue outside the needle structure (PscF-reverse) (**Figure 6**). Optimal models were subjected to a brief structural minimization protocol using the Chimera molecular modeling/visualization package (Pettersen et al., 2004) (default parameters) to remove atomic clashes (VDW overlap). Pre- and post-minimization structures were analyzed using the PSVS webserver (Bhattacharya et al., 2007) to evaluate the structural improvements in the monomeric models. After minimization, all homology models showed significant improvements in both clash scores and favorable Ramachandran angles. The energetically minimized structures were then used to reconstruct PrgI-like T3SS needles, and were built up from 29 monomers to form the needle filaments. To compare the two models of PscF to the needle architecture in *Salmonella* we also constructed a PrgI-inverted needle (PrgI-reverse).

The three resulting needle architectures: PscF-reverse, PscF-forward and PrgI-reverse are shown in **Figure 6**. We then tried to understand if one of the two PscF needle models (PscF-reverse or PscF-forward) was more favorable. To do so, we computed several parameters related to the global architecture: surface electrostatic potential (**Figure 6A**), position of conserved residues (**Figure 6B**) and hydrophobicity (**Figure 6C**) and compared them to the experimental solid-state NMR *Salmonella* PrgI needle structure. Surprisingly none of the PscF needle models showed

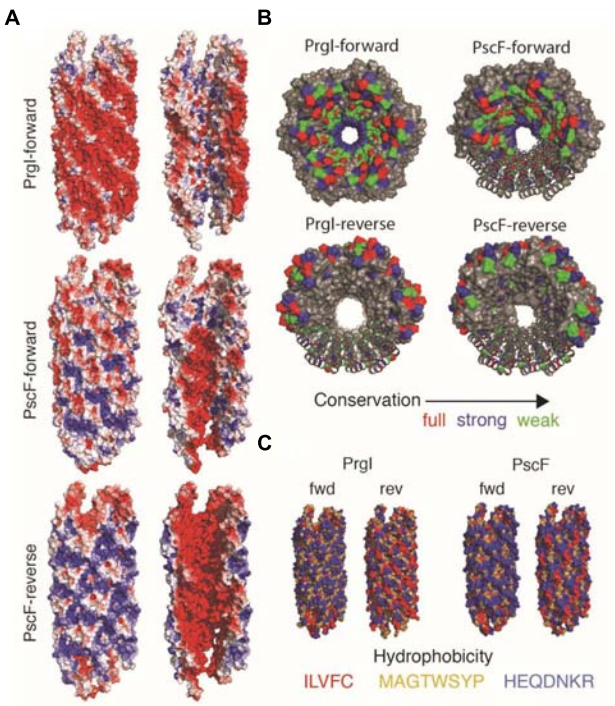

FIGURE 6 | Needle reconstruction for PscF wild-type and mutants. **(A)** The PrgI Solid-state NMR structure was used as a model for the construction of PscF in the Forward and Reverse orientations. Mutants D76A and P74A/Q54A were constructed on the PscF-forward model. The exterior view (left) and lumen view (right) of the T3SS needle models are colored by surface electrostatic potentials, at pH 7, using the APBS plugin for PyMol. **(B)** Distribution of conserved residues distribution on PrgI and PscF needle models in Forward and Reverse orientations. **(C)** Hydrophobicity distribution of the different models shown in **(B)**.

the same electrostatic distribution as the experimental PrgI needle structure (top in **Figure 6A**), displaying an astonishing pattern of circular succession of negative/positive charges at the lumen surface, while the external surface was predominantly negatively charged. Both PscF needle models showed a strong negative charge distribution at the inner surface, while the external surfaces were much more positively charged compared to PrgI needles. In addition, no particular succession of positively/negatively charged patterns could be seen for either PscF model. In PrgI needles, this lumen pattern arises mostly from D70 and Q77 (negative) and K66 and R80 (positive). Equivalent amino acid positions in PscF D76, Q83, and R72 are conserved (**Figures 1**, **6B**); however, R80, the last residue in PrgI, is absent from PscF, leading to a pronounced change in the electrostatic charge distribution at the lumen surface.

Next, we investigated the hydrophobic surface of the models (**Figure 6C**) considering that the PrgI needle is characterized by a strong network of hydrophobic interactions at the lateral interfaces between subunit i and i+5/6 (Loquet et al., 2012). PscF-reverse and PrgI-reverse models both exhibit an unfavorable hydrophobic external surface while the PscF-forward model shows a favorable hydrophilic surface, strengthening the energetic relevance of the PscF-forward model. Finally, we examined the distribution of the conserved residues on the different needle models (**Figure 6B**). The PrgI needle structure has been defined by a typical distribution of conserved residues among the T3SS needle subunits, with almost all conserved residues pointing inside the needle pore while the external surface is made of non-conserved amino acids. Visualization of these conserved needle residues on the PscF models lead to two distinct situations: PscF-forward presents many conserved residues at the lumen surface, while this lumen surface in the PscF-reverse model is mostly composed of non-conserved residues. It has been suggested that the presence of non-conserved residues exposed to the external surface of PrgI could provide a way to evade immune response of the host cell (Loquet et al., 2012). The same distribution is observed for the PscF-forward model, and together with our observations on the hydrophobic and electrostatic surfaces it provides a substantial hint toward the relevance of the PscF-forward model compared to the PscF-reverse model.

Subsequently, we constructed PscF needle models for the two mutants: D76A and P47A/Q54A (**Figure 7B**), adopting the forward model orientation. In the D76A model, the distribution of the charges is drastically affected by the point mutation; D76 is located in the central hollow section of the needle and the mutation into alanine modifies the overall negative charge distribution, which could be an explanation to the lack of polymerization *in vitro* of this mutant. The P47A/Q54A model, however, suggests that the mutated residues are buried in the subunit–subunit interfaces and the overall charges are more similar to the wild-type PscF-forward model. According to the atomic depth measurements (Chen and Pellequer, 2013), the regions 45–47 is the deepest, farthest away from the solvent, in the whole needle. Any change in deeply buried residues is expected to impact proteins stability (Chakravarty and Varadarajan, 1999), that could explain the significant difference in the number of needle on bacteria surface. Considering the equivalent amino acids in PrgI (i.e., P41 and Q48), we examined the residues involved in the subunit–subunit interfaces by taking into account the solid-state NMR restraints used for the PrgI needle structure determination (see **Figure 2** in Loquet et al., 2012). P41 in PrgI is involved in strong contacts between subunit i to i+11 forming the so-called axial interface, while Q48 is weakly involved in the intramolecular fold. This suggests that the double P47A/Q54A mutation in PscF could lead just to a moderate perturbation of the needle arrangement that could explain why this mutant still polymerizes *in vitro*.

We then used the data obtained from trypsin proteolysis and MS analysis to explore the structural differences between wild-type and mutant P47A/Q54A filaments and to validate our model. As mentioned above, we monitored trypsin digestion of both fibers by LC/ESI-MS (**Figure 3C** and **Table 1**). This experiment allowed us to conclude that the residues that were the most accessible to trypsin digestion, and thus were solvent exposed are: Lys36, Lys21, and Lys56 (and probably Lys29, absent in MS digested-fragments). Interestingly, these experimental results are only in agreement with the PscF-forward wild-type model (with the N-termini exposed toward the outside), where Lys36, Lys29, and Lys21 are expected to be the most exposed

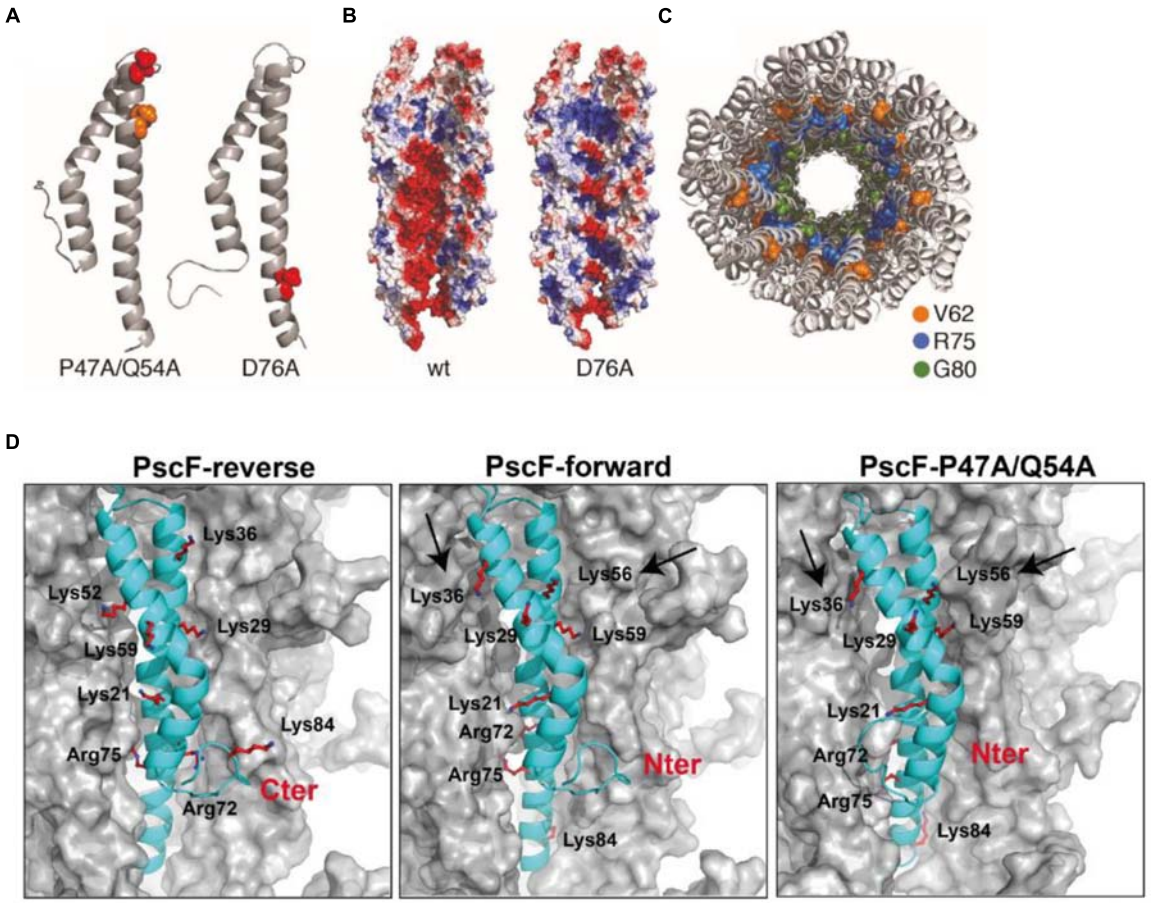

FIGURE 7 | Model of the PscF P47A/Q54A and PscF D76 assembled filament. **(A)** Ribbon representation of PscF monomer carrying the two mutations: D76A and P47A/Q54A. **(B)** Electrostatic surface representation of the two mutant reconstituted filaments with a channel view. **(C)** Top view of a PscF-forward wild-type model, colors show residues implicated in binding of the T3SS-inhibitor phenoxyacetamide (Bowlin et al., 2014). **(D)** Comparison between reverse and forward PscF and PscF-P47A/Q54A filaments. PscF-forward model (with the N-termini exposed toward the outside), with Lys36, Lys29, and Lys21 solvent-exposed, Lys56 and Lys59 less accessible, and Lys84, Arg72, and Arg75 completely buried. PscF-reverse model (with the C-termini exposed toward the outside), with solvent accessible residues: Lys84, Arg75, Lys59, and Lys36. The PscF-P47A/Q54A forward model showing accessibility of the same residues as compared to the PscF-forward wild-type model except for the Lys56 and Lys36 that are slightly less or more trypsin-accessible, respectively (indicated by two arrows). All needle models are represented as surfaces with one monomer of PscF represented as a cyan ribbon. All trypsin-cleavable sites are shown as sticks.

to the solvent, Lys56 and Lys59 are less accessible, and Lys84, Arg72 and Arg75 are completely buried (middle in **Figure 7D**). On the other hand, in the PscF-reverse wild-type model (with the C-termini exposed toward the outside), the residues that would be solvent accessible are: Lys84, Arg75, Lys59, and Lys36 (left in **Figure 7D**). Lys84, in particular, is located just before the C-terminus. In this configuration, the C-terminal 6His-tag would have been expected to be quickly cleaved by trypsin, but no fragment corresponding to this cleavage was observed for any of the peptides analyzed by LC/ESI-MS (**Table 1**). Moreover, the PscF-forward P47A/Q54A model with Lys56 less solvent-exposed and Lys36 more solvent-exposed (right in **Figure 7D**) is also in agreement with our trypsin digestion results. The digestion-fragment at 4,454 Da (corresponding to a cleavage after Lys56) was less abundant in the mutant compared to the wild-type (1.1 vs. 10.5%), while the digestion fragment corresponding to a cleavage after Lys36 was more abundant in the mutant compared to the wild-type (10.7 vs. 2.5%) as discussed above (**Figure 3C** and **Table 1**).

Thus, based on our biochemical, structural and molecular modeling data, we hypothesize that the T3SS needle of *P. aeruginosa* follows the PscF-forward model with the N-terminus pointing toward the outside of the fiber and the C-terminus consequently hidden inside the needle's hollow cavity. Our results imply that the overall architecture of the needle is therefore conserved between *Pseudomonas*, *Salmonella*, and *Shigella* spp., highlighting the importance of the orientation of the small 9-kDa protein inside the oligomeric structure. D76A and P47A/Q54A mutations are located at the C-terminal helix, which is well-conserved in the sequence among bacterial species. Their effects on needle polymerization and stability as well as their importance for functional regulation of needle assembly as shown by our analyses of electrostatic charges present at the lumen surface point to an important role of the C-terminal

helix in the assembly mechanism. The impact of the mutations D76A and P47A/Q54A, and their homologs in T3SS needles of other bacteria, suggests that regions facing the inner cavity or deeply buried within the needle play a significant role in needle stability and/or function. It also suggests that local changes of the sequence of the subunit protein in crucial regions, as exemplified here for the two mutants and in previous studies, might lead to important perturbations on different aspects of the needle structure-function interplay, on both a structural (e.g., structural instability, surface electrostatic distribution) and functional basis. Moreover, the charge distribution in the lumen may be critical in needle assembly as suggest by the defect in polymerization in the D76A variant and the previous observation that the PscF-D76A protein overexpressed in *P. aeruginosa* CHA strain has a dominant-negative effect on assembly of the wild-type PscF needle (Quinaud et al., 2007).

Understanding the Mode of Action of T3SS Inhibitors

To go further we used our proposed *P. aeruginosa* T3SS needle model to understand the mode of action of T3SS-inhibitors, such as the phenoxyacetamide family, that was hypothesized to act inside the cavity of PscF (Bowlin et al., 2014). In this work, the authors suggested that PscF residues V62, R75 and G80 were involved in direct binding of phenoxyacetamide. In our model, only G80 is exposed to the lumen surface (**Figure 7C** in green), while V62 (in orange) and R75 (in blue) are located at subunit interfaces. These observations suggest that the three amino acid positions, upon binding with phenoxyacetamide, may decrease needle stability (for V62 and R75); in addition, it is also possible that binding could change the surface of the lumen (G80). These three residues appear to be close enough in our PscF needle model to speculate the presence of a single binding site, as suggested by the Moir group (Bowlin et al., 2014). We therefore suggest that it is possible to design other molecules that interact with multiple residues starting from the lumen structure model in order to block T3SS action.

The T3SS needle represents an excellent and promising molecular target in the fight against Gram-negative pathogens, since it is easily accessible to small molecules that do not need to cross bacterial membranes, and is non-essential for survival. Thus, small molecules affecting its function could block virulence without eliciting high levels of antibiotic resistance.

Our work provides a new model for the *P. aeruginosa* PscF-needle, that was validated *in vitro* by experimental data combining mutagenesis, proteolysis, and Mass Spectrometry experiments. Moreover, the phenotypic characterization of PscF mutants *in vivo* showed that the majority of the single mutations introduced in the needle have no effect on T3SS-toxicity and are not sufficient to disrupt needle polymerization, with the exception of D76A. This underlines the importance of the charge in the face of the lumen for assembly of a functional needle.

A detailed molecular comprehension of the structure–function relationship of the T3SS needle should advance future developments of anti-virulence molecules.

MATERIALS AND METHODS

Bacterial Strains and Culture Conditions for T3SS Expression

Strains and plasmids used in this study are presented in **Supplementary Table S2**. Cytotoxic *P. aeruginosa* cystic fibrosis isolate CHA carrying appropriate chromosomal deletions of *pscF* gene (Δ*pscF)* was transformed with plasmid pIApG-*pscF* wild-type or mutants that expressed *pscF* with a T3SS inducible promoter. Cultures were grown overnight in Luria-Bertani (LB) at 37°C at 300 rpm in the presence of 300 μg/ml of carbenicillin. Then next day, they were diluted to an optical density measured at 600 nm (OD_{600}) of 0.1 A.U. in LB in T3SS-inducing conditions by adding 5 mM EGTA and 20 mM $MgCl_2$ (Pastor et al., 2005; Dasgupta et al., 2006). When the OD_{600} reached 1.0 A.U., cells were centrifuged, and then the pellet (entire bacterial protein content) and the supernatant (the secreted protein fraction) was analyzed by Western blotting. Anti-PopB and anti-PcrV antibodies (Goure et al., 2004) were diluted to 1:10,000 and 1:3,000, respectively. Anti-PscF antibodies were raised in rabbits (Covalab, France) using monomeric 6His-PscF (Quinaud et al., 2005). The antibodies were further purified on Protein-A column and diluted 1:500 for Western blot analysis. As a loading control we used LasB (a secreted protein) and DsbA (a periplasmic protein) diluted to 1:2,000 and 1:10,000, respectively. Lysis control was done on secreted protein fractions using DsbA antibodies. All mutants were produced using the Quick-Change site-directed mutagenesis II kit (Stragatene). Primers are listed in **Supplementary Table S2**.

Cytotoxicity Assay

Lactate dehydrogenase release into the supernatant was measured using the Cytotoxicity Detection Kit by Roche Applied Science, following the recommended protocol. Briefly, J774 cells were seeded at 2×10^5 in 48-well plates the day prior to the experiment, and infected in DMEM medium at MOI of 5 with *P. aeruginosa*Δ*pscF*-pIApG-*pscF* constructs at OD_{600} = 1 A.U. After 2 and 3 h, 30 μL of cell supernatants were mixed with 100 μl of reaction mix and the OD was read at 490 nm. OD values were subtracted from that of uninfected cells. The 100% cell death value was quantified after addition of 1% Triton X-100, in duplicates. The experiment was performed in triplicate wells (except for the P47A/Q54A mutant for which six replicates were performed). Results represent the means and standard deviations of the triplicates. Statistics were calculated using SigmaPlot software. For multiple comparisons, a one-way analysis of variance (ANOVA) test was performed, followed by Tukey's test for pairwise comparisons.

Immunofluorescence

Two different *P. aeruginosa* genetic backgrounds were used: CHAΔ*pcrV* complemented or not with pIApG-*pcrV*-wt, and CHAΔ*pscF* complemented with all pIApG-*pscF* constructs or with the wild-type *pscF*. Cells were grown under T3SS-inducing conditions up to an optical density measured at 600 nm (OD_{600}) of 1 A.U. and then culture was fixed with 4% PFA in 25 mM

HEPES pH 7.4 overnight at 4°C. After centrifugation at 6,000 rpm for 15 min the pellet was washed three times with 1 ml PBS, then incubated for 30 min at RT in 1 ml PBS with 0.5% BSA (BS, Blocking Solution). Then cells were divided into two Eppendorf tubes and spin down, each pellet was resuspended and incubated for 30 min at room temperature in 50 µl of BS containing of anti-PcrV (1:200) (Goure et al., 2004) or 50 µl BS with anti-PscF (1:50). Anti-PscF antibodies were produced in rabbits (Biotem) from the PscF fibers purified under native conditions from *E. coli* BL21 (DE3). After three washing steps with 1 ml PBS, the pellet was resuspended into 50 µl of BS containing anti-rabbit coupled to Cy3 (Jackson ImmunoResearch Laboratories) with a final dilution of (1:500) and SYTO24-Green (Life Technologies) with a final dilution of (1:2000) and further incubated 30 min at RT. After three final washes, the cells were resuspended into BS. One drop of each sample was deposited on a 8-chambered labteck (Thermo Fisher Scientific) and liquid 1.5% low-melting agarose at 37°C or 1.5% agar pad was added on the top of the drop and visualized on a IX71 Olympus microscope controlled by the CellR Olympus system and driven by Xcellence software (Olympus). Images were captured with a Hammamatsu Orca-ER camera using a 100x (N.A. 1,30) oil objective.

To investigate for the presence of PscF inside the cells in PscF- mutants, cells were fixed with 4% PFA, washed as previously described, then permeabilized with 0.25% Triton X-100 for 5 min at room temperature to allow the anti-PscF to enter cells (method adapted from Cimino et al., 2006). Triton X-100 was then washed out three times with 1 ml PBS before continuing the protocol as described above from BS incubation.

Quantification of Fluorescent Spots Associated With Bacteria

Quantification was done using the MicrobeJ plugin of ImageJ (Ducret et al., 2016)[1] and [2]. Briefly, for bacterial identification we used the same setting (area, length, width, curvature of bacteria) for all images. For PcrV and PscF spot analyses a Tolerance of 100 was used, and only in the case of PscF a filter of intensity between 250-max was added in order to eliminate background noise and unrelated spots. For the final step of analyses by MicrobeJ, namely the association between each identified bacterium and the spots, we used two filters: inside and outside with "exclusive" settings, in order to associate each spot (that could be inside or outside the bacteria) with just one bacterium. Averages were calculated from the results of 5 to 11 independent images taken for each mutant. The frequency was considered as being the percentage of cells with at least one spot.

Statistics were calculated using SigmaPlot. For multiple comparisons, a one-way analysis of variance (ANOVA) test was performed, followed by Dunn's test.

PscF Expression and Purification and Mutant Construction

Escherichia coli BL21 (DE3) cells were transformed with pET22b-PscF (wild-type, D76A and P47A/Q54A) that generated a protein with a 6His-tag at the C terminus (Quinaud et al., 2005). Cells were grown in LB media supplemented with 100 µg/ml ampicillin at 37°C, under agitation (200 rpm) until they reached an OD_{600} = 0.7–0.8 A.U. Protein expression was induced by addition of 1 mM IPTG and growth was continued for up to 3 h, then cells were centrifuged for 30 min at 5,500 rpm at 4°C. Pellets were resuspended at 4°C in 25 ml of lysis buffer (25 mM Tris-HCl pH 8.0, 200 mM NaCl, 25 mM Imidazole) containing benzonase. Cells were lysed at 18 kPsi in a cell disrupter and centrifuged for 30 min at 15,000 rpm at 4°C. The soluble fraction was applied on a 1 ml resin Ni-NTA superflow (QIAGEN) in a batch column. The column was washed with lysis buffer and eluted the same buffer containing 200 mM imidazole. Sample purity was checked by SDS-PAGE and Mass Spectrometry. Mutants were produced using the Quick-Change site-directed mutagenesis II kit (Stragatene) and verified by DNA sequencing. Primers are listed in the **Supplementary Table S2**.

Trypsin Digestion

PscF-wt and PscF-P47A/Q54A proteins were purified as described above. Trypsin digestion was carried out according to the following procedure: trypsin was dissolved into a buffer containing 25 mM Tris-HCl pH 8.0, 200 mM NaCl and digestion was performed using a (trypsin:protein) ratio of 1:500 (w/w). The reaction was performed at RT and samples were collected at different time points (10 min, 30 min, 1 h 30 min, 6 h, ON) and analyzed by 16.5% Tris-Tricine gel and by LC/ESI-MS.

Electron Microscopy

Four µl of the protein samples were absorbed to the clean side of a carbon film on mica, stained with sodium silico tungstate and transferred to a 400-mesh copper grid. The images were taken under low dose conditions ($<10\ e^{-}/Å^2$) at a magnification of 23,000 and 49,000 times with defocus values between 1.2 and 2.5 µm on a Tecnai 12 LaB6 electron microscope at 120 kV accelerating voltage using a CCD Camera Gatan Orius 1000. Size determination of the PscF filaments was performed in Gwyddion (Nečas and Klapetek, 2012) using the raw.dm3 EM files, measurements were done at different positions along the filaments using the "Measure distance" tool. Additional measurements were performed in ImageJ (Schneider et al., 2012). Statistics were calculated using SigmaPlot. For single comparisons, a Mann–Whitney Rank Sum Test was used.

Atomic Force Microscopy

A 2.5 µl drop of reconstituted filaments in deionized water (dilution 1/5000) was deposited on freshly cleaved mica, incubated for 3 min, washed with 1 ml of water with 80 µl drop steps to remove excessive salt crystals, and finally dried with nitrogen gas. Imaging was performed on a Multimode 8, Nanoscope V (Bruker) equipped with NanoScope software (Bruker, Santa Barbara, CA, United States). Imaging was done with peak force imaging mode at ∼1 Hz rate, with 512 or 1024 pixel sampling and other parameters were adjusted automatically with ScanAsyst mode in air. A ScanAsyst-air (Bruker) cantilever with nominal 2 nm tip radius, 70 kHz frequency and 0.4 N/m spring constant was used. Images

[1] https://imagej.nih.gov/ij/

[2] http://www.microbej.com/

were processed with Gwyddion (Nečas and Klapetek, 2012), and if needed stripe noise was removed using DeStripe (Chen and Pellequer, 2011). Size determination of the filaments was performed in Gwyddion by using manual cross-sections (3px thick) and by measuring their maximum heights. Average values and standard deviations are reported. The computation of atomic depth was performed using the Adepth server (Chen and Pellequer, 2013).

LC/ESI Mass Spectrometry

Liquid Chromatography Electrospray Ionization Mass Spectrometry (LC/ESI-MS) was performed using a 6210 LC/ESI-TOF mass spectrometer interfaced with an HPLC binary pump system (Agilent Technologies). The mass spectrometer was calibrated in the mass-to-charge (*m/z*) 300–3200 range with standard calibrants (ESI-L, Low concentration tuning mix, Agilent Technologies) before measurements and mass spectra were recorded in the 300–3200 *m/z* range. MS acquisition was carried out in the positive ion mode with spectra in the profile mode. The MS instrument was operated with the following experimental settings: the ESI source temperature was set at 300°C; nitrogen was used as drying gas (7 l/min) and as nebulizer gas (10 psi); the capillary needle voltage was set at 4000 V. Spectra acquisition rate was of 1.03 spectra/s. All solvents used were HPLC grade (Chromasolv, Sigma-Aldrich), trifluoroacetic acid (TFA) was from Acros Organics (puriss., p.a.). Solvent A was 0.03% TFA in water, solvent B was 95% acetonitrile-5% water-0.03% TFA. The MS spectra were acquired and the data processed with MassHunter workstation software (*v.* B.02.00, Agilent Technologies) and with GPMAW software (v. 7.00b2, Lighthouse Data, Denmark).

Just before analysis each trypsin digested protein was diluted with solvent A to a final concentration of 5 μM and thermostatted at 10°C in the autosampler; 8 μl of each sample were injected. Samples were first trapped and desalted on a reverse phase-C8 cartridge (Zorbax 300SB-C8, 5 μm, 300 μm ID × 5 mm, Agilent Technologies) for 3 min at a flow rate of 50 μl/min with 100% solvent A and then eluted and separated onto a RP-C8 column (Jupiter, 5 μm, 300 Å, 1 mm ID × 50 mm, Phenomenex) at a flow rate of 50 μl/min using the following linear gradient: from 5 to 95% solvent B in 15 min, then remaining 2 min at 100% solvent B and finally re-equilibrating the column at 5% solvent B for 10 min.

Modeling

Optimal models of PscF-forward, PscF-reverse and PrgI-reverse protomers were built based on the PrgI protomer structure of the *Salmonella* needle structure by extracting chain A from the 2LPZ pdb file. MODELLER (Eswar et al., 2007), version 9.16, was used to individually align the forward (N-C:N-C) and reverse (N-C:C-N) PscF sequences to PrgI as well as a reverse (N-C:C-N) variant of PrgI for comparison (align2d.py). Initial single-chain models for the D76A and P47A/Q54A were prepared in the same way. The resulting alignment files and the PrgI subunit model were used as additional input to MODELLER to construct subunit models with secondary structure corresponding to that of PrgI (model-single.py). Ten models were calculated in each case and an overall assessment was manually carried out, judging energetic qualities and alignment to PrgI, to derive single optimal models for all cases. In the case of both forward and reverse PscF models, C-terminal helices were additionally enforced by alteration of the Phi and Psi backbone angles with PyMOL. Optimal models were subjected to a brief structural minimization protocol using the Chimera molecular modeling/visualization package (Pettersen et al., 2004) (default parameters) to remove atomic clashes (VDW overlap). PrgI-like T3SS needles were reconstructed in PyMol by aligning the constructed subunit models, by secondary structure, to the 29 chains of the PrgI (PDB code: 2LPZ) needle model.

The complete 29-chain needle structures, for wild-type (forward and reverse) and mutated subunits, were refined using a cluster-based installation of Rosetta (Das and Baker, 2008) (relax.mpi.linuxgccrelease – relax:fast), wherein the backbone heavy atoms were fixed in space but the positions of side-chains were allowed to evolve with respect to energetic minimization. The best resulting structures (as determined by overall Rosetta energy), calculated from a pool of 3 were then submitted to the MolProbity webserver (Davis et al., 2007) in a protonated form for validation (**Supplementary Table S1**).

DATA AVAILABILITY

Publicly available datasets were analyzed in this study. This data can be found here: https://www.nature.com/articles/nature11079.

AUTHOR CONTRIBUTIONS

VJ, IA, and AL designed the study and assembled the results. CL performed protein purifications and sample preparations for biochemical, EM and AFM experiments. DF and J-MT performed the EM and AFM experiments, respectively. J-LP analyzed and interpreted both images. All model building, computer minimizations and structure interpretations were performed by JT, with the supervision of AL and BH. CG constructed plasmids and mutants and perform initial cytotoxicity assays under the supervision of IA and EF. Macrophages cultures were prepared by SB. VJ performed cytotoxicity, florescence microscopy and biochemical experiments, with data analysis and interpretation. SB and DL contributed to the microscopy experiments and ImageJ/MicrobeJ analysis, while JB helped with Western blots. LS performed mass spectrometry experiments, data analysis, and interpretation. VJ, AD, and AL wrote the paper, with input from all authors.

FUNDING

This work used the platforms of the Grenoble Instruct-ERIC Center (ISBG: UMS 3518 CNRS-CEA-UGA-EMBL) with support from FRISBI (ANR-10 INBS-05-02) and GRAL (ANR-10-LABX-49-01) within the Grenoble Partnership for

Structural Biology (PSB). The electron microscope facility is supported by the Rhône-Alpes Region, the Fondation Recherche Médicale (FRM), the fonds FEDER, the Centre National de la Recherche Scientifique (CNRS), the CEA, the University of Grenoble, EMBL, and the GIS-Infrastrutures en Biologie Santé et Agronomie (IBISA). The authors wish to acknowledge ERC Starting Grant No. 639020, ANR-14-CE09-0020-01 and the Fondation pour la Recherche Médicale (FRM)—AJE20140630090 to AL, as well as grant VLM (RF20150501349) to EF, Fondation pour la Recherche Médicale (DEQ20170336705) to IA, and VLM (RIF20150501457) to AD.

ACKNOWLEDGMENTS

The authors thank Michel Ragno for antibody purification. This work acknowledges the AFM platform at the IBS.

SUPPLEMENTARY MATERIAL

The Supplementary Material for this article can be found online at: https://www.frontiersin.org/articles/10.3389/fmicb.2019.00573/full#supplementary-material

REFERENCES

Bergeron, J. R. C., Fernández, L., Wasney, G. A., Vuckovic, M., Reffuveille, F., Hancock, R. E. W., et al. (2016). The structure of a type 3 secretion system (T3SS) ruler protein suggests a molecular mechanism for needle length sensing. *J. Biol. Chem.* 291, 1676–1691. doi: 10.1074/jbc.M115.684423

Berube, B. J., Murphy, K. R., Torhan, M. C., Bowlin, N. O., Williams, J. D., Bowlin, T. L., et al. (2017). Impact of type III secretion effectors and of phenoxyacetamide inhibitors of type III secretion on abscess formation in a mouse model of *Pseudomonas aeruginosa* infection. *Antimicrob. Agents Chemother.* 61, e1202–e1217. doi: 10.1128/AAC.01202-17

Bhattacharya, A., Tejero, R., and Montelione, G. T. (2007). Evaluating protein structures determined by structural genomics consortia. *Proteins* 66, 778–795. doi: 10.1002/prot.21165

Bowlin, N. O., Williams, J. D., Knoten, C. A., Torhan, M. C., Tashjian, T. F., Li, B., et al. (2014). Mutations in the *Pseudomonas aeruginosa* needle protein gene pscF confer resistance to phenoxyacetamide inhibitors of the type III secretion system. *Antimicrob. Agents Chemother.* 58, 2211–2220. doi: 10.1128/AAC.02795-13

Chakravarty, S., and Varadarajan, R. (1999). Residue depth: a novel parameter for the analysis of protein structure and stability. *Struct. Lond. Engl.* 7, 723–732. doi: 10.1016/S0969-2126(99)80097-5

Charro, N., and Mota, L. J. (2015). Approaches targeting the type III secretion system to treat or prevent bacterial infections. *Expert Opin. Drug Discov.* 10, 373–387. doi: 10.1517/17460441.2015.1019860

Chen, S. W., and Pellequer, J.-L. (2011). DeStripe: frequency-based algorithm for removing stripe noises from AFM images. *BMC Struct. Biol.* 11:7. doi: 10.1186/1472-6807-11-7

Chen, S. W., and Pellequer, J.-L. (2013). Adepth: New Representation and its implications for atomic depths of macromolecules. *Nucleic Acids Res.* 41, W412–W416. doi: 10.1093/nar/gkt299

Cimino, M., Alamo, L., and Salazar, L. (2006). Permeabilization of the mycobacterial envelope for protein cytolocalization studies by immunofluorescence microscopy. *BMC Microbiol.* 6:35. doi: 10.1186/1471-2180-6-35

Cornelis, G. R. (2006). The type III secretion injectisome. *Nat. Rev. Microbiol.* 4, 811–825. doi: 10.1038/nrmicro1526

Das, R., and Baker, D. (2008). Macromolecular modeling with rosetta. *Annu. Rev. Biochem.* 77, 363–382. doi: 10.1146/annurev.biochem.77.062906.171838

Dasgupta, N., Ashare, A., Hunninghake, G. W., and Yahr, T. L. (2006). Transcriptional induction of the *Pseudomonas aeruginosa* type III secretion system by low Ca2+ and host cell contact proceeds through two distinct signaling pathways. *Infect. Immun.* 74, 3334–3341. doi: 10.1128/IAI.00090-06

Davis, A. J., and Mecsas, J. (2007). Mutations in the *Yersinia pseudotuberculosis* type III secretion system needle protein, YscF, that specifically abrogate effector translocation into host cells. *J. Bacteriol.* 189, 83–97. doi: 10.1128/JB.01396-06

Davis, I. W., Leaver-Fay, A., Chen, V. B., Block, J. N., Kapral, G. J., Wang, X., et al. (2007). MolProbity: all-atom contacts and structure validation for proteins and nucleic acids. *Nucleic Acids Res.* 35, W375–W383. doi: 10.1093/nar/gkm216

Deane, J. E., Roversi, P., Cordes, F. S., Johnson, S., Kenjale, R., Daniell, S., et al. (2006). Molecular model of a type III secretion system needle: implications for host-cell sensing. *Proc. Natl. Acad. Sci. U.S.A.* 103, 12529–12533. doi: 10.1073/pnas.0602689103

Demers, J.-P., Habenstein, B., Loquet, A., Kumar Vasa, S., Giller, K., Becker, S., et al. (2014). High-resolution structure of the *Shigella* type-III secretion needle by solid-state NMR and cryo-electron microscopy. *Nat. Commun.* 5:4976. doi: 10.1038/ncomms5976

Demers, J.-P., Sgourakis, N. G., Gupta, R., Loquet, A., Giller, K., Riedel, D., et al. (2013). The common structural architecture of *Shigella flexneri* and *Salmonella typhimurium* type three secretion needles. *PLoS Pathog.* 9:e1003245. doi: 10.1371/journal.ppat.1003245

Discola, K. F., Förster, A., Boulay, F., Simorre, J.-P., Attree, I., Dessen, A., et al. (2014). Membrane and chaperone recognition by the major translocator protein PopB of the type III secretion system of *Pseudomonas aeruginosa*. *J. Biol. Chem.* 289, 3591–3601. doi: 10.1074/jbc.M113.517920

Ducret, A., Quardokus, E. M., and Brun, Y. V. (2016). MicrobeJ, a tool for high throughput bacterial cell detection and quantitative analysis. *Nat. Microbiol.* 1:16077. doi: 10.1038/nmicrobiol.2016.77

Eswar, N., Webb, B., Marti-Renom, M. A., Madhusudhan, M. S., Eramian, D., Shen, M.-Y., et al. (2007). Comparative protein structure modeling using MODELLER. *Curr. Protoc. Protein Sci.* 50, 2.9.1–2.9.31. doi: 10.1002/0471140864.ps0209s50 Unit 2.9,

Fujii, T., Cheung, M., Blanco, A., Kato, T., Blocker, A. J., and Namba, K. (2012). Structure of a type III secretion needle at 7-Å resolution provides insights into its assembly and signaling mechanisms. *Proc. Natl. Acad. Sci. U.S.A.* 109, 4461–4466. doi: 10.1073/pnas.1116126109

Galán, J. E., and Collmer, A. (1999). Type III secretion machines: bacterial devices for protein delivery into host cells. *Science* 284, 1322–1328. doi: 10.1126/science.284.5418.1322

Galán, J. E., Lara-Tejero, M., Marlovits, T. C., and Wagner, S. (2014). Bacterial type III secretion systems: specialized nanomachines for protein delivery into target cells. *Annu. Rev. Microbiol.* 68, 415–438. doi: 10.1146/annurev-micro-092412-155725

Godon, C., Teulon, J.-M., Odorico, M., Basset, C., Meillan, M., Vellutini, L., et al. (2017). Conditions to minimize soft single biomolecule deformation when imaging with atomic force microscopy. *J. Struct. Biol.* 197, 322–329. doi: 10.1016/j.jsb.2016.12.011

Goure, J., Pastor, A., Faudry, E., Chabert, J., Dessen, A., and Attree, I. (2004). The V antigen of *Pseudomonas aeruginosa* is required for assembly of the functional PopB/PopD translocation pore in host cell membranes. *Infect. Immun.* 72, 4741–4750. doi: 10.1128/IAI.72.8.4741-4750.2004

Harmon, D. E., Murphy, J. L., Davis, A. J., and Mecsas, J. (2013). A mutant with aberrant extracellular LcrV-YscF interactions fails to form pores and translocate Yop effector proteins but retains the ability to trigger Yop secretion in response to host cell contact. *J. Bacteriol.* 195, 2244–2254. doi: 10.1128/JB.02011-12

Hoiczyk, E., and Blobel, G. (2001). Polymerization of a single protein of the pathogen *Yersinia enterocolitica* into needles punctures eukaryotic cells. *Proc. Natl. Acad. Sci. U.S.A.* 98, 4669–4674. doi: 10.1073/pnas.071065798

Hu, J., Worrall, L. J., Hong, C., Vuckovic, M., Atkinson, C. E., Caveney, N., et al. (2018). Cryo-EM analysis of the T3S injectisome reveals the structure of the needle and open secretin. *Nat. Commun.* 9:3840. doi: 10.1038/s41467-018-06298-8

Izoré, T., Job, V., and Dessen, A. (2011). Biogenesis, regulation, and targeting of the type III secretion system. *Struct. Lond. Engl.* 1993, 603–612. doi: 10.1016/j.str.2011.03.015

Jneid, B., Moreau, K., Plaisance, M., Rouaix, A., Dano, J., and Simon, S. (2016). Role of T3SS-1 SipD protein in protecting mice against Non-typhoidal *Salmonella* typhimurium. *PLoS Negl. Trop. Dis.* 10:e0005207. doi: 10.1371/journal.pntd.0005207

Job, V., Matteï, P.-J., Lemaire, D., Attree, I., and Dessen, A. (2010). Structural basis of chaperone recognition of type III secretion system minor translocator proteins. *J. Biol. Chem.* 285, 23224–23232. doi: 10.1074/jbc.M110.111278

Journet, L., Agrain, C., Broz, P., and Cornelis, G. R. (2003). The needle length of bacterial injectisomes is determined by a molecular ruler. *Science* 302, 1757–1760. doi: 10.1126/science.1091422

Kato, J., Dey, S., Soto, J. E., Butan, C., Wilkinson, M. C., De Guzman, R. N., et al. (2018). A protein secreted by the *Salmonella* type III secretion system controls needle filament assembly. *eLife* 7:e35886. doi: 10.7554/eLife.35886

Kenjale, R., Wilson, J., Zenk, S. F., Saurya, S., Picking, W. L., Picking, W. D., et al. (2005). The needle component of the type III secreton of *Shigella* regulates the activity of the secretion apparatus. *J. Biol. Chem.* 280, 42929–42937. doi: 10.1074/jbc.M508377200

Koroleva, E. A., Kobets, N. V., Shcherbinin, D. N., Zigangirova, N. A., Shmarov, M. M., Tukhvatulin, A. I., et al. (2017). Chlamydial type III secretion system needle protein induces protective immunity against *Chlamydia muridarum* intravaginal infection. *Biomed Res. Int.* 2017:3865802. doi: 10.1155/2017/3865802

Kubori, T., Matsushima, Y., Nakamura, D., Uralil, J., Lara-Tejero, M., Sukhan, A., et al. (1998). Supramolecular structure of the *Salmonella* typhimurium type III protein secretion system. *Science* 280, 602–605. doi: 10.1126/science.280.5363.602

Kubori, T., Sukhan, A., Aizawa, S. I., and Galán, J. E. (2000). Molecular characterization and assembly of the needle complex of the *Salmonella* typhimurium type III protein secretion system. *Proc. Natl. Acad. Sci. U.S.A.* 97, 10225–10230. doi: 10.1073/pnas.170128997

Kuhlen, L., Abrusci, P., Johnson, S., Gault, J., Deme, J., Caesar, J., et al. (2018). Structure of the core of the type III secretion system export apparatus. *Nat. Struct. Mol. Biol.* 25, 583–590. doi: 10.1038/s41594-018-0086-9

Loquet, A., Sgourakis, N. G., Gupta, R., Giller, K., Riedel, D., Goosmann, C., et al. (2012). Atomic model of the type III secretion system needle. *Nature* 486, 276–279. doi: 10.1038/nature11079

Matteï, P.-J., Faudry, E., Job, V., Izoré, T., Attree, I., and Dessen, A. (2011). Membrane targeting and pore formation by the type III secretion system translocon. *FEBS J.* 278, 414–426. doi: 10.1111/j.1742-4658.2010.07974.x

Nariya, M. K., Israeli, J., Shi, J. J., and Deeds, E. J. (2016). Mathematical model for length control by the timing of substrate switching in the type III secretion system. *PLoS Comput. Biol.* 12:e1004851. doi: 10.1371/journal.pcbi.1004851

Nečas, D., and Klapetek, P. (2012). Gwyddion: an open-source software for SPM data analysis. *Open Phys.* 10, 181–188. doi: 10.2478/s11534-011-0096-2

Nguyen, V. S., Jobichen, C., Tan, K. W., Tan, Y. W., Chan, S. L., Ramesh, K., et al. (2015). Structure of AcrH-AopB chaperone-translocator complex reveals a role for membrane hairpins in type III secretion system translocon assembly. *Struct. Lond. Engl.* 23, 2022–2031. doi: 10.1016/j.str.2015.08.014

Park, D., Lara-Tejero, M., Waxham, M. N., Li, W., Hu, B., Galán, J. E., et al. (2018). Visualization of the type III secretion mediated *Salmonella*-host cell interface using cryo-electron tomography. *eLife* 7:e39514. doi: 10.7554/eLife.39514

Pastor, A., Chabert, J., Louwagie, M., Garin, J., and Attree, I. (2005). PscF is a major component of the *Pseudomonas aeruginosa* type III secretion needle. *FEMS Microbiol. Lett.* 253, 95–101. doi: 10.1016/j.femsle.2005.09.028

Perdu, C., Huber, P., Bouillot, S., Blocker, A., Elsen, S., Attrée, I., et al. (2015). ExsB is required for correct assembly of the *Pseudomonas aeruginosa* type III secretion apparatus in the bacterial membrane and full virulence in vivo. *Infect. Immun.* 83, 1789–1798. doi: 10.1128/IAI.00048-15

Pettersen, E. F., Goddard, T. D., Huang, C. C., Couch, G. S., Greenblatt, D. M., Meng, E. C., et al. (2004). UCSF Chimera–a visualization system for exploratory research and analysis. *J. Comput. Chem.* 25, 1605–1612. doi: 10.1002/jcc.20084

Poyraz, O., Schmidt, H., Seidel, K., Delissen, F., Ader, C., Tenenboim, H., et al. (2010). Protein refolding is required for assembly of the type three secretion needle. *Nat. Struct. Mol. Biol.* 17, 788–792. doi: 10.1038/nsmb.1822

Quinaud, M., Chabert, J., Faudry, E., Neumann, E., Lemaire, D., Pastor, A., et al. (2005). The PscE-PscF-PscG complex controls type III secretion needle biogenesis in *Pseudomonas aeruginosa*. *J. Biol. Chem.* 280, 36293–36300. doi: 10.1074/jbc.M508089200

Quinaud, M., Plé, S., Job, V., Contreras-Martel, C., Simorre, J.-P., Attree, I., et al. (2007). Structure of the heterotrimeric complex that regulates type III secretion needle formation. *Proc. Natl. Acad. Sci. U.S.A.* 104, 7803–7808. doi: 10.1073/pnas.0610098104

Radics, J., Königsmaier, L., and Marlovits, T. C. (2014). Structure of a pathogenic type 3 secretion system in action. *Nat. Struct. Mol. Biol.* 21, 82–87. doi: 10.1038/nsmb.2722

Robert, X., and Gouet, P. (2014). Deciphering key features in protein structures with the new ENDscript server. *Nucleic Acids Res.* 42, W320–W324. doi: 10.1093/nar/gku316

Sal-Man, N., Setiaputra, D., Scholz, R., Deng, W., Yu, A. C. Y., Strynadka, N. C. J., et al. (2013). EscE and EscG are cochaperones for the type III needle protein EscF of enteropathogenic *Escherichia coli*. *J. Bacteriol.* 195, 2481–2489. doi: 10.1128/JB.00118-13

Schneider, C. A., Rasband, W. S., and Eliceiri, K. W. (2012). NIH Image to ImageJ: 25 years of image analysis. *Nat. Methods* 9, 671–675. doi: 10.1038/nmeth.2089

Sun, P., Tropea, J. E., Austin, B. P., Cherry, S., and Waugh, D. S. (2008). Structural characterization of the *Yersinia pestis* type III secretion system needle protein YscF in complex with its heterodimeric chaperone YscE/YscG. *J. Mol. Biol.* 377, 819–830. doi: 10.1016/j.jmb.2007.12.067

Tamano, K., Aizawa, S., Katayama, E., Nonaka, T., Imajoh-Ohmi, S., Kuwae, A., et al. (2000). Supramolecular structure of the *Shigella* type III secretion machinery: the needle part is changeable in length and essential for delivery of effectors. *EMBO J.* 19, 3876–3887. doi: 10.1093/emboj/19.15.3876

Torruellas, J., Jackson, M. W., Pennock, J. W., and Plano, G. V. (2005). The *Yersinia pestis* type III secretion needle plays a role in the regulation of Yop secretion. *Mol. Microbiol.* 57, 1719–1733. doi: 10.1111/j.1365-2958.2005.04790.x

Veenendaal, A. K. J., Hodgkinson, J. L., Schwarzer, L., Stabat, D., Zenk, S. F., and Blocker, A. J. (2007). The type III secretion system needle tip complex mediates host cell sensing and translocon insertion. *Mol. Microbiol.* 63, 1719–1730. doi: 10.1111/j.1365-2958.2007.05620.x

Verasdonck, J., Shen, D.-K., Treadgold, A., Arthur, C., Böckmann, A., Meier, B. H., et al. (2015). Reassessment of MxiH subunit orientation and fold within native *Shigella* T3SS needles using surface labelling and solid-state NMR. *J. Struct. Biol.* 192, 441–448. doi: 10.1016/j.jsb.2015.10.005

Wagner, S., Grin, I., Malmsheimer, S., Singh, N., Torres-Vargas, C. E., and Westerhausen, S. (2018). Bacterial type III secretion systems: a complex device for the delivery of bacterial effector proteins into eukaryotic host cells. *FEMS Microbiol. Lett.* 365:fny201. doi: 10.1093/femsle/fny201

Wagner, S., Stenta, M., Metzger, L. C., Dal Peraro, M., and Cornelis, G. R. (2010). Length control of the injectisome needle requires only one molecule of Yop secretion protein P (YscP). *Proc. Natl. Acad. Sci. U.S.A.* 107, 13860–13865. doi: 10.1073/pnas.1006985107

Wang, Y., Ouellette, A. N., Egan, C. W., Rathinavelan, T., Im, W., and De Guzman, R. N. (2007). Differences in the electrostatic surfaces of the type III secretion needle proteins PrgI, BsaL, and MxiH. *J. Mol. Biol.* 371, 1304–1314. doi: 10.1016/j.jmb.2007.06.034

Conflict of Interest Statement: The authors declare that the research was conducted in the absence of any commercial or financial relationships that could be construed as a potential conflict of interest.

Copyright © 2019 Lombardi, Tolchard, Bouillot, Signor, Gebus, Liebl, Fenel, Teulon, Brock, Habenstein, Pellequer, Faudry, Loquet, Attrée, Dessen and Job. This is an open-access article distributed under the terms of the Creative Commons Attribution License (CC BY). The use, distribution or reproduction in other forums is permitted, provided the original author(s) and the copyright owner(s) are credited and that the original publication in this journal is cited, in accordance with accepted academic practice. No use, distribution or reproduction is permitted which does not comply with these terms.

frontiers in Microbiology

MINI REVIEW
published: 03 May 2019
doi: 10.3389/fmicb.2019.00921

Versatility of the BID Domain: Conserved Function as Type-IV-Secretion-Signal and Secondarily Evolved Effector Functions Within *Bartonella*-Infected Host Cells

*Alexander Wagner, Colin Tittes and Christoph Dehio**

Biozentrum, University of Basel, Basel, Switzerland

Bartonella spp. are facultative intracellular pathogens that infect a wide range of mammalian hosts including humans. In order to subvert cellular functions and the innate immune response of their hosts, these pathogens utilize a VirB/VirD4 type-IV-secretion (T4S) system to translocate *Bartonella* effector proteins (Beps) into host cells. Crucial for this process is the Bep intracellular delivery (BID) domain that together with a C-terminal stretch of positively charged residues constitutes a bipartite T4S signal. This function in T4S is evolutionarily conserved with BID domains present in bacterial toxins and relaxases. Strikingly, some BID domains of Beps have evolved secondary functions to modulate host cell and innate immune pathways in favor of *Bartonella* infection. For instance, BID domains mediate F-actin-dependent bacterial internalization, inhibition of apoptosis, or modulate cell migration. Recently, crystal structures of three BID domains from different Beps have been solved, revealing a conserved fold formed by a four-helix bundle topped with a hook. While the conserved BID domain fold might preserve its genuine role in T4S, the highly variable surfaces characteristic for BID domains may facilitate secondary functions. In this review, we summarize our current knowledge on evolutionary and structural traits as well as functional aspects of the BID domain with regard to T4S and pathogenesis.

Keywords: Type-IV-secretion, VirB/VirD4, Bartonella, α-proteobacteria, Bartonella effector proteins, relaxases, BID domain, pathogenesis

OPEN ACCESS

Edited by:
Ignacio Arechaga, University of Cantabria, Spain

Reviewed by:
Peter J. Christie, University of Texas Health Science Center at Houston, United States
Jack Christopher Leo, University of Oslo, Norway

***Correspondence:**
Christoph Dehio
christoph.dehio@unibas.ch

Specialty section:
This article was submitted to Microbial Physiology and Metabolism, a section of the journal Frontiers in Microbiology

Received: *13 March 2019*
Accepted: *11 April 2019*
Published: *03 May 2019*

Citation:
Wagner A, Tittes C and Dehio C (2019) Versatility of the BID Domain: Conserved Function as Type-IV-Secretion-Signal and Secondarily Evolved Effector Functions Within Bartonella-Infected Host Cells. Front. Microbiol. 10:921. doi: 10.3389/fmicb.2019.00921

INTRODUCTION

Type-IV-secretion (T4S) systems are multiprotein complexes embedded in the cell envelope of Gram-negative and Gram-positive bacteria and some archaea (Berge et al., 2017). They represent versatile nanomachines that fulfill diverse functions including (1) contact-dependent transfer of DNA (conjugation), (2) contact-dependent transfer of bacterial effector proteins into eukaryotic host cells, (3) contact-dependent toxin delivery into bacterial cells, (4) secretion of DNA into the extracellular milieu, and (5) uptake of DNA from the environment (Waksman, 2019). T4S systems can be, based on their architectural complexity, categorized into

two classes: T4AS (12 subunits) and T4BS (>25 subunits) systems (Waksman, 2019). Based on the paradigmatic *Agrobacterium tumefaciens* VirB/VirD4 T4AS system, the subunits are named VirB1–11 and VirD4 (Li and Christie, 2018). VirB2–11 are essential for the assembly of the T4S system machinery and substrate translocation. The membrane-bound ATPase VirD4—also known as the T4S coupling protein (T4CP)—is crucial for the recognition of T4S substrates prior to translocation.

The majority of T4S substrates possess a non-cleavable T4S signal at their C-termini consisting of only a few positively charged or hydrophobic residues (Christie et al., 2014). However, some T4S signals form a larger structural scaffold, as for instance, the globular TSA domain of conjugative relaxase TraI encoded by plasmid R1 (Redzej et al., 2013). Another example constitutes the approximately 100-aa-long BID (Bep intracellular delivery) domain that together with a short positively charged C-terminal tail forms a bipartite T4S signal proposed to interact with the T4CP (Schulein et al., 2005; Stanger et al., 2017). The BID domain is present in α-proteobacterial toxins, relaxases, and Beps (*Bartonella* effector proteins) (**Figure 1A**), the latter representing numerous host cell-targeted effectors of pathogenic *Bartonella* species (Wagner and Dehio, 2019). The vast majority of BID domain-containing T4S substrates are genetically linked to a T4S system that resembles the canonical *A. tumefaciens* VirB/VirD4 T4S system (**Figure 1B**). VirD4-T4CPs associated with BID domain-containing T4S substrates form a monophyletic group among T4CP subtypes, indicating a coevolutionary trajectory to maintain interaction of this sublineage with BID domains (Schulein et al., 2005). Multiple studies with the model pathogen *Bartonella henselae* (*Bhe*) showed that Beps are translocated *via* a VirB/VirD4 T4S system into various host cell types to modulate diverse cellular and innate immune functions allowing *Bartonella* to spread and establish long-lasting hemotrophic infections in its mammalian host (Schulein et al., 2005; Schmid et al., 2006; Truttmann et al., 2011a; Okujava et al., 2014).

Beps are multi-domain proteins. A majority of Beps possess an N-terminal FIC (Filamentation induced by cAMP) domain that confers posttranslational modifications, a central connecting OB (oligonucleotide binding) fold, and a C-terminal BID domain (Engel et al., 2011; Harms et al., 2017b). A previous genome analysis revealed that 70% of all Beps and the interbacterial toxin VbhT (present on conjugative plasmid pVbh encoding the Vbh (VirB homologous) T4S system in certain *Bartonella* spp.) display the canonical FIC-OB-BID architecture (Engel et al., 2011). Furthermore, all Bep repertoires present in the *Bartonella* genus harbor Beps with a derived domain composition, which likely evolved from a single primordial FIC-OB-BID ancestor *via* repeated gene duplication and diversification events. The diversification of Bep repertoires occurred independently in three distinct *Bartonella* lineages, resulting in Bep197–234 in *B. ancashensis* of lineage 1 (L-1), Bep1–10 in lineage 3 (L-3), and BepA-I in the most species-rich lineage 4 (L-4) (Harms et al., 2017). Instead of a FIC domain, the derived Beps possess tandem-repeated tyrosine phosphorylation (pY) motifs that are phosphorylated by endogenous host cell kinases, and/or additional BID domains (Wagner and Dehio, 2019). While the original function as T4S signal is preserved among C-terminal BID domains, some BID domains have secondarily evolved effector functions within host cells. These functions include inhibition of apoptosis, bacterial uptake *via* rearrangement of the F-actin cytoskeleton, and modulation of cell migration of infected host cells (Truttmann et al., 2011a; Pulliainen et al., 2012; Okujava et al., 2014).

In this review, we will focus on the evolution and classification of BID domains based on their presence in different T4S substrates. We will furthermore discuss structural and functional aspects of the BID domain with regard to T4S and the subversion of host cell function.

CLASSIFICATION AND STRUCTURAL FEATURES OF BID DOMAINS

Classification of BID Domains

BID domains display high sequence variability. Their classification is mainly based on their position within the multi-domain relaxases and Beps (**Figure 1A**; Stanger et al., 2017). C-terminal BID domains that serve as part of the T4S signal are designated as tBIDx and nonterminal BID domains as BIDx, with "x" representing a number indicating whether this BID domain is the first, second, third, or fourth BID domain counted from the N-terminus (**Figure 1A**). In the Beps, tBIDs have been further subclassified into ancestral tBIDs found in the canonical FIC-OB-BID architecture and derived tBIDs of pY- and multi-BID domain-containing Beps (Stanger et al., 2017).

A recent study reported the presence of BID domains fused to toxin domains (PezT and Zeta) of toxin/antitoxin modules (Harms et al., 2017a). These PezT/Zeta-BID proteins are encoded by conjugative plasmids that are prevalent in various α-proteobacterial genera such as *Agrobacterium*, *Chelativorans*, *Ochrobactrum*, and *Sinorhizobium*. Although it is not clear whether these PezT/Zeta-BID proteins are translocated through a T4S system, their genetic conservation to a *virB/virD4*-like T4S system locus suggests that these proteins are *bona fide* T4S substrates (**Figure 1B**; Harms et al., 2017a; Wagner and Dehio, 2019). Therefore, we extend the classification of BID domains by introducing tBIDα for those present in toxins found in various α-proteobacterial species. In a phylogenetic tree, tBIDα domains form a monophyletic group similar to tBID2 domains of α-proteobacterial relaxases, tBID1 domains of *Bartonella* TraA-relaxases/VbhTs, and the ancient and derived tBID domains found in Beps, confirming that the tBIDα domains form a new class of BID domains (**Figure 1C**, left). Interestingly, tBIDα domains are more closely related to the tBID domains of Beps than to tBID2 domains of α-proteobacterial relaxases, even though PezT/Zeta-BID proteins are encoded adjacent to the latter (**Figure 1B**). Thus, tBIDα domains are likely not the result of gene duplication and reshuffling events of relaxase tBID1/2 domains as proposed for the tBID1 domain of VbhT that is virtually identical to the tBID1 domains of *Bartonella* TraA relaxases (Harms et al., 2017a).

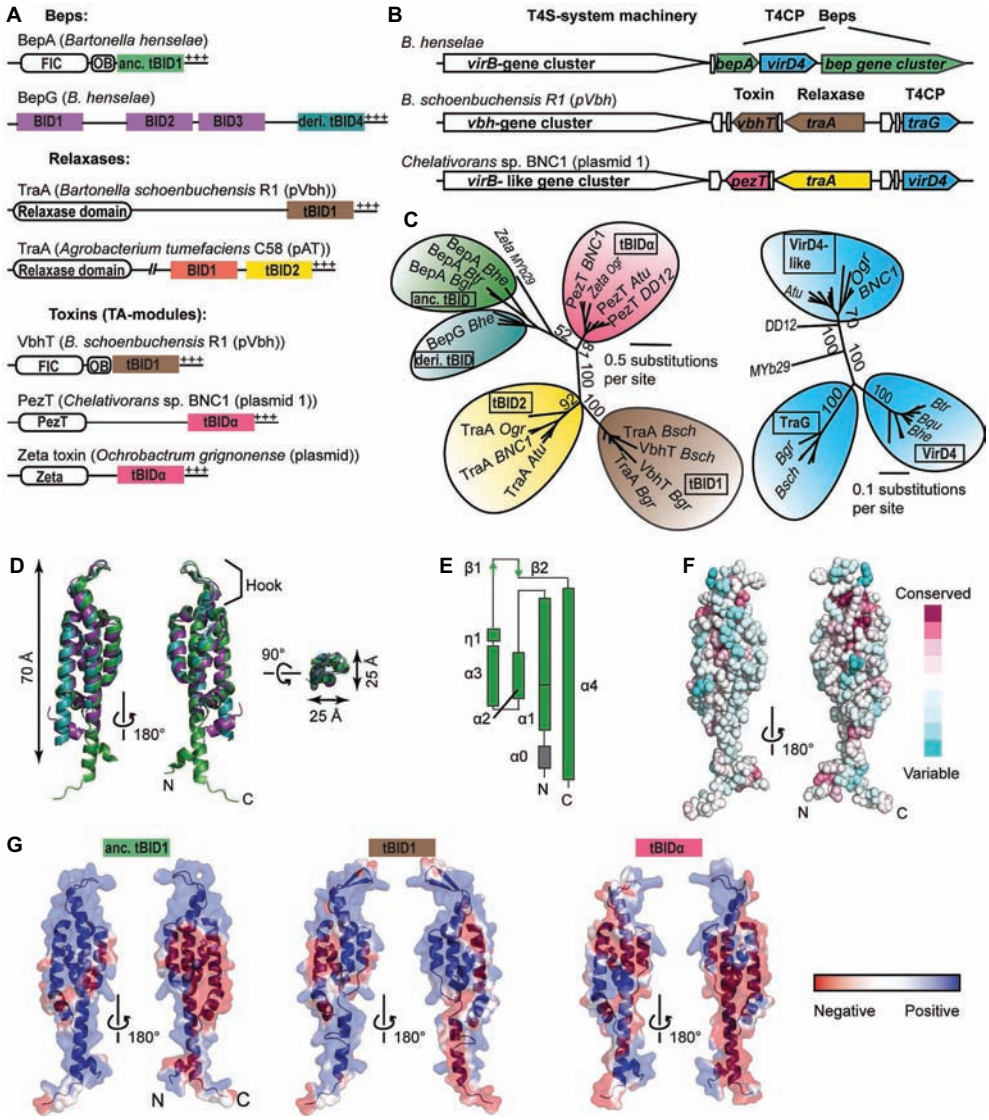

FIGURE 1 | Classification and structural features of BID domains. **(A)** Domain architecture of BID domain-containing type-IV-secretion (T4S) substrates found within α-proteobacteria. N-terminal, catalytic domains (FIC, relaxase domain, PezT, Zeta) and the OB (oligonucleotide binding) fold are displayed as white rectangles, respectively. BIDx and tBIDx domains are colored based on the subclass. +++, positively charged tail; anc., ancestral; deri., derived. **(B)** Synteny of representative BID domain-containing T4S substrate genes and adjacent *virB/virD4-like* T4S-system locus and genes involved in plasmid conjugation (the latter two are represented in white). The color code of BID domain-encoding genes is the same as of the respective BID domains displayed in **(A)**. Homologs of T4S coupling protein (T4CP) are depicted in blue. **(C)** Simplified neighbor-joining distance-based tree representations of the multiple sequence alignment of (left) terminal BIDs [tBIDs, color code as in **(A)**] and (right) the soluble domains of VirD4-like T4CPs that are associated with the tBIDs. Highlighted are representative proteins (per subfamily) encoded by: *B. grahamii* (*Bgr*), *B. tribocorum* (*Btr*), *B. henselae* (*Bhe*), *B. schoenbuchensis pVbh* (*Bsch*), *Agrobacterium tumefaciens* C58 pAT (*Atu*), *Chelativorans* sp. BNC1 plasmid 1 (BNC1), *Ochrobactrum grignonense* plasmid (*Ogr*), *Ochrobactrum sp.* MYb29 (MYb29), and *Shinella sp*. DD12 (DD12). **(D)** The similarity and compact nature of the BID fold is highlighted through superposition of the three solved BID domains: *Bro*Bep6_tBID1 (green; PDB: 4YK1), *Bcl*Bep9_tBID1 (cyan; PDB: 4YK2), and *Bhe*BepE_BID1 (purple; PDB: 4YK3). **(E)** Topology representation of *Bro*Bep6_tBID1. **(D,E)** are redrawn from Stanger et al. (2017) to adapt the color code to the remaining figure. **(F)** Residue conservation is rather low among BID domains of Beps. Depicted is the overall conservation score of BID domains mapped on the surface representation of *Bro*Bep6_tBID1. The color code is based on the ConSurf color scale (Ashkenazy et al., 2016). **(G)** Electrostatic potential mapped on the surfaces of experimentally determined (anc. tBID1 of *Bro*Bep6) and modeled (tBID1 of VbhT from *Bsch* and tBIDα from PezT from BNC1) tBID domains. Protein backbones are depicted as cartoon representation. The color code highlighting the electrostatic potential ranges from red (negative) to blue (positive).

The coevolutionary trajectory of tBID domains with their cognate T4CP is evident for tBID1 domains (TraA/VbhT) and TraG and for ancestral/derived tBIDs (Beps) with VirD4 (**Figure 1C**). In contrast, tBID2 (α-proteobacterial relaxases)- and tBIDα (PezT/Zeta-BID)-containing proteins supposedly interact with the same VirD4-like T4CP (**Figure 1C**, right), although these tBID domains are as distantly related to each other as tBID1 domains and ancestral/derived tBID domains (**Figure 1C**, left). It is worth mentioning that translocation of tBID-containing substrates through heterologous VirB/VirD4 T4S systems has

been experimentally proven in multiple instances (e.g., Schulein et al., 2005; Harms et al., 2017a). For instance, the tBID2 domain of α-proteobacterial relaxase TraA (encoded on *Atu* pAT) fused to Cre-recombinase (Cre) translocates through the *Bhe* VirB/VirD4 T4S system with similar efficiency as Cre-tBID-fusions of different *Bhe*-Beps (Schulein et al., 2005). We therefore believe that coevolution of tBID domains with their BID-associated VirD4-T4CPs has not yet led to the establishment of discrete specificities in recognition – despite the remarkable sequence variability of BID domains.

Structural Features of BID Domains

Recently, the crystal structures of BID domains representative for three different classes have been solved, including an ancestral tBID1 domain of *B. rochalimae* Bep6, a derived tBID1 domain of *B. clarridgeiae* Bep9, and a derived BID1 domain of *Bhe*-BepE (Stanger et al., 2017). All three BID domains are folded to a rigid, antiparallel four-helix bundle topped with a hook that accommodates a position opposite to both termini (**Figures 1D,E**). The shape of the three BID domains is elongated with a length of approximately 70 Å and a diameter of 25 Å, suggesting that this conserved fold might be crucial for the primary secretion signal function of the BID domain in T4S (Stanger et al., 2017). It is tempting to speculate that the hook might play a role in the interaction with the T4CP and/or other components of the VirB/VirD4 T4S machinery. Helix-1 (α1) and helix-4 (α4) can either be straight or kinked (**Figure 1D**). This conformational variability of BID domains at their extremities might be the result of different domain compositions in the remaining part of the protein and/or facilitate novel interactions with host target proteins. Interestingly, the T4S activity of a Cre-tBID1-fusion lacking α1 was reduced to 30% compared to full-length Cre-tBID1, suggesting an important role of α1 in translocation (Schulein et al., 2005).

While the hydrophobic core of BID domains is conserved, their surfaces are highly variable. The plasticity of BID domains is highlighted by the fact that BID domains of relaxases and Beps display on average 14% similarity (Stanger et al., 2017). Sequence similarity is also rather low within the various BID domain classes (**Figure 1F**), with the highest degree of similarity observed within tBID1 domains of *Bartonella* TraA and VbhT, respectively. In general, tBIDx subclasses display a higher degree of conservation than BIDx classes, which might be due to a relieved selection pressure of BIDx domains to interact with the T4CP. Although the surface composition among BID domains is poorly conserved, their surface charge distribution seems to be rather consistent, displaying two highly positively charged areas separated by a negatively charged patch (Stanger et al., 2017). This mainly positive charge distribution suggests that BID domains likely interact with a negatively charged surface on the interaction partner. Furthermore, slight differences in the charge distribution between BID domain classes and even among closely related BID domain orthologs can be observed (**Figure 1G**), suggesting subtle functional differences with respect to T4S efficiency (tBIDx) and effector function (BIDx/tBIDx).

Summarizing, we believe that the conserved rigid fold of the BID domain facilitates its role as T4S signal, whereas the highly variable surface might enable the evolution of secondary functions within host cells.

BID DOMAIN-MEDIATED HOST CELL MODULATIONS

The remarkable degree of host adaptation of pathogenic *Bartonella* spp. to their mammalian hosts has been attributed to a large extent to the VirB/VirD4 T4S system and its translocated Beps (Siamer and Dehio, 2015; Dehio and Tsolis, 2017; Wagner and Dehio, 2019). Most of the Bep-mediated host cell modulations are BID domain dependent and include apoptosis inhibition, F-actin rearrangements, and host cell migration. BID domain-mediated phenotypes are best understood on the molecular and cellular level for human pathogenic *Bhe* and *B. quintana* (*Bqu*). Both species belong to L-4 and thus their Beps are designated with a letter code (BepA, BepB, and so on, **Figure 2A**).

BepA-tBID1 Mediates Apoptosis Inhibition in a Host-Specific Manner

Bhe and *Bqu* enhance the proliferation of human endothelial cells (ECs) by inhibiting apoptosis (Kirby and Nekorchuk, 2002; Schmid et al., 2006; Pulliainen et al., 2012). The antiapoptotic activity was assigned to the ancestral tBID1 domain of *Bhe*-BepA and *Bqu*-BepA.2, respectively (**Figure 2B**). *Bhe*-BepA-tBID1 physically interacts with the catalytic subunit C2 of human adenylyl cyclase isoform 7 (AC7) to potentiate cAMP production (Pulliainen et al., 2012). AC7 is a plasma membrane-bound enzyme, which requires activation and association of its two catalytic subunits C1 and C2 to convert ATP into cAMP (Sadana and Dessauer, 2009). *Bhe*-BepA-tBID1 potentiates the cAMP-triggering effect of GTP-bound $G\alpha_S$ in a physiological context and in a pharmacological context together with the plant-derived drug forskolin, which intercalates C1 and C2 into a catalytically active form (Pulliainen et al., 2012). Thus, it is plausible to assume that *Bhe*-BepA-tBID1 allosterically enhances C1 and C2 subunit association in order to elevate cAMP production. The molecular restraints of the *Bhe*-BepA-tBID1 interaction with C2 (AC7) are currently unknown. However, a *Bhe*-BepA construct consisting only of helix-4 of the ancestral tBID1 domain and the adjacent C-terminal stretch did not inhibit apoptosis, suggesting that helix-4 alone is not sufficient for the antiapoptotic activity mediated by *Bhe*-BepA-BID (Schmid et al., 2006).

Interestingly, neither the BepA paralogs BepB or BepC of *Bhe* nor the BepA ortholog from the rat-associated *B. tribocorum* (*Btr*) displayed antiapoptotic activity (Schmid et al., 2006). The latter is in line with previous observations that only L-4 species associated with significant clinical manifestations in humans (e.g., *Bhe* and *Bqu*) possess antiapoptotic activity toward human ECs (Kirby and Nekorchuk, 2002).

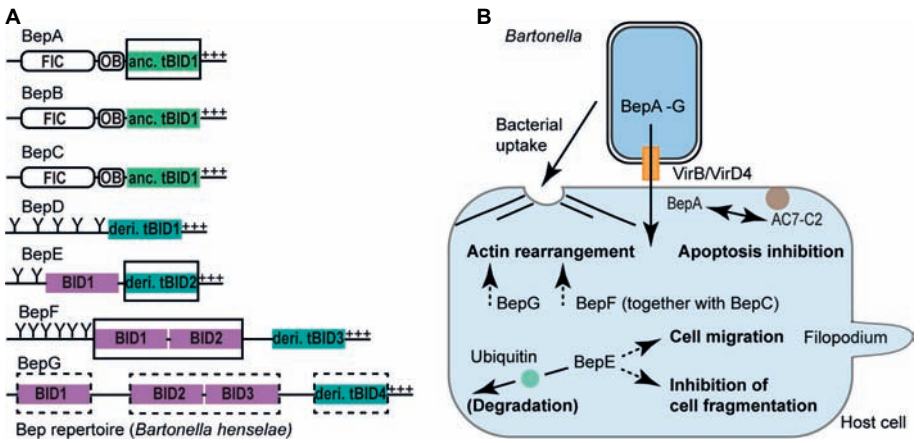

FIGURE 2 | BID domain-mediated host cell modulations. **(A)** Representative Bep repertoire of the model organism *Bartonella henselae* highlighting various classes of BID domains. BID domains with experimentally proven or suspected host-modulating function are highlighted with a full or dashed rectangle, respectively. OB, Oligonucleotide binding fold; Y, Tyrosine phosphorylation motif; +++, positively charged tail; anc., ancestral; deri., derived. **(B)** Schematic representation of BID-mediated host cell modulations. Following the VirB/VirD4 T4S system-mediated translocation into host cells, distinct BID domains [highlighted in **(A)**] alter host cell signaling processes allowing *Bartonella* to survive and propagate within the mammalian host. Host cells can counteract Bep-mediated functions by degrading the effectors following ubiquitination of their BID domains as shown for the BID domains of *Bqu*-BepE. Confirmed BID-target interactions are displayed with a continuous arrow, whereas dashed arrows indicate BID-mediated host cell modulations for which the target protein(s) are currently unknown. AC7-C2, catalytic subunit C2 of human adenylyl cyclase isoform 7 (AC7).

Multi-BID Domain-Containing Effectors BepG and BepF Trigger Invasome Formation

Bhe cells are internalized into ECs either individually *via* endocytosis or as bacterial aggregates in the course of the formation of a unique cellular structure, the invasome (Dehio et al., 1997). Invasome formation is a multistep process, that, following bacterial accumulation at the EC surface, involves F-actin rearrangements and stress fiber formation underneath the engulfed bacterial aggregate (Dehio et al., 1997). Furthermore, in contrast to the T4S system-independent endocytic uptake of *Bhe* into ECs, invasome formation is strictly VirB/VirD4 dependent (Schmid et al., 2004) and is redundantly triggered by either BepG or through the combined action of BepC and BepF (**Figure 2B**; Rhomberg et al., 2009; Truttmann et al., 2011b).

BepG of *Bhe* consists solely of four BID domains that are connected *via* short linker sequences. Hence, BepG likely promotes invasome formation *via* at least one of these four BID domains through interaction with yet unknown host target protein(s) (Rhomberg et al., 2009). Similarly, invasome formation mediated by BepF (together with BepC) is triggered by its two nonterminal BID domains BID1 and BID2, but not by its derived tBID3 domain (Truttmann et al., 2011a). Interestingly, BID2 and tBID3 are more similar to each other than to BID1. The overall low sequence conservation of these three BID domains allows no conclusion on why BID1 and BID2 contribute to invasome formation, but tBID3 is negligible in this process. We speculate that, besides certain, non-conserved residues at the surface of BID domains, also the relative position of BID domains within multi-domain architectures may be critical for effector function.

BepE-BID Domains Antagonize Cell Fragmentation and Promote Host Cell Migration

Bartonella spp. supposedly infect dendritic cells at the dermal site of inoculation and exploit these migratory cells as Trojan horses in order to reach the bloodstream, where bacteria infect, replicate, and persist within erythrocytes (Scherer et al., 1993; Schulein et al., 2001; Okujava et al., 2014; Vieira-Damiani et al., 2016). *In vivo* dissemination into the bloodstream is VirB/VirD4 dependent and relies on the function of BepE (**Figure 2B**; Okujava et al., 2014). *Bhe*-BepE is a pY-containing Bep that contains two BID domains (**Figure 2A**). Although *Bhe*-BepE interacts *via* its pY motifs with several host cell signaling proteins (Selbach et al., 2009), the dissemination of the bacteria into the bloodstream is exclusively dependent on the BID domains. *In vitro*, the derived tBID2 domain of *Bhe*-BepE interferes with a deleterious cell fragmentation phenotype triggered by other Beps (Okujava et al., 2014). Inhibition of the cell fragmentation phenotype is not only restricted to *Bhe*-BepE but appears to be a conserved function among BepE homologs including *Bqu*-BepE and *Btr*-BepE (Okujava et al., 2014).

Besides the cytoprotective effect against other Beps, translocated *Bhe*-BepE promotes the migratory capability of dendritic cells (Okujava et al., 2014). It needs to be determined whether this effect is mediated by the BID domains of BepE or by its pY motifs. However, it is conceivable that the promotion of cell migration is BID dependent, as BID domains of *Bhe*-BepE are sufficient to enable *Bartonella* cells to reach the bloodstream *in vivo* (Okujava et al., 2014).

A recent study showed that the tandemly repeated BID domains of *Bqu*-BepE but not of *Bhe*-BepE become ubiquitinated within

host cells followed by proteasomal degradation (Wang et al., 2018). Whether or not this ubiquitination plays a role in effector function of *Bqu*-BepE needs to be addressed in future research.

CONCLUDING REMARKS

The BID domain constitutes together with a positively charged C-terminal tail a T4S-signal that is crucial for the interbacterial transfer of relaxases (alongside plasmid conjugation) and protein toxins by various α-proteobacteria and for the interkingdom transfer of effectors by pathogenic *Bartonella* spp. Besides its genuine role in T4S, several BID domains have adopted secondary functions within host cells such as apoptosis inhibition and F-actin rearrangements. On the basis of the recently solved BID domain structures, their conserved fold may play a crucial role in T4S, whereas the plasticity of the surfaces seems to have facilitated novel interaction areas with host target proteins (Stanger et al., 2017). Future structure/function-related studies should aim to systematically determine key residues of BID domain interactions with the T4CP and/or other T4S system components and with host target proteins. Regarding the latter, comparative analyses of BID domain-host protein interactions evolved in specific *Bartonella*-mammal pairs will enable us to address the role of Beps in host adaptation.

Independent studies showed that T4S substrates are translocated to the recipient cytosol in an unfolded state (Amyot et al., 2013; Trokter and Waksman, 2018). Due to its structural similarity with the intramolecular chaperone IpaD of type-III-secretion systems, the BID domain might similarly act as an unfoldase to prime toxins, relaxases, and Beps for translocation (Stanger et al., 2017). Future work may address the question if BID domains indeed function as chaperones prior to and after T4S. Furthermore, using multidisciplinary approaches such as X-ray crystallography and cryo-electron tomography, future efforts could pave the way for elucidating long-lasting questions regarding the T4S pathway(s) of relaxases and effectors by using BID domain-containing T4S substrates.

AUTHOR CONTRIBUTIONS

AW and CT designed the figures. AW, CT, and CD wrote the manuscript.

FUNDING

This work was supported by grant 31003A_173119 to CD from the Swiss National Science Foundation (SNSF, www.snf.ch).

REFERENCES

Amyot, W. M., Dejesus, D., and Isberg, R. R. (2013). Poison domains block transit of translocated substrates via the *Legionella pneumophila* Icm/Dot system. *Infect. Immun.* 81, 3239–3252. doi: 10.1128/iai.00552-13

Ashkenazy, H., Abadi, S., Martz, E., Chay, O., Mayrose, I., Pupko, T., et al. (2016). ConSurf 2016: an improved methodology to estimate and visualize evolutionary conservation in macromolecules. *Nucleic Acids Res.* 44, W344–W350. doi: 10.1093/nar/gkw408

Berge, C., Waksman, G., and Terradot, L. (2017). Structural and molecular biology of type IV secretion systems. *Curr. Top. Microbiol. Immunol.* 413, 31–60. doi: 10.1007/978-3-319-75241-9_2

Christie, P. J., Whitaker, N., and Gonzalez-Rivera, C. (2014). Mechanism and structure of the bacterial type IV secretion systems. *Biochim. Biophys. Acta* 1843, 1578–1591. doi: 10.1016/j.bbamcr.2013.12.019

Dehio, C., Meyer, M., Berger, J., Schwarz, H., and Lanz, C. (1997). Interaction of *Bartonella henselae* with endothelial cells results in bacterial aggregation on the cell surface and the subsequent engulfment and internalisation of the bacterial aggregate by a unique structure, the invasome. *J. Cell Sci.* 110, 2141–2154.

Dehio, C., and Tsolis, R. M. (2017). Type IV effector secretion and subversion of host functions by *Bartonella* and *Brucella* species. *Curr. Top. Microbiol. Immunol.* 413, 269–295. doi: 10.1007/978-3-319-75241-9_11

Engel, P., Salzburger, W., Liesch, M., Chang, C. C., Maruyama, S., Lanz, C., et al. (2011). Parallel evolution of a type IV secretion system in radiating lineages of the host-restricted bacterial pathogen *Bartonella*. *PLoS Genet.* 7:e1001296. doi: 10.1371/journal.pgen.1001296

Harms, A., Liesch, M., Korner, J., Quebatte, M., Engel, P., and Dehio, C. (2017). A bacterial toxin-antitoxin module is the origin of inter-bacterial and inter-kingdom effectors of *Bartonella*. *PLoS Genet.* 13:e1007077. doi: 10.1371/journal.pgen.1007077

Harms, A., Segers, F. H., Quebatte, M., Mistl, C., Manfredi, P., Korner, J., et al. (2017). Evolutionary dynamics of pathoadaptation revealed by three independent acquisitions of the VirB/D4 type IV secretion system in *Bartonella*. *Genome Biol. Evol.* 9, 761–776. doi: 10.1093/gbe/evx042

Kirby, J. E., and Nekorchuk, D. M. (2002). *Bartonella*-associated endothelial proliferation depends on inhibition of apoptosis. *Proc. Natl. Acad. Sci. USA* 99, 4656–4661. doi: 10.1073/pnas.072292699

Li, Y. G., and Christie, P. J. (2018). The agrobacterium VirB/VirD4 T4SS: mechanism and architecture defined through in vivo mutagenesis and chimeric systems. *Curr. Top. Microbiol. Immunol.* 418, 233–260. doi: 10.1007/82_2018_94

Okujava, R., Guye, P., Lu, Y. Y., Mistl, C., Polus, F., Vayssier-Taussat, M., et al. (2014). A translocated effector required for *Bartonella* dissemination from derma to blood safeguards migratory host cells from damage by co-translocated effectors. *PLoS Pathog.* 10:e1004187. doi: 10.1371/journal.ppat.1004187

Pulliainen, A. T., Pieles, K., Brand, C. S., Hauert, B., Bohm, A., Quebatte, M., et al. (2012). Bacterial effector binds host cell adenylyl cyclase to potentiate Galphas-dependent cAMP production. *Proc. Natl. Acad. Sci. USA* 109, 9581–9586. doi: 10.1073/pnas.1117651109

Redzej, A., Ilangovan, A., Lang, S., Gruber, C. J., Topf, M., Zangger, K., et al. (2013). Structure of a translocation signal domain mediating conjugative transfer by type IV secretion systems. *Mol. Microbiol.* 89, 324–333. doi: 10.1111/mmi.12275

Rhomberg, T. A., Truttmann, M. C., Guye, P., Ellner, Y., and Dehio, C. (2009). A translocated protein of *Bartonella henselae* interferes with endocytic uptake of individual bacteria and triggers uptake of large bacterial aggregates via the invasome. *Cell. Microbiol.* 11, 927–945. doi: 10.1111/j.1462-5822.2009.01302.x

Sadana, R., and Dessauer, C. W. (2009). Physiological roles for G protein-regulated adenylyl cyclase isoforms: insights from knockout and overexpression studies. *Neurosignals* 17, 5–22. doi: 10.1159/000166277

Scherer, D. C., Deburon-Connors, I., and Minnick, M. F. (1993). Characterization of *Bartonella bacilliformis* flagella and effect of antiflagellin antibodies on invasion of human erythrocytes. *Infect. Immun.* 61, 4962–4971.

Schmid, M. C., Scheidegger, F., Dehio, M., Balmelle-Devaux, N., Schulein, R., Guye, P., et al. (2006). A translocated bacterial protein protects vascular endothelial cells from apoptosis. *PLoS Pathog.* 2:e115. doi: 10.1371/journal.ppat.0020115

Schmid, M. C., Schulein, R., Dehio, M., Denecker, G., Carena, I., and Dehio, C. (2004). The VirB type IV secretion system of *Bartonella henselae* mediates

invasion, proinflammatory activation and antiapoptotic protection of endothelial cells. *Mol. Microbiol.* 52, 81–92. doi: 10.1111/j.1365-2958.2003.03964.x

Schulein, R., Guye, P., Rhomberg, T. A., Schmid, M. C., Schroder, G., Vergunst, A. C., et al. (2005). A bipartite signal mediates the transfer of type IV secretion substrates of *Bartonella henselae* into human cells. *Proc. Natl. Acad. Sci. USA* 102, 856–861. doi: 10.1073/pnas.0406796102

Schulein, R., Seubert, A., Gille, C., Lanz, C., Hansmann, Y., Piemont, Y., et al. (2001). Invasion and persistent intracellular colonization of erythrocytes. A unique parasitic strategy of the emerging pathogen *Bartonella*. *J. Exp. Med.* 193, 1077–1086. doi: 10.1084/jem.193.9.1077

Selbach, M., Paul, F. E., Brandt, S., Guye, P., Daumke, O., Backert, S., et al. (2009). Host cell interactome of tyrosine-phosphorylated bacterial proteins. *Cell Host Microbe* 5, 397–403. doi: 10.1016/j.chom.2009.03.004

Siamer, S., and Dehio, C. (2015). New insights into the role of *Bartonella* effector proteins in pathogenesis. *Curr. Opin. Microbiol.* 23, 80–85. doi: 10.1016/j.mib.2014.11.007

Stanger, F. V., De Beer, T. A. P., Dranow, D. M., Schirmer, T., Phan, I., and Dehio, C. (2017). The BID domain of type IV secretion substrates forms a conserved four-helix bundle topped with a hook. *Structure* 25, 203–211. doi: 10.1016/j.str.2016.10.010

Trokter, M., and Waksman, G. (2018). Translocation through the conjugative type 4 secretion system requires unfolding of its protein substrate. *J. Bacteriol.* 200:e00615-17. doi: 10.1128/jb.00615-17

Truttmann, M. C., Guye, P., and Dehio, C. (2011). BID-F1 and BID-F2 domains of *Bartonella henselae* effector protein BepF trigger together with BepC the formation of invasome structures. *PLoS One* 6:e25106. doi: 10.1371/journal.pone.0025106

Truttmann, M. C., Rhomberg, T. A., and Dehio, C. (2011). Combined action of the type IV secretion effector proteins BepC and BepF promotes invasome formation of *Bartonella henselae* on endothelial and epithelial cells. *Cell. Microbiol.* 13, 284–299. doi: 10.1111/j.1462-5822.2010.01535.x

Vieira-Damiani, G., Ericson, M. E., Da Silva, M. N., Gupta, K., Soares, T. B., De Almeida, A. R., et al. (2016). *Bartonella henselae* initial infection of mature human erythrocytes observed in real time using bacterial endogenous fluorescence. *J. Trop. Dis. Public Health* 4:207. doi: 10.4172/2329-891x.1000207

Wagner, A., and Dehio, C. (2019). Role of distinct type-IV-secretion systems and secreted effector sets in host adaptation by pathogenic *Bartonella* species. *Cell. Microbiol.* 21:e13004. doi: 10.1111/cmi.13004

Waksman, G. (2019). From conjugation to T4S systems in Gram-negative bacteria: a mechanistic biology perspective. *EMBO Rep.* 20:e47012. doi: 10.15252/embr.201847012

Wang, C., Fu, J., Wang, M., Cai, Y., Hua, X., Du, Y., et al. (2018). *Bartonella quintana* type IV secretion effector BepE-induced selective autophagy by conjugation with K63 polyubiquitin chain. *Cell. Microbiol.* 21:e12984. doi: 10.1111/cmi.12984

Conflict of Interest Statement: The authors declare that the research was conducted in the absence of any commercial or financial relationships that could be construed as a potential conflict of interest.

Copyright © 2019 Wagner, Tittes and Dehio. This is an open-access article distributed under the terms of the Creative Commons Attribution License (CC BY). The use, distribution or reproduction in other forums is permitted, provided the original author(s) and the copyright owner(s) are credited and that the original publication in this journal is cited, in accordance with accepted academic practice. No use, distribution or reproduction is permitted which does not comply with these terms.

frontiers in Microbiology

ORIGINAL RESEARCH
published: 07 May 2019
doi: 10.3389/fmicb.2019.00958

Enterococcal PcfF Is a Ribbon-Helix-Helix Protein That Recruits the Relaxase PcfG Through Binding and Bending of the *oriT* Sequence

*Saima Rehman[1], Yang Grace Li[2], Andreas Schmitt[1], Lena Lassinantti[1], Peter J. Christie[2] and Ronnie P.-A. Berntsson[1,3]**

[1] Department of Medical Biochemistry and Biophysics, Umeå University, Umeå, Sweden, [2] Department of Microbiology and Molecular Genetics, McGovern Medical School, Houston, TX, United States, [3] Wallenberg Centre for Molecular Medicine, Umeå University, Umeå, Sweden

The conjugative plasmid pCF10 from *Enterococcus faecalis* encodes a Type 4 Secretion System required for plasmid transfer. The accessory factor PcfF and relaxase PcfG initiate pCF10 transfer by forming the catalytically active relaxosome at the plasmid's origin-of-transfer (*oriT*) sequence. Here, we report the crystal structure of the homo-dimeric PcfF, composed of an N-terminal DNA binding Ribbon-Helix-Helix (RHH) domain and a C-terminal stalk domain. We identified key residues in the RHH domain that are responsible for binding pCF10's *oriT* sequence *in vitro*, and further showed that PcfF bends the DNA upon *oriT* binding. By mutational analysis and pull-down experiments, we identified residues in the stalk domain that contribute to interaction with PcfG. PcfF variant proteins defective in *oriT* or PcfG binding attenuated plasmid transfer *in vivo*, but also suggested that intrinsic or extrinsic factors might modulate relaxosome assembly. We propose that PcfF initiates relaxosome assembly by binding *oriT* and inducing DNA bending, which serves to recruit PcfG as well as extrinsic factors necessary for optimal plasmid processing and engagement with the pCF10 transfer machine.

Keywords: T4SS, accessory factor, conjugation, relaxosome, X-ray crystallography, protein structural and functional analysis

OPEN ACCESS

Edited by:
Eric Cascales, Aix-Marseille Université, France

Reviewed by:
Adam Redzej, Birkbeck, University of London, United Kingdom
Matxalen Llosa, University of Cantabria, Spain

***Correspondence:**
Ronnie P.-A. Berntsson
ronnie.berntsson@umu.se

Specialty section:
This article was submitted to Microbial Physiology and Metabolism, a section of the journal Frontiers in Microbiology

Received: *09 January 2019*
Accepted: *16 April 2019*
Published: *07 May 2019*

Citation:
Rehman S, Li YG, Schmitt A, Lassinantti L, Christie PJ and Berntsson RP-A (2019) Enterococcal PcfF Is a Ribbon-Helix-Helix Protein That Recruits the Relaxase PcfG Through Binding and Bending of the oriT Sequence. Front. Microbiol. 10:958. doi: 10.3389/fmicb.2019.00958

INTRODUCTION

Enterococcus faecalis can transfer pheromone-inducible plasmids in a highly efficient manner upon sensing the peptide pheromones produced by recipient cells. These plasmids encode three functional modules of importance for plasmid transfer: (i) the Dtr (DNA transfer and replication) proteins responsible for processing of the plasmid for transfer, (ii) the Mpf (mating-pair formation) proteins that assemble as the translocation channel or type IV secretion system (T4SS), and (iii) cell-wall anchored adhesins that facilitate formation of donor-recipient cell mating pairs (Alvarez-Martinez and Christie, 2009). Over the past decade, studies have advanced our understanding of the mechanisms of action and structures of T4SSs and Dtr factors functioning in Gram-negative (G^-) species (Grohmann et al., 2017). Systems functioning in Gram-positive (G^+) species,

however, remain less well-understood. While some mechanistic and architectural features are likely conserved among all conjugative machines, key steps of substrate processing and recruitment, mating pair formation, and substrate transfer can be expected to differ substantially between systems functioning in diderm vs. monoderm species (Bhatty et al., 2013; Grohmann et al., 2017).

The tetracycline-resistance plasmid pCF10 from *E. faecalis* is a member of the highly transmissible pheromone-responsive family of mobile genetic elements (MGEs) found in enterococci. The encoded T4SSs of these pheromone regulated MGEs are tightly regulated at the transcriptional level by sensing of peptide pheromones originating from recipient cells (Dunny, 2013; Dunny and Berntsson, 2016). The broad medical importance of this large family of pheromone-inducible plasmids is underscored by the fact that they serve as reservoirs for genes encoding many different virulence factors, adhesins and antibiotic resistance. Additionally, they can mobilize other MGEs to both enterococcal and non-enterococcal recipients (Antiporta and Dunny, 2002; Staddon et al., 2006).

In this study we focused on two of the Dtr proteins, the PcfF accessory factor and the PcfG relaxase. PcfF binds to double stranded DNA (dsDNA) and is specific for inverted repeat sequences located within pCF10's origin of transfer (*oriT*) sequence (Chen et al., 2007). PcfG exhibits no intrinsic affinity for the *oriT* sequence, or any dsDNA, in the absence of PcfF. PcfF-*oriT* complexes, however, recruit PcfG to form the relaxosome, as evidenced by supershifting of PcfF-*oriT* complexes in the presence of PcfG to higher molecular mass complexes in electrophoretic mobility shift assay (EMSA) experiments (Chen et al., 2007). PcfG then catalyzes strand-specific nicking at *oriT* and generation of the single-stranded transfer intermediate (T-strand) (Chen et al., 2007, 2008; Li et al., 2012). After cleaving the substrate, PcfG remains covalently bound to the 5′ end of the T strand and likely pilots it through the conjugation channel and into the recipient cell, as has been shown for relaxases functioning in G^- systems (Alvarez-Martinez and Christie, 2009). PcfG also catalyzes the re-joining of cleaved *nic* sites *in vitro*, a reaction thought to direct T strand re-circularization, second-strand synthesis and plasmid stabilization in the recipient cell (Chen et al., 2007; Alvarez-Martinez and Christie, 2009).

Some G^- accessory factors have been well studied, including the TraM and TraY proteins of the F plasmid, MbeC from the ColE1 plasmid, TrwA of the R388 plasmid and NikA from the R64 plasmid (Luo et al., 1994; Moncalian and de la Cruz, 2004; Yoshida et al., 2008; Varsaki et al., 2009; Wong et al., 2011). These proteins have all been shown to contain a Ribbon-Helix-Helix (RHH) domain responsible for binding to DNA. RHH domains are a well-characterized family of transcriptional repressors in bacteria, first characterized with the bacterial MetJ and Arc repressors (Somers and Phillips, 1992; Raumann et al., 1994; Schreiter and Drennan, 2007). In contrast to the common helix-turn-helix motif for DNA binding, RHH domains bind DNA via a small N-proximal β-sheet composed of one β-strand from each monomer (Schreiter and Drennan, 2007). So far, no accessory factors of G^+ origin have been structurally characterized, albeit one *in silico* analysis has indicated that many of them also contain RHH-binding domains (Miguel-Arribas et al., 2017).

Here, we determined the structure of PcfF and show that it contains an N-terminal RHH domain and a C-terminal stalk domain. PcfF is a dimer in solution and structure-guided mutational analyses identified residues involved in DNA binding and residues required for interaction with PcfG. Together, our findings expand our knowledge of how accessory factors coordinate assembly of the relaxosome in G^+ bacteria. They also suggest the importance of other intrinsic, e.g., DNA bending, and extrinsic factors for relaxosome assembly *in vivo*.

EXPERIMENTAL PROCEDURES

Bacterial Strains and Plasmids

The *Escherichia coli* pET plasmid pCY33 carrying wild-type *pcfF* listed in **Supplementary Table S1** were used to generate plasmids harboring the following *pcfF* mutations: R13L (pYGL194), R13L/I14A (pYGL196), I70S (pYGL197), 1-54 (pYGL199). Mutated genes were confirmed by sequencing using the T7F primer. The *pcfF* alleles on pYGL194, 196, 197, and 199 were then amplified with primers XhoI_pcfF_F and SphI_pcfF_R, the PCR products were digested with XhoI and SphI, and the digested products were introduced into similarly digested pDL278p23 to generate plasmids carrying the *pcfF* variants: R13L (pYGL202), R13L/I14A (pYGL203), I70S (pYGL205), 1-54 (pYGL205). Constructs were confirmed by sequencing with the M13F primer. These plasmids introduced by electroporation into *E. faecalis* strain CK104 (pCF10Δ*pcfF*).

For protein production, *pcfF* (GeneBank accession AAW51324) was PCR amplified using pCF10 as a template and cloned into pGEX-6P-2 using BamHI/XhoI. The truncated version $PcfF_{1-54}$ (lacking residues 55–118) was made by mutation of Tyr 55 to a stop codon. QuikChange mutagenesis was used to generate single, double, and triple mutations of *pcfF* (R13L, I14A, R16L, R13L/I14A, R13L/R16L, R13L/I14A/R16L, I70S, N73A/Q74A, R77S, I70S/R77S, Q105A/W) with *pcfF* expression vectors as templates. *pcfG* (GeneBank accession AAW51325) was PCR amplified from pCF10 and inserted into pBAD expression vectors via the FX cloning system (Geertsma and Dutzler, 2011).

Protein Expression and Purification

PcfG (with a C-terminal deca-histidine tag), PcfF and variants thereof (all with a N-terminal GST tag) were produced in *E. coli* BL21(DE3). For PcfF and the variants of PcfF the cells were grown at 37°C in 2 × YT medium until they reached an OD_{600} of ca 1.0. At that time, the temperature was lowered to 18°C and expression was induced by the addition of 0.4 mM IPTG. Cells were grown for 16 h before harvesting. Production of selenomethionine derivatized PcfF was carried out in *E. coli* BL21(DE3) grown in M9 minimal media supplemented with 50 mg/mL L-Selenomethionine as described previously (Vanduyne et al., 1993). Derivatized PcfF was purified as described below for wild type PcfF, with the addition of

0.5 mM TCEP [tris(2-carboxyethyl)-phosphine] to all buffers after affinity purification. PcfG was produced in the same way as PcfF, with the exception that TB medium was used instead of 2 × YT and that the cells were induced by the addition of 10^{-2}% (w/v) L-arabinose at an OD_{600} of 0.8. The cells were resuspended in lysis buffer (20 mM Tris/HCl pH 7.5, 300 mM NaCl, 0.02 mg/ml DNase I, and 0.5 mM proteinase inhibitor AEBSF) before disrupting them using a Constant Cell Disruptor (Constant Systems) at 25 kPsi and 4°C. Cell debris was removed by centrifugation at 16000 × *g* for 15 min.

Wild type and variant forms of GST-PcfF were incubated for 1 h at 4°C with Glutathione-Agarose bead (Protino). The beads were packed in a gravity flow column and washed with 20 mM Tris/HCl pH 7.5, 200 mM NaCl, before eluting the protein with elution buffer (20 mM Tris/HCl pH 8.0, 200 mM NaCl, 30 mM reduced Glutathione, and 10% Glycerol). Subsequently, the proteins were run on a Superdex 200 10/300 GL Increase column (GE Healthcare) in SEC buffer (20 mM Tris/HCl pH 7.5, 200 mM NaCl). For GST-tag cleavage, 3C protease was added in a ratio of 1:100 and incubated for 16 h at 4°C. To isolate the cleaved sample a second gel-filtration step was performed in SEC buffer. The free-GST tag coeluted with cleaved PcfF, and therefore reverse-purification was performed by passing the purified sample through pre-equilibrated Glutathione-Agarose beads. The single, double and triple variants of PcfF (R13L, I14A, R16L, R13L/I14A, R13L/R16L, R13L/I14A/R16L, I70S, N73A/Q74A, R77S, I70S/R77S, Q105A, and Q105W) all behaved virtually the same as wild type PcfF, with identical elution volume on the SEC. $PcfF_{1-54}$ has a molecular mass of 7 kDa for a monomer (PcfF residues 1-54 plus 4 extra residues left on after cleaving off the GST). $PcfF_{1-54}$ eluted with an apparent molecular mass of 17 kDa on a Superdex 75 10/300 GL column. Due to the absence of Trp in PcfF, the concentration of the protein was determined using a BCA assay (Pierce).

PcfG-His was purified via refolding as previously described (Chen et al., 2007). Briefly, the protein was dissolved in binding buffer (8 M Urea, 20 mM Tris/HCl pH 7.5, 200 mM NaCl, 15 mM Imidazole pH 7.8) and bound to Ni-NTA sepharose beads (Macherey-Nagel) at 4°C. The column was washed with 10 column volumes (CV) wash buffer (8 M Urea, 20 mM Tris/HCl pH 7.5, 200 mM NaCl, and 50 mM Imidazole pH 7.8) before being eluted. PcfG-His was then refolded via a 4-step dialysis to decrease the Urea and Imidazole concentrations. The refolded PcfG-His was subsequently run on a Superdex 200 10/300 GL Increase column, where the protein eluted at the expected volume for a monomer.

Gas-Phase Electrophoretic Mobility Macromolecule Analysis

Gas-phase electrophoretic mobility macromolecule analysis (GEMMA) on PcfF was performed as previously described (Rofougaran et al., 2008). Briefly, the peak of wild type PcfF from size exclusion chromatography (SEC) was dialyzed against 100 mM ammonium acetate, pH 7.8 and then diluted to a concentration of 0.025 mg/mL in a buffer containing 100 mM ammonium acetate, pH 7.8 and 0.005% Tween-20. This protein sample was then analyzed by GEMMA.

Crystallization and Structure Determination

Crystals of selenomethionine incorporated PcfF were grown at 20°C by sitting drop vapor diffusion in a condition containing 0.2 M Lithium sulfate, 0.1 M Bis-Tris pH 6.5, 25% (w/v) PEG 3350 with a protein concentration of 16 mg/mL and a protein:reservoir ratio of 1:1. Crystals were flash-frozen in liquid nitrogen without additional cryo-protectant. X-ray diffraction data of SeMet-PcfF was collected on ID30A-3 ESRF, France at the selenium edge. The data were processed using XDS (Kabsch, 2010). The crystallographic phase-problem was solved using the single anomalous diffraction data and the selenium sites were found and refined by the Auto-Rickshaw software (Panjikar et al., 2005) with an initial model being built by ARP/wARP (Cohen et al., 2008). The PcfF crystals belonged to space group $P2_1$ and contained 4 molecules in the asymmetric unit. The structure was further built in Coot and refined at 1.9 Å using PHENIX refine (Adams et al., 2002; Emsley and Cowtan, 2004), to R_{work}/R_{free} values of 19.0/23.0%. For complete data collection and refinement statistics see **Supplementary Table S2**. The structure has been deposited in the Protein Data Band (PDB code: 6QEQ).

Electrophoretic Mobility Shift Assay

Electrophoretic mobility shift assays were performed as described elsewhere (Hellman and Fried, 2007). Different versions of single stranded *oriT* DNA were purchased from Eurofins Genomics, with the sense strand labeled at the 5′ end with fluorescein isothiocyanate (FITC). The sequences of different DNA segments used in this study are presented in **Supplementary Table S3**. Double-stranded DNA was obtained by mixing equimolar concentration of the sense and antisense strand in annealing buffer (10 mM Tris, 1 mM EDTA, 50 mM NaCl, pH 8.0). The annealing reaction was carried out by incubation at 94°C for 2 min followed by gradual cooling. For further purification, the annealed DNA was run on a 20% polyacrylamide gel, the band containing the fluorescent double strand was excised and the DNA eluted from the gel. Duplex *oriT* DNA (30 nM) was mixed with increasing concentrations of PcfF between 0 to 960 nM in buffer containing 10 mM Tris/HCL pH 7.5, 200 mM NaCl. For the binding studies with PcfF and PcfG, 30 nM of DNA, 100 nM of the PcfF variants and 300 nM of PcfG were mixed in 10 mM Tris/HCL pH 7.5, 150 mM NaCl. The DNA-protein mixtures were incubated at room temperature for 15 min and subsequently loaded on to a 20% native-PAGE made in TAE buffer (40 mM Tris, 20 mM acetic acid, 1 mM EDTA, pH 8.0). Electrophoresis was carried out for 70 min at 110 V and 4°C. The gel was imaged on a Typhoon scanner. The bands were visualized using a 488 nm excitation filter. ImageQuant software was used to quantify the fluorescent signal of the bands, and the curves from the resulting data were fitted to a non-linear fit (Specific binding with Hill slope) using GraphPad Prism.

DNA Bending Assay

Purified PcfF/PcfF$_{1-54}$ and 120 bp long DNA fragments, each containing the *oriT* sequence at varying positions (**Supplementary Table S3**) were mixed in 20 μl of 10 mM Tris/HCl (pH 7.5), 150 mM NaCl to a final protein and DNA concentration of 300 and 30 nM, respectively. After incubation at room temperature for 20 min, the reaction mixtures were loaded onto a 5% (w/v) polyacrylamide gel (acrylamide/bisacrylamide in a ratio of 37.5:1. w/w) in buffer (40 mM Tris–acetate (pH 7.8), 1 mM EDTA) and were electrophoresed at 10 V/cm and 4°C. Following electrophoresis, the DNA fragments in the gel were stained with GelRed and visualized under UV light.

In vitro Pull-Down Assay

For GST-pull-down experiments, 2 nmol of GST-PcfF fusion protein (or variants thereof) were immobilized on GSH-Sepharose beads, while 4 nmol PcfG-His were used as pray protein. Purified proteins were incubated with pre-equilibrated 50 μl Protino® Glutathione-Agarose 4B beads. BSA and purified GST were used as controls. All proteins were dialyzed against the same buffer (20 mM Tris/HCl pH 7.5, 200 mM NaCl). After binding, the beads were washed extensively (5 × 10 CV) and subsequently eluted by elution buffer (20 mM Tris/HCl pH 8.0, 200 mM NaCl, 30 mM reduced Glutathione). Samples from wash and elution steps were analyzed on 15% SDS-PAGE and stained with Coomassie Brilliant Blue G-250.

Detection of PcfF Mutant Proteins in *E. faecalis*

Exponential-phase cultures (10 ml) of *E. faecalis* OG1RF strains carrying pCF10Δ*pcfF* without and with plasmids producing wild type or mutant PcfF proteins were normalized to an OD_{600} of 0.3. The cells were pelleted by centrifugation at 13,200 × *g* for 15 min at 4°C and washed once with cold 1X physiological buffer saline (PBS). The pellet was resuspended in 125 μl of SMM buffer (0.5 M sucrose, 0.02 M $MgCl_2$, 0.02 M maleate, pH 6.5) containing 60 μl ml^{-1} of mutanolysin (Sigma-Aldrich) and 10 mg ml^{-1} of lysozyme (Sigma-Aldrich), and the resulting mix was incubated for 1 h at 37°C with shaking. Material released from the digested cell wall was separated from cell-bound material by centrifugation at 13.200 × *g* for 15 min at 4°C. PcfF variants were detected by Western transfer and immunostaining with the anti-PcfF antibodies (Chen et al., 2008). Blots were probed with antibodies against the β-subunit of RNA polymerase as a protein loading control (Christie et al., 1988; Chen et al., 2007, 2008).

Conjugation Assays

Enterococcus faecalis donor and recipient cultures grown overnight were diluted 1:10 in BHI (Brain Heart Infusion broth; Sigma) and incubated for 1 h at 37°C without shaking. Donor and recipient cells were mixed in a ratio of 1:1 and allowed to mate in liquid without shaking for 1 h at 37°C. Mating mixtures were serially diluted in BHI, and the numbers of donors and transconjugants were obtained by plating on selective BHI agar plates. The plasmid transfer frequencies were calculated as the number of transconjugants per donor cell (Chen et al., 2008). The results are reported as an average of three replicates of each experiment.

RESULTS

PcfF Is a Dimer in Solution

Full-length PcfF (14 kDa) was produced in *E. coli* and purified to homogeneity. It eluted as a single peak on SEC, with an apparent molecular mass of ∼48 kDa. The molecular mass of wild type PcfF from the SEC peak was determined by gas-phase electrophoretic mobility macromolecule analysis (GEMMA, also termed Macroion mobility spectrometer) to be ∼32 kDa, very close an apparent dimer (**Figure 1A**; Kaufman et al., 1996; Bacher et al., 2001). PcfF$_{Q105A/W}$ variants that were made to probe potential differences in oligomerization state, showed no difference in elution volume on SEC as compared to wt PcfF. PcfF$_{1-54}$ eluted as a single peak on SEC, with an apparent molecular weight of 17 kDa (**Figure 1B**), close to the expected 14 kDa weight of a dimer.

We next crystallized full-length selenomethionine-incorporated PcfF for structural analysis. Crystals belonged to space group $P2_1$ and contained 4 molecules in the asymmetric unit. X-ray diffraction data was collected at the selenium edge and the phase problem solved by SAD phasing (**Supplementary Table S2**). The structure was refined at a resolution of 1.9 Å. The electron density accounted for the entire PcfF protein, with the exception of 1–7 residues that were missing at the N terminus and one residue at the C terminus, the exact number varying between each of the 4 protein chains in the structure. PcfF crystallized as a tetramer (dimer of dimers in a head to toe organization) (**Supplementary Figure S1**). However, the tetrameric interface is weak and deemed unstable by PISA calculations (Krissinel, 2015). The biologically relevant oligomer was suggested to be dimeric, in agreement with results from the SEC and GEMMA experiments. The dimeric structure is extended in one dimension, which explains why in size exclusion chromatography PcfF elutes at a higher apparent molecular mass than expected. Functional analysis described in the next section also points toward PcfF functioning as a dimer. From here onward, we base our structural analysis on one of the dimers, made up by chains A and C.

PcfF Contains a DNA-Binding RHH Domain

PcfF contains a RHH domain at the N terminus and a 2-helix bundle, here termed the stalk domain, at the C terminus. These two domains are connected by a hinge region (**Figure 2A**). In the dimer, the RHH and stalk domains are built up by secondary structure elements from both monomers in the dimer. By superimposition of PcfF's RHH domain on other RHH motifs associated with DNA, we determined that 3 residues, R13, I14, and R16, likely are involved in DNA binding (**Figures 2B,C** and **Supplementary Figure S2**). These residues were mutated and effects on DNA binding were assessed using an EMSA. Wild

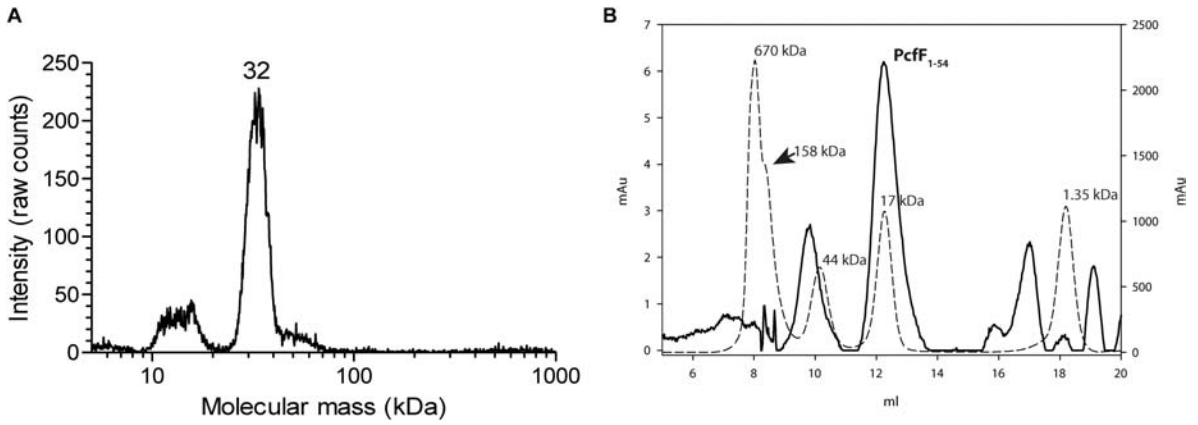

FIGURE 1 | Oligomeric state of PcfF. **(A)**: GEMMA analysis of PcfF. The sample was taken from the elution peak of the size exclusion chromatography fraction. The GEMMA analysis was performed with a protein concentration of 0.025 mg/mL. The determined molecular masses (in kDa) are written above the peak. **(B)**: SEC analysis of $PcfF_{1-54}$ on a Superdex 75 10/300 GL column, with molecular mass standards as dashed lines and $PcfF_{1-54}$ as a solid line. The molecular mass in kDa is written above each standard in the graph. Since $PcfF_{1-54}$ does not have any Tryptophan residues, the left Y axis denotes the absorbance at 254 nm for $PcfF_{1-54}$, while the right y-axis shows the absorbance at 280 nm for the standards. The main peak for $PcfF_{1-54}$ elutes at 17 kDa, with the earlier peak corresponding to free GST after the cleavage of the protein as confirmed by SDS-PAGE analysis.

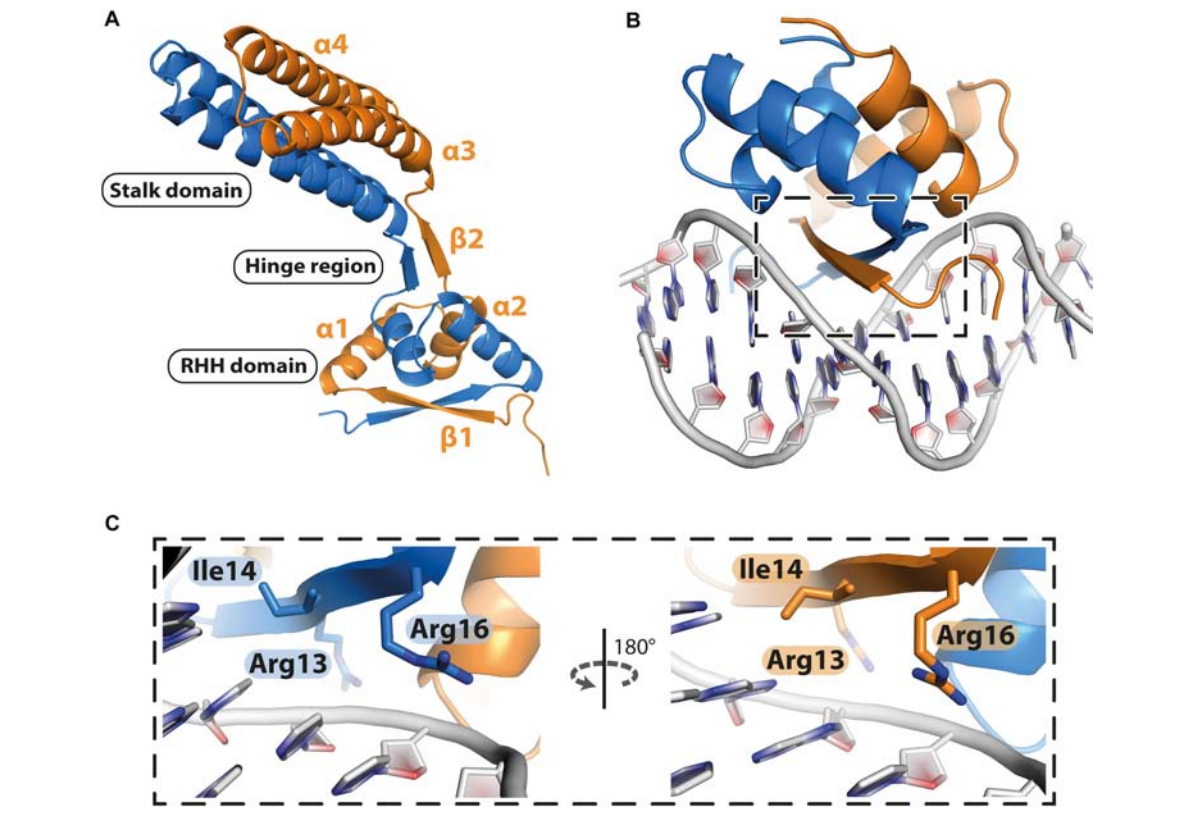

FIGURE 2 | Structure of PcfF. **(A)**: Overall representation of the dimeric PcfF structure, with the RHH and stalk domains connected by a hinge region. Both monomers contribute to the formation of the RHH domain. **(B)**: Model of PcfF with bound DNA, based on superposition with ArcA structure (**Supplementary Figure S2**). **(C)**: Enlarged view of the box from panel **B**, with the conserved DNA binding residues R13, I14, and R16 highlighted as sticks.

type PcfF bound a 40 bp *oriT* sequence, composed of double-stranded inverted repeats and the *nic*-site, with an estimated K_D of ∼100 nM, in agreement with previous findings (Chen et al., 2007; **Figures 3A,B**). PcfF did not bind a random DNA sequence, verifying a specificity for *oriT* binding (**Supplementary Figure S3**). PcfF variants with single (R13L, I14A, R16L),

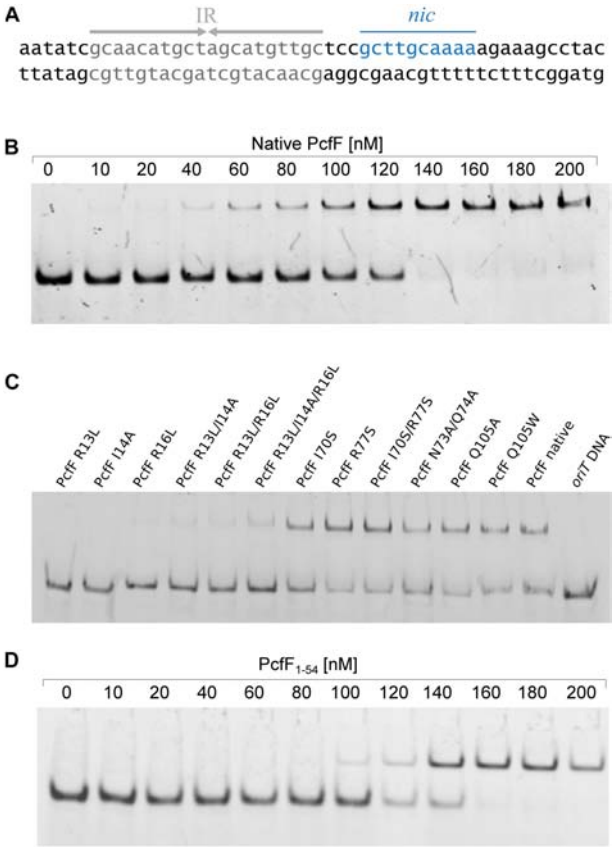

FIGURE 3 | EMSA of PcfF variants binding to *oriT.* In all cases the 30 nM of the 40 bp long double stranded *oriT* substrate was used. **(A)**: Sequence of the *oriT* (40 bp) from pCF10. The inverted repeats (IR), which PcfF binds to, and the nic-site are highlighted. **(B)**: Wild type PcfF binds to a 40 bp *oriT* substrate. The increasing concentrations of PcfF added are indicated above the lanes. **(C)**: PcfF variants bind with varying degrees to the 40 bp *oriT* sequence. Reaction mixtures contained 100 nM PcfF. **(D)**: $PcfF_{1-54}$ binds to *oriT*. The increasing concentrations of PcfF added are indicated above the gel. The reactions were analyzed on 20% native polyacrylamide gels. Protein components in each lane are shown on the top of the lane.

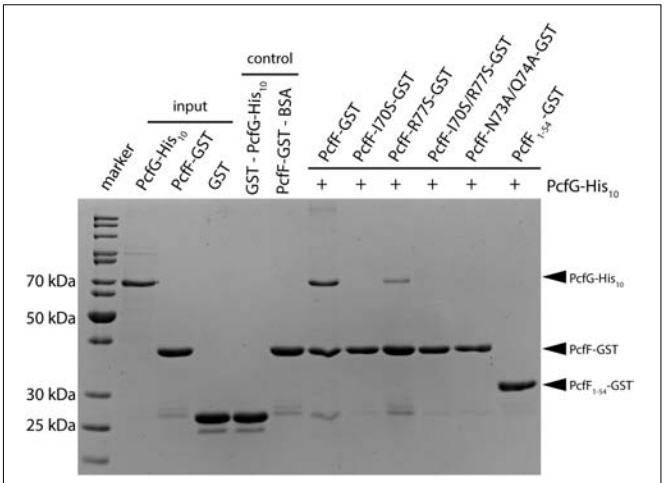

FIGURE 4 | SDS-PAGE analysis of GST pull-down of PcfG. GST-tagged PcfF and variants thereof were compared for their ability to bind PcfG-His_{10}. As controls, GST alone was assayed for binding of PcfG-His_{10}, and PcfF-GST was assayed for binding of BSA. Protein bands were visualized by staining with Coomassie Blue.

double (R13L/I14A, R13L/R16L), or triple (R13L/I14A/R16L) substitution mutations showed marked decreases in *oriT* binding (**Figure 3C**). We also confirmed that the RHH domain ($PcfF_{1-54}$) without the associated stalk domain bound *oriT* with little reduction in affinity (**Figure 3D**).

The Stalk Domain of PcfF Binds PcfG

PcfF binds the relaxase PcfG, as determined by EMSAs and affinity pull-down assays (Chen et al., 2007, 2008). PcfF possesses a sequence-motif NINQ in a surface-exposed region of the C-terminal stalk; this motif is semi-conserved among other T4SSs accessory proteins associated with conjugation systems in Gram-negative and -positive bacteria (**Supplementary Figure S4A**) (Varsaki et al., 2009). In the PcfF X-ray structure, the NINQ motif forms a patch within a small groove (**Supplementary Figure S4B**). We hypothesized that this motif might comprise the binding surface for PcfG. To test this model, we introduced several mutations (I70S, R77S, I70S/R77S, N73A/Q74A) in and around this conserved surface patch. These PcfF variants, as well as $PcfF_{1-54}$ lacking the entire stalk domain, behaved as wild type PcfF with respect to purification as dimers and binding of *oriT* DNA (**Figures 3C,D**). We next tested for effects of the mutations on PcfF binding to PcfG using affinity pull-down assays. GST-PcfF and variants thereof were incubated with PcfG-His and Glutathione-Agarose beads. Following extensive washing, proteins were eluted and analyzed for the presence of GST-PcfF and PcfG-His. As shown previously, wild type GST-PcfF pulled down PcfG-His (**Figure 4**; Chen et al., 2008). None of the GST-PcfF variants detectably bound PcfG-His, except for the R77S mutant which showed a low level of binding. We further assayed for the ability of PcfG-His to bind to PcfF-*oriT* or $PcfF_{1-54}$-*oriT* complexes via EMSAs, but did not observe any additional supershifted bands upon the addition of PcfG-His (**Supplementary Figure S5**).

PcfF Binding Induces DNA Bending

Other T4SS accessory factors with RHH domains have been shown to induce bending of DNA (Yoshida et al., 2008; Wong et al., 2011). To determine if PcfF induces a bend in the pCF10 *oriT* sequence, we capitalized on findings that bent DNA fragments exhibit an anomalous electrophoretic mobility behavior, which is most pronounced when the bending locus is located close to the center of the fragment (Thompson and Landy, 1988; Levene and Zimm, 1989). We performed these DNA bending experiments using 120 bp fragments of random DNA with the *oriT* positioned at the 5′ end, middle or 3′ end of the DNA (**Supplementary Table S3**) (Crothers et al., 1991). Binding of PcfF induced a more pronounced shift in the DNA fragment containing the central *oriT* sequence compared with fragments in which *oriT* was positioned at either end. These

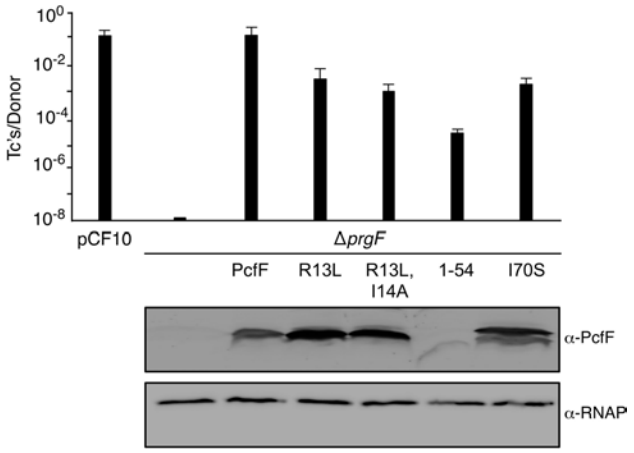

FIGURE 5 | Effects of PcfF mutations on pCF10 transfer. Upper graph: CK104 donors harboring pCF10Δ*pcfF* and producing wild type and mutant variants of PcfF from the constitutive P_{23} promoter were mated with OG1ES recipients for 1 h in BHI media at 37°C without shaking. Transfer frequencies are presented as the number of transconjugants (Tc's) per donor. Experiments were repeated at least three times in triplicate, and results from a representative experiment with standard deviations are shown. Lower panels: Steady-state levels of PcfF proteins in exponentially growing strains. Immunoblots were developed with α-PcfF antibodies for detection of PcfF variants or α-RNAP antibodies for detection of the β-subunit of RNA polymerase as a loading control. Protein extracts were loaded on a per-cell equivalent basis. Strains for both panels: CK104 (pCF10ΔpcfF) alone (ΔpcfF) or with plasmids producing PcfF (pCY33), $PcfF_{R13L}$ (pYGL202), $PcfF_{R13L/I14A}$ (pYGL203), $PcfF_{1-54}$ (pYGL204), $pcfF_{I70S}$ (pYGL205).

findings support a conclusion that PcfF does indeed induce bending of DNA at the *oriT* site (**Supplementary Figure S6**). A similar trend could be seen for $PcfF_{1-54}$ as for PcfF. However, for unknown reasons, $PcfF_{1-54}$ bound to the 120 bp long DNA yielded smeary band shifts and therefore prevent firm conclusions regarding the capacity of PcfF's RHH domain to induce DNA bending.

PcfF DNA Binding and Relaxase Recruitment Is Not Essential for Conjugation *in vivo*

Finally, we determined the effects of the PcfF mutations on pCF10 transfer *in vivo* (**Figure 5**). *E. faecalis* strain CK104(pCF10D*pcfF*) does not transfer the mutant plasmid unless it additionally carries pCY16, which produces wild type PcfF from the constitutive P_{23} promoter. Interestingly, CK104(pCF10D*pcfF*) harboring plasmids producing the RHH mutant proteins $PcfF_{R13L}$ and $PcfF_{R13L/I14A}$ which fail to bind *oriT* DNA *in vitro*, also transferred pCF10D*pcfF* albeit at reduced frequencies of 1 to 2 orders of magnitude compared with CK104(pCF10D*pcfF*, pCY16). Similarly, the CK104(pCF10D*pcfF*) donor with plasmids producing variants defective in binding PcfG *in vitro* ($PcfF_{1-54}$, $PcfF_{I70S}$) mutant also were transfer-proficient, although at reduced levels. In CK104 donor strains, the full-length mutant proteins accumulated at levels comparable to or even higher than wild type PcfF. $PcfF_{1-54}$ was detected at low levels, possibly reflecting instability or poor recognition by the anti-PcfF polyclonal antibodies. Formation of the PcfF/PcfG/*oriT* relaxosome on pCF10 thus appears to depend not only on PcfF residues responsible for binding *oriT* and PcfG *in vitro*, but on DNA structures formed *in vivo* or other unidentified host-encoded factors.

DISCUSSION

Conjugative transfer of MGEs happens by: (i) assembly of the relaxosome at *oriT* sequences, (ii) relaxase-catalyzed nicking of the DNA strand destined for transfer (T-strand), (iii) relaxosome recruitment to the type IV coupling protein (T4CP), and (iv) translocation of the relaxase/T-strand intermediate through the transfer channel (Alvarez-Martinez and Christie, 2009; Wong et al., 2012; Grohmann et al., 2017). Dtr accessory factors are known to be required for assembly of the relaxosome, but in most cases the molecular details surrounding this early stage reaction are unknown. Here, we have solved the structure of the accessory factor PcfF, which binds the pCF10 *oriT* sequence and recruits the PcfG relaxase for relaxosome assembly. Like several other accessory factors, albeit far from all, PcfF is essential for conjugation. We showed that PcfF is composed of an N-terminal RHH domain and a C-terminal a-helical stalk domain. Although residues in both of these domains contribute to dimerization of PcfF, the RHH domain also dimerizes in the absence of the stalk domain. We further confirmed structure-based predictions that β-strands within PcfF's RHH domain contribute to *oriT* binding and gained evidence that a specific patch on the C-terminal stalk of PcfF mediates binding of PcfG.

Prior to this study, only three T4SS encoded accessory factors (TraM, NikA, and VirC2) have been structurally determined to our knowledge (Yoshida et al., 2008; Lu et al., 2009; Wong et al., 2011). Each belong to the RHH superfamily whose members are best known as bacterial transcription factors. Superimposition of these proteins with PcfF reveal that their RHH domains have overall similar structures, with RMSD values of 1.5 – 4 Å (**Figure 6A**). These proteins bind DNA through intercalation of their small two-stranded β-sheet within the RHH domain into the major groove of double stranded DNA; this interaction contributes both to affinity and specificity of DNA substrate binding (Schreiter and Drennan, 2007). Structurally, this β-sheet is made up by the first β-strand of each monomer in the RHH domain. Within this β-strand, a few structurally equivalent residues are (semi)conserved among the various accessory factors (**Figure 6B**). These residues have been implicated to be important for DNA binding, as established by solved structures of TraM or ArcA bound to DNA substrates (Raumann et al., 1994; Wong et al., 2011). In agreement with findings from other RHH accessory factors, we determined that PcfF binds pCF10's *oriT* sequence via its RHH-domain, and that mutation of the surface-exposed charged residues R13 and R16, as well as I14, in the β-sheet strongly abrogate *oriT* binding *in vitro*. Deletion of the stalk domain does not impair *oriT* binding, confirming the RHH domain is both necessary and sufficient for binding the DNA substrate.

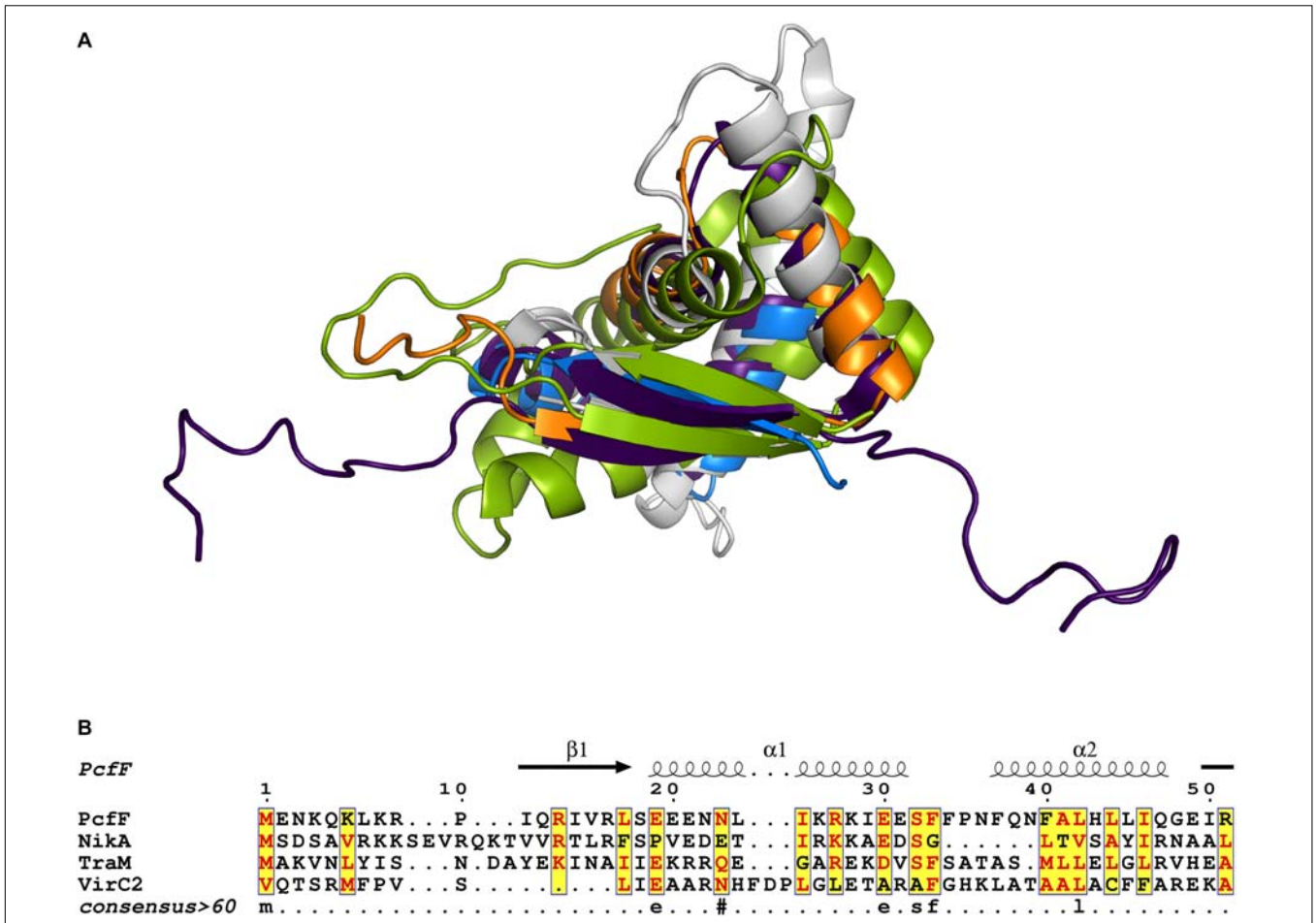

FIGURE 6 | Structural and sequence comparison of four T4SS accessory proteins. **(A)** Superimposed structures of the RHH domain of PcfF (blue and orange), TraM (PDB code 3ON0, gray), NikA (PDB code 2BA3, purple), and VirC2 (PDB code 2RH3, green). PcfF and NikA have similar overall RHH domain structures, with RMSD of ca 1.5 Å. TraM and VirC2 vary more with RMSDs of ca 4.5 Å, but clearly share the same overall fold. **(B)** Sequence alignment of the RHH domains of the four proteins, with the secondary structure elements indicated above the alignment. The alignment file was generated through T-COFFEE server, followed by ESPript3 for rendering alignments (Armougom et al., 2006; Robert and Gouet, 2014). Text in red denotes conserved residues within a group. Blue frame with yellow background highlights similarity across groups and lowercase character denotes the consensus residue for consensus level >0.6.

F plasmid-encoded TraM and another RHH domain-containing protein, TraY, bend and induce localized denaturation upon binding of DNA substrates (Luo et al., 1994; Karl et al., 2001; Fekete and Frost, 2002). Like PcfF, TraM comprises an RHH- and a C-terminal stalk domain. However, in contrast to what seems to be the case for PcfF, TraM assembles as a tetramer with two RHH domains and one larger 8-helical bundle stalk domain forming the tetramerization interface (**Supplementary Figure S7**). TraM binds to its cognate DNA cooperatively, which induces DNA bending (Wong et al., 2011). Here, we showed that PcfF also bends its *oriT* substrate, although seemingly by a mechanism different than TraM. Specifically, in contrast to TraM, which assembles as tetramers in solution, PcfF is dimeric as shown by GEMMA analyses and further supported by the SEC and functional assays. Besides the other evidence, the weak tetramerization interface in the crystal structure only supports a head to tail tetramer, where the two RHH domains sit rotated 180 from each other with the stalk domain in between them (**Supplementary Figure S1**). This organization of the RHH domains is unlikely to be biologically relevant. The stalk domain, which is responsible for tetramerization of TraM, likely supports only dimerization of PcfF in solution. In our EMSAs, binding induced a DNA shift to a single species with higher molecular mass, as has been shown previously (Chen et al., 2007, 2008), indicating that there is only one DNA binding site per functional PcfF molecule. If PcfF would have been a tetramer, it would have contained two RHH domains and thus be able to bind two independent *oriT* probes in the EMSA. If that was the case one would expect to see a state of two independent retarded species in the EMSA, especially around the concentration corresponding to the apparent dissociation constant (K_D). Independent of the PcfF concentration used we only observe a single retarded species, indicating that it is the dimeric PcfF that binds to *oriT*. Although we cannot exclude that PcfF can under some circumstances function as a tetramer, e.g., upon relaxosome assembly, our data points toward that the dimeric form of PcfF is the functional unit.

In view of these findings, we propose that a single PcfF dimer suffices to bind and bend pCF10's *oriT* sequence.

Structural and sequence analysis revealed that the stalk domain possesses a conserved sequence motif, NINQ. These residues, together with a few flanking residues (I70, N73, Q74, and R77), form a patch on the surface of PcfF (**Supplementary Figure S4**). We gained evidence that this patch mediates binding of PcfF to PcfG by showing that a single point mutation (I70S) abolishes PcfF-PcfG binding (**Figure 4**). Other mutations around this site also completely (N73A/Q74A) or partially (R77S) disrupt this interaction. Finally, $PcfF_{1-54}$, (lacking the entire stalk domain) does not bind PcfG, firmly establishing the importance of the stalk domain for the PcfF-PcfG interaction (**Figure 4**). In EMSAs, we do not observe any significant additional retarded species upon the addition of PcfG-His to the reaction mix of PcfF-*oriT* or $PcfF_{1-54}$-*oriT*, in contrast to what was previously shown (Chen et al., 2007). We attribute the differences observed between the previous study and our results to different experimental conditions and protein constructs.

Our finding that mutations in, or a complete deletion of, the stalk domain of PcfF attenuates but does not totally abolish pCF10 transfer *in vivo* (**Figure 5**) indicates that PcfF might be able to indirectly recruit PcfG. We speculate that this could be facilitated via bending and unwinding of the DNA upon PcfF binding. Another accessory factor, TrwA, also binds its cognate *oriT* sequence via an N-terminal RHH domain, whereas its C-terminal domain (which has not been structurally characterized) was shown to not bind to the TrwC relaxase but rather to TrwB (Tato et al., 2007). TrwB is a member of the superfamily of ATPases known as coupling proteins, which are associated with the T4SSs and function in recruitment of cognate substrates for delivery into the transfer channel (Grohmann et al., 2017). Our finding that the $PcfF_{1-54}$ variant supports pCF10 transfer *in vivo* establishes that the stalk domain is not only dispensable for relaxosome assembly but is also not required for docking of the relaxosome with the PcfC coupling protein in *E. faecalis*.

It is more difficult to reconcile the lack of strong effects of the RHH-domain mutations (R13L, R13L/I14A), which abolish PcfF-*oriT* binding *in vitro*, on pCF10 transfer *in vivo* (**Figure 5**). Equivalent mutations in conserved polar, charged residues in the β-sheets of other RHH accessory factors diminish plasmid transfer by more than 3 orders of magnitude (Moncalian and de la Cruz, 2004; Yoshida et al., 2008; Varsaki et al., 2009), although mutant accessory factors can still support a modest level (10^{-5} – 10^{-6} Tc's/D) of plasmid transfer. Even though PcfF homodimers stably bind *oriT* sequences *in vitro,* it is possible that additional binding surfaces or residues are exposed when PcfF binds PcfG, which can contribute to *oriT* binding *in vivo*. Alternatively, PcfF might be capable of binding *oriT* secondary structures that form only *in vivo* through surface-exposed residues other than those mutated in our study. Finally, we cannot exclude the possibility that other unidentified plasmid- or host-encoded factors, e.g., IHF-like proteins, contribute to relaxosome assembly *in vivo* (Nelson et al., 1995; Karl et al., 2001). Discriminating between these possibilities will require further investigations.

CONCLUSION

In summary, RHH domains of several accessory factors associated with conjugation have now been solved and functionally characterized. However, besides PcfF reported here, only one other structure exists for a full-length accessory factor. The structural basis for PcfF binding to pCF10's *oriT* sequence resembles that identified for other RHH domain containing proteins. However, in contrast to most other members, PcfF forms dimers instead of tetramers in solution and does not show cooperative binding. Furthermore, mutations in conserved charged, polar residues in the DNA binding b-sheet motif do not block *oriT* substrate binding *in vivo*. We also showed that the α-helical stalk domain contributes to binding of the relaxase PcfG, despite the fact that the dimeric RHH domain alone retains the capacity to orchestrate assembly of the functional relaxosome and support plasmid transfer *in vivo*. Together, our findings underscore both the structural conservation and functional plasticity of accessory factors as nucleators of relaxosome assembly among the conjugation systems.

AUTHOR CONTRIBUTIONS

SR, AS, and RB performed the cloning, protein purification and structure determination. SR and AS collected the diffraction data. SR, AS, and LL performed the EMSA experiments and protein size determination via GEMMA and SEC. AS performed the DNA bending experiments. YL performed the cloning in *E. faecalis* and the *in vivo* conjugation experiments. SR, PC, and RB planned the experiments, performed the data analysis and wrote the manuscript with input from all authors.

FUNDING

This work was supported by grants from the Swedish Research Council (2016–03599), Åke Wibergs Foundation, Carl Tryggers Foundation, Knut and Alice Wallenberg Foundation and Kempestiftelserna (JCK-1524) to RB and by NIH grant GM48746 to PC.

ACKNOWLEDGMENTS

We thank the beamline scientists at MaxIV, Lund for their support in data collection. We acknowledge the ESRF for provision of synchrotron radiation facilities and we also thank Guillaume Gotthard for assistance in using beamline ID30A-3. We are very grateful to Dr. Anders Hofer for his help with the GEMMA measurements.

SUPPLEMENTARY MATERIAL

The Supplementary Material for this article can be found online at: https://www.frontiersin.org/articles/10.3389/fmicb.2019.00958/full#supplementary-material

REFERENCES

Adams, P. D., Grosse-Kunstleve, R. W., Hung, L. W., Ioerger, T. R., McCoy, A. J., Moriarty, N. W., et al. (2002). PHENIX: building new software for automated crystallographic structure determination. *Acta Crystallogr. D Biol. Crystallogr.* 58, 1948–1954.

Alvarez-Martinez, C. E., and Christie, P. J. (2009). Biological diversity of prokaryotic type IV secretion systems. *Microbiol. Mol. Biol. R.* 73, 775–808. doi: 10.1128/MMBR.00023-09

Antiporta, M., and Dunny, G. (2002). ccfA, the genetic determinant for the cCF10 peptide pheromone in *Enterococcus faecalis* OG1RF. *J. Bacteriol.* 184, 1155–1162.

Armougom, F., Moretti, S., Poirot, O., Audic, S., Dumas, P., Schaeli, B., et al. (2006). Expresso: automatic incorporation of structural information in multiple sequence alignments using 3D-Coffee. *Nucleic Acids Res.* 34, W604–W608. doi: 10.1093/nar/gkl092

Bacher, G., Szymanski, W. W., Kaufman, S. L., Zollner, P., Blaas, D., and Allmaier, G. (2001). Charge-reduced nano electrospray ionization combined with differential mobility analysis of peptides, proteins, glycoproteins, noncovalent protein complexes and viruses. *J. Mass Spectrom.* 36, 1038–1052. doi: 10.1002/jms.208

Bhatty, M., Laverde Gomez, J. A., and Christie, P. J. (2013). The Expanding bacterial type IV secretion lexicon. *Res. Microbiol.* 164, 620–639. doi: 10.1016/j.resmic.2013.03.012

Chen, Y., Staddon, J. H., and Dunny, G. M. (2007). Specificity determinants of conjugative DNA processing in the *Enterococcus faecalis* plasmid pCF10 and the *Lactococcus lactis* plasmid pRS01. *Mol. Microbiol.* 63, 1549–1564. doi: 10.1111/j.1365-2958.2007.05610.x

Chen, Y., Zhang, X., Manias, D., Yeo, H.-J., Dunny, G. M., and Christie, P. J. (2008). *Enterococcus faecalis* PcfC, a spatially localized substrate receptor for type IV secretion of the pCF10 transfer intermediate. *J. Bacteriol.* 190, 3632–3645. doi: 10.1128/JB.01999-07

Christie, P. J., Kao, S. M., Adsit, J. C., and Dunny, G. M. (1988). Cloning and expression of genes encoding pheromone-inducible antigens of *Enterococcus (Streptococcus) faecalis*. *J. Bacteriol.* 170, 5161–5168.

Cohen, S. X., Ben Jelloul, M., Long, F., Vagin, A. A., Knipscheer, P., Lebbink, J., et al. (2008). ARP/wARP and molecular replacement: the next generation. *Acta Crystallogr. D Biol. Crystallogr.* 64, 49–60.

Crothers, D. M., Gartenberg, M. R., and Shrader, T. E. (1991). Dna Bending in protein-Dna complexes. *Methods Enzymol.* 208, 118–146.

Dunny, G. M. (2013). Enterococcal sex pheromones: signaling, social behavior, and evolution. *Annu. Rev. Genet.* 47, 457–482. doi: 10.1146/annurev-genet-111212-133449

Dunny, G. M., and Berntsson, R. P.-A. (2016). Enterococcal sex pheromones: evolutionary pathways to complex, two-signal systems. *J. Bacteriol.* 198, 1556–1562. doi: 10.1128/JB.00128-16

Emsley, P., and Cowtan, K. (2004). Coot: model-building tools for molecular graphics. *Acta Crystallogr. D Biol. Crystallogr.* 60, 2126–2132.

Fekete, R. A., and Frost, L. S. (2002). Characterizing the DNA contacts and cooperative binding of F plasmid TraM to its cognate sites at oriT. *J. Biol. Chem.* 277, 16705–16711. doi: 10.1074/jbc.M111682200

Geertsma, E. R., and Dutzler, R. (2011). A versatile and efficient high-throughput cloning tool for structural biology. *Biochemistry* 50, 3272–3278. doi: 10.1021/bi200178z

Grohmann, E., Christie, P. J., Waksman, G., and Backert, S. (2017). Type IV secretion in gram-negative and gram-positive bacteria. *Mol. Microbiol.* 107, 455–471. doi: 10.1111/mmi.13896

Hellman, L. M., and Fried, M. G. (2007). Electrophoretic mobility shift assay (EMSA) for detecting protein-nucleic acid interactions. *Nat. Protoc.* 2, 1849–1861. doi: 10.1038/nprot.2007.249

Kabsch, W. (2010). XDS. *Acta Crystallogr. D Biol Crystallogr.* 66, 125–132. doi: 10.1107/S0907444909047337

Karl, W., Bamberger, M., and Zechner, E. L. (2001). Transfer protein TraY of plasmid R1 stimulates TraI-catalyzed oriT cleavage in vivo. *J. Bacteriol.* 183, 909–914. doi: 10.1128/JB.183.3.909-914.2001

Kaufman, S. L., Skogen, J. W., Dorman, F. D., Zarrin, F., and Lewis, K. C. (1996). Macromolecule analysis based on electrophoretic mobility in air: globular proteins. *Anal. Chem.* 68, 1895–1904. doi: 10.1021/ac951128f

Krissinel, E. (2015). Stock-based detection of protein oligomeric states in jsPISA. *Nucleic Acids Res.* 43, W314–W319. doi: 10.1093/nar/gkv314

Levene, S. D., and Zimm, B. H. (1989). Understanding the anomalous electrophoresis of bent DNA molecules: a reptation model. *Science* 245, 396–399.

Li, F., Alvarez-Martinez, C., Chen, Y., Choi, K.-J., Yeo, H.-J., and Christie, P. J. (2012). *Enterococcus faecalis* PrgJ, a VirB4-like ATPase, Mediates pCF10 conjugative transfer through substrate binding. *J. Bacteriol.* 194, 4041–4051. doi: 10.1128/JB.00648-12

Lu, J., den Dulk-Ras, A., Hooykaas, P. J. J., and Glover, J. N. M. (2009). *Agrobacterium tumefaciens* VirC2 enhances T-DNA transfer and virulence through its C-terminal ribbon-helix-helix DNA-binding fold. *Proc. Natl. Acad. Sci. U.S.A.* 106, 9643–9648. doi: 10.1073/pnas.0812199106

Luo, Y., Gao, Q., and Deonier, R. C. (1994). Mutational and physical analysis of F plasmid tray protein-binding to orit. *Mol. Microbiol.* 11, 459–469.

Miguel-Arribas, A., Hao, J. A., Luque-Ortega, J. R., Ramachandran, G., Val-Calvo, J., Gago-Córdoba, C., et al. (2017). The *Bacillus subtilis* conjugative plasmid pLS20 encodes two ribbon-helix-helix type auxiliary relaxosome proteins that are essential for conjugation. *Front. Microbiol.* 8:2138. doi: 10.3389/fmicb.2017.02138

Moncalian, G., and de la Cruz, F. (2004). DNA binding properties of protein TrwA, a possible structural variant of the Arc repressor superfamily. *Biochim. Biophys. Acta* 1701, 15–23. doi: 10.1016/j.bbapap.2004.05.009

Nelson, W. C., Howard, M. T., Sherman, J. A., and Matson, S. W. (1995). The traY gene product and integration host factor stimulate *Escherichia coli* DNA helicase I-catalyzed nicking at the F plasmid oriT. *J. Biol. Chem.* 270, 28374–28380.

Panjikar, S., Parthasarathy, V., Lamzin, V. S., Weiss, M. S., and Tucker, P. A. (2005). Auto-Rickshaw: an automated crystal structure determination platform as an efficient tool for the validation of an X-ray diffraction experiment. *Acta Crystallogr. D Biol. Crystallogr.* 61, 449–457. doi: 10.1107/S0907444905001307

Raumann, B. E., Rould, M. A., Pabo, C. O., and Sauer, R. T. (1994). DNA recognition by beta-sheets in the Arc repressor-operator crystal structure. *Nature* 367, 754–757. doi: 10.1038/367754a0

Robert, X., and Gouet, P. (2014). Deciphering key features in protein structures with the new ENDscript server. *Nucleic Acids Res.* 42, W320–W324. doi: 10.1093/nar/gku316

Rofougaran, R., Crona, M., Vodnala, M., Sjöberg, B.-M., and Hofer, A. (2008). Oligomerization status directs overall activity regulation of the *Escherichia coli* class Ia ribonucleotide reductase. *J. Biol. Chem.* 283, 35310–35318. doi: 10.1074/jbc.M806738200

Schreiter, E. R., and Drennan, C. L. (2007). Ribbon-helix-helix transcription factors: variations on a theme. *Nat. Rev. Microbiol.* 5, 710–720. doi: 10.1038/nrmicro1717

Somers, W. S., and Phillips, S. E. (1992). Crystal structure of the met repressor-operator complex at 2.8 A resolution reveals DNA recognition by beta-strands. *Nature* 359, 387–393. doi: 10.1038/359387a0

Staddon, J. H., Bryan, E. M., Manias, D. A., Chen, Y., and Dunny, G. M. (2006). Genetic characterization of the conjugative DNA processing system of enterococcal plasmid pCF10. *Plasmid* 56, 102–111. doi: 10.1016/j.plasmid.2006.05.001

Tato, I., Matilla, I., Arechaga, I., Zunzunegui, S., de la Cruz, F., and Cabezón, E. (2007). The ATPase activity of the DNA transporter TrwB is modulated by protein TrwA - implications for a common assembly mechanism of DNA translocating motors. *J. Biol. Chem.* 282, 25569–25576. doi: 10.1074/jbc.M703464200

Thompson, J. F., and Landy, A. (1988). Empirical estimation of protein-induced DNA bending angles: applications to lambda site-specific recombination complexes. *Nucleic Acids Res.* 16, 9687–9705.

Vanduyne, G. D., Standaert, R. F., Karplus, P. A., Schreiber, S. L., and Clardy, J. (1993). Atomic structures of the human immunophilin Fkbp-12 complexes with Fk506 and rapamycin. *J. Mol. Biol.* 229, 105–124. doi: 10.1006/jmbi.1993.1012

Varsaki, A., Moncalian, G., Garcillan-Barcia, M. D. P., Drainas, C., and de la Cruz, F. (2009). Analysis of colE1 MbeC unveils an extended ribbon-helix-helix family of nicking accessory proteins. *J. Bacteriol.* 191, 1446–1455. doi: 10.1128/JB.01342-08

Wong, J. J. W., Lu, J., Edwards, R. A., Frost, L. S., and Glover, J. N. M. (2011). Structural basis of cooperative DNA recognition by the plasmid conjugation factor, TraM. *Nucleic Acids Res.* 39, 6775–6788. doi: 10.1093/nar/gkr296

Wong, J. J. W., Lu, J., and Glover, J. N. M. (2012). Relaxosome function and conjugation regulation in F-like plasmids - a structural biology perspective. *Mol. Microbiol.* 85, 602–617. doi: 10.1111/j.1365-2958.2012.08131.x

Yoshida, H., Furuyal, N., Lin, Y.-J., Guentert, P., Komano, T., and Kainosho, M. (2008). Structural basis of the role of the NikA ribbon-helix-helix domain in initiating bacterial conjugation. *J. Mol. Biol.* 384, 690–701. doi: 10.1016/j.jmb.2008.09.067

Conflict of Interest Statement: The authors declare that the research was conducted in the absence of any commercial or financial relationships that could be construed as a potential conflict of interest.

Copyright © 2019 Rehman, Li, Schmitt, Lassinantti, Christie and Berntsson. This is an open-access article distributed under the terms of the Creative Commons Attribution License (CC BY). The use, distribution or reproduction in other forums is permitted, provided the original author(s) and the copyright owner(s) are credited and that the original publication in this journal is cited, in accordance with accepted academic practice. No use, distribution or reproduction is permitted which does not comply with these terms.

frontiers in Microbiology

REVIEW
published: 21 May 2019
doi: 10.3389/fmicb.2019.01078

Bacteria-Killing Type IV Secretion Systems

Germán G. Sgro[1†], Gabriel U. Oka[1†], Diorge P. Souza[1‡], William Cenens[1], Ethel Bayer-Santos[1‡], Bruno Y. Matsuyama[1], Natalia F. Bueno[1], Thiago Rodrigo dos Santos[1], Cristina E. Alvarez-Martinez[2], Roberto K. Salinas[1] and Chuck S. Farah[1]*

[1] Departamento de Bioquímica, Instituto de Química, Universidade de São Paulo, São Paulo, Brazil, [2] Departamento de Genética, Evolução, Microbiologia e Imunologia, Instituto de Biologia, University of Campinas (UNICAMP), Campinas, Brazil

OPEN ACCESS

Edited by:
Ignacio Arechaga,
University of Cantabria, Spain

Reviewed by:
Elisabeth Grohmann,
Beuth Hochschule für Technik Berlin, Germany
Xiancai Rao,
Army Medical University, China

***Correspondence:**
Chuck S. Farah
chsfarah@iq.usp.br

[†] These authors have contributed equally to this work

[‡] **Present address:**
Diorge P. Souza,
MRC Laboratory for Molecular Cell Biology, University College London, London, United Kingdom
Ethel Bayer-Santos,
Departamento de Microbiologia, Instituto de Ciências Biomédicas, Universidade de São Paulo, São Paulo, Brazil

Specialty section:
This article was submitted to Microbial Physiology and Metabolism, a section of the journal Frontiers in Microbiology

Received: 15 March 2019
Accepted: 29 April 2019
Published: 21 May 2019

Citation:
Sgro GG, Oka GU, Souza DP, Cenens W, Bayer-Santos E, Matsuyama BY, Bueno NF, dos Santos TR, Alvarez-Martinez CE, Salinas RK and Farah CS (2019) Bacteria-Killing Type IV Secretion Systems. Front. Microbiol. 10:1078. doi: 10.3389/fmicb.2019.01078

Bacteria have been constantly competing for nutrients and space for billions of years. During this time, they have evolved many different molecular mechanisms by which to secrete proteinaceous effectors in order to manipulate and often kill rival bacterial and eukaryotic cells. These processes often employ large multimeric transmembrane nanomachines that have been classified as types I–IX secretion systems. One of the most evolutionarily versatile are the Type IV secretion systems (T4SSs), which have been shown to be able to secrete macromolecules directly into both eukaryotic and prokaryotic cells. Until recently, examples of T4SS-mediated macromolecule transfer from one bacterium to another was restricted to protein-DNA complexes during bacterial conjugation. This view changed when it was shown by our group that many *Xanthomonas* species carry a T4SS that is specialized to transfer toxic bacterial effectors into rival bacterial cells, resulting in cell death. This review will focus on this special subtype of T4SS by describing its distinguishing features, similar systems in other proteobacterial genomes, and the nature of the effectors secreted by these systems and their cognate inhibitors.

Keywords: bacterial competition, Xanthomonadales, type IV immunity protein, type IV secretion effector, type IV secretion system, X-Tfe, X-Tfi, X-T4SS

INTRODUCTION

Type IV secretion systems (T4SSs) have been studied since the birth of modern molecular biology, starting with the description of bacterial conjugation over 70 years ago (Lederberg and Tatum, 1946). It quickly became evident that the T4SS-mediated horizontal transfer of genetic material is a major contributor to bacterial evolution, making it necessary to consider lateral connections between lineages for a complete description of the bacterial tree of life (de la Cruz and Davies, 2000). Horizontal gene transfer is also one of the principal mechanisms for the spread of genes conferring resistance to antibiotics (Cabezon et al., 2015). Moreover, many pathogenic bacteria use T4SSs to facilitate their proliferation and survival inside eukaryotic hosts, typically by the secretion of protein effectors or protein-DNA complexes (Gonzalez-Rivera et al., 2016). T4SSs are thus important virulence factors in a variety of human diseases, including whooping cough (*Bordetella pertussis*; Locht et al., 2011; Carbonetti, 2015), cat-scratch fever (*Bartonella henselae*; Siamer and Dehio, 2015), brucellosis (*Brucella* spp.; Ke et al., 2015), Legionnaire's pneumonia (*Legionella pneumophila*;

Finsel and Hilbi, 2015), Q fever (*Coxiella burnetii*; Moffatt et al., 2015) and peptic ulcer and gastric cancer (*Helicobacter pylori*; Naumann et al., 2017). One of the most well-characterized T4SSs is that of *Agrobacterium tumefaciens* which injects nucleoprotein complexes and protein factors into plant cells (Alvarez-Martinez and Christie, 2009; Li and Christie, 2018). Furthermore, specialized T4SSs from *Neisseria gonorrhoeae* or *H. pylori* secrete DNA to the extracellular milieu or uptake DNA from the environment to the bacterial cytoplasm, respectively (Hofreuter et al., 2001; Hamilton et al., 2005; Callaghan et al., 2017). Finally, the plant pathogen *Xanthomonas citri* (Oliveira et al., 2016; Sgro et al., 2018; Souza et al., 2015) and, more recently, the opportunistic human pathogen *Stenotrophomonas maltophilia* (preprint: Bayer-Santos et al., 2019), have been shown to use a T4SS to inject toxic effectors into target bacteria, thus inducing the death of rival cells (**Figure 1**).

T4SSs are structurally very diverse. For example, the related pKM101 and R388 plasmid-encoded conjugation systems (Chandran et al., 2009; Fronzes et al., 2009; Rivera-Calzada et al., 2013) and the pathogenic *Legionella* Dot/Icm (Ghosal et al., 2017; Chetrit et al., 2018) and *H. pylori* Cag (Frick-Cheng et al., 2016; Chang et al., 2018) effector-secreting systems, while all exhibiting an outer membrane-associated core complex with 14-fold or 13-fold symmetry, present significantly different features in terms of their overall size. These systems also display a varied set of both functional and structural subunits, and even the homologous subunits have very low sequence similarity and frequently present modified domain architectures (Alvarez-Martinez and Christie, 2009; Christie et al., 2014; Guglielmini et al., 2014; Christie, 2016; Grohmann et al., 2017). For these reasons, the T4SSs from Gram-negative bacteria have been divided into two major classes, denoted A and B (Christie and Vogel, 2000), and classification systems based on detailed phylogenetic analysis have divided Gram-negative and Gram-positive T4SSs into up to 8 classes (Guglielmini et al., 2014).

The canonical class A, best represented by the *A. tumefaciens vir* system and those coded by conjugative plasmids pKM101, R388, and RP4, have the basic set of 12 conserved subunits, named VirB1 to VirB11 plus VirD4 (Tzfira and Citovsky, 2006). The overall organization of the canonical class A T4SSs has been revealed in electron microscopy studies (Low et al., 2014; Redzej et al., 2017) and can be divided into two general (sub)complexes (**Figure 1**). The inner membrane complex is made up of subunits embedded in, or associated with, the inner membrane: VirB3, VirB4, VirB6, VirB8, VirB11, and VirD4. The outer membrane or "core" complex is comprised of the subunits VirB7, VirB9, and VirB10. These two complexes are connected by a flexible "stalk" of unknown composition, though it has been proposed to be made up, at least in part, by the disordered N-terminal domain of VirB10 (which also has an N-terminal transmembrane helix embedded in the inner membrane) and/or the C-terminal domain of VirB8 (Christie, 2016; Waksman, 2019). In addition to this transmembrane structure, there are extracellular pili made of subunits VirB2 and VirB5, that are presumably involved in making contact with the membrane of the target cell or organelle (Alvarez-Martinez and Christie, 2009). Even within the class A T4SSs, a large degree of sequence and size diversity has been observed for many of the subunits in different species. This is perhaps most starkly exemplified when considering the *H. pylori* Cag T4SS which, in addition to orthologs of the basic set of canonical class A subunits, possesses another five subunits that are required for proper function (Backert et al., 2015; Frick-Cheng et al., 2016).

The even more distantly related class B includes T4SSs found in the pathogens *L. pneumophila*, *C. burnetii*, and *Rickettsiella grylli* as well as in the IncI conjugative plasmids R64 and ColIb-P9 (Sexton and Vogel, 2002). *L. pneumophila* causes Legionnaire's disease in humans by infecting alveolar macrophages where it replicates within a specialized vacuole (Backert and Meyer, 2006; Ensminger and Isberg, 2009). Its Dot/Icm T4SS is made up of 27 components and secretes more than 300 effector proteins that manipulate signal transduction pathways in the host cell, primarily affecting organelle trafficking (Hilbi et al., 2017; Qiu and Luo, 2017). The bacteria-killing T4SSs, which is the topic of this review, belong to the canonical class A T4SSs, although they do have some structurally distinguishing features as described below.

The Xanthomonadales order of Gammaproteobacteria (Saddler and Bradbury, 2007), recently divided into two orders, Xanthomonadales (families *Xanthomonadaceae* and *Rhodanobacteraceae*) and Nevskiales (Naushad et al., 2015), include several hundred phytopathogenic species of the genera *Xanthomonas* and *Xylella* as well as important and ubiquitous soil, water and plant-associated bacteria of the genera *Stenotrophomonas*, *Lysobacter*, *Luteimonas*, *Pseudoxanthomonas*, *Rhodanobacter*, *Luteibacter*, *Dyella*, *Frateuria*, *Aquimonas*, and others (Van Sluys et al., 2002; Saddler and Bradbury, 2007; Looney et al., 2009; Mansfield et al., 2012). Some *Stenotrophomonas* strains are opportunistic pathogens of immunosuppressed human patients (Chang et al., 2015) and some *Stenotrophomonas* and *Lysobacter* strains have been recognized as potential biological control agents in combating plant diseases caused by fungi or other bacteria (Hayward et al., 2010; Mukherjee and Roy, 2016; Panthee et al., 2016). Other species from the genera *Lysobacter* and *Luteimonas* have been isolated from extreme environments (Brito et al., 2013; Zhang et al., 2015). Although the role of types II and III secretion systems in the virulence of species of the genus *Xanthomonas* is already well established (Buttner and Bonas, 2010), until a few years ago there was little information available on the functions of other secretion systems in these bacterial species. An accompanying article in this series deals with the recently discovered role of the *X. citri* Type VI secretion system (T6SS) in protection against predation by phagocytic amoebas (Bayer-Santos et al., 2018). In this review, we will focus on the special characteristics of the Xanthomonadales Type IV secretion systems, first described in *X. citri*, and their role in the contact-dependent killing of rival Gram-negative species. The review will focus on describing the distinguishing structural features of the T4SS components encoded by the chromosomal *virB* locus of *X. citri*, their conservation in homologous systems in the order Xanthomonadales and other proteobacterial genomes, the nature of the effectors secreted by these systems and the cognate inhibitors of these effectors.

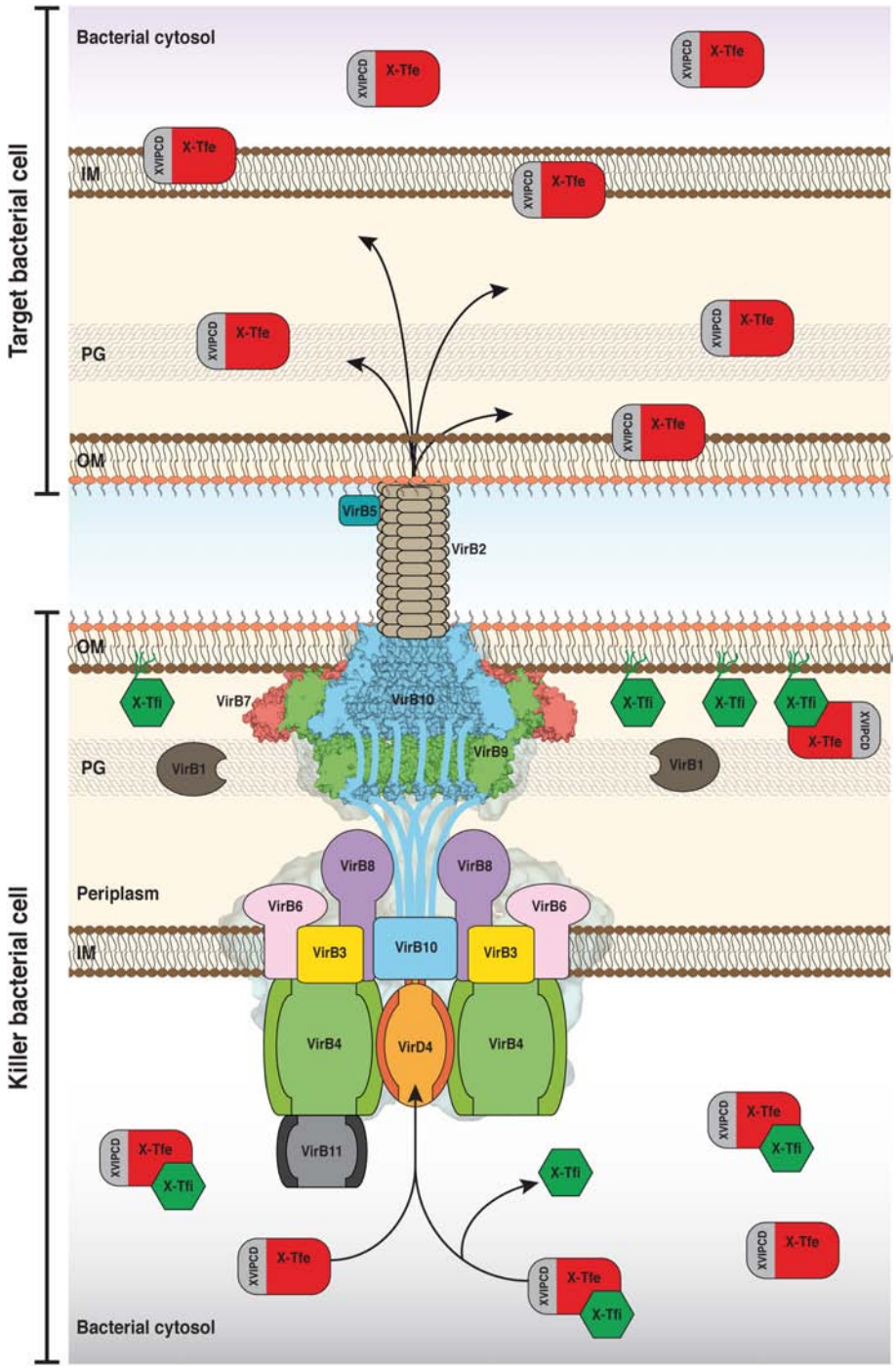

FIGURE 1 | Schematic model of the structure and function of the bacteria-killing Xanthomonadales-like Type IV secretion systems (X-T4SSs). The model shows the interface between two bacterial cells. The killer cell (below) is armed with an X-T4SS whose general architecture is based on the negative-stained electron microscope map of the R388 T4SS shown in the background (Low et al., 2014; Redzej et al., 2017) and the cryo-EM structure of the *X. citri* core complex (VirB7, VirB9, and VirB10; Sgro et al., 2018) associated with the outer membrane (OM). The disordered N-terminal domains of the VirB10 subunits extend down from the core complex and pass through the inner membrane. The inner membrane (IM) complex is made up of VirB3, VirB6, VirB8, the three ATPases VirB4, VirB11, and VirD4 as well as the aforementioned N-terminal segments of VirB10. Pili, made up of VirB2 and VirB5, mediate intercellular contacts. X-T4SS effectors (X-Tfes) interact, via their XVIPCD domains, with VirD4 and are subsequently transferred to the T4SS for translocation into the target cell where they will degrade target structures such as membrane phospholipids or carbohydrate and peptide linkages in the peptidoglycan (PG) layer. Prior to secretion, X-Tfes whose activities could target cytosolic substrates can be inhibited by cytosolic variants of their cognate immunity proteins (X-Tfis). If X-Tfes make their way into the periplasm, either by leakage from the secretion channel or by injection by neighboring cells of the same species, they will be inhibited by the periplasmic lipoprotein forms of the cognate X-Tfi. Portions of the Figure were adapted from Low et al. (2014) and Sgro et al. (2018) with permission from the publishers.

THE CHROMOSOMALLY CODED T4SS OF *Xanthomonas citri*

The T4SS encoded by the chromosomal *vir* locus of *X. citri* contains the canonical set of 12 structural components found in other class A T4SSs (**Figure 2**; Alegria et al., 2005; Souza et al., 2011). The presence of chromosomally encoded homologs in several other *Xanthomonas* species (see below) suggested an important function in *Xanthomonas* biology. A role in bacterial conjugation or nucleic acid transfer was deemed unlikely since the chromosomal *virB* locus does not contain genes coding for homologs of the DNA processing components of the relaxosome or characteristic palindromic *oriT* sites (Alegria et al., 2005). Furthermore, a knockout of the *virB7* gene in *X. citri* did not affect the development of canker symptoms in citrus plants (Souza et al., 2011) and the deletion of a large part of the homologous operon in *Xanthomonas campestris* pv. *campestris* 8004 did not modify the phenotype of infection in several plants of the *Brassicaceae* family (He et al., 2007), ruling out a direct involvement of the T4SS in *Xanthomonas* virulence (at least in these two species). Our group subsequently demonstrated that this secretion system confers to *X. citri* the capacity to kill other Gram-negative cells in a contact-dependent manner (Souza et al., 2015). The first bacterial killing experiments were performed by confronting *X. citri* with common laboratory strains of *Escherichia coli* as well as the Betaproteobacterium *Chromobacterium violaceum* (Souza et al., 2015) and subsequent experiments demonstrated similar T4SS-dependent killing of several other Gram-negative bacteria but not Gram-positive bacteria (DPS, GUO, WC, and CSF; unpublished). Recently, a CPRG-based colorimetric assay has been employed to monitor the real time kinetics of T4SS-dependent bacterial killing by both *X. citri* (Sgro et al., 2018) and *S. maltophilia* (Preprint: Bayer-Santos et al., 2019). Time-lapse microscopy clearly showed that bacterial killing by *X. citri* and *S. maltophilia* requires cell-cell contact and that the death of target cells is evidenced by the loss of cell turgor and contents over a very short period of time (Souza et al., 2015; Preprint: Bayer-Santos et al., 2019). These T4SSs share with some T6SSs the ability to transfer their toxic effectors directly into rival bacterial species of different orders and phyla and so are important factors for interspecies competition. In this sense, they differ from contact-dependent growth inhibition (CDI) systems (Hayes et al., 2014) and the *Staphylococcus aureus* Type VII secretion system (T7SS; Cao et al., 2016) that seem to be important for competition between cells of the same or closely related species (intraspecies competition).

IDENTIFICATION OF HOMOLOGOUS SYSTEMS IN THE ORDER XANTHOMONADALES AND OTHER PROTEOBACTERIAL GENOMES

Several of the *X. citri* T4SS components have some interesting features that distinguish them from their homologs in other more distantly related class A T4SSs involved in horizontal transfer of genetic material. For example, the VirB7 and VirB8 subunits have C-terminal extensions absent in most of their more distantly related homologs (see below). Genes coding for T4SSs with similar characteristics to that of *X. citri* can be identified in the chromosomes of many other *Xanthomonas* species (**Figure 2** and **Table 1**), for example *Xanthomonas campestris* pv. *campestris* B100 (Vorholter et al., 2008), *Xanthomonas albilineans* GPEPC73 (Pieretti et al., 2009), *X. campestris* pv. *vasculorum* NCPPB702 (Studholme et al., 2010) and *X. campestris* pv. *musacearum* NCPPB2005 (Wasukira et al., 2012). The corresponding locus is fragmented in *X. campestris* pv. *campestris* strains ATCC33913 (Da Silva et al., 2002) and 8004 (Qian et al., 2005), with the *virB5* and *virB6* genes found in other regions of the genomes. *X. campestris* pv. *vesicatoria* 85-10 (Thieme et al., 2005) lacks a significant part of the *vir* locus (all that remains is the 5′ region coding for VirD4, VirB7, VirB8, and VirB9). The system is also absent in *Xanthomonas oryzae* strains KACC10331 (Lee et al., 2005), MAFF311018 (Ochiai et al., 2005), PXO99A (Salzberg et al., 2008), and BLS256 (Salzberg et al., 2007), in *Xanthomonas fuscans* subsp. *aurantifolii* strains 10535 and 11122 (Moreira et al., 2010) and in all *Xylella* species sequenced to date. Homologous loci can be found in some Xanthomonadales species of the genera *Stenotrophomonas*, *Pseudoxanthomonas*, *Luteimonas*, *Lysobacter*, *Thermomonas*, *Rhodanobacter*, *Dyella*, *Frateuria*, and *Luteibacter* (**Table 1**). Interestingly, homologous systems are also found in some species of the Betaproteobacteria orders Burkholderiales (genera *Hydrogenophaga*, *Variovorax*) and Neisseriales (genera *Neisseria* and *Morococcus*) (**Table 1**). This is consistent with the observation that in some phylogenetic analyses, Xanthomonadales species are observed to branch anomalously with Betaproteobacteria, most probably due to horizontal gene transfer events (Martins-Pinheiro et al., 2004; Comas et al., 2006; Naushad and Gupta, 2013). We will therefore employ the term X-T4SS to designate all Xanthomonadales-like Type IV secretion systems.

Figure 2 presents the organization of genetic loci, homologous to the *X. citri* chromosomal *vir* locus, that are found in the genomes of a few bacterial species selected from genera of the *Xanthomonadaceae* family (*Xanthomonas*, *Stenotrophomonas*, and *Lysobacter*), and *Rhodanobacteraceae* family (*Dyella* and *Luteibacter*) within the order Xanthomonadales. Also shown are examples of genetic loci that code for X-T4SSs found in the more distant Betaproteobacteria genera of the *Comamonadaceae* family (*Hydrogenophaga*) and *Neisseriaceae* family (*Neisseria*). One interesting observation is that the loci in species from the Xanthomonadales order seem to have one operon coding for all 11 VirB components, beginning with the *virB7* gene. On the other hand, in *Hydrogenophaga crassostreae*, the operon has been divided into two segments (*virB7-11* and *virB1-6*) and in *Neisseria mucosa* and *N. flavescens* it has been divided into three or more segments (**Figure 2**). The positions of the *virD4* genes also vary: in most *Xanthomonas* and *Stenotrophomonas* species it is found immediately upstream of the *virB7* gene while in the more distantly related species it appears upstream, downstream or inserted between segments coding for the *virB* genes (**Figure 2**).

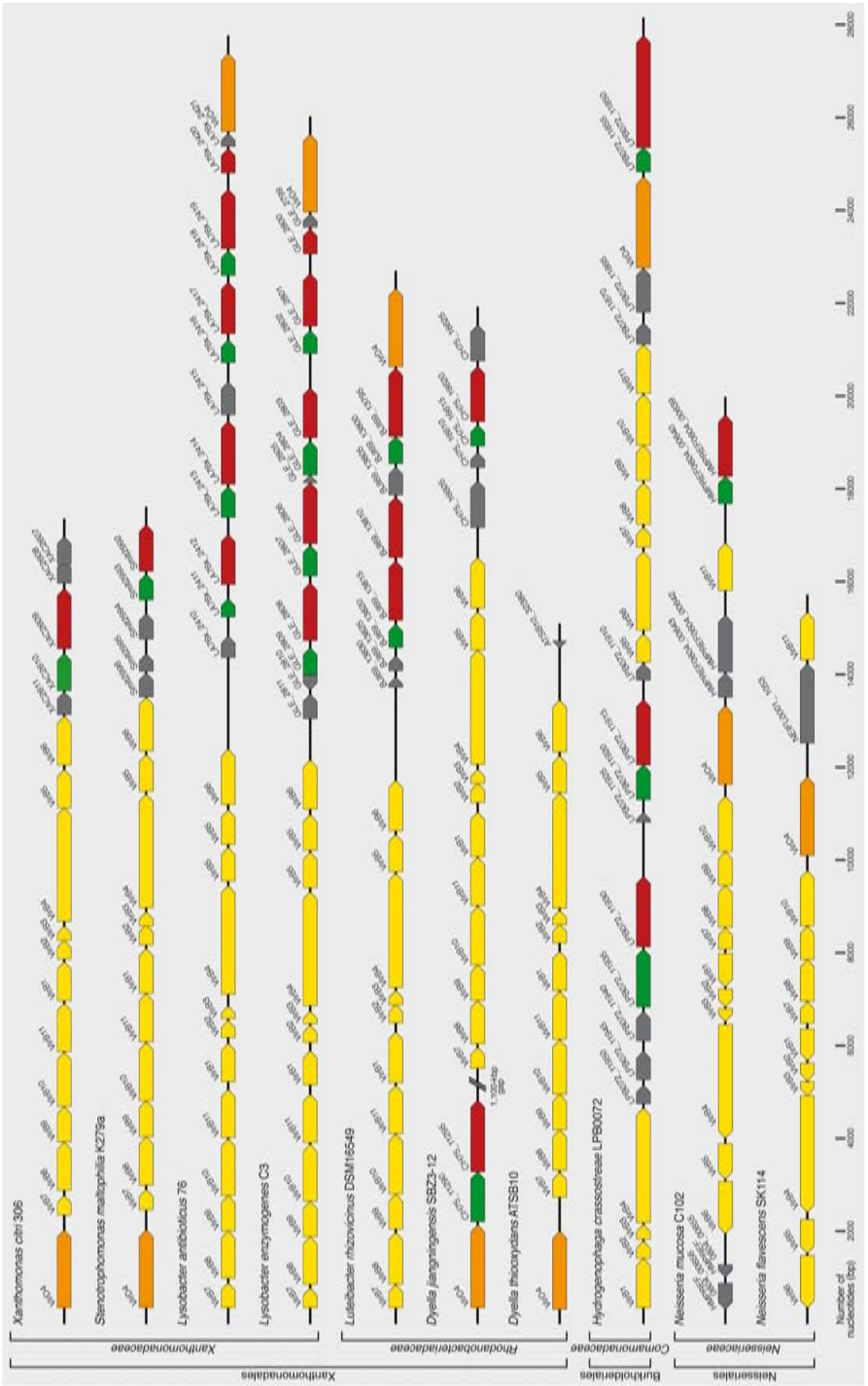

FIGURE 2 | *Xanthomonas citri* chromosomal *vir* locus and its homologs in other species. The top line presents the T4SS encoded by the chromosomal *vir* locus of *X. citri* 306 (Da Silva et al., 2002; Alegria et al., 2005). It contains the canonical set of 12 components found in other class A T4SSs. Genes coding for T4SSs with similar characteristics to that of *X. citri* can be identified in the chromosomes of many other species (see **Table 1** for an extensive list). Shown here are representative examples from *Stenotrophomonas maltophilia* K279a (Crossman et al., 2008), *Lysobacter antibioticus* 76 (de Bruijn et al., 2015), *Lysobacter enzymogenes* C3 (unpublished; GenBank accession CP013140), *Luteibacter rhizovicinus* DSM16549 (unpublished; GenBank accession CP017480), *Dyella jiangningensis* SBZ3-12 (Bao et al., 2014), *Dyella thiooxydans* ATSB10 (unpublished; GenBank accession CP014841), *Hydrogenophaga crassostreae* LPB0072 (unpublished; GenBank accession LWWD01000013), *Neisseria mucosa* C102 (unpublished, GenBank accession GCA_000186165) and *Neisseria flavescens* SK114 (unpublished; GenBank accession ACQV01000009). VirB and VirD4 genes are shown in yellow and orange, respectively. Xanthomonadales-like T4SS effectors (X-Tfes) and immunity proteins (X-Tfis) are colored red and green, respectively. Other open reading frames coding for proteins of unknown function are shown in gray.

DISTINGUISHING STRUCTURAL FEATURES OF THE BACTERIA-KILLING XANTHOMONADALES-LIKE T4SSs (X-T4SSs)

Supplementary Figures S1–S12 present multiple amino acid sequence alignments of VirB1–VirB11 and VirD4 (respectively) X-T4SS components coded by the homologous loci presented in **Figure 2**. What follows in this section is a brief description of some interesting structural features that can be identified from these alignments and, in some cases, their correlations with known structures and site-directed mutagenesis studies. The observations gleaned from these comparisons are likely to apply to most of the X-T4SSs listed in **Table 1**.

VirB7, VirB9, and VirB10: Components of the Core Complex

The 2.9 Å resolution crystal structure of the outer membrane layer of the pKM101 core complex (Chandran et al., 2009) and the recently published 3.3 Å resolution cryo-electron microscopy (cryo-EM) structure of the complete *X. citri* core complex (Sgro et al., 2018), along with the lower resolution EM maps of the complete pKM101 (Fronzes et al., 2009; Rivera-Calzada et al., 2013), R388 (Low et al., 2014) and *A. tumefaciens* (Gordon et al., 2017) core complexes have provided us with the greatest detail as yet of the periplasmic channel that connects the inner and outer membranes of class A T4SSs. These structures, are all made of 14 copies of VirB7–VirB9–VirB10 heterotrimers (named TraN-TraO-TraF in pKM101 and TrwH-TrwF-TrwE in R388) and can be divided into two layers: the O-layer associated with the outer membrane, consisting of VirB7 and the C-terminal domains of VirB9 and VirB10, and the I-layer made up of the N-terminal domains of VirB9 and VirB10 (**Figures 3**, **4**; Fronzes et al., 2009).

The VirB7 lipoprotein component of X-T4SSs is much larger (ranging from 130 to 185 amino acids; **Supplementary Figure S7**) than that found in other class A T4SSs (normally ∼40 amino acids). This large size is due to an extra globular C-terminal domain called N0 (Souza et al., 2011). Interestingly, similar N0 domains are also found in a myriad of transport systems located in Gram-negative bacterial outer membranes, ranging from secretins of T2SSs, Type IV pilus biogenesis machineries (Korotkov et al., 2009), T3SSs (Spreter et al., 2009), filamentous phages (Spagnuolo et al., 2010), long-tailed bacteriophages (Kanamaru et al., 2002; Kondou et al., 2005), signal-transduction domains in TonB-dependent receptors (Garcia-Herrero and Vogel, 2005; Ferguson et al., 2007) and membrane-penetrating devices in T6SSs (Leiman et al., 2009). The N0 domain is also the C-terminal domain of the outer membrane lipoprotein DotD of the class B T4SSs found in the human pathogens *L. pneumophila* and *C. burnetii* (Nakano et al., 2010). The presence of this domain in many outer membrane transport systems could reflect an unexplored evolutionary relationship between them (Souza et al., 2011). The function of the VirB7 N0 domain is possibly related to the observation that it mediates VirB7 oligomerization and, as the VirB7 subunits are highly concentrated in the context of the core complex, it was predicted that the VirB7 domain could assemble an extra peripheral ring in the O-layer of the X-T4SS (Souza et al., 2011), subsequently confirmed by the resolution of the *X. citri* core complex structure (Sgro et al., 2018). This external ring of N0 domains give the *X. citri* core complex its characteristic profile that resembles a flying saucer (**Figure 3**; Sgro et al., 2018). The motifs that mediate VirB7 oligomerization (specific residues in the N0 domain and a [T/S]EIPL) motif that immediately precedes it, contribute to T4SS assembly in the *X. citri* periplasm and are essential for its antibacterial activity (Souza et al., 2011; Oliveira et al., 2016; Sgro et al., 2018). The multiple sequence alignment in **Supplementary Figure S7** shows that these motifs, as well as the region involved in interaction with VirB9, are conserved among X-T4SS VirB7 proteins.

Like their homologs in other class A T4SSs, the X-T4SS VirB9 proteins have two domains connected by a central linker. They all possess an N-terminal signal peptide with a cleavage site immediately after a highly conserved alanine residue (**Supplementary Figure S9**). The cryo-EM structure of the *X. citri* core complex (Sgro et al., 2018) and the NMR solution structure of the *X. citri* VirB7–VirB9 binary complex (Oliveira et al., 2016) showed that the *X. citri* VirB9 C-terminal domain interacts with VirB7 and with the VirB10 C-terminal domain in the O-layer of the core complex in a manner similar to that observed for pKM101 (**Figure 4**). The *X. citri* core complex structure provided us with the first high resolution structure of the I-layer, composed of 14 VirB9 N-terminal β-sandwich domains that pack against each other side-by-side, forming a ring with an internal diameter of 80 Å (**Figure 3**; Sgro et al., 2018). At the base of the I-layer, small 12-residue helices from the N-terminal domains of VirB10 fit into grooves at the interfaces between VirB9 subunits (Sgro et al., 2018). The multiple sequence alignment of X-T4SS VirB9 proteins shows that the N- and C-terminal domains are quite well conserved but the central linker is variable in both sequence and length (**Supplementary Figure S9**). This is consistent with the observation that deletion of six residues in the linker region did not affect the stability or function of the T4SS in *X. citri* (Sgro et al., 2018).

VirB10 subunits in class A T4SSs can be divided into three substructures: the N-terminal cytosolic portion with its contiguous transmembrane helix that spans the bacterial inner membrane, the periplasmic portion of the N-terminal domain that is largely unstructured in the NMR analysis of the isolated domain and the cryo-EM structure of the *X. citri* core complex (Sgro et al., 2018) and the C-terminal domain localized in the O-layer of the core complex. The alignments shown in **Supplementary Figure S10** reveal that the C-terminal domains of X-T4SS VirB10 subunits are very well conserved. The sequences are also very similar to their counterparts in pKM101, R388 and *A. tumefaciens* (Sgro et al., 2018). One region in this domain that presents a relatively high degree of variability is the "antenna" (Chandran et al., 2009), made up of two alpha helices (α1 and α2) that form the actual pore through the outer membrane. **Figure 4** presents a comparison of the relative orientations of the VirB10 antennae when the *X. citri* core complex and pKM101 O-layer structures are superposed. In the *X. citri* core complex

TABLE 1 | Bacterial strains that code for a putative X-T4SS and X-Tfes substrates.

Organism	Accession[#]	Organism	Accession[#]
Xanthomonadaceae			
Luteimonas sp. 83-4	NZ_CP029556.1	*Xanthomonas axonopodis* pv. *citrumelo* F1	CP002914.1
***Lysobacter antibioticus* 76**	NZ_CP011129.1	*Xanthomonas axonopodis* pv. *melhusii* LMG9050	LOJW01000012.1
Lysobacter capsici AZ78	JAJA02000001.1	*Xanthomonas axonopodis* pv. *vasculorum* NCPPB900	KN173625.1
***Lysobacter enzymogenes* C3**	CP013140.1	*Xanthomonas axonopodis* Xac29-1	CP004399.1
Lysobacter gummosus 3.2.11	CP011131.1	*Xanthomonas campestris* pv. *campestris* B100	NC_010688.1
Lysobacter maris HZ9B	CP029843.1	*Xanthomonas campestris* pv. *campestris* str. 8004	CP000050.1
Lysobacter silvestris AM20-91	NZ_NPZB01000002.1	*Xanthomonas campestris* pv. *campestris* str. ATCC33913	NC_003902.1
Lysobacter sp. 4284/11	NZ_RFLY01000011.1	*Xanthomonas campestris* pv. *musacearum* NCPPB2005	AKBE01000043.1
Lysobacter sp. cf310	FOSS01000003.1	*Xanthomonas campestris* pv. *raphani* 756C	CP002789.1
Lysobacter sp. Root494	NZ_LMFH01000005.1	*Xanthomonas campestris* pv. *vitiscarnosae* LMG939	LOKI01000031.1
Lysobacter sp. Root604	LMGS01000001.1	*Xanthomonas campestris* pv. *durantae* LMG696	LOKP01000030.1
Lysobacter sp. TY2-98	NZ_CP031413.1	*Xanthomonas cannabis* pv. *cannabis* NCPPB3753	JSZF01000027.1
Lysobacter sp. yr284	FNPT01000001.1	***Xanthomonas citri* 306**	AE008923.1
Lysobacter sp. zong2l5	NZ_QTSU01000001.1	*Xanthomonas citri* pv. *fuscans* str. 4834-R	FO681494.1
[Pseudomonas] geniculata N1	AJLO02000016.1	*Xanthomonas citri* pv. *glycines* str. 8ra	JDSU01000002.1
Pseudoxanthomonas sp. CF125	NZ_FNLD01000002.1	*Xanthomonas citri* pv. *malvacearum* MSCT	CP017020.1
Pseudoxanthomonas sp. GM95	FOAX01000001.1	*Xanthomonas citri* pv. *phaseoli* var. *fuscans*	CP020979.1
Pseudoxanthomonas sp. KAs_5_3	PKSO01000004.1	*Xanthomonas citri* pv. *vignicola* CFBP7113	CP022270.1
Pseudoxanthomonas spadix DSM18855	NZ_RDQN01000004.1	*Xanthomonas codiaei* CFBP4690	NZ_MDEC01000025.1
Pseudoxanthomonas suwonensis S2	QFNC01000012.1	*Xanthomonas cynarae* CFBP4188	NZ_MDFM01000055.1
Pseudoxanthomonas wuyuanensis CGMCC1.10978	NZ_OCND01000011.1	*Xanthomonas dyei* CFBP7245	NZ_MDEE01000016.1
Stenotrophomonas chelatiphaga DSM21508	NZ_LDJK01000096.1	*Xanthomonas euvesicatoria* 66b	JSZG01000018.1
Stenotrophomonas daejeonensis JCM16244	NZ_LDJP01000037.1	*Xanthomonas euvesicatoria* pv. *citrumelonis* CFBP3371	MDCC01000019.1
Stenotrophomonas ginsengisoli DSM24757	NZ_LDJM01000025.1	*Xanthomonas floridensis* WHRI8848	NZ_LXNG01000007.1
Stenotrophomonas indicatrix WS40	NZ_PEJS01000001.1	*Xanthomonas fragariae* PD5205	LT853885.1
Stenotrophomonas koreensis DSM17805	NZ_LDJH01000013.1	*Xanthomonas gardneri* ATCC19865	AEQX01000084.1
Stenotrophomonas lactitubi M15	NZ_PHQX01000001.1	*Xanthomonas hortorum* pv. *hederae* CFBP4925	MDEF01000040.1
Stenotrophomonas maltophilia Ab55555	JH791780.1	*Xanthomonas hyacinthi* CFBP1156	NZ_MDEG01000039.1
***Stenotrophomonas maltophilia* K279a**	NC_010943.1	*Xanthomonas hyacinthi* DSM19077	JPLD01000728.1
Stenotrophomonas maltophilia MF89	ATAP01000112.1	*Xanthomonas melonis* CFBP4644	MDEH01000006.1
Stenotrophomonas maltophilia R551-3	CP001111.1	*Xanthomonas nasturtii* WHRI8853	NZ_LYMI01000032.1
Stenotrophomonas maltophilia RA8	CALM01000806.1	*Xanthomonas perforans* Xp4-20	JZUZ01000033.1
Stenotrophomonas maltophilia WJ66	KN849114.1	*Xanthomonas phaseoli* pv. *dieffenbachiae* LMG25940	JPYI02000041.1
Stenotrophomonas pavanii DSM25135	LDJN01000042.1	*Xanthomonas phaseoli* pv. *manihotis* LMG784	LKKP01000141.1
Stenotrophomonas rhizophila OG2	NZ_NCWX01000002.1	*Xanthomonas phaseoli* pv. *phaseoli* NCPPB1158	JSBS02000062.1
Stenotrophomonas sp. 92mfcol6.1	FWEU01000001.1	*Xanthomonas pisi* CFBP4643	NZ_MDEI01000004.1
Stenotrophomonas sp. AG209	QXDB01000001.1	*Xanthomonas prunicola* CFBP8355	NZ_PHKX01000001.1
Stenotrophomonas sp. CC120222-04	FZQI01000004.1	*Xanthomonas sacchari* R1	NZ_CP010409.1
Stenotrophomonas sp. BIIR7	NZ_MKCZ01000002.1	*Xanthomonas* sp. CFBP7698	PRDN01000001.1
Thermomonas fusca DSM15424	NZ_AUIV01000008.1	*Xanthomonas* sp. CFBP7912	MDSN01000006.1
Xanthomonas albilineans GPEPC73	FP565176.1	*Xanthomonas* sp. Leaf131	LMOG01000019.1
Xanthomonas alfalfae GEV-Rose-07	MIKD01000086.1	*Xanthomonas* sp. Leaf148	LMOP01000008.1
Xanthomonas arboricola pv. *arracaciae* CFBP7407	MIGU01000001.1	*Xanthomonas* sp. NCPPB1128	NZ_LFME01000006.1
Xanthomonas arboricola pv. *corylina* CFBP2565	MDSJ01000034.1	*Xanthomonas theicola* CFBP4691	NZ_MIGX01000080.1
Xanthomonas arboricola pv. *fragariae* CFBP6773	OEQD01000019.1	*Xanthomonas translucens* pv. *arrhenatheri* LMG727	CXOI01000012.1
Xanthomonas arboricola pv. *guizotiae* CFBP7408	MDSK01000048.1	*Xanthomonas translucens* pv. *phlei* LMG730	CXOJ01000010.1
Xanthomonas arboricola pv. *juglandis* Xaj417	CP012251.1	*Xanthomonas translucens* pv. *poae* B99	LWSU01000053.1
Xanthomonas arboricola pv. *populi* CFBP 3122	MIGV01000035.1	*Xanthomonas translucens* pv. *translucens* DSM18974	CAPJ01000354.1
Xanthomonas arboricola pv. *pruni* MAFF301420	BAVC01000014.1	*Xanthomonas vasicola* NCPPB1060	CP034649.1
Xanthomonas arboricola pv. *pruni* str. MAFF311562	BAVB01000420.1	*Xanthomonas vasicola* pv. *vasculorum* NCPPB702	NZ_GG699328.2
Xanthomonas axonopodis pv. *begoniae* CFBP2524	MPSX01000020.1	*Xanthomonas vesicatoria* ATCC35937	AEQV01000175.1

(Continued)

TABLE 1 | Continued

Organism	Accession[#]	Organism	Accession[#]
Rhodanobacteraceae			
***Dyella jiangningensis* SBZ3-12**	CP007444.1	*Luteibacter* sp. 329MFSha	NZ_FOJE01000001.1
Dyella marensis UNC178MFTsu3.1	FONH01000012.1	*Luteibacter* sp. OK325	QAOX01000004.1
Dyella sp. 333MFSha	FNBR01000009.1	*Luteibacter* sp. UNCMF331Sha3.1	FOBU01000002.1
Dyella sp. 4MSK11	NZ_QRBF01000004.1	*Luteibacter* sp. UNCMF366Tsu5.1	FPIS01000002.1
Dyella sp. AD56	NRDP01000015.1	*Luteibacter yeojuensis* SU11	JZRB01000062.1
Dyella sp. AtDHG13	NZ_QICJ01000003.1	*Rhodanobacter fulvus* Jip2	NZ_AJXU01000014.1
Dyella sp. OK004	FOZI01000001.1	*Rhodanobacter* sp. 67-28	MKTU01000080.1
***Dyella thiooxydans* ATSB10**	CP014841.1	*Rhodanobacter* sp. C01	NZ_MUNR01000011.1
Frateuria terrea CGMCC1.7053	FOXL01000004.1	*Rhodanobacter* sp. C06	NZ_MUNP01000039.1
***Luteibacter rhizovicinus* DSM16549**	CP017480.1	*Rhodanobacter* sp. OK091	FRCH01000001.1
Luteibacter sp. 22Crub2.1	FUYT01000025.1	*Rhodanobacter* sp. Root627	NZ_LMGW01000002.1
Neisseriaceae			
Morococcus cerebrosus CIP81.93	NZ_JUFZ01000115.1	*Neisseria* sp. HMSC069H12	NZ_KV810249.1
Neisseria dentiae NCTC13012	NZ_UGQR01000001.1	*Neisseria* sp. HMSC06F02	KQ001448.1
***Neisseria flavescens* SK114**	ACQV01000009.1	*Neisseria* sp. HMSC070A01	LTII01000031.1
***Neisseria mucosa* C102**	GL635793.1	*Neisseria* sp. HMSC071C03	KV836738.1
Neisseria sp. HMSC056A03	KV821597.1	*Neisseria* sp. oral taxon 014 str. F0314	GL349413.1
Neisseria sp. HMSC064D07	KV831649.1	*Neisseria subflava* C2012011976	NZ_POXP01000001.1
Comamonadaceae			
***Hydrogenophaga crassostreae* LPB0072**	LVWD01000013.1	*Hydrogenophaga* sp. H7	MCIC01000014.1
Hydrogenophaga sp. A37	MUNZ01000181.1	*Variovorax* sp. Root318D1	NZ_LMCQ01000008.1
Others			
Acinetobacter baumannii 4300STDY7045681	UFGS01000006.1	*Burkholderiales* bacterium GWF1_66_17	MERT01000006.1
Bacillus sp. SRB_336	NZ_NADW01000001.1	*Xanthomonadales* bacterium RIFOXYA1FULL_69_10	MIDV01000097.1
Bacterium AM6	MUYX01000125.1	*Xanthomonadales* bacterium 14-68-21	NCKH01000003.1
Betaproteobacteria bacterium HGW	PHCC01000002.1		

X-T4SSs were identified according to the following criteria: (i) located in chromosomal DNA, (ii) VirB7 subunits have C-terminal N0 domains, (iii) genes for all twelve class A T4SS subunits are present, and (iv) the genomes carry genes for putative effectors (X-Tfes) with C-terminal XVIPCD required for recognition by X-T4SS VirD4. Species names are organized in alphabetical order within each bacterial family. Species discussed in more detail in the main text are shown in bold. [#]NCBI Reference Sequences or GenBank accession number.

structure, the antenna helices are twisted clockwise (∼50°) and tilted vertically (∼20°) with respect to the corresponding helices in pKM101, producing a more open outer membrane pore in the *X. citri* structure (45 Å versus 35 Å; **Figure 4**; Sgro et al., 2018). We also observe variability in sequence and length of the linker between the alpha helices that is expected to form a loop on the extracellular side of the outer membrane. This loop is particularly rich in threonine, serine and glycine residues and is longer in the Xanthomonadales VirB10 proteins than in their counterparts in *A. tumefaciens* and pKM101 (**Supplementary Figure S10**; Sgro et al., 2018). In both *X. citri* core complex and pKM101 O-layer structures, these loops are disordered with no significant density in the corresponding maps. Since 14 such loops are expected to be in close proximity at the extracellular face of the outer membrane, they could interact to facilitate closing and opening of the pore. However, an *X. citri* VirB10-msfGFP chimera with an 11 residue deletion in this loop is still partially functional (Sgro et al., 2018).

In contrast to the VirB10 C-terminal domain, its N-terminal domain is known to be highly variable in size and sequence. Xanthomonadales VirB10 proteins have relatively long N-terminal cytosolic segments that precede the transmembrane helix that passes through the inner membrane. While this cytosolic peptide is only 38 or 22 residues long and lacks proline residues in pKM101 and *A. tumefaciens*, it is 57–68 residues long and is rich in proline residues (around 15%) in most X-T4SS VirB10 subunits (**Supplementary Figure S10**). The N-terminal region of VirB10 has been observed to interact with VirD4 of the T4SSs from *A. tumefaciens* (Garza and Christie, 2013) and plasmids R388 (Llosa et al., 2003; Segura et al., 2013) and R27 (Gilmour et al., 2003). Whether similar interactions occur in the X-T4SS remains to be investigated.

The periplasmic portions of the N-terminal domains (NTDs) of VirB10 subunits in many T4SSs are particularly rich in prolines (Jakubowski et al., 2009) and this is also the case for the X-T4SSs (**Supplementary Figure S10**; Sgro et al., 2018). NMR studies of the periplasmic VirB10 NTD revealed it to be intrinsically disordered but with a 12 residue segment that samples a helical conformation and suffers conformational perturbations when mixed with a near 2:1 excess of isolated N-terminal domain of VirB9 at sub-millimolar concentrations (Sgro et al., 2018). This VirB10 N-terminal helix (residues 151–162 in *X. citri*; **Supplementary Figure S10**) fits into the groove between two VirB9 N-terminal domains in the

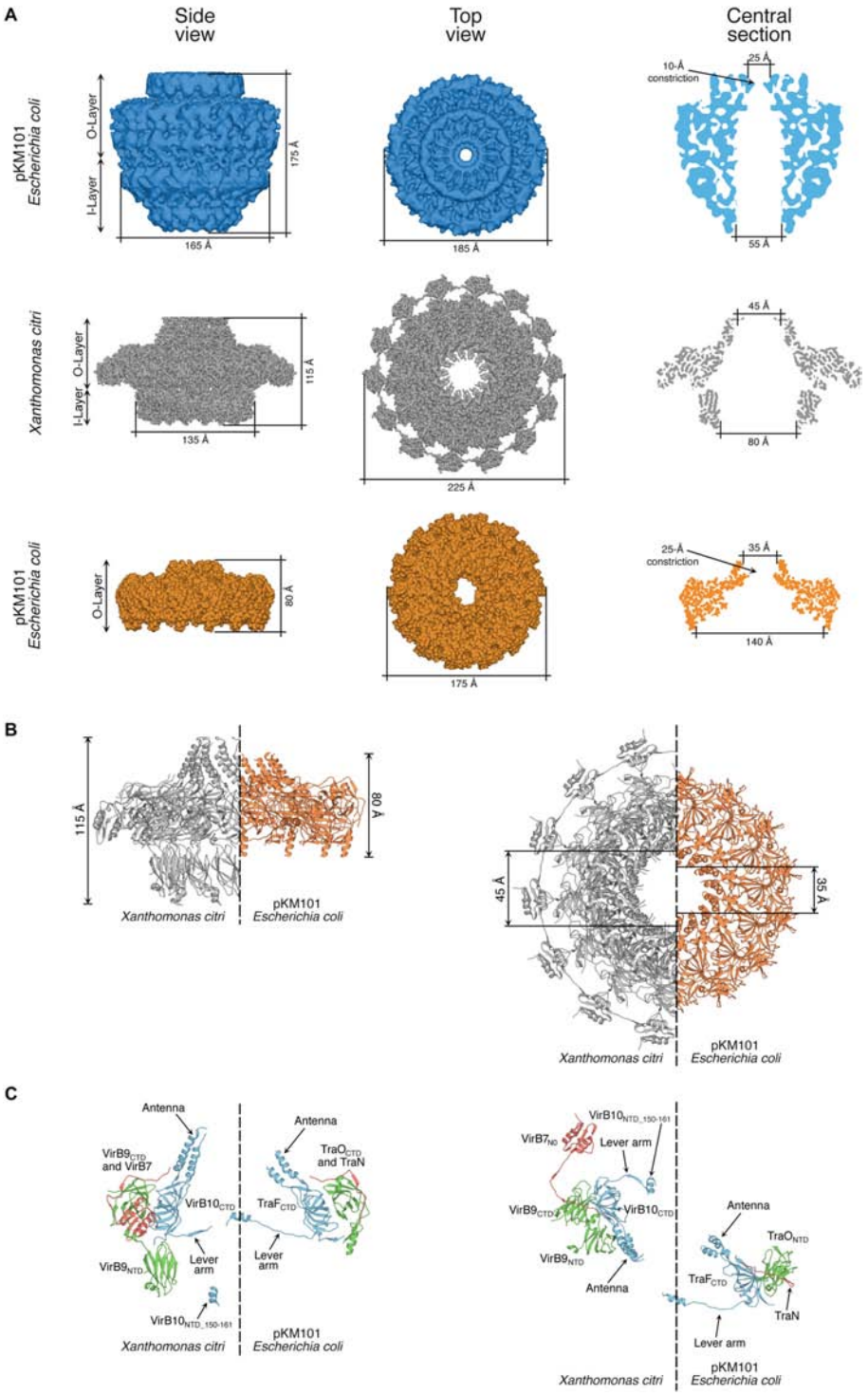

FIGURE 3 | Comparison of core complex structures. **(A)** Comparison of the electron microscopy maps of the full-length core complexes from pKM101 (12.4 Å resolution; top row; Rivera-Calzada et al., 2013) and *X. citri* T4SSs (3.3 Å resolution; middle row; Sgro et al., 2018). Also shown is the electron density map of the O-layer of the pKM101 core complex obtained by X-ray crystallography (2.9 Å resolution; lower row; Chandran et al., 2009). General features and dimensions are shown for side and top views, and for a central section. **(B)** Side-by-side comparison of the atomic models of the *X. citri* core complex (gray) and pKM101 (orange) O-layers. General features and dimensions are shown for side and top views. **(C)** Side-by-side comparison of the atomic models of the VirB7–VirB9–VirB10 trimer and TraN-TraO-TraF trimer in the *X. citri* core complex and pKM101 O-layer, respectively. Colors: VirB10 and TraF (blue), VirB9 and TraO (green), VirB7 and TraN (red). Side (left) and top (right) views are shown of diametrically opposed trimers taken from the side-by-side comparisons shown in **B**. NTD, N-terminal domain; CTD, C-terminal domain. Portions of the Figure were adapted from Rivera-Calzada et al. (2013) and Sgro et al. (2018) with permission from the publishers.

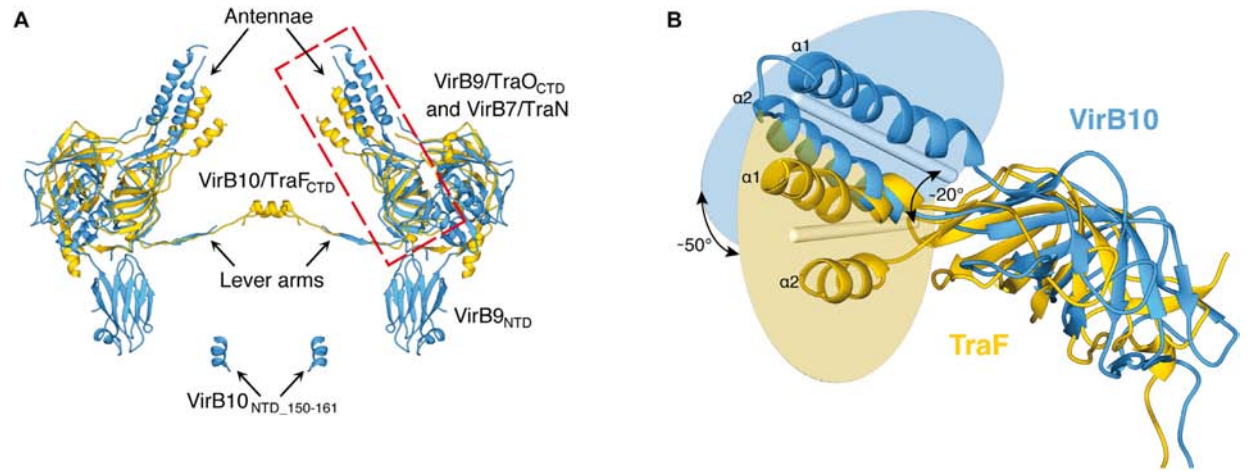

FIGURE 4 | Relative orientations of the antennae that form the outer membrane pore in the *X. citri* and pKM101 core complexes. **(A)** Superposition of the atomic models of diametrically opposed VirB7–VirB9–VirB10 trimers of the *X. citri* core complex (blue) and TraN-TraO-TraF trimers of the pKM101 O-layer (yellow). **(B)** Details of the relative orientations of the VirB10 and TraF C-terminal domains. The structures shown correspond to the red rectangle in **(A)**. The blue and yellow circles represent the planes that contain the central axes of the two antenna helices (α1 and α2). The blue and yellow rods represent the average vector between the two helices in each protein. The angles between the planes (~50°) and between the rods (~20°) are shown. Figure derived from Sgro et al. (2018) with modifications. NTD, N-terminal domain; CTD, C-terminal domain. This Figure was adapted from and Sgro et al. (2018) with permission from the publishers.

X. citri core complex structure (Sgro et al., 2018). The VirB9$_{NTD}$-VirB10$_{NTD}$ interaction, in addition to the VirB7–VirB7 interactions mentioned above (Souza et al., 2011) are two examples of interactions that are relatively weak when measured in isolation but reveal themselves to be physiologically relevant in the context of a large multi-subunit complex whose assembly is expected to be highly cooperative. The helical region is in fact the only well-conserved sequence in the N-terminal domains of the Xanthomonadales and *H. crassostreae* X-T4SS VirB10 subunits and can be described as a P[S/T]Lh[E/D/Q]RRh motif where h is a hydrophobic residue (**Supplementary Figure S10**). The VirB10 subunits from the two *Neisseria* species shown in **Supplementary Figure S10** do not seem to carry this motif.

One interesting observation is the very small number of stereospecific contacts between the I- and O-layers in the *X. citri* core complex. This immediately brings up the question as to what maintains the relative orientations between the two layers. The answer may be that individually weak interactions, multiplied fourteen times in the mature complex, could together be strong enough to favor specific conformational states between the two layers. Another interesting observation is that the long flexible N-terminal linkers that emerge from the VirB9 and VirB10 C-terminal domains in the direction of the I-layer point in opposite directions and pass by each other with their main chain atoms coming within 7 Å of each other (**Figure 3C**; Sgro et al., 2018). Therefore, the covalent linkages between the VirB9 and VirB10 N- and C-domains can be looked upon as forming an intricate cross-weave pattern at the interface of the I- and O-layers. This detail could have a role in maintaining the two layers in a preferential orientation by restricting the excessive relative rotations in both clockwise and counter-clockwise directions. Enigmatically, however, small (6 or 8 residue) deletions in these linkers had only moderate effects on T4SS-dependent bacterial killing by *X. citri* (Sgro et al., 2018).

VirB1

In *A. tumefaciens*, VirB1 undergoes cleavage of its N-terminal signal peptide upon transport to the periplasm and a second cleavage reaction that produces two fragments: (i) an N-terminal SLT (soluble lytic transglycosylase) domain predicted to be involved in peptidoglycan remodeling during T4SS biogenesis and (ii) a 76 residue C-terminal fragment (named VirB1*) that is subsequently transported to the extracellular milieu (Baron et al., 1997; Llosa et al., 2000). The VirB1 proteins in the X-T4SSs all have a well-conserved 150 residue N-terminal domain with predicted SLT activity (**Supplementary Figure S1**). These proteins lack an N-terminal signal sequence, however, and so their mechanism of transport into the periplasm is not yet known. The X-T4SSs VirB1 C-terminal domains vary in length from 130 to over 200 residues and are highly variable in sequence (**Supplementary Figure S1**). Whether X-T4SS VirB1 proteins undergo C-terminal processing in a manner analogous to that observed in *A. tumefaciens* remains to be investigated.

VirB2 and VirB5: The Components of the T4SS Pilus

The VirB2 pilin subunits in the Xanthomonadales species and more distant *H. crassostreae*, *N. flavescens*, and *N. mucosa* all have similar sizes and a very well conserved central hydrophobic region as well as a predicted cleavable 31–39 residue long N-terminal signal peptide (**Supplementary Figure S2**). After removal of the signal peptide, these pilins are predicted to have lengths between 80 and 104 residues. This is significantly greater than the 70 and 64 residue long mature F-pilin and its close homolog from plasmid pED208 (respectively) whose cryo-EM

structures have been determined in the context of the assembled sex pilus (Costa et al., 2016). Sequence-based secondary structure predictions for the X-T4SS VirB2 subunits correspond well with the two pilin structures and this allowed us to predict the positions of the two major helices (α2 and α3) in X-T4SS VirB2 as well as the intervening positively charged loop which interacts with the head groups of bound phospholipids in the pilus lumen (**Supplementary Figure S2**; Costa et al., 2016). The larger size of the X-T4SS VirB2 subunits is due to highly variable C-terminal extensions (**Supplementary Figure S2**). It is not clear whether these C-terminal extensions decorate the external pilus surface in X-T4SSs, perhaps providing binding sites for species-specific targets, or whether they are processed as has been observed for some P-pili (Eisenbrandt et al., 1999).

VirB5 is thought to be associated with the T4SS pilus, perhaps as a minor pilin at the pilus tip (Schmidt-Eisenlohr et al., 1999; Aly and Baron, 2007; Alvarez-Martinez and Christie, 2009). Due to the very high sequence variability in VirB5 proteins, its annotation as a bona-fide T4SS component in deposited genomic sequences is often ambiguous. In the bacteria-killing T4SSs under consideration here, these proteins have between 200 and 280 residues and are highly variable in sequence. They all have a predicted N-terminal cleavable signal peptide as well as a pair of cysteine residues found in the central portion of the amino acid sequence that are separated by 11 to 33 residues (**Supplementary Figure S5**). Interestingly, the genetic loci coding for X-T4SSs in the two *Lysobacter* species shown in **Figure 2** each carry two *virB5* genes in tandem. These protein pairs are 73% and 43% identical in *Lysobacter antibioticus* and *Lysobacter enzymogenes*, respectively. The predicted involvement of VirB5 in mediating the binding of the pilus to specific structures on the target cell (Alvarez-Martinez and Christie, 2009), could be a causative factor in this subunit's accelerated evolution.

VirB8, VirB6, and VirB3: Integral Membrane Proteins of the Inner Membrane Complex

VirB8 is an integral membrane protein with an N-terminal cytosolic peptide, a transmembrane helix and a globular C-terminal domain localized in the periplasm, the latter of which has been shown to interact with several other T4SS components, including VirB6, VirB9, and VirB10 (Alvarez-Martinez and Christie, 2009; Sivanesan et al., 2010; Villamil Giraldo et al., 2012). High resolution structures of the soluble C-terminal region of VirB8 proteins and homologs from diverse T4SSs have been determined: *A. tumefaciens* (Bailey et al., 2006), pKM101 (Casu et al., 2016), *H. pylori* (ComB10) and *Brucella suis* (Terradot et al., 2005), *Clostridium perfringens*, *Rickettsia typhi* and several *Bartonella* species (Gillespie et al., 2015), *L. pneumophila* and plasmid R64 (Kuroda et al., 2015). All these structures present the same fold, a β-sheet juxtaposed against a group of α-helices, and in most cases have been shown to oligomerize to different degrees (see references above). Since there are an estimated 12 copies of VirB8 in each class A T4SS (Low et al., 2014), these domains could associate to form an as-yet unknown structure in the bacterial periplasm. Interestingly, the bacteria-killing X-T4SSs have highly distinctive VirB8 components that are significantly longer (between 290 and 370 residues in length) than the canonical VirB8 components observed in the species listed above (all less than 250 residues). This greater size is, in large part, due to a C-terminal extension enriched in Ala, Gln, Gly, and Pro (AQGP) residues (**Table 2** and **Supplementary Figure S8**). The length of this extension and its enrichment in these residues are particularly evident in the Xanthomonadales order (53–73%) and *H. crassostreae* (45%) and less so in the X-T4SS VirB8 proteins of *Neisseria* species (**Table 2**). The role, if any, of the AQGP-rich extensions in these proteins is not yet known.

VirB6 is predicted to be a polytopic integral protein. In both *A. tumefaciens* and *B. suis*, the VirB6 N-terminus is located in the periplasm and the C-terminus is located in the cytosol, implying an odd number of transmembrane helices, estimated to be five in *A. tumefaciens* (Jakubowski et al., 2004) and seven in *B. suis* (Villamil Giraldo et al., 2015). **Supplementary Figure S6** presents the multiple sequence alignment of X-T4SS VirB6 proteins that also align well with their homologs in *A. tumefaciens* and *B. suis* (data not shown). The precise number and positions of the transmembrane helices is again ambiguous since transmembrane helix pairs 3/4 and 5/6 could alternatively be longer single helices (**Supplementary Figure S6**). Another common feature of these proteins is a large loop between transmembrane helices 2 and 3, predicted to be localized in the periplasm for both *A. tumefaciens*

TABLE 2 | Characteristics of C-terminal extensions in VirB8 proteins from X-T4SSs.

Organism	Extension size (aa)	% Ala	% Gln	% Gly	% Pro	% AQGP
Xanthomonas citri 306	98	21	25	11	15	72
Stenotrophomonas maltophilia K279a	104	19	19	12	15	65
Lysobacter antibioticus 76	97	26	4	10	32	72
Lysobacter enzymogenes C3	100	25	7	10	31	73
Luteibacter rhizovicinus DSM16549	129	26	11	12	22	71
Dyella jiangningensis SBZ3-12	70	16	9	11	17	53
Dyella thiooxydans ATSB10	48	33	2	8	27	70
Hydrogenophaga crassostreae LPB0072	53	13	6	11	15	45
Neisseria mucosa C102	55	6	16	4	13	39
Neisseria flavescens SK114	52	6	14	6	6	32

Analysis is based on the alignment shown in ***Supplementary Figure S8****.*

and *B. suis*. The periplasmic loops of the estimated 24 copies of VirB6 per T4SS (Low et al., 2014) are expected to interact with other periplasmic components of the inner membrane complex (**Figure 1**; Ding et al., 2003; Alvarez-Martinez and Christie, 2009; Villamil Giraldo et al., 2012, 2015; Christie, 2016).

X-T4SS VirB3 proteins are predicted to be bitopic or polytopic membrane proteins with one or two transmembrane helices located within the region encompassed by residues 15 and 57 (see **Supplementary Figure S3** for details). This is consistent with the difficulty in defining VirB3 topology in other T4SSs (Alvarez-Martinez and Christie, 2009). In some organisms, gene fusions have been observed between VirB3 and VirB4 (Batchelor et al., 2004) but this does not seem to be the case in the X-T4SSs. These gene fusions and the highly conserved synteny of *virB3* and *virB4* genes in most organisms suggests that these two proteins could interact with each other at or within the inner membrane (Peña et al., 2012). This hypothesis is supported by the observation that *A. tumefaciens* VirB4 is required to maintain normal levels of VirB3 (Jones et al., 1994) and that recombinant R388 VirB4 and VirB3 can be co-purified as a 1:1 complex (Low et al., 2014).

VirB4, VirB11, and VirD4: The ATPases of the Inner Membrane Complex

VirB4, VirB11, and VirD4 are P-loop ATPases with conserved Walker A and Walker B motifs and, in most T4SSs characterized to date, all three proteins are required for biogenesis and/or function (Alvarez-Martinez and Christie, 2009; Christie et al., 2014; Christie, 2016). These proteins use the hydrolysis of ATP to carry out mechanical work, expected to manifest itself in substrate unfolding, transfer and/or extrusion through the T4SS channel (Atmakuri et al., 2004).

VirB4 is the most well conserved T4SS subunit and has been used in phylogenetic analyses to trace evolutionary relationships and propose models for the emergence of T4SS subclasses (Guglielmini et al., 2014). Studies on different T4SSs have reported evidence that VirB4 interacts, at least transiently, with all of the other inner membrane complex components (Jones et al., 1994; Atmakuri et al., 2004; Cascales and Christie, 2004; Jakubowski et al., 2004; Paschos et al., 2006; Ripoll-Rozada et al., 2013; Low et al., 2014; Christie, 2016).

VirB4 has been localized to two 3-tiered barrel-like pedestals at the base of the inner membrane complex in EM reconstructions of the complete R388 T4SS, with each barrel corresponding to a VirB4 hexamer (Low et al., 2014; Redzej et al., 2017). VirB4 proteins can be divided into N- and C-terminal domains. The C-terminal domain carries all the conserved motifs required for nucleotide binding and hydrolysis (Walker A and Walker B boxes and motifs C, D, and E) and these motifs are present in X-T4SS VirB4 proteins (**Supplementary Figure S4**). The N-terminal domain, known to mediate interactions with the inner membrane, is expected to correspond to the upper tier in the R388 T4SS structure (Low et al., 2014; Redzej et al., 2017). One variable in the family of VirB4 proteins is the presence or absence of one or more predicted N-terminal transmembrane helices and the question as to their requirement for VirB4 function has proven to be controversial (Rabel et al., 2003), with the additional caveat that VirB4/TraB from pKM101 can be purified in soluble and membrane-bound forms (Durand et al., 2010). Therefore, it is not clear whether VirB4 should be considered an integral or peripheral membrane protein, or both (Arechaga et al., 2008; Christie, 2016; Waksman, 2019). The X-T4SS VirB4 proteins do not have predicted transmembrane helices using the TMHMM v2.0 (Krogh et al., 2001) and PSort (Nakai and Horton, 1999) prediction algorithms.

VirB11 is a soluble membrane-associated AAA+ ATPase that has been shown to interact with both VirD4 and VirB4 (Ripoll-Rozada et al., 2013). The crystal structures of VirB11 homologs from *B. suis* (Hare et al., 2006) and *H. pylori* (Yeo et al., 2000) are both two-tiered hexameric rings in which each ring layer consists of six N- or C-terminal domains from the constituent monomers. Within VirB11 monomers, the domains are connected by a central linker of varying length, short in *H. pylori* and 17 residues longer (linker B and α2C) in *B. suis*, resulting in a domain-swapped architecture in the latter (Hare et al., 2006). As a consequence, the nucleotide binding site in *H. pylori* VirB11 is located at the interface between the two domains of the same monomer while in *B. suis* the nucleotide binds at the interface between the N-terminal domain of one monomer and the C-terminal domain of the neighboring monomer (Hare et al., 2006). VirB11 proteins from X-T4SSs show a high degree of sequence similarity and all have the long version of the linker, which aligns well with the *B. suis* linker B and α2C sequences (**Supplementary Figure S11**). We can therefore expect that the X-T4SS VirB11 proteins exhibit a domain-swapped structure similar to that of *B. suis* (Hare et al., 2006).

The VirD4 ATPase and its homologs are often called coupling proteins due to their role in selecting substrates for export by the T4SS. Analysis of the X-T4SS VirD4 proteins suggests that they have a canonical VirD4-like architecture (Llosa and Alkorta, 2017) with two N-terminal transmembrane helices with a predicted intervening ∼30 amino acid periplasmic loop and a cytosolic C-terminal domain. The cytosolic domain can be separated into a nucleotide binding domain (NBD), with conserved Walker A and Walker B motifs, and a so-called all alpha domain (AAD) (**Supplementary Figure S12**; Gomis-Ruth et al., 2002). The VirD4 N-terminal transmembrane domain helices have been implicated in interacting with the VirB10 N-terminal region that includes its transmembrane helix (Segura et al., 2013) and the VirD4 all alpha domain is involved in substrate recognition (Gomis-Ruth et al., 2002; Whitaker et al., 2015). TrwB, the VirD4 homolog of the conjugative plasmid R388, has been crystallized as a hexameric ring (Gomis-Ruth et al., 2002). It has been proposed that VirB4 and VirD4 could form transient heterohexameric complexes during substrate transport (Peña et al., 2012; Waksman, 2019) and low resolution electron microscopy studies of the intact VirB3-B10/D4 T4SS from R388 observed VirD4 dimers sandwiched between the two hexameric VirB4 barrels (Redzej et al., 2017). Therefore, the oligomeric structure of VirD4 in a fully assembled and functioning T4SS is still not clear (Redzej et al., 2017; Chetrit et al., 2018; Waksman, 2019).

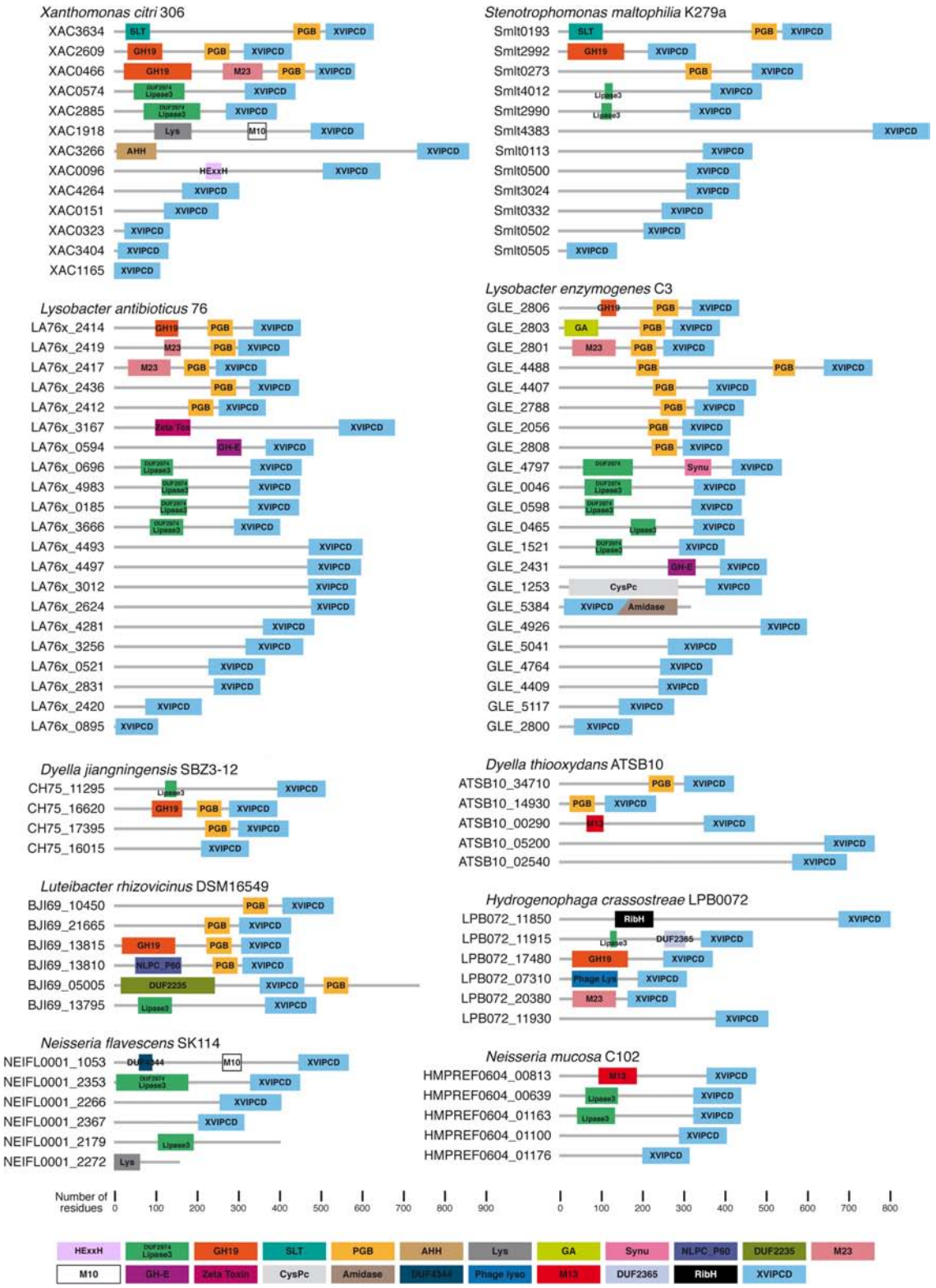

FIGURE 5 | Putative Xanthomonadales-like T4SS effectors (X-Tfes) found in selected species that carry an X-T4SS. Shown here are representative examples from *Xanthomonas citri* 306 (Da Silva et al., 2002), *Stenotrophomonas maltophilia* K279a (Crossman et al., 2008), *Lysobacter antibioticus* 76 (de Bruijn et al., 2015), *Lysobacter enzymogenes* C3 (unpublished; GenBank accession CP013140), *Luteibacter rhizovicinus* DSM16549 (unpublished; GenBank accession CP017480), *(Continued)*

FIGURE 5 | Continued
Dyella jiangningensis SBZ3-12 (Bao et al., 2014), *Dyella thiooxydans* strain ATSB10 (unpublished; GenBank accession CP014841), *Hydrogenophaga crassostreae* LPB0072 (unpublished; GenBank accession LVWD01000013), *Neisseria mucosa* C102 (unpublished, GenBank accession GCA_000186165) and *Neisseria flavescens* SK114 (unpublished; GenBank accession ACQV01000009). Protein domains were identified by sequence comparison with the Pfam (El-Gebali et al., 2019) and/or CDD databases (Marchler-Bauer et al., 2015) and are colored according to the scheme presented at the bottom of the Figure. Domain abbreviations: M10 (Pfam accession PF08548), M13 (Pfam accession PF01431), M23 (Pfam accession PF01551), Lipase3 (Pfam accession PF01764), DUF2974 (Pfam accession PF11187), GH-E (Pfam accession PF14410), GH19 (Pfam accession PF00182), Zeta Toxin (Pfam accession PF06414), SLT (CDD accession cd00254), CysPc (CDD accession cd00044), PGB (Pfam accession PF01471), Amidase (Pfam accession PF01510), AHH (Pfam accession PF14412), DUF4344 (Pfam accession PF14247), Lys (CDD accession cl00222), Phage lyso (Pfam accession PF00959), GA (Pfam accession PF01832), Synu (CDD accession cl03193), DUF2365 (Pfam accession PF10157), NLPC_P60 (Pfam accession PF00877), RibH (Pfam accession PF02267), DUF2235 (Pfam accession PF09994), HExxH (HExxH motif in putative metalloprotease domain; Firczuk and Bochtler, 2007).

XANTHOMONADALES-LIKE T4SS EFFECTORS (X-Tfes) AND THEIR COGNATE INHIBITORS (X-Tfis)

X-Tfes

The first clues regarding the physiological role of the *X. citri* T4SS came from the identification of T4SS substrates using the VirD4 coupling protein as a bait in yeast two-hybrid assays against a *Xanthomonas* genomic library (Alegria et al., 2005). The strategy was based on the reasoning that in other well-characterized T4SSs, the VirD4 component is known to interact with the macromolecular substrates prior to transport (Llosa and Alkorta, 2017). This screening originally identified 12 so-called "*Xanthomonas* VirD4 interacting proteins," or XVIPs (Alegria et al., 2005), later called *Xanthomonadaceae* T4SS effectors (Souza et al., 2015) and from here on Xanthomonadales-like T4SS effectors (X-Tfes, **Figure 5**). In *X. citri*, the gene for one X-Tfe (XAC2609) is found in the *vir* locus while the remaining X-Tfe genes are dispersed throughout the genome. Interestingly, all of these proteins have a common C-terminal domain entitled "XVIP conserved domain" or XVIPCD (**Figures 1**, **5**), typically around 120 residues long, required for interaction with VirD4 (Alegria et al., 2005) and for secretion in a T4SS-dependent manner (Souza et al., 2015). The XVIPCD is characterized by a few conserved motifs in its N-terminal region and a glutamine-rich C-terminal region (Alegria et al., 2005).

The discovery of the XVIPCD as the secretion signal for the *X. citri* X-Tfes allowed for a large-scale bioinformatics identification of X-Tfe genes present in other bacterial genomes (Souza et al., 2015). **Figure 5** shows the domain architectures of the X-Tfes identified by bioinformatics analysis of bacterial genomes whose X-T4SSs are described in **Figure 2**. The N-terminal portions of the *X. citri* X-Tfes are highly variable in size and architecture and most are predicted to function within the periplasm as peptidoglycan (PG) glycohydrolases, lytic transglycosylases, PG peptidases or lipases (**Figure 5**). Therefore, these bacterial species probably use their X-T4SSs to inject not one, but a diverse cocktail of X-Tfes that will simultaneously attack multiple structures in the target cell (**Figure 1**). Two purified *X. citri* X-Tfes (XAC2609 and XAC0466) with predicted PG hydrolase activities have been shown to lyse PG and induce the lysis of Gram-positive cells, which have exposed bacterial cell walls (Souza et al., 2015). It is interesting that a considerable fraction of X-Tfes have N-terminal sequences with no identifiable domains, opening the possibility that new domain families with antibacterial activities could be characterized in the future. One such X-Tfe, Smlt3024 from *S. maltophilia* K279a (**Figure 5**), has been shown to inhibit *E. coli* growth when heterologously expressed and directed to the periplasm (preprint: Bayer-Santos et al., 2019).

It is worth noting that we often encounter several open reading frames that code for small proteins, sometimes possessing little more than an intact XVIPCD; for example XAC0323, XAC1165, and XAC3404 in *X. citri* (respectively 136, 127, and 132 residues in length; **Figure 5**; Souza et al., 2015). In some cases, these open reading frames appear to be fragments of ancestral X-Tfes genes that suffered frameshift mutations. One example of this phenomenon is provided by the XAC1165 gene whose first 37 nucleotides overlap with the 3′ end of the upstream XAC1164 gene which codes for a 437 protein of unknown function. The amino acid sequences of XAC1164 and XAC1165 align very well with the N-terminal and XVIPCD regions, respectively, of the Smlt0113 X-Tfe protein from *S. maltophilia* (**Figure 5**). Thus *X. citri* XAC1164 and XAC1165 proteins are homologous, and probably the non-functional, fragments of a functional X-Tfe (Smlt0113) in *S. maltophilia*.

X-Tfis

To protect against the toxicity of endogenous or exogenous X-Tfes, *X. citri* and *S. maltophilia* produce specific immunity proteins that bind to their cognate toxins (Alegria et al., 2005; Souza et al., 2015; preprint: Bayer-Santos et al., 2019). These inhibitors have been termed *Xanthomonadaceae* T4SS immunity proteins (Souza et al., 2015) and from here on Xanthomonadales-like T4SS immunity proteins (X-Tfis). The genes coding for X-Tfis are usually found upstream and are probably co-transcribed with their cognate X-Tfe (Souza et al., 2015; preprint: Bayer-Santos et al., 2019). All bacterial species identified so far that carry an X-T4SS also code for multiple X-Tfe/X-Tfi pairs and, in most cases, the genes for at least one pair is found within, or in close proximity to, the locus that codes for the structural components of the X-T4SS (see **Figure 2**). Furthermore, in almost all cases where the X-Tfe is predicted to act upon periplasmic structures (glycosidic and peptide bonds in peptidoglycan or ester linkages in phospholipids), the cognate X-Tfi carries an N-terminal signal peptide and lipobox for periplasmic localization and anchoring in the outer membrane (Souza et al., 2015; preprint: Bayer-Santos et al., 2019). On the other hand, some X-Tfes with N-terminal

X-Tfe	X-Tfi	N-terminal amino acid sequence of X-Tfi	Putative alternative X-Tfi initiation codon and RBS
XAC3634	XAC3633	**MLVRKISLVLALATIAAC**TQATPDATAPKTAAAAAGTPTKPSEKDASPM...	agaaaaggatgcatctcccatg
XAC2609	XAC2610	**MLTRELARAVAGVIYLICVVSITAC**SPSNAPSAEADGEKSPAKNQASKKPEYELQKDLKM...	aaaaggatttgaaaatg
XAC0466	XAC0467	**MPPFRLLIPILAVALVAC**NGPQAADAPETPANAPAAAAQPPSPAASPPATPTQGTVPM...	aagggactgtacccatg
XAC0096	XAC0097	**MRFPRAALLFLTALCAPALSAC**AHGPLKPLPKEHADM...	gaaggagcacgctgacatg
XAC0574	XAC0573	**MAAHLPRRPALRQMLTPSLLALLLTAC**HSPETSM...	cggagaccagcatg
XAC2885	XAC2884	**MQPRFPALLVLATSFFAVSC**TASPGAKEQTTM...	aaggagcaaaccaccatg
XAC1918	XAC1917	**MKIKSVGCVALALFFITGC**TVVSAGADM...	gcgggcgcggacatg

FIGURE 6 | Possible alternative translation start codons that could lead to the production of soluble cytosolic X-Tfis in *Xanthomonas citri*. The first two columns list the names of *X. citri* X-Tfe/X-Tfi pairs in which the X-Tfi is predicted to be a lipoprotein (Souza et al., 2015). The third column presents the N-terminal amino acid sequence of the X-Tfi in which the signal sequence and Lipobox are shown in bold. The basic nucleotides at the N-terminus of the signal sequence are shown in blue. The four Lipobox residues are shown in red. Underlined residues are those from the absolutely conserved Cys residue at the site of cleavage in the Lipobox to the next Met residue (green) in the protein sequence. The last column presents the nucleotide sequence (lowercase letters) immediately upstream of the putative alternative start codon (green). The putative Shine–Dalgarno sequence (ribosome binding site) for this alternative start codon is shown in red.

TABLE 3 | List of proteins in the KEGG database with greatest similarity[a] to the N-terminal domain (residues 1–240) of Smlt0332 from *S. maltophilia* K279a.

Organism	Accession[b]	*E*-value	Description
Xanthomonas campestris pv. *campestris* B100	xcc-b100_0624	3 E-88	X-T4SS X-Tfe
Xanthomonas campestris pv. *campestris* 8004	XC_3909	2 E-83	X-T4SS X-Tfe
Xanthomonas campestris pv. *campestris* ATCC33913	XCC3567	2 E-83	X-T4SS X-Tfe
Xanthomonas vasicola pv. *vasculorum* SAM119	C7V42_12340	2 E-79	X-T4SS X-Tfe
Xanthomonas vesicatoria ATCC35937	BJD12_15640	2 E-76	X-T4SS X-Tfe
Metakosakonia sp. MRY16-398	MRY16398_33930	2 E-26	Type VI secretion system secreted protein VgrG
Pantoea ananatis LMG20103	PANA_2352	9 E-26	Type VI secretion system secreted protein VgrG
Pantoea vagans FDAARGOS_160	AL522_12495	4 E-25	Type VI secretion system secreted protein VgrG
Kosakonia radicincitans GXGL-4A	A3780_13240	4 E-22	Type VI secretion system secreted protein VgrG/Rhs
Enterobacter hormaechei subsp. *xiangfangensis* LMG27195	BFV63_12735	4 E-21	Type VI secretion system secreted protein VgrG/Rhs
Enterobacter hormaechei subsp. *xiangfangensis* 34399	LI66_12735	9 E-21	Type VI secretion system secreted protein VgrG/Rhs
Enterobacter hormaechei subsp. *hoffmannii* ECR091	ECR091_12370	9 E-21	Type VI secretion system secreted protein VgrG
Enterobacter hormaechei subsp. *hoffmannii* ECNIH3	ECNIH3_12435	2 E-20	Type VI secretion system secreted protein VgrG
Enterobacter cloacae ECNIH5	ECNIH5_12380	3 E-20	Type VI secretion system secreted protein VgrG/Rhs
Burkholderia stabilis ATCCBAA-67	BBJ41_25130	2 E-20	Type VI secretion system secreted protein VgrG
Enterobacter hormaechei subsp. *hormaechei* 34983	LI64_12500	2 E-20	Type VI secretion system secreted protein VgrG/Rhs
Methylocaldum marinum S8	sS8_3556	6 E-20	Type VI secretion system secreted protein VgrG
Ralstonia solanacearum FQY_4	F504_2863	2 E-19	Type VI secretion system secreted protein VgrG
Ralstonia solanacearum Po82	RSPO_c00015	2 E-19	Type VI secretion system secreted protein VgrG
Burkholderia territorii RF8-non-BP5	WS51_08400	4 E-19	Type VI secretion system secreted protein VgrG
Cronobacter turicensis z3032	CTU_00910	3 E-19	Type VI secretion system secreted protein VgrG
Ralstonia pseudosolanacearum RS 476	CDC45_17535	5 E-19	Type VI secretion system secreted protein VgrG
Ralstonia solanacearum GMI1000	RSc3430	5 E-19	Type VI secretion system secreted protein VgrG
Ralstonia solanacearum PSI07	RPSI07_0016	1 E-17	Type VI secretion system secreted protein VgrG
Burkholderia stagnalis MSMB735WGS	WT74_22275	3 E-17	Type VI secretion system secreted protein VgrG
Xanthomonas fragariae Fap21	BER92_04245	2 E-17	Type VI secretion system secreted protein VgrG
Ralstonia solanacearum FQY_4	F504_3476	4 E-17	Type VI secretion system secreted protein VgrG
Xanthomonas campestris pv. *raphani* 756C	XCR_2915	4 E-17	Hypothetical protein
Mycolicibacterium hassiacum DSM44199	MHAS_03665	1 E-16	Hypothetical protein
Burkholderia ubonensis MSMB22	BW23_4367	3 E-16	Type VI secretion system secreted protein VgrG/Rhs
Enterobacter sp. R4-368	H650_00935	2 E-12	Type VI secretion system secreted protein VgrG
Kosakonia cowanii 888-76	BWI95_18245	7 E-09	Type VI secretion system secreted protein VgrG/Rhs

[a] *only proteins with significant coverage in the alignment are shown.*
[b] *KEGG (Kyoto Encyclopedia of Genes and Genomes) accession number.*

domains predicted to act in the cytosol of the target cell (for example the *X. citri* X-Tfe XAC3266 with an N-terminal AHH domain with predicted nuclease activity; **Figure 5**) have a cognate X-Tfi (for example XAC3267) lacking a lipoprotein signal (Souza et al., 2015). Finally, some X-Tfes are expected to be active in both the cytosol and periplasm, as are the cases of the X-Tfes with predicted lipase domains with phospholipase activities (NFB, DPS, BM, and CSF, manuscript in preparation; **Figure 5**). This brings up the question regarding the cellular localization of the X-Tfis. An analysis of the *X. citri* X-Tfis with putative N-terminal signal peptide and Lipobox sites indicates that their coding genes have potential alternative downstream start (ATG) codons with associated ribosome binding sites (**Figure 6**). This raises the possibility that many X-Tfes can be produced in two versions: (i) a membrane-associated periplasmic lipoprotein and (ii) a soluble cytosolic protein (**Figure 1**). Thus, if X-Tfes make their way into the periplasm, either by leakage from the secretion channel or by injection by neighboring cells of the same species, they will be inhibited by the periplasmic lipoprotein forms of the cognate X-Tfi. On the other hand, X-Tfes whose activities could target cytosolic substrates can be inhibited by cytosolic variants of their cognate X-Tfis. If this is in fact the case, for at least this latter subset of X-Tfes, transport will necessarily involve previous dissociation of the X-Tfe/X-Tfi cytosolic pair.

Parallels Between X-T4SS X-Tfe/X-Tfi, T6SS Effector/Immunity Protein and Plasmid-Encoded Toxin/Antitoxin (TA) Pairs

X-Tfe/X-Tfi pairs share many of the characteristics observed for T6SS effectors and their inhibitors (Russell et al., 2011, 2013). For example, one immunity protein from *X. citri* (X-Tfi^{XAC2610}) inhibits the GH19 family PG hydrolase X-Tfe^{XAC2609} and has a very similar topology, though very little sequence similarity, to the PG hydrolase inhibitors PliI and Tsi1 (Van Herreweghe et al., 2010; Russell et al., 2011) the latter of which is an inhibitor of the T6SS effector Tse1 from *Pseudomonas aeruginosa* (Souza et al., 2015). Another example is provided by the X-Tfe Smlt0332 from *S. maltophilia* K279a, which has many X-Tfe homologs in other Xanthomonadales species (data not shown) but whose N-terminal region has no similarity with annotated domains in the Pfam or CCD databases. Interestingly, Blast searches against the curated KEGG database (Kanehisa et al., 2017) using this domain identified a large number of homologous sequences fused to VgrG domains in effectors predicted to be secreted by T6SSs of *Metakosakonia*, *Pantoea*, *Kosakonia*, *Enterobacter*, *Burkholderia*, *Methylocaldum*, *Ralstonia*, *Cronobacter*, and *Xanthomonas* species (**Table 3**). Searches against the non-redundant protein sequence database (Altschul et al., 1990) identified many more such homologs in other bacterial species (data not shown). These findings raise interesting questions regarding the evolution, distribution and exchange of T4SS and T6SS effectors in the biosphere. In fact, we can make a general observation that anti-bacterial Type IV and Type VI secretion systems share many enzymatic effector and cognate inhibitory modules and differ only in the specific sequences recognized for transport. It also raises the possibility that the acquisition of immunity proteins could be advantageous even in the absence of the cognate effector by offering a defense against the toxic activity of substrates launched by both T4SS and T6SSs during encounters with rival bacteria. We have in fact recently observed the reciprocal T4SS-dependent dueling between *S. maltophilia* and *X. citri* cells which could mimic similar encounters between soil- and/or plant-associated bacteria in the environment (preprint: Bayer-Santos et al., 2019). The differences in X-Tfe and X-Tfi repertoires between rival species will contribute to the outcome of these encounters.

Effector/immunity protein pairs associated with T4SS and T6SSs show intriguing parallels with toxin/anti-toxin modules that function to guarantee vertical transmission of mobile elements (Jensen and Gerdes, 1995). For example, Harms et al. (2017) have shown that the pVbh plasmid of *Bartonella schoenbuchensis*, codes for a toxin/antitoxin module in which the toxin component, VbhT, acquired a C-terminal BID (Bep Intracellular Delivery) domain that confers its transfer to recipient cells during conjugation. They propose that its function may be to support intercellular DNA transfer by pre-emptively addicting the recipient cell to the plasmid, which also carries the gene for the antitoxin antidote. It is not difficult to imagine a scenario in which the T4SS coded by such a plasmid could lose its capacity to transfer DNA but retain its capacity to transfer the toxin, and in this way evolve into a single-purpose bacteria-killing T4SS. Therefore, we can expect bactericidal T4SSs, perhaps with very different recognition signals, to have arisen on multiple occasions in distantly related bacterial species.

CLOSING REMARKS

These are early days in the characterization of antibacterial T4SSs. The structure of the *X. citri* core complex has provided a good reference for comparison with other T4SSs, and has illustrated the structural variability that we can expect to encounter even within the class A T4SSs. While X-T4SS activities have only been experimentally verified for *X. citri* and *S. maltophilia*, bioinformatics analysis allowed us to confidently expand the list of bacterial families both within the Gammaproteobacteria class as well as to other families within the Betaproteobacteria (**Table 1**) that carry proteins with many of the characteristic X-T4SSs features, including VirB7 proteins with N0 domains, VirB8 proteins with AQGP-rich extensions as well as recognizable X-Tfe/X-Tfi pairs in which the effector carries a C-terminal XVIPCD. The list of X-T4SSs will most surely expand significantly in the future. However, it is unlikely that bactericidal T4SSs are restricted to the X-T4SSs described here. It is more probable that many other bacterial species carry as yet uncharacterized and perhaps unrecognized T4SSs that recruit effectors with recognition signals significantly different from the XVIPCDs associated with X-T4SSs as predicted (Souza et al., 2015) and as illustrated by the results obtained for the T4SS encoded by the *B. schoenbuchensis* pVbh plasmid (Harms et al., 2017).

AUTHOR CONTRIBUTIONS

GS, GO, EB-S, and CF produced the figures and tables. CF wrote the manuscript. All authors contributed with critical discussions and revisions that led to the final version of the manuscript.

FUNDING

This work was supported by grants from the Fundação de Amparo à Pesquisa do Estado de São Paulo (FAPESP) to CF (Grant # 2017/17303-7), CA-M (Grant # 2018/01852-4), and EB-S (Grant # 2017/02178-2).

ACKNOWLEDGMENTS

GS, GO, DS, WC, BM, and EB-S acknowledge scholarships from FAPESP. DS, TdS, and NB acknowledge fellowships from Coordenação de Aperfeiçoamento de Pessoal de Nível Superior (CAPES).

SUPPLEMENTARY MATERIAL

The Supplementary Material for this article can be found online at: https://www.frontiersin.org/articles/10.3389/fmicb.2019.01078/full#supplementary-material

REFERENCES

Alegria, M. C., Souza, D. P., Andrade, M. O., Docena, C., Khater, L., Ramos, C. H. I., et al. (2005). Identification of new protein-protein interactions involving the products of the chromosome- and plasmid-encoded type IV secretion loci of the phytopathogen *Xanthomonas axonopodis* pv. *citri*. *J. Bacteriol.* 187, 2315–2325. doi: 10.1128/JB.187.7.2315-2325.2005

Altschul, S. F., Gish, W., Miller, W., Myers, E. W., and Lipman, D. J. (1990). Basic local alignment search tool. *J. Mol. Biol.* 215, 403–410. doi: 10.1016/S0022-2836(05)80360-2

Alvarez-Martinez, C. E., and Christie, P. J. (2009). Biological diversity of prokaryotic type IV secretion systems. *Microbiol. Mol. Biol. Rev.* 73, 775–808. doi: 10.1128/MMBR.00023-09

Aly, K. A., and Baron, C. (2007). The VirB5 protein localizes to the T-pilus tips in *Agrobacterium tumefaciens*. *Microbiology* 153, 3766–3775. doi: 10.1099/mic.0.2007/010462-0

Arechaga, I., Pena, A., Zunzunegui, S., del Carmen Fernandez-Alonso, M., Rivas, G., and de la Cruz, F. (2008). ATPase activity and oligomeric state of TrwK, the VirB4 homologue of the plasmid R388 type IV secretion system. *J. Bacteriol.* 190, 5472–5479. doi: 10.1128/JB.00321-08

Atmakuri, K., Cascales, E., and Christie, P. J. (2004). Energetic components VirD4, VirB11 and VirB4 mediate early DNA transfer reactions required for bacterial type IV secretion. *Mol. Microbiol.* 54, 1199–1211. doi: 10.1111/j.1365-2958.2004.04345.x

Backert, S., and Meyer, T. F. (2006). Type IV secretion systems and their effectors in bacterial pathogenesis. *Curr. Opin. Microbiol.* 9, 207–217. doi: 10.1016/j.mib.2006.02.008

Backert, S., Tegtmeyer, N., and Fischer, W. (2015). Composition, structure and function of the *Helicobacter pylori* cag pathogenicity island encoded type IV secretion system. *Future Microbiol.* 10, 955–965. doi: 10.2217/fmb.15.32

Bailey, S., Ward, D., Middleton, R., Grossmann, J. G., and Zambryski, P. C. (2006). *Agrobacterium tumefaciens* VirB8 structure reveals potential protein-protein interaction sites. *Proc. Natl. Acad. Sci. U.S.A.* 103, 2582–2587. doi: 10.1073/pnas.0511216103

Bao, Y., Kwok, A. H. Y., He, L., Jiang, J., Huang, Z., Leung, F. C. C., et al. (2014). Complete genome sequence of *Dyella jiangningensis* strain SBZ3-12, isolated from the surfaces of weathered rock. *Genome Announc.* 2:e00416-14. doi: 10.1128/genomeA.00416-14

Baron, C., Llosa, M., Zhou, S., and Zambryski, P. C. (1997). VirB1, a component of the T-complex transfer machinery of *Agrobacterium tumefaciens*, is processed to a C-terminal secreted product, VirB1. *J. Bacteriol.* 179, 1203–1210. doi: 10.1128/jb.179.4.1203-1210.1997

Batchelor, R. A., Pearson, B. M., Friis, L. M., Guerry, P., and Wells, J. M. (2004). Nucleotide sequences and comparison of two large conjugative plasmids from different *Campylobacter* species. *Microbiology* 150(Pt 10), 3507–3517. doi: 10.1099/mic.0.27112-0

Bayer-Santos, E., Cenens, W., Matsuyama, B. Y., Di Sessa, G., Mininel, I. D. V., and Farah, C. S. (2019). The opportunistic pathogen *Stenotrophomonas maltophilia* utilizes a type IV secretion system for interbacterial killing. *bioRxiv* [Preprint]. doi: 10.1101/557322

Bayer-Santos, E., Lima, L., dos, P., Ceseti, L., de, M., Ratagami, C. Y., et al. (2018). *Xanthomonas citri* T6SS mediates resistance to *Dictyostelium* predation and is regulated by an ECF σ factor and cognate Ser/Thr kinase. *Environ. Microbiol.* 20, 1562–1575. doi: 10.1111/1462-2920.14085

Brito, E. M., Pinon-Castillo, H. A., Guyoneaud, R., Caretta, C. A., Gutierrez-Corona, J. F., Duran, R., et al. (2013). Bacterial biodiversity from anthropogenic extreme environments: a hyper-alkaline and hyper-saline industrial residue contaminated by chromium and iron. *Appl. Microbiol. Biotechnol.* 97, 369–378. doi: 10.1007/s00253-012-3923-5

Buttner, D., and Bonas, U. (2010). Regulation and secretion of *Xanthomonas* virulence factors. *FEMS Microbiol. Rev.* 34, 107–133. doi: 10.1111/j.1574-6976.2009.00192.x

Cabezon, E., Ripoll-Rozada, J., Pena, A., de la Cruz, F., and Arechaga, I. (2015). Towards an integrated model of bacterial conjugation. *FEMS Microbiol. Rev.* 39, 81–95. doi: 10.1111/1574-6976.12085

Callaghan, M. M., Heilers, J. H., van der Does, C., and Dillard, J. P. (2017). Secretion of chromosomal DNA by the *Neisseria gonorrhoeae* type IV secretion system. *Curr. Top. Microbiol. Immunol.* 413, 323–345. doi: 10.1007/978-3-319-75241-9_13

Cao, Z., Casabona, M. G., Kneuper, H., Chalmers, J. D., and Palmer, T. (2016). The type VII secretion system of *Staphylococcus aureus* secretes a nuclease toxin that targets competitor bacteria. *Nat. Microbiol.* 2:16183. doi: 10.1038/nmicrobiol.2016.183

Carbonetti, N. H. (2015). Contribution of pertussis toxin to the pathogenesis of pertussis disease. *Pathog. Dis.* 73:ftv073. doi: 10.1093/femspd/ftv073

Cascales, E., and Christie, P. J. (2004). Definition of a bacterial type IV secretion pathway for a DNA substrate. *Science* 304, 1170–1173. doi: 10.1126/science.1095211

Casu, B., Smart, J., Hancock, M. A., Smith, M., Sygusch, J., and Baron, C. (2016). Structural analysis and inhibition of TraE from the pKM101 type IV secretion system. *J. Biol. Chem.* 291, 23817–23829. doi: 10.1074/jbc.M116.753327

Chandran, V., Fronzes, R., Duquerroy, S., Cronin, N., Navaza, J., and Waksman, G. (2009). Structure of the outer membrane complex of a type IV secretion system. *Nature* 462, 1011–1015. doi: 10.1038/nature08588

Chang, Y. T., Lin, C. Y., Chen, Y. H., and Hsueh, P. R. (2015). Update on infections caused by *Stenotrophomonas maltophilia* with particular attention to resistance mechanisms and therapeutic options. *Front. Microbiol.* 6:893. doi: 10.3389/fmicb.2015.00893

Chang, Y. W., Shaffer, C. L., Rettberg, L. A., Ghosal, D., and Jensen, G. J. (2018). In vivo structures of the *Helicobacter pylori* cag type IV secretion system. *Cell Rep.* 23, 673–681. doi: 10.1016/j.celrep.2018.03.085

Chetrit, D., Hu, B., Christie, P. J., Roy, C. R., and Liu, J. (2018). A unique cytoplasmic ATPase complex defines the *Legionella pneumophila* type IV secretion channel. *Nat. Microbiol.* 3, 678–686. doi: 10.1038/s41564-018-0165-z

Christie, P. J. (2016). The mosaic type IV secretion systems. *EcoSal Plus* 7:ecosalplus.ESP-0020-2015. doi: 10.1128/ecosalplus.ESP-0020-2015

Christie, P. J., and Vogel, J. P. (2000). Bacterial type IV secretion: conjugation systems adapted to deliver effector molecules to host cells. *Trends Microbiol.* 8, 354–360. doi: 10.1016/s0966-842x(00)01792-3

Christie, P. J., Whitaker, N., and González-Rivera, C. (2014). Mechanism and structure of the bacterial type IV secretion systems. *Biochim. Biophys. Acta* 1843, 1578–1591. doi: 10.1016/j.bbamcr.2013.12.019

Comas, I., Moya, A., Azad, R. K., Lawrence, J. G., and Gonzalez-Candelas, F. (2006). The evolutionary origin of Xanthomonadales genomes and the nature of the horizontal gene transfer process. *Mol. Biol. Evol.* 23, 2049–2057. doi: 10.1093/molbev/msl075

Costa, T. R. D., Ilangovan, A., Ukleja, M., Redzej, A., Santini, J. M., Smith, T. K., et al. (2016). Structure of the bacterial sex F pilus reveals an assembly of a stoichiometric protein-phospholipid complex. *Cell* 166, 1436–1444.e10. doi: 10.1016/j.cell.2016.08.025

Crossman, L. C., Gould, V. C., Dow, J. M., Vernikos, G. S., Okazaki, A., Sebaihia, M., et al. (2008). The complete genome, comparative and functional analysis of *Stenotrophomonas maltophilia* reveals an organism heavily shielded by drug resistance determinants. *Genome Biol.* 9:R74. doi: 10.1186/gb-2008-9-4-r74

Da Silva, A. C. R., Ferro, J. A., Reinach, F. C., Farah, C. S., Furlan, L. R., Quaggio, R. B., et al. (2002). Comparison of the genomes of two *Xanthomonas* pathogens with differing host specificities. *Nature* 417, 459–463. doi: 10.1038/417459a

de Bruijn, I., Cheng, X., de Jager, V., Expósito, R. G., Watrous, J., Patel, N., et al. (2015). Comparative genomics and metabolic profiling of the genus *Lysobacter*. *BMC Genomics* 16:991. doi: 10.1186/s12864-015-2191-z

de la Cruz, F., and Davies, J. (2000). Horizontal gene transfer and the origin of species: lessons from bacteria. *Trends Microbiol.* 8, 128–133. doi: 10.1016/s0966-842x(00)01703-0

Ding, Z., Atmakuri, K., and Christie, P. J. (2003). The outs and ins of bacterial type IV secretion substrates. *Trends Microbiol.* 11, 527–535. doi: 10.1016/j.tim.2003.09.004

Durand, E., Oomen, C., and Waksman, G. (2010). Biochemical dissection of the ATPase TraB, the VirB4 homologue of the *Escherichia coli* pKM101 conjugation machinery. *J. Bacteriol.* 192, 2315–2323. doi: 10.1128/JB.01384-09

Eisenbrandt, R., Kalkum, M., Lai, E. M., Lurz, R., Kado, C. I., and Lanka, E. (1999). Conjugative pili of IncP plasmids, and the Ti plasmid T pilus are composed of cyclic subunits. *J. Biol. Chem.* 274, 22548–22555. doi: 10.1074/jbc.274.32.22548

El-Gebali, S., Mistry, J., Bateman, A., Eddy, S. R., Luciani, A., Potter, S. C., et al. (2019). The Pfam protein families database in 2019. *Nucleic Acids Res.* 47, D427–D432. doi: 10.1093/nar/gky995

Ensminger, A. W., and Isberg, R. R. (2009). *Legionella pneumophila* Dot/Icm translocated substrates: a sum of parts. *Curr. Opin. Microbiol.* 12, 67–73. doi: 10.1016/j.mib.2008.12.004

Ferguson, A. D., Amezcua, C. A., Halabi, N. M., Chelliah, Y., Rosen, M. K., Ranganathan, R., et al. (2007). Signal transduction pathway of TonB-dependent transporters. *Proc. Natl. Acad. Sci. U.S.A.* 104, 513–518. doi: 10.1073/pnas.0609887104

Finsel, I., and Hilbi, H. (2015). Formation of a pathogen vacuole according to *Legionella pneumophila*: how to kill one bird with many stones. *Cell. Microbiol.* 17, 935–950. doi: 10.1111/cmi.12450

Firczuk, M., and Bochtler, M. (2007). Folds and activities of peptidoglycan amidases. *FEMS Microbiol. Rev.* 31, 676–691. doi: 10.1111/j.1574-6976.2007.00084.x

Frick-Cheng, A. E., Pyburn, T. M., Voss, B. J., McDonald, W. H., Ohi, M. D., and Cover, T. L. (2016). Molecular and structural analysis of the *Helicobacter pylori* cag type IV secretion system core complex. *mBio* 7:e02001-15. doi: 10.1128/mBio.02001-15

Fronzes, R., Schafer, E., Wang, L., Saibil, H. R., Orlova, E. V., and Waksman, G. (2009). Structure of a type IV secretion system core complex. *Science* 323, 266–268. doi: 10.1126/science.1166101

Garcia-Herrero, A., and Vogel, H. J. (2005). Nuclear magnetic resonance solution structure of the periplasmic signalling domain of the TonB-dependent outer membrane transporter FecA from *Escherichia coli*. *Mol. Microbiol.* 58, 1226–1237. doi: 10.1111/j.1365-2958.2005.04889.x

Garza, I., and Christie, P. J. (2013). A putative transmembrane leucine zipper of *Agrobacterium* VirB10 is essential for T-Pilus biogenesis but not type IV secretion. *J. Bacteriol.* 195, 3022–3034. doi: 10.1128/JB.00287-13

Ghosal, D., Chang, Y. W., Jeong, K. C., Vogel, J. P., and Jensen, G. J. (2017). *In situ* structure of the *Legionella* Dot/Icm type IV secretion system by electron cryotomography. *EMBO Rep.* 18, 726–732. doi: 10.15252/embr.201643598

Gillespie, J. J., Phan, I. Q. H., Scheib, H., Subramanian, S., Edwards, T. E., Lehman, S. S., et al. (2015). Structural insight into how bacteria prevent interference between multiple divergent type IV secretion systems. *mBio* 6:e01867-15. doi: 10.1128/mBio.01867-15

Gilmour, M. W., Gunton, J. E., Lawley, T. D., and Taylor, D. E. (2003). Interaction between the IncHI1 plasmid R27 coupling protein and type IV secretion system: TraG associates with the coiled-coil mating pair formation protein TrhB. *Mol. Microbiol.* 49, 105–116. doi: 10.1046/j.1365-2958.2003.03551.x

Gomis-Ruth, F. X., Moncalian, G., de la Cruz, F., and Coll, M. (2002). Conjugative plasmid protein TrwB, an integral membrane type IV secretion system coupling protein. Detailed structural features and mapping of the active site cleft. *J. Biol. Chem.* 277, 7556–7566. doi: 10.1074/jbc.m110462200

Gonzalez-Rivera, C., Bhatty, M., and Christie, P. J. (2016). Mechanism and function of type IV secretion during infection of the human host. *Microbiol. Spectr.* 4:VMBF-0024-2015. doi: 10.1128/microbiolspec.VMBF-0024-2015

Gordon, J. E., Costa, T. R. D., Patel, R. S., Gonzalez-Rivera, C., Sarkar, M. K., Orlova, E. V., et al. (2017). Use of chimeric type IV secretion systems to define contributions of outer membrane subassemblies for contact-dependent translocation. *Mol. Microbiol.* 105, 273–293. doi: 10.1111/mmi.13700

Grohmann, E., Christie, P. J., Waksman, G., and Backert, S. (2017). Type IV secretion in Gram-negative and Gram-positive bacteria. *Mol. Microbiol.* 107, 455–471. doi: 10.1111/mmi.13896

Guglielmini, J., Neron, B., Abby, S. S., Garcillan-Barcia, M. P., de la Cruz, F., and Rocha, E. P. (2014). Key components of the eight classes of type IV secretion systems involved in bacterial conjugation or protein secretion. *Nucleic Acids Res.* 42, 5715–5727. doi: 10.1093/nar/gku194

Hamilton, H. L., Dominguez, N. M., Schwartz, K. J., Hackett, K. T., and Dillard, J. P. (2005). *Neisseria gonorrhoeae* secretes chromosomal DNA via a novel type IV secretion system. *Mol. Microbiol.* 55, 1704–1721. doi: 10.1111/j.1365-2958.2005.04521.x

Hare, S., Bayliss, R., Baron, C., and Waksman, G. (2006). A large domain swap in the VirB11 ATPase of *Brucella suis* leaves the hexameric assembly intact. *J. Mol. Biol.* 360, 56–66. doi: 10.1016/j.jmb.2006.04.060

Harms, A., Liesch, M., Körner, J., Québatte, M., Engel, P., and Dehio, C. (2017). A bacterial toxin-antitoxin module is the origin of inter-bacterial and inter-kingdom effectors of *Bartonella*. *PLoS Genet.* 13:e1007077. doi: 10.1371/journal.pgen.1007077

Hayes, C. S., Koskiniemi, S., Ruhe, Z. C., Poole, S. J., and Low, D. A. (2014). Mechanisms and biological roles of contact-dependent growth inhibition systems. *Cold Spring Harb. Perspect. Med.* 4:a010025. doi: 10.1101/cshperspect.a010025

Hayward, A. C., Fegan, N., Fegan, M., and Stirling, G. R. (2010). *Stenotrophomonas* and Lysobacter: ubiquitous plant-associated gamma-proteobacteria of developing significance in applied microbiology. *J. Appl. Microbiol.* 108, 756–770. doi: 10.1111/j.1365-2672.2009.04471.x

He, Y. Q., Zhang, L., Jiang, B. L., Zhang, Z. C., Xu, R. Q., Tang, D. J., et al. (2007). Comparative and functional genomics reveals genetic diversity and determinants of host specificity among reference strains and a large collection of Chinese isolates of the phytopathogen *Xanthomonas campestris* pv. *campestris*. *Genome Biol.* 8:R218.

Hilbi, H., Nagai, H., Kubori, T., and Roy, C. R. (2017). Subversion of host membrane dynamics by the legionella Dot/Icm type IV secretion system. *Curr. Top. Microbiol. Immunol.* 413, 221–242. doi: 10.1007/978-3-319-75241-9_9

Hofreuter, D., Odenbreit, S., and Haas, R. (2001). Natural transformation competence in *Helicobacter pylori* is mediated by the basic components of a type IV secretion system. *Mol. Microbiol.* 41, 379–391. doi: 10.1046/j.1365-2958.2001.02502.x

Jakubowski, S. J., Kerr, J. E., Garza, I., Krishnamoorthy, V., Bayliss, R., Waksman, G., et al. (2009). *Agrobacterium* VirB10 domain requirements for type IV secretion and T pilus biogenesis. *Mol. Microbiol.* 71, 779–794. doi: 10.1111/j.1365-2958.2008.06565.x

Jakubowski, S. J., Krishnamoorthy, V., Cascales, E., and Christie, P. J. (2004). *Agrobacterium tumefaciens* VirB6 domains direct the ordered export of a DNA substrate through a type IV secretion system. *J. Mol. Biol.* 341, 961–977. doi: 10.1016/j.jmb.2004.06.052

Jensen, R. B., and Gerdes, K. (1995). Programmed cell death in bacteria: proteic plasmid stabilization systems. *Mol. Microbiol.* 17, 205–210. doi: 10.1111/j.1365-2958.1995.mmi_17020205.x

Jones, A. L., Shirasu, K., and Kado, C. I. (1994). The product of the VirB4 gene of *Agrobacterium tumefaciens* promotes accumulation of VirB3 protein. *J. Bacteriol.* 176, 5255–5261. doi: 10.1128/jb.176.17.5255-5261.1994

Kanamaru, S., Leiman, P. G., Kostyuchenko, V. A., Chipman, P. R., Mesyanzhinov, V. V., Arisaka, F., et al. (2002). Structure of the cell-puncturing device of bacteriophage T4. *Nature* 415, 553–557. doi: 10.1038/415553a

Kanehisa, M., Furumichi, M., Tanabe, M., Sato, Y., and Morishima, K. (2017). KEGG: new perspectives on genomes, pathways, diseases and drugs. *Nucleic Acids Res.* 45, D353–D361. doi: 10.1093/nar/gkw1092

Ke, Y., Wang, Y., Li, W., and Chen, Z. (2015). Type IV secretion system of *Brucella* spp. and its effectors. *Front. Cell. Infect. Microbiol.* 5:72. doi: 10.3389/fcimb.2015.00072

Kondou, Y., Kitazawa, D., Takeda, S., Tsuchiya, Y., Yamashita, E., Mizuguchi, M., et al. (2005). Structure of the central hub of bacteriophage Mu baseplate determined by X-ray crystallography of gp44. *J. Mol. Biol.* 352, 976–985. doi: 10.1016/j.jmb.2005.07.044

Korotkov, K. V., Pardon, E., Steyaert, J., and Hol, W. G. (2009). Crystal structure of the N-terminal domain of the secretin GspD from ETEC determined with the assistance of a nanobody. *Structure* 17, 255–265. doi: 10.1016/j.str.2008.11.011

Krogh, A., Larsson, B., von Heijne, G., and Sonnhammer, E. L. (2001). Predicting transmembrane protein topology with a hidden Markov model: application to complete genomes. *J. Mol. Biol.* 305, 567–580. doi: 10.1006/jmbi.2000.4315

Kuroda, T., Kubori, T., Thanh Bui, X., Hyakutake, A., Uchida, Y., Imada, K., et al. (2015). Molecular and structural analysis of *Legionella* DotI gives insights into an inner membrane complex essential for type IV secretion. *Sci. Rep.* 5:10912. doi: 10.1038/srep10912

Lederberg, J., and Tatum, E. L. (1946). Gene recombination in *Escherichia coli*. *Nature* 158:558. doi: 10.1038/158558a0

Lee, B. M., Park, Y. J., Park, D. S., Kang, H. W., Kim, J. G., Song, E. S., et al. (2005). The genome sequence of *Xanthomonas oryzae* pathovar oryzae KACC10331, the bacterial blight pathogen of rice. *Nucleic Acids Res.* 33, 577–586. doi: 10.1093/nar/gki206

Leiman, P. G., Basler, M., Ramagopal, U. A., Bonanno, J. B., Sauder, J. M., Pukatzki, S., et al. (2009). Type VI secretion apparatus and phage tail-associated protein complexes share a common evolutionary origin. *Proc. Natl. Acad. Sci. U.S.A.* 106, 4154–4159. doi: 10.1073/pnas.0813360106

Li, Y. G., and Christie, P. J. (2018). The *Agrobacterium* VirB/VirD4 T4SS: mechanism and architecture defined through in vivo mutagenesis and chimeric systems. *Curr. Top. Microbiol. Immunol.* 418, 233–260. doi: 10.1007/82_2018_94

Llosa, M., and Alkorta, I. (2017). Coupling proteins in type IV secretion. *Curr. Top. Microbiol. Immunol.* 413, 143–168. doi: 10.1007/978-3-319-75241-9_6

Llosa, M., Zunzunegui, S., and de la Cruz, F. (2003). Conjugative coupling proteins interact with cognate and heterologous VirB10-like proteins while exhibiting specificity for cognate relaxosomes. *Proc. Natl. Acad. Sci. U.S.A.* 100, 10465–10470. doi: 10.1073/pnas.1830264100

Llosa, M., Zupan, J., Baron, C., and Zambryski, P. (2000). The N- and C-terminal portions of the *Agrobacterium* VirB1 protein independently enhance tumorigenesis. *J. Bacteriol.* 182, 3437–3445. doi: 10.1128/jb.182.12.3437-3445.2000

Locht, C., Coutte, L., and Mielcarek, N. (2011). The ins and outs of pertussis toxin. *FEBS J.* 278, 4668–4682. doi: 10.1111/j.1742-4658.2011.08237.x

Looney, W. J., Narita, M., and Mühlemann, K. (2009). *Stenotrophomonas maltophilia*: an emerging opportunist human pathogen. *Lancet Infect. Dis.* 9, 312–323. doi: 10.1016/S1473-3099(09)70083-0

Low, H. H., Gubellini, F., Rivera-Calzada, A., Braun, N., Connery, S., Dujeancourt, A., et al. (2014). Structure of a type IV secretion system. *Nature* 508, 550–553. doi: 10.1038/nature13081

Mansfield, J., Genin, S., Magori, S., Citovsky, V., Sriariyanum, M., Ronald, P., et al. (2012). Top 10 plant pathogenic bacteria in molecular plant pathology. *Mol. Plant Pathol.* 13, 614–629. doi: 10.1111/j.1364-3703.2012.00804.x

Marchler-Bauer, A., Derbyshire, M. K., Gonzales, N. R., Lu, S., Chitsaz, F., Geer, L. Y., et al. (2015). CDD: NCBI's conserved domain database. *Nucleic Acids Res.* 43, D222–D226. doi: 10.1093/nar/gku1221

Martins-Pinheiro, M., Galhardo, R. S., Lage, C., Lima-Bessa, K. M., Aires, K. A., and Menck, C. F. M. (2004). Different patterns of evolution for duplicated DNA repair genes in bacteria of the Xanthomonadales group. *BMC Evol. Biol.* 4:29. doi: 10.1186/1471-2148-4-29

Moffatt, J. H., Newton, P., and Newton, H. J. (2015). *Coxiella burnetii*: turning hostility into a home. *Cell. Microbiol.* 17, 621–631. doi: 10.1111/cmi.12432

Moreira, L. M., Almeida, N. F. Jr., Potnis, N., Digiampietri, L. A., Adi, S. S., Bortolossi, J. C., et al. (2010). Novel insights into the genomic basis of citrus canker based on the genome sequences of two strains of *Xanthomonas fuscans* subsp. *aurantifolii*. *BMC Genomics* 11:238. doi: 10.1186/1471-2164-11-238

Mukherjee, P., and Roy, P. (2016). Genomic potential of *Stenotrophomonas maltophilia* in bioremediation with an assessment of its multifaceted role in our environment. *Front. Microbiol.* 7:967. doi: 10.3389/fmicb.2016.00967

Nakai, K., and Horton, P. (1999). PSORT: a program for detecting sorting signals in proteins and predicting their subcellular localization. *Trends Biochem. Sci.* 24, 34–35. doi: 10.1016/S0968-0004(98)01336-X

Nakano, N., Kubori, T., Kinoshita, M., Imada, K., and Nagai, H. (2010). Crystal structure of *Legionella* DotD: insights into the relationship between type IVB and type II/III secretion systems. *PLoS Pathog.* 6:e1001129. doi: 10.1371/journal.ppat.1001129

Naumann, M., Sokolova, O., Tegtmeyer, N., and Backert, S. (2017). *Helicobacter pylori*: a paradigm pathogen for subverting host cell signal transmission. *Trends Microbiol.* 25, 316–328. doi: 10.1016/j.tim.2016.12.004

Naushad, H. S., and Gupta, R. S. (2013). Phylogenomics and molecular signatures for species from the plant pathogen-containing order Xanthomonadales. *PLoS One* 8:e55216. doi: 10.1371/journal.pone.0055216

Naushad, S., Adeolu, M., Wong, S., Sohail, M., Schellhorn, H. E., and Gupta, R. S. (2015). A phylogenomic and molecular marker based taxonomic framework for the order *Xanthomonadales*: proposal to transfer the families *Algiphilaceae* and *Solimonadaceae* to the order *Nevskiales* ord. nov. and to create a new family within the order *Xanthomonadales*, the family *Rhodanobacteraceae* fam. nov., containing the genus *Rhodanobacter* and its closest relatives. *Antonie Van Leeuwenhoek* 107, 467–485. doi: 10.1007/s10482-014-0344-8

Ochiai, H., Inoue, V., Takeya, M., Sasaki, A., and Kaku, H. (2005). Genome sequence of *Xanthomonas oryzae* pv. *oryzae* suggests contribution of large numbers of effector genes and insertion sequences to its race diversity. *Jpn. Agric. Res. Q.* 39, 275–287. doi: 10.6090/jarq.39.275

Oliveira, L. C., Souza, D. P., Oka, G. U., Lima, F., da, S., Oliveira, R. J., et al. (2016). VirB7 and VirB9 interactions are required for the assembly and antibacterial activity of a type IV secretion system. *Structure* 24, 1707–1718. doi: 10.1016/j.str.2016.07.015

Panthee, S., Hamamoto, H., Paudel, A., and Sekimizu, K. (2016). *Lysobacter* species: a potential source of novel antibiotics. *Arch. Microbiol.* 198, 839–845. doi: 10.1007/s00203-016-1278-5

Paschos, A., Patey, G., Sivanesan, D., Gao, C., Bayliss, R., Waksman, G., et al. (2006). Dimerization and interactions of *Brucella suis* VirB8 with VirB4 and VirB10 are required for its biological activity. *Proc. Natl. Acad. Sci. U.S.A.* 103, 7252–7257. doi: 10.1073/pnas.0600862103

Peña, A., Matilla, I., Martín-Benito, J., Valpuesta, J. M., Carrascosa, J. L., De La Cruz, F., et al. (2012). The hexameric structure of a conjugative VirB4 protein ATPase provides new insights for a functional and phylogenetic relationship with DNA translocases. *J. Biol. Chem.* 287, 39925–39932. doi: 10.1074/jbc.M112.413849

Pieretti, I., Royer, M., Barbe, V., Carrere, S., Koebnik, R., Cociancich, S., et al. (2009). The complete genome sequence of *Xanthomonas albilineans* provides new insights into the reductive genome evolution of the xylem-limited *Xanthomonadaceae*. *BMC Genomics* 10:616. doi: 10.1186/1471-2164-10-616

Qian, W., Jia, Y., Ren, S. X., He, Y. Q., Feng, J. X., Lu, L. F., et al. (2005). Comparative and functional genomic analyses of the pathogenicity of phytopathogen *Xanthomonas campestris* pv. *campestris*. *Genome Res.* 15, 757–767. doi: 10.1101/gr.3378705

Qiu, J., and Luo, Z. Q. (2017). *Legionella* and *Coxiella* effectors: strength in diversity and activity. *Nat. Rev. Microbiol.* 15, 591–605. doi: 10.1038/nrmicro.2017.67

Rabel, C., Grahn, A. M., Lurz, R., and Lanka, E. (2003). The VirB4 family of proposed traffic nucleoside triphosphatases: common motifs in plasmid RP4 TrbE are essential for conjugation and phage adsorption. *J. Bacteriol.* 185, 1045–1058. doi: 10.1128/JB.185.3.1045-1058.2003

Redzej, A., Ukleja, M., Connery, S., Trokter, M., Felisberto-Rodrigues, C., Cryar, A., et al. (2017). Structure of a VirD4 coupling protein bound to a VirB type IV secretion machinery. *EMBO J.* 36, 3080–3095. doi: 10.15252/embj.201796629

Ripoll-Rozada, J., Zunzunegui, S., de la Cruz, F., Arechaga, I., and Cabezón, E. (2013). Functional interactions of VirB11 traffic ATPases with VirB4 and VirD4 molecular motors in type IV secretion systems. *J. Bacteriol.* 195, 4195–4201. doi: 10.1128/JB.00437-13

Rivera-Calzada, A., Fronzes, R., Savva, C. G., Chandran, V., Lian, P. W., Laeremans, T., et al. (2013). Structure of a bacterial type IV secretion core complex at subnanometre resolution. *EMBO J.* 32, 1195–1204. doi: 10.1038/emboj.2013.58

Russell, A. B., Hood, R. D., Bui, N. K., LeRoux, M., Vollmer, W., and Mougous, J. D. (2011). Type VI secretion delivers bacteriolytic effectors to target cells. *Nature* 475, 343–347. doi: 10.1038/nature10244

Russell, A. B., LeRoux, M., Hathazi, K., Agnello, D. M., Ishikawa, T., Wiggins, P. A., et al. (2013). Diverse type VI secretion phospholipases are functionally plastic antibacterial effectors. *Nature* 496, 508–512. doi: 10.1038/nature12074

Saddler, G. S., and Bradbury, J. F. (2007). "Xanthomonadales ord. nov," in *Bergey's Manual of Systematic Bacteriology*, eds D. J. Brenner, N. R. Krieg, J. T. Staley, G. M. Garrity, D. R. Boone, P. Vos, et al. (Boston, MA: Springer). doi: 10.1007/0-387-28022-7_3

Salzberg, S., Schatz, M., Delcher, A., Roberts, M., Rabinowicz, P., Inman, J., et al. (2007). *Xanthomonas oryzae* pv. oryzicola BLS256, whole genome shotgun sequencing project. Submitt. to GenBank database (AAQN00000000.1).

Salzberg, S. L., Sommer, D. D., Schatz, M. C., Phillippy, A. M., Rabinowicz, P. D., Tsuge, S., et al. (2008). Genome sequence and rapid evolution of the rice pathogen *Xanthomonas oryzae* pv. *oryzae* PXO99A. *BMC Genomics* 9:204. doi: 10.1186/1471-2164-9-204

Schmidt-Eisenlohr, H., Domke, N., Angerer, C., Wanner, G., Zambryski, P. C., and Baron, C. (1999). Vir proteins stabilize VirB5 and mediate its association with the T pilus of *Agrobacterium tumefaciens*. *J. Bacteriol.* 181, 7485–7492.

Segura, R. L., Águila-Arcos, S., Ugarte-Uribe, B., Vecino, A. J., De La Cruz, F., Goñi, F. M., et al. (2013). The transmembrane domain of the T4SS coupling protein TrwB and its role in protein-protein interactions. *Biochim. Biophys. Acta* 1828, 2015–2025. doi: 10.1016/j.bbamem.2013.05.022

Sexton, J. A., and Vogel, J. P. (2002). Type IVB secretion by intracellular pathogens. *Traffic* 3, 178–185. doi: 10.1034/j.1600-0854.2002.030303.x

Sgro, G. G., Costa, T. R. D., Cenens, W., Souza, D. P., Cassago, A., Coutinho de Oliveira, L., et al. (2018). Cryo-EM structure of the bacteria-killing type IV secretion system core complex from *Xanthomonas citri*. *Nat. Microbiol.* 3, 1429–1440. doi: 10.1038/s41564-018-0262-z

Siamer, S., and Dehio, C. (2015). New insights into the role of *Bartonella* effector proteins in pathogenesis. *Curr. Opin. Microbiol.* 23, 80–85. doi: 10.1016/j.mib.2014.11.007

Sivanesan, D., Hancock, M. A., Villamil Giraldo, A. M., and Baron, C. (2010). Quantitative analysis of VirB8-VirB9-VirB10 interactions provides a dynamic model of type IV secretion system core complex assembly. *Biochemistry* 49, 4483–4493. doi: 10.1021/bi902201y

Souza, D. P., Andrade, M. O., Alvarez-Martinez, C. E., Arantes, G. M., Farah, C. S., and Salinas, R. K. (2011). A component of the Xanthomonadaceae type IV secretion system combines a VirB7 motif with a N0 domain found in outer membrane transport proteins. *PLoS Pathog.* 7:e1002031. doi: 10.1371/journal.ppat.1002031

Souza, D. P., Oka, G. U., Alvarez-Martinez, C. E., Bisson-Filho, A. W., Dunger, G., Hobeika, L., et al. (2015). Bacterial killing via a type IV secretion system. *Nat. Commun.* 6:6453. doi: 10.1038/ncomms7453

Spagnuolo, J., Opalka, N., Wen, W. X., Gagic, D., Chabaud, E., Bellini, P., et al. (2010). Identification of the gate regions in the primary structure of the secretin pIV. *Mol. Microbiol.* 76, 133–150. doi: 10.1111/j.1365-2958.2010.07085.x

Spreter, T., Yip, C. K., Sanowar, S., Andre, I., Kimbrough, T. G., Vuckovic, M., et al. (2009). A conserved structural motif mediates formation of the periplasmic rings in the type III secretion system. *Nat. Struct. Mol. Biol.* 16, 468–476. doi: 10.1038/nsmb.1603

Studholme, D. J., Kemen, E., Maclean, D., Schornack, S., Aritua, V., Thwaites, R., et al. (2010). Genome-wide sequencing data reveals virulence factors implicated in banana *Xanthomonas* wilt. *FEMS Microbiol. Lett.* 310, 182–192. doi: 10.1111/j.1574-6968.2010.02065.x

Terradot, L., Bayliss, R., Oomen, C., Leonard, G. A., Baron, C., and Waksman, G. (2005). Structures of two core subunits of the bacterial type IV secretion system, VirB8 from *Brucella suis* and ComB10 from *Helicobacter pylori*. *Proc. Natl. Acad. Sci. U.S.A.* 102, 4596–4601. doi: 10.1073/pnas.0408927102

Thieme, F., Koebnik, R., Bekel, T., Berger, C., Boch, J., Buttner, D., et al. (2005). Insights into genome plasticity and pathogenicity of the plant pathogenic bacterium *Xanthomonas campestris* pv. vesicatoria revealed by the complete genome sequence. *J. Bacteriol.* 187, 7254–7266. doi: 10.1128/JB.187.21.7254-7266.2005

Tzfira, T., and Citovsky, V. (2006). Agrobacterium-mediated genetic transformation of plants: biology and biotechnology. *Curr. Opin. Biotechnol.* 17, 147–154. doi: 10.1016/j.copbio.2006.01.009

Van Herreweghe, J. M., Vanderkelen, L., Callewaert, L., Aertsen, A., Compernolle, G., Declerck, P. J., et al. (2010). Lysozyme inhibitor conferring bacterial tolerance to invertebrate type lysozyme. *Cell. Mol. Life Sci.* 67, 1177–1188. doi: 10.1007/s00018-009-0241-x

Van Sluys, M. A., Monteiro-Vitorello, C. B., Camargo, L. E. A., Menck, C. F. M., da Silva, A. C., Ferro, J. A., et al. (2002). Comparative genomic analysis of plant-associated bacteria. *Annu. Rev. Phytopathol.* 40, 169–189. doi: 10.1146/annurev.phyto.40.030402.090559

Villamil Giraldo, A. M., Mary, C., Sivanesan, D., and Baron, C. (2015). VirB6 and VirB10 from the *Brucella* type IV secretion system interact via the N-terminal periplasmic domain of VirB6. *FEBS Lett.* 589, 1883–1889. doi: 10.1016/j.febslet.2015.05.051

Villamil Giraldo, A. M., Sivanesan, D., Carle, A., Paschos, A., Smith, M. A., Plesa, M., et al. (2012). Type IV secretion system core component VirB8 from *Brucella* binds to the globular domain of VirB5 and to a periplasmic domain of VirB6. *Biochemistry* 51, 3881–3890. doi: 10.1021/bi300298v

Vorholter, F. J., Schneiker, S., Goesmann, A., Krause, L., Bekel, T., Kaiser, O., et al. (2008). The genome of *Xanthomonas campestris* pv. campestris B100 and its use for the reconstruction of metabolic pathways involved in xanthan biosynthesis. *J. Biotechnol.* 134, 33–45. doi: 10.1016/j.jbiotec.2007.12.013

Waksman, G. (2019). From conjugation to T4S systems in Gram-negative bacteria: a mechanistic biology perspective. *EMBO Rep.* 20:e47012. doi: 10.15252/embr.201847012

Wasukira, A., Tayebwa, J., Thwaites, R., Paszkiewicz, K., Aritua, V., Kubiriba, J., et al. (2012). Genome-wide sequencing reveals two major sub-lineages in the genetically monomorphic pathogen *Xanthomonas campestris* pathovar musacearum. *Genes* 3, 361–377. doi: 10.3390/genes3030361

Whitaker, N., Chen, Y., Jakubowski, S. J., Sarkar, M. K., Li, F., and Christie, P. J. (2015). The all-alpha domains of coupling proteins from the *Agrobacterium tumefaciens* VirB/VirD4 and *Enterococcus faecalis* pCF10-encoded type IV secretion systems confer specificity to binding of cognate DNA substrates. *J. Bacteriol.* 197, 2335–2349. doi: 10.1128/JB.00189-15

Yeo, H. J., Savvides, S. N., Herr, A. B., Lanka, E., and Waksman, G. (2000). Crystal structure of the hexameric traffic ATPase of the *Helicobacter pylori* type IV secretion system. *Mol. Cell* 6, 1461–1472. doi: 10.1016/s1097-2765(00)00142-8

Zhang, L., Wang, X., Yu, M., Qiao, Y., and Zhang, X. H. (2015). Genomic analysis of *Luteimonas abyssi* XH031(T): insights into its adaption to the subseafloor environment of South Pacific Gyre and ecological role in biogeochemical cycle. *BMC Genomics* 16:1092. doi: 10.1186/s12864-015-2326-2

Conflict of Interest Statement: The authors declare that the research was conducted in the absence of any commercial or financial relationships that could be construed as a potential conflict of interest.

Copyright © 2019 Sgro, Oka, Souza, Cenens, Bayer-Santos, Matsuyama, Bueno, dos Santos, Alvarez-Martinez, Salinas and Farah. This is an open-access article distributed under the terms of the Creative Commons Attribution License (CC BY). The use, distribution or reproduction in other forums is permitted, provided the original author(s) and the copyright owner(s) are credited and that the original publication in this journal is cited, in accordance with accepted academic practice. No use, distribution or reproduction is permitted which does not comply with these terms.

frontiers in Microbiology

REVIEW
published: 22 May 2019
doi: 10.3389/fmicb.2019.01134

Regulation of Gram-Positive Conjugation

*Verena Kohler[1], Walter Keller[1] and Elisabeth Grohmann[2]**

[1]Institute of Molecular Biosciences, BioTechMed Graz, University of Graz, Graz, Austria, [2]Life Sciences and Technology, Beuth University of Applied Sciences Berlin, Berlin, Germany

Type IV Secretion Systems (T4SSs) are membrane-spanning multiprotein complexes dedicated to protein secretion or conjugative DNA transport (conjugation systems) in bacteria. The prototype and best-characterized T4SS is that of the Gram-negative soil bacterium *Agrobacterium tumefaciens*. For Gram-positive bacteria, only conjugative T4SSs have been characterized in some biochemical, structural, and mechanistic details. These conjugation systems are predominantly encoded by self-transmissible plasmids but are also increasingly detected on integrative and conjugative elements (ICEs) and transposons. Here, we report regulatory details of conjugation systems from *Enterococcus* model plasmids pIP501 and pCF10, *Bacillus* plasmid pLS1, *Clostridium* plasmid pCW3, and staphylococcal plasmid pSK41. In addition, regulation of conjugative processes of ICEs (ICE*Bs*1, ICE*St*1, ICE*St*3) by master regulators belonging to diverse repressor families will be discussed. A special focus of this review lies on the comparison of regulatory mechanisms executed by proteins belonging to the RRNPP family. These regulators share a common fold and govern several essential bacterial processes, including conjugative transfer.

Keywords: Gram-positive bacteria, type IV secretion system, conjugation system, regulation, plasmid, integrative and conjugative element

OPEN ACCESS

Edited by:
Eric Cascales,
Aix-Marseille Université, France

Reviewed by:
Joshua Peter Ramsay,
Curtin University, Australia
Keith Weaver,
University of South Dakota, United States

****Correspondence:***
Elisabeth Grohmann
egrohmann@beuth-hochschule.de

Specialty section:
This article was submitted to Microbial Physiology and Metabolism, a section of the journal Frontiers in Microbiology

Received: *01 March 2019*
Accepted: *03 May 2019*
Published: *22 May 2019*

Citation:
Kohler V, Keller W and Grohmann E (2019) Regulation of Gram-Positive Conjugation. Front. Microbiol. 10:1134. doi: 10.3389/fmicb.2019.01134

INTRODUCTION

Horizontal gene transfer (HGT) is leadingly involved not only in the evolution of bacteria but also in the dissemination of antibiotic resistances and pathogenicity determinants. This process can be subdivided into three mechanisms: transformation, transduction, and conjugation (Daubin and Szöllősi, 2016), with the latter being the most common type involved in spreading of traits that are beneficial under distinct environmental conditions (Davies and Davies, 2010; Sultan et al., 2018). Conjugative transport of DNA from a donor to a recipient cell requires direct cell-to-cell contact and the formation of a pore, where the DNA molecule can be transported through (Perry and Wright, 2013). Conjugation has been described over large taxonomic distances between unrelated bacterial species (Tamminen et al., 2012). Two different conjugative mechanisms are known to date: the transport of single-stranded (ss) DNA, found in both Gram-positive (G+) and Gram-negative (G−) systems vs. the transport of double-stranded DNA. The second mechanism has been described for G+ actinomycetes, and recent work summarizes this process extensively (Thoma and Muth, 2016; Pettis, 2018). Factors needed for conjugative processes can be encoded on plasmids or integrative and conjugative elements (ICEs). The basic mechanism of conjugation is conserved in most G+ conjugative

systems, which facilitate the transport of ss-DNA *via* a molecular machinery encoded by multiple genes that are mostly organized in a single operon. These systems comprise a relaxase, a coupling protein and a mating pair formation (MPF) complex. Relaxases are essential factors in the process of conjugative transfer. They initiate the process by site- and strand-specific cleavage at the *nic*-site of the origin of transfer (*oriT*), forming a covalent complex with the cleaved DNA. For G+ systems, only two relaxases have been structurally characterized so far (Edwards et al., 2013; Pluta et al., 2017). Together with potential accessory factors, the relaxase-DNA complex is called the relaxosome. The coupling protein brings the relaxosome to the MPF complex that forms the actual channel. Conjugation systems usually consist of several mating pair formation proteins, one or more ATPases and proteins facilitating the contact with recipients. In contrast to G-systems that rely on conjugative pili, the contact between donor and recipient is formed *via* surface adhesins in G+ systems. Simultaneously with transfer processes, DNA replication ensures that both donor and new host have a double-stranded version of the plasmid or ICE (Guglielmini et al., 2011; Grohmann et al., 2017).

Transfer of DNA *via* conjugative processes needs to be stringently regulated to reduce the metabolic burden on the host (Koraimann and Wagner, 2014; Singh and Meijer, 2014). Thus, gene products required for conjugation are either kept in a default "OFF" state and are induced by signaling molecules from potential recipients/the environment or conjugative genes are constitutively produced at low abundance to keep fitness costs for the host at a minimum (Frost and Koraimann, 2010; Bañuelos-Vazquez et al., 2017; Stingl and Koraimann, 2017). In this review, we will summarize the current knowledge on the regulation of conjugative processes, focusing on selected conjugation systems from G+ bacteria.

PLASMIDS VS. INTEGRATIVE AND CONJUGATIVE ELEMENTS: SIMILARITIES AND DIFFERENCES

Conjugative plasmids and ICEs harbor all necessary genetic information for conjugative transfer processes (Bañuelos-Vazquez et al., 2017). The principal difference between conjugative plasmids and ICEs lies in their respective maintenance mechanisms within a bacterial cell. While plasmids replicate autonomously, ICEs must integrate into bacterial chromosomes for stable inheritance (**Figure 1**; Perry and Wright, 2013; Burrus, 2017).

Plasmids are autonomously replicating elements that can be categorized into incompatibility (Inc) groups according to their replication and partitioning systems. The spreading of plasmids between unrelated genera is involved in the emergence of antibiotic-resistant bacteria (Sultan et al., 2018). These elements generally carry non-essential genetic features, which might become important under distinct environmental conditions, e.g. in the presence of antibiotic selection pressure (Bañuelos-Vazquez et al., 2017). Plasmids that carry all necessary factors for mobilization and transfer processes are denoted as self-transmissible or conjugative. Biofilm formation plays a substantial role in transfer and dissemination of conjugative plasmids. Conjugative transfer was shown to be considerably higher in biofilms (Kelly et al., 2009).

ICEs are omnipresent in bacterial genomes and were found to be the most abundant conjugative elements in prokaryotes (Ghinet et al., 2011; Guglielmini et al., 2011; Guédon et al., 2017). The exact processes of ICE conjugation are not completely elucidated. It is supposed that these events resemble the ss-plasmid DNA shuttling *via* conjugation systems encoded on plasmids. Since two additional steps, excision and re-integration, are required, ICEs harbor genes that resemble factors of lysogenic phages (Wozniak and Waldor, 2010). These elements show a modular structure with genes of the same/similar function clustered together and usually consist of a maintenance module (responsible for integration and excision), a dissemination module (required for conjugative transfer), and a regulation module (Burrus and Waldor, 2004). An integrated ICE shows a behavior reminiscent of prophages, with most mobility genes suppressed and passively inherited along with the chromosome. Depending on the ICE family, an intra-/intercellular/environmental signal triggers its excision and formation of a circular plasmid-like form, serving as a substrate for the conjugative transfer machinery. After successful transport, the ICE re-integrates into the recipient's chromosome. Integration into and excision from the host chromosome are catalyzed by dedicated enzymes. An integrase (frequently a tyrosine recombinase) governs the reaction between a sequence of the recombination module of the ICE (*attP*) and a sequence on the host chromosome (*attB*), yielding the attachment sites (*attL* and *attR*) that border the ICE after successful integration. In most cases, an excisionase aids in reverting this reaction, forming again an *attP* site on the circularized ICE and an *attB* site on the host's chromosome. As plasmids, ICEs also harbor genes beneficial for their host under specific conditions, e.g. mediating resistance to antimicrobial drugs, heavy metals, and infections by phages (Burrus and Waldor, 2004; Burrus, 2017).

SELECTED MOBILE GENETIC ELEMENTS AND THEIR REGULATION OF CONJUGATIVE PROCESSES

The following sections concentrate on selected plasmids or ICEs from different G+ species, ranging from broad-host range plasmids that produce their conjugative systems constitutively at low levels to inducible/repressible plasmids responding to stimuli from small peptides, called pheromones or autoinducers. These small peptides frequently regulate cellular signaling processes according to the population density, a process denoted as quorum sensing (QS). QS is described to govern essential processes, like virulence, sporulation, and gene transfer. It enables bacteria to sense information about the surrounding species composition and to adapt their expression profiles. This process encompasses the production, release, and detection of autoinducers, the latter is done by a specific sensor component

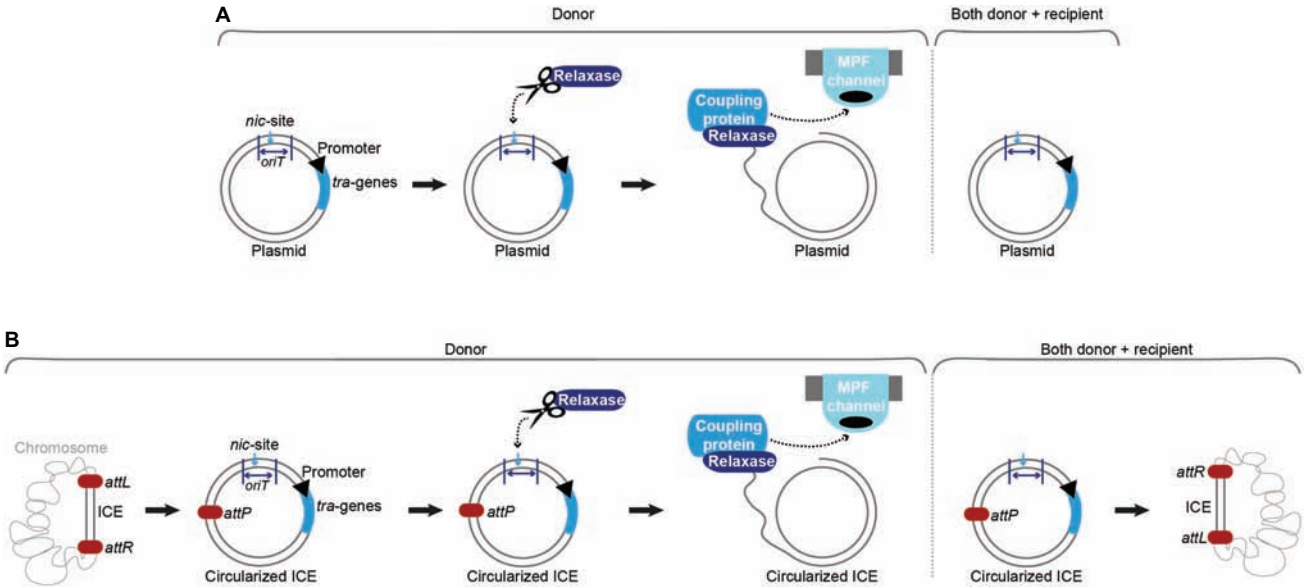

FIGURE 1 | Conjugation of plasmids and integrative and conjugative elements (ICEs). **(A)** Upon a signal (internal or external), the relaxase introduces a single-strand (ss) break at the *nic*-site of the origin of transfer (*oriT*) in the donor cell and covalently binds the ss-DNA. The coupling protein interacts with the relaxosome (relaxase, accessory factors and ss-plasmid DNA) and brings the relaxase-DNA complex to the mating pair formation (MPF) channel. The ss-DNA (most likely covalently bound by the relaxase) is shuttled to the recipient cell. In parallel, replication processes ensure that both donor and recipient harbor a double-stranded version of the conjugative plasmid. **(B)** With the aid of an excisionase and an integrase, the integrative and conjugative element (ICE) is excised from the host's chromosome at *attL* and *attR* attachment sites, forming an *attP* site on the circularized ICE and an *attB* site on the bacterial chromosome. Processing of the DNA, transport and replication follow a comparable mechanism as described for conjugative plasmids in **(A)**. After successful conjugation and replication, the ICE is again integrated into the host's chromosome.

(Papenfort and Bassler, 2016). G+ bacteria usually use oligopeptides as signaling molecules, and the receptor protein interacts directly with the signaling peptide (Monnet et al., 2016). Once a certain level of the pheromone (the quorum) in the external environment is reached, a target sensor kinase or a response regulator is either activated or repressed. Downstream processes then lead to altered expression of QS-dependent genes (Rocha-Estrada et al., 2010).

Pheromone-sensor receptors of the RRNPP-family are found in distantly related G+ bacteria among others on plasmids and ICEs harboring conjugation systems (e.g. pCF10, pLS20 and ICE*Bs*1) (Perez-Pascual et al., 2016). This protein family is named after its prototypical members, Rap, Rgg, NprR, PlcR, and PrgX that despite low sequence homology displays remarkable structural similarities. The defining feature of this group is the C-terminal domain that directly interacts with the pheromone and forms a tetratricopeptide repeat (TPR) domain-like conformation. Structural characterization of these receptors revealed a right-handed super-helical architecture, where the respective ligand is bound to an inner concave binding site of the helix-turn-helix (HTH) repeats (Zeytuni and Zarivach, 2012; Do and Kumaraswami, 2016).

An additional unifying feature of these sensor receptors is the structure of the secreted signaling peptides that are usually linear, 5–10 amino acids long, unmodified, and produced from a longer precursor protein. Pheromones are synthesized *via* the conventional path of ribosomal translation, processing/cleavage, and secretion. Since RRNPP sensor receptors are present inside a cell, the secreted pheromone must be taken up *via* oligopeptide permeases. These enzymes are sometimes aided by accessory proteins that provide high selectivity for the respective peptide (e.g. PrgZ of pCF10; Leonard et al., 1996; Neiditch et al., 2017).

Sex-Pheromone Responsive Plasmid pCF10 From *Enterococcus faecalis*

An increasing number of clinical *E. faecalis* isolates carry conjugative plasmids that are transferred upon induction of peptide pheromones and code for antibiotic resistances (Dunny and Berntsson, 2016). Sex-pheromone responsive plasmids include the tetracycline-resistance plasmid pCF10, one of the best-characterized representatives of this plasmid family, and pAD1. Both plasmids serve as model systems for pheromone-responsive conjugative systems in enterococci (Chen et al., 2017).

prgQ is the conjugative operon of pCF10. It consists of three cassettes. One cassette encodes three surface adhesins required for contacting recipients and *prgU* (Bhatty et al., 2017), encoding a regulator that will be described in further details below. The second cassette harbors the Prg/Pcf MPF and the third cassette codes for factors required for processing the pCF10 plasmid DNA. Several transcriptional and post-transcriptional processes regulate the expression of the *prgQ*

operon to guarantee strict control of the Prg/Pcf conjugation system assembly and conjugative transfer (Johnson et al., 2010).

The transcriptional regulator PrgX that belongs to the RRNPP-family binds to the P_Q promoter and represses transcription (**Figure 2A**; Nakayama et al., 1994; Kozlowicz et al., 2004). PrgX further controls its own expression. Unlike other QS-systems (including the Rap-Phr cassettes from pLS20 and ICE*Bs1*), the signal that is sensed by PrgX originates from two different cell types (donor and recipient). This enables the plasmid donor to control conjugation in response to recipient population density (Kozlowicz et al., 2006). PrgX can bind two different heptapeptides, the inducer peptide cCF10 produced from *ccfA* on the bacterial chromosome and the inhibitor iCF10 that is encoded on pCF10 plasmid solely in donor cells (Antiporta and Dunny, 2002). Both inducer and inhibitor peptides are produced by cleavage of precursor proteins, secreted, and imported by the peptide-binding protein PrgZ and chromosomally encoded permeases (Leonard et al., 1996). Inside cells, these pheromones compete for PrgX binding, as both bind to the same cleft within the PrgX C-terminal dimerization domain while interacting with different residues (**Figure 3**; Shi et al., 2005). Interestingly, in contrast to canonical transcription factors that are usually low abundant and modulated by higher-abundant ligands, pCF10-harboring cells usually display an excess of PrgX (15-fold excess of PrgX to its binding site), while the pheromones are present at low concentrations (Mori et al., 1988; Nakayama et al., 1994; Caserta et al., 2012). While its apo-form is indeed able to bind DNA and repress P_Q transcriptional activity at high protein concentrations, PrgX complexed with both the inducer peptide as well as the inhibitor peptide leads to shifted/supershifted DNA complexes with much higher affinities than the unbound form (Caserta et al., 2012; Chen et al., 2017). Thus, following the import of inhibitor/inducer peptide, DNA-bound apo-PrgX is replaced by its complexed form. It is further suggested that the binding affinity of the pheromone (both inhibitor and inducer peptide) for

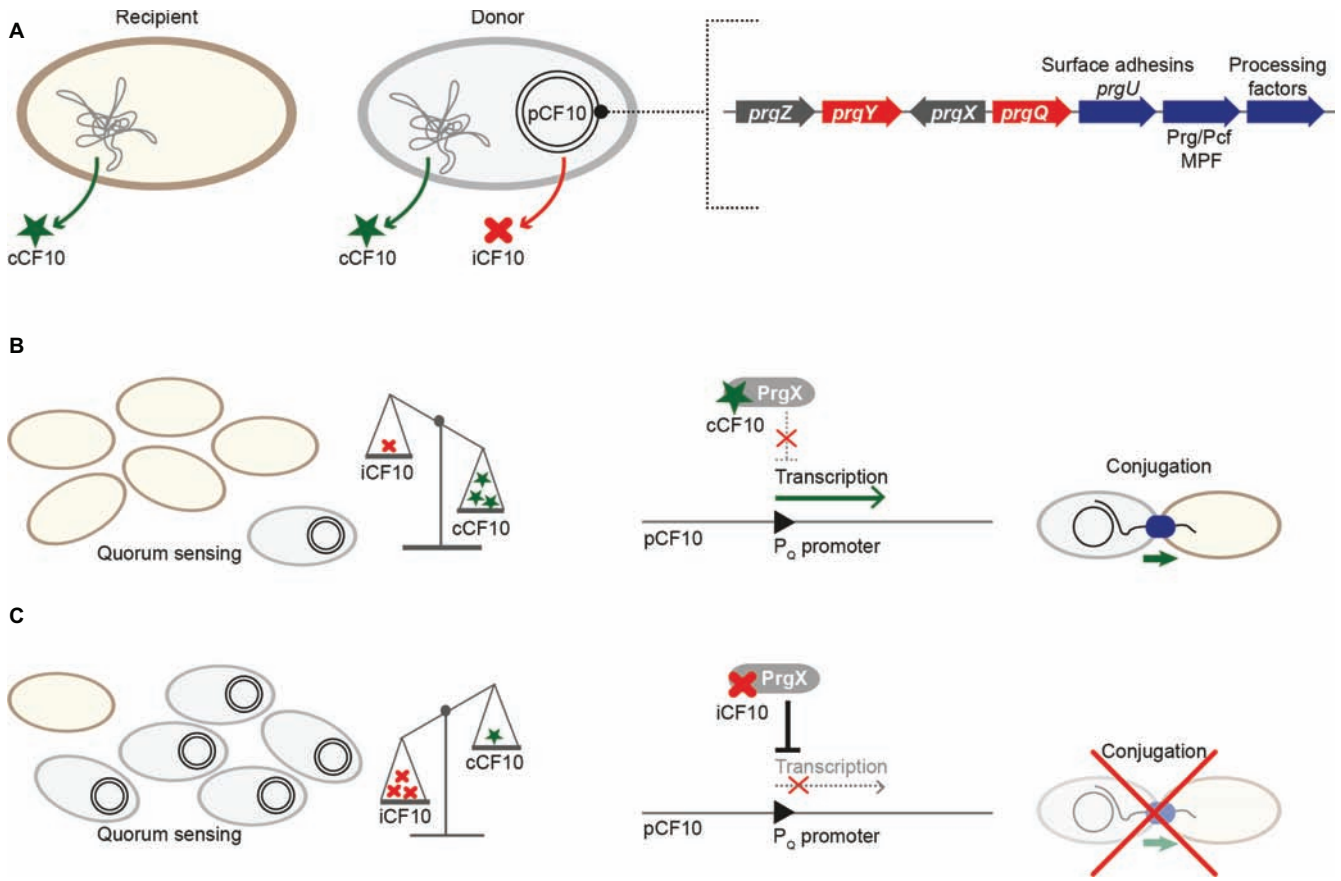

FIGURE 2 | Regulation of pCF10 conjugative transfer. **(A)** While both recipient and donor cell produce the pheromone cCF10 from *ccfA* on the chromosome, only cells harboring pCF10 secrete the inhibitor iCF10 that is produced from *prgQ*. *prgQ* lies upstream of the three cassettes responsible for conjugative transfer: The first cassette codes for the surface adhesins PrgA, PrgB, and PrgC and the regulator PrgU, the second harbors members of the Prg/Pcf conjugation system, and the third is composed of genes for processing factors (including the relaxase). The RRNPP-family protein PrgX is the master regulator and PrgY aids in reducing cCF10 pheromone activity. *prgZ* codes for a permease that imports both cCF10 and iCF10. **(B)** The relative ratio between cCF10 and iCF10 increases with a higher proportion of potential recipients present. This leads to increased import of cCF10, which binds to PrgX, thus interfering with its ability to repress the P_Q promoter. Transcription of genes required for conjugative transfer is activated, and conjugation takes place. **(C)** The cCF10/iCF10 ratio decreases with a lower proportion of potential recipients present, which leads to increased import of the inhibitor peptide iCF10. iCF10-PrgX complexes repress the P_Q promoter, thus downregulating transcription of genes required for conjugative transfer and ultimately inhibiting conjugation.

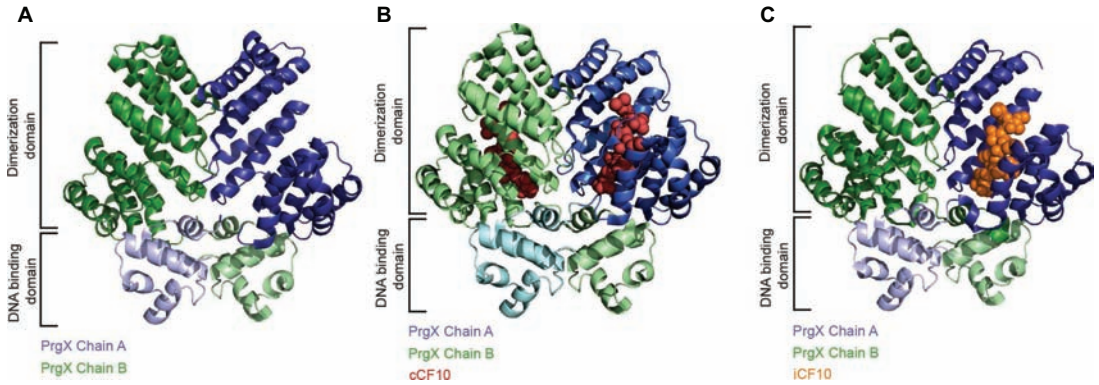

FIGURE 3 | Structural basis for the regulation of the P_Q promoter. **(A)** The PrgX protein forms tetramers, which repress transfer gene expression by binding to two adjacent operator sites, one of which overlaps with the P_Q promoter. The tetramer is built as a dimer of dimers with each dimer occupying one operator site with the N-terminal DNA-binding domain, whereas the C-terminal domain accommodates the dimerization and pheromone-binding function. The dimer of apo-PrgX (PDB: 2AXU) is shown in a cartoon presentation with the chains colored in blue and green, respectively. **(B)** Binding of the pheromone cCF10 (red spheres) leads to a conformational change in the C-terminal region of PrgX (PDB: 2AXZ), alleviating the repression of the P_Q promoter. **(C)** A surplus of iCF10 (orange spheres), which competes with cCF10 for the same binding site (PDB: 2GRL), reinstates the repressed state of the P_Q promoter.

PrgX is considerably stronger than that of complexed PrgX to its DNA binding site. Thus, changes of the donor's induction state most likely come from the exchange of the PrgX apoform for a complexed PrgX form on the DNA (Chen et al., 2017). X-ray crystallography revealed that PrgX exists as a tetramer formed by two dimers. PrgX dimers bind to two operators present on pCF10, O1 and O2. Thus, it has been proposed that the two dimers bound to O1 and O2 interact with each other and form a stable DNA loop. This DNA loop restrains the RNA polymerase from accessing the *prgQ* promoter. When cCF10 binds to the C-terminal domain of PrgX, conformational changes of PrgX are induced. These structural alterations are suggested to break up the tetramers, thus allowing the polymerase to bind to the *prgQ* promoter. By contrast, while iCF10 is thought to compete with cCF10 for the binding site, the inhibitor peptide most likely does not induce structural changes and the tetramer should not be destabilized (Shi et al., 2005). Since the iCF10 precursor is encoded within the *prgQ* locus, enhanced transcription from the *prgQ* promoter increases iCF10 levels, resulting in repression of the transcription of the *prgQ* locus (Kozlowicz et al., 2006). Interestingly, in contrast to other Rap protein-dependent pheromones, neither cCF10 nor iCF10 harbors a positively charged amino acid at the second position (Rocha-Estrada et al., 2010).

In the absence of inducer pheromone sensing, several mechanisms control transcription of the *prgQ* operon (Bae et al., 2004). These comprise PrgX-mediated repression of the P_Q promoter, elevated PrgX repression by binding of the small inhibitor peptide iCF10 that is expressed from a gene directly downstream of the P_Q promoter and production of *anti-Q*, an antisense RNA produced from the convergent P_X promoter, that binds *prgQ* transcripts and induces formation of a termination structure, which blocks transcriptional elongation of *prgQ* transcripts (Nakayama et al., 1994; Shokeen et al., 2010; Chatterjee et al., 2013). Uninduced donor cells show transcriptional activity of the *prgQ* promoter, leading to short (approximately 380 nucleotide long) transcripts. Upon cCF10 binding to PrgX and destabilization of the PrgX tetramer, the number of short *prgQ* transcripts increases, leading to transcription of the whole operon. Within the first 30 min of cCF10 pheromone-exposure, donor cells synthesize the Prg/Pcf conjugation system, form intercellular aggregates due to production of PrgB, one of the surface adhesins, and transfer pCF10 at high frequencies with up to one transconjugant per recipient (**Figure 2B**). In the following 1–2 h, *prgQ* transcription returns to pre-induction levels (Hirt et al., 2005; Chatterjee et al., 2013). Two processes ensure that pCF10-harboring cells do not undergo self-induction. PrgY, a plasmid-encoded membrane protein, reduces pheromone activity produced by donor cells. The extracellular domain of PrgY was proposed to interact with and modify/degrade cCF10 heptapeptides, thus reducing endogenous pheromone activity in donor cells (Chandler et al., 2005). Residual pheromone activity is neutralized by the inhibitor peptide iCF10 encoded by *prgQ* (Nakayama et al., 1994). This inhibitor not only plays a crucial role in returning induced donor cells to the pre-induction state but also serves as a sensor of donor cell density (**Figure 2C**; Chatterjee et al., 2013). After 30–60 min, iCF10 levels reach a certain threshold and consequently reduce transcriptional activity to pre-induction levels. Genes located between *prgQ* and *prgA* (e.g., *prgR*, *prgS*) code for factors modulating transcription and translation of genes required for conjugation (Chung and Dunny, 1992; Bensing et al., 1997).

It was recently demonstrated that cCF10 induction is highly toxic for cells without *prgU*, a small gene downstream of *prgB*, encoding an essential surface adhesin (Bhatty et al., 2017). These *prgU* mutants displayed impaired cell envelope integrity and overproduction of Prg adhesins. By contrast, PrgU overproduction rendered cells insensitive to the sex pheromone and blocked surface adhesin production. PrgU was found to belong to a novel class of RNA binding regulators, reducing toxicity by overproduced surface adhesins. Thus, PrgU exerts another layer of negative regulation of pCF10 conjugative

processes. Modeling studies showed that PrgU most likely exists as a tetramer and comprises a PUA (pseudouridine synthase and archaeosine transglycosylase) fold, domains widely distributed and usually interacting with RNA substrates (Pérez-Arellano et al., 2007). Thus, it is hypothesized that PrgU controls Prg adhesin production by binding of RNA substrates, likely regulating trans-acting sRNAs or *prgQ* transcripts. Interestingly, *prgB-prgU* gene pairs were identified in many *E. faecalis* strains and several other enterococci and staphylococci, suggesting that this genetic linkage has evolved to regulate the production of PrgB-like adhesins (Bhatty et al., 2017).

pLS20 From *Bacillus subtilis*

pLS20 is a 65-kbp conjugative plasmid originally isolated from *B. subtilis natto*. It was shown to considerably influence the physiology of its host, e.g. by inhibition of natural competence by the plasmid-encoded repressor ComK (Singh et al., 2012). An operon encoding more than 40 genes responsible for conjugative processes lies downstream of a divergently oriented gene, encoding Rco_{LS20}, the master regulator that keeps conjugative processes in a default "OFF" state, reminiscent of PrgX from pCF10 (**Figure 4A**). Activation of conjugation requires the RRNPP-family protein Rap_{LS20}, the anti-repressor, which is regulated by the signaling pentapeptide Phr^*_{LS20}. Conjugative transfer of pLS20 takes place only during exponential growth (Itaya et al., 2006). pLS20-encoded conjugative proteins are regulated on three levels: first, expression of conjugative proteins and the key transcriptional regulator Rco_{LS20} is controlled by two overlapping divergent promoters of different strengths. Second, Rco_{LS20} exerts three different functions. It is not only a repressor of the main promoter but also an autoregulator of its own promoter, either negatively or positively depending on its abundance. Third, a DNA loop is formed by binding of tetrameric Rco_{LS20} to two operators, overlapping with the divergent promoters (**Figure 4B**; Ramachandran et al., 2014). This scenario is similar to that described for PrgX in the pCF10 system. In contrast to sex-pheromone responsive plasmids like pCF10, pLS20 is not activated by recipient's signaling (*via* an activator peptide like cCF10), but by factors encoded on the plasmid itself. A Rap-Phr module regulates the transfer of pLS20 (Singh et al., 2013). Most Rap-Phr cassettes known to date govern processes like sporulation, competence, or protease/antibiotic synthesis, where the RRNPP-family protein Rap inhibits these events by interacting with a factor required for activating genes involved in these processes. The *phr* gene codes for a protein that is processed into a penta/hexapeptide after Sec-dependent secretion. Following re-uptake, the peptide binds and inactivates its cognate Rap protein (Pottathil and Lazazzera, 2003). The anti-repressor Rap_{LS20} directly binds to the helix-turn-helix domain of Rco_{LS20} in an equimolar stoichiometry, thus most likely interfering with DNA binding of Rco_{LS20} (**Figure 4C**). The pheromone Phr^*_{LS20}, produced as a precursor molecule, directly interacts with Rap_{LS20}, inducing a conformational change of this regulator, which leads to dissociation from Rco_{LS20} (**Figure 4D**). This pheromone is secreted and re-imported into the cells; thus, it is a signal that underlies cell density (Rösch and Graumann, 2015). Interestingly, in contrast to pheromone-induction of pCF10 and processes where QS activates gene expression, genes required for pLS20 conjugation are repressed when the signaling molecule produced by the conjugative plasmid itself reaches a certain quorum. Consequently, when a large number of donor cells is present in the population and thus high levels of the pheromone Phr^*_{LS20}, conjugative processes are inhibited, while plasmid dissemination is activated when more recipient cells are around (and thus lower pheromone levels; Singh and Meijer, 2014). Further, Phr^*_{LS20} plays an essential role in returning conjugative processes to the default "OFF"-state (Singh et al., 2013). This results in heterogeneity of the bacterial population, where up to 30% of the cells induce expression of the operon responsible for conjugation. Several other plasmids, including pX01 of *B. anthracis*, and pBS32 as well as pTA1060 from *B. subtilis*, carry Rap-Phr modules, pointing toward a similar mode of regulation (Koetje et al., 2003; Bongiorni et al., 2006; Parashar et al., 2013).

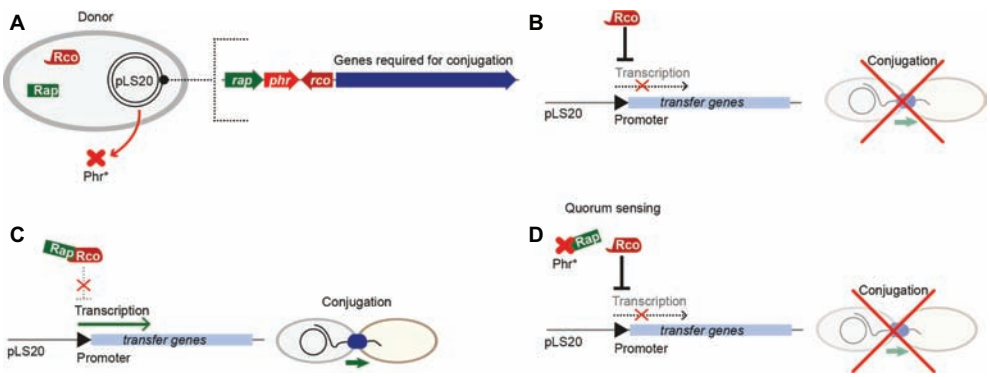

FIGURE 4 | Regulation of pLS20 conjugative transfer. **(A)** Key players involved in regulation are encoded on the pLS20 plasmid, including the master regulator Rco_{LS20} and the Rap_{LS20}-Phr_{LS20} sensor-pheromone cassette upstream of genes required for conjugation. **(B)** The master regulator Rco_{LS20} represses transcription of transfer genes, thus ultimately inhibiting conjugation. **(C)** Binding of Rap_{LS20} to the master regulator Rco_{LS20} leads to conformational changes of Rco_{LS20}, interfering with transcriptional repression of transfer genes, thus conjugation can take place. **(D)** Upon a distinct pheromone concentration (the quorum), the pheromone Phr^*_{LS20} interacts with Rap_{LS20} and interferes with its binding to the master regulator Rco_{LS20}. In consequence, Rco_{LS20} represses transcription of transfer genes and inhibits conjugation.

ICE*Bs*1 From *Bacillus subtilis*

ICE*Bs*1 is a 20.5-kbp ICE that is found on the chromosome of diverse *B. subtilis* strains. The genes required for conjugative transfer are related to those from ICE*St*1 and Tn*916*. This ICE has one of the highest transfer rates in Firmicutes. ICE*Bs*1 harbors more than 20 ORFs and integrates into a locus coding for a tRNA. ICE*Bs*1 cannot only transfer itself, but it can mobilize non-conjugative plasmids as well (Lee et al., 2012). ICE*Bs*1's transfer rate was reported to be considerably higher in biofilms, even though the presence of donor cells in a biofilm did not change the frequency of ICE excision (Lécuyer et al., 2018). Interestingly, regulatory processes of ICE*Bs*1 resemble those of plasmid pLS20. In both systems, conjugation is kept in a default "OFF" state by a master regulator that represses expression of the conjugation genes. ImmR is the master regulator of ICE*Bs*1 that can be modulated by the RapI-PhrI cassette, reminiscent of the Rap-Phr module in pLS20 (**Figures 5A,B**). ImmR inhibits the expression of the excisionase and further downstream genes that are required for ICE*Bs*1 excision and transfer. The RRNPP-family protein RapI induces the production of proteins governing conjugation by interfering with ImmR-mediated repression *via* the anti-repressor ImmA. RapI has been proposed to increase the specific activity of the metalloprotease ImmA that cleaves and thus inactivates ImmR (Bose et al., 2008). In turn, the signaling peptide produced from PhrI inhibits RapI activity. PhrI is encoded downstream of the *rapI* gene within ICE*Bs1* (Auchtung et al., 2005). *phrI* is both expressed from the *rapI* promoter and also produced from its own promoter that is regulated by the sigma factor σ^H (McQuade et al., 2001). Thus, *phrI* transcription increases with enhanced cell density. PhrI is secreted and cleaved by host-encoded factors. After pheromone import *via* the oligopeptide permease Opp, PhrI binds RapI, thus inhibiting its activity and subsequently reducing ICE*Bs1* excision and transfer (Auchtung et al., 2005). Similar to iCF10 from pCF10, extracellular concentrations of PhrI correlate with the number of cells harboring ICE*Bs1*. Thus, when only donors harboring ICE*Bs1* are present, PhrI blocks activation of conjugation *via* interaction with RapI. When potential recipient cells without ICE*Bs1* are present, they take up the pheromone PhrI. This then leads to reduced pheromone levels in donor cells, resulting in RapI-dependent activation of excision, *tra*-gene transcription, and consequently conjugative transfer (Auchtung et al., 2005). RapI not only activates conjugative transfer of ICE*Bs*1 but also inhibits sporulation (Auchtung et al., 2005; Bose et al., 2008). De-repression of ICE*Bs*1, followed by excision and conjugative processes, also takes place upon global DNA damage and is mediated by the DNA-repair protein RecA (Auchtung et al., 2005; Bose and Grossman, 2011), the key mediator of the SOS response. It remains elusive, whether RecA can directly influence the activity of the protease ImmA or acts as stabilization factor (**Figures 5C,D**; Bose and Grossman, 2011).

pIP501 From *Enterococcus faecalis*

The Inc18-family plasmid pIP501 was originally isolated from a clinical *Streptococcus agalactiae* strain and – due to its small size and simplicity – has become the paradigm to study broad host-range plasmids in G+ bacteria with a low G + C content. Inc18 plasmids, including pRE25, pAMß1 and pIP501, have been isolated from clinically relevant *E. faecalis* and *E. faecium* strains and are thought to disseminate resistance to the last-line antimicrobial drug vancomycin, to methicillin-resistant lineages of *Staphylococcus aureus* (Kohler et al., 2018b). The region responsible for conjugative transfer processes is organized as a single operon of 14 kbp, and seven transfer proteins were identified as functional/structural homologs of the G- prototype *A. tumefaciens* T4SS. The *tra*-genes of the pIP501 plasmid were found to be co-transcribed, and mRNA levels remained mostly unchanged

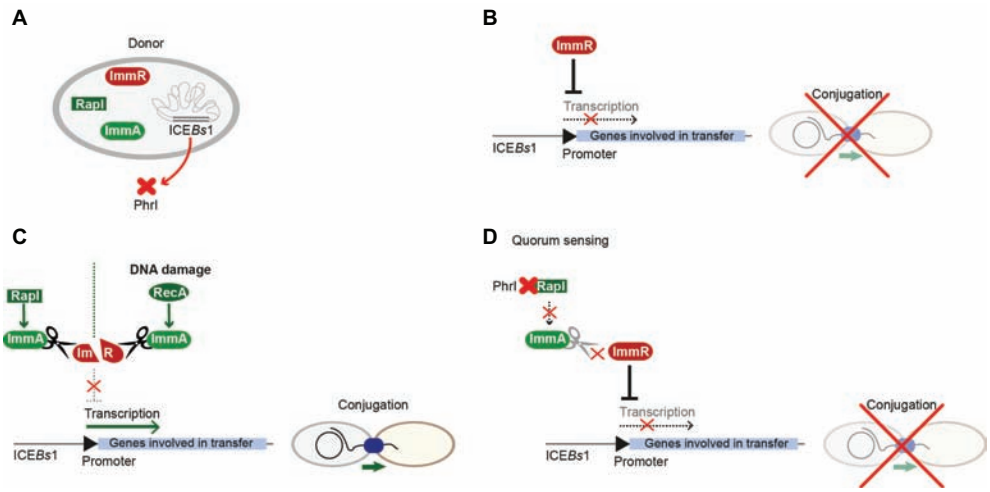

FIGURE 5 | Regulation of ICE*Bs*1 conjugative transfer. **(A)** ICE*Bs*1 harbors most key players involved in regulation of conjugative processes, including the master-regulator ImmR, the metalloprotease ImmA, and the RapI-PhrI sensor-pheromone cassette. **(B)** Similar to processes in pLS20, the master-regulator ImmR represses transcription of genes involved in mobilization and transfer, which ultimately leads to inhibition of conjugation. **(C)** RapI or RecA that is activated by general DNA damage control proteolytic cleavage of ImmR by the metalloprotease ImmA. Thus, transcription is activated and conjugation can take place. **(D)** Upon a distinct concentration (the quorum), the signal peptide PhrI binds to RapI, interfering with its ability to activate ImmA; thus, ImmR can exert repression of the promoter as described in **(A)**.

until late stationary phase. The relaxase TraA, encoded as the first *tra*-gene of the operon, was described to be leadingly involved in regulation of conjugative transfer. TraA was shown to bind to the P_{tra} promoter, thereby negatively regulating transcription of the *tra*-operon (Kurenbach et al., 2006). Recently, TraN, a small cytosolic transfer protein, was identified as additional repressor of the pIP501 conjugation system by binding to its cognate binding site upstream of the P_{tra} promoter and the *oriT nic*-site (Kohler et al., 2018a). TraN is an internal dimer containing two structurally equivalent domains, which belong to the family of winged-helix fold proteins. Its recognition helices protrude into two adjoining major grooves. The wings are required for formation of the interface between the two domains of the internal dimer and insert into the central minor groove. This composition differs from the DNA binding mode of homo-dimeric winged-helix transcription factors (e.g., LysR-type transcriptional regulators; **Figure 6A**; Brown et al., 2003). In contrast to the relaxase TraA that shows autoregulation, TraN's regulatory processes appear to be multi-layered. In addition to the P_{tra} promoter, a second promoter P_{traNO} upstream of the *traN* gene was identified. It was shown to be also negatively regulated by TraN (**Figure 7**). Thus, it was hypothesized that while the P_{tra} promoter was most likely controlled by a concerted action of the relaxase TraA and TraN, TraN binding to P_{traNO} might not only tune its own production but might also be required to regulate levels of TraO, the proposed surface adhesin needed for contacting potential recipients (Kohler et al., 2018a). Toxicity due to overproduction of surface adhesins was demonstrated for other G+ conjugation systems (Bhatty et al., 2017). Nevertheless, the nature of the signal either from potential recipients and/or the environment preceding the nicking of the plasmid DNA by TraA has not been identified so far. Since TraN-homologs and potential TraN binding sites were identified on several Inc18-like and other related multi-resistance plasmids, a similar mechanism of repression was postulated for those plasmids highlighting the potential applicability of TraN as a pharmacological target to combat the dissemination of antibiotic resistances (Kohler et al., 2018a).

pCW3 From *Clostridium perfringens*

The tetracycline resistance plasmid pCW3 from *Clostridium perfringens* belongs to a class of related antibiotic resistance

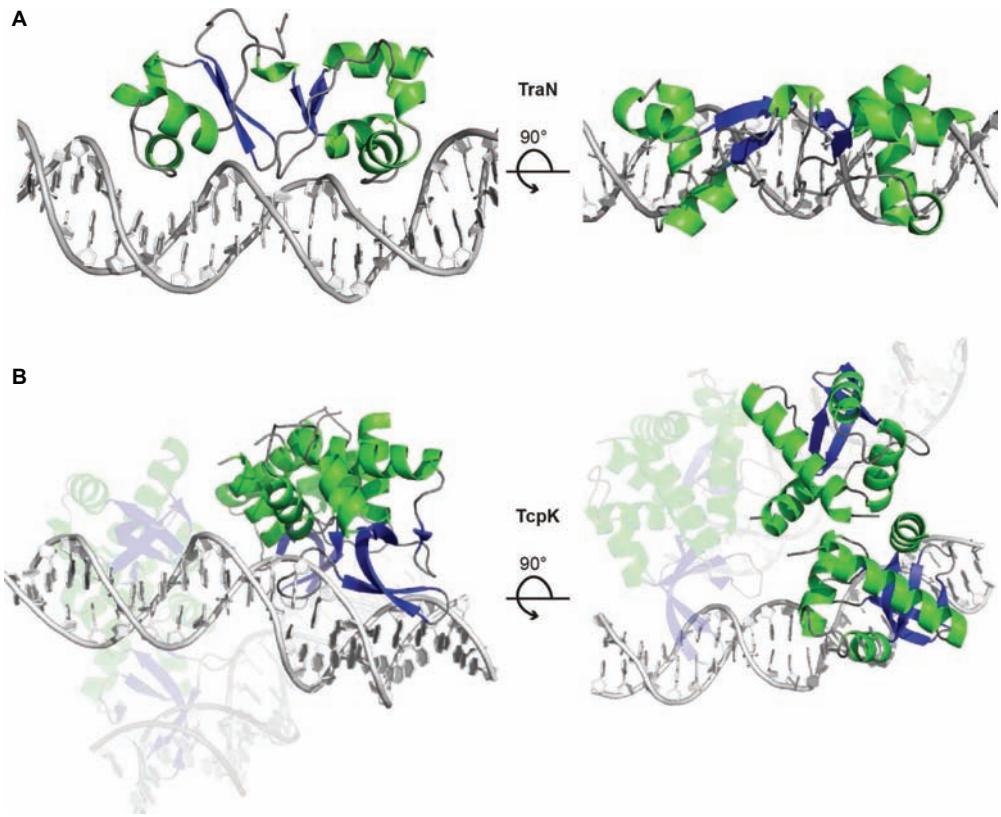

FIGURE 6 | TraN and TcpK are small regulatory proteins exhibiting a winged-helix-turn-helix (wHTH) fold motif. **(A)** TraN is a potent repressor of transcription of the pIP501 *tra*-operon. The TraN protein forms an internal dimer with one wHTH motif in each the N- and C-terminal domain. The TraN-DNA complex (PDB: 6G1T) is shown in cartoon representation, with TraN colored according to secondary structure (α-helices green, β-strands blue) and the DNA in grey. The view is along the recognition helices inserted in the major grooves of the recognition site (left panel) and along the pseudo-two-fold axis of the TraN molecule (right panel). **(B)** The TcpK-DNA complex (PDB: 5VFX) contains two protein dimers bridging two double-stranded DNA molecules with two direct-repeat recognition sequences. The color scheme is the same as in panel **(A)**, and the orientation is chosen to show the DNA-binding mode with the β-ribbon of the wing inserted in the major groove of the double-stranded DNA (left panel) and the bridging of the two double-stranded DNA pieces by one of the TcpK dimers (right panel).

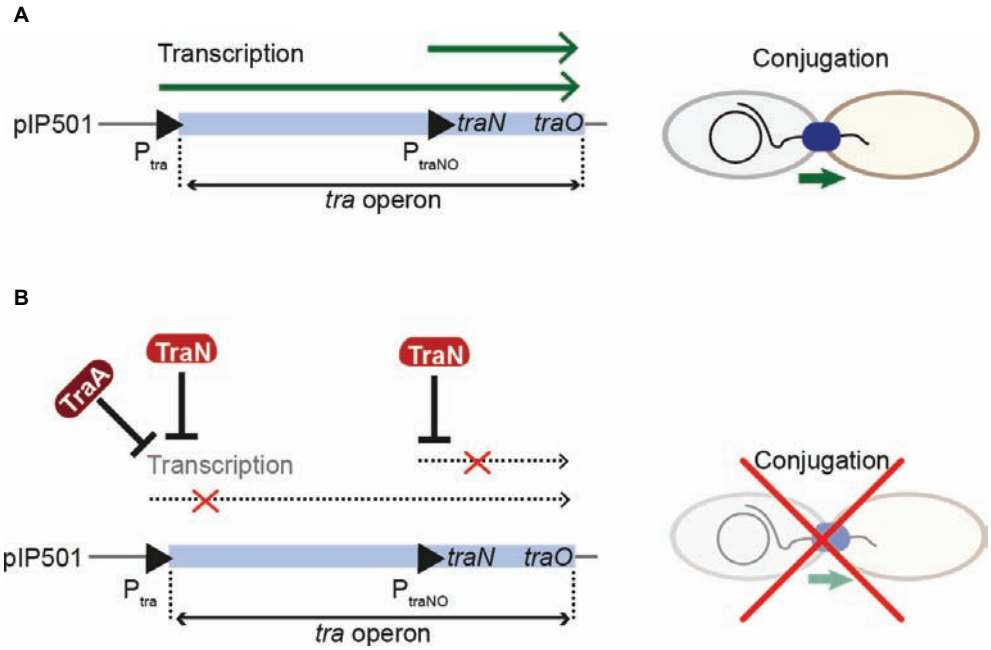

FIGURE 7 | Regulation of pIP501 conjugative transfer. **(A)** Transcription of the pIP501 transfer genes is executed by two promoters, P_{tra} and P_{traNO}, leading to the production of factors required for conjugative transfer. **(B)** By a concerted action between the relaxase TraA and TraN, transcription from the P_{tra} promoter is reduced. Further, TraN can repress the P_{traNO} promoter upstream of its own gene. These regulative processes lead to inhibition of conjugative transfer.

and toxin plasmids (Li et al., 2013). The transfer of clostridial plasmids (*tcp*) locus encoding 11 genes mediates conjugative transfer, with eight proteins essential for these processes (Wisniewski and Rood, 2017). Recently, the structure of TcpK was solved, an essential protein encoded upstream of the *oriT* and shown to be involved in efficient conjugation of pCW3 (Traore et al., 2018). Similar to TraN from pIP501, TcpK is a member of the winged helix-turn-helix protein family and binds specifically to tandem repeats within the pCW3 *oriT*. The complex structure of TcpK with its binding site DNA revealed a binding mode, completely different from other known winged helix-turn-helix proteins. Interestingly, while the wing protrudes into the major groove, the recognition helix makes only a single contact to the binding site DNA. Further, each TcpK dimer binds two binding boxes on different DNA molecules, thus suggesting that TcpK dimers bridge across two DNA molecules (**Figure 6B**). It was suggested that TcpK is an accessory factor of the pCW3 relaxosome, most likely binding to the *oriT* by directly interacting with sequences only present in this region of the plasmid, thus aiding in the proper recruitment of the relaxase TcpM (Traore et al., 2018). Even though the binding mode of TcpK has been uncovered and described in extensive detail, the exact mechanism of regulation remains to be elucidated.

pMV158 From *Streptococcus agalactiae*

pMV158 is a rolling-circle plasmid and was originally isolated from *S. agalactiae* (Burdett, 1980). This 5.5-kbp plasmid is not conjugative but can be mobilized among diverse G+ and G- species by several Inc18-family plasmids including pIP501 and pAMß1 (Priebe and Lacks, 1989; Van der Lelie et al., 1990; Grohmann et al., 1999). MobM is the relaxase of pMV158 and belongs to the MOB_V family of relaxases (Garcillán-Barcia et al., 2009). The full-length MobM as well as the relaxase domain specifically bind to $oriT_{pMV158}$ and are able to perform ss-cleavage of supercoiled pMV158 DNA at the *nic*-site (Grohmann et al., 1999; de Antonio et al., 2004; Lorenzo-Díaz et al., 2011, 2014). Recently, the structure of MobM in complex with different DNA substrates was solved (Pluta et al., 2017). The structures reveal a tight network of protein-DNA interactions involving base-specific as well as backbone interactions. Besides its role in mobilization, MobM is able to repress its own transcription by binding to the *oriT* region, which contains two promoter sequences, one directly overlapping the *oriT* and the second adjacent to the *oriT* (Lorenzo-Díaz et al., 2012), in a similar mode as observed for TraA of pIP501 (Kurenbach et al., 2006). MobM not only autoregulates its own synthesis but is also involved in regulating the pMV158 copy number by binding to the promoter region of the antisense RNAII consequently alleviating the repression of the replication initiator RepB (Lorenzo-Díaz et al., 2017).

pSK41 From *Staphylococcus aureus*

pSK41 and pGO1 are two well-characterized representatives of a large family of low-copy number multi-resistance plasmids from *S. aureus* (Liu et al., 2013). pSK41-like plasmids are self-transmissible and comprise a compact conjugation system with a 14-kbp *tra* region, which consists of two operons, *traA-K* and *traL-M* (Firth et al., 1993), and an additional, divergently transcribed gene, *artA* (*trsN* in pGO1), which will be discussed in detail

below (Ni et al., 2009). However, in contrast to the architecture of Inc18-like plasmids, encoding the relaxase as the first open reading frame of the operon, the relaxase gene of pSK41-like plasmids is outside of the *tra* region. The product of the conversely oriented gene, ArtA, is a global transcriptional regulator of pSK41 with six binding sites present on the plasmid, repressing the transcription of conjugative genes as well as those of the segregation system. All three *tra* promoters (P_{artA}, P_{traA}, and P_{traL}) contain these specific ArtA recognition sites and exhibit ArtA binding affinities in the nanomolar range. The crystal structure of ArtA in complex with its cognate DNA binding site reveals that ArtA belongs to the family of ribbon-helix-helix DNA-binding proteins with a lysine-rich N-terminal stretch, which supposedly contributes to additional binding strength (**Figure 8**; Ni et al., 2009).

Other Mobile Genetic Elements

ICEs similar to ICE*Bs*1 include Tn*916*, ICE*St*1, and ICE*St*3. Tn*916* shows a wide host range and is frequently encountered in clinical isolates of *E. faecalis*, *Clostridium difficile*, and *Streptococcus pneumoniae* (Roberts and Mullany, 2009). This ICE is one of the smallest and least complex conjugative elements and carries a tetracycline resistance gene. It can replicate autonomously in *B. subtilis*, which depends on its relaxase. Tn*916* shows its maximal excision frequency during late exponential phase (Celli et al., 1997), thus activation of the element depends on the respective growth phase. Circularization of Tn*916* is required for conjugative transfer, since distinct transcripts can only be produced when the *att* sites are covalently joined (Celli and Trieu-Cuot, 1998). Interestingly, when exposed to tetracycline conjugative transfer frequencies increase 19-fold in *B. subtilis*, while excision frequencies were apparently not affected (Showsh and Andrews, 1992; Celli et al., 1997).

ICE*St*1 with a size of 35 kbp and ICE*St*3 with 28 kbp are closely related ICEs that are found in streptococci. While ICE*St*3 was shown to be transferred to other species including *S. pyogenes* and *E. faecalis*, it is still a matter of debate whether ICE*St*1 is functional or was acquired by transformation (Bellanger et al., 2009; Fontaine et al., 2010). The dissemination module of these ICEs is a 14-kbp polycistronic operon under the control of the P_{cr} promoter (Carraro et al., 2011). It is suggested that the mobility of this ICE family relies on the activity of the P_{cr} promoter (Carraro et al., 2011). The actual DNA-processing machinery is suggested to involve a putative relaxase, which, in addition to the *oriT*, seems to be conserved between these ICEs, ICE*Bs*1 and Tn*916* (Jaworski and Clewell, 1995; Burrus et al., 2002; Rocco and Churchward, 2006). The *arp2* gene encodes a protein reminiscent of the master-regulator ImmR of ICE*Bs*1, while *orfQ* might encode an ImmA-like metalloprotease. Interestingly, while ICEs are usually controlled by one central repressor belonging to unrelated families, cI or ImmR, ICE*St*1/ICE*St*3 family members harbor both repressors (Bellanger et al., 2009; Carraro et al., 2011).

CONCLUSIONS AND PERSPECTIVES

Assembly and operation of multiprotein complexes such as bacterial conjugation systems require large amounts of energy, provided by one or more ATPases encoded by the conjugation system itself. To minimize energy costs of DNA-protein complex transport, expression and/or activity of single crucial components or the whole conjugation system need to be tightly controlled. This is exerted at different levels by different modes (1) at the transcriptional level by controlling the expression of components, such as the conjugative relaxase and/or accessory relaxosome components, or by controlling the production of surface adhesins required for contacting potential recipient cells, (2) *via* cell density sensing (QS) and sex pheromone-induced surface adhesin production, or (3) *via* a master regulator encoded by the plasmid or ICE itself that keeps the conjugative process in a default "OFF" state until the respective antirepressor gets activated, which turns "ON" the conjugative process.

Some plasmids or ICEs dispose only one of these regulatory modes, and others use combinations of them to maintain conjugative activity at an optimum level. Additionally, conjugative processes of some plasmids as well as ICEs are highly growth-phase dependent, with transfer taking place exclusively during exponential growth or exhibiting maximum rates only during (late) exponential growth. Several well-known conjugative

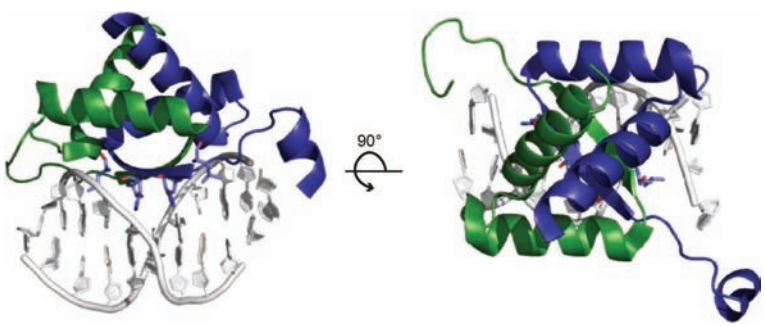

FIGURE 8 | Structure of the ArtA-DNA complex (PDB: 3GXQ). ArtA, the master regulator of the plasmid pSK41, exhibits a ribbon-helix-helix fold. The dimeric repressor is shown in cartoon representation, with chains A and B colored in green and blue, respectively. The anti-parallel β-ribbon permeates the major groove of the binding-site DNA and exerts base-specific interactions (left panel). The view along the twofold axis of the ArtA dimer and the pseudo-palindromic double-stranded DNA site is shown in the right panel.

plasmids and ICEs of G+ origin use pheromone-sensor receptors of the RRNPP family to regulate the conjugation process. Although all members of the RRNPP family display remarkable structural similarity, the downstream reactions often differ widely. Therefore, even though construction of pheromone mimicries would be doable based on the extensive information gathered for this protein family, their structural similarity combined with their differing effects on conjugation would cause problems. Precise data on the regulatory mechanism combined with extensive testing of potential pheromone analogues for diverse conjugation systems would be a first step to solve this problem.

Conjugation is one of the most important means in the dissemination of antibiotic resistance and virulence factors among pathogenic bacteria. Thus, elucidating mechanistic and regulatory details of these large nanomachines is crucial for developing novel approaches to combat multi-resistant pathogens: Important advancements in this direction have been made recently by solution of the cryo-EM structure of the first bacteria-killing T4SS core complex from the G- phytopathogen *Xanthomonas citri* (Sgro et al., 2018) and by the experimental proof that the relaxase has to unfold for efficient translocation through the conjugative T4SS complex (Trokter and Waksman, 2018). Although the abundance of ICEs seems to largely exceed that of conjugative plasmids (Guédon et al., 2017), mechanistic details of their transfer remain elusive. Thus, the aim of future research should lie on the elucidation of the spreading mechanism of ICEs to enable the development/design of specific inhibitors reducing their dissemination.

AUTHOR CONTRIBUTIONS

VK, WK, and EG drafted the manuscript. VK designed the figures. All authors approved the final version of the manuscript.

FUNDING

Work in the Grohmann lab was supported by DLR grants 50WB1166 and 50WB1466, and work in the Keller lab was supported by FWF grant P 27383.

REFERENCES

Antiporta, M. H., and Dunny, G. M. (2002). *ccfa*, the genetic determinant for the cCF10 peptide pheromone in *Enterococcus faecalis* OG1RF. *J. Bacteriol.* 184, 1155–1162. doi: 10.1128/jb.184.4.1155-1162.2002

Auchtung, J. M., Lee, C. A., Monson, R. E., Lehman, A. P., and Grossman, A. D. (2005). Regulation of a *Bacillus subtilis* mobile genetic element by intercellular signaling and the global DNA damage response. *Proc. Natl. Acad. Sci.* 102, 12554–12559. doi: 10.1073/pnas.0505835102

Bae, T., Kozlowicz, B. K., and Dunny, G. M. (2004). Characterization of cis-acting *prgQ* mutants: evidence for two distinct repression mechanisms by Qa RNA and PrgX protein in pheromone-inducible enterococcal plasmid pCF10. *Mol. Microbiol.* 51, 271–281. doi: 10.1046/j.1365-2958.2003.03832.x

Bañuelos-Vazquez, L. A., Torres Tejerizo, G., and Brom, S. (2017). Regulation of conjugative transfer of plasmids and integrative conjugative elements. *Plasmid* 91, 82–89. doi: 10.1016/j.plasmid.2017.04.002

Bellanger, X., Roberts, A. P., Morel, C., Choulet, F., Pavlovic, G., Mullany, P., et al. (2009). Conjugative transfer of the integrative conjugative elements ICE*St*1 and ICE*St*3 from *Streptococcus thermophilus*. *J. Bacteriol.* 191, 2764–2775. doi: 10.1128/JB.01412-08

Bensing, B. A., Manias, D. A., and Dunny, G. M. (1997). Pheromone cCF10 and plasmid pCF10-encoded regulatory molecules act post-transcriptionally to activate expression of downstream conjugation functions. *Mol. Microbiol.* 24, 285–294. doi: 10.1046/j.1365-2958.1997.3301710.x

Bhatty, M., Camacho, M. I., Gonzalez-Rivera, C., Frank, K. L., Dale, J. L., Manias, D. A., et al. (2017). PrgU: a suppressor of sex pheromone toxicity in *Enterococcus faecalis*. *Mol. Microbiol.* 103, 398–412. doi: 10.1111/mmi.13563

Bongiorni, C., Stoessel, R., Shoemaker, D., and Perego, M. (2006). Rap phosphatase of virulence plasmid pXO1 inhibits *Bacillus anthracis* sporulation. *J. Bacteriol.* 188, 487–498. doi: 10.1128/JB.188.2.487-498.2006

Bose, B., Auchtung, J. M., Lee, C. A., and Grossman, A. D. (2008). A conserved anti-repressor controls horizontal gene transfer by proteolysis. *Mol. Microbiol.* 70, 570–582. doi: 10.1111/j.1365-2958.2008.06414.x

Bose, B., and Grossman, A. D. (2011). Regulation of horizontal gene transfer in *Bacillus subtilis* by activation of a conserved site-specific protease. *J. Bacteriol.* 193, 22–29. doi: 10.1128/JB.01143-10

Brown, N. L., Stoyanov, J. V., Kidd, S. P., and Hobman, J. L. (2003). The MerR family of transcriptional regulators. *FEMS Microbiol. Rev.* 27, 145–163. doi: 10.1016/S0168-6445(03)00051-2

Burdett, V. (1980). Identification of tetracycline-resistant R-plasmids in *Streptococcus agalactiae* (group B). *Antimicrob. Agents Chemother.* 18, 753–760. doi: 10.1128/AAC.18.5.753

Burrus, V. (2017). Mechanisms of stabilization of integrative and conjugative elements. *Curr. Opin. Microbiol.* 38, 44–50. doi: 10.1016/j.mib.2017.03.014

Burrus, V., Pavlovic, G., Decaris, B., and Guédon, G. (2002). The ICE*St*1 element of *Streptococcus thermophilus* belongs to a large family of integrative and conjugative elements that exchange modules and change their specificity of integration. *Plasmid* 48, 77–97. doi: 10.1016/S0147-619X(02)00102-6

Burrus, V., and Waldor, M. K. (2004). Shaping bacterial genomes with integrative and conjugative elements. *Res. Microbiol.* 155, 376–386. doi: 10.1016/j.resmic.2004.01.012

Carraro, N., Libante, V., Morel, C., Decaris, B., Charron-Bourgoin, F., Leblond, P., et al. (2011). Differential regulation of two closely related integrative and conjugative elements from *Streptococcus thermophilus*. *BMC Microbiol.* 11:238. doi: 10.1186/1471-2180-11-238

Caserta, E., Haemig, H. A. H., Manias, D. A., Tomsic, J., Grundy, F. J., Henkin, T. M., et al. (2012). In vivo and in vitro analyses of regulation of the pheromone-responsive *prgQ* promoter by the PrgX pheromone receptor protein. *J. Bacteriol.* 194, 3386–3394. doi: 10.1128/JB.00364-12

Celli, J., Poyart, C., and Trieu-Cuot, P. (1997). Use of an excision reporter plasmid to study the intracellular mobility of the conjugative transposon *Tn916* in Gram-positive bacteria. *Microbiology* 143, 1253–1261. doi: 10.1099/00221287-143-4-1253

Celli, J., and Trieu-Cuot, P. (1998). Circularization of Tn*916* is required for expression of the transposon-encoded transfer functions: characterization of long tetracycline-inducible transcripts reading through the attachment site. *Mol. Microbiol.* 28, 103–117. doi: 10.1046/j.1365-2958.1998.00778.x

Chandler, J. R., Flynn, A. R., Bryan, E. M., and Dunny, G. M. (2005). Specific control of endogenous cCF10 pheromone by a conserved domain of the pCF10-encoded regulatory protein PrgY in *Enterococcus faecalis*. *J. Bacteriol.* 187, 4830–4843. doi: 10.1128/JB.187.14.4830-4843.2005

Chatterjee, A., Cook, L. C. C., Shu, C.-C., Chen, Y., Manias, D. A., Ramkrishna, D., et al. (2013). Antagonistic self-sensing and mate-sensing signaling controls antibiotic-resistance transfer. *Proc. Natl. Acad. Sci.* 110, 7086–7090. doi: 10.1073/pnas.1212256110

Chen, Y., Bandyopadhyay, A., Kozlowicz, B. K., Haemig, H. A. H., Tai, A., Hu, W. S., et al. (2017). Mechanisms of peptide sex pheromone regulation of conjugation in *Enterococcus faecalis*. *Microbiology* 6:e00492. doi: 10.1002/mbo3.492

Chung, J. W., and Dunny, G. M. (1992). Cis-acting, orientation-dependent, positive control system activates pheromone-inducible conjugation functions at distances greater than 10 kilobases upstream from its target in *Enterococcus faecalis*. *Proc. Natl. Acad. Sci.* 89, 9020–9024. doi: 10.1073/pnas.89.19.9020

Daubin, V., and Szöllősi, G. J. (2016). Horizontal gene transfer and the history of life. *Cold Spring Harb. Perspect. Biol.* 8:a018036. doi: 10.1101/cshperspect.a018036

Davies, J., and Davies, D. (2010). Origins and evolution of antibiotic resistance. *Microbiol. Mol. Biol. Rev.* 74, 417–433. doi: 10.1128/MMBR.00016-10

de Antonio, C., Farías, M. E., de Lacoba, M. G., and Espinosa, M. (2004). Features of the plasmid pMV158-encoded MobM, a protein involved in its mobilization. *J. Mol. Biol.* 335, 733–743. doi: 10.1016/J.JMB.2003.11.017

Do, H., and Kumaraswami, M. (2016). Structural mechanisms of peptide recognition and allosteric modulation of gene regulation by the RRNPP family of quorum-sensing regulators. *J. Mol. Biol.* 428, 2793–2804. doi: 10.1016/J.JMB.2016.05.026

Dunny, G. M., and Berntsson, P. (2016). Enterococcal sex pheromones: evolutionary pathways to complex, two-signal systems. *J. Bacteriol.* 198, 1556–1562. doi: 10.1128/JB.00128-16

Edwards, J. S., Betts, L., Frazier, M. L., Pollet, R. M., Kwong, S. M., Walton, W. G., et al. (2013). Molecular basis of antibiotic multiresistance transfer in *Staphylococcus aureus*. *Proc. Natl. Acad. Sci. USA* 110, 2804–2809. doi: 10.1073/pnas.1219701110

Firth, N., Ridgway, K. P., Byrne, M. E., Fink, P. D., Johnson, L., Paulsen, I. T., et al. (1993). Analysis of a transfer region from the staphylococcal conjugative plasmid pSK41. *Gene* 136, 13–25. doi: 10.1016/0378-1119(93)90442-6

Fontaine, L., Boutry, C., de Frahan, M. H., Delplace, B., Fremaux, C., Horvath, P., et al. (2010). A novel pheromone quorum-sensing system controls the development of natural competence in *Streptococcus thermophilus* and *Streptococcus salivarius*. *J. Bacteriol.* 192, 1444–1454. doi: 10.1128/JB.01251-09

Frost, L. S., and Koraimann, G. (2010). Regulation of bacterial conjugation: balancing opportunity with adversity. *Future Microbiol* 5, 1057–1071. doi: 10.2217/fmb.10.70

Garcillán-Barcia, M. P., Francia, M. V., and de La Cruz, F. (2009). The diversity of conjugative relaxases and its application in plasmid classification. *FEMS Microbiol. Rev.* 33, 657–687. doi: 10.1111/j.1574-6976.2009.00168.x

Ghinet, M. G., Bordeleau, E., Beaudin, J., Brzezinski, R., Roy, S., and Burrus, V. (2011). Uncovering the prevalence and diversity of integrating conjugative elements in actinobacteria. *PLoS One* 6:e27846. doi: 10.1371/journal.pone.0027846

Grohmann, E., Christie, P. J., Waksman, G., and Backert, S. (2017). Type IV secretion in Gram-negative and Gram-positive bacteria. *Mol. Microbiol.* 107, 455–471. doi: 10.1111/mmi.13896

Grohmann, E., Guzmán, L. M., and Espinosa, M. (1999). Mobilisation of the streptococcal plasmid pMV158: interactions of MobM protein with its cognate *oriT* DNA region. *Mol. Gen. Genet.* 261, 707–715. doi: 10.1007/s004380050014

Guédon, G., Libante, V., Coluzzi, C., Payot, S., and Leblond-Bourget, N. (2017). The obscure world of integrative and mobilizable elements, highly widespread elements that pirate bacterial conjugative systems. *Genes* 8:337. doi: 10.3390/genes8110337

Guglielmini, J., Quintais, L., Garcillán-Barcia, M. P., de la Cruz, F., and Rocha, E. P. C. (2011). The repertoire of ICE in prokaryotes underscores the unity, diversity, and ubiquity of conjugation. *PLoS Genet.* 7:e1002222. doi: 10.1371/journal.pgen.1002222

Hirt, H., Manias, D. A., Bryan, E. M., Klein, J. R., Marklund, J. K., Staddon, J. H., et al. (2005). Characterization of the pheromone response of the *Enterococcus faecalis* conjugative plasmid pCF10: complete sequence and comparative analysis of the transcriptional and phenotypic responses of pCF10-containing cells to pheromone induction. *J. Bacteriol.* 187, 1044–1054. doi: 10.1128/JB.187.3.1044-1054.2005

Itaya, M., Sakaya, N., Matsunaga, S., Fujita, K., and Kaneko, S. (2006). Conjugational transfer kinetics of pLS20 between *Bacillus subtilis* in liquid medium. *Biosci. Biotechnol. Biochem.* 70, 740–742. doi: 10.1271/bbb.70.740

Jaworski, D. D., and Clewell, D. B. (1995). A functional origin of transfer (*oriT*) on the conjugative transposon *Tn*916. *J. Bacteriol.* 177, 6644–6651. doi: 10.1128/JB.177.22.6644-6651.1995

Johnson, C. M., Manias, D. A., Haemig, H. A. H., Shokeen, S., Weaver, K. E., Henkin, T. M., et al. (2010). Direct evidence for control of the pheromone-inducible *prgQ* operon of *Enterococcus faecalis* plasmid pCF10 by a countertranscript-driven attenuation mechanism. *J. Bacteriol.* 192, 1634–1642. doi: 10.1128/JB.01525-09

Kelly, B. G., Vespermann, A., and Bolton, D. J. (2009). The role of horizontal gene transfer in the evolution of selected foodborne bacterial pathogens. *Food Chem. Toxicol.* 47, 951–968. doi: 10.1016/j.fct.2008.02.006

Koetje, E. J., Hajdo-Milasinovic, A., Kiewiet, R., Bron, S., and Tjalsma, H. (2003). A plasmid-borne Rap-Phr system of *Bacillus subtilis* can mediate cell-density controlled production of extracellular proteases. *Microbiology* 149, 19–28. doi: 10.1099/mic.0.25737-0

Kohler, V., Goessweiner-Mohr, N., Aufschnaiter, A., Fercher, C., Probst, I., Pavkov-Keller, T., et al. (2018a). TraN: a novel repressor of an enterococcus conjugative type IV secretion system. *Nucleic Acids Res.* 46, 9201–9219 doi: 10.1093/nar/gky671

Kohler, V., Vaishampayan, A., and Grohmann, E. (2018b). Broad-host-range Inc18 plasmids: occurrence, spread and transfer mechanisms. *Plasmid* 99, 11–21. doi: 10.1016/J.PLASMID.2018.06.001

Koraimann, G., and Wagner, M. A. (2014). Social behavior and decision making in bacterial conjugation. *Front. Cell. Infect. Microbiol.* 4:54. doi: 10.3389/fcimb.2014.00054

Kozlowicz, B. K., Bae, T., and Dunny, G. M. (2004). *Enterococcus faecalis* pheromone-responsive protein PrgX: genetic separation of positive autoregulatory functions from those involved in negative regulation of conjugative plasmid transfer. *Mol. Microbiol.* 54, 520–532. doi: 10.1111/j.1365-2958.2004.04286.x

Kozlowicz, B. K., Shi, K., Gu, Z. Y., Ohlendorf, D. H., Earhart, C. A., and Dunny, G. M. (2006). Molecular basis for control of conjugation by bacterial pheromone and inhibitor peptides. *Mol. Microbiol.* 62, 958–969. doi: 10.1111/j.1365-2958.2006.05434.x

Kurenbach, B., Kopeć, J., Mägdefrau, M., Andreas, K., Keller, W., Bohn, C., et al. (2006). The TraA relaxase autoregulates the putative type IV secretion-like system encoded by the broad-host-range *Streptococcus agalactiae* plasmid pIP501. *Microbiology* 152, 637–645. doi: 10.1099/mic.0.28468-0

Lécuyer, F., Bourassa, J.-S., Gélinas, M., Charron-Lamoureux, V., Burrus, V., and Beauregard, P. B. (2018). Biofilm formation drives transfer of the conjugative element ICE*Bs*1 in *Bacillus subtilis*. *mSphere* 3, 1–12. doi: 10.1128/mSphere.00473-18

Lee, C. A., Thomas, J., and Grossman, A. D. (2012). The *Bacillus subtilis* conjugative transposon ICE*Bs*1 mobilizes plasmids lacking dedicated mobilization functions. *J. Bacteriol.* 194, 3165–3172. doi: 10.1128/JB.00301-12

Leonard, B. A., Podbielski, A., Hedberg, P. J., and Dunny, G. M. (1996). *Enterococcus faecalis* pheromone binding protein, PrgZ, recruits a chromosomal oligopeptide permease system to import sex pheromone cCF10 for induction of conjugation. *Proc. Natl. Acad. Sci. USA* 93, 260–264. doi: 10.1073/PNAS.93.1.260

Li, J., Adams, V., Bannam, T. L., Miyamoto, K., Garcia, J. P., Uzal, F. A., et al. (2013). Toxin plasmids of *Clostridium perfringens*. *Microbiol. Mol. Biol. Rev.* 77, 208–233. doi: 10.1128/MMBR.00062-12

Liu, M. A., Kwong, S. M., Jensen, S. O., and Brzoska, A. J. (2013). Biology of the staphylococcal conjugative multiresistance plasmid pSK41. *Plasmid* 70, 42–51. doi: 10.1016/J.PLASMID.2013.02.001

Lorenzo-Díaz, F., Dostál, L., Coll, M., Schildbach, J. F., Menéndez, M., and Espinosa, M. (2011). The MobM relaxase domain of plasmid pMV158: thermal stability and activity upon Mn^{2+} and specific DNA binding. *Nucleic Acids Res.* 39, 4315–4329. doi: 10.1093/nar/gkr049

Lorenzo-Díaz, F., Espinosa, M., Solano-Collado, V., Garsin, D. A., Bravo, A., Ruiz-Cruz, S., et al. (2014). Mobilizable rolling-circle replicating plasmids from Gram-positive bacteria: a low-cost conjugative transfer. *Microbiol. Spectr.* 2. doi: 10.1128/microbiolspec.PLAS-0008-2013

Lorenzo-Díaz, F., Fernández-López, C., Lurz, R., Bravo, A., and Espinosa, M. (2017). Crosstalk between vertical and horizontal gene transfer: plasmid replication control by a conjugative relaxase. *Nucleic Acids Res.* 45, 7774–7785. doi: 10.1093/nar/gkx450

Lorenzo-Díaz, F., Solano-Collado, V., Lurz, R., Bravo, A., and Espinosa, M. (2012). Autoregulation of the synthesis of the MobM relaxase encoded by the promiscuous Plasmid pMV158. *J. Bacteriol.* 194, 1789–1799. doi: 10.1128/JB.06827-11

McQuade, R. S., Comella, N., and Grossman, A. D. (2001). Control of a family of phosphatase regulatory genes (*phr*) by the alternate sigma factor sigma-H of *Bacillus subtilis*. *J. Bacteriol.* 183, 4905–4909. doi: 10.1128/JB.183.16.4905-4909.2001

Monnet, V., Juillard, V., and Gardan, R. (2016). Peptide conversations in Gram-positive bacteria. *Crit. Rev. Microbiol.* 42, 339–351. doi: 10.3109/1040841X.2014.948804

Mori, M., Sakagamis, Y., Ishiis, Y., Isogais, A., Kitadaj, C., Fujinoj, M., et al. (1988). Structure of cCF10, a peptide sex pheromone which induces conjugative transfer of the *Streptococcus faecalis* tetracycline resistance plasmid, pCF10. *J. Biol. Chem.* 263, 14574–14578.

Nakayama, J., Ruhfel, R. E., Dunny, G. M., Isogai, A., and Suzuki, A. (1994). The *prgQ* gene of the *Enterococcus faecalis* tetracycline resistance plasmid pCF10 encodes a peptide inhibitor, iCF10. *J. Bacteriol.* 176, 7405–7408. doi: 10.1128/jb.176.23.7405-7408.1994

Neiditch, M. B., Capodagli, G. C., Prehna, G., and Federle, M. J. (2017). Genetic and structural analyses of RRNPP intercellular peptide signaling of Gram-positive bacteria. *Annu. Rev. Genet.* 51, 311–333. doi: 10.1146/annurev-genet-120116-023507

Ni, L., Jensen, S. O., Ky Tonthat, N., Berg, T., Kwong, S. M., Guan, F. H. X., et al. (2009). The *Staphylococcus aureus* pSK41 plasmid-encoded ArtA protein is a master regulator of plasmid transmission genes and contains a RHH motif used in alternate DNA-binding modes. *Nucleic Acids Res.* 37, 6970–6983. doi: 10.1093/nar/gkp756

Papenfort, K., and Bassler, B. L. (2016). Quorum sensing signal-response systems in Gram-negative bacteria. *Nat. Rev. Microbiol.* 14, 576–588. doi: 10.1038/nrmicro.2016.89

Parashar, V., Konkol, M. A., Kearns, D. B., and Neiditch, M. B. (2013). A plasmid-encoded phosphatase regulates *Bacillus subtilis* biofilm architecture, sporulation, and genetic competence. *J. Bacteriol.* 195, 2437–2448. doi: 10.1128/JB.02030-12

Pérez-Arellano, I., Gallego, J., and Cervera, J. (2007). The PUA domain–a structural and functional overview. *FEBS J.* 274, 4972–4984. doi: 10.1111/j.1742-4658.2007.06031.x

Perez-Pascual, D., Monnet, V., and Gardan, R. (2016). Bacterial cell-cell communication in the host via RRNPP peptide-binding regulators. *Front. Microbiol.* 7:706. doi: 10.3389/fmicb.2016.00706

Perry, J. A., and Wright, G. D. (2013). The antibiotic resistance "mobilome": searching for the link between environment and clinic. *Front. Microbiol.* 4:138. doi: 10.3389/fmicb.2013.00138

Pettis, G. S. (2018). Spreading the news about the novel conjugation mechanism in *Streptomyces* bacteria. *Environ. Microbiol. Rep.* 10, 503–510. doi: 10.1111/1758-2229.12659

Pluta, R., Boer, D. R., Lorenzo-Díaz, F., Russi, S., Gómez, H., Fernández-López, C., et al. (2017). Structural basis of a histidine-DNA nicking/joining mechanism for gene transfer and promiscuous spread of antibiotic resistance. *Proc. Natl. Acad. Sci. USA* 114, E6526–E6535. doi: 10.1073/pnas.1702971114

Pottathil, M., and Lazazzera, B. A. (2003). The extracellular phr peptide-Rap phosphatase signaling circuit of Bacillus subtilis. *Front. Biosci.* 8, 32–45. doi: 10.2741/913

Priebe, S. D., and Lacks, S. A. (1989). Region of the streptococcal plasmid pMV158 required for conjugative mobilization. *J. Bacteriol.* 171, 4778–4784. doi: 10.1128/jb.171.9.4778-4784.1989

Ramachandran, G., Singh, P. K., Luque-Ortega, J. R., Yuste, L., Alfonso, C., Rojo, F., et al. (2014). A complex genetic switch involving overlapping divergent promoters and DNA looping regulates expression of conjugation genes of a Gram-positive plasmid. *PLoS Genet.* 10:e1004733. doi: 10.1371/journal.pgen.1004733

Roberts, A. P., and Mullany, P. (2009). A modular master on the move: the Tn*916* family of mobile genetic elements. *Trends Microbiol.* 17, 251–258. doi: 10.1016/j.tim.2009.03.002

Rocco, J. M., and Churchward, G. (2006). The integrase of the conjugative transposon Tn*916* directs strand- and sequence-specific cleavage of the origin of conjugal transfer, *oriT*, by the endonuclease Orf20. *J. Bacteriol.* 188, 2207–2213. doi: 10.1128/JB.188.6.2207-2213.2006

Rocha-Estrada, J., Aceves-Diez, A. E., Guarneros, G., and De La Torre, M. (2010). The RNPP family of quorum-sensing proteins in Gram-positive bacteria. *Appl. Microbiol. Biotechnol.* 87, 913–923. doi: 10.1007/s00253-010-2651-y

Rösch, T. C., and Graumann, P. L. (2015). Induction of plasmid conjugation in *Bacillus subtilis* is bistable and driven by a direct interaction of a Rap/Phr quorum-sensing system with a master repressor. *J. Biol. Chem.* 290, 20221–20232. doi: 10.1074/jbc.M115.664110

Sgro, G. G., Costa, T. R. D., Cenens, W., Souza, D. P., Cassago, A., Coutinho de Oliveira, L., et al. (2018). Cryo-EM structure of the bacteria-killing type IV secretion system core complex from *Xanthomonas citri*. *Nat. Microbiol.* 3, 1429–1440. doi: 10.1038/s41564-018-0262-z

Shi, K., Brown, C. K., Gu, Z.-Y., Kozlowicz, B. K., Dunny, G. M., Ohlendorf, D. H., et al. (2005). Structure of peptide sex pheromone receptor PrgX and PrgX/pheromone complexes and regulation of conjugation in *Enterococcus faecalis*. *Proc. Natl. Acad. Sci.* 102, 18596–18601. doi: 10.1073/pnas.0506163102

Shokeen, S., Johnson, C. M., Greenfield, T. J., Manias, D. A., Dunny, G. M., and Weaver, K. E. (2010). Structural analysis of the Anti-Q-Qs interaction: RNA-mediated regulation of *E. faecalis* plasmid pCF10 conjugation. *Plasmid* 64, 26–35. doi: 10.1016/j.plasmid.2010.03.002

Showsh, S. A., and Andrews, R. E. (1992). Tetracycline enhances *Tn*916-mediated conjugal transfer. *Plasmid* 28, 213–224. doi: 10.1016/0147-619X(92)90053-D

Singh, P. K., and Meijer, W. J. J. (2014). Diverse regulatory circuits for transfer of conjugative elements. *FEMS Microbiol. Lett.* 358, 119–128. doi: 10.1111/1574-6968.12526

Singh, P. K., Ramachandran, G., Durán-Alcalde, L., Alonso, C., Wu, L. J., and Meijer, W. J. J. (2012). Inhibition of *Bacillus subtilis* natural competence by a native, conjugative plasmid-encoded ComK repressor protein. *Environ. Microbiol.* 14, 2812–2825. doi: 10.1111/j.1462-2920.2012.02819.x

Singh, P. K., Ramachandran, G., Ramos-Ruiz, R., Peiró-Pastor, R., Abia, D., Wu, L. J., et al. (2013). Mobility of the native *Bacillus subtilis* conjugative plasmid pLS20 is regulated by intercellular signaling. *PLoS Genet.* 9:e1003892. doi: 10.1371/journal.pgen.1003892

Stingl, K., and Koraimann, G. (2017). "Prokaryotic information games: how and when to take up and secrete DNA" in *Type IV Secretion in Gram-Negative and Gram-Positive Bacteria. Current topics in microbiology and immunology*. Vol. 413, eds. S. Backert and E. Grohmann (Cham: Springer), 61–92.

Sultan, I., Rahman, S., Jan, A. T., Siddiqui, M. T., Mondal, A. H., and Haq, Q. M. R. (2018). Antibiotics, resistome and resistance mechanisms: a bacterial perspective. *Front. Microbiol.* 9:2066. doi: 10.3389/fmicb.2018.02066

Tamminen, M., Virta, M., Fani, R., and Fondi, M. (2012). Large-scale analysis of plasmid relationships through gene-sharing networks. *Mol. Biol. Evol.* 29, 1225–1240. doi: 10.1093/molbev/msr292

Thoma, L., and Muth, G. (2016). Conjugative DNA-transfer in *Streptomyces*, a mycelial organism. *Plasmid* 87, 1–9. doi: 10.1016/j.plasmid.2016.09.004

Traore, D. A. K., Wisniewski, J. A., Flanigan, S. F., Conroy, P. J., Panjikar, S., Mok, Y. F., et al. (2018). Crystal structure of TcpK in complex with *oriT* DNA of the antibiotic resistance plasmid pCW3. *Nat. Commun.* 9:3732. doi: 10.1038/s41467-018-06096-2

Trokter, M., and Waksman, G. (2018). Translocation through the conjugative Type 4 secretion system requires unfolding of its protein substrate. *J. Bacteriol.* 200. pii: JB.00615-617. doi: 10.1128/JB.00615-17

Van der Lelie, D., Wosten, H. A. B., Bron, S., Oskam, L., and Venema, G. (1990). Conjugal mobilization of streptococcal plasmid pMV158 between strains of *Lactococcus lactis* subsp. *lactis*. *J. Bacteriol.* 172, 47–52. doi: 10.1128/jb.172.1.47-52.1990

Wisniewski, J. A., and Rood, J. I. (2017). The Tcp conjugation system of *Clostridium perfringens*. *Plasmid* 91, 28–36. doi: 10.1016/j.plasmid.2017.03.001

Wozniak, R. A. F., and Waldor, M. K. (2010). Integrative and conjugative elements: mosaic mobile genetic elements enabling dynamic lateral gene flow. *Nat. Rev. Microbiol.* 8, 552–563. doi: 10.1038/nrmicro2382

Zeytuni, N., and Zarivach, R. (2012). Structural and functional discussion of the tetra-trico-peptide repeat, a protein interaction module. *Structure* 20, 397–405. doi: 10.1016/J.STR.2012.01.006

Conflict of Interest Statement: The authors declare that the research was conducted in the absence of any commercial or financial relationships that could be construed as a potential conflict of interest.

Copyright © 2019 Kohler, Keller and Grohmann. This is an open-access article distributed under the terms of the Creative Commons Attribution License (CC BY). The use, distribution or reproduction in other forums is permitted, provided the original author(s) and the copyright owner(s) are credited and that the original publication in this journal is cited, in accordance with accepted academic practice. No use, distribution or reproduction is permitted which does not comply with these terms.

frontiers in Microbiology

REVIEW
published: 31 May 2019
doi: 10.3389/fmicb.2019.01163

Type V Secretion Systems: An Overview of Passenger Domain Functions

*Ina Meuskens, Athanasios Saragliadis, Jack C. Leo and Dirk Linke**

Department of Biosciences, Section for Genetics and Evolutionary Biology, University of Oslo, Oslo, Norway

Bacteria secrete proteins for different purposes such as communication, virulence functions, adhesion to surfaces, nutrient acquisition, or growth inhibition of competing bacteria. For secretion of proteins, Gram-negative bacteria have evolved different secretion systems, classified as secretion systems I through IX to date. While some of these systems consist of multiple proteins building a complex spanning the cell envelope, the type V secretion system, the subject of this review, is rather minimal. Proteins of the Type V secretion system are often called autotransporters (ATs). In the simplest case, a type V secretion system consists of only one polypeptide chain with a β-barrel translocator domain in the membrane, and an extracellular passenger or effector region. Depending on the exact domain architecture of the protein, type V secretion systems can be further separated into sub-groups termed type Va through e, and possibly another recently identified subtype termed Vf. While this classification works well when it comes to the architecture of the proteins, this is not the case for the function(s) of the secreted passenger. In this review, we will give an overview of the functions of the passengers of the different AT classes, shedding more light on the variety of functions carried out by type V secretion systems.

Keywords: secretion systems, AT, virulence, bacterial outer membrane, Gram-negative microorganisms

OPEN ACCESS

Edited by:
Eric Cascales,
Aix-Marseille Université, France

Reviewed by:
Kim Rachael Hardie,
University of Nottingham,
United Kingdom
Timothy James Wells,
The University of Queensland,
Australia

***Correspondence:**
Dirk Linke
dirk.linke@ibv.uio.no

Specialty section:
This article was submitted to Microbial Physiology and Metabolism, a section of the journal Frontiers in Microbiology

Received: *29 March 2019*
Accepted: *07 May 2019*
Published: *31 May 2019*

Citation:
Meuskens I, Saragliadis A, Leo JC and Linke D (2019) Type V Secretion Systems: An Overview of Passenger Domain Functions. Front. Microbiol. 10:1163. doi: 10.3389/fmicb.2019.01163

INTRODUCTION

Bacteria in general display a great variety of proteins on their cell surface, serving functions in nutrient transport, signaling, adhesion, or virulence. The proteins and protein complexes responsible for secretion in Gram-negative bacteria can be divided into categories, termed type I through type IX secretion systems (Costa et al., 2015; Green and Mecsas, 2016). These secretion systems differ in their complexity, with some of them consisting of only one polypeptide chain, like some of the type V secretion systems, to very intricate machineries consisting of multiple proteins building a complex, sometimes spanning several membranes. Compared with multi-subunit secretion systems, type V secretion systems seem somewhat peculiar. In comparison to most of the other secretion systems, they are much smaller, and only span the Gram-negative outer membrane (OM) (Leo et al., 2012). Type V secretion systems have no obvious energy source for transport, as there is no chemical energy such as ATP available in the periplasm, and no stable proton or other ion gradients exist across the OM. This has led to the name "autotransporter" (AT) that suggests a completely self-sufficient system for secretion (Klauser et al., 1993). Today we know of multiple factors that are involved in the secretion of ATs, but the source of energy for the secretion

is still a matter of debate (Thanassi et al., 2005; Kang'ethe and Bernstein, 2013; Drobnak et al., 2015; Oberhettinger et al., 2015).

Type V secretion systems come in different forms depending on their structural features and domain organization (**Figure 1**). Type V ATs are therefore divided into sub-classes, type Va through type Ve, and possibly the very recently suggested type Vf (Grijpstra et al., 2013). While sub-classification according to the domain structure of ATs is useful to show differences in general principles of their organization and biogenesis, this does not usually reflect the secreted passengers' function(s). AT passengers function in very diverse ways, ranging from adhesins or enzymes to toxic proteins. **Table 1** gives a general overview of functionalities of passengers from the different subclasses. While many reviews concentrate on the topology and biogenesis of ATs, we deliberately focus on the functions of the passenger domains of ATs. We also give a short overview of the different topologies of AT sub-classes and their biogenesis.

TOPOLOGY OF ATs

Autotransporters consist of two distinct regions, a secreted passenger and a β-barrel domain that resides in the bacterial OM. The transmembrane domain typically is C-terminal to the passenger, but in type Ve ATs this domain order is inverted (**Figure 1**). Both regions are found in a single polypeptide chain with the exception of type Vb secretion systems, where the moieties are separate polypeptide chains (Guérin et al., 2017). While this broad separation into two functional regions is conserved among all type V systems, additional functional features have been identified. Examples include the PL-region (pertactin-like region), stable core or autochaperone region, all describing the same features of the membrane-proximal part of AT passengers that have special functions in folding and transport of the rest of the passenger (Drobnak et al., 2015). To further complicate the issue, the passenger itself has been referred to as the α-domain and the transmembrane β-barrel as the translocator or β-domain (Pohlner et al., 1995; Henderson et al., 2004; Drobnak et al., 2015). To avoid confusion, we will only refer to the β-barrel and the passenger in this review according to Drobnak et al. (2015). In the following section, we will give a short overview over the different structural features of the different sub-classes of ATs.

Type Va (Classical Autotransporters)

Type Va ATs are commonly known as classical ATs. They have been studied extensively, both functionally and structurally. Well studied members are the IgA protease from *Neisseria meningitidis* and EstA, a lipase from *Pseudomonas aeruginosa* (Henderson et al., 2004). Type Va ATs consist of a 12-stranded β-barrel domain, which functions as a C-terminal anchor in the OM and which is required for the transport of the N-terminal passenger to the extracellular environment. The passenger usually adopts a repetitive β-helix fold extending away from the bacterial cell surface, as demonstrated by the crystal structure of the Pertactin passenger (Emsley et al., 1996). Other forms of passengers are possible as well, as exemplified by EstA folding into a predominantly α-helical passenger (Brzuszkiewicz et al., 2009). The passenger harbors the specific function of the protein, and most model systems that have been studied in different species are important virulence factors. The diversity of passenger functions and specifically of protease functions among type Va passengers has given rise to classifications into SPATE (serine protease autotransporters of Enterobacteriaceae) proteases, SPATE-like and non-SPATE proteases (Yen et al., 2008; Ruiz-Perez and Nataro, 2014). In some cases the passenger domain of type Va ATs can be cleaved off after secretion. Passengers with enzymatic activity, like SPATE proteases, more often belong to the group of cleaved passengers than adhesin passengers, though cleavage has been observed also in adhesins such as AIDA-I (Charbonneau et al., 2006; Barnard et al., 2007; Dautin et al., 2007). Other examples are the SAATs (self-aggregating ATs) such as Ag43 from *E. coli* (Klemm et al., 2004).

Type Vb (Two-Partner Secretion)

Type Vb secretion systems consist of two distinct polypeptide chains encoded in one operon, e.g., the *Bordetella* filamentous hemagglutinin FHA (Chevalier et al., 2004; Jacob-Dubuisson et al., 2013). Due to this, they are also called two-partner secretion systems (TPSSs). TPSSs are composed of two proteins, one functioning as the translocator (TpsB) and the other as the secreted passenger (TpsA). TpsB is a 16-stranded, OM integral β-barrel protein with two periplasmic POTRA (polypeptide transport-associated) domains (Kajava et al., 2001). Due to the separation of the β-barrel and the passenger into two separate polypeptide chains, the passenger is released into the cell's environment after transport without any need for release by proteolytic cleavage. The fate of the passenger after secretion can differ. Some TpsB proteins stay attached to the OM in a non-covalently bound manner as exemplified by the *Haemophilus influenzae* proteins HMW1 and HMW2, while others are secreted, such as the *Serratia marcescens* protein ShlA (Braun et al., 1993; St. Geme, 1994).

Type Vc (Trimeric Autotransporter Adhesins)

Type Vc secretion systems have the same topology as type Va systems, but form highly intertwined trimeric structures. For this reason, and because all examples studied so far are adhesins, they are often referred to as trimeric autotransporter adhesins (TAAs). YadA, the *Yersinia* adhesin A from *Yersinia enterocolitica* and *Yersinia pseudotuberculosis* is the best studied member of this class of ATs (Mühlenkamp et al., 2015). These proteins consist of three identical polypeptide chains, and in their final folded form are composed of a C-terminal 12 stranded β-barrel (4 β-strands per monomer), and a passenger, which is also trimeric and typically folds into a lollipop-like structure with a coiled coil stalk and a globular head domain at the N-terminus of the protein (Hoiczyk, 2000; Linke et al., 2006; Wollmann et al., 2006).

Type Vd

The type Vd ATs are a fairly recently discovered class of ATs that resembles a hybrid of type Va and type Vb systems with PlpD

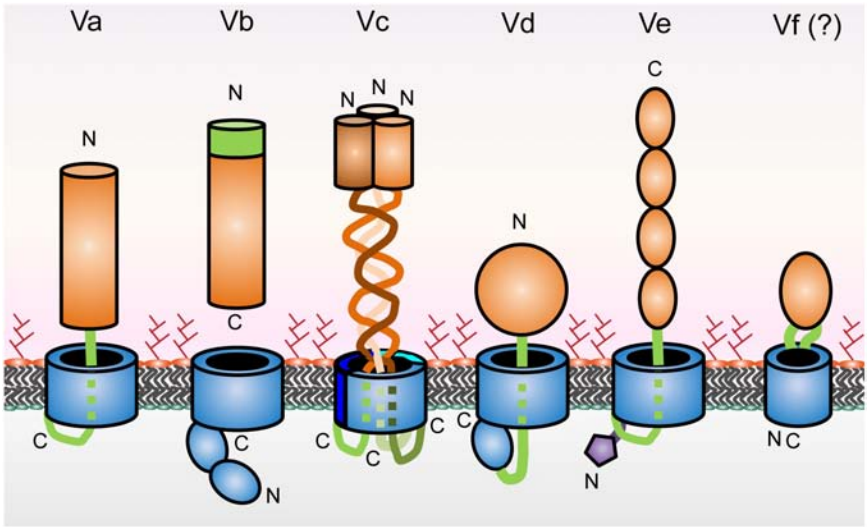

FIGURE 1 | Schematic of type V secretion system subclasses. β-barrels and POTRA domains are shown in blue, linkers and TPS domains in green, and passengers in orange. The periplasmic extension of type Ve proteins is in purple. The positions of the N- and C-termini are indicated. Type Vf is not fully established as part of the type V secretion scheme; this is denoted by the question mark.

from *P. aeruginosa* and FplA from *Fusobacterium nucleatum* as prototypical members (Salacha et al., 2010; Casasanta et al., 2017). The C-terminal β-barrel domain of type Vd ATs consist of 16 β-strands which is similar to the β-barrel of TpsB proteins. However, type Vd ATs have only one POTRA domain, whereas TpsB proteins have two POTRA domains for binding their TpsA substrate for secretion (Leo et al., 2012). Whereas type Va ATs have a passenger that typically folds into a β-helical structure, the passenger domains of type Vd ATs, which have been found to harbor lipase activity, adopt an α/β-hydrolase fold (Emsley et al., 1996; Da Mata Madeira et al., 2016). Note though that there are also some type Va ATs with passengers that have an α/β hydrolase fold, e.g., EstA (Brzuszkiewicz et al., 2009). A key difference between Va and type Vd passengers seems to be that type Va passengers have a multitude of different folds and functionalities, while type Vd passengers characterized so far only function as lipases/esterases (Da Mata Madeira et al., 2016; Casasanta et al., 2017).

Type Ve (Inverse Autotransporters)

Type Ve ATs share obvious similarities to type Va ATs, with a modular architecture including a 12-stranded β-barrel domain and a secreted, monomeric passenger that remains attached after translocation. The major difference to type Va ATs is that the type Ve ATs have an inverted domain order, with the β-barrel at the N-terminal end and the passenger at the C-terminus as shown for intimin and invasin from *Escherichia coli* and *Y. enterocolitica* (Leo et al., 2012, 2015b). This has led to the name "inverse autotransporters" (Oberhettinger et al., 2015). The passenger of inverse ATs typically contains domains with Ig-like or lectin-like folds, and some exemplars have long, repetitive stretches of Ig-like domains that are capped with a lectin-like domain (Leo et al., 2015b). Some type Ve ATs have an additional periplasmic domain which is not found in other types of ATs. This periplasmic domain aids in dimerization as well as in interactions with peptidoglycan, possibly anchoring it and helping in receptor interactions during host invasion (Leo et al., 2015a).

Type Vf?

The type Vf secretion systems were very recently described as a new class of ATs, with BapA as the prototypical member, and appear to be unique to *Helicobacter pylori*. This proposed class of ATs has a surface-exposed domain inserted into the N-terminal region between the first and second β-strand of an 8-stranded β-barrel domain, and contains no additional passenger at either terminus of the protein. Thus, the proposed passenger actually is an extended loop of the β-barrel domain and the β-barrel is smaller than that of any other AT (Coppens et al., 2018). Though BapA and related proteins have been proposed to be part of the AT family, their topology is very different from the other types of ATs. It is therefore questionable whether these proteins should be considered ATs, and further investigation of the secretion mechanism is required to find out whether these proteins actually self-export in a similar fashion to other ATs.

BIOGENESIS OF ATs

Transport Across Membranes and β-Barrel Insertion

Like most OM proteins, ATs follow a conserved pathway in their biogenesis.

Autotransporters are translated in the cytosol where the polypeptide chain is kept in an unfolded state by the help of chaperones and translocated across the inner membrane (IM) into the periplasm by the SecYEG translocon (Sijbrandi et al., 2003; Tsirigotaki et al., 2017). An N-terminal signal sequence ensures proper recognition of the AT as a Sec target, and targeting

TABLE 1 | Functions of type V secretion system passenger domains.

Function		Mode of action	Example		AT-Type	References
Enzyme	Protease	SPATE	Group I	EspC (*Escherichia coli*)	Va	Stein et al., 1996
				EspP (*Escherichia coli*)		Roman-Hernandez et al., 2014
			Group II	Hbp (*Escherichia coli*)	Va	Soprova et al., 2010
				Pic (*Escherichia coli*)		Abreu et al., 2016
		SPATE-like	IgA protease (*Neisseria gonorrhoeae*)		Va	Hulks and Plaut, 1978; Diebel et al., 2004
		Non-SPATE	NalP (*Neisseria meningitidis*)		Va	Arenas et al., 2013
			Ssph1/2 (*Serratia marcescens*)			Ohnishi et al., 1997; Kida et al., 2008
			LepA (*Pseudomonas aeruginosa*)		Vb	Ohnishi and Horinouchi, 2009
	Lipase/esterase	EstA (*Pseudomonas aeruginosa*)			Va	Wilhelm et al., 2007
		McaP (*Moraxella catarrhalis*)				Lipski et al., 2007
		EstA (*Serratia liquefaciens*)				Riedel et al., 2003
		ApeE (*Salmonella* Typhimurium)				Carinato et al., 1998
		PlpD (*Pseudomonas aeruginosa*)			Vd	Salacha et al., 2010; Da Mata Madeira et al., 2016
		FplA (*Fusobacteriumnucleatum*)				Casasanta et al., 2017
CDI	Growth-inhibition of competing bacteria	CdiA/B (Enterobacteriaceae)			Vb	Diner et al., 2012
		BcpA/B (*Burkholderia pseudomallei*)				Garcia et al., 2013
Alteration of Host Cell Processes		BadA (*Bartonella henselae*)			Vb	Riess et al., 2004
		InvD (*Yersinia pseudotuberculosis*)			Ve	Sadana et al., 2018
Immune evasion	Circumventing host immune response	IgA protease (*Escherichia coli*)			Va	Zinchenko et al., 2018
		EtpA (*Escherichia coli*)			Vb	Roy et al., 2009
		YadA (*Yersinia* spp.)			Vc	Schindler et al., 2012
		Eib (*Escherichia coli*)				Leo and Goldman, 2009; Leo et al., 2011
Cyto-/Hemolysis		VacA (*Helicobacterpylori*)			Va	Cover and Blanke, 2005
		ShlA (*Serratia marcescens*)			Vb	Reboud et al., 2017
		ExlA (*Pseudomonas aeruginosa*)				Yang and Braun, 2000
Adhesin	Adhesion to surfaces/receptors	AIDA-I (*Escherichia coli*)			Va	Laarmann and Schmidt, 2003; Charbonneau et al., 2006
		EhaA (*Escherichia coli*)				
		Pertactin (*Bordetella pertussis*)				Aricò et al., 1993
		FHA (*Bordetella pertussis*)			Vb	Serra et al., 2011
		HMW1/2 (*Haemophilus influenzae*)				Buscher et al., 2006
		YadA (*Yersinia* spp.)			Vc	Tertti et al., 1992; Mühlenkamp et al., 2017
		Eib (*Escherichia coli*)				Leo and Goldman, 2009
		Intimin (*Escherichia coli*)			Ve	Kenny et al., 1997
		InvA (*Yersinia* spp.)				Isberg et al., 2000
	Auto-Agglutination and biofilm formation	Ag43 (*Escherichia coli*)			Va	Sherlock et al., 2006
		FHA (*Bordetella pertussis*)			Vb	Serra et al., 2011
		EtpA (*Escherichia coli*)				Roy et al., 2009
		YadA (*Yersinia enterocolitica*)			Vc	Trunk et al., 2018
		Eib (*Escherichia coli*)				Leo and Goldman, 2009
Intracellular motility	Activation of actin polymerases	IcsA (*Shigella flexneri*)			Va	Goldberg and Theriot, 1995
		YapV (*Yersinia* spp.)				Besingi et al., 2013
		BimA (*Burkholderia* spp.)			Vc	Benanti et al., 2015

and secretion through the IM and signal peptide cleavage after transport works in the same way as for other Sec-secreted proteins (Papanikou et al., 2007). Some ATs, like Hbp and AIDA-I, show an extended Sec signal sequence which might aid in slowing down IM translocation and thus in prevention of premature folding and aggregation of the AT within the periplasm (Henderson et al., 1998; Szabady et al., 2005; Jacob-Dubuisson et al., 2013). For type Vb systems, it has been shown that some TpsA passengers aggregate much faster than others and therefore retaining the AT bound to the Sec is beneficial; Otp is a protein which is not prone to aggregation and therefore does not require fast transport to the OM (Choi and Bernstein, 2010). In other systems like FHA, quick secretion is of importance as degradation of unfolded FHA by DegP is more likely due to the length of the FHA precursor (Baud et al., 2009).

In the periplasm, ATs are kept unfolded but in a folding-competent state, shielded from aggregation by periplasmic chaperones like SurA, Skp and DegP (Baud et al., 2009; Ieva and Bernstein, 2009; Oberhettinger et al., 2012; Pavlova et al., 2013; Weirich et al., 2017). Insertion of the β-barrel domain of ATs is then facilitated by the β-barrel assembly machinery (BAM) complex (Jain and Goldberg, 2007; Leo et al., 2012). In *E. coli*, it is composed of five subunits, BamA through BamE. This complex interacts with most if not all OM integral β-barrel proteins (Lee et al., 2018). The 16-stranded β-barrel integral membrane protein BamA helps in insertion of the substrate barrel into the OM by a not yet entirely understood mechanism (Schiffrin et al., 2017). For type Va ATs, it has been clearly shown by crosslinking experiments that the 12-stranded β-barrel membrane anchor folds and inserts into the OM aided directly by the BAM complex. The passenger of EspP, an *E. coli* AT, for example, can be crosslinked to periplasmic chaperones, as well as to its β-barrel domain and to BamA (Ieva and Bernstein, 2009; Pavlova et al., 2013). Similarly, type Vc and Ve ATs interact with the Bam complex, as shown for YadA and Invasin (Roggenkamp et al., 2003; Oberhettinger et al., 2015).

Passenger Secretion

While most other bacterial secretion systems have access to energy sources like proton gradients across the IM or are directly energized by cytoplasmic ATP, ATs only span the OM, which is too leaky for ion gradients, and the periplasm is devoid of ATP (Nikaido and Vaara, 1985; Silhavy et al., 2006). Various models for how the secretion and folding process of passengers is energized have been proposed. One plausible explanation is that the energy for transport comes from the intrinsic folding capacity of the AT itself, either directly driving export or leading to a Brownian ratchet model where, once secreted, the passenger cannot slide back into the periplasm and is therefore driven to move outside the cell and fold (Henderson et al., 2004; Choi and Bernstein, 2010). Furthermore, asymmetric charge distribution within the passenger has been put forward as a possible driving factor for passenger secretion (Kang'ethe and Bernstein, 2013).

Passenger transport and secretion differ slightly between the various AT subclasses due to differences in domain organization. In type Va ATs, the passenger is transported via a C-terminus-first mechanism. According to the widely accepted hairpin-loop model of secretion, a hairpin-loop is formed at the C-terminus of the passenger in the interior of the β-barrel, followed by sequential folding of the passenger on the cell surface starting from the C-terminus (Junker et al., 2006). This was shown for multiple members of the type Va AT subclass, including Pertactin, Hbp and EspP (Junker et al., 2009; Peterson et al., 2010; Soprova et al., 2010).

For type Vb secretion, models are somewhat different since in the TPSSs the β-barrel domain is separated from the passenger domain. After the TpsB transporter is properly inserted into the OM by the BAM complex, recognition of TpsA by TpsB is provided by interaction of the TpsB POTRAs and the N-terminal TPS signal of TpsA (Baud et al., 2009). The TPS signal is a conserved stretch with an amphipathic character that remains unfolded in the periplasm. Association and dissociation rates of the TPS signal with the TpsB POTRA domains are high based on surface plasmon resonance experiments, making the interaction transient, and helping in later release of the TpsA substrate from its transporter (Delattre et al., 2010; Guérin et al., 2017). NMR experiments have shown similar highly dynamic interactions (Garnett et al., 2015). Crosslinking experiments have further shown that the TPS signal interacts with the TpsB POTRA domains, as well as some central amino acids within the barrel lumen (Baud et al., 2014). Similarly to all other Type V secretion systems, it is assumed that during transport, TpsA is unfolded as it passes through the central pore of the TpsB barrel and that folding of the substrate occurs during exit from the transporter barrel.

There are two different models for how the export of the TpsA is initiated: one is that, like in other ATs, a hairpin is formed within the barrel pore driving folding of the secreted substrate in a C-to-N direction. Release of the TpsB-bound TPS domain would then occur at the end of secretion, after major parts of TpsA have already folded (Pavlova et al., 2013; Norell et al., 2014). In this case, the high on/off rate between the PORTA domains and the TPS signal domain would facilitate the release that is based on the pulling forces generated by the folding process itself (Guérin et al., 2017). According to the second model, the N-terminal TPS domain nucleates folding, i.e., the TPS domain is exported first and the rest of the protein folds N-to-C (Hodak and Jacob-Dubuisson, 2007). The fact that the TpsA proteins' N-terminal domain can also fold independently bolsters this argument (Clantin et al., 2004, 2007).

In type Vc ATs, passenger secretion is more intricate due to the trimeric nature of the proteins. Three passenger polypeptide chains have to be orchestrated through a comparatively narrow β-barrel domain. After formation of the 12-stranded β-barrel, the passenger is transported to the exterior of the cell starting with the formation of a hairpin loop of each of the three passenger domains followed by folding of the coiled coil stalk (Linke et al., 2006; Szczesny and Lupas, 2008; Mikula et al., 2012; Chauhan et al., 2019). Transport of three distinct polypeptide chains in a hairpin loop conformation across a comparably small barrel might be sterically challenging. The interior of

type Vc β-barrels contains many glycine and alanine residues which have small side chains, and it has been suggested that this facilitates passage of multiple chains though the barrel interior (Mikula et al., 2012). Additionally, β-barrel proteins are not necessarily fully rigid pores. The capacity of "breathing" movement without breakage of the hydrogen bonding has already been shown for the usher protein FimD, which in its apo-structure is more narrow than when bound to a transport substrate (Phan et al., 2011). Similar breathing behavior would be necessary in type Vc autotransport to accommodate all chains simultaneously. An additional problem comes with the highly intertwined passenger structure in type Vc systems. Sequential folding after initial hairpin formation would build up mechanical strain. It has been shown for some examples that an YxD/RxD motif toward the C-terminus of the passenger helps in initiation of passenger folding and folding outside the membrane anchor, potentially by releasing mechanical strain. YxD motifs furthermore stabilize right-handed coiled-coils whereas RxD motifs support left-handed coiled-coils (Alvarez et al., 2010). In addition, while the core residues of coiled-coil proteins are generally hydrophobic, some trimeric AT passengers contain hydrophilic residues in these positions. These residues can coordinate anions, which might allow sequences that are otherwise not easily folded to interact and stabilize (Hartmann et al., 2009; Leo et al., 2011).

It is not yet entirely clear how passenger secretion works in type Vd systems, and what role the POTRA domain plays in this (Salacha et al., 2010). It might function either as a chaperone for the passenger, aiding in secretion, or aiding in the recruitment of proteases for passenger cleavage. In some strains of *F. nucleatum* the passenger domain of FplA seems to be cleaved off while in other strains this could not be shown (Casasanta et al., 2017). It is unclear whether proteolytic cleavage of the passenger of type Vd ATs is achieved via autoproteolysis, like in some type Va ATs, or via an independent protease, like in the example of the NalP cleaving the type Va AT IgA protease for release from its β-barrel domain (Salacha et al., 2010; Casasanta et al., 2017). However, the fact that type Vd passengers remain uncleaved in some strains and when heterologously expressed in *E. coli* supports the latter interpretation (Salacha et al., 2010).

The biogenesis of type Ve ATs is similar to the one of type Va ATs. Although the topology of type Ve ATs is inverted, the β-barrel functions as a transport pore in an analogous way via formation of a hairpin-loop, and the passenger is secreted in a very similar fashion to the passenger secretion of classical ATs, but in the opposite direction (N-to-C rather than C-to-N) (Oberhettinger et al., 2012, 2015). Folding is energized by sequential folding of the extracellular Ig-like domains, as shown for the example of Intimin (Leo et al., 2016).

FUNCTIONS OF AT PASSENGERS

Research on ATs has traditionally focused on a single protein and its function (often in pathogenesis) (**Figure 2**), or on individual subclasses based on topology and biogenesis (**Figure 1**). The latter has led to the systematic sub-classification into type Va to Ve secretion systems, but this classification does not reflect the function of the passenger. Passengers from different subclasses can have similar functions despite structural differences, and some individual passengers mediate multiple functions. Therefore, a systematic differentiation between passenger functions is harder to achieve (Dautin and Bernstein, 2007; Drobnak et al., 2015). Furthermore, while some functions can be described as general virulence traits and can be found in a wide variety of Gram-negative bacteria, such as protease activity (Yen et al., 2008; Dautin, 2010), other functions are rather unique and are involved in tasks specific to the bacterium and its lifestyle, such as intracellular mobility and nutrient acquisition in limited environments (Luckett et al., 2012; Benanti et al., 2015).

Tables 1, **2** show an overview of the functions and exemplary members of the functional groups.

Enzymatic Activities

Passengers with enzymatic functions can directly alter host cell processes, be involved in immune evasion or help in the establishment and colonization of niches. The large diversity of possible enzymatic functions includes protease activity, lipase activity, but also contact-dependent growth inhibition (CDI) mediated by ADP ribosyl cyclases, adenosine deaminases, or nicking endonucleases.

Lipases and Esterases

Lipase and esterase activity can be found in type Va as well as in type Vd passenger domains. It has been proposed that these enzymes aid in niche establishment especially for intracellular bacteria, but also in alteration of host cell signaling by phosphoinositide (PI) cleavage (Casasanta et al., 2017). Though there are some ideas and models for the role that ATs with lipase and esterase function play in virulence, their exact function is not clear, and it is quite possible that AT lipases of different bacteria act on different targets in the host (Da Mata Madeira et al., 2016; Casasanta et al., 2017).

A prototypical example for a passenger with a lipase domain is EstA, a type Va AT of *P. aeruginosa.* In this protein, the passenger is not cleaved from its β-barrel domain (Wilhelm et al., 1999). EstA is implicated in the cleavage of rhamnolipids, which by themselves are important for biofilm formation and have toxic properties (Davey et al., 2003; Klausen et al., 2003). When deleting the *estA* gene, rhamnolipids in biofilms shifted from di-rhamnolipids to mono-rhamnolipids, indicating that rhamnolipids might be a target of EstA (Wilhelm et al., 2007; Tielen et al., 2010). Knockouts of *estA* also showed alterations in motility. While swimming and swarming are absent in *estA* deletion strains, twitching motility is enhanced, which seems somewhat puzzling taking into account that only swarming, not swimming or twitching motility is influenced by the rhamnolipid content of a biofilm (Kohler et al., 2000; Déziel et al., 2003; Wilhelm et al., 2007). Other differences in motility can thus not be explained by rhamnolipids as targets of EstA alone (Wilhelm et al., 2007). Other type Va AT with comparable lipolytic functions can be found in *Moraxella catarrhalis* (Mcap), *Serratia liquefaciens* (EstA) and also *Salmonella typhimurium*

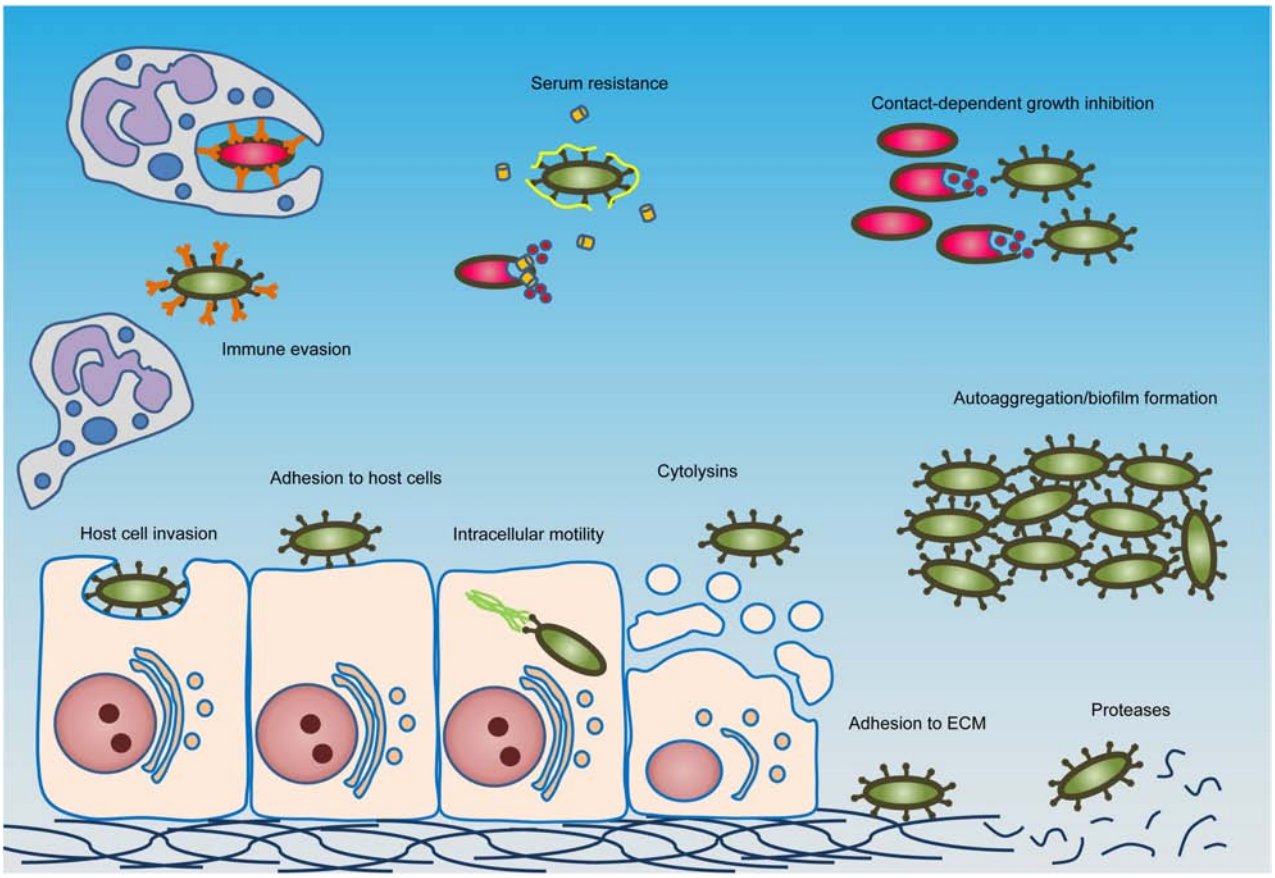

FIGURE 2 | Typical activities of autotransporter proteins. The major activities found in autotransporters are shown schematically. Green bacteria express autotransporters, but red bacteria do not. Autotransporters mediate activities such as adhesion to host cells or the extracellular matrix (ECM), invasion of host cells, immune evasion and serum resistance, contact-dependent growth inhibition, toxicity toward host cells, intracellular mobility, protease activity, and autoaggregation and biofilm formation. Cytolysin activity can be mediated by lipases or pore-forming toxins. Immune evasion can be accomplished by a variety of mechanisms, such as by binding to the constant regions of antibodies to prevent opsonisation (depicted here), cleavage of antibodies, mediating phagocytosis resistance or modulating immune cell signaling and gene regulation. In serum resistance, bacteria become resistant to the bactericidal effects of complement (shown as orange cylinders) by binding to complement-regulatory factors such as Factor H (shown as yellow ribbons). For full descriptions, see main text.

(ApeE) (Carinato et al., 1998). EstA of *S. liquefaciens*, for example, is involved in cellular signaling by providing the cells with enough lipids for synthesis of second messenger molecules (Riedel et al., 2003). This function could not be verified for EstA in *P. aeruginosa*, however (Wilhelm et al., 2007).

In type Vd ATs, all passengers described so far have lipase activity. Though lipase activity can also be found in type Va ATs, the structure and domain organization of type Vd ATs is very distinct with a single POTRA domain fusing the β-barrel and the passenger even though both passengers have a α/β hydrolase fold (Salacha et al., 2010; Casasanta et al., 2017). Furthermore, the catalytically active site in type Va lipases like the GDSL lipase EstA usually consists of a catalytic triad while type Vd ATs show a catalytic dyad (Desvaux et al., 2005; Brzuszkiewicz et al., 2009; van den Berg, 2010). Prototypic for type Vd ATs are PlpD from *P. aeruginosa* and FplA from *F. nucleatum* (Salacha et al., 2010; Casasanta et al., 2017). The name of the *Pseudomonas* proteins comes from structural similarity of the passenger to patatin from potatoes; hence the name patatin-like protein D. So far more than 200 Gram-negative bacterial species have been found to encode PlpD orthologues, including a wide variety of pathogenic as well as non-pathogenic, environmental bacteria (Salacha et al., 2010). The patatin-like domain of PlpD harbors A1 phospholipase activity (Da Mata Madeira et al., 2016). Similarly, the PlpD homologue from *F. nucleatum*, FplA, has phospholipase A1 activity and displays very high hydrolytic activity toward artificial substrates (Casasanta et al., 2017). The structure of the PlpD passenger has been solved, and the active site offers enough space to accommodate C16 to C20 acyl chains (Da Mata Madeira et al., 2016). The catalytic dyad in PlpD consists of Ser60 and Asp207, which are in close proximity to a hydrophobic helix within the cleft containing the active site, which probably stabilizes the lipid interaction (Casasanta et al., 2017). Similarly, in FplA, the catalytic residues are Ser98 and Asp243 (Casasanta et al., 2017). Biochemical experiments with FplA showed no binding affinity for phospholipids like phosphatidycholine (PC), phosphatidyethanolamine (PE), and phospatidic acid (PA) but

TABLE 2 | Adhesins and adhesion targets of autotransporters.

Type	Host bacterium	Binding partners	References
Va			
AIDA-I	*Escherichia coli*	glycoprotein	Laarmann and Schmidt, 2003
EhaB		collagen, laminin	Chagnot et al., 2012
Tsh		collagen, fibronectin	Kostakioti and Stathopoulos, 2004
Hap	*Haemophilus influenzae*	fibronectin, laminin, collagen	Fink et al., 2003
MisL	*Salmonella enterica*	collagen, fibronectin	Dorsey et al., 2005
ShdA			Kingsley et al., 2002, 2004
Vb			
FHA	*Bordetella* spp.	heparin, dextran	Menozzi et al., 1994
EtpA	*Escherichia coli*	flagellin	Roy et al., 2009
HMW1/2	*Haemophilus influenzae*	sialylated glycoprotein/ unknown	St. Geme, 1994; St. Geme and Yeo, 2009
MhaB1	*Moraxella catarrhalis*	mammalian cells	Balder et al., 2007
HrpA	*Neisseria meningitidis*	mammalian cells	Schmitt et al., 2007
Vc			
BadA	*Bartonella henselae*	collagen, laminin, fibronectin	Riess et al., 2004
EhaG	*Escherichia coli*	laminin, fibronectin, fibrinogen, collagen	Totsika et al., 2012
UpaG			Valle et al., 2008; Totsika et al., 2012
DsrA	*Haemophilus ducreyi*	fibronectin	Leduc et al., 2008
NcaA		Collagen	Fulcher et al., 2006
Hia	*Haemophilus influenzae*	cells	Spahich, 2011
UspA	*Moraxella catharralis*	fibronectin, laminin	Tan et al., 2005, 2006
NadA	*Neisseria meningiditis*	cells	Tavano et al., 2011
NhhA		laminin, heparan sulfate, cells	Scarselli et al., 2006
SadA	*Salmonella typhimurium*	cells (no ECM)	Raghunathan et al., 2011
YadA	*Yersinia enterocolitica*	collagen, fibronectin, laminin	El Tahir and Skurnik, 2001
Ve			
FdeC	*Escherichia coli*	cells, collagen	Nesta et al., 2012
Intimin		Tir protein	Batchelor et al., 2000
Invasin	*Yersinia* spp.	β1-integrins	Isberg et al., 2000
InvD		IgG/IgA	Sadana et al., 2018

it seems to bind to phosphatidyinositol (PI) phosphates which acts in signaling of host cells (Casasanta et al., 2017). It has been proposed that lipase activity is important for establishing a niche especially for intracellularly living bacteria by recognizing phosphorylated PIs and by their cleavage altering cell signaling (Casasanta et al., 2017). Furthermore, this lipase activity might also help in cytosolic release of the bacteria from the vacuole and phagosomal survival within the host cell, which are important for niche establishment and an intracellular lifestyle of this bacterium (Casasanta et al., 2017).

Proteolytic Activity

Proteolytic cleavage of host target proteins can be beneficial for the bacterium in terms of virulence. A number of proteolytically active type Va AT passengers have been discovered. The first AT discovered is Immunoglobulin A (IgA) protease from *Neisseria gonorrhoeae* and *N. meningitidis.* The passenger of IgA protease can be divided into a 106 kDa protease domain, a more C-terminal 3 kDa γ-peptide, a 12–44 kDa α-peptide, a linker region and the C-terminal β-barrel membrane anchor (Halter et al., 1984). Following export, the passenger is cleaved off from the β-barrel transporter to function as a protease in virulence. Cleavage of the passenger can happen in different ways: either the passenger is autoproteolyzed or cleaved by another AT called NalP in a phase-dependent fashion (Roussel-Jazédé et al., 2010). NalP-dependent cleavage results in the release of the full passenger domain, including the protease domain, the α-peptide, the γ-peptide and the linker region, while autoproteolysis results in the release of fragments of different sizes: either the protease, the protease and the γ-peptide or the complete passenger. The autoproteolytic cleavage seems to be strain-dependent and can have different effects on the role the released passenger has in virulence.

More recently, it has been shown that IgA protease can also modulate host gene expression (Hulks and Plaut, 1978). If the passenger is cleaved off together with the α-peptide, the α-peptide via its nuclear localization-like sequence can guide the IgA protease domain to the host cell nucleus. The IgA protease domain can then cleave NF-κB and p65/RelA in the nucleus and thereby modulate the entire host cell response to pathogenic stressors (Pohlner et al., 1995; Besbes et al., 2015).

Furthermore, IgA proteases have been shown to cleave LAMP1, a highly glycosylated endosomal and lysosomal membrane protein which normally protects the membrane from degradation (Hauck and Meyer, 1997). Degradation of LAMP1 in turn seems beneficial for the growth of intracellular bacteria, as *Neisseria* lacking IgA protease grow slower intracellularly than wild-type bacteria (Lin et al., 1997). *Neisseria* pilus proteins and porins influence the calcium intake of epithelial cells, leading to the exocytosis of endosomes (Ayala et al., 2002). This shows that IgA proteases secreted by *Neisseria* have multiple targets and play an important role in survival and growth of *Neisseria* in infection contexts.

Autotransporter proteases do not only play a role in host immune response circumvention and establishing a niche in the host, but also in nutrient acquisition. As an example, AaaA from *P. aeruginosa* is involved in nitrogen acquisition from peptides in chronic infections. It acts as an aminopeptidase aiding in long-term infections in mice (Luckett et al., 2012). Another group of type Va ATs with protease activity are the SPATEs (Serine Protease Autotransporters of *Enterobacteriaceae*) proteins. Their targets can be very diverse; one prominent example is Hbp (hemoglobin protease or hemoglobin binding protein) from *E. coli.* Hbp employs an active Ser residue for cleavage of hemoglobin, but shows no specificity for other proteins such as

albumin (Otto et al., 2005). Hbp, like all SPATEs, is cleaved off after passenger transport (Dautin, 2010). Functionally, Hbp is used by enterohemorrhagic *E. coli* strains for heme acquisition (Dautin, 2010).

Contact-Dependent Growth Inhibition (CDI)

Enzymatically active passenger domains can also be found in type Vb ATs. Like in the type Va ATs, there can be dramatic differences in enzymatic functions. One major function of the passengers of type Vb ATs is CDI. Here, the passenger domains can function as nucleases, deaminases, and also as metallopeptidases. The name of this functional class of type Vb ATs is potentially misleading, since it is still unclear whether growth inhibition of competing bacterial strains is the main evolutionary purpose of this system (Guérin et al., 2017).

Contact-dependent growth inhibitions are transporter-effector pairs called CdiB/A pairs, where CdiA corresponds to TpsA and CdiB to TpsB (see section on type Vb transport, above) (Ruhe et al., 2013a). Upon secretion of CdiA by CdiB, CdiA acts as a toxin that can inhibit the growth of other bacteria, typically of the same species. In order to render themselves immune against their own CdiA toxin, the *cdi* gene cluster encodes an additional immunity protein named CdiI (Aoki et al., 2005). The receptor for *E. coli* CdiA is BamA, the β-barrel protein of the BAM (Aoki et al., 2008). BamA is an essential protein in all bacterial species, but shows considerable sequence variability in its extracellular loops, allowing discrimination between closely and more distantly or unrelated species for CDI (Ruhe et al., 2013b).

Growth inhibition by the cytotoxic C-terminus of CdiA (CdiA-CT) is then facilitated by diverse mechanisms such as nuclease activity, adenosine deaminase activity, metallopeptidase activity, or ADP ribosyl cyclase activity (Ruhe et al., 2013a). One well-studied example of a CDI system is the system of *E. coli* UPEC 536, which encodes a CdiA-CT that harbors tRNase activity (Aoki et al., 2010). Interestingly, this protein is not active until in its host, where it binds to CysK, a protein involved in the catalysis of L-serine to L-cysteine (Diner et al., 2012). Only upon binding to CysK is CdiA able to cleave tRNA. Normally, CysK interacts with CysE, but CdiA has a common amino acid motif with CysE that allows it to bind CysK and become active (Diner et al., 2012).

Another example of a CDI system is the *cdiAIB* system of *Burkholderia pseudomallei* coding for BcpAIB. Here, BcpA is the secreted protein that plays a role in cooperative bacterial communication during biofilm formation. Architecturally, BcpA also harbors a toxic C-terminus, but secretion of BcpA enhances the formation of stable biofilms, possibly by influencing the amount of extracellular DNA as part of the stable biofilm. It has also been proposed that BcpA has nickase activity which might consolidate the microbial community in a biofilm by crosslinking eDNA or attaching the bacteria to eDNA within a biofilm (Garcia et al., 2013; Ruhe et al., 2013a). This example suggests that CDI systems not only provide a growth advantage over other bacterial strains in a competitive environment, but can also play more complex roles.

Immune Evasion

Immune evasion is a collective term for a number of highly specialized mechanisms employed by some bacteria to escape from host immune responses. ATs can participate in immune evasion by interfering with different components of the host immune system.

The first level of immune evasion is serum resistance, which means the ability to survive the action of the complement system that is part of the innate immune response. Serum resistance is achieved by binding to and/or inactivating different components of the complement cascade, such as by binding to Factor H and C3 through C9 products. Binding complement proteins via adhesins like the YadA from *Y. enterocolitica* or the classical AT Vag8 from *Bordetella pertussis* inhibit the full cascade and thus formation of the terminal complement complex which would lead to lysis of the pathogen (Marr et al., 2011; Schindler et al., 2012). YadA is able to sequester different factors, like Factor H and C4b-binding protein, involved in complement regulation (Grosskinsky et al., 2007; Biedzka-Sarek et al., 2008; Kirjavainen et al., 2008). In addition, YadA can bind directly to C3b and iC3b, which in turn promotes Factor H binding and allows *Y. enterocolitica* to escape killing by complement (Schindler et al., 2012). YadA-expressing *Yersinia* can also bind to a variety of host surfaces, initiating virulence processes like secretion of *Yersinia* outer proteins (Yops) via the type III secretion system and thereby killing host immune cells like neutrophils (Rosqvist et al., 1991; Bliska et al., 1993).

Another, more indirect means of host immune evasion is the disguise of immunogenic structures on the bacterial surface. EtpA from *E. coli* for example binds to flagella, which may serve in protection against the host immune system by covering FliC, the main flagellar protein, as an antigen; this may help the bacterium to colonize the host (Roy et al., 2009). EtpA serves a double purpose here, as it also mediates binding to host surfaces and thus bacterial adhesion and biofilm formation (Roy et al., 2009). ATs can also bind factors of the adaptive immune response. The Eib proteins from *E. coli* evade the host immune system by binding to Fc antibody fragments of IgG, possibly in order to avoid opsonization and subsequent phagocytosis (Leo and Goldman, 2009). A more prominent and well-studied example for interactions of ATs with the adaptive immune system is IgA protease of *Neisseria* spp. Here, the serine protease domain exerts endopeptidase activity, recognizing and cleaving the TPPTPSPS motif in the hinge region of human IgA1 and IgA2 and releasing the antigen-binding Fab region from the Fc region. This allows the bacteria to evade opsonization (Plaut et al., 1975, 1977).

Alteration of Other Host Cell Processes

Autotransporters can also influence other host processes beyond the host immune response, typically to promote pathogenic processes. A well-studied example is the TAA BadA, which activates hypoxia-inducible factor 1 (HIF-1), which in turn leads to the release of vaso-endothelial growth factor (VEGF) inducing endothelial proliferation (Kempf et al., 2001). Interaction of BadA-expressing *Bartonella henselae* with endothelial cells has

been shown to inhibit apoptosis, supporting the effect of VEGF induced vaso-endothelial proliferation (Kempf et al., 2005). Interestingly, a comparative study investigating the interplay of BadA with the type IV secretion system VirB/D4 in different clinical isolates showed that the enormous length of the BadA stalk (240 nm) might interfere with injection of toxic proteins into the host cell by the type IV secretion system in *B. henselae* (Riess et al., 2004; Müller et al., 2011). This at first seems puzzling, but in light of the intracellular lifestyle of these bacteria, encouraging endothelial growth and inhibiting apoptosis as a natural host cell reaction to infection would benefit the bacteria in a way that the bacteria promote host cell growth for intracellular replication (Schülein et al., 2001).

Alterations in host immune responses not only benefit bacteria with an intracellular lifestyle but also bacteria invading deeper tissues, such as some *Yersiniae*. InvD from *Y. pseudotuberculosis* has recently been shown to utilize host antibody binding during acute infections of the intestinal tract for virulence (Sadana et al., 2018). InvD is a type Ve AT which specifically binds to the Fab region of IgA antibodies. This binding might enable InvD expressing *Yersinia* to alter the host immune response. This way immune exclusion, normally preventing bacteria from crossing the mucosal barrier, can be circumvented and thus allows the bacteria to invade deeper tissues (Sadana et al., 2018). Similarly, the *Shigella flexneri* AT SIgA is involved in invasion of the Peyer's patches, though *Shigella* is not usually found in underlying tissues (Mantis et al., 2002; Favre et al., 2005).

Cyto- and Hemolysins

Passenger domains functioning as cyto- and hemolysins are so far mostly known in type Vb ATs. Here, toxins like ShlA from *S. marcescens* and ExlA from *P. aeruginosa* are secreted and lead to leakage from or lysis of host cells. The cyto- and hemolytic activity of the TpsA C-termini is most often conferred by pore formation within the target cell membrane, triggering a cascade of downstream events that cause the cells to lose their intercellular integrity and to die of ATP depletion. Both ShlA and ExlA form pores in epithelial and endothelial cells causing a massive influx of cations that reduces or abolishes the membrane potential. This leads to ATP depletion and to the activation of eukaryotic proteases cleaving cadherin, leading to breakage of the epithelial barrier (Hertle et al., 1999; Reboud et al., 2017). A classical AT with a cytotoxic passenger can be found in *H. pylori* and is named VacA (vacuolating cytotoxin A). The passenger of VacA is cleaved off and acts in induction of host cell vacuolation, which does not seem to be lethal for the host cell but is important for efficient colonization of the bacteria within the host (Cover and Blanke, 2005). VacA can also act on mitochondria and thus induce apoptosis as part of VacA cell toxicity (Cover and Blanke, 2005).

Adhesion

Adhesion to host cells is a major attribute of many different ATs. Interactions with host cells are usually conferred by adhesins belonging to ATs of types Va, b, c, and e. Importantly, "adhesin" serves as a collective term for different types of interactions, with host cells, tissues, or non-living surfaces. In pathogenesis, depending on the individual adhesin and host organism, this can range from diffuse adhesion to a variety of surface molecules to very specific, high-affinity interactions with a given receptor as shown in **Table 2**.

Adhesion to Surfaces

In order for bacteria to thrive in a competitive environment or during an ongoing infection, the ability to adhere to biotic and abiotic surfaces is pivotal to the bacteria, both in direct contact with host cells and as a first step toward biofilm formation. Being able to adhere to a surface ensures not only interaction with a target cell or surface but also helps the bacteria to regulate gene expression optimal for biofilm conditions. AIDA-I is a major adhesin in *E. coli* that belongs to the class of classical ATs (Benz and Schmidt, 1989). It has been shown to confer diffuse adhesion to human cells and also to other cell types by interaction with surface glycoproteins of the host cells (Laarmann and Schmidt, 2003; Sherlock et al., 2004). Both the receptors and AIDA-I itself are glycosylated. The protein responsible for glycosylation of AIDA-I is encoded directly upstream of the *aidA* gene and is named *aah* (Benz and Schmidt, 2001). Without glycosylation, AIDA-I does not function as an adhesin anymore, though glycosylation appears to be dispensable for autoaggregation, another virulence trait conferred by AIDA-I (Benz and Schmidt, 2001; Sherlock et al., 2004). The passenger of AIDA-I can be cleaved *in vitro*, and it has been hypothesized that cleavage of the passenger might contribute to persistence of the bacterial infection as released AIDA-I passengers facilitate host cell entry (Charbonneau et al., 2006; Pizarro-Cerdá and Cossart, 2006).

In contrast to the diversity of target structures of AIDA-I, the type Vb adhesins FHA from *B. pertussis* and EtpA from *E. coli* target a smaller set of host cell structures in order to confer adhesion. FHA binds specifically to certain surface glycans in human lung epithelial cells (Tuomanen et al., 1988; Relman et al., 1990). FHA favors some carbohydrates over others on the surface of ciliated cells, leading to adhesion to the target and later infection of the lung epithelial cells. Also, EtpA has a more specific mode of action by binding to flagellin, as described in Section "Immune Evasion" (Roy et al., 2009).

Adhesin functions have also been found in essentially all type Vc ATs studied so far, leading to the term trimeric autotransporter adhesin ("TAA") (Linke et al., 2006). The best-studied adhesin belonging to this group is YadA, the *Yersinia* Adhesin A. This protein is encoded on the 70 kb pYV virulence plasmid in all human pathogenic *Yersinia* species including *Y. enterocolitica*, *Y. pseudotuberculosis*, and *Y. pestis*. However, in *Y. pestis* YadA is not expressed at all due to a frameshift in its gene (Rosqvist et al., 1988; Skurnik and Wolf-Watz, 1989), and the role of *Y. pseudotuberculosis* YadA has been elusive since it seems to be dispensable for full virulence (Bolin and Wolf-Watz, 1984). In *Y. enterocolitica*, YadA is important for a multitude of virulence-associated traits. The YadA β-roll head domain at the very N-terminus of the passenger plays an important role

in binding to different ECM proteins in the host (El Tahir and Skurnik, 2001). YadA associates with general binding to ECM molecules, including collagen, laminin, fibronectin, and vitronectin (Emody et al., 1989; Flügel et al., 1994; El Tahir et al., 2000; Heise and Dersch, 2006; Mühlenkamp et al., 2017). The interaction of YadA with collagen relies on binding to a triple-helical structure of collagen rich in iminoacids and poor in charged residues (Leo et al., 2008). Because of the high density of YadA on the cell surface during infections it is possible for YadA to bind to collagen strongly despite the low affinity of the interaction (Leo et al., 2010).This contributes to host cell attachment and tissue invasion. For the latter, expression of both YadA and Invasin seems important (Bliska et al., 1993; Eitel et al., 2002). Entry into epithelial cells is needed to further disseminate to underlying tissues and to Peyer's patches and subsequent infection of the liver and spleen (Isberg et al., 1987). BadA from *B. henselae* is among the largest characterized trimeric AT adhesins, with an overall length of 240 nm and a molecular weight of 984 kDa of the trimer (Riess et al., 2004). Similarly, to YadA, BadA binds to ECM proteins including collagen, fibronectin, and laminin (Goldman and Linke, 2011; Müller et al., 2011). The stalk domain of BadA is important for binding to fibronectin, as BadA mutants lacking most of the stalk cannot bind fibronectin anymore (Kaiser et al., 2012). Apart from the stalk binding to fibronectin, most of the adhesive properties lie within the BadA head domain (Müller et al., 2011; Kaiser et al., 2012).

Adhesion to Receptors

Not all ATs bind to multiple surfaces in a promiscuous fashion. Some ATs also bind to specific host receptors, or even to bacterial receptors injected into the host. Intimate contact initiated by Intimin, an *E. coli* type Ve AT, employs such a bacterial receptor inserted into the host membrane named Translocated intimin receptor (Tir). During infection of the small intestine of the host, enteropathogenic *E. coli* and enterohemorrhagic *E. coli* (EHEC and EPEC) induce attaching and effacing (A/E) lesions of the mucosal membrane. These A/E lesions are characterized by polymerization of actin and other cytoskeletal proteins leading to the demise of the cells and at the same time to building an actin pedestal for adhesion of the pathogen. In order for the bacterium to achieve this infection platform, EHEC and EPEC genomes include a pathogenicity island termed LEE (locus of enterocyte effacement), which among other factors encodes for the Tir receptor and intimin (Kenny et al., 1997; Deibel et al., 1998; Gauthier et al., 2000). Though the exact mechanism by which the Tir receptor is inserted into the host cell plasma membrane is still unclear, host cell delivery is facilitated by the bacterial type III secretion system, which is also encoded within the LEE island (Gauthier et al., 2000; Frankel et al., 2001). While Tir is important as a receptor for the Intimin passenger, the Intimin-Tir complex also has implications in cytoskeletal dynamics in the host cell and is thus a multifactorial virulence factor of *E. coli* (Kenny, 1999; Goosney et al., 2001).

Another important member of the type Ve ATs is Invasin of *Yersinia* spp. In contrast to Intimin, it does not bind via a bacterial receptor in the host cell, but instead binds directly to β_1-integrins expressed on the apical side of gut epithelial cells (Isberg et al., 1987, 2000; Schulte et al., 2000). As a consequence of this binding, *Yersinia* spp. are internalized into the cell via endocytosis and can infect the underlying tissue (Isberg and Leong, 1990; Pepe, 1993; Grassl et al., 2003). Subsequently, Invasin-expressing bacteria can infect the lymph nodes and disseminate into other tissue types (Isberg et al., 2000).

Other subclasses of ATs can also use specific receptors expressed on host cells for adhesion. UspA1, a *M. catarrhalis* TAA, binds to carcinoembryonic antigen-related cell adhesion molecule 1 (CAECAM-1), a cell surface protein displayed by epithelial cells (Hill and Virji, 2003). Interestingly, UspA1 is an example of an AT where the binding function lies within the coiled-coil stalk of the protein (Conners et al., 2008). Due to the length of UspA1 and the density with which UspA1 covers the surface of *M. catarrhalis*, this interaction requires bending of the stalk in order to interact with CAECAM-1 as a receptor (Conners et al., 2008). In addition to the interaction with CAECAM-1, UspA1 also binds to laminin and fibronectin via the head domain in a similar fashion as other type Vc ATs (Tan et al., 2005).

Autoaggregation and Biofilm Formation

Biofilms act as a protective mesh that protects bacterial communities from outside influences. Biofilms are a lifestyle that is distinct from that of planktonic bacteria; this is reflected in very different gene expression patterns and by signaling processes inside the biofilm that lead to this adaption. Once established, biofilms can be very hard to remove and are a special challenge in infection and hygiene contexts (Monds and O'Toole, 2009; Trunk et al., 2018).

Both initial adhesion to surfaces and autoaggregation are necessary for establishing biofilms on surfaces. A model system for self-recognition leading to autoaggregation of the bacteria is Ag43 (Antigen 43), a type Va AT from *E. coli*. Ag43 confers intercellular binding by a self-recognizing handshake interaction. By this mechanism the bacteria flocculate, which is beneficial in colonization, immune evasion and persistence in the host (Klemm et al., 2004; Sherlock et al., 2006).

Also FHA aids in the formation of biofilms and thus directly contributes to host colonization and persistence during pathogenesis in *B. pertussis*, together with other proteinaceous factors regulated by the BvgAS system, like fimbriae and ACY, which negatively regulates biofilm formation by interaction with FHA (Irie et al., 2004). In this context, FHA seems to be important in initiation of the attachment of bacteria to the surface, thereby aiding in building micro-colonies that later become part of a bacterial biofilm. FHA also seems to play a major role in maintaining the integrity of the biofilm (Serra et al., 2011). Surprisingly, free FHA actually inhibits the formation of biofilms. This has been speculated to play a regulatory role in biofilm formation during pathogenesis of *B. pertussis* (Serra et al., 2011). In *E. coli*, the type Vb protein EtpA plays a major role in adhesion and biofilm formation. In contrast to free FHA that regulates biofilm formation, secreted EtpA plays a bridging role, aiding in the interaction of flagella with intestinal cells during enterobacterial infection. EtpA binds conserved domains of the

flagellar protein FliC at the tip of the flagellum. EtpA then guides the bacterium to gut epithelial cells, where it interacts with mucin producing cells and aids in biofilm formation (Roy et al., 2009).

YadA form entero-pathogenic *Yersiniae* contributes to the induction of microabscesses by autoaggregation. Bacteria expressing YadA tend to aggregate following a zipper-like interaction of YadA proteins displayed on the bacterial surface. This autoaggregation seems beneficial during infection of the Peyer's patches since induction of microabscesses aids in bacterial persistence (El Tahir and Skurnik, 2001). Autoaggregation by YadA also seems to play a role in general biofilm formation, which in turn contributes to persistence of the infection and immune evasion (Trunk et al., 2018). Thus, YadA is a premier example of how trimeric AT adhesins can take part in multiple virulence-associated tasks including adhesion, immune evasion, autoaggregation, and biofilm formation.

Adhesion to Abiotic Surfaces

Adhesion to abiotic surfaces such as rubber, glass, or plastic is a major problem when it comes to working with primary, sterile material in hospital settings or the food industry as adhesion to surfaces is the first step in formation of stable biofilms (Lindsay and von Holy, 2006). Some ATs are universally sticky and interact with a variety of surfaces. Especially TAAs, for example YadA and BadA, interact with various surfaces such as plastic and glass (Schulze-Koops et al., 1993; Müller et al., 2011; Berne et al., 2015). This depends on various factors including the nature of the surface as well as the growth conditions (static vs. flow). There are also specific differences: BadA, for example, interacts more strongly with plastic than YadA (Müller et al., 2011). Together with other modes of surface adhesion and auto-aggregation, YadA, and BadA can thus induce formation of biofilms on a variety of materials. Another well-studied TAA, AtaA from *Acinetobacter* sp., does not appear to have specific binding partners. Like YadA, AtaA has been shown to function in adhesion to collagen and laminin but in general displays low specificity for any particular substrate – instead, it seems to be "universally sticky" adhering strongly to a variety of biotic and abiotic surfaces, including, e.g., polyurethane, steel, and glass (Ishikawa et al., 2012; Hori et al., 2015; Koiwai et al., 2016). Similar features are known for YeeJ, a type Ve inverse AT from *E. coli* involved in adhesion to numerous abiotic surfaces and biofilm formation (Moriel et al., 2017). Unfortunately, though many AT adhesins exhibit the ability to interact with abiotic surfaces, information regarding affinities and systematic studies on which surface materials are preferred are sparse.

INTRACELLULAR MOTILITY

Some bacteria have the ability to invade cells and live within the host cells. This is beneficial for virulence because the bacterium is protected from host immune responses, has access to nutrients, and is influenced less by the harsh environment within the host. Examples of ATs involved in this process have already been mentioned above, including YadA and IgA protease that are implicated in tissue invasion and in release into the host cytosol after uptake into the host cells, respectively. Once inside the cell, bacteria can use ATs in different ways to confer intracellular motility employing the host cell actin cytoskeleton. This motility can be conveyed through the interaction with actin polymerases of the host or by mimicking polymerizing factors themselves (Sitthidet et al., 2011). Both mechanisms can be found in BimA, a type Vc AT of *B. pseudomallei*, *Burkholderia mallei*, and *Burkholderia thailandensis* (Stevens et al., 2005). The mechanism employed for actin polymerization differs slightly between the different species. *B. mallei* and *B. pseudomallei* BimA have a WH2 domain (Wiskott-Aldrich syndrome protein homology domain) that directly mimics WASP (Wiskott-Aldrich syndrome protein) as an actin polymerase. The *B. thailandensis* BimA has a CA domain (central and acidic) that can bind and activate Arp2/3, a complex that activates actin polymerization, in addition to a WH2 domain (Sitthidet et al., 2011; Benanti et al., 2015).

A slightly different mechanism for actin polymerization is used by IcsA, also called VirG, a type Va AT of *S. flexneri* and YapV, a type Va AT of *Y. pseudotuberculosis* and *Y. pestis*. While BimA either binds Arp2/3 by mimicking WASP through a WH2 domain or activate actin polymerization directly by a CA domain, IcsA and YapV seem to interact with N-WASP (neural WASP) (Besingi et al., 2013; Chauhan et al., 2016). IcsA is mostly located at the bacterial pole (Goldberg et al., 1993). Its passenger binds to N-WASP which then can activate Arp2/3 which subsequently functions as an actin polymerase (Bernardini et al., 1989; Goldberg and Theriot, 1995). YapV from *Y. pestis* functions in a similar fashion. Like IcsA, YapV also binds to N-WASP, an actin polymerization factor in order to influence actin polymerization and utilize it for intracellular movement (Besingi et al., 2013; Chauhan et al., 2016; Leupold et al., 2017).

CONCLUSION AND OUTLOOK

The different subclasses of type V secretion systems, or ATs, display similarities in their biogenesis and mode of passenger secretion, but the functional implications of their passengers in virulence as well as in symbiosis are very diverse. These functions can extend from surface adhesion via enzymatic activity to complex interactions with cellular factors directly influencing host cell behavior. These diverse functions do not cluster with the secretion system (sub)classification; similar functions can be found across some or all subclasses. Detailed mechanistic knowledge about functions of AT passengers is available only for a few well-studied examples, and while the biogenesis pathway(s) are conserved across all species that harbor AT genes, the specific AT functions are often not.

Though well studied, open questions remain in the biogenesis of ATs. It is not entirely clear how the β-barrel domain is inserted

into the membrane, and specifically, what role the BAM complex plays in this. BAM is involved in the insertion of all β-barrel membrane proteins in the OM of Gram-negative bacteria, but several AT biogenesis models suggest additional functions for BAM also in passenger secretion (Sauri et al., 2009; Leo et al., 2012; Leo and Linke, 2018). Partly as a consequence of this debate, the mechanism of passenger secretion by the β-barrel is not fully understood. While type Va and Ve ATs secrete their passengers via a hairpin-loop intermediate, the question of how this works, e.g., in trimeric ATs is still under debate (Leo and Linke, 2018). As to whether all three passenger polypeptides are transported at the same time or sequentially has still to be shown. The presence of trimeric helper proteins that may act as chaperones to coordinate export of type Vc ATs suggest simultaneous export and recent study points toward contemporaneous transport of all passenger polypeptides (Grin et al., 2014; Chauhan et al., 2019).

Likewise, the molecular mechanisms of many AT functions have still not been entirely elucidated.

In many cases of adhesins bind to a variety of surfaces promiscuously, but it is still not known as to whether different affinities toward different ECM molecules have a biological consequence. Furthermore, it is still not known how exactly differential binding works and which residues plays a role in differentiation of the binding targets. Another example for how ill-defined the functions of some passenger domains are protease and lipase targets. Although ATs with protease and lipase function have been studied for decades – and in fact belong to the best studied ATs – most of the host cellular targets have not been found yet. Even if targets have been defined in many cases the implications of targeting these structures is mostly unclear.

A lot of virulence potential lies within the secreted passengers of ATs, which would make many ATs potential targets for, e.g., drug and vaccine development (Xin et al., 2010; Olvera et al., 2011; Bentancor et al., 2012). Currently, there are already two major recombinant vaccines using ATs on the market. These contain FHA and Pertactin of *B. pertussis*, as well as NadA from *N. meningitidis* (Hellwig et al., 2003; Malito et al., 2014). Since ATs oftentimes belong to the virulence factors initiating an infection, for example Intimin and Invasin, one could also think of them as targets for anti-infective drugs (Durand et al., 2009; Heras et al., 2015).

In this review, we picked some prominent examples to illustrate the variety of passenger functions in ATs. Future research will undoubtedly lead to a more detailed picture of the variety of passenger functions and their involvement in infections as well as in symbiotic or environmental lifestyles.

AUTHOR CONTRIBUTIONS

IM wrote the first draft. All the authors contributed to complete the manuscript.

FUNDING

This work was funded by the Horizon 2020 Innovative Training Network "ViBrANT" (to DL) and the Norwegian Research Council (to JL). Contributions by the University of Oslo are gratefully acknowledged. AS is partly funded from Novo Nordisk Fonden grant NNF18OC0032818.

REFERENCES

Abreu, A. G., Abe, C. M., Nunes, K. O., Moraes, C. T. P., Chavez-Dueñas, L., Navarro-Garcia, F., et al. (2016). The serine protease Pic as a virulence factor of atypical enteropathogenic *Escherichia coli*. *Gut Microbes* 7, 115–125. doi: 10.1080/19490976.2015.1136775

Alvarez, B. H., Gruber, M., Ursinus, A., Dunin-Horkawicz, S., Lupas, A. N., and Zeth, K. (2010). A transition from strong right-handed to canonical left-handed supercoiling in a conserved coiled-coil segment of trimeric autotransporter adhesins. *J. Struct. Biol.* 170, 236–245. doi: 10.1016/j.jsb.2010.02.009

Aoki, S. K., Diner, E. J., De Roodenbeke, C. T. K., Burgess, B. R., Poole, S. J., Braaten, B. A., et al. (2010). A widespread family of polymorphic contact-dependent toxin delivery systems in bacteria. *Nature* 468, 439–442. doi: 10.1038/nature09490

Aoki, S. K., Malinverni, J. C., Jacoby, K., Thomas, B., Pamma, R., Trinh, B. N., et al. (2008). Contact-dependent growth inhibition requires the essential outer membrane protein BamA (YaeT) as the receptor and the inner membrane transport protein AcrB. *Mol. Microbiol.* 70, 323–340. doi: 10.1111/j.1365-2958.2008.06404.x

Aoki, S. K., Pamma, R., and Hernday, A. D. (2005). Contact-dependent inhibition of growth in *Escherichia coli*. *Science* 309, 1245–1249.

Arenas, J., Nijland, R., Rodriguez, F. J., Bosma, T. N. P., and Tommassen, J. (2013). Involvement of three meningococcal surface-exposed proteins, the heparin-binding protein NhbA, the α-peptide of IgA protease and the autotransporter protease NalP, in initiation of biofilm formation. *Mol. Microbiol.* 87, 254–268. doi: 10.1111/mmi.12097

Aricò, B., Nuti, S., Scarlato, V., and Rappuoli, R. (1993). Adhesion of *Bordetella pertussis* to eukaryotic cells requires a time-dependent export and maturation of filamentous hemagglutinin. *Proc. Natl. Acad. Sci. U.S.A.* 90, 9204–9208. doi: 10.1073/pnas.90.19.9204

Ayala, P., Vasquez, B., Wetzler, L., and So, M. (2002). *Neisseria gonorrhoeae* Porin P1.B induces endosome exocytosis and a redistribution of lamp1 to the plasma membrane. *Infect. Immun.* 70, 5965–5971. doi: 10.1128/iai.70.11.5965-5971.2002

Balder, R., Hassel, J., Lipski, S., and Lafontaine, E. R. (2007). *Moraxella* catarrhalis strain O35E expresses two filamentous hemagglutinin-like proteins that mediate adherence to human epithelial cells. *Infect. Immun.* 75, 2765–2775. doi: 10.1128/iai.00079-07

Barnard, T. J., Dautin, N., Lukacik, P., Bernstein, H. D., and Buchanan, S. K. (2007). Autotransporter structure reveals intra-barrel cleavage followed by conformational changes. *Nat. Struct. Mol. Biol.* 14, 1214–1220. doi: 10.1038/nsmb1322

Batchelor, M., Prasannan, S., Daniell, S., Reece, S., Connerton, I., Bloomberg, G., et al. (2000). Structural basis for recognition of the translocated intimin receptor (Tir) by intimin from enteropathogenic *Escherichia coli*. *EMBO J.* 19, 2452–2464. doi: 10.1093/emboj/19.11.2452

Baud, C., Guérin, J., Petit, E., Lesne, E., Dupré, E., Locht, C., et al. (2014). Translocation path of a substrate protein through its Omp85 transporter. *Nat. Commun.* 5:5271. doi: 10.1038/ncomms6271

Baud, C., Hodak, H., Willery, E., Drobecq, H., Locht, C., Jamin, M., et al. (2009). Role of DegP for two-partner secretion in Bordetella. *Mol. Microbiol.* 74, 315–329. doi: 10.1111/j.1365-2958.2009.06860.x

Benanti, E. L., Nguyen, C. M., and Welch, M. D. (2015). Virulent burkholderia species mimic host actin polymerases to drive actin-based motility. *Cell* 161, 348–360. doi: 10.1016/j.cell.2015.02.044

Bentancor, L. V., Routray, A., Bozkurt-Guzel, C., Camacho-Peiro, A., Pier, G. B., and Maira-Litrán, T. (2012). Evaluation of the trimeric autotransporter ata as a vaccine candidate against *Acinetobacter baumannii* infections. *Infect. Immun.* 80, 3381–3388. doi: 10.1128/IAI.06096-11

Benz, I., and Schmidt, M. A. (1989). Cloning and expression of an adhesin (AIDA-I) involved in diffuse adherence of enteropathogenic *Escherichia coli*. *Infect. Immun.* 57, 1506–1511.

Benz, I., and Schmidt, M. A. (2001). Glycosylation with heptose residues mediated by the aah gene product is essential for adherence of the AIDA-I adhesin. *Mol. Microbiol.* 40, 1403–1413. doi: 10.1046/j.1365-2958.2001.02487.x

Bernardini, M. L., Mounier, J., d'Hauteville, H., Coquis-Rondon, M., and Sansonetti, P. J. (1989). Identification of icsA, a plasmid locus of *Shigella* flexneri that governs bacterial intra- and intercellular spread through interaction with F-actin. *Proc. Natl. Acad. Sci. U.S.A.* 86, 3867–3871. doi: 10.1073/pnas.86.10.3867

Berne, C., Ducret, A., Hardy, G. G., and Brun, Y. V. (2015). Adhesins involved in attachment to abiotic surfaces by Gram-negative bacteria. *Microbiol. Spectr.* 3, 1–45. doi: 10.1128/microbiolspec.MB-0018-2015

Besbes, A., Le Goff, S., Antunes, A., Terrade, A., Hong, E., Giorgini, D., et al. (2015). Hyperinvasive Meningococci Induce Intra-nuclear Cleavage of the NF-κB Protein p65/RelA by Meningococcal IgA Protease. *PLoS Pathog.* 11:e1005078. doi: 10.1371/journal.ppat.1005078

Besingi, R. N., Chaney, J. L., and Clark, P. L. (2013). An alternative outer membrane secretion mechanism for an autotransporter protein lacking a C-terminal stable core. *Mol. Microbiol.* 90, 1028–1045. doi: 10.1111/mmi.12414

Biedzka-Sarek, M., Jarva, H., Hyytiäinen, H., Meri, S., and Skurnik, M. (2008). Characterization of complement factor H binding to *Yersinia enterocolitica* serotype O:3. *Infect. Immun.* 76, 4100–4109. doi: 10.1128/IAI.00313-08

Bliska, J. B., Copass, M. C., and Falkow, S. (1993). The *Yersinia pseudotuberculosis* adhesin YadA mediates intimate bacterial attachment to and entry into HEp-2 cells. *Infect. Immun.* 61, 3914–3921.

Bolin, I., and Wolf-Watz, H. (1984). Molecular cloning of the temperature-inducible outer membrane protein 1 of *Yersinia pseudotuberculosis*. *Infect. Immun.* 43, 72–78.

Braun, V., Ondraczek, R., and Hobbie, S. (1993). Activation and secretion of Serratia hemolysin. *Zentralbl. Bakteriol.* 278, 306–315. doi: 10.1016/s0934-8840(11)80847-9

Brzuszkiewicz, A., Nowak, E., Dauter, Z., Dauter, M., Cieśliski, H., Dłługołł?cka, A., et al. (2009). Structure of esta esterase from psychrotrophic pseudoalteromonas sp. 643A covalently inhibited by monoethylphosphonate. *Acta Crystallogr. Sect. F Struct. Biol. Cryst. Commun.* 65, 862–865. doi: 10.1107/S1744309109030826

Buscher, A. Z., Grass, S., Heuser, J., Roth, R., and St. Geme, J. W. (2006). Surface anchoring of a bacterial adhesin secreted by the two-partner secretion pathway. *Mol. Microbiol.* 61, 470–483. doi: 10.1111/j.1365-2958.2006.05236.x

Carinato, M. E., Collin-Osdoby, P., Yang, X., Knox, T. M., Conlin, C. A., and Miller, C. G. (1998). The apeE gene of *Salmonella* typhimurium encodes an outer membrane esterase not present in *Escherichia coli*. *J. Bacteriol.* 180, 3517–3521.

Casasanta, M. A., Yoo, C. C., Smith, H. B., Duncan, A. J., Cochrane, K., Varano, A. C., et al. (2017). A chemical and biological toolbox for Type Vd secretion: characterization of the phospholipase A1 autotransporter FplA from *Fusobacterium nucleatum*. *J. Biol. Chem.* 292, 20240–20254. doi: 10.1074/jbc.M117.819144

Chagnot, C., Listrat, A., Astruc, T., and Desvaux, M. (2012). Bacterial adhesion to animal tissues: protein determinants for recognition of extracellular matrix components. *Cell. Microbiol.* 14, 1687–1696. doi: 10.1111/cmi.12002

Charbonneau, M. È, Berthiaume, F., and Mourez, M. (2006). Proteolytic processing is not essential for multiple functions of the *Escherichia coli* autotransporter adhesin involved in diffuse adherence (AIDA-I). *J. Bacteriol.* 188, 8504–8512. doi: 10.1128/jb.00864-06

Chauhan, N., Hatlem, D., Orwick-Rydmark, M., Schneider, K., Floetenmeyer, M., van Rossum, B., et al. (2019). Insights into the autotransport process of a trimeric autotransporter, Yersinia Adhesin A (YadA). *Mol. Microbiol.* 111, 844–862. doi: 10.1111/mmi.14195

Chauhan, N., Wrobel, A., Skurnik, M., and Leo, J. C. (2016). *Yersinia* adhesins: an arsenal for infection. *Proteomics Clin. Appl.* 10, 949–963. doi: 10.1002/prca.201600012

Chevalier, N., Moser, M., Koch, H. G., Schimz, K. L., Willery, E., Locht, C., et al. (2004). Membrane targeting of a bacterial virulence factor harbouring an extended signal peptide. *J. Mol. Microbiol. Biotechnol.* 8, 7–18. doi: 10.1159/000082076

Choi, P. S., and Bernstein, H. D. (2010). Sequential translocation of an Escherchia coli two-partner secretion pathway exoprotein across the inner and outer membranes. *Mol. Microbiol.* 75, 440–451. doi: 10.1111/j.1365-2958.2009.06993.x

Clantin, B., Delattre, A., Rucktooa, P., Saint, N., Méli, A. C., Locht, C., et al. (2007). Structure of the membrane protein transporter superfamily. *Science* 416, 3–7.

Clantin, B., Hodak, H., Willery, E., Locht, C., Jacob-Dubuisson, F., and Villeret, V. (2004). The crystal structure of filamentous hemagglutinin secretion domain and its implications for the two-partner secretion pathway. *Proc. Natl. Acad. Sci. U.S.A.* 101, 6194–6199. doi: 10.1073/pnas.0400291101

Conners, R., Hill, D. J., Borodina, E., Agnew, C., Daniell, S. J., Burton, N. M., et al. (2008). The *Moraxella* adhesin UspA1 binds to its human CEACAM1 receptor by a deformable trimeric coiled-coil. *EMBO J.* 27, 1779–1789. doi: 10.1038/emboj.2008.101

Coppens, F., Castaldo, G., Debraekeleer, A., Subedi, S., Moonens, K., Lo, A., et al. (2018). Hop-family *Helicobacter* outer membrane adhesins form a novel class of Type 5-like secretion proteins with an interrupted β-barrel domain. *Mol. Microbiol.* 110, 33–46. doi: 10.1111/mmi.14075

Costa, T. R. D., Felisberto-Rodrigues, C., Meir, A., Prevost, M. S., Redzej, A., Trokter, M., et al. (2015). Secretion systems in Gram-negative bacteria: Structural and mechanistic insights. *Nat. Rev. Microbiol.* 13, 343–359. doi: 10.1038/nrmicro3456

Cover, T. L., and Blanke, S. R. (2005). *Helicobacter* pylori VacA, a paradigm for toxin multifunctionality. *Nat. Rev. Microbiol.* 3, 320–332. doi: 10.1038/nrmicro1095

Da Mata Madeira, P. V., Zouhir, S., Basso, P., Neves, D., Laubier, A., Salacha, R., et al. (2016). Structural basis of lipid targeting and destruction by the type v secretion system of *Pseudomonas aeruginosa*. *J. Mol. Biol.* 428, 1790–1803. doi: 10.1016/j.jmb.2016.03.012

Dautin, N. (2010). Serine protease autotransporters of *Enterobacteriaceae* (SPATEs): Biogenesis and function. *Toxins* 2, 1179–1206. doi: 10.3390/toxins2061179

Dautin, N., Barnard, T. J., Anderson, D. E., and Bernstein, H. D. (2007). Cleavage of a bacterial autotransporter by an evolutionarily convergent autocatalytic mechanism. *EMBO J.* 26, 1942–1952. doi: 10.1038/sj.emboj.7601638

Dautin, N., and Bernstein, H. D. (2007). Protein secretion in gram-negative bacteria via the autotransporter pathway. *Annu. Rev. Microbiol.* 61, 89–112. doi: 10.1146/annurev.micro.61.080706.093233

Davey, M. E., Caiazza, N. C., and O'Toole, G. A. (2003). Rhamnolipid surfactant production affects biofilm architecture in *Pseudomonas aeruginosa* PAO1. *J. Bacteriol.* 185, 1027–1036. doi: 10.1128/jb.185.3.1027-1036.2003

Deibel, C., Krämer, S., Chakraborty, T., and Ebel, F. (1998). EspE, a novel secreted protein of attaching and effacing bacteria, is directly translocated into infected host cells, where it appears as a tyrosine-phosphorylated 90 kDa protein. *Mol. Microbiol.* 28, 463–474. doi: 10.1046/j.1365-2958.1998.00798.x

Delattre, A. S., Clantin, B., Saint, N., Locht, C., Villeret, V., and Jacob-Dubuisson, F. (2010). Functional importance of a conserved sequence motif in FhaC, a prototypic member of the TpsB/Omp85 superfamily. *FEBS J.* 277, 4755–4765. doi: 10.1111/j.1742-4658.2010.07881.x

Desvaux, M., Khan, A., Beatson, S. A., Scott-Tucker, A., and Henderson, I. R. (2005). Protein secretion systems in *Fusobacterium nucleatum*: Genomic identification of Type 4 piliation and complete Type V pathways brings new insight into mechanisms of pathogenesis. *Biochim. Biophys. Acta* 1713, 92–112. doi: 10.1016/j.bbamem.2005.05.002

Déziel, E., Lépine, F., Milot, S., and Villemur, R. (2003). rhlA is required for the production of a novel biosurfactant promoting swarming motility in *Pseudomonas aeruginosa*: 3-(3-hydroxyalkanoyloxy)alkanoic acids (HAAs), the precursors of rhamnolipids. *Microbiology* 149, 2005–2013. doi: 10.1099/mic.0.26154-0

Diebel, L. N., Liberati, D. M., Baylor, A. E., Brown, W. J., and Devlin, J. (2004). Immunoglobulin A protease is a virulence factor for gram-negative pneumonia. *Surgery* 136, 937–943. doi: 10.1016/j.surg.2004.06.029

Diner, E. J., Beck, C. M., Webb, J. S., Low, D. A., and Hayes, C. S. (2012). Identification of a target cell permissive factor required for contact-dependent growth inhibition (CDI). *Genes Dev.* 26, 515–525. doi: 10.1101/gad.182345.111

Dorsey, C. W., Laarakker, M. C., Humphries, A. D., Weening, E. H., and Bäumler, A. J. (2005). *Salmonella enterica* serotype Typhimurium MisL is an intestinal colonization factor that binds fibronectin. *Mol. Microbiol.* 57, 196–211. doi: 10.1111/j.1365-2958.2005.04666.x

Drobnak, I., Braselmann, E., Chaney, J. L., Leyton, D. L., Bernstein, H. D., Lithgow, T., et al. (2015). Of linkers and autochaperones: an unambiguous nomenclature to identify common and uncommon themes for autotransporter secretion. *Mol. Microbiol.* 95, 1–16. doi: 10.1111/mmi.12838

Durand, E., Verger, D., Rêgo, A. T., Chandran, V., Meng, G., Fronzes, R., et al. (2009). Structural biology of bacterial secretion systems in gram-negative pathogens - Potential for new drug targets. *Infect. Disord. Drug Targets* 9, 518–547. doi: 10.2174/187152609789105722

Eitel, J., Eitel, J., Dersch, P., and Dersch, P. (2002). The YadA protein of *Yersinia pseudotuberculosis* mediates high-efficiency uptake into human cells under environmental conditions in which Invasin is repressed. *Society* 70, 4880–4891. doi: 10.1128/iai.70.9.4880-4891.2002

El Tahir, Y., Kuusela, P., and Skurnik, M. (2000). Functional mapping of the *Yersinia enterocolitica* adhesin YadA. Identification of eight NSVAIG - S motifs in the amino-terminal half of the protein involved in collagen binding. *Mol. Microbiol.* 37, 192–206. doi: 10.1046/j.1365-2958.2000.01992.x

El Tahir, Y., and Skurnik, M. (2001). YadA, the multifaceted *Yersinia* adhesin. *Int. J. Med. Microbiol.* 291, 209–218. doi: 10.1078/1438-4221-00119

Emody, L., Heesemann, J., Wolf-Watz, H., Skurnik, M., Kapperud, G., O'Toole, P., et al. (1989). Binding to collagen by *Yersinia enterocolitica* and *Yersinia pseudotuberculosis*: evidence for yopA-mediated and chromosomally encoded mechanisms. *J. Bacteriol.* 171, 6674–6679. doi: 10.1128/jb.171.12.6674-6679.1989

Emsley, P., Charles, I. G., Fairweather, N. F., and Isaacs neil, W. (1996). Structure of *Bordatella pertussis* virulence factor P.69 pertactin. *Nature* 381, 90–92. doi: 10.1038/381090a0

Favre, L., Spertini, F., and Corthesy, B. (2005). Secretory IgA possesses intrinsic modulatory properties stimulating mucosal and systemic immune responses. *J. Immunol.* 175, 2793–2800. doi: 10.4049/jimmunol.175.5.2793

Fink, D. L., Buscher, A. Z., Green, B., Fernsten, P., and St. Geme, J. W. (2003). The *Haemophilus influenzae* Hap autotransporter mediates microcolony formation and adherence to epithelial cells and extracellular matrix via binding regions in the C-terminal end of the passenger domain. *Cell. Microbiol.* 5, 175–186. doi: 10.1046/j.1462-5822.2003.00266.x

Flügel, A., Schulze-Koops, H., Heesemann, J., Kühn, K., Sorokin, L., Burkhardt, H., et al. (1994). Interaction of enteropathogenic *Yersinia enterocolitica* with complex basement membranes and the extracellular matrix proteins collagen type IV, laminin-1 and -2, and nidogen/entactin. *J. Biol. Chem.* 269, 29732–29738.

Frankel, G., Phillips, A. D., Trabulsi, L. R., Knutton, S., Dougan, G., and Matthews, S. (2001). Intimin and the host cell - Is it bound to end in Tir(s)? *Trends Microbiol.* 9, 214–218. doi: 10.1016/s0966-842x(01)02016-9

Fulcher, R. A., Cole, L. E., Janowicz, D. M., Toffer, K. L., Fortney, K. R., Katz, B. P., et al. (2006). Expression of *Haemophilus ducreyi* collagen binding outer membrane protein NcaA is required for virulence in swine and human challenge models of chancroid. *Infect. Immun.* 74, 2651–2658. doi: 10.1128/iai.74.5.2651-2658.2006

Garcia, E. C., Anderson, M. S., Hagar, J. A., and Cotter, P. A. (2013). BurkholderiaBcpA mediates biofilm formation independently of interbacterial contact-dependent growth inhibition. *Mol. Microbiol.* 89, 1213–1225. doi: 10.1111/mmi.12339

Garnett, J. A., Muhl, D., Douse, C. H., Hui, K., Busch, A., Omisore, A., et al. (2015). Structure-function analysis reveals that the *Pseudomonas aeruginosa* Tps4 two-partner secretion system is involved in CupB5 translocation. *Protein Sci.* 24, 670–687. doi: 10.1002/pro.2640

Gauthier, A., De Grado, M., and Finlay, B. B. (2000). Mechanical fractionation reveals structural requirements for enteropathogenic *Escherichia coli* Tir insertion into host membranes. *Infect. Immun.* 68, 4344–4348. doi: 10.1128/iai.68.7.4344-4348.2000

Goldberg, M. B., Barzu, O., Parsot, C., and Sansonetti, P. J. (1993). Unipolar localization and ATPase activity of IcsA, a *Shigella* flexneri protein involved in intracellular movement. *J. Bacteriol.* 175, 2189–2196. doi: 10.1128/jb.175.8.2189-2196.1993

Goldberg, M. B., and Theriot, J. A. (1995). *Shigella* flexneri surface protein IcsA is sufficient to direct actin-based motility. *Proc. Natl. Acad. Sci. U.S.A.* 92, 6572–6576. doi: 10.1073/pnas.92.14.6572

Goldman, A., and Linke, D. (2011). Bacterial Adhesion. *Adva. Exp. Med. Biol.* 715, 271–284. doi: 10.1007/978-94-007-0940-9_17

Goosney, D. L., DeVinney, R., and Finlay, B. B. (2001). Recruitment of cytoskeletal and signaling proteins to enteropathogenic and enterohemorrhagic *Escherichia coli* pedestals. *Infect. Immun.* 69, 3315–3322. doi: 10.1128/iai.69.5.3315-3322.2001

Grassl, G. A., Bohn, E., Müller, Y., Bühler, O. T., and Autenrieth, I. B. (2003). Interaction of *Yersinia enterocolitica* with epithelial cells: Invasin beyond invasion. *Int. J. Med. Microbiol.* 293, 41–54. doi: 10.1078/1438-4221-00243

Green, E. R., and Mecsas, J. (2016). Bacterial Secretion Systems – An overview CHAPTER SUMMARY. *Microbiol. Spectr.* 4, 1–32.

Grijpstra, J., Arenas, J., Rutten, L., and Tommassen, J. (2013). Autotransporter secretion: varying on a theme. *Res. Microbiol.* 164, 562–582. doi: 10.1016/j.resmic.2013.03.010

Grin, I., Hartmann, M. D., Sauer, G., Alvarez, B. H., Schütz, M., Wagner, S., et al. (2014). A trimeric lipoprotein assists in trimeric autotransporter biogenesis in enterobacteria. *J. Biol. Chem.* 289, 7388–7398. doi: 10.1074/jbc.M113.513275

Grosskinsky, U., Schütz, M., Fritz, M., Schmid, Y., Lamparter, M. C., Szczesny, P., et al. (2007). A conserved glycine residue of trimeric autotransporter domains plays a key role in *Yersinia* adhesin A autotransport. *J. Bacteriol.* 189, 9011–9019. doi: 10.1128/jb.00985-07

Guérin, J., Bigot, S., Schneider, R., Buchanan, S. K., and Jacob-Dubuisson, F. (2017). Two-partner secretion: combining efficiency and simplicity in the secretion of large proteins for bacteria-host and bacteria-bacteria interactions. *Front. Cell. Infect. Microbiol.* 7:148. doi: 10.3389/fcimb.2017.00148

Halter, R., Pohlner, J., and Meyer, T. F. (1984). IgA protease of *Neisseria gonorrhoeae*: isolation and characterization of the gene and its extracellular product. *EMBO J.* 3, 1595–1601. doi: 10.1002/j.1460-2075.1984.tb02016.x

Hartmann, M. D., Ridderbusch, O., Zeth, K., Albrecht, R., Testa, O., Woolfson, D. N., et al. (2009). A coiled-coil motif that sequesters ions to the hydrophobic core. *Proc. Natl. Acad. Sci. U.S.A.* 106, 16950–16955. doi: 10.1073/pnas.0907256106

Hauck, C. R., and Meyer, T. F. (1997). The lysosomal/phagosomal membrane protein h-lamp-1 is a target of the IgA1 protease of *Neisseria gonorrhoeae*. *FEBS Lett.* 405, 86–90. doi: 10.1016/S0014-5793(97)00163-4

Heise, T., and Dersch, P. (2006). Identification of a domain in Yersinia virulence factor YadA that is crucial for extracellular matrix-specific cell adhesion and uptake. *Proc. Natl. Acad. Sci. U.S.A.* 103, 3375–3380. doi: 10.1073/pnas.0507749103

Hellwig, S. M. M., Rodriguez, M. E., Berbers, G. A. M., van de Winkel, J. G. J., and Mooi, F. R. (2003). Crucial role of antibodies to Pertactin in *Bordetella pertussis* immunity. *J. Infect. Dis.* 188, 738–742.

Henderson, I. R., Navarro-Garcia, F., Desvaux, M., Fernandez, R. C., and Ala'Aldeen, D. (2004). Type V protein secretion pathway: the autotransporter story. *Microbiol. Mol. Biol. Rev.* 68, 692–744. doi: 10.1128/mmbr.68.4.692-744.2004

Henderson, I. R., Navarro-García, F., and Nataro, J. P. (1998). The great escape: structure and function of the autotransporter proteins. *Trends Microbiol.* 6, 370–378. doi: 10.1016/s0966-842x(98)01318-3

Heras, B., Scanlon, M. J., and Martin, J. L. (2015). Targeting virulence not viability in the search for future antibacterials. *Br. J. Clin. Pharmacol.* 79, 208–215. doi: 10.1111/bcp.12356

Hertle, R., Hilger, M., Weingardt-Kocher, S., and Walev, I. (1999). Cytotoxic action of *Serratia marcescens* hemolysin on human epithelial cells. *Infect. Immun.* 67, 817–825.

Hill, D. J., and Virji, M. (2003). A novel cell-binding mechanism of *Moraxella* catarrhalis ubiquitous surface protein UspA: specific targeting of the N-domain of carcinoembryonic antigen-related cell adhesion molecules by UspA1. *Mol. Microbiol.* 48, 117–129. doi: 10.1046/j.1365-2958.2003.03433.x

Hodak, H., and Jacob-Dubuisson, F. (2007). Current challenges in autotransport and two-partner protein secretion pathways. *Res. Microbiol.* 158, 631–637. doi: 10.1016/j.resmic.2007.08.001

Hoiczyk, E. (2000). Structure and sequence analysis of *Yersinia* YadA and *Moraxella* UspAs reveal a novel class of adhesins. *EMBO J.* 19, 5989–5999. doi: 10.1093/emboj/19.22.5989

Hori, K., Ohara, Y., Ishikawa, M., and Nakatani, H. (2015). Effectiveness of direct immobilization of bacterial cells onto material surfaces using the bacterionanofiber protein AtaA. *Appl. Microbiol. Biotechnol.* 99, 5025–5032. doi: 10.1007/s00253-015-6554-9

Hulks, M. H., and Plaut, A. G. (1978). IgA protease production as a characteristic distinguishing pathogenic from harmless Neisseriaceae. *N. Engl. J. Med.* 299, 973–976. doi: 10.1056/nejm197811022991802

Ieva, R., and Bernstein, H. D. (2009). Interaction of an autotransporter passenger domain with BamA during its translocation across the bacterial outer membrane. *Proc. Natl. Acad. Sci. U.S.A.* 106, 19120–19125. doi: 10.1073/pnas.0907912106

Irie, Y., Mattoo, S., and Yuk, M. H. (2004). The Bvg virulence control system regulates biofilm formation in Bordetella bronchiseptica. *J. Bacteriol.* 186, 5692–5698. doi: 10.1128/jb.186.17.5692-5698.2004

Isberg, R. R., Hamburger, Z., and Dersch, P. (2000). Signaling and invasin-promoted uptake via integrin receptors. *Microbes Infect.* 2, 793–801. doi: 10.1016/s1286-4579(00)90364-2

Isberg, R. R., and Leong, J. M. (1990). Multiple β1 chain integrins are receptors for invasin, a protein that promotes bacterial penetration into mammalian cells. *Cell* 60, 861–871. doi: 10.1016/0092-8674(90)90099-z

Isberg, R. R., Voorhis, D. L., and Falkow, S. (1987). Identification of invasin: a protein that allows enteric bacteria to penetrate cultured mammalian cells. *Cell* 50, 769–778. doi: 10.1016/0092-8674(87)90335-7

Ishikawa, M., Nakatani, H., Hori, K., Hori, K., Matsumoto, S., Soto, G., et al. (2012). AtaA, a new member of the Trimeric Autotransporter Adhesins from *Acinetobacter* sp. Tol 5 mediating high adhesiveness to various abiotic surfaces. *PLoS One* 7:e48830. doi: 10.1371/journal.pone.0048830

Jacob-Dubuisson, F., Guérin, J., Baelen, S., and Clantin, B. (2013). Two-partner secretion: As simple as it sounds? *Res. Microbiol.* 164, 583–595. doi: 10.1016/j.resmic.2013.03.009

Jain, S., and Goldberg, M. B. (2007). Requirement for YaeT in the outer membrane assembly of autotransporter proteins. *J. Bacteriol.* 189, 5393–5398. doi: 10.1128/jb.00228-07

Junker, M., Besingi, R. N., and Clark, P. L. (2009). Vectorial transport and folding of an autotransporter virulence protein during outer membrane secretion. *Mol. Microbiol.* 71, 1323–1332. doi: 10.1111/j.1365-2958.2009.06607.x

Junker, M., Schuster, C. C., McDonnell, A. V., Sorg, K. A., Finn, M. C., Berger, B., et al. (2006). Pertactin beta-helix folding mechanism suggests common themes for the secretion and folding of autotransporter proteins. *Proc. Natl. Acad. Sci. U.S.A.* 103, 4918–4923. doi: 10.1073/pnas.0507923103

Kaiser, P. O., Linke, D., Schwarz, H., Leo, J. C., and Kempf, V. A. J. (2012). Analysis of the BadA stalk from *Bartonella henselae* reveals domain-specific and domain-overlapping functions in the host cell infection process. *Cell. Microbiol.* 14, 198–209. doi: 10.1111/j.1462-5822.2011.01711.x

Kajava, A. V., Cheng, N., Cleaver, R., Kessel, M., Simon, M. N., Willery, E., et al. (2001). Beta-helix model for the filamentous haemagglutinin adhesin of *Bordetella pertussis* and related bacterial secretory proteins. *Mol. Microbiol.* 42, 279–292. doi: 10.1046/j.1365-2958.2001.02598.x

Kang'ethe, W., and Bernstein, H. D. (2013). Charge-dependent secretion of an intrinsically disordered protein via the autotransporter pathway. *Proc. Natl. Acad. Sci. U.S.A.* 110, E4246–E4255. doi: 10.1073/pnas.1310345110

Kempf, V. A. J., Schairer, A., Neumann, D., Grassl, G. A., Lauber, K., Lebiedziejewski, M., et al. (2005). *Bartonella henselae* inhibits apoptosis in Mono Mac 6 cells. *Cell. Microbiol.* 7, 91–104. doi: 10.1111/j.1462-5822.2004.00440.x

Kempf, V. A. J., Volkmann, B., Schaller, M., Sander, C. A., Alitalo, K., Rieß, T., et al. (2001). Evidence of a leading role for VEGF in *Bartonella henselae*-induced endothelial cell proliferations. *Cell. Microbiol.* 3, 623–632. doi: 10.1046/j.1462-5822.2001.00144.x

Kenny, B. (1999). Phosphorylation of tyrosine 474 of the enteropathogenic *Escherichia coli* (EPEC) Tir receptor molecule is essential for actin nucleating activity and is preceded by additional host modifications. *Mol. Microbiol.* 31, 1229–1241. doi: 10.1046/j.1365-2958.1999.01265.x

Kenny, B., DeVinney, R., Stein, M., Reinscheid, D. J., Frey, E. A., and Finlay, B. B. (1997). Enteropathogenic *E. coli* (EPEC) transfers its receptor for intimate adherence into mammalian cells. *Cell* 91, 511–520. doi: 10.1016/s0092-8674(00)80437-7

Kida, Y., Higashimoto, Y., Inoue, H., Shimizu, T., and Kuwano, K. (2008). A novel secreted protease from *Pseudomonas aeruginosa* activates NF-KB through protease-activated receptors. *Cell. Microbiol.* 10, 1491–1504. doi: 10.1111/j.1462-5822.2008.01142.x

Kingsley, R. A., Ghanem, D. A., Puebla-Osorio, N., Keestra, A. M., Berghman, L., and Bäumler, A. J. (2004). Fibronectin binding to the *Salmonella enterica* serotype typhimurium ShdA autotransporter protein is inhibited by a monoclonal antibody recognizing the A3 repeat. *J. Bacteriol.* 186, 4931–4939. doi: 10.1128/jb.186.15.4931-4939.2004

Kingsley, R. A., Santos, R. L., Keestra, A. M., Adams, L. G., and Bäumler, A. J. (2002). *Salmonella enterica* serotype Typhimurium ShdA is an outer membrane fibronectin-binding protein that is expressed in the intestine. *Mol. Microbiol.* 43, 895–905. doi: 10.1046/j.1365-2958.2002.02805.x

Kirjavainen, V., Jarva, H., Biedzka-Sarek, M., Blom, A. M., Skurnik, M., and Meri, S. (2008). *Yersinia enterocolitica* serum resistance proteins YadA and ail bind the complement regulator C4b-binding protein. *PLoS Pathog.* 4:e1000140. doi: 10.1371/journal.ppat.1000140

Klausen, M., Aaes-Jørgensen, A., Molin, S., and Tolker-Nielsen, T. (2003). Involvement of bacterial migration in the development of complex multicellular structures in *Pseudomonas aeruginosa* biofilms. *Mol. Microbiol.* 50, 61–68. doi: 10.1046/j.1365-2958.2003.03677.x

Klauser, T., Pohlner, J., and Meyer, T. F. (1993). The secretion pathway of IgA protease-type proteins in gram-negative bacteria. *Bioessays* 15, 799–805. doi: 10.1002/bies.950151205

Klemm, P., Hjerrild, L., Gjermansen, M., and Schembri, M. A. (2004). Structure-function analysis of the self-recognizing Antigen 43 autotransporter protein from *Escherichia coli*. *Mol. Microbiol.* 51, 283–296. doi: 10.1046/j.1365-2958.2003.03833.x

Kohler, T., Curty, L. K., Barja, F., Van Delden, C., and Pechere, J. C. (2000). Swarming of *Pseudomonas aeruginosa* is dependent on cell-to-cell signaling and requires flagella and pili. *J. Bacteriol.* 182, 5990–5996. doi: 10.1128/jb.182.21.5990-5996.2000

Koiwai, K., Hartmann, M. D., Linke, D., Lupas, A. N., and Hori, K. (2016). Structural basis for toughness and flexibility in the C-terminal passenger domain of an *Acinetobacter* trimeric autotransporter adhesin. *J. Biol. Chem.* 291, 3705–3724. doi: 10.1074/jbc.M115.701698

Kostakioti, M., and Stathopoulos, C. (2004). Functional analysis of the Tsh autotransporter from an avian pathogenic *Escherichia coli* strain. *Infect. Immun.* 72, 5548–5554. doi: 10.1128/iai.72.10.5548-5554.2004

Laarmann, S., and Schmidt, M. A. (2003). The *Escherichia coli* AIDA autotransporter adhesin recognizes an integral membrane glycoprotein as receptor. *Microbiology* 149, 1871–1882. doi: 10.1099/mic.0.26264-0

Leduc, I., White, C. D., Nepluev, I., Throm, R. E., Spinola, S. M., and Elkins, C. (2008). Outer membrane protein DsrA is the major fibronectin-binding determinant of *Haemophilus ducreyi*. *Infect. Immun.* 76, 1608–1616. doi: 10.1128/IAI.00994-07

Lee, J., Sutterlin, H. A., Wzorek, J. S., Mandler, M. D., Hagan, C. L., Grabowicz, M., et al. (2018). Substrate binding to BamD triggers a conformational change in BamA to control membrane insertion. *Proc. Natl. Acad. Sci. U.S.A.* 115, 201711727. doi: 10.1073/pnas.1711727115

Leo, C. J., and Linke, D. (2018). A unified model for BAM function that takes into account type Vc secretion and species differences in BAM composition. *AIMS Microbiol.* 4, 455–468. doi: 10.3934/microbiol.2018.3.455

Leo, J. C., Elovaara, H., Bihan, D., Pugh, N., Kilpinen, S. K., Raynal, N., et al. (2010). First analysis of a bacterial collagen-binding protein with collagen toolkits: promiscuous binding of YadA to collagens may explain how YadA interferes with host processes. *Infect. Immun.* 78, 3226–3236. doi: 10.1128/IAI.01057-09

Leo, J. C., Elovaara, H., Brodsky, B., Skurnik, M., and Goldman, A. (2008). The *Yersinia* adhesin YadA binds to a collagenous triple-helical conformation but without sequence specificity. *Protein Eng. Des. Sel.* 21, 475–484. doi: 10.1093/protein/gzn025

Leo, J. C., and Goldman, A. (2009). The immunoglobulin-binding Eib proteins from *Escherichia coli* are receptors for IgG Fc. *Mol. Immunol.* 46, 1860–1866. doi: 10.1016/j.molimm.2009.02.024

Leo, J. C., Grin, I., and Linke, D. (2012). Type V secretion: mechanism(S) of autotransport through the bacterial outer membrane. *Philos. Trans. R. Soc. B Biol. Sci.* 367, 1088–1101. doi: 10.1098/rstb.2011.0208

Leo, J. C., Lyskowski, A., Hattula, K., Hartmann, M. D., Schwarz, H., Butcher, S. J., et al. (2011). The structure of *E. coli* IgG-binding protein D suggests a general model for bending and binding in trimeric autotransporter adhesins. *Structure* 19, 1021–1030. doi: 10.1016/j.str.2011.03.021

Leo, J. C., Oberhettinger, P., Chaubey, M., Schütz, M., Kühner, D., Bertsche, U., et al. (2015a). The Intimin periplasmic domain mediates dimerisation and binding to peptidoglycan. *Mol. Microbiol.* 95, 80–100. doi: 10.1111/mmi.12840

Leo, J. C., Oberhettinger, P., Schütz, M., and Linke, D. (2015b). The inverse autotransporter family: intimin, invasin and related proteins. *Int. J. Med. Microbiol.* 305, 276–282. doi: 10.1016/j.ijmm.2014.12.011

Leo, J. C., Oberhettinger, P., Yoshimoto, S., Gupta Udatha, D. B. R. K., Morth, J. P., Schu, M., et al. (2016). Secretion of the intimin passenger domain is driven by protein folding. *J. Biol. Chem.* 291, 20096–20112. doi: 10.1074/jbc.M116.731497

Leupold, S., Büsing, P., Mas, P. J., Hart, D. J., and Scrima, A. (2017). Structural insights into the architecture of the *Shigella flexneri* virulence factor IcsA/VirG and motifs involved in polar distribution and secretion. *J. Struct. Biol.* 198, 19–27. doi: 10.1016/j.jsb.2017.03.003

Lin, L., Ayala, P., Larson, J., Mulks, M., Fukuda, M., Carlsson, S. R., et al. (1997). The Neisseria type 2 IgA1 protease cleaves LAMP1 and promotes survival of bacteria within epithelial cells. *Mol. Microbiol.* 24, 1083–1094. doi: 10.1046/j.1365-2958.1997.4191776.x

Lindsay, D., and von Holy, A. (2006). Bacterial biofilms within the clinical setting: what healthcare professionals should know. *J. Hosp. Infect.* 64, 313–325. doi: 10.1016/j.jhin.2006.06.028

Linke, D., Riess, T., Autenrieth, I. B., Lupas, A., and Kempf, V. A. J. (2006). Trimeric autotransporter adhesins: variable structure, common function. *Trends Microbiol.* 14, 264–270. doi: 10.1016/j.tim.2006.04.005

Lipski, S. L., Akimana, C., Timpe, J. M., Wooten, R. M., and Lafontaine, E. R. (2007). The *Moraxella* catarrhalis autotransporter McaP is a conserved surface protein that mediates adherence to human epithelial cells through its N-terminal passenger domain. *Infect. Immun.* 75, 314–324. doi: 10.1128/iai.01330-06

Luckett, J. C. A., Darch, O., Watters, C., AbuOun, M., Wright, V., Paredes-Osses, E., et al. (2012). A novel virulence strategy for *Pseudomonas aeruginosa* mediated by an autotransporter with arginine-specific aminopeptidase activity. *PLoS Pathog.* 8:e1002854. doi: 10.1371/journal.ppat.1002854

Malito, E., Biancucci, M., Faleri, A., Ferlenghi, I., Scarselli, M., Maruggi, G., et al. (2014). Structure of the meningococcal vaccine antigen NadA and epitope mapping of a bactericidal antibody. *Proc. Natl. Acad. Sci. U.S.A.* 111, 17128–17133. doi: 10.1073/pnas.1419686111

Mantis, N. J., Cheung, M. C., Koteswara, R., Rey, J., Corthésy, B., and Neutra, R. (2002). Selective adherence of IgA to Murine Peyer's Patch M cells: evidence for a novel IgA receptor. *J. Immunol.* 169, 1844–1851. doi: 10.4049/jimmunol.169.4.1844

Marr, N., Shah, N. R., Lee, R., Kim, E. J., and Fernandez, R. C. (2011). *Bordetella pertussis* autotransporter Vag8 binds human C1 esterase inhibitor and confers serum resistance. *PLoS One* 6:e20585. doi: 10.1371/journal.pone.0020585

Menozzi, F. D., Mutombo, R., Renauld, G., Gantiez, C., Hannah, J. H., Leininger, E., et al. (1994). Heparin-inhibitable lectin activity of the filamentous hemagglutinin adhesin of *Bordetella pertussis*. *Infect. Immun.* 62, 769–778.

Mikula, K. M., Leo, J. C., Łyskowski, A., Kedracka-Krok, S., Pirog, A., and Goldman, A. (2012). The translocation domain in *trimeric autotransporter adhesins* is necessary and sufficient for trimerization and autotransportation. *J. Bacteriol.* 194, 827–838. doi: 10.1128/JB.05322-11

Monds, R. D., and O'Toole, G. A. (2009). The developmental model of microbial biofilms: ten years of a paradigm up for review. *Trends Microbiol.* 17, 73–87. doi: 10.1016/j.tim.2008.11.001

Moriel, D. G., Rackaityte, E., Goh, K. G. K., Martinez-Gil, M., Audrain, B., Sakamoto, C., et al. (2017). YeeJ is an inverse autotransporter from *Escherichia coli* that binds to peptidoglycan and promotes biofilm formation. *Sci. Rep.* 7:11326. doi: 10.1038/s41598-017-10902-0

Mühlenkamp, M., Oberhettinger, P., Leo, J. C., Linke, D., and Schütz, M. S. (2015). Yersinia adhesin A (YadA) - Beauty & beast. *Int. J. Med. Microbiol.* 305, 252–258. doi: 10.1016/j.ijmm.2014.12.008

Mühlenkamp, M. C., Hallström, T., Autenrieth, I. B., Bohn, E., Linke, D., Rinker, J., et al. (2017). Vitronectin binds to a specific stretch within the head region of *Yersinia* adhesin a and thereby modulates *Yersinia enterocolitica* host interaction. *J. Innate Immun.* 9, 33–51. doi: 10.1159/000449200

Müller, N. F., Kaiser, P. O., Linke, D., Schwarz, H., Riess, T., Schäfer, A., et al. (2011). Trimeric autotransporter adhesin-dependent adherence of *Bartonella henselae*, *Bartonella quintana*, and *Yersinia enterocolitica* to matrix components and endothelial cells under static and dynamic flow conditions. *Infect. Immun.* 79, 2544–2553. doi: 10.1128/IAI.01309-10

Nesta, B., Spraggon, G., Alteri, C., Moriel, D. G., Rosini, R., Veggi, D., et al. (2012). FdeC, a novel broadly conserved *Escherichia coli* adhesin eliciting protection against urinary tract infections. *mBio* 3:e00010-12.

Nikaido, H., and Vaara, M. (1985). Molecular basis of bacterial outer membrane permeability. *Microbiol. Rev.* 49, 1–32.

Norell, D., Heuck, A., Tran-Thi, T.-A., Götzke, H., Jacob-Dubuisson, F., Clausen, T., et al. (2014). Versatile in vitro system to study translocation and functional integration of bacterial outer membrane proteins. *Nat. Commun.* 5:5396. doi: 10.1038/ncomms6396

Oberhettinger, P., Leo, J. C., Linke, D., Autenrieth, I. B., and Schütz, M. S. (2015). The inverse autotransporter intimin exports its passenger domain via a hairpin intermediate. *J. Biol. Chem.* 290, 1837–1849. doi: 10.1074/jbc.M114.604769

Oberhettinger, P., Schütz, M., Leo, J. C., Heinz, N., Berger, J., Autenrieth, I. B., et al. (2012). Intimin and invasin export their C-terminus to the bacterial cell surface using an inverse mechanism compared to classical autotransport. *PLoS One* 7:e47069. doi: 10.1371/journal.pone.0047069

Ohnishi, Y., Beppu, T., and Horinouchi, S. (1997). Two genes encoding serine protease homologues in *Serratia marcescens* and characterization of their products in *Escherichia coli*. *J. Biochem.* 121, 902–913. doi: 10.1093/oxfordjournals.jbchem.a021672

Ohnishi, Y., and Horinouchi, S. (2009). Extracellular production of a *Serratia marcescens* serine protease in *Escherichia coli*. *Biosci. Biotechnol. Biochem.* 60, 1551–1558.

Olvera, A., Pina, S., Pérez-Simó, M., Aragón, V., Segalés, J., and Bensaid, A. (2011). Immunogenicity and protection against Haemophilus parasuis infection after vaccination with recombinant virulence associated trimeric autotransporters (VtaA). *Vaccine* 29, 2797–2802. doi: 10.1016/j.vaccine.2011.01.105

Otto, B. R., Sijbrandi, R., Luirink, J., Oudega, B., Heddle, J. G., Mizutani, K., et al. (2005). Crystal structure of hemoglobin protease, a heme binding autotransporter protein from pathogenic *Escherichia coli*. *J. Biol. Chem.* 280, 17339–17345. doi: 10.1074/jbc.m412885200

Papanikou, E., Karamanou, S., and Economou, A. (2007). Bacterial protein secretion through the translocase nanomachine. *Nat. Rev. Microbiol.* 5, 839–851. doi: 10.1038/nrmicro1771

Pavlova, O., Peterson, J. H., Ieva, R., and Bernstein, H. D. (2013). Mechanistic link between barrel assembly and the initiation of autotransporter secretion. *Proc. Natl. Acad. Sci. U.S.A.* 110, E938–E947. doi: 10.1073/pnas.1219076110

Pepe, J. C. (1993). *Yersinia enterocolitica* invasin: a primary role in the initiation of infection. *Proc. Natl. Acad. Sci. U.S.A.* 90, 6473–6477. doi: 10.1073/pnas.90.14.6473

Peterson, J. H., Tian, P., Ieva, R., Dautin, N., and Bernstein, H. D. (2010). Secretion of a bacterial virulence factor is driven by the folding of a C-terminal segment. *Proc. Natl. Acad. Sci. U.S.A.* 107, 17739–17744. doi: 10.1073/pnas.1009491107

Phan, G., Remaut, H., Wang, T., Allen, W. J., Pirker, K. F., Lebedev, A., et al. (2011). Crystal structure of the FimD usher bound to its cognate FimC-FimH substrate. *Nature* 474, 49–53. doi: 10.1038/nature10109

Pizarro-Cerdá, J., and Cossart, P. (2006). Bacterial adhesion and entry into host cells. *Cell* 124, 715–727. doi: 10.1016/j.cell.2006.02.012

Plaut, A. G., Gilbert, J. V., Artenstein, M. S., and Capra, J. D. (1975). *Neisseria gonorrhoeae* and *Neisseria meningitidis*: extracellular enzyme cleaves human immunoglobulin A. *Science* 190, 1103–1105. doi: 10.1126/science.810892

Plaut, A. G., Gilbert, J. V., and Wistar, R. (1977). Loss of antibody activity in human immunoglobulin A exposed to extracellular immunoglobulin A proteases of *Neisseria gonorrhoeae* and *Streptococcus sanguis*. *Infect. Immun.* 17, 130–135.

Pohlner, J., Langenberg, U., Wölk, U., Beck, S. C., and Meyer, T. F. (1995). Uptake and nuclear transport of Neisseria IgA1 protease-associated α-proteins in human cells. *Mol. Microbiol.* 17, 1073–1083. doi: 10.1111/j.1365-2958.1995.mmi_17061073.x

Raghunathan, D., Wells, T. J., Morris, F. C., Shaw, R. K., Bobat, S., Peters, S. E., et al. (2011). SadA, a trimeric autotransporter from *Salmonella enterica* serovar Typhimurium, can promote biofilm formation and provides limited protection against infection. *Infect. Immun.* 79, 4342–4352. doi: 10.1128/IAI.05592-11

Reboud, E., Bouillot, S., Patot, S., Béganton, B., Attrée, I., and Huber, P. (2017). *Pseudomonas aeruginosa* ExlA and *Serratia marcescens* ShlA trigger cadherin cleavage by promoting calcium influx and ADAM10 activation. *PLoS Pathog.* 13:e1006579. doi: 10.1371/journal.ppat.1006579

Relman, D., Tuomanen, E., Falkow, S., Golenbock, D. T., Saukkonen, K., and Wright, S. D. (1990). Recognition of a bacterial adhesin by an integrin: Macrophage CR3 (αMβ2, CD11b CD18) binds filamentous hemagglutinin of *Bordetella pertussis*. *Cell* 61, 1375–1382. doi: 10.1016/0092-8674(90)90701-f

Riedel, K., Talker-Huiber, D., Givskov, M., Schwab, H., and Eberl, L. (2003). Identification and characterization of a GDSL esterase gene located proximal to the swr quorum-sensing system of *Serratia liquefaciens* MG1. *Appl. Environ. Microbiol.* 69, 3901–3910. doi: 10.1128/aem.69.7.3901-3910.2003

Riess, T., Andersson, S. G. E., Lupas, A., Schaller, M., Schäfer, A., Kyme, P., et al. (2004). *Bartonella* adhesin a mediates a proangiogenic host cell response. *J. Exp. Med.* 200, 1267–1278. doi: 10.1084/jem.20040500

Roggenkamp, A., Ackermann, N., Jacobi, C. A., Truelzsch, K., Hoffmann, H., and Heesemann, J. (2003). Molecular analysis of transport and oligomerization of the *Yersinia enterocolitica* adhesin YadA. *J. Bacteriol.* 185, 3735–3744. doi: 10.1128/jb.185.13.3735-3744.2003

Roman-Hernandez, G., Peterson, J. H., and Bernstein, H. D. (2014). Reconstitution of bacterial autotransporter assembly using purified components. *eLife* 3:e04234. doi: 10.7554/eLife.04234

Rosqvist, R., Forsberg, A., and Wolf-Watz, H. (1991). Intracellular targeting of the *Yersinia* YopE cytotoxin in mammalian cells induces actin microfilament disruption. *Infect. Immun.* 59, 4562–4569.

Rosqvist, R., Skurnik, M., and Wolf-Watz, H. (1988). Increased virulence of *Yersinia pseudotuberculosis* by two independent mutations. *Nature* 334, 522–525. doi: 10.1038/334522a0

Roussel-Jazédé, V., Jongerius, I., Bos, M. P., Tommassen, J., and Van Ulsen, P. (2010). NalP-mediated proteolytic release of lactoferrin-binding protein B from the meningococcal cell surface. *Infect. Immun.* 78, 3083–3089. doi: 10.1128/IAI.01193-09

Roy, K., Hilliard, G. M., Hamilton, D. J., Luo, J., Ostmann, M. M., and Fleckenstein, J. M. (2009). Enterotoxigenic *Escherichia coli* EtpA mediates adhesion between flagella and host cells. *Nature* 457, 594–598. doi: 10.1038/nature07568

Ruhe, Z. C., Low, D. A., and Hayes, C. S. (2013a). Bacterial contact-dependent growth inhibition. *Trends Microbiol.* 21, 230–237. doi: 10.1016/j.tim.2013.02.003

Ruhe, Z. C., Wallace, A. B., Low, D. A., and Hayes, C. S. (2013b). Receptor polymorphism restricts contact-dependent growth inhibition to members of the same species. *mBio* 4:e00480-13. doi: 10.1128/mBio.00480-13

Ruiz-Perez, F., and Nataro, J. P. (2014). Bacterial serine proteases secreted by the autotransporter pathway: classification, specificity, and role in virulence. *Cell. Mol. Life Sci.* 71, 745–770. doi: 10.1007/s00018-013-1355-8

Sadana, P., Geyer, R., Pezoldt, J., Helmsing, S., Huehn, J., Hust, M., et al. (2018). The invasin D protein from *Yersinia pseudotuberculosis* selectively binds the Fab region of host antibodies and affects colonization of the intestine. *J. Biol. Chem.* 293, 8672–8690. doi: 10.1074/jbc.RA117.001068

Salacha, R., Kovačić, F., Brochier-Armanet, C., Wilhelm, S., Tommassen, J., Filloux, A., et al. (2010). The *Pseudomonas aeruginosa* patatin-like protein PlpD is the archetype of a novel Type V secretion system. *Environ. Microbiol.* 12, 1498–1512. doi: 10.1111/j.1462-2920.2010.02174.x

Sauri, A., Soprova, Z., Wickström, D., de Gier, J. W., Van der Schors, R. C., Smit, A. B., et al. (2009). The Bam (Omp85) complex is involved in secretion of the autotransporter haemoglobin protease. *Microbiology* 155, 3982–3991. doi: 10.1099/mic.0.034991-0

Scarselli, M., Serruto, D., Montanari, P., Capecchi, B., Adu-Bobie, J., Veggi, D., et al. (2006). Neisseria meningitidis NhhA is a multifunctional trimeric autotransporter adhesin. *Mol. Microbiol.* 61, 631–644. doi: 10.1111/j.1365-2958.2006.05261.x

Schiffrin, B., Brockwell, D. J., and Radford, S. E. (2017). Outer membrane protein folding from an energy landscape perspective. *BMC Biol.* 15:123. doi: 10.1186/s12915-017-0464-5

Schindler, M. K. H., Schutz, M. S., Muhlenkamp, M. C., Rooijakkers, S. H. M., Hallstrom, T., Zipfel, P. F., et al. (2012). *Yersinia enterocolitica* YadA mediates complement evasion by recruitment and inactivation of C3 products. *J. Immunol.* 189, 4900–4908. doi: 10.4049/jimmunol.1201383

Schmitt, C., Turner, D., Boesl, M., Abele, M., Frosch, M., and Kurzai, O. (2007). A functional two-partner secretion system contributes to adhesion of *Neisseria meningitidis* to epithelial cells. *J. Bacteriol.* 189, 7968–7976. doi: 10.1128/jb.00851-07

Schülein, R., Seubert, A., Gille, C., Lanz, C., Hansmann, Y., Piémont, Y., et al. (2001). Invasion and persistent intracellular colonization of erythrocytes. *J. Exp. Med.* 193, 1077–1086. doi: 10.1084/jem.193.9.1077

Schulte, R., Kerneis, S., Klinke, S., Bartels, H., Preger, S., Kraehenbuhl, J. P., et al. (2000). Translocation of *Yersinia enterocolitica* across reconstituted intestinal epithelial monolayers is triggered by *Yersinia* invasin binding to? beta1 integrins apically expressed on M-like cells. *Cell. Microbiol.* 2, 173–185. doi: 10.1046/j.1462-5822.2000.00047.x

Schulze-Koops, H., Burkhardt, H., Heesemann, J., Kirsch, T., Swoboda, B., Bull, C., et al. (1993). Outer membrane protein YadA of enteropathogenic yersiniae mediates specific binding to cellular but not plasma fibronectin. *Infect. Immun.* 61, 2513–2519.

Serra, D. O., Conover, M. S., Arnal, L., Sloan, G. P., Rodriguez, M. E., Yantorno, O. M., et al. (2011). FHA-mediated cell-substrate and cell-cell adhesions are critical for *Bordetella pertussis* biofilm formation on abiotic surfaces and in the mouse nose and the trachea. *PLoS One* 6:e28811. doi: 10.1371/journal.pone.0028811

Sherlock, O., Dobrindt, U., Jensen, J. B., Vejborg, R. M., and Klemm, P. (2006). Glycosylation of the self-recognizing *Escherichia coli* Ag43 autotransporter protein. *J. Bacteriol.* 188, 1798–1807. doi: 10.1128/jb.188.5.1798-1807.2006

Sherlock, O., Schembri, M. A., Reisner, A., and Klemm, P. (2004). Novel roles for the AIDA adhesin from diarrheagenic *Escherichia coli*: cell aggregation and biofilm formation. *J. Bacteriol.* 186, 8058–8065. doi: 10.1128/jb.186.23.8058-8065.2004

Sijbrandi, R., Urbanus, M. L., Ten Hagen-Jongman, C. M., Bernstein, H. D., Oudega, B., Otto, B. R., et al. (2003). Signal recognition particle (SRP)-mediated targeting and Sec-dependent translocation of an extracellular *Escherichia coli* protein. *J. Biol. Chem.* 278, 4654–4659. doi: 10.1074/jbc.m211630200

Silhavy, T. J., Ruiz, N., and Kahne, D. (2006). Advances in understanding bacterial outer-membrane biogenesis. *Nat. Rev. Microbiol.* 4, 57–66. doi: 10.1038/nrmicro1322

Sitthidet, C., Korbsrisate, S., Layton, A. N., Field, T. R., Stevens, M. P., and Stevens, J. M. (2011). Identification of motifs of *Burkholderia pseudomallei* BimA required for intracellular motility, actin binding, and actin polymerization. *J. Bacteriol.* 193, 1901–1910. doi: 10.1128/JB.01455-10

Skurnik, M., and Wolf-Watz, H. (1989). Analysis of the yopA gene encoding the Yop1 virulence determinants of *Yersinia* spp. *Mol. Microbiol.* 3, 517–529. doi: 10.1111/j.1365-2958.1989.tb00198.x

Soprova, Z., Sauri, A., Van Ulsen, P., Tame, J. R. H., Den Blaauwen, T., Jong, W. S. P., et al. (2010). A conserved aromatic residue in the autochaperone domain of the autotransporter Hbp is critical for initiation of outer membrane translocation. *J. Biol. Chem.* 285, 38224–38233. doi: 10.1074/jbc.M110.180505

Spahich, N. (2011). Structure and function of the *Haemophilus influenzae* autotransporters. *Front. Cell. Infect. Microbiol.* 1:5. doi: 10.3389/fcimb.2011.00005

St. Geme, J. W. (1994). The HMW1 adhesin of nontypeable *Haemophilus influenzae* recognizes sialylated glycoprotein receptors on cultured human epithelial cells. *Infect. Immun.* 62, 3881–3889.

St. Geme, J. W., and Yeo, H. J. (2009). A prototype two-partner secretion pathway: the *Haemophilus influenzae* HMW1 and HMW2 adhesin systems. *Trends Microbiol.* 17, 355–360. doi: 10.1016/j.tim.2009.06.002

Stein, M., Kenny, B., Stein, M. A., and Finlay, B. B. (1996). Characterization of EspC, a 110-kilodalton protein secreted by enteropathogenic *Escherichia coli* which is homologous to members of the immunoglobulin A protease-like family of secreted proteins. *J. Bacteriol.* 178, 6546–6554. doi: 10.1128/jb.178.22.6546-6554.1996

Stevens, M. P., Stevens, J. M., Jeng, R. L., Taylor, L. A., Wood, M. W., Hawes, P., et al. (2005). Identification of a bacterial factor required for actin-based motility

of *Burkholderia pseudomallei*. *Mol. Microbiol.* 56, 40–53. doi: 10.1111/j.1365-2958.2004.04528.x

Szabady, R. L., Peterson, J. H., Skillman, K. M., and Bernstein, H. D. (2005). From The Cover: an unusual signal peptide facilitates late steps in the biogenesis of a bacterial autotransporter. *Proc. Natl. Acad. Sci. U.S.A.* 102, 221–226. doi: 10.1073/pnas.0406055102

Szczesny, P., and Lupas, A. (2008). Domain annotation of trimeric autotransporter adhesins - daTAA. *Bioinformatics* 24, 1251–1256. doi: 10.1093/bioinformatics/btn118

Tan, T. T., Forsgren, A., and Riesbeck, K. (2006). The respiratory pathogen *moraxella* catarrhalis binds to laminin via ubiquitous surface proteins A1 and A2. *J. Infect. Dis.* 194, 493–497. doi: 10.1086/505581

Tan, T. T., Nordström, T., Forsgren, A., and Riesbeck, K. (2005). The respiratory pathogen *Moraxella catarrhalis* adheres to epithelial cells by interacting with fibronectin through ubiquitous surface proteins A1 and A2. *J. Infect. Dis.* 1029–1038. doi: 10.1086/432759

Tavano, R., Capecchi, B., Montanari, P., Franzoso, S., Marin, O., Sztukowska, M., et al. (2011). Mapping of the *Neisseria meningitidis* NadA cell-binding site: Relevance of predicted?α-helices in the NH2-terminal and dimeric coiled-coil regions. *J. Bacteriol.* 193, 107–115. doi: 10.1128/jb.00430-10

Tertti, R., Skurnik, M., Vartio, T., and Kuusela, P. (1992). Adhesion protein YadA of *Yersinia* species mediates binding of bacteria to fibronectin. *Infect. Immun.* 60, 3021–3024.

Thanassi, D. G., Stathopoulos, C., Karkal, A., and Li, H. (2005). Protein secretion in the absence of ATP: the autotransporter, two-partner secretion and chaperone/usher pathways of Gram-negative bacteria. *Mol. Membr. Biol.* 22, 63–72. doi: 10.1080/09687860500063290

Tielen, P., Rosenau, F., Wilhelm, S., Jaeger, K. E., Flemming, H. C., and Wingender, J. (2010). Extracellular enzymes affect biofilm formation of mucoid *Pseudomonas aeruginosa*. *Microbiology* 156, 2239–2252. doi: 10.1099/mic.0.037036-0

Totsika, M., Wells, T. J., Beloin, C., Valle, J., Allsopp, L. P., King, N. P., et al. (2012). Molecular characterization of the EhaG and UpaG trimeric autotransporter proteins from pathogenic *Escherichia coli*. *Appl. Environ. Microbiol.* 78, 2179–2189. doi: 10.1128/AEM.06680-11

Trunk, T., Khalil, H. S., and Leo, J. C. (2018). Bacterial autoaggregation. *AIMS Microbiol.* 4, 140–164. doi: 10.3934/microbiol.2018.1.140

Tsirigotaki, A., De Geyter, J., Šoštarić, N., Economou, A., and Karamanou, S. (2017). Protein export through the bacterial Sec pathway. *Nat. Rev. Microbiol.* 15, 21–36. doi: 10.1038/nrmicro.2016.161

Tuomanen, E., Towbin, H., Rosenfelder, G., Braun, D., Larson, G., Hansson, G. C., et al. (1988). Receptor analogs and monoclonal antibodies that inhibit adherence of *Bordetella pertussis* to human ciliated respiratory epithelial cells. *J. Exp. Med.* 168, 267–277. doi: 10.1084/jem.168.1.267

Valle, J., Mabbett, A. N., Ulett, G. C., Toledo-Arana, A., Wecker, K., Totsika, M., et al. (2008). UpaG, a new member of the trimeric autotransporter family of adhesins in uropathogenic *Escherichia coli*. *J. Bacteriol.* 190, 4147–4161. doi: 10.1128/JB.00122-08

van den Berg, B. (2010). Crystal structure of a full-length autotransporter. *J. Mol. Biol.* 396, 627–633. doi: 10.1016/j.jmb.2009.12.061

Weirich, J., Bräutigam, C., Mühlenkamp, M., Franz-Wachtel, M., Macek, B., Meuskens, I., et al. (2017). Identifying components required for OMP biogenesis as novel targets for antiinfective drugs. *Virulence* 8, 1170–1188. doi: 10.1080/21505594.2016.1278333

Wilhelm, S., Gdynia, A., Tielen, P., Rosenau, F., and Jaeger, K. E. (2007). The autotransporter esterase EstA of *Pseudomonas aeruginosa* is required for rhamnolipid production, cell motility, and biofilm formation. *J. Bacteriol.* 189, 6695–6703. doi: 10.1128/jb.00023-07

Wilhelm, S., Tommassen, J., and Jaeger, K. E. (1999). A novel lipolytic enzyme located in the outer membrane of *Pseudomonas aeruginosa*. *J. Bacteriol.* 181, 6977–6986.

Wollmann, P., Zeth, K., Lupas, A. N., and Linke, D. (2006). Purification of the YadA membrane anchor for secondary structure analysis and crystallization. *Int. J. Biol. Macromol.* 39, 3–9. doi: 10.1016/j.ijbiomac.2005.11.009

Xin, K. W., Chow, V. T. K., and Alonso, S. (2010). Exploring the versatility of the autotransporter BrkA for the presentation of enterovirus 71 vaccine candidates at the surface of attenuated *Bordetella pertussis*. *Procedia Vaccinol.* 2, 64–70.

Yang, F. L., and Braun, V. (2000). ShlB mutants of *Serratia marcescens* allow uncoupling of activation and secretion of the ShlA hemolysin. *Int. J. Med. Microbiol.* 290, 529–538. doi: 10.1016/S1438-4221(00)80018-1

Yen, Y. T., Kostakioti, M., Henderson, I. R., and Stathopoulos, C. (2008). Common themes and variations in serine protease autotransporters. *Trends Microbiol.* 16, 370–379. doi: 10.1016/j.tim.2008.05.003

Zinchenko, A. A., Kotelnikova, O. V., Gordeeva, E. A., Prokopenko, Y. A., Razgulyaeva, O. A., Serova, O. V., et al. (2018). Immunogenic and protective properties of *Neisseria meningitidis* IgA1 protease and of its truncated fragments. *Russ. J. Bioorg. Chem.* 44, 64–72. doi: 10.1134/s1068162018010193

Conflict of Interest Statement: The authors declare that the research was conducted in the absence of any commercial or financial relationships that could be construed as a potential conflict of interest.

Copyright © 2019 Meuskens, Saragliadis, Leo and Linke. This is an open-access article distributed under the terms of the Creative Commons Attribution License (CC BY). The use, distribution or reproduction in other forums is permitted, provided the original author(s) and the copyright owner(s) are credited and that the original publication in this journal is cited, in accordance with accepted academic practice. No use, distribution or reproduction is permitted which does not comply with these terms.

frontiers in Microbiology

ORIGINAL RESEARCH
published: 05 June 2019
doi: 10.3389/fmicb.2019.01218

A Type VI Secretion System Trans-Kingdom Effector Is Required for the Delivery of a Novel Antibacterial Toxin in *Pseudomonas aeruginosa*

*Benjamin Berni, Chantal Soscia, Sarah Djermoun, Bérengère Ize and Sophie Bleves**

LISM, IMM (Institut de Microbiologie de la Méditerranée), CNRS and Aix-Marseille Univ, Marseille, France

Pseudomonas aeruginosa has evolved multiple strategies to disarm and take advantage of its host. For this purpose, this opportunist pathogen has particularly developed protein secretion in the surrounding medium or injection into host cells. Among this, the type VI secretion system (T6SS) is utilized to deliver effectors into eukaryotic host as well as target bacteria. It assembles into a contractile bacteriophage tail-like structure that functions like a crossbow, injecting an arrow loaded with effectors into the target cell. The repertoire of T6SS antibacterial effectors of *P. aeruginosa* is remarkably broad to promote environmental adaptation and survival in various bacterial communities, and presumably in the eukaryotic host too. Here, we report the discovery of a novel pair of antibacterial effector and immunity of *P. aeruginosa*, Tle3 and Tli3. Tli3 neutralizes the toxicity of Tle3 in the periplasm to protect from fratricide intoxication. The characterization of the secretion mechanism of Tle3 indicates that it requires a cytoplasmic adaptor, Tla3, to be targeted and loaded onto the VgrG2b spike and thus delivered by the H2-T6SS machinery. Tla3 is different from the other adaptors discovered so far and defines a novel family among T6SS with a DUF2875. Interestingly, this led us to discover that VgrG2b that we previously characterized as an anti-eukaryotic effector possesses an antibacterial activity as well, as it is toxic towards *Escherichia coli*. Excitingly Tli3 can counteract VgrG2b toxicity. VgrG2b is thus a novel trans-kingdom effector targeting both bacteria and eukaryotes. VgrG2b represents an interesting target for fighting against *P. aeruginosa* in the environment and in the context of host infection.

Keywords: virulence, type VI secretion system, bacterial competition, VgrG, Tle, immunity, adaptor, chaperone

OPEN ACCESS

Edited by:
Ignacio Arechaga, University of Cantabria, Spain

Reviewed by:
Yosuke Tashiro, Shizuoka University, Japan
Paola Sperandeo, University of Milan, Italy

***Correspondence:**
Sophie Bleves
bleves@imm.cnrs.fr

Specialty section:
This article was submitted to Microbial Physiology and Metabolism, a section of the journal Frontiers in Microbiology

Received: *25 February 2019*
Accepted: *15 May 2019*
Published: *05 June 2019*

Citation:
Berni B, Soscia C, Djermoun S, Ize B and Bleves S (2019) A Type VI Secretion System Trans-Kingdom Effector Is Required for the Delivery of a Novel Antibacterial Toxin in Pseudomonas aeruginosa. Front. Microbiol. 10:1218. doi: 10.3389/fmicb.2019.01218

INTRODUCTION

Pseudomonas aeruginosa is one of the most virulent opportunistic pathogens, being responsible for various diseases such as acute infections of lungs and burned skin that can lead to septicemia more particularly in immunocompromized patients, or broncho-alveolar colonization in cystic fibrosis sufferers. *P. aeruginosa* has been classified in 2017 as critical by the WHO in the top

three lists of antibiotic resistant bacteria (WHO, 2019). *P. aeruginosa* has developed various pathogenicity strategies among which protein secretion or protein delivery into target cells is key. Indeed, this pathogen possesses five of the six secretion systems so far identified among Gram-negative bacteria, if we exclude the T9SS (type IX secretion system) restricted to one phylum, and remarkably in several copies for most of them (Bleves et al., 2010).

The type VI secretion system (T6SS) was first discovered in the context of eukaryotic host infection (Mougous et al., 2006; Pukatzki et al., 2006) and later during bacterial competition (Hood et al., 2010), which seems to be its primary function (Cianfanelli et al., 2016b). The T6SS confers a fitness advantage (1) in environmental niches against rival bacteria (inter- and intraspecies competitiveness have been described) and (2) in the eukaryotic host towards commensal bacteria (Cianfanelli et al., 2016b). Indeed, recent studies have highlighted a novel role for T6SS-dependent antibacterial responses in interbacterial competition in the mammalian gut (Hecht et al., 2016; Sana et al., 2016b), suggesting that T6SSs may be important not only in shaping microbial community composition but also in governing interactions between the microbiota and invading pathogens. Interestingly, several T6SSs are also known to target both cell type genus such as the T6SS of *Vibrio cholera* (Pukatzki et al., 2006; MacIntyre et al., 2010) and *P. aeruginosa* (Sana et al., 2012) (Russell et al., 2013). Even more remarkably, three T6SS effectors of *P. aeruginosa*, namely, PldA (also called Tle5a), PldB (Tle5b), and TplE (Tle4) (Jiang et al., 2014, 2016) have been called "trans-kingdom effectors" since these toxins can target both prokaryotic and eukaryotic cells (Bleves, 2016). Indeed, toxins are usually directed against eukaryotic cells (like AB toxins or RTX pore-forming toxins) or against rival bacteria (like bacteriocins).

The T6SS functions as a dynamic contractile phage tail-like structure anchored in the bacterial cell envelope that delivers effector proteins directly into the target cell in a one-step manner. T6SS includes a contractile sheath that cover a nanotube of stacked Hcp topped with a membrane-puncturing spike made of VgrG and PAAR (proline-alanine-alanine-arginine repeat) proteins (Basler, 2015). The sheath can contract and inject the arrow loaded with effectors into the target cell. Characterizing the repertoire of effectors delivered by the T6SS has highlighted a great diversity in terms of effector activities, host cell targets, and mode of recruitment by the T6SS machinery. In brief, there are two broad effector categories: the "specialized" effectors fused to components of the machinery (evolved VgrG, evolved PAAR, and evolved Hcp have been described so far) and the "cargo" effectors (Cianfanelli et al., 2016b). The later are addressed to the T6SS machinery by binding directly one of the arrow components (VgrG, PAAR, and Hcp) or by being targeted through cytoplasmic adaptor proteins also called chaperones. To date, three families of adaptor have been described, the first one harboring a DUF4123 (Miyata et al., 2013; Salomon et al., 2014; Liang et al., 2015; Unterweger et al., 2015), the second a DUF1795 (Alcoforado Diniz and Coulthurst, 2015; Whitney et al., 2015), and the third one a DUF2169 (Bondage et al., 2016). In line with this, many effector-encoding genes are found in close proximity to *vgrG*, *hcp*, and *paar* or adaptor genes. Finally to protect themselves from self-intoxication or from antibacterial toxins injected by neighboring sibling cells, bacteria always synthesize immunity proteins, which are encoded by adjacent genes (Benz and Meinhart, 2014).

P. aeruginosa encodes three distinct T6SS loci, H1- to H3-T6SS. While H1-T6SS has only been involved in antibacterial activity so far (Sana et al., 2016a; LaCourse et al., 2018), H2-T6SS and H3-T6SS can target both bacterial and eukaryotic cells possessing even as said earlier trans-kingdom effectors (Sana et al., 2012, 2015; Russell et al., 2013; Jiang et al., 2014, 2016; Burkinshaw et al., 2018). We discovered the anti-eukaryotic function of the H2-T6SS machinery that promotes the uptake of *P. aeruginosa* by non-phagocytic cells (Sana et al., 2012). The two phospholipases D mentioned earlier, PldA (Tle5a) and PldB (Tle5b), delivered, respectively, by H2-T6SS and H3-T6SS machineries participate in the host kinase pathway hijacking that facilitates further entry of *P. aeruginosa* (Jiang et al., 2014). The evolved VgrG2b effector (Sana et al., 2015) is delivered by H2-T6SS into epithelial cells where it targets the γ-tubulin ring complex, a microtubule-nucleating multiprotein complex to promote a microtubule-dependent internalization of *P. aeruginosa*. Finally TplE (Tle4), which is secreted by the H2-T6SS machinery, promotes autophagy in epithelial cells once localized to the endoplasmic reticulum (Jiang et al., 2016). Interestingly, PldA (Tle5a), PldB (Tle5b), and TplE (Tle4) have also been identified as antibacterial phospholipases of the Tle (type VI lipase effectors) family (Russell et al., 2013). They work by affecting membrane integrity of the rival bacteria (Russell et al., 2013; Jiang et al., 2014, 2016). More precisely, PldA degrades the major constituent of bacterial membranes, the phosphatidylethanolamine (Russell et al., 2013).

In the present study, we have discovered a novel antibacterial toxin, Tle3, and its cognate immunity, Tli3, whose genes are encoded downstream of *vrgG2b*. By characterizing the secretion mechanism of Tle3 by H2-T6SS, we showed that it requires Tla3, a cytoplasmic adaptor of a unique family, to be targeted to the VgrG2b spike. Interestingly, we also found that the C-terminal extension of VgrG2b is toxic towards *Escherichia coli* making VgrG2b a new trans-kingdom effector of *P. aeruginosa*.

MATERIALS AND METHODS

Bacterial Strains, Growth Conditions, and Plasmid Construction

All *P. aeruginosa* and *E. coli* strains used in this study are described in **Supplementary Table S1**. Briefly, the *E. coli* K-12 DH5α and CC118λPir were used for cloning procedures. The BL21(DE3)pLysS and BTH101 were used for protein production and BACTH analyses, respectively. Strains were grown in LB or in TSB medium (for *P. aeruginosa*) at 37 or 30°C. Specific growth conditions are specified in the text when necessary. Recombinant plasmids were introduced into *P. aeruginosa* by triparental mating

using the conjugative properties of the helper plasmid pRK2013 (**Supplementary Table S1**). Plasmids were maintained by the addition of ampicillin (50 μg/ml), kanamycin (50 μg/ml), chloramphenicol (30 μg/ml), streptomycin (30 μg/ml for *E. coli* and 2,000 μg/ml for *P. aeruginosa*), or gentamicin (30 μg/ml for *E. coli* and 115 μg/ml for *P. aeruginosa*). Expression of genes from pT7 in BL21(DE3)pLysS was blocked with 0.4% of glucose and induced in exponential phase (OD_{600} = 0.4–0.6) for 3 h with 1 mM of IPTG. Cloning procedures were described in Sana et al. (2015). The plasmids used and constructed are described in **Supplementary Table S1**, the list of oligonucleotides (synthesized by Eurogentec or IDT) is given in **Supplementary Table S2**.

Cloning Procedures for *P. aeruginosa* Mutants

To generate *P. aeruginosa* mutants, 500 bp upstream and 500 bp downstream of the gene to be deleted were amplified by overlapping PCR with Q5 high fidelity DNA polymerase (NEB) using primers listed in **Supplementary Table S1**. The PCR product was cloned in pKNG101 suicide vector by one-step sequence and ligation-independent cloning (SLIC) (Jeong et al., 2012), which was then sequenced. pKNG101 derivatives, maintained in the *E. coli* CC118λpir strain, were mobilized in *P. aeruginosa* strains. The mutants, in which the double recombination events occurred, were confirmed by PCR analysis.

Heterologous Toxicity Assays

E. coli BL21(DE3)pLysS containing plasmids producing cytoplasmic or periplasmic targeted proteins were grown overnight at 37°C in LB with 0.4% of glucose. About 10 μl drops of bacterial suspensions serially diluted were spotted onto LB agar plates containing 0.1 mM IPTG or 0.4% glucose and cells were grown for 16 h at 37°C.

Bacterial Two-Hybrid Assay

Protein-protein interactions were assessed with the adenylate cyclase-based two-hybrid technique using protocols published previously (Karimova et al., 1998; Battesti and Bouveret, 2012). Briefly, the proteins to be tested were fused to the isolated T18 and T25 catalytic domains of the *Bordetella* adenylate cyclase. After introduction of the two plasmids producing the fusion proteins into the reporter BTH101 strain, plates were incubated at 30°C for 24 h. Three independent colonies for each transformation were inoculated into 600 μl of LB medium supplemented with ampicillin (50 μg/ml), kanamycin (50 μg/ml), and IPTG (0.5 mM). After overnight growth at 30°C, 5 μl of each culture was spotted onto LB agar plates supplemented with ampicillin, kanamycin, IPTG, and 5-bromo-4-chloro-3-indonyl-D-galactopyrannoside (X-gal, 40 μg/ml) and incubated for 16 h at 30°C.

Protein Purification by Affinity Chromatography

E. coli BL21(DE3)plysS cells carrying the pRSFDUET-1 and pETDUET-1 derivatives were grown at 37°C in LB to an OD_{600}~0.5 and the expression of the PA0262, PA0261, PA0260, or PA0259 genes was induced with IPTG (1 mM) for 3 h at 37°C. Cells were harvested by centrifugation at 1,914 × *g* for 30 min at 4°C. The cell pellet was resuspended in Tris–HCl 50 mM pH 8.0, NaCl 150 mM, Triton X-100 0.1%, lysozyme 0.5 mg/ml, and EDTA 1 mM and stored at −80°C. Cells were supplemented with DNase (20 μg/ml), $MgCl_2$, and phenylmethylsulfonyl fluoride 1 mM and cells were lysed by three passages at the Emulsiflex-C5 (Avestin), and lysates were clarified by centrifugation at 16,000 × *g* for 30 min. The supernatant was loaded onto a 5-ml StrepTrap HP (GE Healthcare) column and then washed with 50 mM Tris-HCl pH 8.0, 150 mM NaCl at 4°C. The fusion protein was eluted in the affinity buffer supplemented with 2.5 mM desthiobiotin. Peak fractions were pooled and loaded onto a Superose 200 10/300 column (GE Healthcare) equilibrated in 50 mM Tris-HCl pH 8.0, 50 mM NaCl.

Fractionation of *P. aeruginosa*

Fractionation of cells into spheroplasts (cytoplasm and membranes) and periplasmic fractions were done as previously described (Ize et al., 2014). Proteins corresponding to the cytoplasm and periplasm fractions or to insoluble material were resuspended in loading buffer.

Protein Secretion

P. aeruginosa strains were grown at 25°C in TBS for 24 h. Cells corresponding to 10 U DO_{600} and extracellular medium were separated by centrifugation at 2,000 × *g* for 10 min at room temperature. 2/3 of the supernatants were collected and centrifuged at 13,000 × *g* for 5 min at room temperature. Proteins contained in the supernatant were precipitated with tricholoro-acetic acid (TCA, 15%) for 3 h at 4°C. Samples were centrifuged at 13,000 × *g* for 30 min at 4°C, pellets washed with 90% acetone, and resuspended in loading buffer.

SDS-PAGE and Western-Blot

Protein samples derived from equivalent amounts of culture (i.e., optical density equivalents) resuspended in loading buffer were boiled and separated by SDS-PAGE. Proteins were then stained by Coomassie-blue or immunodetected as described before (Sana et al., 2015) using primary polyclonal antibodies directed against His6 epitope-tag (Penta His, Qiagen, dilution 1:1,000), V5 epitope-tag (Bethyl Laboratories, dilution 1:1,000), Strep epitope-tag (IBA StrepMAB Classic, dilution 1:000), DsbA (kindly gifted by K. E. Jaeger – university of Heinrich-Heine, dilution 1:25,000), or monoclonal antibodies directed against EF-Tu (Hycult-biotech, dilution 1:20,000), XcpY (laboratory collection, dilution 1:5,000), and TolB (laboratory collection, dilution 1:500). Peroxidase-conjugated anti-Mouse or anti-Rabbit IgGs (Sigma, dilution 1:5,000) were used as secondary antibodies. Nitrocellulose membranes were revealed with homemade enhanced chemiluminescence and were scanned using ImageQuant LAS4000 analysis software (GE Healthcare Life sciences).

Protein samples equivalent to 0.1 OD_{600} units were loaded for whole cell and spheroplasts analysis while protein samples

equivalent to 0.2 OD_{600} units were used for cytoplasm or periplasm analysis and protein samples equivalent to 1 OD_{600} units were used for extracellular medium analysis.

Bacterial Competition Assays

Intraspecific competition assays between *P. aeruginosa* strains were performed as previously described (Jiang et al., 2014) with modifications. The prey cells carry pJN105 vector (Gm^R) to allow counterselection. Overnight cultures of *P. aeruginosa* attacker and prey cells were mixed in a 10:1 (attacker:prey) ratio and harvested by centrifugation at 3,724 × *g* for 5 min. The pellet was resuspended in 200 µl of PBS 1X and spotted onto 0.45-µm nitrocellulose membranes overlaid on a 1% bactoagar plate. After 24 h of incubation at 37°C, cells were resuspended in 2 ml of PBS 1X, normalized to an OD_{600nm} of 0.5, and 10 µl of bacterial serially diluted (10^{-1} to 10^{-6}) were spotted onto selective LB agar plates containing gentamicin (125 µg/ml). Significant growth difference of the prey bacteria for each competition assay was computed by one-way ANOVA (Stat Plus) and unpaired Student's Test (Excel).

RESULTS

Tle3 Is a Novel Antibacterial Toxin of *P. aeruginosa*

The analysis of the *vgrG2b* genetic environment revealed the presence of the PA0260 gene encoding a protein with a α/β hydrolase domain (PF00561) and a putative Ser-Asp-His catalytic triad used by various esterase enzymes and has thus been classified in the Tle3 family of antibacterial Tle toxins (**Figure 1A**; Russell et al., 2013). The immunities of Tle proteins, which are lipolytic toxins active in the periplasm of the prey bacterium, are localized in or exposed to the periplasm where they neutralize the cognate toxin (Russell et al., 2013; Jiang et al., 2014, 2016; Flaugnatti et al., 2016). The two genes surrounding *tle3*, PA0259 and PA0261, are good candidates as Tle3 immunity. Indeed, sequence comparisons of PA0259 and PA0261 showed that PA0261 is homologous to Tsi6, the immunity protein of a H1-T6SS effector called Tse6, and PA0259 to TplEi (Tli4), the immunity of TlpE (Tle4), a H2-T6SS effector (Lu et al., 2014; Jiang et al., 2016). We used the SignalP 4.1 server (Nielsen, 2017) to predict the cellular localization of the two immunity candidates. While a Sec signal sequence is predicted at the N-terminal extremity of PA0261, the analysis of the PA0259 sequence did not reveal any. However, three upstream ATG can be found in frame with the annotated ATG of PA0259 (**Supplementary Figure S1**). The sequence of the proteins synthesized from the two first ATG (ATG_1 and ATG_2) presents then a N-terminal signal peptide, while the protein synthesized from the last codon (ATG_3) does not. Moreover, a ribosome-binding sequence (RBS) can be found only upstream of ATG_1 and with a significant Kolaskar score that indicates a strong probability to be used as an initiation codon (Kolaskar and Reddy, 1985). Altogether, these data tend to indicate an incorrect annotation of the start codon of PA0259 and that ATG_1 should be considered for the initiation of PA0259 translation. Such a correction has been already seen for Tli5 (PA3488) the immunity protein of PldA (Tle5a) of *P. aeruginosa* (Russell et al., 2013). In conclusion of this *in silico* analysis, the two putative immunities may harbor a Sec signal peptide that suggests a periplasmic localization in agreement with Tle3 activity in this compartment.

To demonstrate the antibacterial activity of Tle3 and to identify its immunity protein, we developed a heterologous toxicity assay in *E. coli* on the basis that Tle3 should be toxic when produced in the periplasm of *E. coli* and that it should be counteracted by the co-production of its immunity protein. In order to artificially address Tle3 to the periplasm of *E. coli* the *tle3* sequence has been cloned in frame with the sequence coding the PelB signal peptide on the pET22b vector under a P_{T7} promoter. PA0259 from ATG_1 and PA0261 were respectively cloned in pRSF-DUET, a higher copy-number vector, to allow a maximal co-expression with *ss-tle3* in the *E. coli* BL21(DE3) pLysS strain. The correct production and localization of all the recombinant proteins in *E. coli* has been verified by western blot after cell fractionation (**Supplementary Figure S2**). The results presented in **Figure 1B** indicate that whereas the cytoplasmic production of Tle3 was not toxic, Tle3 targeting to the periplasm led to *E. coli* killing. Moreover, while PA0259 had no effect, the coproduction of PA0261 in the periplasm protected the cells against the toxicity of Tle3. We verified that the sole overproduction of PA0259 and PA0261 was not toxic to *E. coli*. As PA0261 neutralized Tle3 toxicity, we called it "Tli3" for Type VI lipase immunity (**Figure 1A**). During this study, we observed that the protection conferred by Tli3 coproduction could be sometimes partial and we solved this issue by cloning in tandem *tli3* and *tle3* on the same plasmid like they are organized on *P. aeruginosa* genome (**Figure 1B**, line 8). The importance of this genetic link is the proof of the close connection between these two proteins as a pair of toxin-antitoxin.

Tli3 (PA0261) Is the Immunity Protein of Tle3

As the immunities bind specifically their effector, which is suggested by the release of Tle3 toxicity by Tli3, we tested the physical interaction between both proteins by co-purification with affinity chromatography (**Figure 2A** and **Supplementary Figure S6**). A cytoplasmic Strep-tagged version of Tli3 was engineered by fusing the tag to the mature domain of Tli3, lacking its signal peptide. The recombinant protein was coproduced in *E. coli* BL21(DE3) pLysS with the cytoplasmic His_{10}-tagged Tle3. The bacterial lysate was loaded to a StrepTactin matrix (see section "Materials and Methods"), and $Tli3^{C}_{Strep}$ was eluted with desthiobiotin. The presence of $Tle3^{C}_{His}$ was controlled in the elution fraction with anti-His antibodies. As showed in **Figure 2A** and **Supplementary Figure S6**, $Tle3^{C}_{His}$ was found in the eluted fraction only upon coproduction with $Tli3^{C}_{Strep}$ (left panel). Indeed when produced alone in *E. coli*, $Tle3^{C}_{His}$ was not purified by affinity chromatography (right panel). As expected for an immunity protein, Tli3 directly interacts with Tle3.

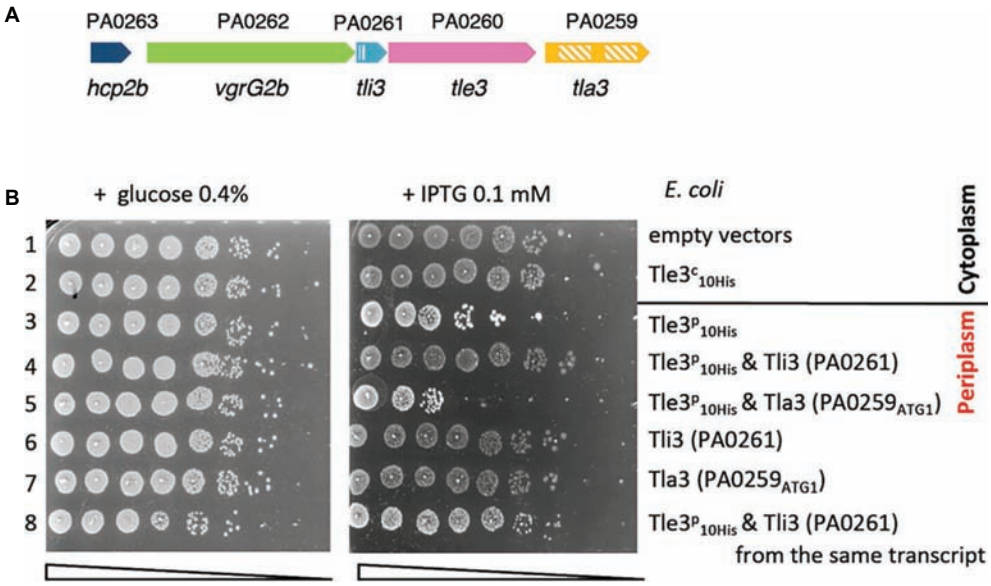

FIGURE 1 | (A) *vgrG2b* island organization. The genes are labeled with the given name (i.e., *hcp2b*) and are indicated by their annotation number (e.g., PA0263). The Sec signal peptide of Tli3 (PA0261) and the two DUF2875 of Tla3 (PA0259) are represented with stripped boxes. **(B)** The Tle3 periplasmic toxicity is counteracted by Tli3 (PA0261). Serial dilutions (from non-diluted to 10^{-7}) of normalized cultures of *E. coli* BL21(DE3)pLysS producing the wild-type Tle3 in the cytoplasm, called Tle3^{c} (from pVT1, a pETDuet-1 derivative) or in the periplasm, called Tle3^{p} [from pSBC81, a pET22b(+) derivative yielding a fusion of Tle3 with a Sec signal peptide] were spotted on LB agar plates supplemented (left panel) with 0.4% glucose or (right panel) with 0.1 mM IPTG. Glucose and IPTG allow respectively repression and induction of the gene encoding the T7 RNA polymerase. When indicated Tli3 (PA0261) or Tla3 (PA0259) were produced in the periplasm from pVT8, pSBC107 and pVT9, respectively, pRSFDuet-1 derivatives. Line 1: pET22b(+) and pRSFDuet-1, line 2: pVT1 and pRSFDuet-1, line 3: pSBC81 and pRSFDuet-1, line 4: pSBC81 and pVT8, line 5: pSBC81 and pVT9, line 6: pVT8 and pET22b(+), line 7: pVT9 and pET22b(+), and line 8: pSBC107 is a pRSFDuet-1 derivative producing Tli3 (PA0261) and Tle3^{p} from the same transcript.

To go further into Tli3 characterization, we chose to determine its cellular localization in *P. aeruginosa*. All the immunity proteins identified so far for Tle proteins are localized in the periplasm or associated to the periplasmic side of the outer membrane (Russell et al., 2013; Jiang et al., 2014, 2016; Flaugnatti et al., 2016) in order to counteract their cognate toxin. A chromosomally encoded Tli3$_{V5}$ translational fusion was engineered in order to specifically immunodetect the protein in *P. aeruginosa* (**Supplementary Table S1**). After fractionation of *P. aeruginosa* (**Figure 2B**), Tli3 was readily observed in the same fraction as DsbA that catalyzes intrachain disulfide bond formation as peptides emerge into the periplasm. This indicates a periplasmic localization for Tli3 in *P. aeruginosa* in agreement with the presence of a Sec signal peptide and our working hypothesis suggesting an immunity function.

Tle3 Protein-Protein Interaction Network

To further characterize Tle3, we performed a bacterial two-hybrid (BACTH) assay with the other gene products of the *vgrG2b* operon hypothesizing that a genetic link could reflect protein-protein interaction. The sequences coding PA0259 and Tli3 (PA0261) after their signal sequences and Tle3 were cloned downstream and upstream the T18 or T25 domains of the *Bordetella adenylate* cyclase. Because of the high molecular weight of VgrG2b and since the interaction of another Tle with a VgrG in entero-aggregative *E. coli* (EAEC) was previously delimitated to the C-terminal domain of VgrG (Flaugnatti et al., 2016), we cloned the sequences encoding the C-terminal extension (domains 1, 2, and 3) and a truncated version harboring only the DUF2345 and the transthyretin-like (TTR) domains (domains 1 and 2) of VgrG2b downstream the T18 and T25 domains (**Figure 3A**).

Unexpectedly, the sole interaction revealed by the BACTH assay for Tle3 was with PA0259 (**Figure 3B**) since only the T18/T25-Tle3 and T18/T25-PA0259 fusion proteins coproduction activated the expression of the reporter gene. This assay did not confirm the interaction between Tle3 and Tli3 observed by copurification and did not evidence an interaction with VgrG2b. Interestingly, Tle3 and PA0259 did not interact anymore when they were fused upstream the T18 and T25 domains suggesting that both proteins interact *via* their C-terminal domains (**Supplementary Figure S3A**). To go further in characterizing the interaction between Tle3 and PA0259, we constructed truncated variants taking into account their domain organization (**Figure 3A**). We further delimitated the interacting domain of Tle3 to its extreme C-terminus (the DUF3274 domain) since only the truncated T18-Tle3D2 construct still interacts with T25-PA0259 (**Figure 3C**). We did not find the domain of interaction within PA0259 as none of the DUF2875 domains alone interacts with Tle3 or this may suggest that both of them are required for the interaction (**Figure 3C**).

Next, we took advantage of all the constructs we made to test other interactions. The BACTH assay also showed that

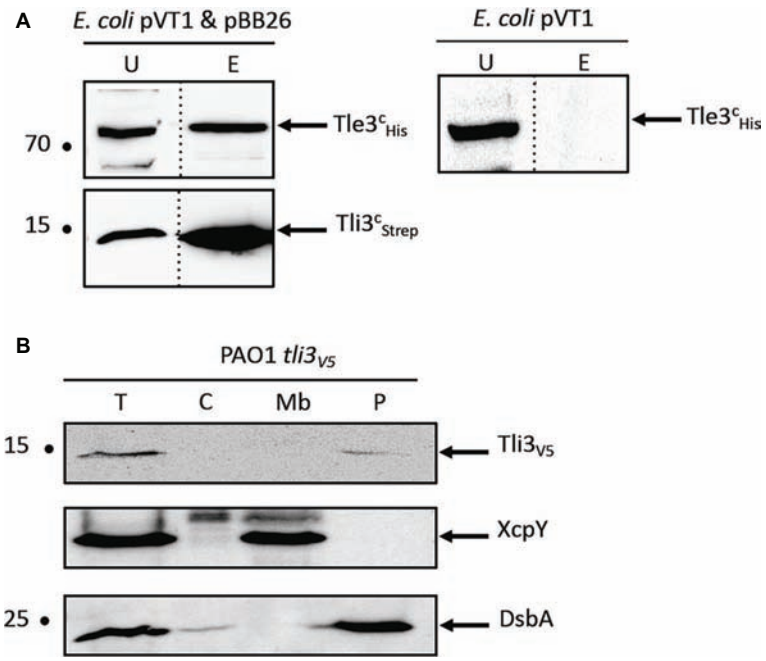

FIGURE 2 | (A) Tli3 (PA0261) interacts with Tle3. Copurification assay on StrepTactin column of $Tli3c_{Strep}$ with $Tle3c10_{His}$ produced in *E. coli* BL21(DE3)pLysS produced from pBB26 and pVT1 respectively. The unbound (U) and eluted (E) fractions were collected and subjected to SDS-PAGE (10.5%) and Western blot analyses using anti-His antibody (Upper) and anti-streptavidin antibody (Lower). The position of the proteins and the molecular mass markers (in kDa) are indicated. **(B)** Tli3 (PA0261) is a periplasmic protein in *P. aeruginosa*. Cells of *P. aeruginosa* PAO1 $tli3_{V5}$ were subjected to fractionation and immunoblotting using antibodies directed against the V5 tag, XcpY and DsbA. XcpY and DsbA were used as membrane and periplasmic controls, respectively. T, whole cell; C, cytoplasm; Mb, total membrane; P, periplasm. The position of the proteins and the molecular mass markers (in kDa) are indicated.

PA0259 interacts with both forms of the VgrG2b C-terminal extension (**Figure 3B**). The domain of interaction on VgrG2b is thus at least constituted by the DUF2345 and TTR domains. We also observed that PA0259 at least dimerizes since all the PA0259 constructs interact with each other whatever the orientation of PA0259 (**Figures 3B,D; Supplementary Figure S3B**). VgrG2b and Tli3 (PA0261) are also able to homomultimerize since all the constructs interact with each other (**Figure 3D; Supplementary Figure S3B**).

Taking into account the interactions revealed by the BACTH assay, we propose that the Tle3 toxin can be addressed to the H2-T6SS machinery VgrG2b component via PA0259. We thus named PA0259 "Tla3" for Type VI lipase adaptor protein.

Tla3 (PA0259) Characterization

To gain insight into the role of Tla3 during Tle3 secretion, we first validated the interactions of Tla3 with Tle3 and VgrG2b by a complementary approach of co-purification by affinity chromatography. Two different tagged versions of Tla3 were engineered by fusing a Strep-tag or a 10His-tag to the mature domain of Tla3 this leading to cytoplasmic tagged Tla3 proteins. The recombinant $Tla3^{C}_{Strep}$ was coproduced in *E. coli* BL21(DE3) pLysS with $Tle3^{C}_{His}$, and the $Tla3^{C}_{His}$ with 3 recombinant forms of Strep-tagged VgrG2b consisting in the full-length VgrG2b, or VgrG2b truncated for the extreme C-terminus (deletion of domain 3 in **Figure 3A**) or VgrG2b truncated for the extreme C-terminus and the TTR domain (deletion of domains 2 and 3 in **Figure 3A**). We initially tried with His-tagged VgrG2b but a problem of protein instability led us to shift for Strep-tagged VgrG2b. The bacterial lysates were loaded on a StrepTactin matrix, and $Tla3^{C}_{Strep}$ or the three recombinant $VgrG2b_{Strep}$ were eluted with desthiobiotin. The presence of $Tle3^{C}_{His}$ and of $Tla3^{C}_{His}$ was visualized in the elution fractions with anti-His antibodies. As shown in **Figures 4A, 2A** right panel and **Supplementary Figure S6**, $Tle3^{C}_{His}$ was only found in the eluted fraction upon coproduction with $Tla3^{C}_{Strep}$. We observed that $Tla3^{C}_{His}$ is copurified only upon coproduction with the full length VgrG2b (**Figure 4B** and **Supplementary Figure S6**) or the VgrG2b truncated for the extreme C-terminus (**Figure 4C** and **Supplementary Figure S6**). Indeed when produced alone (**Figure 4B** and **Supplementary Figure S6**) or with VgrG2b truncated for the extreme C-terminus and the TTR domain (**Figure 4D** and **Supplementary Figure S6**), $Tla3^{C}_{His}$ was not purified by affinity chromatography. Since VgrG2b truncated for the extreme C-terminus still copurified with Tla3 we can exclude that this domain is required for the interaction. This is in line with the BACTH assay that showed an interaction between Tla3 and a truncated VgrG2b consisting in only the DUF2345 and TTR domains (domains 1 and 2, **Figure 3A**). Moreover, the deletion of the TTR domain affecting the copurification, one can conclude that this domain is key for the interaction.

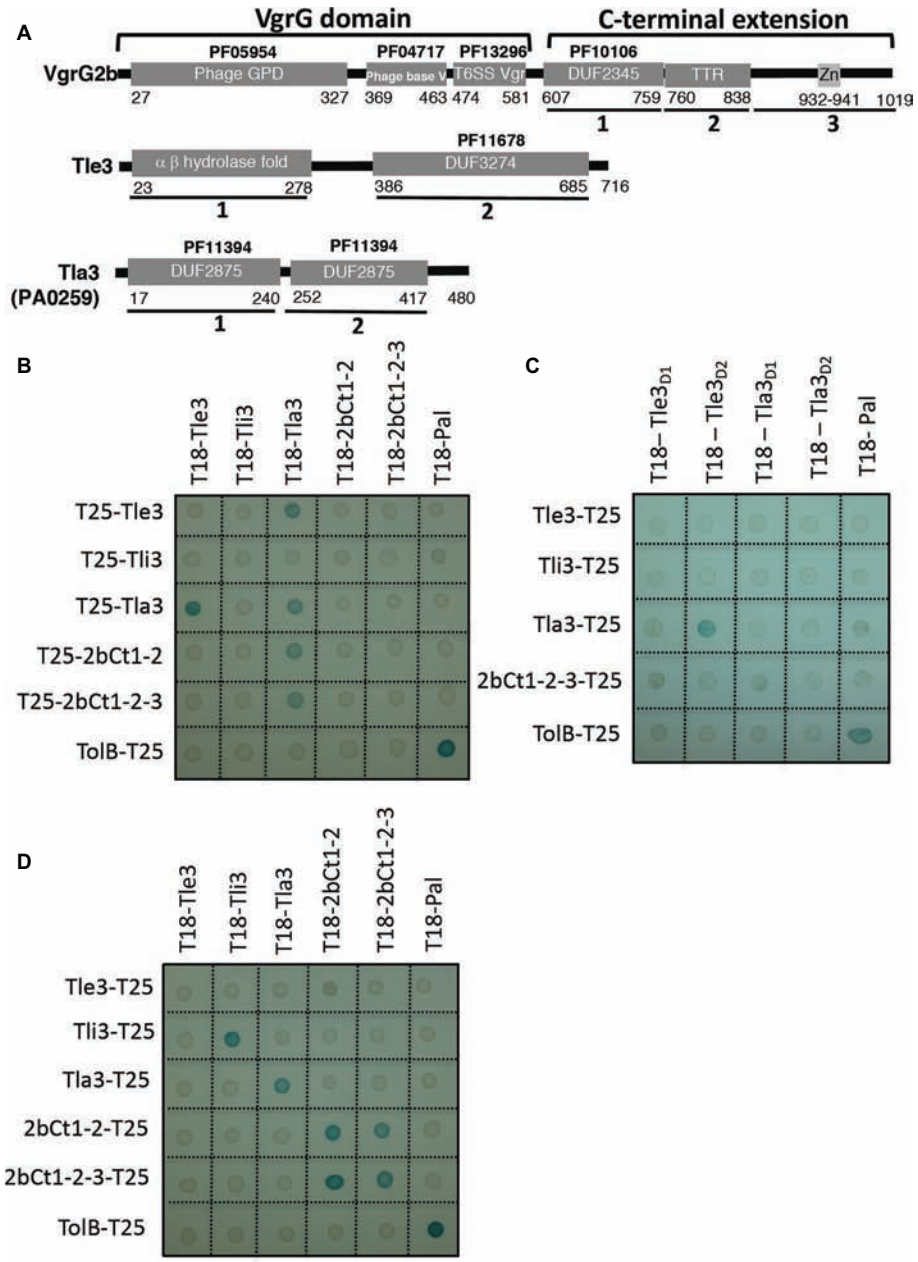

FIGURE 3 | (A) Tla3 (PA0259) interacts with the Tle3 toxin and with VgrG2b. Domain organization of VgrG2b, Tle3, and Tla3 (PA0259). The first 581 residues of VgrG2b carry the VgrG domain homologous to gp27 and gp5 phage tail proteins and consisting of three sub-domains. This is followed by the C-terminal extension, composed of a conserved domain of uncharacterized proteins (DUF2345, PF10106) (2bCt1), a TTR (transthyretin-like region) (2bCt2), and a putative zinc-dependent metallopeptidase pattern (LFIHEMTHVW signature, PS00142) (2bCt3). Tle3 architecture consists of an α,β hydrolase fold domain ($Tle3_{D1}$) followed by a DUF3274 ($Tle3_{D2}$), Tla3 of a tandem of DUF2875 ($Tla3_{D1}$ and $Tla3_{D2}$). **(B–D)** Bacterial two-hybrid assay. BTH101 reporter cells producing the indicated proteins or domains fused to the T18 or T25 domain of the *Bordetella* adenylate cyclase were spotted on X-gal indicator plates. The blue color of the colony reflects the interaction between the two proteins. TolB and Pal are two proteins known to interact but unrelated to the T6SS. The experiment was performed in triplicate and a representative result is shown.

Taken together these data confirmed a direct interaction of Tla3 with Tle3 on one side and with VgrG2b on the other side. By taking into account the BACTH data and the copurification with two truncated forms of VgrG2b, the domain of interaction of VgrG2b with Tla3 can be delimitated to the TTR domain.

We then analyzed the cellular localization of Tla3 in *P. aeruginosa* that, according to its interactions with Tle3 and VgrG2b, should be cytoplasmic. As for Tli3, we engineered a chromosomally encoded $Tla3_{V5}$ translational fusion (**Supplementary Table S1**). Tla3 was indeed immunodetected in the cytoplasmic fraction (**Figure 5A**). One could note that

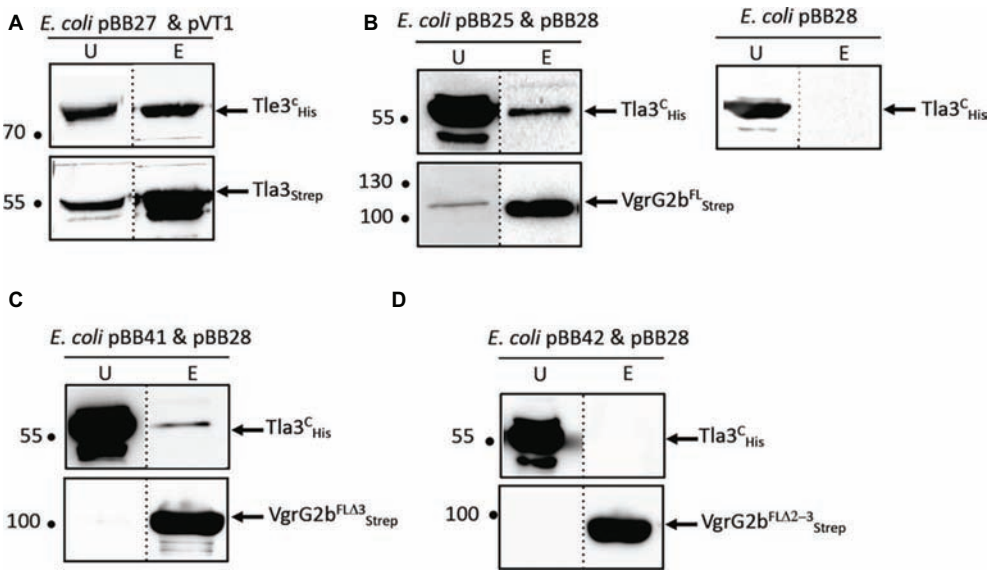

FIGURE 4 | Tla3 interaction with Tle3 **(A)** and VgrG2b **(B–D)**. Copurification assay on StrepTactin column of $Tla3^{c}_{STREP}$ with $Tle3^{c}_{His}$ produced *in E. coli* BL21(DE3) pLysS from pBB27 and pVT1, respectively, **(A)** or of $Tla3^{c}_{His}$ with $VgrG2b^{FL}_{STREP}$ **(B)** or $VgrG2b^{FLD3}_{STREP}$ **(C)** or $VgrG2b^{FLD2\text{-}3}_{STREP}$ **(D)** produced from pBB28 and pBB25 **(B)** or pBB41**(C)** or pBB42 **(D)**. The unbound (U) and eluted (E) fractions were collected and subjected to SDS-PAGE (10.5%) and Western blot analysis using anti-His antibody (upper) and anti-streptavidin antibody (lower). The dashed line separates lanes from non-adjacent part of the same gel. The position of the proteins and the molecular mass markers (in kDa) are indicated.

in contrast with our first hypothesis suggesting an incorrect start codon for *tla3* and our observation of the recombinant protein in the periplasm of *E. coli* (**Supplementary Figure S1**), Tla3 was totally absent from the periplasmic fraction of *P. aeruginosa*. To strengthen this result, each putative ATG was individually mutated on the chromosome of the PAO1 strain encoding the $Tla3_{V5}$ translational fusion (**Figure 5B**). In agreement with its cytoplasmic localization in *P. aeruginosa*, Tla3 was only produced if the fourth ATG was intact. Accordingly the Tla3 protein synthesized from this ATG is not predicted to possess a N-terminal signal peptide (**Supplementary Figure S1**). In conclusion, Tla3 is a cytoplasmic protein synthesized from the annotated translation start[1] and this localization is in agreement with a role in the targeting of the toxin to the secretion machinery.

Next, we asked whether Tla3 is specific for Tle3 or if it can be required for the secretion of other substrates of the H2-T6SS machinery. Since Hcp secretion is the hallmark of a functional secretion system, we studied the secretion of Hcp2b whose gene is upstream *vgrG2b* (**Figure 1A**). Like Allsopp et al. (2017), we deleted the *rsmA* gene to enable Hcp2b production and thus secretion by a PAO1 strain encoding a $Hcp2b_{His}$ translational fusion (**Figure 5C**, compare lines 1 and 2). RsmA is a posttranscriptional regulator known to repress all three T6SS clusters of *P. aeruginosa* (Allsopp et al., 2017). This results in a massive secretion since $Hcp2b_{His}$ can be observed in the extracellular protein samples by Coomassie-blue staining (**Figure 5C**, lower panel). While $Hcp2b_{His}$ secretion was abolished in a *rsmA clpV2* mutant, a H2-T6SS mutant, we observed that $Hcp2b_{His}$ is still secreted in the absence of Tla3 (**Figure 5C**, compare line 3 with line 4), suggesting that Tla3 is specific for the secretion of Tle3 but not for other H2-T6SS proteins. In line with this specific adaptor-toxin pair, $Tla3^{C}_{Strep}$ did not copurify TplE (Tle4), another antibacterial phospholipase delivered by the H2-T6SS machinery (**Figure 5D** and **Supplementary Figure S6**).

Finally as the interaction with a VgrG can suggest that Tla3 is itself a T6SS effector, we studied whether Tla3 is secreted by *P. aeruginosa*. To this end, the *rsmA* gene was deleted from the PAO1 strain encoding a $Tla3_{V5}$ translational fusion. Whereas $Tla3_{V5}$ was better produced upon *rsmA* deletion (**Figure 5E**), this did not lead to immunodetection of $Tla3_{V5}$ in the extracellular medium although Hcp2b was readily observed by Coomassie-blue staining of the same samples. Tla3 is thus not an effector *per se*.

In conclusion, the cytoplasmic localization of Tla3 in *P. aeruginosa* is appropriate with a recruiting role of Tle3 to the H2-T6SS machinery through an interaction with the TTR domain of VgrG2b. Tla3 is not co-secreted with Tle3. Tla3 role seems specific to Tle3 since it is not required for a functional H2-T6SS machinery and does not interact with TplE (Tle4), another H2-T6SS effector.

Tle3 Secretion Mechanism by the H2-T6SS Machinery of *P. aeruginosa*

In order to study the antibacterial role and the secretion of Tle3 by *P. aeruginosa*, we performed intra-species bacterial competition assays between *P. aeruginosa* strains. This consists in studying the survival of prey bacteria lacking the *tli3* immunity gene (by CFU counting of antibiotic resistant bacteria) co-cultivated

[1]pseudomonas.com

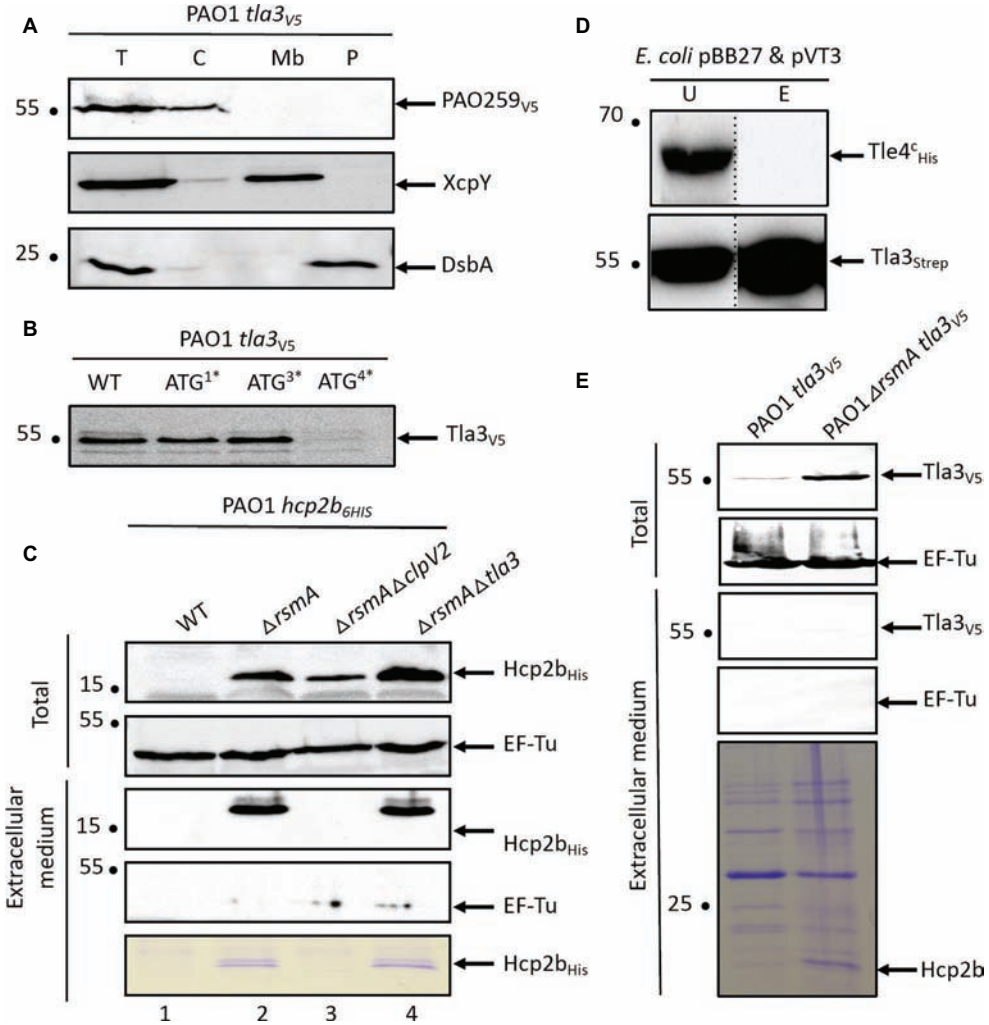

FIGURE 5 | (A) Tla3(PA0259) is a cytoplasmic protein of *P. aeruginosa*. Cells of *P. aeruginosa* PAO1 $tla3_{V5}$ were subjected to fractionation and immunoblotting using antibodies directed against the V5 tag, XcpY and DsbA. XcpY and DsbA were used as membrane and periplasmic controls, respectively. T, whole cell; C, cytoplasm; Mb, total membrane; P, periplasm. **(B)** The annotated ATG drives the initiation of translation of *tla3* in *P. aeruginosa*. Immunodetection of $Tla3_{V5}$ with anti-V5 antibodies produced in a WT background or in strains in which one of the four predicted ATG in *tla3* have been substituted in ATA. The number followed by a star indicates which ATG from **Supplementary Figure S1** ATG_4 corresponds to the annotated ATG. **(C)** Tla3 is not required for Hcp2b secretion. Immunodetection of $Hcp2b_{6His}$ with anti-His antibodies produced in a WT background (line 1) or in strains deleted for *rsmA* (lines 2–4) and *clpV2* (line 3) or *tla3* (line 4). The strains were grown at 25°C for 24 h and total bacteria were separated from extracellular medium. Anti-EF-Tu is used as a lysis control. The extracellular medium proteins were also stained with Coomassie-blue. **(D)** Tla3 does not interact with Tle4. Copurification assay on StrepTactin column of $Tla3^{c}_{STREP}$ with $Tle4_{His}$ produced *in E. coli* BL21(DE3)pLysS from pBB27 and pVT3 respectively. Legend is as in **Figure 4**. **(E)** Tla3 is not secreted. Immunodetection of $Tla3_{V5}$ with anti-HV5 antibodies produced in a WT background (line 1) or in strain deleted for *rsmA* (line 2). The strains were grown at 25°C for 24 h and total bacteria were separated from extracellular medium. Anti-EF-Tu is used as a lysis control. The extracellular medium proteins were also stained with Coomassie-blue. **(A-E)** The position of the proteins and the molecular mass markers (in kDa) are indicated.

24 hours at 37°C on plate with various attackers. As immunity genes are essential genes (protection from fratricide intoxication), both toxin and immunity genes have been deleted in order to construct a *via*ble Δ*tli3*Δ*tle3* mutant strain (**Supplementary Table S1**). **Figure 6** first confirms the antibacterial function of Tle3 and the immunity role of Tli3 since the growth of the immunity mutant was affected by the WT strain because it cannot resist Tle3 toxicity, while the Δ*tle3* mutant had no effect (**Figure 6** compare line 1 with line 2). The use of the Δ*clpV2* strain, a H2-T6SS mutant, and of Δ*vgrG2b* and Δ*tla3* mutants allowed to demonstrate that Tle3 is delivered to prey bacteria through the H2-T6SS machinery and confirms that VgrG2b and Tla3 participate in Tle3 targeting to the H2-T6SS machinery (**Figure 6** compare line 1 with lines 4, 5, and 6). Indeed Δ*clpV2*, Δ*vgrG2b* and Δ*tla3* mutants had no effect on the immunity mutant growth since they cannot deliver Tle3 into prey bacteria. The complementation *in cis* of *tle3* and *tla3* deletions (the mutants have been constructed for this study) restored a WT phenotype (**Figure 6** compare line 2 with line 3, and line 6 with line 7) this demonstrating no polar effect on downstream

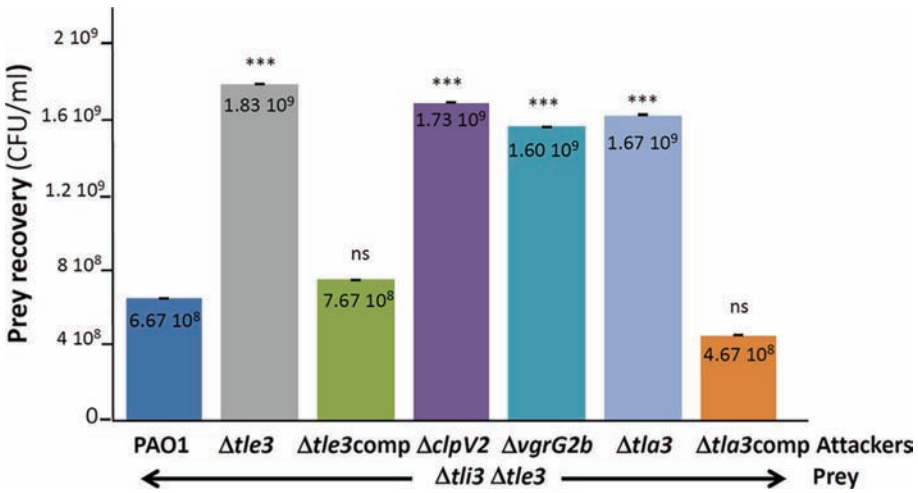

FIGURE 6 | *P. aeruginosa* growth competition. The *P. aeruginosa* prey strain (Δ*tli3*Δ*tle3*) was incubated with various *P. aeruginosa* attacker strains as indicated in the figure for 24 h at 37°C. The number of recovered prey bacteria is indicated in CFU/ml. "comp" stand for *cis* complementation of the corresponding mutation with a wild-type copy inserted at the *attB* site on *P. aeruginosa* chromosome. Error bars represent ± SEM ($n = 3$); ***$p < 0.001$, ns not significant.

genes. Furthermore, the introduction of a wild-type copy of *tli3* at the *attB* site on *P. aeruginosa* chromosome of the Δ*tli3*Δ*tle3* mutant restores wild-type competition capacity to this strain (**Supplementary Figure S4A**). This confirms that the absence of the immunity was responsible of the phenotypes observed for the Δ*tli3*Δ*tle3* strain (**Figure 6**). Finally, the Δ*tla3* mutant has been used as a prey and was not affected by the WT strain or any of the mutants excluding definitively a role of immunity as proposed by its annotation (see text footnote 1) and confirming its adaptor function (**Supplementary Figure S4B**).

Taken together, these results demonstrated that Tle3 is an effective H2-T6SS-dependent antibacterial toxin loaded onto the VgrG2b puncturing device *via* Tla3 and neutralized by Tli3 in resistant prey bacteria.

VgrG2b Is a Trans-Kingdom Toxin

A putative neutral zinc metallopeptidase domain has been predicted at the extreme C-terminus of VgrG2b by Pukatzki and colleagues (**Figure 3A**; Pukatzki et al., 2007). This motif (Prosite PS00142, PFAM04298) consists in a metal-binding consensus motif HExxH, the two histidine residues being ligands of the catalytic Zn^{2+} and the glutamic acid residue involved in nucleophilic attack. As an effector with a protease activity can target both eukaryotic and bacterial proteins, we searched for an antibacterial activity of the VgrG2b C-terminal extension. To do this, we performed the same heterologous toxicity assay in *E. coli* as with Tle3. As shown in **Figure 7**, whereas the production of $VgrG2b_{Cter}$ in the cytoplasm did not impact *E. coli* growth, its periplasmic production killed *E. coli* (**Figure 7**, compare lines 2 and 5). Moreover substitution of the histidine in position 935 and of the glutamic acid 936 for an alanine relieves $VgrG2b_{Cter}$ toxicity this showing that VgrG2b is a novel antibacterial protease active in the periplasm.

Finally because of their genetic proximity, we tested whether Tli3 can be the immunity of $VgrG2b_{Cter}$. Indeed, the coproduction of Tli3 counteracts $VgrG2b_{Cter}$ toxicity whether it is coproduced from a second plasmid (**Figure 7**, line 6) or from the same transcript (**Figure 7**, line 7). In conclusion Tli3 serves two toxins and protects also from the antibacterial activity of VgrG2b.

DISCUSSION

Here, we report the existence of a novel pair of antibacterial effector and immunity of the H2-T6SS of *P. aeruginosa*, Tle3 (PA0260) and Tli3 (PA0261), and we propose a chronology of Tle3 secretion process that includes a cytoplasmic adaptor protein, Tla3 (PA0259) to load the toxin onto the VgrG2b spike (a model is proposed in **Figure 8**). Through heterologous toxicity assay and bacterial competition, we show that Tle3 was toxic once delivered in the periplasm of prey bacteria and that Tli3 can neutralize the toxin in this compartment. Interestingly, this led us to discover that VgrG2b that we previously recognized as an anti-eukaryotic effector possesses an antibacterial activity as well.

The VgrG-recruitment of cargo effectors has been previously evidenced for several antibacterial effectors among them two toxins of the Tle family, TseL (Tle2) of *V. cholerae* (Dong et al., 2013; Liang et al., 2015; Unterweger et al., 2015) and Tle1 of EAEC (Flaugnatti et al., 2016). In both cases, the *tle* genes were just downstream the *vgrG* genes like the organization of *vgrG2b* and *tle3* of *P. aeruginosa*. TseL and Tle1 have been shown to directly bind a dedicated VgrG, VgrG3 and VgrG1 respectively (Dong et al., 2013; Flaugnatti et al., 2016). The domain of interaction within EAEC VgrG1 has been delimitated to the TTR domain and may also include the DUF2345, both of which are present in the *P. aeruginosa* VgrG2b. In line with this, and despite Tle3 requiring an adaptor to be targeted to VgrG2b, we have shown that Tla3 interacts with the TTR domain of VgrG2b. Taken together these data demonstrate that TTR domains of VgrGs are involved in recruitment

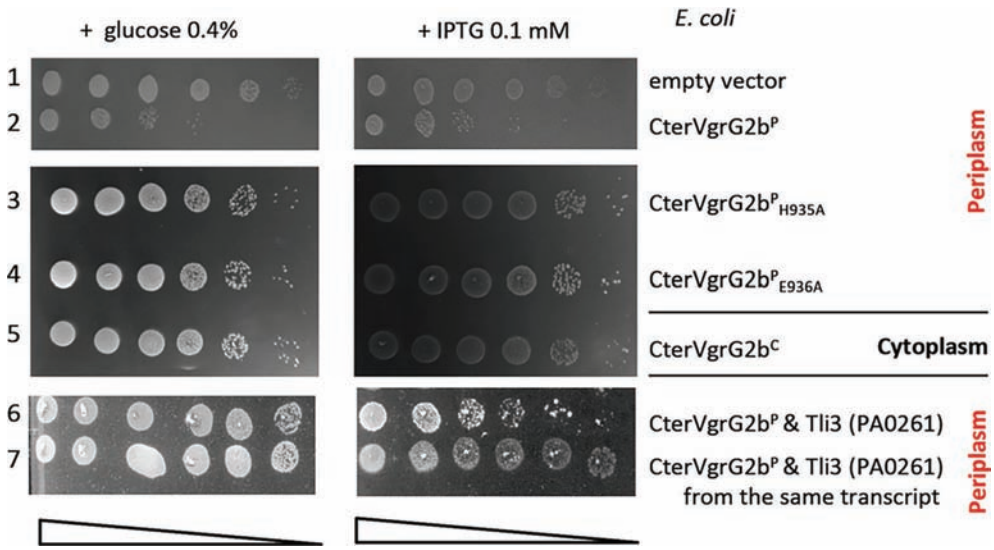

FIGURE 7 | The protease domain of VgrG2b is required for its antibacterial activity. Serial dilutions (from non-diluted to 10^{-5}) of normalized cultures of *E. coli* BL21(DE3)pLys producing the wild-type C-terminal domain of VgrG2b in the cytoplasm, called CterVgrG2b^{C} (from pBB43, a pETDuet-1 derivative, line 5) or in the periplasm, called CterVgrG2b^{P} (from pBB44, a pET22b(+) derivative yielding a fusion of the C-terminal domain with a Sec signal peptide, line 2) or two variants CterVgr2b$^{P}_{H935A}$ (from pBB45, line 3) and CterVgr2b$^{P}_{E936A}$ (from pBB46, line 4) were spotted on LB agar plates supplemented (left panel) with 0.4% glucose or (right panel) with 0.1 mM IPTG. In line 6, the CterVgrG2b^{P} (from pBB44) was coproduced with Tli3 (from pVT8) and in line 7, the CterVgrG2b^{P} and Tli3 were coproduced from the same transcript (from pSBC110). Glucose and IPTG allow respectively repression and induction of the gene encoding the T7 RNA polymerase.

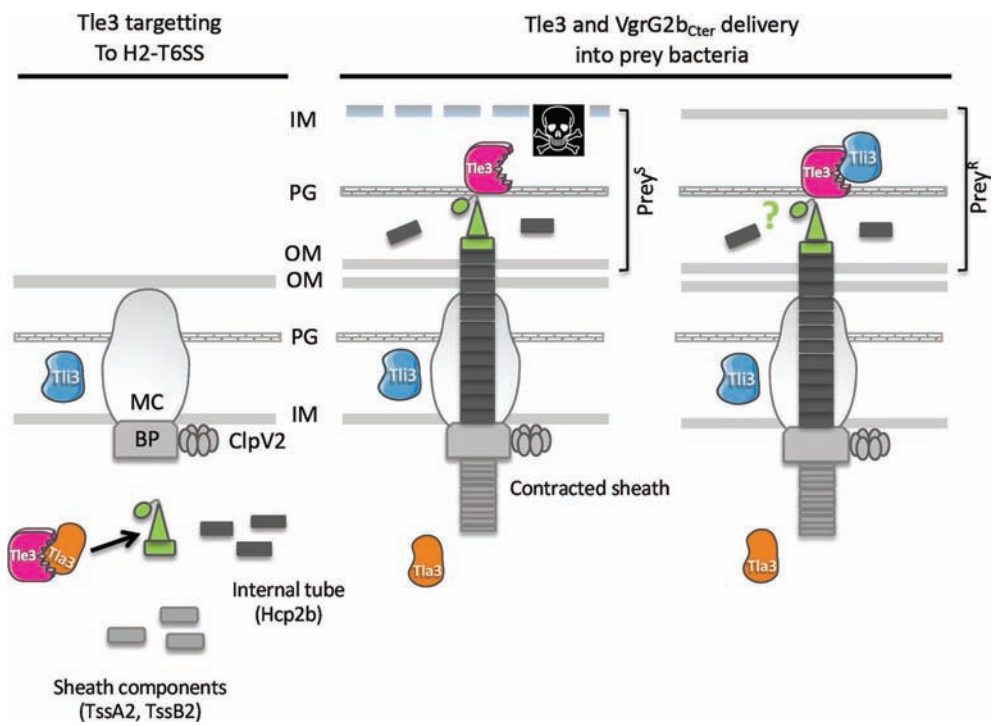

FIGURE 8 | Working model: Tle3 targeting to the H2-T6SS machinery (left panel) Tle3 (in pink) is taken in charge in the cytoplasm by Tla3 (in orange) that binds VgrG2b (green). Upon Hcp2b (in dark grey) assembly into the growing sheath (light grey), the VgrG2b loaded with the Tle3 is placed at the tip of the Hcp arrow. Tle3 and VgrG2b$_{Cter}$ delivery into bacteria (right panel). The sheath contraction in the cytoplasm propels the Hcp arrow towards the target bacterium. Tle3 associated with this expelled structure is thus translocated into target cells, as well as VgrG2b$_{Cter}$ (green circle). The prey is killed (Prey^{S}) except if it has the Tli3 immunity (in blue) in the periplasm (Prey^{R}). The mechanism of resistance to VgrG2b$_{Cter}$ is still unknown. OM, outer membrane; PG, peptidoglycan; IM, inner membrane; BP, base plate; MC, membrane complex. Prey^{S}, sensitive prey; Prey^{R}, resistant prey.

and transport of Tle effectors, directly or through adaptor. Likewise, C-terminal extensions of VgrG1 and VgrG2 of *Agrobacterium tumefaciens* were identified as specifically required for the delivery of each cognate DNAse toxins, named Tde1 and Tde2, respectively (Bondage et al., 2016). C-terminal domains of VgrGs can thus be considered more generally as specificity determinants for T6SS effector loading and transport.

Interestingly, TseL of *V. cholerae* requires also Tap-1 (Tec) as an adaptor protein to be delivered to another VgrG, called VgrG1 (Liang et al., 2015; Unterweger et al., 2015), showing that a sole toxin can be targeted directly and indirectly to two different VgrG proteins. Tap-1 (Tec) belongs to the DUF4123 family of adaptor proteins that contains also VasW of *V. cholerae* (Miyata et al., 2013) and several uncharacterized gene products linked to effector genes with a MIX (marker for type VI effectors) motif in *Proteus mirabilis* or *B. thailandensis* for instance (Salomon et al., 2014). Interestingly TecT, a DUF4123 adaptor of *P. aeruginosa*, has been shown to require a co-adaptor, called co-TecT, to deliver the TseT effector to the PAAR4 protein (Burkinshaw et al., 2018). This is the first example of an adaptor-co-adaptor module. Taken together, these data suggest a conserved role for DUF4123 adaptors in the recruitment of a number of T6SS effectors. Remarkably Tla3 of *P. aeruginosa* does not belong to the DUF4123 adaptor family, or to that of the two other unrelated families, the DUF1795 adaptor family, reported with EagR (effector-associated gene with Rhs) in *Serratia marcescens* (Alcoforado Diniz and Coulthurst, 2015) or EagT6 in *P. aeruginosa* (Whitney et al., 2015), and the DUF2169 adaptor family reported with Atu3641 in *A. tumefaciens* (Bondage et al., 2016). Nor Tla3 is a PAAR protein, the last class of effector targeting mode to a VgrG (Shneider et al., 2013; Whitney et al., 2014; Bondage et al., 2016; Cianfanelli et al., 2016a; Burkinshaw et al., 2018). Instead, we find that Tla3 harbors two DUF2875 domains (**Figure 3A**) that are both required for the interaction with the toxin. Moreover, genes coding DUF2875 containing proteins can be find at the vicinity of *tle*, *tli*, *vgrG*, or PAAR genes, but they are restricted to α and β proteobacteria (**Supplementary Figure S5**). We thus hypothesize that DUF2875 might assist in T6SS-mediated effector delivery. Like the three other adaptor families (DUF4123, DUF1795, and DUF2169), we have observed that Tla3 is not required for the H2-T6SS functionality since the Δ*tla3* mutant still secrete Hcp2b and can compete with a WT strain, and that Tla3 is specific for the Tle3 toxin since it did not interact with another H2-T6SS effector, TplE (Tle4). Finally, as we did not detect Tla3 secretion under constitutive H2-T6SS condition, we propose that Tla3 hands over Tle3 to VgrG2b in the cytoplasm prior to its loading to the baseplate and further recruitment to the central Hcp tube in preparation (**Figure 8**). Overall, the existence of various modes of effector recruitment, further refined with adaptors, likely explains how the T6SS is able to deliver numerous and structurally diverse proteins.

Five families of Tle, Tle1–5, have been identified among Gram-negative bacteria (Russell et al., 2013) and four Tle have been studied in *P. aeruginosa* so far. Our demonstration of the activity of Tle3 in the periplasm is consistent with the observations that the heterologous periplasmic production of PldA (Tle5a) (Russell et al., 2013; Jiang et al., 2014), PldB (Tle5b) (Jiang et al., 2014), Tle1 (Hu et al., 2014), and TplE (Tle4) (Jiang et al., 2016) is toxic. The reason of the periplasmic activity of Tle proteins is still unclear although several hypothesis have been proposed (Flaugnatti et al., 2016), the most likely being an activation of the toxin in this compartment. Very recently this has nicely been exemplified with the hijacking of DsbA in the target cells of *S. marcescens* for the activation of incoming effectors (Mariano et al., 2018). No member of the Tle3 family has yet been enzymatically characterized. Our attempts to efficiently purify Tle3 from *E. coli* or from *P. aeruginosa* have been unsuccessful, even if we have noticed that the presence of the Tla3 adaptor stabilized Tle3, it still formed inclusion bodies. In the future, we will decipher the enzymatic activity of Tle3, which is presumably active on membrane phospholipids as our preliminary data of thin-layer chromatography tend to show.

The periplasmic activity of Tle toxins is counteracted by the synthesis of a cognate immunity protein that is usually a periplasmic soluble protein, as we showed for Tli3 in *P. aeruginosa*, or a membrane-anchored lipoprotein (Russell et al., 2013). Interestingly the genetic organization of the *tli3* gene upstream of the *tle3* gene observed in *E. coli*, *K. pneumoniae*, *B. cenocepacia*, or *R. solanacearum* (Russell et al., 2013) is conserved in *P. aeruginosa*. The fact that the two genes are co-transcribed (the immunity being the first) is key for the protection against toxicity. Indeed, we have observed systematic protection against the periplasmic toxicity of Tle3 in *E. coli* when the two genes were expressed from the same promoter under the same plasmid, whereas it was not as efficient when the genes were on two plasmids. This genetic link reinforces the connection within the toxin/immunity pair. This has previously been noticed with a T7SS antibacterial toxin and its immunity in *Staphylococcus aureus* (Cao et al., 2016). Other immunities of Tle characterized so far have been shown to inhibit the action of the effector by direct protein-protein contacts (Russell et al., 2013; Jiang et al., 2014; Flaugnatti et al., 2016). Our copurification assay in *E. coli* demonstrates a direct interaction between Tle3 and Tli3 that was already suggested with the release of Tle3 toxicity upon coproduction of Tli3 in the periplasm. A crystal structure of the *P. aeruginosa* TplE (Tle4) effector in complex with its immunity protein TplEI (Tli4) revealed that the immunity uses a grasp mechanism to prevent the interfacial activation of the toxin (Lu et al., 2014).

Like two other H2-T6SS-related orphan *vgrG* loci, the *vgrG4b* cluster encoding PldA (Tle5a) and the *vgrG2a* encoding TplE (Tle4), we show here that the *vgrG2b* cluster has both antibacterial activities (through Tle3 and VgrG2b) and anti-eukaryotic (through VgrG2b; Sana et al., 2015). Interestingly, VgrG2b is thus (1) a structural component of the H2-T6SS puncturing device since our bacterial competition showed its requirement for Tle3 delivery, (2) an anti-eukaryotic effector through an interaction with the microtubule nucleating complex (Sana et al., 2015), and (3) an antibacterial effector as suggested by our toxicity assay in *E. coli*. We have shown that two conserved residues of the putative metallopeptidase motif (a histidine and a glutamic acid) are essential for the VgrG2b antibacterial activity. This is consistent with an antibacterial protease activity for VgrG2b that will be, to our knowledge, the first case in the T6SS effector literature.

The discovery of the VgrG2b immunity is even more exciting since we observed that Tli3 also relieves $VgrG2b_{Cter}$ toxicity. To our knowledge, Tli3 is the first example of a T6SS immunity serving two different proteins. But one can cite the chaperones of the type III secretion translocators that form a pore in the eukaryotic target cell membrane (Neyt and Cornelis, 1999). Indeed the chaperone SycD from *Yersinia* enterocolitica and its homologues from other Gram-negative bacteria bind the two translocators to prevent their premature interaction in the inner membrane and avoid further toxicity.

DATA AVAILABILITY

All datasets generated for this study are included in the manuscript and/or the **Supplementary Files**.

AUTHOR CONTRIBUTIONS

BB and SB designed and conceived the experiments. BB, CS, and SD performed the experiments. SB supervised the execution of the experiments. BB, CS, BI, and SB analyzed and discussed the data. SB wrote the paper with contribution from BB and reading from BI.

FUNDING

This work was supported by recurrent funding from the CNRS and Aix-Marseille University. The project leading to this publication has received funding from the Excellence Initiative of Aix-Marseille University-A*Midex, a French "Investissements d'Avenir" program ("Emergence & Innovation" A-M-AAP-EI-17-139-170301-10.31-BLEVES-HLS).

ACKNOWLEDGMENTS

We thank V. Tutagata for pVT1, pVT8, and pVT9 constructs, and B. Douzi for all the advices during protein purification and members of B.B. PhD committee for helpful discussion and support. We are grateful to M. Ba, I. Bringer, A. Brun, and O. Uderso for technical assistance. BB was financed with a PhD fellowship from the French Research Ministry.

SUPPLEMENTARY MATERIAL

The Supplementary Material for this article can be found online at: https://www.frontiersin.org/articles/10.3389/fmicb.2019.01218/full#supplementary-material

REFERENCES

Alcoforado Diniz, J., and Coulthurst, S. J. (2015). Intraspecies competition in *Serratia marcescens* is mediated by type VI-secreted Rhs effectors and a conserved effector-associated accessory protein. *J. Bacteriol.* 197, 2350–2360. doi: 10.1128/JB.00199-15

Allsopp, L. P., Wood, T. E., Howard, S. A., Maggiorelli, F., Nolan, L. M., Wettstadt, S., et al. (2017). RsmA and AmrZ orchestrate the assembly of all three type VI secretion systems in *Pseudomonas aeruginosa*. *Proc. Natl. Acad. Sci. USA* 114, 7707–7712. doi: 10.1073/pnas.1700286114

Basler, M. (2015). Type VI secretion system: secretion by a contractile nanomachine. *Philos. Trans. R. Soc. Lond. Ser. B Biol. Sci.* 370. doi: 10.1098/rstb.2015.0021

Battesti, A., and Bouveret, E. (2012). The bacterial two-hybrid system based on adenylate cyclase reconstitution in *Escherichia coli*. *Methods* 58, 325–334. doi: 10.1016/j.ymeth.2012.07.018

Benz, J., and Meinhart, A. (2014). Antibacterial effector/immunity systems: it's just the tip of the iceberg. *Curr. Opin. Microbiol.* 17, 1–10. doi: 10.1016/j.mib.2013.11.002

Bleves, S. (2016). Game of trans-kingdom effectors. *Trends Microbiol.* 24, 773–774. doi: 10.1016/j.tim.2016.08.002

Bleves, S., Viarre, V., Salacha, R., Michel, G. P. F., Filloux, A., and Voulhoux, R. (2010). Protein secretion systems in *Pseudomonas aeruginosa*: a wealth of pathogenic weapons. *Int. J. Med. Microbiol.* 300, 534–543. doi: 10.1016/j.ijmm.2010.08.005

Bondage, D. D., Lin, J.-S., Ma, L.-S., Kuo, C.-H., and Lai, E.-M. (2016). VgrG C terminus confers the type VI effector transport specificity and is required for binding with PAAR and adaptor-effector complex. *Proc. Natl. Acad. Sci. USA* 113, E3931–E3940. doi: 10.1073/pnas.1600428113

Burkinshaw, B. J., Liang, X., Wong, M., Le, A. N. H., Lam, L., and Dong, T. G. (2018). A type VI secretion system effector delivery mechanism dependent on PAAR and a chaperone-co-chaperone complex. *Nat. Microbiol.* 3, 632–640. doi: 10.1038/s41564-018-0144-4

Cao, Z., Casabona, M. G., Kneuper, H., Chalmers, J. D., and Palmer, T. (2016). The type VII secretion system of *Staphylococcus aureus* secretes a nuclease toxin that targets competitor bacteria. *Nat. Microbiol.* 2:16183. doi: 10.1038/nmicrobiol.2016.183

Cianfanelli, F. R., Alcoforado Diniz, J., Guo, M., De Cesare, V., Trost, M., and Coulthurst, S. J. (2016a). VgrG and PAAR proteins define distinct versions of a functional type VI secretion system. *PLoS Pathog.* 12:e1005735. doi: 10.1371/journal.ppat.1005735

Cianfanelli, F. R., Monlezun, L., and Coulthurst, S. J. (2016b). Aim, load, fire: the type VI secretion system, a bacterial nanoweapon. *Trends Microbiol.* 24, 51–62. doi: 10.1016/j.tim.2015.10.005

Dong, T. G., Ho, B. T., Yoder-Himes, D. R., and Mekalanos, J. J. (2013). Identification of T6SS-dependent effector and immunity proteins by Tn-seq in *Vibrio cholerae*. *Proc. Natl. Acad. Sci. USA* 110, 2623–2628. doi: 10.1073/pnas.1222783110

Flaugnatti, N., Le, T. T. H., Canaan, S., Aschtgen, M.-S., Nguyen, V. S., Blangy, S., et al. (2016). A phospholipase A1 antibacterial Type VI secretion effector interacts directly with the C-terminal domain of the VgrG spike protein for delivery. *Mol. Microbiol.* 99, 1099–1118. doi: 10.1111/mmi.13292

Hecht, A. L., Casterline, B. W., Earley, Z. M., Goo, Y. A., Goodlett, D. R., and Bubeck Wardenburg, J. (2016). Strain competition restricts colonization of an enteric pathogen and prevents colitis. *EMBO Rep.* 17, 1281–1291. doi: 10.15252/embr.201642282

Hood, R. D., Singh, P., Hsu, F., Güvener, T., Carl, M. A., Trinidad, R. R. S., et al. (2010). A type VI secretion system of *Pseudomonas aeruginosa* targets a toxin to bacteria. *Cell Host Microbe* 7, 25–37. doi: 10.1016/j.chom.2009.12.007

Hu, H., Zhang, H., Gao, Z., Wang, D., Liu, G., Xu, J., et al. (2014). Structure of the type VI secretion phospholipase effector Tle1 provides insight into its hydrolysis and membrane targeting. *Acta Crystallogr. D Biol. Crystallogr.* 70, 2175–2185. doi: 10.1107/S1399004714012899

Ize, B., Viarre, V., and Voulhoux, R. (2014). Cell fractionation. *Methods Mol. Biol.* 1149, 185–191. doi: 10.1007/978-1-4939-0473-0_15

Jeong, J.-Y., Yim, H.-S., Ryu, J.-Y., Lee, H. S., Lee, J.-H., Seen, D.-S., et al. (2012). One-step sequence- and ligation-independent cloning as a rapid and versatile cloning method for functional genomics studies. *Appl. Environ. Microbiol.* 78, 5440–5443. doi: 10.1128/AEM.00844-12

Jiang, F., Wang, X., Wang, B., Chen, L., Zhao, Z., Waterfield, N. R., et al. (2016). The *Pseudomonas aeruginosa* type VI secretion PGAP1-like effector induces host autophagy by activating endoplasmic reticulum stress. *Cell Rep.* 16, 1502–1509. doi: 10.1016/j.celrep.2016.07.012

Jiang, F., Waterfield, N. R., Yang, J., Yang, G., and Jin, Q. (2014). A *Pseudomonas aeruginosa* type VI secretion phospholipase D effector targets both prokaryotic and eukaryotic cells. *Cell Host Microbe* 15, 600–610. doi: 10.1016/j.chom.2014.04.010

Karimova, G., Pidoux, J., Ullmann, A., and Ladant, D. (1998). A bacterial two-hybrid system based on a reconstituted signal transduction pathway. *Proc. Natl. Acad. Sci. USA* 95, 5752–5756.

Kolaskar, A. S., and Reddy, B. V. (1985). A method to locate protein coding sequences in DNA of prokaryotic systems. *Nucleic Acids Res.* 13, 185–194. doi: 10.1093/nar/13.1.185

LaCourse, K. D., Peterson, S. B., Kulasekara, H. D., Radey, M. C., Kim, J., and Mougous, J. D. (2018). Conditional toxicity and synergy drive diversity among antibacterial effectors. *Nat. Microbiol.* 3, 440–446. doi: 10.1038/s41564-018-0113-y

Liang, X., Moore, R., Wilton, M., Wong, M. J. Q., Lam, L., and Dong, T. G. (2015). Identification of divergent type VI secretion effectors using a conserved chaperone domain. *Proc. Natl. Acad. Sci. USA* 112, 9106–9111. doi: 10.1073/pnas.1505317112

Lu, D., Zheng, Y., Liao, N., Wei, L., Xu, B., Liu, X., et al. (2014). The structural basis of the Tle4-Tli4 complex reveals the self-protection mechanism of H2-T6SS in *Pseudomonas aeruginosa*. *Acta Crystallogr. D Biol. Crystallogr.* 70, 3233–3243. doi: 10.1107/S1399004714023967

MacIntyre, D. L., Miyata, S. T., Kitaoka, M., and Pukatzki, S. (2010). The *Vibrio cholerae* type VI secretion system displays antimicrobial properties. *Proc. Natl. Acad. Sci. USA* 107, 19520–19524. doi: 10.1073/pnas.1012931107

Mariano, G., Monlezun, L., and Coulthurst, S. J. (2018). Dual role for DsbA in attacking and targeted bacterial cells during type VI secretion system-mediated competition. *Cell Rep.* 22, 774–785. doi: 10.1016/j.celrep.2017.12.075

Miyata, S. T., Unterweger, D., Rudko, S. P., and Pukatzki, S. (2013). Dual expression profile of type VI secretion system immunity genes protects pandemic *Vibrio cholerae*. *PLoS Pathog.* 9:e1003752. doi: 10.1371/journal.ppat.1003752

Mougous, J. D., Cuff, M. E., Raunser, S., Shen, A., Zhou, M., Gifford, C. A., et al. (2006). A virulence locus of *Pseudomonas aeruginosa* encodes a protein secretion apparatus. *Science* 312, 1526–1530. doi: 10.1126/science.1128393

Neyt, C., and Cornelis, G. R. (1999). Role of SycD, the chaperone of the *Yersinia* Yop translocators YopB and YopD. *Mol. Microbiol.* 31, 143–156. doi: 10.1046/j.1365-2958.1999.01154.x

Nielsen, H. (2017). "Predicting secretory proteins with SignalP" in *Protein function prediction*. ed. D. Kihara (New York, NY: Springer), 59–73.

Pukatzki, S., Ma, A. T., Revel, A. T., Sturtevant, D., and Mekalanos, J. J. (2007). Type VI secretion system translocates a phage tail spike-like protein into target cells where it cross-links actin. *Proc. Natl. Acad. Sci. USA* 104, 15508–15513. doi: 10.1073/pnas.0706532104

Pukatzki, S., Ma, A. T., Sturtevant, D., Krastins, B., Sarracino, D., Nelson, W. C., et al. (2006). Identification of a conserved bacterial protein secretion system in *Vibrio cholerae* using the Dictyostelium host model system. *Proc. Natl. Acad. Sci. USA* 103, 1528–1533. doi: 10.1073/pnas.0510322103

Russell, A. B., LeRoux, M., Hathazi, K., Agnello, D. M., Ishikawa, T., Wiggins, P. A., et al. (2013). Diverse type VI secretion phospholipases are functionally plastic antibacterial effectors. *Nature* 496, 508–512. doi: 10.1038/nature12074

Salomon, D., Kinch, L. N., Trudgian, D. C., Guo, X., Klimko, J. A., Grishin, N. V., et al. (2014). Marker for type VI secretion system effectors. *Proc. Natl. Acad. Sci. USA* 111, 9271–9276. doi: 10.1073/pnas.1406110111

Sana, T. G., Baumann, C., Merdes, A., Soscia, C., Rattei, T., Hachani, A., et al. (2015). Internalization of *Pseudomonas aeruginosa* strain PAO1 into epithelial cells is promoted by interaction of a T6SS effector with the microtubule network. *MBio* 6:e00712. doi: 10.1128/mBio.00712-15

Sana, T. G., Berni, B., and Bleves, S. (2016a). The T6SSs of *Pseudomonas aeruginosa* strain PAO1 and their effectors: beyond bacterial-cell targeting. *Front. Cell. Infect. Microbiol.* 6:61. doi: 10.3389/fcimb.2016.00061

Sana, T. G., Flaugnatti, N., Lugo, K. A., Lam, L. H., Jacobson, A., Baylot, V., et al. (2016b). Salmonella Typhimurium utilizes a T6SS-mediated antibacterial weapon to establish in the host gut. *Proc. Natl. Acad. Sci. USA* 113, E5044–E5051. doi: 10.1073/pnas.1608858113

Sana, T. G., Hachani, A., Bucior, I., Soscia, C., Garvis, S., Termine, E., et al. (2012). The second type VI secretion system of *Pseudomonas aeruginosa* strain PAO1 is regulated by quorum sensing and Fur and modulates internalization in epithelial cells. *J. Biol. Chem.* 287, 27095–27105. doi: 10.1074/jbc.M112.376368

Shneider, M. M., Buth, S. A., Ho, B. T., Basler, M., Mekalanos, J. J., and Leiman, P. G. (2013). PAAR-repeat proteins sharpen and diversify the type VI secretion system spike. *Nature* 500, 350–353. doi: 10.1038/nature12453

Unterweger, D., Kostiuk, B., Ötjengerdes, R., Wilton, A., Diaz-Satizabal, L., and Pukatzki, S. (2015). Chimeric adaptor proteins translocate diverse type VI secretion system effectors in *Vibrio cholerae*. *EMBO J.* 34, 2198–2210. doi: 10.15252/embj.201591163

Whitney, J. C., Beck, C. M., Goo, Y. A., Russell, A. B., Harding, B. N., De Leon, J. A., et al. (2014). Genetically distinct pathways guide effector export through the type VI secretion system. *Mol. Microbiol.* 92, 529–542. doi: 10.1111/mmi.12571

Whitney, J. C., Quentin, D., Sawai, S., LeRoux, M., Harding, B. N., Ledvina, H. E., et al. (2015). An interbacterial NAD(P)(+) glycohydrolase toxin requires elongation factor Tu for delivery to target cells. *Cell* 163, 607–619. doi: 10.1016/j.cell.2015.09.027

WHO (2019). WHO publishes list of bacteria for which new antibiotics are urgently needed. Available at: https://www.who.int/news-room/detail/27-02-2017-who-publishes-list-of-bacteria-for-which-new-antibiotics-are-urgently-needed (Accessed January 21, 2019).

Conflict of Interest Statement: The authors declare that the research was conducted in the absence of any commercial or financial relationships that could be construed as a potential conflict of interest.

Copyright © 2019 Berni, Soscia, Djermoun, Ize and Bleves. This is an open-access article distributed under the terms of the Creative Commons Attribution License (CC BY). The use, distribution or reproduction in other forums is permitted, provided the original author(s) and the copyright owner(s) are credited and that the original publication in this journal is cited, in accordance with accepted academic practice. No use, distribution or reproduction is permitted which does not comply with these terms.

frontiers in Microbiology

MINI REVIEW
published: 19 June 2019
doi: 10.3389/fmicb.2019.01217

The Dynamic ATP-Driven Mechanism of Bacterial Protein Translocation and the Critical Role of Phospholipids

*Ian Collinson**

School of Biochemistry, University of Bristol, Bristol, United Kingdom

Protein secretion from the cell cytoplasm to the outside is essential for life. Bacteria do so for a range of membrane associated and extracellular activities, including envelope biogenesis, surface adherence, pathogenicity, and degradation of noxious chemicals such as antibiotics. The major route for this process is *via* the ubiquitous Sec system, residing in the plasma membrane. Translocation across (secretion) or into (insertion) the membrane is driven through the translocon by the action of associated energy-transducing factors or translating ribosomes. This review seeks to summarize the recent advances in the dynamic mechanisms of protein transport and the critical role played by lipids in this process. The article will include an exploration of how lipids are actively involved in protein translocation and the consequences of these interactions for energy transduction from ATP hydrolysis and the trans-membrane proton-motive-force (PMF).

Keywords: SecA ATPase, bacteria, SecY translocon, lipids, protein secretion

OPEN ACCESS

Edited by:
Eric Cascales,
Aix-Marseille Université, France

Reviewed by:
Ray A. Larsen,
Bowling Green State University, United States
Iain Sutcliffe,
Northumbria University, United Kingdom

***Correspondence:**
Ian Collinson
ian.collinson@bristol.ac.uk

Specialty section:
This article was submitted to Microbial Physiology and Metabolism, a section of the journal Frontiers in Microbiology

Received: *15 March 2019*
Accepted: *15 May 2019*
Published: *19 June 2019*

Citation:
Collinson I (2019) The Dynamic ATP-Driven Mechanism of Bacterial Protein Translocation and the Critical Role of Phospholipids. Front. Microbiol. 10:1217. doi: 10.3389/fmicb.2019.01217

PROTEIN SECRETION THROUGH THE BACTERIAL SEC MACHINERY

Protein secretion, from the cell cytoplasm to the outside, is essential for life. Bacteria secrete proteins for enveloping biogenesis, surface adherence, and pathogenicity and degrading noxious chemicals (including antibiotics), among a range of many other membrane and extracellular activities. The major route for protein secretion is *via* the ubiquitous Sec translocon: a conserved hetero-trimeric core-complex of the inner membrane. This machinery is also responsible for membrane protein insertion, whereby proteins containing **T**rans-**M**embrane α-**H**elices (TMH) are threaded laterally into the bilayer rather than across it. Therefore, the interaction of the machinery with lipids is critical in that they interface with the protein complex through which proteins cross and enter the membrane. Moreover, it turns out that phospholipids play direct and critical roles in the active energy transducing process driving protein transport.

Secretory and membrane proteins are targeted to the Sec machinery with the aid of an N-terminal signal sequence (Chang et al., 1978; Walter et al., 1981b). These proteins then translocate through the apparatus in an unfolded conformation (Arkowitz et al., 1993), either during their synthesis (co-translationally), or afterwards (post-translationally). The former is a ubiquitous process in which the signal sequence at the N-terminus of the nascent polypeptide emerging from the ribosome exit tunnel is recognized by the signal recognition particle (SRP) and targeted to the membrane-associated SRP-receptor (Walter et al., 1981a,b,c; Poritz et al., 1990). The ribosome nascent chain complex (RNC) is then shuttled to the Sec complex for translocation

(Jomaa et al., 2016), where the growing polypeptide is forced through the membrane. In the bacterial model *Escherichia coli* (**Figure 1**), the co-translational pathway is generally utilized for membrane protein insertion (Ulbrandt et al., 1997; Müller et al., 2001), while transport across the membrane (secretion) tends to be post-translational. In the latter process, cytosolic chaperones, such as SecB, deliver the pre-protein in a translocation competent (unfolded) state to the SecA motor protein and channel complex SecYEG for secretion (Hartl et al., 1990; Cranford-Smith and Huber, 2018).

STRUCTURE OF THE CORE-TRANSLOCON

The pathway for translocation of the mature region of the pre-protein – the protein-conducting channel – is formed through the center of SecY, between two pseudo-symmetrical halves, each with five TMHs (Van den Berg et al., 2004; Cannon et al., 2005). When at rest, the channel is kept sealed by a short α-helix (the plug) and a sphincter of six hydrophobic residues, usually isoleucine (Van den Berg et al., 2004). Separation of the two halves opens a channel across the membrane (for secretion) as well as a lateral gate (LG) for entry of TMHs into the bilayer (insertion). Multiple rounds of ATP hydrolysis and the trans-membrane proton-motive-force (PMF) then drive protein transport across the membrane (Brundage et al., 1990; Schiebel et al., 1991; Economou and Wickner, 1994).

MECHANISM OF SECA-DRIVEN PROTEIN TRANSLOCATION

Today, we understand a great deal about the structure and activity of Sec machinery, particularly the bacterial counterpart (almost exclusively through the study of the *E. coli* system). During SecA-driven secretion, the association of SecA with the pre-protein causes the signal sequence to bind at the LG of SecY, at the interface with the lipid bilayer (Hizlan et al., 2012; Li et al., 2016). Many studies have shown that this interaction causes a conformational change in both SecA and the protein channel (Hizlan et al., 2012; Corey et al., 2016; Li et al., 2016), and a priming of SecA for increased ATPase activity (Gouridis et al., 2009; Robson et al., 2009; Gold et al., 2013). In this "unlocked" state, the channel opens slightly and the plug, which helps keep the Sec-complex closed, retracts from its central position (Zimmer et al., 2008; Hizlan et al., 2012; Corey et al., 2016; Li et al., 2016).

Our understanding of this reaction has been aided by recent single-molecule fluorescence studies (Allen et al., 2016;

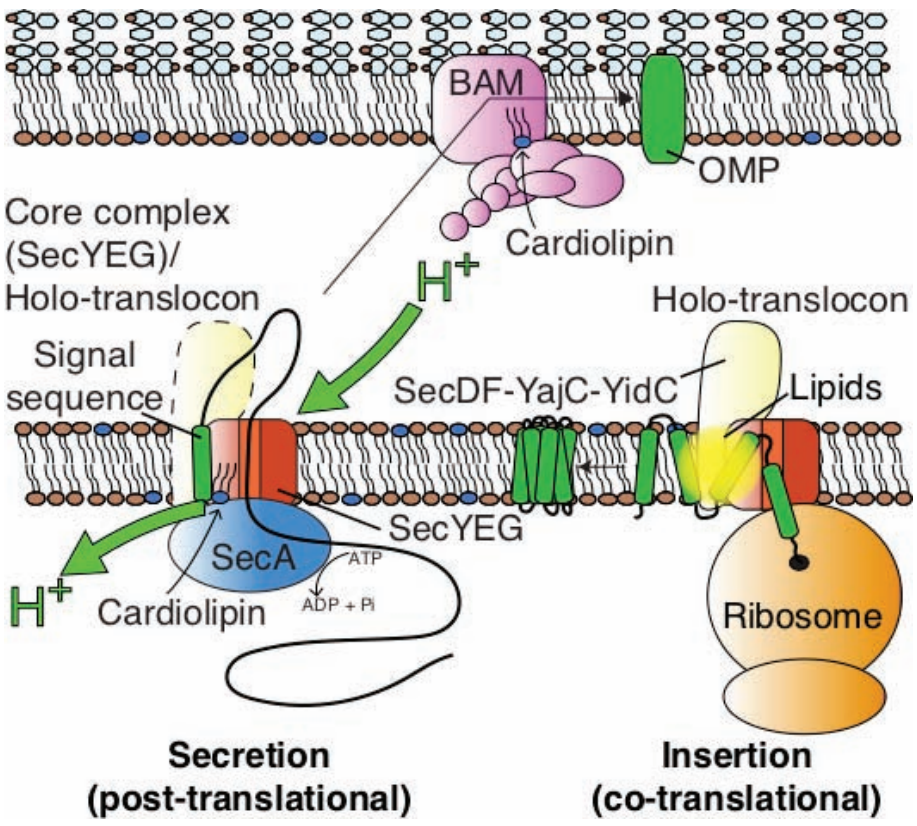

FIGURE 1 | Pathways for protein transport across and into the Gram-negative inner membrane and further across the periplasm for outer-membrane insertion and folding. The figure also highlights the action of lipids on the SecYEG-SecA complex (see **Figure 3**), the holo-translocon (HTL), and the BAM complex.

Fessl et al., 2018). These applications enable the dissection and analysis of different stages of the reaction, which would otherwise be blurred in the reaction ensemble. The analysis demonstrates that the initiation process requires the signal sequence and mature regions of the pre-protein, as well as ATP (Fessl et al., 2018). The initiation involves an ATP-driven transport step, independent of pre-protein length, likely to be the intercalation of the signal sequence and early mature regions of the polypeptide (presumably as a loop with the N-terminus pointing towards the cytosol; **Figures 1, 2**) into the "unlocked" translocon, as was previously proposed (Hizlan et al., 2012). At this point, the ATPase becomes fully activated and translocation across the membrane can begin through SecYEG; the kinetics of which depend on the length of the substrate (see Fessl et al., 2018 and Figure 6 therein; Tomkiewicz et al., 2006).

MODEL FOR PROTEIN TRANSLOCATION

For the transport process *per* se, a stochastic Brownian ratchet model for the ATP-driven reaction has been proposed wherein the free energy available from ATP binding and hydrolysis helps bias the random diffusional flow of polypeptide to favor an outward direction (see Figure 8 and associated movie in Allen et al., 2016).

A follow-up study proposed how this stochastic process could be further enhanced. ATP-dependent control of protein folding has been well documented in the protein chaperone field (Clarke, 1996). We have introduced this concept into the protein transport field whereby the translocon utilizes the hydrolytic cycle of ATP to exert an asymmetric control of pre-protein folding (Corey et al., 2019). Preventing partial folding at the cytosolic interface of the ATPase SecA with SecY, while enabling it at the outward facing exit site, would prevent back sliding of the translocating polypeptide (**Figure 2**), thus favoring outward flow of the pre-protein. This concept is consistent with independent findings that the folding propensity (or lack of it) of the mature regions of the pre-protein has profound effects on the secretion efficiency (Gonsberg et al., 2017; Jung and Tatzelt, 2018; Tsirigotaki et al., 2018).

An alternative "push-and-slide" model invokes both diffusional and ATP-driven power-stroke components, involving the 2-helix finger (2HF) motif of SecA moving up and down to physically push polypeptides across the membrane (Erlandson et al., 2008; Zimmer et al., 2008; Bauer et al., 2014). A recent follow-up study, based on single-molecule fluorescence, confirms that the 2HF is indeed conformationally mobile throughout the ATP-driven transport cycle (Catipovic et al., 2019). The differences in fluorescence were equated to a very large apparent change in energy transfer efficiency (~0.1 to ~0.9). The main contention here is if the observations are really due to **F**örster **R**esonance **E**nergy **T**ransfer (FRET), or to **P**rotein-**I**nduced **F**luorescent **E**nhancement (PIFE; Stennett et al., 2015). In the former case, this would require an extraordinarily large movement of >20 Å. Otherwise, the affect may be due to changes of the dye environment, for example, the formation of steric constraints at alternative conformations. This phenomenon is a known feature of some fluorescent reporters, particularly Cy3 (Stennett et al., 2015), used in this new study (Catipovic et al., 2019). Consequently, more subtle movements could also be responsible for these large fluorescent fluctuations, which would be more concordant with the limited space available for the 2HF to move (Zimmer et al., 2008; Li et al., 2016).

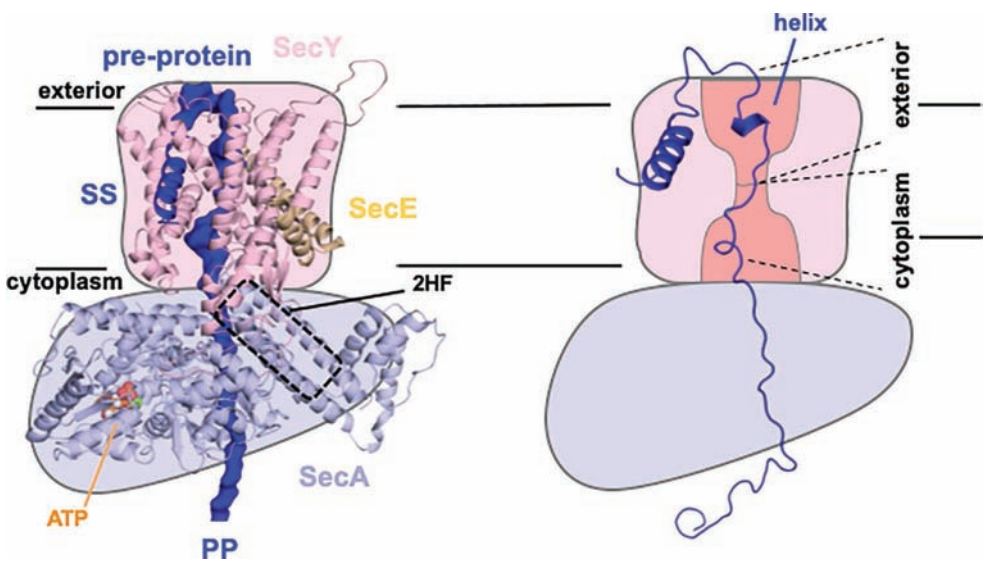

FIGURE 2 | Sec control of protein folding as a driver for transport. Model structure of SecYEG-SecA^{ATP} based on Li et al. (2016) with key features labeled accordingly; SS, signal sequence; 2HF, 2 helix finger (left). Schematic of same (right), showing only the simulated structure of the pre-protein, with a partial folding in the exterior cavity (helix) and unfolded regions in the cytoplasmic cavity and hence favoring transport to the exterior, as required. Adapted from figures shown previously, used with permission (Corey et al., 2019).

Either way, whether a diffusional ratchet (Allen et al., 2016) or power stroke/diffusional hybrid (Bauer et al., 2014; Catipovic et al., 2019) is at play, the core ATP-driven process is further stimulated by the PMF (Brundage et al., 1990) in order to achieve the high rates of secretion required for rapid growth. Presently, it is not known if or how the electrical ($\Delta\psi$) or chemical (ΔpH) components of the PMF achieve this enhancement. The PMF may indeed also operate to favor the outward flow of polypeptide in a Brownian ratchet-type mechanism.

During the final stages of transport, the signal sequence of the pre-protein is proteolytically cleaved to release the mature protein on the other side of the membrane (Josefsson and Randall, 1981). The terminal closure of the translocon is apparently independent of ATP (Fessl et al., 2018).

THE HOLO-TRANSLOCON (HTL)

To complicate matters further, the SecYEG core complex also associates with a number of accessory proteins: the membrane protein "insertase" YidC and the sub-complex SecDF (Duong and Wickner, 1997; Schulze et al., 2014). In a large number of cases, including *E. coli*, this complex also contains the YajC protein of obscure function (Duong and Wickner, 1997; Schulze et al., 2014). YidC facilitates the lateral insertion of TMHs from SecY into the bilayer (Houben et al., 2000; Samuelson et al., 2000; Scotti et al., 2000; Kumazaki et al., 2014), while SecDF makes an additional use of the PMF to help drive the transport of secretory proteins (Arkowitz and Wickner, 1994; Duong and Wickner, 1997; Tsukazaki et al., 2011; Botte et al., 2016; Furukawa et al., 2017). Thus, the resultant super-complex – the **H**olo-**T**rans**L**ocon (HTL) – associates with co-translating ribosomes for efficient membrane protein insertion and SecA for ATP/PMF-driven secretion (**Figure 1**; Schulze et al., 2014; Komar et al., 2016).

TRANSPORT THROUGH THE CELL ENVELOPE

For many proteins, transport across the inner membrane is only the first step. Following passage through the Sec-translocon proteins are either retained in the cell envelope or find their way to the external medium. Gram-negative bacteria have the added complexity of an outer membrane with an inter-membrane periplasm containing the peptidoglycan layer. Therefore, proteins must either be folded and retained in the periplasm or be further trafficked into or across the outer membrane. This is no mean feat.

There are a number of periplasmic shock proteins that are transported to the periplasm and folded in enormous quantities, e.g., Spy and HdeI (Tapley et al., 2009; Quan et al., 2011). Moreover, the demand for the insertion and folding of β-barrel **O**uter **M**embrane **P**roteins (OMPs) in rapidly dividing cells is vast. The process is facilitated by the periplasmic chaperones SurA and Skp (Sklar et al., 2007; McMorran et al., 2013), which presumably collect proteins as they emerge from the translocon for folding or for delivery to the outer membrane. How the chaperoned OMPs negotiate the peptidoglycan layer is unclear. We know that when they get there, they are welcomed by the β-**B**arrel **A**ssembly **M**achinery (BAM) – a complex of five proteins BamABCDE, responsible for the insertion and folding of OMPs (**Figure 1**; Voulhoux et al., 2003; Wu et al., 2005). But how this is achieved for very large fluxes of proteins, without aggregation, and in the absence of an energy source is not easily reconciled. Many structures of the BAM complex have been determined (Bakelar et al., 2016; Gu et al., 2016; Iadanza et al., 2016); despite this, the mechanism for energy-independent OMP insertion and folding has yet to emerge.

THE ROLE OF SPECIFIC PHOSPHOLIPIDS IN PROTEIN TRANSPORT

While the dynamic mechanism for protein secretion through the protein machinery of the bacterial energy conserving, inner membrane has been the focus of our attention, it is becoming increasingly clear that the resident lipids also play a critical role in the transport proteins across, as well as into the membrane (**Figure 1**).

This post-translational reaction has been known for many years to require acidic phospholipids. Mutants defective in acidic phospholipid – cardiolipin (CL) and phosphatidyl-glycerol (PG) – synthesis have protein export deficiencies (Tommassen et al., 1989). Moreover, these lipids are required for functional association of SecA to the inner membrane (Hendrick and Wickner, 1991). Later work showed that the CL and, to a lesser extent, PG are important for stability of the SecYEG complex and to stimulate SecA ATPase activity (Bessonneau et al., 2002; Gold et al., 2010) – but the mechanism of action was unclear. Recent progress on this subject is beginning to unravel the mysterious action of this unique lipid.

Course-Grain Molecular Dynamics (CGMD) simulations have identified SecYEG sites, which transiently interacted with CL, which were validated empirically (**Figure 3**; Corey et al., 2018): native mass spectrometry demonstrated that variants in which the positive surface charges of the putative binding sites were diminished, bound CL less effectively. Remarkably, it turns out that these specific CL interactions confer the stimulation of SecA ATPase activity and PMF enhancement of secretion (**Figures 1, 3**; Corey et al., 2018); the latter may be achieved by proton carriage by the lipid itself. If true, this would be the first description of a direct involvement of a phospholipid in the process of energy coupling.

Furthermore, the interaction of the translocon with CL has profound consequences for the structure of the protein complex. Interestingly, specific sites on SecYEG, used to monitor the opening and closure of the protein channel (Fessl et al., 2018), are strongly dependent on CL for SecA promoted channel opening (Figure 5 and Supplementary Figure 2 in Corey et al., 2019).

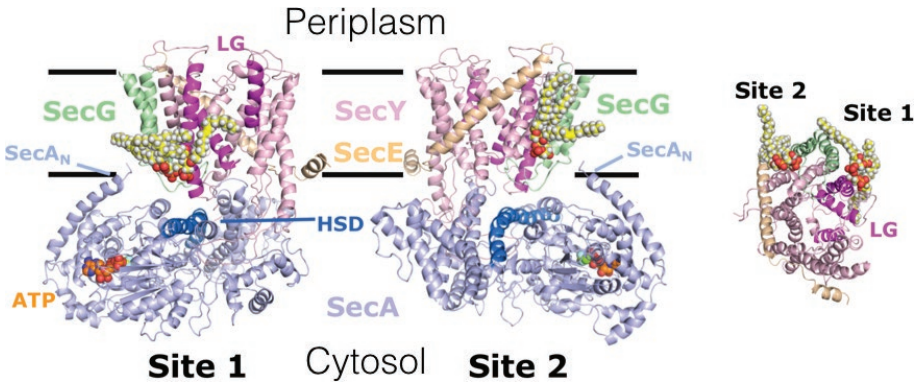

FIGURE 3 | Interaction of cardiolipin (CL) with the bacterial translocon. 2 CL (yellow, white, and red spheres) – binding sites 1 & 2 – on SecYEG; identified by CGMD, validated and shown to be critical for ATP and PMF-driven secretion (Corey et al., 2018). Left and middle, side view of SecYEG bound to the motor ATPase SecA; right, cytosolic view of SecYEG alone. In SecA: ATP, $SecA_N$ – N-terminus; HSD (including the 2HF) – helical scaffold domain, at the entrance to the protein channel in SecY. In SecYEG: LG – lateral gate, which opens during transport of proteins across and into the membrane. Adapted from Corey et al. (2018), used with permission.

A LIPID POOL IN THE HTL

Co-translational transport of proteins into the membrane occurs through the HTL (see above; **Figure 1**). Lipids, again CL in particular, are required to stabilize the holo-complex (Schulze et al., 2014), and critically, lipids also form an encapsulated pool at its center (**Figure 1**; Botte et al., 2016; Martin et al., 2019). This remarkable feature could provide an enclosed lipidic environment to promote efficient membrane protein insertion and assembly, protecting the translocating membrane protein from aggregation and proteolysis. This is a familiar concept for promoting folding of globular proteins within a chamber of the chaperonin GroEL (Ranson et al., 1997; Xu et al., 1997).

OTHER PROTEIN TRANSLOCATION SYSTEMS

It is very interesting that other protein translocation systems have also been implicated in the association with CL, including the BAM complex of the outer membrane (**Figure 1**; Chorev et al., 2018), and the mitochondrial Tim23 import machinery (Malhotra et al., 2017), but apparently not the TAT machinery responsible for the export of fully folded proteins in bacteria (Rathmann et al., 2017). Given the well-known dependence of CL for many proton translocating energy transducing systems, such as the ATP synthase (Duncan et al., 2016), and the electron transfer chain complexes I, III, and IV (Fry and Green, 1981; Pfeiffer et al., 2003; Fiedorczuk et al., 2016; Malkamäki and Sharma, 2019), one could surmise a critical role for proton-driven protein transport too.

CONCLUSION

Finally, our understanding of the dynamic mechanism underlying ATP-driven secretion through the Sec machinery is approaching clarity, while its augmentation by the PMF is a mystery shortly to be resolved, after nearly 30 years since its discovery (Brundage et al., 1990; Schiebel et al., 1991). In this context, CL seems to play essential and multifarious roles, for the structure and for both ATP and PMF-driven protein translocation activity. This warrants further investigation and exploitation. The essential lipid-protein interface could be a prime target for infiltration by small molecules for prospective antibiotic development.

AUTHOR CONTRIBUTIONS

The author confirms being the sole contributor of this work and has approved it for publication.

FUNDING

Our work on bacterial secretion is funded by the BBSRC (BB/S008349/1, BB/N015126/1, and BB/M003604/1). The author is indebted to Drs. Robin Corey, Phillip Stansfeld, and Daniel Watkins for preparing the figures.

REFERENCES

Allen, W. J., Corey, R. A., Oatley, P., Sessions, R. B., Baldwin, S. A., Radford, S. E., et al. (2016). Two-way communication between SecY and SecA suggests a Brownian ratchet mechanism for protein translocation. *eLife* 5. doi: 10.7554/eLife.15598

Arkowitz, R. A., Joly, J. C., and Wickner, W. (1993). Translocation can drive the unfolding of a preprotein domain. *EMBO J.* 12, 243–253. doi: 10.1002/j.1460-2075.1993.tb05650.x

Arkowitz, R. A., and Wickner, W. (1994). SecD and SecF are required for the proton electrochemical gradient stimulation of preprotein translocation. *EMBO J.* 13, 954–963. doi: 10.1002/j.1460-2075.1994.tb06340.x

Bakelar, J., Buchanan, S. K., and Noinaj, N. (2016). The structure of the β-barrel assembly machinery complex. *Science* 351, 180–186. doi: 10.1126/science.aad3460

Bauer, B. W., Shemesh, T., Chen, Y., and Rapoport, T. A. (2014). A "push and slide" mechanism allows sequence-insensitive translocation of secretory proteins by the SecA ATPase. *Cell* 157, 1416–1429. doi: 10.1016/j.cell.2014.03.063

Bessonneau, P., Besson, V., Collinson, I., and Duong, F. (2002). The SecYEG preprotein translocation channel is a conformationally dynamic and dimeric structure. *EMBO J.* 21, 995–1003. doi: 10.1093/emboj/21.5.995

Botte, M., Zaccai, N. R., Nijeholt, J. L. À., Martin, R., Knoops, K., Papai, G., et al. (2016). A central cavity within the holo-translocon suggests a mechanism for membrane protein insertion. *Sci. Rep.* 6:38399. doi: 10.1038/srep38399

Brundage, L., Hendrick, J. P., Schiebel, E., Driessen, A. J., and Wickner, W. (1990). The purified *E. coli* integral membrane protein SecY/E is sufficient for reconstitution of SecA-dependent precursor protein translocation. *Cell* 62, 649–657. doi: 10.1016/0092-8674(90)90111-Q

Cannon, K. S., Or, E., Clemons, W. M., Shibata, Y., and Rapoport, T. A. (2005). Disulfide bridge formation between SecY and a translocating polypeptide localizes the translocation pore to the center of SecY. *J. Cell Biol.* 169, 219–225. doi: 10.1083/jcb.200412019

Catipovic, M. A., Bauer, B. W., Loparo, J. J., and Rapoport, T. A. (2019). Protein translocation by the SecA ATPase occurs by a power-stroke mechanism. *EMBO J.* 38. doi: 10.15252/embj.2018101140

Chang, C. N., Blobel, G., and Model, P. (1978). Detection of prokaryotic signal peptidase in an *Escherichia coli* membrane fraction: endoproteolytic cleavage of nascent f1 pre-coat protein. *Proc. Natl. Acad. Sci. USA* 75, 361–365.

Chorev, D. S., Baker, L. A., Wu, D., Beilsten-Edmands, V., Rouse, S. L., Zeev-Ben-Mordehai, T., et al. (2018). Protein assemblies ejected directly from native membranes yield complexes for mass spectrometry. *Science* 362, 829–834. doi: 10.1126/science.aau0976

Clarke, A. R. (1996). Molecular chaperones in protein folding and translocation. *Curr. Opin. Struct. Biol.* 6, 43–50. doi: 10.1016/S0959-440X(96)80093-5

Corey, R. A., Ahdash, Z., Shah, A., Pyle, E., Allen, W. J., Fessl, T., et al. (2019). ATP-induced asymmetric pre-protein folding as a driver of protein translocation through the sec machinery. *eLife* 8. doi: 10.7554/eLife.41803

Corey, R. A., Allen, W. J., Komar, J., Masiulis, S., Menzies, S., Robson, A., et al. (2016). Unlocking the bacterial SecY translocon. *Structure* 24, 518–527. doi: 10.1016/j.str.2016.02.001

Corey, R. A., Pyle, E., Allen, W. J., Watkins, D. W., Casiraghi, M., Miroux, B., et al. (2018). Specific cardiolipin-SecY interactions are required for proton-motive force stimulation of protein secretion. *Proc. Natl. Acad. Sci. USA* 115, 7967–7972. doi: 10.1073/pnas.1721536115

Cranford-Smith, T., and Huber, D. (2018). The way is the goal: how SecA transports proteins across the cytoplasmic membrane in bacteria. *FEMS Microbiol. Lett.* 365. doi: 10.1093/femsle/fny093

Duncan, A. L., Robinson, A. J., and Walker, J. E. (2016). Cardiolipin binds selectively but transiently to conserved lysine residues in the rotor of metazoan ATP synthases. *Proc. Natl. Acad. Sci. USA* 113, 8687–8692. doi: 10.1073/pnas.1608396113

Duong, F., and Wickner, W. (1997). Distinct catalytic roles of the SecYE, SecG and SecDFyajC subunits of preprotein translocase holoenzyme. *EMBO J.* 16, 2756–2768. doi: 10.1093/emboj/16.10.2756

Economou, A., and Wickner, W. (1994). SecA promotes preprotein translocation by undergoing ATP-driven cycles of membrane insertion and deinsertion. *Cell* 78, 835–843. doi: 10.1016/S0092-8674(94)90582-7

Erlandson, K. J., Miller, S. B. M., Nam, Y., Osborne, A. R., Zimmer, J., and Rapoport, T. A. (2008). A role for the two-helix finger of the SecA ATPase in protein translocation. *Nature* 455, 984–987. doi: 10.1038/nature07439

Fessl, T., Watkins, D., Oatley, P., Allen, W. J., Corey, R. A., Horne, J., et al. (2018). Dynamic action of the Sec machinery during initiation, protein translocation and termination. *eLife* 7. doi: 10.7554/eLife.35112

Fiedorczuk, K., Letts, J. A., Degliesposti, G., Kaszuba, K., Skehel, M., and Sazanov, L. A. (2016). Atomic structure of the entire mammalian mitochondrial complex I. *Nature* 538, 406–410. doi: 10.1038/nature19794

Fry, M., and Green, D. E. (1981). Cardiolipin requirement for electron transfer in complex I and III of the mitochondrial respiratory chain. *J. Biol. Chem.* 256, 1874–1880.

Furukawa, A., Yoshikaie, K., Mori, T., Mori, H., Morimoto, Y. V., Sugano, Y., et al. (2017). Tunnel formation inferred from the I-form structures of the proton-driven protein secretion motor SecDF. *Cell Rep.* 19, 895–901. doi: 10.1016/j.celrep.2017.04.030

Gold, V. A. M., Robson, A., Bao, H., Romantsov, T., Duong, F., and Collinson, I. (2010). The action of cardiolipin on the bacterial translocon. *Proc. Natl. Acad. Sci. USA* 107, 10044–10049. doi: 10.1073/pnas.0914680107

Gold, V. A. M., Whitehouse, S., Robson, A., and Collinson, I. (2013). The dynamic action of SecA during the initiation of protein translocation. *Biochem. J.* 449, 695–705. doi: 10.1042/BJ20121314

Gonsberg, A., Jung, S., Ulbrich, S., Origi, A., Ziska, A., Baier, M., et al. (2017). The Sec61/SecY complex is inherently deficient in translocating intrinsically disordered proteins. *J. Biol. Chem.* 292, 21383–21396. doi: 10.1074/jbc.M117.788067

Gouridis, G., Karamanou, S., Gelis, I., Kalodimos, C. G., and Economou, A. (2009). Signal peptides are allosteric activators of the protein translocase. *Nature* 462, 363–367. doi: 10.1038/nature08559

Gu, Y., Li, H., Dong, H., Zeng, Y., Zhang, Z., Paterson, N. G., et al. (2016). Structural basis of outer membrane protein insertion by the BAM complex. *Nature* 531, 64–69. doi: 10.1038/nature17199

Hartl, F. U., Lecker, S., Schiebel, E., Hendrick, J. P., and Wickner, W. (1990). The binding cascade of SecB to SecA to SecY/E mediates preprotein targeting to the *E. coli* plasma membrane. *Cell* 63, 269–279. doi: 10.1016/0092-8674(90)90160-G

Hendrick, J. P., and Wickner, W. (1991). SecA protein needs both acidic phospholipids and SecY/E protein for functional high-affinity binding to the *Escherichia coli* plasma membrane. *J. Biol. Chem.* 266, 24596–24600.

Hizlan, D., Robson, A., Whitehouse, S., Gold, V. A., Vonck, J., Mills, D., et al. (2012). Structure of the SecY complex unlocked by a preprotein mimic. *Cell Rep.* 1, 21–28. doi: 10.1016/j.celrep.2011.11.003

Houben, E. N., Scotti, P. A., Valent, Q. A., Brunner, J., de Gier, J. L., Oudega, B., et al. (2000). Nascent Lep inserts into the *Escherichia coli* inner membrane in the vicinity of YidC, SecY and SecA. *FEBS Lett.* 476, 229–233. doi: 10.1016/S0014-5793(00)01735-X

Iadanza, M. G., Higgins, A. J., Schiffrin, B., Calabrese, A. N., Brockwell, D. J., Ashcroft, A. E., et al. (2016). Lateral opening in the intact β-barrel assembly machinery captured by cryo-EM. *Nat. Commun.* 7:12865. doi: 10.1038/ncomms12865

Jomaa, A., Boehringer, D., Leibundgut, M., and Ban, N. (2016). Structures of the *E. coli* translating ribosome with SRP and its receptor and with the translocon. *Nat. Commun.* 7:10471. doi: 10.1038/ncomms10471

Josefsson, L. G., and Randall, L. L. (1981). Different exported proteins in *E. coli* show differences in the temporal mode of processing in vivo. *Cell* 25, 151–157. doi: 10.1016/0092-8674(81)90239-7

Jung, S., and Tatzelt, J. (2018). Impaired transport of intrinsically disordered proteins through the Sec61 and SecY translocon; implications for prion diseases. *Prion* 12, 88–92. doi: 10.1080/19336896.2018.1435936

Komar, J., Alvira, S., Schulze, R. J., Martin, R., Lycklama A Nijeholt, J. A., Lee, S. C., et al. (2016). Membrane protein insertion and assembly by the bacterial holo-translocon SecYEG-SecDF-YajC-YidC. *Biochem. J.* 473, 3341–3354. doi: 10.1042/BCJ20160545

Kumazaki, K., Chiba, S., Takemoto, M., Furukawa, A., Nishiyama, K.-I., Sugano, Y., et al. (2014). Structural basis of sec-independent membrane protein insertion by YidC. *Nature* 509, 516–520. doi: 10.1038/nature13167

Li, L., Park, E., Ling, J., Ingram, J., Ploegh, H., and Rapoport, T. A. (2016). Crystal structure of a substrate-engaged SecY protein-translocation channel. *Nature* 531, 395–399. doi: 10.1038/nature17163

Malhotra, K., Modak, A., Nangia, S., Daman, T. H., Gunsel, U., Robinson, V. L., et al. (2017). Cardiolipin mediates membrane and channel interactions of the mitochondrial TIM23 protein import complex receptor Tim50. *Sci. Adv.* 3:e1700532. doi: 10.1126/sciadv.1700532

Malkamäki, A., and Sharma, V. (2019). Atomistic insights into cardiolipin binding sites of cytochrome c oxidase. *Biochim. Biophys. Acta Bioenerg.* 1860, 224–232. doi: 10.1016/j.bbabio.2018.11.004

Martin, R., Larsen, A. H., Corey, R. A., Midtgaard, S. R., Frielinghaus, H., Schaffitzel, C., et al. (2019). Structure and dynamics of the central lipid

pool and proteins of the bacterial holo-translocon. *Biophys. J.* 116, 1931–1940. doi: 10.1016/j.bpj.2019.04.002

McMorran, L. M., Bartlett, A. I., Huysmans, G. H. M., Radford, S. E., and Brockwell, D. J. (2013). Dissecting the effects of periplasmic chaperones on the in vitro folding of the outer membrane protein PagP. *J. Mol. Biol.* 425, 3178–3191. doi: 10.1016/j.jmb.2013.06.017

Müller, M., Koch, H. G., Beck, K., and Schäfer, U. (2001). Protein traffic in bacteria: multiple routes from the ribosome to and across the membrane. *Prog. Nucleic Acid Res. Mol. Biol.* 66, 107–157.

Pfeiffer, K., Gohil, V., Stuart, R. A., Hunte, C., Brandt, U., Greenberg, M. L., et al. (2003). Cardiolipin stabilizes respiratory chain supercomplexes. *J. Biol. Chem.* 278, 52873–52880. doi: 10.1074/jbc.M308366200

Poritz, M. A., Bernstein, H. D., Strub, K., Zopf, D., Wilhelm, H., and Walter, P. (1990). An *E. coli* ribonucleoprotein containing 4.5S RNA resembles mammalian signal recognition particle. *Science* 250, 1111–1117. doi: 10.1126/science.1701272

Quan, S., Koldewey, P., Tapley, T., Kirsch, N., Ruane, K. M., Pfizenmaier, J., et al. (2011). Genetic selection designed to stabilize proteins uncovers a chaperone called Spy. *Nat. Struct. Mol. Biol.* 18, 262–269. doi: 10.1038/nsmb.2016

Ranson, N. A., Burston, S. G., and Clarke, A. R. (1997). Binding, encapsulation and ejection: substrate dynamics during a chaperonin-assisted folding reaction. *J. Mol. Biol.* 266, 656–664. doi: 10.1006/jmbi.1996.0815

Rathmann, C., Schlösser, A. S., Schiller, J., Bogdanov, M., and Brüser, T. (2017). Tat transport in *Escherichia coli* requires zwitterionic phosphatidylethanolamine but no specific negatively charged phospholipid. *FEBS Lett.* 591, 2848–2858. doi: 10.1002/1873-3468.12794

Robson, A., Gold, V. A. M., Hodson, S., Clarke, A. R., and Collinson, I. (2009). Energy transduction in protein transport and the ATP hydrolytic cycle of SecA. *Proc. Natl. Acad. Sci. USA* 106, 5111–5116. doi: 10.1073/pnas.0809592106

Samuelson, J. C., Chen, M., Jiang, F., Möller, I., Wiedmann, M., Kuhn, A., et al. (2000). YidC mediates membrane protein insertion in bacteria. *Nature* 406, 637–641. doi: 10.1038/35020586

Schiebel, E., Driessen, A. J., Hartl, F. U., and Wickner, W. (1991). Delta mu H+ and ATP function at different steps of the catalytic cycle of preprotein translocase. *Cell* 64, 927–939. doi: 10.1016/0092-8674(91)90317-R

Schulze, R. J., Komar, J., Botte, M., Allen, W. J., Whitehouse, S., Gold, V. A. M., et al. (2014). Membrane protein insertion and proton-motive-force-dependent secretion through the bacterial holo-translocon SecYEG-SecDF-YajC-YidC. *Proc. Natl. Acad. Sci. USA* 111, 4844–4849. doi: 10.1073/pnas.1315901111

Scotti, P. A., Urbanus, M. L., Brunner, J., de Gier, J. W., Heijne, von, G., van der Does, C., et al. (2000). YidC, the *Escherichia coli* homologue of mitochondrial Oxa1p, is a component of the Sec translocase. *EMBO J.* 19, 542–549. doi: 10.1093/emboj/19.4.542

Sklar, J. G., Wu, T., Kahne, D., and Silhavy, T. J. (2007). Defining the roles of the periplasmic chaperones SurA, Skp, and DegP in *Escherichia coli*. *Genes Dev.* 21, 2473–2484. doi: 10.1101/gad.1581007

Stennett, E. M. S., Ciuba, M. A., Lin, S., and Levitus, M. (2015). Demystifying PIFE: the photophysics behind the protein-induced fluorescence enhancement phenomenon in Cy3. *J. Phys. Chem. Lett.* 6, 1819–1823. doi: 10.1021/acs.jpclett.5b00613

Tapley, T. L., Körner, J. L., Barge, M. T., Hupfeld, J., Schauerte, J. A., Gafni, A., et al. (2009). Structural plasticity of an acid-activated chaperone allows promiscuous substrate binding. *Proc. Natl. Acad. Sci. USA* 106, 5557–5562. doi: 10.1073/pnas.0811811106

Tomkiewicz, D., Nouwen, N., van Leeuwen, R., Tans, S., and Driessen, A. J. M. (2006). SecA supports a constant rate of preprotein translocation. *J. Biol. Chem.* 281, 15709–15713. doi: 10.1074/jbc.M600205200

Tommassen, J., de Vrije, T., de Cock, H., Bosch, D., and de Kruijff, B. (1989). Involvement of membrane lipids in protein export in Escherichia coli. *J. Cell Sci.* 11, 73–83.

Tsirigotaki, A., Chatzi, K. E., Koukaki, M., De Geyter, J., Portaliou, A. G., Orfanoudaki, G., et al. (2018). Long-lived folding intermediates predominate the targeting-competent Secretome. *Structure* 26, 695.e5–707.e5. doi: 10.1016/j.str.2018.03.006

Tsukazaki, T., Mori, H., Echizen, Y., Ishitani, R., Fukai, S., Tanaka, T., et al. (2011). Structure and function of a membrane component SecDF that enhances protein export. *Nature* 474, 235–238. doi: 10.1038/nature09980

Ulbrandt, N. D., Newitt, J. A., and Bernstein, H. D. (1997). The *E. coli* signal recognition particle is required for the insertion of a subset of inner membrane proteins. *Cell* 88, 187–196. doi: 10.1016/S0092-8674(00)81839-5

Van den Berg, B., Clemons, W. M., Collinson, I., Modis, Y., Hartmann, E., Harrison, S. C., et al. (2004). X-ray structure of a protein-conducting channel. *Nature* 427, 36–44. doi: 10.1038/nature02218

Voulhoux, R., Bos, M. P., Geurtsen, J., Mols, M., and Tommassen, J. (2003). Role of a highly conserved bacterial protein in outer membrane protein assembly. *Science* 299, 262–265. doi: 10.1126/science.1078973

Walter, P., Ibrahimi, I., and Blobel, G. (1981a). Translocation of proteins across the endoplasmic reticulum. I. Signal recognition protein (SRP) binds to in-vitro-assembled polysomes synthesizing secretory protein. *J. Cell Biol.* 91, 545–550.

Walter, P., Walter, P., Blobel, G., and Blobel, G. (1981b). Translocation of proteins across the endoplasmic reticulum III. Signal recognition protein (SRP) causes signal sequence-dependent and site-specific arrest of chain elongation that is released by microsomal membranes. *J. Cell Biol.* 91, 557–561.

Walter, P., Walter, P., Blobel, G., and Blobel, G. (1981c). Translocation of proteins across the endoplasmic reticulum. II. Signal recognition protein (SRP) mediates the selective binding to microsomal membranes of in-vitro-assembled polysomes synthesizing secretory protein. *J. Cell Biol.* 91, 551–556.

Wu, T., Malinverni, J., Ruiz, N., Kim, S., Silhavy, T. J., and Kahne, D. (2005). Identification of a multicomponent complex required for outer membrane biogenesis in *Escherichia coli*. *Cell* 121, 235–245. doi: 10.1016/j.cell.2005.02.015

Xu, Z., Horwich, A. L., and Sigler, P. B. (1997). The crystal structure of the asymmetric GroEL-GroES-(ADP)7 chaperonin complex. *Nature* 388, 741–750. doi: 10.1038/41944

Zimmer, J., Nam, Y., and Rapoport, T. A. (2008). Structure of a complex of the ATPase SecA and the protein-translocation channel. *Nature* 455, 936–943. doi: 10.1038/nature07335

Conflict of Interest Statement: The author declares that the research was conducted in the absence of any commercial or financial relationships that could be construed as a potential conflict of interest.

Copyright © 2019 Collinson. This is an open-access article distributed under the terms of the Creative Commons Attribution License (CC BY). The use, distribution or reproduction in other forums is permitted, provided the original author(s) and the copyright owner(s) are credited and that the original publication in this journal is cited, in accordance with accepted academic practice. No use, distribution or reproduction is permitted which does not comply with these terms.

frontiers in Microbiology

ORIGINAL RESEARCH
published: 21 June 2019
doi: 10.3389/fmicb.2019.01391

Prediction of T4SS Effector Proteins for *Anaplasma phagocytophilum* Using OPT4e, A New Software Tool

Zhila Esna Ashari[1]*, *Kelly A. Brayton*[1,2,3†] and *Shira L. Broschat*[1,2,3†]

[1] School of Electrical Engineering and Computer Science, Washington State University, Pullman, WA, United States, [2] Department of Veterinary Microbiology and Pathology, Washington State University, Pullman, WA, United States, [3] Paul G. Allen School for Global Animal Health, Washington State University, Pullman, WA, United States

Type IV secretion systems (T4SS) are used by a number of bacterial pathogens to attack the host cell. The complex protein structure of the T4SS is used to directly translocate effector proteins into host cells, often causing fatal diseases in humans and animals. Identification of effector proteins is the first step in understanding how they function to cause virulence and pathogenicity. Accurate prediction of effector proteins via a machine learning approach can assist in the process of their identification. The main goal of this study is to predict a set of candidate effectors for the tick-borne pathogen *Anaplasma phagocytophilum*, the causative agent of anaplasmosis in humans. To our knowledge, we present the first computational study for effector prediction with a focus on *A. phagocytophilum*. In a previous study, we systematically selected a set of optimal features from more than 1,000 possible protein characteristics for predicting T4SS effector candidates. This was followed by a study of the features using the proteome of *Legionella pneumophila* strain Philadelphia deduced from its complete genome. In this manuscript we introduce the OPT4e software package for Optimal-features Predictor for T4SS Effector proteins. An earlier version of OPT4e was verified using cross-validation tests, accuracy tests, and comparison with previous results for *L. pneumophila*. We use OPT4e to predict candidate effectors from the proteomes of *A. phagocytophilum* strains HZ and HGE-1 and predict 48 and 46 candidates, respectively, with 16 and 18 deemed most probable as effectors. These latter include the three known validated effectors for *A. phagocytophilum*.

Keywords: T4SS effector proteins, machine learning, *Anaplasma phagocytophilum*, protein prediction, OPT4e software

OPEN ACCESS

Edited by:
Eric Cascales,
Aix-Marseille Université, France

Reviewed by:
Sukanya Narasimhan,
Yale University School of Medicine, United States
Paul Dean,
Teesside University, United Kingdom

***Correspondence:**
Zhila Esna Ashari
z.esnaashariesfahan@wsu.edu

†These authors have contributed equally to this work

Specialty section:
This article was submitted to Microbial Physiology and Metabolism, a section of the journal Frontiers in Microbiology

Received: *05 March 2019*
Accepted: *03 June 2019*
Published: *21 June 2019*

Citation:
Esna Ashari Z, Brayton KA and Broschat SL (2019) Prediction of T4SS Effector Proteins for Anaplasma phagocytophilum Using OPT4e, A New Software Tool. Front. Microbiol. 10:1391. doi: 10.3389/fmicb.2019.01391

1. INTRODUCTION

Anaplasma phagocytophilum is a tick-borne zoonotic Gram-negative pathogen that causes Human Granulocytic Anaplasmosis (HGA). Incidence of this potentially fatal disease is rising in the United States, with the number of cases increasing from 348 in 2000 to 5,762 in 2017 and incidence rates increasing from 1.4 cases per million people in 2000 to 17.9 cases per million in 2017. The number of cases in the United States increased 39% from 2016 to 2017 alone (CDC, 2019). Moreover, the geographic range of *A. phagocytophilum* seems to be increasing along with the range expansion of the tick vector *Ixodes scapularis* (blacklegged tick). HGA is now the third most common vector-borne infection in the United States (Dumler et al., 2005; Dumler, 2012; Bakken and Dumler, 2015; Sinclair et al., 2015; CDC, 2019).

The geographic distribution of HGA is mainly focused in the upper midwest and northeastern United States, which coincides with Lyme disease and other *I. scapularis*-transmitted diseases (CDC, 2019). The agent of Lyme disease, *Borrelia burgdorferi*, and other human pathogens such as *Babesia microti*, *Borrelia mayonii*, *Borrelia miyamotoi*, and *Ehrlichia muris eauclairensis* are also transmitted by *I. scapularis*, with co-infections with *A. phagocytophilum* reported in <10% of cases (CDC, 2019).

Some Gram-negative bacteria such as *A. phagocytophilum* have evolved specialized secretion systems, secreting proteins that interact with host cells. The type IV secretion system (T4SS) is a macromolecular complex composed of proteins that are responsible for secreting effector proteins directly into the cytosol of eukaryotic host cells. The transported proteins, called effector proteins, are instrumental agents of virulence and pathogenesis and play a key role in altering environmental niches to allow pathogen replication (Voth et al., 2010, 2012; Abby et al., 2016; Han et al., 2016), yet relatively little is known about them. A critical goal is to understand how effectors cause infection in humans and animals which requires knowledge of the function of each effector. The first step toward this goal is identifying the effectors from among the entire set of proteins in the complete genome of a bacterial pathogen with a T4SS.

In addition to experimentally validating effector proteins by means of fusion protein reporter assays in translocation studies (Voth et al., 2012; Maturana et al., 2013), a time-consuming and expensive process, several computational methods have been proposed for the prediction of effectors (Burstein et al., 2009; Yu et al., 2010; Lockwood et al., 2011; Meyer et al., 2013; Zou et al., 2013; Wang et al., 2014, 2018a,b). Accurate prediction of effector proteins greatly limits the number of proteins requiring experimental verification which reduces costs. Current computational methods use either a scoring method (Meyer et al., 2013) or a machine learning approach (Burstein et al., 2009; Zou et al., 2013; Wang et al., 2014, 2018a,b) to predict a set of candidate effectors. For example, Meyer et al. (2013) used a scoring method to predict effectors for *Legionella pneumophila* and other pathogens. Burstein et al. (2009) used machine learning to focus on the *L. pneumophila* genome while (Wang et al., 2014) studied *Helicobacter pylori* effectors. In addition, there are several reviews on T4SS effector prediction and the progress made in this area (McDermott et al., 2011; Wang et al., 2017a; An et al., 2018; Zeng and Zou, 2019) as well as several databases for curating experimentally validated effector proteins for some species (Bi et al., 2013).

The computational methods previously reported for T4SS effector prediction used different sets of protein characteristics as features for their methods. We suspect that the use of these differing feature sets explains the differences in effector predictions by the different algorithms. As a result of the disparities between the results of earlier methods, we assembled all the features used in prior studies and used a multi-level, statistical approach to determine which were the most effective in predicting effector proteins (Esna Ashari et al., 2017, 2018). Because of the number of validated effectors available for *L. pneumophila*, we then ran a number of experiments on the whole genome of *L. pneumophila* using our optimal set of features (Esna Ashari et al., 2019). A comparison of our results with the list of validated effectors and those of previous studies was highly encouraging.

Although *A. phagocytophilum* employs the T4SS to invade human cells and cause anaplasmosis, a disease sometimes fatal to humans, it has just three experimentally verified effector proteins. As such, in order to conduct further research on this increasingly important human pathogen, there is a need to identify more effector proteins. Accurate prediction of effectors will assist in this identification. In this paper we turn our attention to the prediction of effector proteins in *A. phagocytophilum*. This pathogen has not been the focus of previous computational studies for effector prediction, in part because of its lack of validated effector proteins. Because of the high accuracy of the prediction results we obtained for *L. pneumophila* using a combination of validated effectors for four different pathogens, we decided to apply our method to *A. phagocytophilum*.

In addition to applying our model for T4SS effector prediction to *A. phagocytophilum*, we also improved it based on what we learned from our previous study (Esna Ashari et al., 2019) and expanded the code to make it easy for microbiologists to use for other bacteria with T4 secretion systems. We created a software package called OPT4e, for Optimal-features Predictor for T4SS Effector proteins, that performs all the steps described in our previous studies as well as incorporating new steps, including automation of feature evaluation which is very time consuming for whole proteomes. OPT4e is specifically designed for T4SS effector protein prediction and for use on Windows, Mac OS X, and Linux operating systems. One of the main characteristics of OPT4e is that it integrates all the tools, scripts, and software needed for calculation of our optimal set of features (Esna Ashari et al., 2018) and automatically creates the set of optimal features for training or test sets. OPT4e predicts candidate effectors and groups them based on their degree of likelihood of being an effector. In addition, OPT4e can be updated to become a stronger predictor over time. Finally, OPT4e has a very simple and intuitive graphical-user interface (GUI) making it easy to use.

The remainder of the manuscript is organized as follows: First, we focus on introducing OPT4e and the steps taken to create its framework and the related algorithms. Next we explain our set of optimal features and the machine learning algorithm used for OPT4e. We then introduce the datasets used in this study for the training and test sets followed by presentation of our results. In the final section, we discuss the results we obtained for OPT4e for two input proteomes.

2. MATERIALS AND METHODS

2.1. OPT4e Software

We designed and created OPT4e as a software package for the purpose of predicting effector proteins in different T4SS bacterial pathogens. OPT4e is an easy-to-use and user-friendly software package written in Python 3. Its specific features are as follows: It is based on usage of a machine learning approach for effector prediction. Each protein characteristic in a sequence is identified as a feature and is assigned the appropriate coefficient by the machine learning algorithm based on its significance

as determined by the training data, and it is not necessary to determine the importance of each feature manually. Moreover, it gathers and connects multiple bioinformatic tools in order to automatically calculate and assign all the needed features and to select the best ones. Therefore, installation is simple, and there is no need to use lots of online tools or to know a specific programming language to be able to use OPT4e as is necessary for some previously developed tools (Burstein et al., 2009; Zou et al., 2013; Wang et al., 2014). In addition, OPT4e predictions are based on protein sequences and are not dependent on an entire bacterial proteome. In fact, the input to OPT4e can be a single protein sequence selected by the user. Also, OPT4e is based on predictions using a specific machine learning algorithm while taking advantage of two additional algorithms in order to present the results in three different groups of more-likely, possible, and less-likely candidate effectors. One of the most important features of OPT4e is that it can be updated over time. Thus, if a user has some new experimentally verified effectors or discovers some critical non-effectors, they can add them to the software using a few mouse clicks. The software will then include them in the training set and update the model automatically. Enriching the set of validated effectors in the software dataset will help with the accuracy of the machine learning predictions, and OPT4e will become increasingly more accurate with time.

2.1.1. Framework

The framework and Graphical User Interface (GUI) for OPT4e are presented in **Figure 1**. First we provide an explanation of the framework, shown in **Figure 1A**, as follows: In the initial step a training set of known effectors and non-effectors is provided, and values for the optimal features are calculated for them automatically (Esna Ashari et al., 2018). OPT4e uses this set as its input. Note that in the first step a user has to select the appropriate button related to the purpose for using the software. If it is being used for effector prediction, the user will need to provide the test file for a protein sequence or a set of sequences in fasta-file format for classification as effectors or non-effectors by the OPT4e software. Then the software will calculate the feature values for each of the sequences provided such that they are available for machine learning prediction. The features used in this package are explained in the next section.

In the next step, OPT4e uses a support vector machine (SVM) algorithm with a radial basis function (RBF) kernel to predict effector protein sequences. This algorithm was found to give the best results as explained in Esna Ashari et al. (2019). In addition, OPT4e uses two additional classifiers (SVM with linear kernel and logistic regression) with the test sequences and uses their results to group the initially predicted effectors into three groups of more-likely (predicted by all three classifiers), possible (predicted by an additional classifier), and less-likely (predicted by just the initial SVM RBF classifier). The predicted groups of effector sequences are given as the output of the program. It should be noted that this methodology was used in the previous version of our algorithm as well (Esna Ashari et al., 2019). However, in our earlier work we used two ensemble classifiers and divided the features into three different groups for each ensemble set in addition to using the SVM with radial basis function with all the features. We found that a single classifier used with all the optimal features gave better results (Esna Ashari et al., 2019). Hence, we have replaced the ensemble classifiers with an SVM with a linear kernel and logistic regression in order to improve the model.

If a user wants to add experimentally verified effectors or some new known non-effectors to the training set to enrich it, they should select the appropriate option when using OPT4e. Then the software will automatically calculate the corresponding feature values for the new sequences and will add them to the feature set of the older training set.

We have added an option in OPT4e in case a user has made changes to the training set incorrectly or decides they do not want to change it. When the user clicks on the last button on the GUI (**Figure 1B**), OPT4e will reset the training data back to the original version. Finally, OPT4e is an open-source package, and users can update it as they wish.

2.2. Features and Feature Selection

As described in the introduction, in our earlier study we analyzed a comprehensive set of features gathered from previous computational studies performed in the field of T4SS effector protein prediction. The total number of features, including elements of vector features, was 1,027. The complete list of these features and the tools and software needed for their computation are presented in Esna Ashari et al. (2017, 2018).

We used a multi-step feature selection algorithm, described briefly in the next paragraph, to generate a set of optimal features for prediction of effector proteins consisting of 370 features. The detailed list of selected features, including the selected vector feature elements, can be found in Esna Ashari et al. (2018). The features can be grouped into chemical properties determining the way proteins interact with their environment and how effectors enter host cells (Yu et al., 2010; Zou et al., 2013), structural properties affecting protein-protein interactions between bacterial pathogens and host cells (Yu et al., 2010; Zou et al., 2013; Wang et al., 2014), compositional properties including the amino acid and dipeptide composition of protein sequences, and position-specific scoring matrix (PSSM)-related properties including PSSM composition and PSSM auto-covariance correlation composition (Zou et al., 2013; Wang et al., 2017b). The compositional properties determine the shapes and motifs of the protein sequences and, therefore, can affect the way they interact with host cells.

The first step in determining our optimal set of features was to use a filtering selection approach. For this purpose we used the *t*-test as a hypothesis testing method to filter features based on their associated *p*-values. Next we used Principal Component Analysis and Factor Analysis for dimensional reduction and to eliminate any redundancy and correlation in our feature set. The final step in our statistical approach was designing a fast backward feature selection method based on a Hosmer-Lemeshow goodness-of-fit test and using binary logistic regression. In this fashion we were able to retrieve a set of optimal features that work well together for effector prediction, and the concordance percentage from the Hosmer-Lemeshow goodness-of-fit test was still high after removal of the less related features.

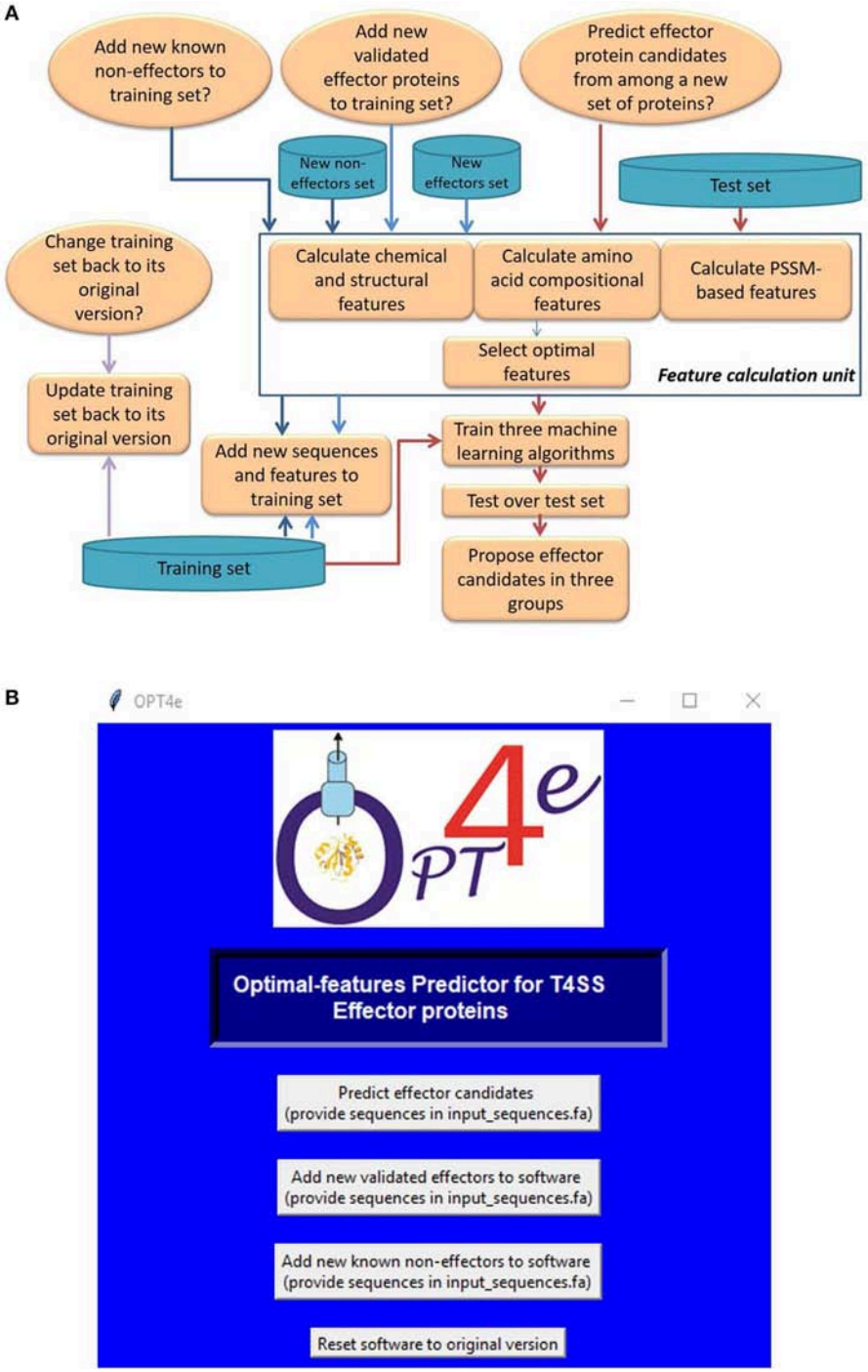

FIGURE 1 | OPT4e Software: **(A)** The framework for OPT4e. **(B)** The Graphical User Interface (GUI) for OPT4e.

2.3. Machine Learning Model

After selecting a set of optimal features, we designed multiple machine learning-based classifiers and tested them in order to select the most accurate predictor with our feature set (Esna Ashari et al., 2019). In due course, we focused on three classifiers. They included the SVM with the RBF kernel which is a well-known classifier and two ensemble classifiers (Esna Ashari et al., 2019). Based on 10-fold cross-validation results for our training set, results for our test set, and comparison with the results of previously developed methods, the SVM with the RBF kernel classifier was selected for further predictions, and it is the main classifier used in the OPT4e software package. As

mentioned earlier, the ensemble classifiers were replaced by an SVM with a linear kernel and logistic regression.

2.4. Dataset

In order to create our training set, we gathered known effectors and non-effectors for four Gram-negative bacterial pathogens from the Alphaproteobacteria and Gammaproteobacteria classes. This set is composed of effectors and non-effectors from: *L. pneumophila*, *Coxiella burnettii*, *Brucella* spp., and *Bartonella* spp. Furthermore, we added the three validated effectors and multiple non-effectors from *A. phagocytophilum* to our training set. The numbers of non-effector sequences added from *A. phagocytophilum* strains HZ and HGE-1 were 115 and 120 sequences, respectively. The final training set included 1,365 sequences consisting of 432 effectors and 933 non-effectors. Moreover, we added four experimentally validated effector proteins for *Anaplasma marginale* to the training set and repeated all the experiments (Lockwood et al., 2011). Therefore, the final training set consisted of 436 effectors. The complete file of protein sequences in fasta format used in the training set is presented in **Supplementary Data Sheet S1**.

For this study we selected two strains of *A. phagocytophilum*, strain HZ (accession number CP000235) and strain HGE-1 (accession number APHH01000001), for use with OPT4e. These strains are composed of 1,352 and 1,148 protein sequences, respectively. We used these two sets of protein sequences as input files for OPT4e. In addition, the proteome for *L. pneumophila* strain Philadelphia with 2,942 sequences was examined. Results for the latter proteome are briefly described later to explain the performance of OPT4e. More details concerning these datasets are given in the next section.

3. RESULTS

In this section we present the results obtained by OPT4e for the proteomes of *A. phagocytophilum* strain HZ and strain HGE-1. First, however, we present a brief discussion on validation of our classifier for the results obtained for the proteome of *L. pneumophila* strain Philadelphia.

3.1. Validation of OPT4e

We performed a thorough validation of the earlier version of our machine learning model as described in Esna Ashari et al. (2019). Briefly, in our previous study we performed 10-fold cross-validation for our training set and achieved an average accuracy of 94.05% over all folds for the SVM with radial basis function. Also, the model was verified using other performance metrics and achieved an average precision of 92.49%, an average recall of 92.00%, an average MCC (Matthews Correlation Coefficient, a measure of correlation between real and predicted values) of 0.87, and an average AUC (area under the curve) of 0.98. For further validation of our method, we tested the algorithm using the proteome for *L. pneumophila* strain Philadelphia and compared our predictions with ones from previous computational methods. Our results for effector candidates considered to be the most likely agreed with 80.5 and 72.2% of candidate effectors predicted using previous methods developed by Burstein et al. (2009) and Meyer et al. (2013), respectively. Also, the results predicted 93.7 and 99.8% of known effectors and non-effectors, respectively, from our training set (Esna Ashari et al., 2019).

TABLE 1 | Number of effector candidate proteins for *A. phagocytophilum* strains HZ and HGE-1 before and after adding *A. marginale* validated effectors to the OPT4e training set.

	Before adding *A. marginale* effectors		After adding *A. Marginale* effectors	
	Ap strain HZ	**Ap strain HGE-1**	**Ap strain HZ**	**Ap strain HGE-1**
More likely	14	17	16	18
Possible	10	6	9	5
Less likely	22	23	23	23
Total	46	46	48	46

A. phagocytophilum is indicated by Ap.

As mentioned earlier, in our previous study we learned that using all the features with a single classifier gave more accurate results than separating the features and using them in an ensemble classifier (Esna Ashari et al., 2019). Thus, for OPT4e we replaced the ensemble classifiers in our model for determining more-likely, possible, and less-likely effectors. To ensure that changing to the SVM with linear kernel and logistic regression classifiers actually does give more accurate results, we used 10-fold cross validation with our *L. pneumophila* strain Philadelphia effector and non-effector proteins. We obtained accuracies of 93.73% for the SVM with linear kernel and 93.79% using logistic regression. This is in contrast to our previous ensemble results for which we obtained average accuracies of 93.64 and 92.44%.

3.2. Predicted Effectors for *A. phagocytophilum* Strains HZ and HGE-1

Anaplasma phagocytophilum strain HZ contains 1,352 protein sequences consisting of 115 known non-effectors including the protein sequences associated with the genes *rpoB* (DNA-directed RNA polymerase subunit beta), *rpoC* (DNA-directed RNA polymerase subunit beta'), and Msp2/P44. For this strain, 14 protein sequences were predicted to be more likely to be an effector protein.

Anaplasma phagocytophilum strain HGE-1 contains 1,148 protein sequences consisting of 120 known non-effectors including DNA pol III, delta subunit (HGE1_05467), DNA-binding protein HGE1_04712 (a helix-turn-helix DNA binding protein somewhat specific to bacteria), MerR transcriptional regulator-HGE1_05592 (a helix-turn-helix DNA binding protein somewhat specific to bacteria), type IV secretion system VirB6-HGE1_01722 (a part of the T4SS structure), putative ABC transporter, permease protein-HGE1_00015 (an outer membrane protein also found in *Escherichia coli*), thiamine biosynthesis protein ThiS-HGE1_00315 (a sulfur carrier protein common in bacterial metablolism), and Msp2/P44 sequences. For this strain, 17 protein sequences were predicted to be more likely to be an effector protein.

Table 1 lists the number of candidate effectors for both strains of *A. phagocytophilum* according to their likelihood as predicted by OPT4e.

TABLE 2 | Effector candidates predicted by OPT4e.

Suggest	HGE1	HGE1 (other)	HZ	HZ (other)	Notes
	HGE1_00145		APH_0033		
*	HGE1_00220	S, T4	APH_0049	S, T4	
*	HGE1_00312	T4	APH_0068	T4	
*	HGE1_00527	S	APH_0117	S, T4	
	HGE1_00815		APH_0189		HZ: 7-aa insert at start
*	HGE1_01135	S, T4	APH_0259	S, T4	
*	HGE1_01175	T4	APH_0267	T4	HGE1: 17-aa insert at start
	HGE1_01752		APH_0382		
*	HGE1_01772		APH_0385	T4	
	HGE1_02100		APH_0385		
	HGE1_01777		APH_0386		
	HGE1_01782		APH_0387		
	HGE1_02092		APH_0452		
	HGE1_02095		APH_0453		
	HGE1_02117		APH_0453		
	HGE1_02107		APH_0455	S	Known effector
*	HGE1_02112		APH_0457	T4	
*	HGE1_02242	T4	APH_0485	T4	
*	HGE1_02492	S, T4	APH_0546	S, T4	
*	HGE1_02802	T4	APH_0633	T4	
*	HGE1_02817	T4	APH_0636	T4	HGE1: 3-aa insert at start
	HGE1_02827		APH_0641		
	HGE1_02947		APH_0670		First aa different
*	HGE1_03022		APH_0688	T4	
*	HGE1_03117		APH_0708	T4	
*	HGE1_03122	S	APH_0709	S, T4	
*	HGE1_03182	S, T4	APH_0726	S, T4	
*	HGE1_03232	S, T4	APH_0740	S, T4	Known effector
	HGE1_03297		APH_0755		
*	HGE1_03432		APH_0792	T4	
*	HGE1_03492	S	APH_0805	S, T4	
*	HGE1_03497		APH_0807	T4	
*	HGE1_03502	T4	APH_0808		
	HGE1_03532		APH_0815		
	HGE1_03557		APH_0820		
	HGE1_03697	S, T4	APH_0859	S, T4	Known effector
*	HGE1_03707	T4	APH_0861	T4	
*	HGE1_02737	T4	APH_0863	S	
*	HGE1_03892	S, T4	APH_0914	S, T4	
*	HGE1_05072	T4	APH_1167	T4	
*	HGE1_03907		APH_0916	T4	
	HGE1_03962		APH_0928		
*	HGE1_04167	T4	APH_0976	T4	
	HGE1_03507				HZ homolog not predicted
	HGE1_05977		APH_1365		First aa different
*	HGE1_05997	T4	APH_1369	T4	HZ: 6-aa insert at start
*	HGE1_06052	S	APH_1379	S	HZ: 14-aa insert in middle
*	HGE1_06067	T4	APH_1383	T4	
			APH_0239		No equivalent sequence in HGE1
			APH_0904		No equivalent sequence in HGE1
			APH_0028		No equivalent sequence in HGE1
			APH_0640		No equivalent sequence in HGE1
			APH_0816		No equivalent sequence in HGE1

HGE1 and HZ homologs are row aligned. Blue, orange, and red text colors indicate More Likely, Possible, and Less Likely effector candidates, respectively. Black text indicates that a sequence was not predicted as an effector. The columns HGE1 (other) and HZ (other) indicate when a sequence was predicted as an effector candidate by S4TE (S) or T4EffPred (T4). The Notes column lists differences between HGE-1 and HZ homologs, and finally the Suggest column indicates effector candidates proposed for initial experimental validation based on the strength of their predictions.

Because *Anaplasma marginale* is more closely related to *A. phagocytophilum* than the bacteria used in our model, we added four experimentally verified effector proteins for *A. marginale* (Lockwood et al., 2011) to our training set and repeated our experiments. Two new candidate effectors were predicted for *A. phagocytophilum* strain HZ. Also, the more likely category of candidate effectors was increased by 2 and 1 for *A. phagocytophilum* strains HZ and HGE-1, respectively. Specific numbers are reported in **Table 1**, and all predicted candidate effectors are presented in **Tables 2–4** by locus number. In addition, **Tables 2–4** present suggestions for the order of experimental verification of candidate effectors as explained in detail in the next section.

4. DISCUSSION

The main goal of this study was predicting a set of candidate effectors for *A. phagocytophilum* using a new package called OPT4e which we developed for this purpose. In fact, OPT4e can be used to give reasonable candidate effector predictions for most T4SS bacteria from the Alphaproteobacteria and Gammaproteobacteria classes. For *A. phagocytophilum* strains HGE-1 and HZ, we predicted 48 and 46 candidate effectors, respectively, with 16 and 18 more likely to be effectors. All three experimentally-verified effector proteins were included in the 16 and 18 more-likely category.

We compared the differences between the predictions for the two strains and found that whenever there was a difference between the category in which an effector was predicted or an effector was not predicted for one of the strains, there was a difference between the homologous protein sequences of the two strains. These differences are noted in **Table 2**. In addition, five effector proteins were predicted in strain HZ for which there is no equivalent protein sequence in strain HGE-1. Strain HZ was the first *A. phagocytophilum* genome to be sequenced, and many small open reading frames (ORFs) were annotated that have not been retained in subsequent annotations (including the RefSeq for HZ). Some of these small ORFs account for the differences between the effector predictions for the two strains. Interestingly, there was one effector predicted in HGE-1 for which there was not an equivalent protein annotated in HZ. However, closer inspection of the HZ genome revealed that the sequence is present.

It should be noted that in machine learning-based prediction, an algorithm tries to fit as many training samples as it can based on the given features, and as the numbers of features and samples increase, the task increases in complexity. Also, it should be noted that the greater part of our positive training set consists of known effectors for *L. pneumophila* because it has the largest number of verified effectors. Moreover, there are only three verified effectors for *A. phagocytophilum* in our dataset. Therefore, it is possible that our set of candidate effectors for *A. phagocytophilum* include the ones that are mostly similar to *L. pneumophila* effectors. In addition, OPT4e may be detecting genes with a different signature from the rest of the genome such as those acquired by horizontal gene transfer in species where this

TABLE 3 | Groups recommended for experimental verification of effector candidates for strain HZ.

Effector candidates	Other models	Notes
Group 1		
APH_0259	S, T4	
APH_0740	S, T4	Known effector
APH_0859	S, T4	Known effector
Group 2		
APH_0239	T4	
APH_0385	T4	
APH_0457	T4	
APH_0636	T4	
APH_0904	T4	
APH_0455	S	Known effector
Group 3		
APH_0033		
APH_0382		
APH_0385		
APH_0386		
APH_0387		
APH_0452		
APH_0453		
APH_0928		
Group 4		
APH_0267	T4	
APH_0633	T4	
APH_0861	T4	
APH_1167	T4	
APH_1369	T4	
APH_0863	S	
APH_1379	S	
Group 5		
APH_0028		
APH_0640		
APH_1365		
Group 6		
APH_0049	S, T4	
APH_0546	S, T4	
APH_0709	S, T4	
APH_0726	S, T4	
APH_0805	S, T4	
APH_0914	S, T4	
Group 7		
APH_0068	T4	
APH_0485	T4	
APH_0688	T4	
APH_0708	T4	
APH_0792	T4	
APH_0807	T4	
APH_0916	T4	
APH_0976	T4	
APH_1383	T4	
APH_0117	S	

(Continued)

TABLE 3 | Continued

Effector candidates	Other models	Notes
Group 8		
APH_0641		
APH_0670		
APH_0755		
APH_0808		
APH_0815		
APH_0816		
APH_0820		
APH_1383		

Groups are based on whether effector candidates are More Likely shown in blue, Probable shown in orange, and Less Likely shown in red, followed by prediction by both S4TE (S) and T4EffPred (T4), prediction by one of them, or prediction by neither. We recommend starting with Group 1 and proceeding successively through Group 8.

occurs. Thus, caution is necessary when evaluating the output. It should be noted, however, that a strength of OPT4e is that it can be updated over time, and a user has the ability to add newly verified effectors to the training dataset. As a result, as new effectors for *A. phagocytophilum* are verified, they can be used in OPT4e to increase its accuracy for predicting effector proteins.

As a final note, we compared our effector candidates for *A. phagocytophilum* with those predicted by S4TE (Noroy et al., 2019) and T4EffPred (Zou et al., 2013) after we used these two programs to predict effectors for both *A. phagocytophilum* strains in our study. For HZ, OPT4e shared 13 of 48 predictions with S4TE and 27 of 92 predictions with T4EffPred. S4TE and T4EffPred shared ten predictions. Two of these were for known effectors. The third known effector was predicted by S4TE but not by T4EffPred. Thus, both OPT4e and S4TE predicted all three known effectors (see **Table 2**). For HGE-1, OPT4e shared 11 of 49 predictions with S4TE and 19 of 45 predictions with T4EffPred. S4TE and T4EffPred shared seven predictions. Two of these were for the homologs of known effectors. The third effector homolog was not predicted by either method; only OPT4e predicted all three.

One strategy for deciding which effector candidates to choose for experimental verification is to select from among the ones predicted by OPT4e for both strains of *A. phagocytophilum* and also predicted by one of the other two methods, S4TE or T4EffPred. There are 28 of these indicated by asterisks in **Table 2**, where HGE1 and HZ homologs are row aligned.

An alternative strategy and more systematic approach is to first group the predicted effectors on the basis of more-likely, probable, and less-likely and then based on predictions by the two methods, S4TE or T4effPred. Experimental verification would begin with Group 1 and proceed in order through successive groups as shown in **Tables 3**, **4**. **Table 3** is for HZ and **Table 4** is for HGE-1, and for both strains Group 1 candidate effectors have literally been predicted by five different algorithms, the three from OPT4e plus S4TE and T4EffPred. For HZ, two of the three sequences in Group 1 are for known effectors, and the third known effector is in Group 2. For HGE-1, two of the sequences in Group 1 are for homologs of known

TABLE 4 | Groups recommended for experimental verification of effector candidates for strain HGE-1.

Effector Candidates	Other Models	Notes
Group 1		
HGE1_01135	S, T4	
HGE1_03232	S, T4	Homolog of known effector
HGE1_03697	S, T4	Homolog of known effector
Group 2		
HGE1_01175	T4	
HGE1_05997	T4	
Group 3		
HGE1_00145		
HGE1_01752		
HGE1_01772		
HGE1_01777		
HGE1_01782		
HGE1_02092		
HGE1_02095		
HGE1_02100		
HGE1_02107		Homolog of known effector
HGE1_02112		
HGE1_02117		
HGE1_03507		
HGE1_03962		
Group 4		
HGE1_02737	T4	
HGE1_02802	T4	
HGE1_02817	T4	
HGE1_03707	T4	
HGE1_05072	T4	
Group 5		
HGE1_00220	S, T4	
HGE1_02492	S, T4	
HGE1_03182	S, T4	
HGE1_03892	S, T4	
Group 6		
HGE1_00312	T4	
HGE1_02242	T4	
HGE1_03502	T4	
HGE1_04167	T4	
HGE1_06067	T4	
HGE1_00527	S	
HGE1_03122	S	
HGE1_03492	S	
HGE1_06052	S	
Group 7		
HGE1_00815		
HGE1_02827		
HGE1_03022		
HGE1_03117		
HGE1_03297		
HGE1_03432		
HGE1_03497		
HGE1_03532		
HGE1_03557		
HGE1_03907		

Groups are based on whether effector candidates are More Likely shown in blue, Probable shown in orange, and Less Likely shown in red, followed by prediction by both S4TE (S) and T4EffPred (T4), prediction by one of them, or prediction by neither. We recommend starting with Group 1 and proceeding successively through Group 7.

effectors, and the third effector homolog is in Group 3. Thus the first three groups for each strain present excellent choices for experimental verification.

DATA AVAILABILITY

The OPT4e software package as well as the datasets used for this study can be found at https://bitbucket.org/zhesna/opt4e/ and http://bcb.eecs.wsu.edu/software.

AUTHOR CONTRIBUTIONS

ZE developed the OPT4e software and performed dataset preparation, machine learning predictions, computational experiments, data analysis, and drafted the manuscript. SB and KB supervised, conceived, and coordinated the study and contributed to the manuscript. All authors gave final approval for publication.

FUNDING

This study was supported by grant R01AI042792 from the National Institutes of Health and by the Carl M. Hansen Foundation. The funders had no role in the study design, data collection and analysis, decision to publish, or preparation of the manuscript.

SUPPLEMENTARY MATERIAL

The Supplementary Material for this article can be found online at: https://www.frontiersin.org/articles/10.3389/fmicb.2019.01391/full#supplementary-material

REFERENCES

Abby, S. S., Cury, J., Guglielmini, J., Néron, B., Touchon, M., and Rocha, E. P. C. (2016). Identification of protein secretion systems in bacterial genomes. *Sci. Rep.* 6:23080. doi: 10.1038/srep23080

An, Y., Wang, J., Li, C., Leier, A., Marquez-Lago, T., Wilksch, J., et al. (2018). Comprehensive assessment and performance improvement of effector protein predictors for bacterial secretion systems III, IV and VI. *Brief. Bioinform.* 19, 148–161. doi: 10.1093/bib/bbw100

Bakken, J. S., and Dumler, S. J. (2015). Human granulocytic anaplasmosis. *Infect. Dis. Clin. North Am.* 29, 341–355. doi: 10.1016/j.idc.2015.02.007

Bi, D., Liu, L., Tai, C., Deng, Z., Rajakumar, K., and Ou, H. Y. (2013). Secret4: a web-based bacterial type iv secretion system resource. *Nucleic Acids Res.* 41, D660–D665. doi: 10.1093/nar/gks1248

Burstein, D., Zusman, T., Degtyar, E., Viner, R., Segal, G., and Pupko, T. (2009). Genome-scale identification of *Legionella pneumophila* effectors using a machine learning approach. *PLoS Pathogens* 5:e1000508. doi: 10.1371/journal.ppat.1000508

CDC (2019). *Centers for Disease Control and Prevention.* Available online at: https://www.cdc.gov/anaplasmosis/index.html

Dumler, S. J. (2012). The biological basis of severe outcomes in *Anaplasma phagocytophilum* infection. *FEMS Immunol. Med. Microbiol.* 64, 13–20. doi: 10.1111/j.1574-695X.2011.00909.x

Dumler, S. J., Choi, K.-S., Garcia-Garcia, J. C., Barat, N. S., Scorpio, D. G., Garyu, J. W., et al. (2005). Human granulocytic anaplasmosis and *Anaplasma phagocytophilum*. *Emerg. Infect. Dis.* 11, 1828–1834. doi: 10.3201/eid1112.050898

Esna Ashari, Z., Brayton, K. A., and Broschat, S. L. (2017). "Determining optimal features for predicting type IV secretion system effector proteins for *Coxiella burnetii*," in *Proceedings of The 8th ACM Conference on Bioinformatics, Computational Biology, and Health Informatics (ACM BCB)* (Boston, MA: ACM), 346–351.

Esna Ashari, Z., Brayton, K. A., and Broschat, S. L. (2018). An optimal set of features for predicting type IV secretion system effector proteins for a subset of species based on a multi-level feature selection approach. *PLoS ONE* 13:e0197041. doi: 10.1371/journal.pone.0197041

Esna Ashari, Z., Brayton, K. A., and Broschat, S. L. (2019). Using an optimal set of features with a machine learning-based approach to predict effector proteins for *Legionella pneumophila*. *PLoS ONE* 9:e0202312. doi: 10.1371/journal.pone.0202312

Han, N., Yu, W., Qiang, Y., and Zhang, W. (2016). T4sp database 2.0: an improved database for type IV secretion systems in bacterial genomes with new online analysis tools. *Comput. Math. Methods Med.* 2016:9415459. doi: 10.1155/2016/9415459

Lockwood, S., Voth, D. E., Brayton, K. A., Beare, P. A., Brown, W. C., Heinzen, R. A., et al. (2011). Identification of *Anaplasma marginale* type IV secretion system effector proteins. *PLoS ONE* 6:e27724. doi: 10.1371/journal.pone.0027724

Maturana, P., Graham, J. G., Sharma, U. M., and Voth, D. E. (2013). Refining the plasmid-encoded type IV secretion system substrate repertoire of *Coxiella burnetii*. *J. Bacteriol.* 195, 3269–3276. doi: 10.1128/JB.00180-13

McDermott, J. E., Corrigan, A., Peterson, E., Oehmen, C., Niemann, G., Cambronne, E. D., et al. (2011). Computational prediction of type III and IV secreted effectors in gram-negative bacteria. Infection and immunity. *Brief. Bioinform.* 79, 23–32. doi: 10.1128/IAI.00537-10

Meyer, D. F., Noroy, C., Moumene, A., Raffaele, S., Albina, E., and Vachiery, N. (2013). Searching algorithm for type IV secretion system effectors 1.0: a tool for predicting type IV effectors and exploring their genomic context. *Nucleic Acids Res.* 41, 9218–9229. doi: 10.1093/nar/gkt718

Noroy, C., Lefrancois, T., and Meyer, D. F. (2019). Searching algorithm for type IV effector proteins (s4te) 2.0: improved tools for type IV effector prediction, analysis and comparison. *PLoS Comput. Biol.* 15:e1006847. doi: 10.1371/journal.pcbi.1006847

Sinclair, S. H. G., Garcia-Garcia, J. C., and Dumler, J. S. (2015). Bioinformatic and mass spectrometry identification of *Anaplasma phagocytophilum* proteins translocated into host cell nuclei. *Front. Microbiol.* 6:55. doi: 10.3389/fmicb.2015.00055

Voth, D. E., Beare, P. A., Howe, D., Sharma, U. M., Samoilis, G., Cockrell, D. C., et al. (2010). The *Coxiella burnetii* cryptic plasmid is enriched in genes encoding type IV secretion system substrate. *J. Bacteriol.* 193, 1493–1503. doi: 10.1128/JB.01359-10

Voth, D. E., Broederdorf, L. J., and Graham, J. G. (2012). Bacterial type IV secretion systems: versatile virulence machines. *Fut. Microbiol.* 7, 241–257. doi: 10.2217/fmb.11.150

Wang, J., Li, J., Yang, B., Xie, R., Marquez-Lago, T. T., Leier, A., et al. (2018a). Bastion3: a two-layer ensemble predictor of type III secreted effectors. *Bioinformatics*. 35, 2017–2028. doi: 10.1093/bioinformatics/bty914

Wang, J., Yang, B., An, Y., Marquez-Lago, T., Leier, A., Wilksch, J., et al. (2017a). Systematic analysis and prediction of type IV secreted effector proteins by machine learning approaches. *Brief. Bioinform.* bbx164, 1–21. doi: 10.1093/bib/bbx164

Wang, J., Yang, B., Leier, A., Marquez-Lago, T. T., Hayashida, M., Rocker, A., et al. (2018b). Bastion6: a bioinformatics approach for accurate prediction of type VI secreted effectors. *Nat. Genet.* 34, 2546–2555. doi: 10.1093/bioinformatics/bty155

Wang, J., Yang, B., Revote, J., Leier, A., Marquez-Lago, T. T., Webb, G., et al. (2017b). POSSUM: a bioinformatics toolkit for generating numerical sequence

feature descriptors based on pssm profiles. *Bioinformatics* 33, 2756–2758. doi: 10.1093/bioinformatics/btx302

Wang, Y., Wei, X., Bao, H., and Liu, S. (2014). Prediction of bacterial type IV secreted effectors by c-terminal features. *BMC Genomics* 15:50. doi: 10.1186/1471-2164-15-50

Yu, L., Guo, Y., Li, Y., Li, G., Li, M., Luo, J., et al. (2010). Secretp: identifying bacterial secreted proteins by fusing new features into chou's pseudo-amino acid composition. *J. Theor. Biol.* 267, 1–6. doi: 10.1016/j.jtbi.2010.08.001

Zeng, C., and Zou, L. (2019). An account of *in silico* identification tools of secreted effector proteins in bacteria and future challenges. *Brief. Bioinform.* 20, 110–129. doi: 10.1093/bib/bbx078

Zou, L., Nan, C., and Hu, F. (2013). Accurate prediction of bacterial type IV secreted effectors using amino acid composition and PSSM profiles. *Bioinformatics* 29, 3135–3142. doi: 10.1093/bioinformatics/btt554

Conflict of Interest Statement: The authors declare that the research was conducted in the absence of any commercial or financial relationships that could be construed as a potential conflict of interest.

Copyright © 2019 Esna Ashari, Brayton and Broschat. This is an open-access article distributed under the terms of the Creative Commons Attribution License (CC BY). The use, distribution or reproduction in other forums is permitted, provided the original author(s) and the copyright owner(s) are credited and that the original publication in this journal is cited, in accordance with accepted academic practice. No use, distribution or reproduction is permitted which does not comply with these terms.

frontiers in Microbiology

MINI REVIEW
published: 28 June 2019
doi: 10.3389/fmicb.2019.01484

Confirmed and Potential Roles of Bacterial T6SSs in the Intestinal Ecosystem

Can Chen[1†], Xiaobing Yang[2†] and Xihui Shen[2]*

[1] Institute of Food and Drug Inspection, College of Life Science and Agronomy, Zhoukou Normal University, Zhoukou, China, [2] State Key Laboratory of Crop Stress Biology for Arid Areas, Shaanxi Key Laboratory of Agricultural and Environmental Microbiology, College of Life Sciences, Northwest A&F University, Yangling, China

The contact-dependent type VI secretion system (T6SS) in diverse microbes plays crucial roles in both inter-bacterial and bacteria-host interactions. As numerous microorganisms inhabit the intestinal ecosystem at a high density, it is necessary to consider the functions of T6SS in intestinal bacteria. In this mini-review, we discuss T6SS-dependent functions in intestinal microbes, including commensal microbes and enteric pathogens, and list experimentally verified species of intestinal bacteria containing T6SS clusters. Several seminal studies have shown that T6SS plays crucial antibacterial roles in colonization resistance, niche occupancy, activation of host innate immune responses, and modulation of host intestinal mechanics. Some potential roles of T6SS in the intestinal ecosystem, such as targeting of single cell eukaryotic competitors, competition for micronutrients, and stress resistance are also discussed. Considering the distinct activities of T6SS in diverse bacteria residing in the intestine, we suggest that T6SS research in intestinal microbes may be beneficial for the future development of new medicines and clinical treatments.

Keywords: type VI secretion system, intestinal microbiota, enteric pathogen, colonization resistance, competition

OPEN ACCESS

Edited by:
Eric Cascales,
Aix-Marseille Université, France

Reviewed by:
Thibault Géry Sana,
École Polytechnique Fédérale de Lausanne, Switzerland
Benjamin Ross,
University of Washington, United States

****Correspondence:***
Xihui Shen
xihuishen@nwsuaf.edu.cn

† These authors have contributed equally to this work

Specialty section:
This article was submitted to Microbial Physiology and Metabolism, a section of the journal Frontiers in Microbiology

Received: *22 January 2019*
Accepted: *14 June 2019*
Published: *28 June 2019*

Citation:
Chen C, Yang X and Shen X (2019) Confirmed and Potential Roles of Bacterial T6SSs in the Intestinal Ecosystem. Front. Microbiol. 10:1484. doi: 10.3389/fmicb.2019.01484

INTRODUCTION

The type VI secretion system (T6SS) is a contact-dependent transmembrane nanomachine that uses a contractile mechanism to inject effectors into adjacent prokaryotic or eukaryotic cells (Hood et al., 2010; Jani and Cotter, 2010; Cianfanelli et al., 2016). A typical T6SS apparatus is composed of 13 core subunits (TssA-TssM) and possesses a structure similar to that of a T4 bacteriophage tail (Boyer et al., 2009; Cascales and Cambillau, 2012; Zoued et al., 2013). In an integral T6SS apparatus, the baseplate complex (TssAEFGK) is anchored to the cell membrane by the membrane complex (TssJLM), providing structural support. The needle sheath (TssBC), tail tube (TssD/Hcp), and spike complex (TssI/VgrG) form the injection apparatus, which is responsible for effector secretion (Cascales and Cambillau, 2012; Silverman et al., 2012). A dynamic T6SS secretion process contains assembly/extension, contraction/puncture, and disassembly of the sheath. Briefly, the membrane complex is formed at the initial stage. Subsequently, baseplate proteins are recruited for sheath/tube anchoring and extension. When attacking, the membrane-puncturing spike pierces target cells through sheath contraction, accompanied by energy consumption and load transportation. Consequently, various effectors are delivered into target cells in a one-step manner (Basler et al., 2012; Brunet et al., 2015; Cianfanelli et al., 2016; Coulthurst, 2019). Although some

pathogen-associated T6SSs have been reported to be involved in bacterial pathogenesis (Pukatzki et al., 2007; Aubert et al., 2016; Jiang et al., 2016), the primary function of T6SSs is to compete against rival bacteria in polymicrobial environments (Durand et al., 2014; Cianfanelli et al., 2016). However, other functions of T6SSs, such as resistance to amoeba predation (Zheng et al., 2011), biofilm formation (Gallique et al., 2017), and stress response (Weber et al., 2009; Zhang W. et al., 2013), have also been reported.

The intestinal ecosystem is composed of a densely populated community of multiple microorganisms that may be beneficial or harmful to host health (Walter and Ley, 2011). In intestinal environments where nutrients and space are limited, microbes must use various strategies to coexist or compete with the host and other bacteria. In recent years, the contact-dependent T6SS nanomachine has attracted much attention for its role in interbacterial competition in the mammalian gut (Sana et al., 2017; Verster et al., 2017). T6SS mediated antagonism in the mammalian gut not only benefits the microbiota-mediated colonization resistance by preventing invasion of pathogens, but also assists some pathogens to battle with the resident microbiota to invade an ecosystem and cause disease. Thus, it was stated that there is secret bacterial warfare in the gut, due to the T6SS roles both in the intestinal commensal microbes and enteric pathogens (Sana et al., 2017; Garcia-Bayona and Comstock, 2018). In this review, we have discussed recent studies on intestinal microorganisms with functional T6SS clusters and T6SS-dependent activities related to the intestinal microbial community and host health.

T6SS-DEPENDENT ACTIVITIES IN INTESTINAL ECOSYSTEM

Interference Competition Mediated by T6SS

Bacterial competition occurs as interference competition (killing of target cells with antibacterial weapons) or exploitation competition (consuming nutrients from the milieu) (Chassaing and Cascales, 2018). As an anti-bacterial weapon, T6SSs were primarily considered to mediate interference competition in the intestinal microbiota. The antibacterial function of T6SSs relies primarily on injection of "anti-bacterial" effectors that target conserved, essential features of the bacterial cell, such as peptidoglycan (Russell et al., 2011), membrane phospholipids (Russell et al., 2013), nucleic acids (Ma L.S. et al., 2014), NAD^+ (Whitney et al., 2015), and the critical cell division protein FtsZ (Ting et al., 2018).

Commensal bacteria form a protective barrier that protects the host from bacterial pathogens (Belkaid and Hand, 2014). In healthy adult individuals, Bacteroidales are the most abundant order of bacteria in the intestinal microbiota (Faith et al., 2013). Recently, by performing extensive bioinformatics analyses and creating hidden Markov models for Bacteroidales Tss proteins, Coyne and colleagues identified 130 T6SS loci within 205 human gut Bacteroidales genomes. As Bacteroidales comprise approximately 50% of all colonic bacteria in many people, this suggested that T6SSs are distributed in about 25% of bacteria in the human colon (Coyne et al., 2014; Coyne et al., 2016). Moreover, more than 10^9 T6SS-firing events were determined per minute per gram of colonic contents, further supporting the importance of this weapon in shaping gut microbiota composition (Wexler et al., 2016). T6SS loci of the human gut Bacteroidales species segregate into three distinct genetic architectures (GA), termed GA1-GA3. GA1 and GA2 loci are present on conserved integrative conjugative elements (ICE) and are transferred between diverse human gut Bacteroidales strains via ICE. GA3 loci are not contained on conserved ICE and are confined to *Bacteroides fragilis* (Coyne et al., 2014, 2016). The GA3 T6SSs of *B. fragilis* antagonizes human gut Bacteroidales species *in vivo* using previously undescribed effectors, likely to create a locally protected niche in the human gut (Wexler et al., 2016). The interbacterial interactions among symbiotic Bacteroidales species could be predicted according to the presence or absence of strain-specific effector/immunity (E/I) repertoires. Further, some of these strains may avoid contact-dependent killing by accumulating immunity genes to neutralize antibacterial effectors that they do not encode to persist in the gut (Wexler et al., 2016). Importantly, symbiotic non-toxigenic *B. fragilis* strains could restrict enteric colonization by an enterotoxigenic *B. fragilis* strain, dependent on a functional T6S, to protect the host against intestinal inflammatory disease, suggesting a novel role of T6SS in colonization resistance (Hecht et al., 2016; Casterline et al., 2017).

Type VI secretion systems are widely distributed and have been proposed to be present in about 25% of all sequenced Gram-negative bacteria (Boyer et al., 2009; Salomon and Orth, 2015), including enteric pathogenic microorganisms, e.g., *Vibrio cholerae*, *Salmonella enterica*, *Shigella sonnei*, and *Yersinia pseudotuberculosis*. Thus, T6SS mediated antagonism in the mammalian gut both benefits microbiota-mediated colonization resistance by preventing pathogen invasion and facilitates some pathogens to battle resident microbiota to invade the ecosystem and cause disease. Some enteric pathogens could utilize T6SS-mediated antibacterial weapons to kill symbionts and establish within the host gut. For example, *S. enterica* Serovar Typhimurium uses T6SS to kill commensal *Klebsiella oxytoca* and enhance colonization of the mouse gut (Sana et al., 2016). With a functional T6SS, *S. sonnei* showed an advantage in competing against *E. coli* and *Shigella flexneri* both *in vitro* and *in vivo*, which may explain the dominance and increasing global prevalence of *S. sonnei* in developed countries worldwide (Anderson et al., 2017). Constitutive T6SS expression provides *V. cholerae* with an advantage in intra-specific and inter-specific competition, such that T6SS-dependent toxicity toward other bacteria could enhance *V. cholerae* survival in the environment and/or during colonization of a host (MacIntyre et al., 2010; Unterweger et al., 2012; Fu et al., 2013). Through transcriptome sequencing (RNA-Seq), T6SSs and their associated toxins in the gut symbiont of 28 *Snodgrassella alvi* strains from diverse *Apis* and *Bombus* species were analyzed. T6SS-associated Rhs toxins with antibacterial activity could mediate both intraspecific and interspecific competition among *S. alvi* strains and other bee gut

microbes. Furthermore, extensive recombination and horizontal transfer of toxin/immunity genes between strains in the gut microbiota have resulted in tremendous diversity in their toxin repertoires, which suggest that T6SS-mediated competition may be an important driver of coevolution (Steele et al., 2017). These studies showed that enteric pathogens could use their T6SSs for interbacterial competition *in vivo* and for niche occupancy.

Besides bacterial competitors, T6SS was also found to target some single cell eukaryotic competitors, including amoebae and fungi. In fact, T6SS was first identified by screening *V. cholerae* mutants that failed to kill the social amoeba *Dictyostelium discoideum*, and the lipid-binding effector VasX was found to be required for T6SS-mediated amoeba killing, possibly through plasma membrane perturbations (Pukatzki et al., 2006; Miyata et al., 2011; Zheng et al., 2011). T6SSs in *Pseudomonas syringae* and *Serratia marcescens* were reported to be required for competition against other single cell eukaryotic organisms, i.e., yeast and fungi (Haapalainen et al., 2012; Trunk et al., 2018). The first anti-fungal T6SS effectors, Tfe1 and Tfe2, were identified in *S. marcescens*. Tfe1 causes plasma membrane depolarization without formation of a specific pore, while Tfe2 disrupts nutrient uptake and amino acid metabolism, and induces autophagy (Trunk et al., 2018). Since single cell eukaryotes are important components of the intestinal microbiota (Coyne and Comstock, 2019), it is not surprising that intestinal bacteria might deploy anti-eukaryotic T6SSs to compete for nutrients and space against co-habiting microbial eukaryotes.

Exploitation Competition Meditated by T6SS

As essential micronutrients are involved in a wide range of cellular processes (e.g., DNA replication, respiration, and energy generation), transit of these metal ions is a crucial component of host-microbe interactions, including those in the gastrointestinal tract (Sorbara and Pamer, 2019). For example, *E. coli* mutants defective in catecholate siderophore production show impaired murine gut colonization (Pi et al., 2012). Without a high-affinity zinc transporter, *Campylobacter jejuni* is unable to replicate or colonize the gastrointestinal tract, as quantities of zinc in the gastrointestinal tract are reduced by the host (Gielda and DiRita, 2012). Thus, competition for micronutrients in the gut is intense.

Type VI secretion system has been reported to be involved in acquisition of essential micronutrients, such as zinc, manganese, and iron, indicating its novel function in increasing bacterial fitness through competition for essential nutrients. In *Pseudomonas aeruginosa*, the H3-T6SS secreted effector TseF facilitates iron acquisition by interacting with the iron-chelating molecule PQS (Pseudomonas quinolone signal) (Lin et al., 2017). In *Burkholderia thailandensis*, T6SS4 secretes zinc- and manganese-scavenging proteins to fulfill the increased cellular demand for these metal ions under oxidative stress (Si et al., 2017a,b). Similarly, in the enteric pathogen *Y. pseudotuberculosis*, T6SS4 functions to combat host nutritional immunity and multiple adverse stresses by translocating a zinc binding effector YezP (Wang et al., 2015). Distinct from the extensively studied contact-dependent "anti-bacterial" and "anti-eukaryotic" T6SSs, the "metal ion transporting" T6SS secretes metal-binding proteins into the extracellular milieu, independent of cell-cell contact (Si et al., 2017a). Thus, T6SS confers survival advantages to bacterium in niches with multiple bacterial species not only by delivering "anti-bacterial" toxins to kill competing cells for interference competition, but also by enhancing its ability to acquire essential micronutrients for exploitation competition. It will be interesting to determine the physiologic consequence of these metal acquisition T6SSs in the intestinal ecosystem in the future.

Interestingly, expression of *Y. pseudotuberculosis* T6SS4 was found to be nutrient status-dependently regulated by the stringent response factor RelA and the nutrient-dependent regulator RovM (Song et al., 2015; Yang et al., 2019). Further research is needed to reveal whether T6SS is involved in competition for other nutrients besides metal ions.

Activation of the Innate Immune Response and Virulence

Although it is well-known that enteric pathogens could utilize the antibacterial T6SS weapon to eradicate competing microbes *in vivo*, little is known about whether the T6SS-dependent interactions with commensal bacteria have additional effects on virulence. Recently, Zhao et al. (2018) discovered that the *V. cholerae* T6SS could compete against commensal *E. coli* strains in the mouse gut to facilitate colonization. Importantly, they found that this microbial antagonistic interaction could improve fitness of *V. cholera* by activating host innate immune responses and improving expression of bacterial virulence genes (i.e., cholera toxin) (Zhao et al., 2018). The authors suggested that the innate immune response was induced by bacterial debris derived from lysed commensals, which together with up-regulated cholera toxin (CT), resulted in elevated disease symptoms and increased fitness of *V. cholerae* as a pathogen. Fast et al. (2018) used the *Drosophila melanogaster* model of cholera to define the contribution of T6SS to *V. cholerae* pathogenesis. They found that interactions between T6SS and the gut commensal *Acetobacter pasteurianus* intensified disease symptoms and accelerated host death. The disease severity was attenuated by inactivation of T6SS, or removal of *A. pasteurianus*. Interestingly, mutation of the Immune Deficiency (IMD) pathway relieved T6SS dependent lethality, implicating innate defenses in T6SS-mediated host death (Fast et al., 2018). These studies established that interactions between T6SS and commensal bacteria activate innate immune responses and promote *V. cholera* pathogenesis.

In addition, a few T6SS toxic effectors result in metabolic disorders or diseases in eukaryotic host cells. VgrG-1 in *V. cholerae* was responsible for T6SS-dependent cytotoxicity of macrophages through covalent cross-linking of host cell actin (Pukatzki et al., 2007; Ma and Mekalanos, 2010). In the diarrheal isolate *Aeromonas hydrophila* SSU, T6SS-secreted VgrG1 exhibited actin ADP-ribosylating activity, which can induce a rounded phenotype in HeLa cells, resulting in apoptosis (Suarez et al., 2010). A non-VgrG T6SS effector in *Edwardsiella tarda*, EvpP, inhibited NLRP3 inflammasome activation through repression of the Ca^{2+}-dependent MAPK-Jnk

pathway (Chen et al., 2017). T6SS effectors with phospholipase activity could cause damage to the cell membrane and accelerate the infection process (Dong et al., 2013; Russell et al., 2013). Notably, a few bacterial pathogens with the T6SS apparatus may spread through the digestive tract but cause diseases outside the gastrointestinal system. For example, in the newborn meningitis *E. coli* (NMEC) K1 strain, the Hcps of T6SS interacts with human brain microvascular endothelial cells (HBMEC) in a coordinated manner, first binding, then invading, and finally causing apoptosis of HBMEC (Zhou et al., 2012). The T6SS-secreted proteins VgrG1 and VgrG2 in *Helicobacter hepaticus* increases cellular innate pro-inflammatory responses, resulting in liver disease and intestinal inflammation (Bartonickova et al., 2013).

Modulation of Host Intestinal Mechanics

Recently, Logan and colleagues used a combination of microbial genetics, *in vitro* experiments, and quantitative *in vivo* imaging in zebrafish to determine the role of *V. cholerae* T6SS in gut colonization. They found that *V. cholerae* can expel resident microbiota of the genus *Aeromonas* in a T6SS-dependent manner. Unexpectedly, T6SS acted primarily to increase the strength of gut contractions, rather than killing the bacterial competitor. Coupling of T6SS activity to host contractions depended on an actin cross-linking domain (ACD) from the T6SS apparatus. When the ACD domain was deleted, *V. cholerae* could no longer induce enhanced host contractions, and dense *Aeromonas* communities remained in the gut. Deleting the ACD domain did not affect the ability of *V. cholerae* to kill *A. veronii in vitro* or enter and occupy the host intestine. These findings reveal a novel strategy by which enteric pathogens can modulate host intestinal mechanics to redefine gut communities and highlights the role of the host fluid-mechanical environment in shaping gut population dynamics (Logan et al., 2018). Whether this is a common tactic for gut-colonizing bacteria to invade the intestinal ecosystem especially in human needs to be verified in the future.

Stress Resistance

Within the intestinal lumen, enteric pathogens encounter severe stresses, such as bile salts, antimicrobial peptides, free fatty acids, enhanced osmolarity, and oxidative stress (Fang et al., 2016). To survive these adverse environments, bacteria have developed various delicate mechanisms. As a versatile molecular machine, T6SS has been found to play crucial roles in the bacterial stress response and contribute to cell survival under multiple environmental challenges. *Vibrio anguillarum* T6SS is regulated by the general stress response regulator RpoS and is involved in its resistance to hydrogen peroxide, ethanol, and low pH (Weber et al., 2009). Upon activation by RpoS and the global oxidative stress regulator OxyR, enterohaemorrhagic *Escherichia coli* (EHEC) uses its T6SS to secrete a Mn-containing catalase, KatN, thus providing a higher resistance to reactive oxygen species (ROS) produced by the host and enhancing survival levels in the host (Wan et al., 2017). *Y. pseudotuberculosis* T6SS4 was required for bacterial survival under osmotic, oxidative, and acidic stress and for resistance to bile salts, and its expression was regulated by various stress response regulators, such as the stationary growth phase stress σ factor RpoS, the global oxidative stress regulator OxyR, and the acid/osmotic regulator OmpR (Gueguen et al., 2013; Zhang W. et al., 2013; Guan et al., 2015; Wang et al., 2015). In *V. cholerae* O1, activation of T6SS has been shown to be dependent on the osmolarity of the milieu (Ishikawa et al., 2012). In addition, in the intestine, *V. cholerae* T6SS genes are overexpressed under mucin (intestinal host factors) and microbiota-modified bile salt conditions (Bachmann et al., 2015). Bile salts can also activate expression of T6SS genes in *Salmonella typhimurium* (Sana et al., 2016) and *C. jejuni* (Lertpiriyapong et al., 2012). These studies on gene expression regulation suggest that T6SS is expressed in the intestine and could provide resistance to multiple stresses, increasing bacterial adaptability or survival in the intestinal ecosystem.

Other Potential Functions

Recently, it was suggested that T6SS in *V. cholerae* serves as a predatory weapon and fosters horizontal gene transfer. For incorporation of DNA released by lysed cells into a competent predator cell, natural transformation and evolution can occur (Borgeaud et al., 2015). Thus, T6SS may promote co-evolution of bacterial microflora within their environments, including intestinal ecosystems.

Compelling data showed that *H. hepaticus* interacts with intestinal epithelial cells (IECs) and employs T6SS to limit within-host growth and virulence (Chow and Mazmanian, 2010). This feature was regarded as T6SS function of anti-virulence (Jani and Cotter, 2010). Nevertheless, this phenomenon is rarely seen.

To summarize, we constructed a schematic diagram showing the functions of T6SS in the intestinal ecosystem (**Figure 1**).

COMMENSAL INTESTINAL MICROBES WITH T6SS CLUSTERS

Bacteroidetes

Bacteroidetes, a phylum of Gram-negative bacteria, is highly abundant in the gastrointestinal tracts of humans and other mammals (Lozupone et al., 2012; Russell et al., 2014; Wexler and Goodman, 2017). Despite Bacteroidales being predominant in the mammalian gut, T6SSs in Bacteroidetes species were not identified until 2014, perhaps because the T6SS in Bacteroidetes does not have sufficient sequence similarity with core T6SS proteins of Proteobacteria for protein-protein comparisons (e.g., BLASTP) or protein-profile comparisons (e.g., Pfam, COG) (Russell et al., 2014; Coyne et al., 2016). Studies have revealed that the T6SS loci are segregated into three distinct genetic architectures (GA1-GA3), among which the T6SS loci GA1 and GA2 are contained on highly similar integrative conjugative element (ICE) (Coyne et al., 2016). Among the numerous mechanisms that compete in the extremely dense ecosystem of the gut, T6SSs are probably very prevalent antagonistic systems in gut Bacteroidales (Wilson et al., 2015; Chatzidaki-Livanis et al., 2016; Coyne et al., 2016; Coyne and Comstock, 2019), as the Bacteroides T6SS genes are widespread in human gut metagenomes (Verster et al., 2017). Given that T6SSs in Bacteroidetes mediate inter-bacterial antagonism against

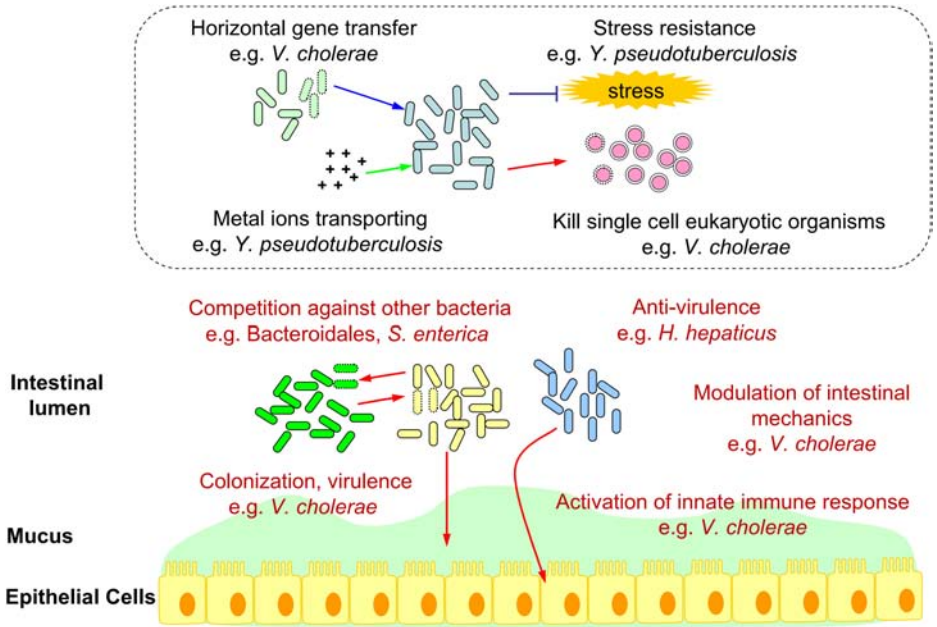

FIGURE 1 | Schematic diagram of bacterial T6SS functions in the intestinal ecosystem. T6SS functions verified in the gut (e.g., Competition against other bacteria, Colonization, Virulence, Anti-virulence, Modulation of intestinal mechanics, and Activation of innate immune response.) were marked in red. Deduced T6SS functions in the gut (e.g., Horizontal gene transfer, Metal ions transporting, Stress resistance, and Kill single cell eukaryotic organisms.) based on *in vitro* analysis were shown in the dotted box.

pathogens and in view of the observed stability of Bacteroidetes in the healthy human intestine, it predicts that T6SS in the stable Bacteroidetes community contributes to intestinal homeostasis. We believe that further research on T6SSs in Bacteroidales species will add to our understanding of microbial stability in the gut and to our ability to diagnose and treat gut microbial infections.

ENTERIC PATHOGENS WITH T6SS CLUSTERS

Vibrio cholerae

Vibrio cholerae is a Gram-negative pathogen consisting of over 200 serogroups that usually cause diarrhoeal diseases ranging from cholera to mild gastroenteritis after ingestion of contaminated food or water containing them (Kitaoka et al., 2011; Unterweger et al., 2014). All *V. cholerae* strains examined to date contain T6SS gene clusters (Unterweger et al., 2012). This microorganism provided several important and initial discoveries about T6SS, including the definition of the contact-dependent secretion model (Pukatzki et al., 2006; Basler et al., 2012), identification of T6SS-dependent effector-immunity pairs (Dong et al., 2013; Russell et al., 2013; Altindis et al., 2015), and induction of intestinal inflammation through actin cross-linking in host cells (Ma and Mekalanos, 2010). Recently, *in vivo* analysis presented new insight on the pathogenic mechanism of *V. cholerae* with T6SS. T6SS in *V. cholerae* acts on commensal bacteria *A. pasteurianus* to accelerate death of the *Drosophila* host (Fast et al., 2018). Another study revealed the roles of *V. cholerae* T6SS in antagonism against host commensal microbiota *in vivo* over their niche, which facilitated bacterial colonization of the mice gut (Zhao et al., 2018). Besides killing host gut bacterial symbionts, *V. cholerae* T6SS could modulate host intestinal mechanics, enhancing intestinal movements that led to expulsion of resident microbiota by the host (Logan et al., 2018).

Vibrio parahaemolyticus

Research indicated that vpT6SS2 contributed to adhesion of *V. parahaemolyticus* to host cells (Yu et al., 2012). In addition, the vpT6SS2 effector could induce autophagy in macrophage cells without causing apparent cytotoxicity (Yu et al., 2015).

Salmonella enterica

Experiments suggested that T6SS contributed to pathogenicity, at least in the *S. enterica* serotypes Gallinarum (Blondel et al., 2013), Enteritidis (Blondel et al., 2010; Troxell, 2018), Typhi (Wang et al., 2011), Dublin (Pezoa et al., 2014), and Typhimurium (Mulder et al., 2012). A recent study provided *in vivo* evidence that *S. typhimurium* used T6SS as a weapon to kill commensal bacteria (*K. oxytoca*) to successfully colonize the mouse gut (Sana et al., 2016).

Yersinia pseudotuberculosis

Studies of *Y. pseudotuberculosis* revealed roles for T6SS in responses to various stressors and identified corresponding regulators, including OmpR (Gueguen et al., 2013; Zhang W. et al., 2013), OxyR (Wang et al., 2015), ZntR (Wang et al., 2017),

RpoS (Guan et al., 2015), RovM (Song et al., 2015), and YpsI/YtbI (Zhang et al., 2011). Notably, T6SS4 in *Y. pseudotuberculosis* was found to be involved in zinc transportation by secreting a zinc-binding protein YezP to mitigate the impact of detrimental hydroxyl radicals under oxidative stress (Wang et al., 2015). The contribution of T6SS to ion transport was also confirmed in *B. thailandensis* and *P. aeruginosa* (Lin et al., 2017; Si et al., 2017a,b).

Escherichia coli

Escherichia coli are model bacteria that have been studied extensively. Although less abundant than Bacteroidales in the gastrointestinal tract, symbiotic gut *E. coli* play important roles in colonization resistance against enteric pathogens of the proteobacterial phylum (Coyne and Comstock, 2019). To date, more than 150 *E. coli* strains have been identified. Most are harmless, but several serotypes have been proposed to be pathogenic and may cause significant diarrheal and extraintestinal diseases (Croxen et al., 2013). The current knowledge regarding the prevalence, the assembly, the regulation, and the roles of the T6SS in *E. coli* has been reviewed (Journet and Cascales, 2016). It has been suggested that T6SS contributes to pathogenesis in *E. coli* strains. For example, T6SS-dependent Hcp1 in *E. coli* K1 induced actin cytoskeleton rearrangement, apoptosis, and release of interleukin-6 (IL-6) and IL-8 in human brain microvascular endothelial cells (HBMEC) (Zhou et al., 2012). Further, T6SS in avian pathogenic *E. coli* (APEC) strains contributes to APEC pathogenesis (Ma et al., 2018). Several

TABLE 1 | Intestinal bacteria with functional T6SSs that have been verified experimentally.

Bacteria species	No. of T6SS loci	Experimental strains	T6SS associated phenotypes	References
Aeromonas hydrophila	1	SSU	Induce host cell toxicity by ADP ribosylation of actin	Suarez et al., 2010
Bacteroides fragilis	1	TM4000, ATCC43858, ATCC43859	Virulence and strain competition	Casterline et al., 2017
		NCTC 9343, 638R	Competition	Chatzidaki-Livanis et al., 2016
		NCTC 9343	Interbacterial antagonism	Russell et al., 2014
Campylobacter jejuni	1	subsp. *jejuni* serotype O:3	Host cell adhesion, invasion, colonization; adaptation to DCA	Lertpiriyapong et al., 2012
		108	Cytotoxicity toward red blood cells	Bleumink-Pluym et al., 2013
Citrobacter freundii	1–2	CF74	Adhesion and cytotoxicity to host cells	Liu et al., 2015
Citrobacter rodentium	1–2	DBS100[ATCC51459]	Interbacterial killing	Gueguen et al., 2014
Edwardsiella tarda	1–2	EIB202	NLRP3 inflammasome inhibition, bacterial colonization *in vivo*	Chen et al., 2017
Enterobacter cloacae	1–2	subsp. *cloacae* ATCC13047	Interbacterial competition	Zhang H. et al., 2013
Escherichia coli	1–3	K12 W3110, EAEC 17-2	Bacterial growth competition	Brunet et al., 2013
		APEC SEPT362	Pathogenesis	de Pace et al., 2010
		APEC SEPT362	Enhance biofilm formation	de Pace et al., 2011
		RS218	Pathogenicity in HBMEC	Zhou et al., 2012
		TW-XM (O2:K1)	Pathogenic pathways	Ma J. et al., 2014
		EHEC EDL933	Virulence	Wan et al., 2017
		STEC	Virulence	Aas et al., 2018
Helicobacter hepaticus	1	ATCC51449	Modulate and exacerbate the innate pro-inflammatory effect	Bartonickova et al., 2013
		ATCC51449	Limiting colonization and intestinal inflammation	Chow and Mazmanian, 2010
Salmonella enterica	1–2	Typhimurium LT2	Pathogenesis	Mulder et al., 2012
		Gallinarum NCTC13346, Enteritidis NCTC13349	Chicken colonization	Blondel et al., 2010
		Typhi GIFU10007	Cytotoxicity of human epithelial cells	Wang et al., 2011
		Typhimurium 14028s	Chicken colonization	Blondel et al., 2013
		Dublin CT_02021853	Colonization of mice and chickens	Pezoa et al., 2014
		Enteritidis	Virulence	Troxell, 2018
		SL1344	Killing of commensal bacteria, Colonization of the host gut	Sana et al., 2016
Shigella sonnei	1	CIP106347	Interbacterial competition, niche occupancy	Anderson et al., 2017
Vibrio alginolyticus	1–2	EPGS, MVP01, ATCC33787	Regulated by QS and RpoN	Sheng et al., 2012
Vibrio anguillarum	1	NB10 serotype O1	Modulates quorum sensing and stress response	Weber et al., 2009

(Continued)

TABLE 1 | Continued

Bacteria species	No. of T6SS loci	Experimental strains	T6SS associated phenotypes	References
Vibrio cholerae	1	C6706	Microbial antagonistic interaction, intestinal colonization, virulence	Zhao et al., 2018
		O37 strain V52	Virulence, competition	Zheng et al., 2011
		O37 strain V52	Intra- and interspecific competition	Unterweger et al., 2012
		A1552	Foster horizontal gene transfer	Borgeaud et al., 2015
		O37 strain V52	Microbial pathogenesis	Pukatzki et al., 2006
		O37 strain V52	Induces an inflammatory diarrhea	Ma and Mekalanos, 2010
		O37 strain V52	Virulence	Miyata et al., 2011
		Multiple strains	Intraspecific competition	Unterweger et al., 2014
		O37 strain V52	Interspecies competition	MacIntyre et al., 2010
		C6706	Intermicrobial competition	Logan et al., 2018
Vibrio fluvialis	2	85003	Environmental survival	Pan et al., 2018
Vibrio parahaemolyticus	1–2	HZ	Cell adhesion and cytotoxicity	Yu et al., 2012
		RIMD 2210633	Enhance environmental fitness in marine environments, anti-bacterial activity	Salomon et al., 2013
		HZ	Induce autophagy in macrophages	Yu et al., 2015
Yersinia enterocolitica	1	subsp. *enterocolitica* 8081	Encumber bacteria invasion and survival in host cells	Jaakkola et al., 2015
Yersinia pseudotuberculosis	4–6	YpIII	Maintain intracellular pH homeostasis	Zhang W. et al., 2013
		IP31758	Survival in high osmolarity, resistance to deoxycholate	Gueguen et al., 2013
		YpIII	Transports Zn^{2+} to combat multiple stresses and host immunity	Wang et al., 2015

structural proteins of T6SS in *E. coli* have been studied to clarify the specific functions of these T6SS components (Felisberto-Rodrigues et al., 2011; Aschtgen et al., 2012; Durand et al., 2012). However, whether *E. coli* gut symbionts have T6SSs that function in colonization resistance against enteric pathogens, and how enteric pathogenic *E. coli* T6SSs function in the intestinal ecosystem still remain enigmatic.

Notably, the T6SS apparatus has a common evolutionary origin with phage tail-associated protein complexes. Yet, the involvement of phages in the evolution of bacterial T6SS remains unclear.

OTHER ENTERIC PATHOGENS

Type VI secretion system in some other enteric pathogens has also been studied. In *C. jejuni*, T6SS mediates host cell adhesion, invasion, colonization, and adaptation to deoxycholic acid (DCA) (Lertpiriyapong et al., 2012). In *Citrobacter freundii*, T6SS plays a wide-ranging role in the regulation of the flagellar system and in motility; it is also involved in the adherence and cytotoxicity to host cells (Liu et al., 2015). T6SS2 in *Vibrio fluvialis* is associated with anti-bacterial activity and contributes to bacteria survival in highly competitive environments (Pan et al., 2018). The T6SS effector VgrG1 from *A. hydrophila* induces host cell toxicity by ADP ribosylation of actin (Suarez et al., 2010). In *E. tarda*, the T6SS effector EvpP significantly inhibits NLRP3 inflammasome activation by inhibiting the Ca^{2+}-dependent MAPK-Jnk pathway (Chen et al., 2017). Additionally, functional T6SSs have been verified in the enteric pathogens *Enterobacter cloacae* (Whitney et al., 2014), *Edwardsiella ictaluri* (Rogge and Thune, 2011), *Yersinia enterocolitica* (Jaakkola et al., 2015), and *V. anguillarum* (Weber et al., 2009). To facilitate retrieval for future research, we have listed the experimentally verified intestinal bacteria that contain functional T6SS loci in **Table 1**.

CONCLUDING REMARKS

Although the composition and function of the intestinal microbiota has been well documented, the underlying mechanisms of its assembly remain poorly understood. T6SS is a contact-dependent molecular weapon primarily used for interbacterial competition. Considering that T6SS loci exist in 50% of intestinal Bacteroidetes, which are the dominant microflora in the gastrointestinal system, and in some other commensal intestinal microbes and enteric pathogens, T6SS might be widely used in the intestinal ecosystem to shape microbiota composition. Actually, several seminal studies have greatly advanced our understanding of the importance of T6SS in the intestine. These studies showed that the T6SS antibacterial weapons are not only used by pathogens to colonize their hosts, but also by gut commensals to prevent pathogen colonization. Interestingly, two studies in *V. cholera* further indicated that microbial antagonistic interactions mediated by T6SS could elevate disease symptoms by activating host innate immune responses (Fast et al., 2018; Zhao et al., 2018). Moreover, using

a zebrafish model, Logan et al. (2018) revealed that the T6SS of *V. cholera* could modulate host intestinal mechanics to redefine the gut microbial composition. These findings provide new insights into the mechanisms used by enteric pathogens for gut colonization. As for the gut commensals, Verster et al. (2017) investigate the prevalence and roles of the T6SS in the human gut microbiome by using metagenomic analyses. In addition to the compatibility with species GA1 and GA2, GA3 is associated with increased Bacteroides abundance in infant microbiomes, and confers an advantage in Bacteroides-rich ecosystems. Thus, it revealed the prevalence and potential role of T6SS-dependent competition in shaping human gut microbial composition (Verster et al., 2017).

It is noteworthy that sometimes a few invertebrate models and small animal models (e.g., Drosophila, zebrafish) were used to analyze T6SS functions in the intestinal ecosystem (Fast et al., 2018; Logan et al., 2018). These results should be further verified in mammalian models. In addition, further *in vivo* studies are urgently needed to confirm whether anti-fungal, stress-resistant and metal ion-acquiring T6SSs are functional in the intestinal ecosystem. Studies of T6SS in the intestinal ecosystem are just beginning and have a long way to go. As T6SS in several bacterial pathogens contributes to virulence against the host, the T6SS apparatus could be exploited as a therapeutic drug target. Based on this possibility, a novel natural antimicrobial was identified that can reduce the pathogenicity of *Campylobacter* T6SS *in vitro* and also decrease its colonization *in vivo* (Sima et al., 2018). These findings suggest that studies on T6SS functions in the intestinal ecosystem may provide a theoretical basis for the development of new medicines for various pathogenic infections in the future.

AUTHOR CONTRIBUTIONS

CC and XY collected and assessed the references. CC and XS contributed in the proposal and guidelines of the review. CC and XY wrote this manuscript.

FUNDING

This work was funded by the National Natural Science Foundation of China (Nos. 31725003 and 31670053) and the Open Project Program of the State Key Laboratory of Pathogen and Biosecurity (No. SKLPBS1825).

REFERENCES

Aas, C. G., Drablos, F., Haugum, K., and Afset, J. E. (2018). Comparative transcriptome profiling reveals a potential role of type VI secretion system and fimbriae in virulence of Non-O157 shiga toxin-producing *Escherichia coli*. *Front. Microbiol.* 9:1416. doi: 10.3389/fmicb.2018.01416

Altindis, E., Dong, T., Catalano, C., and Mekalanos, J. (2015). Secretome analysis of *Vibrio cholerae* type VI secretion system reveals a new effector-immunity pair. *mBio* 6:e00075. doi: 10.1128/mBio.00075-15

Anderson, M. C., Vonaesch, P., Saffarian, A., Marteyn, B. S., and Sansonetti, P. J. (2017). *Shigella sonnei* encodes a functional T6SS used for interbacterial competition and niche occupancy. *Cell Host Microbe* 21, 769.e3–776.e3. doi: 10.1016/j.chom.2017.05.004

Aschtgen, M. S., Zoued, A., Lloubes, R., Journet, L., and Cascales, E. (2012). The C-tail anchored TssL subunit, an essential protein of the enteroaggregative *Escherichia coli* Sci-1 Type VI secretion system, is inserted by YidC. *Microbiologyopen* 1, 71–82. doi: 10.1002/mbo3.9

Aubert, D. F., Xu, H., Yang, J., Shi, X., Gao, W., Li, L., et al. (2016). A *Burkholderia* type VI effector deamidates Rho GTPases to activate the pyrin inflammasome and trigger inflammation. *Cell Host Microbe* 19, 664–674. doi: 10.1016/j.chom.2016.04.004

Bachmann, V., Kostiuk, B., Unterweger, D., Diaz-Satizabal, L., Ogg, S., and Pukatzki, S. (2015). Bile salts modulate the mucin-activated type VI secretion system of pandemic *Vibrio cholerae*. *PLoS Negl. Trop. Dis.* 9:e0004031. doi: 10.1371/journal.pntd.0004031

Bartonickova, L., Sterzenbach, T., Nell, S., Kops, F., Schulze, J., Venzke, A., et al. (2013). Hcp and VgrG1 are secreted components of the *Helicobacter hepaticus* type VI secretion system and VgrG1 increases the bacterial colitogenic potential. *Cell Microbiol.* 15, 992–1011. doi: 10.1111/cmi.12094

Basler, M., Pilhofer, M., Henderson, G. P., Jensen, G. J., and Mekalanos, J. J. (2012). Type VI secretion requires a dynamic contractile phage tail-like structure. *Nature* 483, 182–186. doi: 10.1038/nature10846

Belkaid, Y., and Hand, T. W. (2014). Role of the microbiota in immunity and inflammation. *Cell* 157, 121–141. doi: 10.1016/j.cell.2014.03.011

Bleumink-Pluym, N. M., van Alphen, L. B., Bouwman, L. I., Wosten, M. M., and van Putten, J. P. (2013). Identification of a functional type VI secretion system in *Campylobacter jejuni* conferring capsule polysaccharide sensitive cytotoxicity. *PLoS Pathog.* 9:e1003393. doi: 10.1371/journal.ppat.1003393

Blondel, C. J., Jimenez, J. C., Leiva, L. E., Alvarez, S. A., Pinto, B. I., Contreras, F., et al. (2013). The type VI secretion system encoded in *Salmonella* pathogenicity island 19 is required for *Salmonella enterica* serotype Gallinarum survival within infected macrophages. *Infect. Immun.* 81, 1207–1220. doi: 10.1128/IAI.01165-12

Blondel, C. J., Yang, H. J., Castro, B., Chiang, S., Toro, C. S., Zaldivar, M., et al. (2010). Contribution of the type VI secretion system encoded in SPI-19 to chicken colonization by *Salmonella enterica* serotypes Gallinarum and Enteritidis. *PLoS One* 5:e11724. doi: 10.1371/journal.pone.0011724

Borgeaud, S., Metzger, L. C., Scrignari, T., and Blokesch, M. (2015). The type VI secretion system of *Vibrio cholerae* fosters horizontal gene transfer. *Science* 347, 63–67. doi: 10.1126/science.1260064

Boyer, F., Fichant, G., Berthod, J., Vandenbrouck, Y., and Attree, I. (2009). Dissecting the bacterial type VI secretion system by a genome wide in silico analysis: what can be learned from available microbial genomic resources? *BMC Genomics* 10:104. doi: 10.1186/1471-2164-10-104

Brunet, Y. R., Espinosa, L., Harchouni, S., Mignot, T., and Cascales, E. (2013). Imaging type VI secretion-mediated bacterial killing. *Cell Rep.* 3, 36–41. doi: 10.1016/j.celrep.2012.11.027

Brunet, Y. R., Zoued, A., Boyer, F., Douzi, B., and Cascales, E. (2015). The Type VI secretion TssEFGK-VgrG phage-like baseplate is recruited to the TssJLM membrane complex via multiple contacts and serves as assembly platform for tail tube/sheath polymerization. *PLoS Genet.* 11:e1005545. doi: 10.1371/journal.pgen.1005545

Cascales, E., and Cambillau, C. (2012). Structural biology of type VI secretion systems. *Philos. Trans. R. Soc. Lond. B Biol. Sci.* 367, 1102–1111. doi: 10.1098/rstb.2011.0209

Casterline, B. W., Hecht, A. L., Choi, V. M., and Bubeck Wardenburg, J. (2017). The *Bacteroides fragilis* pathogenicity island links virulence and strain competition. *Gut Microbes* 8, 374–383. doi: 10.1080/19490976.2017.1290758

Chassaing, B., and Cascales, E. (2018). antibacterial weapons: targeted destruction in the microbiota. *Trends Microbiol.* 26, 329–338. doi: 10.1016/j.tim.2018.01.006

Chatzidaki-Livanis, M., Geva-Zatorsky, N., and Comstock, L. E. (2016). *Bacteroides fragilis* type VI secretion systems use novel effector and immunity proteins to antagonize human gut Bacteroidales species. *Proc. Natl. Acad. Sci. U.S.A.* 113, 3627–3632. doi: 10.1073/pnas.1522510113

Chen, H., Yang, D., Han, F., Tan, J., Zhang, L., Xiao, J., et al. (2017). The bacterial T6SS effector EvpP prevents NLRP3 inflammasome activation by inhibiting the Ca2+-dependent MAPK-Jnk pathway. *Cell Host Microbe* 21, 47–58. doi: 10.1016/j.chom.2016.12.004

Chow, J., and Mazmanian, S. K. (2010). A pathobiont of the microbiota balances host colonization and intestinal inflammation. *Cell Host Microbe* 7, 265–276. doi: 10.1016/j.chom.2010.03.004

Cianfanelli, F. R., Monlezun, L., and Coulthurst, S. J. (2016). Aim, load, fire: the type VI secretion system, a bacterial nanoweapon. *Trends Microbiol.* 24, 51–62. doi: 10.1016/j.tim.2015.10.005

Coulthurst, S. (2019). The Type VI secretion system: a versatile bacterial weapon. *Microbiology* 165, 503–515. doi: 10.1099/mic.0.000789

Coyne, M. J., and Comstock, L. E. (2019). Type VI secretion systems and the gut microbiota. *Microbiol Spectr* 7:PSIB–0009–2018. doi: 10.1128/microbiolspec.PSIB-0009-2018

Coyne, M. J., Roelofs, K. G., and Comstock, L. E. (2016). Type VI secretion systems of human gut Bacteroidales segregate into three genetic architectures, two of which are contained on mobile genetic elements. *BMC Genomics* 17:58. doi: 10.1186/s12864-016-2377-z

Coyne, M. J., Zitomersky, N. L., McGuire, A. M., Earl, A. M., and Comstock, L. E. (2014). Evidence of extensive DNA transfer between bacteroidales species within the human gut. *mBio* 5, e01305–e01314. doi: 10.1128/mBio.01305-14

Croxen, M. A., Law, R. J., Scholz, R., Keeney, K. M., Wlodarska, M., and Finlay, B. B. (2013). Recent advances in understanding enteric pathogenic *Escherichia coli*. *Clin. Microbiol. Rev.* 26, 822–880. doi: 10.1128/CMR.00022-13

de Pace, F., Boldrin de Paiva, J., Nakazato, G., Lancellotti, M., Sircili, M. P., Guedes Stehling, E., et al. (2011). Characterization of IcmF of the type VI secretion system in an avian pathogenic *Escherichia coli* (APEC) strain. *Microbiology* 157(Pt 10), 2954–2962. doi: 10.1099/mic.0.050005-0

de Pace, F., Nakazato, G., Pacheco, A., de Paiva, J. B., Sperandio, V., and da Silveira, W. D. (2010). The type VI secretion system plays a role in type 1 fimbria expression and pathogenesis of an avian pathogenic *Escherichia coli* strain. *Infect. Immun.* 78, 4990–4998. doi: 10.1128/IAI.00531-10

Dong, T. G., Ho, B. T., Yoder-Himes, D. R., and Mekalanos, J. J. (2013). Identification of T6SS-dependent effector and immunity proteins by Tn-seq in *Vibrio cholerae*. *Proc. Natl. Acad. Sci. U.S.A.* 110, 2623–2628. doi: 10.1073/pnas.1222783110

Durand, E., Cambillau, C., Cascales, E., and Journet, L. (2014). VgrG, Tae, Tle, and beyond: the versatile arsenal of Type VI secretion effectors. *Trends Microbiol.* 22, 498–507. doi: 10.1016/j.tim.2014.06.004

Durand, E., Zoued, A., Spinelli, S., Watson, P. J., Aschtgen, M. S., Journet, L., et al. (2012). Structural characterization and oligomerization of the TssL protein, a component shared by bacterial type VI and type IVb secretion systems. *J. Biol. Chem.* 287, 14157–14168. doi: 10.1074/jbc.M111.338731

Faith, J. J., Guruge, J. L., Charbonneau, M., Subramanian, S., Seedorf, H., Goodman, A. L., et al. (2013). The long-term stability of the human gut microbiota. *Science* 341:1237439. doi: 10.1126/science.1237439

Fang, F. C., Frawley, E. R., Tapscott, T., and Vazquez-Torres, A. (2016). Bacterial stress responses during host infection. *Cell Host Microbe* 20, 133–143. doi: 10.1016/j.chom.2016.07.009

Fast, D., Kostiuk, B., Foley, E., and Pukatzki, S. (2018). Commensal pathogen competition impacts host viability. *Proc. Natl. Acad. Sci. U.S.A.* 115, 7099–7104. doi: 10.1073/pnas.1802165115

Felisberto-Rodrigues, C., Durand, E., Aschtgen, M. S., Blangy, S., Ortiz-Lombardia, M., Douzi, B., et al. (2011). Towards a structural comprehension of bacterial type VI secretion systems: characterization of the TssJ-TssM complex of an *Escherichia coli* pathovar. *PLoS Pathog.* 7:e1002386. doi: 10.1371/journal.ppat.1002386

Fu, Y., Waldor, M. K., and Mekalanos, J. J. (2013). Tn-Seq analysis of *Vibrio cholerae* intestinal colonization reveals a role for T6SS-mediated antibacterial activity in the host. *Cell Host Microbe* 14, 652–663. doi: 10.1016/j.chom.2013.11.001

Gallique, M., Decoin, V., Barbey, C., Rosay, T., Feuilloley, M. G., Orange, N., et al. (2017). Contribution of the *Pseudomonas* fluorescens MFE01 Type VI secretion system to biofilm formation. *PLoS One* 12:e0170770. doi: 10.1371/journal.pone.0170770

Garcia-Bayona, L., and Comstock, L. E. (2018). Bacterial antagonism in host-associated microbial communities. *Science* 361:eaat2456. doi: 10.1126/science.aat2456

Gielda, L. M., and DiRita, V. J. (2012). Zinc competition among the intestinal microbiota. *mBio* 3:e00171-12. doi: 10.1128/mBio.00171-12

Guan, J., Xiao, X., Xu, S., Gao, F., Wang, J., Wang, T., et al. (2015). Roles of RpoS in *Yersinia pseudotuberculosis* stress survival, motility, biofilm formation and type VI secretion system expression. *J. Microbiol.* 53, 633–642. doi: 10.1007/s12275-015-0099-6

Gueguen, E., Durand, E., Zhang, X. Y., d'Amalric, Q., Journet, L., and Cascales, E. (2013). Expression of a *Yersinia pseudotuberculosis* type VI secretion system is responsive to envelope stresses through the OmpR transcriptional activator. *PLoS One* 8:e66615. doi: 10.1371/journal.pone.0066615

Gueguen, E., Wills, N. M., Atkins, J. F., and Cascales, E. (2014). Transcriptional frameshifting rescues *Citrobacter rodentium* type VI secretion by the production of two length variants from the prematurely interrupted tssM gene. *PLoS Genet.* 10:e1004869. doi: 10.1371/journal.pgen.1004869

Haapalainen, M., Mosorin, H., Dorati, F., Wu, R. F., Roine, E., Taira, S., et al. (2012). Hcp2, a secreted protein of the phytopathogen *Pseudomonas syringae* pv. tomato DC3000, is required for fitness for competition against bacteria and yeasts. *J. Bacteriol.* 194, 4810–4822. doi: 10.1128/JB.00611-12

Hecht, A. L., Casterline, B. W., Earley, Z. M., Goo, Y. A., Goodlett, D. R., and Bubeck Wardenburg, J. (2016). Strain competition restricts colonization of an enteric pathogen and prevents colitis. *EMBO Rep.* 17, 1281–1291. doi: 10.15252/embr.201642282

Hood, R. D., Singh, P., Hsu, F., Guvener, T., Carl, M. A., Trinidad, R. R., et al. (2010). A type VI secretion system of *Pseudomonas aeruginosa* targets a toxin to bacteria. *Cell Host Microbe* 7, 25–37. doi: 10.1016/j.chom.2009.12.007

Ishikawa, T., Sabharwal, D., Broms, J., Milton, D. L., Sjostedt, A., Uhlin, B. E., et al. (2012). Pathoadaptive conditional regulation of the type VI secretion system in *Vibrio cholerae* O1 strains. *Infect. Immun.* 80, 575–584. doi: 10.1128/IAI.05510-11

Jaakkola, K., Somervuo, P., and Korkeala, H. (2015). Comparative genomic hybridization analysis of *Yersinia enterocolitica* and *Yersinia pseudotuberculosis* identifies genetic traits to elucidate their different ecologies. *Biomed. Res. Int.* 2015:760494. doi: 10.1155/2015/760494

Jani, A. J., and Cotter, P. A. (2010). Type VI secretion: not just for pathogenesis anymore. *Cell Host Microbe* 8, 2–6. doi: 10.1016/j.chom.2010.06.012

Jiang, F., Wang, X., Wang, B., Chen, L., Zhao, Z., Waterfield, N. R., et al. (2016). The *Pseudomonas aeruginosa* type VI secretion PGAP1-like effector induces host autophagy by activating endoplasmic reticulum stress. *Cell Rep.* 16, 1502–1509. doi: 10.1016/j.celrep.2016.07.012

Journet, L., and Cascales, E. (2016). The type VI secretion system in *Escherichia coli* and related species. *EcoSal Plus* 7, 1–20. doi: 10.1128/ecosalplus.ESP-0009-2015

Kitaoka, M., Miyata, S. T., Unterweger, D., and Pukatzki, S. (2011). Antibiotic resistance mechanisms of *Vibrio cholerae*. *J. Med. Microbiol.* 60(Pt 4), 397–407. doi: 10.1099/jmm.0.023051-0

Lertpiriyapong, K., Gamazon, E. R., Feng, Y., Park, D. S., Pang, J., Botka, G., et al. (2012). *Campylobacter jejuni* type VI secretion system: roles in adaptation to deoxycholic acid, host cell adherence, invasion, and in vivo colonization. *PLoS One* 7:e42842. doi: 10.1371/journal.pone.0042842

Lin, J., Zhang, W., Cheng, J., Yang, X., Zhu, K., Wang, Y., et al. (2017). A *Pseudomonas* T6SS effector recruits PQS-containing outer membrane vesicles for iron acquisition. *Nat. Commun.* 8:14888. doi: 10.1038/ncomms14888

Liu, L., Hao, S., Lan, R., Wang, G., Xiao, D., Sun, H., et al. (2015). The type VI secretion system modulates flagellar gene expression and secretion in *Citrobacter freundii* and contributes to adhesion and cytotoxicity to host cells. *Infect. Immun.* 83, 2596–2604. doi: 10.1128/IAI.03071-14

Logan, S. L., Thomas, J., Yan, J., Baker, R. P., Shields, D. S., Xavier, J. B., et al. (2018). The *Vibrio cholerae* type VI secretion system can modulate host intestinal mechanics to displace gut bacterial symbionts. *Proc. Natl. Acad. Sci. U.S.A.* 115, E3779–E3787. doi: 10.1073/pnas.1720133115

Lozupone, C. A., Stombaugh, J. I., Gordon, J. I., Jansson, J. K., and Knight, R. (2012). Diversity, stability and resilience of the human gut microbiota. *Nature* 489, 220–230. doi: 10.1038/nature11550

Ma, A. T., and Mekalanos, J. J. (2010). *In vivo* actin cross-linking induced by *Vibrio cholerae* type VI secretion system is associated with intestinal inflammation. *Proc. Natl. Acad. Sci. U.S.A.* 107, 4365–4370. doi: 10.1073/pnas.0915156107

Ma, J., Bao, Y., Sun, M., Dong, W., Pan, Z., Zhang, W., et al. (2014). Two functional type VI secretion systems in avian pathogenic *Escherichia coli* are involved in

different pathogenic pathways. *Infect. Immun.* 82, 3867–3879. doi: 10.1128/IAI.01769-14

Ma, L. S., Hachani, A., Lin, J. S., Filloux, A., and Lai, E. M. (2014). *Agrobacterium tumefaciens* deploys a superfamily of type VI secretion DNase effectors as weapons for interbacterial competition in planta. *Cell Host Microbe* 16, 94–104. doi: 10.1016/j.chom.2014.06.002

Ma, J., Sun, M., Pan, Z., Song, W., Lu, C., and Yao, H. (2018). Three Hcp homologs with divergent extended loop regions exhibit different functions in avian pathogenic *Escherichia coli*. *Emerg. Microbes Infect.* 7:49. doi: 10.1038/s41426-018-0042-0

MacIntyre, D. L., Miyata, S. T., Kitaoka, M., and Pukatzki, S. (2010). The *Vibrio cholerae* type VI secretion system displays antimicrobial properties. *Proc. Natl. Acad. Sci. U.S.A.* 107, 19520–19524. doi: 10.1073/pnas.1012931107

Miyata, S. T., Kitaoka, M., Brooks, T. M., McAuley, S. B., and Pukatzki, S. (2011). Vibrio cholerae requires the type VI secretion system virulence factor VasX to kill *Dictyostelium discoideum*. *Infect. Immun.* 79, 2941–2949. doi: 10.1128/IAI.01266-10

Mulder, D. T., Cooper, C. A., and Coombes, B. K. (2012). Type VI secretion system-associated gene clusters contribute to pathogenesis of *Salmonella enterica serovar Typhimurium*. *Infect. Immun.* 80, 1996–2007. doi: 10.1128/IAI.06205-11

Pan, J., Zhao, M., Huang, Y., Li, J., Liu, X., Ren, Z., et al. (2018). Integration host factor modulates the expression and function of T6SS2 in *Vibrio fluvialis*. *Front. Microbiol.* 9:962. doi: 10.3389/fmicb.2018.00962

Pezoa, D., Blondel, C. J., Silva, C. A., Yang, H. J., Andrews-Polymenis, H., Santiviago, C. A., et al. (2014). Only one of the two type VI secretion systems encoded in the *Salmonella enterica* serotype Dublin genome is involved in colonization of the avian and murine hosts. *Vet. Res.* 45:2. doi: 10.1186/1297-9716-45-2

Pi, H., Jones, S. A., Mercer, L. E., Meador, J. P., Caughron, J. E., Jordan, L., et al. (2012). Role of catecholate siderophores in gram-negative bacterial colonization of the mouse gut. *PLoS One* 7:e50020. doi: 10.1371/journal.pone.0050020

Pukatzki, S., Ma, A. T., Revel, A. T., Sturtevant, D., and Mekalanos, J. J. (2007). Type VI secretion system translocates a phage tail spike-like protein into target cells where it cross-links actin. *Proc. Natl. Acad. Sci. U.S.A.* 104, 15508–15513. doi: 10.1073/pnas.0706532104

Pukatzki, S., Ma, A. T., Sturtevant, D., Krastins, B., Sarracino, D., Nelson, W. C., et al. (2006). Identification of a conserved bacterial protein secretion system in *Vibrio cholerae* using the *Dictyostelium* host model system. *Proc. Natl. Acad. Sci. U.S.A.* 103, 1528–1533. doi: 10.1073/pnas.0510322103

Rogge, M. L., and Thune, R. L. (2011). Regulation of the *Edwardsiella ictaluri* type III secretion system by pH and phosphate concentration through EsrA, EsrB, and EsrC. *Appl. Environ. Microbiol.* 77, 4293–4302. doi: 10.1128/AEM.00195-11

Russell, A. B., Hood, R. D., Bui, N. K., LeRoux, M., Vollmer, W., and Mougous, J. D. (2011). Type VI secretion delivers bacteriolytic effectors to target cells. *Nature* 475, 343–347. doi: 10.1038/nature10244

Russell, A. B., LeRoux, M., Hathazi, K., Agnello, D. M., Ishikawa, T., Wiggins, P. A., et al. (2013). Diverse type VI secretion phospholipases are functionally plastic antibacterial effectors. *Nature* 496, 508–512. doi: 10.1038/nature12074

Russell, A. B., Wexler, A. G., Harding, B. N., Whitney, J. C., Bohn, A. J., Goo, Y. A., et al. (2014). A type VI secretion-related pathway in *Bacteroidetes* mediates interbacterial antagonism. *Cell Host Microbe* 16, 227–236. doi: 10.1016/j.chom.2014.07.007

Salomon, D., Gonzalez, H., Updegraff, B. L., and Orth, K. (2013). *Vibrio parahaemolyticus* type VI secretion system 1 is activated in marine conditions to target bacteria, and is differentially regulated from system 2. *PLoS One* 8:e61086. doi: 10.1371/journal.pone.0061086

Salomon, D., and Orth, K. (2015). Type VI secretion system. *Curr. Biol.* 25, R265–R266. doi: 10.1016/j.cub.2015.02.031

Sana, T. G., Flaugnatti, N., Lugo, K. A., Lam, L. H., Jacobson, A., Baylot, V., et al. (2016). *Salmonella Typhimurium* utilizes a T6SS-mediated antibacterial weapon to establish in the host gut. *Proc. Natl. Acad. Sci. U.S.A.* 113, E5044–E5051. doi: 10.1073/pnas.1608858113

Sana, T. G., Lugo, K. A., and Monack, D. M. (2017). T6SS: the bacterial "fight club" in the host gut. *PLoS Pathog.* 13:e1006325. doi: 10.1371/journal.ppat.1006325

Sheng, L., Gu, D., Wang, Q., Liu, Q., and Zhang, Y. (2012). Quorum sensing and alternative sigma factor RpoN regulate type VI secretion system I (T6SSVA1) in fish pathogen *Vibrio alginolyticus*. *Arch. Microbiol.* 194, 379–390. doi: 10.1007/s00203-011-0780-z

Si, M., Wang, Y., Zhang, B., Zhao, C., Kang, Y., Bai, H., et al. (2017a). The type VI secretion system engages a redox-regulated dual-functional heme transporter for zinc acquisition. *Cell Rep.* 20, 949–959. doi: 10.1016/j.celrep.2017.06.081

Si, M., Zhao, C., Burkinshaw, B., Zhang, B., Wei, D., Wang, Y., et al. (2017b). Manganese scavenging and oxidative stress response mediated by type VI secretion system in *Burkholderia thailandensis*. *Proc. Natl. Acad. Sci. U.S.A.* 114, E2233–E2242. doi: 10.1073/pnas.1614902114

Silverman, J. M., Brunet, Y. R., Cascales, E., and Mougous, J. D. (2012). Structure and regulation of the type VI secretion system. *Annu. Rev. Microbiol.* 66, 453–472. doi: 10.1146/annurev-micro-121809-151619

Sima, F., Stratakos, A. C., Ward, P., Linton, M., Kelly, C., Pinkerton, L., et al. (2018). A novel natural antimicrobial can reduce the *in vitro* and *in vivo* pathogenicity of T6SS positive *Campylobacter jejuni* and *Campylobacter coli* chicken isolates. *Front. Microbiol.* 9:2139. doi: 10.3389/fmicb.2018.02139

Song, Y., Xiao, X., Li, C., Wang, T., Zhao, R., Zhang, W., et al. (2015). The dual transcriptional regulator RovM regulates the expression of AR3- and T6SS4-dependent acid survival systems in response to nutritional status in *Yersinia pseudotuberculosis*. *Environ. Microbiol.* 17, 4631–4645. doi: 10.1111/1462-2920.12996

Sorbara, M. T., and Pamer, E. G. (2019). Interbacterial mechanisms of colonization resistance and the strategies pathogens use to overcome them. *Mucosal Immunol.* 12, 1–9. doi: 10.1038/s41385-018-0053-0

Steele, M. I., Kwong, W. K., Whiteley, M., and Moran, N. A. (2017). Diversification of type VI secretion system toxins reveals ancient antagonism among bee gut microbes. *MBio* 8:e01630-17. doi: 10.1128/mBio.01630-17

Suarez, G., Sierra, J. C., Erova, T. E., Sha, J., Horneman, A. J., and Chopra, A. K. (2010). A type VI secretion system effector protein, VgrG1, from *Aeromonas hydrophila* that induces host cell toxicity by ADP ribosylation of actin. *J. Bacteriol.* 192, 155–168. doi: 10.1128/JB.01260-09

Ting, S. Y., Bosch, D. E., Mangiameli, S. M., Radey, M. C., Huang, S., Park, Y. J., et al. (2018). Bifunctional immunity proteins protect bacteria against FtsZ-targeting ADP-ribosylating toxins. *Cell* 175, 1380.e14–1392.e14. doi: 10.1016/j.cell.2018.09.037

Troxell, B. (2018). A type 6 secretion system (T6SS) encoded gene within *Salmonella enterica* serovar Enteritidis contributes to virulence. *Virulence* 9, 585–587. doi: 10.1080/21505594.2017.1421829

Trunk, K., Peltier, J., Liu, Y. C., Dill, B. D., Walker, L., Gow, N. A. R., et al. (2018). The type VI secretion system deploys antifungal effectors against microbial competitors. *Nat. Microbiol.* 3, 920–931. doi: 10.1038/s41564-018-0191-x

Unterweger, D., Kitaoka, M., Miyata, S. T., Bachmann, V., Brooks, T. M., Moloney, J., et al. (2012). Constitutive type VI secretion system expression gives *Vibrio cholerae* intra- and interspecific competitive advantages. *PLoS One* 7:e48320. doi: 10.1371/journal.pone.0048320

Unterweger, D., Miyata, S. T., Bachmann, V., Brooks, T. M., Mullins, T., Kostiuk, B., et al. (2014). The *Vibrio cholerae* type VI secretion system employs diverse effector modules for intraspecific competition. *Nat. Commun.* 5:3549. doi: 10.1038/ncomms4549

Verster, A. J., Ross, B. D., Radey, M. C., Bao, Y., Goodman, A. L., Mougous, J. D., et al. (2017). The landscape of type VI secretion across human gut microbiomes reveals its role in community composition. *Cell Host Microbe* 22, 411.e14–419.e14. doi: 10.1016/j.chom.2017.08.010

Walter, J., and Ley, R. (2011). The human gut microbiome: ecology and recent evolutionary changes. *Annu. Rev. Microbiol.* 65, 411–429. doi: 10.1146/annurev-micro-090110-102830

Wan, B., Zhang, Q., Ni, J., Li, S., Wen, D., Li, J., et al. (2017). Type VI secretion system contributes to Enterohemorrhagic *Escherichia coli* virulence by secreting catalase against host reactive oxygen species (ROS). *PLoS Pathog.* 13:e1006246. doi: 10.1371/journal.ppat.1006246

Wang, M., Luo, Z., Du, H., Xu, S., Ni, B., Zhang, H., et al. (2011). Molecular characterization of a functional type VI secretion system in *Salmonella enterica* serovar Typhi. *Curr. Microbiol.* 63, 22–31. doi: 10.1007/s00284-011-9935-z

Wang, T., Chen, K., Gao, F., Kang, Y., Chaudhry, M. T., Wang, Z., et al. (2017). ZntR positively regulates T6SS4 expression in *Yersinia pseudotuberculosis*. *J. Microbiol.* 55, 448–456. doi: 10.1007/s12275-017-6540-2

Wang, T., Si, M., Song, Y., Zhu, W., Gao, F., Wang, Y., et al. (2015). Type VI secretion system transports Zn2+ to combat multiple stresses and host immunity. *PLoS Pathog.* 11:e1005020. doi: 10.1371/journal.ppat.1005020

Weber, B., Hasic, M., Chen, C., Wai, S. N., and Milton, D. L. (2009). Type VI secretion modulates quorum sensing and stress response in *Vibrio anguillarum*. *Environ. Microbiol.* 11, 3018–3028. doi: 10.1111/j.1462-2920.2009.02005.x

Wexler, A. G., Bao, Y., Whitney, J. C., Bobay, L. M., Xavier, J. B., Schofield, W. B., et al. (2016). Human symbionts inject and neutralize antibacterial toxins to persist in the gut. *Proc. Natl. Acad. Sci. U.S.A.* 113, 3639–3644. doi: 10.1073/pnas.1525637113

Wexler, A. G., and Goodman, A. L. (2017). An insider's perspective: *Bacteroides* as a window into the microbiome. *Nat. Microbiol.* 2:17026. doi: 10.1038/nmicrobiol.2017.26

Whitney, J. C., Beck, C. M., Goo, Y. A., Russell, A. B., Harding, B. N., De Leon, J. A., et al. (2014). Genetically distinct pathways guide effector export through the type VI secretion system. *Mol. Microbiol.* 92, 529–542. doi: 10.1111/mmi.12571

Whitney, J. C., Quentin, D., Sawai, S., LeRoux, M., Harding, B. N., Ledvina, H. E., et al. (2015). An interbacterial NAD(P)(+) glycohydrolase toxin requires elongation factor Tu for delivery to target cells. *Cell* 163, 607–619. doi: 10.1016/j.cell.2015.09.027

Wilson, M. M., Anderson, D. E., and Bernstein, H. D. (2015). Analysis of the outer membrane proteome and secretome of *Bacteroides fragilis* reveals a multiplicity of secretion mechanisms. *PLoS One* 10:e0117732. doi: 10.1371/journal.pone.0117732

Yang, X., Song, Y., Dai, Q., Zhang, H., Song, L., Wang, Z., et al. (2019). The stringent response factor, RelA, positively regulates T6SS4 expression through the RovM/RovA pathway in *Yersinia pseudotuberculosis*. *Microbiol. Res.* 220, 32–41. doi: 10.1016/j.micres.2018.12.002

Yu, Y., Fang, L., Zhang, Y., Sheng, H., and Fang, W. (2015). VgrG2 of type VI secretion system 2 of *Vibrio parahaemolyticus* induces autophagy in macrophages. *Front. Microbiol.* 6:168. doi: 10.3389/fmicb.2015.00168

Yu, Y., Yang, H., Li, J., Zhang, P., Wu, B., Zhu, B., et al. (2012). Putative type VI secretion systems of *Vibrio parahaemolyticus* contribute to adhesion to cultured cell monolayers. *Arch. Microbiol.* 194, 827–835. doi: 10.1007/s00203-012-0816-z

Zhang, H., Gao, Z. Q., Wei, Y., Xu, J. H., and Dong, Y. H. (2013). Insights into the cross-immunity mechanism within effector families of bacteria type VI secretion system from the structure of StTae4-EcTai4 complex. *PLoS One* 8:e73782. doi: 10.1371/journal.pone.0073782

Zhang, W., Wang, Y., Song, Y., Wang, T., Xu, S., Peng, Z., et al. (2013). A type VI secretion system regulated by OmpR in *Yersinia pseudotuberculosis* functions to maintain intracellular pH homeostasis. *Environ. Microbiol.* 15, 557–569. doi: 10.1111/1462-2920.12005

Zhang, W., Xu, S., Li, J., Shen, X., Wang, Y., and Yuan, Z. (2011). Modulation of a thermoregulated type VI secretion system by AHL-dependent quorum sensing in *Yersinia pseudotuberculosis*. *Arch. Microbiol.* 193, 351–363. doi: 10.1007/s00203-011-0680-2

Zhao, W., Caro, F., Robins, W., and Mekalanos, J. J. (2018). Antagonism toward the intestinal microbiota and its effect on *Vibrio cholerae* virulence. *Science* 359, 210–213. doi: 10.1126/science.aap8775

Zheng, J., Ho, B., and Mekalanos, J. J. (2011). Genetic analysis of anti-amoebae and anti-bacterial activities of the type VI secretion system in *Vibrio cholerae*. *PLoS One* 6:e23876. doi: 10.1371/journal.pone.0023876

Zhou, Y., Tao, J., Yu, H., Ni, J., Zeng, L., Teng, Q., et al. (2012). Hcp family proteins secreted via the type VI secretion system coordinately regulate *Escherichia coli* K1 interaction with human brain microvascular endothelial cells. *Infect. Immun.* 80, 1243–1251. doi: 10.1128/IAI.05994-11

Zoued, A., Durand, E., Bebeacua, C., Brunet, Y. R., Douzi, B., Cambillau, C., et al. (2013). TssK is a trimeric cytoplasmic protein interacting with components of both phage-like and membrane anchoring complexes of the type VI secretion system. *J. Biol. Chem.* 288, 27031–27041. doi: 10.1074/jbc.M113.499772

Conflict of Interest Statement: The authors declare that the research was conducted in the absence of any commercial or financial relationships that could be construed as a potential conflict of interest.

Copyright © 2019 Chen, Yang and Shen. This is an open-access article distributed under the terms of the Creative Commons Attribution License (CC BY). The use, distribution or reproduction in other forums is permitted, provided the original author(s) and the copyright owner(s) are credited and that the original publication in this journal is cited, in accordance with accepted academic practice. No use, distribution or reproduction is permitted which does not comply with these terms.

frontiers in Microbiology

ORIGINAL RESEARCH
published: 11 July 2019
doi: 10.3389/fmicb.2019.01482

A Potential Late Stage Intermediate of Twin-Arginine Dependent Protein Translocation in *Escherichia coli*

*Hendrik Geise, Eyleen Sabine Heidrich, Christoph Stefan Nikolin, Denise Mehner-Breitfeld and Thomas Brüser**

Institute of Microbiology, Leibniz University Hannover, Hannover, Germany

The twin-arginine translocation (Tat) system transports folded proteins across membranes of prokaryotes, plant plastids, and some mitochondria. According to blue-native polyacrylamide gel electrophoresis after solubilization with digitonin, distinct interactions between the components TatA, TatB, and TatC result in two major TatBC-containing complexes in *Escherichia coli* that can bind protein substrates. We now report the first detection of a TatABC complex that likely represents the state at which transport occurs. This complex was initially found when the photo cross-linking amino acid *p*-benzoyl-L-phenylalanine (Bpa) was introduced at position I50 on the periplasmic side of the first trans-membrane domain of TatC. Cross-linking of $TatC_{I50Bpa}$ resulted in TatC-TatC-cross-links, indicating a close proximity to neighboring TatC in the complex. However, the new complex was not caused by cross-links but rather by non-covalent side chain interactions, as it was also detectable without UV-cross-linking or with an I50Y exchange. The new complex did not contain any detectable substrate. It was slightly upshifted relative to previously reported substrate-containing TatABC complexes. In the absence of TatA, an inactive $TatBC_{I50Bpa}$ complex was formed of the size of wild-type substrate-containing TatABC complexes, suggesting that TatB occupies TatA-binding sites at $TatC_{I50Bpa}$. When substrate binding was abolished by point mutations, this $TatBC_{I50Bpa}$ complex shifted analogously to active $TatABC_{I50Bpa}$ complexes, indicating that a defect substrate-binding site further enhances TatB association to TatA-binding sites. Only TatA could shift the complex with an intact substrate-binding site, which explains the TatA requirement for substrate transport by TatABC systems.

Keywords: twin-arginine translocation, membrane protein complexes, protein translocation, *Escherichia coli*, photo cross-linking

OPEN ACCESS

Edited by:
Eric Cascales, Aix-Marseille Université, France

Reviewed by:
Bérengère Ize, Centre National de la Recherche Scientifique, France
Roland Freudl, Forschungszentrum Jülich GmbH, Germany

***Correspondence:**
Thomas Brüser
brueser@ifmb.uni-hannover.de

Specialty section:
This article was submitted to Microbial Physiology and Metabolism, a section of the journal Frontiers in Microbiology

Received: *04 March 2019*
Accepted: *14 June 2019*
Published: *11 July 2019*

Citation:
Geise H, Heidrich ES, Nikolin CS, Mehner-Breitfeld D and Brüser T (2019) A Potential Late Stage Intermediate of Twin-Arginine Dependent Protein Translocation in Escherichia coli. Front. Microbiol. 10:1482. doi: 10.3389/fmicb.2019.01482

INTRODUCTION

The twin-arginine translocation (Tat) system transports folded proteins across the cytoplasmic membrane of prokaryotes, the thylakoid membrane of plant plastids, and the inner membrane in some mitochondria (Hou and Brüser, 2011; Hamsanathan and Musser, 2018; Petrů et al., 2018). The Tat-dependent translocation is driven by the membrane potential that is generated by ionic gradients at energy-transducing membranes, which is why this system is restricted

to such membranes (Cline, 2015). In *Escherichia coli*, a fully functional Tat-translocon assembles from the three components TatA, TatB, and TatC (Sargent et al., 1999). A second paralog of TatA, TatE, can mix into these systems or substitute TatA, without being specifically required for the transport of a known Tat substrate (Sargent et al., 1999). TatA/E and TatB are evolutionary related and share the same principle structural organization in their functionally important N-terminal half (Yen et al., 2002; Hu et al., 2010; Zhang et al., 2014). They are N-terminally membrane anchored by a short hydrophobic region, followed by a hinge and an amphipathic helix on the cytoplasmic surface of the membrane. This amphipathic helix is followed by some negatively charged residues and regions that are not really conserved anymore between TatA/B family proteins (Hou and Brüser, 2011). TatC consists of six transmembrane helices (TM1–6) with cytoplasmic N- and C-termini and loops on the cytoplasmic and periplasmic sides of the membrane (Rollauer et al., 2012; Ramasamy et al., 2013). Tat substrates contain N-terminal signal peptides with the eponymous highly conserved twin-arginine motif, which is recognized by a binding site that is formed by the N-terminus and the first cytoplasmic loop of TatC (Ramasamy et al., 2013). TatC binds TatB and also TatA, and corresponding binding sites have been identified (Alcock et al., 2016). TatB and TatC interact tightly, and earlier studies with the homologous TatABC systems in plants and *E. coli* were suggestive for a substrate-induced recruitment of TatA to TatBC (Cline and Mori, 2001; Mori and Cline, 2002; Alami et al., 2003). While cross-linking and co-purification analyses later demonstrated that TatA also interacts with TatBC independently of substrate binding (Aldridge et al., 2014; Behrendt and Brüser, 2014), active transport apparently increases the affinity of TatA to TatBC, as reflected by a recruitment of TatA-XFP fusion proteins to TatBC in response to substrate overproduction (Alcock et al., 2013; Rose et al., 2013). Besides TatBC, also TatA interacts with the signal peptide of precursor proteins, but this interaction contributes to transport without being involved in the RR-motif recognition by TatBC (Taubert et al., 2015). The Tat complexes are usually analyzed by BN-PAGE in combination with Western-blotting or other labeling methods. Solubilized TatA tends to form multiple homooligomers that are visible as a dense ladder in BN-PAGE (Oates et al., 2005; Richter and Brüser, 2005). These highly abundant TatA homooligomers so far prevented the direct identification of TatA as constituent of any of the TatBC-containing complexes by BN-PAGE (Behrendt and Brüser, 2014). However, cross-linking experiments showed that TatA and TatB share the same binding sites of TatC, and positions of TatA and TatB are believed to switch in course of transport (Habersetzer et al., 2017). As TatA is required for Tat transport, it is important to reveal the complexes that contain all three components.

TatB and TatC have been detected in two substrate-free and two substrate-associated complexes in the range of 400–700 kDa (Behrendt and Brüser, 2014). As the migration behavior of solubilized membrane protein complexes in BN-PAGE is influenced by the detergent and lipid content of solubilized complexes, the BN-PAGE deduced molecular masses do not permit the estimation of individual subunit numbers. Some variation of reported Tat complex molecular masses in BN-PAGE analyses may have been caused by lot variations of the commonly used mild detergent digitonin, which is enriched from extractions of foxglove (*Digitalis purpurea*). For a clear assignment, it is therefore important to include the wild-type complexes in each study. To clarify the designation of Tat complexes, we now name the smaller substrate-free TatBC-containing complex of *E. coli* Tat-complex 1 (TC1; previously termed 370, 430, or 440 kDa complex; Oates et al., 2005; Richter and Brüser, 2005; Orriss et al., 2007; Huang et al., 2017) and the larger substrate-free TatBC-containing complex Tat-complex 2 (TC2; previously termed 580 kDa or "higher molecular weight variant" TatBC complex; Richter and Brüser, 2005; Huang et al., 2017). As mentioned above, both of these complexes can in principle also contain TatA, but the continuous dissociation of TatA from TatBC during solubilization and purification and the accompanying formation of homooligomeric TatA associations in a wide range of sizes prevented so far the assignment of TatA to these complexes. Both complexes are easily identified by BN-PAGE without overproduction of Tat substrates (Richter and Brüser, 2005; Behrendt and Brüser, 2014). Due to harsher BN-PAGE conditions, other groups detected TC2 only with transport-enhancing mutations (Huang et al., 2017). The corresponding substrate-bound shifted complexes, now termed TC1S or TC2S, can so far only be detected upon substrate overproduction (Behrendt and Brüser, 2014). To facilitate comparisons, we suggest the use of this nomenclature for future studies.

During characterizations of TatC variants with individual residues substituted by the artificial cross-linking amino acid *p*-benzoyl-L-phenylalanine (Bpa), we found with a $TatC_{I50Bpa}$ mutation a new TatBC-containing complex larger than TC2S. The formation of this complex did not relate to a Bpa cross-link and depended on TatA. Mutational inactivation of the substrate-binding site permitted the formation of this complex in the absence of TatA, suggesting that TatB can be recruited to TatA-binding sites in such inactive complexes. The data indicate that subtle changes in the substrate-binding site can shift the TatBC complex to a higher associated state in the absence of TatA, but TatA is required for this shift when the substrate-binding site is functional. As the $TatABC_{I50Bpa}$ system is active, and as the complex does not contain substrate anymore, it is likely that the described new complex represents a late translocation state, kinetically stabilized by the $TatC_{I50Bpa}$ mutation.

MATERIALS AND METHODS

Strains and Growth Conditions

The *tatABCDE* deficient *E. coli* strain DADE D6 ara^R (Lindenstrauss et al., 2010) was used for physiological and biochemical analyses, and *E. coli* XL1-Blue MRF' Tet (Agilent) was used for cloning. Strains were grown aerobically at 37°C in LB medium [1% (w/v) tryptone, 1% (w/v) NaCl, 0.5% (w/v) yeast extract] in the presence of appropriate antibiotics (100 μg/ml

ampicillin, 25 μg/ml chloramphenicol, and 12.5 μg/ml tetracycline) and harvested after 5 h. Cultures carrying pABS- or pDE-derived plasmids were normalized to an OD_{600} of 1.0 and cultures carrying pZX31-derived plasmids to an OD_{600} of 2.0. Cultures containing pBW-*efeB-strep* were harvested after 3 h growth with 0.05% (w/v) rhamnose added at an OD_{600} of 0.6. For incorporation of Bpa at amber stop codons in strains carrying the pEVOL-*p*BpF system, 100 μM Bpa was added simultaneously with 100 μM arabinose. For optional cross-linking, cultures were grown for 5 h before irradiation with UV light at 365 nm for 30 min at ambient temperature, normalization, and further processing.

Plasmids and Genetic Methods

pEVOL-*p*BpF-tet, which encodes an orthogonal Bpa-specific suppressor tRNA/aminoacyl tRNA synthetase pair used for incorporation of Bpa at introduced amber stop codons, was donated by Peter G. Schultz (Young et al., 2010). The vector pDE-*tatABC-h6*, used for constitutive *tatABC* expression in pEVOL-*p*BpF-tet-containing strains, was generated by cloning the NheI-XbaI digested *ori* ColA from pCOLAduet-1 (Novagen) into the corresponding sites of pABS-*tatABC-h6*. pABS-*tatABC-h6* was generated by substituting *pspC* in pABS-*pspC-h6* (Mehner et al., 2012) with *tatABC*, using NdeI and BamHI restriction sites and the primer pair *tatA*-NdeI-F 5′-TCT TCT CAT ATG GGT GGT ATC AGT ATT TGG C-3′ and *tatC*-BamHI-R 5′-CAA GCG GAT CCT TCT TCA GTT TTT TCG CTT TCT GCT TC-3′. pABS-*tatABC-h6* results in constitutive P_{tatA}-dependent expression of the *tatABC* genes, with TatC produced as C-terminally hexahistidine-tagged protein. The plasmid pZX31-*tatBC-h6*, used for constitutive *tatBC* expression, was generated by cloning *ori* ColA into AvrII-SpeI digested pZA31-*tatBC-h6* using the primer pair ColA-AvrII-F 5′-GAT CCC TAG GAA ACG TCC TAG AAG ATG CCA GGA GGA TA-3′ and ColA-SpeI-R 5′-GAT CAC TAG TTG GTG TCG GGA ATC CGT AAA GG-3′. For generation of pZA31-*tatBC-h6*, *tatBC* was amplified using the primer pair *tatB*-EcoRI-F 5′-GAA GAC GCG AAT TCC CAC GAT AAA GAG C-3′/*tatC-h6*-PstI-R 5′-TAG CCA CTG CAG TTA ATG GTG ATG GTG ATG GTG TTC TTC AGT TTT TTC GCT TTC-3′ and cloned into the corresponding sites of pZA31MCS (Expressys, Bammental). Single amino acid exchanges in TatC were introduced by QuikChange™ mutagenesis (Stratagene) of pDE-*tatABC-h6* or pZX31-*tatBC-h6*, using the forward primers *tatC*-A47Bpa-F 5′-CAT CTA TCA CCT GGT ATC CTA GCC ATT GAT CAA GCA GTT G-3′, *tatC*-P48Bpa-F 5′-CTA TCA CCT GGT ATC CGC GTA GTT GAT CAA GCA GTT GCC G-3′, *tatC*-L49Bpa-F 5′-GGT ATC CGC GCC ATA GAT CAA GCA GTT GC-3′, *tatC*-I50Bpa-F 5′-CAC CTG GTA TCC GCG CCA TTG TAG AAG CAG TTG CCG CAA GGT TC-3′, *tatC*-I50Y-F 5′-GGT ATC CGC GCC ATT GTA TAA GCA GTT GCC GCA AG-3′, *tatC*-I50F-F 5′-GTA TCC GCG CCA TTG TTC AAG CAG TTG CCG-3′, *tatC*-I50W-F GTA TCC GCG CCA TTG TGG AAG CAG TTG CCG CAA G-3′, *tatC*-K51Bpa-F 5′-CCG CGC CAT TGA TCT AGC AGT TGC CGC AAG-3′, *tatC*-Q52Bpa-F 5′-GCG CCA TTG ATC AAG TAG TTG CCG CAA GGT TC-3′, *tatC*-F94Q-F 5′-CTA TCA GGT GTG GGC ACA GAT CGC CCC AGC GCT G-3′, and *tatC*-E103A-F 5′-CGC TGT ATA AGC ATG CGC GTC GCC TGG TGG TG-3′ in conjunction with reverse primers that cover the identical sequence region. The vector pBW-*ycdB-strep* (Sturm et al., 2006) was used for the overexpression of *efeB* (formerly called *ycdB*). All genetic constructs were confirmed by sequencing.

Biochemical Methods

BN-PAGE was performed as described previously (Richter and Brüser, 2005), but without β-mercaptoethanol in the buffers. TatABC complexes were solubilized with 1% digitonin and purified by Ni-NTA affinity chromatography using 50 mM Bis-Tris pH 7.0, 20% (w/v) sucrose, 10 mM $MgCl_2$, 0.1% digitonin as buffer system, and 250 mM imidazole containing buffer for elution. When indicated, an additional size exclusion chromatography purification step was applied using the same buffer. Sodium dodecyl sulfate-polyacrylamide gel electrophoresis (SDS-PAGE) analysis was carried out by standard methods (Laemmli, 1970). For immunoblots, proteins were semi-dry blotted on nitrocellulose membranes and blots were developed using antibodies directed against synthetic C-terminal peptides of TatA, TatB, TatC, or purified EfeB, using the ECL system (GE Healthcare) for signal detection. HRP-conjugated goat anti rabbit anti-bodies (Roth) served as secondary antibodies. For stripping, blots were incubated with 100 mM glycine pH 2.8, 1% SDS, 0.2% Tween 20 for 30 min, followed by three washing steps with PBS and a second blocking (PBS with 5% skim milk). Stripped blots were again incubated with the secondary antibody and developed to ensure that they gave no detectable background and thereafter used for new detections. The chain formation phenotype was assessed by phase contrast microscopy. SDS sensitivity was determined by aerobic growth in LB medium containing 4% (w/v) sodium dodecyl sulfate (SDS), using the quotient of the OD_{600} with/without SDS after 3 h of growth (Ize et al., 2003).

RESULTS

The Region Around Position I50 of TatC Contacts Neighboring TatC Protomers

In the course of *in vivo* photo-cross-linking analyses of TatC interactions with single TatC amino acids exchanged to *p*-benzoyl-L-phenylalanine (Bpa), we identified that a $TatC_{I50Bpa}$ construct efficiently cross-linked to other TatC protomers, giving rise to a strong UV-induced shifted TatC band at ~55 kDa (**Figure 1A**, compare −UV/+UV). TatB is known to tightly interact with TatC, and TatB-TatC cross-links would have resulted in shifts of similar size, but as no TatB was detectable in these bands, it is likely that the shifted bands represented TatC-TatC cross-links. TatC is only present in oligomeric complexes in *E. coli*, and the position of the I50Bpa exchange must be therefore in close proximity to neighboring TatC protomers within Tat complexes. Within the first periplasmic loop (PPL1) of TatC, Ile50 is located in an α-helix oriented almost parallel to the

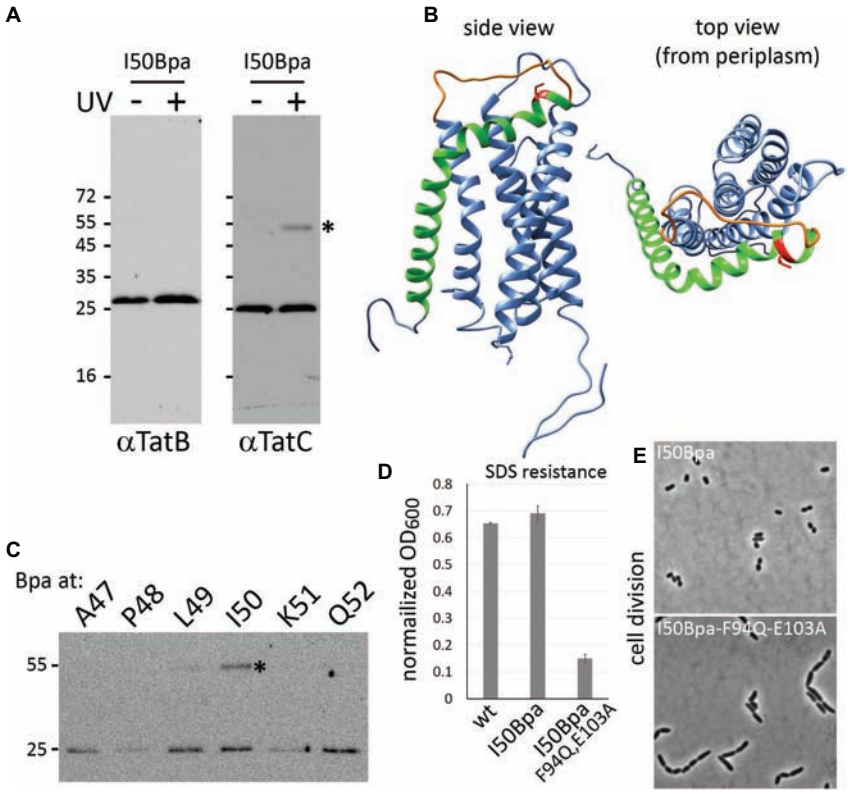

FIGURE 1 | $TatC_{I50Bpa}$ is functional and its cross-linking results in TatC dimers. **(A)** Immunoblot detection of Bpa photo cross-links in a strain producing $TatABC_{I50Bpa}$. Irradiation by UV light results in formation of a ~55 kDa TatC homodimer (*) that is detected in the TatC blot (right) but not in the TatB blot (left). **(B)** Model of *E. coli* TatC. I50 of TatC is highlighted in red and is located at the end of TM1 (green) in transition to a less structured region of the first periplasmic loop (orange). The model is based on the *Aquifex aeolicus* TatC structure (PDB 4HTS; Ramasamy et al., 2013) and was modeled using RaptorX (Peng and Xu, 2011; Källberg et al., 2014). Molecular graphics and analyses were performed using UCSF Chimera (Pettersen et al., 2004). **(C)** Analysis of photo cross-links with Bpa exchanges at indicated TatC positions in the vicinity of I50. The position of the cross-link is indicated by an asterisk. SDS-solubilized membranes were used for the detection of Tat components as described previously (Taubert et al., 2015). **(D,E)** Activity of $TatABC_{I50Bpa}$ as monitored by complementation of the SDS sensitivity **(D)** and chain formation phenotypes **(E)** of Tat deficient strains. SDS sensitivity results in lowered cell density, which is given as normalized OD_{600}, the quotient of OD_{600} after 3 h of growth in 4% SDS/OD after 3 h of growth in 0% SDS. As control for these phenotypes, the same system was analyzed with a mutated Tat substrate-binding site. The mutations F94Q/E103A completely inactivate Tat systems (Huang et al., 2017, and this study).

surface of the membrane directly following TM1 (**Figure 1B**). Previous studies showed that other residues located in this region are crucial for Tat complex assembly or functionality (Allen et al., 2002; Barrett et al., 2005; Kneuper et al., 2012). Already in early studies, an exchange of the close-by residue Pro48 to Ala has been shown to inactivate the Tat system, which has been explained by a destabilization of protomer interactions within the complex (Allen et al., 2002; Behrendt and Brüser, 2014). While Pro48 is directed inward and thus likely positions the helix at its place, Ile50 is directed outward, which likely enables the contacts to neighboring TatC subunits. To examine potential TatC cross-links with Bpa exchanges in the vicinity of Ile50, we included cross-link analyses of TatABC systems with TatC exchanges A47Bpa, P48Bpa, L49Bpa, K51Bpa, and Q52Bpa (**Figure 1C**). In case of P48Bpa and K51Bpa, the abundance of TatC was reduced, most likely due to destabilization and degradation effects. A cross-link was also observed with L49Bpa, but I50Bpa gave the strongest cross-link. In further analyses, we therefore concentrated on I50Bpa. The $TatABC_{I50Bpa}$ system was active, as shown by the complementation of SDS sensitivity and chain formation phenotypes of a *tatABCDE* mutant strain (**Figures 1D,E**).

p-Benzoylphenylalanine or Tyrosine at Position I50 of TatC Influence the Equilibrium Between Three Assembly States of Twin-Arginine Translocation Complexes

Previous studies had already indicated a strong influence of P48, which is located only half a helical turn away from I50, on the stability of TatBC complexes (Allen et al., 2002; Barrett et al., 2005; Kneuper et al., 2012; Behrendt and Brüser, 2014). To our knowledge, mutations of I50 have never been analyzed. To address complex stability of Tat systems containing I50Bpa, membranes were solubilized with 1% (w/v) digitonin and subjected to BN-PAGE/Western-blot analysis (**Figure 2**). While wild-type TatABC produced the two known TatB- and TatC-containing complexes (TC1 and TC2), $TatABC_{I50Bpa}$ predominantly formed a new complex that was clearly shifted to a higher molecular

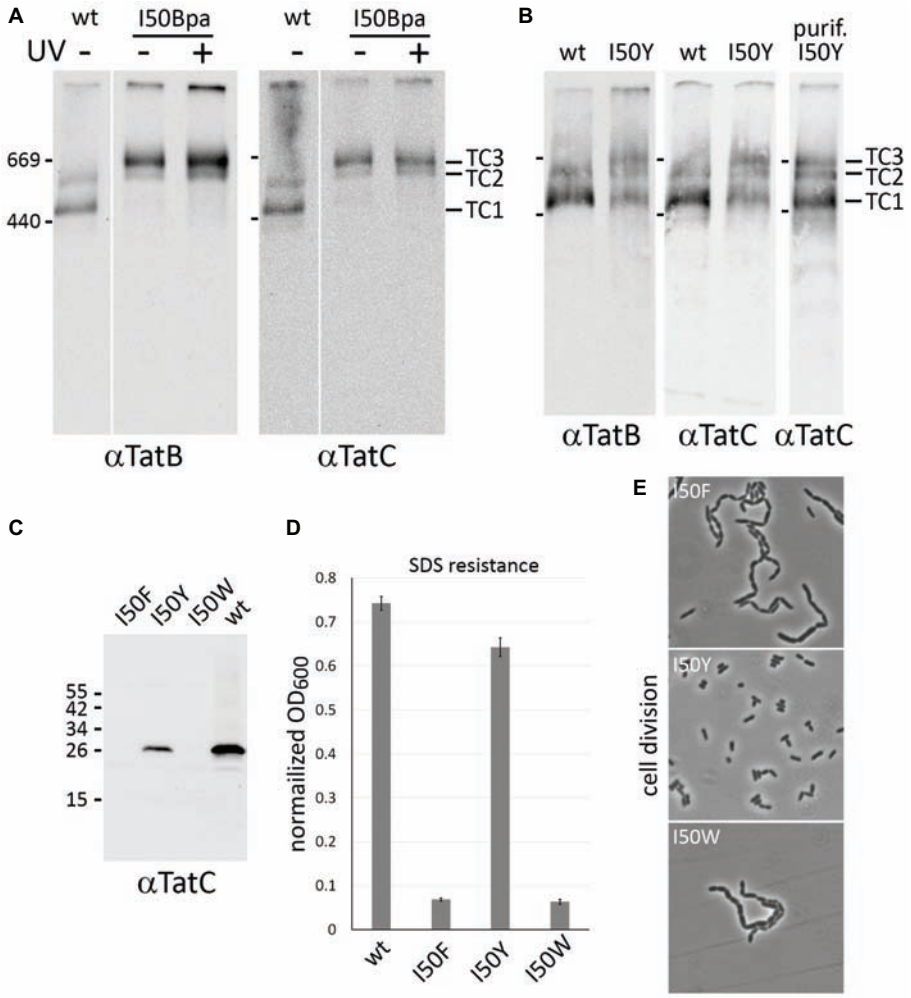

FIGURE 2 | An equilibrium between three Tat complexes is influenced by Bpa or Tyr exchanges at position I50. **(A)** BN-PAGE/Western-blot analysis of Tat complexes formed by wild-type TatABC and $TatABC_{I50Bpa}$ systems. As indicated, blots were developed using TatB or TatC specific antibodies. Positions of marker proteins are indicated on the left of the blots, positions of the three Tat complexes are indicated on the right. White lines separate lanes from one blot that were not directly neighboring. **(B)** BN-PAGE/Western-blot analysis of Tat complexes formed by wild-type TatABC and by $TatABC_{I50Y}$ systems. The Tat complexes of the latter were also enriched by affinity chromatography (lane purif. I50Y). **(C)** SDS-PAGE/Western-blot analysis of TatC with I50 exchanged by indicated aromatic natural amino acids. TatC from the non-mutated system is analyzed for comparison. **(D,E)** Activity of Tat systems with wild-type TatC or indicated TatC variants, as monitored by complementation of the SDS sensitivity **(D)** and chain formation phenotype **(E)** of Tat deficient strains. The SDS sensitivity is reflected by the normalized OD_{600} as described in **Figure 1**.

mass and also contained TatB and TatC (**Figure 2A**). In addition, a less dominant complex with the size of TC2 or TC2S of the wild-type Tat system was observed, which will be assigned later (see below). The shifted complex did not result from UV-cross-linking, as the pattern did not change without UV illumination. This suggested that most likely a non-covalent interaction of the aromatic benzophenone side chain was causing the shift. To analyze whether aromatic side chains of natural amino acids can cause the same shift, we substituted Ile50 by tyrosine, tryptophan, or phenylalanine. Before analyzing the corresponding Tat complexes, we examined the activity and formation of the mutated components (**Figures 2C–E**). The I50W and I50F substitutions resulted in inactivation and absence of TatC, and thus, most likely caused a complete degradation of TatC. Notably, an I50Y substitution lowered the abundance of TatC but did not inactivate the system. The data underlined the importance of that position for the structural integrity of the Tat system. The active $TatABC_{I50Y}$ system was then analyzed by BN-PAGE (**Figure 2B**). The usual complexes TC1 and TC2 were formed that can be also observed by non-mutated Tat systems, but there was clearly the additional band of the shifted complex (TC3) that had been previously observed with $TatABC_{I50Bpa}$. Together, these analyses indicated that an equilibrium exists between three Tat complexes in active Tat systems, and this equilibrium is strongly influenced by I50 exchanges to either Bpa or Tyr, which introduces benzophenone or hydroxyphenol moieties, respectively. Both side chains allow aromatic contacts as well as hydrogen bonding (mediated by

the keto group of benzophenone or the hydroxy group in tyrosine), and this combination is likely responsible for the stabilization of TC3, which apparently otherwise is likely only a short-lived complex. As cross-links were irrelevant for TC3-formation, we did not apply cross-linking for all further analyses with Bpa-containing constructs.

TC3 Requires TatA to Be Formed

A reason for the I50Bpa-induced stabilization of a Tat complex at a higher molecular mass could have been an enhanced affinity of TatA to TatBC. A reduced TatA-dissociation would explain the observed depletion of TC1. We therefore addressed this potential role of TatA by comparing the BN-PAGE detectable complexes formed in the presence or absence of TatA (**Figure 3**). The absence of TatA resulted in the formation of a complex of the size of TC2 or TC2S, which would need a substrate detection for clear differentiation (see below), but TC3 was clearly absent. Notably, the $TatBC_{I50Bpa}$ system did not result in TC1, which is the complex usually formed in the absence of TatA (Behrendt and Brüser, 2014), indicating that the I50Bpa mutation in TatC also results in an increased affinity of TatB to TatA-binding sites. It is established that TatB can in principle bind to TatA-binding sites in active Tat systems (Habersetzer et al., 2017), and apparently, the I50Bpa mutation enhances this interaction to an extent that no TC1 is detected anymore. The data also clearly show that TatA is required for the formation of TC3 in $TatABC_{I50Bpa}$ systems, implying that TatA was likely a constituent of the new complex. To address this aspect directly, we purified TatC-h6-tagged Tat complexes in a strain producing the $TatABC_{I50Bpa}$ components, using a combination of immobilized metal affinity chromatography (IMAC) and size exclusion chromatography (SEC). Thus, the enriched complexes were analyzed by BN-PAGE/Western-blotting (**Figure 3**). Non-bound TatA, which is known to form homooligomeric assemblies that are detected as a "ladder" over a broad range of sizes in BN-PAGE (Barrett et al., 2005; Richter and Brüser, 2005; Behrendt et al., 2007), was efficiently removed by the purification. We now were able to detect TatA in a weak band of the size of the two TatBC-containing complexes, likely indicating the presence of TatA in these complexes. Based on the TatA dependence of TC3 in conjunction with the detection of TatA in a BN-PAGE band of that size, we suggest that both detected complexes contain significant amounts of TatA, which likely explains the shift of these complexes in comparison with TC1. Consequently, the I50Bpa exchange likely enhanced the stability of a TatA-assembled state of the Tat system.

Substrate Is Likely Already Transported by the Detected TC3

To clearly differentiate, whether the detected $TatBC_{I50Bpa}$ complex that is formed in the absence of TatA contains substrate or not, we examined the complex after recombinant production of the *E. coli* Tat substrate EfeB (formerly known as YcdB). EfeB has been shown to bind Tat complexes with sufficient affinity to detect the interaction by BN-PAGE/Western-blot analysis (Behrendt and Brüser, 2014). EfeB could be clearly detected in the $TatBC_{I50Bpa}$ complex, indicating that it represented the substrate-bound TC2S (**Figure 4A**). Note that, due to the lack of TatA, the $TatBC_{I50Bpa}$ system is inactive (**Figure 4B**),

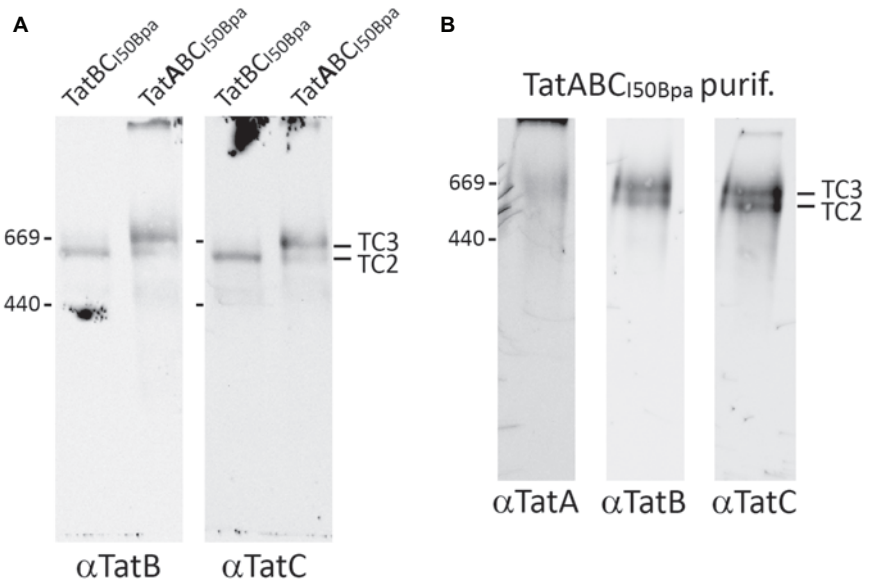

FIGURE 3 | TatA is required for the formation of TC3. **(A)** BN-PAGE/Western-blotting detection of Tat complexes in the absence or presence of TatA. Analyses of Tat complexes in strains producing $TatABC_{I50Bpa}$ or $TatBC_{I50Bpa}$. **(B)** Detection of the three Tat components within TC3 after a two-step purification (Ni-affinity purification and size exclusion chromatography using a Superose 6 column). Positions of TC2 and TC3 are indicated on the right, size markers on the left, and the used antibodies below the corresponding blots.

and EfeB accumulates strongly in the membranes, whereas the active transport by the $TatABC_{I50Bpa}$ system markedly reduces the abundance of EfeB in the membranes (**Figure 4C**, compare free EfeB signals, lanes 2 and 4). The TC2 complex was also present in $TatABC_{I50Bpa}$ systems, migrating as a second band below TC3, but the complex was less abundant, and no substrate was detectable. Also TC3 of the $TatABC_{I50Bpa}$ system contained no detectable substrate, although it was more abundant than TC2S of the $TatBC_{I50Bpa}$ system (**Figure 4C**), in line with the generally accepted idea that transport occurs upon TatA recruitment. The detected TC3 therefore likely represents a stabilized active state of the Tat system in which the complexes have already accomplished transport.

To examine whether TC3 depends also on substrate binding, we analyzed the $TatABC_{I50Bpa}$ system with an inactivated twin-arginine motif-binding site, achieved by a F94Q/E103A double exchange in TatC. The inactivity of that system has been previously established by others (Huang et al., 2017) and was confirmed in our hands (see negative control in **Figures 1D,E**). BN-PAGE analyses demonstrated that the inactivation of the substrate-binding site did not diminish TC3, clearly demonstrating that substrate binding was not a prerequisite for the shift (**Figure 4C**). When we introduced the same inactive substrate-binding site into the $TatBC_{I50Bpa}$ system, we found in analogous BN-PAGE/Western-blotting analyses that a small portion of the $TatBC_{I50Bpa/F94Q/E103A}$ complex had shifted to TC3, which is normally only found in the presence of TatA (**Figure 4C**). Apparently, TatB associated with $TatBC_{I50Bpa/F94Q/E103A}$ just like TatA to $TatBC_{I50Bpa}$. In conclusion, the F94Q/E103A mutations of the substrate-binding site caused a relaxed, not TatA or TatB differentiating enhanced association of TatA or TatB to TatC, leading to increased amounts of the TC3 with $TatABC_{I50Bpa/F94Q/E103A}$ systems and even a TC3 in $TatBC_{I50Bpa/F94Q/E103A}$ systems.

DISCUSSION

In this study, we analyzed in some detail a third Tat complex, termed TC3, that became the dominant Tat complex if only one TatC position, I50, was mutated to the artificial aromatic amino acid Bpa. We could demonstrate that side chain properties and not a photo activatable cross-link were the basis for the detection of this complex. The complex was active, suggesting

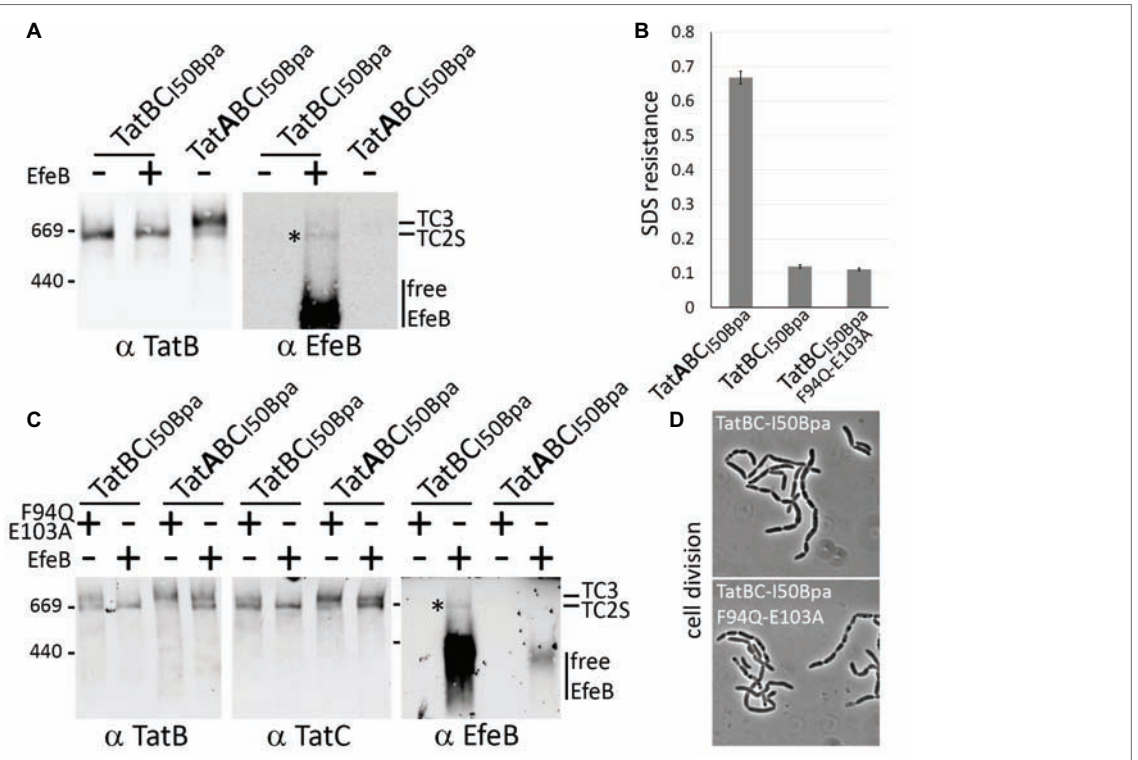

FIGURE 4 | A mutated substrate-binding site can result in TC3 formation in the absence of TatA. **(A)** Detection of recombinant Tat substrate EfeB in TC2. Overproduction of EfeB leads to the detectability of this Tat substrate in TC2 formed by $TatBC_{I50Bpa}$. After development of the blot using antibodies directed against TatB (left blot), the blot was stripped (see methods) and developed again with antibodies recognizing EfeB (right blot). **(B,D)** The absence of TatA inactivates the Tat system also in case of $TatBC_{I50Bpa}$. As monitored by SDS resistance **(B)** and the cell division **(D)**, $TatBC_{I50Bpa}$ does not complement the deficiency phenotypes of the *E. coli* Tat mutant strain DADE. The SDS sensitivity is reflected by the normalized OD_{600} as described in **Figure 1**. We used the $TatABC_{I50Bpa}$ as positive control, which behaved like the wild type (see **Figure 1D** or **2D**). **(C)** Mutational inactivation of the twin-arginine motif-binding site in TatC influences the formation of TC2 and TC3. Comparison of systems with inactivated Tat substrate-binding sites (F94Q, E103A) with systems in which the Tat substrate EfeB has been overproduced. After development of the blot using TatC antibodies, the blot was stripped and developed using antibodies recognizing EfeB. Note that EfeB is not detected in the TC2 formed by the active $TatABC_{I50Bpa}$ system, most likely due to active transport that is likely the reason for the lowered abundance of EfeB in the membranes.

that it likely represents a naturally occurring association of Tat components that is stabilized by the amino acid exchange (**Figure 1**). As additional evidence for this, we found that the exchange of I50 by the natural amino acid Tyr could stabilize TC3, too. In case of this I50Y exchange, which was active as well, all three Tat complexes were clearly detectable (**Figure 2**), suggesting that there is an equilibrium between Tat associations that can be influenced by single amino acid exchanges at position I50. The fact that the I50Bpa exchange can be photo cross-linked to neighboring TatC subunits supports the idea that certain TatC-TatC interactions stabilize the association that is detected as TC3. If there is an equilibrium between TC1, TC2, and TC3, this means that either TC3 is a lowly populated transiently formed complex in the wild-type system or it disassembles upon solubilization to TC2 or TC1, if it is not stabilized. The fact that the complex depends on TatA and that TatA can be co-purified with that complex (**Figure 3**) suggests that TC3 may be the active translocon association. In agreement with the idea that TC3 transports and therefore releases Tat substrates, we found that this complex did not contain any detectable Tat substrate (**Figure 4**). In the absence of TatA, when no transport can take place, a TC2S is formed. However, a TC2 band that is detected below the TC3 band in the active $TatABC_{I50BPA}$ system did not contain any detectable substrate. This indicates that either TC2 with or without substrate cannot be differentiated by BN-PAGE migration behavior with I50Bpa TatC variants, or substrate does not accumulate to a detectable extent at TC2 in active (TatA-containing) systems (**Figure 4**). The detection of translocon bound substrate in TC2 of $TatBC_{I50BPA}$ systems may thus be facilitated by the accumulation of substrates due to the absence of TatA, which is evidenced by the large amounts of EfeB in the membranes of that strain.

An older study questioned the physiological relevance of the Tat complexes that are detected by BN-PAGE analyses (Barrett et al., 2007). The authors used mutated TatA that significantly improved Tat functionality in systems lacking TatB (Blaudeck et al., 2005). However, the mutations were in the N-terminus of TatA and cannot be expected to influence the low detergent resistance of the TatA-TatC interaction, which is mediated mainly by the trans-membrane domain (Habersetzer et al., 2017). It is well known that *E. coli* TatA and TatC catalyze translocation with extremely low efficiency (Ize et al., 2002; Blaudeck et al., 2005). Although no easily detectable detergent-stable TatAC complexes are formed, TatA depletes TatC-only complexes in the absence of TatB, indicating that the TatA-TatC interaction engages most TatC *in vivo* and thereby does not permit the formation of TatC-only complexes (Behrendt et al., 2007). The interaction is also supported by *in vitro* TatAC cross-links in the absence of TatB (Blümmel et al., 2015). The absence of BN-PAGE-detectable detergent-solubilized TatAC complexes in systems lacking TatB therefore should not be taken as argument against the relevance of identified Tat complexes in TatABC systems. TC1 and TC2 can bind substrates, resulting in TC1S and TC2S (Behrendt and Brüser, 2014). Substrates were bound *in vivo*, supporting the physiological relevance of these complexes. Now we found a third complex (TC3) that became detectable due to stabilizing interactions of altered side chains. We propose that this is the association that actually delivered the substrate across the membrane.

The knowledge about the three *E. coli* Tat complexes detected so far can be summarized in the following assembly pathway model (**Figure 5**): TC1 can be formed without TatA and may be regarded as the core unit. TC2 is detectable when TatA is present in the system and we think that this likely represents the resting state (Behrendt and Brüser, 2014). Harsh solubilization conditions deplete TC2 in favor of TC1. When TatB is recombinantly overproduced, complexes of the size of TC2 can also be formed without TatA in the system (Behrendt et al., 2007), which agrees with the finding that TatB can occupy TatA-binding sites at TatC under certain conditions (Habersetzer et al., 2017). As both, TC1 and TC2, can bind Tat substrates (Behrendt and Brüser, 2014), it is unclear whether TatA is recruited to TatBC upon substrate binding or whether substrates

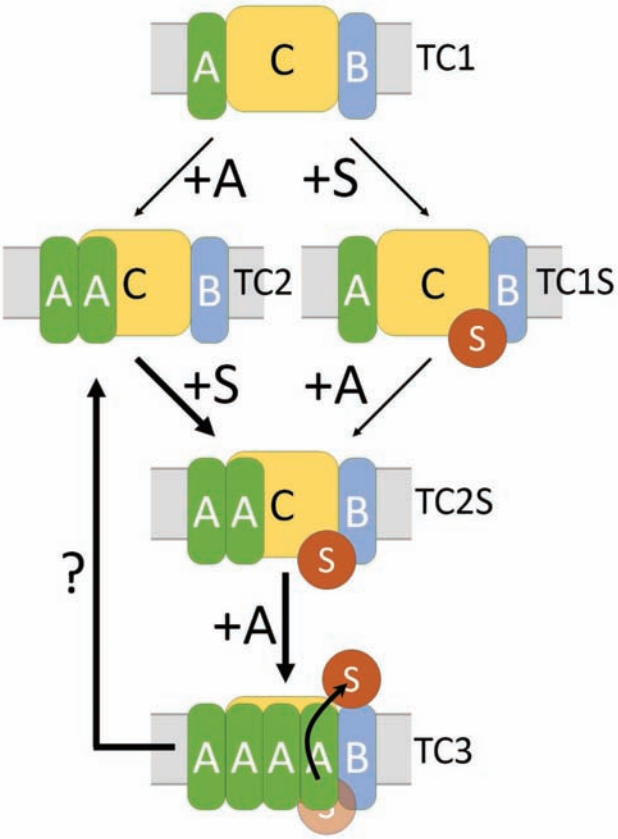

FIGURE 5 | Integrative model for the assembly of active TatABC complexes. Based on the data of this study, in combination with the published work, we propose the following assembly model for active Tat complexes: TC1 represents a Tat complex that can in principle be formed in the absence of TatA and likely is the core complex. TC2 is less stable in detergent solution but already present in wild-type TatABC systems. Both, TC1 and TC2 can in principle bind Tat substrates. Substrate-bound TC2 (TC2S) can switch to TC3, which has an increased affinity to TatA. When TC3 is formed, the substrate can be translocated through the membrane, most likely in an TatA-influenced environment. In the model, "+A" at arrows indicates that more detergent-resistant TatA is bound. "+S" indicates the binding of the twin-arginine motif to its binding site at the TatBC core.

are recruited to TC2 that already contains TatA. Both scenarios can explain the previously observed co-localization of TatA-XFP fusion proteins with TatBC upon substrate overproduction (Alcock et al., 2013; Rose et al., 2013). A stabilization of the TatA-TatBC interaction by substrate binding may compensate for a destabilization that can result from the XFP fusion to the tightly interacting smaller TatA protomers, which would also explain the observations that have been interpreted as substrate-induced assembly. Substrate binding clearly influences the interaction of TatBC with TatA, which can be monitored by cross-linking (Dabney-Smith et al., 2006), but TatA is always directly or indirectly associated with TatBC also under resting conditions (Aldridge et al., 2014; Behrendt and Brüser, 2014). The TatA-dependent rearrangement or conformational transition within Tat complexes likely paves the way for Tat transport. It could be demonstrated that a substrate interaction with TatA results in conformational transitions that destabilize the membrane, and this has been suggested to enable the translocation (Brüser and Sanders, 2003; Hou et al., 2018). All published data suggest that there exists a transiently enhanced affinity to TatA during transport, and it is a matter of kinetic stability, whether or not this active TatABC translocon can be detected. Our analyses now suggest that single amino acid exchanges at position I50, which is positioned at a TatC-TatC interface, can stabilize this active complex. This third Tat complex (TC3) likely switches back to the TC2 state when transport has taken place (question mark in **Figure 5**), and the kinetics of this transition is apparently slowed down by the amino acid exchange, thereby allowing the detection of TC3. The stabilization of TC3 does not require substrate binding and therefore is only a matter of TatABC interactions. As Bpa cross-linking indicates a close proximity of the I50 position to neighboring TatC protomers in the complex, a conformational transition that relies on TatC-TatC interactions is likely responsible for higher TatA affinity. Substrate binding may trigger the switch to this altered interaction in the native, non-mutated system, which explains why TC3 is normally very transient. The data that we obtained with TatBC systems indicate that the I50Bpa mutation enhances not only the TatA affinity but also the TatB affinity to TatC. In contrast to the $TatABC_{I50Bpa}$ system, the $TatBC_{I50Bpa}$ system is not active, indicating that TatB cannot substitute for TatA. However, an inactivated substrate-binding site can trigger the transformation of TC2 to TC3 even in the absence of TatA (**Figure 4**). The conformation of the substrate-binding site might therefore be important for a selective binding of TatA to this site, which is crucial for the transport process. In agreement with this observation, cross-linking studies with the plant TatABC system have shown in the past that TatA associates with the substrate-binding site (Aldridge et al., 2014).

DATA AVAILABILITY

All datasets generated for this study are included in the manuscript.

AUTHOR CONTRIBUTIONS

HG obtained all presented data, except the analysis shown in **Figure 1C**, which was done by CN. DM-B and EH were involved in early stages of the project and did initial experiments. TB designed and supervised the study and wrote the manuscript together with HG. All authors contributed to the final manuscript.

FUNDING

This work was funded by the German Research Foundation (DFG grant BR2285/4-2).

ACKNOWLEDGMENTS

We thank Sybille Traupe and Inge Reupke for excellent technical assistance and Jana Behrendt for discussions and seminal contributions to the methods.

REFERENCES

Alami, M., Lüke, I., Deitermann, S., Eisner, G., Koch, H. G., Brunner, J., et al. (2003). Differential interactions between a twin-arginine signal peptide and its translocase in *Escherichia coli*. *Mol. Cell* 12, 937–946. doi: 10.1016/S1097-2765(03)00398-8

Alcock, F., Baker, M. A. B., Greene, N. P., Palmer, T., Wallace, M. I., and Berks, B. C. (2013). Live cell imaging shows reversible assembly of the TatA component of the twin-arginine protein transport system. *Proc. Natl. Acad. Sci. USA* 110, E3650–E3659. doi: 10.1073/Pnas.1306738110

Alcock, F., Stansfeld, P. J., Basit, H., Habersetzer, J., Baker, M. A., Palmer, T., et al. (2016). Assembling the tat protein translocase. *elife* 5:e20718. doi: 10.7554/eLife.20718

Aldridge, C., Ma, X., Gerard, F., and Cline, K. (2014). Substrate-gated docking of pore subunit Tha4 in the TatC cavity initiates tat translocase assembly. *J. Cell Biol.* 205, 51–65. doi: 10.1083/jcb.201311057

Allen, S. C., Barrett, C. M., Ray, N., and Robinson, C. (2002). Essential cytoplasmic domains in the *Escherichia coli* TatC protein. *J. Biol. Chem.* 277, 10362–10366. doi: 10.1074/Jbc.M109135200

Barrett, C. M. L., Freudl, R., and Robinson, C. (2007). Twin arginine translocation (tat)-dependent export in the apparent absence of TatABC or TatA complexes using modified *Escherichia coli* TatA subunits that substitute for TatB. *J. Biol. Chem.* 282, 36206–36213. doi: 10.1074/Jbc.M704127200

Barrett, C. M., Mangels, D., and Robinson, C. (2005). Mutations in subunits of the *Escherichia coli* twin-arginine translocase block function via differing effects on translocation activity or tat complex structure. *J. Mol. Biol.* 347, 453–463. doi: 10.1016/J.Jmb.2005.01.026

Behrendt, J., and Brüser, T. (2014). The TatBC complex of the tat protein translocase in *Escherichia coli* and its transition to the substrate-bound TatABC complex. *Biochemistry* 53, 2344–2354. doi: 10.1021/bi500169s

Behrendt, J., Lindenstrauss, U., and Brüser, T. (2007). The TatBC complex formation suppresses a modular TatB-multimerization in *Escherichia coli*. *FEBS Lett.* 581, 4085–4090. doi: 10.1016/j.febslet.2007.07.045

Blaudeck, N., Kreutzenbeck, P., Müller, M., Sprenger, G. A., and Freudl, R. (2005). Isolation and characterization of bifunctional *Escherichia coli* TatA mutant proteins that allow efficient tat-dependent protein translocation in the absence of TatB. *J. Biol. Chem.* 280, 3426–3432. doi: 10.1074/Jbc.M411210200

Blümmel, A.-S., Haag, L. A., Eimer, E., Müller, M., and Fröbel, J. (2015). Initial assembly steps of a translocase for folded proteins. *Nat. Commun.* 6:7234. doi: 10.1038/Ncomms8234

Brüser, T., and Sanders, C. (2003). An alternative model of the twin arginine translocation system. *Microbiol. Res.* 158, 7–17. doi: 10.1078/0944-5013-00176

Cline, K. (2015). Mechanistic aspects of folded protein transport by the twin arginine translocase (tat). *J. Biol. Chem.* 290, 16530–16538. doi: 10.1074/Jbc.R114.626820

Cline, K., and Mori, H. (2001). Thylakoid Δph-dependent precursor proteins bind to a Cptatc-Hcf106 complex before Tha4-dependent transport. *J. Cell Biol.* 154, 719–729. doi: 10.1083/Jcb.200105149

Dabney-Smith, C., Mori, H., and Cline, K. (2006). Oligomers of Tha4 organize at the thylakoid tat translocase during protein transport. *J. Biol. Chem.* 281, 5476–5483. doi: 10.1074/Jbc.M512453200

Habersetzer, J., Moore, K., Cherry, J., Buchanan, G., Stansfeld, P. J., and Palmer, T. (2017). Substrate-triggered position switching of TatA and TatB during tat transport in *Escherichia coli*. *Open Biol.* 7:170091. doi: 10.1098/rsob.170091

Hamsanathan, S., and Musser, S. M. (2018). The tat protein transport system: intriguing questions and conundrums. *FEMS Microbiol. Lett.* 365:fny123. doi: 10.1093/femsle/fny123

Hou, B., and Brüser, T. (2011). The tat-dependent protein translocation pathway. *Biomol. Concepts* 2, 507–523. doi: 10.1515/BMC.2011.040

Hou, B., Heidrich, E. S., Mehner-Breitfeld, D., and Brüser, T. (2018). The TatA component of the twin-arginine translocation system locally weakens the cytoplasmic membrane of *Escherichia coli* upon protein substrate binding. *J. Biol. Chem.* 293, 7592–7605. doi: 10.1074/jbc.RA118.002205

Hu, Y., Zhao, E., Li, H., Xia, B., and Jin, C. (2010). Solution NMR structure of the TatA component of the twin-arginine protein transport system from gram-positive bacterium *Bacillus subtilis*. *J. Am. Chem. Soc.* 132, 15942–15944. doi: 10.1021/Ja1053785

Huang, Q., Alcock, F., Kneuper, H., Deme, J. C., Rollauer, S. E., Lea, S. M., et al. (2017). A signal sequence suppressor mutant that stabilizes an assembled state of the twin arginine translocase. *Proc. Natl. Acad. Sci. USA* 114, E1958–E1967. doi: 10.1073/Pnas.1615056114

Ize, B., Gerard, F., Zhang, M., Chanal, A., Voulhoux, R., Palmer, T., et al. (2002). *In vivo* dissection of the tat translocation pathway in *Escherichia coli*. *J. Mol. Biol.* 317, 327–335. doi: 10.1006/Jmbi.2001.5431

Ize, B., Stanley, N. R., Buchanan, G., and Palmer, T. (2003). Role of the *Escherichia coli* tat pathway in outer membrane integrity. *Mol. Microbiol.* 48, 1183–1193. doi: 10.1046/j.1365-2958.2003.03504.x

Källberg, M., Margaryan, G., Wang, S., Ma, J., and Xu, J. (2014). Raptorx server: a resource for template-based protein structure modeling. *Methods Mol. Biol.* 1137, 17–27. doi: 10.1007/978-1-4939-0366-5_2

Kneuper, H., Maldonado, B., Jäger, F., Krehenbrink, M., Buchanan, G., Keller, R., et al. (2012). Molecular dissection of TatC defines critical regions essential for protein transport and a TatB-TatC contact site. *Mol. Microbiol.* 85, 945–961. doi: 10.1111/j.1365-2958.2012.08151.x

Laemmli, U. K. (1970). Cleavage of structural proteins during the assembly of the head of bacteriophage T4. *Nature* 227, 680–685. doi: 10.1038/227680a0

Lindenstrauss, U., Matos, C. F. R. O., Graubner, W., Robinson, C., and Brüser, T. (2010). Malfolded recombinant tat substrates are tat-independently degraded in *Escherichia coli*. *FEBS Lett.* 584, 3644–3648. doi: 10.1016/J.Febslet.2010.07.039

Mehner, D., Osadnik, H., Lünsdorf, H., and Brüser, T. (2012). The tat system for membrane translocation of folded proteins recruits the membrane-stabilizing Psp machinery in *Escherichia coli*. *J. Biol. Chem.* 287, 27834–27842. doi: 10.1074/jbc.M112.374983

Mori, H., and Cline, K. (2002). A twin arginine signal peptide and the Ph gradient trigger reversible assembly of the thylakoid Δph/tat translocase. *J. Cell Biol.* 157, 205–210. doi: 10.1083/jcb.200202048

Oates, J., Barrett, C. M., Barnett, J. P., Byrne, K. G., Bolhuis, A., and Robinson, C. (2005). The *Escherichia coli* twin-arginine translocation apparatus incorporates a distinct form of TatABC complex, spectrum of modular TatA complexes and minor TatAB complex. *J. Mol. Biol.* 346, 295–305. doi: 10.1016/j.jmb.2004.11.047

Orriss, G. L., Tarry, M. J., Ize, B., Sargent, F., Lea, S. M., Palmer, T., et al. (2007). TatBC, TatB, and TatC form structurally autonomous units within the twin arginine protein transport system of *Escherichia coli*. *FEBS Lett.* 581, 4091–4097. doi: 10.1016/j.febslet.2007.07.044

Peng, J., and Xu, J. (2011). Raptorx: exploiting structure information for protein alignment by statistical inference. *Proteins* 79, 161–171. doi: 10.1002/prot.23175

Petrů, M., Wideman, J., Moore, K., Alcock, F., Palmer, T., and Doležal, P. (2018). Evolution of mitochondrial tat translocases illustrates the loss of bacterial protein transport machines in mitochondria. *BMC Biol.* 16:141. doi: 10.1186/s12915-018-0607-3

Pettersen, E. F., Goddard, T. D., Huang, C. C., Couch, G. S., Greenblatt, D. M., Meng, E. C., et al. (2004). UCSF chimera–a visualization system for exploratory research and analysis. *J. Comput. Chem.* 25, 1605–1612. doi: 10.1002/jcc.20084

Ramasamy, S., Abrol, R., Suloway, C. J. M., and Clemons, W. M. (2013). The glove-like structure of the conserved membrane protein TatC provides insight into signal sequence recognition in twin-arginine translocation. *Structure* 21, 777–788. doi: 10.1016/j.str.2013.03.004

Richter, S., and Brüser, T. (2005). Targeting of unfolded Phoa to the tat translocon of *Escherichia coli*. *J. Biol. Chem.* 280, 42723–42730. doi: 10.1074/jbc.M509570200

Rollauer, S. E., Tarry, M. J., Graham, J. E., Jaaskelainen, M., Jager, F., Johnson, S., et al. (2012). Structure of the TatC core of the twin-arginine protein transport system. *Nature* 492, 210–214. doi: 10.1038/Nature11683

Rose, P., Fröbel, J., Graumann, P. L., and Müller, M. (2013). Substrate-dependent assembly of the tat translocase as observed in live *Escherichia coli* cells. *PLoS One* 8:E69488. doi: 10.1371/journal.pone.0069488

Sargent, F., Stanley, N. R., Berks, B. C., and Palmer, T. (1999). Sec-independent protein translocation in *Escherichia coli*. A distinct and pivotal role for the TatB protein. *J. Biol. Chem.* 274, 36073–36082. doi: 10.1074/Jbc.274.51.36073

Sturm, A., Schierhorn, A., Lindenstrauss, U., Lilie, H., and Brüser, T. (2006). Ycdb from *Escherichia coli* reveals a novel class of tat-dependently translocated hemoproteins. *J. Biol. Chem.* 281, 13972–13978. doi: 10.1074/Jbc.M511891200

Taubert, J., Hou, B., Risselada, H. J., Mehner, D., Lünsdorf, H., Grubmüller, H., et al. (2015). TatBC-independent TatA/tat substrate interactions contribute to transport efficiency. *PLoS One* 10:E0119761. doi: 10.1371/journal.pone.0119761

Yen, M. R., Tseng, Y. H., Nguyen, E. H., Wu, L. F., and Saier, M. H. Jr. (2002). Sequence and phylogenetic analyses of the twin-arginine targeting (tat) protein export system. *Arch. Microbiol.* 177, 441–450. doi: 10.1007/s00203-002-0408-4

Young, T. S., Ahmad, I., Yin, J. A., and Schultz, P. G. (2010). An enhanced system for unnatural amino acid mutagenesis in *E. coli*. *J. Mol. Biol.* 395, 361–374. doi: 10.1016/j.jmb.2009.10.030

Zhang, Y., Wang, L., Hu, Y., and Jin, C. (2014). Solution structure of the TatB component of the twin-arginine translocation system. *Biochim. Biophys. Acta* 1838, 1881–1888. doi: 10.1016/J.Bbamem.2014.03.015

Conflict of Interest Statement: The authors declare that the research was conducted in the absence of any commercial or financial relationships that could be construed as a potential conflict of interest.

Copyright © 2019 Geise, Heidrich, Nikolin, Mehner-Breitfeld and Brüser. This is an open-access article distributed under the terms of the Creative Commons Attribution License (CC BY). The use, distribution or reproduction in other forums is permitted, provided the original author(s) and the copyright owner(s) are credited and that the original publication in this journal is cited, in accordance with accepted academic practice. No use, distribution or reproduction is permitted which does not comply with these terms.

frontiers in Microbiology

MINI REVIEW
published: 17 July 2019
doi: 10.3389/fmicb.2019.01635

Distribution, Function and Regulation of Type 6 Secretion Systems of Xanthomonadales

*Ethel Bayer-Santos[1], Lucas de Moraes Ceseti[2], Chuck Shaker Farah[3] and Cristina Elisa Alvarez-Martinez[2]**

[1] Departamento de Microbiologia, Instituto de Ciências Biomédicas, Universidade de São Paulo, São Paulo, Brazil, [2] Departamento de Genética, Evolução, Microbiologia e Imunologia, Instituto de Biologia, Universidade Estadual de Campinas, Campinas, Brazil, [3] Departamento de Bioquímica, Instituto de Química, Universidade de São Paulo, São Paulo, Brazil

OPEN ACCESS

Edited by:
Eric Cascales,
Aix-Marseille Université, France

Reviewed by:
María A. Llamas,
Spanish National Research Council (CSIC), Spain
Thibault Géry Sana,
École Polytechnique Fédérale de Lausanne, Switzerland
Badreddine Douzi,
INRA Centre Nancy-Lorraine, France

***Correspondence:**
Cristina Elisa Alvarez-Martinez
ceamarti@unicamp.br

Specialty section:
This article was submitted to Microbial Physiology and Metabolism, a section of the journal Frontiers in Microbiology

Received: 04 March 2019
Accepted: 02 July 2019
Published: 17 July 2019

Citation:
Bayer-Santos E, Ceseti LM, Farah CS and Alvarez-Martinez CE (2019) Distribution, Function and Regulation of Type 6 Secretion Systems of Xanthomonadales. Front. Microbiol. 10:1635. doi: 10.3389/fmicb.2019.01635

Members of the Xanthomonadales order include several plant pathogens of significant economic and agricultural impact, such as *Xanthomonas* spp. Type 6 secretion systems (T6SSs) are contractile nanomachines used by many bacterial species to inject protein effectors into target prokaryotic and eukaryotic cells and provide a competitive advantage for bacteria in different environments. Effectors with antibacterial properties include peptidoglycan hydrolases, lipases and phospholipases that break down structural components of the cell envelope, promoting target-cell lysis; and RNases, DNAses, and NADases that affect target-cell metabolism, arresting growth. Effectors with anti-eukaryotic properties are functionally more diverse. The T6SS of *Xanthomonas citri* is the only example experimentally characterized so far within the Xanthomonadales order and displays anti-eukaryotic function by providing resistance to predation by amoeba. This T6SS is regulated at the transcriptional level by a signaling cascade involving a Ser/Thr kinase and an extracytoplasmic function (ECF) sigma factor. In this review, we performed *in silico* analyses of 35 genomes of Xanthomonadales and showed that T6SSs are widely distributed and phylogenetically classified into three major groups. *In silico* predictions identified a series of proteins with known toxic domains as putative T6SS effectors, suggesting that the T6SSs of Xanthomonadales display both anti-prokaryotic and anti-eukaryotic properties depending on the phylogenetic group and bacterial species.

Keywords: Xanthomonadales, *Xanthomonas*, T6SS, bacterial killing, amoeba predation, effectors, toxins

INTRODUCTION

The order Xanthomonadales includes many Gram-negative rod-shaped bacteria with very diverse physiological characteristics and habitats. Members of this group range from plant and human pathogens to non-pathogenic environmental bacteria that are able to survive in adverse conditions such as contaminated soil and hot springs (Saddler and Bradbury, 2005). Xanthomonadales is

an early diverging branch of the Gammaproteobacteria (Williams et al., 2010). The taxonomy of the order is controversial, but a recent phylogenetic analysis has divided Xanthomonadales into two main branches comprising the families *Xanthomonadaceae* and *Rhodanobacteraceae* (Naushad et al., 2015). *Xanthomonadaceae* includes genera *Xanthomonas*, *Xylella*, *Stenotrophomonas*, *Pseudoxanthomonas*, *Luteimonas*, *Lysobacter*, *Thermomonas*, *Arenimonas*, and *Silanimonas*; while *Rhodanobacteraceae* includes genera *Rhodanobacter*, *Dyella*, *Frateuria*, *Luteibacter*, *Fulvimonas*, *Pseudofulvimonas*, *Aquimonas*, *Dokdonella*, and *Rudaea* (Naushad et al., 2015).

Species of the *Xanthomonadaceae* family have been by far the most studied due to their importance as plant pathogens. The genera *Xanthomonas* and *Xylella* contain species that promote disease in more than 400 economically important crops, including citrus, tomato, rice, cabbage, pepper, coffee, grapes, and olives (Leyns et al., 1984; Rapicavoli et al., 2018). Species within both genera vary in their ability to colonize different plant tissues and show a high degree of host specificity (Ryan et al., 2011). *Stenotrophomonas* is another important genus in *Xanthomonadaceae*. *Stenotrophomonas maltophilia* include several strains that are nosocomial pathogens, causing bacteremia, endocarditis and pneumonia in immunocompromised and cystic fibrosis patients (Adegoke et al., 2017). Conversely, species like *Stenotrophomonas rhizophila* are environmental bacteria found in association with plants and have a well-documented ability to promote plant growth, suppress colonization by plant pathogens and degrade a wide variety of xenobiotics, making them potential agents for biocontrol and bioremediation (Berg and Martinez, 2015). The genus *Lysobacter* comprises gliding predatory bacteria that display broad-spectrum lytic activity against nematodes, fungi, Gram-negative and Gram-positive bacteria (Christensen and Cook, 2009), including species of significant biotechnological and biocontrol interest (Ko et al., 2009; Hayward et al., 2010).

Availability of genomic data from an increasing number of Xanthomonadales species has provided important insights into environmental adaptations and physiological diversity. Gene clusters encoding bacterial secretion systems are recognized as key virulence factors of pathogenic species within the order (Büttner and Bonas, 2010). The type 6 secretion system (T6SS) is a molecular nanomachine that provides increased fitness to bacteria by firing a series of toxic effector proteins into neighbor competitor species, thus shaping bacterial communities. The T6SS of the biocontrol agent *Pseudomonas putida* kills phytopathogens upon co-infection *in planta*, and the *Agrobacterium tumefaciens* T6SS promotes plant colonization by providing a competitive advantage (Ma et al., 2014; Bernal et al., 2017). Anti-eukaryotic T6SSs are important for virulence in mammalian hosts, as well as for bacterial survival in the environment by providing resistance to predation by amoebas and exhibiting killing activity against fungi (Hachani et al., 2016; Bayer-Santos et al., 2018; Trunk et al., 2018). A role of T6SS in nutrient acquisition by the secretion of metal-scavenging proteins in the extracellular milieu has also been reported (Si et al., 2017a,b).

The sole T6SS representative of the Xanthomonadales order experimentally characterized to date from *Xanthomonas citri* pv. *citri* is required for resistance against predation by the soil amoeba *Dictyostelium discoideum* (Bayer-Santos et al., 2018), a yet unexplored aspect of xanthomonad biology that can be expected to be an important factor for environmental survival and dissemination. The secreted effectors and dynamics of *X. citri*-amoeba interactions are still elusive. The *X. citri* T6SS does not confer a competitive advantage in encounters with other Gram-negative bacteria and *X. citri* antibacterial activity is dependent on a type 4 secretion system (T4SS) (Souza et al., 2015; Bayer-Santos et al., 2018).

T6SSs are encoded in the genome of several species within Xanthomonadales. In this review, we performed *in silico* analyses of Xanthomonadales T6SSs to describe the distribution and genomic organization of T6SSs clusters in these species. Furthermore, we identified putative T6SS effectors that provided clues about the function of uncharacterized T6SS clusters in several Xanthomonadales species.

TYPE 6 SECRETION SYSTEM

The T6SS is a contractile machinery composed of 13 core structural proteins. This system is evolutionarily related to the tail of bacteriophages (Basler and Mekalanos, 2012) and assembles into three major complexes: the *trans*-membrane complex, the baseplate and the tail. The *trans*-membrane complex is composed of three proteins TssM, TssL, and TssJ. The baseplate is formed by TssE, TssF, TssG, and TssK, and represents an adaptor between the *trans*-membrane complex and the tail. The tail has an internal tube formed by Hcp topped with VgrG and is enveloped by a contractile sheath composed of TssB and TssC (Nguyen et al., 2018). The assembly of the tail requires TssA, which interacts with baseplate, inner tube and sheath components and stabilizes the distal extremity of the tube (Planamente et al., 2016; Zoued et al., 2016; Dix et al., 2018). After contraction, the T6SS tail is recycled via the ATPase ClpV that disassembles the sheath into monomeric components (Kapitein et al., 2013). In addition to the core structural proteins described above, T6SS gene clusters also encode accessory proteins, which comprise components required for the assembly of the secretion apparatus, regulatory subunits acting transcriptionally or post-translationally to control the expression or the activity of the T6SS, and effectors and immunity proteins required for its function (Silverman et al., 2012).

T6SSs deliver protein effectors into diverse cell types including prokaryotic and eukaryotic cells in a contact-dependent manner (Cianfanelli et al., 2016; Hachani et al., 2016). T6SSs were also reported to display contact-independent functions in which secreted effectors facilitate the acquisition of nutrients (Wang et al., 2015; Si et al., 2017a,b). T6SS gene clusters have been classified into four subtypes ($T6SS^{i-iv}$) (Boyer et al., 2009; Bröms et al., 2010; Russell et al., 2014; Bock et al., 2017): (i) the majority of T6SSs belong to subtype $T6SS^{i}$ and are present

in Proteobacteria; (ii) the *Francisella* pathogenicity island-like systems were classified as T6SS^{ii} (Bröms et al., 2010); (iii) Bacteroidetes T6SSs are distinct from the first two and were classified as T6SS^{iii} (Russell et al., 2014); and (iv) a contractile system from *Amoebophilus asiaticus* was classified T6SS^{iv} (Bock et al., 2017). Proteobacteria T6SS^{i} are the most diverse and have been further subdivided into five phylogenetic clades (Boyer et al., 2009). Xanthomonadales harbor three subtypes of T6SS^{i} belonging to clades 1, 3, and 4, which will be discussed below.

GENOMIC ARCHITECTURE OF XANTHOMONADALES T6SS CLUSTERS

From 71 Xanthomonadales species genomes retrieved from the KEGG database (Kanehisa and Goto, 2000), we identified 35 genomes harboring one or two T6SS clusters (**Supplementary Table S1**). Distribution of T6SS does not show a clear correlation with species lifestyles and they are found in several environmental bacteria and phytopathogenic species that colonize distinct plant tissues (vascular and non-vascular pathogens) (**Supplementary Table S1**). T6SS clusters are absent in xylem-limited phytopathogens with reduced genomes, including *X. albilineans* (3.78 Mb) and all members of the *Xylella* genus (2.5 Mb).

According to phylogenetic analyses using the sheath component TssC, T6SSs clusters separate into three groups matching clades/groups 1, 3, and 4 proposed by Boyer et al. (2009) (**Figure 1A**). Similarly, analysis of T6SS distribution in plant-associated bacteria that included several members of the *Xanthomonas* genus has shown an overrepresentation of these three clades (Bernal et al., 2018). Group 3 presents the most heterogeneous distribution among plant-associated bacteria and the Xanthomonadales representatives are clustered in a clade that includes *Burkholderia* species (Bernal et al., 2018). Xanthomonadales group 4 T6SSs belong to subgroup 4B2 described by Bernal et al. (2018), which also includes *Ralstonia* and *Burkholderia* species. The sole member of group 1 is found in a *Stenotrophomonas* sp. isolated from the phyllosphere and a phylogenetic analysis showed that it belongs to the subclade 1.2A described by Bernal et al. (2018), which includes *P. putida* species. Each group displays a unique genetic architecture, contains different T6SS-associated genes (Tag proteins) and present variable regions within or in the vicinity of the structural gene clusters, which contain putative effectors and/or regulatory proteins (**Figure 1B**). The characteristics of each group are further described in detail below.

Group 3 presents two main clusters of structural genes separated by an insertion in which the content varies depending on the bacterial species, ranging from ∼2.2 to 15.6 kb (**Figure 1B**). Group 3 was further divided into three subclades (hereafter referred to as subgroup 3*, 3**, and 3***) (**Figures 1A,B**). Division of *Xanthomonas* group 3 T6SSs in two subclades is also observed in the phylogenetic analysis by Bernal et al. (2018), which did not include *Dyella* species. Group 3* contains the only Xanthomonadales T6SS functionally characterized to date from *X. citri* (**Figure 1A**) (Bayer-Santos et al., 2018) and is restricted to *Xanthomonas* species, a few of them also containing a second T6SS from subgroup 3*** (**Figure 1**). The presence of one representative from each subgroup in some species may indicate distinct functions in bacterial physiology, despite similarities in cluster organization.

Group 3 shows unique features such as the presence of components from the PpkA-PppA-FHA post-translational phosphorylation pathway (Mougous et al., 2007) and its repressor TagF (Silverman et al., 2011; Lin et al., 2018). It also contains TagJ, which interacts with the ATPase ClpV and the sheath component TssB to control the disassembly of the contracted sheath (Forster et al., 2014). TagJ co-evolved with a specific subset of the TssB/TssC/ClpV gene cluster (Forster et al., 2014). The TssA component from group 3 is closely related to homologs from group 4 T6SSs, belonging to the same phylogenetic clade 1 (TssA1) (Dix et al., 2018), while TssA from group 1 T6SS shows a divergent C-terminal region and belongs to clade 2 (Dix et al., 2018). In *X. citri*, the variable region is ∼15.6 kb and contains the extracytoplasmic function (ECF) sigma factor EcfK and its cognate kinase PknS, which were shown to be required for T6SS activation and function (Bayer-Santos et al., 2018). Curiously, EcfK/PknS are not present in the most similar T6SS cluster from *Dyella japonica* and *Dyella thiooxydans* (**Figure 1A**), which has an intermediate-size variable region of ∼5.2 kb. Despite the differences in the variable region, T6SS from *D. japonica* and *D. thiooxydans* are very similar to *X. citri* T6SS and present conserved genes of unknown function downstream of the *PAAR* and *vgrG* genes (**Figure 1B**, white arrows). A third genetic architecture within group 3 can be observed in a branch comprising *Xanthomonas oryzae* pv. *oryzae*, *Xanthomonas oryzae* pv. *oryzicola*, and *Lysobacter enzymogenes* (subgroup 3***). These species contain even smaller insertions in the variable region (∼2.2 kb) and *tssA* appears in a different orientation (**Figure 1B**). Bacterial species carrying this subtype of T6SS usually have a second T6SS belonging to group 4 or subgroup 3* (**Figure 1A**, blue).

T6SSs classified as group 4 display two genetic architectures. In the majority of species, the structural core genes are organized in conserved clusters and variability is found in the vicinity of *vgrG* genes. These variable regions are very large – ranging from 40 kb to 75 kb – and contain several duplications of *vgrG* (up to 6), proteins with domains of unknown functions (DUFs) and proteins with putative toxic domains (**Table 1**). In some species, such as *Xanthomonas fragariae*, the cluster of structural genes composed of *tssM*, *tagF*, *tagN*, and *tssA* are located ∼300 kb from the other structural cluster composed of *tssJ*, *tssK*, *tssL*, *vgrG*. Another interesting and unique feature of T6SSs from group 4 is the presence of a gene encoding TagX, which is a membrane-associated peptidoglycan hydrolase proposed to help degrade the bacterial wall for the insertion of T6SS machinery (Weber et al., 2016). Group 4 T6SSs also contain the associated genes *tagN* and *tagM*, but their role in T6SS biogenesis or regulation was not yet clarified. *Lysobacter gummosus* is the only example belonging to group 4 that contains

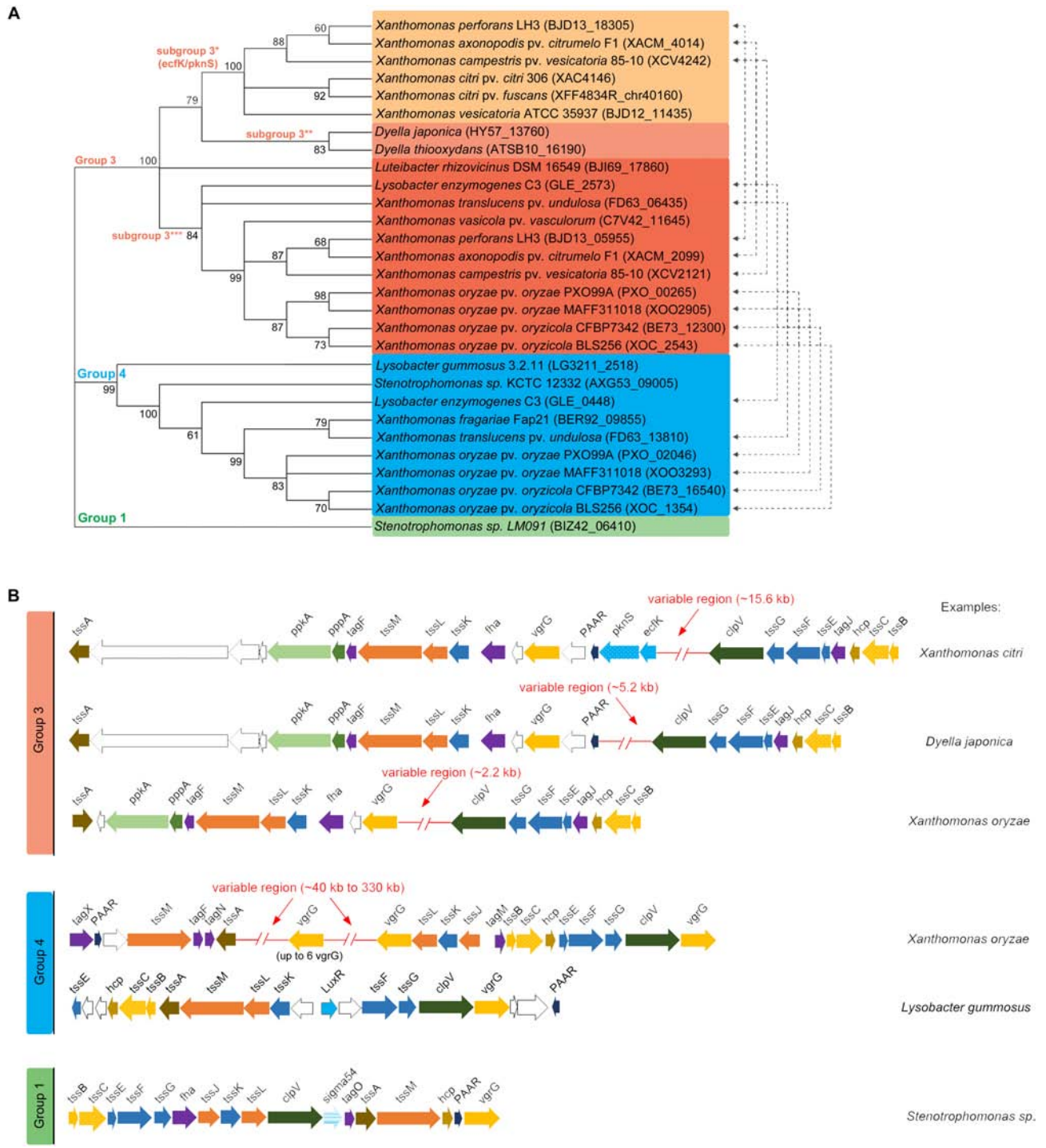

FIGURE 1 | Phylogenetic classification of T6SSs within Xanthomonadales and genomic organization of T6SS gene clusters. **(A)** Phylogenetic distribution of Xanthomonadales T6SS clusters. Maximum-likelihood consensus tree with 1000 bootstrap replicates built with amino acid sequence of TssC (XAC4146) homologs aligned and grouped using MEGA 7.0 (Kumar et al., 2016). **(B)** Schematic representation of genomic regions encoding the different subtypes of T6SSs.

a divergent version of T6SS, displaying a different genetic architecture (**Figure 1B**).

The only example of a Group 1 T6SS is found in *Stenotrophomonas* sp. LM91. This system is very similar to the T6SS from *Vibrio cholerae* and contains the sigma factor σ^{54} transcriptional regulator, which was reported to control the expression of T6SS in other bacteria (Bernard et al., 2011). Group 1 T6SS also contains a gene

TABLE 1 | List of PAAR and VgrG proteins from Xanthomonadales and putative toxic effectors identified by Bastion6 software.

Species	T6SS Group	PAAR	Orphan PAAR	VgrG (class)	Orphan VgrG (class)	Bastion6 predicted T6SS effectors	
						N	Description[1,2]
X. vesicatoria ATCC 35937	3*	1	0	1 (I)	0	4	Hypothetical
X. vasicola pv. *vasculorum* SAM119	3***	0	0	1 (I)	0	1	Hypothetical
X. translucens pv. *undulosa* Xtu 4699	3***	0	2	1 (I)	0	1	Hypothetical
	4	1		2 (II)		12[#]	Tle1-like, DUF3304 (2), neuraminidase
						2 orphans	Tox-REase-5 (2)
X. perforans LH3	3*	1	0	1 (I)	0	3	Acid phosphatase, EEP endo/exonuclease/phosphatase
	3***	0		1 (I)		2	TIR_2 superfamily
X. oryzae pv. *oryzicola* CFBP7342	3***	0	3	1 (I) and 1 (II)	1 (I) and 10 (II)	3	Hypothetical
	4	1		4 (II)		19	Tle1-like (4), DUF3304 (5), hydrolase
						55 orphans	Tle1-like (2), Tle3-like (2), Tle4-like (2), DUF2875 (5), DUF3304 (4), DUF1800, DUF1501, catalase, peptidase (2), PAAR/Rhs MafB19-deaminase, haemolysin, Tox-REase-5
X. oryzae pv. *oryzicola* BLS256	3***	0	1	2 (I) and 1 (II)	3 (I) and 5 (II)	1	Hypothetical
	4	1		2 (I) and 3 (II)		14	Tle1-like (4), DUF3304 (3), hydrolase
						39 orphans	Tle1-like (2), Tle3-like (4), Tle4-like (3), DUF2875 (5), DUF3304 (5), DUF493, peptidase, transglycosylase, carboxypeptidase, Rhs repeat proteins (2), oxidoreductase
X. oryzae pv. *oryzae* PXO99A	3***	0	5	1 (I) and 1 (II)	1 (I) and 5 (II)	2	Hypothetical
	4	1		3 (II)		12	Tle1-like (2), DUF3304 (2), transglycosylase
						13 orphans	Tle3-like (5), DUF2875 (4)
X. oryzae pv. *oryzae* MAFF 311018	3***	0	3	1 (I)	2 (I) and 7 (II)	0	
	4	1		5 (II)		14	Tle1-like (2), DUF3304 (5), DUF2345
						51 orphans	Tle1-like (4), DUF3304 (6), Tle3-like (5), DUF2875 (5), murein hydrolase D, muraminidase (2), carboxypeptidase, peptidase, PAAR/Rhs XOO_2897-like deaminase, Tox-REase-5 (2)
X. fragariae Fap21	4	1	0	4 (II)	2 (I) and 4 (II)	12	Hypothetical
						27 orphans	Tle1-like (2), DUF3304 (6), glycoside hydrolase, Rhs repeat protein, PAAR/DUF4150 Colicin-DNAse
X. citri pv. *fuscans*	3*	1	0	1 (I)	0	4	Acid phosphatase, EEP endo/exonuclease/phosphatase
X. citri pv. *citri* 306	3*	1	0	1 (I)	0	4	Acid phosphatase, EEP endo/exonuclease/phosphatase, adhesin
X. campestris pv. *vesicatoria* 85-10	3*	1	0	1 (I)	0	4	Acid phosphatase, EEP endo/exonuclease/phosphatase
	3***	0		1 (I)		4	TIR_2 superfamily
X. axonopodis pv. *citrumelo* F1	3*	1	0	1 (I)	0	4	Acid phosphatase, EEP endo/exonuclease/phosphatase
	3***	0		1 (I)		3	TIR_2 superfamily
Stenotrophomonas sp. LM091	1	1	0	1 (II)	0	5	Tle3-like (2), DUF4274, DUF2875
Stenotrophomonas sp. KCTC 12332	4	1	2	1 (I) and 1 (II)	1 (II)	4	Hypothetical
						6 orphans	Tle1-like, Tle4-like, DUF4287
L. rhizovicinus DSM 16549	3***	0	0	1 (I)	0	1	Hypothetical
L. gummosus 3.2.11	4	1	2	1 (I)	1 (I)	4	Transglycosylase, peptidoglycan-binding protein
						7 orphans	DUF4157, peptidase, DUF3244/DUF3218

(Continued)

TABLE 1 | Continued

Species	T6SS Group	PAAR	Orphan PAAR	VgrG (class)	Orphan VgrG (class)	Bastion6 predicted T6SS effectors	
						N	Description[1,2]
L. enzymogenes C3	3***	0	3	1 (I)	1 (I)	0	
	4	0		3 (II)		7	Tle4-like protein, hydrolase, peptidase, phospholipase
						3 orphans	GTP-binding protein, TPR-repeat protein
D. thyooxidans ATSB10	3**	1	0	1 (I)	0	1	Hypothetical
D. japonica A8	3**	1	0	1 (I)	2 (II)	2	DUF5636, amidase
						7 orphans	Phospholipase, muraminidase, peptidase, TPR repeat proteins (3)

[#]*All genes flanking the two VgrGs were analyzed.* [1]*Only proteins with putative toxic domains or DUFs previously associated with T6SS are described.* [2]*Number of proteins with identical domains are indicated in brackets when >1.*

encoding the associated protein TagO, but its function is still unknown.

FUNCTION OF PUTATIVE XANTHOMONADALES T6SS EFFECTORS

T6SSs translocate effectors by decorating the Hcp-VgrG-PAAR puncturing device that is propelled against target cells, thus delivering a cocktail of effectors after each contraction event. The current model suggests that effectors can either interact with one of these three proteins, named "cargo" effectors, or be presented as an extra domain within the same proteins, named "specialized" effectors (Durand et al., 2014; Cianfanelli et al., 2016).

In order to assess the repertoire of Xanthomonadales T6SSs effectors, we manually analyzed the genomic regions encoding the structural components Hcp, VgrG, and PAAR to search for specialized effectors. All Xanthomonadales species analyzed display only one copy of Hcp that is associated with a T6SS structural cluster, and these Hcps do not present a C-terminal extension (**Supplementary Table S2A**). The VgrG repertoire of Xanthomonadales seems to be more diverse. VgrGs are categorized into three classes (De Maayer et al., 2011): the first is composed of proteins with a N-terminal VgrG domain; the second class is formed by VgrG proteins carrying a C-terminal domain of unknown function DUF2345, which is required for interaction with cargo effectors (Flaugnatti et al., 2016); and the third class comprises the evolved- or specialized-VgrG that carry a C-terminal toxic domain. In Xanthomonadales, class I VgrGs seem to be predominantly associated with the T6SSs belonging to group 3 (**Table 1** and **Supplementary Table S2B**). Class II VgrGs are more abundant in species that carry a T6SS belonging to group 4 (**Table 1** and **Supplementary Table S2B**). In addition, Xanthomonadales species that contain T6SS clusters from group 4 usually have orphan VgrGs scattered in the genome (**Supplementary Table S2B**), while species with T6SSs from subgroup 3* do not harbor orphan VgrGs. Interestingly, a high number of orphan VgrGs are found in the genomes of *X. oryzae* from different strains. Moreover, no bona fide specialized VgrGs (class III) were detected in the analyzed genomes (**Table 1** and **Supplementary Table S2B**). PAAR proteins were associated with T6SS structural gene clusters in all groups, except species from subgroup 3*** (**Figure 1**, **Table 1**, and **Supplementary Table S2C**). Most species harboring a subgroup 3*** T6SS that lack a PAAR protein also encode an additional T6SS cluster in their genomes, either from subgroup 3* or 4 (**Figure 1A**). At this point, it is unclear whether PAAR-like proteins could be shared between two systems or whether subgroup 3*** systems are non-functional due to the loss of an associated PAAR protein. Nevertheless, none of the Xanthomonadales PAAR proteins associated with T6SS clusters have extended domains coding for putative toxic proteins (**Supplementary Table S2C**). Orphan PAAR proteins are present in genomes that contain a group 4 T6SS cluster, some of them with extended sizes that might encode effector functions (**Supplementary Table S2C**). Among them, three proteins that belong to the modular PAAR-Rhs-toxin group of antibacterial toxins (Ma et al., 2017) are present in the genomes of *X. fragarie*, *X. oryzae* pv. *oryzae*, and *X. oryzae* pv. *oryzicola* (**Supplementary Tables S2C**, **S3**).

To search for cargo effectors using *in silico* analyses, we arbitrarily chose to analyze a fixed number of 10 genes immediately flanking all T6SS VgrGs using Bastion6 software (Wang et al., 2018). We also searched for genes encoding DUF4123, DUF2169 or DUF1795-containing proteins, which act as adaptors for effector recruitment by T6SSs (Liang et al., 2015; Unterweger et al., 2015; Bondage et al., 2016). Genes encoding DUF1795 are not present in Xanthomonadales genomes, while DUF2169 genes are located in association with VgrG (**Supplementary Table S2D**), as previously described (Liang et al., 2015; Unterweger et al., 2015). Fourteen DUF4123-containing proteins were found encoded in Xanthomonadales genomes, not associated with structural clusters or orphan VgrGs (**Supplementary Table S2E**). We retrieved the two genes located immediately downstream from each DUF4123-encoding gene for effector prediction using Bastion6. Antibacterial cargo effectors are usually encoded in bicistronic units with genes encoding cognate immunity proteins, targeting components of the bacterial cell-envelope and/or nucleic acids, such as peptidoglycan hydrolases, amidases, lipases, and nucleases (Lien and Lai, 2017).

Effectors with anti-eukaryotic properties are less studied and functionally more diverse and include proteins involved in actin-crosslinking, lipases, deaminases and catalases (Jiang et al., 2014; Lien and Lai, 2017).

Analysis of the set of predicted T6SS effectors from Xanthomonadales showed a high number of putative antibacterial toxins associated with group 4 T6SS, which display hydrolase, lipase, carboxypeptidase and muraminidase domains (**Table 1** and **Supplementary Table S3**). Interestingly, most genomes harbouring a group 4 T6SS present multiple copies of members of the superfamily of antibacterial T6SS lipase effectors (Tle), more specifically from families Tle1, Tle3, and Tle 4 (Russell et al., 2013) (**Table 1** and **Supplementary Table S3**). Furthermore, Tle1 copies are found in association with T6SS clusters from group 4 in most genomes (**Table 1** and **Supplementary Table S3**). Tle1 homologs from *Burkholdeia thailandensis* and *Escherichia coli* EAEC Sci-1 T6SS were shown to have antibacterial activity (Russell et al., 2013; Flaugnatti et al., 2016). In *X. fragariae*, putative antibacterial toxins containing hydrolase domains and a colicin-DNAse domain are associated with orphan VgrGs (**Table 1** and **Supplementary Table S3**). Similarly, a variety of putative effectors with hydrolase and phospholipase domains were found associated to the variable regions of *L. enzymogenes* group 4 cluster, which has 3 class II *vgrG* genes (**Table 1** and **Supplementary Table S3**). Interestingly, five putative predicted effectors belonging to the Tox-REase-5 family of restriction endonucleases that includes TseT, a previously described antibacterial toxin from *Pseudomonas aeruginosa* H2-T6SS (Burkinshaw et al., 2018) are present in association with orphan DUF4123-containing proteins in *X. oryzae* strains and *Xanthomonas translucens* pv. *undulosa* (**Table 1**). As no example belonging to Xanthomonadales group 4 T6SS has been functionally characterized to date, based on the domains of putative effectors secreted by these systems, we hypothesize that members of group 4 might display antibacterial activity rather than anti-eukaryotic activity as observed for the *X. citri* T6SS from group 3* (Bayer-Santos et al., 2018). Interestingly, group 4 T6SSs are mostly found in Xanthomonadales genomes that lack the antibacterial T4SS (Souza et al., 2015; Sgro et al., 2019), as exemplified by all *X. oryzae* strains.

Prediction of T6SS effectors associated with VgrGs from group 3 identified a limited number of proteins of unknown function (**Table 1** and **Supplementary Table S3**). For the T6SSs from subgroup 3*, which are homologous to the anti-amoeba T6SS from *X. citri*, two proteins were frequently identified in the vicinity of VgrGs: an acid phosphatase and a protein with lectin and phosphodiesterase domains from the EEP family (endo/exonuclease/phosphatase) (**Table 1**). A distinct set of conserved hypothetical proteins were identified in subgroup 3***, including some with a TIR_2 domain typical of Toll-like receptors. Bacterial proteins containing these domains have been originally implicated in virulence by subversion of host immune responses, but recent work showed their roles as NADases that cleave NAD^+ and interfere with cellular metabolism (Cirl et al., 2008; Essuman et al., 2018). On the other hand, *D. japonica* group 3 T6SS is the sole representative in the group that presents several predicted antibacterial T6SS effectors (proteins containing amidase, muraminidase, and phospholipase domains) in the vicinity of VgrG, suggesting a role as an anti-prokaryotic weapon (**Table 1**). These observations lead us to speculate that distinct subgroups within group 3 might display diverse functions in Xanthomonadales.

REGULATION OF T6SSS

Regulation of T6SSs assembly and firing events occur at different levels: transcriptional, posttranscriptional, and post-translational. Transcriptional regulation of T6SS genes is highly variable among species and several components have been implicated in this activity, including the nucleoid-structuring protein H-NS, σ^{54} and regulators of nutrient acquisition pathways such as Fur and PhoB-PhoR (Brunet et al., 2011, 2015; Silverman et al., 2012). The *X. citri* T6SS is regulated at the transcriptional level by a mechanism involving an alternative sigma factor of the ECF family named EcfK and a transmembrane eukaryotic-like serine-threonine kinase (PknS), which is required for activation of EcfK (Bayer-Santos et al., 2018).

Interestingly, T6SS clusters from subgroup 3*** that do not contain EcfK/PknS carry a gene for a LysR-type transcriptional regulator that is predicted to be co-transcribed with the *tssA* gene (**Figure 1** and **Supplementary Table S4**). Genes encoding a VirA/VirG-like two-component system are also found in a putative operon associated with *lysR-tssA* in all subgroup 3*** T6SS, except for *Luteibacter rhizovicinus* that form a distinct branch within the group (**Figure 1** and **Supplementary Table S4**). This conservation in genome organization and the absence of *ecfK/pknS* suggest that these regulators might be involved in the control of subgroup 3*** T6SS gene expression. T6SS from *Dyella* spp. form a distinct branch in group 3 and do not present *ecfK/pknS* homologs or *lysR*-type genes near their T6SS clusters. No conserved gene encoding a transcriptional regulator was identified in T6SS clusters from group 4, except for a LuxR homolog that is present in the divergent *L. gummosus* cluster.

Distribution of T6SS putative post-translational regulators also differ among distinct clades. T6SS clusters from group 3 contain *tagF-pppA-ppkA-fha* genes, suggesting that activation of T6SS assembly and firing is dependent on the activation of the kinase PpkA, as originally described in *P. aeruginosa* (Mougous et al., 2007; Casabona et al., 2013). Recent work has demonstrated that PpkA acts by counteracting the inhibitory effect of TagF on T6SS activity, and the distinction between defensive and offensive T6SSs is mainly determined by the upstream input from protein(s) responsible for activation of PpkA (Lin et al., 2018; Ostrowski et al., 2018). In the defensive T6SS of *P. aeruginosa*, an incoming attack is sensed in the periplasm by TagQRST, while in the offensive *Serratia marcensens* T6SS, the signal is sensed by RtkS (Ostrowski et al., 2018). The offensive/defensive model has been described in only a few antibacterial T6SS and the mechanism of post-translational activation of anti-eukaryotic machines is possibly different.

Whether the post-translational regulatory cascade depending on tagF-pppA-ppkA-fha genes are functional in Xanthomonadales remains to be determined experimentally. Interestingly, T6SS clusters from group 4 do not encode *ppkA* or *pppA*, but instead contain a *tagF* gene (**Figure 1**), suggesting that a yet undescribed mechanism may be involved in relieving repression imposed by TagF in this group. The group 1 T6SS clusters from *Stenotrophomonas* sp. do not encode any component of the post-translational regulatory pathway, suggesting that activation occurs at the transcriptional level through σ^{54}.

PERSPECTIVES

Studies on the function, regulation and characterization of effector repertoire of T6SSs from Xanthomonadales is only just beginning. Much work is still required to understand how these systems contribute to the biology and pathogenesis of members of these important groups of bacteria. Further experimental evidence is needed to clarify whether the different subtypes of T6SSs pointed out in this review function as antibacterial and/or anti-eukaryotic weapons and whether the predicted putative effectors identified here are bona fide cargo proteins.

AUTHOR CONTRIBUTIONS

EB-S and CA-M performed *in silico* analysis, wrote and edited the review. LC performed *in silico* analysis and wrote the review. CF wrote and edited the review.

FUNDING

This work was supported by grants from the São Paulo Research Foundation (FAPESP) to EB-S (2017/02178-2), CF (2017/17303-7), and CA-M (2018/01852-4). EB-S (2018/04553-8) and LC (2017/02318-9) was supported by FAPESP. CF received a research fellowship award from the National Council for Scientific and Technological Development (CNPq). This study was also supported partly by the Coordenação de Aperfeiçoamento de Pessoal de Nível Superior – Brasil (CAPES) – Finance Code 001.

SUPPLEMENTARY MATERIAL

The Supplementary Material for this article can be found online at: https://www.frontiersin.org/articles/10.3389/fmicb.2019.01635/full#supplementary-material

REFERENCES

Adegoke, A. A., Stenström, T. A., and Okoh, A. I. (2017). *Stenotrophomonas maltophilia* as an emerging ubiquitous pathogen: looking beyond contemporary antibiotic therapy. *Front. Microbiol.* 8:2276. doi: 10.3389/fmicb.2017.02276

Basler, M., and Mekalanos, J. (2012). Type 6 secretion dynamics within and between bacterial cells. *Science* 337:815. doi: 10.1126/science.1222901

Bayer-Santos, E., Lidia dos Passos, L., de Moraes Ceseti, L., Ratagami, C. Y., de Santana, E. S., da Silva, A. M., et al. (2018). Xanthomonas citri T6SS mediates resistance to *Dictyostelium* predation and is regulated by an ECF σ factor and cognate Ser/Thr kinase. *Environ. Microbiol.* 20, 1562–1575. doi: 10.1111/1462-2920.14085

Berg, G., and Martinez, J. L. (2015). Friends or foes: can we make a distinction between beneficial and harmful strains of the *Stenotrophomonas maltophilia* complex? *Front. Microbiol.* 6:241. doi: 10.3389/fmicb.2015.00241

Bernal, P., Allsopp, L. P., Filloux, A., and Llamas, M. A. (2017). The *Pseudomonas putida* T6SS is a plant warden against phytopathogens. *ISME J.* 11, 972–987. doi: 10.1038/ismej.2016.169

Bernal, P., Llamas, M. A., and Filloux, A. (2018). Type VI secretion systems in plant-associated bacteria. *Environ. Microbiol.* 20, 1–15. doi: 10.1111/1462-2920.13956

Bernard, C. S., Brunet, Y. R., Gavioli, M., Lloubès, R., and Cascales, E. (2011). Regulation of type VI secretion gene clusters by σ^{54} and cognate enhancer binding proteins. *J Bacteriol.* 193, 2158–2167. doi: 10.1128/JB.00029-11.

Bock, D., Medeiros, J., Tsao, H., Penz, T., Weiss, G., Aistleitner, K., et al. (2017). *In situ* architecture, function, and evolution of a contractile injection system. *Science* 357, 713–717. doi: 10.1126/science.aan7904

Bondage, D. D., Lin, J., Ma, L., Kuo, C., and Lai, E. (2016). VgrG C terminus confers the type VI effector transport specificity and is required for binding with PAAR and adaptor – effector complex. *Proc. Natl. Acad. Sci. U.S.A.* 113, E3931–E3940. doi: 10.1073/pnas.1600428113

Boyer, F., Fichant, G., Berthod, J., Vandenbrouck, Y., and Attree, I. (2009). Dissecting the bacterial type VI secretion system by a genome wide *in silico* analysis: what can be learned from available microbial genomic resources? *BMC Genomics* 10:104. doi: 10.1186/1471-2164-10-104

Bröms, J. E., Sjöstedt, A., and Lavander, M. (2010). The role of the *Francisella tularensis* pathogenicity island in type VI secretion, intracellular survival, and modulation of host cell signaling. *Front. Microbiol.* 1:136. doi: 10.3389/fmicb.2010.00136

Brunet, Y. R., Bernard, C. S., Gavioli, M., Lloubès, R., and Cascales, E. (2011). An epigenetic switch involving overlapping fur and DNA methylation optimizes expression of a type VI secretion gene cluster. *PLoS Genet.* 7:e1002205. doi: 10.1371/journal.pgen.1002205

Brunet, Y. R., Khodr, A., Logger, L., Aussel, L., Mignot, T., Rimsky, S., et al. (2015). H-NS silencing of the *salmonella* pathogenicity island 6-encoded type VI secretion system limits *Salmonella enterica* serovar typhimurium interbacterial killing. *Infect. Immun.* 83, 2738–2750. doi: 10.1128/IAI.00198-15

Burkinshaw, B. J., Liang, X., Wong, M., Le, A. N. H., Lam, L., and Dong, T. G. (2018). A type VI secretion system effector delivery mechanism dependent on PAAR and a chaperone–co-chaperone complex. *Nat. Microbiol.* 3, 632–640. doi: 10.1038/s41564-018-0144-4.

Büttner, D., and Bonas, U. (2010). Regulation and secretion of *Xanthomonas* virulence factors. *FEMS Microbiol. Rev.* 34, 107–133. doi: 10.1111/j.1574-6976.2009.00192.x

Casabona, M. G., Silverman, J. M., Sall, K. M., Boyer, F., Couté, Y., Poirel, J., et al. (2013). An ABC transporter and an outer membrane lipoprotein participate in posttranslational activation of type VI secretion in *Pseudomonas aeruginosa*. *Environ. Microbiol.* 15, 471–486. doi: 10.1111/j.1462-2920.2012.02816.x

Christensen, P., and Cook, F. D. (2009). *Lysobacter*, a new genus of nonfruiting. gliding bacteria with a high base ratio. *Int. J. Syst. Bacteriol.* 28, 367–393. doi: 10.1099/00207713-28-3-367

Cianfanelli, F. R., Monlezun, L., and Coulthurst, S. J. (2016). Aim. load, fire: the type VI secretion system, a bacterial nanoweapon. *Trends Microbiol.* 24, 51–62. doi: 10.1016/j.tim.2015.10.005

Cirl, C., Wieser, A., Yadav, M., Duerr, S., Schubert, S., Fischer, H., et al. (2008). Subversion of toll-like receptor signaling by a unique family of bacterial Toll/interleukin-1 receptor domain-containing proteins. *Nat. Med.* 14:399. doi: 10.1038/nm1734

De Maayer, P., Venter, S., Kamber, T., Duffy, B., Coutinho, T., and Smits, T. (2011). Comparative genomics of the Type VI secretion systems of *Pantoea* and *Erwinia* species reveals the presence of putative effector islands that may

be translocated by the VgrG and Hcp proteins. *BMC Genomics* 12:576. doi: 10.1186/1471-2164-12-576

Dix, S. R., Owen, H. J., Sun, R., Ahmad, A., Shastri, S., Spiewak, H. L., et al. (2018). Structural insights into the function of type VI secretion system TssA subunits. *Nat. Commun.* 9:4765. doi: 10.1038/s41467-018-07247-1

Durand, E., Cambillau, C., Cascales, E., and Journet, L. (2014). VgrG. Tae, Tle, and beyond: the versatile arsenal of Type VI secretion effectors. *Trends Microbiol.* 22, 498–507. doi: 10.1016/j.tim.2014.06.004

Essuman, K., Summers, D., Sasaki, Y., Mao, X., Yim, A., DiAntonio, A., et al. (2018). TIR domain proteins are an ancient family of NAD(+)-consuming enzymes. *Curr. Biol.* 28, 421–430. doi: 10.1016/j.cub.2017.12.024

Flaugnatti, N., Le, T., Canaan, S., Aschtgen, M., Nguyen, V., Blangy, S., et al. (2016). A phospholipase A1 antibacterial type VI secretion effector interacts directly with the C-terminal domain of the VgrG spike protein for delivery. *Mol. Microbiol.* 99, 1099–1118. doi: 10.1111/mmi.13292

Forster, A., Planamente, S., Manoli, E., Lossi, N. S., Freemont, P. S., and Filloux, A. (2014). Coevolution of the ATPase ClpV, the sheath proteins TssB and TssC and the accessory protein TagJ/HsiE1 distinguishes type VI secretion classes. *J. Biol. Chem.* 289, 33032–33043. doi: 10.1074/jbc.M114.600510

Hachani, A., Wood, T. E., and Filloux, A. (2016). Type VI secretion and anti-host effectors. *Curr. Opin. Microbiol.* 29, 81–93. doi: 10.1016/j.mib.2015.11.006

Hayward, A. C., Fegan, N., Fegan, M., and Stirling, G. R. (2010). *Stenotrophomonas* and *Lysobacter*: ubiquitous plant-associated gamma-*proteobacteria* of developing significance in applied microbiology. *J. Appl. Microbiol.* 108, 756–770. doi: 10.1111/j.1365-2672.2009.04471.x

Jiang, F., Waterfield, N. R., Yang, J., Yang, G., and Jin, Q. (2014). A *Pseudomonas aeruginosa* type VI secretion phospholipase D effector targets both prokaryotic and eukaryotic cells. *Cell Host Microbe* 15, 600–610. doi: 10.1016/j.chom.2014.04.010

Kanehisa, M., and Goto, S. (2000). KEGG: kyoto encyclopedia of genes and genomes. *Nucleic Acids Res.* 28, 27–30. doi: 10.1093/nar/28.1.27

Kapitein, N., Bönemann, G., Pietrosiuk, A., Seyffer, F., Hausser, I., Locker, J. K., et al. (2013). ClpV recycles VipA/VipB tubules and prevents non-productive tubule formation to ensure efficient type VI protein secretion. *Mol. Microbiol.* 87, 1013–1028. doi: 10.1111/mmi.12147

Ko, H. S., Jin, R., De Krishnan, H. B., Lee, S. B., and Kim, K. Y. (2009). Biocontrol ability of *Lysobacter antibioticus* HS124 against phytophthora blight is mediated by the production of 4-hydroxyphenylacetic acid and several lytic enzymes. *Curr. Microbiol.* 59, 608–615. doi: 10.1007/s00284-009-9481-0

Kumar, S., Stecher, G., and Tamura, K. (2016). MEGA7: molecular evolutionary genetics analysis version 7.0 for bigger datasets. *Mol. Biol. Evol.* 33, 1870–1874. doi: 10.1093/molbev/msw054

Leyns, F., De Cleene, M., Swings, J. G., and De Ley, J. (1984). The host range of the genus *Xanthomonas*. *Bot. Rev.* 5, 308–356. doi: 10.1007/BF02862635

Liang, X., Moore, R., Wilton, M., Wong, M. J. Q., Lam, L., and Dong, T. G. (2015). Identification of divergent type VI secretion effectors using a conserved chaperone domain. *Proc. Natl. Acad. Sci. U.S.A.* 112, 9106–9111. doi: 10.1073/pnas.1505317112

Lien, Y.-W., and Lai, E.-M. (2017). Type VI secretion effectors: methodologies and biology. *Front. Cell. Infect. Microbiol.* 7:254. doi: 10.3389/fcimb.2017.00254

Lin, J. S., Pissaridou, P., Wu, H. H., Tsai, M. D., Filloux, A., and Lai, E. M. (2018). TagF-mediated repression of bacterial type VI secretion systems involves a direct interaction with the cytoplasmic protein Fha. *J. Biol. Chem.* 293, 8829–8842. doi: 10.1074/jbc.RA117.001618

Ma, J., Sun, M., Dong, W., Pan, Z., Lu, C., and Yao, H. (2017). PAAR-Rhs proteins harbor various C-terminal toxins to diversify the antibacterial pathways of type VI secretion systems. *Environ. Microbiol.* 19, 345–360. doi: 10.1111/1462-2920.13621

Ma, L.-S., Hachani, A., Lin, J.-S., Filloux, A., and Lai, E.-M. (2014). *Agrobacterium tumefaciens* deploys a superfamily of type VI secretion DNase effectors as weapons for interbacterial competition in planta. *Cell Host Microbe* 16, 94–104. doi: 10.1016/j.chom.2014.06.002

Mougous, J. D., Gifford, C. A., Ramsdell, T. L., and Mekalanos, J. J. (2007). Threonine phosphorylation post-translationally regulates protein secretion in *Pseudomonas aeruginosa*. *Nat. Cell Biol.* 9, 797–803. doi: 10.1038/ncb1605

Naushad, S., Adeolu, M., Wong, S., Sohail, M., Schellhorn, H. E., and Gupta, R. S. (2015). A phylogenomic and molecular marker based taxonomic framework for the order Xanthomonadales: proposal to transfer the families *Algiphilaceae* and *Solimonadaceae* to the order Nevskiales ord. nov. and to create a new family within the order Xanthomonadales. Antonie van Leeuwenhoek. *Int. J. Gen. Mol. Microbiol.* 107, 467–485. doi: 10.1007/s10482-014-0344-8

Nguyen, V., Douzi, B., Durand, E., Roussel, A., Cascales, E., and Cambillau, C. (2018). Towards a complete structural deciphering of type VI secretion system. *Curr. Opin. Struct. Biol.* 49, 77–84. doi: 10.1016/j.sbi.2018.01.007

Ostrowski, A., Cianfanelli, F. R., Porter, M., Mariano, G., Peltier, J., Wong, J. J., et al. (2018). Killing with proficiency: integrated post-translational regulation of an offensive Type VI secretion system. *PLoS Pathog.* 14:e1007230. doi: 10.1371/journal.ppat.1007230

Planamente, S., Salih, O., Manoli, E., Albesa-Jové, D., Freemont, P. S., and Filloux, A. (2016). TssA forms a gp6-like ring attached to the type VI secretion sheath. *EMBO J.* 35, 1613–1627. doi: 10.15252/embj.201694024

Rapicavoli, J., Ingel, B., Blanco-Ulate, B., Cantu, D., and Roper, C. (2018). *Xylella fastidiosa*: an examination of a re-emerging plant pathogen. *Mol. Plant Pathol.* 19, 786–800. doi: 10.1111/mpp.12585

Russell, A. B., Leroux, M., Hathazi, K., Agnello, D. M., Ishikawa, T., Wiggins, P. A., et al. (2013). Diverse type VI secretion phospholipases are functionally plastic antibacterial effectors. *Nature* 496, 508–512. doi: 10.1038/nature12074

Russell, A. B., Wexler, A. G., Harding, B. N., Whitney, J. C., Bohn, A. J., Goo, Y. A., et al. (2014). A Type VI secretion-related pathway in bacteroidetes mediates interbacterial antagonism. *Cell Host Microbe* 16, 227–236. doi: 10.1016/j.chom.2014.07.007

Ryan, R. P., Vorhölter, F. J., Potnis, N., Jones, J. B., Van Sluys, M. A., Bogdanove, A. J., et al. (2011). Pathogenomics of *Xanthomonas*: understanding bacterium-plant interactions. *Nat. Rev. Microbiol.* 9, 344–355. doi: 10.1038/nrmicro2558

Saddler, G., and Bradbury, J. (2005). "Order III. Xanthomonadales ord. nov," in *Bergey's Manual of Systematic Bacteriology*. ed D. J. Brenner et al. Austin: Springer, 63–122. doi: 10.1007/0-387-28022-7_3

Sgro, G. G., Oka, G. U., Souza, D. P., Cenens, W., Bayer-Santos, E., Matsuyama, B. Y., et al. (2019). Bacteria-killing type IV secretion systems. *Front. Microbiol.* 10:1078. doi: 10.3389/fmicb.2019.01078

Si, M., Wang, Y., Zhang, B., Zhao, C., Kang, Y., Bai, H., et al. (2017a). The type VI secretion system engages a redox-regulated dual-functional heme transporter for zinc acquisition. *Cell Rep.* 20, 949–959. doi: 10.1016/j.celrep.2017.06.081

Si, M., Zhao, C., Burkinshaw, B., Zhang, B., Wei, D., Wang, Y., et al. (2017b). Manganese scavenging and oxidative stress response mediated by type VI secretion system in *Burkholderia thailandensis*. *Proc. Natl. Acad. Sci. U.S.A.* 114, E2233–E2242. doi: 10.1073/pnas.1614902114

Silverman, J. M., Austin, L. S., Hsu, F., Hicks, K. G., Hood, R. D., and Mougous, J. D. (2011). Separate inputs modulate phosphorylation-dependent and -independent type VI secretion activation. *Mol. Microbiol.* 82, 1277–1290. doi: 10.1111/j.1365-2958.2011.07889.x

Silverman, J. M., Brunet, Y. R., Cascales, E., and Mougous, J. D. (2012). Structure and regulation of the type VI secretion system. *Annu. Rev. Microbiol.* 66, 453–472. doi: 10.1146/annurev-micro-121809-151619

Souza, D. P., Oka, G. U., Alvarez-Martinez, C. E., Bisson-Filho, A. W., Dunger, G., Hobeika, L., et al. (2015). Bacterial killing via a type IV secretion system. *Nat. Commun.* 6, 1–9. doi: 10.1038/ncomms7453

Trunk, K., Peltier, J., Liu, Y., Dill, B., Walker, L., Gow, N., et al. (2018). The type VI secretion system deploys antifungal effectors against microbial competitors. *Nat. Microbiol.* 3, 920–931. doi: 10.1038/s41564-018-0191-x

Unterweger, D., Kostiuk, B., Otjengerdes, R., Wilton, A., Diaz-Satizabal, L., and Pukatzki, S. (2015). Chimeric adaptor proteins translocate diverse type VI secretion system effectors in *Vibrio cholerae*. *EMBO J.* 34, 2198–2210. doi: 10.15252/embj.201591163

Wang, J., Yang, B., Leier, A., Marquez-Lago, T., Hayashida, M., Rocker, A., et al. (2018). Bastion6: a bioinformatics approach for accurate prediction of type VI secreted effectors. *Bioinformatics* 34, 2546–2555. doi: 10.1093/bioinformatics/bty155

Wang, T., Si, M., Song, Y., Zhu, W., Gao, F., Wang, Y., et al. (2015). Type VI secretion system transports Zn2+ to combat multiple stresses and host immunity. *PLoS Pathog.* 11:e1005020. doi: 10.1371/journal.ppat.1005020

Weber, B., Hennon, S., Wright, M., Scott, N., de Berardinis, V., Foster, L., et al. (2016). Genetic dissection of the type vi secretion system in *Acinetobacter* and identification of a novel peptidoglycan hydrolase. tagx, required for its biogenesis. *MBio* 7, e1253–e1216. doi: 10.1128/mBio.01253-16

Williams, K. P., Gillespie, J. J., Sobral, B. W. S., Nordberg, E. K., Snyder, E. E., Shallom, J. M., et al. (2010). Phylogeny of gamma proteobacteria. *J. Bacteriol.* 192, 2305–2314. doi: 10.1128/JB.01480-09

Zoued, A., Durand, E., Brunet, Y. R., Spinelli, S., Douzi, B., Guzzo, M., et al. (2016). Priming and polymerization of a bacterial contractile tail structure. *Nature* 531, 59–63. doi: 10.1038/nature17182

Conflict of Interest Statement: The authors declare that the research was conducted in the absence of any commercial or financial relationships that could be construed as a potential conflict of interest.

Copyright © 2019 Bayer-Santos, Ceseti, Farah and Alvarez-Martinez. This is an open-access article distributed under the terms of the Creative Commons Attribution License (CC BY). The use, distribution or reproduction in other forums is permitted, provided the original author(s) and the copyright owner(s) are credited and that the original publication in this journal is cited, in accordance with accepted academic practice. No use, distribution or reproduction is permitted which does not comply with these terms.

frontiers in Microbiology

ORIGINAL RESEARCH
published: 18 July 2019
doi: 10.3389/fmicb.2019.01615

Baseplate Component TssK and Spatio-Temporal Assembly of T6SS in *Pseudomonas aeruginosa*

David Liebl[1]†, Mylène Robert-Genthon[1], Viviana Job[1,2], Valentina Cogoni[1] and Ina Attrée[1]**

[1] Univ. Grenoble Alpes, CNRS, Bacterial Pathogenesis and Cellular Responses, ERL 5261, INSERM, UMR-S 1036, CEA, Grenoble, France, [2] Univ. Grenoble Alpes, CEA, CNRS, Institut de Biologie Structurale (IBS), Grenoble, France

OPEN ACCESS

Edited by:
Eric Cascales,
Aix-Marseille Université, France

Reviewed by:
Thierry Doan,
UMR7255 Laboratoire d'Ingénierie des Systèmes Macromoléculaires (LISM), France
Erh-Min Lai,
Academia Sinica, Taiwan

***Correspondence:**
David Liebl
David_Liebl@sris.a-star.edu.sg
Ina Attrée
ina.attree-delic@cea.fr

†Present address:
David Liebl,
A*STAR Microscopy Platform, Skin Research Institute of Singapore (SRIS), Agency for Science, Technology and Research (A*STAR), Singapore, Singapore

Specialty section:
This article was submitted to Microbial Physiology and Metabolism, a section of the journal Frontiers in Microbiology

Received: 10 April 2019
Accepted: 28 June 2019
Published: 18 July 2019

Citation:
Liebl D, Robert-Genthon M, Job V, Cogoni V and Attrée I (2019) Baseplate Component TssK and Spatio-Temporal Assembly of T6SS in Pseudomonas aeruginosa. Front. Microbiol. 10:1615. doi: 10.3389/fmicb.2019.01615

The Gram-negative bacteria use the contractile multi-molecular structure, called the Type VI Secretion System (T6SS) to inject toxic products into eukaryotic and prokaryotic cells. In this study, we use fluorescent protein fusions and time-lapse microscopy imaging to study the assembly dynamics of the baseplate protein TssK in *Pseudomonas aeruginosa* T6SS. TssK formed transient higher-order structures that correlated with dynamics of sheath component TssB. Assembly of peri-membrane TssK structures occurred *de novo* upon contact with competing bacteria. We show that this assembly required presence of TagQ-TagR envelope sensors, activity of PpkA kinase and anchoring to the inner membrane *via* TssM. Disassembly and repositioning of TssK component was dependent on PppA phosphatase and indispensable for repositioning and deployment of the entire contractile apparatus toward a new target cell. We also show that TssE is necessary for correct elongation and stability of TssB-sheath, but not for TssK assembly. Therefore, in *P. aeruginosa*, assembly of the TssK-containing structure relays on the post-translational regulatory envelope module and acts as spatio-temporal marker for further recruitment and subsequent assembly of the contractile apparatus.

Keywords: molecular nanomachine, T4 bacteriophage, bacterial competition, T6SS, baseplate assembly

INTRODUCTION

Gram-negative bacteria deploy a number of complex envelope-embedded multi-protein nanomachines adjusted exclusively for protein export across bacterial membrane and interaction with eukaryotic and prokaryotic species (Filloux et al., 2008; Hayes et al., 2010). One of these is Type VI secretion system (T6SS), originally identified in *Vibrio cholerae* using *Dictyostelium* host (Pukatzki et al., 2006). The T6SS is a versatile protein exporting machinery implicated in virulence as well as competition and cooperation in microbial communities and it is capable of targeting both bacteria and eukaryotic cells (Alcoforado Diniz et al., 2015; Bleves, 2016; Jani and Cotter, 2010). Thirteen essential core proteins are conserved in all T6SSs (Shalom et al., 2007; Cascales, 2008; Filloux et al., 2008; Boyer et al., 2009); the membrane associated complex TssJ-TssL-TssM, the baseplate proteins TssE, TssF, TssG, and TssK, the bacteriophage-related puncturing complex composed of the tube (Hcp), the tip/puncturing device VgrG, and the contractile sheath structure

(TssB and TssC) (Coulthurst, 2013; Ho et al., 2014; Cianfanelli et al., 2016). Finally, the starfish-shaped dodecameric protein, TssA, limits contractile sheath polymerization at its distal part when TagA captures TssA (Planamente et al., 2016; Santin et al., 2018).

T6SS function involves a highly dynamic process of TssB/TssC sheath assembly, contraction and disassembly (Basler and Mekalanos, 2012; Basler et al., 2012; Forster et al., 2014), where recycling of the sheath subunits depends on ClpV ATPase (Bonemann et al., 2009; Pietrosiuk et al., 2011). Analogous to the T4 bacteriophage tail structure, the T6SS sheath assembles around an inner Hcp tube with membrane-puncturing device (VgrG) positioned at its proximal end (Leiman et al., 2009; Shneider et al., 2013; Silverman et al., 2013). Current model assumes that the positioning and contraction of the apparatus and subsequent ejection of effectors is strictly dependent on transient yet firm anchoring of the contractile device to precise loci within the bacteria membrane. Upon activation of the system, certain components such as Hcp and VgrG, could be exchanged between neighboring bacteria to launch rapid response to external stimuli (Vettiger and Basler, 2016).

Biogenesis of T6SS baseplate start with the association of two molecules of TssF, one molecule of TssG and two TssK trimers to form a stable complex, that then oligomerize further around the VrgG hub (Cherrak et al., 2018; Park et al., 2018). The composition of the whole 1.15 megadalton baseplate is proposed to be $(TssE)_6$-$(TssF)_{12}$-$(TssG)_6$ with eighteen TssK subunits (Nazarov et al., 2018) connecting the whole assembly to the membrane-embedded 1.7 megadalton TssJLM complex (Brunet et al., 2015; Durand et al., 2015), where it stabilizes and initiates tube/sheath polymerization probably through interactions with TssE, as it is the case for its homolog gp25 in the phage (Yap et al., 2010; Nazarov et al., 2018).

Although the structural components of the T6SS machinery are conserved in several organisms, regulatory pathways controlling the expression and assembly of the apparatus differ. *Pseudomonas aeruginosa*, a major human opportunistic pathogen and causative agent of chronic infections in cystic fibrosis patients possesses three T6SS-encoding loci and a number of effector-encoding genes spread through the genome (Filloux et al., 2008). The machinery encoded by the Hcp secretion island I-encoded T6SS (H1-T6SS) (Mougous et al., 2006) is used for bacterial warfare and can translocate multiple effectors into target bacteria (Russell et al., 2011, 2012). The expression and activity of H1-T6SS is controlled at the transcriptional and translational level by a regulatory network including membrane sensors (RetS, LadS, and GacS) (Brencic and Lory, 2009; Brencic et al., 2009), small regulatory RNAs (Brencic and Lory, 2009; Brencic et al., 2009) and di-cGMP signaling (Moscoso et al., 2011). At the post-translational level, eukaryotic-like threonine kinase/phosphatase pair (PpkA-PppA) and a signal-transmission module (TagQ-TagR-TagS-TagT) embedded within the bacterial envelope are required for the T6SS activity (Mougous et al., 2007; Hsu et al., 2009; Basler et al., 2013). The Tag proteins are found in the so-called "defensive" T6SS and modulate the T6SS activity in response to an attack from a competitor, while the "offensive" system is always active, ready to fire on any surrounding bacteria as in the case of *V. cholera* (Basler et al., 2013; Ostrowski et al., 2018).

The aim of this study was to examine the role of signal-transmission module and threonine kinase/phosphatase pair on initial T6SS baseplate assembly. To that purpose, we used quantitative time-lapse microscopy imaging to investigate the spatio-temporal recruitment and assembly of two baseplate proteins, TssK, TssE and the sheath component, TssB. Although the fusion constructs compromised the very last step of T6SS action, i.e., prey killing, they reflected the dynamics of all initial steps of machinery function, including sensing, baseplate and contractile apparatus assembly and firing. As the exploring behavior of TssK/TssB fusions was possible only in the wild-type background, we propose that assembly of baseplate/sheet structure still required a pool of endogenous (non-tagged) TssK/TssB to co-assemble with exogenous (tagged) TssK/TssB. Our results show dynamic assembly of the T6SS baseplate structure that depends on *P. aeruginosa* post-translational signaling cascade, as well as the key functions the baseplate provides for assembly and relocation of the T6SS nanomachinery to a site of contact with competing bacteria.

RESULTS

TssK Assembles Into Peri-Membrane Higher-Order Structures in Response to TagQRST-Mediated Activation of T6SS

To examine whether the environmental signals, transmitted by TagQRST, influence the baseplate assembly we engineered fusions between genes encoding several baseplate proteins (*tssE*, *tssF*, *tssG* and *tssK*) with *sfGFP* and *tssB-GFP*. The plasmids carrying the fusion under arabinose-inducible promoter were introduced in the wild-type *P. aeruginosa* strain PAO1. We were unable to exploit any florescent signal with TssG-sfGFP and TssF-sfGFP. However, in a subpopulation of bacteria, TssK-sfGFP assembled into discernible foci localized to the bacterial periphery, reminiscent to TssK foci observed in *Escherichia coli* (Brunet et al., 2015; Cherrak et al., 2018), whereas TssB-GFP assembled into elongated rod-like structures with substantially higher fluorescence intensity relative to TssK foci (**Figure 1A**). In *P. aeruginosa*, T6SS assemble preferentially upon the attack by neighboring bacteria in a behavior named "T6SS dueling" (Basler and Mekalanos, 2012; Basler et al., 2013). We analyzed *P. aeruginosa* cells expressing TssK-sfGFP grown in presence of *Acetinobacter baumannii* and found that spots formed by TssK-sfGFP were mostly positioned specifically toward contacts with *A. baumannii* (**Figure 1B**), as would be expected for a "defensive" T6SS apparatus. Notably, quantification revealed that incidence of TssK-sfGFP spots in *P. aeruginosa* increased significantly in mixed culture with wild type *A baumannii* but not with a *tssM* mutant (*Ab*Δ*tssM*) with an inactive T6SS (Weber et al., 2013); showing that TssK-sfGFP spot formation correlates specifically with a response of *P. aeruginosa* to T6SS-mediated attack by competitor bacteria. Thus, TssK has the capacity to assemble from the cytosolic pool into perimembrane higher order structures

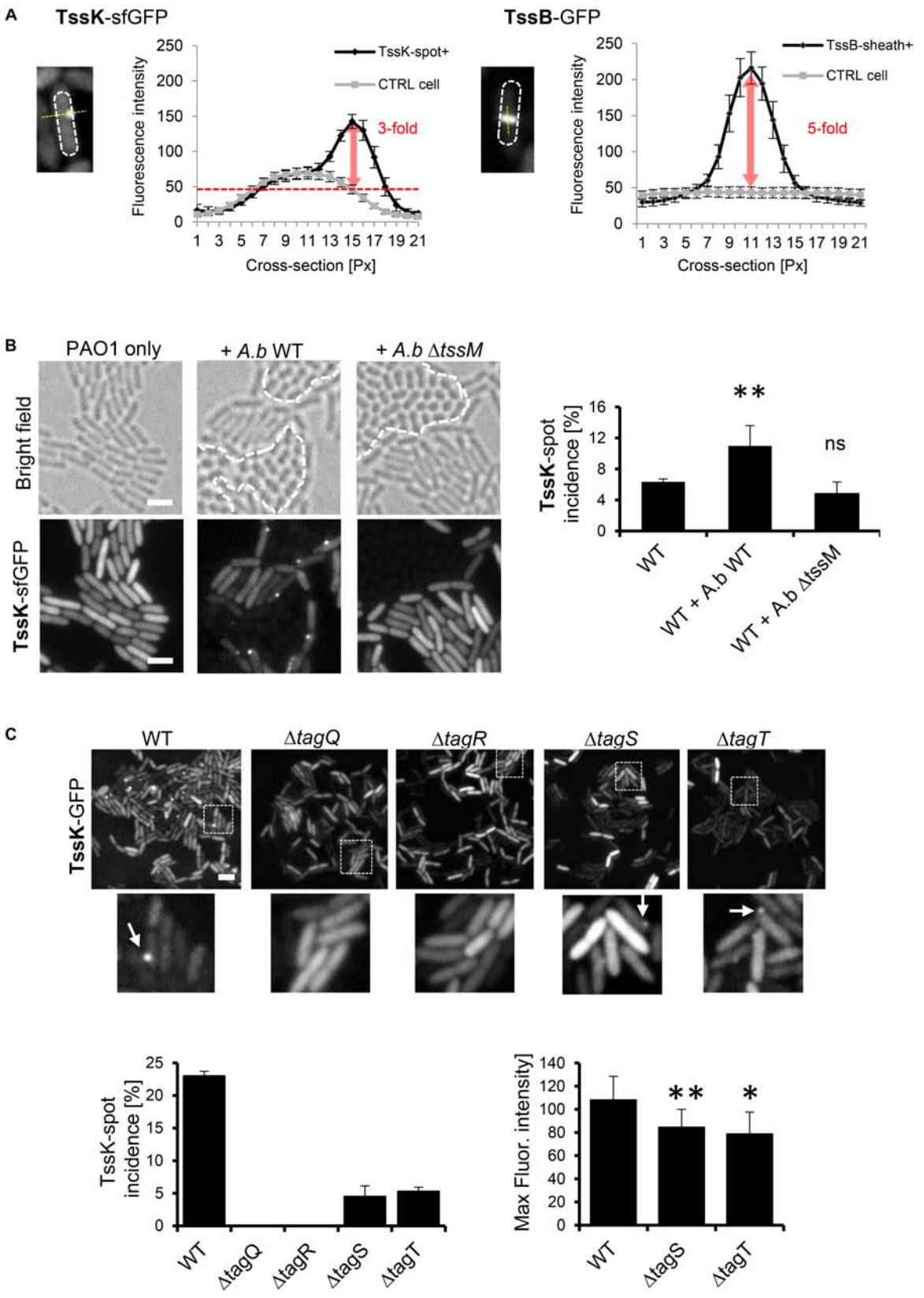

FIGURE 1 | Continued

FIGURE 1 | TssK assembles into discernible perimembrane structures in response to T6SS activation. **(A)** Fluorescent intensities of TssK-sfGFP rounded foci and TssB-GFP elongated rods observed in PAO1 strain after arabinose-induction. Note the 3-fold and 5-fold higher intensity compared to the cytoplasmic levels for TssK and TssB, respectively. **(B)** Assembly of TssK-sfGFP increases in mixed culture with wild type *A. baumannii* but not with T6SS-inactive *A. baumannii* mutant Δ*tssM*. Note that *A. baumannii* can be discriminated from *P. aeruginosa* by its rounded-cell morphology in bright field images (borders between two species are depicted by dashed lines). Representative bright field and fluorescent images are shown with quantification of TssK-spot incidence. Average and SD values were calculated for each group from 4 to 6 ROI each containing between 400 and 1000 of cells. Two-tail *t*-test, $^{*}P = 0.038$. **(C)** Role of TagQRST sensor module in TssK assembly. Fluorescence images are shown for each *tag* mutant. Histograms showing quantification of TssK-spot (white arrows in images) incidence and fluorescence intensity measurements of TssK-sfGFP structures are shown below. No spots of TssK-sfGFP were found in Δ*tagQ* and Δ*tagR* mutants and deletion of *tagS* or *tagT* lead to a significant reduction of the incidence of TssK-spot formation. Note that fluorescence intensity of TssK-sfGFP spots in Δ*tagS* and Δ*tagT* mutants was significantly decreased. Average and SD values were calculated from 20 spots for each sample. Two-tail *t*-test, $^{**}P = 0.03$ (Δ*tagS*) and $^{*}P = 0.09$ (Δ*tagT*). ns, non significant. Bar = 2 μm.

with the incidence that increases specifically during interaction with competitor bacteria. In competition assays with *E. coli* DH5α, the killing capacity of the PAO1 strain expressing TssK-sfGFP toward the pray was diminished compared to PAO1 (wild type) (**Supplementary Figure S1**). This suggest that TssK-sfGFP incorporates within the baseplate with native TssK but limits the capacity of T6SS to inject effectors. Similar dominant-negative effect on T6SS activity was already observed for single domains of TssK in enteroaggregative *E. coli* (Cherrak et al., 2018).

However, the TssK-sfGFP protein fusion construct could be used to study T6SS assembly kinetics, as demonstrated in the following experiments.

A unique feature of post-translational regulation of T6SS activity in *P. aeruginosa* is the sensory module composed of TagQ, TagR, TagS, and TagT proteins encoded together with other T6SS core components within the HSI-1 locus (Cascales, 2008; Filloux et al., 2008; Boyer et al., 2009). TagQ is an outer-membrane lipoprotein required for recruitment of periplasmic TagR which in turn activates a Threonine Protein Phosphorylation (TPP) pathway promoting assembly of the T6SS apparatus (Mougous et al., 2007; Hsu et al., 2009). TagS and TagT form a classical ABC transporter embedded within the inner membrane of bacteria, and all four proteins are necessary for optimal T6SS activation *in vitro* (Casabona et al., 2013). We used previously characterized Δ*tagQ*, Δ*tagR*, Δ*tagS* and Δ*tagT* mutants (Casabona et al., 2013) and analyzed TssK-sfGFP localization and its incidence in these cells mixed with *A. baumannii*. Unlike the wild type, no TssK-assemblies were detected in Δ*tagQ* and Δ*tagR* mutants (**Figure 1C**). Interestingly, deletion of *tagS* or *tagT* did not lead to complete block of TssK assembly, yet significantly reduced the incidence of TssK-assembling cells so as the overall spot size (fluorescence intensity) of TssK-structures relative to the control (**Figure 1C**). Consequently, we found that assembly of TssK into a baseplate structure within a particular site at the plasma membrane is dependent on TagQ and TagR. We established that presence of TagS and TagT was dispensable for TssK assembly but may have modulatory/accessory function in the process of TssK recruitment into functional entities, in agreement with previous findings that TagT was required for "dueling" behavior and reposition of the apparatus toward neighboring sister cells (Basler et al., 2013). We conclude that observed TssK-sfGFP foci represent protein complexes within T6SS apparatus that are assembled in post-translational manner and can be used as a marker for monitoring T6SS baseplate assembly.

TssK Undergoes Dynamic Assembly-Disassembly

We then analyzed *P. aeruginosa* cells expressing TssK-sfGFP by time-lapse imaging to examine its dynamic features including assembly/disassembly and/or lateral displacement or motility. Real-time detection of transient appearance-growth-decay-disappearance of discernible perimembrane-localized fluorescent spot(s) was measured as described in Section "Materials and Methods," and reported as assembly/disassembly. Intensity measurements started prior structure appearance (except for TssK in *pppA* mutant) where values at T0 (normalized to 1) correspond to fluorescence intensity of cytosolic pool of the fusion protein. We typically observed multiple rounds of assembly disassembly occurring at the same location before assembly was detected at another location of the same bacteria. Interestingly, no more than one TssK-sfGFP spot was found per single cell at a given time. Kinetic measurements of fluorescence intensity revealed that assembly of the TssK-sfGFP occurred within 39 ± 6 s whereas disassembly of the structures lasted in average 61 ± 10 s (**Figure 2A**), implying that these transient structures undergo frequent assembly-disassembly as a dynamic component of T6SS baseplate structure.

Downstream of TagQRST sensory module, the T6SS activity is post-translationally regulated by the threonine kinase PpkA whose activity is antagonized by the phosphatase PppA (Mougous et al., 2007; Ostrowski et al., 2018). We detected TssK-sfGFP assemblies in the Δ*pppA* mutant but never in the Δ*ppkA* mutant of *P. aeruginosa* (**Figure 2A** and **Supplementary Figure S2**), despite the same expression levels of corresponding constructs as revealed by immunoblot analysis (**Supplementary Figure S3**). Similar result was reported for TssB and Fha foci in Δ*pppA* and Δ*ppkA* mutants in *S. marcescens* (Ostrowski et al., 2018). Kinetic measurements showed that in Δ*pppA,* structures formed by TssK-sfGFP were static, permanently retained at one perimembrane site without *de novo* assembly at another location (**Figure 2A**). This suggests that the dephosphorylation of Fha, a target of PpkA kinase and PppA dephosphatase, is necessary for repositioning of the TssK-containing baseplate, but not for its assembly *per se*. Otherwise, PppA could have another, yet unidentified target. To note, in the wild-type *E. coli*, TssK foci also seem to be static at a given time but several of them were detected per cell, which may be explained by the absence of post-translational regulatory module in this system (Brunet et al., 2015).

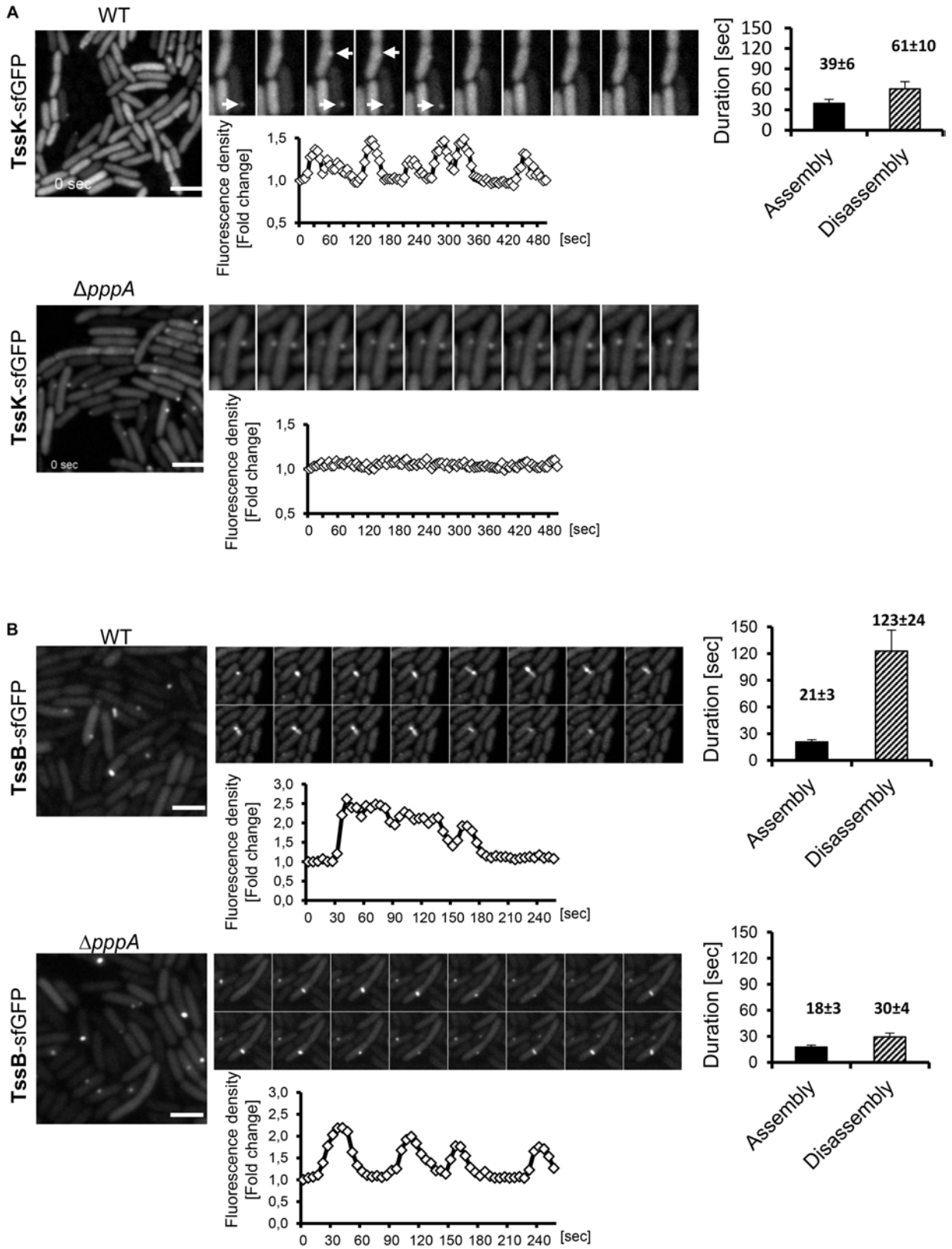

FIGURE 2 | Continued

FIGURE 2 | Assembly of TssK baseplate component requires activity of PpkA kinase while disassembly and repositioning is dependent on PppA phosphatase. Time-lapse series of *P. aeruginosa* PA01 (WT) and PppA-deficient mutant (Δ*pppA*) expressing TssK-sfGFP **(A)** or TssB-GFP **(B)**. Series of fluorescence images are shown (10 s between frames) with kinetic measurements of relative fluorescence intensity in ROI containing TssK-sfGFP/TssB-GFP structures (below) and quantification of an average duration of assembly/disassembly of these structures (on right). Bars = 2 μm. **(A)** In wild type cells, individual TssK-sfGFP structures (white arrows) assemble/disassemble within an average 100 ± 10 s. Note that lack of PppA impaired recycling and re-positioning of TssK structures but not their assembly *per se*. **(B)** A single round of assembly-contraction-disassembly of individual TssB-GFP sheaths in wild type occurs within an average 144 ± 24 s period. Note that in Δ*pppA*, the TssB-sheath assembles repeatedly at the same location and exhibits an aberrant kinetics with significantly faster rate of disassembly (30 ± 4 s) relative to the wild type control (123 ± 24 s).

To investigate how TssK dynamics relates to the assembly, contraction and disassembly of the contractile sheath in *P. aeruginosa* we first analyzed the sheath dynamics in *P. aeruginosa* expressing TssB-GFP construct. Similar to TssK, the TssB-GFP exhibited homogenous cytosolic localization in a vast majority of cells but elongated sheath-like structures were readily detected in mixed cultures with *A. baumanni*. As for TssK foci, we have never detected more than one TssB-sheath structure per individual cell at a given time. Quantitative measurements of assembly-disassembly revealed distinct kinetics features for TssB-sheaths, relative to TssK structures, where assembly occurred within 21 ± 3 s followed by disassembly at a slower rate of 123 ± 24 s resulting in an average 140 s lifetime for an individual TssB-structure (**Figure 2B**), similar to value found by others (Basler and Mekalanos, 2012; Basler et al., 2012). Kinetic profiles of TssK-baseplate in homogenous culture of *P. aeruginosa* were similar to corresponding profiles in competition conditions where the assembly of TssK structures was targeted preferentially toward the contact with competing *A. baumannii* (**Supplementary Figure S4**). Like TssK assemblies, several rounds of assembly-contraction of TssB-sheaths were detected at the same site of the bacteria prior complete disassembly of the structure. The dynamic feature of the contractile sheath (TssB-GFP) was not lost in *P. aeruginosa* mutant Δ*pppA* but led to significantly faster (likely premature) disassembly of the sheath relative to wild-type (30 ± 4 vs. 123 ± 24 s, respectively).

We conclude that similarly to contractile sheath component TssB, the baseplate component TssK also undergoes regulated periodic assembly and disassembly during deployment of the T6SS apparatus. This implies that in cells primed for T6SS activity, TssK does not assemble into multiple rigid baseplate structures per cell, but instead assembles transiently *ad hoc* at a specific site of the inner membrane toward the contact with neighbor attacking bacteria. We provide evidence that PppA phosphatase functions downstream of this TssK assembly and is essential for its disassembly and relocation to a new site for subsequent *de novo* assembly of the contractile apparatus.

TssK Functions as a Spatio-Temporal Marker for Assembly of Contractile Apparatus

Because both, TssK-sfGFP structures and TssB-GFP sheaths exhibited similar yet distinct dynamic phenotype, we examined TssK as a spatio-temporal cue for recruitment of contractile sheath components TssB. We analyzed colocalization between TssK and TssB and measured the kinetics of their assembly-disassembly in *P. aeruginosa* co-expressing TssK-RFPT and TssB-GFP. Correspondent with our previous observations with individually expressed proteins, TssK only assembled into rounded spots at the periphery of bacteria, whereas TssB assembled into rod-like structure often spanning the entire width of the cell (in an extended conformation) (**Figure 3A**). It is noteworthy that in bacteria with discernible TssK and TssB assemblies the TssK structure co-localized exclusively with the proximal tip of the TssB structure at the perimembrane site (**Figures 3A,B**), in agreement with proposed baseplate localization and function as a platform for sheath polymerization (Brunet et al., 2015; Cianfanelli et al., 2016; Cherrak et al., 2018; Nazarov et al., 2018).

Importantly, in the wild-type strain co-expressing both fusions the incidence of discernible TssK structures at random time points (as captured on still images) was more frequent than that of TssB-sheaths and consequently a vast majority (95%) of TssB sheaths was marked by discernible TssK-structure, while only a subpopulation of cells with TssK structure (40%) also exhibited assembled TssB-sheath (not shown). This suggests that both components assemble sequentially rather than simultaneously into the apparatus and that only a fraction of TssK assemblies gives rise to TssB-sheath assembly, similarly to a study in *E. coli* (Santin et al., 2018). We then examined relative timing of TssK and TssB assembly by time-lapse analysis of individual bacteria followed by quantitative measurement of fluorescence intensity within a region of interest (ROI) covering the site of TssK/TssB assembly. Although the incidence of TssK and TssB assemblies exhibited a spatial correlation within individual cells, their temporal co-localization was mutually exclusive. Quantitative fluorescence intensity measurements also revealed consistent interval of 20 ± 10 s between kinetic fluorescence maxima of TssK and TssB assemblies (**Figure 3B**), suggesting that TssK component of the baseplate is involved in the initial stage of TssB-sheath nucleation rather than in subsequent steps of sheath elongation, contraction or disassembly.

TssK Requires TssM to Trigger TssB-Assembly

To determine the impact of the membrane component TssM on the kinetics of TssK assembly, we analyzed the incidence of TssK and TssB assemblies in *P. aeruginosa* PAO1Δ*tssM*. We found that although deletion of *tssM* significantly decreased the incidence of bacteria positive for TssK foci (from 10% in the parental strain to 3.7% in Δ*tssM*) the assembly of TssK structures and their localization to the membrane was not completely abolished (**Figure 4A**). In contrast, elongated TssB rod-shaped assemblies were detected only in wild-type bacteria

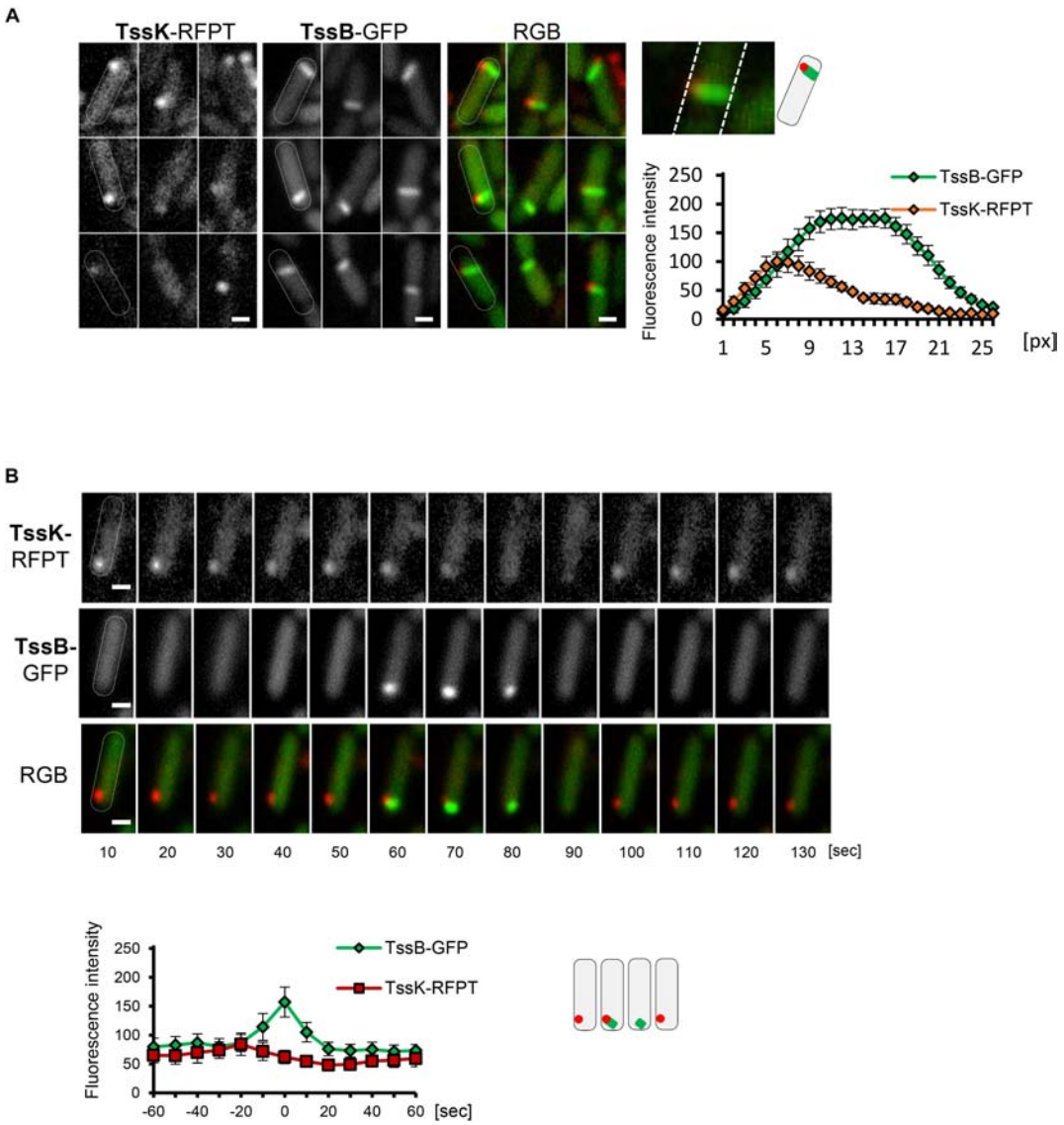

FIGURE 3 | TssK functions as essential positional marker for recruitment, nucleation and assembly of contractile apparatus. **(A)** TssK assembles into discrete structure at the proximal tip of TssB-sheath. Several representative fluorescence images of WT cells co-expressing TssK-RFPT and TssB-GFP. Note that fully elongated TssB-sheath spans the entire width of bacteria. Fluorescence intensity profile of structures positive for both TssK-RFPT and TssB-GFP measured on line cross-section from proximal to distal pole with average values and SD calculated from 20 structures ($N = 20$). Schematic representation of bacteria with TssK (in red) and TssB (in green). **(B)** TssK and TssB assemblies within individual bacteria exhibit spatial correlation, but differential temporal co-localization. Time-lapse of fluorescence images of representative bacteria co-expressing TssB-GFP and TssK-RFPT (top panel). Note that TssK structure transiently disappears after the onset of TssB assembly at that site. Kinetics of fluorescence intensity measured at ROI containing nascent TssK/TssB structure indicates an interval (20 ± 10 s) between fluorescence maxima of TssK-RFPT and TssB-GFP. SD were calculated from ROI of 20 bacteria ($N = 20$). Bars = 0.5 μm. Schematic representation of bacteria from time lapse in B, with TssK (in red) and TssB (in green).

and never in Δ*tssM*. We noted however, that in less than 0.6% of Δ*tssM* bacteria the TssB assembled into low-intensity round-shaped fluorescent spot(s) localizing to the membrane but these structures never extended into a shape of an extended sheath-like structure (**Figure 4A**). To assess possible impact of *tssM* deletion on dynamic properties of TssK we quantified an average time span of TssK structure (period between onset of assembly and complete disassembly/disappearance) by measuring the TssK-GFP fluorescence intensity in time-lapse of Δ*tssM* relative to wild-type bacteria. We found kinetics of TssK assembly-disassembly to be almost identical in both genetic backgrounds (140 ± 30 s per single round of assembly-disassembly) (**Figure 4B**). However, in a contrast to the wild-type, TssK-assemblies in Δ*tssM* often "detached" from the original perimembrane site and exhibited lateral movement along the membrane before their complete disassembly (**Figure 4C**).

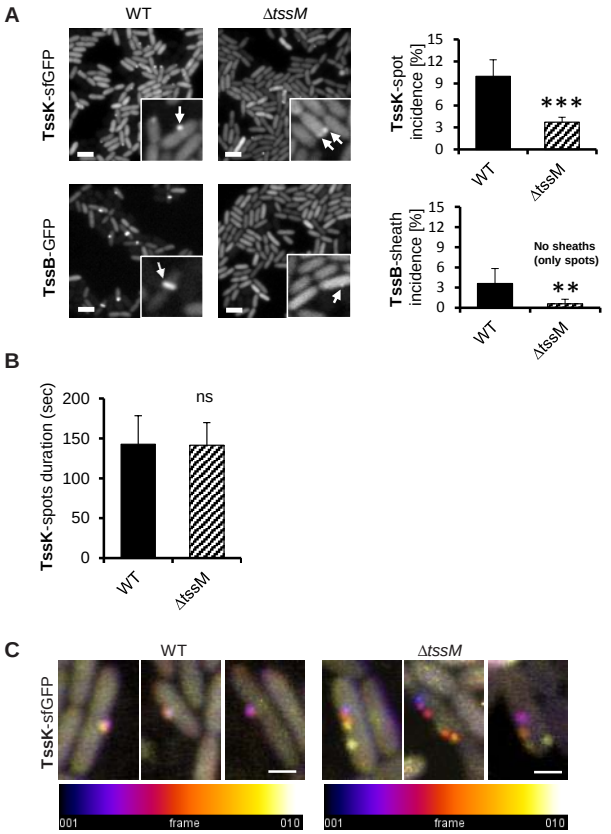

FIGURE 4 | Assembly of TssK baseplate is essential but not sufficient to trigger TssB-assembly and requires stable anchor *via* TssM. **(A)** Assembly of TssK-baseplate and TssB-sheath in *P. aeruginosa* PAO1 lacking transmembrane component of T6SS apparatus, TssM. Representative fluorescence images (left) and quantification of TssK or TssB assemblies (right). Note that incidence of TssK structures (white arrows) in Δ*tssM* cells is significantly reduced, but not completely abolished, while elongated TssB-sheaths (white arrows) are only visible in PAO1 and only minor subpopulation of Δ*tssM* bacteria (<0.6%) was found with a spot-like structure of TssB-GFP. Two-tail *t*-test, ***P = 0.002 (TssK) and **P = 0.015 (TssB). Bars = 2 μm. **(B)** Quantification of TssK-spot duration as a time between appearance and disappearance of discernible TssK-sfGFP structure over the background fluorescence intensity of the fusion construct. Note that kinetics of TssK-sfGFP baseplate assembly-disassembly is not impaired in Δ*tssM* relative to the WT cells (140 ± 30 s). Average values and SD were calculated from 30 cells (N = 30). Two-tail *t*-test. ns, non-significant. **(C)** Three representative time-lapse series (10 s between frames, 10 frames) of WT and Δ*tssM* cells expressing TssK-sfGFP. Each series were superimposed and color-coded (fire LUT) to visualize TssK structure stability/displacement over time. Note that TssK-structure in Δ*tssM* undergoes lateral displacement. Bars = 0.5 μm.

Together, these results show that (i) TssM is not necessary for assembly of TssK *per se*, (ii) TssM is essential for stabilization of assembled TssK structure at a fixed perimembrane site and (iii) in the absence of TssM, the TssB protein is still recruited to the structure containing TssK, but the assembly of TssB-sheath is aborted (likely at the nucleation stage). This implies that TssM provides a necessary anchor, probably through the outer membrane lipoprotein TssJ (Felisberto-Rodrigues et al., 2011) for transient assembly of TssK-oligomeric structure. This could restrict its lateral movement along cell periphery, which in turn is required for subsequent recruitment, assembly and elongation of TssB-sheath.

TssE Functions Downstream of TssK and Prevents Detachment of TssB-Sheath and Its Premature Disassembly

TssE is the structural homolog of the T4 phage baseplate components gp25 (Leiman et al., 2009; Lossi et al., 2011). TssE oligomerises within the baseplate together with TssF and TssG, interacts with the sheath element TssB (Cherrak et al., 2018; Nazarov et al., 2018) and was proposed to act as an initiator of sheath polymerization (Kudryashev et al., 2015; Yap et al., 2010). To check contribution of TssE in TssK-mediated assembly of TssB-sheath in *P. aeruginosa*, we generated *P. aeruginosa* mutant Δ*tssE* expressing TssK-sfGFP and analyzed TssK-assemblies. TssK-sfGFP retained the capacity to assemble into foci in Δ*tssE* mutant and in the strain Δ*tssE/tssE* (**Supplementary Figure S5**). Similar to TssK-GFP, the TssE-sfGFP fusion protein also exhibited homogenous cytosolic localization in a majority of bacteria with a minor subpopulation of cells where TssE-sfGFP assembled into discernible perimembrane spots (**Figure 5A**). To confirm that TssK and TssE assemble into the same spot-like structure we generated bacteria co-expressing TssE-sfGFP with TssK-RFPT. Analysis of *P. aeruginosa* co-expressing TssE-sfGFP and TssK-RFPT (**Figure 5A**) revealed that all discernible TssE assemblies colocalized with TssK (upper panel) while not all TssK-RFPT assemblies were positive for TssE-sfGFP (lower panel). We generated also a Δ*tssE* strain expressing TssB-GFP. As already reported (Basler and Mekalanos, 2012; Vettiger and Basler, 2016), very low number of TssB-structures were seen in the mutant bacteria, and this was corrected by complementation (**Supplementary Figure S5C**). The time-lapse analysis of TssB-sheaths in Δ*tssE* revealed an aberrant phenotype, where the sheaths were unusually elongated and curved, not perpendicular to the membrane, and their dissociation from the inner membrane followed by disintegration into fragments was readily observed (**Figure 5B**), suggesting a weak or inefficient connection to the baseplate. This aberrant phenotype may explain the extremely low activity of the T6SS machinery in the absence of TssE observed in *Vibrio* (Basler and Mekalanos, 2012; Vettiger and Basler, 2016).

From these results, we conclude that (i) TssK component of the baseplate assembles independently of TssE, (ii) TssE is recruited to the baseplate complex at later stages as already suggested, and (iii) TssE is dispensable for TssB-sheath assembly *per se* but is required for stabilization of the connection between the sheath and the baseplate.

DISCUSSION

The access to assembly of multi-protein, membrane-bound architectures in live cells is extremely challenging in the context of spatial and temporal resolution. Here we focused on dynamic and regulatory aspects of assembly/disassembly

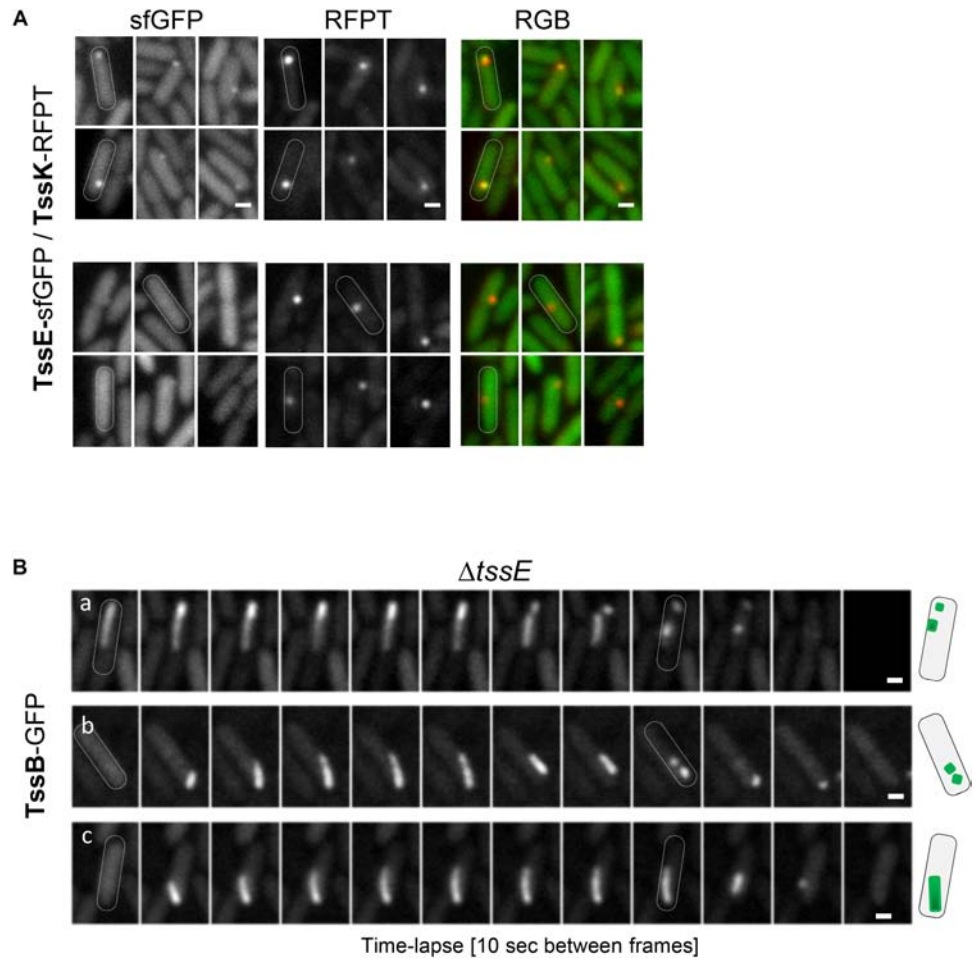

FIGURE 5 | Role of TssE in baseplate assembly and elongation of TssB-sheath. **(A)** TssE-sfGFP assembles into discernible perimembrane structures and colocalizes with TssK in *P. aeruginosa* PAO1 co-expressing *tssE-sfGFP* with *tssK-RFPT* (upper panel). In some cases, TssK-RFPT assembles into spots without TssE-sfGFP (lower panel). Six representative fluorescence images are shown. Bars = 0.5 μm. **(B)** Aberrant phenotype of contractile sheath (TssB-GFP) in PA01 Δ*tssE* strain. Fluorescence images from three representative time-lapse series of Δ*tssE* cells are shown. Note that the TssB-sheath is unusually elongated and curved and breaks off from the membrane. Bars = 0.5 μm. Schematic representation of bacteria with TssB (green) in PAO1 Δ*tssE*.

of the T6SS baseplate components, TssK and TssE, and TssB by microscopy imaging of intact bacteria. We followed their capability to assemble into discernible higher order structure(s) depending on post-transcriptional regulatory module, their subcellular localization and spatial orientation and their dynamic characteristics (assembly/disassembly).

We found that TssK assembles into higher-ordered structure localizing to discrete foci at the cell periphery in the proximity of exogenous attacker and initiates further assembly of the contractile sheath, in agreement with its higher-ordered oligomerization capacity within the T6SS baseplate. In the complex baseplate-extended sheath forms TssK the connector ring between the membrane complex TssJLM and the rest of the baseplate. The overall structure has a six fold symmetry in the center, and is composed by two TssF interconnected by one TssG. TssG then contacts two TssK trimers trough extended loops to form a final structure containing 18 subunits of TssK (Cherrak et al., 2018; Nazarov et al., 2018; Park et al., 2018).

Based on those structural studies and observations by others, the C-terminal fusion construct is not sterically incompatible and should not impede TssK binding to its partners (TssL, TssM, TssG, and TssF). TssK-sfGFP used in our work is probably not competent for *E. coli* killing because of the GFP molecule hindering structural movements in TssK oligomer required to trigger final VgrG-toxin expulsion, although we could still observe the dueling.

The main finding in this study is the transient characteristic of TssK structures suggesting that they assemble *ad hoc* as structural entities and disassemble together with the contractile sheath TssB to recycle the components for *de novo* assembly of the apparatus in another site of the cell. Results of our kinetic analysis propose that TssK assembles upstream of TssE, the major transmembrane anchoring component TssM, and contractile sheath component TssB. It also requires presence of at least two essential components of the membrane-embedded sensory module, TagQ and TagR. This is in agreement with previous

findings showing that TagQ-TagR-PppK-Fha-PppA pathway recognizes an external signal to activate the T6SS (Mougous et al., 2007; Basler et al., 2012; Ho et al., 2014). Our laboratory found that the sensory module in *P. aeruginosa* has additional components TagS and TagT that form an inner membrane ABC transporter with TagT having an ATPase activity (Casabona et al., 2013). Here we show that mutants in any of these two components are still capable to assemble TssK structures even if with lower incidence within the cell population. This opens a possibility that TagQ and TagR represent the core unit of the sensory complex able alone to trigger assembly of the TssK component of the baseplate whereas TagS and TagT probably through their ATPase activity may have a role in promoting higher-order oligomerization of proteins within the baseplate to adopt and stabilize the whole sheath/tube entity. TagT was indeed required for assembly of T6SS sheaths upon activation by polymyxin B treatment (Ho et al., 2013), or upon attack by a neighboring T6SS-positive bacteria (Basler et al., 2013), as assessed by the ClpV-GFP fusion. This observation could be a consequence of TagT effect on capacity of TssK to oligomerize in higher-ordered structures. We previously found that fusion construct TagQ-mCherry expressed in *P. aeruginosa* localizes to the outer membrane, but no discernible structures could be detected (Casabona et al., 2013). We thus hypothesize that multiple TagQRST modules may be scattered throughout the surface of bacteria and function as receptors sensing physical contract with kin or prey cells to trigger rapid assembly of the T6SS apparatus by recruitment of baseplate components at close proximity to assure effective attack toward a predatory species. Intriguingly, the *E. coli* TssK assemblies are static component of the baseplate (Brunet et al., 2015). This difference in TssK behavior may reflect the difference in regulatory features between *E. coli* and *P. aeruginosa* T6SSs, notably the absence of TagQRST-PpkA-PppA signaling in the *E. coli* system (Boyer et al., 2009).

What provides the link to the transmembrane anchoring complex of the T6SS once the baseplate begins to assemble? Previous studies using bacterial two-hybrid analysis identified direct interactions between TssK and TssM and between TssK and TssL, but only the TssK/TssL interaction was confirmed by co-immunoprecipitation (Zoued et al., 2013). In our study, we showed that membrane protein TssM is essential for lateral stabilization of TssK foci but not for the TssK assembly. It is possible that TssL alone assures TssK recruitment from the cytosolic pool into the perimembrane site. Biochemistry and bacterial two-hybrid screen revealed that TssK physically interacts with N-terminal cytoplasmic domain of TssL, residues 1–184 (Zoued et al., 2013). Moreover, study of T6-secretion in *A. tumefaciens* (Lin et al., 2014) proposed a model for the TssL-TssM complex where TssL is first phosphorylated by PpkA leading to ATP-binding dependent conformational switch in TssM followed by direct binding of FHA domain of Fha to the TssL. As thus the TssM-p-TssL-Fha complex powered by TssM-mediated ATP hydrolysis (Ma et al., 2012) may initiate recruitment of tube core component Hcp for assembly. Analysis of TssK behavior in specific mutants, either lacking domains of interactions between those components, mutants deficient in TssM ATPase activity, or bearing Fha unable to be phosphorylated, should bring more insights into molecular mechanisms governing the initial recruitments of TssK.

Our data suggest that although TssE assembles into a single perimembrane structure similar to TssK, it does so independently and downstream of assembly of TssK baseplate component. TssE homolog in bacteriophage T4, gp25, is essential to initiate assembly of the tube (Wagenknecht and Bloomfield, 1977). TssE assembles in the outermost structure of the baseplate hub around the membrane-puncturing device (Cherrak et al., 2018; Nazarov et al., 2018), as does gp25 (Kostyuchenko et al., 2003; Leiman et al., 2009). In contrast to TssK, we found that, in *P. aeruginosa*, TssE was not essential for TssB assembly into a sheath-like structure, although the sheath in a Δ*tssE* mutant exhibited an aberrant phenotype and break itself in smaller pieces, in agreement with almost undetectable activity of T6SS in competition assays found by others (Vettiger and Basler, 2016). In some Δ*tssE* bacteria where the TssB-sheath elongated parallel (or in a certain angle) to the membrane, the elongation of the apparatus was not spatially limited by cell width and TssB-sheath thus often assembled to an extreme length. This implies that although TssE and TssK co-assemble into a baseplate structure they adopt distinct functions where TssE incorporation into the baseplate may fortify the physical link between tube-sheath complex and the baseplate. Access to spatio-temporal behavior of two other baseplate proteins, TssG and TssF, should provide in the future global picture of the role of the baseplate in T6SS function.

In conclusion, our work shows the role of transmembrane post-translational regulatory cascade in activation and/or localization of T6SS baseplate assembly and the role of TssK and TssE in spatio-temporal organization and stabilization of T6SS contractile sheath in *P. aeruginosa*. Despite the fact that due to the low fluorescence intensities we could not examine the assembly of TssF and TssG, we present a model (**Figure 6**) where trimers of TssK associate with TssF/TssG complex transiently at the perimembrane site in contact with prey bacteria. The baseplate assembly occurs downstream of TagQRST activation and PpkA activity and functions as an essential spatio-temporal cue for subsequent recruitment of other components of the machinery including TssE, Hcp, and TssB/TssC leading to assembly of functional contractile apparatus with stable anchor within bacterial membrane. Our model also highlights the role of TssK in PppA-mediated recycling and repositioning of the machinery through *de novo* assembly at different perimembrane location defined by local activation of TagQRST module upon contact with the target cell.

MATERIALS AND METHODS

Bacterial Strains and Genetic Constructions

All bacterial strains are listed in the **Supplementary Table S1**. Wild-type *Acinetobacter bauamnnii* and its Δ*tssM* mutant was kindly provided by Brent Weber (Alberta Glycomics Centre, University of Alberta, Canada) and described earlier

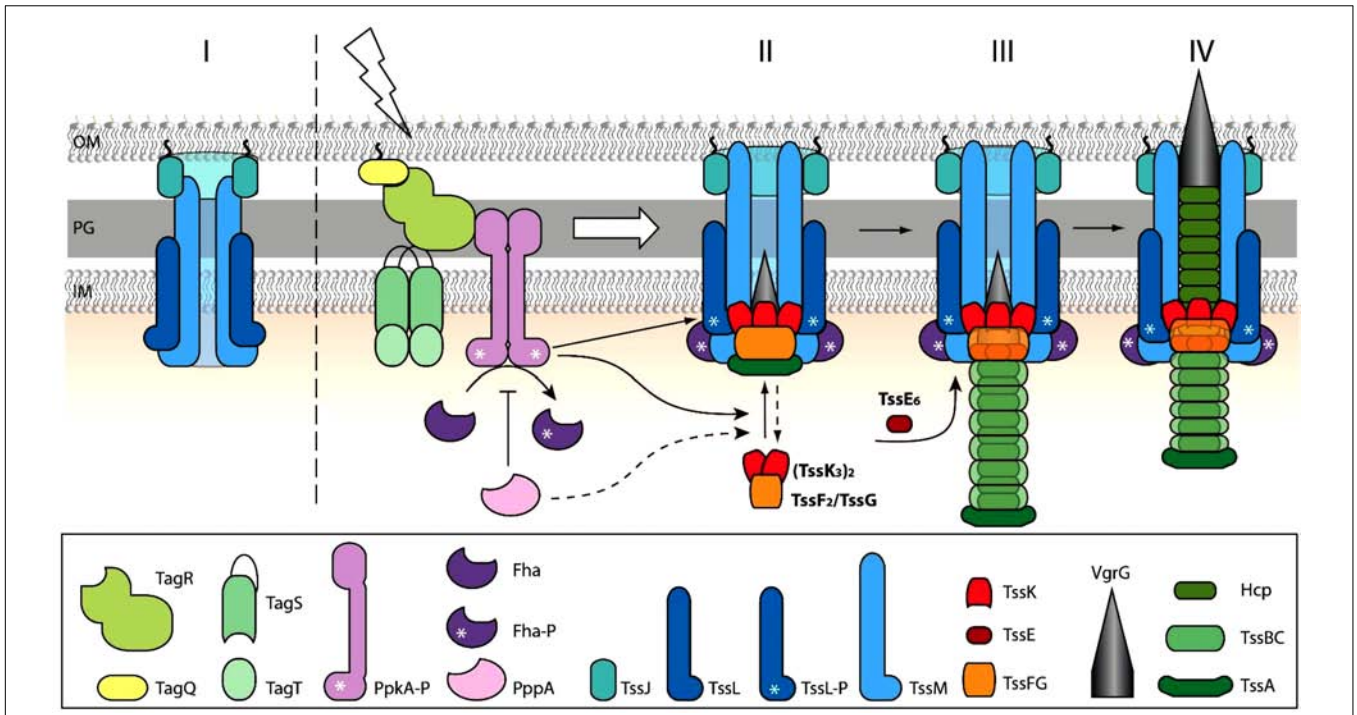

FIGURE 6 | Schematic model for TssK/TssE baseplate assembly and function. **(I)** In a steady state, the baseplate components TssK and TssE are present in the cytosol. **(II)** Upon contact with target cell and activation of TagQRST (lightning) the Fha is phosphorylated by activated PpkA and binds TssL associated with the inner membrane. Upon activation of TagQ, TagR, and TssK oligomerizes, probably concurrently with TssF and TssG, around VrgG and the whole complex ($VrgG(TssK_3)_6(TssF_2/TssG)_6$) is recruited into the baseplate and anchored to the transmembrane complex TssJLM. The TssK oligomers disassemble upon action of PppA (shown in dashed lines). Stoichiometry $(TssK_3)_2(TssF_2/TssG)$ in accordance with cryo-EM structure (PDB 6N38) is shown. **(III)** Nucleation of the tube-sheath assembly begins by recruitment of Hcp-TssB/C subunits. TssE joins the TssF-TssG complex to form a more stable tube-sheath structure. **(IV)** The fully extended state is ready to "fire". Outer membrane (OM), peptidoglycan (PG), inner membrane (IM).

(Weber et al., 2013). *P. aeruginosa* wild type and mutants Δ*tssM* (PA0077), Δ*tagQ* (PA0070), Δ*tagR* (PA0071), Δ*tagS* (PA0072), Δ*tagT* (PA0073), Δ*pppA* (PA0074), and Δ*ppkA* (PA0075) were kindly provided by J. Mougous Laboratory (University of Washington, United States) and described earlier (Silverman et al., 2011). Original plasmids and plasmid constructs used in this study are summarized in **Supplementary Table S2.** Fusion constructs *tssK*-sfGFP and *tssE*-sfGFP were generated as follows. First, the gene sequence encoding sfGFP [GenBank: HQ873313.1] was synthesized (Genscript, United States) to contain 5′ terminal *Spe*I and 3′ terminal *Sac*I restriction sites. This product was subcloned into pJN105 plasmid (Newman and Fuqua, 1999) via *Spe*I/*Sac*I restriction sites to generate pJN105-sfGFP. Second, genes encoding TssK (PA0079) and TssE (PA0087) without stop codon were amplified from *P. aeruginosa* PAO1 genomic DNA by PCR using primers listed in (**Supplementary Table S3**) and subcloned into pJN105-sfGFP via *Eco*RI/*Spe*I restriction sites. Fusion construct TssB-GFP was synthesized (ProteoGenix, France) to contain 5′ terminal *Eco*RI restriction site followed by 20nt 5′ TCGCGCGAGGGAGAAACAAG including ribosome-binding site, gene encoding TssB (PA0083), a linker sequence (5′ GCCGCCGCCGGCGGCGGC 3′), gene encoding GFP [GenBank: LN515608.1] and 3′ terminal *Sma*I restriction site. This synthetic product was subcloned into pJN105 via *Eco*RI/*Sma*I restriction sites to generate pJN105-*tssB-GFP*. Fusion construct *tssK-RFPT* was generated as follows. First, gene sequence encoding TagRFP-T (RFPT in this manuscript) [GenBank: EU582019.1] without ATG start codon was codon optimized for expression in *P. aeruginosa* and synthesized (Genescript, Unites States) to contain 5′ terminal *Spe*I restriction site followed by a linker sequence (5′ GCCGCCGCCGGCGGCGGC 3′), gene encoding TagRFP-T and 3′ terminal *Sac*I restriction site. This synthetic product was subcloned into pSW196 plasmid *via Spe*I/*Sac*I restriction sites to generate pSW196-RFPT. Second, gene encoding TssK was subcloned from pJN105-*tssK-sfGFP* into pSW196-*RFPT* via *EcoR*I/*Spe*I restriction sites to generate pSW196-*tssK-RFPT*. Plasmids encoding fusion constructs were introduced into *P. aeruginosa* strains by heat-shock transformation for pJN105-derived plasmids or by triparental mating for pSW196 integrative plasmids. To generate an in-frame deletion of *tssE* (PA0087) in *P. aeruginosa*, sequences corresponding to upstream and downstream flanking regions of the genes was synthesized (Genscript, United States) to contain *Sac*I and *Xba*I restriction sites on 5′ and 3′ terminus, respectively. This synthetic product was subcloned into pEXG2 plasmid (Rietsch et al., 2005) for subsequent *sacB*-mediated allelic exchange as

described earlier (Metcalf et al., 1996). Deletion was confirmed by PCR using primers listed in **Supplementary Table S3**. The similar level of expression of fusions in different strains was confirmed by immunoblotting (**Supplementary Figure S3**). For complementation experiments, gene of interest was cloned into a pminiCTX1-derivative plasmid pSW196 containing arabinose-inducible promotor pBAD. Then, pSW196 plasmid containing *tssE* or *tssK* gene was introduced in *P. aeruginosa* by triparental mating (Hmelo et al., 2015).

Competition Assays

The competition assays were performed as previously described (Hachani et al., 2013). *P. aeruginosa* and *E. coli* (pBlueScript) were grown overnight in 3 ml LB medium supplemented with appropriate antibiotics. Diluted overnight cultures were inoculated in the same medium containing 0.025% arabinose (to induce the expression of specific fusion) and the culture was grown until OD_{600} = 1. Then 1 ml of each culture were spin down and pellet was resuspended in 100 μl LB with arabinose 0.025%. Indicated *P. aeruginosa* strains (predator) were mixed with *E. coli* (prey) in ratio 1:2 (predator:prey). Competition reactions (20 μl), realized in triplicate, were spotted onto LB agar plates containing 50 μg/ml ampicillin and incubated 5 h at 37°C. The totality of bacteria was recover in LB and dilutions were plated in triplicates onto LB plates containing Xgal (40 μg/ml) and IPTG (100 μM) to visualize *E. coli* (blue colonies).

Western Blotting

The expression levels of protein fusions in different mutants were assessed by immunoblotting. For the Western blot, total bacterial samples (OD_{600} = 1) were separated on Criterion 4–20% TGX precasted gels, BioRad and transferred onto a PVDF membrane (GE.Healthcare) by electrotransfert in 20% Laemmli buffer. After blocking step in 5% milk, polyclonal anti-GFP antibodies (diluted 1/5000 in PBS buffer with 0.1% Tween20) were incubated one hour at room temperature, followed with a second antibodies incubation (anti-rabbit HRP, dilution 1/20 000, Sigma). Detection was performed using Luminata Classico HRP-substrate (Millipore) using BioRad ChemiDoc apparatus.

Time Lapse Video Microscopy

Bacteria were grown over night in LB with appropriate selection antibiotics, then sub-cultured 1:100 in LB with arabinose (0.025–0.25%) for induction of fusion construct expression and grown for additional 3 h to reach OD_{600} = 2. To immobilize bacteria for acquisition of still images or a time-lapse series, a drop of bacterial culture was applied on top of agarose pads [1.5% Low melting agarose in Hanks' balanced salt solution (Gibco)] and transferred into the glass-bottom imaging dishes (WillCo Wells BV) so that bacteria were grown in interphase between glass bottom and semi-solid medium of agarose pad for another 1 h prior imaging. For competing conditions, culture of *P. aeruginosa* was mixed 1:1 with competing bacteria (*A. baumannii*) prior applying onto agarose pads. Still images or time-lapse image acquisitions was performed within 1–3 h post mixing competing bacteria – a time frame when we observed the peak activity of TssK/TssB assemblies. Fluorescence and bright field images were acquired at a rate of 6 frames per min (10 s between frames) for 5–15 min using OLYMPUS inverted microscope IX71 equipped with UPlanFLN 100× NA1.3 objective and 16-bit Hamamatsu ORCA-ER CCD camera, operated by Xcellence RT2.0 acquisition software (OLYMPUS). Digital image processing and analysis including measurements of fluorescent intensity and kinetic profiles was made using ImageJ 1.47v (Wayne Rusband, NIH, United States). Where necessary, the *x*–*y* drift in time-lapse series was corrected by StackReg plugin using Rigid body transformation algorithm. Statistic evaluation was done in MS Excel 2010.

Foci Quantification

Because rarely more than one discernible fluorescent structure of the fusion construct of TssK or TssB was detected per cell at a time, still images of live bacteria were used to quantify the incidence of assembly as a fraction (%) of cells that exhibit discernible fluorescent structure relative to the total amount of bacteria in the view field. For every sample and condition analyzed, a set of images was acquired from random fields of view using fixed exposure settings to allow quantitative comparison between samples. Because the expression levels of the fusion construct was usually heterogeneous within the same population of bacteria, automated particle counting on binary images using thresholding, filtering and segmentation algorithm was not reliable and thus manual counting from images was used instead after 16-bit to 8-bit conversion and background subtraction. Average and SD values were calculated for each group from 4 to 6 ROI each containing between 400 and 1000 of cells.

Kinetic Measurements of Fluorescence Intensity

Kinetic changes of fluorescence intensity were measured on a stack of images from a time-lapse. First, a set of ROI of fixed size (500×500 nm) covering area where discernible TssK/TssB-structures appear during the time-lapse was selected and fluorescence integrated density within these ROI was measured using ROI manager and multiple measurements plugin (ImageJ). Illustrative results for a typical profile were plotted as a fold-increase/decrease in fluorescence intensity relative to ROI intensity in frame 1 (T0) of the time-lapse (set as nominal value 1). Average duration of assembly was assessed as a time between the onset of fluorescence increase over the background level (rel. value = 1.0) and the peak fluorescence values. On contrary, average duration of disassembly was assessed as a time between fluorescence peak and its decrease to the background levels. Average values and SD were calculated from 20 to 40 ROI for each group. For an assessment of spatio-temporal colocalization between TssK-RFPT and TssB-GFP

the fluorescence intensity for both channels (RFPT and GFP) was first measured at multiple ROI of several independent time lapse series. The resulting kinetic plot profiles were then aligned along *y*-axis so that maximum peak values for GFP channel (fully extended TssB-sheath) fit to $T = 0$ s and fluorescence intensity values of RFPT corresponding to each time point of GFP values were plotted accordingly. Average values and SD were calculated from 20 kinetic profiles for each channel.

Fluorescence Intensity Measurements of Protein Assemblies

For measurement of fluorescence intensity profile of TssK and TssB structures (**Figure 1A**) images were acquired with fixed exposure settings and fluorescence intensity plot profile was measured on line cross-section through the structures. Maximum fluorescence intensity (Max gray values) of TssK spots in *tagS* and *tagT* mutants (**Figure 1C**) was measured by ImageJ in fixed-size square ROI drawn around the fluorescent spots. Average and SD values were calculated from 20 plot profile measurements for each group. For an assessment of spatial co-localization between TssK-RFPT and TssB-GFP in elongated TssB-sheaths, fluorescence intensity plot profile was measured along the long axis of the structure with proximal end of the ROI crossing perimembrane TssK structure.

DATA AVAILABILITY

The raw data supporting the conclusions of this manuscript will be made available by the authors, without undue reservation, to any qualified researcher.

AUTHOR CONTRIBUTIONS

DL, MR-G, VJ, and VC performed the experiments and prepared the figures. DL and IA designed the study, analyzed the data, and wrote the manuscript.

FUNDING

This project received funding from the Laboratory of Excellence GRAL, financed within the University Grenoble Alpes graduate school (Ecoles Universitaires de Recherche) CBH-EUR-GS (ANR-17-EURE-0003). DL was funded by a grant from the Laboratory of Excellence GRAL (ANR-10-LABX-49-01). VC was funded by FINOVI (Fondation Innovation en Infectiologie).

ACKNOWLEDGMENTS

We thank to Brent Weber (Alberta Glycomics Centre, University of Alberta, Canada) and Joseph Mougous (University of Washington, United States) for providing bacterial strains and mutants used in this study. We also thank to Sylvie Elsen, Yohann Couté, and Maria Guillermina Casabona (CEA, Grenoble) for input in initial design of the project, sharing the unpublished data and interesting discussions, and to Brian T. Ho (Harvard Medical School, Boston, United States) for critical reading of the initial manuscript.

SUPPLEMENTARY MATERIAL

The Supplementary Material for this article can be found online at: https://www.frontiersin.org/articles/10.3389/fmicb.2019.01615/full#supplementary-material

REFERENCES

Alcoforado Diniz, J., Liu, Y. C., and Coulthurst, S. J. (2015). Molecular weaponry: diverse effectors delivered by the Type VI secretion system. *Cell Microbiol.* 17, 1742–1751. doi: 10.1111/cmi.12532

Basler, M., Ho, B. T., and Mekalanos, J. J. (2013). Tit-for-tat: type VI secretion system counterattack during bacterial cell-cell interactions. *Cell* 152, 884–894. doi: 10.1016/j.cell.2013.01.042

Basler, M., and Mekalanos, J. J. (2012). Type 6 secretion dynamics within and between bacterial cells. *Science* 337:815. doi: 10.1126/science.1222901

Basler, M., Pilhofer, M., Henderson, G. P., Jensen, G. J., and Mekalanos, J. J. (2012). Type VI secretion requires a dynamic contractile phage tail-like structure. *Nature* 483, 182–186. doi: 10.1038/nature10846

Bleves, S. (2016). Game of trans-kingdom effectors. *Trends Microbiol.* 24, 773–774. doi: 10.1016/j.tim.2016.08.002

Bonemann, G., Pietrosiuk, A., Diemand, A., Zentgraf, H., and Mogk, A. (2009). Remodelling of VipA/VipB tubules by ClpV-mediated threading is crucial for type VI protein secretion. *EMBO J.* 28, 315–325. doi: 10.1038/emboj.2008.269

Boyer, F., Fichant, G., Berthod, J., Vandenbrouck, Y., and Attree, I. (2009). Dissecting the bacterial type VI secretion system by a genome wide in silico analysis: what can be learned from available microbial genomic resources? *BMC genomics* 10:104. doi: 10.1186/1471-2164-10-104

Brencic, A., and Lory, S. (2009). Determination of the regulon and identification of novel mRNA targets of *Pseudomonas aeruginosa* RsmA. *Mol. Microbiol.* 72, 612–632. doi: 10.1111/j.1365-2958.2009.06670.x

Brencic, A., McFarland, K. A., McManus, H. R., Castang, S., Mogno, I., Dove, S. L., et al. (2009). The GacS/GacA signal transduction system of *Pseudomonas aeruginosa* acts exclusively through its control over the transcription of the RsmY and RsmZ regulatory small RNAs. *Mol. Microbiol.* 73, 434–445. doi: 10.1111/j.1365-2958.2009.06782.x

Brunet, Y. R., Zoued, A., Boyer, F., Douzi, B., and Cascales, E. (2015). The type VI secretion TssEFGK-VgrG phage-like baseplate is recruited to the TssJLM membrane complex via multiple contacts and serves as assembly platform for tail tube/sheath polymerization. *PLoS Genet.* 11:e1005545. doi: 10.1371/journal.pgen.1005545

Casabona, M. G., Silverman, J. M., Sall, K. M., Boyer, F., Coute, Y., Poirel, J., et al. (2013). An ABC transporter and an outer membrane lipoprotein participate in posttranslational activation of type VI secretion in *Pseudomonas aeruginosa*. *Environ. Microbiol.* 15, 471–486. doi: 10.1111/j.1462-2920.2012.02816.x

Cascales, E. (2008). The type VI secretion toolkit. *EMBO Rep.* 9, 735–741. doi: 10.1038/embor.2008.131

Cherrak, Y., Rapisarda, C., Pellarin, R., Bouvier, G., Bardiaux, B., Allain, F., et al. (2018). Biogenesis and structure of a type VI secretion baseplate. *Nat. Microbiol.* 3, 1404–1416. doi: 10.1038/s41564-018-0260-1

Cianfanelli, F. R., Monlezun, L., and Coulthurst, S. J. (2016). Aim, load, fire: the type VI secretion system, a Bacterial Nanoweapon. *Trends Microbiol.* 24, 51–62. doi: 10.1016/j.tim.2015.10.005

Coulthurst, S. J. (2013). The type VI secretion system - a widespread and versatile cell targeting system. *Res. Microbiol.* 164, 640–654. doi: 10.1016/j.resmic.2013.03.017

Durand, E., Nguyen, V. S., Zoued, A., Logger, L., Pehau-Arnaudet, G., Aschtgen, M. S., et al. (2015). Biogenesis and structure of a type VI secretion membrane core complex. *Nature* 523, 555–560. doi: 10.1038/nature14667

Felisberto-Rodrigues, C., Durand, E., Aschtgen, M. S., Blangy, S., Ortiz-Lombardia, M., Douzi, B., et al. (2011). Towards a structural comprehension of bacterial type VI secretion systems: characterization of the TssJ-TssM complex of an *Escherichia coli* pathovar. *PLoS Pathogens.* 7:e1002386. doi: 10.1371/journal.ppat.1002386

Filloux, A., Hachani, A., and Bleves, S. (2008). The bacterial type VI secretion machine: yet another player for protein transport across membranes. *Microbiology* 154(Pt 6), 1570–1583. doi: 10.1099/mic.0.2008/016840-0

Forster, A., Planamente, S., Manoli, E., Lossi, N. S., Freemont, P. S., and Filloux, A. (2014). Coevolution of the ATPase ClpV, the sheath proteins TssB and TssC, and the accessory protein TagJ/HsiE1 distinguishes type VI secretion classes. *J. Biol. Chem.* 289, 33032–33043. doi: 10.1074/jbc.M114.600510

Hachani, A., Lossi, N. S., and Filloux, A. (2013). A visual assay to monitor T6SS-mediated bacterial competition. *J. Vis. Exp.* 73:e50103. doi: 10.3791/50103

Hayes, C. S., Aoki, S. K., and Low, D. A. (2010). Bacterial contact-dependent delivery systems. *Annu. Rev. Genet.* 44, 71–90. doi: 10.1146/annurev.genet.42.110807.091449

Hmelo, L. R., Borlee, B. R., Almblad, H., Love, M. E., Randall, T. E., Tseng, B. S., et al. (2015). Precision-engineering the *Pseudomonas aeruginosa* genome with two-step allelic exchange. *Nat. protoc.* 10, 1820–1841. doi: 10.1038/nprot.2015.115

Ho, B. T., Basler, M., and Mekalanos, J. J. (2013). Type 6 secretion system-mediated immunity to type 4 secretion system-mediated gene transfer. *Science* 342, 250–253. doi: 10.1126/science.1243745

Ho, B. T., Dong, T. G., and Mekalanos, J. J. (2014). A view to a kill: the bacterial type VI secretion system. *Cell Host Microbe* 15, 9–21. doi: 10.1016/j.chom.2013.11.008

Hsu, F., Schwarz, S., and Mougous, J. D. (2009). TagR promotes PpkA-catalysed type VI secretion activation in *Pseudomonas aeruginosa*. *Mol. Microbiol.* 72, 1111–1125. doi: 10.1111/j.1365-2958.2009.06701.x

Jani, A. J., and Cotter, P. A. (2010). Type VI secretion: not just for pathogenesis anymore. *Cell Host Microbe* 8, 2–6. doi: 10.1016/j.chom.2010.06.012

Kostyuchenko, V. A., Leiman, P. G., Chipman, P. R., Kanamaru, S., van Raaij, M. J., Arisaka, F., et al. (2003). Three-dimensional structure of bacteriophage T4 baseplate. *Nat. Struct. Biol.* 10, 688–693.

Kudryashev, M., Wang, R. Y., Brackmann, M., Scherer, S., Maier, T., Baker, D., et al. (2015). Structure of the type VI secretion system contractile sheath. *Cell* 160, 952–962. doi: 10.1016/j.cell.2015.01.037

Leiman, P. G., Basler, M., Ramagopal, U. A., Bonanno, J. B., Sauder, J. M., Pukatzki, S., et al. (2009). Type VI secretion apparatus and phage tail-associated protein complexes share a common evolutionary origin. *Proc. Natl. Acad. Sci. U.S.A.* 106, 4154–4159. doi: 10.1073/pnas.0813360106

Lin, J. S., Wu, H. H., Hsu, P. H., Ma, L. S., Pang, Y. Y., Tsai, M. D., et al. (2014). Fha interaction with phosphothreonine of TssL activates type VI secretion in *Agrobacterium tumefaciens*. *PLoS Pathog.* 10:e1003991. doi: 10.1371/journal.ppat.1003991

Lossi, N. S., Dajani, R., Freemont, P., and Filloux, A. (2011). Structure-function analysis of HsiF, a gp25-like component of the type VI secretion system, in *Pseudomonas aeruginosa*. *Microbiology* 157(Pt 12), 3292–3305. doi: 10.1099/mic.0.051987-0

Ma, L. S., Narberhaus, F., and Lai, E. M. (2012). IcmF family protein TssM exhibits ATPase activity and energizes type VI secretion. *J. Biol. Chem.* 287, 15610–15621. doi: 10.1074/jbc.M111.301630

Metcalf, W. W., Jiang, W., Daniels, L. L., Kim, S. K., Haldimann, A., and Wanner, B. L. (1996). Conditionally replicative and conjugative plasmids carrying lacZ alpha for cloning, mutagenesis, and allele replacement in bacteria. *Plasmid* 35, 1–13. doi: 10.1006/plas.1996.0001

Moscoso, J. A., Mikkelsen, H., Heeb, S., Williams, P., and Filloux, A. (2011). The *Pseudomonas aeruginosa* sensor RetS switches type III and type VI secretion via c-di-GMP signalling. *Environ. Microbiol.* 13, 3128–3138. doi: 10.1111/j.1462-2920.2011.02595.x

Mougous, J. D., Cuff, M. E., Raunser, S., Shen, A., Zhou, M., Gifford, C. A., et al. (2006). A virulence locus of *Pseudomonas aeruginosa* encodes a protein secretion apparatus. *Science* 312, 1526–1530. doi: 10.1126/science.1128393

Mougous, J. D., Gifford, C. A., Ramsdell, T. L., and Mekalanos, J. J. (2007). Threonine phosphorylation post-translationally regulates protein secretion in *Pseudomonas aeruginosa*. *Nat. Cell Biol.* 9, 797–803. doi: 10.1038/ncb1605

Nazarov, S., Schneider, J. P., Brackmann, M., Goldie, K. N., Stahlberg, H., and Basler, M. (2018). Cryo-EM reconstruction of Type VI secretion system baseplate and sheath distal end. *EMBO J.* 37:e97103. doi: 10.15252/embj.201797103

Newman, J. R., and Fuqua, C. (1999). Broad-host-range expression vectors that carry the L-arabinose-inducible *Escherichia coli* araBAD promoter and the araC regulator. *Gene* 227, 197–203. doi: 10.1016/s0378-1119(98)00601-5

Ostrowski, A., Cianfanelli, F. R., Porter, M., Mariano, G., Peltier, J., Wong, J. J., et al. (2018). Killing with proficiency: integrated post-translational regulation of an offensive Type VI secretion system. *PLoS pathogens* 14:e1007230. doi: 10.1371/journal.ppat.1007230

Park, Y. J., Lacourse, K. D., Cambillau, C., DiMaio, F., Mougous, J. D., and Veesler, D. (2018). Structure of the type VI secretion system TssK-TssF-TssG baseplate subcomplex revealed by cryo-electron microscopy. *Nat. Commun.* 9:5385. doi: 10.1038/s41467-018-07796-5

Pietrosiuk, A., Lenherr, E. D., Falk, S., Bonemann, G., Kopp, J., Zentgraf, H., et al. (2011). Molecular basis for the unique role of the AAA + chaperone ClpV in type VI protein secretion. *J. Biol. Chem.* 286, 30010–30021. doi: 10.1074/jbc.M111.253377

Planamente, S., Salih, O., Manoli, E., Albesa-Jove, D., Freemont, P. S., and Filloux, A. (2016). TssA forms a gp6-like ring attached to the type VI secretion sheath. *EMBO J.* 35, 1613–1627. doi: 10.15252/embj.201694024

Pukatzki, S., Ma, A. T., Sturtevant, D., Krastins, B., Sarracino, D., Nelson, W. C., et al. (2006). Identification of a conserved bacterial protein secretion system in *Vibrio cholerae* using the Dictyostelium host model system. *Proc. Natl. Acad. Sci. U.S.A.* 103, 1528–1533. doi: 10.1073/pnas.0510322103

Rietsch, A., Vallet-Gely, I., Dove, S. L., and Mekalanos, J. J. (2005). ExsE, a secreted regulator of type III secretion genes in *Pseudomonas aeruginosa*. *Proc. Natl. Acad. Sci. U.S.A.* 102, 8006–8011. doi: 10.1073/pnas.0503005102

Russell, A. B., Hood, R. D., Bui, N. K., LeRoux, M., Vollmer, W., and Mougous, J. D. (2011). Type VI secretion delivers bacteriolytic effectors to target cells. *Nature* 475, 343–347. doi: 10.1038/nature10244

Russell, A. B., Singh, P., Brittnacher, M., Bui, N. K., Hood, R. D., Carl, M. A., et al. (2012). A widespread bacterial type VI secretion effector superfamily identified using a heuristic approach. *Cell Host Microbe* 11, 538–549. doi: 10.1016/j.chom.2012.04.007

Santin, Y. G., Doan, T., Lebrun, R., Espinosa, L., Journet, L., and Cascales, E. (2018). In vivo TssA proximity labelling during type VI secretion biogenesis reveals TagA as a protein that stops and holds the sheath. *Nat. Microbiol.* 3, 1304–1313. doi: 10.1038/s41564-018-0234-3

Shalom, G., Shaw, J. G., and Thomas, M. S. (2007). In vivo expression technology identifies a type VI secretion system locus in Burkholderia pseudomallei that is induced upon invasion of macrophages. *Microbiology* 153(Pt 8), 2689–2699. doi: 10.1099/mic.0.2007/006585-0

Shneider, M. M., Buth, S. A., Ho, B. T., Basler, M., Mekalanos, J. J., and Leiman, P. G. (2013). PAAR-repeat proteins sharpen and diversify the type VI secretion system spike. *Nature* 500, 350–353. doi: 10.1038/nature12453

Silverman, J. M., Agnello, D. M., Zheng, H., Andrews, B. T., Li, M., Catalano, C. E., et al. (2013). Haemolysin coregulated protein is an exported receptor and chaperone of type VI secretion substrates. *Mol. Cell.* 51, 584–593. doi: 10.1016/j.molcel.2013.07.025

Silverman, J. M., Austin, L. S., Hsu, F., Hicks, K. G., Hood, R. D., and Mougous, J. D. (2011). Separate inputs modulate phosphorylation-dependent and -independent type VI secretion activation. *Mol. Microbiol.* 82, 1277–1290. doi: 10.1111/j.1365-2958.2011.07889.x

Vettiger, A., and Basler, M. (2016). Type VI secretion system substrates are transferred and reused among sister cells. *Cell* 167, 99–110.e112. doi: 10.1016/j.cell.2016.08.023

Wagenknecht, T., and Bloomfield, V. A. (1977). In vitro polymerization of bacteriophage T4D tail core subunits. *J. Mol. Biol.* 116, 347–359. doi: 10.1016/0022-2836(77)90074-2

Weber, B. S., Miyata, S. T., Iwashkiw, J. A., Mortensen, B. L., Skaar, E. P., Pukatzki, S., et al. (2013). Genomic and functional analysis of the type VI secretion system in Acinetobacter. *PLoS One* 8:e55142. doi: 10.1371/journal.pone.0055142

Yap, M. L., Mio, K., Leiman, P. G., Kanamaru, S., and Arisaka, F. (2010). The baseplate wedges of bacteriophage T4 spontaneously assemble into hubless baseplate-like structure in vitro. *J. Mol. Biol.* 395, 349–360. doi: 10.1016/j.jmb.2009.10.071

Zoued, A., Durand, E., Bebeacua, C., Brunet, Y. R., Douzi, B., Cambillau, C., et al. (2013). TssK is a trimeric cytoplasmic protein interacting with components of both phage-like and membrane anchoring complexes of the type VI secretion system. *J. Biol. Chem.* 288, 27031–27041. doi: 10.1074/jbc.M113.499772

Conflict of Interest Statement: The authors declare that the research was conducted in the absence of any commercial or financial relationships that could be construed as a potential conflict of interest.

Copyright © 2019 Liebl, Robert-Genthon, Job, Cogoni and Attrée. This is an open-access article distributed under the terms of the Creative Commons Attribution License (CC BY). The use, distribution or reproduction in other forums is permitted, provided the original author(s) and the copyright owner(s) are credited and that the original publication in this journal is cited, in accordance with accepted academic practice. No use, distribution or reproduction is permitted which does not comply with these terms.

frontiers in Microbiology

ORIGINAL RESEARCH
published: 23 July 2019
doi: 10.3389/fmicb.2019.01511

Enhancing Recombinant Protein Yields in the *E. coli* Periplasm by Combining Signal Peptide and Production Rate Screening

*Alexandros Karyolaimos[1†], Henry Ampah-Korsah[1†], Tamara Hillenaar[1], Anna Mestre Borras[1], Katarzyna Magdalena Dolata[2], Susanne Sievers[2], Katharina Riedel[2], Robert Daniels[1] and Jan-Willem de Gier[1]**

[1] Department of Biochemistry and Biophysics, Center for Biomembrane Research, Stockholm University, Stockholm, Sweden, [2] Institute of Microbiology, University of Greifswald, Greifswald, Germany

OPEN ACCESS

Edited by:
Eric Cascales, Aix-Marseille Université, France

Reviewed by:
Hans-Georg Koch, University of Freiburg, Germany
Mehmet Berkmen, New England Biolabs, United States

***Correspondence:**
Jan-Willem de Gier
degier@dbb.su.se

[†] *These authors have contributed equally to this work*

Specialty section:
This article was submitted to Microbial Physiology and Metabolism, a section of the journal Frontiers in Microbiology

Received: *17 March 2019*
Accepted: *17 June 2019*
Published: *23 July 2019*

Citation:
Karyolaimos A, Ampah-Korsah H, Hillenaar T, Mestre Borras A, Dolata KM, Sievers S, Riedel K, Daniels R and de Gier J-W (2019) Enhancing Recombinant Protein Yields in the E. coli Periplasm by Combining Signal Peptide and Production Rate Screening. Front. Microbiol. 10:1511. doi: 10.3389/fmicb.2019.01511

Proteins that contain disulfide bonds mainly mature in the oxidative environment of the eukaryotic endoplasmic reticulum or the periplasm of Gram-negative bacteria. In *E. coli*, disulfide bond containing recombinant proteins are often targeted to the periplasm by an N-terminal signal peptide that is removed once it passes through the Sec-translocon in the cytoplasmic membrane. Despite their conserved targeting function, signal peptides can impact recombinant protein production yields in the periplasm, as can the production rate. Here, we present a combined screen involving different signal peptides and varying production rates that enabled the identification of more optimal conditions for periplasmic production of recombinant proteins with disulfide bonds. The data was generated from two targets, a single chain antibody fragment (BL1) and human growth hormone (hGH), with four different signal peptides and a titratable rhamnose promoter-based system that enables the tuning of protein production rates. Across the screen conditions, the yields for both targets significantly varied, and the optimal signal peptide and rhamnose concentration differed for each protein. Under the optimal conditions, the periplasmic BL1 and hGH were properly folded and active. Our study underpins the importance of combinatorial screening approaches for addressing the requirements associated with the production of a recombinant protein in the periplasm.

Keywords: *Escherichia coli*, recombinant protein, periplasm, signal peptide, protein production rate, protein production screen

INTRODUCTION

The bacterium *Escherichia coli* is one of the most widely used hosts to produce recombinant proteins (Rosano and Ceccarelli, 2014). While the majority of recombinant proteins are produced in the cytoplasm of *E. coli*, it is common to produce recombinant proteins that contain disulfide bonds in the periplasm. By targeting these proteins to the periplasm, it is possible to take advantage of the oxidizing environment and the resident disulfide bond formation (Dsb)-system to facilitate the proper disulfide bonds (Bardwell et al., 1991; Baneyx and Mujacic, 2004; Landeta et al., 2018). Although using the periplasm is more ideal for disulfide bond containing recombinant proteins, the

bottlenecks associated with the targeting across the cytoplasmic membrane can substantially limit periplasmic yields (Baneyx and Mujacic, 2004; De Geyter et al., 2016).

To reach the periplasm, recombinant proteins are most often equipped with an N-terminal signal peptide that guides it to the Sec-translocon, which is a protein-conducting channel in the cytoplasmic membrane (Denks et al., 2014; Crane and Randall, 2017; Tsirigotaki et al., 2017). The targeting to the Sec-translocon can occur either co-translationally *via* the SRP-pathway or post-translationally in a chaperone-dependent or -independent manner (Kim et al., 2000; Tsirigotaki et al., 2017). Currently, it is not clear how the particular signal peptide, the mature part of the secretory protein, or even the mRNA affect the mode of targeting to the Sec-translocon (Gouridis et al., 2009; Chatzi et al., 2017; Tsirigotaki et al., 2018). Independent of the targeting pathway, proteins directed to the Sec-translocon are ultimately translocated across the cytoplasmic membrane in an unfolded conformation (Arkowitz et al., 1993), and the signal peptide is removed by leader peptidase (Paetzel, 2014; Tsirigotaki et al., 2017). Due to the requirements for translocation, the folding reaction is limited until these proteins reach the periplasm where the Dsb-system can mediate disulfide bond formation and various catalysts can guide the folding process (Inaba, 2009; Landeta et al., 2018). Different signal peptides from both targeting pathways as well as engineered signal peptides have been used for the production of recombinant proteins in the periplasm (Low et al., 2013; Zhou et al., 2016; Freudl, 2018; Selas Castineiras et al., 2018; Zhang et al., 2018). Thus far, it has not been possible to predict which signal peptide is optimal for the production of a particular recombinant protein in the periplasm.

Usually, the gene encoding a recombinant protein is expressed at the highest level possible (Wagner et al., 2008). For recombinant proteins that carry a signal peptide this can lead to saturation of the Sec-translocon capacity which can negatively affect biomass formation and protein production yields (Schlegel et al., 2013; Hjelm et al., 2017; Baumgarten et al., 2018). To overcome this bottleneck, our laboratory developed a rhamnose promoter-based system, which enables the precise regulation of protein production rates (Hjelm et al., 2017). Recently, we have shown that when a rhamnose promoter is used to govern the expression of the gene encoding a recombinant protein in a RhaT-mediated rhamnose transport and rhamnose catabolism deficient double mutant background, rhamnose promoter-based protein production rates can be regulated in a rhamnose concentration-dependent manner. This setup has successfully been used to avoid saturation of the Sec-translocon capacity during the production of a secretory recombinant protein, which leads to enhanced periplasmic protein production levels.

Numerous studies have shown that signal peptides and secretory protein production rates can independently influence the yields of periplasmic proteins, but these two aspects have not been examined in combination. The aim of this study was to examine the effects on periplasmic protein production when combining these two aspects. Hence, we produced two recombinant proteins containing disulfide bonds, the single chain variable fragment (scFv) BL1 and human growth hormone (hGH), using four signal peptides at different protein production rates. To vary the protein production rates aforementioned rhamnose promoter-based setup was used. For both target proteins a setup for enhanced production was identified using the signal peptide and production rate-based combinatorial screening approach.

MATERIALS AND METHODS

Construction of *E. coli* W3110Δ*rha*Δ*lac*

To delete the *rha* operon and the *lac* operon in W3110 (obtained from the American Type Culture Collection) the Red-swap-method was used (Datsenko and Wanner, 2000). In short, kanamycin cassettes with regions homologous to the 5′ and 3′ flanking regions of the *rha* operon and the *lac* operon were generated by PCR using the pKD13 plasmid as a template and the primer pairs listed in **Supplementary Table S1**. The template was digested with *Dpn*I (NEB cutsmart) and the molecular weight of the PCR products were verified using an agarose gel and isolated using the Thermo Fisher Scientific gel extraction kit. To generate the W3110*rha*::Km^R and W3110*lac*::Km^R strains, the purified PCR products were electroporated into W3110 cells harboring pKD46 that had been cultured at 30°C in standard Lysogeny broth (LB) medium (Difco) containing 0.2% arabinose. Kanamycin-resistant clones (kan: 50 μg/ml final concentration) were then screened for the proper kanamycin cassette insertion by PCR using the primer pairs listed in **Supplementary Table S1**. Using P1-mediated generalized transduction, the region of interest of the strains exposed to the lambda Red system were transferred to cells that had not been exposed to the lambda Red system (Thomason et al., 2007). Upon successful transduction of the genetic region of interest, cells were transformed with pCP20 to remove the kanamycin cassette from the genome using FLP-recombinase (Datsenko and Wanner, 2000) and removal of the cassette was verified by PCR/sequencing. Finally, the cells were cured from pCP20 by a prolonged cultivation at 37°C. To generate the W3110Δ*rha*Δ*lac* strain, which is referred to in the text as *E. coli*Δ*rha*, the *rha* operon in W3110 was deleted and then the *lac* operon was deleted from the resulting strain. It is of note that the removal of the *lac* operon prevents any secondary effects on the model recombinant protein scFv BL1 that could occur from binding to its substrate *E. coli* β-galactosidase (Schlegel et al., 2013).

Construction of Expression Vectors

To create the expression vectors for the signal peptide-BL1-His_6 constructs, i.e., $DsbA_{sp}BL1His_6$, $Hbp_{sp}BL1His_6$, $OmpA_{sp}BL1His_6$, and $PhoA_{sp}BL1His_6$ the gene encoding BL1 was amplified with forward primers containing the signal peptide coding sequence with an *Eco*RI site as an overhang (**Supplementary Table S1**) and a reverse primer that contained the His_6-tag coding sequence with a *Hin*dIII site overhang (Schlegel et al., 2013). The PCR products encoding BL1 with a C-terminal His_6-tag and the four different N-terminal signal peptides were then cloned into

a pRha67Km^R-derived vector (Giacalone et al., 2006; Hjelm et al., 2017). To create the expression vectors for the signal peptide-hGH-His$_6$ fusion constructs, i.e., DsbA$_{sp}$hGHHis$_6$, Hbp$_{sp}$hGHHis$_6$, OmpA$_{sp}$hGHHis$_6$, and PhoA$_{sp}$hGHHis$_6$ and, the BL1 plasmids described above were used as templates for Gibson assembly where the BL1 coding region was replaced by a gene encoding hGH that is optimized for expression in *E. coli* (Browning et al., 2017). This resulted in four plasmids where hGH was N-terminally fused to a different signal peptide and C-terminally fused to a His$_6$-tag. The primers for the Gibson assembly are listed in **Supplementary Table S1**. All plasmids were verified by sequencing. Plasmid sequences will be provided upon request.

Protein Production Experiments

For all protein production experiments the *E. coli* strain W3110Δ*rha*Δ*lac* (referred to as *E. coli*Δ*rha* in the main text) was used. Cells were transformed with the expression vectors described in the previous section or an empty expression vector that served as a control. Protein production screening was done in a standard 24-well plate format (culture volume 4 ml). Cells were grown aerobically at 30°C and 200 rpm (New Brunswick Innova 42R shaker with an orbit diameter of 1.9 cm), in LB medium supplemented with 50 μg/ml kanamycin. To precultures, 0.2% glucose was added to prevent background expression of the genes encoding the target proteins. Growth was monitored by measuring the A_{600} with a UV-1300 spectrophotometer (Shimadzu). At an A_{600} of ∼0.5 target gene expression was induced by the addition of rhamnose. For scFv BL1 production screening the following rhamnose concentrations were used: 0, 50, 100, 250, 500, and 5000 μM. For hGH production screening the following rhamnose concentrations were used: 0, 10, 50, 100, 250, and 5000 μM. Cells were harvested at the indicated time points for further analysis. Standard deviations shown in figures of culturing experiments are based on at least three independent biological replicates. Cultures for the isolation of hGH and BL1 were done in 2.5 L shake flasks (Tunair^{TM}) containing 1 L of LB medium.

SDS-PAGE, Coomassie Staining and Immuno-Blotting

To monitor the production of the scFv BL1 and hGH, proteins in whole-cell lysates were separated by sodium dodecyl sulfate-polyacrylamide gel electrophoresis (SDS-PAGE) followed by either Coomassie blue staining or immuno-blotting. scFv BL1 was analyzed on Tris Glycine 8–16% (Invitrogen) gels and hGH was analyzed using Tricine 16% (Invitrogen) gels. Lysates equivalent to 0.04 A_{600} units were loaded onto gels for Coomassie staining and lysates equivalent to 0.02 A_{600} units were loaded onto gels that were analyzed by immuno-blotting. For volumetric comparisons, cell pellets derived from 1 ml of culture were solubilized in 300 μl of sample buffer and 8 μl was loaded for Coomassie blue staining and 4 μl for immuno-blotting. In the blotting experiments, secretory/secreted BL1 and hGH were detected based on their C-terminal His$_6$-tag using HisProbe-HRP Conjugate (Pierce) or the AlexaFluor 647 conjugated anti-HIS antibody (Invitrogen). The HisProbe-HRP Conjugate was used for mere detection and the AlexaFluor 647 conjugated anti-HIS antibody for quantification. The Western Bright Sirius kit (Advansta) was used to visualize immuno-blots stained with the HisProbe-HRP Conjugate. Chemiluminescence and fluorescence signals were detected using an Azure c600 imaging system (Azure Biosystems).

Protein Isolation

Cells producing the scFv BL1 and hGH from 1 L cultures were sedimented at 6000 × *g* for 20 min, 4°C. The supernatant was discarded and the cell pellets were stored at −80°C. The cell pellets were thawed on ice and subsequently lysed in 25 ml buffer A [50 mM Tris–HCl pH 7.4 (for BL1) or pH 8 (for hGH), 0.1% Triton X-100, 1 mg/ml lysozyme, 1× Roche protease inhibitor cocktail, 1 mM phenylmethylsulfonyl fluoride (PMSF)] using the EmusiFlex C3 homogenizer (Avestin) in a cold room. The cell lysate was sedimented (10.000 × *g* for 20 min, 4°C) and the supernatant was transferred into a 70 Ti ultracentrifugation tube and sedimented again (100.000 × *g* for 1 h, 4°C). The high-spin supernatant was transferred to a 50 ml falcon tube, adjusted to a final concentration of 10 mM imidazole and 1 ml of a Ni-NTA agarose beads slurry was added that was pre-equilibrated with buffer B [1× phosphate buffered saline (PBS) pH 7.4, 150 mM NaCl, 0.1% Triton X-100, 10% Glycero]) containing 10 mM imidazole. The mixture was incubated in a cold room overnight with gentle tumbling and then transferred into a 10 ml polyprep chromatographic column. The column was washed with 20 column volumes (CV) of buffer B supplemented with 20 mM imidazole and the BL1 or hGH was eluted with buffer B supplemented with 300 mM imidazole. The eluted protein samples were pooled and loaded onto a HiLoad 16/60 Superdex 200 size exclusion chromatography (SEC) column mounted on an ÄKTAprime plus (GE Healthcare) that was pre-equilibrated with buffer C (50 mM Tris–HCl pH 7.4 (for BL1) or pH 8 (for hGH), 150 mM NaCl, 10% Glycerol). The column was run at a flow-rate of 1 ml/min, the protein was monitored at a wavelength of 280 nm, and the fractions corresponding to the peak were collected and stored at −20°C. All purification steps were done in the cold room. Protein concentration and purity were determined with the BCA method (Pierce) and SDS-PAGE followed by Coomassie staining. Protein folding was monitored using reducing and non-reducing SDS-PAGE followed by Coomassie staining and immuno-blotting. For BL1 analysis 2 μg of protein was loaded for Coomassie staining and 0.5 μg of protein for immuno-blotting and for hGH analysis 2 μg of protein was loaded for Coomassie staining and 1 μg of protein for immuno-blotting.

BL1 Activity Assay

The proper folding of the isolated BL1 was assayed by the recognition of its substrate, *E. coli* β-galactosidase, using a dot-blot assay (Schlegel et al., 2013). For the activity assay, 100 μl of a 1:2 serial dilution of β-galactosidase (100, 50, 25, 12.5, 6.25, 3.125, 1.563, and 0 μg/ml) was spotted directly onto a

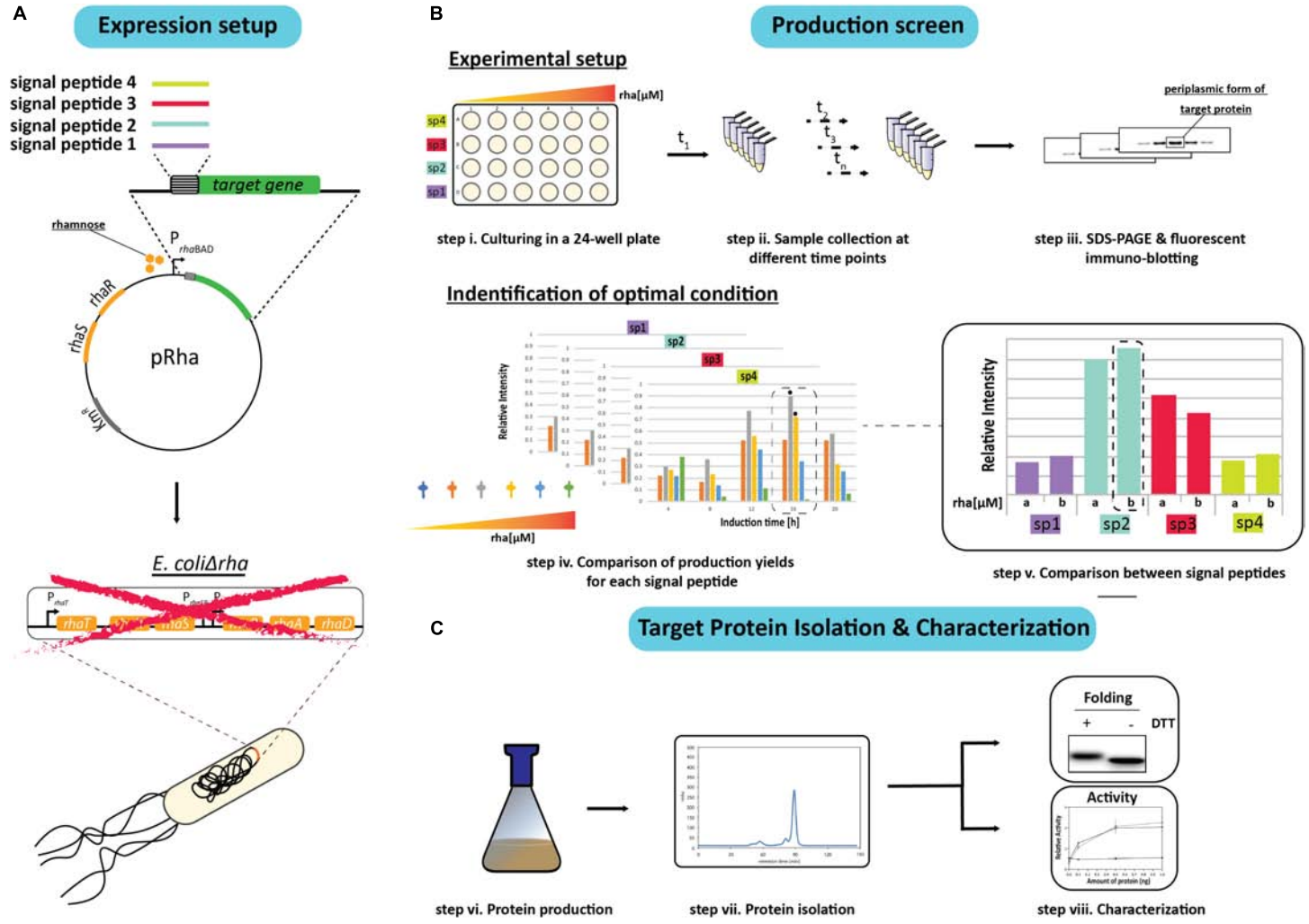

FIGURE 1 | Setup of the signal peptide and production rate-based combinatorial screening approach to enhance periplasmic protein production yields in *E. coli*. **(A)** The gene encoding the protein to be produced in the periplasm is fused to the genetic information encoding different signal peptides. The genetic fusions are subsequently cloned in a rhamnose promoter-based expression vector (pRha). The expression vectors harboring the genes encoding the different signal peptide target protein fusions are subsequently transformed into an *E. coli* strain lacking the rhamnose operon (*E. coli*Δ*rha*). **(B)** Protein production screening is done in standard 24-well plates (step i). Expression of the genes encoding the different signal peptide target protein fusions is induced using varying amounts of rhamnose. Protein production in the periplasm is monitored over time (t_1, t_n) (step ii) by separating proteins present in equal volumes of culture by SDS-PAGE followed by immuno-blotting using a fluorescently labeled antibody recognizing the target protein (step iii). This enables to make for each of the used signal peptides a relative comparison of the protein production yields in the periplasm (step iv). The two highest periplasmic protein production yields are indicated with a black hexagon. For each signal peptide the two setups leading to the highest production yields are compared directly (step v). **(C)** This exercise is used to pick the condition used for scaling up target protein production (step vi) and the subsequent isolation of the target protein (step vii). The isolated protein is analyzed using SDS-PAGE in the presence and absence of the reductant DTT followed by Coomassie staining and immuno-blotting as well as a protein specific activity assay (step viii).

nitrocellulose membrane (Millipore) using a BIO-DOT device (Bio-Rad). As a negative control, equal amounts of bovine serum albumin (BSA) were spotted on the same membrane. The membranes were blocked with a solution of tris buffered saline containing 0.05% Tween 20 (TBS-T) and 5% milk for 1 h at room temperature (RT), washed three times for 15 min with TBS-T and incubated overnight at 4°C with 17 μg/ml of the isolated BL1 in buffer C. The bound BL1 was labeled with the HisProbe-HRP Conjugate and the membrane was developed using the Western Bright Sirius kit and an Azure c600 imaging system.

Human Growth Hormone Activity Assay

The activity of the purified hGH protein was ascertained by its ability to promote the growth of prolactin-dependent Nb2 lymphoma cell line (Nb2-11 cells) as previously described with slight modifications (Sonoda and Sugimura, 2008; Kim et al., 2013). Nb2-11 cells (Sigma) were cultured in RPMI 1640 medium (Gibco/Thermo Fisher Scientific) containing 10% fetal bovine serum (FBS), 10% horse serum (Gibco/Thermo Fisher Scientific) and 1% penicillin-streptomycin (Gibco/Thermo Fisher Scientific) at 37°C in a humidified atmosphere containing 5% CO_2. To begin the assay, the cells were sedimented (500 × *g* for 3 min), washed once in medium without FBS and re-suspended in medium without FBS. The cell density was then determined with a Countess II automated cell counter (Life Technologies), diluted to approximately 2×10^5 cells/ml and 100 μl of the cell suspension was added to each well of a 96 well plate. Each well then received the following amounts of the purified hGH protein: 0, 0.1, 0.5, and 1 ng. After mixing the solution on a shaker at 100 rpm for 1 min, the cells were placed in the 37°C humidified incubator and the cell proliferation 48 h after the hGH addition was used to determine its activity. To measure the cell growth, 20 μl of CellTiter 96®aqueous one solution reagent (Promega) was added to each well, the plate was placed back in the 37°C humidified incubator for 2.5 h and then the absorbance was measured at 490 nm using a SpectraMax M2e microplate reader (Molecular Devices).

Quantification of the scFv BL1 and hGH Amounts Produced in the Periplasm

Cells from 1 ml of either a 4 ml or 1 L culture were sedimented and lysed using 0.3 ml of sample buffer. The amounts of periplasmic BL1 and hGH in the samples were determined by measuring the mature levels of the proteins by immuno-blotting as follows. For BL1 samples a Tris Glycine 8–16% gel was loaded with 3 μl and a two-fold dilution of the whole cell lysate followed by a two-fold dilution series of the isolated BL1 containing 2, 1, 0.5, 0.25, 0.1, and 0.05 μg of protein. The samples were then resolved, transferred to a PVDF membrane, and the BL1 was detected with a fluorescently labeled antibody that recognizes the His_6-tag. Images were acquired using an Azure c600 system. The band intensities were quantified with ImageJ and the values from the standard curve were used to determine the amount of BL1 in the two samples. The amount of hGH was determined similarly with the exception that a Bis Tris 4–12% gel was loaded with 10 μl and a two-fold dilution of the whole cell lysate and the dilution series of isolated hGH had the following amounts of protein: 3, 2, 1, 0.5, 0.25, 0.1, and 0.05 μg.

RESULTS AND DISCUSSION

Combinatorial Signal Peptide and Production Rate Screening Approach

In an effort to identify the ideal condition for producing an oxidized recombinant protein in the *E. coli* periplasm, a combinatorial screen was set up using a panel of different signal peptides and a titratable rhamnose promoter system for controlling protein production rates. To initiate the screen, the genes encoding the target proteins with a C-terminal His_6-tag were fused to sequences encoding for the signal peptides from the *E. coli* proteins DsbA, OmpA, PhoA, and the hemoglobin protease (Hbp) autotransporter, and inserted into the rhamnose promoter-based expression vector pRha (**Figure 1A**). These signal peptides were chosen because they are (i) from *E. coli* proteins, (ii) are commonly used for periplasmic targeting of recombinant proteins, and/or (iii) the corresponding mature proteins are reported to be rather abundant in the *E. coli* cell (Kendall et al., 1986; Schierle et al., 2003; Sijbrandi et al., 2003; Schlegel et al., 2013; Schmidt et al., 2016; Hjelm et al., 2017; Baumgarten et al., 2018) (see for more information **Supplementary Table S2**). The plasmids were then transformed into an *E. coli* strain (W3110Δ*rha*Δ*lac*) that enables tuning of the target production rates by varying the rhamnose concentration. The rhamnose tunability of the strain, herein referred to as *E.coli*Δ*rha*, was achieved by deleting the whole *rha* operon, which includes the removal of the genes involved in rhamnose transport (*rhaT*) and catabolism (*rhaB*) that were previously shown to create a rhamnose titratable protein production strain (Hjelm et al., 2017).

Due to sample number limitations, the initial screen for each target protein with a particular signal peptide was analyzed independently using 24-well plates and a range of rhamnose concentrations to induce the target gene expression (**Figure 1B**). Following the induction, the cells from equal culture volumes were harvested at different time intervals and the periplasmic protein production was monitored by measuring the mature protein amounts using immuno-blots stained with fluorescently labeled antibodies (**Figure 1B**). The resulting data was then used to identify the best conditions for producing the target protein with each of the four signal peptides. To validate that the observed improvements in periplasmic production were not associated with the culture volume analysis, the production levels in equal

cell amounts was also examined using Coomassie staining and immuno-blotting.

Based on the results from the initial screen, the two best conditions for each target protein and signal peptide combination were compared directly to determine the rhamnose concentration and signal peptide that provided the highest periplasmic yields (**Figure 1B**). The most effective signal peptide and rhamnose concentration was then tested using large scale cultures where the target proteins were isolated, quantified and characterized for disulfide bond formation and activity (Francis et al., 2002; **Figure 1C**). Two targets were used throughout this study, the single chain antibody fragment BL1 (scFv BL1), which recognizes the *E. coli* β-galactosidase (Schlegel et al., 2013), and human growth hormone (hGH), which stimulates cell proliferation (Kim et al., 2013). Both targets were chosen because they contain two disulfide bonds in their native state and a C-terminal His_6-tag was incorporated for isolation and detection.

ScFv BL1 Production Screen

During the initial screen the temporal production of the scFv BL1 in *E. coli*Δ*rha* was examined using the four different signal peptides ($DsbA_{sp}$, Hbp_{sp}, $OmpA_{sp}$, and $PhoA_{sp}$) and a range of rhamnose concentrations (**Figure 2**). The BL1 amounts, which were determined for equal culture volumes by SDS-PAGE immune-blots (**Figure 1B**), showed that for all signal peptides the highest BL1 yields were obtained 16 h post-induction with rhamnose. The production of BL1 with each signal peptide was then examined at 16 h post-induction using equal amounts of biomass (**Supplementary Figures S1**, **S2**). While the optimal rhamnose concentration slightly changed for some signal peptides in the equal biomass analysis based on Coomassie staining and immuno-blotting against the C-terminal His_6, the preference for lower rhamnose concentrations was confirmed.

Next, the BL1 production yields for each signal peptide at the two best rhamnose conditions were directly compared using equal culture volumes (**Figure 3A**). The results from this volumetric analysis revealed that for BL1 the highest periplasmic production yields were achieved with the OmpA signal peptide and 100 μM rhamnose. To monitor if BL1 produced with the OmpA signal peptide had formed disulfide bonds in the periplasm, the whole cell lysates were separated by SDS-PAGE in the presence and the absence of the reductant DTT followed by Coomassie staining and immuno-blotting (**Figure 3B**). Indicative that BL1 is properly folded with two intramolecular disulfide bonds, BL1 migrated more slowly when it was reduced by DTT.

To more thoroughly examine the periplasmic BL1 that was produced with the most optimal signal peptide and rhamnose concentration, BL1 was produced in a larger scale culture and subsequently isolated using immobilized-metal affinity chromatography (IMAC) followed by size exclusion chromatography (SEC). The isolated BL1 showed the expected migration shift in the presence of DTT (**Figure 4A**). To confirm that the isolated BL1 is indeed properly folded, we examined its ability to bind β-galactosidase (**Figure 4B**; Schlegel et al., 2013). For this analysis, β-galactosidase and BSA were spotted in decreasing concentrations on a nitrocellulose membrane.

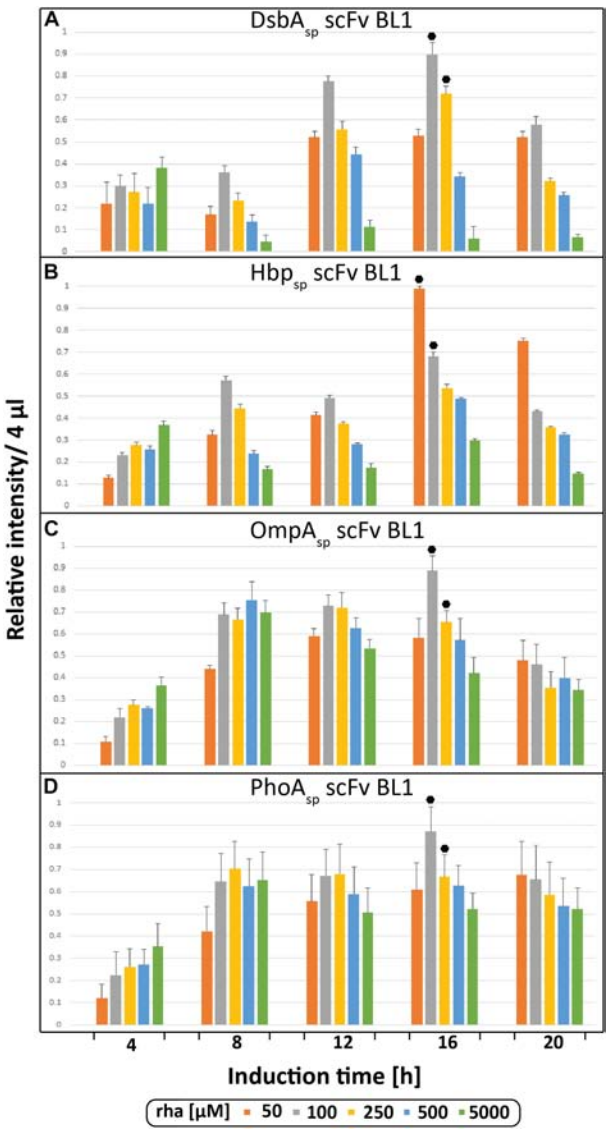

FIGURE 2 | Periplasmic production of the scFv BL1 using different signal peptides and inducer concentrations monitored volumetrically over time. Production of the scFv BL1 N-terminally fused to the DsbA **(A)**, the Hbp **(B)**, the OmpA **(C),** and the PhoA **(D)** signal peptide, in *E. coli*Δ*rha* using varying amounts of rhamnose, was monitored over time (4, 8, 12, 16, and 20 h after induction of target gene expression). Proteins present in equal amounts of culture volume were separated by SDS-PAGE followed by immuno-blotting using a fluorescently labeled antibody recognizing the His_6-tag fused to the C-terminus of BL1 (see section "Materials and Methods"). Fluorescent signals representing BL1 (i.e., the processed/periplasmic form of the protein) were quantified using ImageJ and peak intensities were used for comparison. To enable the comparison of BL1 production between different time-points for each signal peptide, standard curves were made using peak intensities from serial dilutions of the optimal condition of each signal peptide. For each signal peptide used the two highest periplasmic BL1 production yields are indicated with a black hexagon.

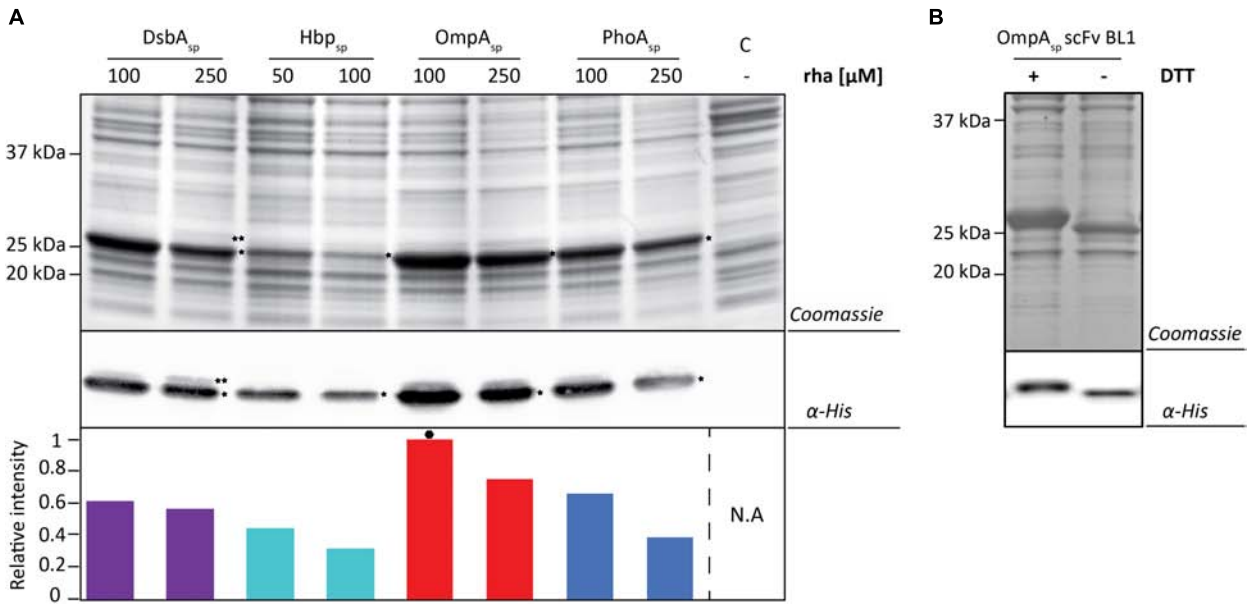

FIGURE 3 | Identifying the optimal setup for the periplasmic production of the scFv BL1. **(A)** For each signal peptide used the two setups leading to the highest periplasmic production yields of BL1 were compared using SDS-PAGE followed by Coomassie staining and immuno-blotting using a fluorescently labeled antibody recognizing the His_6-tag at the C-terminus of BL1. Importantly, equal amounts of culture volume were loaded per lane since this enables to directly compare the amount of BL1 produced in the periplasm volumetrically. Relative intensities of the fluorescent signals are shown below the blot. The highest periplasmic BL1 production yield is indicated with a black hexagon (see also **Supplementary Figure S3**). The precursor form, i.e., BL1 with the signal peptide still attached, is indicated with ** and the mature form, i.e., BL1 without signal peptide, is indicated with *. **(B)** The use of the OmpA-BL1 fusion resulted in the highest production of BL1 in the periplasm. To assess the folding of the BL1 produced in the periplasm cells were solubilized in sample buffer with and without the reductant DTT prior to SDS-PAGE followed by Coomassie staining and immuno-blotting using HisProbe.

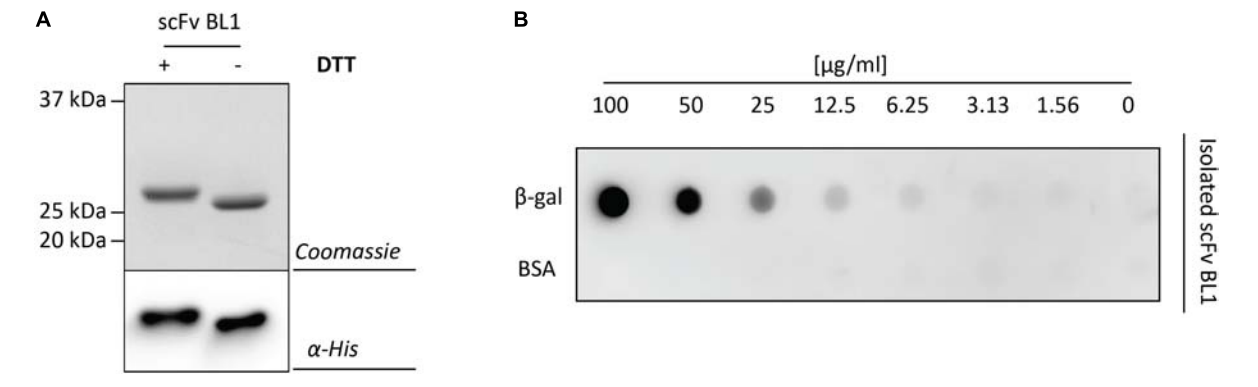

FIGURE 4 | Characterization of the isolated scFv BL1. For the isolation of BL1, the OmpA signal peptide and 100 µM of rhamnose for the induction of target gene expression were used (see **Figure 3A**). BL1 was isolated using a combination of IMAC and SEC. **(A)** The isolated BL1 was incubated in sample buffer with and without the reductant DTT prior to SDS-PAGE followed by Coomassie staining and immuno-blotting using HisProbe. **(B)** A nitrocellulose membrane containing increasing amounts of β-galactosidase as well as increasing amounts of BSA (control) was incubated with the isolated BL1. Binding of BL1 to the β-galactosidase spotted on the nitrocellulose membrane was detected using HisProbe recognizing the His_6-tag at the C-terminus of BL1.

The membrane was then incubated with the isolated BL1 and the bound BL1 was detected using HisProbe (see section "Materials and Methods"). As expected, the BL1 produced under the optimal conditions was capable of binding to its substrate and showed no affinity for the BSA negative control.

Together, these results show that by screening different signal peptides and protein production rates for the scFv BL1 we were able to identify conditions capable of producing functional BL1 in the periplasm at around 200 µg per ml of culture (**Supplementary Figure S4**).

hGH Production Screen

To test if the target can have an influence on the yields obtained with each signal peptide and the different production rates, the screen was repeated using hGH and

the two best production conditions were identified for each signal peptide (**Figure 5A** and **Supplementary Figures S5**, **S6**). Similar to the results using BL1, the highest hGH yields were observed at 16 h post-induction with rhamnose for all of the signal peptides. For hGH the use of the Hbp signal peptide and 50 μM rhamnose resulted in the highest production of hGH in the periplasm. To monitor if hGH produced with the Hbp signal peptide had formed disulfide bonds in the periplasm whole cell lysates were analyzed using SDS-PAGE in the presence and absence of DTT (**Figure 5B**). As expected, the mature hGH showed slower mobility in the presence of DTT, indicating that it likely folds correctly and obtains its two intramolecular disulfide bonds. Thus, both signal peptide and rhamnose concentration leading to the highest production of hGH in the periplasm are different from the ones observed for BL1.

The optimal Hbp-signal peptide-based hGH production setup was scaled up and a combination of IMAC and SEC was used to isolate hGH. Isolated hGH was analyzed by means of SDS-PAGE in the presence and the absence of the reductant DTT followed by Coomassie staining and immuno-blotting (**Figure 6A**). The shift of isolated hGH toward a lower molecular weight upon omitting DTT is an indication that the hGH produced is properly folded. Next, we examined the ability of the isolated hGH to promote the growth of prolactin-dependent Nb2 lymphoma cell line (Nb2-11 cells) using commercially available hGH as a reference and BSA as a negative control (**Figure 6B**). Using this set-up, we showed that hGH produced under the optimal conditions was capable of promoting the growth of prolactin-dependent Nb2 lymphoma cell line equally well as commercially purchased hGH.

Taken together, here we show for hGH that screening different signal peptides and protein production rates leads to the identification of a setup that enables to produce functional hGH in the periplasm at around 30 μg per ml of culture.

CONCLUDING REMARKS

Here, to enhance the production of the scFv BL1 and hGH in the periplasm we used a combinatorial screening approach using four different signal peptides and a rhamnose promoter-based setup enabling to precisely set protein production rates. Main finding is that the signal peptide and rhamnose concentration that provide the highest production yields in the periplasm are different for the two target proteins that were tested. Although the induction times for the optimal conditions are the same for both targets, this may be a mere coincidence and

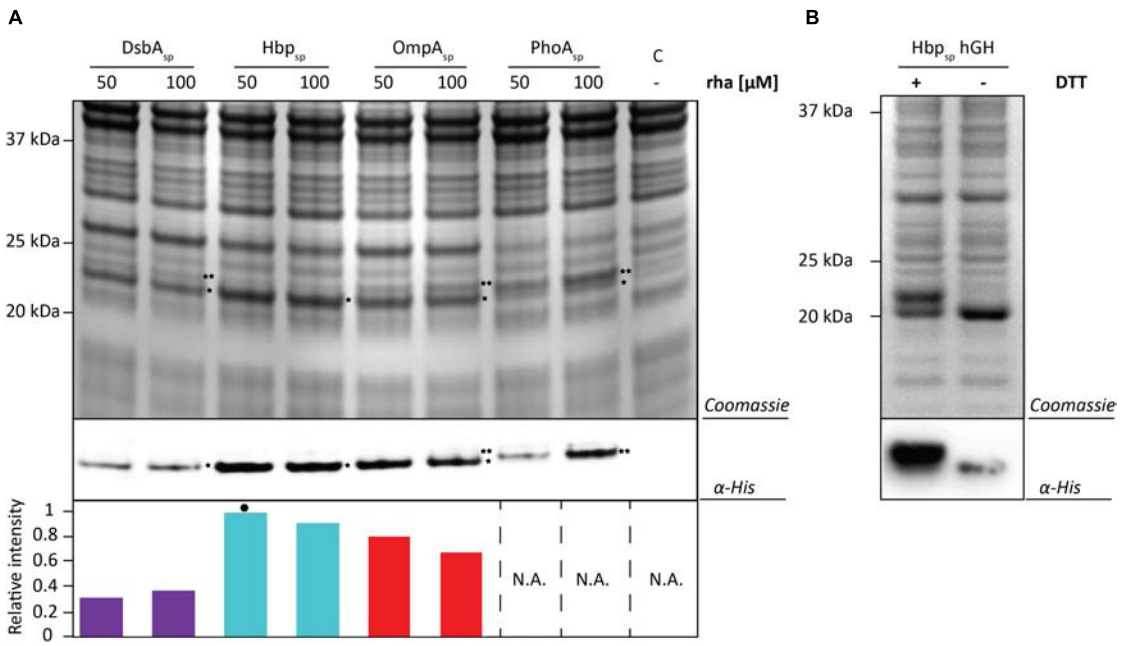

FIGURE 5 | Identifying the optimal setup for the periplasmic production of hGH. **(A)** For each signal peptide used, the two setups leading to the highest periplasmic production yields of hGH were compared by SDS-PAGE followed by Coomassie staining and immuno-blotting using a fluorescently labeled antibody recognizing the His_6-tag at the C-terminus of hGH Importantly, equal amounts of culture volume were loaded per lane since this enables to compare the amount of hGH produced in the periplasm volumetrically. Relative intensities of the fluorescent signals are shown below the blot. The highest periplasmic hGH production yield is indicated with a black hexagon (see also **Supplementary Figure S7**). The precursor form, i.e., hGH with the signal peptide still attached, is indicated with ** and the mature form, i.e., hGH without signal peptide, is indicated with *. **(B)** Whole cell lysates derived from cells producing hGH fused to the Hbp signal peptide at 50 μM of rhamnose isolated 16 h after the addition of rhamnose, were analyzed by means of SDS-PAGE followed by Coomassie staining and immuno-blotting (see section "Materials and Methods"). To assess the folding of the hGH produced in the periplasm cells were dissolved in sample buffer with and without the reductant DTT prior to SDS-PAGE (see also **Supplementary Figure S8**).

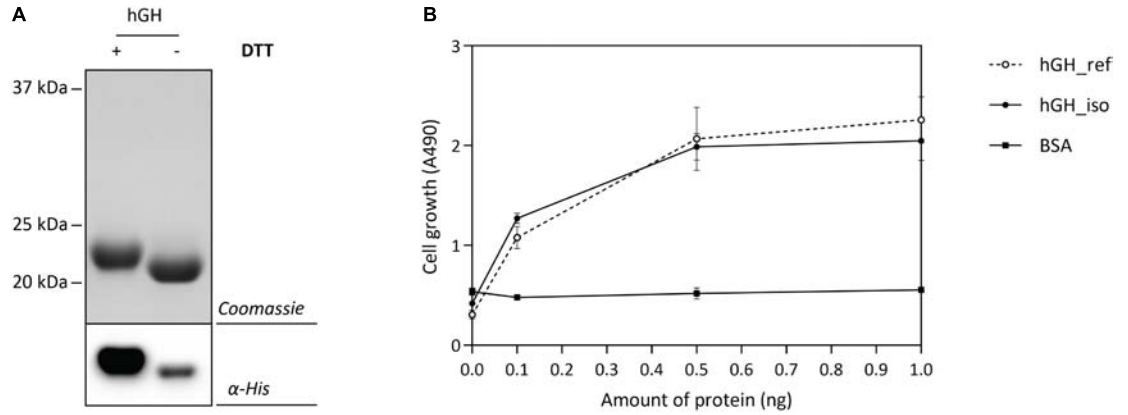

FIGURE 6 | Characterization of isolated hGH. For the isolation of hGH, the Hbp signal peptide and 50 μM of rhamnose for the induction of target gene expression were used (see **Figure 5**). hGH was isolated using a combination of IMAC and SEC. **(A)** To assess the folding of the isolated hGH, it was solubilized in sample buffer with and without the reductant DTT prior to SDS-PAGE followed by Coomassie staining and immuno-blotting using HisProbe (see also **Supplementary Figure S8**). **(B)** The activity of the isolated hGH was assessed by monitoring its ability to promote growth of an Nb2-11 cell line. Resuspended Nb2-11 cells in medium without FBS were incubated with various amounts of isolated hGH (filled circle), hGH reference (empty circle), and BSA (filled square) in a 96-well plate and cultured at 37°C in a humidified, 5% CO_2 atmosphere for 48 h. Cell proliferation was determined colorimetrically with MTT reagent. hGH reference and BSA were used as positive and negative control, respectively. All experiments were done in triplicate and standard deviations are depicted by error bars.

needs to be confirmed using additional targets before this parameter can be fixed.

Previously, it has been shown that the mature part of *E. coli* secretory proteins can contain information that is important for their secretion and that a signal peptide can affect the folding/targeting of a protein destined for the periplasm (Liu et al., 1989; Rusch et al., 2002; Gouridis et al., 2009; Singh et al., 2013; Chatzi et al., 2017; Tsirigotaki et al., 2018). How these observations translate to the production of heterologous proteins in the periplasm of *E. coli* is still *terra incognita*. However, the effects observed for BL1 and hGH production using different signal peptides strongly suggest that signal peptide - target protein combinations can have a profound effect on the production of a protein in the periplasm. Striking example is that the use of the PhoA signal peptide leads to good - although not the best – periplasmic production of BL1, whereas hardly any hGH is produced in the periplasm when the PhoA signal peptide is used. Recently, for PhoA it has been shown that its efficient translocation depends on so-called mature domain targeting signals (Chatzi et al., 2017). Interestingly, using the MatureP predictor, which was trained using the *E. coli* proteome, such a mature domain targeting signal in BL1 could be identified, whereas in hGH such a signal could not be identified (Orfanoudaki et al., 2017). This may explain why the PhoA signal peptide only promotes the efficient export of BL1. These observations raise the question if it would be possible to develop predictors which can streamline screening for the enhanced production of recombinant proteins in the periplasm.

In conclusion, our study shows that combinatorial screening of different signal peptides and protein production rates opens up a new avenue to enhance protein production yields in the periplasm of *E. coli*.

DATA AVAILABILITY

The raw data supporting the conclusion of this manuscript will be made available by the authors, without undue reservation, to any qualified researcher.

AUTHOR CONTRIBUTIONS

AK, HA-K, RD, and J-WG conceived and designed the experiments. AK, HA-K, TH, AM, and KD conducted the experiments. AK, HA-K, TH, AM, KD, RD, and J-WG analyzed the data. AK, HA-K, KMD, SS, KR, RD, and J-WG wrote the manuscript.

FUNDING

This work was supported by grants from the Swedish Research Council (2015-05288) and the Carl Tryggers Foundation (CTS17:114) to J-WG, a Marie Curie Initial Training Network Grants (Horizon 2020, ProteinFactory, 642863) to the Stockholm University (AK) and the University of Greifswald (KD), grants from the Swedish Research Council (K2015-57-21980-04-4) and the Carl Tryggers Foundation (CTS17:111) as well as Federal funds from the National Institute of Allergy and Infectious Diseases, the National Institutes of Health, and the United States Department of Health and Human Services, under the CEIRS contract number HHSN272201400005C to RD.

SUPPLEMENTARY MATERIAL

The Supplementary Material for this article can be found online at: https://www.frontiersin.org/articles/10.3389/fmicb.2019.01511/full#supplementary-material

REFERENCES

Arkowitz, R. A., Joly, J. C., and Wickner, W. (1993). Translocation can drive the unfolding of a preprotein domain. *EMBO J.* 12, 243–253. doi: 10.1002/j.1460-2075.1993.tb05650.x

Baneyx, F., and Mujacic, M. (2004). Recombinant protein folding and misfolding in *Escherichia coli*. *Nat. Biotechnol.* 22, 1399–1408. doi: 10.1038/nbt1029

Bardwell, J. C., Mcgovern, K., and Beckwith, J. (1991). Identification of a protein required for disulfide bond formation *in vivo*. *Cell* 67, 581–589. doi: 10.1016/0092-8674(91)90532-4

Baumgarten, T., Ytterberg, A. J., Zubarev, R. A., and De Gier, J. W. (2018). Optimizing recombinant protein production in the *Escherichia coli* periplasm alleviates stress. *Appl. Environ. Microbiol.* 84, e00270-18. doi: 10.1128/AEM.00270-18

Browning, D. F., Richards, K. L., Peswani, A. R., Roobol, J., Busby, S. J. W., and Robinson, C. (2017). *Escherichia coli* "TatExpress" strains super-secrete human growth hormone into the bacterial periplasm by the Tat pathway. *Biotechnol. Bioeng.* 114, 2828–2836. doi: 10.1002/bit.26434

Chatzi, K. E., Sardis, M. F., Tsirigotaki, A., Koukaki, M., Sostaric, N., Konijnenberg, A., et al. (2017). Preprotein mature domains contain translocase targeting signals that are essential for secretion. *J. Cell Biol.* 216, 1357–1369. doi: 10.1083/jcb.201609022

Crane, J. M., and Randall, L. L. (2017). The sec system: protein export in *Escherichia coli*. *EcoSal Plus* 7, 1–44. doi: 10.1128/ecosalplus.ESP-0002-2017

Datsenko, K. A., and Wanner, B. L. (2000). One-step inactivation of chromosomal genes in *Escherichia coli* K-12 using PCR products. *Proc. Natl. Acad Sci. U.S.A.* 97, 6640–6645. doi: 10.1073/pnas.120163297

De Geyter, J., Tsirigotaki, A., Orfanoudaki, G., Zorzini, V., Economou, A., and Karamanou, S. (2016). Protein folding in the cell envelope of *Escherichia coli*. *Nat. Microbiol.* 1:16107. doi: 10.1038/nmicrobiol.2016.107

Denks, K., Vogt, A., Sachelaru, I., Petriman, N. A., Kudva, R., and Koch, H. G. (2014). The sec translocon mediated protein transport in prokaryotes and eukaryotes. *Mol. Membr. Biol.* 31, 58–84. doi: 10.3109/09687688.2014.907455

Francis, E., Daniels, R., and Hebert, D. N. (2002). Analysis of protein folding and oxidation in the endoplasmic reticulum. *Curr. Protoc. Cell Biol.* 14, 15.6.1–15.6.29. doi: 10.1002/0471143030.cb1506s14

Freudl, R. (2018). Signal peptides for recombinant protein secretion in bacterial expression systems. *Microb. Cell Fact.* 17:52. doi: 10.1186/s12934-018-0901-3

Giacalone, M. J., Gentile, A. M., Lovitt, B. T., Berkley, N. L., Gunderson, C. W., and Surber, M. W. (2006). Toxic protein expression in *Escherichia coli* using a rhamnose-based tightly regulated and tunable promoter system. *Biotechniques* 40, 355–364. doi: 10.2144/000112112

Gouridis, G., Karamanou, S., Gelis, I., Kalodimos, C. G., and Economou, A. (2009). Signal peptides are allosteric activators of the protein translocase. *Nature* 462, 363–367. doi: 10.1038/nature08559

Hjelm, A., Karyolaimos, A., Zhang, Z., Rujas, E., Vikstrom, D., Slotboom, D. J., et al. (2017). Tailoring *Escherichia coli* for the l-rhamnose PBAD promoter-based production of membrane and secretory proteins. *ACS Synth Biol.* 6, 985–994. doi: 10.1021/acssynbio.6b00321

Inaba, K. (2009). Disulfide bond formation system in *Escherichia coli*. *J. Biochem.* 146, 591–597. doi: 10.1093/jb/mvp102

Kendall, D. A., Bock, S. C., and Kaiser, E. T. (1986). Idealization of the hydrophobic segment of the alkaline phosphatase signal peptide. *Nature* 321, 706–708. doi: 10.1038/321706a0

Kim, J., Luirink, J., and Kendall, D. A. (2000). SecB dependence of an exported protein is a continuum influenced by the characteristics of the signal peptide or early mature region. *J. Bacteriol.* 182, 4108–4112. doi: 10.1128/jb.182.14.4108-4112.2000

Kim, M. J., Park, H. S., Seo, K. H., Yang, H. J., Kim, S. K., and Choi, J. H. (2013). Complete solubilization and purification of recombinant human growth hormone produced in *Escherichia coli*. *PLoS One* 8:e56168. doi: 10.1371/journal.pone.0056168

Landeta, C., Boyd, D., and Beckwith, J. (2018). Disulfide bond formation in prokaryotes. *Nat. Microbiol.* 3, 270–280. doi: 10.1038/s41564-017-0106-2

Liu, G., Topping, T. B., and Randall, L. L. (1989). Physiological role during export for the retardation of folding by the leader peptide of maltose-binding protein. *Proc. Natl. Acad Sci. U.S.A.* 86, 9213–9217. doi: 10.1073/pnas.86.23.9213

Low, K. O., Muhammad Mahadi, N., and Md Illias, R. (2013). Optimisation of signal peptide for recombinant protein secretion in bacterial hosts. *Appl. Microbiol. Biotechnol.* 97, 3811–3826. doi: 10.1007/s00253-013-4831-z

Orfanoudaki, G., Markaki, M., Chatzi, K., Tsamardinos, I., and Economou, A. (2017). MatureP: prediction of secreted proteins with exclusive information from their mature regions. *Sci. Rep.* 7:3263. doi: 10.1038/s41598-017-03557-4

Paetzel, M. (2014). Structure and mechanism of *Escherichia coli* type I signal peptidase. *Biochim. Biophys. Acta* 1843, 1497–1508. doi: 10.1016/j.bbamcr.2013.12.003

Rosano, G. L., and Ceccarelli, E. A. (2014). Recombinant protein expression in *Escherichia coli*: advances and challenges. *Front. Microbiol.* 5:172. doi: 10.3389/fmicb.2014.00172

Rusch, S. L., Mascolo, C. L., Kebir, M. O., and Kendall, D. A. (2002). Juxtaposition of signal-peptide charge and core region hydrophobicity is critical for functional signal peptides. *Arch. Microbiol.* 178, 306–310. doi: 10.1007/s00203-002-0453-z

Schierle, C. F., Berkmen, M., Huber, D., Kumamoto, C., Boyd, D., and Beckwith, J. (2003). The DsbA signal sequence directs efficient, cotranslational export of passenger proteins to the *Escherichia coli* periplasm via the signal recognition particle pathway. *J. Bacteriol.* 185, 5706–5713. doi: 10.1128/jb.185.19.5706-5713.2003

Schlegel, S., Rujas, E., Ytterberg, A. J., Zubarev, R. A., Luirink, J., and De Gier, J. W. (2013). Optimizing heterologous protein production in the periplasm of *E. coli* by regulating gene expression levels. *Microb. Cell Fact* 12:24. doi: 10.1186/1475-2859-12-24

Schmidt, A., Kochanowski, K., Vedelaar, S., Ahrne, E., Volkmer, B., Callipo, L., et al. (2016). The quantitative and condition-dependent *Escherichia coli* proteome. *Nat. Biotechnol.* 34, 104–110. doi: 10.1038/nbt.3418

Selas Castineiras, T., Williams, S. G., Hitchcock, A., Cole, J. A., Smith, D. C., and Overton, T. W. (2018). Development of a generic beta-lactamase screening system for improved signal peptides for periplasmic targeting of recombinant proteins in *Escherichia coli*. *Sci. Rep.* 8:6986. doi: 10.1038/s41598-018-25192-3

Sijbrandi, R., Urbanus, M. L., Ten Hagen-Jongman, C. M., Bernstein, H. D., Oudega, B., Otto, B. R., et al. (2003). Signal recognition particle (SRP)-mediated targeting and Sec-dependent translocation of an extracellular *Escherichia coli* protein. *J. Biol. Chem.* 278, 4654–4659. doi: 10.1074/jbc.M211630200

Singh, P., Sharma, L., Kulothungan, S. R., Adkar, B. V., Prajapati, R. S., Ali, P. S., et al. (2013). Effect of signal peptide on stability and folding of *Escherichia coli* thioredoxin. *PLoS One* 8:e63442. doi: 10.1371/journal.pone.0063442

Sonoda, H., and Sugimura, A. (2008). Improved solubilization of recombinant human growth hormone inclusion body produced in *Escherichia coli*. *Biosci. Biotechnol. Biochem.* 72, 2675–2680. doi: 10.1271/bbb.80332

Thomason, L. C., Costantino, N., and Court, D. L. (2007). *E. coli* genome manipulation by P1 transduction. *Curr. Protoc. Mol. Biol.* 79, 1.17.1–1.17.8. doi: 10.1002/0471142727.mb0117s79

Tsirigotaki, A., Chatzi, K. E., Koukaki, M., De Geyter, J., Portaliou, A. G., Orfanoudaki, G., et al. (2018). Long-lived folding intermediates predominate the targeting-competent secretome. *Structure* 26, 695.e5–707.e5. doi: 10.1016/j.str.2018.03.006

Tsirigotaki, A., De Geyter, J., Sostaric, N., Economou, A., and Karamanou, S. (2017). Protein export through the bacterial Sec pathway. *Nat. Rev. Microbiol.* 15, 21–36. doi: 10.1038/nrmicro.2016.161

Wagner, S., Klepsch, M. M., Schlegel, S., Appel, A., Draheim, R., Tarry, M., et al. (2008). Tuning *Escherichia coli* for membrane protein overexpression.

Proc. Natl. Acad Sci. U.S.A. 105, 14371–14376. doi: 10.1073/pnas.0804090105

Zhang, W., Lu, J., Zhang, S., Liu, L., Pang, X., and Lv, J. (2018). Development an effective system to expression recombinant protein in E. coli via comparison and optimization of signal peptides: expression of *Pseudomonas fluorescens* BJ-10 thermostable lipase as case study. *Microb. Cell Fact* 17:50. doi: 10.1186/s12934-018-0894-y

Zhou, Y., Liu, P., Gan, Y., Sandoval, W., Katakam, A. K., Reichelt, M., et al. (2016). Enhancing full-length antibody production by signal peptide engineering. *Microb. Cell Fact* 15:47. doi: 10.1186/s12934-016-0445-3

Conflict of Interest Statement: The authors declare that the research was conducted in the absence of any commercial or financial relationships that could be construed as a potential conflict of interest.

Copyright © 2019 Karyolaimos, Ampah-Korsah, Hillenaar, Mestre Borras, Dolata, Sievers, Riedel, Daniels and de Gier. This is an open-access article distributed under the terms of the Creative Commons Attribution License (CC BY). The use, distribution or reproduction in other forums is permitted, provided the original author(s) and the copyright owner(s) are credited and that the original publication in this journal is cited, in accordance with accepted academic practice. No use, distribution or reproduction is permitted which does not comply with these terms.

frontiers in Microbiology

ORIGINAL RESEARCH
published: 31 July 2019
doi: 10.3389/fmicb.2019.01718

Delivery of the *Pseudomonas aeruginosa* Phospholipase Effectors PldA and PldB in a VgrG- and H2-T6SS-Dependent Manner

*Sarah Wettstadt†, Thomas E. Wood†, Selina Fecht and Alain Filloux**

MRC Centre for Molecular Bacteriology and Infection, Department of Life Sciences, Imperial College London, London, United Kingdom

OPEN ACCESS

Edited by:
Eric Cascales, Aix-Marseille Université, France

Reviewed by:
Tao Dong, University of Calgary, Canada
John Whitney, McMaster University, Canada

***Correspondence:**
Alain Filloux
a.filloux@imperial.ac.uk

†Present address:
Sarah Wettstadt, Department of Environmental Protection, Estación Experimental del Zaidín-Consejo Superior de Investigaciones Científicas, Granada, Spain
Thomas E. Wood, Department of Medicine, Division of Infectious Diseases, Massachusetts General Hospital, Cambridge, MA, United States; Department of Microbiology & Immunobiology, Harvard Medical School, Boston, MA, United States

Specialty section:
This article was submitted to Microbial Physiology and Metabolism, a section of the journal Frontiers in Microbiology

Received: *20 December 2018*
Accepted: *11 July 2019*
Published: *31 July 2019*

Citation:
Wettstadt S, Wood TE, Fecht S and Filloux A (2019) Delivery of the Pseudomonas aeruginosa Phospholipase Effectors PldA and PldB in a VgrG- and H2-T6SS-Dependent Manner. Front. Microbiol. 10:1718. doi: 10.3389/fmicb.2019.01718

The bacterial pathogen *Pseudomonas aeruginosa* uses three type VI secretion systems (T6SSs) to drive a multitude of effector proteins into eukaryotic or prokaryotic target cells. The T6SS is a supramolecular nanomachine, involving a set of 13 core proteins, which resembles the contractile tail of bacteriophages and whose tip is considered as a puncturing device helping to cross membranes. Effectors can attach directly to the T6SS spike which is composed of a VgrG (valine-glycine-rich proteins) trimer, of which *P. aeruginosa* produces several. We have previously shown that the master regulator RsmA controls the expression of all three T6SS gene clusters (H1-, H2- and H3-T6SS) and a range of remote *vgrG* and effector genes. We also demonstrated that specific interactions between VgrGs and various T6SS effectors are prerequisite for effector delivery in a process we called "à la carte delivery." Here, we provide an in-depth description on how the two H2-T6SS-dependent effectors PldA and PldB are delivered *via* their cognate VgrGs, VgrG4b and VgrG5, respectively. We show that specific recognition of the VgrG C terminus is required and effector specificity can be swapped by exchanging these C-terminal domains. Importantly, we established that effector recognition by a cognate VgrG is not always sufficient to achieve successful secretion, but it is crucial to provide effector stability. This study highlights the complexity of effector adaptation to the T6SS nanomachine and shows how the VgrG tip can possibly be manipulated to achieve effector delivery.

Keywords: type VI secretion system, bacterial toxin, phospholipase, VgrG, *Pseudomonas aeruginosa*

INTRODUCTION

The type VI secretion system (T6SS) is a sophisticated protein secretion system that is found in about 25% of Gram-negative bacteria (Bingle et al., 2008). Resembling the contractile tail of bacteriophage (Kanamaru et al., 2002), the T6SS is used by bacteria to drive effector proteins directly into nearby cells, which can be of eukaryotic or prokaryotic nature (Basler et al., 2013). The T6SS is placed onto the bacterial cytoplasmic membrane *via* a membrane complex consisting of TssL, TssM and TssJ proteins (Durand et al., 2012, 2015). The membrane complex is connected to a so-called T6SS baseplate, sitting at the cytosolic side of the inner membrane and made of TssA, TssE, TssF, TssG, TssK, and VgrG (Brunet et al., 2015; Planamente et al., 2016). From the baseplate, the

T6SS sheath is built and polymerizes into the cytoplasm. Composed of TssB and TssC subunits (Leiman et al., 2009), this helical contractile sheath envelops an inner tube, that consists of stacked hexamers of Hcp proteins (Brunet et al., 2014) which are topped by the VgrG spike (Renault et al., 2018). Contraction of the sheath toward the baseplate leads to extracellular release of the VgrG spike and the Hcp tube, where presence of Hcp in the supernatant fraction of bacterial cultures is a standard readout for T6SS activity, since it is a direct measure of a functional T6SS machinery (Pukatzki et al., 2006).

The spike atop the Hcp tube is composed of a trimer of VgrG proteins forming a rigid needle-like structure due to intertwining C-terminal hydrophobic β-sheets (Kanamaru et al., 2002). At the tip of the T6SS VgrG trimer sits a PAAR protein (Shneider et al., 2013) whose conical fold is thought to facilitate the puncturing of target membranes (Browning et al., 2012). One PAAR protein likely binds on top of one VgrG trimer in a way that it interacts with the last β-sheet derived from each VgrG monomer (Shneider et al., 2013).

Pseudomonas aeruginosa contains three T6SS clusters (H1-, H2- and H3-T6SS) each encoding all core T6SS components. The three clusters could be expressed simultaneously (Hachani et al., 2011; Allsopp et al., 2017) while each system delivers different sets of effector proteins into prokaryotic or eukaryotic cells (Russell et al., 2011; Hachani et al., 2014; Jiang et al., 2014; Whitney et al., 2014). Additionally, the *P. aeruginosa* genome contains multiple remote satellite islands, likely acquired *via* horizontal gene transfer, encoding different *vgrG, paar* and effector genes co-regulated with the core T6SS clusters (Jones et al., 2013; Allsopp et al., 2017). Effector genes are usually encoded together with immunity genes allowing the survival of the effector producing strain (Russell et al., 2011) as well as preventing T6SS-dependent intoxication by neighboring sibling cells (MacIntyre et al., 2010).

In some cases, the effector is a covalent extension of a structural component and thus called evolved VgrG-, PAAR-, or Hcp-effector (Ma et al., 2009, 2017; Whitney et al., 2015). If separated, a genetic link between an effector gene and a gene encoding a VgrG-, PAAR-, or Hcp-protein suggests a functional association (Hachani et al., 2014). Indeed, the delivery of many effectors was shown to be dependent on the nearby encoded VgrG, PAAR or Hcp component. In these cases, the effector protein specifically interacts non-covalently with a cognate Hcp hexamer, like Tse2 with Hcp1 in *P. aeruginosa* (Silverman et al., 2013); a PAAR protein, for example TseT with PAAR4 in *P. aeruginosa* (Burkinshaw et al., 2018); or the VgrG spike, as Tle1 with VgrG1 in *Escherichia coli* (Flaugnatti et al., 2015); a concept coined as "à la carte" effector delivery (Hachani et al., 2014). In some instances, the presence of so-called adaptor or chaperone proteins are required to connect effectors to the T6SS spike. These adaptor proteins can be of the DUF4123, DUF1795 or DUF2169 family. The DUF4123 proteins, denoted Tap1 (T6SS adaptor protein 1) from *Agrobacterium tumefaciens* and *Vibrio cholerae* were shown to be required for the recruitment of the effectors Tde1 and TseL, respectively, onto the cognate VgrG1 spikes (Liang et al., 2015; Unterweger et al., 2015; Bondage et al., 2016). DUF1795 proteins were termed Eag proteins and bind to the N-terminal half of PAAR effectors, chaperoning them in the producing cell before recruiting the PAAR effector to the T6SS tip (Diniz and Coulthurst, 2015; Whitney et al., 2015; Quentin et al., 2018). DUF2169 proteins seem to be less prevalent and their involvement in effector delivery has only been shown for Tde2 in *A. tumefaciens* (Bondage et al., 2016).

Pseudomonas aeruginosa encodes the two phospholipases PldA and PldB that were shown to be delivered into prey cells in a T6SS-dependent manner (Russell et al., 2013; Jiang et al., 2014; Boulant et al., 2018). Both effector genes are directly located downstream of two *vgrG* genes and no adaptor gene is encoded in their direct vicinity. This suggests that both effectors are recruited directly to the VgrG spike by a yet undefined mechanism. Here, we elucidated the effector delivery mechanisms of PldA and PldB *via* the T6SS of *P. aeruginosa* and describe an interesting new concept which shows that PldA delivery is not only dependent on one but two VgrG proteins.

MATERIALS AND METHODS

Bacterial Strains and Growth Conditions

Bacterial strains used in this study are described in **Table 1**. *P. aeruginosa* strains were grown in tryptone soy broth (TSB) or LB supplemented with antibiotics where appropriate (streptomycin 2000 μg mL^{-1}, spectinomycin 2000 μg mL^{-1}, carbenicillin 100 μg mL^{-1}, tetracycline 200 μg mL^{-1}) at 37°C with agitation. *E. coli* strains were grown in LB broth supplemented with antibiotics where appropriate (streptomycin 50 μg mL^{-1}, kanamycin 50 μg mL^{-1}, spectinomycin 100 μg mL^{-1}, carbenicillin 50 μg mL^{-1}, tetracycline 15 μg mL^{-1}).

DNA Manipulation

DNA purification was performed using PureLink Genomic DNA mini kit (Life Technologies). Isolation of plasmid DNA was carried out using the QIAprep spin miniprep kit (Qiagen). Restriction endonucleases were used according to the manufacturer's specifications (New England Biolabs or Roche). Oligonucleotides used are listed in **Table 2** and were purchased from Sigma, United Kingdom. The genes or DNA fragments used for the construction of mutator plasmids and deletion mutants were amplified with KOD Hot Start DNA Polymerase (Novagen) as described by the manufacturer with the inclusion of 0.5 M betaine (Sigma). Colony PCR was performed with Taq polymerase (New England Biolabs). DNA sequencing was performed by GATC Biotech.

Construction of *P. aeruginosa* Mutants

Pseudomonas aeruginosa deletion mutants were constructed as described previously (Vasseur et al., 2005) using the suicide plasmid pKNG101 (Herrero et al., 1990; Kaniga et al., 1991). Briefly, to create PAO1Δ*gene-of-interest* (*GOI*), 500-bp DNA fragments of the 5′ (up) and 3′ (down) ends of the target gene were obtained by PCR using PAO1 chromosomal DNA as a template with two pairs of oligonucleotides (Up5′/Up3′ and Down5′/Down3′) (**Table 2**). To create chimeric genes, splicing by overlap extension PCRs was performed. Briefly, approximately 500 bp upstream and downstream of the locus

TABLE 1 | Strains and plasmids used in this work.

Strain or plasmid	Relevant characteristics[a]	Source/References
Strain		
E. coli		
DH5α	F– Φ80*lacZ*ΔM15 Δ(*lacZYA-argF*) U169 *rec*A1 *end*A1 *hsd*R17 (rK–, mK+) *pho*A *sup*E44 λ– *thi*-1 *gyr*A96 *rel*A1	Laboratory collection
CC118(λpir)	Host strain for pKNG101 replication; Δ(*ara-leu*) *araD*Δ*lacX74 galE galK-phoA20 thi-1 rpsE rpoB argE* (Am) *recA1* Rf^Rλ*pir)*	Laboratory collection
P. aeruginosa		
PAO1	PAO1 wild type strain	Laboratory collection
PAO1 Δ*rsmA*	Deletion in *rsmA* (*PA0905*)	Allsopp et al., 2017
PAO1::*pldA-bla*$_{TEM-1}$	Insertion of *bla*$_{TEM-1}$ before *pldA (PA3487)* STOP codon	Allsopp et al., 2017
PAO1::*pldB-bla*$_{TEM-1}$	Insertion of *bla*$_{TEM-1}$ before *pldB (PA5089)* STOP codon	Allsopp et al., 2017
PAO1 ΔrsmAΔ*pldAtli5a*	Deletion in *rsmA*, *pldA-tli5a* (*PA3487-PA3488*)	This work
PAO1 ΔrsmAΔ*pldAtli5a::lacZ*	Deletion in *rsmA*, *pldA-tli5a PA3487-PA3488*, chromosomal insertion of *lacZ* at *att* site	This work
PAO1 ΔrsmAΔ*pldBtli5b*$_{123}$*::lacZ*	Deletion in *rsmA*, *pldB-tli5b*$_{123}$ (*PA5089-PA5086*), chromosomal insertion of *lacZ* at *att* site	This work
PAO1 ΔrsmAΔ*pldAtli5a* Δ*pldBtli5b*$_{123}$*::lacZ*	Deletion in *rsmA*, *pldA-tli5a PA3487-PA3488*, *pldB-tli5b*$_{123}$ *PA5089-PA5086*, chromosomal insertion of *lacZ* at *att* site	This work
PAO1 Δ*rsmA*Δ*tssE2*	Deletions in *rsmA* and *tssE2* (*PA1657*)	This work
PAO1 Δ*rsmA*Δ*tssK3*	Deletions in *rsmA* and *tssK3* (*PA2363*)	This work
PAO1 Δ*rsmA*Δ*tssE2::pldA-bla*$_{TEM-1}$	Deletions in *rsmA*, *tssE2* and insertion of *bla*$_{TEM-1}$ before *pldA* STOP codon	Allsopp et al., 2017
PAO1 Δ*rsmA*Δ*tssE2::pldB-bla*$_{TEM-1}$	Deletions in *rsmA*, *tssE2* and insertion of *bla*$_{TEM-1}$ before *pldB* STOP codon	This work
PAO1 Δ*rsmA*Δ*tssK3::pldA-bla*$_{TEM-1}$	Deletions in *rsmA*, *tssK3* and insertion of *bla*$_{TEM-1}$ before *pldA* STOP codon	This work
PAO1 Δ*rsmA*Δ*vgrG4b*	Deletions in *rsmA* and *vgrG4b* (*PA3486*)	Allsopp et al., 2017
PAO1 Δ*rsmA*Δ*vgrG4b*Δ*pldBtli5b*$_{123}$	Deletions in *rsmA, vgrG4b PA3486* and *pldB-tli5b*$_{123}$ *PA5089-PA5086*	This work
PAO1 Δ*rsmA*Δ*vgrG4b::pldA-bla*$_{TEM-1}$	Deletions in *rsmA*, *vgrG4b* and insertion of *bla*$_{TEM-1}$ before *pldA* STOP codon	This work
PAO1 Δ*rsmA*Δ*vgrG4b::pldB-bla*$_{TEM-1}$	Deletions in *rsmA*, *vgrG4b* and insertion of *bla*$_{TEM-1}$ before *pldB* STOP codon	This work
PAO1 Δ*rsmA::vgrG4b*^{618}*-vgrG5*^{169}	Deletion in *rsmA* and substitution of gene portion corresponding to *vgrG4b*^{187} with gene portion for *vgrG5*^{169}	This work
PAO1 Δ*rsmA::vgrG4b*^{618}*-vgrG5*^{169} *::pldA-bla*$_{TEM-1}$	Deletion in *rsmA*, insertion of *bla*$_{TEM-1}$ before *pldA* STOP codon, substitution of gene portion corresponding to *vgrG4b*^{187} with gene portion for *vgrG5*^{169}	This work
PAO1 Δ*rsmA*Δ*vgrG4b::vgrG5*^{623}*-vgrG4b*^{187}	Deletions in *rsmA*, *vgrG4b*, substitution of gene portion corresponding to *vgrG4b*^{187} with gene portion for *vgrG5*^{169}	This work
PAO1 Δ*rsmA*Δ*vgrG4b::vgrG5*^{623}*-vgrG4b*^{187}*::pldA-bla*$_{TEM-1}$	Deletions in *rsmA* and *vgrG4b*, insertion of *bla*$_{TEM-1}$ before *pldA* STOP codon, substitution of gene portion corresponding to *vgrG4b*^{187} with gene portion for *vgrG5*^{169}	This work
PAO1 Δ*rsmA*Δ*vgrG4b*Δ*tssE2::vgrG4b*^{618}*-vgrG5*^{169}*::pldA-bla*$_{TEM-1}$	Deletions in *rsmA*, *vgrG4b, tssE2* and insertion of *bla*$_{TEM-1}$ before *pldA* STOP codon and a substitution of gene portion corresponding to *vgrG4b*^{187} with gene portion for *vgrG5*^{169}	This work
PAO1 Δ*rsmA*Δ*vgrG4b*Δ*tssK3::vgrG4b*^{618}*-vgrG5*^{169}*::pldA-bla*$_{TEM-1}$	Deletions in *rsmA*, *vgrG4b, tssK3* and an insertion of *bla*$_{TEM-1}$ before *pldA* STOP codon and a substitution of gene portion corresponding to *vgrG4b*^{187} with gene portion for *vgrG5*^{169}	This work
PAO1 Δ*rsmA*Δ*vgrG4b*Δ*vgrG5*	Deletions in *rsmA*, *vgrG4b* and *vgrG5*	This work
PAO1 Δ*rsmA*Δ*vgrG5*	Deletions in *rsmA* and *vgrG5 (PA5090)*	This work
PAO1 Δ*rsmA*Δ*vgrG5::pldA-bla*$_{TEM-1}$	Deletions in *rsmA* and *vgrG5* and insertion of *bla*$_{TEM-1}$ before *pldA* STOP codon	This work
PAO1 Δ*rsmA*Δ*vgrG5::pldB-bla*$_{TEM-1}$	Deletions in *rsmA* and *vgrG5* and insertion of *bla*$_{TEM-1}$ before *pldB* STOP codon	This work
PAO1 Δ*rsmA*Δ*vgrG5::vgrG4b*^{618}*-vgrG5*^{169}	Deletions in *rsmA* and *vgrG5*, substitution of gene portion corresponding to *vgrG4b*^{187} with gene portion for *vgrG5*^{169}	This work
PAO1 Δ*rsmA*Δ*vgrG5::vgrG4b*^{618}*-vgrG5*^{169}*::pldB-bla*$_{TEM-1}$	Deletions in *rsmA* and *vgrG5,* substitution of gene portion corresponding to *vgrG4b*^{187} with gene portion for *vgrG5*^{169} and insertion of *bla*$_{TEM-1}$ before *pldB* STOP codon	This work

(Continued)

TABLE 1 | Continued

Strain or plasmid	Relevant characteristics[a]	Source/References
PAO1 Δ*rsmA* Δ*TAA*^{vgrG4b}-*ATG*^{pldA}	Deletion in *rsmA,* deletion of STOP codon of *vgrG4b*, 16bp intergenic region and START codon of *pldA*	This work
PAO1 Δ*rsmA* Δ*tssE2* Δ*TAA*^{vgrG4b}-*ATG*^{pldA}	Deletions in *rsmA* and *tssE2,* deletion of STOP codon of *vgrG4b*, 16bp intergenic region and START codon of *pldA*	This work
Plasmids		
pRK2013	Tra$^+$Mob$^+$, Km^R	Laboratory collection
pCR2.1	TA cloning vector, Ap^R, Km^R	Invitrogen
pCR-BluntII-TOPO	Blunt cloning vector, Zeo^R, Km^R	Invitrogen
pKNG101	Suicide vector, *sacB*, Str^R	(39)
pKNG101-*vgrG4b*	pKNG101-*vgrG4b* deletion construct	Allsopp et al., 2017
pKNG101-*vgrG5*	pKNG101-*vgrG5* deletion construct	This work
pKNG101-*pldA-bla*$_{TEM-1}$	pKNG101 deletion construct to fuse *bla*$_{TEM-1}$ to *pldA* gene	This work
pKNG101-*pldB-bla*$_{TEM-1}$	pKNG101 deletion construct to fuse *bla*$_{TEM-1}$ to *pldB* gene	This work
pKNG101- *vgrG5*^{623}-*vgrG4b*^{187}	pKNG101 deletion construct to substitute final 493 bp of *vgrG5* with 564 bp from *vgrG4b*	This work
pKNG101- *vgrG4b*^{621}-*vgrG5*^{169}	pKNG101 deletion construct to substitute final 564 bp of vgrG4b with 493 bp from *vgrG5*	This work
pKNG1010 Δ*TAA*^{vgrG4b}-*ATG*^{pldA}	pKNG101 deletion construct to delete the STOP codon of *vgrG4b*, 16bp intergenic region and START codon of *pldA*	This work
pKNG101-*tssE2*	pKNG101-*tssE2* deletion construct	Allsopp et al., 2017
pKNG101-*tssK3*	pKNG101-*tssK3* deletion construct	Allsopp et al., 2017
pTrc200	Broad host range pVS1 derivative plasmid, *lacIq*, *pTrc* promoter, Sm^R/Sp^R	Schmidt-Eisenlohr et al., 1999; Gift from Erh-Min Lai
p *vgrG4b*	pTrc200 producing full length VgrG4b, Sm^R/Sp^R	This work
pBBR1-mcs4	Broad host range vector, with constitutive *PLAC* promoter, Ap^R/Cb^R	Kovach et al., 1995
p *vgrG5*-HA	pBBR1-MCS-4 encoding *vgrG5* with a C-terminal quadruple HA-tag, Ap^R, Cb^R	This work
p *vgrG5*^{628}-HA	pBBR1-MCS-4 encoding *vgrG5*^{628} with a C-terminal quadruple HA-tag, Ap^R, Cb^R	This work
miniCTX::*lacZ*	Mini-CTX1 harboring the *lacZ* with constitutive promoter, Tc^R	Becher and Schweizer, 2000

[a] *Ap^R, ampicillin resistant; Str^R, Streptomycin resistant; Km^R, Kanamycin resistant; Tc^R, Tetracycline resistant, Cb^R carbenicillin resistant, Sp^R spectinomycin resistant.*

of interest was amplified using the internal primers 3′up and 5′down. Two additional primers, 3′down and 5′up, were used that contain complementary sequences to the opposing side of the splice junction and amplified to yield a fusion fragment. Thus, two subsequent overlap extension PCR steps were undertaken, employing an equimolar ratio of the upstream and downstream fragments as the DNA template. The gene fragments were cloned into pCR-BluntII-TOPO (Invitrogen), their sequences confirmed and sub-cloned into pKNG101 suicide vector. The pKNG-derivatives were maintained in the *E. coli* strain CC118λpir and mobilized into *P. aeruginosa* PAK using *E. coli* 1047 carrying the conjugative plasmid pRK2013 (Figurski and Helinski, 1979). Clones, in which double recombination events occurred, resulting in the deletion of *GOI* or fusion to *GOI*, were isolated using counterselection on sucrose plates as previously described (Vasseur et al., 2005). Gene deletion or fusion was verified by PCR using external primers and western blot analysis where appropriate.

Secretion Assay

Secretion assays were performed similarly as previously described (Hachani et al., 2011). Bacterial suspension was diluted from overnight cultures in TSB to OD_{600} of 0.1 and grown at 25°C to an OD_{600} of 4, unless otherwise stated. A bacterial culture sample adjusted to OD_{600} of 1 was harvested by centrifugation and served as the whole cell sample. Simultaneously, 13 mL of culture was centrifuged at 4 000 *g* for 20 min at 4°C to separate the bacterial cells from culture supernatant. 10 ml of the supernatant was transferred into falcon tubes and centrifuged again; 7 mL of the uppermost supernatant was transferred into new tubes and centrifuged. To 1.8 mL supernatant fraction, we added 200 µl trichloroacetic acid to precipitate proteins overnight at 4°C. The protein precipitate was centrifugated at 16 000 *g* for 30 min at 4°C and washed with cold 90% (v/v) acetone before further centrifugation. After removing the supernatant, the washed pellet was air-dried for 30 min and resuspended in 1× Laemmli buffer to an OD_{600} equivalent of 20.

Western Blot Analysis and SDS-PAGE

For SDS-PAGE analysis, cell extracts were loaded onto SDS polyacrylamide gels, migrated and transferred to a nitrocellulose membrane at 3 mA/cm^2. Following transfer, membranes were incubated overnight in blocking buffer (5% milk powder, 0.1% Tween 20 in Tris–buffered saline, pH 8.0). Polyclonal antibodies

TABLE 2 | Oligonucleotides used in this study.

Deleted gene/ Oligonucleotide	Oligonucleotide sequence[a]
vgrG5	
Up5′	ACAGCCATGTGCTCAACG
Up3′	GGTAGGCGTGGCGAACATTCACTGTCC
Down5′	ATGTTCGCCACGCCTACCGGCGCGACG
Down3′	CGCGATGAGGTTGAGGTT
pldAtli5a	
Up5′	GCGATCAAGATGCCGTTGAC
Up3′	TACTTCTTCCTTCTTCTGCAACATGGA TCAGTC
Down5′	CAGAAGAAGGAAGAAGTACTG CCCCGCC
Down3′	TTCTTCACCAGCATCTCGGT
pldBtli5b$_{123}$	
Up5′	CCTGAAGCAGCCGGAACA
Up3′	CCGCAAACCTATCCTCTGCCTCCTCATCC
Down5′	CAGAGGATAGGTTTGCGGTTTGTACAGGT
Down3′	TAGTGATCGAGGCAGGCATG
TAA^{vgrG4b}*-ATG*^{pldA}	
Up5′	CAAGGACCAGAAGAAGCCCTACAA
Up3′	GGCTTCTTCTGGTCCTTGGCC
Gene fusions/ Oligonucleotide	
pldA-bla$_{TEM-1}$	
Up5′	AAGCATCGCACAGCGGCCAGCCT
Up3′	AGGCTGGCCGCTGTGCGATG
Down5′	ATCGCACATGAAAAGGGTTTTGAT
Down3′	TACCTTCGCAGTTTGGCATG
pldB-bla$_{TEM-1}$	
Up5′	CAAGATCGAGGCGCTCGAAG
Up3′	GTCAAAATCTTACGGTGGACGCGG CCAGCCTGGAAG
Down5′	GCATCGCTCAGTCCACCGTTACCAA TGCTTAATCAG
Down3′	ACAGAGCACGGCCCAAAGTC
vgrG5^{623}*-vgrG4b*^{187}	
Up5′	GGCGCCCTGGCACGGATCAAT
Up3′	GTGCCAGGGCGCCGTCGAGGGTG
Down5′	GCCAAGGACTGACAAGGATGAGC
Down3′	TCCTTGTCAGTCCTTGGCCAGT
vgrG4b^{621}*-vgrG5*^{169}	
Up5′	CGGCCCGCAGGTGATGATCAAC
Up3′	TCATCACCTGCGGGCCGCTGATGGC
Down5′	CGCCATGAGCCAAGGACTGAT
Down3′	CTCATGGCGTGGGCTCAT
Amplified gene/ Oligonucleotide	
vgrG4b	
5′	GCATACTCTAGAGTTGATCTGGTTGAGT TCCTTTTC
3′	GCATACGAGCTCTTTTCGAGAAACAGG GGACAG
vgrG5-HA	
5′	atgGTCGACGAATACGCCAGGAACGCAC
3′	tagGCTAGCGCCGCCGCTGTTGATCATCA
vgrG5^{628}	
5′	atgGTCGACGAATACGCCAGGAACGCAC
3′	tagGCTAGCGCCGCCGCTGTTGATCATCA

[a] *Oligonucleotides are presented in the orientation 5′-3′.*

against the C-terminal extension domain of VgrG4b (VgrG4b^{C}) were used at a dilution of 1:1000, against Hcp2 at 1:1000 (Jones et al., 2013), against LasB 1:1000 (Gift from Romé Voulhoux). Monoclonal anti-Bla$_{TEM-1}$ (BioLegend) and anti-HA antibodies (BioLegend) were used at a dilution of 1:5000. Monoclonal antibodies against the β subunit of RNA polymerase (RpoB, NeoClone) were used at 1:5000. Secondary antibodies conjugated to horseradish peroxidase were used at a dilution of 1:5000. Western blots were developed using Super-Signal West Pico Chemiluminescent Substrate (Pierce) and visualized on a LAS3000 Fuji Imager.

Interbacterial Competition Assays

Interbacterial competition assays were conducted on solid media due to the contact-dependent killing of the T6SS (Hachani et al., 2013). *P. aeruginosa* prey strains contained the Mini-CTX-lacZ plasmid integrated at the *att* site, consequently giving rise to blue colonies on 5-bromo-4-chloro-3-indolyl-D-galactopyranoside (X-gal)-containing media. Overnight cultures in TSB were collected by centrifugation at 8 000 *g* for 3 min before washing twice in 1 ml sterile PBS and normalized to OD_{600} of 3.0. 100 μl of attacker and 100 μl prey strains for a ratio of 1:1 were mixed. This mixture was centrifuged at 8 000 *g* for 3 min and 100 μl supernatant was removed. 5 μl of each competition mix was spotted in duplicates onto LB-agar, the spots dried, and the Petri dish lids secured using parafilm M (Bemis). Competition plates were inverted and incubated at 25°C for 24 h under H2-T6SS-inducive killing conditions (Allsopp et al., 2017).

The input competitions were serially diluted to 10^{-7}, plated on selective media for both attacker and prey (LB agar with 100 μg mL^{-1} X-gal for blue/white differentiation) of *P. aeruginosa* prey/attacker and grown overnight at 37°C to confirm the input ratios. Competition spots were gathered using 5 μl inoculation loops (VWR) and resuspended in 1 mL PBS. The competition output mixture was serially diluted to 10^{-7}, plated on selective media and grown overnight at 37°C similarly, to the input. Both attacker and prey colony forming units were enumerated on both input and output dilution plates. All competition assays were repeated three times unless otherwise stated and the mean colony forming unit (cfu) of surviving prey strains obtained from all experiments was plotted with the standard deviation.

RESULTS AND DISCUSSION

PldA and PldB Are Delivered Into Prey Cells *via* Their Cognate VgrGs and in a H2-T6SS-Dependent Manner

The tandemly organized genes encoding the T6SS effector phospholipase PldA, also known as Tle5a (Russell et al., 2013), and the structural component VgrG4b are upregulated in an *rsmA* mutant and both proteins are secreted by the H2-T6SS in *P. aeruginosa* PAO1 (**Supplementary Figure S1**; Russell et al., 2013; Allsopp et al., 2017). Yet, this genetic link (**Figure 1A**, top panel) suggested PldA to be delivered as a VgrG4b-dependent effector, which we recently demonstrated by monitoring secretion

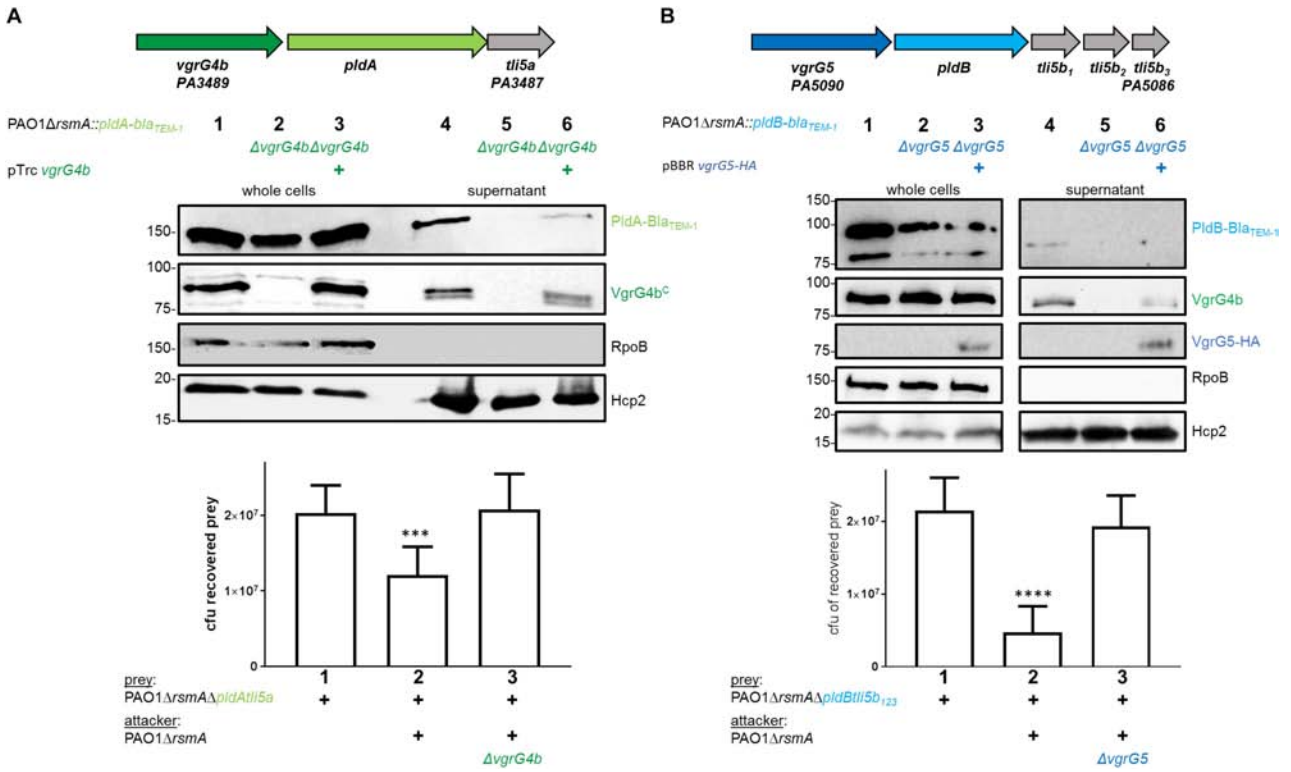

FIGURE 1 | *P. aeruginosa* encodes two phospholipases delivered *via* their cognate VgrGs. **(A)** *vgrG4b* (PA3489, green) is encoded directly upstream of *pldA* (PA3488, bright green). **(B)** *vgrG5* (PA5090, blue) is encoded directly upstream of *pldB* (PA5089, cyan). Second panel: Representative figures of western blots from secretion assays using PAO1 Δ*rsmA* expressing Bla_{TEM-1}-tagged versions of PldA **(A)** or PldB **(B)**. The absence (Δ) of the native *vgrG4b* **(A)** or *vgrG5* **(B)** are indicated. For complementation experiments of the **(A)** *vgrG4b* and **(B)** *vgrG5* mutants, the introduction *in trans* of **(A)** *vgrG4b* (pTrc-*vgrG4b*) and **(B)** *vgrG5* (pBBR1-mcs5-*vgrG5-HA*) are marked with (+). Membranes in **(A)** and **(B)** were revealed, from top to bottom, using antibodies against Bla_{TEM-1}, the C-terminal extension domain of VgrG4b (αVgrG4b^C), the HA-tag, RpoB and Hcp2 as indicated on the right. In the bottom panel, bacterial competition outcomes are shown by plots of recovered cfu of prey strains susceptible to PldA delivery, PAO1 Δ*rsmA* Δ*pldAtli5a::lacZ* **(A)**, or PldB delivery, PAO1 Δ*rsmA* Δ*pldBtli5b*$_{123}$*::lacZ* **(B)**, after contact with the attacker strain PAO1 Δ*rsmA* encoding or lacking (Δ) the native *vgrG4b* **(A)** or *vgrG5* **(B)**. Spots were incubated for 24 h at 25 °C in a 1:1 ratio. One-Way ANOVA analysis with Dunnett's multiple comparisons test was conducted on the data set obtained from recovered prey in the absence of an attacker strain with ****$p < 0.0001$.

of a chimeric fusion protein PldA-Bla_{TEM-1} (Allsopp et al., 2017). Here, we show that the lack of PldA secretion is solely due to the absence of VgrG4b since PldA release is restored by complementing the *vgrG4b* mutant (**Figure 1A**, middle panel, lane 6). PldA displays antibacterial activity (Russell et al., 2013) and we aimed at elucidating whether VgrG4b would facilitate PldA delivery into neighboring prey cells. We constructed prey strains lacking genes encoding PldA and its immunity Tli5a rendering them susceptible to PldA delivery. When in contact with the parental strain, the prey survival was challenged (**Figure 1A**, lower panel, lane 2), which was not the case when the attacker strain lacked *vgrG4b* (**Figure 1A**, lower panel, lane 3).

Interestingly, *P. aeruginosa* PAO1 produces a second T6SS phospholipase, PldB, also known as Tle5b (Russell et al., 2013), whose corresponding gene is found in a remote locus and downstream of a gene encoding VgrG5 (**Figure 1B**, top panel). To monitor PldB production and secretion using western blot analysis, we engineered a chimeric gene encoding a fusion between PldB and the β-lactamase, Bla_{TEM-1}. Production of the PldB-Bla_{TEM-1} fusion protein is relieved in absence of RsmA (**Supplementary Figure S2**; Allsopp et al., 2017) and we assessed whether PldB delivery is mediated by VgrG5. Remarkably, PldB secretion was abrogated in absence of VgrG5 (**Figure 1B**, middle panel, lane 5), while PldB-mediated killing was abolished when using attacker strains lacking *vgrG5* (**Figure 1B**, bottom panel, lane 3). Complementation of PldB secretion with VgrG5 *in trans* could not be detected (**Figure 1B**, middle panel, lane 6) likely due to low abundance of PldB-Bla_{TEM-1} in complemented cells (lane 3). However, the used VgrG5 construct was functional since it was able to restore VgrG4b secretion, as will be discussed at a later point. Interestingly, secreted PldB-Bla_{TEM-1} was always detected as a smaller band (**Figure 1B**, lane 4) than in the whole cell fraction (lane 1). This is likely to be due to N-terminal processing of the effector as the detected Bla_{TEM-1} domain is fused to the C-terminus of PldB and can still be detected.

A previous study suggested that PldB is delivered into prey cells by the H3-T6SS (Jiang et al., 2014). Here, not only do we show that PldB secretion is dependent on VgrG5, but we observed that VgrG5 secretion is more likely H2-T6SS-dependent. This statement is supported by our analysis

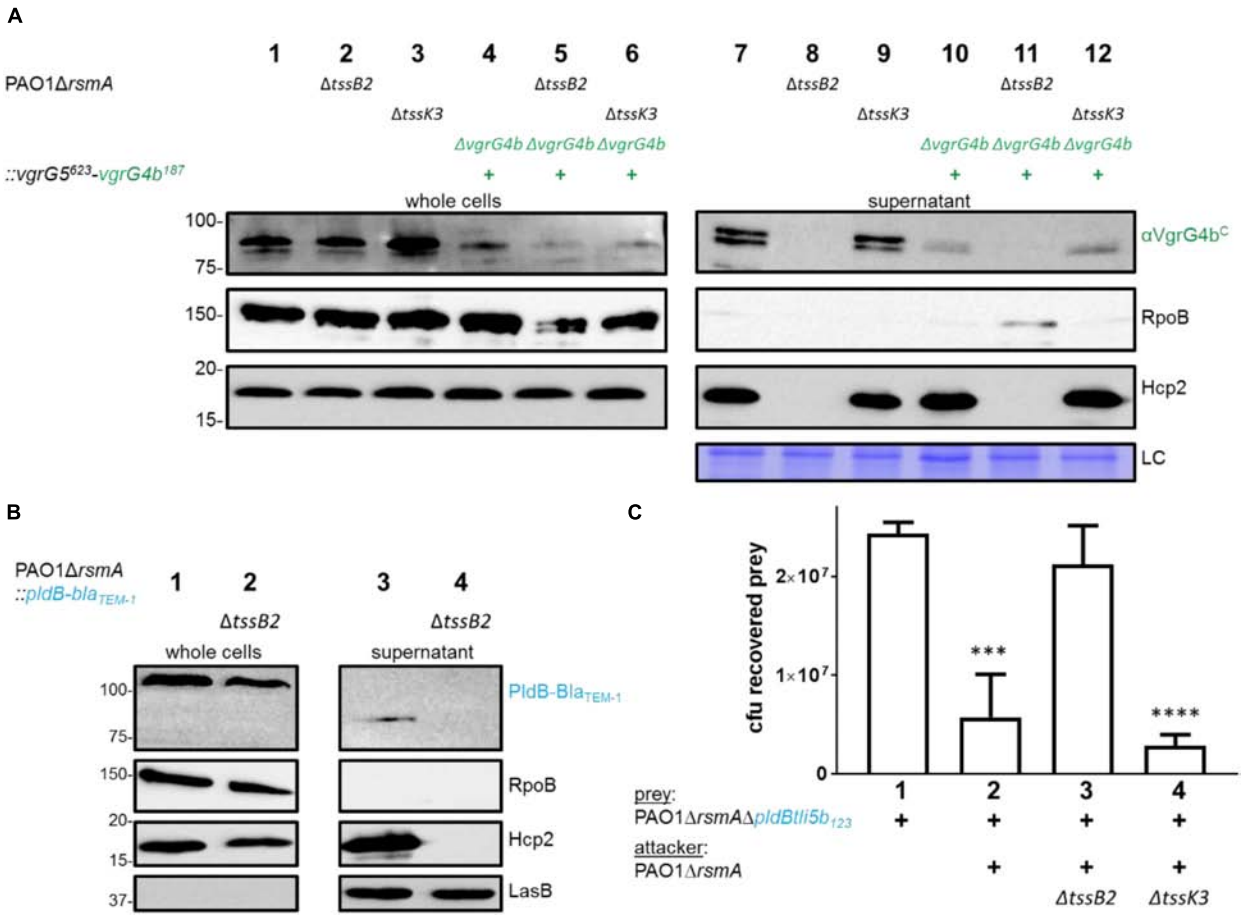

FIGURE 2 | VgrG5 secretion and PldB delivery are H2-T6SS dependent. **(A)** Representative figure of a western blot from a secretion assay using PAO1Δ*rsmA*. Strains encode native *vgrG4b* or the *vgrG5*^{623}-*vgrG4b*^{187} chimera (+) as well as an active or inactive (Δ) H2-T6SS (Δ*tssB2*) or H3-T6SS (Δ*tssK3*). Antibodies used (from top to bottom) are against VgrG4b^{C}, RpoB and Hcp2 as indicated on the right. A section from a Coomassie gel was included to serve as a loading control (LC) for the supernatant fraction. **(B)** Representative figure of a western blot from a secretion assay using PAO1Δ*rsmA* expressing a Bla$_{TEM-1}$-tagged version of PldB. Strains produce an active or inactive (Δ*tssB2*) H2-T6SS. Antibodies used (from top to bottom) are against Bla$_{TEM-1}$, RpoB, Hcp2 and LasB as indicated on the right. **(C)** Bacterial competition represented by plots of recovered cfu of prey strain PAO1Δ*rsmA*Δ*pldBtli5b*$_{123}$::*lacZ* after contact with the attacker strain that encodes a non-functional H2-T6SS (Δ*tssB2*) or H3-T6SS (Δ*tssK3*). As a positive control for PldB-mediated killing, PAO1Δ*rsmA* was included. Spots were incubated for 24 h at 25 °C in a 1:1 ratio. One-Way ANOVA analysis with Dunnett's multiple comparisons test was conducted on the data set obtained from recovered prey on its own with ****$p < 0.0001$.

of the secretion of a VgrG5^{623}-VgrG4b^{187} chimera (first 623 amino acids of VgrG5, VgrG5^{625} and last 187 aa of VgrG4b, VgrG4b^{187}, **Supplementary Figure S3C**). The VgrG5 portion of the chimera is the core gp27/gp5 domain while the C terminus has been replaced with the C terminus of VgrG4b, which we will describe in further sections. We reasoned that the N-terminal hub domains of the trimeric VgrG spike interact with the top Hcp hexamer of the Hcp tube likely mediating its affiliation to a specific T6SS (Renault et al., 2018). Hence, modifying the C-terminal domain of a VgrG tip protein would have no impact on its affiliation to a specific T6SS. The rationale for using this fusion is that in absence of a VgrG5 antibody we could monitor VgrG5 secretion by western blot analysis using an antibody against the C-terminal domain of VgrG4b. We used PAO1 wild type and mutant strains and showed that the VgrG5^{623}-VgrG4b^{187} chimera is detected in the supernatant of H3-T6SS-inactive (**Figure 2A**, lane 12) but not of H2-T6SS-inactive mutants (**Figure 2A**, lane 11). We further reasoned that if VgrG5 is H2-T6SS-dependent then PldB might also be (**Figure 2B**). We assessed PldB secretion and showed that it was indeed abrogated when using H2-T6SS-inactive mutants (**Figure 2B**, lane 4). Finally, we performed bacterial competition assays (**Figure 2C**) and observed that PldB-mediated killing was only diminished from H2-T6SS inactive attackers (**Figure 2C**, lane 3) but not from those lacking an active H3-T6SS (**Figure 2C**, lane 4).

In all, we demonstrate that VgrG4b and VgrG5 do mediate delivery of their cognate effectors, PldA and PldB, respectively, which agrees with the "à la carte" delivery concept for genetically linked VgrG and cognate T6SS effector. We also showed that these two remote pairs, which are not genetically linked with other core T6SS genes, are H2-T6SS-dependent.

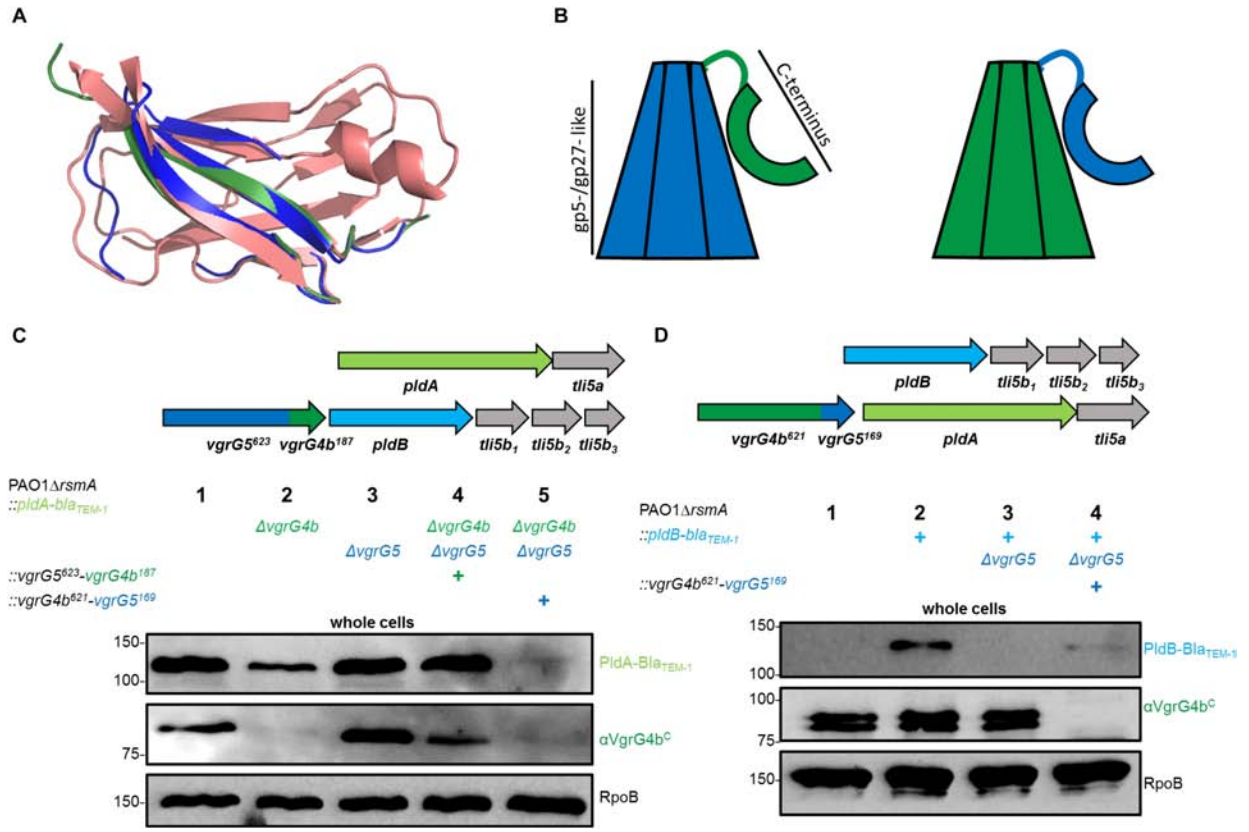

FIGURE 3 | The C-terminal domain of a VgrG specifically stabilizes its cognate effector protein. **(A)** Structural models of the C termini of VgrG4b (green) and VgrG5 (blue) as compared to the transthyretin-like protein from *Salmonella dublin* (red, pdb: 2gpz). **(B)** Schematic of the here used chimerae between VgrG5 (blue) and VgrG4b (green). Highlighted are each the gp5-/gp27-like domains of VgrG4b and VgrG5 as well as the C-terminal domain consisting of the TTR-like domains (aa 648 – 770, see **Supplementary Figure S3** for more details) as shown with an arc form. **(C,D)** Mutant strains carry Bla_{TEM-1}-tagged version of PldA **(C)** or PldB **(D)** as well as the gene clusters as sketched in the top panels and using the color code as in **Figure 1**. **(C)** Strains express one of the following *vgrG* genes: native *vgrG5* (lane 2), native *vgrG4b* (lane 3), $vgrG5^{623}$-$vgrG4b^{187}$ chimera (lane 4) or $vgrG4b^{629}$-$vgrG5^{169}$ chimera (lane 5). Representative figures of western blots from whole cell fractions of PAO1Δ*rsmA* derivates as indicated by (+). **(D)** $vgrG4b^{629}$-$vgrG5^{169}$ chimera replaces the native *vgrG4b* and the native *vgrG5* gene is deleted. Controls for native effector stability are shown with the parental strains in **(C)** lane 1 and **(D)** lane 2, while the negative controls lack the cognate *vgrG* locus in **(C)** lane 2 or in **(D)** lane 3. Antibodies used (top to bottom) are against Bla_{TEM-1}, $VgrG4b^{C}$ and RpoB as indicated on the right of each panel.

The C-Terminal TTR-Like Domains of VgrG4b and VgrG5 Differ and Are Specific for Recognition of PldA and PldB

Recognition of T6SS effectors by a cognate VgrG could be direct or involve adaptor proteins facilitating the interaction. In *A. tumefaciens* it has been shown that the two VgrGs, VgrG1 and VgrG2, specifically bind and recognize their cognate effectors Tde1 and Tde2 (Bondage et al., 2016). In this case, Tde1 and Tde2 recognition involves two distinct adaptor proteins, Tap1, a DUF4123 protein, and Atu3641, a DUF2169 protein, respectively. The adaptor genes *tap1* and *atu3641* are genetically linked with the cognate effector genes *tde1* and *tde2*, respectively, and the adaptor proteins bind their cognate effectors to recruit them at the C-terminal regions of VgrG1 and VgrG2, respectively (Bondage et al., 2016).

No adaptor genes are located in the vicinity of *pldA* or *pldB* suggesting that the corresponding effectors bind directly to their respective VgrG spikes. Using bioinformatic analysis, we identified transthyretin (TTR)-like folds within the C-terminal domains of both VgrG4b and VgrG5 (**Figure 3A**). Importantly, TTR-like domains within VgrG proteins have been shown to mediate binding of the cognate effector to the VgrG C terminus, as is the case in enteroaggregative *E. coli* and the VgrG1-dependent delivery of Tle1 (Flaugnatti et al., 2015).

The TTR-like domains of VgrG4b and VgrG5 share 25 % sequence identity, while their N-terminal gp5-/gp27-like domains share 69 % identity (**Supplementary Figure S3A**). From these observations, we hypothesized that specificity for PldA and PldB lies within the C-terminal domains of VgrG4b and VgrG5, respectively. To assess this concept, we swapped the C-terminal domains between VgrG4b (the C-terminal 187 amino acids) and VgrG5 (the C-terminal 169 amino acids) as depicted in **Supplementary Figures S3B,C** leading to chimeric VgrG proteins (**Figure 3B**). For VgrG protein detection we used an antibody that specifically recognizes the C terminus of VgrG4b as shown already in **Figure 2A**. As such, from the

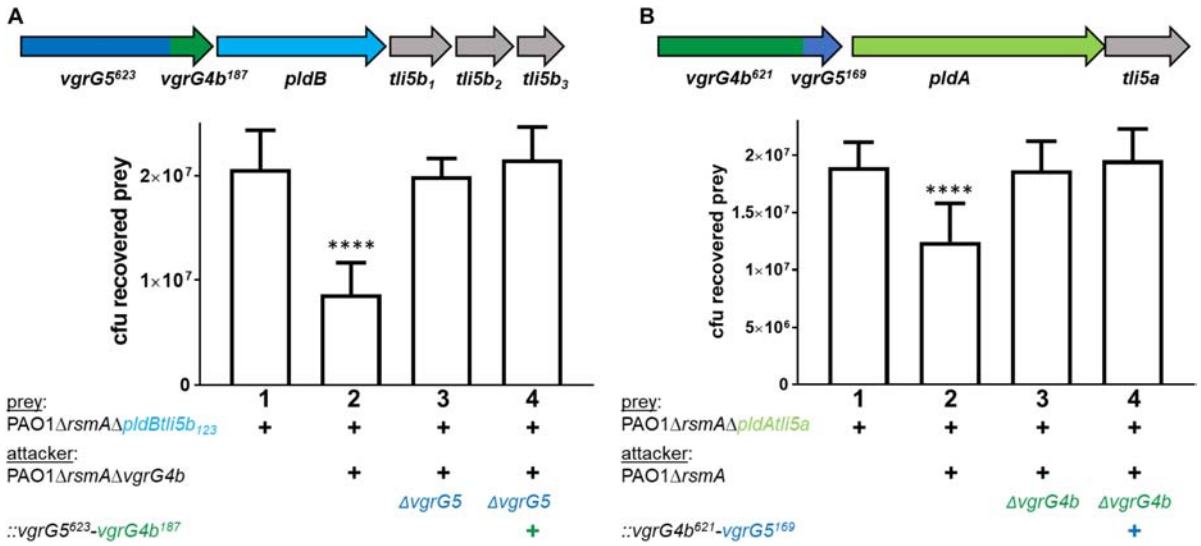

FIGURE 4 | Modifying the VgrG C-terminus abrogates delivery of cognate effectors. The *vgrG* cluster color code is as in **Figure 1**. The mutant strains used carry the gene sequence for **(A)** *vgrG5*^{623}-*vgrG4b*^{187} chimera and **(B)** *vgrG4b*^{621}-*vgrG5*^{169} chimera. Note that mutants in **(A)** encode the N terminal 623 amino acids of VgrG5 (blue) and the last C-terminal 187 amino acids of VgrG4b (+, green, **Supplementary Figure S4B**) and mutants in **(B)** encode the N terminal 621 amino acids of VgrG4b and the last C-terminal 169 amino acids of VgrG5 (+, **Supplementary Figure S4C**). Bottom panels: bacterial competition experiments and plots of recovered cfu of prey strains as described in **Figure 1**. Recovery is after contact with the attacker strain that encodes **(A)** native *vgrG5* or the *vgrG5*^{623}-*vgrG4b*^{187} chimera (+) or **(B)** native *vgrG4b* or the *vgrG4b*^{621}-*vgrG5*^{169} (+). As a positive control for effector-mediated killing, the parental strains were included (lanes 2), while the negative control lacked the cognate *vgrG* (lanes 3). Spots were incubated for 24 h at 25 °C in a 1:1 ratio. One-Way ANOVA analysis with Dunnett's multiple comparisons test was conducted on data set obtained from recovered prey on their own with $^{****}p < 0.0001$.

two chimeric VgrGs, that we engineered, the antibody could detect the VgrG5^{623}-VgrG4b^{187} chimera (**Figure 3C**, lane 4), but not the VgrG4b^{621}-VgrG5^{169} chimera (**Figure 3D**, lane 4). We also used strains that produce Bla$_{TEM-1}$-tagged versions of PldA or PldB (**Figures 3C,D**, upper panels) so that production of these T6SS effectors could be followed with an antibody directed against the Bla$_{TEM-1}$ portion of the chimeric proteins. We performed western blot analysis of whole cell lysates derived from various strains and observed that in absence of VgrG4b, there is a consistent decrease in the amount of the cognate effector PldA (**Figure 3C**, lane 2). A stable PldA protein is only seen in presence of VgrG4b (**Figure 3C**, lanes 1 and **3**) or its C-terminal domain (**Figure 3C**, lane 4). Instead, the sole presence of VgrG5 (**Figure 3C**, lane 2) or its C-terminal domain (**Figure 3C**, lane 5) had no stabilizing effect on PldA. On the other hand, the absence of VgrG5 has an even more drastic impact on the abundance of its cognate effector PldB (**Figure 3D**, lane 3). Interestingly, PldB stability was partly restored when the C terminus of the cognate VgrG5 was expressed as part of a VgrG4b chimera (**Figure 3D**, lane 4), which would suggest that the cognate VgrG C terminus is sufficient to help stabilizing the effector.

Here, it is interesting to observe that stability of the T6SS effectors PldA and PldB depends on the C-terminal domains of their cognate VgrGs. On multiple occasions, it has been experimentally validated that T6SS effectors require the presence of cognate T6SS components for their stability. Tse2 from *P. aeruginosa* was shown to be degraded in absence of its receptor Hcp1 (Silverman et al., 2013), while purification of the effector Tde1 from *A. tumefaciens* led to higher yields in presence of its adaptor protein Tap1 (Ma et al., 2014). Furthermore, substrates from other bacterial secretion systems require the presence of dedicated chaperone proteins for stability. For example, the T3SS substrate YopE from *Y. pseudotuberculosis* (Birtalan et al., 2002) as well as the T4SS substrate VirE2 from *A. tumefaciens* (Zhao et al., 2001; Sutherland et al., 2012) require chaperones to connect to the cognate secretion machinery. For PldA and PldB, the C-terminal domains of their cognate VgrGs likely act as chaperone domains.

The mechanism involving specific binding and stabilization of a toxic protein by a secretion component prior to its export likely represents a survival strategy in addition to the presence of cognate immunity proteins. Upon binding of the toxic protein by the secretion component, the cell ensures to rapidly deliver the toxin out of the cell where it can execute its damaging effect. However, when lacking the cognate secretion component, the toxin would accumulate within the cell likely leading to cellular damage. In this case, the cell would trigger degradation of the toxin to quickly prevent deleterious outcomes.

All our results indicate that PldA and PldB are specifically stabilized, and likely chaperoned, by the C-terminal TTR domains of their cognate VgrG proteins. If this were the case, a modified VgrG C-terminal extension domain would jeopardize the cognate effector delivery. We tested this hypothesis and used appropriate *P. aeruginosa* strains producing VgrG4b^{621}-VgrG5^{169} or VgrG5^{623}-VgrG4b^{187} chimera to challenge prey cells susceptible to PldB (**Figure 4A**) or PldA (**Figure 4B**) injection. Note that the susceptibility is conferred by the deletion of appropriate immunity genes, *tli5b*$_{123}$ or *tli5a* in the prey

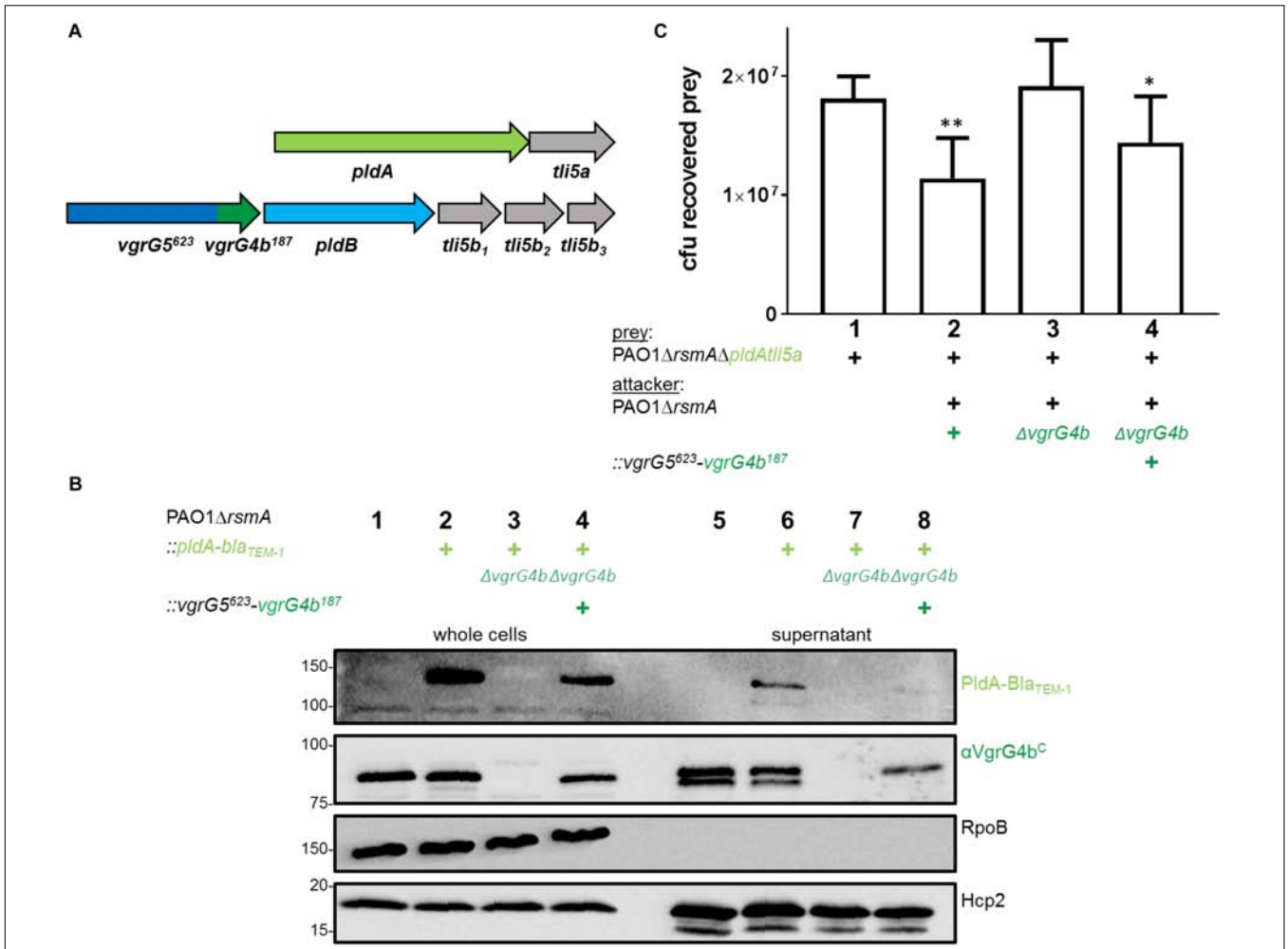

FIGURE 5 | Substitution of the VgrG5 C-terminus with the VgrG4b C-terminus restores PldA delivery. **(A)** Schematic depicting a strain carrying the *vgrG5*^{623}-*vgrG4b*^{187} chimeric gene at the native *vgrG5*. The native *vgrG4b* is deleted. **(B)** Representative figure of a western blot from a secretion assay using PAO1Δ*rsmA* or PAO1Δ*rsmA::pldA-bla*$_{TEM-1}$ (+) encoding native *vgrG4b* or the *vgrG5*^{623}-*vgrG4b*^{187} chimera (+). As a control for PldA-Bla$_{TEM-1}$ secretion, the parental strain was included (lane 6), while the negative control lacked the native *vgrG4b* (lane 7). Antibodies used (from top to bottom) are against Bla$_{TEM-1}$, VgrG4b^{C}, RpoB and Hcp2 as indicated on the right. **(C)** Bacterial competition represented by plots of recovered cfu of prey strain PAO1Δ*rsmA*Δ*pldAtli5a::lacZ* after contact with the attacker strain that encodes native *vgrG4b* or the *vgrG5*^{623}-*vgrG4b*^{187} chimera (+). As a positive control for PldA-mediated killing, PAO1Δ*rsmA* was included (lane 2), while the negative control lacked *vgrG4b* (lane 3). Spots were incubated for 24 h at 25 °C in a 1:1 ratio. One-Way ANOVA analysis with Dunnett's multiple comparisons test was conducted on data set obtained from recovered prey on their own with ****$p < 0.0001$.

cells. Remarkably, attacker strains with a modified cognate VgrG (**Figure 4**, lanes 4, respectively) failed to outcompete corresponding susceptible prey cells thus confirming that the C-terminal domain of VgrG is instrumental for effector recognition and delivery.

Swapping the C-Terminal TTR-Like Domain to Redirect Effectors to the VgrG Tip

We then sought to exploit the concept of VgrG C-terminal specificity to force PldA to use a VgrG5 vehicle carrying the VgrG4b C terminus, i.e., a VgrG5^{623}-VgrG4b^{187} chimera (**Figure 5A**). Remarkably, PldA was identified in the supernatant fraction of cells expressing VgrG5^{623}-VgrG4b^{187}, which was also secreted (**Figure 5B**, lane 8). We also performed competition assays and showed that cells expressing VgrG5^{623}-VgrG4b^{187} display a competitive advantage toward prey cells lacking the *pldAtli5a* effector-immunity locus, which are thus PldA-sensitive (**Figure 5C**). These results suggest that presence of the C-terminal domain of VgrG4b at the VgrG5 tip is sufficient to adapt VgrG5 for PldA delivery and that it is possible to redirect an effector to a non-cognate VgrG vehicle.

Interdependent VgrG Secretion Compromises the Swapping Specificity Hypothesis

We further aimed to test whether the same concept would hold true to adapt the effector PldB to a non-cognate VgrG

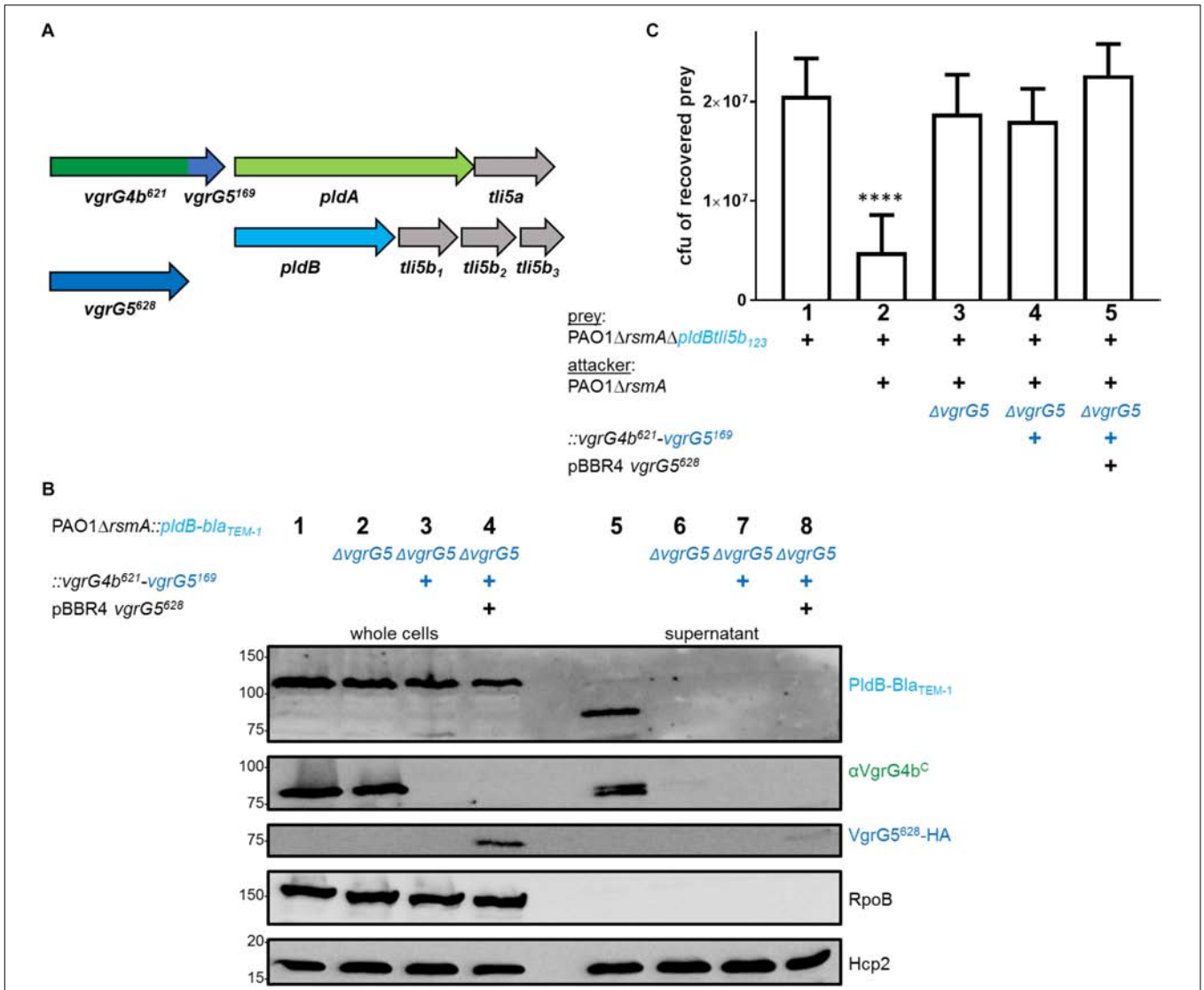

FIGURE 6 | Production of the VgrG5 N-terminus (VgrG5^{628}) does not support PldB secretion. **(A)** Schematic depicting a strain carrying the chimeric gene *vgrG4b*^{629}-*vgrG5*^{169} at the native *vgrG4b* locus and in absence of the native *vgrG5* gene. A construct encoding a quadruple HA-tagged version of VgrG5^{628} is expressed from *pBBR1-mcs4* (pBBR4-*vgrG5*^{628}). **(B)** Representative figure of a western blot of a secretion assay using PAO1 Δ*rsmA::pldB-bla*$_{TEM-1}$ in presence of the native *vgrG5*, encoding the *vgrG4b*^{629}-*vgrG5*^{169} chimera (+) or carrying pBBR4-*vgrG5*^{628} (+). Antibodies used (from top to bottom) are against Bla$_{TEM-1}$, VgrG4b^{C}, HA, RpoB and Hcp2 as indicated on the right. **(C)** Bacterial competition represented by plot of recovered cfu of prey strain PAO1 Δ*rsmA* Δ*pldBtli5b*$_3$*::lacZ* after contact with the attacker strain that encoded native *vgrG5* or the *vgrG4b*^{629}-*vgrG5*^{169} chimera (+) or pBBR1-*mcs4 vgrG5*^{628} (+). As a positive control for PldB-mediated killing, PAO1 Δ*rsmA* was included (lane 2), while the negative control lacked the native *vgrG5* locus (lane 3). Spots were incubated for 24 h at 25 °C in a 1:1 ratio. One-Way ANOVA analysis with Dunnett's multiple comparisons test was conducted on data set obtained from recovered prey on their own with ****$p < 0.0001$.

vehicle. Indeed, when using the VgrG4b^{621}-VgrG5^{169} chimera to specifically bind and deliver PldB (**Figure 6A**), neither secretion (**Figure 6B**, lane 7) nor delivery into prey cells (**Figure 6C**, lane 4) could be observed. One plausible explanation is that VgrG4b secretion is abolished in absence of VgrG5 (**Figure 6B**, lane 6 and **Figure 1B**, lane 5). This would further impact secretion of the VgrG4b^{621}-VgrG5^{169} chimera as it is expressed in a *vgrG5*-deficient background to avoid cross specificity for the cognate effector PldB. Nevertheless, absence of neither VgrG4b nor VgrG4b^{621}-VgrG5^{169} secretion is due to an inactive H2-T6SS, as Hcp2 is efficiently secreted (**Figure 1B**, lane 5 and **Figure 6B**, lane 6). This result challenged our concept that an effector can be delivered *via* any VgrG vehicle solely by equipping it with the appropriate C-terminal domain.

Since VgrG4b mediates PldA delivery, we hypothesized that VgrG5 absence would thus in turn affect PldA delivery into prey cells, which appeared to be the case (**Figure 7A**, lane 4). A straightforward explanation for VgrG4b secretion being dependent on VgrG5 would be that both might be part of a hetero-trimer. Indeed, in both *P. aeruginosa* and *V. cholerae,*

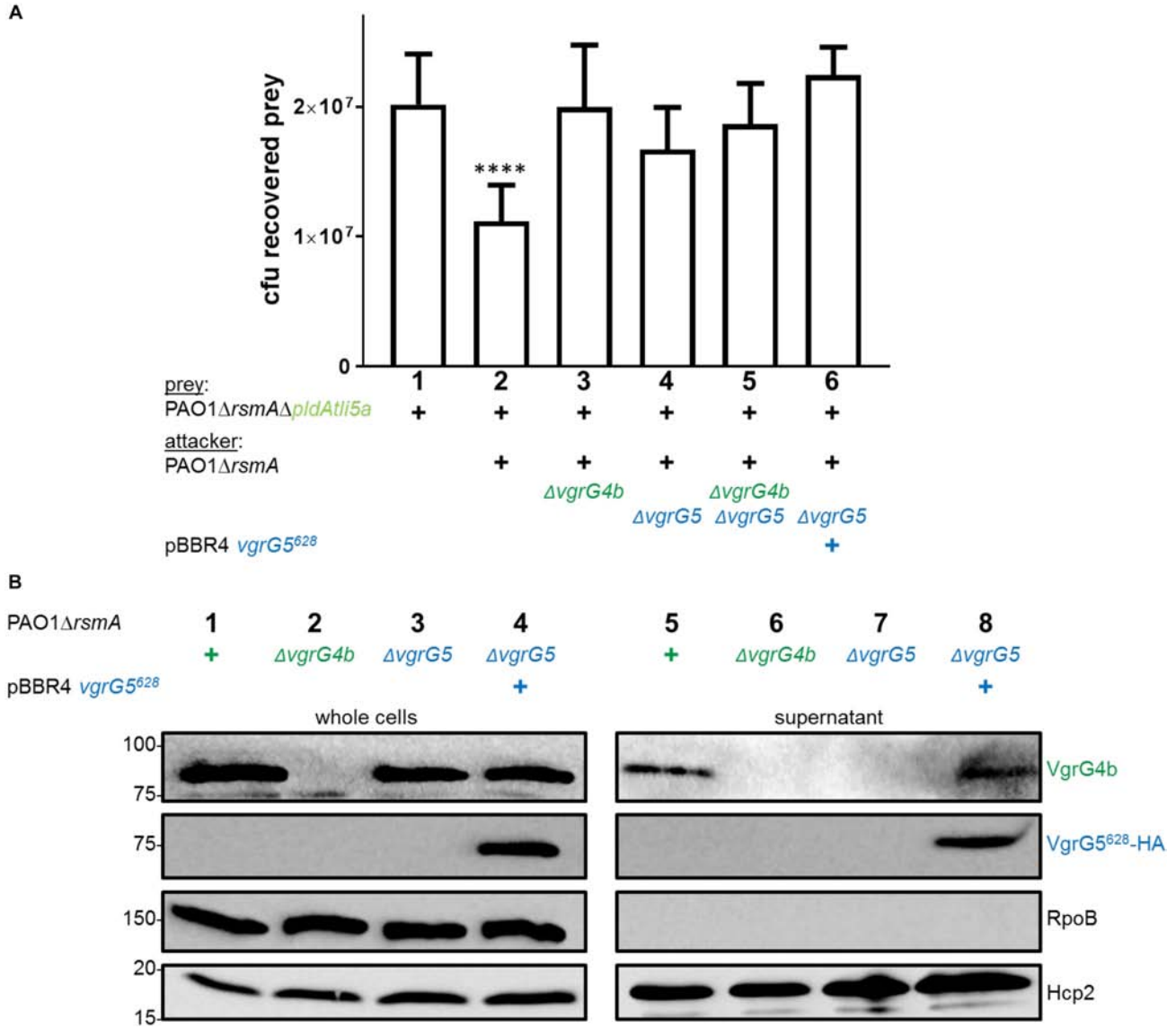

FIGURE 7 | VgrG5 mediates delivery of both PldA and PldB. **(A)** Plots of recovered cfu of prey strains susceptible for PldA delivery upon bacterial competition assays. Prey strains are as described in **Figure 1**. PAO1Δ*rsmA* attacking strains either lacked (Δ) *vgrG4b*, *vgrG5* or both, or expressed *vgrG5*^{628} *in trans* (+). Spots were incubated for 24 h at 25 °C in a 1:1 ratio. One-Way ANOVA analysis with Dunnett's multiple comparisons test was conducted on the data set obtained from recovered prey on their own with ****$p < 0.0001$. **(B)** Representative figure of western blot from a secretion assay using PAO1Δ*rsmA*. The absence (Δ) of the native *vgrG5* or *vgrG4b* is shown as well as when expressing an HA-tagged version of *vgrG5*^{628} *in trans* (+). Antibodies (from top to bottom) against the C-terminal portion of VgrG4b (VgrG4b), HA, RpoB and Hcp2 were used as indicated on the right.

it has been suggested that the spike can be made of a hetero-complex of various VgrG proteins (Pukatzki et al., 2007; Hachani et al., 2011). Hence, we investigated whether VgrG4b could be secreted as part of a hetero-trimer with VgrG5. In **Figure 1B**, middle panel, lane 6, we showed that presence of full length VgrG5 is sufficient to restore VgrG4b secretion. Since trimerization of VgrG proteins to a functional spike is mediated by their gp5/gp27-like domains (Spinola-Amilibia et al., 2016), we hypothesized that expression of solely the VgrG5 N-terminal domain (first 628 amino acids, VgrG5^{628}) would suffice to form a functional spike. By performing a secretion assay using a *vgrG5* mutant, we indeed verified that VgrG4b secretion is restored in presence of VgrG5^{628} only (**Figure 7B**, lane 8). This also confirmed that the C terminus of VgrG5 is not required to support VgrG4b secretion.

Since VgrG4b is secreted in presence of VgrG5^{628}, we reasoned that this construct would restore PldA delivery, which was not observed (**Figure 7A**, lane 6). There are potential explanations for this observation. One would be the existence of an effector delivery hierarchy. For example, VgrG5 homotrimer-dependent delivery of PldB might be initially required for subsequent VgrG4b homotrimer-dependent delivery of PldA.

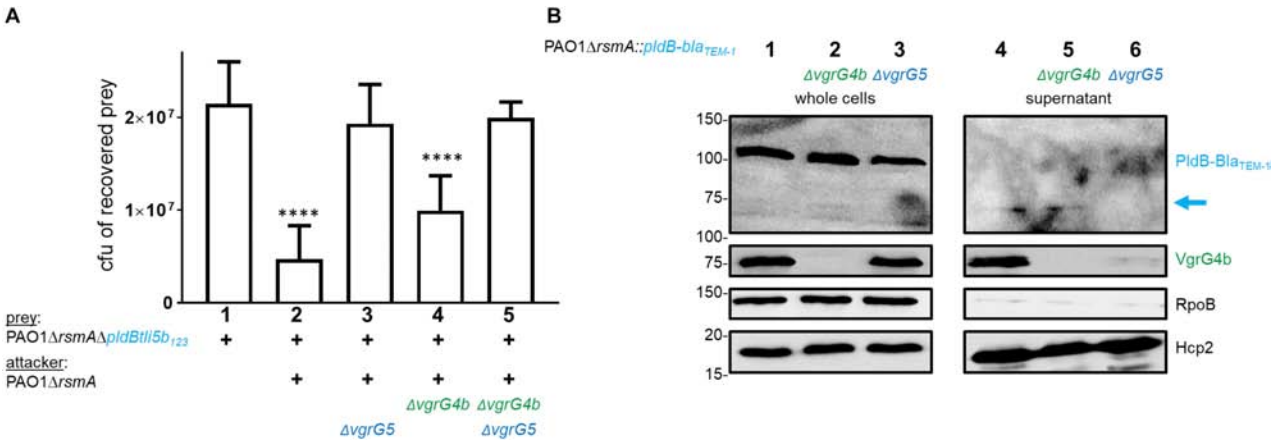

FIGURE 8 | Absence of VgrG4b has no impact on PldB delivery. **(A)** Plots of recovered cfu of prey strains susceptible for PldB delivery upon bacterial competition assays. Prey strains are as described in **Figure 1**. PAO1Δ*rsmA* attacking strains either lacked (Δ) *vgrG4b*, *vgrG5* or both. Spots were incubated for 24 h at 25°C in a 1:1 ratio. One-Way ANOVA analysis with Dunnett's multiple comparisons test was conducted on the data set obtained from recovered prey on their own with ****$p < 0.0001$. **(B)** Representative figure of a western blot from a secretion assay using PAO1Δ*rsmA::pldB-bla*$_{TEM-1}$. Strains lack (Δ) native *vgrG4b* or *vgrG5*. The blue arrow on the right indicates the secretion product of PldB-Bla$_{TEM-1}$, which is not visible when *vgrG5* is deleted. Antibodies used (from top to bottom) are against Bla$_{TEM-1}$, VgrG4b^{C}, RpoB and Hcp2 as indicated on the right.

As such, using the truncated VgrG5^{628} would not suffice to trigger VgrG4b-PldA delivery since PldB was not delivered. We tested this hypothesis by monitoring PldA delivery in absence of PldB (**Supplementary Figure S4**). An attacking strain lacking PldB showed to have the same competitive advantage toward a PldA-lacking strain (lane 5) as the parental strain (lane 2). Hence, the effector hierarchy concept is not fully supported by this observation.

An alternative possibility could be that another T6SS component, such as an adaptor or chaperone, binds the C-terminal domains of VgrG5 and VgrG4b in a VgrG4b-VgrG5 hetero-trimer and thus triggers binding of PldA toward the spike. There is for example evidence suggesting that the chaperone TecT connects the effector TseT to a VgrG4b-VgrG6 hetero-trimer (Burkinshaw et al., 2018). A similar concept could be possible for a VgrG4b-VgrG5-PldA complex. However, the finding that PldA is delivered from a VgrG5^{623}-VgrG4b^{187} chimera lacking the C-terminal domain of VgrG5 (**Figure 5**) is not in full agreement with this hypothesis. Yet it is clear that VgrG5 does not need another VgrG for its secretion and is able to deliver any effector as long as it carries a cognate C-terminal domain, here PldA through the Vgr4b C-terminal domain.

We hypothesized that co-expression of the VgrG5^{628} construct would also facilitate delivery of the VgrG4b^{621}-VgrG5^{169} chimera, which in turn would mediate PldB delivery (**Figure 6A**). However, neither PldB secretion (**Figure 6B**, lane 8) nor PldB-mediated killing (**Figure 6C**, lane 5) could be observed. This result might be explained by the lack of recognition of a cognate PAAR protein, which specifically binds the VgrG tip (Shneider et al., 2013). Here, we starkly modified the PAAR recognition site, which might have rendered this tip unrecognizable for its cognate PAAR protein and thus unsuitable for secretion.

Due to the impact of VgrG5 on PldA delivery, we finally questioned whether VgrG4b would be involved in PldB delivery (**Figure 8**). We challenged PldB-sensitive prey strains with attackers deficient for *vgrG4b*, *vgrG5* or both and observed that VgrG4b absence reduced PldB delivery, while significant killing could still be observed (**Figure 8A**, lane 4). We confirmed these data with a secretion assay demonstrating that PldB is still secreted into the supernatant in VgrG4b absence (**Figure 8B**, lane 5). From these results we conclude that VgrG5 alone suffices for PldB delivery, while PldA delivery depends on both VgrG4b and VgrG5.

VgrG4b Can Deliver PldA When Covalently Linked to the Spike

In the previous sections we made clear that a VgrG spike can recognize its cognate effector likely through specific protein-protein interaction. It is also known that many VgrGs, called "evolved" VgrGs display an effector domain fused at their C terminus (Ma et al., 2009; Sana et al., 2015). We wonder whether there is a rationale behind having the effector fused to the VgrG C terminus versus a protein-protein interaction delivery mode, or whether this is only the result of a fortuitous evolutionary process.

We demonstrated that PldA is delivered as a cargo effector dependent on VgrG4b and here assessed whether delivery is compromised if PldA is covalently linked to the VgrG4b C terminus. Hence, we deleted the STOP codon of *vgrG4b*, the intergenic region and the START codon of *pldA* (**Figure 9A**). Expression of this gene would thus lead to production of one single polypeptide consisting of VgrG4b and PldA, which we could readily detect using western blot analysis (**Figure 9B**, lane 3). The same product was detected in the supernatant fraction of H2-T6SS active strains (**Figure 9B**, lane 7), but not of H2-T6SS inactive strains (**Figure 9B**, lane 8) suggesting that secretion of

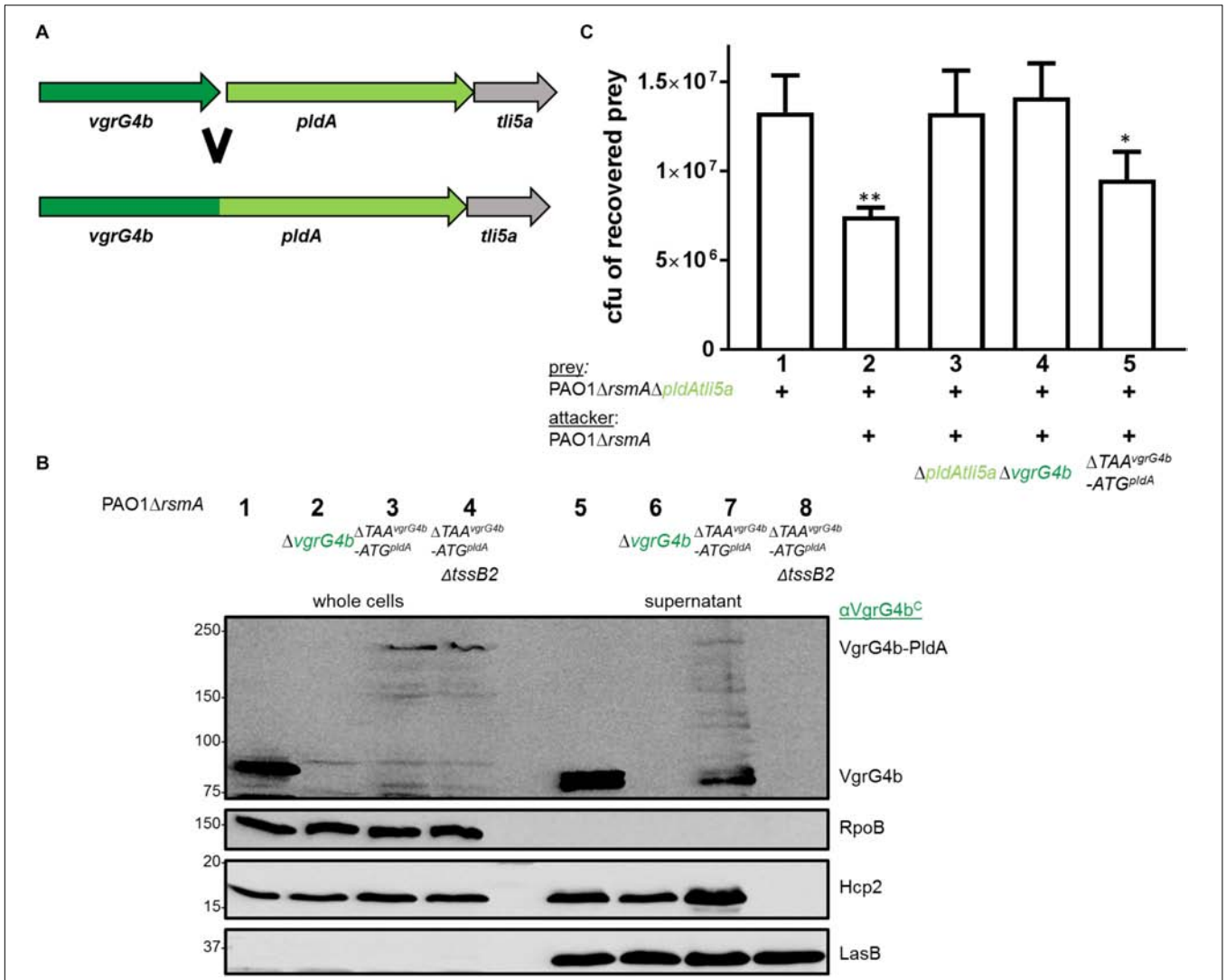

FIGURE 9 | VgrG4b can deliver PldA when fused to its C-terminus. **(A)** The STOP codon of *vgrG4b*, the intergenic region and START-codon of *pldA* were deleted resulting in a single chimeric gene product. **(B)** Representative figure of a western blot from a secretion assay using PAO1Δ*rsmA* with an active or inactive H2-T6SS (Δ*tssB2*) encoding VgrG4b-PldA (Δ*TAA*^{vgrG4b}-*ATG*^{pldA}). As a positive control for VgrG4b secretion, PAO1Δ*rsmA* (lane 1) was included, while the negative control lacked *vgrG4b* (lane 2). Antibodies used (from top to bottom) are against VgrG4b^{C}, RpoB, Hcp2 and LasB, a T2SS substrate (Olson and Ohman, 1992) acting as a loading control for the supernatant, as indicated on the right. **(C)** Bacterial competition represented by plots of recovered cfu of prey strain PAO1Δ*rsmA*Δ*pldAtli5a*:: *lacZ* after contact with the attacker strain encoding WT PldA, WT VgrG4b or the fusion VgrG4b-PldA (Δ*TAA*^{vgrG4b}-*ATG*^{pldA}) as indicated. As a positive control for PldA-mediated killing, PAO1Δ*rsmA* was included (lane 2) while the negative controls lacked *pldAtli5a* (lane 3) or *vgrG4b* (lane 4). Spots were incubated for 24 h at 25 °C in a 1:1 ratio. One-Way ANOVA analysis with Dunnett's multiple comparisons test was conducted on the data set obtained from the recovered prey on its own with $*p < 0.05$ and $**p < 0.01$.

the VgrG4b-PldA fusion remains H2-T6SS-dependent. Note, that additional bands most likely representing VgrG4b degradation products can be detected in the supernatant fraction but to a lesser amount as in the whole cells. This suggests that the artificially evolved VgrG4b-PldA protein becomes prone for proteolysis once secreted into the environment.

We further investigated whether such a fusion could be injected into bacterial prey cells. We challenged PldA-sensitive preys against *P. aeruginosa* strains expressing the VgrG4b-PldA fusion (**Figure 9C**, lane 5) and observed that they are outcompeted to a similar extent as when in competition with the parental strain (**Figure 9C**, lane 2). This led us to conclude that the VgrG4b-PldA fusion protein can be delivered by *P. aeruginosa* both into the extracellular milieu and into neighboring bacteria.

The H2-T6SS Could Be a Core System for the Delivery of Remote VgrG Spikes

We previously showed that *P. aeruginosa* uses its H1-T6SS to deliver at least three different VgrG-dependent antibacterial effectors into target prey cells, namely Tse5, Tse6 and Tse7

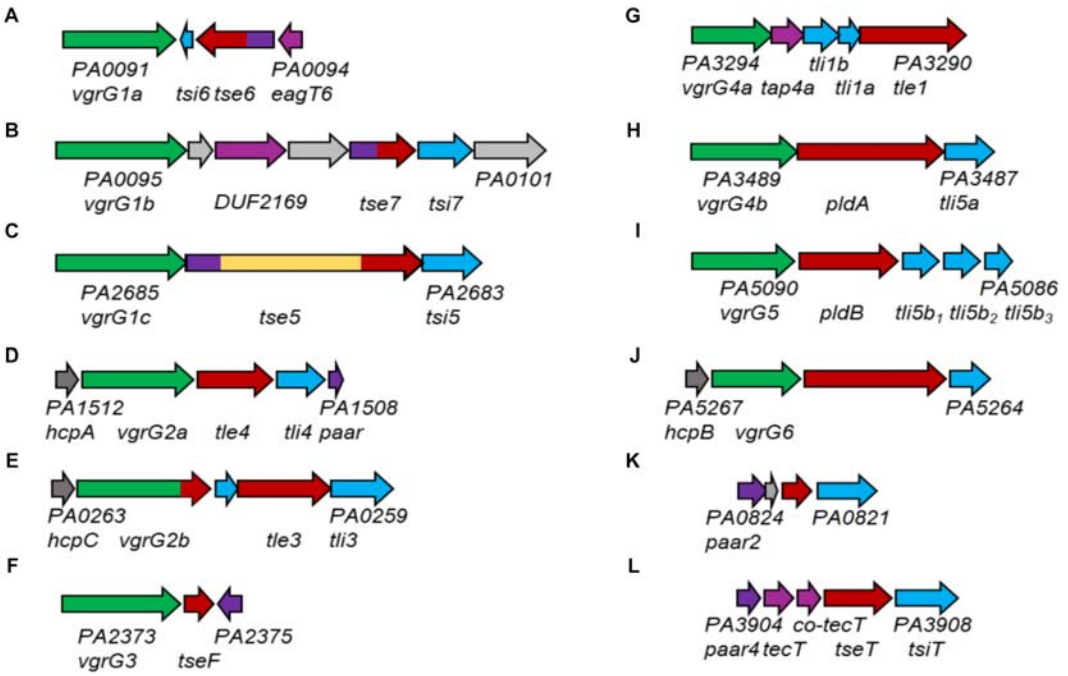

FIGURE 10 | Genomic loci containing *vgrG* or *paar* genes of *P. aeruginosa* PAO1. *vgrG* genes are shown in green, effector genes in red, cognate immunities in cyan, *hcp* genes in dark gray, *paar* genes in purple, *tap* genes in magenta and genes of unknown function in gray. For all examples, the PA numbers of the two outer genes are shown. Effector genes close to their (putative) cognate vgrG or PAAR genes are the following: **(A)** tse6; **(B)** tse7; **(C)** tse5; **(D)** tle4; **(E)** tle3; **(F)** tseF; **(G)** tle1; **(H)** pldA; **(I)** pldB; **(J)** PA5265; **(K)** PA0822; **(L)** tseT.

(Hachani et al., 2014; Pissaridou et al., 2018). All of these effectors are evolved PAARs that interact with their cognate VgrGs, VgrG1c, VgrG1a and VgrG1b (**Figures 10A–C**), respectively, *via* their N-terminal PAAR domains (Shneider et al., 2013; Whitney et al., 2015). In case of the H3-T6SS, information about associated effectors is scarce. In the H3-T6SS cluster, *vgrG3* as well as the effector *tseF* are encoded (**Figure 10F**) and it is proposed that TseF secretion is H3-T6SS-dependent (Lin et al., 2017). Although not experimentally demonstrated, it is likely that considering the genetic linkage, TseF delivery might also be VgrG3-dependent. Previous reports have also suggested that PldB delivery is H3-T6SS-dependent (Jiang et al., 2014), however, here we show that this effector is secreted in a H2-T6SS-dependent fashion and requires the cognate VgrG5.

There is experimental evidence that the H2-T6SS is responsible for delivery of VgrG4b (Allsopp et al., 2017), VgrG5 (this study), VgrG2a and VgrG2b (Sana et al., 2015). We here provide functional evidence, that VgrG4b specifically delivers PldA (**Figure 10H**) and VgrG5 delivers PldB (**Figure 10I**). VgrG2a and VgrG2b are genetically linked to the effector proteins Tle4 (**Figure 10D**) and Tle3 (**Figure 10E**; Jiang et al., 2016), however, their functional links require further investigations. Additionally, VgrG4a, which is encoded on a separate satellite *vgrG* island, is likely affiliated with the H2-T6SS due to a sequence identity of 97% with VgrG4b within the N-terminal gp5/gp27-like domains (Allsopp et al., 2017). Downstream of *vgrG4a*, another effector, Tle1, is encoded (**Figure 10G**), and because of the genetic linkage, most likely delivered in a VgrG4a-dependent manner. VgrG6, encoded on yet another satellite *vgrG* island, is genetically linked to *hcpB* (**Figure 10J**). This might be an indication for its association with the H2-T6SS (Burkinshaw et al., 2018) because the HcpB amino acids sequence is 100 % identical to HcpA and HcpC (Jones et al., 2013), which are genetically linked to genes encoding H2-T6SS spike proteins VgrG2a (**Figure 10D**) and VgrG2b (**Figure 10E**), respectively. Additionally, there is a putative effector gene linked to *vgrG6* whose role has not been studied yet. A remote *paar* cluster (**Figure 10L**) has also been connected to the H2-T6SS, whose gene product PAAR4 mediates delivery of the effector TseT in a TecT, Co-TecT-, VgrG4b- and VgrG6-dependent fashion (Burkinshaw et al., 2018). PAAR2, encoded on yet another orphan island (**Figure 10K**), was shown to be able to functionally replace PAAR4 (Burkinshaw et al., 2018), hence its affiliation with the H2-T6SS is also implicated.

Combining these data and observations, we propose that *P. aeruginosa* uses its H2-T6SS machinery to deliver a multitude of different spikes decorated with various effectors. Interestingly, five (PldA, PldB, Tle3, Tle4 and Tle1) out of seven postulated H2-T6SS-dependent effectors are lipases that have been either experimentally proven (Russell et al., 2013; Jiang et al., 2014, 2016) or proposed due to the presence of the lipase-specific DUF2235 domain. The affiliation of at least five lipases, even though with different substrate specificities (Russell et al., 2013), with one T6SS machinery begs the question of why there would be such effector redundancy. In any case, with such a broad spike repertoire, *P. aeruginosa* has many options for

loading its H2-T6SS weapon in order to confer a competitive advantage in a polymicrobial environment. This also mitigates the presumption of the H1-T6SS being the major antibacterial T6SS of *P. aeruginosa* (Hachani et al., 2014; Allsopp et al., 2017) while the H2-T6SS provides *P. aeruginosa* with the versatility to fire various effectors into competing prey cells.

CONCLUSION

The T6SS is a potent bacterial weapon that delivers an arsenal of toxins into eukaryotic and prokaryotic prey cells. All *P. aeruginosa* strains sequenced so far carry three distinct T6SSs, namely H1-, H2- and H3-T6SS, which could act in concert to inject a lethal cocktail of enzymes targeting essential functions in living organisms. Among these are phospholipases, and notably PldA and PldB, which are described in this study and which are considered as trans-kingdom effectors since they challenge the survival of eukaryotic cells as much as bacterial cells. The effector delivery strategy of the T6SS has been shown to be quite variable, and one mode we described here involves an exquisite recognition specificity between the toxin and the cognate T6SS spike, known as a VgrG trimer. The effector specificity lies within the C-terminal domain of a VgrG and we showed that such region in VgrG4b and VgrG5 is a TTR-like domain providing chaperone activity on PldA and PldB, respectively, which is instrumental for efficient secretion of these effectors (**Supplementary Figure S5**). PldA and PldB are encoded remotely from other T6SS core genes but are genetically linked to their cognate VgrG, supporting the concept of *vgrG* islands. As such, the *pldA/vgrG4b* or *pldB/vgrG5* genes, remotely and spread on the entire chromosome, exclusively carry the genes needed to load the T6SS spike (e.g., VgrG/effector or VgrG/Effector/Adaptor) at the tip of the T6SS nanomachine. It thus remains quite elusive on which T6SS core system each of the spike is loaded. Here we showed that both VgrG4b/PldA and VgrG5/PldB are delivered in an H2-T6SS-dependent manner and propose that most *vgrG* island-encoded effectors might actually use the H2-T6SS rather than the H1- or H3-T6SS. It is likely that fitting of the VgrG protein onto the T6SS machine would require specific interactions with the Hcp tube, as was shown recently (Renault et al., 2018). It is thus likely that acquisition of single effectors from other bacterial species by horizontal gene transfer would have to obey a number of rules before they can be fitted on and fired by endogenous T6SSs.

AUTHOR CONTRIBUTIONS

AF and SW conceived the study, participated in its design and coordination and wrote the manuscript. TW engineered the *P. aeruginosa* prey strains and optimized the bacterial killing assay conditions. SW performed most of the experiments and SF contributed to additional experiments. All authors discussed, reviewed and approved the final manuscript.

FUNDING

AF work on T6SS was supported by the MRC grants MR/K001930/1 and MR/N023250/1 and the BBSRC grant BB/I019871/1. SW was supported by the Imperial College President's Scholarship, TW by the Wellcome Trust and Selina Fecht by the Medical Research Council.

ACKNOWLEDGMENTS

We would like to thank Silvia D'Arcangelo for contributing the engineering of the *tssK3* mutant, as well as the parental strains of this study, PAO1 *rsmA*.

SUPPLEMENTARY MATERIAL

The Supplementary Material for this article can be found online at: https://www.frontiersin.org/articles/10.3389/fmicb.2019.01718/full#supplementary-material

REFERENCES

Allsopp, L. P., Wood, T. E., Howard, S. A., Maggiorelli, F., Nolan, L. M., Wettstadt, S., et al. (2017). RsmA and AmrZ orchestrate the assembly of all three type VI secretion systems in *Pseudomonas aeruginosa*. *Proc. Nat. Acad. Sci. U. S. A.* 114, 7707–7712. doi: 10.1073/pnas.1700286114

Basler, M., Ho, B. T., and Mekalanos, J. J. (2013). Tit-for-tat: type VI secretion system counterattack during bacterial cell-cell interactions. *Cell* 152, 884–894. doi: 10.1016/j.cell.2013.01.042

Becher, A., and Schweizer, H. P. (2000). Integration-proficient *Pseudomonas aeruginosa* vectors for isolation of single-copy chromosomal lacZ and lux gene fusions. *Biotechniques* 29, 952.

Bingle, L. E., Bailey, C. M., and Pallen, M. J. (2008). Type VI secretion: a beginner's guide. *Curr. Opin. Microbiol.* 11, 3–8. doi: 10.1016/j.mib.2008.01.006

Birtalan, S. C., Phillips, R. M., and Ghosh, P. (2002). Three-dimensional secretion signals in chaperone-effector complexes of bacterial pathogens. *Mol. cell* 9, 971–980. doi: 10.1016/s1097-2765(02)00529-4

Bondage, D. D., Lin, J. S., Ma, L. S., Kuo, C. H., and Lai, E. M. (2016). VgrG C terminus confers the type VI effector transport specificity and is required for binding with PAAR and adaptor-effector complex. *Proc. Nat. Acad. Sci. U. S. A.* 113, E3931–E3940. doi: 10.1073/pnas.1600428113

Boulant, T., Boudehen, Y. M., Filloux, A., Plesiat, P., Naas, T., and Dortet, L. (2018). Higher prevalence of PldA, a *Pseudomonas aeruginosa* trans-kingdom H2-Type VI secretion system effector, in clinical isolates responsible for acute infections and in multidrug resistant strains. *Front. Microbiol.* 9:2578. doi: 10.3389/fmicb.2018.02578

Browning, C., Shneider, M. M., Bowman, V. D., Schwarzer, D., and Leiman, P. G. (2012). Phage pierces the host cell membrane with the iron-loaded spike. *Structure* 20, 326–339. doi: 10.1016/j.str.2011.12.009

Brunet, Y. R., Henin, J., Celia, H., and Cascales, E. (2014). Type VI secretion and bacteriophage tail tubes share a common assembly pathway. *EMBO Rep.* 15, 315–321. doi: 10.1002/embr.201337936

Brunet, Y. R., Zoued, A., Boyer, F., Douzi, B., and Cascales, E. (2015). The type VI secretion TssEFGK-VgrG phage-like baseplate is recruited to the TssJLM membrane complex via multiple contacts and serves as assembly platform for tail tube/sheath polymerization. *PLoS Genet.* 11:e1005545. doi: 10.1371/journal.pgen.1005545

Burkinshaw, B. J., Liang, X., Wong, M., Le, A. N. H., Lam, L., and Dong, T. G. (2018). A type VI secretion system effector delivery mechanism dependent on PAAR and a chaperone-co-chaperone complex. *Nat. Microbiol.* 3, 632–640. doi: 10.1038/s41564-018-0144-4

Diniz, J. A., and Coulthurst, S. J. (2015). Intra-species competition in *Serratia marcescens* is mediated by type VI secretion Rhs effectors and a conserved effector-associated accessory protein. *J. Bacteriol.* 197, 2350–2360. doi: 10.1128/jb.00199-15

Durand, E., Nguyen, V. S., Zoued, A., Logger, L., Pehau-Arnaudet, G., Aschtgen, M. S., et al. (2015). Biogenesis and structure of a type VI secretion membrane core complex. *Nature* 523, 555–560. doi: 10.1038/nature14667

Durand, E., Zoued, A., Spinelli, S., Watson, P. J., Aschtgen, M. S., Journet, L., et al. (2012). Structural characterization and oligomerization of the TssL protein, a component shared by bacterial type VI and type IVb secretion systems. *J. Biol. Chem.* 287, 14157–14168. doi: 10.1074/jbc.M111.338731

Figurski, D. H., and Helinski, D. R. (1979). Replication of an origin-containing derivative of plasmid RK2 dependent on a plasmid function provided in trans. *Proc. Nat. Acad. Sci.U. S. A.* 76, 1648–1652. doi: 10.1073/pnas.76.4.1648

Flaugnatti, N., Le, T. T., Canaan, S., Aschtgen, M. S., Nguyen, V. S., Blangy, S., et al. (2015). A phospholipase a anti-bacterial T6SS effector interacts directly with the C-terminal domain of the VgrG spike protein for delivery. *Mol. Microbiol.* 99, 1099–1118. doi: 10.1111/mmi.13292

Hachani, A., Allsopp, L. P., Oduko, Y., and Filloux, A. (2014). The VgrG proteins are "á la carte" delivery systems for bacterial type VI effectors. *J. Biol. Chem.* 289, 17872–17884. doi: 10.1074/jbc.M114.563429

Hachani, A., Lossi, N. S., and Filloux, A. (2013). A visual assay to monitor T6SS-mediated bacterial competition. *J. Vis. Exp.* 73:e50103.

Hachani, A., Lossi, N. S., Hamilton, A., Jones, C., Bleves, S., Albesa-Jove, D., et al. (2011). Type VI secretion system in *Pseudomonas aeruginosa*: secretion and multimerization of VgrG proteins. *J. Biol. Chem.* 286, 12317–12327. doi: 10.1074/jbc.M110.193045

Herrero, M., de Lorenzo, V., and Timmis, K. N. (1990). Transposon vectors containing non-antibiotic resistance selection markers for cloning and stable chromosomal insertion of foreign genes in gram-negative bacteria. *J. Bacteriol.* 172, 6557–6567. doi: 10.1128/jb.172.11.6557-6567.1990

Jiang, F., Wang, X., Wang, B., Chen, L., Zhao, Z., Waterfield, N. R., et al. (2016). The *Pseudomonas aeruginosa* type VI secretion PGAP1-like effector induces host autophagy by activating endoplasmic reticulum stress. *Cell Rep.* 16, 1502–1509. doi: 10.1016/j.celrep.2016.07.012

Jiang, F., Waterfield, N. R., Yang, J., Yang, G., and Jin, Q. (2014). A *Pseudomonas aeruginosa* type VI secretion phospholipase D effector targets both prokaryotic and eukaryotic cells. *Cell Host Microbe* 15, 600–610. doi: 10.1016/j.chom.2014.04.010

Jones, C., Hachani, A., Manoli, E., and Filloux, A. (2013). An *rhs* gene linked to the second type VI secretion cluster is a feature of the *Pseudomonas aeruginosa* strain PA14. *J. Bacteriol.* 196, 800–810. doi: 10.1128/JB.00863-13

Kanamaru, S., Leiman, P. G., Kostyuchenko, V. A., Chipman, P. R., Mesyanzhinov, V. V., Arisaka, F., et al. (2002). Structure of the cell-puncturing device of bacteriophage T4. *Nature* 415, 553–557. doi: 10.1038/415553a

Kaniga, K., Delor, I., and Cornelis, G. R. (1991). A wide-host-range suicide vector for improving reverse genetics in gram-negative bacteria: inactivation of the blaA gene of Yersinia enterocolitica. *Gene* 109, 137–141. doi: 10.1016/0378-1119(91)90599-7

Kovach, M. E., Elzer, P. H., Hill, D. S., Robertson, G. T., Farris, M. A., Roop, R. M. II, et al. (1995). Four new derivatives of the broad-host-range cloning vector pBBR1MCS, carrying different antibiotic-resistance cassettes. *Gene* 166, 175–176. doi: 10.1016/0378-1119(95)00584-1

Leiman, P. G., Basler, M., Ramagopal, U. A., Bonanno, J. B., Sauder, J. M., Pukatzki, S., et al. (2009). Type VI secretion apparatus and phage tail-associated protein complexes share a common evolutionary origin. *Proc. Nat. Acad. Sci. U. S. A.* 106, 4154–4159. doi: 10.1073/pnas.0813360106

Liang, X., Moore, R., Wilton, M., Wong, M. J., Lam, L., and Dong, T. G. (2015).). Identification of divergent type VI secretion effectors using a conserved chaperone domain. *Proc. Nat. Acad. Sci. U. S. A* 112, 9106–9111. doi: 10.1073/pnas.1505317112

Lin, J., Zhang, W., Cheng, J., Yang, X., Zhu, K., Wang, Y., et al. (2017). A *Pseudomonas* T6SS effector recruits PQS-containing outer membrane vesicles for iron acquisition. *Nat. Commun.* 8:14888. doi: 10.1038/ncomms14888

Ma, A. T., McAuley, S., Pukatzki, S., and Mekalanos, J. J. (2009). Translocation of a *Vibrio cholerae* type VI secretion effector requires bacterial endocytosis by host cells. *Cell Host Microbe* 5, 234–243. doi: 10.1016/j.chom.2009.02.005

Ma, J., Pan, Z., Huang, J., Sun, M., Lu, C., and Yao, H. (2017). The Hcp proteins fused with diverse extended-toxin domains represent a novel pattern of antibacterial effectors in type VI secretion systems. *Virulence* 8, 1189–1202. doi: 10.1080/21505594.2017.1279374

Ma, L. S., Hachani, A., Lin, J. S., Filloux, A., and Lai, E. M. (2014). *Agrobacterium tumefaciens* deploys a superfamily of type VI secretion DNase effectors as weapons for interbacterial competition in planta. *Cell Host Microbe* 16, 94–104. doi: 10.1016/j.chom.2014.06.002

MacIntyre, D. L., Miyata, S. T., Kitaoka, M., and Pukatzki, S. (2010). The *Vibrio cholerae* type VI secretion system displays antimicrobial properties. *Proc. Nat. Acad. Sci. U. S. A.* 107, 19520–19524. doi: 10.1073/pnas.1012931107

Olson, J. C., and Ohman, D. E. (1992). Efficient production and processing of elastase and LasA by *Pseudomonas aeruginosa* require zinc and calcium ions. *J. Bacteriol.* 174, 4140–4147. doi: 10.1128/jb.174.12.4140-4147.1992

Pissaridou, P., Allsopp, L. P., Wettstadt, S., Howard, S. A., Mavridou, D. A. I., and Filloux, A. (2018). The *Pseudomonas aeruginosa* T6SS-VgrG1b spike is topped by a PAAR protein eliciting DNA damage to bacterial competitors. *Proc. Nat. Acad. Sci. U. S. A.* 115, 12519–12524. doi: 10.1073/pnas.1814181115

Planamente, S., Salih, O., Manoli, E., Albesa-Jove, D., Freemont, P. S., and Filloux, A. (2016). TssA forms a gp6-like ring attached to the type VI secretion sheath. *EMBO J.* 35, 1613–1627. doi: 10.15252/embj.201694024

Pukatzki, S., Ma, A. T., Revel, A. T., Sturtevant, D., and Mekalanos, J. J. (2007). Type VI secretion system translocates a phage tail spike-like protein into target cells where it cross-links actin. *Proc. Nat. Acad. Sci. U. S. A.* 104, 15508–15513. doi: 10.1073/pnas.0706532104

Pukatzki, S., Ma, A. T., Sturtevant, D., Krastins, B., Sarracino, D., Nelson, W. C., et al. (2006). Identification of a conserved bacterial protein secretion system in *Vibrio cholerae* using the dictyostelium host model system. *Proc. Nat. Acad. Sci. U. S. A.* 103, 1528–1533. doi: 10.1073/pnas.0510322103

Quentin, D., Ahmad, S., Shanthamoorthy, P., Mougous, J. D., Whitney, J. C., and Raunser, S. (2018). Mechanism of loading and translocation of type VI secretion system effector Tse6. *Nat. Microbiol.* 3, 1142–1152. doi: 10.1038/s41564-018-0238-z

Renault, M. G., Zamarreno Beas, J., Douzi, B., Chabalier, M., Zoued, A., Brunet, Y. R., et al. (2018). The gp27-like Hub of VgrG Serves as Adaptor to Promote Hcp Tube Assembly. *J. Mol. Biol.* 430(18 Pt B), 3143–3156. doi: 10.1016/j.jmb.2018.07.018

Russell, A. B., Hood, R. D., Bui, N. K., LeRoux, M., Vollmer, W., and Mougous, J. D. (2011). Type VI secretion delivers bacteriolytic effectors to target cells. *Nature* 475, 343–347. doi: 10.1038/nature10244

Russell, A. B., LeRoux, M., Hathazi, K., Agnello, D. M., Ishikawa, T., Wiggins, P. A., et al. (2013). Diverse type VI secretion phospholipases are functionally plastic antibacterial effectors. *Nature* 496, 508–512. doi: 10.1038/nature12074

Sana, T. G., Baumann, C., Merdes, A., Soscia, C., Rattei, T., Hachani, A., et al. (2015). Internalization of Pseudomonas aeruginosa strain PAO1 into epithelial cells is promoted by interaction of a T6SS effector with the microtubule network. *MBio* 6:e00712. doi: 10.1128/mBio.00712-15

Schmidt-Eisenlohr, H., Domke, N., and Baron, C. (1999). TraC of IncN plasmid pKM101 associates with membranes and extracellular high-molecular-weight structures in *Escherichia coli*. *J Bacteriol* 181, 5563–5571.

Shneider, M. M., Buth, S. A., Ho, B. T., Basler, M., Mekalanos, J. J., and Leiman, P. G. (2013). PAAR-repeat proteins sharpen and diversify the type VI secretion system spike. *Nature* 500, 350–353. doi: 10.1038/nature12453

Silverman, J. M., Agnello, D. M., Zheng, H., Andrews, B. T., Li, M., Catalano, C. E., et al. (2013). Haemolysin coregulated protein is an exported receptor and chaperone of type VI secretion substrates. *Mol. Cell* 51, 584–593. doi: 10.1016/j.molcel.2013.07.025

Spinola-Amilibia, M., Davo-Siguero, I., Ruiz, F. M., Santillana, E., Medrano, F. J., and Romero, A. (2016). The structure of VgrG1 from *Pseudomonas aeruginosa*, the needle tip of the bacterial type VI secretion system. *Acta. Crystallogr. D Struct. Biol.* 72, 22–33. doi: 10.1107/S2059798315021142

Sutherland, M. C., Nguyen, T. L., Tseng, V., and Vogel, J. P. (2012). The *Legionella* IcmSW complex directly interacts with DotL to mediate translocation of adaptor-dependent substrates. *PLoS Pathog.* 8:e1002910. doi: 10.1371/journal.ppat.1002910

Unterweger, D., Kostiuk, B., Otjengerdes, R., Wilton, A., Diaz-Satizabal, L., and Pukatzki, S. (2015). Chimeric adaptor proteins translocate diverse type VI secretion system effectors in *Vibrio cholerae*. *EMBO J.* 34, 2198–2210. doi: 10.15252/embj.201591163

Vasseur, P., Vallet-Gely, I., Soscia, C., Genin, S., and Filloux, A. (2005). The pel genes of the *Pseudomonas aeruginosa* PAK strain are involved at early and late stages of biofilm formation. *Microbiology* 151, 985–997. doi: 10.1099/mic.0.27410-0

Whitney, J. C., Beck, C. M., Goo, Y. A., Russell, A. B., Harding, B. N., De Leon, J. A., et al. (2014). Genetically distinct pathways guide effector export through the type VI secretion system. *Mol. Microbiol.* 92, 529–542. doi: 10.1111/mmi.12571

Whitney, J. C., Quentin, D., Sawai, S., LeRoux, M., Harding, B. N., Ledvina, H. E., et al. (2015). An interbacterial NAD(P)(+) glycohydrolase toxin requires elongation factor Tu for delivery to target cells. *Cell* 163, 607–619. doi: 10.1016/j.cell.2015.09.027

Zhao, Z., Sagulenko, E., Ding, Z., and Christie, P. J. (2001). Activities of virE1 and the VirE1 secretion chaperone in export of the multifunctional VirE2 effector via an *Agrobacterium* type IV secretion pathway. *J. Bacteriol.* 183, 3855–3865. doi: 10.1128/jb.183.13.3855-3865.2001

Conflict of Interest Statement: The authors declare that the research was conducted in the absence of any commercial or financial relationships that could be construed as a potential conflict of interest.

Copyright © 2019 Wettstadt, Wood, Fecht and Filloux. This is an open-access article distributed under the terms of the Creative Commons Attribution License (CC BY). The use, distribution or reproduction in other forums is permitted, provided the original author(s) and the copyright owner(s) are credited and that the original publication in this journal is cited, in accordance with accepted academic practice. No use, distribution or reproduction is permitted which does not comply with these terms.

frontiers in Microbiology

ORIGINAL RESEARCH
published: 13 September 2019
doi: 10.3389/fmicb.2019.02128

Life After Secretion—*Yersinia enterocolitica* Rapidly Toggles Effector Secretion and Can Resume Cell Division in Response to Changing External Conditions

*Bailey Milne-Davies, Carlos Helbig, Stephan Wimmi, Dorothy W. C. Cheng†, Nicole Paczia and Andreas Diepold**

Department of Ecophysiology, Max Planck Institute for Terrestrial Microbiology, Marburg, Germany

OPEN ACCESS

Edited by:
Eric Cascales, Aix-Marseille Université, France

Reviewed by:
Luís Jaime Mota, New University of Lisbon, Portugal
Victoria Auerbuch, University of California, Santa Cruz, United States

***Correspondence:**
Andreas Diepold andreas.diepold@mpi-marburg.mpg.de

†Present address:
Dorothy W. C. Cheng, Department of Chemistry, Reed College, Portland, OR, United States

Specialty section:
This article was submitted to Microbial Physiology and Metabolism, a section of the journal Frontiers in Microbiology

Received: *04 March 2019*
Accepted: *29 August 2019*
Published: *13 September 2019*

Citation:
Milne-Davies B, Helbig C, Wimmi S, Cheng DWC, Paczia N and Diepold A (2019) Life After Secretion—Yersinia enterocolitica Rapidly Toggles Effector Secretion and Can Resume Cell Division in Response to Changing External Conditions. Front. Microbiol. 10:2128. doi: 10.3389/fmicb.2019.02128

Many pathogenic bacteria use the type III secretion system (T3SS) injectisome to manipulate host cells by injecting virulence-promoting effector proteins into the host cytosol. The T3SS is activated upon host cell contact, and its activation is accompanied by an arrest of cell division; hence, many species maintain a T3SS-inactive sibling population to propagate efficiently within the host. The enteric pathogen *Yersinia enterocolitica* utilizes the T3SS to prevent phagocytosis and inhibit inflammatory responses. Unlike other species, almost all *Y. enterocolitica* are T3SS-positive at 37°C, which raises the question, how these bacteria are able to propagate within the host, that is, when and how they stop secretion and restart cell division after a burst of secretion. Using a fast and quantitative *in vitro* secretion assay, we have examined the initiation and termination of type III secretion. We found that effector secretion begins immediately once the activating signal is present, and instantly stops when this signal is removed. Following effector secretion, the bacteria resume division within minutes after being introduced to a non-secreting environment, and the same bacteria are able to re-initiate effector secretion at later time points. Our results indicate that *Y. enterocolitica* use their type III secretion system to promote their individual survival when necessary, and are able to quickly switch their behavior toward replication afterwards, possibly gaining an advantage during infection.

Keywords: bacterial protein secretion, host-pathogen interaction, regulation of virulence mechanisms, protein translocation, *Yersinia enterocolitica*, enteropathogens

INTRODUCTION

Bacteria use their type III secretion systems (T3SS) in a variety of ways to survive in different environments. The virulence-associated T3SS[1] is a membrane-spanning nanosyringe that is used by various Gram-negative bacteria to export effector proteins into the cytoplasm of eukaryotic host cells, allowing them to modify host cell behavior (Cornelis, 2006; Galán, 2009; Pha, 2016).

[1]In this manuscript, T3SS refers to virulence-associated T3SS. The common "Sct" nomenclature (Hueck, 1998; Portaliou et al., 2016) is used for T3SS components, see (Diepold and Wagner, 2014) for species-specific names.

The T3SS protein complex, commonly named the injectisome, is comprised of an extracellular needle, a series of membrane rings embedding an export apparatus, and several cytosolic components (**Figure 1A**). The needle creates a continuous channel that connects the bacterium to the host cytoplasm with the help of translocator proteins that form a needle tip and a pore within the host cell membrane (Håkansson et al., 1996; Nauth et al., 2018; Park et al., 2018), thus allowing the translocation of effector proteins. The membrane rings anchor the injectisome in the peptidoglycan and the inner and outer membrane, while the export apparatus facilitates the transfer of effectors from the bacterial cytosol through the needle (Kuhlen et al., 2018). The cytosolic components, which shuttle between the cytosol and the injectisome, bind to chaperone-effector complexes and govern the order of secretion (Akeda and Galán, 2005; Lara-Tejero et al., 2011; Diepold et al., 2015). During the assembly and function of the T3SS, three substrate classes are subsequently exported. The early substrates include the needle subunit and a ruler protein that determines the length of the needle. Once the correct needle length is reached, the hydrophilic translocator, classified as intermediate substrate, is exported and assembles a needle tip (Mueller et al., 2005). At this stage, the T3SS is in a standby mode (Enninga and Rosenshine, 2009), and secretion of the late substrates, the pore-forming hydrophobic translocators and the virulence effectors, can be induced, for example by host cell contact.

Pathogens including *Salmonella*, *Shigella, Pseudomonas*, and *Yersinia* use their T3SS to promote survival and enhance pathogenicity within the host (Büttner, 2012; Deng et al., 2017). In some pathogenic species, such as *Salmonella enterica* and *Pseudomonas aeruginosa*, T3SS are heterogeneously expressed resulting in two subpopulations (Rietsch and Mekalanos, 2006; Sturm et al., 2011; Rundell et al., 2016). The resulting mixed populations can allow bacteria that express the T3SS to promote the survival of their siblings that do not. This is evident for the T3SS encoded by the *Salmonella* pathogenicity island (SPI)-1, where bacteria utilize their T3SS to promote entry into host cells, but also to induce inflammation of the intestinal lumen and remove competition of the intestinal flora (Stecher et al., 2007; Müller et al., 2009; Knodler et al., 2010; Behnsen et al., 2014). The SPI-1-utilizing bacteria display a retarded growth rate, which is a common trait of actively type III-secreting bacteria (Kupferberg and Higuchi, 1958; Mehigh et al., 1989; Fowler and Brubaker, 1994; Sturm et al., 2011). As a result, bacteria that do not express their T3SS outgrow the SPI-1-active population, which can be interpreted as an investment of the SPI-1-active bacteria into increased chances for their genetically identical SPI-1-inactive siblings (Sturm et al., 2011; Diard et al., 2013; Sánchez-Romero and Casadesús, 2018; Weigel and Dersch, 2018).

Yersinia enterocolitica is considered a largely extracellular pathogen that uses its T3SS mainly to prevent phagocytosis, inhibit inflammatory responses and promote dissemination (Navarro et al., 2005; Cornelis, 2006; Galán, 2009; Pha, 2016). Once *Yersinia* are exposed to a temperature of 37°C (e.g., after entering a host organism), they start expressing T3SS components (Skurnik et al., 1984; Lambert de Rouvroit et al., 1992). During infection, *Y. enterocolitica* can come into contact with host cells, such as macrophages, dissociate, and possibly establish contact with further host cells. Contact with a host cell activates the secretion of effectors, called Yops (*Yersinia* outer proteins), by the T3SS (Cornelis, 2002). *In vitro*, this activation can be achieved by the chelation of calcium (Ca^{2+}) from the extracellular environment. Under these conditions, the bacteria begin exporting their effectors and upregulate effector expression (Cornelis et al., 1987; Wiley et al., 2007; Dewoody et al., 2013). In this study, we used strains based on wild-type *Y. enterocolitica* expressing all virulence effectors (MRS40), as well as on a strain lacking the six main virulence effectors YopH,O,P,E,M,T, as well as the aspartate-beta-semialdehyde dehydrogenase gene (ΔHOPEMTasd), which is consequently avirulent, auxotrophic for the cell wall component diaminopimelic acid, and can be analyzed under safety class 1 conditions.

Prior studies have mainly focused on the activation of the T3SS by host cell contact or Ca^{2+} chelation. However, the post-secretion events like deactivation, reestablishment of bacterial division and the possibility of reactivation of the T3SS are likely to play an equally essential role in promoting bacterial survival and pathogenesis within the host. We therefore used a fast and quantitative *in vitro* secretion assay to examine the initiation and termination of type III secretion in *Y. enterocolitica*, monitored the rate of cell growth and division throughout these steps, and assessed whether previously T3SS-active bacteria can initiate further secretion events. Our results show that activation and deactivation occur immediately in response to changing external conditions, and that after secretion, bacteria transition back to division within short time, while remaining able to reactivate their T3SS.

RESULTS

Expression and Assembly of the *Y. enterocolitica* T3SS Is Uniform and Stable Under Different Conditions

Earlier visualizations of T3SS components within *Y. enterocolitica* showed that most bacteria express T3SS, which are localized in a non-random pattern of small patches visible as fluorescent foci at the bacterial surface (Diepold et al., 2010, 2017; Kudryashev et al., 2015). To quantify the fraction of T3SS-positive *Y. enterocolitica*, we analyzed how many bacteria within a population displayed this standard pattern of fluorescence for functional EGFP-labeled versions of a T3SS inner membrane ring protein (SctD), and a cytosolic protein (SctQ) at 37°C. Both under non-secreting conditions (presence of 5 mM Ca^{2+} in the medium) and secreting conditions (chelation of Ca^{2+} by addition of 5 mM EGTA), all or almost all bacteria were T3SS-positive (**Figure 1B**, **Supplementary Figure 1**). Even after long-term incubation under secreting conditions for 3 h, the vast majority of bacteria (>98%) were T3SS-positive (**Figure 1C**).

Activation Kinetics of the *Y. enterocolitica* T3SS by Ca^{2+} Chelation

The previous results showed that *Y. enterocolitica* populations almost uniformly assemble T3SS injectisomes. We next analyzed

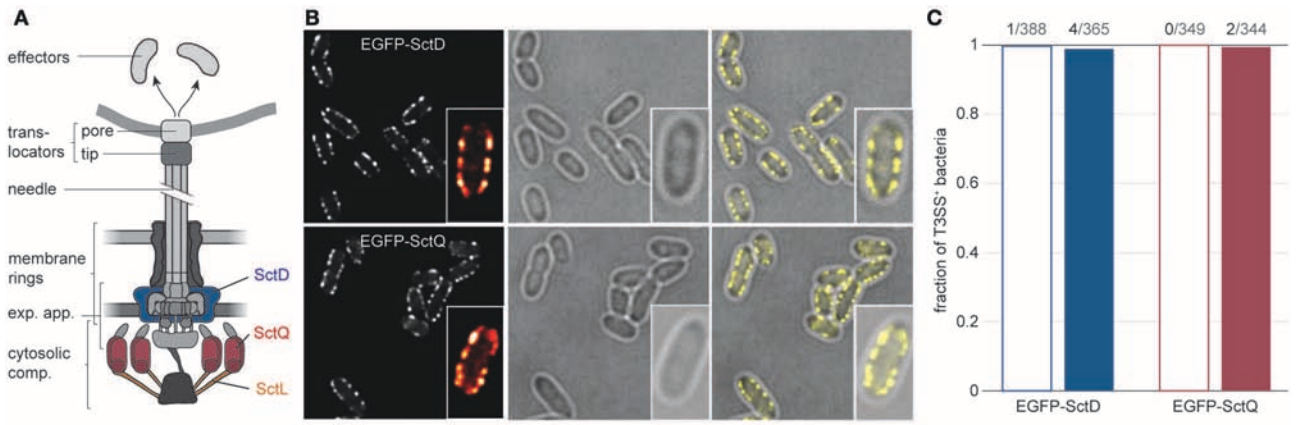

FIGURE 1 | The type III secretion system is expressed in almost all *Y. enterocolitica*, both under secreting and non-secreting conditions. **(A)** Schematic overview of the different substructures of the T3SS (left). Positions of the labeled proteins analyzed in this study are indicated (right). exp. app, export apparatus. **(B)** Micrographs of *Y. enterocolitica* ΔHOPEMTasd expressing EGFP-SctD (top) or EGFP-SctQ (bottom) from their native genetic localization. Three hours after induction of T3SS expression by temperature shift to 37°C under non-secreting conditions, bacteria were subjected to secreting conditions, and imaged. Left, EGFP fluorescence (insets show fluorescence intensity for one enlarged bacterium in ImageJ red-hot coloring scale); center, corresponding phase contrast images; right, overlay. Larger fields of view and images of bacteria under non-secreting conditions are shown in **Supplementary Figure 1**. **(C)** Fraction of bacteria with standard expression and distribution of T3SS (multiple membrane foci) for the indicated fusion protein, 3 h after induction of expression of the T3SS under non-secreting conditions (empty bars) or secreting conditions (filled bars) $n = 344–388$. Numbers on top indicate the number of bacteria that do not display multiple visible T3SS, and the number of analyzed bacteria. Secreting and non-secreting conditions refer to incubation in medium with addition of 5 mM EGTA or $CaCl_2$, respectively.

the activation and deactivation of these injectisomes in more detail, using an improved version of a previously published enzymatic export assay (Diepold et al., 2015), which measures the export of the reporter construct $YopH_{1-17}$-β-lactamase (Charpentier and Oswald, 2004; Marketon et al., 2005). The updated protocol utilizes the pACYC184 plasmid instead of pBAD, which removes background β-lactamase activity (**Supplementary Figure 2A**). The higher signal/noise ratio of the modified assay allowed us to reliably quantify secretion in intervals of down to 5 min, and we confirmed that the enzymatic assay itself is not strongly influenced by the used concentration of $CaCl_2$ or EGTA (**Supplementary Figure 2B**). We therefore were able to quantify the initiation of secretion in *Y. enterocolitica* ΔHOPEMTasd within the first 15 min after Ca^{2+} chelation. Within this time range, secretion is difficult to quantify even in an accumulative standard *in vitro* secretion assay (**Figure 2A**). For the reporter export assay, bacteria were grown at 37°C under non-secreting conditions, allowing for assembly, but not activation of T3SS. Secretion was then activated by resuspension in medium lacking Ca^{2+} and samples were taken every 5 min, and tested for export of the reporter substrate into the supernatant within the following 5 min. The results of the reporter assay clearly show that secretion is fully active at the earliest time range after activation (0–5 min) (**Figure 2B**), suggesting that effector secretion is initiated immediately by Ca^{2+} chelation. To test whether this fast activation of effector secretion impacts the cellular ATP levels, we determined the adenylate energy charge (([ATP]+0.5[ADP])/([ATP]+[ADP]+[AMP])) of wild-type *Y. enterocolitica* ΔHOPEMTasd, incubated under the same conditions, 10 min after activation of the T3SS. We found that the energy charge of the secreting cultures was not significantly decreased in this time range (**Supplementary Figure 3**). In line with these findings, the level of secretion of the reporter substrate remained constant throughout the first 2 h after secretion (**Figure 2B**, **Supplementary Figure 4** and data not shown). Secretion activity in a freshly activated wild-type strain was comparable to that of a SctW (YopN) deletion strain, which is calcium-blind and continuously secretes effectors (**Supplementary Figure 4**), underlining that the level of protein secretion immediately after activation is comparable to the level during ongoing secretion.

T3SS Effector Secretion Ceases Within Minutes After Removal of the Activating Signal

Next, we measured if and how fast the T3SS is inactivated upon reintroduction of Ca^{2+} into the medium. Wild-type *Y. enterocolitica* that had been secreting for 2 h were subjected to non-secreting medium, and the export of the reporter substrate was measured in 10-min intervals afterwards. Already within the first period after Ca^{2+} addition, the export of the reporter strongly dropped compared to the control that was left under secreting conditions (**Figure 3A**, **Supplementary Figure 4**). Based on the amount of exported reporter substrate under non-secreting conditions over time (green bars in **Figure 3A**), deactivation is likely to occur within the first minutes after the removal of the activating signal. Similar to the activation, deactivation of secretion did not increase the energy charge of the bacteria within these time ranges (**Supplementary Figure 3**).

To further investigate the inactivation of secretion, we aimed to determine, which factor, temperature or Ca^{2+} concentration, has a greater effect on the export of different substrate classes.

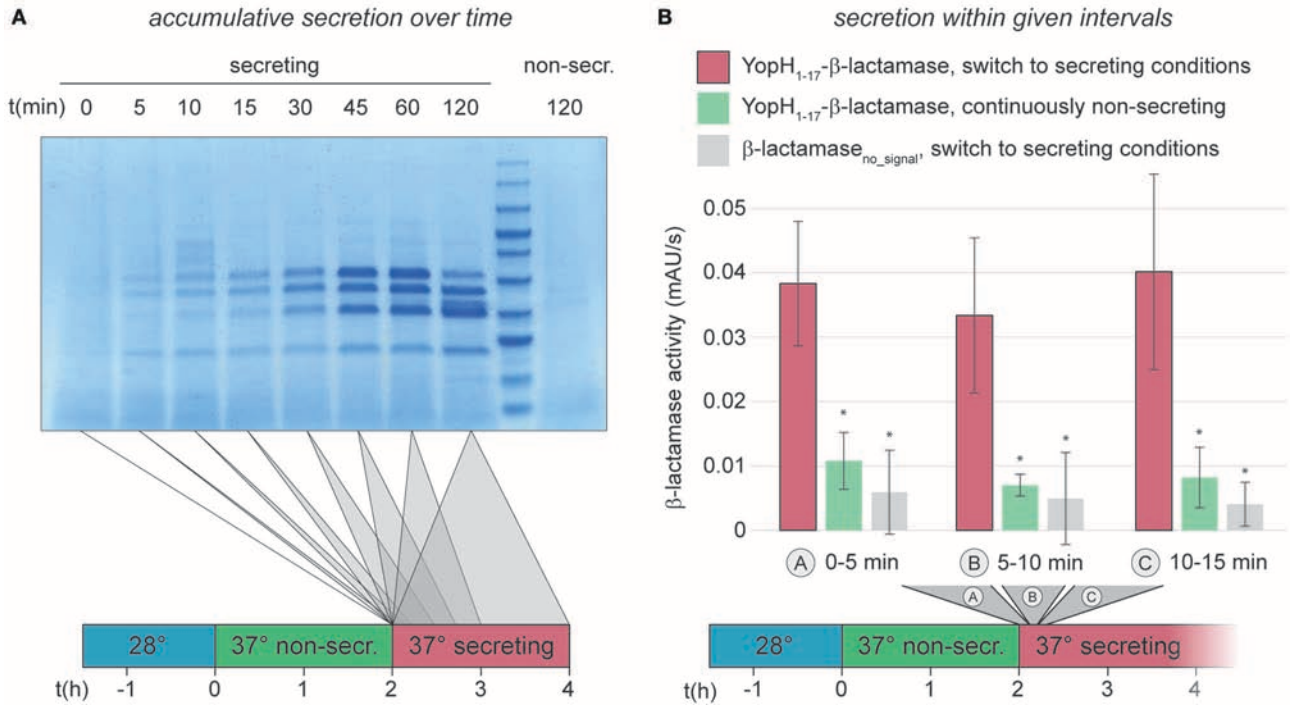

FIGURE 2 | Immediate activation of the T3SS can be measured by an *in vitro* β-lactamase assay. **(A)** Accumulative effector secretion into the culture supernatant during a standard *in vitro* secretion assay using *Y. enterocolitica* MRS40. At the time points indicated (0 min = activation of T3SS secretion by resuspension of bacteria in secreting medium, see also time line at bottom), the culture supernatant of 3×10^9 bacteria was removed and visualized by Coomassie staining of an SDS-PAGE gel. Control (far right), bacteria resuspended in non-secreting medium. **(B)** Quantification of effector export in the indicated time ranges after resuspension of *Y. enterocolitica* ΔHOPEMTasd in secreting medium (see also time line at bottom). Red bars, β-lactamase activity indicative of export of the reporter T3SS substrate $YopH_{1-17}$-β-lactamase; green bars, non-secreting control; gray bars, β-lactamase lacking a T3SS secretion signal under secreting conditions. Error bars indicate standard deviation of the averages of technical triplicates between three biological replicates. *$p < 0.05$ vs. the $YopH_{1-17}$-β-lactamase, switch to secreting conditions, sample (red bars) in a two-tailed homoscedastic *t*-test. Secreting and non-secreting (non-secr.) conditions refer to incubation in medium with addition of 5 mM EGTA or $CaCl_2$, respectively.

We therefore analyzed the export of virulence effectors (YopE and YopM), the needle protein SctF, the hydrophilic translocator SctA (=LcrV), and the ruler protein SctP in a wild-type strain expressing all virulence effectors (MRS40). Cultures were grown in secreting conditions and after 3 h, the previously secreting cultures were exposed to non-secreting or secreting conditions, at 26 or 37°C. Our results show that while export of the virulence effectors was strongly repressed by the addition of Ca^{2+}, they were secreted in the absence of Ca^{2+}, irrespective of the temperature (**Figures 3B,C**). Export of the needle, translocator and ruler protein, in contrast, was more strongly influenced by the temperature than by the Ca^{2+} level, although this effect was not statistically significant for SctF and SctP (**Figures 3B,C**). The resuspension steps used in our protocol do not affect assembled needles, and in all cases, cell lysis was negligible; differences in expression levels cannot explain the observed export phenotype (**Supplementary Figures 5–7**).

Y. enterocolitica Can Resume Growth or Engage in New Secretion Activity After Secretion Has Ended

Having analyzed the activation and deactivation of type III secretion by external signals, we turned our interest to the events after secretion. Specifically, we wanted to find out whether and when post-secretion *Y. enterocolitica* can resume division and/or re-initiate secretion. To answer the first question, we compared the optical culture density of wild-type *Y. enterocolitica* (MRS40) bacteria that had previously been secreting, and were then either kept under secreting conditions, or subjected to non-secreting conditions. Compared to the non-secreting control, secreting bacteria slow down their division (**Figures 4A,B**, "first incubation"). Strikingly, previously secreting bacteria that were subjected to non-secreting conditions resumed division within a short time (**Figures 4A,B**, "second incubation"). This phenotype is linked to T3SS activity, as indicated by the steady division of T3SS-negative ΔSctD bacteria under all tested conditions (**Figures 4A,B**). As expected, constantly secreting bacteria (the "Ca^{2+} blind" ΔSctW (ΔYopN) strain (Yother and Goguen, 1985), **Supplementary Figure 7**) displayed growth curves similar to wild-type under secreting conditions, irrespective of the medium. Similar results were obtained on solid medium, where T3SS-positive bacteria did not divide, and only slightly increased their cell volume, under sustained secreting conditions, in contrast to T3SS-negative bacteria (**Figure 4C**, **Supplementary Figure 8**). Under non-secreting conditions, both populations displayed a higher rate of growth and division

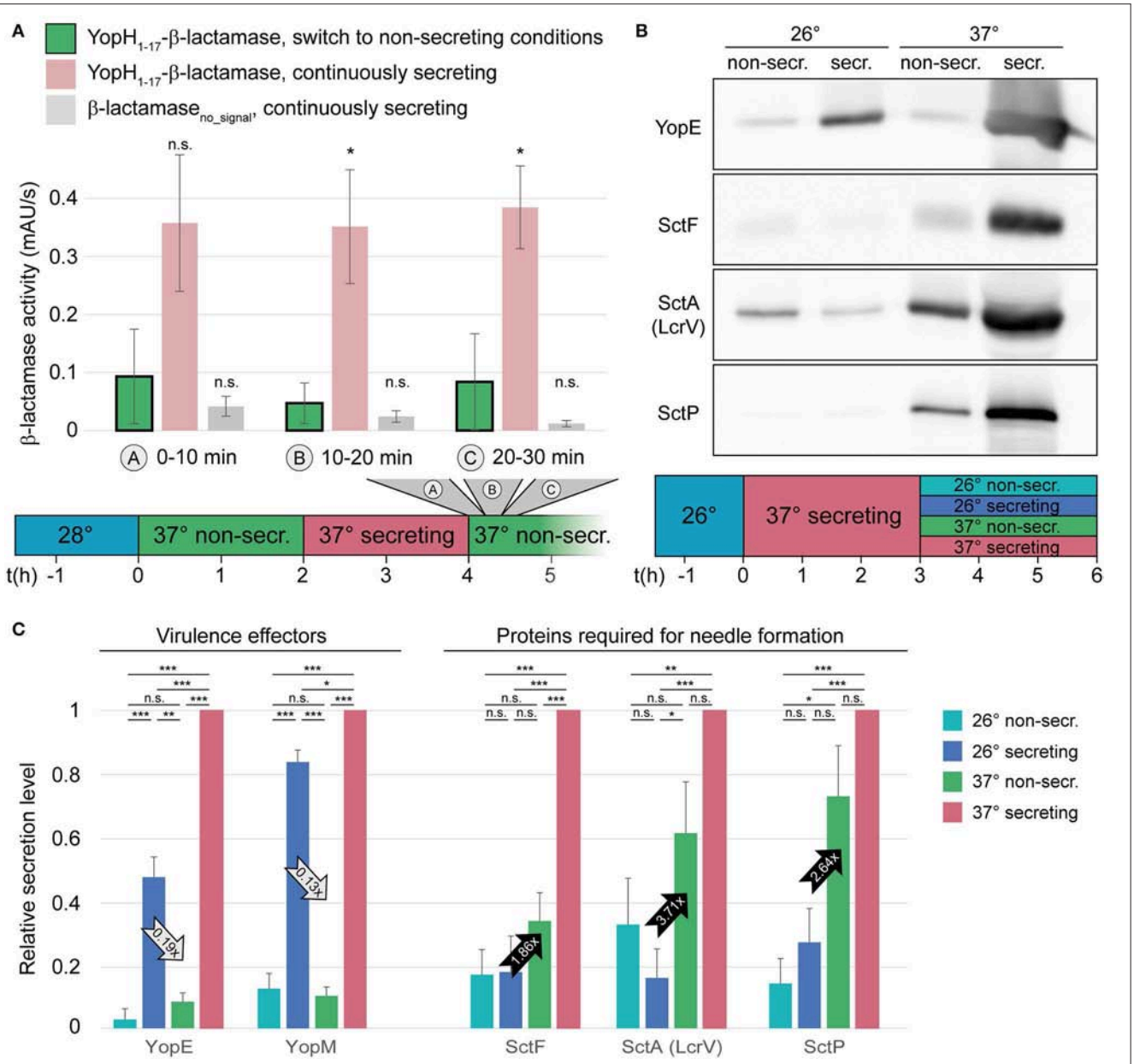

FIGURE 3 | Type III secretion, but not needle formation, is stopped within short time in the absence of activating signal. **(A)** Quantification of effector export in the indicated time ranges after resuspension of *Y. enterocolitica* ΔHOPEMTasd in non-secreting medium (see also time line at bottom). Green bars, β-lactamase activity indicative of export of the reporter T3SS substrate $YopH_{1-17}$-β-lactamase; red bars, secreting control; gray bars, β-lactamase lacking a T3SS secretion signal under secreting conditions. Error bars indicate standard deviation of the averages of technical triplicates between three biological replicates. $^*p < 0.05$ vs. the $YopH_{1-17}$-β-lactamase, switch to non-secreting conditions, sample in a two-tailed homoscedastic *t*-test; n.s., difference not statistically significant. **(B)** The export of different substrate classes is influenced differently by the temperature and the external calcium concentration. Wild-type *Y. enterocolitica* expressing all effectors (MRS40) were grown at 26°C for 1.5 h, and subsequently at 37°C under secreting conditions for 3 h. Afterwards, they were resuspended in different conditions, as indicated (top and time line at bottom) for another 3 h. Proteins secreted by 3×10^9 bacteria were separated on an SDS-PAGE gel and analyzed by immunoblot using antibodies against the indicated proteins, the effector YopE, the needle subunit SctF, the hydrophilic translocator SctA (LcrV), and the ruler protein SctP ($n = 4$, image representative). The respective analysis for bacteria directly subjected to the indicated conditions after incubation at 26°C, Coomassie-based analysis of all secreted proteins, and protein expression controls are displayed in **Supplementary Figure 6**. **(C)** Relative secretion levels of indicated virulence effectors (left) and proteins required for needle export (right) under the indicated conditions [see time line in **(B)**]. Secretion levels were quantified by densitometric analysis of the bands for the respective proteins in Coomassie-stained SDS-PAGE gels for YopE and YopM ($n = 3$) and immunoblots for YopE (one additional analysis), SctF, SctA (LcrV), and SctP ($n = 4$ in each case), and normalized to the respective secretion level at 37°C under secreting conditions. Error bars display the standard error of the mean; arrows indicate the difference between the influence of the temperature (28°C, secreting conditions) and calcium levels (37°C, non-secreting conditions) and the ratio of secretion under these conditions. Secreting and non-secreting (non-secr.) conditions refer to incubation in medium with addition of 5 mM EGTA or $CaCl_2$, respectively. $^*p < 0.05$, $^{**}p < 0.01$, $^{***}p < 0.001$ in a two-tailed homoscedastic *t*-test; n.s., difference not statistically significant.

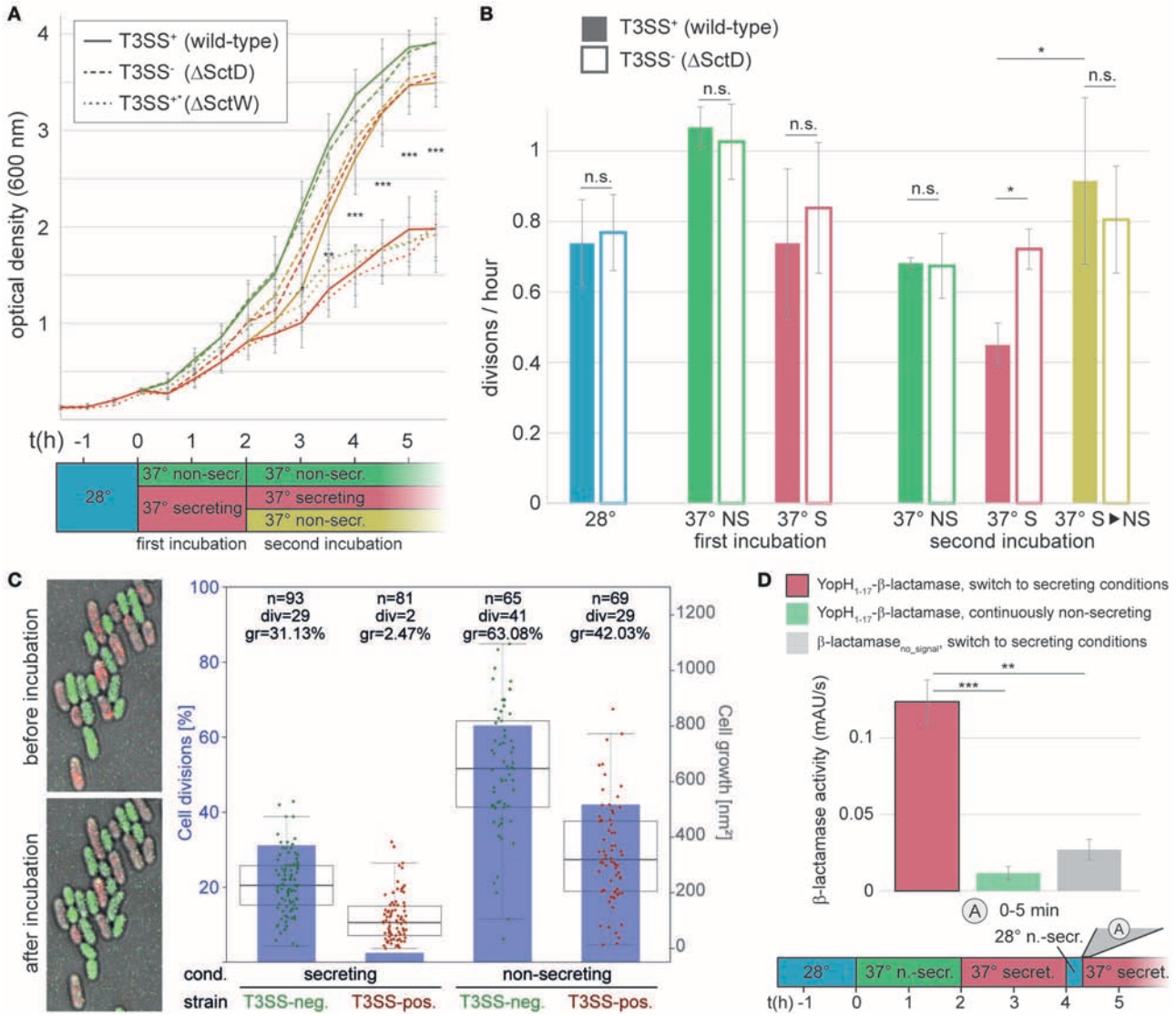

FIGURE 4 | Bacteria can resume division, or engage in another round of secretion after deactivation of secretion. **(A)** Growth curves (optical culture density at 600 nm) of T3SS-positive *Y. enterocolitica* wild-type MRS40 expressing all virulence effectors ($T3SS^+$, continuous lines), T3SS-negative bacteria ($T3SS^-$, dashed lines), and Ca^{2+}-blind constantly secreting bacteria ($T3SS^{+*}$, dotted lines) incubated under the conditions indicated in the time line (bottom). **(B)** Number of bacterial divisions per hour during the different phases, colors as in **(A)**. Filled bars, T3SS-positive bacteria; open bars, T3SS-negative bacteria. Error bars indicate the standard deviation of the averages of technical triplicates between three independent biological replicates. **(C)** Growth and division of T3SS-positive (mCherry-SctL, red) and T3SS-negative (EGFP-SctL ΔSctD, green) *Y. enterocolitica* ΔHOPEMTasd on LB-agarose pads under secreting conditions during the first 2 h of the second incubation period [see **(A)**]. Left, fluorescence micrographs showing growth and division of green (T3SS-negative), but not of red (T3SS-positive) bacteria within the analysis period. Right, quantification of fraction of cell divisions (blue bars and axis on left side) and cell growth (increase in two-dimensional cell area on micrographs) per initial bacterium (box charts and single data points, right axis) for the indicated strains and conditions. Each data point represents a single measurement. The boxes show the median and quartiles (75th and 25th percentile). The whiskers extend 1.5 times the interquartile range until the furthest data point within this range. No standard deviation is displayed. n, number of analyzed bacteria; div, number of bacteria dividing within analysis period; gr, average growth (increase of cell area) within analysis period. Cell growth is statistically significantly different ($p < 0.001$ in a two-tailed homoscedastic *t*-test) for all pairwise comparisons of strains and conditions. **(D)** Quantification of effector export in the indicated time range after resuspension of *Y. enterocolitica* ΔHOPEMTasd in secreting medium after a 15 min incubation in non-secreting medium at 28°C (see time line at bottom). Red bar, β-lactamase activity indicative of export of the reporter T3SS substrate $YopH_{1-17}$-β-lactamase; green bar, non-secreting control; gray bar, β-lactamase lacking a T3SS secretion signal under secreting conditions. Error bars indicate standard deviation of the averages of technical triplicates between three biological replicates. Secreting and non-secreting conditions refer to incubation in medium with addition of 5 mM EGTA or $CaCl_2$, respectively. The incubation steps at 28°C (blue bars) are performed in medium with 5 mM $CaCl_2$. *$p < 0.05$; **$p < 0.01$; ***$p < 0.001$ in a two-tailed homoscedastic *t*-test; n.s., difference not statistically significant. For **(A)**, this statistical analysis applies to the difference between wild-type and ΔSctD under secreting conditions (continuous and dashed red lines), other time points were not statistically significantly different.

(**Figure 4C**, **Supplementary Figure 8**). Taken together, these results indicate that individual *Y. enterocolitica* cells not only can disengage from secretion within a short time, but also quickly resume division in the absence of further stimulating signals.

To determine if *Y. enterocolitica* can also go through repeated cycles of secretion activation and deactivation, we tested the reactivation of secretion in bacteria that had been secreting for 2 h, and where secretion was stopped afterwards by addition of $CaCl_2$. These bacteria were incubated in the presence of Ca^{2+} for 15 min at 28°C to suppress the formation of new injectisomes (**Figure 3B**), and then again subjected to secreting conditions (37°C, absence of Ca^{2+}). The secretion of effectors started within the first 5 min after the renewed incubation under secreting conditions (**Figure 4D**), which shows that type III secretion can be reactivated, and that this occurs within a similarly short time as the initial activation of secretion.

DISCUSSION

Life after secretion—the deactivation of the T3SS, the recovery of division, and possible additional encounters with host cells—is incompletely understood in *Yersinia*, despite the critical role of these events in the infection process. In this study, we therefore explored the kinetics of activation and, most crucially, deactivation of secretion by external cues, as well as the potential of *Y. enterocolitica* to restart division and to re-initiate secretion afterwards. During infection, when *Y. enterocolitica* enter the Peyer's Patches, bacteria may come into contact with immune cells. In this situation, fast initiation of effector export provides essential defense against phagocytosis and inflammatory signals to the immune system (Grosdent et al., 2002; Navarro et al., 2005; Galán, 2009; Pha, 2016; Philip et al., 2016). Such fast activation of type III secretion has indeed been shown for various bacteria (Enninga et al., 2005; Schlumberger et al., 2005; Mills et al., 2008). Following the interaction with the host, however, *Y. enterocolitica* conceivably benefit from stopping effector export, which may allow them to resume division and disseminate within the host (where the bacteria may again face contact with immune cells). To study T3SS activation and deactivation kinetics in a fast, reproducible and quantitative manner, we used an *in vitro* secretion assay for the reporter substrate β-lactamase in *Y. enterocolitica*, fused to the minimal secretion signal for the native *Y. enterocolitica* virulence effector YopH (Sory et al., 1995). Low and high calcium levels, as used in the assay, have been proposed to mimic the intracellular environment within host cells (low Ca^{2+}), and the extracellular host environment (high Ca^{2+}), respectively (Fowler and Brubaker, 1994). Our results show that just like activation of secretion (**Figure 2**), deactivation (**Figure 3A**) occurs immediately when introduced into secreting or non-secreting media, respectively.

The ability of *Y. enterocolitica* to respond quickly to these external stimuli suggests one or several highly sensitive regulation mechanisms. How exactly host cell contact and changes in the environment, such as the Ca^{2+} levels, are sensed, is still unclear. A number of studies, predominantly performed in *Shigella flexneri* and *Pseudomonas aeruginosa*, suggest that the needle tip senses host cell contact (Veenendaal et al., 2007; Roehrich et al., 2013; Armentrout and Rietsch, 2016), and that the signal is transmitted through rearrangements of the needle subunits to the cytosolic interface of the T3SS (Kenjale et al., 2005; Torruellas et al., 2005; Davis and Mecsas, 2006). Other external factors, such as the Ca^{2+} level and factors inducing other T3SS such as Congo Red might also be sensed at the needle tip and be transmitted the same way. However, the composition of the cytosolic complex of the *Y. enterocolitica* T3SS was shown to be influenced by external Ca^{2+} levels in strains lacking SctD (and therefore also not assembling needles), suggesting a direct sensing mechanism (Diepold et al., 2017). The Ca^{2+}-dependent interaction of the ruler SctP and the cytosolic gatekeeper protein SctW in enteropathogenic *E. coli* (EPEC) supports yet another model in which the export of effectors is inhibited as long as a local influx of Ca^{2+} ions occurs through T3SS needles which are not in contact to a host cell (Shaulov et al., 2017).

Notably, in our deactivation experiments, not all substrate classes were affected equally by the Ca^{2+} level. While export of the tested effectors (YopE and YopM) was strongly suppressed upon addition of Ca^{2+}, the export of early and intermediary substrates, required for the formation of new needles, continued, albeit at a lower rate. In contrast, a reduction of the temperature to 26°C at continuous low Ca^{2+} levels strongly decreased the export of early and intermediary substrates, but allowed the continued export of the effectors (**Figure 3B**). This phenotype is most likely not a mere effect of the expression levels of the exported proteins: While the initial expression of all T3SS export substrates is strongly regulated by the temperature, as a consequence of the temperature-dependent expression of the main transcriptional regulator of the T3SS, VirF (Cornelis et al., 1989; Hoe and Goguen, 1993; Böhme et al., 2012), this effect is far less pronounced in a system that has previously been activated by incubation at 37°C under secreting conditions (**Supplementary Figures 6A,B**). This indicates that in the latter case, mRNA and proteins levels are sufficient for continuous effector secretion at low Ca^{2+} levels, even at 26°C. The secretion of the proteins required for needle formation is more strongly repressed at 26°C (although this effect is only statistically significant for SctA=LcrV), suggesting that the inhibition of the secretion of needle-related proteins and effectors are controlled by additional, and different, regulatory pathways. A similar differential regulation of secretion of the different substrate classes has been shown for *P. aeruginosa* (Cisz et al., 2008) and EPEC (Shaulov et al., 2017), suggesting that this mechanism is conserved amongst different T3SS.

Regulating the events after secretion is particularly important for *Y. enterocolitica*, which differ from other pathogens in that they homogeneously express the T3SS when exposed to 37°C (**Figure 1**, **Supplementary Figure 1**), and that the complete population can activate secretion *in vitro* (Wiley et al., 2007). The low fraction of T3SS-negative bacteria even after prolonged *in vitro* secretion (**Figure 1C**), despite the lower replication rate of these bacteria, highlights the important role of T3SS function during infection in *Y. enterocolitica*. What then happens after a bacterium has survived an encounter with an immune cell? Once effector secretion has ceased, *Y.*

enterocolitica benefit from re-initiating faster replication, but have to remain guarded for additional interactions with immune cells. It has been an open question whether re-initiation of replication can be observed *in vitro*, where all injectisomes are activated (Wiley et al., 2007), which might differ from the situation during an infection (Heroven and Dersch, 2014; Avican et al., 2015). We found that *Y. enterocolitica* can quickly resume division when exposed to a non-secreting environment after prior incubation in a secretion-activating environment (**Figures 4A–C**). This recovery (as well as the cessation of growth and division upon secretion initiation) appears independent of the cellular energy levels, which did not significantly drop under secreting conditions within the tested time range in the used effector-less strain (**Supplementary Figure 3**). At this point, renewed contact with host cells, especially immune cells, is possible. We have shown that accordingly, previously secreting *Y. enterocolitica* continue to assemble new needles (**Figure 3B**), and that reactivation of the T3SS is possible and occurs immediately when introduced from non-secreting media back into secreting media (**Figure 4D**). Reestablishing secretion likely allows the bacteria to defend themselves during future interactions with immune cells. Notably, the experiments to investigate the kinetics of secretion start and stop, as well as the re-initiation of growth and division, were performed in an effector-less strain background (ΔHOPEMTasd). The observed effects are therefore independent of any additional regulatory role of the effectors themselves (Dewoody et al., 2013).

Effector translocation into macrophages prevents phagocytosis and inflammation, which both the interacting bacterium and bystanders benefit from. However, the ability to quickly restart growth after interaction with immune cells implies that *Y. enterocolitica* do not sacrifice to combat immune cells in an altogether altruistic manner, but also attempt to increase individual fitness. Other pathogens deviate from this strategy, and utilize their T3SS differently. In the well-studied example of *Salmonella* Typhimurium SPI-1, only a fraction of bacteria express the T3SS, while the remaining bacteria do not express the T3SS. The SPI-1 activity elicits an inflammatory response that reduces competition with established microflora. Due to the inflammation and the decreased growth rate of the population expressing the SPI-1 T3SS genes, the subpopulation not expressing the SPI-1 genes outgrows both the SPI-1-expressing population and competing bacteria (Sturm et al., 2011; Diard et al., 2013; Weigel and Dersch, 2018). The cooperative virulence of *Salmonella* therefore allows for SPI-1 negative bacteria to colonize the intestinal lumen and thus promotes the competitiveness of the population and efficient invasion of the host (Stecher et al., 2007; Müller et al., 2009; Knodler et al., 2010; Ramos-Morales, 2012; Behnsen et al., 2014).

It is currently unclear whether the suppression of growth during secretion is based on the leakage of ions and amino acids, which might be either co-transported with the secreted proteins or passively diffuse through the T3SS during secretion (Fowler and Brubaker, 1994; Fowler et al., 2009), the metabolic burden caused by biosynthesis, assembly and operation of the T3SS (Brubaker, 2005; Sturm et al., 2011; Wilharm and Heider, 2014; Wang et al., 2016), yet unknown specific regulatory mechanisms, or a combination thereof. Wang et al. showed that in the related *Y. pseudotuberculosis*, activation of the T3SS by Ca^{2+} chelation or host cell contact leads to an increased copy number of the virulence plasmid (Wang et al., 2016). A decrease in virulence plasmid copy number upon deactivation of secretion could therefore increase the amount of energy available for growth and division; however, it is unclear whether such an effect could account for the rather quick recovery of growth and division presented in this study (**Figures 4A,C**). Notably, on solid medium, cell growth differs between secreting and non-secreting conditions (addition of 5 mM EGTA or $CaCl_2$, respectively) even for a T3SS-deficient strain (**Figure 4C**), which indicates an additional T3SS-independent effect of calcium or other divalent cations on growth on solid medium. Taken together, the finding that growth and cell division are restored within short time after secretion has ceased is most compatible with a direct effect of ion leakage, or a specific regulatory mechanism.

The results of this study describe important parameters of *Y. enterocolitica*'s life after secretion. They show the ability to stop type III secretion and re-initiate growth and division within short time after the loss of the activating signal, while remaining able to enter another round of secretion, and support the notion that *Y. enterocolitica* applies the T3SS in an individual rather than a purely altruistic manner.

MATERIALS AND METHODS

Bacterial strains and constructs used in this study are listed in **Table 1**.

E. coli Top10 was used for cloning and grown on Luria-Bertani (LB) agar plates or in LB medium at 37°C. Chloramphenicol and streptomycin were used to select for expression and suicide vectors at concentrations of 10 and 50 μg/ml, respectively.

Yersinia enterocolitica strains were grown over night at 28°C in brain heart infusion (BHI) medium containing nalidixic acid (35 μg/ml), and diaminopimelic acid (60 μg/ml) for ΔHOPEMTasd strains. Day cultures were grown in BHI supplemented with nalidixic acid, diaminopimelic acid where required, $MgCl_2$ (20 mM), and glycerol (0.4% v/v). For non-secreting conditions, 5 mM $CaCl_2$ was added to the medium, whereas for secreting conditions, residual Ca^{2+} was chelated by addition of 5 mM EGTA.

Plasmids were constructed using Phusion polymerase (New England Biolabs). Mutators for exchange of genes on the pYV virulence plasmid were created as previously described (Diepold et al., 2011). Inserted sequences were confirmed by sequencing (Eurofin Genomics). *Y. enterocolitica* mutants were generated by allelic exchange, resulting in the exchange of wild-type gene sequences with the mutated gene (Kaniga et al., 1991).

β-Lactamase Assay

ΔHOPEMTasd-based *Y. enterocolitica* were used for the β-lactamase (bla) assays to allow handling in a biological safety level 1 environment. *Y. enterocolitica* harboring pAD626 (pACYC184::$YopH_{1-17}$-bla) or pAD627 (pACYC184::bla) were inoculated from overnight cultures to an optical density at 600 nm (OD_{600}) of 0.10 (0.12 in validation experiment) in

TABLE 1 | Bacterial strains and genetic constructs used in this study.

Strain	Relevant characteristics of virulence plasmid	References
***Y. enterocolitica* strains**		
MRS40	Wild-type pYV plasmid of *Y. enterocolitica* E40 (pYVe40) ΔblaA	Sory et al., 1995
IML421*asd* (ΔHOPEMTasd)	pYVmrs40 $yopO_{\Delta 2-427}$ $yopE_{21}$ $yopH_{\Delta 1-352}$ $yopM_{23}$ $yopP_{23}$ $yopT_{135}$ Δ*asd*	Kudryashev et al., 2013
AD4051	pYVmrs40 Δ*sctD*	Diepold et al., 2010
AD4085	pYViml421asd *egfp-sctQ*	Kudryashev et al., 2013
AD4306	pYViml421asd *egfp-sctD*	Diepold et al., 2015
AD4483	pYViml421asd *egfp-sctL* Δ*sctD*	Diepold et al., 2017
ADTM4521	pYViml421asd *mCherry-sctL*	This study
IM41	pYVmrs40 $sctW_{45}$ (does not encode *sctW=yopN*)	Boland et al., 1996
CH4006	pYViml421asd $sctF_{S5C}$	This study
Plasmid	**Relevant characteristics**	**References**
Plasmids		
pACYC184	Expression vector	New England Biolabs
pKNG101	oriR6K sacBR$^+$ oriTRK2 strAB$^+$ (suicide vector)	Kaniga et al., 1991
pAD626	pACYC184::$yopH_{1-17}$-*bla* (β-lactamase from pBAD::His-B cloned in-frame with first 17 amino acids of *Y. enterocolitica* yopH)	This study
pAD627	pACYC184::*bla*	This study
pADTM521	pKNG101 *mCh-sctL* (*pamCherry* and flexible linker cloned in-frame at the N-terminus of *sctL*)	Diepold et al., 2017
pCH06	pKNG101 $sctF_{S5C}$ (serine to cysteine point mutation of amino acid 5 in *sctF*)	This study

Strains and constructs used in this study. Y. enterocolitica strains are based on either the wild-type strain MRS40 or the multi-effector knock-out strain ΔHOPEMTasd (IML421asd), which lacks the virulence effectors YopH, YopO, YopP, YopE, YopM, and YopT, and is auxotrophic for diaminopimelic acid as result from a mutation in the aspartate-β-semialdehyde (asd) gene. The knock-out of the virulence effectors and the asd mutation is used for biosafety purposes, allowing these strains to be handled in a biosafety 1 level environment.

non-secreting BHI medium. After shaking incubation at 28°C for 1.5 h, the culture was shifted to 37°C to induce the *yop* regulon. After 2 h (1.5 h in the initial validation experiment) of incubation at 37°C, bacteria were collected (unless stated differently, bacteria were collected by centrifugation (2,400 g, 4 min, 37°C), and resuspended in an equal amount of fresh medium pre-warmed to 37°C throughout the protocol), and resuspended in secreting BHI medium. Over the next 15 min, the activation kinetics analysis was performed (see below). To determine the deactivation kinetics, cultures were incubated for 2 h at 37°C in secreting medium and were then collected and resuspended in non-secreting medium. Over the next 30 min, the deactivation kinetics analysis was performed (see below). To determine the reactivation kinetics, cultures were incubated in the secreting medium for 2 h at 37°C and were then collected and resuspended in non-secreting medium pre-warmed to 28°C. Cultures were incubated at 28°C for 15 min, collected and resuspended in secreting medium at 37°C, where the reactivation kinetics analysis was performed.

Samples for the kinetics analysis of activation, deactivation, and reactivation of secretion were treated as follows: after resuspension, 400–800 μl samples were removed from the culture at the indicated time points (0, 5, 10 min for activation; 0, 10, 20 min for deactivation; 0 min for reactivation), collected, resuspended in fresh medium as indicated and incubated in a table top shaking incubator at 37°C, 800 rpm for 5 min (activation and reactivation) or 10 min (deactivation). After this incubation, bacteria were removed by centrifugation (16,000 g, 2 min), and the supernatant was stored at room temperature until all samples of one experiment were collected. For each sample, 100 μl supernatant were added to a Sarstedt TC-Platte 96 well plate in triplicates. 10 μl/well of β-lactamase substrate solution (10 μM Nitrocefin (Merck) in phosphate buffered saline) were added. β-lactamase activity was quantified by the increase in absorbance at 483 nm, caused by β-lactamase catalyzed hydrolysis of Nitrocefin, for 40 rounds of 30 s each at 30°C using a Tecan Infinite 200 Pro photometer. The results are averages of β-lactamase activity, determined by linear regression within the linear range of the absorbance, of three independent experiments that were run in technical triplicates for each experiment.

The initial validation assay was performed as described above with the following modifications: 200 μl supernatant was added to a Sarstedt TC-Platte 96 well plate in triplicates, and 20 μl/well of β-lactamase substrate solution (20 μM Fluorocillin Green 495/525 (Life Technologies in 0.1 M Tris-HCl pH 7.5) was added. β-lactamase activity was quantified by the increase in fluorescence caused by β-lactamase catalyzed hydrolysis of the substrate, measured at 495 ± 5 nm excitation and 525 ± 10 nm emission for 30 rounds every 30 s using a Tecan Infinite 200 Pro photometer. The result is the increase of fluorescence over time of one experiment that was run in a technical triplicate.

In vitro Secretion Time Course

Yersinia enterocolitica (MRS40) were selected for the *in vitro* secretion assay to compare the effector export over time. *Y. enterocolitica* were grown as stated above for the β-lactamase assay. At each indicated time point (0, 5, 10, 15, 30, 45, 60, and 120 min secreting; 120 min non-secreting) following activation,

2 ml of culture samples were taken for further analysis (see secretion analysis).

Growth Curve Experiment

Yersinia enterocolitica MRS40, AD4051 (ΔSctD), and IM41 (ΔSctW=YopN) cultures for growth curve experiments were inoculated from overnight cultures to an OD_{600} of 0.12 in non-secreting BHI medium. After incubating at 28°C for 1.5 h, the culture was divided in three parts and collected (2,400 g, 4 min, 37°C). The pellet was then resuspended in either non-secreting medium (one part) or secreting medium (two parts), both pre-warmed at 37°C, to induce the *yop* regulon. The cultures were incubated at 37°C for 2 h, and collected again (2,400 g, 4 min, 37°C). One previously secreting culture was resuspended in secreting medium and the second was resuspended in non-secreting medium; the previously non-secreting culture was resuspended in fresh non-secreting medium, all pre-warmed at 37°C. Cultures were incubated at 37°C for 3.5 h. Throughout the experiment, the optical density at 600 nm wavelength (OD_{600}) of all cultures was measured every 30 min in a 1:3 dilution. The number of divisions per time for each culture was determined using the OD_{600} values for −1.5 h and 0 h (28°C), 0 h and 2 h (first incubation), and 2 h and 4 h (second incubation).

Secretion Analysis

Culture samples were centrifuged (20,000 g, 5 min, 4°C) and 1.8 ml of the supernatant (SN) was collected. SN proteins were precipitated using trichloroacetic acid 10% (w/v) final for 24–48 h at 4°C. Proteins were separated on 4–20% gradient SDS-PAGE gels (BioRad). Samples were normalized to contain the proteins secreted by 0.4 OD units of bacteria (the equivalent of 0.4 ml culture at an OD_{600} of 1). Secreted proteins were stained with "Instant Blue," Coomassie-based staining solution (Expedeon). Immunoblots were carried out using rabbit polyclonal primary antibodies against *Y. enterocolitica* SctP (MIPA57, 1:3000), YopE (MIPA73, 1:1000), SctA (LcrV) (MIPA220, 1:2000), or SctF (MIPA223, 1:1000), goat anti-rabbit secondary antibodies conjugated to horseradish peroxidase (Dako, 1:5000), and ECL chemiluminescent substrate (Pierce).

Fluorescence Microscopy—Visualization of Growth Under Secreting and Non-secreting Conditions

Yersinia enterocolitica AD4483 (ΔHOPEMTasd EGFP-SctL ΔSctD) (Diepold et al., 2017) and ADTM4521 (ΔHOPEMTasd mCherry-SctL) cultures for microscopy were inoculated from overnight cultures to an OD_{600} of 0.15 in secreting medium. Cultures were incubated at 28°C for 1.5 h and then shifted to 37°C for 2 h. Next, 750 μl of each culture were centrifuged (2,400 g, 3 min), and resuspended in 100 μl of either secreting or non-secreting medium for both strains. 2 μl of resuspended culture were spotted on preheated (37°C) agarose pads containing 1.5% (w/v) low melting agarose, LB, nalidixic acid (35 μg/ml), glycerol (0.4% v/v), $MgCl_2$ (20 mM) and either oxalate (20 mM) for secreting conditions, or $CaCl_2$ (5 mM) for non-secreting conditions. Bright field images were taken every 5 min and fluorescence images were taken every 20 min for 2 h at 37°C with a Deltavision Spectris optical sectioning microscope (Applied Precision) using a 100x oil immersion objective (Olympus) with a numerical aperture of 1.40. The exposure time was set to 0.2 s, with a light intensity of 32% for bright field, 587 nm and 485 nm excitation lights. Following image acquisition, images were deconvolved using softWoRx 5.5 (standard "conservative" settings). Images were further processed with ImageJ-Fiji (National Institute of Health) using a binary mask for measuring cell growth. Red and green fluorescence was manually adjusted to discriminate T3SS-positive and T3SS-negative bacteria, respectively.

Fluorescence Microscopy—Quantification of Assembled T3SS Under Secreting and Non-secreting Conditions

ΔHOPEMTasd-based *Y. enterocolitica* AD4085 (EGFP-SctQ) and AD4306 (EGFP-SctD) cultures for microscopy (Kudryashev et al., 2013; Diepold et al., 2015) were inoculated from an overnight culture to an OD_{600} of 0.12. Cultures were incubated at 28°C for 1.5 h. After incubation, cultures were shifted to 37°C for 3 h. Next, 400 μl of culture was centrifuged (2,400 g, 2 min) and concentrated in 200 μl microscopy imaging buffer (100 mM HEPES pH 7.2, 100 mM NaCl, 5 mM ammonium sulfate, 20 mM sodium glutamate, 10 mM $MgCl_2$, 5 mM K_2SO_4, 0.5% (w/v) casamino acids) containing diaminopimelic acid (60 μg/ml) and $CaCl_2$ (5 mM) or EGTA (5 mM) according to the imaging conditions (non-secreting or secreting). To test for possible loss of T3SS during extended secretion, cultures were incubated under secreting or non-secreting conditions at 28°C for 1.5 h, and then shifted to 37°C for 3 h. For visualization, 2 μl of resuspended culture where mounted on a 1.5% (w/v) agar pad casted with the same buffer in a depression slide and visualized in a Deltavision Spectris Optical Sectioning Microscope (Applied Precision), equipped with a UApo N 100x/1.49 oil TIRF UIS2 objective (Olympus), using an Evolve EMCCD Camera (Photometrics). The sample was illuminated for 0.15 s with a 488 laser in a TIRF depth of 3440.0, except for the extended secretion assay, where the exposure time was 0.3 s under non-TIRF conditions. The micrographs where then deconvolved using softWoRx 5.5 (standard "conservative" settings) and further processed for presentation with ImageJ-Fiji. Cells were manually counted in several fields of view.

Needle Staining Protocol

MRS40-based *Y. enterocolitica* CH4006 ($SctF_{S5C}$) and a MRS40 wild-type control were inoculated from overnight cultures to an OD_{600} of 0.15 in secreting medium. Cultures were incubated at 28°C for 1.5 h and then shifted to 37°C for 2 h. At this point, 500 μl were transferred to a 2 ml tube and washed with minimal medium adjusted for secreting conditions. The cells were concentrated in 100 μl microscopy imaging buffer containing EGTA (5 mM) and CF-633 maleimide dye (Sigma-Aldrich, USA) (5 μM) for 5 min. The cells were then collected and washed with microscopy imaging buffer containing EGTA (5 mM) once or four times, as indicated. Images were acquired as z stacks of 11 images with a stacking of 0.15 μm. The micrographs where

then deconvolved using softWoRx 5.5 (standard "conservative" settings) and further processed for presentation with ImageJ-Fiji.

Energy Charge Determination

Intracellular metabolites were extracted from the total cellular biomass of wildtype ΔHOPEMTasd cultures, used in this experiment for biosafety reasons, based on a sequential quenching–extraction approach. 3 ml culture aliquots were pipetted into 9 ml of 60% (v/v) cold methanol (−60°C). Cells were immediately pelleted by centrifugation (10 min, −10°C, 20,000 x g), and the supernatant was removed. Pellets were stored at −80°C until extracted. Intracellular metabolites were extracted by adding a volume equivalent to 300 µl per 3 ml of a sample at an OD_{600} of 1 of both extraction fluid {50% (v/v) methanol, 50% (v/v) TE buffer [10 mM TRIZMA (pH 7.0), 1 mM EDTA]; −20°C} and chloroform (−20°C) to each cell pellet. The resulting mixture was incubated at 4°C for 2 h on a shaking device (Eppendorf shaker) and centrifuged (10 min, −10°C, 20,000 x g). The upper phase of the two-phase system was filtered (0.22 µm, PTFE, 4 mm diameter, Phenomenex) and stored at −80°C until the polar metabolites were analyzed.

Quantification of nucleotides was performed using a LC-MS/MS. The chromatographic separation was performed on an Agilent Infinity II 1290 HPLC system using a SeQuant ZIC-HILIC column (150 × 2.1 mm; 3.5 µm, 100 Å, Merck, Germany) equipped with a 20 × 2.1 mm guard column of similar specificity (Merck, Germany) at a constant flow rate of 0.4 ml/min with mobile phase A being 20 mM ammonium acetate (Sigma-Aldrich, USA) adjusted to pH 9.2 with ammonium hydroxide (Honeywell, USA) and phase B being acetonitrile (Honeywell, USA).

The injection volume was 3 µl. The mobile phase profile consisted of the following steps and linear gradients: 0–1 min from 20% B to 25% B; 1–4 min from 25 to 35% B; 4–5 min from 35 to 80% B; 5–6 min constant at 80% B; 6–7 min from 80 to 20% B; 7–8 min constant at 20% B. An Agilent 6495 ion funnel mass spectrometer was used in negative mode with an electrospray ionization source and the following conditions: ESI spray voltage 3,500 V, sheath gas 350°C at 11 l/min, nebulizer pressure 20 psig and drying gas 225°C at 14 l/min. Compounds were identified based on their exact mass and retention time compared to standards. Extracted ion chromatograms of the [M-H]- forms were integrated using MassHunter software (Agilent, Santa Clara, CA, USA). Absolute concentrations were calculated based on an external calibration curve.

DATA AVAILABILITY

All datasets generated for this study are included in the manuscript and/or the **Supplementary Files**.

AUTHOR CONTRIBUTIONS

BM-D and AD conceived, designed experiments, and wrote the paper. BM-D, CH, SW, DC, NP, and AD performed the experiments. BM-D, CH, SW, NP, and AD analyzed the data.

ACKNOWLEDGMENTS

This work was supported by the Max Planck Society. Nucleotide analysis was performed by the Core Facility for Metabolomics and Small Molecules of the Max Planck Institute for Terrestrial Microbiology. We thank Kai Thormann, University of Gießen, for support with the visualization of needles.

SUPPLEMENTARY MATERIAL

The Supplementary Material for this article can be found online at: https://www.frontiersin.org/articles/10.3389/fmicb.2019.02128/full#supplementary-material

REFERENCES

Akeda, Y., and Galán, J. E. (2005). Chaperone release and unfolding of substrates in type III secretion. *Nature* 437, 911–915. doi: 10.1038/nature03992

Armentrout, E. I., and Rietsch, A. (2016). The type III secretion translocation pore senses host cell contact. *PLOS Pathog.* 12:e1005530. doi: 10.1371/journal.ppat.1005530

Avican, K., Fahlgren, A., Huss, M., Heroven, A. K., Beckstette, M., Dersch, P., et al. (2015). Reprogramming of yersinia from virulent to persistent mode revealed by complex *in vivo* RNA-seq analysis. *PLoS Pathog.* 11:e1004600. doi: 10.1371/journal.ppat.1004600

Behnsen, J., Jellbauer, S., Wong, C. P., Edwards, R. A., George, M. D., Ouyang, W., et al. (2014). The cytokine IL-22 promotes pathogen colonization by suppressing related commensal bacteria. *Immunity* 40, 262–273. doi: 10.1016/j.immuni.2014.01.003

Böhme, K., Steinmann, R., Kortmann, J., Seekircher, S., Heroven, A. K., Berger, E., et al. (2012). Concerted actions of a thermo-labile regulator and a unique intergenic RNA thermosensor control Yersinia virulence. *PLoS Pathog.* 8:e1002518. doi: 10.1371/journal.ppat.1002518

Boland, A., Sory, M.-P., Iriarte, M., Kerbourch, C., Wattiau, P., and Cornelis, G. R. (1996). Status of YopM and YopN in the yersinia yop virulon: YopM of Y.enterocolitica is internalized inside the cytosol of PU5-1.8 macrophages by the YopB, D, N delivery apparatus. *EMBO J.* 15, 5191–5201. doi: 10.1002/j.1460-2075.1996.tb00904.x

Brubaker, R. R. (2005). Influence of Na(+), dicarboxylic amino acids, and pH in modulating the low-calcium response of *Yersinia pestis*. *Infect. Immun.* 73, 4743–4752. doi: 10.1128/IAI.73.8.4743-4752.2005

Büttner, D. (2012). Protein export according to schedule: architecture, assembly, and regulation of type III secretion systems from plant- and animal-pathogenic bacteria. *Microbiol. Mol. Biol. Rev.* 76, 262–310. doi: 10.1128/MMBR.05017-11

Charpentier, X., and Oswald, E. (2004). Identification of the secretion and translocation domain of the enteropathogenic and enterohemorrhagic *Escherichia coli* effector Cif, using TEM-1 beta-lactamase as a new fluorescence-based reporter. *J. Bacteriol.* 186, 5486–5495. doi: 10.1128/JB.186.16.5486-5495.2004

Cisz, M., Lee, P. C., and Rietsch, A. (2008). ExoS controls the cell contact-mediated switch to effector secretion in *Pseudomonas aeruginosa*. *J. Bacteriol.* 190, 2726–2738. doi: 10.1128/JB.01553-07

Cornelis, G., Vanooteghem, J., and Sluiters, C. (1987). Transcription of the yop regulon from *Y. enterocolitica* requires trans acting pYV and chromosomal genes. *Microb. Pathog.* 2, 367–379. doi: 10.1016/0882-4010(87)90078-7

Cornelis, G. R. (2002). Yersinia type III secretion: send in the effectors. *J. Cell Biol.* 158, 401–408. doi: 10.1083/jcb.200205077

Cornelis, G. R. (2006). The type III secretion injectisome. *Nat. Rev. Microbiol.* 4, 811–825. doi: 10.1038/nrmicro1526

Cornelis, G. R., Biot, T., Lambert de Rouvroit, C., Michiels, T., Mulder, B., Sluiters, C., et al. (1989). The Yersinia yop regulon. *Mol. Microbiol.* 3, 1455–1459. doi: 10.1111/j.1365-2958.1989.tb00129.x

Davis, A. J., and Mecsas, J. (2006). Mutations in the Yersinia pseudotuberculosis type III secretion system needle protein, YscF, that specifically abrogate effector translocation into host cells. *J. Bacteriol.* 189, 83–97. doi: 10.1128/JB.01396-06

Deng, W., Marshall, N. C., Rowland, J. L., McCoy, J. M., Worrall, L. J., Santos, A. S., et al. (2017). Assembly, structure, function and regulation of type III secretion systems. *Nat. Rev. Microbiol.* 15, 323–337. doi: 10.1038/nrmicro.2017.20

Dewoody, R. S., Merritt, P. M., and Marketon, M. M. (2013). Regulation of the Yersinia type III secretion system: traffic control. *Front. Cell. Infect. Microbiol.* 3:4. doi: 10.3389/fcimb.2013.00004

Diard, M., Garcia, V., Maier, L., Remus-Emsermann, M. N. P., Regoes, R. R., Ackermann, M., et al. (2013). Stabilization of cooperative virulence by the expression of an avirulent phenotype. *Nature* 494, 353–356. doi: 10.1038/nature11913

Diepold, A., Amstutz, M., Abel, S., Sorg, I., Jenal, U., and Cornelis, G. R. (2010). Deciphering the assembly of the Yersinia type III secretion injectisome. *EMBO J.* 29, 1928–1940. doi: 10.1038/emboj.2010.84

Diepold, A., Kudryashev, M., Delalez, N. J., Berry, R. M., and Armitage, J. P. (2015). Composition, formation, and regulation of the cytosolic c-ring, a dynamic component of the type III secretion injectisome. *PLOS Biol.* 13:e1002039. doi: 10.1371/journal.pbio.1002039

Diepold, A., Sezgin, E., Huseyin, M., Mortimer, T., Eggeling, C., and Armitage, J. P. (2017). A dynamic and adaptive network of cytosolic interactions governs protein export by the T3SS injectisome. *Nat. Commun.* 8:15940. doi: 10.1038/ncomms15940

Diepold, A., and Wagner, S. (2014). Assembly of the bacterial type III secretion machinery. *FEMS Microbiol. Rev.* 38, 802–822. doi: 10.1111/1574-6976.12061

Diepold, A., Wiesand, U., and Cornelis, G. R. (2011). The assembly of the export apparatus (YscR,S,T,U,V) of the Yersinia type III secretion apparatus occurs independently of other structural components and involves the formation of an YscV oligomer. *Mol. Microbiol.* 82, 502–514. doi: 10.1111/j.1365-2958.2011.07830.x

Enninga, J., Mounier, J., Sansonetti, P., Tran Van Nhieu, G., and Van Nhieu, G. T. (2005). Secretion of type III effectors into host cells in real time. *Nat. Methods* 2, 959–965. doi: 10.1038/nmeth804

Enninga, J., and Rosenshine, I. (2009). Imaging the assembly, structure and activity of type III secretion systems. *Cell. Microbiol.* 11, 1462–1470. doi: 10.1111/j.1462-5822.2009.01360.x

Fowler, J. M., and Brubaker, R. R. (1994). Physiological basis of the low calcium response in *Yersinia pestis*. *Infect. Immun.* 62, 5234–5241.

Fowler, J. M., Wulff, C. R., Straley, S., and Brubaker, R. R. (2009). Growth of calcium-blind mutants of *Yersinia pestis* at 37 C in permissive Ca2+-deficient environments. *Microbiology* 155, 2509–2521. doi: 10.1099/mic.0.028852-0

Galán, J. E. (2009). Common themes in the design and function of bacterial effectors. *Cell Host Microbe* 5, 571–579. doi: 10.1016/j.chom.2009.04.008

Grosdent, N., Maridonneau-Parini, I., Sory, M.-P., and Cornelis, G. R. (2002). Role of yops and adhesins in resistance of yersinia enterocolitica to phagocytosis. *Infect. Immun.* 70, 4165–4176. doi: 10.1128/IAI.70.8.4165-4176.2002

Håkansson, S., Schesser, K., Persson, C., Galyov, E. E., Rosqvist, R., Hombl,é, F., et al. (1996). The YopB protein of Yersinia pseudotuberculosis is essential for the translocation of Yop effector proteins across the target cell plasma membrane and displays a contact-dependent membrane disrupting activity. *EMBO J.* 15, 5812–5823. doi: 10.1002/j.1460-2075.1996.tb00968.x

Heroven, A. K., and Dersch, P. (2014). Coregulation of host-adapted metabolism and virulence by pathogenic yersiniae. *Front. Cell. Infect. Microbiol.* 4:146. doi: 10.3389/fcimb.2014.00146

Hoe, N., and Goguen, J. D. (1993). Temperature sensing in *Yersinia pestis*: translation of the LcrF activator protein is thermally regulated. *J. Bacteriol.* 175, 7901–7909. doi: 10.1128/jb.175.24.7901-7909.1993

Hueck, C. J. (1998). Type III protein secretion systems in bacterial pathogens of animals and plants. *Microbiol. Mol. Biol. Rev.* 62, 379–433.

Kaniga, K., Delor, I., and Cornelis, G. R. (1991). A wide-host-range suicide vector for improving reverse genetics in Gram-negative bacteria: inactivation of the blaA gene of Yersinia enterocolitica. *Gene* 109, 137–141. doi: 10.1016/0378-1119(91)90599-7

Kenjale, R., Wilson, J., Zenk, S., Saurya, S., Picking, W. L., and Blocker, A. J. (2005). The needle component of the type III secreton of Shigella regulates the activity of the secretion apparatus. *J. Biol. Chem.* 280, 42929–42937. doi: 10.1074/jbc.M508377200

Knodler, L. A., Vallance, B. A., Celli, J., Winfree, S., Hansen, B., Montero, M., et al. (2010). Dissemination of invasive Salmonella via bacterial-induced extrusion of mucosal epithelia. *Proc. Natl. Acad. Sci. U.S.A.* 107, 17733–17738. doi: 10.1073/pnas.1006098107

Kudryashev, M., Diepold, A., Amstutz, M., Armitage, J. P., Stahlberg, H., and Cornelis, G. R. (2015). Yersinia enterocolitica type III secretion injectisomes form regularly spaced clusters, which incorporate new machines upon activation. *Mol. Microbiol.* 95, 875–884. doi: 10.1111/mmi.12908

Kudryashev, M., Stenta, M., Schmelz, S., Amstutz, M., Wiesand, U., Castaño-Díez, D., et al. (2013). In situ structural analysis of the Yersinia enterocolitica injectisome. *Elife* 2:e00792. doi: 10.7554/eLife.00792

Kuhlen, L., Abrusci, P., Johnson, S., Gault, J., Deme, J., Caesar, J., et al. (2018). Structure of the core of the type III secretion system export apparatus. *Nat. Struct. Mol. Biol.* 25, 583–590. doi: 10.1038/s41594-018-0086-9

Kupferberg, L. L., and Higuchi, K. (1958). Role of calcium ions in the stimulation of growth of virulent strains of Pasteurella pestis. *J. Bacteriol.* 76, 120–121.

Lambert de Rouvroit, C., Sluiters, C., and Cornelis, G. R. (1992). Role of the transcriptional activator, VirF, and temperature in the expression of the pYV plasmid genes of Yersinia enterocolitica. *Mol. Microbiol.* 6, 395–409. doi: 10.1111/j.1365-2958.1992.tb01483.x

Lara-Tejero, M., Kato, J., Wagner, S., Liu, X., and Galán, J. E. (2011). A sorting platform determines the order of protein secretion in bacterial type III systems. *Science* 331, 1188–1191. doi: 10.1126/science.1201476

Marketon, M. M., DePaolo, R. W., DeBord, K. L., Jabri, B., and Schneewind, O. (2005). Plague bacteria target immune cells during infection. *Science* 309, 1739–1741. doi: 10.1126/science.1114580

Mehigh, R. J., Sample, A. K., and Brubaker, R. R. (1989). Expression of the low calcium response in *Yersinia pestis*. *Microb. Pathog.* 6, 203–217. doi: 10.1016/0882-4010(89)90070-3

Mills, E., Baruch, K., Charpentier, X., Kobi, S., and Rosenshine, I. (2008). Real-time analysis of effector translocation by the type III secretion system of enteropathogenic *Escherichia coli*. *Cell Host Microbe* 3, 104–113. doi: 10.1016/j.chom.2007.11.007

Mueller, C. A., Broz, P., Müller, S. A., Ringler, P., Erne-Brand, F., Sorg, I., et al. (2005). The V-antigen of Yersinia forms a distinct structure at the tip of injectisome needles. *Science* 310, 674–676. doi: 10.1126/science.1118476

Müller, A. J., Hoffmann, C., Galle, M., Van Den Broeke, A., Heikenwalder, M., Falter, L., et al. (2009). The, *S. typhimurium* effector sope induces caspase-1 activation in stromal cells to initiate gut inflammation. *Cell Host Microbe* 6, 125–136. doi: 10.1016/j.chom.2009.07.007

Nauth, T., Huschka, F., Schweizer, M., Bosse, J. B., Diepold, A., Failla, A. V., et al. (2018). Visualization of translocons in Yersinia type III protein secretion machines during host cell infection. *PLOS Pathog.* 14:e1007527. doi: 10.1371/journal.ppat.1007527

Navarro, L., Alto, N. M., and Dixon, J. E. (2005). Functions of the Yersinia effector proteins in inhibiting host immune responses. *Curr. Opin. Microbiol.* 8, 21–27. doi: 10.1016/j.mib.2004.12.014

Park, D., Lara-Tejero, M., Waxham, M. N., Li, W., Hu, B., Galán, J. E., et al. (2018). Visualization of the type III secretion mediated Salmonella-host cell interface using cryo-electron tomography. *Elife* 7:e39514. doi: 10.7554/eLife.39514

Pha, K. (2016). *Yersinia* type III effectors perturb host innate immune responses. *World, J. Biol. Chem.* 7:1. doi: 10.4331/wjbc.v7.i1.1

Philip, N. H., Zwack, E. E., and Brodsky, I. E. (2016). Activation and evasion of inflammasomes by yersinia. *Curr. Top. Microbiol. Immunol.* 397, 69–90. doi: 10.1007/978-3-319-41171-2_4

Portaliou, A. G., Tsolis, K. C., Loos, M. S., Zorzini, V., and Economou, A. (2016). Type III secretion: building and operating a remarkable nanomachine. *Trends Biochem. Sci.* 41, 175–189 doi: 10.1016/j.tibs.2015.09.005

Ramos-Morales, F. (2012). Impact of *Salmonella enterica* type III secretion system effectors on the eukaryotic host cell. *ISRN Cell Biol.* 2012, 1–36. doi: 10.5402/2012/787934

Rietsch, A., and Mekalanos, J. J. (2006). Metabolic regulation of type III secretion gene expression in *Pseudomonas aeruginosa*. *Mol. Microbiol.* 59, 807–820. doi: 10.1111/j.1365-2958.2005.04990.x

Roehrich, A. D., Guillossou, E., Blocker, A. J., and Martinez-Argudo, I. (2013). Shigella IpaD has a dual role: signal transduction from the type III secretion system needle tip and intracellular secretion regulation. *Mol. Microbiol.* 87, 690–706. doi: 10.1111/mmi.12124

Rundell, E. A., McKeithen-Mead, S. A., and Kazmierczak, B. I. (2016). Rampant cheating by pathogens? *PLOS Pathog.* 12:e1005792. doi: 10.1371/journal.ppat.1005792

Sánchez-Romero, M. A., and Casadesús, J. (2018). Contribution of SPI-1 bistability to *Salmonella enterica* cooperative virulence: insights from single cell analysis. *Sci. Rep.* 8:14875. doi: 10.1038/s41598-018-33137-z

Schlumberger, M. C., Müller, A., Ehrbar, K., Winnen, B., Duss, I., Stecher, B., et al. (2005). Real-time imaging of type III secretion: salmonella SipA injection into host cells. *Proc. Natl. Acad. Sci. U.S.A.* 102, 12548–12553. doi: 10.1073/pnas.0503407102

Shaulov, L., Gershberg, J., Deng, W., Finlay, B. B., and Sal-Man, N. (2017). The ruler protein escp of the enteropathogenic *Escherichia coli* type III secretion system is involved in calcium sensing and secretion hierarchy regulation by interacting with the gatekeeper protein SepL. *MBio* 8:e01733–e01716. doi: 10.1128/mBio.01733-16

Skurnik, M., Bölin, I., Heikkinen, H., Piha, S., and Wolf-Watz, H. (1984). Virulence plasmid-associated autoagglutination in Yersinia spp. *J. Bacteriol.* 158, 1033–1036.

Sory, M.-P., Boland, A., Lambermont, I., and Cornelis, G. R. (1995). Identification of the YopE and YopH domains required for secretion and internalization into the cytosol of macrophages, using the cyaA gene fusion approach. *Proc. Natl. Acad. Sci. U.S.A.* 92, 11998–12002. doi: 10.1073/pnas.92.26.11998

Stecher, B., Robbiani, R., Walker, A. W., Westendorf, A. M., Barthel, M., Kremer, M., et al. (2007). *Salmonella enterica* serovar typhimurium exploits inflammation to compete with the intestinal microbiota. *PLoS Biol.* 5, 2177–2189. doi: 10.1371/journal.pbio.0050244

Sturm, A., Heinemann, M., Arnoldini, M., Benecke, A., Ackermann, M., Benz, M., et al. (2011). The cost of virulence: retarded growth of Salmonella Typhimurium cells expressing type III secretion system 1. *PLoS Pathog.* 7:e1002143. doi: 10.1371/journal.ppat.1002143

Torruellas, J., Jackson, M. W., Pennock, J. W., and Plano, G. V. (2005). The *Yersinia pestis* type III secretion needle plays a role in the regulation of Yop secretion. *Mol. Microbiol.* 57, 1719–1733. doi: 10.1111/j.1365-2958.2005.04790.x

Veenendaal, A. K. J., Hodgkinson, J., Schwarzer, L., Stabat, D., Zenk, S., and Blocker, A. J. (2007). The type III secretion system needle tip complex mediates host cell sensing and translocon insertion. *Mol. Microbiol.* 63, 1719–1730. doi: 10.1111/j.1365-2958.2007.05620.x

Wang, H., Avican, K., Fahlgren, A., Erttmann, S. F., Nuss, A. M., Dersch, P., et al. (2016). Increased plasmid copy number is essential for Yersinia T3SS function and virulence. *Science* 353, 492–495. doi: 10.1126/science.aaf7501

Weigel, W. A., and Dersch, P. (2018). Phenotypic heterogeneity: a bacterial virulence strategy. *Microbes Infect.* 20, 570–577. doi: 10.1016/j.micinf.2018.01.008

Wiley, D. J., Rosqvist, R., and Schesser, K. (2007). Induction of the yersinia type 3 secretion system as an all-or-none phenomenon. *J. Mol. Biol.* 373, 27–37. doi: 10.1016/j.jmb.2007.07.077

Wilharm, G., and Heider, C. (2014). Interrelationship between type three secretion system and metabolism in pathogenic bacteria. *Front. Cell. Infect. Microbiol.* 4:150. doi: 10.3389/fcimb.2014.00150

Yother, J., and Goguen, J. D. (1985). Isolation and characterization of Ca2+-blind mutants of *Yersinia pestis*. *J. Bacteriol.* 164, 704–711.

Conflict of Interest Statement: The authors declare that the research was conducted in the absence of any commercial or financial relationships that could be construed as a potential conflict of interest.

Copyright © 2019 Milne-Davies, Helbig, Wimmi, Cheng, Paczia and Diepold. This is an open-access article distributed under the terms of the Creative Commons Attribution License (CC BY). The use, distribution or reproduction in other forums is permitted, provided the original author(s) and the copyright owner(s) are credited and that the original publication in this journal is cited, in accordance with accepted academic practice. No use, distribution or reproduction is permitted which does not comply with these terms.

frontiers in Microbiology

ORIGINAL RESEARCH
published: 30 October 2019
doi: 10.3389/fmicb.2019.02450

Identification of a Contact-Dependent Growth Inhibition (CDI) System That Reduces Biofilm Formation and Host Cell Adhesion of *Acinetobacter baumannii* DSM30011 Strain

Morgane Roussin[1], Sedera Rabarioelina[1], Laurence Cluzeau[1], Julien Cayron[2], Christian Lesterlin[2], Suzana P. Salcedo[1]† and Sarah Bigot[1,2]*†*

[1] Cell Biology of Bacterial Pathogenicity Team, Laboratory of Molecular Microbiology and Structural Biochemistry, CNRS UMR 5086, University of Lyon, Lyon, France, [2] Cell to Cell DNA Transfer Team, Laboratory of Molecular Microbiology and Structural Biochemistry, CNRS UMR 5086, University of Lyon, Lyon, France

OPEN ACCESS

Edited by:
Ignacio Arechaga,
University of Cantabria, Spain

Reviewed by:
Alfonso Soler-Bistue,
CONICET Institute of Biotechnological Research (IIB-INTECH), Argentina
Marco Maria D'Andrea,
University of Rome Tor Vergata, Italy

***Correspondence:**
Suzana P. Salcedo
suzana.salcedo@ibcp.fr
Sarah Bigot
sarah.bigot@ibcp.fr

†These authors share last authorship

Specialty section:
This article was submitted to Microbial Physiology and Metabolism, a section of the journal Frontiers in Microbiology

Received: 25 July 2019
Accepted: 11 October 2019
Published: 30 October 2019

Citation:
Roussin M, Rabarioelina S, Cluzeau L, Cayron J, Lesterlin C, Salcedo SP and Bigot S (2019) Identification of a Contact-Dependent Growth Inhibition (CDI) System That Reduces Biofilm Formation and Host Cell Adhesion of Acinetobacter baumannii DSM30011 Strain. Front. Microbiol. 10:2450. doi: 10.3389/fmicb.2019.02450

Acinetobacter baumannii is a multidrug-resistant nosocomial opportunistic pathogen that is becoming a major health threat worldwide. In this study, we have focused on the *A. baumannii* DSM30011 strain, an environmental isolate that retains many virulence-associated traits. We found that its genome contains two loci encoding for contact-dependent growth inhibition (CDI) systems. These systems serve to kill or inhibit the growth of non-sibling bacteria by delivering toxins into the cytoplasm of target cells, thereby conferring the host strain a significant competitive advantage. We show that one of the two toxins functions as a DNA-damaging enzyme, capable of inducing DNA double-stranded breaks to the chromosome of *Escherichia coli* strain. The second toxin has unknown catalytic activity but stops the growth of *E. coli* without bactericidal effect. In our conditions, only one of the CDI systems was highly expressed in the *A. baumannii* DSM30011 strain and was found to mediate interbacterial competition. Surprisingly, the absence of this CDI system promotes adhesion of *A. baumannii* DSM30011 to both abiotic and biotic surfaces, a phenotype that differs from previously described CDI systems. Our results suggest that a specific regulation mediated by this *A. baumannii* DSM30011 CDI system may result in changes in bacterial physiology that repress host cell adhesion and biofilm formation.

Keywords: type V secretion system, contact-dependent growth inhibition, *Acinectobacter baumannii*, biofilm, cell adhesion ability

INTRODUCTION

In Gram-negative bacteria, the two-partner secretion (TPS) pathway, also known as type Vb secretion system (T5bSS), mediates the translocation across the outer membrane of large, mostly virulence-related, TpsA proteins (Guérin et al., 2017). Functions of the TpsA secreted through the TPS pathway are diverse ranging from cytolysis, adhesion, and iron acquisition to

contact-dependent growth inhibition (CDI) (van Ulsen et al., 2014). CDI system was the first secretion system identified to deliver toxin into neighboring cells, arming bacteria with a killing mechanism for outcompeting non-kin cells and establishment of self-communities (Aoki et al., 2005). Growth inhibition involves direct physical contact between bacteria and depends on the production of toxin–antitoxin pairs (Willett et al., 2015). This mechanism exploits the CdiA/CdiB subfamily of TPS systems to export CdiA to the surface through the cognate CdiB transporter and deliver into the cytosol of the target bacterium the last ∼300 C-terminal toxic residues of the CdiA proteins, called CdiA-CT. The C-terminal domain is delimited by conserved motifs of unknown function such as (Q/E)LYN in *Burkholderia*, VENN in most bacteria, or yet other motifs in *Pseudomonas* (Aoki et al., 2005; Anderson et al., 2012; Mercy et al., 2016). The presence of the cytoplasmic immunity protein CdiI protects CDI^+ bacteria by interacting with the cognate CdiA-CT toxin and neutralizing its toxic activity. CdiA-CT is highly variable and shows various folds and activities (tRNase, DNase, and pore forming), allowing for a wide diversity of distinct toxins to be deployed to target bacteria (Zhang et al., 2011).

Contact-dependent growth inhibition systems are widespread among Gram-negative bacteria, as *cdi* gene clusters are found in several α-, β-, and γ-proteobacteria. They have been extensively studied in Enterobacteria and *Burkholderia* species, and recent work investigated their role in *Acinetobacter* species (Harding et al., 2017). *Acinetobacter baumannii* can be found associated with severe infections in humans, exhibiting multidrug resistance and causing fatal infections in susceptible hosts, such as patients in intensive care units. *A. baumannii* resists desiccation and forms biofilms that may contribute to its persistence in the clinical devices, causing acute infections. The molecular mechanisms implicated in infection by *A. baumannii* and the virulence factors associated with this process are still unclear. Recent studies investigated the potential implication of TPS systems in *A. baumannii* pathogenesis. The TpsA proteins characterized in strains *A. baumannii* ATCC 19606(T) and clinical AbH12O-A2 are both adhesins that mediate adherence to eukaryotic cells (Darvish Alipour Astaneh et al., 2014; Pérez et al., 2016), and TpsA of *A. baumannii* AbH12O-A2 was shown to contribute to virulence in models of mouse systemic infection and *Caenorhabditis elegans* (Pérez et al., 2016). Interestingly, our *in silico* analysis revealed that these two adhesins associated with their respective CdiB and CdiI partners constitute putative CDI systems, suggesting a potential involvement of these systems in the virulence of *A. baumannii*. This is in line with studies in other organisms suggesting a role for CDI systems beyond bacterial competition. Indeed, several CdiA promotes bacterial auto-aggregation and biofilm formation in *Escherichia coli*, *Pseudomonas aeruginosa*, and *Burkholderia thailandensis* (Garcia et al., 2013; Ruhe et al., 2015; Mercy et al., 2016), as well as intracellular escape and immune evasion of *Neisseria meningitidis* (Talà et al., 2008), functions that are required for the virulence of several pathogens (Gallagher and Manoil, 2001; Rojas et al., 2002; Guilhabert and Kirkpatrick, 2005; Gottig et al., 2009). Recently, *in silico* analysis revealed the identification of more than 40 different CDI systems in pathogenic *Acinetobacter* genomes that have been sorted into type I and II groups (De Gregorio et al., 2019). While sequencing the genome from *A. baumannii* DSM30011 strain (Repizo et al., 2017), we have also identified two *cdiBAI* loci potentially encoding type I and II CDI systems. *A. baumannii* DSM30011, an environmental strain isolated in 1944 from resin-producing guayule plants, has many of the characteristics of clinical strains and was shown to use a type 6 secretion system (T6SS) for bacterial competition and colonization in the model organism *Galleria mellonella* (Repizo et al., 2015). In this study, we used live-cell microscopy to characterize the function of CdiA-CT toxins when produced in *E. coli* cells. Using transcriptional fusions, we show that only one CDI system is expressed in *A. baumannii* DSM30011 and promotes interbacterial competition but is surprisingly a limiting factor for the adhesion process.

RESULTS

The *Acinetobacter baumannii* DSM30011 Genome Contains Two Predicted CDI Systems

In the course of this study, we performed a bioinformatic search to obtain the global repartition and representation of TPS systems among *A. baumannii* species. Each subset of TpsA was used to blast against the *A. baumannii* sequence database. Based on their sequence, TpsA proteins can be phylogenetically classified into at least five subfamilies with distinct functions: (i) the CDI CdiA proteins (Aoki et al., 2005), (ii) the hemolysins/cytolysins such as ShlA of *Serratia marcescens* (Braun et al., 1992), (iii) the adhesins such as filamentous hemagglutinin (FHA) of *Bordetella pertussis* (Relman et al., 1989), (iv) HxuA-type proteins involved in iron acquisition (Fournier et al., 2011), and (v) TpsA with unknown specific activities (Faure et al., 2014). The blast search revealed that the CDI system subfamily is predominantly represented within *A. baumannii* strains with the exception of some genomes comprising Hxu system homologues. We detected two loci in our *A. baumannii* DSM30011 laboratory model strain containing gene organization related to the "*Escherichia coli*"-type CDI systems (**Figure 1A**). We renamed them as $cdi_1^{Ab30011}$ (encoding proteins PNH15603.1, PNH15604.1, and PNH15605.1) and $cdi_2^{Ab30011}$ (encoding proteins PNH14818.1, PNH14817.1, and PNH14816.1). The CdiA proteins of these systems share only 9.6% identity overall, but both contain the highly conserved VENN motif (PF04829) that delimits the N- and C-terminal (CT) domains. The sequence analysis of $CdiA_1$ revealed that the N-terminal domain of this very large protein (532 kDa) harbors long stretches of imperfect repeats predicted to form β-helix folds, that is, β-strand structure organized in fibrous (Kajava et al., 2001), which classifies it as a type II CdiA protein (De Gregorio et al., 2019). $CdiA_1$-CT does not contain any conserved domain. The smaller $CdiA_2$ protein (204 kDa) belongs to the type I CdiA and its $CdiA_2$-CT preceded by the small-helical DUF637 domain found in many CdiA proteins (Iyer et al., 2011) contains a Tox-REase7 nuclease domain. Three potential orphan *cdiI* genes encoding the PNH15606.1,

PNH15607.1, and PNH15608.1 proteins are located downstream of the cdi_1 locus. Indeed, PNH15606.1 and PNH15607.1 proteins contain an Imm23 domain, and PNH15608.1 protein has a Smi1/Knr4 superfamily domain typically found in immunity proteins present in bacterial polymorphic toxin systems (Iyer et al., 2011; Zhang et al., 2011).

CdiA$_1$-CT/CdiI$_1$ and CdiA$_2$-CT/CdiI$_2$ Are Two Non-interchangeable Toxin–Antitoxin Pairs

To address the toxicity of CT domains, we generated pBAD33 plasmid derivatives producing each CdiA-CT (from the VENN motif to the stop codon) in the presence of arabinose. To assess the CdiI immunity property, nucleotide sequences encoding CdiI fused to 6xHis tag were introduced in pTrc99a plasmid and induced with isopropyl-β-D-1-thiogalactopyranoside (IPTG). The production of CdiA$_1$-CT alone stops the growth of the *E. coli* DH5α strain after 4 h of induction (**Figure 1B**). Unlike CdiA$_1$-CT, CdiA$_2$-CT is highly toxic in *E. coli* where its induction inhibits the growth (**Figure 1C**). Cells coproducing CdiI$_1$ and CdiA$_1$-CT or CdiI$_2$ and CdiA$_2$-CT are protected from the toxic effect of the toxins and exhibited growth equivalent to that of cells containing the empty vector (**Figures 1B,C**). In contrast, the production of CdiI$_1$ or CdiI$_2$ with CdiA$_2$-CT or CdiA$_1$-CT, respectively, does not suppress toxicity. Both CdiI-6xHis were detected in *E. coli* cells in the presence or absence of CdiA-CT using Western blot experiment (**Figure 1D**) showing that the inability to rescue the growth defect caused by a non-cognate CdiA-CT is not due to a lack of CdiI production. CdiA$_1$-CT/CdiI$_1$ and CdiA$_2$-CT/CdiI$_2$ therefore function as pairs of toxin–antitoxin, and these systems are not interchangeable.

CdiA$_2$-CT^{Ab30011} Toxin Induces DNA Damage in *E. coli*

CdiA$_2$-CT contains a restriction endonuclease-like domain belonging to the Tox-REase7 family (Pfam PF15649) mostly found in CdiA of *Pseudomonas* and *Acinetobacter* species (Zhang et al., 2012; Mercy et al., 2016). To determine whether CdiA$_2$-CT displays nuclease activity when expressed in *E. coli* cells, we performed real-time microscopy visualization of the nucleoid-associated HU protein after induction of the toxin. HU is a widely conserved histone-like protein very abundant in the bacterial cytoplasm that binds to DNA in a non-specific manner. Owing to its nucleoid association, HU localization reveals the global organization of the chromosome and potential alterations. We grew a CdiA$_2$-CT-producing *E. coli* MG1655 strain in which the *hupA* gene encoding the α-subunit of HU is fused to the *mcherry* gene at the endogenous locus. Twenty minutes after CdiA$_2$-CT induction, the majority of the cells contain organized and well-segregated nucleoids (**Figure 2** and **Supplementary Movie S1**). However, after 60 min, the nucleoids condense as a dense mass at midcell of the bacteria or show a diffused localization pattern. This global nucleoid disorganization is followed by cell filamentation indicative of cell division inhibition. These chromosome alterations are associated with cell death, as CdiA$_2$-CT-producing cells are not able to form viable colony units (**Supplementary Figure S1A**). No filamentation is observed after induction of the CdiA$_2$-CT in *recA*- cells showing that cell division arrest depends on the homologous recombination RecA protein (**Supplementary Figure S1B**). In contrast to bacteria producing only CdiA$_2$, cells coproducing the CdiI$_2$ immunity protein suffer no loss of viability and retain normal chromosome organization and cell division (**Figure 2**, **Supplementary Movie S2**, and **Supplementary Figure S1A**). The perturbation of DNA organization together with the RecA-dependent filamentation observed in the presence of CdiA$_2$-CT suggests that this toxin induces DNA damage to the chromosomal DNA. To test this hypothesis, we examined the localization pattern of the RecA protein, which has been reported to polymerize into large intracellular structures in response to DNA lesions (Lesterlin et al., 2014). To do so, we used an *E. coli* MG1655 strain expressing a carboxy-terminal fusion of RecA to green fluorescent protein (GFP) and wild-type (wt) RecA, both expressed from wt chromosome *recA* promoters. Before induction of CdiA$_2$-CT, RecA-GFP fluorescence appears uniformly distributed in most cells (**Figure 3**; t = 0 h and **Supplementary Movie S3**). From 20 min after production of CdiA$_2$-CT, fluorescent RecA-GFP structures form in the majority of cells, and we observed the formation of RecA bundles reported to promote homologous recombination repair between distant regions of homology (Lesterlin et al., 2014). As expected, RecA-GFP fluorescence is diffuse when CdiA$_2$-CT is co-expressed with CdiI$_2$, reflecting the absence of DNA damage (**Figure 3** and **Supplementary Movie S4**). Altogether, these results demonstrate that CdiA$_2$-CT creates multiple DNA breaks that cannot be repaired by the cells leading to growth inhibition, loss of chromosome organization, and eventual cell death.

CdiA$_1$-CT Toxin Inhibits the Growth of *E. coli*

In order to get insight into the mechanism of growth inhibition generated by the production of CdiA$_1$-CT in *E. coli* (**Figure 1B**), we analyzed in real-time microscopy the localization pattern of the recombinant HU-mCherry and RecA-GFP proteins after induction of CdiA$_1$-CT in the presence or absence of its cognate CdiI$_1$ immunity protein. Microscopy analysis showed no diffusion of the HU-mCherry in CdiA$_1$-CT-producing cells and RecA-GFP formed no spot or bundle, indicating that the toxin does not induce nucleoid disruption nor DNA damage (**Figure 4A** and **Supplementary Movies S5–S8**). However, we noticed CdiA$_1$-CT production led to increased cell size (**Figure 4B**) and division arrest in more than half of the cell population (**Figure 4C**). These results are consistent with the observed cell viability decrease 2 h post production of the CdiA$_1$-CT followed by a plateau of the number of colony-forming unit (CFU)/ml indicating a cell growth defect (**Supplementary Figure S2A**). To assess if these arrested cells are alive, we used the Live/Dead assay on the basis of the green fluorescent SYTO9 entering all cells to stain nucleic acid and the propidium iodide entering only dead cells with damaged cytoplasmic membranes. Our results showed the CdiA$_1$-CT-producing cells are not dying once they have stopped growing and that the percentage of cell

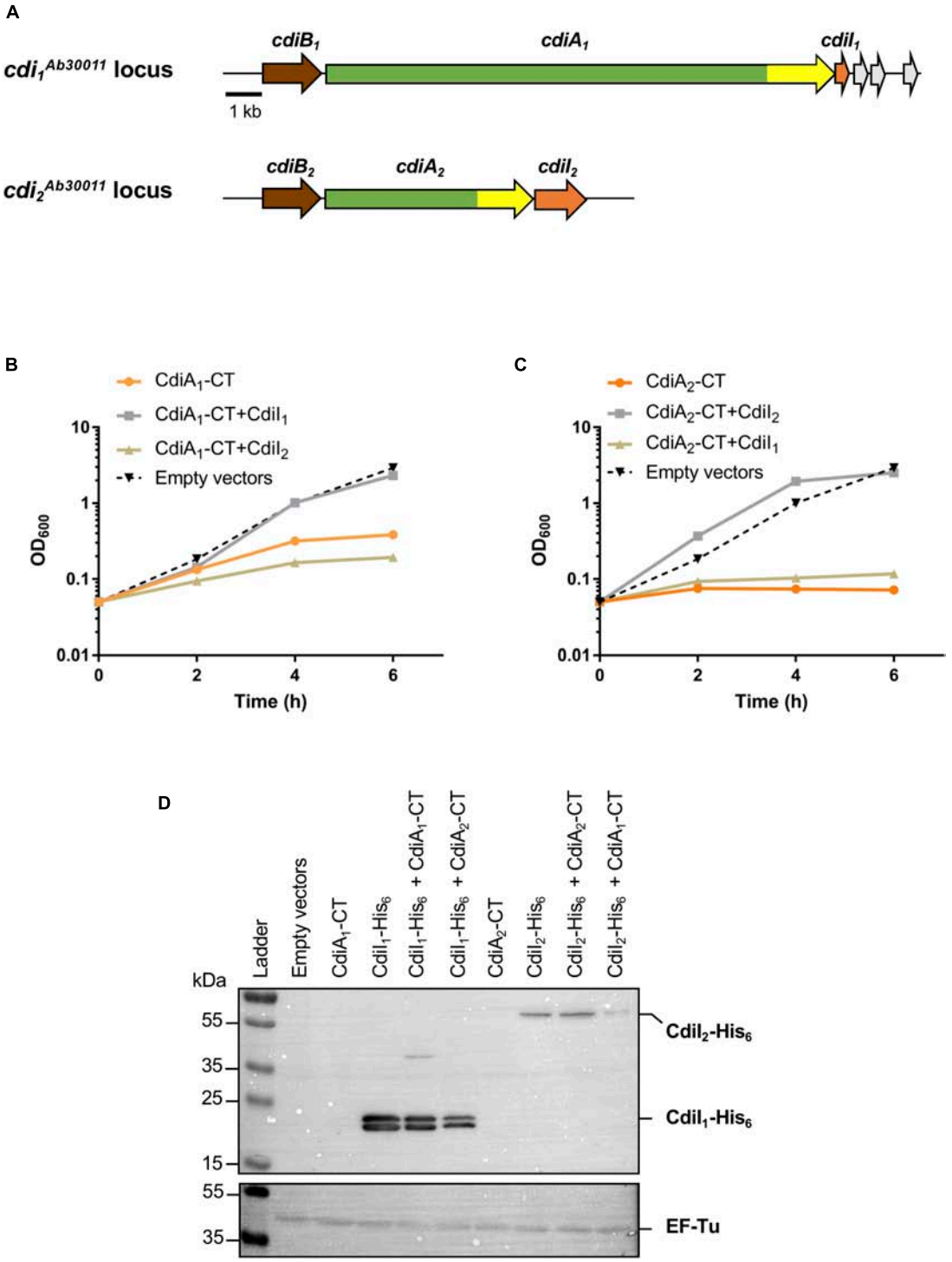

FIGURE 1 | The production of CT domains of $CdiA_1$ or $CdiA_2$ in *Escherichia coli* is toxic, and *cdiI* genes encode immunity proteins. **(A)** Schematic of the $cdi_1^{Ab30011}$ and $cdi_2^{Ab30011}$ loci. Genes encoding putative CdiB transporters, CdiA exoproteins, and CdiI immunity proteins are colored, respectively, in brown, green, and orange. Gray arrows represent putative orphan immunity genes. The highly variable nucleotide regions encoding CdiA-CT domains are highlighted in yellow. Black bar represents the 1-kb scale. Based on sequenced *Acinetobacter baumannii* DSM30011 genome (Repizo et al., 2017), $CdiB_1$, $CdiA_1$, and $CdiI_1$ correspond, respectively, to PNH15603.1, PNH15604.1, and PNH15605.1 proteins and $CdiB_2$, $CdiA_2$, and $CdiI_2$ to PNH14818.1, PNH14817.1, and PNH14816.1 proteins. **(B,C)** Effect of $CdiA_1$-CT **(B)** or $CdiA_2$-CT **(C)** production in *E. coli* DH5α strain. CdiA-CT production was induced at 0 min with or without CdiI, and growth was monitored by measuring the optical density at 600 nm (OD_{600}). **(D)** After 6 h of culture, *E. coli* cell extracts containing an indicated set of produced proteins were analyzed to probe the production of CdiI-His_6 and the cytoplasmic EF-Tu control using the anti-pentaHis (top panel) and anti-EF-Tu monoclonal antibodies (bottom panel). Molecular weight marker (kDa) is indicated on the left.

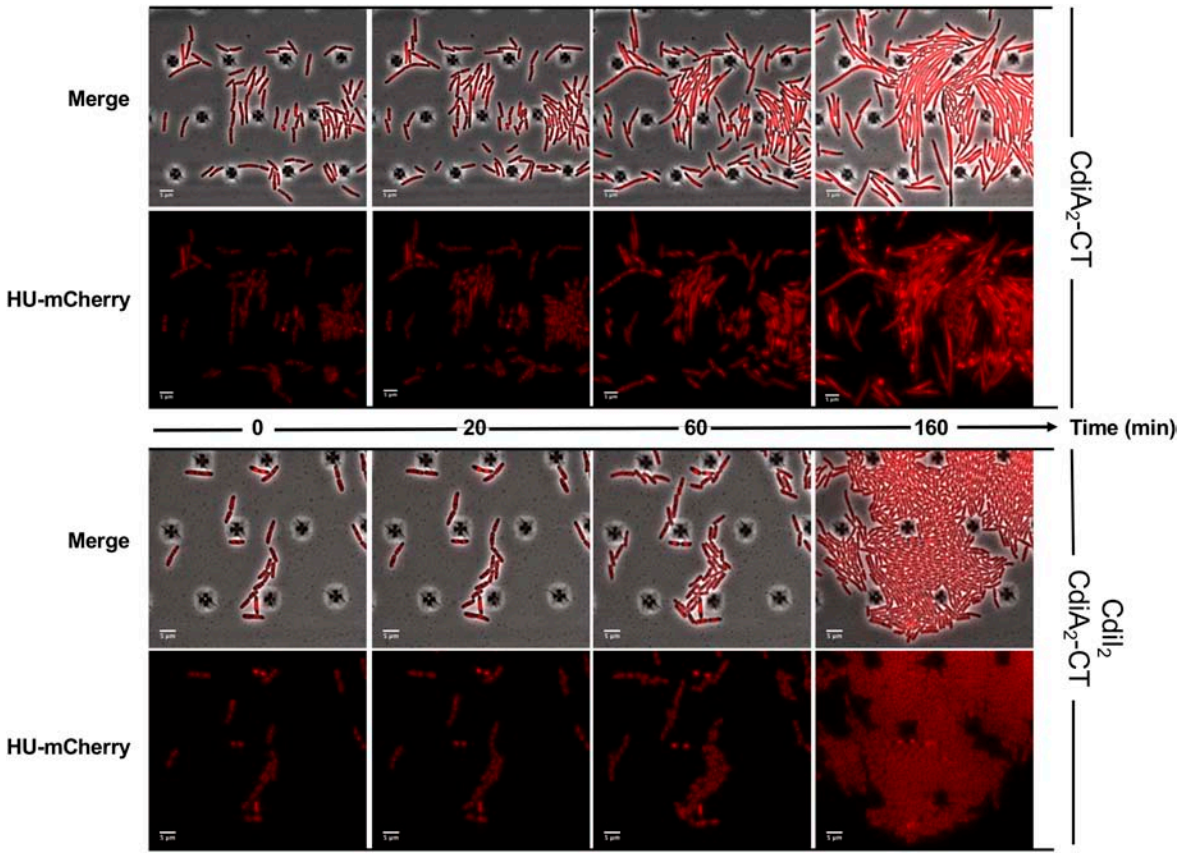

FIGURE 2 | The production of $CdiA_2$-CT in *Escherichia coli* disorganizes the nucleoid localization. Time-lapse fluorescence microscopy of the recombinant HU-mCherry protein produced by *E. coli* MG1655 strain after induction of the $CdiA_2$-CT in the absence or in presence of its cognate $CdiI_2$ immunity protein. The scale bar corresponds to 5 μm.

death was similar to that of cells producing $CdiA_1$-CT in the presence of $CdiI_1$ (**Supplementary Figure S2B**).

Unlike the *cdiBAI*$_2$ Locus, the *cdiBAI*$_1$ Genes Are Expressed in *A. baumannii* DSM30011

Most of the *cdi* genes are not expressed in laboratory growth conditions (Cope et al., 1994; Rojas et al., 2002; Mercy et al., 2016). In order to get insight into the expression profile of *cdi* genes present in *A. baumannii* DSM30011, we constructed plasmids containing transcriptional fusions between DNA region upstream of these genes and the *gfp* reporter. *A. baumannii* DSM30011 reporter strains were grown in liquid Luria–Bertani (LB)-rich medium at 37°C with agitation and static conditions, and the GFP fluorescence intensity was measured at 6 and 8 h, respectively. Equivalent results were obtained for each growth condition (**Figure 5A**). The level of GFP fluorescence of P*cdiB*$_2$, P*cdiA*$_2$, and P*cdiI*$_2$ fusions is identical to that of the promoterless fusion, indicating that DNA regions upstream of these genes do not have any promoter activity and that the *cdi*$_2$ locus might not be expressed under the growth conditions tested (**Figure 5A**). In contrast, the P*cdiB*$_1$ fusion produces a really high level of GFP compared to the regions upstream the *cdiA*$_1$ and *cdiI*$_1$ genes that do not exhibit any promoter activity (**Figure 5A**). In addition, the GFP fluorescence is quite homogeneous within the population, as all individual bacteria produce high levels of GFP fluorescence (**Figure 5B**). In order to determine whether $CdiA_1$ is produced in the tested conditions, we tried to detect this protein using sodium dodecyl sulfate polyacrylamide gel electrophoresis (SDS-PAGE). Overnight cultures were fractionated to analyze the protein profile of the whole cell lysate and secreted fraction. A band with a slower mobility than 250-kDa molecular weight marker was detected in the secreted fraction of the wt strain, which was identified as $CdiA_1$ protein by mass spectrometry (**Figure 5C**). For controls, we confirmed that this band disappeared in the Δ*cdiA*$_1$ mutant and that the $CdiA_1$ transport required $CdiB_1$ because no $CdiA_1$ is secreted in a Δ*cdiB*$_1$ mutant probably owing to the instability of the protein that is trapped in the periplasm, which is consistent with previous reports on FHA undergoing a rapid proteolytic degradation in the periplasm in the absence of its transporter FhaC (Jacob-Dubuisson et al., 1997; Guédin et al., 1998). Furthermore, the secretion of $CdiA_1$ is not due to cell lysis, as the cytoplasmic EF-Tu protein is only found in the whole cell fraction and Hcp, identified by mass spectrometry, the main component of the T6SS, is detected in the secreted fraction

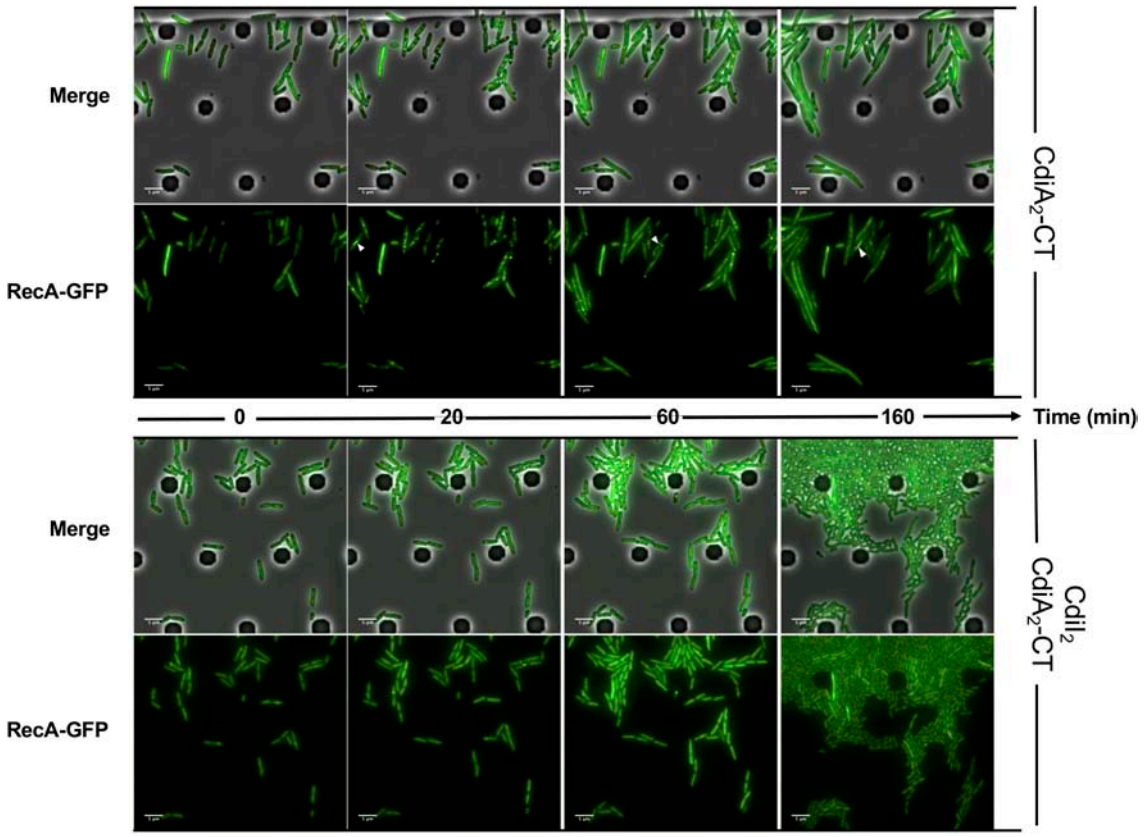

FIGURE 3 | The production of $CdiA_2$-CT in *Escherichia coli* induces DNA damages. Time-lapse fluorescence microscopy of the recombinant RecA-GFP protein produced by *E. coli* MG1655 strain after induction of the $CdiA_2$-CT in the absence or in the presence of its cognate $CdiI_2$ immunity protein. White arrows indicate examples of bundles of RecA-GFP. The scale bar corresponds to 5 μm. GFP, green fluorescent protein.

(**Figure 5C**). Knowing that $CdiA_1$ is highly produced and can be visualized by Coomassie blue staining, this suggests that the three *cdiBAI*$_1$ genes are transcribed as a polycistronic mRNA from the same promoter upstream *cdiB*$_1$.

The *cdiBAI*$_1$ Locus Mediates Bacterial Competition

As only the CDI_1 system is turned on under the tested conditions and we have not yet determined the regulatory pathway of the *cdi*$_2$ locus, we pursued in *A. baumannii* the characterization of the *cdiBAI*$_1$ system. To determine whether this system functions as a CDI system, the entire locus was replaced by a kanamycin cassette or deleted generating the Δ*cdiBAI*$_1$:*kn* and Δ*cdiBAI*$_1$ mutants. Next, we performed competition experiments by mixing the wt or Δ*cdiBAI*$_1$ attacker strains with the Δ*cdiBAI*$_1$:*kn* target strain and measure the CFU/ml of the target over time. As seen in **Figure 6**, wt strain inhibits the growth of the isogenic Δ*cdiBAI*$_1$:*kn* target strain by ∼1 log after 6 h of growth competition, whereas no growth inhibition is observed with the Δ*cdiBAI*$_1$ attacker strain. No significant viability defect between the wt and mutant strains was observed, indicating that the ability of wt strain to outcompete the Δ*cdiBAI*$_1$ is not due to a growth rate difference (**Supplementary Figure S3**).

cdi$_1$ Locus Decreases *A. baumannii* DSM30011 Biofilm Formation and Adhesion to Epithelial Cells

CdiA proteins can promote biofilm formation and/or attachment to eukaryotic cells (Rojas et al., 2002; Plamondon et al., 2007; Schmitt et al., 2007; Gottig et al., 2009; Neil and Apicella, 2009; Garcia et al., 2013; Ruhe et al., 2015; Mercy et al., 2016). To investigate whether *cdi*$_1$ locus contributes to biofilm formation, we quantified in 96-well polystyrene plates over a 24-h time period the biofilm biomass formed by the wt and *cdiBAI*$_1$ mutant strains. After 3 h, the capacity to form biofilm of the mutant was lower than that of the wt (**Figure 7A**). Surprisingly, *cdiBAI*$_1$ mutant generated twice as much biofilm mass as the wt after 5 and 24 h (**Figure 7A**). Analysis of the depth bacterial growth on glass-bottom slides by confocal microscopy confirmed that the *cdiBAI*$_1$ mutant exhibited the highest ability to form a bacterial 3D structured layer especially after 5 h (**Figure 7B** and **Supplementary Figure S4**). To determine whether the *cdi*$_1$ locus is also implicated in the adhesion of *A. baumannii* DSM30011 to biotic surfaces, we compared the adhesiveness of wt and isogenic *cdiBAI*$_1$ mutant strains to A549 epithelial cells by CFU measurement and confocal microscopy analysis to directly visualize *A. baumannii* strains and confirm CFU

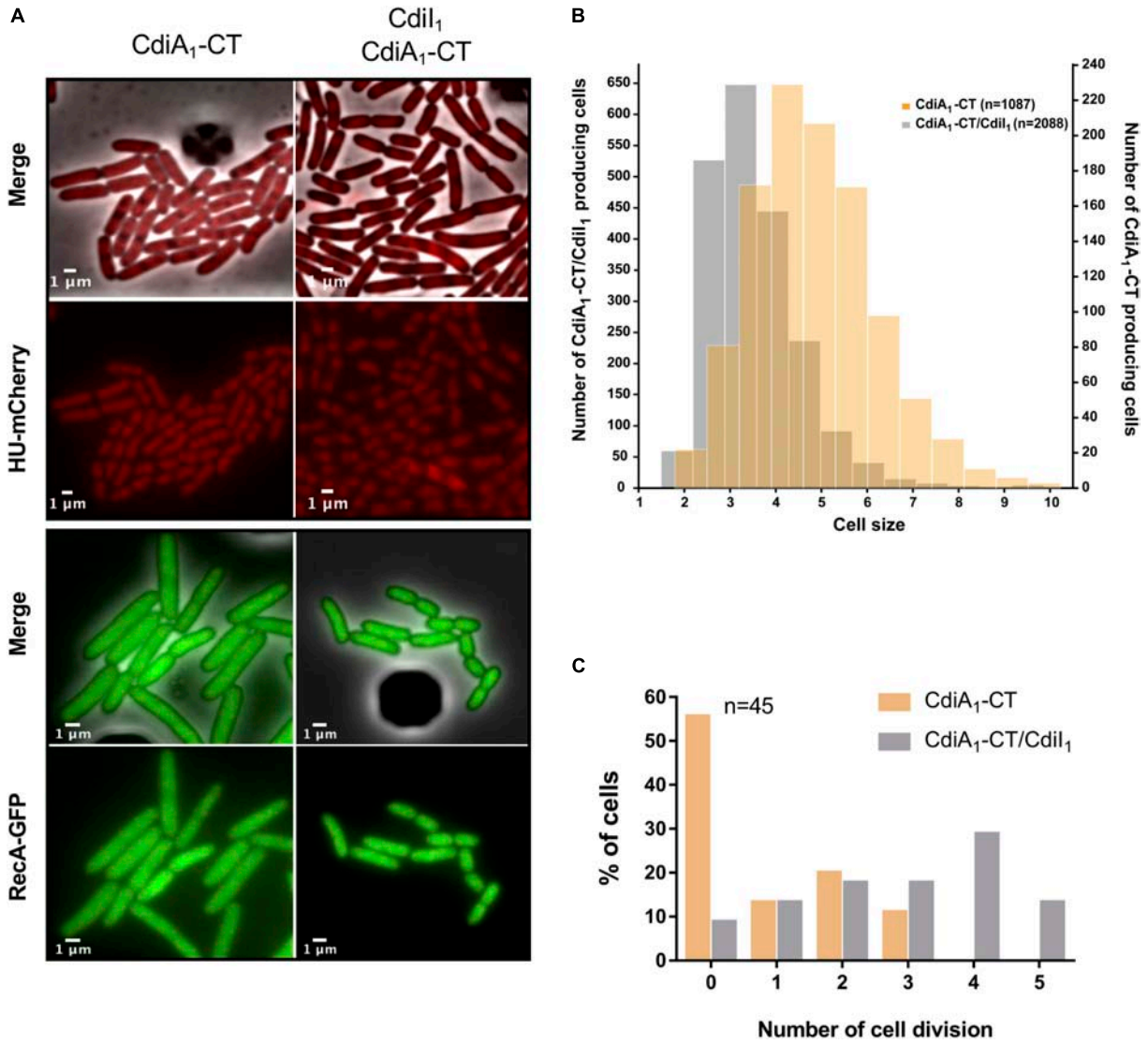

FIGURE 4 | The $CdiA_1$-CT toxin stops the growth of *Escherichia coli*. **(A)** Fluorescence microscopy of recombinant HU-mCherry or RecA-GFP produced by *E. coli* MG1655 strains 130 min after induction of $CdiA_1$-CT in the absence or in the presence of its cognate $CdiI_1$ immunity protein. The scale bar is indicated on the lower left. **(B)** Cell length analysis of RecA-GFP producing *E. coli* MG1655 strains 3 h after induction of $CdiA_1$-CT in the absence or in the presence of its cognate $CdiI_1$ immunity protein. *n* indicates the number of analyzed cells. **(C)** HU-mCherry producing *E. coli* MG1655 strains were grown in M9-casa after induction of $CdiA_1$-CT with or without $CdiI_1$, and real-time microscopy was performed in order to calculate the number of division over 45 single bacteria. GFP, green fluorescent protein.

counts. No difference between strains was observed after 2 h of infection with exponential cultures grown in LB liquid medium (**Figure 7C**; exponential). The biofilm increase is a late phenotype (**Figure 7A**), and we noticed that on agar plate the Δ*cdiBAI*$_1$ colonies were slightly smaller than those of the wt, reflecting a potential change in physiology depending on the growth condition. For these reasons, we directly analyzed the capacity of bacteria scratched from the agar plate to bind to host cells. As seen in **Figure 7C** (solid), the deletion of the *cdi*$_1$ locus led to a significant 2.5-fold increase in the proportion of cell-associated bacteria 2-h post infection. Furthermore, the number of cell-attached bacteria detected by immunofluorescence using an anti-*Acinetobacter* antibody was also higher for the *cdiBAI*$_1$ mutant (**Figure 7D**). Z-stack reconstruction confirmed that the bacteria are well attached to the cell surface and not endocyted by the host cells (**Supplementary Figure S5**).

DISCUSSION

The knowledge on virulence mechanisms and factors contributing to the pathogenic potential of *Acinetobacter baumannii* is limited, and a deeper understanding of its infection mechanisms may shed light on new strategies for drug development. On the basis of recent studies that characterized the potential implication of secretion systems including the TPS

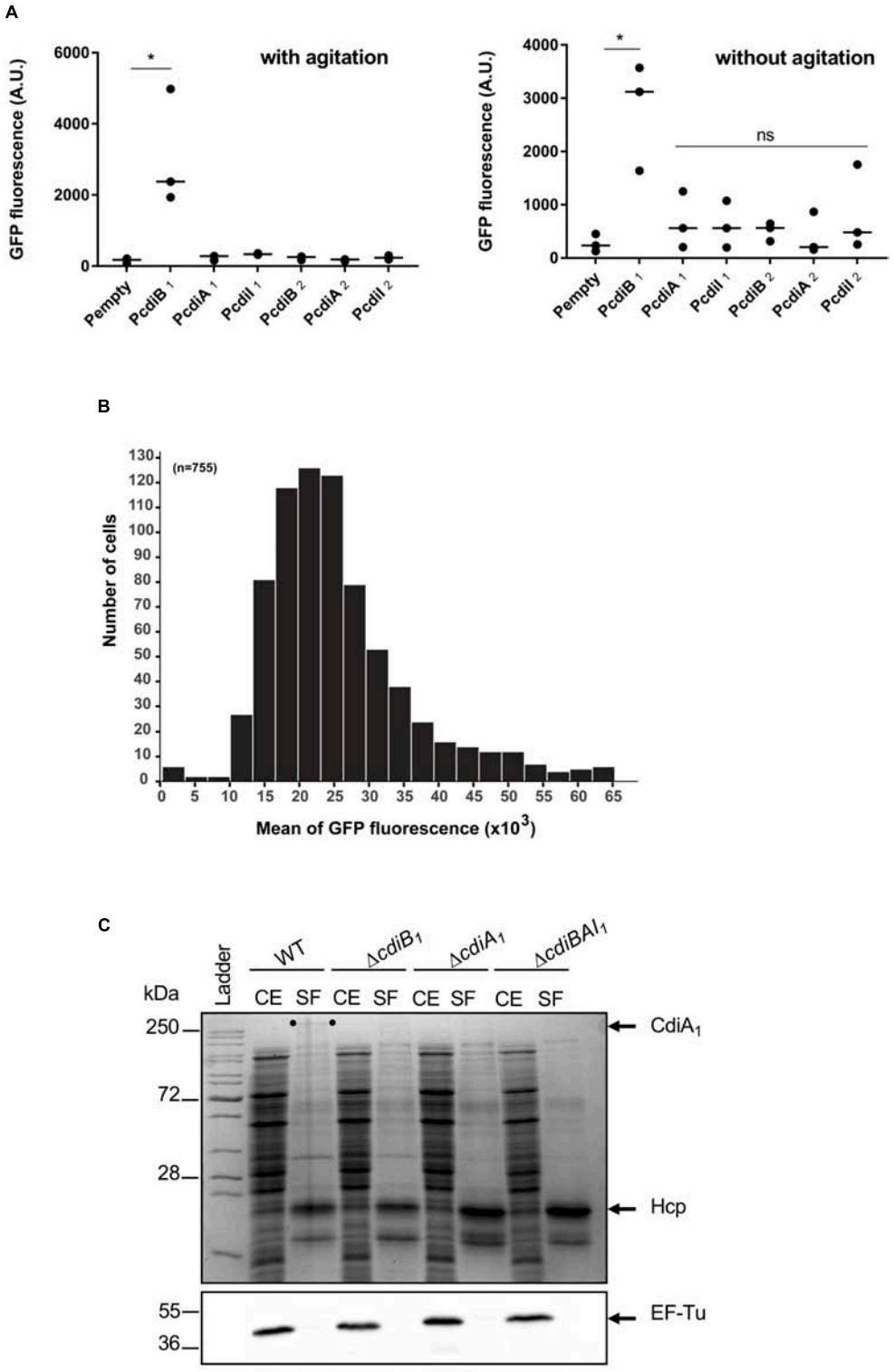

FIGURE 5 | Only the *cdiBAI*$_1$ genes are expressed in *Acinetobacter baumannii* DSM3011. **(A)** GFP fluorescence measurements for potential promoter regions of *cdi* genes. A strain harboring plasmid with a *gfp* reporter gene without a promoter (Pempty) served as a negative control. For statistical analyses, a non-parametric one-way ANOVA with Dunn's multiple comparison test was performed. *p = 0.0184 (with agitation) and p = 0.028 (without agitation); ns: not significant. **(B)** Repartition of the GFP fluorescence intensities within a sibling population harboring the P*cdiB*$_1$ fusion. n = number of analyzed cells. **(C)** Cell extract (CE) and secreted fraction (SF) of wild-type and mutant strains grown overnight were analyzed by Coomassie blue staining and Western blot analysis using anti-EF-Tu antibody. The migration position of CdiA$_1$ protein is indicated by two dots. Molecular marker (kDa) is indicated on the left. GFP, green fluorescent protein.

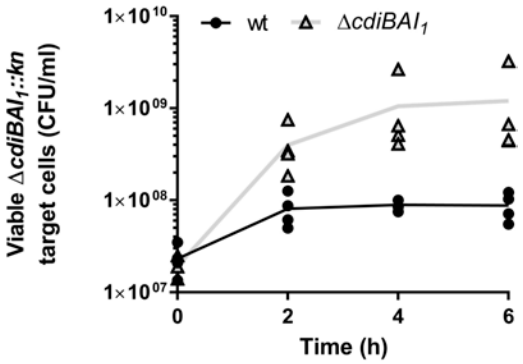

FIGURE 6 | Growth inhibition mediated by the CDI_1 system of strain *Acinetobacter baumannii* DSM30011. Both attacker and target strains were grown in LB separately to OD_{600} = 0.35 and mixed to a 4:1 (attacker:target) ratio. At various times of co-incubation, the *cdiBAI*$_1$*:kn* target was spread on LB agar supplemented with kanamycin to measure the colony-forming unit (CFU)/ml. For statistical analyses, a non-parametric Mann–Whitney test was performed. **p* = 0.0286 at 4 and 6 h. GFP, green fluorescent protein; LB, Luria–Bertani.

pathway, we performed a blast search using TpsA of diverse functions to evaluate their distribution within *A. baumannii*. The basic pattern reflected in this search was that several *cdi* loci could be identified in a large number of *A. baumannii* species and confirmed a previous study (De Gregorio et al., 2019). Strikingly, other subfamilies of TPS systems were absent with the exception of HxuA homologues found in some *A. baumannii* strains, which are TpsA involved in iron acquisition (Cope et al., 1994, 1995, 1998). These findings suggest that CDI systems may be significant players in *A. baumannii.* In this work, we used the environmental *A. baumannii* DSM30011 strain with two CDI systems.

Most of the *cdi* genes appear to be under tight regulatory control (Mercy et al., 2016) or only expressed during infection (Rojas et al., 2002; Aoki et al., 2010). Our results show that *A. baumannii* DSM30011 cells differentially produce its CDI systems. Indeed, *cdi*$_2$ locus is not expressed under the rich medium and growth conditions used in this study and undergoes negative regulation. Interestingly, we noticed the presence of a putative pho box in the *cdiB*$_2$ promoter region, suggesting a potential regulation by the transcriptional regulator PhoB through a differential phosphate level, as it has already been characterized for the *Pseudomonas aeruginosa tps* genes (Faure et al., 2013). Although additional experiments will be necessary to identify the regulatory circuits controlling the expression of this *cdiA* gene and its role in *A. baumannii*, we were able to show that $CdiA_2$-CT, produced intracellularly in *Escherichia coli*, induces multiple DNA damages that the target cell cannot repair, leading to its death. This finding is consistent with the presence of a Tox-REase-7-fold domain and strongly suggests that $CdiA_2$-CT functions as a cytoplasmic DNase to degrade nucleic acids like several other CdiA toxins (Willett et al., 2015). In contrast, the $CdiA_1$ protein is highly secreted in *A. baumannii*, and the expression of *cdiBAI*$_1$ genes is quite homogeneous within the population, in comparison with *Burkholderia thailandensis*, which expresses a high level of *cdi* genes in a stochastic manner (Anderson et al., 2012). In addition, in the *A. baumannii* SDF strain, we also observed the presence of two CDI systems, one of which is not repressed (**Supplementary Figures S6, S7**), and other studies have shown the constitutive activation of CDI systems within several *Acinetobacter* species in growth laboratory conditions (Perez et al., 2007; Darvish Alipour Astaneh et al., 2014; Harding et al., 2017), suggesting that *Acinetobacter* might not keep CDI system in an inactive state. Interestingly, we and others have shown that several *Acinetobacter* species often coproduce the CDI and the T6SS (Carruthers et al., 2013; Repizo et al., 2015; Harding et al., 2017; unpublished data), and in *Pseudomonas aeruginosa*, they are both regulated by the post-transcriptional RsmA regulator (Mercy et al., 2016; Allsopp et al., 2017). These observations might reflect that a co-regulation exists between these two systems, but additional work is needed to understand the real link between CDI and T6SS co-regulation in *Acinetobacter*.

Although we established that the CDI_1 system is functional and arrests the growth of neighboring *A. baumannii* bacteria that do not contain the *cdi*$_1$ locus, we have not yet investigated the mechanisms involved. However, we have shown that the production of $CdiA_1$-CT in the cytoplasm of *E. coli* stops bacterial growth by inhibiting cell division rather than cell death, indicating that this domain might be responsible for the *A. baumannii* growth arrest during bacterial competition. $CdiA_1$-CT does not contain any known conserved domains, but the use of fluorescent proteins reporting chromosome compaction state and DNA damage allowed us to exclude that this toxin functions as a DNase. The induction of growth arrest by $CdiA_1$-CT can arise from different mechanisms of action. Many CdiA toxins act as nucleases that degrade tRNA or rRNA arresting growth by blocking the translation (Willett et al., 2015), whereas $CdiA^{EC93}$ from *E. coli* EC93, a ionophore that dissipates the proton motive force, inhibits the growth by depleting ATP levels (Aoki et al., 2009). Further investigation will be necessary to identify the functional activity of $CdiA_1$ toxin of *A. baumannii* DSM30011.

CdiA proteins might be multifunctional, which would be quite conceivable given their large sizes and might therefore have a broader role than bacterial competition. Indeed, studies in *A. baumannii* but also in other bacteria show that CdiA functions as adhesins mediating adhesion to epithelial cells or structuring a biofilm through bacteria–bacteria interactions (Balder et al., 2007; Plamondon et al., 2007; Darvish Alipour Astaneh et al., 2014; Ruhe et al., 2015; Pérez et al., 2016). Interestingly, $CdiA_1$ of *A. baumannii* DSM30011 is a very large protein whose amino acid sequence is mostly constituted of β-helical and FHA repeats found in a number of TpsA adhesins (Jacob-Dubuisson et al., 2001). However, we found that CDI_1 system does not promote biofilm formation nor adhesion to eukaryotic cells, but instead, its absence increases the adhesiveness of *A. baumannii*. The mechanism enabling the limitation of cell–cell or surface adhesion by the CDI_1 system is not yet understood and remains to be discovered. Recent studies suggest a role for CDI beyond bacterial competition in collective

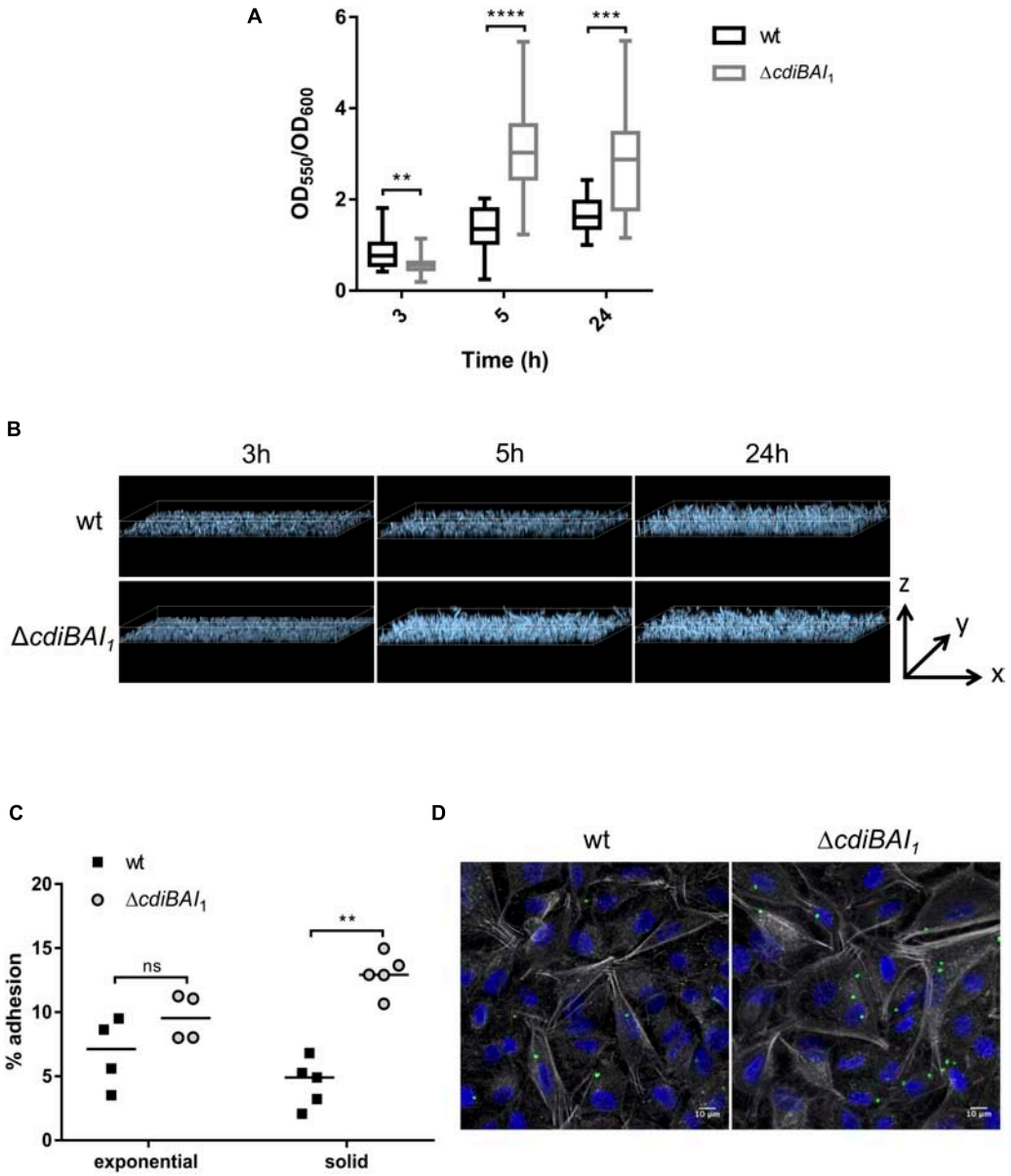

FIGURE 7 | The adhesive properties of *Acinetobacter baumannii* DSM30011 is enhanced in the absence of *cdiBAI*$_1$ locus. **(A)** Biofilm formation assayed by crystal violet staining. *A. baumannii* DSM30011 wild-type (wt) and Δ*cdiBAI*$_1$ strains were statically grown at 37°C for 3, 5, and 24 h. The biofilm biomass was estimated by calculating the OD_{550}/OD_{600} ratio from three independent experimental replicates. For statistical analyses, a non-parametric Mann–Whitney test was performed. $^{**}p = 0.0045$, $^{***}p = 0.0004$, $^{****}p < 0.0001$. **(B)** Confocal microscopy of biofilm formed by the wild-type and Δ*cdiBAI*$_1$ strains grown on glass-bottom slides in static conditions. Images correspond to the depth analysis of a 3D reconstruction of z-stacks obtained for the different strains at 3, 5, and 24 h. The height of the *z* axis is between 0 and 10 μm. Bacteria were labeled with DAPI. **(C)** Adhesion assay in which A549 cells were infected with *A. baumannii* DSM30011 wt or Δ*cdiBAI*$_1$ strains at a MOI of 100 for 2 h. Data are expressed as a percentage of *A. baumannii* adhesion obtained from the ratio between CFU/ml before and after infection. For statistical analyses, a non-parametric Mann–Whitney test was performed. $^{**}p = 0.0079$, ns: not significant. **(D)** Representative immunofluorescence images obtained by confocal microscopy and analyzed with ImageJ of A549 cells infected with bacteria grown in solid. Images correspond to Z-projections at average intensity. *A. baumannii* strains were detected with an anti-*A. baumannii* antibody (green). The actin cytoskeleton and nucleus were labeled with phalloidin (white) and DAPI (blue), respectively. MOI, multiplicity of infection.

behavior between sibling immune cells. In *P. aeruginosa*, the deletion of *cdi* locus increases the production of cyanide and swarming motility potentially via post-transcriptional regulation (Melvin et al., 2017). *Burkholderia* uses the contact-dependent signaling (CDS) mechanism to modulate gene expression in immune recipient bacteria that are dependent on the activity of the CdiA-CT toxin but independent of CDI growth inhibitory function (Garcia et al., 2016); and in *E. coli*, CDI modulates the cellular (p)ppGpp levels to increase the number of persister cells (Ghosh et al., 2018). It is therefore possible that the *A. baumannii*

CDI_1 system could also impact overall bacterial physiology by fine-tuning cellular responses.

EXPERIMENTAL PROCEDURES

Growth Conditions, Strains, Plasmids, and Primers

Strains/plasmids and primers used in this study are listed in **Supplementary Tables S1, S2**, respectively. *Acinetobacter baumannii* and *Escherichia coli* strains were grown in LB, EZ-Rich Defined Medium (RDM), or M9 medium containing 0.2% glucose and 0.4% casamino acid (M9-casa) supplemented with appropriate antibiotics: 30 μg/ml of chloramphenicol (Cm), 50 μg/ml of ampicillin (Amp), 50 μg/ml of kanamycin (Kn), 15 μg/ml of gentamycin (Gm), and 50 (liquid) or 200 μg/ml (solid) of carbenicillin (Cb).

Strain Construction

Gene insertion in the *E. coli* chromosome was performed by λRed recombination (Datsenko and Wanner, 2000; Yu et al., 2000). Mutant alleles were transferred by phage P1 transduction to generate the final strains. The *kan* and *cat* genes were removed using site-specific recombination induced by expression of the Flp recombinase from plasmid pCP20 (Datsenko and Wanner, 2000).

cdiBAI$_1$ mutants were constructed following the Tucker et al. (2014) protocol. Briefly, the FRT (Flippase Recognition Target) site-flanked kanamycin resistance cassette was amplified from the pKD4 plasmid with primers containing 100-nt extension with homology to the flanking regions of *cdiBAI* locus. After the PCR product was electroporated into *A. baumannii* competent cells carrying pAT02 plasmid, which produces the $RecA_b$ recombinase, mutants were selected on Kn 50 μg/ml, and the presence of integrated kanamycin cassette was verified by PCR. The *kan* gene was removed using site-specific recombination induced by expression of the Flp recombinase from plasmid pFLP2 (Hoang et al., 2000).

cdiA$_1$ and *cdiB*$_1$ mutants were constructed by amplifying 2 kb with homology to the flanking regions of the genes. PCR products were combined by overlapping extension PCR and cloned into pUC18T-mini-Tn7-Ap *Sac*I/*Bam*HI. The apramycin (Apr) resistance cassette was then amplified from pMHL2-2 and cloned between the 2-kb-flanking regions with *Nco*I/*Sac*I restriction site. Then, the 2-kb-flanked apramycin cassette was amplified by PCR and electroporated into *A. baumannii* competent cells, and mutants were selected on Apr 50 μg/ml. The presence of integrated cassette was verified by PCR.

Toxicity Assays in *E. coli*

CdiA-CT domains were cloned with the artificial Shine-Dalgarno sequence into the pBAD33 plasmid using *Sac*I and *Sal*I. The *cdiI* genes were PCR amplified with a reverse primer encoding a 6xHis C-terminal tag and cloned into the pTrc99a plasmid using *Nco*I and *Bam*HI. Plasmid cloning was verified by Sanger sequencing (GATC Biotech). To perform toxicity assay, an overnight culture in LB with 0.5% glucose was washed in LB and diluted to an OD_{600} ∼ 0.05 in LB with 100 μM of IPTG and 1% arabinose to produce the immunity protein and the CdiA-CT domain, respectively. At indicated time of culture at 37°C, cells were washed in LB, and CFU/ml was calculated by plating onto LB agar plates containing Cm, Amp, and glucose 0.5%. The production of immunity proteins was verified by Western blot analyses. Briefly, the cell extract was separated on 12% SDS-PAGE, transferred onto polyvinylidene difluoride (PVDF) membranes, and probed with primary mouse anti-pentaHis (Qiagen) or anti EF-Tu.

Live-Cell Microscopy Experiment

Live and Dead Assay

Overnight cultures in RDM supplemented with 0.5% glucose were washed and diluted to OD_{600} of 0.05 with 100 μM of IPTG and 1% arabinose and grown further at 37°C for 3 h 30 min before treatment with the LIVE/DEAD® BacLight™ Bacterial Viability Kit. To control the functionality of the Live/Dead assay, we treated the samples with ethanol to kill the bacteria, and as expected, the percentage of cell death reaches ∼100% in this condition (**Supplementary Figure S2B**). Cells were stained for 20 min, washed, resuspended in RDM, and spread over a RDM or M9-casa 1% agarose pad.

Time-Lapse Experiments

Overnight cultures in RDM or M9-casa media supplemented with 0.5% glucose were diluted to OD_{600} of 0.05 with 0.5% glucose and grown further to OD_{600} = 0.1. Cultures were loaded to B04A microfluidic chamber (ONIX, CellASIC®) with 5 psi for 1 min. Medium supplemented with 1% arabinose was maintained at 1 psi with a constant temperature of 37°C. Cells were imaged every 10 min for 6 h.

Image Acquisition and Analysis

Conventional wide-field fluorescence microscopy imaging was carried out on an Eclipse Ti-E microscope (Nikon), equipped with ×100/1.45 oil Plan Apo Lambda phase objective, FLash4 V2 CMOS camera (Hamamatsu), and using NIS software for image acquisition. Acquisition setting was 10 ms for Syto9, 100 ms for GFP, 10 ms for propidium iodide, and 100 ms for mCherry, using 50% power of a fluo LED Spectra X light source at 488- and 560-nm excitation wavelengths, respectively. Cell counting and length analysis were performed using MicrobeJ (Ducret et al., 2016).

Quantification of Promoter Activities

The P_{empty} transcriptional fusion was constructed by cloning the *gfpmut2* gene from pUA66 plasmid as an *Eco*RI/*Bgl*II PCR fragment cloned into pWH1266. To construct transcriptional fusions, 500 bp corresponding to the putative promoter regions was amplified as a *Bam*HI/*Sac*I PCR fragment and cloned into pWH1266-P_{empty}-*gfp*. To quantify promoter activities, overnight cultures in LB were diluted to an OD_{600} of 0.05 and grown at 37°C for 6 h. Two hundred microliters of cells was transferred into well of a black 96-well plate (Greiner), and the absorbance at 600 nm and fluorescence (excitation 485 nm, emission 530 nm) were measured using TECAN Spark multimode plate reader. The relative fluorescence was expressed as the intensity

of fluorescence divided by the absorbance at 600 nm after subtracting the values of blank sample. Fluorescence repartition of the P*cdiB*$_1$-*gfp* was performed by diluting an overnight culture in RDM to an OD_{600} of 0.05 and grown further at 37°C to an OD_{600} ∼ 0.8 before spreading the cells over a RDM 1% agarose pad. The analysis was performed using MicrobeJ (Ducret et al., 2016).

Detection of CdiA$_1$

Cell extract and secreted fractions were prepared as follows. Bacterial cells from overnight culture grown in LB were harvested by centrifugation at 4,000 × *g* for 20 min, and pellets (cell extracts) were resuspended in loading buffer. The supernatant fraction was centrifuged at 13,000 × *g* for 20 min at 4°C. Proteins from the supernatant (secreted fraction) were then precipitated with 12% (w/v) trichloroacetic acid (TCA), washed with acetone, air-dried, and resuspended in loading buffer. The protein samples were then heated to 95°C for 10 min, separated by SDS-PAGE, and revealed by Coomassie blue staining or immunoblotting.

Growth Competition Assays

The attackers and target strains were grown overnight separately in LB medium without antibiotic at 37°C. Overnight cultures were diluted to an OD_{600} of 0.05 in LB medium without antibiotic and grown at 37°C with shaking to an OD_{600} ∼ 0.35. Strains were then mixed at an attacker to target cell ratio of 4:1, and the mixed bacteria were grown at 37°C with agitation at 160 rpm. At indicated times, the mix was serially diluted and plated onto kanamycin-containing LB agar plates to determine the CFU/ml of the target strain.

Biofilm Assays

Biofilm assays were performed following the O'Toole (2011) protocol. Briefly, overnight cultures were inoculated into LB at a final OD_{600} of 0.1. One hundred microliters of culture was added to 96-well polystyrene plates and incubated over a 5-h period without shaking. At the indicated times, cells in suspension were removed, and the wells washed twice with distilled water. One hundred twenty-five microliters of 0.1% crystal violet was then added to the wells, incubated for 10 min, and washed three times with 125 µl of distilled water. To solubilize the crystal violet, 125 µl of 30% acetic acid was added and the absorbance measured at 550 nm. The ratio OD_{550}/OD_{600} was calculated to normalize the biofilm formation due to variation in bacterial growth.

For biofilm imaging, bacteria were grown in BM2 minimal medium (Repizo et al., 2015) supplemented with 10 mM of potassium glutamate (BM2G) as carbon source in a glass-bottom 24-well µ-plate. Cultures were inoculated at an initial OD_{600} of 0.1 from an overnight culture grown in LB and then incubated at 37°C under static conditions. At indicated times, the biofilm was labeled with DAPI, and images were taken with a confocal Zeiss LSM800 Airyscan microscope and analyzed with ImageJ and Imaris software.

A. baumannii Infection of A549 Cells

A549 cells were grown in Dulbecco's modified Eagle medium (DMEM) supplemented with 10% of fetal calf serum and 1% L-glutamine at 37°C with 5% CO_2 atmosphere. For adhesion assays and microscopy analysis, A549 cells were first seeded into 24-well tissue culture plates at 5 × 10^5 cells/well to obtain a monolayer. *A. baumannii* strains were grown on LB agar plate for 24 h at 37°C to form a "lawn" covering. Bacteria were scraped from the agar surface and resuspended in 1 ml of LB to form a homogeneous suspension of ∼10^8 CFU/ml. Cells were then infected at a multiplicity of infection (MOI) of 100 of *A. baumannii* in 500 µl of complete medium per well. Plates were centrifuged at 400 × *g* for 5 min and then incubated for 2 h at 37°C with 5% CO_2 atmosphere. Cells were then washed five times with phosphate-buffered saline (PBS) 1 × and either lysed with 0.1% sodium deoxycholate (5-min incubation) or fixed with 3% paraformaldehyde (15 min incubation). The number of CFU/ml before and after infection was determined to calculate the percentage of bacterial adhesion. The number of CFU/ml of the inocula was also used to verify the MOI and ensure equivalent numbers of bacteria were used for wt and mutant strains.

Immunofluorescence Labeling and A549 Cell Microscopy

After fixation, cells were incubated at room temperature for 1 h in a PBS 1 × 0.1% saponin and 10% horse serum solution for permeabilization and blocking. Cells were then labeled at room temperature with primary rabbit anti-*Acinetobacter* antibody mix diluted at 1/20,000 in the same solution for 1 h followed by two washes in PBS 1 × 0.1% saponin. Secondary antibodies (anti-rabbit Alexa-488 [1/1,000], phalloidin-568 [1/250], and DAPI nuclear dye [1/1,000] to label *A. baumannii*, actin cytoskeleton, and host cell nucleus, respectively) were then mixed and incubated for 45 min, followed by two washes in PBS 1 × 0.1% saponin, one wash in PBS 1×, and one wash in distilled water before mounting with ProLong Gold. Coverslips were examined on a Zeiss LSM800 laser scanning confocal microscopes and analyzed with ImageJ software (Schindelin et al., 2012). Z-stack tool and Z-projection for maximum intensity were used for image presentation.

DATA AVAILABILITY STATEMENT

All datasets generated for this study are included in the article/**Supplementary Material**.

AUTHOR CONTRIBUTIONS

MR performed the majority of the experiments. SR, LC, JC, and CL also conducted the experiments. MR, SS, and CL participated in the experimental design and data analysis. SB conceived the project, designed and undertook experiments, interpreted data, and wrote the manuscript. All authors read and approved the manuscript.

FUNDING

This work was funded by a FINOVI young principal investigator grant awarded to SS. MR has a Ph.D. fellowship from the French

Ministry of Research. JC was funded by the FINOVI Foundation in partnership to the ATIP-Avenir grant to CL. SS and CL was supported by an INSERM staff scientist contract. SB was supported by the CNRS staff scientist contract.

ACKNOWLEDGMENTS

We thank E. Gueguen at the MAP, University of Lyon, for helpful discussions and support and for providing pUA66 plasmid. We are grateful to B. Davies at the University of Texas at Austin for providing the pAT02 plasmid, to X. Charpentier at the CIRI (INSERM, University of Lyon, CNRS, ENS) for the pMHL2-2 plasmid, and to R. Voulhoux at the CNRS-Aix-Marseille University for the anti EF-Tu antibody. We thank the proteomic facility of the Protein Science Facility of the SFR Biosciences for the mass spectrometry.

SUPPLEMENTARY MATERIAL

The Supplementary Material for this article can be found online at: https://www.frontiersin.org/articles/10.3389/fmicb.2019.02450/full#supplementary-material

REFERENCES

Allsopp, L. P., Wood, T. E., Howard, S. A., Maggiorelli, F., Nolan, L. M., Wettstadt, S., et al. (2017). RsmA and AmrZ orchestrate the assembly of all three type VI secretion systems in *Pseudomonas aeruginosa*. *Proc. Natl. Acad. Sci. U.S.A.* 114, 7707–7712. doi: 10.1073/pnas.1700286114

Anderson, M. S., Garcia, E. C., and Cotter, P. A. (2012). The burkholderia bcpAIOB genes define unique classes of two-partner secretion and contact dependent growth inhibition systems. *PLoS Genet.* 8:e1002877. doi: 10.1371/journal.pgen.1002877

Aoki, S. K., Diner, E. J., de Roodenbeke, C., Burgess, B. R., Poole, S. J., Braaten, B. A., et al. (2010). A widespread family of polymorphic contact-dependent toxin delivery systems in bacteria. *Nature* 468, 439–442. doi: 10.1038/nature09490

Aoki, S. K., Pamma, R., Hernday, A. D., Bickham, J. E., Braaten, B. A., and Low, D. A. (2005). Contact-dependent inhibition of growth in *Escherichia coli*. *Science* 309, 1245–1248. doi: 10.1126/science.1115109

Aoki, S. K., Webb, J. S., Braaten, B. A., and Low, D. A. (2009). Contact-dependent growth inhibition causes reversible metabolic downregulation in *Escherichia coli*. *J. Bacteriol.* 191, 1777–1786. doi: 10.1128/JB.01437-1438

Balder, R., Hassel, J., Lipski, S., and Lafontaine, E. R. (2007). *Moraxella* catarrhalis strain O35E expresses two filamentous hemagglutinin-like proteins that mediate adherence to human epithelial cells. *Infect. Immun.* 75, 2765–2775. doi: 10.1128/IAI.00079-77

Braun, V., Hobbie, S., and Ondraczek, R. (1992). *Serratia marcescens* forms a new type of cytolysin. *FEMS Microbiol. Lett.* 100, 299–305. doi: 10.1016/0378-1097(92)90225-d

Carruthers, M. D., Nicholson, P. A., Tracy, E. N., and Munson, R. S. (2013). *Acinetobacter baumannii* utilizes a type VI secretion system for bacterial competition. *PLoS One* 8:e59388. doi: 10.1371/journal.pone.0059388

Cope, L. D., Thomas, S. E., Hrkal, Z., and Hansen, E. J. (1998). Binding of heme-hemopexin complexes by soluble HxuA protein allows utilization of this complexed heme by *Haemophilus influenzae*. *Infect. Immun.* 66, 4511–4516.

Cope, L. D., Thomas, S. E., Latimer, J. L., Slaughter, C. A., Müller-Eberhard, U., and Hansen, E. J. (1994). The 100 kDa haem:haemopexin-binding protein of *Haemophilus influenzae*: structure and localization. *Mol. Microbiol.* 13, 863–873. doi: 10.1111/j.1365-2958.1994.tb00478.x

Cope, L. D., Yogev, R., Muller-Eberhard, U., and Hansen, E. J. (1995). A gene cluster involved in the utilization of both free heme and heme:hemopexin by *Haemophilus influenzae* type b. *J. Bacteriol.* 177, 2644–2653. doi: 10.1128/jb.177.10.2644-2653.1995

Darvish Alipour Astaneh, S., Rasooli, I., and Mousavi Gargari, S. L. (2014). The role of filamentous hemagglutinin adhesin in adherence and biofilm formation in *Acinetobacter baumannii* ATCC19606(T). *Microb. Pathog.* 74, 42–49. doi: 10.1016/j.micpath.2014.07.007

Datsenko, K., and Wanner, B. (2000). One-step inactivation of chromosomal genes in *Escherichia coli* K-12 using PCR products. *Proc. Natl. Acad. Sci. U.S.A.* 97, 6640–6645. doi: 10.1073/pnas.120163297

De Gregorio, E., Zarrilli, R., and Di Nocera, P. P. (2019). Contact-dependent growth inhibition systems in acinetobacter. *Sci. Rep.* 9:154. doi: 10.1038/s41598-018-36427-36428

Ducret, A., Quardokus, E. M., and Brun, Y. V. (2016). MicrobeJ, a tool for high throughput bacterial cell detection and quantitative analysis. *Nat. Microbiol.* 1:16077. doi: 10.1038/nmicrobiol.2016.77

Faure, L. M., Garvis, S., de Bentzmann, S., and Bigot, S. (2014). Characterization of a novel two-partner secretion system implicated in the virulence of *Pseudomonas aeruginosa*. *Microbiol. Read. Engl.* 160, 1940–1952. doi: 10.1099/mic.0.079616-79610

Faure, L. M., Llamas, M. A., Bastiaansen, K. C., de Bentzmann, S., and Bigot, S. (2013). Phosphate starvation relayed by PhoB activates the expression of the *Pseudomonas aeruginosa* σvreI ECF factor and its target genes. *Microbiol. Read. Engl.* 159, 1315–1327. doi: 10.1099/mic.0.067645-67640

Fournier, C., Smith, A., and Delepelaire, P. (2011). Haem release from haemopexin by HxuA allows *Haemophilus influenzae* to escape host nutritional immunity: HxuA releases haem from haemopexin. *Mol. Microbiol.* 80, 133–148. doi: 10.1111/j.1365-2958.2011.07562.x

Gallagher, L. A., and Manoil, C. (2001). *Pseudomonas aeruginosa* PAO1 kills *Caenorhabditis elegans* by cyanide poisoning. *J. Bacteriol.* 183, 6207–6214. doi: 10.1128/JB.183.21.6207-6214.2001

Garcia, E. C., Anderson, M. S., Hagar, J. A., and Cotter, P. A. (2013). BcpA mediates biofilm formation independently of interbacterial contact-dependent growth inhibition: CDI system protein-mediated biofilm. *Mol. Microbiol.* 89, 1213–1225. doi: 10.1111/mmi.12339

Garcia, E. C., Perault, A. I., Marlatt, S. A., and Cotter, P. A. (2016). Interbacterial signaling via burkholderia contact-dependent growth inhibition system proteins. *Proc. Natl. Acad. Sci. U.S.A.* 113, 8296–8301. doi: 10.1073/pnas.1606323113

Ghosh, A., Baltekin, Ö, Wäneskog, M., Elkhalifa, D., Hammarlöf, D. L., Elf, J., et al. (2018). Contact-dependent growth inhibition induces high levels of antibiotic-tolerant persister cells in clonal bacterial populations. *EMBO J.* 37:e98026. doi: 10.15252/embj.201798026

Gottig, N., Garavaglia, B. S., Garofalo, C. G., Orellano, E. G., and Ottado, J. (2009). A filamentous hemagglutinin-like protein of *Xanthomonas axonopodis* pv. citri, the phytopathogen responsible for citrus canker, is involved in bacterial virulence. *PloS One* 4:e4358. doi: 10.1371/journal.pone.0004358

Guédin, S., Willery, E., Locht, C., and Jacob-Dubuisson, F. (1998). Evidence that a globular conformation is not compatible with FhaC-mediated secretion of the *Bordetella pertussis* filamentous haemagglutinin. *Mol. Microbiol.* 29, 763–774. doi: 10.1046/j.1365-2958.1998.00970.x

Guérin, J., Bigot, S., Schneider, R., Buchanan, S. K., and Jacob-Dubuisson, F. (2017). Two-partner secretion: combining efficiency and simplicity in the secretion of large proteins for bacteria-host and bacteria-bacteria interactions. *Front. Cell. Infect. Microbiol.* 7:148. doi: 10.3389/fcimb.2017.00148

Guilhabert, M. R., and Kirkpatrick, B. C. (2005). Identification of Xylella fastidiosa antivirulence genes: hemagglutinin adhesins contribute a biofilm maturation to X. fastidios and colonization and attenuate virulence. *Mol. Plant Microb. Interact. MPMI* 18, 856–868. doi: 10.1094/MPMI-18-0856

Harding, C. M., Pulido, M. R., Di Venanzio, G., Kinsella, R. L., Webb, A. I., Scott, N. E., et al. (2017). Pathogenic acinetobacter species have a functional type i secretion system and contact-dependent inhibition systems. *J. Biol. Chem.* 292, 9075–9087. doi: 10.1074/jbc.M117.781575

Hoang, T. T., Kutchma, A. J., Becher, A., and Schweizer, H. P. (2000). Integration-proficient plasmids for *Pseudomonas aeruginosa*: site-specific integration and use for engineering of reporter and expression strains. *Plasmid* 43, 59–72. doi: 10.1006/plas.1999.1441

Iyer, L. M., Zhang, D., Rogozin, I. B., and Aravind, L. (2011). Evolution of the deaminase fold and multiple origins of eukaryotic editing and mutagenic nucleic acid deaminases from bacterial toxin systems. *Nucleic Acids Res.* 39, 9473–9497. doi: 10.1093/nar/gkr691

Jacob-Dubuisson, F., Buisine, C., Willery, E., Renauld-Mongénie, G., and Locht, C. (1997). Lack of functional complementation between Bordetella pertussis filamentous hemagglutinin and *Proteus mirabilis* HpmA hemolysin secretion machineries. *J. Bacteriol.* 179, 775–783. doi: 10.1128/jb.179.3.775-783.1997

Jacob-Dubuisson, F., Locht, C., and Antoine, R. (2001). Two-partner secretion in Gram-negative bacteria: a thrifty, specific pathway for large virulence proteins. *Mol. Microbiol.* 40, 306–313. doi: 10.1046/j.1365-2958.2001.02278.x

Kajava, A. V., Cheng, N., Cleaver, R., Kessel, M., Simon, M. N., Willery, E., et al. (2001). Beta-helix model for the filamentous haemagglutinin adhesin of Bordetella pertussis and related bacterial secretory proteins. *Mol. Microbiol.* 42, 279–292. doi: 10.1046/j.1365-2958.2001.02598.x

Lesterlin, C., Ball, G., Schermelleh, L., and Sherratt, D. J. (2014). RecA bundles mediate homology pairing between distant sisters during DNA break repair. *Nature* 506, 249–253. doi: 10.1038/nature12868

Melvin, J. A., Gaston, J. R., Phillips, S. N., Springer, M. J., Marshall, C. W., Shanks, R. M. Q., et al. (2017). *Pseudomonas aeruginosa* contact-dependent growth inhibition plays dual role in host-pathogen interactions. *mSphere* 2, e336–e317. doi: 10.1128/mSphere.00336-317

Mercy, C., Ize, B., Salcedo, S. P., de Bentzmann, S., and Bigot, S. (2016). Functional characterization of *Pseudomonas* contact dependent growth inhibition (CDI) systems. *PLoS One* 11:e0147435. doi: 10.1371/journal.pone.0147435

Neil, R. B., and Apicella, M. A. (2009). Role of HrpA in biofilm formation of *Neisseria meningitidis* and regulation of the hrpBAS transcripts. *Infect. Immun.* 77, 2285–2293. doi: 10.1128/IAI.01502-1508

O'Toole, G. A. (2011). Microtiter dish biofilm formation assay. *J. Vis. Exp.* 47, e2437. doi: 10.3791/2437

Pérez, A., Merino, M., Rumbo-Feal, S., Álvarez-Fraga, L., Vallejo, J. A., Beceiro, A., et al. (2016). The FhaB/FhaC two-partner secretion system is involved in adhesion of *Acinetobacter baumannii* AbH12O-A2 strain. *Virulence* 8, 959–974. doi: 10.1080/21505594.2016.1262313

Perez, F., Hujer, A. M., Hujer, K. M., Decker, B. K., Rather, P. N., and Bonomo, R. A. (2007). Global challenge of multidrug-resistant *Acinetobacter baumannii*. *Antimicrob. Agents Chemother.* 51, 3471–3484. doi: 10.1128/AAC.01464-1466

Plamondon, P., Luke, N. R., and Campagnari, A. A. (2007). Identification of a novel two-partner secretion locus in *Moraxella catarrhalis*. *Infect. Immun.* 75, 2929–2936. doi: 10.1128/IAI.00396-397

Relman, D. A., Domenighini, M., Tuomanen, E., Rappuoli, R., and Falkow, S. (1989). Filamentous hemagglutinin of Bordetella pertussis: nucleotide sequence and crucial role in adherence. *Proc. Natl. Acad. Sci. U.S.A.* 86, 2637–2641. doi: 10.1073/pnas.86.8.2637

Repizo, G. D., Gagné, S., Foucault-Grunenwald, M.-L., Borges, V., Charpentier, X., Limansky, A. S., et al. (2015). Differential Role of the T6SS in *Acinetobacter baumannii* virulence. *PLoS One* 10:e0138265. doi: 10.1371/journal.pone.0138265

Repizo, G. D., Viale, A. M., Borges, V., Cameranesi, M. M., Taib, N., Espariz, M., et al. (2017). The environmental *Acinetobacter baumannii* isolate DSM30011 reveals clues into the preantibiotic era genome diversity, virulence potential, and niche range of a predominant nosocomial pathogen. *Genome Biol. Evol.* 9, 2292–2307. doi: 10.1093/gbe/evx162

Rojas, C. M., Ham, J. H., Deng, W.-L., Doyle, J. J., and Collmer, A. (2002). HecA, a member of a class of adhesins produced by diverse pathogenic bacteria, contributes to the attachment, aggregation, epidermal cell killing, and virulence phenotypes of erwinia chrysanthemi EC16 on *Nicotiana clevelandii* seedlings. *Proc. Natl. Acad. Sci. U.S.A.* 99, 13142–13147. doi: 10.1073/pnas.202358699

Ruhe, Z. C., Townsley, L., Wallace, A. B., King, A., Van der Woude, M. W., Low, D. A., et al. (2015). CdiA promotes receptor-independent intercellular adhesion. *Mol. Microbiol.* 98, 175–192. doi: 10.1111/mmi.13114

Schindelin, J., Arganda-Carreras, I., Frise, E., Kaynig, V., Longair, M., Pietzsch, T., et al. (2012). Fiji: an open-source platform for biological-image analysis. *Nat. Methods* 9, 676–682. doi: 10.1038/nmeth.2019

Schmitt, C., Turner, D., Boesl, M., Abele, M., Frosch, M., and Kurzai, O. (2007). A functional two-partner secretion system contributes to adhesion of *Neisseria meningitidis* to epithelial cells. *J. Bacteriol.* 189, 7968–7976. doi: 10.1128/JB.00851-857

Talà, A., Progida, C., De Stefano, M., Cogli, L., Spinosa, M. R., Bucci, C., et al. (2008). The HrpB-HrpA two-partner secretion system is essential for intracellular survival of *Neisseria meningitidis*. *Cell. Microbiol.* 10, 2461–2482. doi: 10.1111/j.1462-5822.2008.01222.x

Tucker, A. T., Nowicki, E. M., Boll, J. M., Knauf, G. A., Burdis, N. C., Trent, M. S., et al. (2014). Defining gene-phenotype relationships in *Acinetobacter baumannii* through one-step chromosomal gene inactivation. *mBio* 5, e1313–e1314. doi: 10.1128/mBio.01313-1314

van Ulsen, P., Rahman, S. U., Jong, W. S. P., Daleke-Schermerhorn, M. H., and Luirink, J. (2014). Type V secretion: from biogenesis to biotechnology. *Biochim. Biophys. Acta* 1843, 1592–1611. doi: 10.1016/j.bbamcr.2013.11.006

Willett, J. L. E., Ruhe, Z. C., Goulding, C. W., Low, D. A., and Hayes, C. S. (2015). Contact-dependent growth inhibition (CDI) and CdiB/CdiA Two-Partner Secretion Proteins. *J. Mol. Biol.* 427, 3754–3765. doi: 10.1016/j.jmb.2015.09.010

Yu, D., Ellis, H. M., Lee, E. C., Jenkins, N. A., Copeland, N. G., and Court, D. L. (2000). An efficient recombination system for chromosome engineering in *Escherichia coli*. *Proc. Natl. Acad. Sci. U.S.A.* 97, 5978–5983. doi: 10.1073/pnas.100127597

Zhang, D., de Souza, R. F., Anantharaman, V., Iyer, L. M., and Aravind, L. (2012). Polymorphic toxin systems: comprehensive characterization of trafficking modes, processing, mechanisms of action, immunity and ecology using comparative genomics. *Biol. Direct.* 7:18. doi: 10.1186/1745-6150-7-18

Zhang, D., Iyer, L. M., and Aravind, L. (2011). A novel immunity system for bacterial nucleic acid degrading toxins and its recruitment in various eukaryotic and DNA viral systems. *Nucleic Acids Res.* 39, 4532–4552. doi: 10.1093/nar/gkr036

Conflict of Interest: The authors declare that the research was conducted in the absence of any commercial or financial relationships that could be construed as a potential conflict of interest.

Copyright © 2019 Roussin, Rabarioelina, Cluzeau, Cayron, Lesterlin, Salcedo and Bigot. This is an open-access article distributed under the terms of the Creative Commons Attribution License (CC BY). The use, distribution or reproduction in other forums is permitted, provided the original author(s) and the copyright owner(s) are credited and that the original publication in this journal is cited, in accordance with accepted academic practice. No use, distribution or reproduction is permitted which does not comply with these terms.

frontiers in Microbiology

ORIGINAL RESEARCH
published: 17 December 2019
doi: 10.3389/fmicb.2019.02864

The *Campylobacter jejuni* Type VI Secretion System Enhances the Oxidative Stress Response and Host Colonization

*Janie Liaw[1], Geunhye Hong[1], Cadi Davies[1], Abdi Elmi[1], Filip Sima[2], Alexandros Stratakos[2], Lavinia Stef[3], Ioan Pet[3], Abderrahman Hachani[1,4], Nicolae Corcionivoschi[2,3], Brendan W. Wren[1], Ozan Gundogdu[1] and Nick Dorrell[1]**

[1] Faculty of Infectious and Tropical Diseases, London School of Hygiene & Tropical Medicine, London, United Kingdom, [2] Bacteriology Branch, Veterinary Sciences Division, Agri-Food and Biosciences Institute, Belfast, United Kingdom, [3] Bioengineering of Animal Science Resources, Banat University of Agricultural Sciences and Veterinary Medicine – King Michael the I of Romania, Timisoara, Romania, [4] The Peter Doherty Institute for Infection and Immunity, Department of Microbiology and Immunology, University of Melbourne, Melbourne, VIC, Australia

The role of the Type VI secretion system (T6SS) in *Campylobacter jejuni* is poorly understood despite an increasing prevalence of the T6SS in recent *C. jejuni* isolates in humans and chickens. The T6SS is a contractile secretion machinery capable of delivering effectors that can play a role in host colonization and niche establishment. During host colonization, *C. jejuni* is exposed to oxidative stress in the host gastrointestinal tract, and in other bacteria the T6SS has been linked with the oxidative stress response. In this study, comparisons of whole genome sequences of a novel human isolate 488 with previously sequenced strains revealed a single highly conserved T6SS cluster shared between strains isolated from humans and chickens. The presence of a functional T6SS in the 488 wild-type strain is indicated by expression of T6SS genes and secretion of the effector TssD. Increased expression of oxidative stress response genes *katA*, *sodB*, and *ahpC*, and increased oxidative stress resistance in 488 wild-type strain suggest T6SS is associated with oxidative stress response. The role of the T6SS in interactions with host cells is explored using *in vitro* and *in vivo* models, and the presence of the T6SS is shown to increase *C. jejuni* cytotoxicity in the *Galleria mellonella* infection model. In biologically relevant models, the T6SS enhances *C. jejuni* interactions with and invasion of chicken primary intestinal cells and enhances the ability of *C. jejuni* to colonize chickens. This study demonstrates that the *C. jejuni* T6SS provides defense against oxidative stress and enhances host colonization, and highlights the importance of the T6SS during *in vivo* survival of T6SS-positive *C. jejuni* strains.

Keywords: campylobacter, type 6 secretion system, oxidative stress, chicken colonization, catalase, superoxide dismutase

OPEN ACCESS

Edited by:
Ignacio Arechaga, University of Cantabria, Spain

Reviewed by:
Carlos J. Blondel, Andres Bello University, Chile
Ina Attree, Centre National de la Recherche Scientifique (CNRS), France

***Correspondence:**
Nick Dorrell
nick.dorrell@lshtm.ac.uk

Specialty section:
This article was submitted to Microbial Physiology and Metabolism, a section of the journal Frontiers in Microbiology

Received: *28 March 2019*
Accepted: *26 November 2019*
Published: *17 December 2019*

Citation:
Liaw J, Hong G, Davies C, Elmi A, Sima F, Stratakos A, Stef L, Pet I, Hachani A, Corcionivoschi N, Wren BW, Gundogdu O and Dorrell N (2019) The Campylobacter jejuni Type VI Secretion System Enhances the Oxidative Stress Response and Host Colonization. Front. Microbiol. 10:2864. doi: 10.3389/fmicb.2019.02864

INTRODUCTION

Campylobacter jejuni, a Gram-negative microaerophilic bacteria, is the leading cause of bacterial foodborne gastroenteritis worldwide. *C. jejuni* infection in humans can lead to diarrhea, vomiting, abdominal pain, fever, with symptoms generally appearing 2–5 days following exposure to an infectious dose as low as 500–900 bacteria (Robinson, 1981; Kaakoush et al., 2015). Disease

presentation can vary depending on geographical region, with infections in low- and middle-income countries typically presenting with watery, non-inflammatory diarrhea whilst infections in high income countries display more severe disease, presenting with bloody inflammatory diarrhea (Coker et al., 2002). Campylobacteriosis is generally self-limiting, however, around 1 in 1,000 cases can develop severe auto-immune complications such as Guillain-Barré syndrome or Miller Fisher syndrome (Ang et al., 2001).

Campylobacter jejuni is most commonly transmitted through the handling and consumption of raw or undercooked poultry, but can also be spread through unpasteurized milk, contaminated water and cross contamination with other foods (Young et al., 2007; Kaakoush et al., 2015). *C. jejuni* colonizes chickens and other avian species and an estimated 70% of raw chicken sold in supermarkets in the United Kingdom will be contaminated with *C. jejuni* (Kaakoush et al., 2015). *C. jejuni* was previously regarded as a harmless commensal in the digestive tract of chickens, but recent studies indicate that colonization by *C. jejuni* is not asymptomatic, resulting in weight loss and slow growth of the infected poultry (Hermans et al., 2012; Wigley, 2015). The spread of *C. jejuni* through chicken flocks in farms can have a vast economic impact on the poultry industry and an increased spread of *C. jejuni* in chickens can subsequently affect the rates of infection in humans (Newell and Fearnley, 2003; Skarp et al., 2016).

During host colonization and infection, *C. jejuni* is exposed to conditions in the host gastrointestinal tract that present as physical and chemical stresses, including oxidative stress (Kim et al., 2015; Flint et al., 2016). Oxidative stress involves the generation of reactive oxygen species (ROS) that cause damage to nucleic acids, membranes and proteins of bacteria. In order to survive in this hostile environment, *C. jejuni* must defend against oxidative stress with enzymes that degrade ROS, such as SodB (superoxide dismutase), KatA (catalase), and AhpC (hydroperoxide reductase) (Kim et al., 2015). Regulation of the *C. jejuni* oxidative stress response is controlled by multiple regulatory mechanisms involving PerR, Fur and CosR to respond to fluctuating levels of ROS. Two MarR-type transcriptional regulators, RrpA and RrpB, also play a role in oxidative stress response regulation (Gundogdu et al., 2015).

The Type VI Secretion System (T6SS) is a contact-dependent secretion machinery capable of delivering effector proteins to both prokaryotic and eukaryotic cells. First identified in *Vibrio cholerae* and *Pseudomonas aeruginosa*, the T6SS has since been found to be present in 25% of Gram-negative bacterial species (Mougous et al., 2006; Pukatzki et al., 2006). The structure of the T6SS resembles an inverted bacteriophage tail with homologous components. The T6SS consists of 13 core components (TssA-TssM) and accessory proteins such as the T6SS-associated gene (Tag) proteins (see **Table 1**). A functioning T6SS complex requires essential components such as the baseplate (TssEFGK), a membrane-anchoring structure (TssJLM), a contractile sheath (TssBC) wrapped around a needle-like tube (TssD) and a puncture tip (TssI) further sharpened by a spike (TagD) (Cianfanelli et al., 2016). Composed of interlocking TssB and TssC components, the contractile sheath is responsible for producing enough energy to force the TssD needle-like structure through the inner membrane out into the extracellular space and puncture a host membrane to deliver effector proteins (Cianfanelli et al., 2016; Salih et al., 2018). The extended contractile sheath is broken down and the components recycled by the TssH ATPase for further sheath assembly (Kapitein et al., 2013).

TABLE 1 | Components of the bacterial Type VI Secretion System.

TSS system	Orthologs	Putative function/location
TssA	VasJ/ImpA	Docks to membrane complex, recruits baseplate complex, initiates/coordinates polymerization of TssD with sheath
TssB	VipA/ImpB	Contractile sheath
TssC	VipB/ImpC	Contractile sheath
TssD	Hcp	Secreted tube, effector
TssE	HsiF	Baseplate
TssF	VasA/ImpG	Baseplate
TssG	VasB/ImpH	Baseplate
TssH	ClpV/VasG	AAA+ATPase, sheath recycling
TssI	VgrG	Expelled spike, effector
TssJ	VasD/Lip/SciN	Membrane complex
TssK	VasE/ImpJ	Baseplate
TssL	IcmH/DotU/VasF	Membrane complex
TssM	IcmF/VasK	Membrane complex
TagD	PAAR	Tip of expelled spike

Delivery of effector proteins by the T6SS to target cells can exert a number of effects including colonization and niche establishment (Kapitein and Mogk, 2014; Ma et al., 2014; Drebes Dorr and Blokesch, 2018). T6SS effectors can target and eliminate bacterial and fungal competitors and also affect eukaryotic host cells (Murdoch et al., 2011; Trunk et al., 2018). To prevent self-intoxication by effector proteins, bacteria with the T6SS possess immunity proteins to neutralize the effects of the toxins (Kirchberger et al., 2017; Ringel et al., 2017; Fitzsimons et al., 2018). In competition with prokaryotic targets, T6SS can act either defensively or offensively; for example, the T6SS of *V. cholerae* and *Serratia marcescens* are offensive, apparently firing constantly and indiscriminately into the surrounding space, whilst the defensive T6SS of *P. aeruginosa* reacts only when fired upon in a "tit-for-tat" response (Gerc et al., 2015). T6SS effectors can subvert host cell processes by manipulating the host cytoskeleton, hindering host defense mechanisms, modulating the host inflammatory response and modifying host membrane structure (Hachani et al., 2016).

The T6SS can also defend against the production of ROS through secretion of effectors. For example, the T6SS-4 of *Yersinia pseudotuberculosis* secretes the effector YezP, which is able to bind to and sequester zinc ions and protect the bacteria from the effects of oxidative stress (Wang et al., 2015). The T6SS-4 of *Burkholderia thailandensis* also secretes effectors TseM for the uptake of manganese ions and TseZ for the uptake of zinc ions to mitigate the effects of oxidative stress. Similarly, enterohemorrhagic *Escherichia coli* secretes a T6SS effector, KatN, which facilitates survival of the bacteria in macrophages through decreasing the level of intracellular ROS (Wan et al., 2017).

Studies examining the prevalence of the T6SS in *C. jejuni* in Asia and Europe found a large variation in prevalence between regions. Harrison et al. (2014) observed in 2014 that up to 70% of isolates from chickens and humans in Vietnam were positive for the T6SS, whilst approximately only 3% of similar isolates from the United Kingdom were T6SS-positive. A further study in 2015 examining chicken isolates in Spain found a prevalence of 14%, whilst another study found that 28.8% of chicken isolates in Northern Ireland were T6SS-positive (Corcionivoschi et al., 2015; Ugarte-Ruiz et al., 2015). Other *Campylobacter* species can also carry the T6SS; the same study in Northern Ireland observed that 56.1% of *C. coli* found in retail chickens were T6SS-positive (Corcionivoschi et al., 2015). However, the large variation in prevalence may be due to differences in sample sizes, sample sources and in detection methods. Recent data suggests that the T6SS is becoming increasingly prevalent in *C. jejuni* strains, with indications that T6SS-positive strains are becoming more prevalent than T6SS-negative strains infecting chickens in farms, on raw poultry in supermarkets and even in hospital patients in the United Kingdom (Carmel Kelly, Agri-Food and Biosciences Institute, Personal Communication). A recent study in 2018 examining the presence of *C. jejuni* in wild birds of Finland observed that 49% of western jackdaw isolates and 72% of mallard duck isolates were T6SS-positive (Kovanen et al., 2018). This emphasizes the need to understand the role of the T6SS in *C. jejuni* and to develop intervention strategies to combat the rise of T6SS-positive *C. jejuni* strains (Sima et al., 2018).

In contrast to *V. cholerae* and *P. aeruginosa*, the role of the T6SS in *C. jejuni* is poorly understood. To date, only one *C. jejuni* T6SS cluster expressing a single TssD has been identified, compared to *P. aeruginosa* and *Yersinia pseudotuberculosis* which both possess multiple T6SS clusters exhibiting different functions (Lertpiriyapong et al., 2012). The structure of the *C. jejuni* T6SS is yet to be solved and TssD is thus far the only effector protein identified to be secreted by the *C. jejuni* T6SS (Lertpiriyapong et al., 2012; Bleumink-Pluym et al., 2013). Previous studies have demonstrated the *C. jejuni* T6SS may be important in host cell adherence and invasion, colonization, survival in bile salts and contact-dependent cytotoxicity toward red blood cells (Lertpiriyapong et al., 2012; Bleumink-Pluym et al., 2013). A recent study examined the structure of the TssD effector in *C. jejuni* and found that TssD is cytotoxic toward HepG2 human liver carcinoma cells (Noreen et al., 2018). However, whether the T6SS plays a role in the survival and infection of *C. jejuni* in poultry, a primary reservoir in humans is still unknown.

In this study, we investigated the role of the *C. jejuni* T6SS through whole genome sequencing of a T6SS-positive 488 wild-type strain (a recent human isolate from Brazil). We also sequenced the T6SS-positive 43431 wild-type strain (a human isolate from Canada) (Penner et al., 1983). We constructed defined isogenic mutants for genes encoding the contractile sheath components TssBC and needle structure TssD in the 488 wild-type strain and performed *in vitro* and *in vivo* characterization experiments in biologically relevant models. Our findings indicate that a functional T6SS is present in the *C. jejuni* 488 wild-type strain and the presence of the T6SS is important in defending against oxidative stress and enhancing *in vivo* survival, potentially thereby allowing strains harboring the T6SS to colonize and dominate in specific niches within a host.

RESULTS

Bioinformatic Analysis of T6SS Gene Clusters in *C. jejuni* 488 and Other T6SS-Positive Wild-Type Strains Reveals Synteny

Whole genome sequencing of *C. jejuni* 488 wild-type strain (a recent human isolate from Brazil) and *C. jejuni* wild-type strain 43431 (a human isolate from Canada) (Penner et al., 1983) was performed. *C. jejuni* wild-type strain RC039 (a chicken isolate from Northern Ireland) was previously sequenced (Corcionivoschi et al., 2015). The presence of a single T6SS cluster was observed in all three strains. All T6SS core components were identified, however, the TssH (ClpV) ATPase responsible for disassembly of the contracted sheath components is absent from the T6SS cluster of all *C. jejuni* strains sequenced thus far. The genome coordinates of the T6SS cluster in the *C. jejuni* 488 strain is listed in **Supplementary Table S1**. Comparisons of the 488, 43431, and RC039 genome sequences with previously published sequences for other T6SS-positive *C. jejuni* strains (Lertpiriyapong et al., 2012; Bleumink-Pluym et al., 2013) revealed a T6SS cluster that is highly conserved, sharing synteny between strains and also with other *Campylobacter* species isolated from humans and chickens (**Figure 1**). The 414 strain, isolated from wild bank voles in the United Kingdom, has a different gene arrangement in the T6SS cluster, but the same core components are still present.

T6SS Genes *tssB*, *tssC tssD* Are Expressed in the 488 Wild-Type Strain

Composed of interlocking TssB and TssC proteins, the contractile sheath is responsible for producing enough energy to force the TssD needle-like structure through the inner membrane out into the extracellular space and across host membranes (Cianfanelli et al., 2016). To investigate whether the *C. jejuni* 488 wild-type strain has a functional T6SS, the expression of the contractile sheath genes *tssB* and *tssC* as well as the *tssD* gene was investigated using RT-PCR. *tssB*, *tssC tssD* were all found to be expressed when the 488 wild-type strain is grown both in broth culture for 16 h and on blood agar for 24 h, indicating that the *C. jejuni* T6SS contractile sheath is produced under different growth conditions (**Figure 2**).

C. jejuni 488 Wild-Type Strain Has a Functional T6SS That Secretes TssD

Previous studies have used the secretion of TssD as evidence that the T6SS is functional in *C. jejuni* (Lertpiriyapong et al., 2012; Bleumink-Pluym et al., 2013). In order to determine whether the T6SS in the 488 wild-type strain is functional,

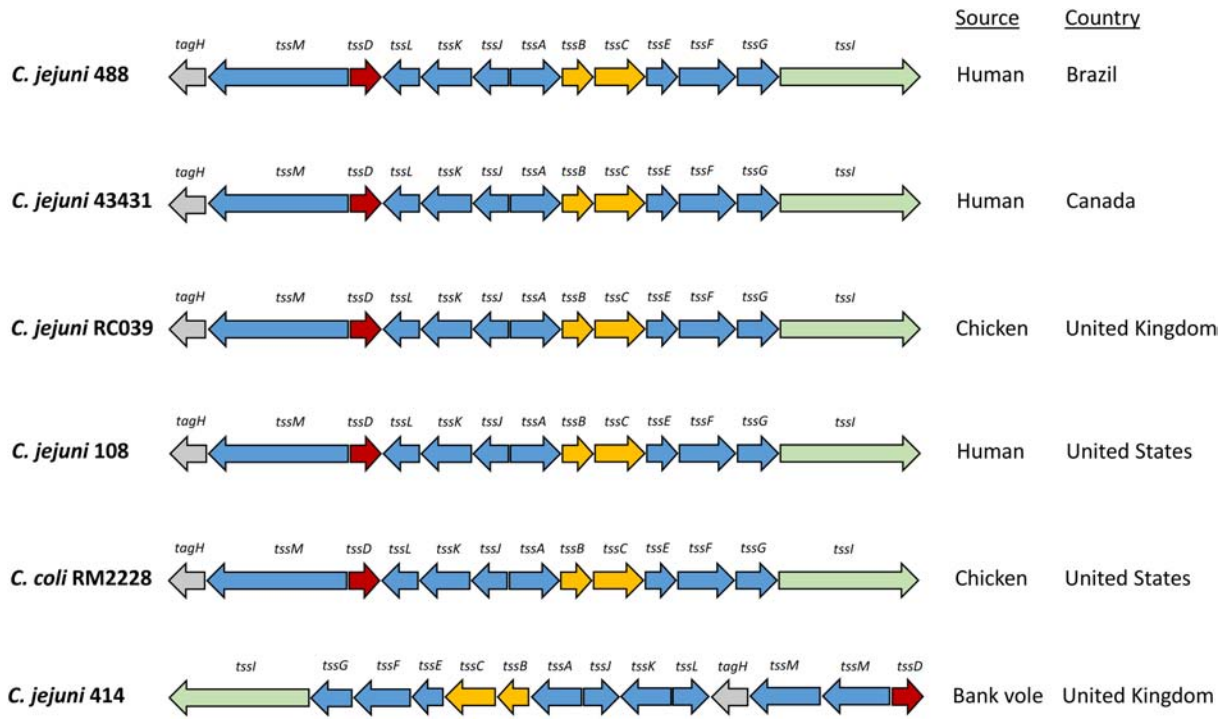

FIGURE 1 | Type VI secretion system gene clusters of *C. jejuni* strains. The *C. jejuni* 488 and 43431 wild-type strains were sequenced using whole genome sequencing in this study. The genome sequence of *C. jejuni* RC039 was published by Corcionivoschi et al. (2015). The genome sequences for *C. jejuni* 108 and *C. coli* RM2228 was published by Bleumink-Pluym et al. (2013). The genome sequence for *C. jejuni* 414 was published by Lertpiriyapong et al. (2012).

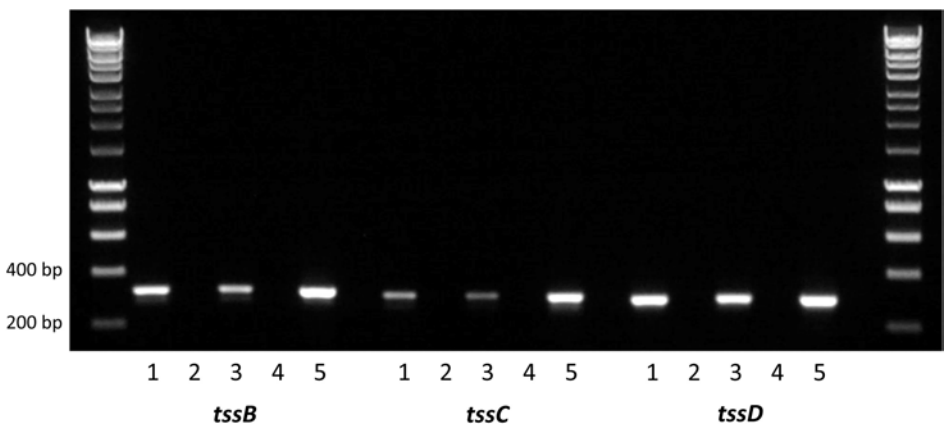

FIGURE 2 | Reverse transcription PCR analysis of T6SS gene expression in the 488 wild-type strain. RNA was isolated from 488 wild-type strain. Plate cultures were grown on blood agar plates and incubated for 24 h under microaerobic conditions. Broth cultures were grown in Brucella broth for 16 h at 37°C with shaking at 75 rpm under microaerobic conditions. Extracted RNA was converted to cDNA. RT-PCR was performed using *tssB*, *tssC*, and *tssD* primers. The first and last lanes are the molecular weight marker (HyperLadder 1 kb, Bioline, United Kingdom). Lane 1: 488 cDNA (plate culture); Lane 2: negative control (488 cDNA from plate culture synthesized without reverse transcriptase); Lane 3: 488 cDNA (broth culture); Lane 4: negative control (488 cDNA from broth culture synthesized without reverse transcriptase); and Lane 5: positive control (488 gDNA). Expected sizes are 316 bp (*tssB*), 300 bp (*tssC*), and 287 bp (*tssD*).

Western blotting was performed using a TssD antibody to detect the secretion of TssD. TssD is an approximately 18 kD protein that makes up the needle-like structure of the T6SS and has been shown in other bacteria to be important in the secretion of effector proteins (Cianfanelli et al., 2016). TssD is present in the whole cell lysate (**Figure 3A**) and also secreted into the supernatant of the 488 wild-type strain (**Figure 3B**), indicating that this strain has a functional T6SS. TssD is absent from both whole cell lysate and supernatant from the 488 *tssD* mutant.

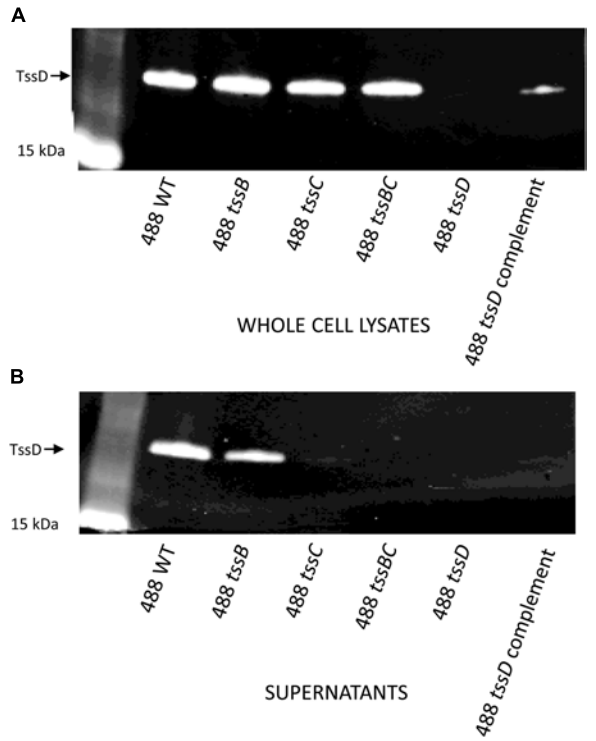

FIGURE 3 | Detection of TssD in *C. jejuni* whole cell lysates and supernatants. **(A)** Detection of TssD in *C. jejuni* whole cell lysates. Whole cell lysate samples were prepared from 16 h cultures of *C. jejuni* 488 wild-type strain, 488 *tssB* mutant, 488 *tssC* mutant, 488 *tssBC* double mutant, 488 *tssD* mutant, and 488 *tssD* complement grown in Brucella broth. 13 μg of samples were loaded onto SDS-PAGE. Western blotting was performed using a TssD antibody, with a recombinant TssD protein used as a positive control. **(B)** Detection of TssD in *C. jejuni* supernatants. Bacterial supernatant samples were prepared from 16 h cultures of *C. jejuni* 488 wild-type strain, 488 *tssB* mutant, 488 *tssC* mutant and 488 *tssBC* double mutant grown in Brucella broth. Supernatant samples were concentrated via TCA precipitation and 30 μg of samples were loaded onto SDS-PAGE. Western blotting was performed using a *C. jejuni* TssD antibody. *C. jejuni* TssD has an estimated molecular weight of 18 kDa.

Inactivation of Individual Contractile Sheath Components Does Not Abolish *C. jejuni* T6SS Function

488 *tssB* and *tssC* single mutants were constructed to investigate whether knocking out a contractile sheath component would result in a non-functional T6SS. Inactivation of either *tssB* or *tssC* reduces but does not completely abolish secretion of TssD (**Figure 3B**), indicating that the absence of one of the contractile sheath components does not result in a completely non-functional T6SS in *C. jejuni*. A 488 *tssBC* double mutant was also constructed to test the hypothesis that function of the *C. jejuni* T6SS is only abolished in the absence of both contractile sheath components. As hypothesized, TssD was present in the whole cell lysate but absent from the supernatant of the 488 *tssBC* double mutant, thereby demonstrating that the *C. jejuni* T6SS is not functional when the entire contractile sheath structure is missing.

T6SS in *C. jejuni* Is Associated With the Oxidative Stress Response

The T6SS has previously been linked with the oxidative stress response in *Y. pseudotuberculosis*, *B. thailandensis*, and enterohemorrhagic *E. coli* (Wang et al., 2015; Si et al., 2017; Wan et al., 2017). To investigate whether the *C. jejuni* T6SS is also associated with the oxidative stress response, the 488 wild-type strain, 488 *tssD* mutant and 81–176 wild-type strain were exposed to hydrogen peroxide (H_2O_2). Following 30 min exposure to 50 mM H_2O_2, the 488 wild-type strain exhibited significantly greater resistance to oxidative stress killing compared to the 488 *tssD* mutant and the 81–176 wild-type strain (**Figure 4A**). In order to investigate whether the increased susceptibility of the 488 *tssD* mutant to H_2O_2 is specific and not due to a potential membrane defect due to improper assembly of the T6SS in the bacterial membrane, antimicrobial susceptibility testing for the 488 wild-type strain, 488 tssD mutant and 488 tssD complement were performed. Disk diffusion assays were performed using ampicillin, amoxycillin/clavulanic acid, tetracycline and polymyxin B. A broth microdilution assay was performed using vancomycin. No differences in antimicrobial susceptibility were observed (**Supplementary Table S2**).

katA, *sodB*, and *ahpC* encode proteins involved directly in the breakdown of ROS. Expression of *katA*, *sodB*, and *ahpC* was investigated in the 488 wild-type strain and 488 *tssD* mutant using qRT-PCR. Expression of all three genes were significantly reduced in the 488 *tssD* mutant compared to the 488 wild-type strain. This data combined with the increased ability of the 488 wild-type strain to survive the effects of oxidative stress suggest that the T6SS is associated with the oxidative stress response in *C. jejuni* (**Figure 4B**).

T6SS Increases *C. jejuni* Cytotoxicity in the *Galleria mellonella* Model of Infection

The larvae of *G. mellonella* (Greater wax moth) are an established model to study the pathogenesis of *C. jejuni* (Senior et al., 2011). In order to investigate whether the presence of a T6SS in *C. jejuni* enhances bacterial cytotoxicity, *G. mellonella* larvae were injected with *C. jejuni* strains and larvae survival examined over a duration of 5 days. Only the T6SS-positive 488 wild-type strain was cytotoxic to *G. mellonella* larvae after 24 h post-injection (**Figure 5**). The T6SS-negative 81–176 wild-type strain also exhibited some cytotoxicity, but at a lower level compared to the 488 wild-type strain after 48 and 72 h. After 96 and 120 h, cytotoxicity of the 488 *tssD* mutant was also observed but at a significantly lower level than the 488 wild-type strain.

T6SS Enhances Both *C. jejuni* Interactions With and Invasion of Chicken Primary Intestinal Cells

Recent studies suggest that the prevalence of T6SS-positive *C. jejuni* strains is on the rise in high-income countries and there are indications that T6SS-positive strains are now prevalent over T6SS-negative strains infecting chickens in farms, on raw chicken in supermarkets and in hospital patients (Ugarte-Ruiz et al., 2015; Sima et al., 2018). To investigate whether the presence of the

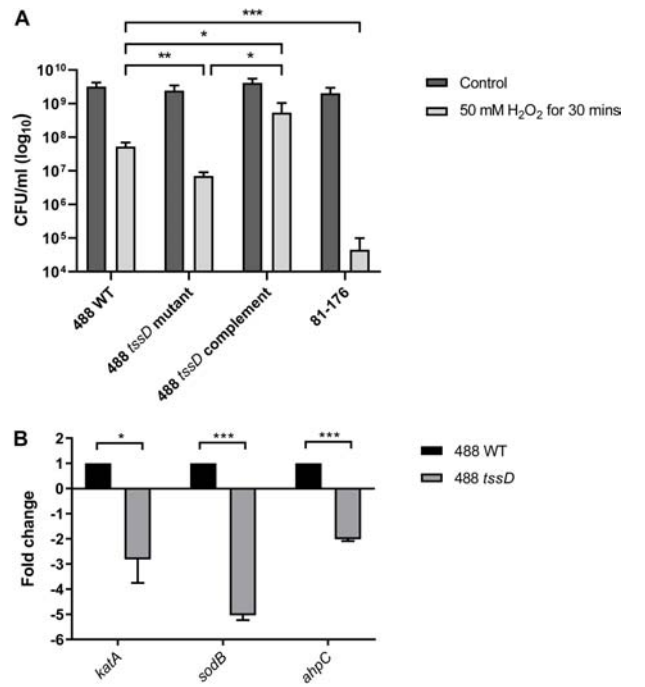

FIGURE 4 | Type VI secretion system of *C. jejuni* is involved in the oxidative stress response. **(A)** Survival of 488 wild-type strain, 488 *tssD* mutant, 488 *tssD* complement, and 81–176 wild-type strain following exposure to oxidative stress. The strains were exposed to 50 mM H_2O_2 for 30 min, then serial dilutions were performed and CFUs/ml counted. Asterisks denote a statistically significant difference (*$p \leq 0.05$, **$p \leq 0.01$, ***$p \leq 0.001$). **(B)** qRT-PCR analysis comparing expression of *katA*, *sodB*, and *ahpC* in the 488 wild-type strain and 488 *tssD* mutant. qRT-PCR analysis was performed using *katA*, *sodB*, and *ahpC* primers. Data was analyzed by the comparative CT method with *gyrA* housekeeping gene as the internal control. The relative expression of *katA*, *sodB*, and *ahpC* are shown. Asterisks denote a statistically significant difference (*$p \leq 0.05$, ***$p \leq 0.001$).

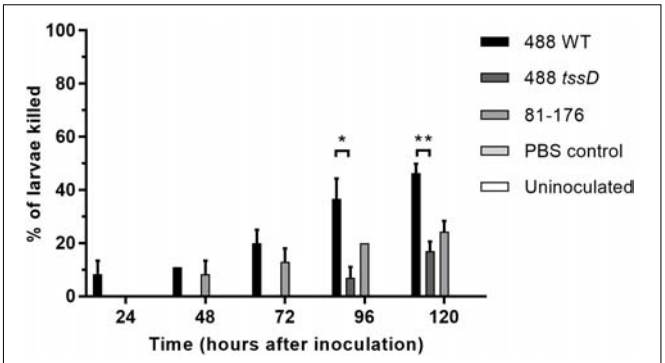

FIGURE 5 | Infection of *Galleria mellonella* larvae with the 488 wild-type strain, 488 *tssD* mutant or 81–176 wild-type strain. Ten *G. mellonella* larvae were injected per bacterial strain with a syringe in the right foremost leg. Controls injected with PBS only were included along with uninoculated controls. Larvae were incubated at 37°C with counts of dead larvae recorded every 24 h over a period of 5 days. Asterisks denote a statistically significant difference (*$p \leq 0.05$, **$p \leq 0.01$).

T6SS plays a role in the ability of *C. jejuni* to infect chickens, an *in vitro* model was used to examine the potential of *C. jejuni* to adhere to and invade chicken primary intestinal cells. The 488 wild-type strain exhibited significantly higher levels of adherence and invasion than the 488 *tssD* mutant. The T6SS-negative 81–176 wild-type strain also exhibited lower levels of adherence and invasion than the 488 wild-type strain, however, these differences were not significant (**Figure 6**).

T6SS Enhances the Ability of *C. jejuni* to Infect Chickens

To further investigate whether the presence of the T6SS plays a role in the ability of *C. jejuni* to infect chickens, chicken infection studies were performed. An identical pattern was observed after *in vivo* infection of 15-day old Ross 308 broiler chickens, where at 3 days post-infection the numbers of the 488 wild-type strain detected in the caeca were significantly higher than the numbers of the 488 *tssD* mutant or 81–176 wild-type strain (**Figure 7**). These results indicate that the presence of the T6SS is important in enhancing the ability of *C. jejuni* to colonize chickens.

DISCUSSION

The *C. jejuni* T6SS is a functional secretory mechanism that appears distinct from the well-elucidated *P. aeruginosa* and *V. cholerae* T6SS model systems. Whole genome sequencing of a novel 488 strain and the T6SS-positive 43431 strain revealed a single T6SS cluster containing one copy of the *tssD* gene that encodes the needle-like tube of the T6SS, but the absence of *tssH* which encodes the ATPase that breaks down and recycles the TssBC contractile sheath. This is in contrast to the T6SS model systems of *P. aeruginosa* and *V. cholerae* where multiple T6SS clusters are present with differing functions. The absence of a *tssH* ortholog had previously been observed in other *C. jejuni* strains in other studies (Lertpiriyapong et al., 2012; Bleumink-Pluym et al., 2013). *Burkholderia* species, *Helicobacter hepaticus*, *Francisella tularensis*, and *Salmonella enterica* also appear to lack a TssH component. Despite the absence of TssH, the presence of a functional T6SS in all these organisms including *C. jejuni* suggests there may be alternate mechanisms for contractile sheath recycling. In *V. cholerae* a study demonstrated that whilst TssH is not essential, it is important in increasing the efficiency of the T6SS in inter-bacterial competition assays (Bachmann et al., 2015).

Comparison of the *C. jejuni* strains sequenced in this study with previously published sequences of other *C. jejuni* strains as well as other *Campylobacter* species revealed a T6SS cluster that is very closely conserved with all core genes present in the same arrangement. *C. jejuni* 488 (human isolate from Brazil), 43431 (human isolate from Canada), 108 (human isolate from the United States), RC039 (chicken isolate from the United Kingdom), and even *C. coli* RM2228 (chicken isolate from the United States) all share the same conserved T6SS cluster. Only *C. jejuni* 414 had a different gene arrangement in the T6SS cluster. 414 is an environmental strain, isolated from a wild bank vole in the United Kingdom (Williams et al., 2010). It is possible that agricultural intensification practices which readily facilitate

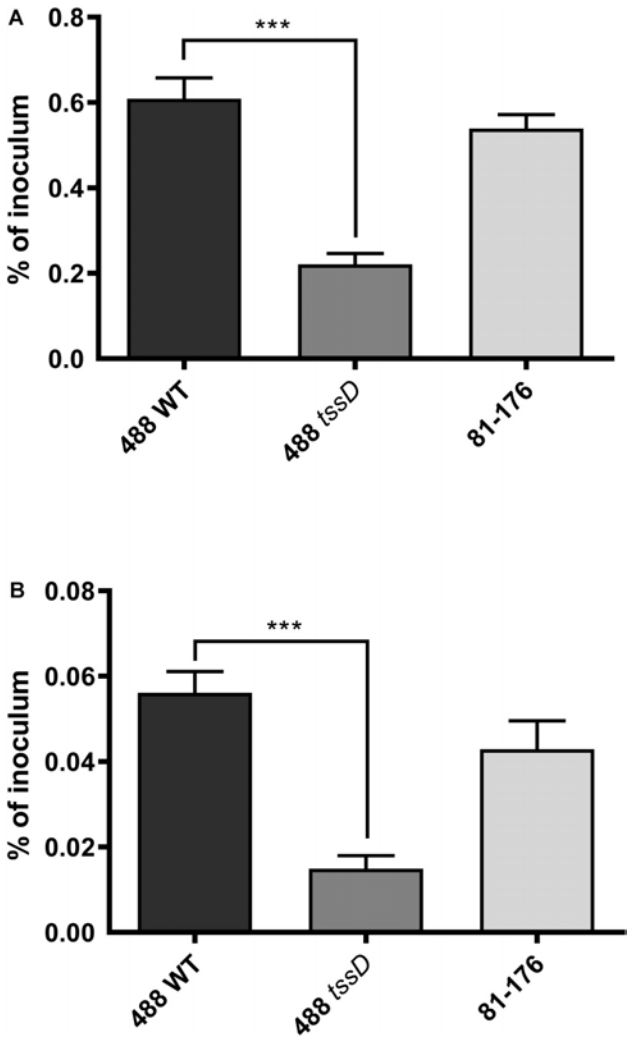

FIGURE 6 | Interactions with and invasion of primary chicken intestinal cells with the 488 wild-type strain, 488 *tssD* mutant or 81–176 wild-type strain. Primary chicken intestinal cells were infected with *C. jejuni* strains at a MOI of 1,000:1. **(A)** For interaction assays, infected monolayers were washed with PBS and treated with 0.1% (v/v) Triton X-100. **(B)** For invasion assays, infected monolayers were washed with PBS and treated with gentamicin (400 μg/ml) for 2 h at 37°C. Cells were then washed with PBS and treated with 0.1% (v/v) Triton X-100. For both experiments, serial dilutions were then performed and the CFUs/ml counted. Asterisks denote a statistically significant difference (***$p \leq 0.001$).

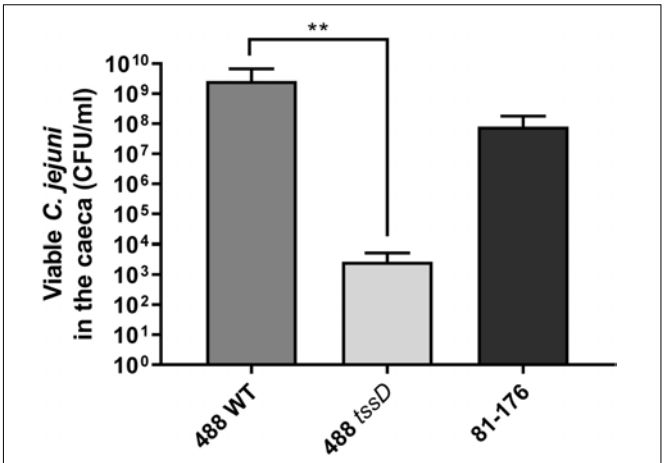

FIGURE 7 | Infection of broiler chickens with the 488 wild-type strain, 488 *tssD* mutant or 81–176 wild-type strain. Ten 15-day old Ross 308 broiler chickens were inoculated with approximately 1×10^8 CFU/ml of either the 488 wild-type strain, the 488 *tssD* mutant or the 81–176 wild-type strain. Chickens were euthanized 3 days post-infection. Caecum contents were plated and counts of viable *C. jejuni* in the samples performed. Asterisks denote a statistically significant difference (**$p \leq 0.01$).

passing of strains between chickens and humans could lead to these strains to share more of a conserved T6SS compared to the 414 environmental strain.

Further investigations indicated that the novel 488 strain has a functional T6SS capable of secreting the TssD effector, corroborating previous studies which have shown TssD to be secreted from 43431 and 108 strains (Lertpiriyapong et al., 2012; Bleumink-Pluym et al., 2013). However, the contractile sheath components TssBC and their function had not previously been studied in *C. jejuni*. In other bacteria, an intact contractile sheath structure is important for a fully functioning T6SS as removal of either TssB/VipA or TssC/VipB from the contractile sheaths described in *V. cholerae* result in a defective T6SS unable to secrete effectors (Basler et al., 2012; Kudryashev et al., 2015; Brackmann et al., 2018). In this study we have shown that both contractile sheath genes are expressed when the 488 strain is cultured in broth and on solid plates. Isogenic 488 *tssB* and *tssC* mutants were constructed and shown to still be able to secrete TssD at a reduced level compared to the wild-type strain. The observation that the *C. jejuni* T6SS does not require both TssB and TssC components to be present for the T6SS to be able to secrete TssD is unusual and differs from previous observations of the T6SS in *V. cholerae*. This suggests that in *C. jejuni*, as long as either TssB or TssC is present, the T6SS remains capable of secreting TssD at a reduced level. However, this does not suggest that the contractile sheath components in *C. jejuni* may differ from those in the T6SS model systems of *P. aeruginosa* and *V. cholerae*, rather that the contractile sheath components may be interchangeable or be able to compensate for the absence of the other component via a yet unknown process.

The importance of the T6SS in countering the effects of oxidative stress has previously been shown in *Y. pseudotuberculosis*, *B. thailandensis*, and enterohemorrhagic *E. coli* (Wang et al., 2015; Si et al., 2017; Wan et al., 2017). In this study, we show that the *C. jejuni* T6SS also appears to play a role, with the genes that encode KatA, SodB, and AhpC that are involved directly in the breakdown of ROS all expressed at significantly higher levels in the 488 wild-type strain compared to the 488 *tssD* mutant. The 488 wild-type strain with an intact T6SS is also more resistant to the effects of oxidative stress compared to the 488 *tssD* mutant. We speculate that TssD positively regulates the expression of genes involved in the breakdown of ROS, and in turn this results in greater resistance to oxidative stress in strains harboring an intact T6SS cluster.

A MarR family transcriptional regulator TctR was recently shown to regulate the T6SS-2 gene cluster in *B. pseudomallei* (Losada et al., 2018). Previous studies have also shown that the MarR family transcriptional regulators RrpA and RrpB are important in regulating both oxidative and aerobic stress responses in *C. jejuni* and therefore play a role in enhancing bacterial survival both in the hosts and in the environment (Gundogdu et al., 2011, 2015, 2016). As our results indicate that the *C. jejuni* T6SS is also associated with the oxidative stress response, it is tempting to speculate that the RrpA and RrpB regulators may in some way be linked to the T6SS. Further studies will be required to investigate this hypothetical link.

Based on our data we propose that presence of the T6SS cluster in *C. jejuni* strains also confers a competitive advantage to these strains within a host. The T6SS-positive 488 wild-type strain is more cytotoxic in the *G. mellonella* model than the T6SS-negative 81–176 wild-type strain and the 488 *tssD* mutant. This suggests that the presence of a T6SS increases the cytotoxicity of *C. jejuni* in the *G. mellonella* model of infection and secreted T6SS effectors may also be important in causing cytotoxicity to other organisms. The 81–176 strain was selected as a negative control in this study due to the absence of the T6SS in this strain. Despite lacking the T6SS, 81–176 is a hypervirulent strain capable of causing severe disease and harbors two plasmids, pTet and pVir, that play a role in increased virulence (Black et al., 1988; Bacon et al., 2000). Therefore, any differences observed between 488 and 81–176 could potentially be due to a diversity of virulence factors in these two strains rather than the presence or absence of the T6SS.

This study is the first to examine the role of T6SS of *C. jejuni* in a biologically relevant model. Lertpiriyapong et al. (2012) utilized a murine model and found that a T6SS-positive strain to be more interactive with and invasive in RAW 264.7 macrophage cells and have a higher colonization potential in IL-10-deficient mice. However, it has previously been shown that *C. jejuni* does not colonize mice in the same manner as in chickens, as *C. jejuni* colonizes mice at a significantly slower rate than chickens and some strains such as 81–176 do not appear to colonize mice at all (Wilson et al., 2010). The *C. jejuni* 488 wild-type strain exhibits higher levels of adherence to and invasion of chicken cells and is also able to infect chickens at a much higher rate that the *tssD* mutant. The results indicate that the ability of *C. jejuni* to infect chickens is enhanced by the presence of the T6SS and the T6SS may be important as a colonization factor in the natural host of *C. jejuni*. The increased ability of *C. jejuni* strains with the T6SS to infect and colonize chickens is a particular concern for the agricultural and food industries tasked with reducing *C. jejuni* load in both live chickens on farms and on raw chicken meat in the supermarket (Sima et al., 2018). From a public health perspective, the rise of T6SS in *C. jejuni* is also problematic as there are indications that strains with the T6SS may cause more severe disease in humans (Harrison et al., 2014).

In summary, in this study we confirmed the presence of a single T6SS cluster among several *C. jejuni* strains and confirmed that the functional T6SS is capable of secreting the TssD effector. Our results indicated that the *C. jejuni* T6SS is involved in the oxidative stress response. Using *in vitro* and *in vivo* models we demonstrated the increased ability of T6SS-positive *C. jejuni* to colonize the natural avian host. Our findings highlight the importance of further understanding the function of the T6SS present in an expanding population of *C. jejuni*, the potential importance of the T6SS in colonization and niche establishment in different hosts and the potential for T6SS-positive *C. jejuni* strains to cause more severe disease in both chickens and humans.

MATERIALS AND METHODS

Bacterial Strains and Growth Conditions

Campylobacter jejuni strains used in this study are listed in **Supplementary Table S3**. *C. jejuni* strains were grown at 37°C under microaerobic conditions (85% N_2, 15% CO_2 5% O_2) in a variable atmosphere chamber (Don Whitley Scientific, United Kingdom). Unless otherwise stated, *C. jejuni* were grown either on Columbia agar with 7% (v/v) horse blood (TCS Biosciences, United Kingdom) with the addition of Skirrow *Campylobacter* selective supplement or in Brucella broth (BD Diagnostics, United Kingdom). *E. coli* strains listed in **Supplementary Table S4** were grown on lysogeny broth (LB) agar plates or in LB broth at 37°C. The appropriate antibiotics were added as required at concentrations of 50 μg/ml kanamycin, 100 μg/ml ampicillin or 10 μg/ml chloramphenicol for *C. jejuni* growth, with the concentration of chloramphenicol for *E. coli* growth increased to 50 μg/ml. All reagents were obtained from Oxoid (United Kingdom) unless otherwise stated.

Whole Genome Sequencing

Genome sequencing of the *C. jejuni* 488 and 43431 (Poly et al., 2004) wild-type strains was performed as previously described by Ugarte-Ruiz et al. (2014). Briefly, sequencing was performed using the Illumina MiSeq 2 × 301 bp paired-end sequencing. To analyze the data quality, FastQC was used (Simon, 2010) followed by read trimming using Trimmomatic (v0.32) (leading' and "trailing" setting of 3, a "sliding window" setting of 4:20 and a "minlength" of 36 nucleotides) (Bolger et al., 2014). Reads were mapped using BWA-MEM (v0.7.7-r441) against the genome sequence of *C. jejuni* NCTC 11168 (AL111168) (Li and Durbin, 2009). Assembly on unmapped regions was performed using Velvet Optimizer (v2.2.5) using n50 optimization (Zerbino and Birney, 2008; Gladman and Seemann, 2012). Contigs were ordered against *C. jejuni* NCTC 11168 (AL111168) strains using ABACAS (v1.3.1) (Assefa et al., 2009). Genome annotation was performed using Prokka (Seemann, 2014). Genomes were visualized using Artemis and ACT software (Carver et al., 2012). T6SS ORFs were identified using BLAST (Altschul et al., 1990; Gish and States, 1993). The 488 and 43431 genome sequences were uploaded to the EBI ENA database (Accession number PRJEB31331).

Reverse Transcription PCR (RT-PCR) and Quantitative Real-Time PCR (qRT-PCR) Analyses

Total RNA was isolated using PureLink RNA Mini Kit (Thermo Fisher Scientific) from *C. jejuni* cultures grown for 16 h at

37°C with shaking at 75 rpm under microaerobic conditions in Brucella broth. TURBO DNA-free kit (Thermo Fisher Scientific) was used to remove DNA contamination and RNA was converted to cDNA using the SuperScript III First-Strand Synthesis System (Thermo Fisher Scientific). Reverse transcription PCR (RT-PCR) was performed according to the manufacturer's instructions with primers listed in **Supplementary Table S5**. Quantitative real-time PCR (qRT-PCR) was performed using primers listed in **Supplementary Table S5**, with SYBR Green Master Mix (Applied Biosystems, United Kingdom) on the ABI 7500 Real-Time PCR System machine (Applied Biosystems). qRT-PCR data was analyzed by the comparative C_T method with *gyrA* housekeeping gene as an internal control (Ritz et al., 2002; Schmittgen and Livak, 2008).

Construction of *tssB*, *tssC*, *tssD* Mutants and *tssBC* Double Mutant

Campylobacter jejuni mutants were constructed as previously described (Gundogdu et al., 2011). Briefly, the appropriate gene specific primers (see **Supplementary Table S5**) were used to amplify the gene of interest from *C. jejuni* genomic DNA. PCR products were cloned into a pGEM-T Easy vector (Promega, United Kingdom) and transformed into *E. coli* XL2-Blue if the unique restriction site was *Bam*HI or *Bgl*II. *E. coli* SCS110 were used if the restriction site was *Bcl*I. If none of these sites were present, inverse PCR mutagenesis was used to introduce a *Bgl*II site (Gundogdu et al., 2015). Plasmid DNA was digested with *Bam*HI, *Bcl*I, or *Bgl*II, a kanamycin or chloramphenicol resistance cassette was inserted and the resulting construct transformed into *E. coli*. Successful constructs were transformed into *C. jejuni* by electroporation and positive clones were confirmed by PCR and Sanger sequencing. For construction of a *C. jejuni tssBC* double mutant, the plasmid DNA construct used for the *C. jejuni tssC* mutant was transformed into *C. jejuni tssB* mutant by electroporation.

Preparation of Whole Cell Lysates and Supernatants for Protein Secretion Assays

Campylobacter jejuni strains from 24 h plate cultures were inoculated to OD_{600} 0.1 in Brucella broth and incubated at 37°C with shaking at 75 rpm under microaerobic conditions until late log phase. The broth cultures were centrifuged at 4,000 rpm at 4°C for 30 min to separate the pellet and the supernatant.

To prepare a whole cell lysate sample, a pellet was re-suspended in PBS and sonicated for 10 min on high setting using a Bioruptor (Diagenode, Belgium). Sonicated samples were centrifuged at 13,000 rpm for 5 min and the resulting supernatant was added to 2X Laemmli sample buffer (Sigma-Aldrich, United Kingdom) then boiled at 95°C for 10 min, followed by centrifugation at 13,000 rpm for 5 min. To prepare a supernatant sample, supernatant was filtered through a 0.2 μm-pore-size filter (Millipore, United Kingdom) to remove remaining cells and the titrate was concentrated using an Amicon Ultra-15 centrifugal filter (10 kDa) (Millipore). Trichloroacetic acid (TCA) precipitation with acetone washes was performed to further concentrate the samples as described previously (Link and LaBaer, 2011). Following acetone washes, the pellet was re-suspended in 2X Laemmli sample buffer and boiled at 95°C for 10 min, followed by centrifugation at 13,000 rpm for 5 min.

SDS-PAGE and Western Blot Analysis

BCA assay was performed to determine protein concentration in samples. 13 μg of whole cell lysate samples and 30 μg of supernatant samples were loaded along with Pageruler Plus Pre-stained Protein Ladder (Thermo Fisher Scientific, United Kingdom) onto NuPAGE Bis-Tris gel (12%) (Thermo Fisher Scientific) with MOPS running buffer (Thermo Fisher Scientific). Membrane transfer was performed using the iBlot 2 Dry Blotting System (Thermo Fisher Scientific). The membrane was blocked with 2% (w/v) milk overnight at 4°C, incubated with the TssD antibody in phosphate buffered saline with 0.1% (v/v) Tween-20 (PBS-T) for 1 h at room temperature, washed with PBS-T then incubated with the secondary goat anti-rabbit antibody in PBS-T for 1 h at room temperature. The membrane was washed twice with PBS-T, once with PBS scanned using the Odyssey Imaging System (LI-COR Biosciences, United Kingdom).

TssD Antibody Production

The polyclonal anti-TssD antibody was produced by Capra Science Antibodies AB (Sweden). The *tssD* gene cloned into an expression vector and recombinant TssD protein was isolated and purified. For production of the TssD antiserum, purified TssD was immunized into a rabbit. Two boosts with the antigen were performed, followed by the first bleed. A further boost with the antigen was performed followed by the second bleed; the process was repeated for a third bleed. Antiserum collected from the third bleed was affinity purified using a peptide-coupled column for the anti-TssD antibody.

Oxidative Stress Assay

Campylobacter jejuni from 24 h plate cultures were re-suspended in PBS, the OD_{600} was measured and the suspension adjusted with PBS to OD_{600} 1.0. Bacterial suspensions were exposed to 50 mM H_2O_2 for 30 min at 37°C stationary under microaerobic conditions. Serial dilutions were performed and dilutions plated onto blood agar plates. Plates were incubated at 37°C under microaerobic conditions and colonies counted after 48 h.

Antimicrobial Susceptibility Assays

The disk diffusion assays were performed with ampicillin (10 μg), amoxycillin/clavulanic acid (2:1, 30 μg), tetracycline (30 μg) or polymyxin B (300 units) disks (Oxoid) following the methodology published by the European Society of Clinical Microbiology (EUCAST) (EUCAST, 2019). Zones of growth inhibition were measured in millimeters and sensitivity (S) determined based on the EUCAST guidelines. Broth microdilution assays were performed with vancomycin (Sigma) and the minimum inhibitory concentration (MIC, μg/ml) was determined according to the methodology published by Wiegand et al. (2008).

Galleria mellonella Model of Infection

Galleria mellonella larvae were purchased from Livefoods Direct (United Kingdom). Bacterial cells harvested from 24 h plate cultures were re-suspended in PBS and OD_{600} adjusted to 0.1. Ten *G. mellonella* larvae per bacterial strain were injected with 10 μl bacterial suspension with a micro syringe (Hamilton, Switzerland) in the right foremost leg. Controls injected with PBS or not injected were also prepared. Larvae were incubated at 37°C, with counts of dead larvae recorded every 24 h for 5 days.

Chicken Cell Interaction and Invasion Assays

Isolation of chicken intestinal primary cells (Byrne et al., 2007) as well as interaction and invasion assays (Corcionivoschi et al., 2009) were performed as described previously. Briefly, biopsies from sections of small intestines from 6 to 12 week-old broiler chickens (Cobb 500) were placed in primary cell culture medium and primary cells were isolated. *C. jejuni* strains were grown for 24 h on Muller-Hinton agar under microaerobic conditions. Bacterial cells were washed and resuspended in tissue culture medium to an OD_{600} of 0.4, then added to chicken intestinal primary cells grown in tissue culture plates to yield a multiplicity of infection of 1000:1. Plates were centrifuged and incubated for 3 h at 37°C in a microaerophilic environment. For interaction assays, infected monolayers were washed with PBS and treated with 0.1% v/v Triton X-100. Serial dilutions were performed and the CFUs/ml were enumerated. For invasion assays, infected monolayers were washed with PBS and treated with gentamicin (400 μg/ml) for 2 h at 37°C. Cells were then washed with PBS and treated with 0.1% v/v Triton X-100. Serial dilutions were performed and the CFUs/ml were enumerated.

Chicken Infection Assay

Thirty male broiler chickens (Ross 308) were housed in isolation units on wood shaving bedding. The temperature in the isolation unit was kept between 22–25°C and thermostatically controlled. Broilers were fed *ad libitum* with a standard diet. *C. jejuni* strains were grown on Muller Hinton plates for 24 h under microaerobic conditions and resuspended in sterile distilled water. At 15 days old, ten broilers were inoculated with approximately 1×10^8 CFU/ml of either the 488 wild-type strain, the 488 *tssD* mutant or the 81–176 wild-type strain. The different batches of infected broilers were kept separated in sterile isolation units. After 3 days of infection, broilers were euthanized and *C. jejuni* was enumerated by analyzing the cecum content using the ISO17025 methodology for plate counting. All broilers were confirmed using cloacal swabs as being *Campylobacter* free at the time of infection. These experiments were performed in triplicate on three separate occasions.

Statistical Analysis

All experiments were performed with at least three biological replicates and three technical replicates, unless otherwise stated. Statistical analyses were performed using GraphPad Prism 7 (GraphPad Software, United States) and data were presented as mean ± SEM. Results were compared using unpaired *t*-test with $^{*}p \leq 0.05$, $^{**}p \leq 0.01$, $^{***}p \leq 0.001$.

DATA AVAILABILITY STATEMENT

The genome sequence datasets generated for this study can be found in EBI ENA, PRJEB31331.

ETHICS STATEMENT

The experiments were performed according to the legislation in place (Law 471/2002 and government ordinance 437/2002) and under the supervision of National Sanitary Veterinary Agency. The Ethics Committee of Banat University of Agricultural Sciences and Veterinary Medicine – King Michael I of Romania approved this work.

AUTHOR CONTRIBUTIONS

OG and ND conceived the study with input from AH and NC. JL, GH, CD, AE, FS, AS, and OG performed the experiments and contributed to this manuscript. JL, OG, and ND wrote the manuscript with significant input from LS, IP, NC, and BW.

FUNDING

The authors gratefully acknowledge the support of the Biotechnology and Biological Sciences Research Council Institute Strategic Programme BB/R012504/1 constituent project BBS/E/F/000PR10349. AH was supported by H2020-MSCA Global Fellowship grant 657766.

SUPPLEMENTARY MATERIAL

The Supplementary Material for this article can be found online at: https://www.frontiersin.org/articles/10.3389/fmicb.2019.02864/full#supplementary-material

REFERENCES

Altschul, S. F., Gish, W., Miller, W., Myers, E. W., and Lipman, D. J. (1990). Basic local alignment search tool. *J. Mol. Biol.* 215, 403–410. doi: 10.1006/jmbi.1990.9999

Ang, C. W., De Klerk, M. A., Endtz, H. P., Jacobs, B. C., Laman, J. D., van der Meche, F. G., et al. (2001). Guillain-Barre syndrome- and miller fisher syndrome-associated campylobacter *jejuni* lipopolysaccharides induce anti-GM1 and anti-GQ1b antibodies in rabbits. *Infect. Immun.* 69, 2462–2469. doi: 10.1128/IAI.69.4.2462-2469.2001

Assefa, S., Keane, T. M., Otto, T. D., Newbold, C., and Berriman, M. (2009). ABACAS: algorithm-based automatic contiguation of assembled sequences. *Bioinformatics* 25, 1968–1969. doi: 10.1093/bioinformatics/btp347

Bachmann, V., Kostiuk, B., Unterweger, D., Diaz-Satizabal, L., Ogg, S., and Pukatzki, S. (2015). Bile salts modulate the mucin-activated type VI secretion system of pandemic *Vibrio cholerae*. *PLoS Negl. Trop. Dis.* 9:e0004031. doi: 10.1371/journal.pntd.0004031

Bacon, D. J., Alm, R. A., Burr, D. H., Hu, L., Kopecko, D. J., Ewing, C. P., et al. (2000). Involvement of a plasmid in virulence of *Campylobacter jejuni* 81-176. *Infect. Immun.* 68, 4384–4390. doi: 10.1128/iai.68.8.4384-4390.2000

Basler, M., Pilhofer, M., Henderson, G. P., Jensen, G. J., and Mekalanos, J. J. (2012). Type VI secretion requires a dynamic contractile phage tail-like structure. *Nature* 483, 182–186. doi: 10.1038/nature10846

Black, R. E., Levine, M. M., Clements, M. L., Hughes, T. P., and Blaser, M. J. (1988). Experimental *Campylobacter jejuni* infection in humans. *J. Infect. Dis.* 157, 472–479. doi: 10.1093/infdis/157.3.472

Bleumink-Pluym, N. M., van Alphen, L. B., Bouwman, L. I., Wosten, M. M., and van Putten, J. P. (2013). Identification of a functional type VI secretion system in *Campylobacter jejuni* conferring capsule polysaccharide sensitive cytotoxicity. *PLoS Pathog.* 9:e1003393. doi: 10.1371/journal.ppat.1003393

Bolger, A. M., Lohse, M., and Usadel, B. (2014). Trimmomatic: a flexible trimmer for Illumina sequence data. *Bioinformatics* 30, 2114–2120. doi: 10.1093/bioinformatics/btu170

Brackmann, M., Wang, J., and Basler, M. (2018). Type VI secretion system sheath inter-subunit interactions modulate its contraction. *EMBO Rep.* 19, 225–233. doi: 10.15252/embr.201744416

Byrne, C. M., Clyne, M., and Bourke, B. (2007). *Campylobacter jejuni* adhere to and invade chicken intestinal epithelial cells in vitro. *Microbiology* 153(Pt 2), 561–569. doi: 10.1099/mic.0.2006/000711-710

Carver, T., Harris, S. R., Berriman, M., Parkhill, J., and McQuillan, J. A. (2012). Artemis: an integrated platform for visualization and analysis of high-throughput sequence-based experimental data. *Bioinformatics* 28, 464–469. doi: 10.1093/bioinformatics/btr703

Cianfanelli, F. R., Monlezun, L., and Coulthurst, S. J. (2016). Aim, load, fire: the type VI secretion system, a bacterial Nanoweapon. *Trends Microbiol.* 24, 51–62. doi: 10.1016/j.tim.2015.10.005

Coker, A. O., Isokpehi, R. D., Thomas, B. N., Amisu, K. O., and Obi, C. L. (2002). Human campylobacteriosis in developing countries. *Emerg. Infect. Dis.* 8, 237–244. doi: 10.3201/eid0803.010233

Corcionivoschi, N., Clyne, M., Lyons, A., Elmi, A., Gundogdu, O., Wren, B. W., et al. (2009). *Campylobacter jejuni* cocultured with epithelial cells reduces surface capsular polysaccharide expression. *Infect. Immun.* 77, 1959–1967. doi: 10.1128/IAI.01239-1238

Corcionivoschi, N., Gundogdu, O., Moran, L., Kelly, C., Scates, P., Stef, L., et al. (2015). Virulence characteristics of hcp (+) *Campylobacter jejuni* and Campylobacter coli isolates from retail chicken. *Gut Pathog.* 7:20. doi: 10.1186/s13099-015-0067-z

Drebes Dorr, N. C., and Blokesch, M. (2018). Bacterial type VI secretion system facilitates niche domination. *Proc. Natl. Acad. Sci. U.S.A.* 115, 8855–8857. doi: 10.1073/pnas.1812776115

EUCAST (2019). *Antimicrobial Susceptibility Testing: EUCAST Disk Diffusion Method*. Available at: http://www.eucast.org/ast_of_bacteria/disk_diffusion_methodology/ (accessed May 10, 2019).

Fitzsimons, T. C., Lewis, J. M., Wright, A., Kleifeld, O., Schittenhelm, R. B., Powell, D., et al. (2018). Identification of novel *Acinetobacter baumannii* Type VI secretion system antibacterial effector and immunity pairs. *Infect. Immun.* 86:e00297-18. doi: 10.1128/IAI.00297-218

Flint, A., Butcher, J., and Stintzi, A. (2016). Stress responses, adaptation, and virulence of bacterial pathogens during host gastrointestinal colonization. *Microbiol. Spectr.* 4:VMBF-0007-2015. doi: 10.1128/microbiolspec.VMBF-0007-2015

Gerc, A. J., Diepold, A., Trunk, K., Porter, M., Rickman, C., Armitage, J. P., et al. (2015). Visualization of the *Serratia* Type VI secretion system reveals unprovoked attacks and dynamic assembly. *Cell Rep.* 12, 2131–2142. doi: 10.1016/j.celrep.2015.08.053

Gish, W., and States, D. J. (1993). Identification of protein coding regions by database similarity search. *Nat. Genet.* 3, 266–272. doi: 10.1038/ng0393-266

Gladman, S., and Seemann, T. (2012). *VelvetOptimiser, v2.2.5*.

Gundogdu, O., da Silva, D. T., Mohammad, B., Elmi, A., Mills, D. C., Wren, B. W., et al. (2015). The *Campylobacter jejuni* MarR-like transcriptional regulators RrpA and RrpB both influence bacterial responses to oxidative and aerobic stresses. *Front. Microbiol.* 6:724. doi: 10.3389/fmicb.2015.00724

Gundogdu, O., da Silva, D. T., Mohammad, B., Elmi, A., Wren, B. W., van Vliet, A. H., et al. (2016). The *Campylobacter jejuni* oxidative stress regulator RrpB is associated with a genomic hypervariable region and altered oxidative stress resistance. *Front. Microbiol.* 7:2117. doi: 10.3389/fmicb.2016.02117

Gundogdu, O., Mills, D. C., Elmi, A., Martin, M. J., Wren, B. W., and Dorrell, N. (2011). The *Campylobacter jejuni* transcriptional regulator Cj1556 plays a role in the oxidative and aerobic stress response and is important for bacterial survival in vivo. *J. Bacteriol.* 193, 4238–4249. doi: 10.1128/JB.05189-5111

Hachani, A., Wood, T. E., and Filloux, A. (2016). Type VI secretion and anti-host effectors. *Curr. Opin. Microbiol.* 29, 81–93. doi: 10.1016/j.mib.2015.11.006

Harrison, J. W., Dung, T. T., Siddiqui, F., Korbrisate, S., Bukhari, H., Tra, M. P., et al. (2014). Identification of possible virulence marker from *Campylobacter jejuni* isolates. *Emerg. Infect. Dis.* 20, 1026–1029. doi: 10.3201/eid2006.130635

Hermans, D., Pasmans, F., Heyndrickx, M., Van Immerseel, F., Martel, A., Van Deun, K., et al. (2012). A tolerogenic mucosal immune response leads to persistent *Campylobacter jejuni* colonization in the chicken gut. *Crit. Rev. Microbiol.* 38, 17–29. doi: 10.3109/1040841X.2011.615298

Kaakoush, N. O., Castano-Rodriguez, N., Mitchell, H. M., and Man, S. M. (2015). Global epidemiology of *Campylobacter* infection. *Clin. Microbiol. Rev.* 28, 687–720. doi: 10.1128/CMR.00006-15

Kapitein, N., Bonemann, G., Pietrosiuk, A., Seyffer, F., Hausser, I., Locker, J. K., et al. (2013). ClpV recycles VipA/VipB tubules and prevents non-productive tubule formation to ensure efficient type VI protein secretion. *Mol. Microbiol.* 87, 1013–1028. doi: 10.1111/mmi.12147

Kapitein, N., and Mogk, A. (2014). Type VI secretion system helps find a niche. *Cell Host Microb.* 16, 5–6. doi: 10.1016/j.chom.2014.06.012

Kim, J. C., Oh, E., Kim, J., and Jeon, B. (2015). Regulation of oxidative stress resistance in *Campylobacter jejuni*, a microaerophilic foodborne pathogen. *Front. Microbiol.* 6:751. doi: 10.3389/fmicb.2015.00751

Kirchberger, P. C., Unterweger, D., Provenzano, D., Pukatzki, S., and Boucher, Y. (2017). Sequential displacement of Type VI secretion system effector genes leads to evolution of diverse immunity gene arrays in *Vibrio cholerae*. *Sci. Rep.* 7:45133. doi: 10.1038/srep45133

Kovanen, S., Rossi, M., Pohja-Mykra, M., Nieminen, T., Raunio-Saarnisto, M., Sauvala, M., et al. (2018). Population genetics and characterization of *Campylobacter jejuni* isolates in western jackdaws and game birds in Finland. *Appl. Environ. Microbiol.* 85:e02365-18. doi: 10.1128/AEM.02365-2318

Kudryashev, M., Wang, R. Y., Brackmann, M., Scherer, S., Maier, T., Baker, D., et al. (2015). Structure of the type VI secretion system contractile sheath. *Cell* 160, 952–962. doi: 10.1016/j.cell.2015.01.037

Lertpiriyapong, K., Gamazon, E. R., Feng, Y., Park, D. S., Pang, J., Botka, G., et al. (2012). *Campylobacter jejuni* type VI secretion system: roles in adaptation to deoxycholic acid, host cell adherence, invasion, and in vivo colonization. *PLoS One* 7:e42842. doi: 10.1371/journal.pone.0042842

Li, H., and Durbin, R. (2009). Fast and accurate short read alignment with burrows-wheeler transform. *Bioinformatics* 25, 1754–1760. doi: 10.1093/bioinformatics/btp324

Link, A. J., and LaBaer, J. (2011). Trichloroacetic acid (TCA) precipitation of proteins. *Cold Spring Harb. Protoc.* 2011, 993–994. doi: 10.1101/pdb.prot5651

Losada, L., Shea, A. A., and DeShazer, D. (2018). A MarR family transcriptional regulator and subinhibitory antibiotics regulate type VI secretion gene clusters in *Burkholderia pseudomallei*. *Microbiology* 164, 1196–1211. doi: 10.1099/mic.0.000697

Ma, L. S., Hachani, A., Lin, J. S., Filloux, A., and Lai, E. M. (2014). *Agrobacterium tumefaciens* deploys a superfamily of type VI secretion DNase effectors as weapons for interbacterial competition in planta. *Cell Host Microb.* 16, 94–104. doi: 10.1016/j.chom.2014.06.002

Mougous, J. D., Cuff, M. E., Raunser, S., Shen, A., Zhou, M., Gifford, C. A., et al. (2006). A virulence locus of *Pseudomonas aeruginosa* encodes a protein secretion apparatus. *Science* 312, 1526–1530. doi: 10.1126/science.1128393

Murdoch, S. L., Trunk, K., English, G., Fritsch, M. J., Pourkarimi, E., and Coulthurst, S. J. (2011). The opportunistic pathogen *Serratia marcescens* utilizes

type VI secretion to target bacterial competitors. *J. Bacteriol.* 193, 6057–6069. doi: 10.1128/JB.05671-5611

Newell, D. G., and Fearnley, C. (2003). Sources of *Campylobacter* colonization in broiler chickens. *Appl. Environ. Microbiol.* 69, 4343–4351. doi: 10.1128/aem.69.8.4343-4351.2003

Noreen, Z., Jobichen, C., Abbasi, R., Seetharaman, J., Sivaraman, J., and Bokhari, H. (2018). Structural basis for the pathogenesis of *Campylobacter jejuni* Hcp1, a structural and effector protein of the Type VI Secretion System. *FEBS J.* 285, 4060–4070. doi: 10.1111/febs.14650

Penner, J. L., Hennessy, J. N., and Congi, R. V. (1983). Serotyping of *Campylobacter jejuni* and *Campylobacter coli* on the basis of thermostable antigens. *Eur. J. Clin. Microbiol.* 2, 378–383. doi: 10.1007/bf02019474

Poly, F., Threadgill, D., and Stintzi, A. (2004). Identification of *Campylobacter jejuni* ATCC 43431-specific genes by whole microbial genome comparisons. *J. Bacteriol.* 186, 4781–4795. doi: 10.1128/JB.186.14.4781-4795.2004

Pukatzki, S., Ma, A. T., Sturtevant, D., Krastins, B., Sarracino, D., Nelson, W. C., et al. (2006). Identification of a conserved bacterial protein secretion system in *Vibrio cholerae* using the *Dictyostelium* host model system. *Proc. Natl. Acad. Sci. U.S.A.* 103, 1528–1533. doi: 10.1073/pnas.0510322103

Ringel, P. D., Hu, D., and Basler, M. (2017). The role of Type VI secretion system effectors in target cell lysis and subsequent horizontal gene transfer. *Cell Rep.* 21, 3927–3940. doi: 10.1016/j.celrep.2017.12.020

Ritz, M., Garenaux, A., Berge, M., and Federighi, M. (2002). Determination of rpoA as the most suitable internal control to study stress response in *C. jejuni* by RT-qPCR and application to oxidative stress. *J. Microbiol. Methods* 76, 196–200. doi: 10.1016/j.mimet.2008.10.014

Robinson, D. A. (1981). Infective dose of *Campylobacter jejuni* in milk. *Br. Med. J.* 282:1584. doi: 10.1136/bmj.282.6276.1584

Salih, O., He, S., Planamente, S., Stach, L., MacDonald, J. T., Manoli, E., et al. (2018). Atomic structure of Type VI contractile sheath from *Pseudomonas aeruginosa*. *Structure* 26, 329–336.e3. doi: 10.1016/j.str.2017.12.005

Schmittgen, T. D., and Livak, K. J. (2008). Analyzing real-time PCR data by the comparative C(T) method. *Nat. Protoc.* 3, 1101–1108. doi: 10.1038/nprot.2008.73

Seemann, T. (2014). Prokka: rapid prokaryotic genome annotation. *Bioinformatics* 30, 2068–2069. doi: 10.1093/bioinformatics/btu153

Senior, N. J., Bagnall, M. C., Champion, O. L., Reynolds, S. E., La Ragione, R. M., Woodward, M. J., et al. (2011). Galleria mellonella as an infection model for *Campylobacter jejuni* virulence. *J. Med. Microbiol.* 60(Pt 5), 661–669. doi: 10.1099/jmm.0.026658-26650

Si, M., Wang, Y., Zhang, B., Zhao, C., Kang, Y., Bai, H., et al. (2017). The Type VI secretion system engages a Redox-regulated dual-functional heme transporter for zinc acquisition. *Cell Rep.* 20, 949–959. doi: 10.1016/j.celrep.2017.06.081

Sima, F., Stratakos, A. C., Ward, P., Linton, M., Kelly, C., Pinkerton, L., et al. (2018). A novel natural antimicrobial can reduce the *in vitro* and *in vivo* Pathogenicity of T6SS positive *Campylobacter jejuni* and *Campylobacter coli* chicken isolates. *Front. Microbiol.* 9:2139. doi: 10.3389/fmicb.2018.02139

Simon, A. (2010). *FastQC*. Available at: http://www.bioinformatics.babraham.ac.uk/projects/fastqc/, v0.11.2 (accessed March 5, 2018).

Skarp, C. P. A., Hanninen, M. L., and Rautelin, H. I. K. (2016). *Campylobacteriosis*: the role of poultry meat. *Clin. Microbiol. Infect.* 22, 103–109. doi: 10.1016/j.cmi.2015.11.019

Trunk, K., Peltier, J., Liu, Y. C., Dill, B. D., Walker, L., Gow, N. A. R., et al. (2018). The type VI secretion system deploys antifungal effectors against microbial competitors. *Nat. Microbiol.* 3, 920–931. doi: 10.1038/s41564-018-0191-x

Ugarte-Ruiz, M., Stabler, R. A., Dominguez, L., Porrero, M. C., Wren, B. W., Dorrell, N., et al. (2014). Prevalence of Type VI secretion system in spanish *Campylobacter jejuni* isolates. *Zoonoses Public Health* 62, 497–500. doi: 10.1111/zph.12176

Ugarte-Ruiz, M., Stabler, R. A., Dominguez, L., Porrero, M. C., Wren, B. W., Dorrell, N., et al. (2015). Prevalence of type VI secretion system in spanish *Campylobacter jejuni* isolates. *Zoonoses Public Health* 62, 497–500. doi: 10.1111/zph.12176

Wan, B., Zhang, Q., Ni, J., Li, S., Wen, D., Li, J., et al. (2017). Type VI secretion system contributes to Enterohemorrhagic *Escherichia coli* virulence by secreting catalase against host reactive oxygen species (ROS). *PLoS Pathog.* 13:e1006246. doi: 10.1371/journal.ppat.1006246

Wang, T., Si, M., Song, Y., Zhu, W., Gao, F., Wang, Y., et al. (2015). Type VI Secretion system transports Zn2+ to combat multiple stresses and host immunity. *PLoS Pathog.* 11:e1005020. doi: 10.1371/journal.ppat.1005020

Wiegand, I., Hilpert, K., and Hancock, R. E. (2008). Agar and broth dilution methods to determine the minimal inhibitory concentration (MIC) of antimicrobial substances. *Nat. Protoc.* 3, 163–175. doi: 10.1038/nprot.2007.521

Wigley, P. (2015). Blurred lines: pathogens, commensals, and the healthy Gut. *Front. Vet. Sci.* 2:40. doi: 10.3389/fvets.2015.00040

Williams, N. J., Jones, T. R., Leatherbarrow, H. J., Birtles, R. J., Lahuerta-Marin, A., Bennett, M., et al. (2010). Isolation of a novel *Campylobacter jejuni* clone associated with the bank vole, *Myodes glareolus*. *Appl. Environ. Microbiol.* 76, 7318–7321. doi: 10.1128/AEM.00511-510

Wilson, D. L., Rathinam, V. A. K., Qi, W. H., Wick, L. M., Landgraf, J., Bell, J. A., et al. (2010). Genetic diversity in *Campylobacter jejuni* is associated with differential colonization of broiler chickens and C57BL/6J IL10-deficient mice. *Microbiology* 156, 2046–2057. doi: 10.1099/mic.0.035717-35710

Young, K. T., Davis, L. M., and Dirita, V. J. (2007). *Campylobacter jejuni*: molecular biology and pathogenesis. *Nat. Rev. Microbiol.* 5, 665–679. doi: 10.1038/nrmicro1718

Zerbino, D. R., and Birney, E. (2008). Velvet: algorithms for de novo short read assembly using de Bruijn graphs. *Genome Res.* 18, 821–829. doi: 10.1101/gr.074492.107

Conflict of Interest: The authors declare that the research was conducted in the absence of any commercial or financial relationships that could be construed as a potential conflict of interest.

Copyright © 2019 Liaw, Hong, Davies, Elmi, Sima, Stratakos, Stef, Pet, Hachani, Corcionivoschi, Wren, Gundogdu and Dorrell. This is an open-access article distributed under the terms of the Creative Commons Attribution License (CC BY). The use, distribution or reproduction in other forums is permitted, provided the original author(s) and the copyright owner(s) are credited and that the original publication in this journal is cited, in accordance with accepted academic practice. No use, distribution or reproduction is permitted which does not comply with these terms.

frontiers in Microbiology

ORIGINAL RESEARCH
published: 14 January 2020
doi: 10.3389/fmicb.2019.03004

Redundancy and Specificity of Type VI Secretion *vgrG* Loci in Antibacterial Activity of *Agrobacterium tumefaciens* 1D1609 Strain

*Mary Nia M. Santos[1,2,3], Shu-Ting Cho[1], Chih-Feng Wu[1†], Chun-Ju Chang[1], Chih-Horng Kuo[1,2,4] and Erh-Min Lai[1,2,4]**

[1] Institute of Plant and Microbial Biology, Academia Sinica, Taipei, Taiwan, [2] Molecular and Biological Agricultural Sciences Program, Taiwan International Graduate Program, National Chung Hsing University and Academia Sinica, Taipei, Taiwan, [3] Graduate Institute of Biotechnology, National Chung Hsing University, Taichung, Taiwan, [4] Biotechnology Center, National Chung Hsing University, Taichung, Taiwan

Type VI secretion system (T6SS) is a contractile nanoweapon employed by many Proteobacteria to deliver effectors to kill or inhibit their competitors. One T6SS gene, *vgrG,* encodes a spike protein for effector translocation and is often present as multiple copies in bacterial genomes. Our phylogenomic analyses sampled 48 genomes across diverse Proteobacteria lineages and found ∼70% of them encode multiple VgrGs, yet only four genomes have nearly identical paralogs. Among these four, *Agrobacterium tumefaciens* 1D1609 has the highest *vgrG* redundancy. Compared to *A. tumefaciens* model strain C58 which harbors two *vgrG* genes, 1D1609 encodes four *vgrG* genes (i.e., *vgrGa-d*) with each adjacent to different putative effector genes. Thus, 1D1609 was selected to investigate the functional redundancy and specificity of multiple *vgrG* genes and their associated effectors. Secretion assay of single and multiple *vgrG* deletion mutants demonstrated that these four *vgrG*s are functionally redundant in mediating T6SS secretion. By analyzing various *vgrG* mutants, we found that all except for the divergent *vgrGb* could contribute to 1D1609's antibacterial activity. Further characterizations of putative effector-immunity gene pairs revealed that *vgrGa*-associated gene 2 (*v2a*) encodes an AHH family nuclease and serves as the major antibacterial toxin. Interestingly, C58's VgrG2 shares 99% amino acid sequence identity with 1D1609's VgrGa, VgrGc and VgrGd. This high sequence similarity allows 1D1609 to use an exogenous VgrG delivered from C58 to kill another competing bacterium. Taken together, *Agrobacterium* can use highly similar VgrGs, either produced endogenously or injected from its close relatives, for T6SS-mediated interbacterial competition.

Keywords: type VI secretion system, VgrG, effector, antibacterial, functional redundancy, *Agrobacterium tumefaciens*

OPEN ACCESS

Edited by:
Ignacio Arechaga, University of Cantabria, Spain

Reviewed by:
Weili Liang, National Institute for Communicable Disease Control and Prevention (China CDC), China
Yong-Qiang He, Guangxi University, China

***Correspondence:**
Erh-Min Lai
emlai@gate.sinica.edu.tw

†Present address:
Chih-Feng Wu, Department of Botany and Plant Pathology, Oregon State University, Corvallis, OR, United States

Specialty section:
This article was submitted to Microbial Physiology and Metabolism, a section of the journal Frontiers in Microbiology

Received: *12 September 2019*
Accepted: *12 December 2019*
Published: *14 January 2020*

Citation:
Santos MNM, Cho S-T, Wu C-F, Chang C-J, Kuo C-H and Lai E-M (2020) Redundancy and Specificity of Type VI Secretion vgrG Loci in Antibacterial Activity of Agrobacterium tumefaciens 1D1609 Strain. Front. Microbiol. 10:3004. doi: 10.3389/fmicb.2019.03004

INTRODUCTION

Bacteria have evolved many survival strategies, including pathogenesis, competition, and cooperation, to thrive in diverse and changing environments. One of the weapons that they use is type VI secretion system (T6SS), a machinery that delivers effectors to both eukaryotic and prokaryotic target cells. Its coding genes are present in approximately 25% of the Gram-negative bacterial genomes sequenced (Bingle et al., 2008).

T6SS has an important role in interbacterial competition and provides T6SS-possessing bacteria with competitive advantage in microbial community. It can deliver a variety of effectors such as nuclease, amidase, phospholipase, peptidoglycan hydrolase, muramidase, glycosidase, NADase, and ADP-ribosyltransferase into the target bacterial cell by a contractile machinery (Russell et al., 2014; Tang et al., 2018; Ting et al., 2018). Contraction of the sheath-like structure drives the inner tube composed of Hcp tipped by VgrG-PAAR and the associated effectors across bacterial membranes to extracellular milieu or into the target cell. After firing, the structure is immediately disassembled into its individual components, which can be recycled to assemble new machinery for continuous firing (Zoued et al., 2014).

The spike component VgrG is homologous to the gp27/gp5 complex or the tail spike of bacteriophage T4 and assembles into a trimeric complex (Leiman et al., 2009). Current knowledge based on studies from several bacterial systems suggests that VgrG is specifically required for delivery of cognate effector(s) encoded in the same *vgrG* genetic module (Hachani et al., 2014; Whitney et al., 2014). Furthermore, the C-terminal variable region of VgrG is the molecular determinant conferring specificity of effector delivery by binding to its cognate effector directly or via adaptor/chaperone that interacts with a specific effector (Bondage et al., 2016; Flaugnatti et al., 2016). T6SS adaptors/chaperones including DUF4123-, DUF1795-, and DUF2169-containing proteins are required for loading a specific effector onto the cognate VgrG for delivery (Lien and Lai, 2017).

Agrobacterium tumefaciens is a soil Alphaproteobacterium that infects a broad range of dicotyledonous plants and transfers T-DNA, an oncogenic DNA fragment, to plant's nuclear chromosomes (Gelvin, 2000; Hwang et al., 2017). *A. tumefaciens* strain C58 encodes a single T6SS gene cluster and is equipped with three toxins namely type VI amidase effector (Tae), type VI DNase effector 1 and 2 (Tde1 and Tde2), in which its toxin activity can be neutralized by its cognate immunity. Tde is a major antibacterial weapon during *in planta* interbacterial competition and its associated VgrG is specifically required for Tde1/2-dependent bacterial killing (Ma et al., 2014; Bondage et al., 2016). A gene which encodes DUF2169 is always found between *vgrG2* and *tde2* orthologs across many Proteobacterial classes (Bondage et al., 2016). In *A. tumefaciens* strain C58, a DUF2169-containing protein encoded upstream of *tde2* is required to stabilize Tde2 and for Tde2-mediated antibacterial activity. For *vgrG1*-associated Tde1, Tap1 (encoded upstream of *tde1*) is the specific chaperone/adaptor interacting with Tde1 prior to loading to VgrG1 for formation of Tde1-Tap1-VgrG-PAAR secretion complex (Bondage et al., 2016).

Aside from the representative *A. tumefaciens* model strain C58, there is little knowledge of T6SS available for other *A. tumefaciens* strains. Our recent comparative analysis of T6SS gene clusters from 11 *A. tumefaciens* strains with complete genome sequences revealed that T6SS is present in all sequenced strains belonging to different genomospecies (Wu et al., 2019b). The *imp* operon (*impA-N*) encoding core structural or regulatory components and the first five genes (*clpV, tai, tae, hcp, vgrG*) encoded in the *hcp* operon are highly conserved but the *vgrG*-associated downstream genes are variable. While all strains only harbor one *vgrG* gene encoded in the main T6SS gene cluster, additional orphan *vgrG* genes not genetically linked to the main T6SS gene cluster were often identified in some strains.

A T6SS-harboring bacterium can encode one to multiple VgrG proteins, in which several of them were demonstrated to be specifically required for delivery of cognate effector(s) encoded in the same *vgrG* genetic module (Hachani et al., 2014; Whitney et al., 2014). However, the prevalence and biological significance of *vgrG* redundancy has not been tackled. In this study, *A. tumefaciens* 1D1609 which has the highest number of nearly identical *vgrG* genes among all sampled Proteobacteria lineages was chosen to address this question. We investigated the functional redundancy and specificity of multiple VgrG in the effector delivery strategies of T6SS in the context of interbacterial competition. We generated single to multiple in-frame deletion of *vgrG* mutants to characterize the role of paralogous VgrG proteins and its associated effectors in 1D1609. We found that the four *vgrGs* are functionally redundant in mediating Hcp secretion but also exert both redundancy and specificity in mediating effector delivery for interbacterial competition. We also demonstrated that 1D1609 employs a nuclease effector as the major antibacterial toxin. Importantly, we provided experimental evidence that *A. tumefaciens* can use T6SS in the context of interbacterial competition to exchange VgrG as an effector carrier between its close siblings.

RESULTS

Majority of T6SS-Possessing Proteobacterial Genomes Harbor Multiple *vgrG* Genes

To survey the number of *vgrG* genes in T6SS-encoding bacterial genomes, 48 representative Proteobacteria harboring T6SS gene cluster(s) were selected for phylogenetic analysis. The result revealed that 33 of these genomes (∼70%) encode multiple *vgrG* genes. The *vgrG* copy numbers have no strong tie to the phylogenetic placement of individual genomes (**Figure 1**), suggesting that the copy number evolution is highly dynamic, even at the intra-genus level (e.g., *Agrobacterium* in Alphaproteobacteria or *Pseudomonas* in Gammaproteobacteria). The *vgrG* gene tree (**Supplementary Figure S1**) is not congruent with the species tree (**Figure 1**) and the patterns suggest that horizontal gene transfers across different classes are not rare events. Nonetheless, the species with multiple VgrG homologs mostly (∼64%) form a monophyletic clade at family levels.

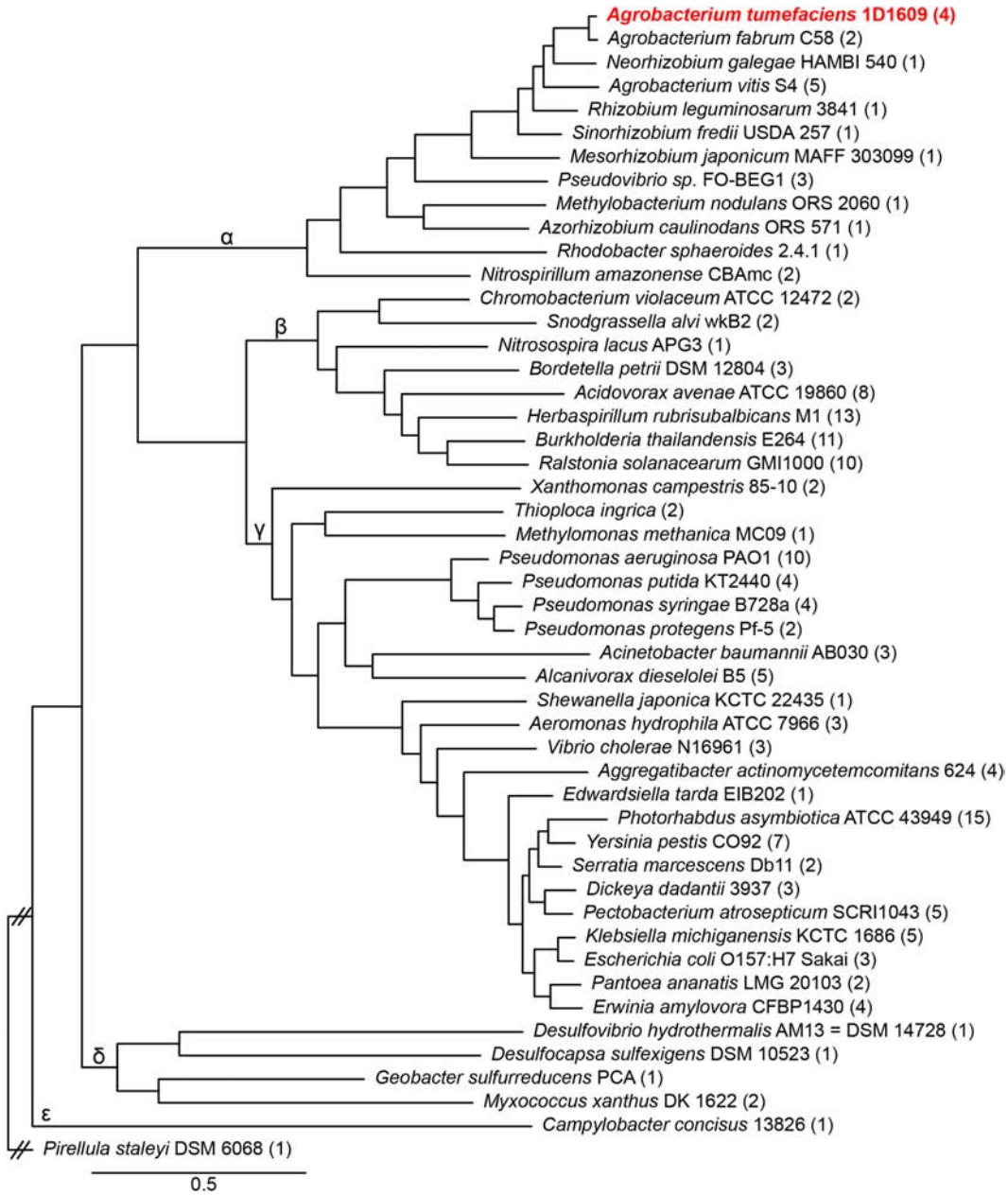

FIGURE 1 | Bayesian phylogeny of representative Proteobacteria based on 120 shared single-copy genes. The labels on the branches indicate the five classes within this phylum: Alphaproteobacteria (α), Betaproteobacteria (β), Deltaproteobacteria (δ), Epsilonproteobacteria (ε) and Gammaproteobacteria (γ). The numbers in parentheses after strain names indicate the *vgrG* copy numbers.

The genome of all the sampled Rhizobiaceae lineages harbors only one main T6SS gene cluster and forms a monophyletic clade except for *Sinorhizobium fredii* (**Supplementary Figure S1**) (Bladergroen et al., 2003; Wu et al., 2019b). This pattern suggests that gene duplication could be the major driving force for copy number increase within families.

We further asked, when there are multiple *vgrG* homologs in a genome, how often can we find highly similar genes that are likely to be functionally redundant. Using protein sequence identity ≥ 95% as the cut-off, only four genomes met the criteria (**Supplementary Table S1**). These include Alphaproteobacterium *A. tumefaciens* strain 1D1609 (three out of four with 99% identity, the remaining one is 93–94% identical), Betaproteobacterium *Acidovorax avenae subsp. avenae* ATCC 19860 (two out of eight with 99% identity), Gammaproteobacterium *Aggregatibacter actinomycetemcomitans* strain 624 (four copies belonging to two types: within-type = 99–100% identity, between-type = 90% identity), and Gammaproteobacterium *Dickeya dadantii* strain

FIGURE 2 | 1D1609 encodes four *vgrG* genes, each is genetically linked with different potential effector gene(s). Genetic organization of *A. tumefaciens* 1D1609 and C58 T6SS gene cluster and *vgrG* genetic modules. C58 *vgrG1* is outlined with green and C58 *vgrG2* and 1D1609's four *vgrG* genes are outlined in orange. The gene encoding DUF2169 domain is highlighted in yellow and DUF4150 (PAAR-like) domain is shown in dark green. The *vgrG-associated genes* (*v*) are numbered according to their position from *vgrG*. The percentage identity, which corresponds to **Supplementary Table S3** is indicated below the gene cluster.

3937 (two out of three with 97% identity, the remaining one is 78% identical). Among them 1D1609 has the highest redundancy.

1D1609 Has Four *vgrG* Genes With Each Genetically Linked to Specific Putative Effector Gene(s)

1D1609 genome encodes one main T6SS gene cluster including *vgrGa* (At1D1609_RS23245) that is encoded in *hcp* operon within the T6SS main gene cluster. The other three *vgrGs* – *vgrGb* (At1D1609_RS26290), *vgrGc* (At1D1609_RS22460) and *vgrGd* (At1D1609_RS18895) are encoded in different loci elsewhere (**Figure 2**). All four *vgrG* genes are genetically linked with distinct potential effector gene(s) and associated genes predicted to function as adaptor/chaperone or immunity (Wu et al., 2019b). The four *vgrG* genetic modules consist of the first three genes with conserved domain and same gene order encoding VgrG-DUF2169-DUF4150. The *vgrGa-*, *vgrGc-*, and *vgrGd*-associated genes (*v2a, v2c, v2d*) encode N-terminal PAAR-like DUF4150 domain followed by C-terminal putative effector domain. The *vgrGb*-linked *v2b* does not encode obvious effector domain and instead followed by downstream genes encoding putative effector domain, as predicted by Phyre or NCBI CDD search and BLASTP (Boratyn et al., 2013; Kelley et al., 2015; Marchler-Bauer et al., 2017) (**Supplementary Table S2**). The *vgrGc*-associated putative effector gene *v2c* does not encode any conserved domain, while the one (*v2d)* associated with *vgrGd* encodes a putative GH25 muramidase domain. Genes encoding DUF2169 domain are commonly found downstream of *vgrG* and upstream of DUF4150-containing effector genes. This gene order in *vgrG* genetic module is highly conserved in the *vgrG2* locus of C58, in which DUF2169-containing protein (Atu3641) may function as adaptor/chaperone of Tde2 due to its requirement for Tde2 stability and Tde2-dependent bacterial killing (Bondage et al., 2016). Thus, DUF2169-containing V1 protein is likely to function as a chaperone/adaptor required for delivery of cognate effectors in conjunction with the associated VgrG.

Unlike VgrG1 and VgrG2 which share 92% identity and are highly divergent at their C-terminus (Bondage et al., 2016),

we found that the three VgrG proteins – VgrGa, VgrGc and VgrGd in 1D1609 share 99% overall amino acid sequence identity (and 100% identity in the C-terminal region). These are also highly similar with VgrG2 of C58 (**Figure 2** and **Supplementary Table S3**). VgrGb shares 93–94% overall identity to the other three VgrGs and has a highly divergent C-terminal region (**Supplementary Figure S2** and **Supplementary Table S3**). Consistent with the VgrG comparisons, the DUF2169 and DUF4150 proteins with *vgrGa*/*c*/*d* also share 98–100% and 99–100% amino acid sequence identity, respectively (**Supplementary Table S3**). In contrast, VgrGb-associated DUF2169 and DUF4150 share only 26 and 35% sequence identities to those encoded in the other three *vgrG* loci respectively. The four predicted effector domains fused to DUF4150 or Rhs do not share high sequence similarity to each other or to known effectors, which could equip 1D1609 with diverse effector activities to fight with a wide range of competing bacteria. Homologs of *vgrGa*-, *vgrGb*-, *vgrGc*-, and *vgrGd*-associated effector genes are widely found in species belonging to Rhizobiales, suggesting that these are common effectors in this group.

Four VgrG Proteins Are Functionally Redundant in Mediating Hcp Secretion

In C58, VgrG1 and VgrG2 are functionally redundant in mediating Hcp secretion but specifically required for delivery of the cognate effectors Tde1 and Tde2, respectively (Lin et al., 2013; Bondage et al., 2016). Each of in-frame deletion mutants of *vgrGa*, *vgrGb*, *vgrGc* and *vgrGd* were generated to determine their functions in mediating Hcp secretion, a hallmark of a functional T6SS assembly. The Δ*tssL* mutant, with deletion of gene encoding the essential T6SS membrane component TssL, is used as a negative control. The secretion assay showed that all single *vgrG* deletion mutants remain active in Hcp secretion, suggesting that they are functionally redundant for assembly of a functional T6SS (**Figure 3A**). We are able to detect secretion of VgrG proteins from 1D1609 using polyclonal antibody against VgrG1 protein of C58, which can recognize all four VgrG proteins produced in 1D1609 and VgrG2 of C58. The Hcp and VgrG proteins are secreted in a T6SS-dependent manner because no Hcp and VgrG signals are detected in the secretion fraction of Δ*tssL* and RpoA (RNA polymerase α-subunit), a non-secreted protein, is not detectable in any secretion fraction. Hcp secretion remains active in double and triple *vgrG* deletion mutants but is only completely abolished when all four *vgrG* genes was deleted (**Figure 3B**). The overexpression of each of all four *vgrG* on a plasmid in the quadruple *vgrG* mutant restores Hcp secretion (**Figure 3C**). Furthermore, trans complementation of each 1D1609 *vgrG* constitutively expressed on a plasmid can also restore Hcp secretion in C58 double *vgrG* deletion mutant (Δ*vgrG*1,2) (**Figure 3D**). This is consistent with a previous study that either VgrG1 or VgrG2 is sufficient in mediating the secretion of Hcp in C58 (Lin et al., 2013). Indeed, all triple *vgrG* mutants wherein only one VgrG is present remains capable of mediating Hcp and VgrG secretion (**Figure 3E**). In Δ*vgrGabd* mutant, wherein only VgrGc is produced, Hcp secretion level is at lesser amount as compared to WT. The transcript expression level of *vgrGc* is also low compared to the other *vgrG*s (Haryono et al., 2019). Altogether, our comprehensive secretion assays demonstrated that the four VgrGs are functionally redundant in mediating Hcp secretion. Single *vgrG* is sufficient for assembly of a functional T6SS although the degree of assembly efficiency may not be the same due to expression level or sequence divergence.

T6SS-Dependent Antibacterial Activity Against *Escherichia coli* Is Mainly Contributed by *vgrGa* and *vgrGd*

We previously showed that all tested *A. tumefaciens* strains including 1D1609 exhibit T6SS-mediated antibacterial activity against T6SS-negative *E. coli* (Wu et al., 2019b). Here, we further investigated the role of the four *vgrG* genes in interbacterial competition against *E. coli*. As a positive control, ∼10x reduction of surviving *E. coli* target cells was observed when co-cultured with 1D1609 WT as compared to that of Δ*tssL*. However, each of single *vgrG* deletion mutants remains to have similar antibacterial activity to WT (**Figure 4A**). Further antibacterial activity assay of double, triple and quadruple *vgrG* mutants showed that the antibacterial activity of 1D1609 is completely lost in Δ*Gacd,* Δ*Gabd,* or Δ*Gabcd,* while Δ*Gbcd* and Δ*Gabc* triple *vgrG* mutants remain similar antibacterial activity to that of WT 1D1609 (**Figures 4B,C**). These results suggest that *vgrGa* and *vgrGd* alone is sufficient to contribute to the antibacterial activity of 1D1609. In contrast, *vgrGb* or *vgrGc* alone cannot exert any detectable antibacterial activity even though either *vgrG* alone (Δ*Gacd,* Δ*Gabd*) is sufficient in mediating Hcp and VgrG secretion (**Figure 3E**). However, when each single *vgrG* is constitutively overexpressed on a plasmid in quadruple *vgrG* mutant, *vgrGa, vgrGc,* and *vgrGd* but not *vgrGb* is able to partially restore antibacterial activity (**Figure 4D**). These results strongly suggest that endogenous *vgrGa* and *vgrGd* indeed play important roles for antibacterial activity while *vgrGb* plays no role in antibacterial activity to *E. coli.* The data that endogenous *vgrGc* plays no role but can exert its function in antibacterial activity when overexpressed are consistent with its low endogenous expression and high amino acid sequence identity to VgrGa and VgrGd.

The *vgrGa*- and *vgrGd*-Associated EI Pairs Are Responsible for Antibacterial Activity of 1D1609 and V2a Is a Nuclease of HNH/ENDO VII Superfamily

We also generated deletion mutants of each putative effector-immunity (EI) gene pairs individually and mutants with deletions in multiple putative EI pairs. Due to failure in generating the *vgrGc*-associated *v2c-v3c* EI pair deletion mutant after several attempts, we instead generated the deletion of the whole *vgrGc* cluster to assay the antibacterial effect of *vgrGc*-associated effector. Deletion of *vgrGa*- and *vgrGd*-associated EI pair partially compromised antibacterial activity against *E. coli* while deletion of *vgrGb*-associated EI pair or *vgrGc* cluster/associated toxin has no effect in compromising 1D1609's killing activity to *E. coli,* as compared to WT (**Figure 5A**). Importantly, any mutant minimally deleting both *vgrGa*- and *vgrGd*-associated EI pairs (*Δ2EIad*, *Δ3EIabd*, or *Δ4EIabcd*) completely abolished the

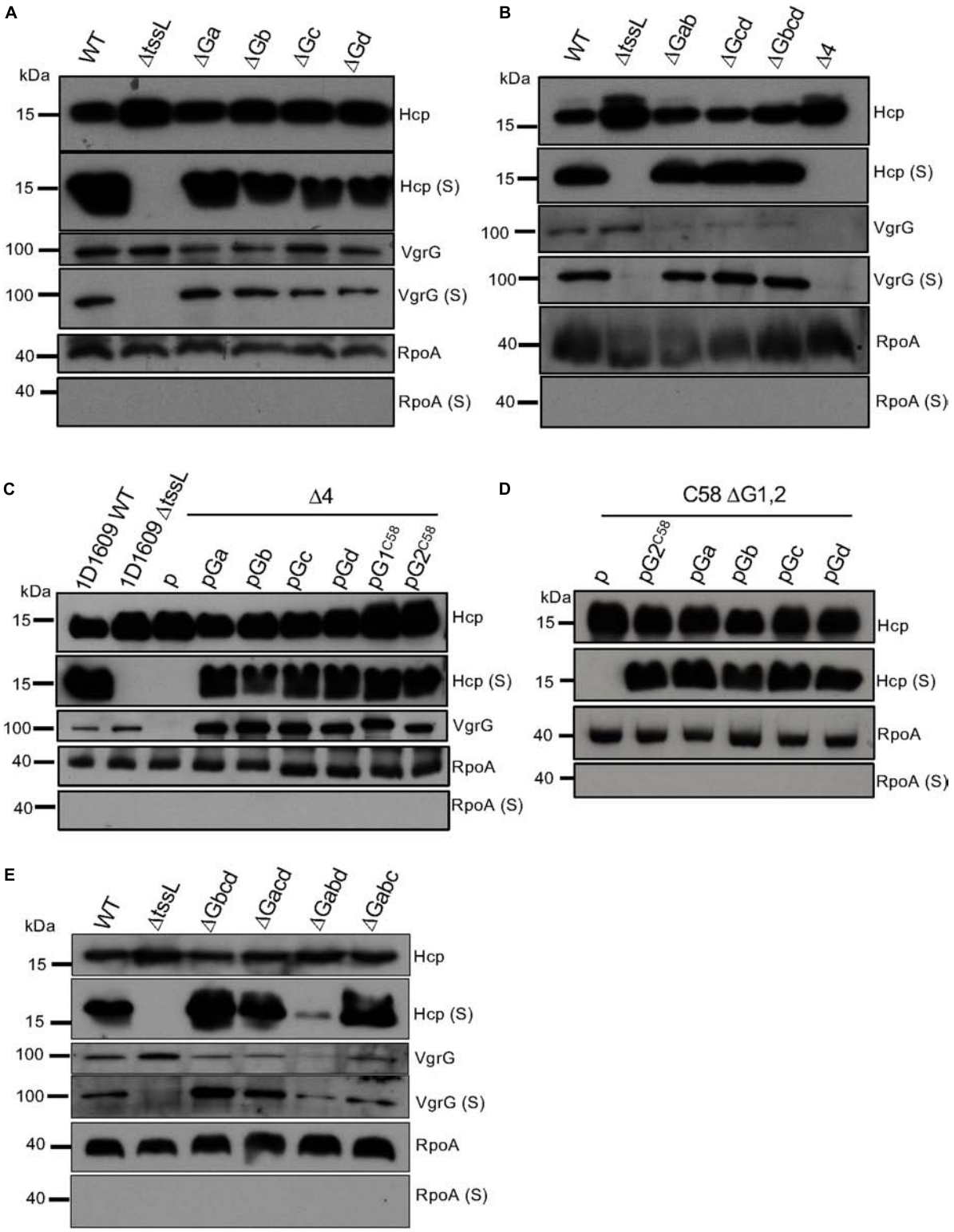

FIGURE 3 | The four VgrG proteins of 1D1609 are functionally redundant for Hcp secretion. Western blot analysis of cellular and secreted (S) proteins from single *vgrG* deletion mutants **(A)**, multiple *vgrG* deletion mutants **(B)**, overexpression of VgrG in 1D1609 quadruple *vgrG* mutant (Δ4) **(C),** and in C58 double *vgrG* deletion mutant (ΔG1,2) **(D),** and triple *vgrG* deletion mutants **(E)**. Various *A. tumefaciens* strains were cultured in LB **(A,B,E)** or AK **(C,E)** broth at 25°C and cellular and secreted (S) fractions were subjected to western blotting using anti-Hcp, anti-VgrG, and RpoA as indicated. The T6SS inactive mutant Δ*tssL* is a negative control and RpoA serves as a non-secreted protein control. Protein markers (in kDa) are indicated on the left. Similar results were obtained from 2–4 independent experiments.

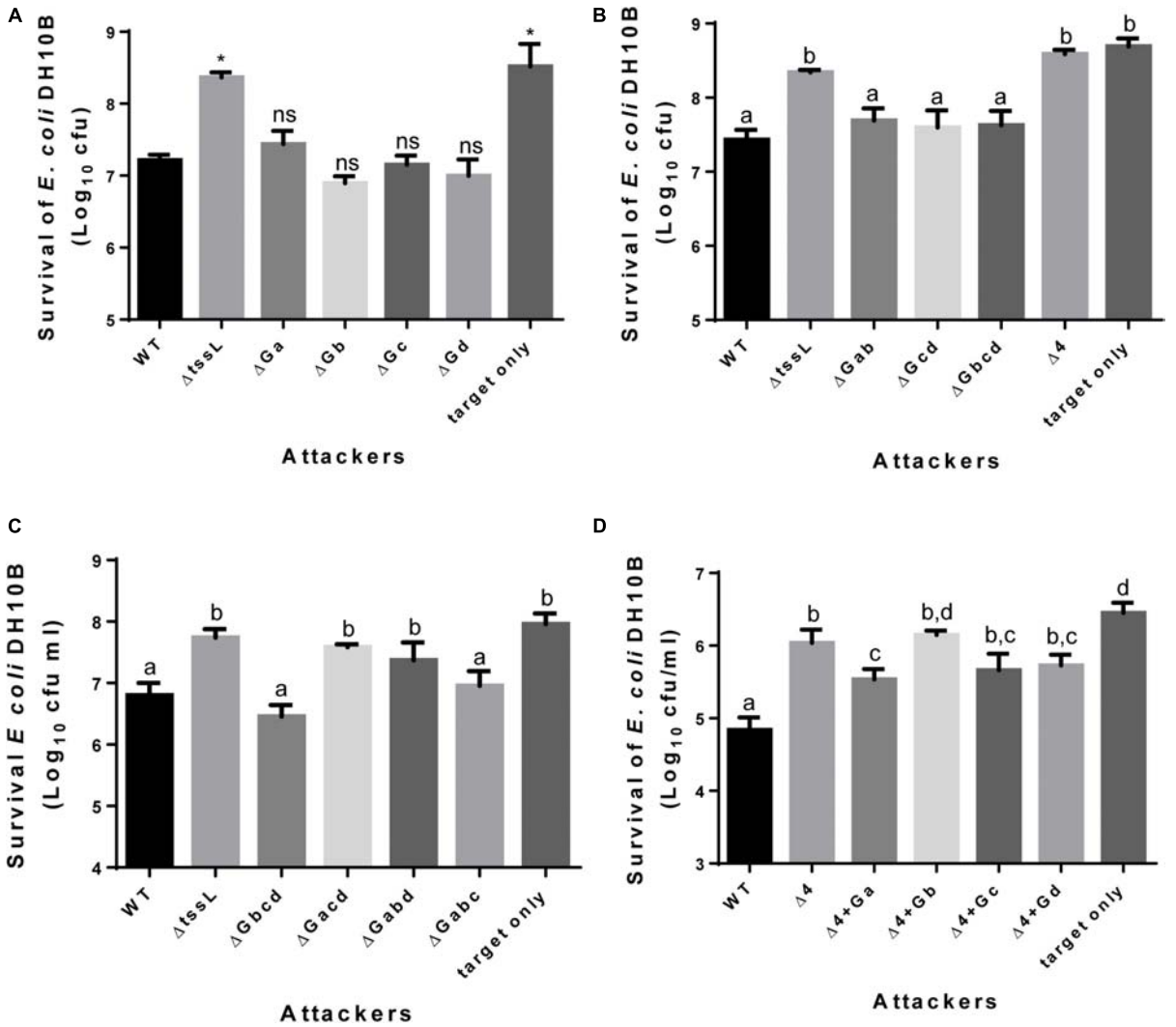

FIGURE 4 | *vgrGa* and *vgrGd* contributes to antibacterial activity of 1D1609. Each of various *A. tumefaciens* 1D1609 strains (indicated in the *x* axis) was mixed with *E. coli* DH10B cells expressing pRL662 to confer gentamicin resistance at 30:1 ratio in LB **(A,B)** or AK **(C,D)** media for 18 h. The survival of *E. coli* cells was quantified as cfu as shown on the *y* axis. **(A)** Antibacterial activity of single *vgrG* deletion mutants. Data are mean ± SEM of three biological replicates, similar results were obtained from three independent experiments. Two-tailed Student's *t*-test was used for statistical analyses. $*p < 0.01$. **(B)** Antibacterial activity in multiple *vgrG* deletion mutants. **(C)** Antibacterial activity using triple *vgrG* mutants. **(D)** Single *vgrG* expressed *in trans* using pRLBla in quadruple *vgrG* mutant (Δ4). Data are mean ± SEM of three biological replicates **(B)** or four biological replicates from two independent experiments **(C,D)**. Different letters above the bar indicate statistically different groups of strains ($P < 0.05$) determined by Tukey's HSD test, based on cfu of surviving *E. coli* cells.

antibacterial activity against *E. coli* (**Figure 5B**). These results suggest that *vgrGa*- and *vgrGd*-associated EI pairs contribute to antibacterial activity to *E. coli*.

Since single deletion of *vgrGa*-associated EI pair (Δ*EIa*) or in combination with additional EI-pair/s showed reduced or abolished antibacterial activity (**Figures 5A,B**), we considered *vgrGa*-associated effector V2a as the primary toxin and characterized its function. The putative effector gene *v2a* was expressed by an arabinose inducible promoter on plasmid pJN105 and its putative cognate immunity gene *v3a* was expressed constitutively on plasmid pTrc200 in *E. coli*. The results showed that the bacterial growth is inhibited when *v2a* is induced as compared to the vector control whereas co-expression with *v3a* restores the growth (**Figure 5C**), indicating their toxin-immunity relationship.

V2a is 522-aa in length and contains a N-terminal PAAR-like DUF4150 domain and a C-terminal nuclease domain belonging to HNH/ENDOVII superfamily (pfam14412) of the treble cleft fold (Marchler-Bauer et al., 2017) (**Figure 5D**). This nuclease family has a conserved motif AHH, which is a predicted toxin module found in bacterial polymorphic toxin systems. In the AHH motif, the first His forms one of the catalytic metal-chelating ligands and the second His contributes to the active site that directs the water for phosphoester hydrolysis (Zhang et al., 2011). Partial sequence alignment of representative nuclease family of HNH/ENDO

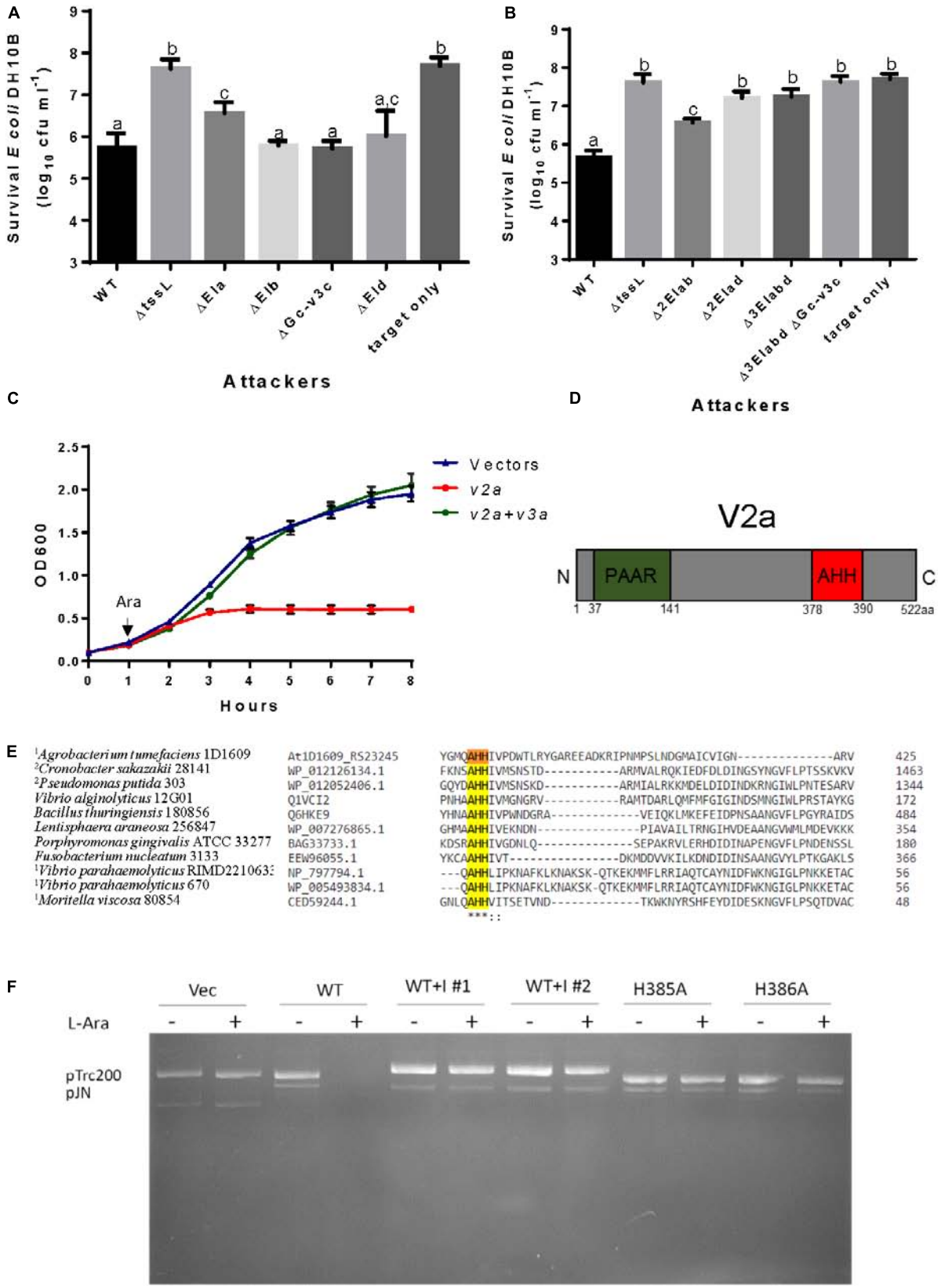

FIGURE 5 | Continued

FIGURE 5 | *vgrGa*- and *vgrGd*-associated EI pairs are responsible for antibacterial activity and V2a is a nuclease. *A. tumefaciens* 1D1609 strains (indicated in the *x* axis) was mixed with *E. coli* DH10B cells expressing pRL662 to confer Gentamicin resistance at 30:1 ratio in LB. The survival of *E. coli* cells was quantified as cfu as shown on the y axis when co-cultured with single **(A)** and multiple **(B)** EI pair deletion mutant. Data are mean ± SEM of four biological repeats from two independent experiments. Different letters above the bar indicate statistically different groups of strains ($P < 0.05$) determined by Tukey's HSD test, based on cfu of surviving *E. coli* cells. **(C)** *E. coli* growth inhibition analysis in *vgrGa*-associated EI pair. *E. coli* cultures were induced with 1 mM IPTG at 0 h for the expression of putative immunity protein expressed on pTrc200 plasmid followed by L-arabinose (Ara) induction at 1 hr to induce putative toxin gene from pJN105 plasmid. Cell growth was recorded every hour at OD_{600}. Empty vectors were used as controls. Data are mean ± SEM of three independent experiments. **(D)** Schematic diagram showing N-terminal PAAR region and C-terminal AHH nuclease domain of *vgrGa*-associated effector V2a. **(E)** Partial sequence alignment of representative nuclease family of HNH/ENDO VII superfamily with conserved AHH motif, modified from NCBI CDD sequence alignment of nuclease family of the HNH/ENDO VII superfamily with conserved AHH (pfam14412). The strain name and locus tag/accession number are on the left, and the conserved amino acid residues are indicated as * (identical) and: (similar) respectively. AHH motif is highlighted in yellow with the two His targeted for mutagenesis. AHH domain linked to DUF4150 domain[1] or Rhs[2] is indicted. **(F)** Nuclease activity assay. *E. coli* cells with pTrc200 and pJN105 plasmid (Vec) or derivatives expressing *v2a* (WT), WT with immunity protein (WT + I; #1 and #2 are two independent constructs) and catalytic site mutants (H385A, H386A) were induced with (+) or without (–) L-arabinose (L-Ara) for 2 h. Plasmid DNA was extracted and the degradation pattern was observed in agarose gel.

VII superfamily with conserved AHH motif is shown in **Figure 5E**.

To determine its nuclease activity, we examined the degradation of the plasmid DNA extracted from *E. coli* cells after *v2a* is induced by arabinose for 2 h. We showed that both pTrc200 and pJN-derived plasmids were not detectable from *v2a*-containing cells induced by arabinose, in contrast to the presence of both plasmids in vector control or *v2a*-containing cells not treated with arabinose (**Figure 5F**). The plasmid degradation is indeed caused by nuclease activity of V2a because the plasmid degradation is no longer detectable when the cells expressing the catalytic site (H385A and H386A) mutant or co-expression of *v3a* (**Figure 5F**). Taken together, we demonstrated that V2a is a T6SS effector that requires its AHH motif for nuclease activity. Moreover, this toxicity can be specifically neutralized by its cognate immunity protein. While this study was under way, a type VI nuclease effector Tse7 with GHH catalytic site (Tox-GHH2, pfam14412) from the same HNH/ENDO VII superfamily was reported in *P. aeruginosa* (Pissaridou et al., 2018). In conclusion, HNH nuclease superfamily appeared to be a widespread T6SS nuclease toxin family for antibacterial activity. These results strongly suggested the *v2a-v3a* toxin-immunity relationship, which supported their contribution to 1D1609's antibacterial activity to *E. coli*.

VgrG Can Be Exchanged Between C58 and 1D1609

Considering that VgrGa, VgrGc and VgrGd of 1D1609 and VgrG2 of C58 are highly similar with identical C-terminal region and their DUF2169 and DUF4150 share high sequence similarity (**Supplementary Table S3**), it is plausible that these VgrG proteins can substitute each other's role in effector delivery. Previous work showed that Hcp and VgrG can be exchanged between *Vibrio cholerae* cells in a T6SS-dependent manner and can be reused to assemble a new T6SS (Vettiger and Basler, 2016). Thus, we hypothesized that *Agrobacterium* may take advantage of having multiple, highly similar VgrG to receive or donate this effector carrier from/to its siblings and the donated VgrG can be used by the recipient cell to kill another competing bacterial cell. To test this hypothesis, we designed a tripartite interbacterial transfer system that will allow us to see the killing of the target *E. coli* cell only when there is a functionally exchangeable VgrG protein translocated from C58 to 1D1609. The nearly identical VgrGs ($G2^{C58}$ and Ga^{1D1609}) expressed on a non-transferable pRL662 plasmid in C58 Δ*tdei1*Δ*G1*Δ*G2op,* a mutant deleting *vgrG1, tde1-tdi1, vgrG2* operon, serves as a donor cell. 1D1609 Δ*4* with deletion of all four *vgrG* genes but is still armed with effectors is designated as a recipient cell as well as an attacker to kill *E. coli* (**Figure 6A**). Since no antibacterial activity can be detected in C58 Δ*tdei1*Δ*G1*Δ*G2op* (Ma et al., 2014) and 1D1609 Δ*4* (**Figure 4B**), 1D1609 Δ*4* can only exhibit antibacterial activity by obtaining VgrG proteins from C58 donor and using it for effector delivery to kill *E. coli*.

During this course of study, our group also discovered that Tde effector loading onto VgrG is critical for T6SS assembly and Hcp secretion (Wu et al., 2019a). Thus, aside from expressing $G2^{C58}$ or Ga^{1D1609} in C58 Δ*tdei*Δ*G1*Δ*G2op* donor strain, a plasmid expressing Tde2 with catalytic site mutation and its cognate DUF2169 chaperone/adaptor ($pTde2^{M}$) was also included to ensure effective T6SS assembly and firing. Hcp secretion and antibacterial activity assays confirmed that the $G2^{C58}$ or Ga^{1D1609} in C58 Δ*tdei*Δ*G1*Δ*G2op* donor strain remained active in Hcp secretion as WT level but completely lost the antibacterial activity against *E. coli* (**Figures 6B,C**). However, the donor-recipient-prey tripartite co-incubation showed that only the experimental set with C58 Δ*tdei*Δ*G1*Δ*G2op* donor strain harboring $G2^{C58}$ or Ga^{1D1609} in the presence of $pTde2^{M}$ can allow 1D1609 Δ*4* to exhibit antibacterial activity to *E. coli* (**Figure 6D**). 1D1609 Δ*4* co-cultured with donor strains C58 Δ*tssL,* Δ*tdei*Δ*G1*Δ*G2op* harboring vector only, $G2^{C58}$ or Ga^{1D1609} alone do not exhibit detectable killing activity to *E. coli*. These results suggest that 1D1609 can use the $VgrG2^{C58}$ and $VgrGa^{1D1609}$ delivered from C58 to kill *E. coli* and $VgrG2^{C58}$ can function as an effector carrier in 1D1609.

DISCUSSION

Functional redundancy is a useful strategy for the pathogen to build a robust system (Galán, 2009). In this study, our phylogenomic analyses revealed that the majority of T6SS-harboring Proteobacteria encode multiple *vgrG* genes. Among them, *A. tumefaciens* strain 1D1609 is unique for having multiple VgrG paralogs (VgrGa, VgrGc, and VgrGd) with high sequence identity (99%). The three *vgrG* genetic modules have the

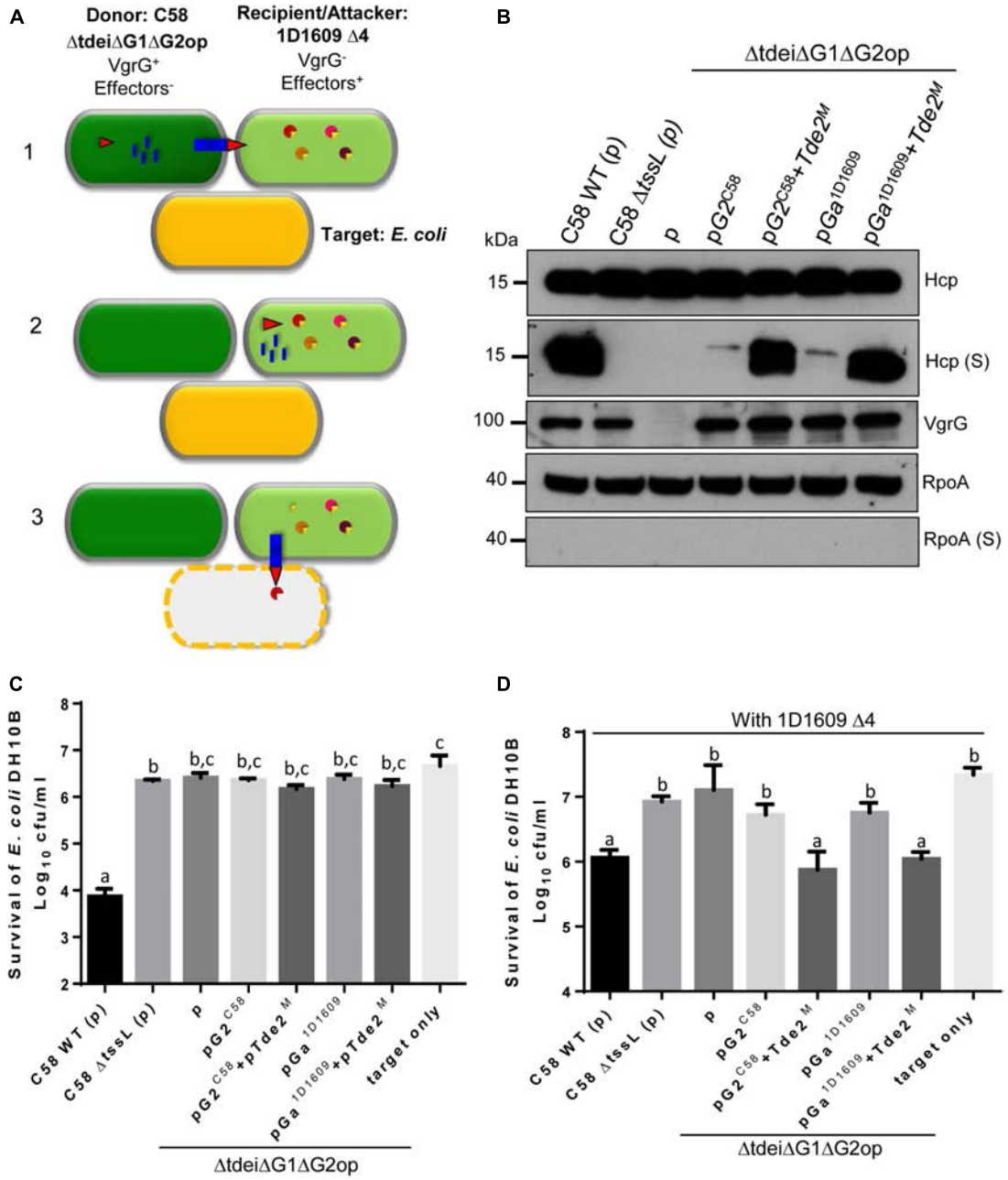

FIGURE 6 | VgrG can be exchanged between C58 and 1D1609 for executing antibacterial activity. **(A)** Schematic diagram for tripartite interaction assay to determine the VgrG exchange/killing of *E. coli* by the recipient *Agrobacterium*. The donor C58 Δ*tdei*Δ*G1*Δ*G2op* was co-cultured with recipient 1D1609 Δ4 and *E. coli* target. The "exchangeable" VgrGs ($G2^{C58}$ or Ga^{1D1609}) was expressed alone or co-expressed with Atu3641 and Tde2 with catalytic site mutation (named as $Tde2^{M}$) in donor C58 cells. The exchange/killing is divided in three steps: (1) Donor C58 expresses T6SS components without active toxin effectors and recipient 1D1609 expresses effectors complexed with cognate immunity proteins (EI pairs shown in circle with triangle) without T6SS assembly. T6SS is assembled in donor C58 for injecting Hcp (blue blocks) and VgrG (red triangle) into recipient 1D1609. (2) Recipient 1D1609 uses the translocated VgrG to assemble a new T6SS machine carrying 1D1609 effector. (3) Recipient 1D1609 injects the toxin effector and kills the target *E. coli.* **(B)** Hcp secretion in the donor C58. *A. tumefaciens* strain C58 or derivatives containing the plasmid only (p) or expressing the indicated genes were cultured in ABMES (pH 5.5) broth at 25°C and cellular and secreted (S) fractions were subjected to immunoblotting using anti-Hcp, anti-VgrG, and RpoA. The T6SS inactive mutant Δ*tssL* is a negative control and RpoA serves as a non-secreted protein control. **(C,D)** *A. tumefaciens* 1D1609 strains (indicated in the *x* axis) was mixed with *E. coli* DH10B cells expressing pRLBla to confer ampicillin resistance at 30:1 ratio in AK medium. The survival of *E. coli* cells was quantified as cfu as shown on the y axis when co-cultured with donor cells only **(C)** or with donor and recipient 1D1609 cells, at 1:10 ratio **(D)**. Data are mean ± SEM of four biological repeats from three independent experiments. Different letters above the bar indicate statistically different groups of strains ($P < 0.05$) determined by Tukey's HSD test, based on cfu of surviving *E. coli* cells.

same gene orders encoding highly conserved VgrG-DUF2169-DUF4150. However the DUF4150-linked effectors do not share significant sequence similarities suggesting that these effectors may have distinct functions. This study provided genetic evidence that these nearly identical VgrG paralogs can carry not only their genetically linked cognate effector but also non-genetically linked effectors sharing the highly similar DUF4150. The functional replacement or exchange can occur for these proteins produced in the same bacterial cells or those taking from its isogenic sibling or close relatives during T6SS attacks. Thus, such functional redundancy may be a beneficial strategy for agrobacteria to compete in their ecological niche.

While several studies clearly demonstrated that VgrG is specifically required for delivery of cognate effector(s) encoded in the same *vgrG* genetic module (Hachani et al., 2014; Whitney et al., 2014) and C-terminal variable region of VgrG is the molecular determinant (Bondage et al., 2016; Flaugnatti et al., 2016), only few studies reveal the roles of highly homologous VgrG proteins in effector delivery. *D. dadantii* 3937 also encodes two highly similar VgrG homologs ($VgrG_A$ and $VgrG_B$, **Supplementary Table S1**) which are both genetically linked to genes encoding homologous DUF1795-containing EagR chaperone and Rhs-linked effectors RhsA and RhsB (Koskiniemi et al., 2013). The homologous DUF1795 shares 97% amino acid sequence identity and RhsA and RhsB share 86% amino acid sequence identity with conserved N-terminal PAAR domain (99% identity). By sharing the highly similar chaperone and PAAR-Rhs regions, RhsA and RhsB effectors each harboring distinct C-terminal nuclease toxin domains could be delivered by not only its cognate but also non-cognate VgrG. Indeed, the competition assay revealed that either $vgrG_A$ or $vgrG_B$ is required for RhsB-mediated inhibition. The inhibitor cells without $vgrG_B$ in $\Delta rhsA/rhsB^+$ background can still have competitive advantage. The advantage is lost when both *vgrG*s are deleted and restored when $vgrG_B$ was expressed in double *vgrG* deletion mutant. Sharing the same VgrG carrier was also found in *Serratia marcescens* Db10, in which two different PAAR-domain containing Rhs effectors (RhS1 and RhS2) can functionally pair with the same VgrG protein (VgrG2) for delivery to target cells (Cianfanelli et al., 2016). The *rhs2* effector gene is not genetically linked to *vgrG2*, but both Rhs1 and Rhs2 have the same DUF1795 (EagR)-PAAR-Rhs gene organization. The EagR1 shares only 26% amino acid sequence identity with EagR2 and each specifically interacts with its cognate Rhs and is required for delivery (Alcoforado Diniz and Coulthurst, 2015; Cianfanelli et al., 2016). VgrG2 can form VgrG2-Rhs1-EagR1 or VgrG2-Rhs2-EagR2 complexes even though the N-terminal PAAR and full-length amino acid sequence of Rhs1 and Rhs2 share only 34 and 30% identity, respectively. In this case, high amino acid sequence identity in chaperone and PAAR is not required for functional exchange. However, they may share structural similarity that is sufficient for interacting with the same VgrG.

A recent study demonstrated that T6SS components, Hcp and VgrG, can be transferred and reused by *V. cholera* cells (Vettiger and Basler, 2016). An isogenic $LacZ^+$ reporter strain was used to measure the level of LacZ released for detection of cell lysis when the isogenic donor cells translocate Hcp and VgrG2 to isogenic recipient cells for T6SS assembly and firing. In our system, a tripartite interbacterial exchange/competition assay was designed to show evidence that highly similar VgrG proteins can be exchanged between two different *A. tumefaciens* genomospecies to kill the co-existing *E. coli*. Different *A. tumefaciens* genomospecies are known to co-exist in the same geographic area (Vogel et al., 2003). Several studies revealed that more than two genomospecies of *A. tumefaciens* can be found in the same crown gall or soil samples (Costechareyre et al., 2010; Bouri et al., 2016). Using tomato and maize seedlings, Gharsa et al. (2018) evaluated the competition of different *A. tumefaciens* genomospecies in soil and rhizosphere and concluded that related ecotypes can coexist. The initial competition alters the relative abundance, but does not eliminate the weaker strain. VgrG exchange may bring the advantages of sympatry and possessing different sets of T6SS gene clusters can maintain balance in sympatry. In *V. cholerae*, the bacterial strains that are incompatible (i.e., with different effector module sets), actively use their T6SS to kill susceptible strain during intra-species competition (Unterweger et al., 2014). However, in *A. tumefaciens* species, compatibility of T6SS EI pairs is not always predictive of competition outcomes (Wu et al., 2019b). C58 and 1D1609, which belongs to different genomospecies, can exhibit antibacterial activity against each other when the attacker is initiated with a higher relative abundance during an *in planta* interbacterial competition assay. However, C58 and 1D1609 can coexist with similar competitiveness when co-cultured at equal ratio despite their distinct EI pairs (**Supplementary Figure S4**). No significant difference of competitiveness (competitive index ∼1) could be observed when C58 WT is co-inoculated with equal number of 1D1609 WT or Δ*tssL*, or vice versa. This indicates that the two strains are proliferating equally *in planta* regardless of the presence or absence of a functional T6SS of *Agrobacterium* in different host plants. Interestingly, highly similar VgrGs are common in different *A. tumefaciens* genomospecies. In genomospecies 1 (G1), all (except 1D1108) share 100% identity while G8 (represented by C58 VgrG1 and two VgrGs in 1D132) share 95.7–99.8%. G7 (three VgrGs in 1D1609) and G8 (C58 VgrG2, 1D132 VgrG and three VgrGs in 1D1609) share 96.9–99.9% identity (**Supplementary Figure S3**). Thus, VgrG exchange might be common between different genomospecies, which may allow them to coexist and could in turn benefit *A. tumefaciens* sympatry in its ecological niche.

While not always evident by statistical analysis, deletion of single *vgrGa* (Δ*vgrGa*) or its associated effector-immunity (Δ*EIa*), but not other single *vgrG* or *EI* pair mutants, showed reduction of antibacterial activity (**Figures 4A**, **5A,B**). The data suggest that *vgrGa* genetic module play the primary role in antibacterial activity of 1D1609. The *vgrGa*-associated effector V2a belongs to different type of nuclease toxin distinct from the Tde1 and Tde2 nuclease toxins (toxin_43 domain with HxxD catalytic motif) identified in C58 (Ma et al., 2014). The use of enzymatic toxins such as nuclease is the most prominent theme in bacterial warfare (Galán, 2009). Using bioinformatics analysis, Ma et al. (2017) found that among more than 2,500 T6SS-dependent Rhs-CTs with N-terminal PAAR in 143 bacterial species, nuclease represents the major group. Among these,

the Rhs-AHH is the most dominant nuclease found in 66 bacterial species. Effectors with predicted AHH nuclease has been reported with antibacterial activity in *V. parahaemolyticus* VP1415 (Salomon et al., 2014) and *Pectobacterium carotovorum subsp. brasiliense* strain PBR 1692 (Bellieny-Rabelo et al., 2019) but no nuclease activity has been tested. In *Acinetobacter baylyi*, it was shown that the genomic DNA was completely degraded when Rhs2 with C-terminal AHH motif is expressed in *E. coli* (Fitzsimons et al., 2018). In this study, we characterize further to show that the AHH motif is indeed responsible for the DNase activity (**Figure 5**). The other conserved motif of HNH/ENDO VII superfamily nuclease has been reported in *P. putida* KT2440 Tke2 (Rhs-Tox-HNH) and Tke4 (Rhs-Tox-SHH) (Bernal et al., 2017) and functional characterization was done only in Tox-GHH2 in Tse7 in *P. aeruginosa* (Pissaridou et al., 2018). Among the 100 Soft-rot Enterobacteriaceae (SRE) genomes surveyed by Bellieny-Rabelo et al. (2019), about a quarter encodes AHH, suggesting that this nuclease is a common weapon deployed by both plant and animal pathogenic bacteria in interbacterial competition.

Among the four *vgrG* clusters encoded in 1D1609, *vgrGb* is distinct from the other three. Our data suggest that *vgrGb* and *v4b* encoding a putative toxin does not seem to play a role in antibacterial activity (**Figures 4**, **5A,B**). This may be due to low expression level of this gene. Alternatively, V4b may target eukaryotic cells because it contains a nuclear localization signal and has an extensive structural similarity to the insecticidal TcdB2-TccC3 toxin of *Photorhabdus luminescens* and YenC2 toxin of *Yersinia entomophaga* (**Supplementary Table S2**). The activity of the remaining effectors remains unknown and is currently under investigation.

In conclusion, *Agrobacterium* has developed a flexible mode of T6SS effector delivery, by using highly similar VgrGs, either produced endogenously or injected from its close relatives, for T6SS assembly and firing. VgrG and PAAR are among the least abundant T6SS components (Lin et al., 2019) and limiting VgrG can result in reduced number of T6SS assemblies (Vettiger and Basler, 2016). Therefore, it is plausible that having multiple highly similar VgrGs may enhance robustness and abundance of T6SS assemblies. This flexibility could allow them to be an ally to its sister cells and an effective weapon against distantly related bacterial competitors. The knowledge gained in this study can help advance the understanding of mechanisms and physiological roles of multiple VgrG proteins and associated effectors and may provide new insights for sympatric speciation.

MATERIALS AND METHODS

Bacterial Strains, Plasmids, and Growth Conditions

The bacterial strains, plasmids and primers used in this study are listed in **Supplementary Tables S4, S5**. *A. tumefaciens* strains were grown in 523 medium at 25°C while *E. coli* strains were grown in LB medium at 37°C. In-frame deletion mutants in *Agrobacterium* were generated using a suicide plasmid via double crossing over by electroporation or by conjugation (Ma et al., 2009). The mutants were confirmed by colony PCR and/or Southern blot analysis (**Supplementary Figure S5**). Site directed mutagenesis was done using overlapping PCR (Ho et al., 1989).

Phylogenetic and Sequence Analysis

All bioinformatics tools were used with the default parameters unless stated otherwise. The function of putative effectors were inferred from NCBI's Conserved Domain Database (CDD) based on BLASTP searches (Boratyn et al., 2013; Marchler-Bauer et al., 2017) and Protein Homology/analogy Recognition Engine (Phyre2) (Kelley et al., 2015). SignalP was used to predict signal peptides (Petersen et al., 2011). PSORTb version 3.0.2 was used to predict sub-cellular localization of proteins (Yu et al., 2010).

For the phylogenomic analysis to investigate the VgrG diversity among Proteobacteria, the VgrG homologs from five representatives (i.e., *A. tumefaciens* 1D1609, *Burkholderia thailandensis* E264, *Geobacter sulfurreducens* PCA, *Helicobacter cinaedi* CCUG 18818, and *P. aeruginosa* PAO1) were used as queries to run BLASTP searches against the NCBI non-redundant protein database (*e*-value cutoff = 1e-15, max target sequences = 100,000). Spurious hits, defined as hits with the high scoring pairs (HSP) accounting for <74% of the query sequence or sequence similarity <48% within the HSP, were removed. The resulting lists from different query species were combined to remove redundant hits. The combined list was further manually curated to keep only the targets with complete genome sequences available in GenBank. Based on the taxonomy information of the targets, the list was iteratively trimmed to achieve a balance taxon sampling with ∼50 genomes to represent all major lineages within Proteobacteria. One Planctomycetes, *Pirellula staleyi* DSM 6068, was included as the outgroup to root the species phylogeny (**Figure 1**). In addition to the aforementioned data set for phylum-level (i.e., Proteobacteria) diversity, a second data set containing 11 *Agrobacterium* genomes (Wu et al., 2019b) was compiled to examine the genus-level VgrG diversity; *Neorhizobium galegae* HAMBI 540 was included as the outgroup for this second data set (**Supplementary Figure S3**).

After genome selection, the procedures for homologous gene identification and molecular phylogenetic analysis were based on those described in our previous studies (Lo et al., 2013; Lo and Kuo, 2017). Briefly, the homologous genes among all genomes were identified by using OrthoMCL (Li et al., 2003). The single-copy genes shared by all genomes were used for inferring the species phylogeny. Additionally, all *vgrG* homologs in these genomes, defined as the genes containing at least 80% of the VgrG domain (TIGR03361), were extracted for inferring the gene tree. The protein sequences were aligned using MUSCLE (Edgar, 2004) and the molecular phylogenies were inferred using MrBayes (Ronquist and Huelsenbeck, 2003). The amino acid substitution model was set to mix with gamma-distributed rate variation across sites and a proportion of invariable sites. The number of rate categories for the gamma distribution was set to four. The Markov chain Monte Carlo analysis was set to run for 1,000,000 generations and sampled every 100 generations. The first 25% of the samples were discarded as the burn-in. Furthermore, the protein sequence identity among all VgrG homologs were calculated using PROTDIST (Felsenstein, 1989). The amino

acid sequence identity and similarity percentage of VgrG and VgrG-associated proteins were determined using Vector NTI Advance 11.5.4.

Secretion Assay

Secretion assay from liquid culture of *A. tumefaciens* grown in either LB rich medium or AB-MES minimal medium was done as previously described (Ma et al., 2009). Proteins from cellular and secreted fractions were resolved by SDS-PAGE and transferred onto a PVDF membrane by using a transfer apparatus (Bio-Rad). The membrane was probed with primary antibody against C58 VgrG1 (1:1,000), which recognizes the C58 VgrG2 and all four VgrGs of 1D1609, Hcp (1:2,500), and RpoA (1:7,500) (Lin et al., 2013), followed by incubation with horseradish peroxidase-conjugated anti-rabbit secondary antibody (1:30,000) and visualized with the ECL system (PerkinElmer).

Interbacterial Competition Assay

Escherichia c*oli* killing assay was performed as described previously (Bondage et al., 2016). In brief, overnight culture of *A. tumefaciens* and *E. coli* strain were adjusted to OD_{600} 0.1 and incubated at 25°C for 4 h. *A. tumefaciens* and *E. coli* cells were mixed at a 30:1 ratio (OD 0.3:0.01) and spotted on LB agar (1.5%) plates. After 18 hr incubation at 25°C, the co-cultured cells were collected, serially diluted and plated on LB agar containing appropriate antibiotics to quantify surviving *E. coli* by counting colony forming unit (cfu). When enhanced killing activity is desired, an optimized growth medium, named as *Agrobacterium* Kill-triggering, AK medium (3 g K_2HPO_4, 1 g NaH_2PO_4, 1 g NH_4Cl, 0.15 g KCl, 9.76 g MES in 900 mL ddH20, pH5.5) modified from AB-MES medium and solidified by 2% (w/v) agar, was used instead. Data are expressed as mean ± SEM (standard error of the mean) from three independent experiments. Statistics was done using one-way ANOVA and Tukey's honestly significance difference (HSD) test[1].

In planta bacterial competition assay was performed as described previously (Ma et al., 2014). *A. tumefaciens* strain C58 transformed with gentamicin resistance-conferring pRL662 plasmid and strain 1D1609 conferring spectinomycin resistance were mixed at 1:1 (OD 1) ratio and infiltrated into 6- to 7-week-old *Nicotiana benthamiana* and *Medicago truncatula* leaves. The competition outcome was quantified at 0 h and 24 h by counting cfu on LB plates with appropriate antibiotics. 1D1609/C58 ratio at t = 24 h was divided by 1D1609/C58 ratio at t = 0h to calculate the competitive index.

Growth Inhibition Assay

Growth inhibition assay was performed as described previously (Ma et al., 2014). In brief, overnight cultures of *E. coli* DH10B strain with vectors or their derivatives were adjusted to OD_{600} 0.1. The expression of the tested immunity protein was induced by 1 mM IPTG for 1 h before L-arabinose (0.2% final concentration) was added to induce expression of the toxin.

[1]http://astatsa.com/OneWay_Anova_with_TukeyHSD/

Plasmid DNA Degradation Analysis in *E. coli* Cells

In vivo plasmid DNA degradation analysis was performed as described previously (Ma et al., 2014). In brief, overnight cultures of *E. coli* DH10B strain with empty vectors or derivatives expressing *v2a* and catalytic site mutant were harvested and adjusted to OD_{600} 0.3. L-arabinose (0.2%, final concentration) was added to induce the expression and cultured for 2 h. Equal amounts of cells were used for plasmid DNA extraction and equal volume of extracted DNA was resolved in agarose gel followed by ethidium bromide staining.

Southern Blot Hybridization

Southern blot hybridization was performed as described (Sambrook, 2001). In brief, genomic DNA (gDNA) was extracted from overnight cultures of selected strains using Genomic DNA purification Kit (Promega) as per manufacturer's instructions. About 35 μg of gDNA was digested using NEB restriction enzymes (Nsil and *Pvu*II) and resolved in 0.8% agarose gel, 50 V, 3 h. The DNA fragments were transferred to a positively charged nylon membrane (Roche Diagnostics). Nylon membranes were cross-linked and used for hybridization with DIG-labeled probe (Roche). Hybridization was done overnight at 65°C using hybridization solution (FastHyb-Hybridization solution, BioChain). The washing, blocking and detection were done using Roche Wash and Block Buffer Set and DIG DNA Labeling and Detection Kit, according to manufacturer's instructions (Roche). The membrane was exposed to X-ray for detection. The probe for the four *vgrGs* (*vgrGa*, *vgrGb*, *vgrGc,* and *vgrGd*) and putative toxin genes (*v2a*, *v2c*, *v2d,* and *v4b*) was prepared using the plasmid DNA *vgrGa*-pJN105, *v2d*-pJN105, and *v4b*-pJN105, respectively. The primer sets used are listed in **Supplementary Table S5**.

DATA AVAILABILITY STATEMENT

All datasets generated for this study are included in the article/**Supplementary Material**.

AUTHOR CONTRIBUTIONS

E-ML and MS conceptualized the study. MS, S-TC, and C-JC worked on the data curation. E-ML, C-HK, C-FW, and MS worked on the methodology. C-HK, S-TC, MS, and C-JC carried out the investigation. E-ML was responsible for project administration and resources. E-ML and C-HK supervised the study. MS, C-HK, and E-ML wrote the manuscript. All authors reviewed and approved the manuscript.

FUNDING

Funding for this project was provided by the Ministry of Science and Technology of Taiwan (MOST) Grant Nos. 104-2311-B-001-025-MY3 and 107-2311-B-001-019-MY3 to E-ML. The funders had no role in study design, data collection and analysis, decision

to publish, or preparation of the manuscript. Open access publication fees will be paid by the Institute of Plant and Microbial Biology, Academia Sinica, Taiwan.

ACKNOWLEDGMENTS

We thank Manda Yu for sharing the recipes of AK medium for enhanced T6SS killing assay and members of Lai lab for their help, encouragement, and stimulating discussion. We are grateful for Genomic Technology Core of Institute of Plant and Microbial Biology for DNA sequencing. This manuscript has been released as a Pre-Print at bioRxiv 740209; doi: 10.1101/740209.

SUPPLEMENTARY MATERIAL

The Supplementary Material for this article can be found online at: https://www.frontiersin.org/articles/10.3389/fmicb.2019.03004/full#supplementary-material

FIGURE S1 | Bayesian phylogeny of the VgrG homologs identified in the representative Proteobacteria genomes presented in **Figure 1**. The color coding is based on the class: Alphaproteobacteria (black), Betaproteobacteria (blue), Deltaproteobacteria (cyan), Epsilonproteobacteria (purple) and Gammaproteobacteria (green). Numbers on the branches indicate the support levels based on posterior probabilities, only values > 60% were shown.

FIGURE S2 | Multiple sequence alignment of VgrG amino acid sequences of 1D1609 and C58. All VgrG homologs were aligned and conserved amino acid residues are shaded in yellow and variable residues are in blue or green, while the C-terminal extension of C58 VgrG1 not homologous to the other VgrGs is unshaded. The red and blue lines indicate the predicted gp27 and gp5 domains, respectively. The amino acid residue number is indicated.

FIGURE S3 | VgrG tree of the 11 *A. tumefaciens* strains. All VgrG homologs in these 11 genomes were extracted for inferring the gene tree. The VgrG orthologs share ≥ 95% identity in amino acid sequence were highlighted. The genomospecies and strain name for each VgrG indicated by a locus tag are shown.

FIGURE S4 | *In planta* competition experiments between C58 and 1D1609 at 1:1 ratio. *A. tumefaciens* strain C58 harboring gentamicin resistance-conferring pRL662 and strain 1D1609 which was selected in spectinomycin plate were mixed at 1:1 ratio and infiltrated into leaves of 6- to 7-week-old *Nicotiana benthamiana* **(A)** and *Medicago truncatula* **(B)**. The competition outcome was quantified at 0 and 24 h post-infection by counting cfu on LB plates with appropriate antibiotics. Data are mean ± SEM, with each data point indicating the competitive index of 4–6 biological replicates from a total of 2–3 independent experiments. No statistical difference ($P > 0.05$) could be detected among different samples as determined by Tukey's HSD test.

FIGURE S5 | Southern blot analysis of mutants generated in this study. Schematic diagram showing probes used for Southern blotting, restriction enzyme cleavage sites and expected sizes. The genomic DNA is hybridized with **(A)** 821-bp *vgrG* probe with homology to all four *vgrG* genes (*vgrGabcd)* was used to confirm *vgrG* mutants; **(B)** 478-bp *v2* probe with homology to *v2acd* was used to confirm *v2a*, *v2c,* and *v2d* mutant and **(C)** 778-bp *v4b* probe was used to confirm *v4b* mutant. Each lane contains 30 μg of genomic DNA digested with *Nsi*I only or combined with *Pvu*II. The expected size (in bp) is indicated on the side of the blot.

TABLE S1 | Percentage identity of VgrG within genomes with highly identical multiple VgrGs. The locus tag of each homolog is shown in rows and column and highlight shows ≥ 95% identity.

TABLE S2 | Predicted functions/domains of toxin/s associated with each *vgrG* based on Phyre or NCBI CDD search and BLASTP.

TABLE S3 | Amino acid sequence similarity/identity among the protein homologs encoded in the *vgrG* genetic modules in *A. tumefaciens* strains C58 and 1D1609.

TABLE S4 | Bacterial strains and plasmids.

TABLE S5 | Primers used in this study.

REFERENCES

Alcoforado Diniz, J., and Coulthurst, S. J. (2015). Intraspecies competition in *Serratia marcescens* is mediated by type VI-secreted Rhs effectors and a conserved effector-associated accessory protein. *J. Bacteriol.* 197, 2350–2360. doi: 10.1128/JB.00199-15

Bellieny-Rabelo, D., Tanui, C. K., Miguel, N., Kwenda, S., Shyntum, D. Y., and Moleleki, L. N. (2019). Transcriptome and comparative genomics analyses reveal new functional insights on key determinants of pathogenesis and interbacterial competition in pectobacterium and *Dickeya* spp. *Appl. Environ. Microbiol.* 85: e02050-018. doi: 10.1128/AEM.02050-18

Bernal, P., Allsopp, L. P., Filloux, A., and Llamas, M. A. (2017). The *Pseudomonas* putida T6SS is a plant warden against phytopathogens. *ISME J.* 11, 972–987. doi: 10.1038/ismej.2016.169

Bingle, L. E., Bailey, C. M., and Pallen, M. J. (2008). Type VI secretion: a beginner's guide. *Curr. Opin. Microbiol.* 11, 3–8. doi: 10.1016/j.mib.2008.01.006

Bladergroen, M. R., Badelt, K., and Spaink, H. P. (2003). Infection-blocking genes of a symbiotic *Rhizobium leguminosarum* strain that are involved in temperature-dependent protein secretion. *Mol. Plant Microbe Interact.* 16, 53–64. doi: 10.1094/mpmi.2003.16.1.53

Bondage, D. D., Lin, J.-S., Ma, L.-S., Kuo, C.-H., and Lai, E.-M. (2016). VgrG C terminus confers the type VI effector transport specificity and is required for binding with PAAR and adaptor–effector complex. *Proc. Natl. Acad. Sci. U.S.A.* 113, E3931–E3940. doi: 10.1073/pnas.1600428113

Boratyn, G. M., Camacho, C., Cooper, P. S., Coulouris, G., Fong, A., Ma, N., et al. (2013). BLAST: a more efficient report with usability improvements. *Nucleic Acids Res.* 41, W29–W33. doi: 10.1093/nar/gkt282

Bouri, M., Chattaoui, M., Gharsa, H. B., McClean, A., Kluepfel, D., Nesme, X., et al. (2016). Analysis of Agrobacterium populations isolated from tunisian soils: genetic structure, avirulent-virulent ratios and characterization of tumorigenic strains. *J. Plant Pathol.* 98, 265–274.

Cianfanelli, F. R., Alcoforado Diniz, J., Guo, M., De Cesare, V., Trost, M., and Coulthurst, S. J. (2016). VgrG and PAAR proteins define distinct versions of a functional type VI secretion system. *PLoS Pathog.* 12:e1005735. doi: 10.1371/journal.ppat.1005735

Costechareyre, D., Rhouma, A., Lavire, C., Portier, P., Chapulliot, D., Bertolla, F., et al. (2010). Rapid and efficient identification of agrobacterium species by recA Allele analysis. *Microb. Ecol.* 60, 862–872. doi: 10.1007/s00248-010-9685-7

Edgar, R. C. (2004). MUSCLE: multiple sequence alignment with high accuracy and high throughput. *Nucleic Acids Res.* 32, 1792–1797. doi: 10.1093/nar/gkh340

Felsenstein, J. (1989). PHYLIP - phylogeny inference package (Version 3.2). *Cladistics* 5, 164–166.

Fitzsimons, T. C., Lewis, J. M., Wright, A., Kleifeld, O., Schittenhelm, R. B., Powell, D., et al. (2018). Identification of novel *Acinetobacter baumannii* Type VI secretion system antibacterial effector and immunity pairs. *Infect. Immun.* 86:e00297-18. doi: 10.1128/IAI.00297-18

Flaugnatti, N., Le, T. T., Canaan, S., Aschtgen, M. S., Nguyen, V. S., Blangy, S., et al. (2016). A phospholipase A1 antibacterial Type VI secretion effector interacts directly with the C-terminal domain of the VgrG spike protein for delivery. *Mol. Microbiol.* 99, 1099–1118. doi: 10.1111/mmi.13292

Galán, J. E. (2009). Common themes in the design and function of bacterial effectors. *Cell Host Microbe* 5, 571–579. doi: 10.1016/j.chom.2009.04.008

Gelvin, S. B. (2000). Agrobacterium and plant genes involved in t-dna transfer and integration. *Annu. Rev. Plant Physiol. Plant Mol. Biol.* 51, 223–256.

Gharsa, H. B., Bouri, M., Glick, B., Gannar, A., Mougou Hamdane, A., and Rhouma, A. (2018). Evaluation of the interspecific competition within *Agrobacterium* spp. in the soil and rhizosphere of tomato (Solanum

lycopersicum) and maize (Zea mays). *J. Plant Pathol.* 100, 505–511. doi: 10.1007/s42161-018-0114-y

Hachani, A., Allsopp, L. P., Oduko, Y., and Filloux, A. (2014). The VgrG proteins are "à la Carte" delivery systems for bacterial type VI effectors. *J. Biol. Chem.* 289, 17872–17884. doi: 10.1074/jbc.M114.563429

Haryono, M., Cho, S.-T., Fang, M.-J., Chen, A.-P., Chou, S.-J., Lai, E.-M., et al. (2019). Differentiations in gene content and expression response to virulence induction between two *Agrobacterium* strains. *Front. Microbiol.* 10:1554. doi: 10.3389/fmicb.2019.01554

Ho, S. N., Hunt, H. D., Horton, R. M., Pullen, J. K., and Pease, L. R. (1989). Site-directed mutagenesis by overlap extension using the polymerase chain reaction. *Gene* 77, 51–59. doi: 10.1016/0378-1119(89)90358-2

Hwang, H.-H., Yu, M., and Lai, E.-M. (2017). Agrobacterium-mediated plant transformation: biology and applications. *Arabidop. Book* 15:e0186. doi: 10.1199/tab.0186

Kelley, L. A., Mezulis, S., Yates, C. M., Wass, M. N., and Sternberg, M. J. (2015). The Phyre2 web portal for protein modeling, prediction and analysis. *Nat. Protoc.* 10, 845–858. doi: 10.1038/nprot.2015.053

Koskiniemi, S., Lamoureux, J. G., Nikolakakis, K. C., t'Kint de Roodenbeke, C., Kaplan, M. D., Low, D. A., et al. (2013). Rhs proteins from diverse bacteria mediate intercellular competition. *Proc. Natl. Acad. Sci. U.S.A.* 110, 7032–7037. doi: 10.1073/pnas.1300627110

Leiman, P. G., Basler, M., Ramagopal, U. A., Bonanno, J. B., Sauder, J. M., Pukatzki, S., et al. (2009). Type VI secretion apparatus and phage tail-associated protein complexes share a common evolutionary origin. *Proc. Natl. Acad. Sci. U.S.A.* 106, 4154–4159. doi: 10.1073/pnas.0813360106

Li, L., Stoeckert, C. J., and Roos, D. S. (2003). OrthoMCL: identification of ortholog groups for eukaryotic genomes. *Genome Res.* 13, 2178–2189. doi: 10.1101/gr.1224503

Lien, Y. W., and Lai, E. M. (2017). Type VI secretion effectors: methodologies and biology. *Front. Cell. Infect. Microbiol.* 7:254. doi: 10.3389/fcimb.2017.00254

Lin, J.-S., Ma, L.-S., and Lai, E.-M. (2013). Systematic dissection of the agrobacterium type VI secretion system reveals machinery and secreted components for subcomplex formation. *PLoS One* 8:e67647. doi: 10.1371/journal.pone.0067647

Lin, L., Lezan, E., Schmidt, A., and Basler, M. (2019). Abundance of bacterial Type VI secretion system components measured by targeted proteomics. *Nat. Commun.* 10:2584. doi: 10.1038/s41467-019-10466-9

Lo, W.-S., Chen, L.-L., Chung, W.-C., Gasparich, G. E., and Kuo, C.-H. (2013). Comparative genome analysis of Spiroplasma melliferum IPMB4A, a honeybee-associated bacterium. *BMC Genomics* 14:22. doi: 10.1186/1471-2164-14-22

Lo, W.-S., and Kuo, C.-H. (2017). Horizontal acquisition and transcriptional integration of novel genes in mosquito-associated spiroplasma. *Genome Biol. Evol.* 9, 3246–3259. doi: 10.1093/gbe/evx244

Ma, J., Sun, M., Dong, W., Pan, Z., Lu, C., and Yao, H. (2017). PAAR-Rhs proteins harbor various C-terminal toxins to diversify the antibacterial pathways of type VI secretion systems. *Environ. Microbiol.* 19, 345–360. doi: 10.1111/1462-2920.13621

Ma, L.-S., Hachani, A., Lin, J.-S., Filloux, A., and Lai, E.-M. (2014). *Agrobacterium tumefaciens* deploys a superfamily of Type VI secretion DNase effectors as weapons for interbacterial competition in planta. *Cell Host Microbe* 16, 94–104. doi: 10.1016/j.chom.2014.06.002

Ma, L. S., Lin, J. S., and Lai, E. M. (2009). An IcmF family protein, ImpLM, is an integral inner membrane protein interacting with ImpKL, and its walker a motif is required for type VI secretion system-mediated Hcp secretion in *Agrobacterium tumefaciens*. *J. Bacteriol.* 191, 4316–4329. doi: 10.1128/JB.00029-09

Marchler-Bauer, A., Bo, Y., Han, L., He, J., Lanczycki, C. J., Lu, S., et al. (2017). CDD/SPARCLE: functional classification of proteins via subfamily domain architectures. *Nucleic Acids Res.* 45, D200–D203. doi: 10.1093/nar/gkw1129

Petersen, T. N., Brunak, S., von Heijne, G., and Nielsen, H. (2011). SignalP 4.0: discriminating signal peptides from transmembrane regions. *Nat. Methods* 8, 785–786. doi: 10.1038/nmeth.1701

Pissaridou, P., Allsopp, L. P., Wettstadt, S., Howard, S. A., Mavridou, D. A. I., and Filloux, A. (2018). The *Pseudomonas* aeruginosaT6SS-VgrG1b spike is topped by a PAAR protein eliciting DNA damage to bacterial competitors. *Proc. Natl. Acad. Sci. U.S.A.* 115, 12519–15524. doi: 10.1073/pnas.1814181115

Ronquist, F., and Huelsenbeck, J. P. (2003). MrBayes 3: Bayesian phylogenetic inference under mixed models. *Bioinformatics* 19, 1572–1574. doi: 10.1093/bioinformatics/btg180

Russell, A. B., Peterson, S. B., and Mougous, J. D. (2014). Type VI secretion system effectors: poisons with a purpose. *Nat. Rev. Micro.* 12, 137–148. doi: 10.1038/nrmicro3185

Salomon, D., Kinch, L. N., Trudgian, D. C., Guo, X., Klimko, J. A., Grishin, N. V., et al. (2014). Marker for type VI secretion system effectors. *Proc. Natl. Acad. Sci. U.S.A.* 111, 9271–9276. doi: 10.1073/pnas.1406110111

Sambrook, J. (2001). *Molecular Cloning: A Laboratory Manual*, 3rd Edn. Cold Spring Harbor, NY: Cold Spring Harbor Laboratory Press.

Tang, J. Y., Bullen, N. P., Ahmad, S., and Whitney, J. C. (2018). Diverse NADase effector families mediate interbacterial antagonism via the type VI secretion system. *J. Biol. Chem.* 293, 1504–1514. doi: 10.1074/jbc.RA117.000178

Ting, S.-Y., Bosch, D. E., Mangiameli, S. M., Radey, M. C., Huang, S., Park, Y.-J., et al. (2018). Bifunctional immunity proteins protect bacteria against FtsZ-Targeting ADP-Ribosylating Toxins. *Cell* 175, 1380.e–1392.e. doi: 10.1016/j.cell.2018.09.037

Unterweger, D., Miyata, S. T., Bachmann, V., Brooks, T. M., Mullins, T., Kostiuk, B., et al. (2014). The *Vibrio cholerae* type VI secretion system employs diverse effector modules for intraspecific competition. *Nat. Commun.* 5:3549. doi: 10.1038/ncomms4549

Vettiger, A., and Basler, M. (2016). Type VI secretion system substrates are transferred and reused among sister cells. *Cell* 167, 99.e12–110.e12. doi: 10.1016/j.cell.2016.08.023

Vogel, J., Normand, P., Thioulouse, J., Nesme, X., and Grundmann, G. L. (2003). Relationship between spatial and genetic distance in *Agrobacterium* spp. in 1 cubic centimeter of soil. *Appl. Environ. Microbiol.* 69, 1482–1487. doi: 10.1128/aem.69.3.1482-1487.2003

Whitney, J. C., Beck, C. M., Goo, Y. A., Russell, A. B., Harding, B. N., De Leon, J. A., et al. (2014). Genetically distinct pathways guide effector export through the type VI secretion system. *Mol. Microbiol.* 92, 529–542. doi: 10.1111/mmi.12571

Wu, C.-F., Lien, Y.-W., Bondage, D., Lin, J.-S., Pilhofer, M., Shih, Y.-L., et al. (2019a). Effector loading onto the VgrG carrier activates type VI secretion system assembly. *EMBO Rep.* e47961. doi: 10.15252/embr.201947961

Wu, C.-F., Santos, M. N. M., Cho, S.-T., Chang, H.-H., Tsai, Y.-M., Smith, D. A., et al. (2019b). Plant-pathogenic *Agrobacterium tumefaciens* strains have diverse type VI effector-immunity pairs and vary in in planta competitiveness. *Mol. Plant Microbe Interact.* 32, 961–971. doi: 10.1094/MPMI-01-19-0021-R

Yu, N. Y., Wagner, J. R., Laird, M. R., Melli, G., Rey, S., Lo, R., et al. (2010). PSORTb 3.0: improved protein subcellular localization prediction with refined localization subcategories and predictive capabilities for all prokaryotes. *Bioinformatics* 26, 1608–1615. doi: 10.1093/bioinformatics/btq249

Zhang, D., Iyer, L. M., and Aravind, L. (2011). A novel immunity system for bacterial nucleic acid degrading toxins and its recruitment in various eukaryotic and DNA viral systems. *Nucleic Acids Res.* 39, 4532–4552. doi: 10.1093/nar/gkr036

Zoued, A., Brunet, Y. R., Durand, E., Aschtgen, M.-S., Logger, L., Douzi, B., et al. (2014). Architecture and assembly of the Type VI secretion system. *Biochim. Biophys. Acta Mol. Cell Res.* 1843, 1664–1673. doi: 10.1016/j.bbamcr.2014.03.018

Conflict of Interest: The authors declare that the research was conducted in the absence of any commercial or financial relationships that could be construed as a potential conflict of interest.

Copyright © 2020 Santos, Cho, Wu, Chang, Kuo and Lai. This is an open-access article distributed under the terms of the Creative Commons Attribution License (CC BY). The use, distribution or reproduction in other forums is permitted, provided the original author(s) and the copyright owner(s) are credited and that the original publication in this journal is cited, in accordance with accepted academic practice. No use, distribution or reproduction is permitted which does not comply with these terms.

frontiers in Microbiology

ORIGINAL RESEARCH
published: 05 February 2020
doi: 10.3389/fmicb.2019.03077

A High-Throughput Interbacterial Competition Screen Identifies ClpAP in Enhancing Recipient Susceptibility to Type VI Secretion System-Mediated Attack by *Agrobacterium tumefaciens*

Hsiao-Han Lin[1,2], Manda Yu[1], Manoj Kumar Sriramoju[3], Shang-Te Danny Hsu[3], Chi-Te Liu[2,4] and Erh-Min Lai[1]**

[1] *Institute of Plant and Microbial Biology, Academia Sinica, Taipei, Taiwan,* [2] *Institute of Biotechnology, National Taiwan University, Taipei, Taiwan,* [3] *Institute of Biological Chemistry, Academia Sinica, Taipei, Taiwan,* [4] *Agricultural Biotechnology Research Center, Academia Sinica, Taipei, Taiwan*

OPEN ACCESS

Edited by:
Ignacio Arechaga, University of Cantabria, Spain

Reviewed by:
Weili Liang, National Institute for Communicable Disease Control and Prevention (China CDC), China
Meriyem Aktas, Ruhr University Bochum, Germany

***Correspondence:**
Chi-Te Liu
chiteliu@ntu.edu.tw
Erh-Min Lai
emlai@gate.sinica.edu.tw

Specialty section:
This article was submitted to Microbial Physiology and Metabolism, a section of the journal Frontiers in Microbiology

Received: *07 October 2019*
Accepted: *19 December 2019*
Published: *05 February 2020*

Citation:
Lin H-H, Yu M, Sriramoju MK, Hsu S-TD, Liu C-T and Lai E-M (2020) A High-Throughput Interbacterial Competition Screen Identifies ClpAP in Enhancing Recipient Susceptibility to Type VI Secretion System-Mediated Attack by Agrobacterium tumefaciens. Front. Microbiol. 10:3077. doi: 10.3389/fmicb.2019.03077

The type VI secretion system (T6SS) is an effector delivery system used by Gram-negative bacteria to kill other bacteria or eukaryotic hosts to gain fitness. The plant pathogen *Agrobacterium tumefaciens* utilizes its T6SS to kill other bacteria, such as *Escherichia coli*. We observed that the *A. tumefaciens* T6SS-dependent killing outcome differs when using different T6SS-lacking, K-12 *E. coli* strains as a recipient cell. Thus, we hypothesized that the *A. tumefaciens* T6SS killing outcome not only relies on the T6SS activity of the attacker cells but also depends on the recipient cells. Here, we developed a high-throughput interbacterial competition platform to test the hypothesis by screening for mutants with reduced killing outcomes caused by *A. tumefaciens* strain C58. Among the 3,909 strains in the *E. coli* Keio library screened, 16 mutants with less susceptibility to *A. tumefaciens* C58 T6SS-dependent killing were identified, and four of them were validated by complementation test. Among the four, the *clpP* encoding ClpP protease, which is universal and highly conserved in both prokaryotes and eukaryotic organelles, was selected for further characterizations. We demonstrated that ClpP is responsible for enhancing susceptibility to the T6SS killing. Because ClpP protease depends on other adapter proteins such as ClpA and ClpX for substrate recognition, further mutant studies followed by complementation tests were carried out to reveal that ClpP-associated AAA^+ ATPase ClpA, but not ClpX, is involved in enhancing susceptibility to *A. tumefaciens* T6SS killing. Moreover, functional and biochemical studies of various ClpP amino acid substitution variants provided evidence that ClpA–ClpP interaction is critical in enhancing susceptibility to the T6SS killing. This study highlights the importance of recipient factors in determining the outcome of the T6SS killing and shows the universal ClpP protease as a novel recipient factor hijacked by the T6SS of *A. tumefaciens*.

Keywords: type VI secretion system, antibacterial activity, recipient cells, ClpP, ClpA, *Agrobacterium tumefaciens*, *Escherichia coli*

INTRODUCTION

Bacteria have evolved broad strategies in secreting antibiotics or protein toxins to antagonize other bacteria and gain fitness to fight for limited nutrients and space. Among them, the Gram-negative bacteria use a variety of protein secretion systems such as type I secretion system (T1SS) (García-Bayona et al., 2017, 2019), type IV secretion system (T4SS) (Souza et al., 2015; Bayer-Santos et al., 2019), contact-dependent inhibition (CDI; belongs to type V secretion system) (Aoki et al., 2005, 2010), and type VI secretion system (T6SS) (LeRoux et al., 2012; Basler et al., 2013) as antibacterial weapons. Bacteria that produce and deliver protein toxins, the effectors, through secretion systems to kill other bacteria are attacker cells, and the attacked cells are the recipient cells (Costa et al., 2015; Filloux and Sagfors, 2015). Attacker cells also produce cognate immunity proteins to neutralize effectors to prevent self-intoxication (Alteri and Mobley, 2016; Lien and Lai, 2017). A recipient cell is intoxicated if it does not have cognate immunity protein to neutralize the toxicity of its effector.

In the CDI system, non-immunity proteins in the recipient cell also participate in the bacterial competition outcome (Aoki et al., 2008, 2010; Diner et al., 2012; Willett et al., 2015; Jones et al., 2017). For example, the CDI effector CdiA-CT^{EC93} utilizes recipient's outer membrane protein BamA and the inner membrane protein AcrB to enter the recipient cell (Aoki et al., 2008). BamA belongs to the BAM complex that functions in outer membrane β-barrel proteins (OMPs) biogenesis. AcrB is an inner membrane protein that belongs to the multidrug efflux pump TolC complex. Another example is the necessity of the recipient *O*-acetylserine sulfhydrylase A (CysK) to the CDI effector CdiA-CT^{EC536} (Diner et al., 2012). In the recipient cell, CdiA-CT^{EC536} binds to CysK to increase its thermostability and its tRNase activity (Johnson et al., 2016). Interestingly, this CysK.CdiA-CT^{EC536} complex mimics the CysK.CysE complex, which is typically formed during *de novo* cysteine biogenesis, with a higher binding affinity (Johnson et al., 2016; Jones et al., 2017). Other examples are the recipient elongation factor Tu (EF-Tu) in activating the toxicity of CdiA-CT^{EC869} and CdiA-CT^{NC101} (Jones et al., 2017; Michalska et al., 2017), and the involvement of recipient PtsG in CdiA-CT^{3006} and CdiA-CT^{NC101} entry (Willett et al., 2015). To summarize, a variety of the non-immunity proteins in the recipient cells affect the CDI antagonizing outcome. As the bacterial secretion systems that serve as an antibacterial weapon share some universal characters, the above phenomenon raised a question of whether non-immunity proteins of the recipient cells also affect the bacterial antagonizing outcome in other secretion systems.

Recently, examples about the involvement of the recipient non-immunity proteins in T6SS competition outcome emerged. The first description is the involvement of the EF-Tu protein of the recipient cell for Tse6 effector-mediated killing by *Pseudomonas aeruginosa* (Whitney et al., 2015). Although recipient's EF-Tu was initially proposed to grant access of Tse6 into the recipient cytoplasm (Whitney et al., 2015), a further study demonstrated that Tse6 could penetrate the double bilayer of the EF-Tu-free liposome and exert its toxicity inside it (Quentin et al., 2018). The role of the recipient EF-Tu involved in an interbacterial competition of Tse6 remains elusive. A T6SS study in *Serratia marcescens* demonstrated that the recipient protein DsbA plays a role in activating *S. marcescens* T6SS effectors Ssp2 and Ssp4, but not Rhs2 (Mariano et al., 2018). The *S. marcescens* T6SS kills its Ssp2-sensitive siblings only when the recipient cells harbor *dsbA* homologs (*dsbA1*$^+$ *dsbA2*$^+$). The same results were also observed using Ssp4-sensitive recipient cells, but not Rhs2-sensitive strain as a recipient cell. The above findings highlight the necessity of a recipient factor to facilitate the T6SS attack. However, a systematic screening of the recipient factors that can either promote or reduce the susceptibility of the T6SS attack is still lacking.

This study aimed to explore the recipient genetic factors that affect the T6SS killing outcome using the well-characterized T6SS-possessing plant pathogen *Agrobacterium tumefaciens*, a causative agent of crown gall disease in many different plants. The *A. tumefaciens* strain C58 harbors three effector proteins: type VI DNase effector 1 (Tde1), Tde2, and putative type VI amidase effector (Tae). The Tde proteins are the main contributor to *A. tumefaciens* T6SS-dependent interbacterial competition (Ma et al., 2014). Using the T6SS-lacking *Escherichia coli* K12 strain as a model recipient cell, we report here a high-throughput, population level, interbacterial competition screening platform for identifying the recipient genetic factors that contribute to *A. tumefaciens* C58 T6SS's killing outcome. Among the 3,909 *E. coli* Keio mutants screened, we confirmed that at least six of them play a role in enhancing susceptibility to *A. tumefaciens* T6SS attack by an interbacterial competition assay and by complementation *in trans*. One of the confirmed genes, *caseinolytic protease P* (*clpP*), was highlighted in this study owing to its prominent phenotype. A functional ClpP complex consists of a tetradodecameric ClpP and its associated AAA$^+$ ATPase substrate-recognizing partner ClpA or ClpX (Olivares et al., 2015). Further mutant studies showed that *clpA*, but not *clpX*, is involved in the outcome of *A. tumefaciens* T6SS killing. Our data also suggest that the ClpAP complex formation mediates the outcome of T6SS killing. This work not only provides a new screening platform for elucidating factors that are involved in the interbacterial competition but also strengthens the importance of recipient genetic factors in the outcome of the T6SS antibacterial activity.

MATERIALS AND METHODS

Bacterial Strains, Plasmids, and Growth Conditions

The complete information about the strains and plasmids used in this study is described in **Table 1**. The *E. coli* Keio mutants (Baba et al., 2006) and the BW25113 wild type were obtained from the Keio collection from NBRP (NIG, Japan) and used as the recipient cells unless otherwise indicated. *A. tumefaciens* C58 wild type and the *tssL* mutants (Δ*tssL*) were used as the attacker cells. *A. tumefaciens* was grown at 25°C in 523 medium, and *E. coli* was grown in lysogeny broth (LB) medium at 37°C unless indicated. The plasmids were maintained in 20 μg/ml of kanamycin (Km),

TABLE 1 | Bacterial strains and plasmids.

Strain/plasmid	Relevant characteristics	Source/references
Agrobacterium tumefaciens		
C58 (EML530)	Wild-type virulence strain containing pTiC58 and pAtC58	Eugene Nester
C58:Δ*atu4333* (EML1073)	*atu4333* (*tssL*) in-frame deletion mutant of C58 background	(Ma et al., 2012)
Escherichia coli		
DH10B	Host for DNA cloning	Invitrogen
BW25113	Wild-type strain of the Keio Collection. *rrnB* DE*lacZ*4787 *HsdR*514 DE(*araBAD*)567 DE(*rhaBAD*)568 *rph*-1.	(Baba et al., 2006)
Keio collection	Systematic single-gene knockout mutants of *E. coli* BW25113	(Baba et al., 2006)
JW0427	BW25113 *clpP*:*kan*	(Baba et al., 2006)
JW0866	BW25113 *clpA*:*kan*	(Baba et al., 2006)
JW0428	BW25113 *clpX*:*kan*	(Baba et al., 2006)
EML5395	DH10B harboring pNptII	This study
EML5393	BW25113 wild-type harboring pNptII	This study
BL21(DE3)	Host for protein expression	(Studier and Moffatt, 1986)
Plasmids		
pTrc200HA	Sp^R, pTrc200 harboring C-terminal influenza hemagglutinin (HA) epitope, P*trc*, $lacI^q$, pVS1 origin	Laboratory collection
pRL662	Gm^R, a non-transferable broad-host range vector derived from pBBR1MCS2	(Vergunst et al., 2000)
pET22b(+)	Ap^R, *E. coli* overexpression vector harboring C-terminal 6xHis epitope	Novagen
pRL-*rpsL*	Gm^R, pRL662 expressing BW25113 *rpsL* gene	This study
pRL-*galk*	Gm^R, pRL662 expressing BW25113 *galK* gene	This study
pRL-*nupG*	Gm^R, pRL662 expressing BW25113 *nupG* gene	This study
pRL-$rpsL^{Str}$	Gm^R, pRL662 expressing DH10B $rpsL^{Str}$ gene	This study
pNptII	Km^R, Gm^R, pRL662 expressing *nptII* gene	This study
pClpP-HA	Sp^R, pTrc200HA expressing ClpP-HA fusion protein	This study
pClpA-HA	Sp^R, pTrc200HA expressing ClpA-HA fusion protein	This study
$pClpP_{S111A}$-HA	Sp^R, pTrc200HA expressing ClpP-HA fusion protein with S111A substitution	This study
$pClpP_{H136A}$-HA	Sp^R, pTrc200HA expressing ClpP-HA fusion protein with H136A substitution	This study
$pClpP_{D185A}$-HA	Sp^R, pTrc200HA expressing ClpP-HA fusion protein with D185A substitution	This study
$pClpP_{R26A}$-HA	Sp^R, pTrc200HA expressing ClpP-HA fusion protein with R26A substitution	This study
$pClpP_{D32A}$-HA	Sp^R, pTrc200HA expressing ClpP-HA fusion protein with D32A substitution	This study
pClpX-ΔN-ter	Plasmid used for purifying ClpX-ΔN	Robert T. Sauer
pGFP-ssrA	Plasmid used for purifying GFP-ssrA	Robert T. Sauer
pClpP-tev-His	Ap^R, pET22b(+) expressing ClpP-tev-His, in which ClpP protein is fused with a TEV protease cleavage site and a His-tag in its C-terminal	Robert T. Sauer
$pClpP_{S111A}$-tev-His	Ap^R, pET22b(+) expressing ClpP-tev-His with ClpP S111A substitution	This study
$pClpP_{H136A}$-tev-His	Ap^R, pET22b(+) expressing ClpP-tev-His with ClpP H136A substitution	This study
$pClpP_{D185A}$-tev-His	Ap^R, pET22b(+) expressing ClpP-tev-His with ClpP D185A substitution	This study

100 μg/ml of spectinomycin (Sp), and 20 μg/ml of gentamycin for *E. coli*.

Plasmid Construction

All plasmids (**Table 1**) were confirmed by sequencing unless otherwise indicated. The complete list of primers used in this study is in **Table 2**. Plasmid pNptII was created by ligating the *Xho*I/*Bam*HI-digested *nptII* PCR product into the same restriction sites of pRL662. The plasmid was transformed into DH10B, and the resulting strain was designated as EML5395. The pRL-*rpsL*, pRL-*galK*, pRL-*nupG*, and pRL-$rpsL^{Str}$ were created by ligating the *Xho*I/*Xba*I-digested PCR product into the same restriction sites of pRL662. The plasmid was transformed into DH10B, and the resulting strain was designated as EML5389, EML5390, EML5391, and EML5392. Plasmids pClpP-HA and pClpA-HA were created by ligating *Sac*I/*Pst*I-digested PCR products (*clpP* and *clpA* from BW25113 wild type without the stop codon, respectively) into pTrc200HA. The $pClpP_{S111A}$-HA was created by amplifying fragments using pTRC99C-F plus ClpP-S111A-rv and pTRC99C-R plus ClpP-S111A-fw as primers. The two fragments were then merged and amplified by PCR-Splicing by Overlapping Extension (SOEing) (Heckman and Pease, 2007). The resulting full-length *clpP*-containing fragment was digested by *Sac*I/*Pst*I and then ligated into pTrc200HA. All other pClpP-HA plasmids with a mutated form of ClpP were created similarly. The plasmid constructs ClpX (ClpX-ΔN-ter), wild-type ClpP-tev-His, and green fluorescent protein (GFP)-ssrA were a kind gift from Dr. Robert T. Sauer (MIT, Cambridge, United States). Site-directed mutagenesis was performed to generate the ClpP variants. All plasmids of pClpP-tev-His with a

TABLE 2 | Primer information.

Primer	Sequence (5′–3′)[a]	Plasmids
T7	TAATACGACTCACTATAGGG	pET22b(+)
T7T	GCTAGTTATTGCTCAGCGG	
pTRC99C-F	TTGCGCCGACATCATAAC	pTrc200HA
pTRC99C-R	CTGCGTTCTGATTTAATCTG	
rpsL-fw	AAAAACTCGAGGCAAAAGCTAAAACCAGGA	(1) pRL-*rpsL*
rpsL-rv	AAAAATCTAGACTTACTTAACGGAGAACCA	(2) pRL-rpsL^{Str}
galK-fw	AAAAACTCGAGCAGTCAGCGATATCCATT	pRL-galk
galK-rv	AAAAATCTAGAGCAAAGTTAACAGTCGGT	
nupG-fw	AAAAACTCGAGTCAAACACTCATCCGCAT	pRL-nupG
nupG-rv	AAAAATCTAGACCCGTTTTTCTTTGCGTAA	
NptII-fw-*Xho*I	AAAAACTCGAGAGACTGGGCGGTTTTATGGA	pNptII
NptII-rv-*Hin*dIII	AAAAAAAGCTTCTCTAGCGAACCCCAGAGTC	
ClpP-*Sac*I-fw	AAAAAGAGCTCATGTCATACAGCGGCGAACGAGATAAC	pClpP-HA
ClpP-*Pst*I-rv	AAAAACTGCAGATTACGATGGGTCAGAATCGAATCGAC	
ClpA-*Sac*I-fw	AAAAAGAGCTCATGCTCAATCAAGAACTGGAACTCAGTTT	pClpA-HA
ClpA-*Pst*I-rv	AAAAACTGCAGATGCGCTGCTTCCGCCTTGTGCTTT	
ClpP-S111A-fw	TGTATGGGCCAGGCGGCC**GCG**ATGGGCGCTTTCTTGCTG	(1) pClpP$_{S111A}$-HA
ClpP-S111A-rv	CAGCAAGAAAGCGCCCAT**CGC**GGCCGCCTGGCCCATACA	(2) pClpP$_{S111A}$-tev-His
ClpP-H136A-fw	AATTCGCGCGTGATGATT**GCC**CAACCGTTGGGCGGCTAC	(1) pClpP$_{H136A}$-HA
ClpP-H136A-rv	GTAGCCGCCCAACGGTTG**GGC**AATCATCACGCGCGAATT	(2) pClpP$_{H136A}$-tev-His
ClpP-D185A-fw	GAACGTGATACCGAGCGC**GCT**CGCTTCCTTTCCGCCCCT	(1) pClpP$_{D185A}$-HA
ClpP-D185A-rv	AGGGGCGGAAAGGAAGCG**AGC**GCGCTCGGTATCACGTTC	(2) pClpP$_{D185A}$-tev-His
ClpP-R26A-fw	GTCATTGAACAGACCTCA**GCC**GGTGAGCGCTCTTTTGAT	pClpP$_{R26A}$-HA
ClpP-R26A-rv	ATCAAAAGAGCGCTCACC**GGC**TGAGGTCTGTTCAATGAC	
ClpP-D32A-fw	CGCGGTGAGCGCTCTTTT**GCT**ATCTATTCTCGTCTACTT	pClpP$_{D32A}$-HA
ClpP-D32A-rv	AAGTAGACGAGAATAGAT**AGC**AAAAGAGCGCTCACCGCG	

[a]*Restriction enzyme sites are underlined, and mutated sequences are indicated in bold type.*

mutated *clpP* gene was constructed similar to that of pClpP$_{S111A}$-HA mentioned above with the differences below: Primer T7 was used instead of pTRC99C-F, and primer T7T was used instead of pTRC99C-R, and the restriction sites used were *Xba*I/*Xho*I.

Interbacterial Competition Assay

The optical densities of the cultured *A. tumefaciens* and *E. coli* were measured and adjusted to OD_{600} equals to 3.0 in 0.9% NaCl (w/v). The recipient *E. coli* cells were then further diluted to OD_{600} equals to 0.3 or 0.1, depending on the need of the assay. Afterward, the attacker and the recipient cultures were mixed in equal volume to make the attacker: recipient ratio 10:1 or 30:1, respectively. Ten microliters of the mixed bacterial culture was then spotted onto *Agrobacterium* Kill-triggering medium (AK medium, 3 g of K_2HPO_4, 1 g of NaH_2PO_4, 1 g of NH_4Cl, 0.15 g of KCl, and 9.76 g of MES, pH 5.5), solidified by 2% (w/v) agar, and then air-dried to enable contact-dependent competition. The competition plates were cultured at 25°C for 16 h. After the competition, bacteria were recovered using a loop and resuspended into 500 μl of 0.9% NaCl. The recovered bacterial suspension was then serially diluted and plated onto LB supplemented with spectinomycin to select recipient *E. coli* cells. After overnight culture at 37°C, the recovered colony formation unit (cfu) was counted and recorded. The T6SS-dependent susceptibility index (SI) was defined as the logarithm of the recovered *E. coli* cfu co-cultured with Δ*tssL* subtracted by that co-cultured with wild-type *A. tumefaciens*.

The High-Throughput Interbacterial Competition Platform

Pipetting steps of the screening platform were performed by the pipetting robot EzMate401 (Arise Biotech, Taiwan) unless otherwise specified. Fifty microliters of the cultured attacker *A. tumefaciens* was pelleted using 8,000 × *g* for 10 min at 15°C. After the medium was removed, the pellet was washed twice using 0.9% NaCl (w/v) and then adjusted to OD_{600} equals to 3.0. The OD_{600}-adjusted attacker cells were then dispensed as 300 μl into each well of a 2.2-ml Deepwell microplate (Basic Life, Taiwan). Each well was then added with 10 μl of the cultured recipient *E. coli* mutants and mixed well to make the attacker:target at 30:1 (v/v). After being mixed, the bacterial mixture was then added onto the competition plate. The competition plate was made by 25 ml of the AK medium with 2% (w/v) agarose solidified in a 96-well lid. The competition plate was then cultured at 25°C for 16 h before recovery. The recovery was performed by stamping a 96-well plate replicator to the competition spots followed by suspending the bacterial cells to a 96-well plate containing 200 μl of 0.9% NaCl in each well. After being mixed, 10 μl of the recovered bacterial suspension was spotted onto LB agar supplemented with kanamycin made in a 96-well lid,

cultured at 37°C overnight, and then was observed. In the first screening, only *A. tumefaciens* C58 wild type was used as the attacker. In the second screening, both wild type and Δ*tssL* were used as the attackers. For the groups co-cultured with *A. tumefaciens* C58 wild type, the recovery suspension was either undiluted or diluted to 5 and 25 times before being spotted onto LB agar with kanamycin plate. For the groups co-cultured with *A. tumefaciens* C58 Δ*tssL*, the recovery suspensions were either undiluted or diluted to 10 and 100 times before spotted onto LB agar with kanamycin plate. At each stage, the *E. coli* mutants that formed multiple colonies were identified as the candidates.

Protein Production and Purification

Escherichia coli BL21(DE3) was used as a host to produce all proteins of interests. Cells were cultured in LB medium supplemented with appropriate antibiotics in 1-L flask. When OD_{600} reached 0.6, the bacterial culture was cooled to 16°C, and IPTG was added (final concentration of 0.5 mM) for the overexpression of the protein. The cells were further allowed to grow for 16 h, followed by centrifugation to pellet them and then resuspended in lysis buffer (50 mM of Tris, pH 8.0, 300 mM of NaCl, 1% Triton X-100, 10 mM of beta-mercaptoethanol, 1 mM of DTT, and 10% glycerol). The cells were lysed by sonication at 4°C (amplitude 10 for 5 s, followed by 15-s breaks; total sonication time was 6 min) (PRO Scientific, United States). The lysates were centrifuged at 20,000 rpm for 30 min at 4°C. The supernatants were collected and loaded onto Ni-NTA column (GE Healthcare, United States) equilibrated with wash buffer (50 mM of Tris, pH 8.0, and 300 mM of NaCl) and eluted by 6 ml of wash buffer containing 250 mM of imidazole. The eluted fractions of the protein were further subjected to size-exclusion chromatography (SEC) by Superdex 200, 16/60 column (GE Life Sciences, United States) in buffer containing 50 mM of Tris, pH 7.5, 100 mM of KCl, 25 mM of $MgCl_2$, 1 mM of DTT, and 10% glycerol. The protein purity was confirmed on 12% sodium dodecyl sulfate–polyacrylamide gel electrophoresis (SDS-PAGE). The samples were flash-frozen and stored in −80°C until further use.

Protein Degradation Assay

Green fluorescent protein (GFP) fluorescence based-degradation assays were carried out in Protein Degradation (PD) buffer (25 mM of HEPES, pH 7.5, 100 mM of KCl, 25 mM of $MgCl_2$, 1 mM of DTT, and 10% glycerol) containing 3 μM of GFP-ssrA as substrate and ATP regeneration system (16 mM of creatine phosphatase and 0.32 mg/ml of creatine kinase) as described previously (Sriramoju et al., 2018). In brief, 0.1 μM of $ClpX_6$ and 0.3 μM of $ClpP_{14}$ or its variants were mixed at 30°C and allowed to stand for 2 min. The protein degradation reaction was started by addition of ATP to a final concentration of 5 mM. The changes in the fluorescence were measured at 511 nm with an excitation wavelength at 467 nm in a 96-well format using Infinite M1000 PRO plate reader (Tecan, Switzerland).

Sodium Dodecyl Sulfate–Polyacrylamide Gel Electrophoresis and Western Blot Analysis

The Δ*clpP*:kan *E. coli* strains harboring appropriate plasmid were grown as the same procedure indicated in the *Interbacterial Competition Assay*. Cells were adjusted to OD_{600} of 5.0, collected at 5,000 × *g* for 5 min, and directly resuspended in 1 × SDS sample buffer. The samples were incubated at 96°C for 10 min and then analyzed by SDS-PAGE. Protein samples separated by SDS-PAGE were transferred to an Immobilon-P membrane (Merck Millipore, United States). The monoclonal anti-HA was used at a dilution of 1:10,000 (Yao-Hong Biotech Inc., Taiwan), and the goat–anti-rabbit conjugated to horseradish peroxidase secondary antibody was used at a dilution of 1:10,000 (GeneTex, Taiwan). The Western Lightning ECL Pro (PerkinElmer Life Sciences, United States) was used for color development and visualized by BioSpectrum 600 Imaging System (UVP, United States).

Statistical Analysis and Figure Production

Statistical analyses and figure production were performed using the R program (version 3.5.1) (R Core Team, 2018) and RStudio (version 1.1.456) (RStudio Team, 2015). R packages plyr (version 1.8.4) (Wickham, 2011) and multcompView (version 0.1-7) (Graves et al., 2015) were used for statistical analyses. Figures were produced using the R packages ggplot2 (version 3.0.0) (Wickham, 2016), Hmisc (version 4.1-1) (Harrell et al., 2018), and ggpubr (version 0.2) (Kassambara, 2018). Student's *t*-test, one-way analysis of variance (one-way ANOVA), and Tukey's honestly significant difference test (Tukey HSD test), in which significant difference threshold set as 0.05, were used in all cases.

RESULTS

The *Agrobacterium tumefaciens* T6SS Killing Outcome Differs Between Different *Escherichia coli* Strains

Using an optimized competition condition (AK medium agar that contains basic minerals at pH 5.5), we noticed that when co-cultured with wild-type *A. tumefaciens* C58, the recovered colony-forming unit (cfu) of *E. coli* BW25113 was always lower than that of DH10B (**Figure 1A**). Meanwhile, the recovered cfu of both *E. coli* strains was the same when co-cultured with Δ*tssL A. tumefaciens* C58 (hereafter referred to Δ*tssL*), a T6SS secretion-deficient mutant (**Figure 1A**). For more intuitive readout, we introduced T6SS-dependent SI, which reflects the strength of the T6SS killing. The SI was defined as the logarithm of the recovered *E. coli* cfu co-cultured with Δ*tssL* subtracted by that co-cultured with wild type. The mean SI between *A. tumefaciens* and BW25113 was significantly higher than that of between *A. tumefaciens* and DH10B with a *P*-value of 0.02 ($T \leq t$, two-tailed, **Figure 1B**). This result suggests that some genetic factors of BW25113 may enhance the *A. tumefaciens* C58 killing outcome in a T6SS-dependent manner.

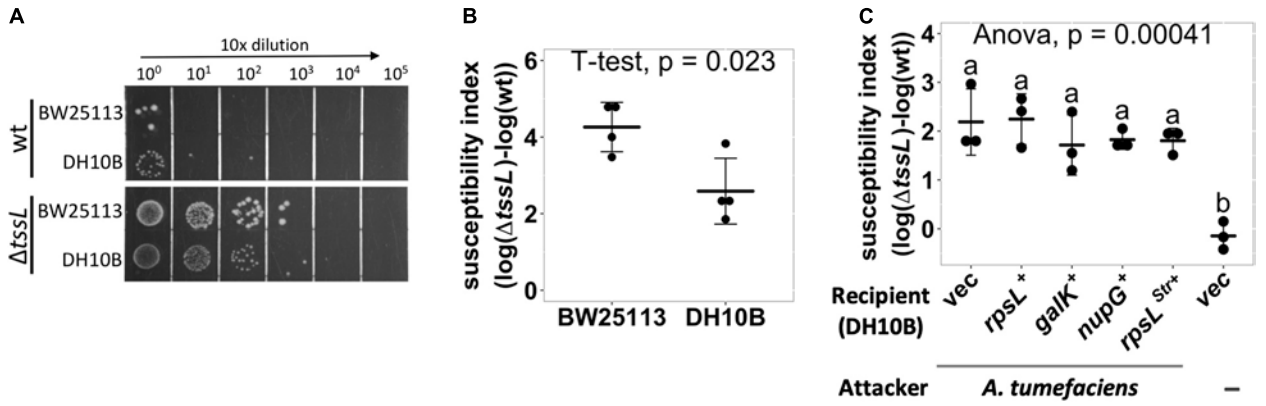

FIGURE 1 | *Agrobacterium tumefaciens* type VI secretion system (T6SS)-dependent antibacterial activity against *Escherichia coli* strains. **(A,B)** *A. tumefaciens* T6SS antibacterial activity against *E. coli* strains DH10B and BW25113. *A. tumefaciens* was co-cultured at a ratio of 30:1 with *E. coli* DH10B or BW25113, both *E. coli* strains harboring vector pRL662, on *Agrobacterium* Kill (AK) agar medium for 16 h. The bacterial mixtures were serially diluted and spotted **(A)** or quantified by counting cfu **(B)** on gentamicin-containing lysogeny broth (LB) agar plates to selectively recover *E. coli*. **(C)** *E. coli* DH10B was complemented by either vector only (vec) or derivative expressing *rpsL*, *galK*, *nupG*, or *rpsL*^{Str} *in trans* before being subjected to *A. tumefaciens* T6SS-dependent antibacterial activity assay as described in **(B)**. Susceptibility index (SI) was defined as the subtraction difference of the recovery log(cfu) of that attacked by Δ*tssL* to that attacked by wild-type *A. tumefaciens* C58. Data are mean ± SD of three independent experiments calculated by *t*-test with $P < 0.05$ for statistical significance **(B)** or single-factor analysis of variance (ANOVA) and Tukey honestly significant difference (HSD), in which two groups with significant differences are indicated with different letters (a and b) **(C)**.

We tested whether the genes that are functional in BW25113 but not in DH10B could be the cause of the higher SI in BW25113. The *galK* and *nupG* genes are functional in BW25113 but are pseudogenes in DH10B. The *rpsL* has a mutation in DH10B (*rpsL*^{Str}), which renders the strain resistant to streptomycin, but not in BW25113. The *rpsL*, *galK*, or *nupG* gene from BW25113 was cloned into pRL662 and expressed by constitutive *lacZ* promoter in DH10B as a recipient for a T6SS interbacterial competition assay (**Figure 1C**). The DH10B expressing the *rpsL*^{Str} (overexpressing *rpsL*^{Str}) was also included. The DH10B harboring empty vector (vec) served as a negative control. A group without attacker was also included to monitor whether the decrease in cfu after the competition solely comes from co-culture with *A. tumefaciens* attacker. The SIs were not significantly different between DH10B and any of the complemented groups, and each had an SI mean of about 2 (**Figure 1C**). The above approach was not able to identify the genetic factors that contributed to the enhanced resistance in DH10B, which may imply that precise control of transgene expression or multiple complementation would be required. Therefore, we developed a high-throughput screening method to identify the individual genes that contribute to the enhanced susceptibility of BW25113.

Establishment of a High-Throughput Interbacterial Competition Platform to Identify Recipient *Escherichia coli* Mutants With Less Susceptibility to *Agrobacterium tumefaciens* C58 T6SS Killing

We decided to screen the BW25113 single-gene mutant library (Keio collection from NBRP [NIG, Japan]: *E. coli*) for strains with less susceptibility to *A. tumefaciens* T6SS-mediated killing. An interbacterial competition assay starts from mixing the attacker and the recipient cells, followed by counting the recovered recipient *E. coli* on selective media (**Figure 2A**). This protocol only allowed screening of 10 mutants per day, which was not efficient enough for screening 3,909 strains of the Keio library.

Therefore, we developed a high-throughput interbacterial competition platform that enables 96 population-level, interbacterial competition simultaneously (**Figure 2B**). The recipient Keio *E. coli* strains were cultured in the 96-well, and the attacker *A. tumefaciens* was cultured in a flask. After the culture, the attacker was adjusted to OD_{600} equals to 3.0 and then dispensed to a 2.2-ml deep-well plate. The recipient cells were added into the attacker-containing plates in a volume ratio of 30 to 1. Ten microliters of the attacker-recipient mixtures were dropped on the competition surface made by agar solidified on a 96-well lid. A microplate replicator was used to stamp on the competition spots to recover the bacterial cells of each competition group. The recovered bacteria were suspended in the saline buffer (0.9% NaCl), mixed, and then spotted on the recipient-selection surface made by agar solidified on a microplate lid. The competition condition was set at the strength that enables *A. tumefaciens* to kill almost all BW25113 wild-type recipients so that only a few or no cells would survive. This setup made recognizing the resistant mutants simple – the ones with the multiple colonies are the candidates (**Figure 2B**).

All the 3,909 strains in the Keio were screened using *A. tumefaciens* C58 wild type as the attacker. In each screening, at least two wild type *E. coli* BW25113 replicates were incorporated and screened in parallel as parental controls. The Keio mutants that formed colonies in this stage were selected, and 196 strains showed enhanced resistant to *A. tumefaciens* C58 attack. The 196 strains were subjected to second screening using both wild

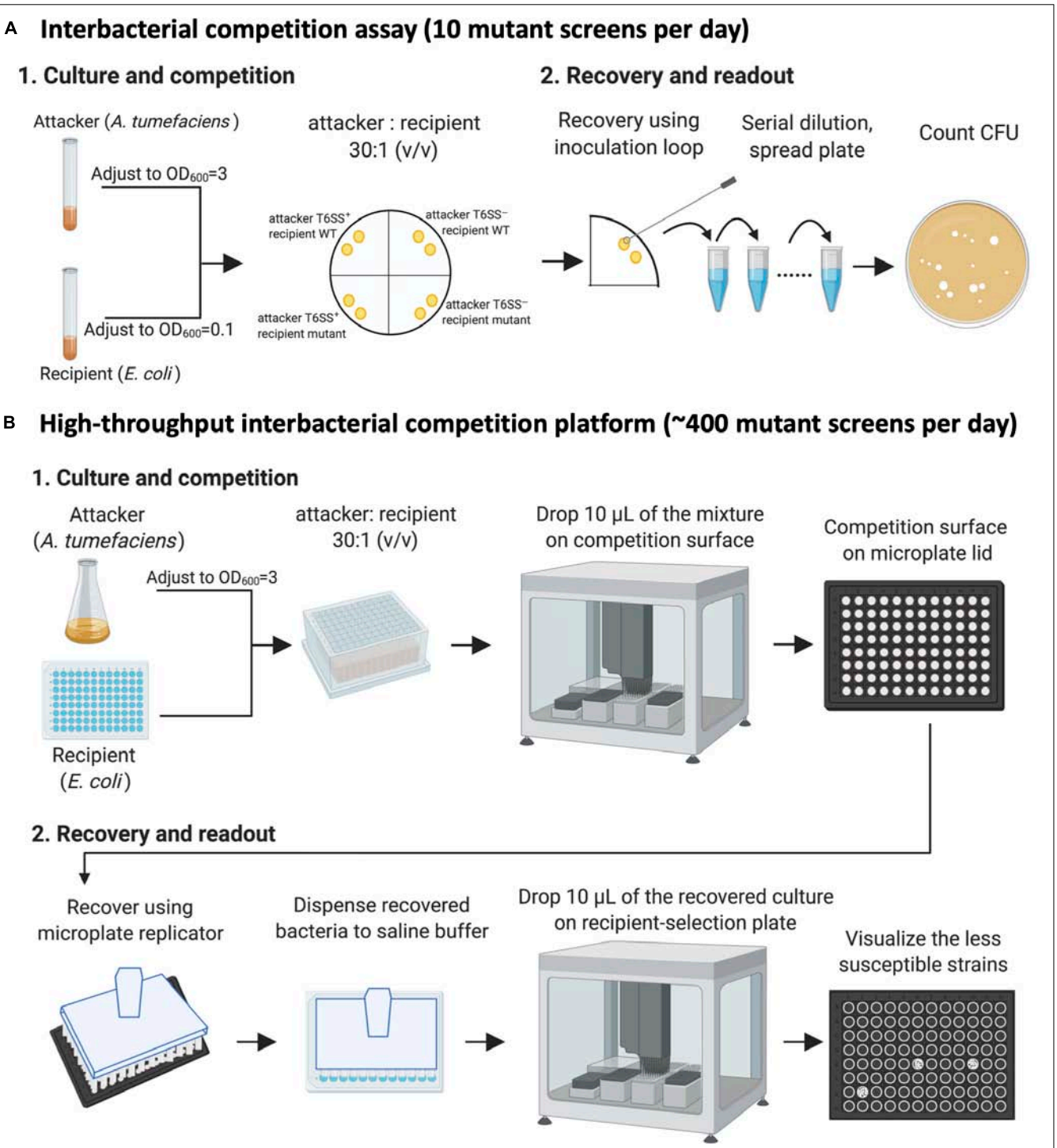

FIGURE 2 | The high-throughput interbacterial competition platform. **(A)** Interbacterial competition assay. Cultured attacker *Agrobacterium tumefaciens* and recipient *Escherichia coli* were mixed and then spotted on the *Agrobacterium* Kill (AK) agar medium to allow interbacterial competition for 16 h at 25°C followed by recovery of mixed cultures, serially diluted, and then spread onto lysogeny broth (LB) plate supplemented with appropriate antibiotics to select for recipient cells. **(B)** High-throughput interbacterial competition screening platform. Recipient cells were grown and mixed with attacker *A. tumefaciens* in a 96-well plate. The bacterial mixture was dropped onto the AK agar medium competition surface using an automated pipetting system. The competition surface was made on a microplate lid. Recovery was performed using microplate replicator. The candidates are the strains that show multiple colonies grown after recovery as opposed to wild-type controls and most strains with no or few colonies. This high-throughput *A. tumefaciens* type VI secretion system (T6SS) killing platform enables ~400 mutant screens per day. This figure was created with BioRender (https://biorender.com/).

type and Δ*tssL* as the attackers. At this stage, we incorporated a grading system: Grade I mutants were at least 25 times less susceptible to C58 T6SS-dependent killing, whereas grade II mutants were at least 10 times less susceptible. Six grade I mutants and 10 grade II mutants were identified.

Confirmation of the *Escherichia coli* Mutants With Less Susceptibility to *Agrobacterium tumefaciens* C58 Type VI Secretion System Killing

The enhanced resistance of the six grade I mutants were further verified by an interbacterial competition assay and by complementation tests. For complementation, wild-type genes from BW25113 were cloned into plasmid pTrc200HA plasmid and expressed by *trc* promoter. Five out of six showed lower susceptibility to *A. tumefaciens* T6SS attack than that of BW25113 wild type (**Table 3** and **Supplementary Figure S1**). These are *clpP*, *gltA*, *ydhS*, *ydaE*, and *cbpA* mutants. The *yeaX* mutant, on the other hand, did not differ when compared with the wild type. The *cbpA* mutant showed a milder phenotype and could not be complemented *in trans* under the condition tested (**Table 3** and **Supplementary Figure S1**). As *cbpA* is the first gene in its operon, the failure in complementation could be due to the requirement of other gene(s) in the operon. Nevertheless, the verification performed above showed that the high-throughput interbacterial competition platform was reliable in identifying the recipient genetic factors that participate in T6SS killing.

The ClpP Protein Plays a Role in Enhancing Susceptibility to *Agrobacterium tumefaciens* Type VI Secretion System Killing

Because known recipient cell factors affecting antibacterial activity are often conserved components, we selected Δ*clpP*:kan (labeled as Δ*clpP*) for further studies. ClpP is a highly conserved, housekeeping AAA^+ serine protease that exists in prokaryotes, plastids, and mitochondria (Alexopoulos et al., 2012; Bhandari et al., 2018; Mahmoud and Chien, 2018). We performed a quantitative interbacterial competition assay using *A. tumefaciens* as the attacker and the BW25113 wild type, Δ*clpP*, or complemented strain $clpP^+$ as the recipient cells (**Figure 3A**). The initial cfu of the *E. coli* at 0 h was about 10^6 in all groups (one-way ANOVA with $P = 0.88$), indicating that any *E. coli* cfu difference at 16 h was not due to initial bacteria titer difference. The cfu among different recipient *E. coli* strains was not significantly different at 16 h when using *A. tumefaciens* Δ*tssL* (one-way ANOVA with $P = 0.67$), indicating that co-culture with T6SS-deficient strain will not cause recipient titer to differ. On the other hand, the recovered cfu of Δ*clpP* was about 10^4, whereas it was about 5×10^2 in BW25113 wild type and in $clpP^+$ after 16-h competition using wild-type *A. tumefaciens* (**Figure 3A**). The mean SI of the BW25113 wild type to *A. tumefaciens* C58 is significantly higher than that of Δ*clpP* (one-way ANOVA with $P = 0.02$, **Figure 3B**). The less susceptible phenotype of the Δ*clpP* can be fully complemented *in trans* ($clpP^+$) ($P = 0.96$ compared with BW25113 wild type). These results confirmed that *clpP* contributes to enhancing susceptibility to T6SS antibacterial activity of *A. tumefaciens* C58.

Effects of ClpP Catalytic Variants in Enhancing *Agrobacterium tumefaciens* Type VI Secretion System Antibacterial Activity and Protease Activity

A functional ClpP complex consists of a tetradodecameric ClpP ($ClpP_{14}$) and its associated AAA^+ ATPase substrate-recognizing partner ClpA or ClpX, both in a hexameric form (Olivares et al., 2015). The protease catalytic triad of the *E. coli* ClpP is composed of S111, H136, and D185 (counted from the Met1) (Maurizi et al., 1990; Wang et al., 1997). We tested whether the ClpP protease is essential in enhancing *E. coli* susceptibility to *A. tumefaciens* C58 T6SS attack. *E. coli*Δ*clpP* complemented with pTrc200HA expressing either wild-type or catalytic variants ClpP S111A, H136A, and D185A was used as a recipient strain. All ClpP variants contain a C-terminal HA tag. Two of the catalytic variants, $S111A^+$ and $H136A^+$, failed to complement, whereas surprisingly, the third catalytic variant, $D185A^+$, can fully complement the phenotype (**Figure 4A**). The difference of ClpP catalytic variants to complement Δ*clpP* was not due to their protein-expression level as determined by Western blot (**Figure 4B**). The protein migration of the $ClpP_{S111A}$ and $ClpP_{H136A}$ was slower than that of the $ClpP_{wt}$ and $ClpP_{D185A}$

TABLE 3 | *Escherichia coli* strains that showed reduced susceptibility to *Agrobacterium tumefaciens* T6SS attack.

No.	Resource (JW ID)	Disrupted gene	Gene products affected by kanamycin cassette insertion[a]	Reduced susceptibility[b]	Trans complementation[c]
1	JS0427	*clpP*	ClpAXP, ClpXP, ClpAP	O	O
2	JW0710	*gltA*	citrate synthase	O	O
3	JW1658	*ydhS*	FAD/NAD(P) binding domain-containing protein YdhS	O	O
4	JW1346	*ydaE*	Rac prophage; zinc-binding protein	O	Δ
5	JW0985	*cbpA*	Curved DNA-binding protein	O	X
6	JW1792	*yeaX*	Carnitine monooxygenase	X	n.d.

n.d., not determined. [a]Gene products information was obtained from the EcoCyc database (Keseler et al., 2016). [b]Mutant strains with reduced susceptibility index (SI) and showed significant difference under $P < 0.05$ was labeled as O; those with no significant difference to that of wild type were labeled in X. [c]Plasmid-born gene that can fully complement the disrupted gene is labeled in O, partially complemented is labeled in Δ, and cannot be complemented is labeled in X.

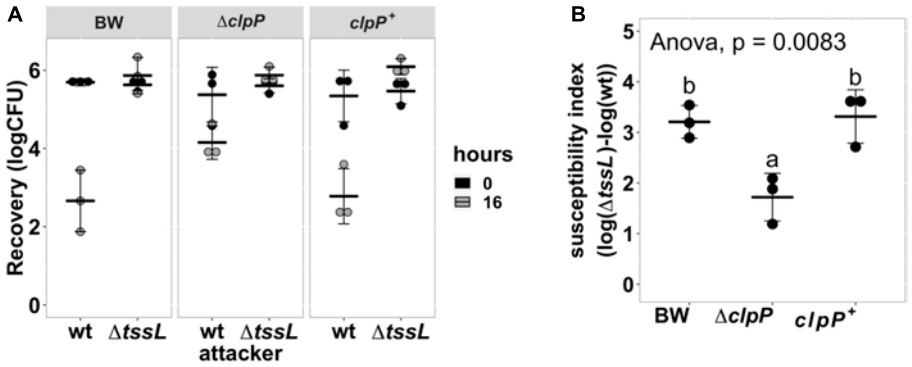

FIGURE 3 | *Agrobacterium tumefaciens* susceptibility to type VI secretion system (T6SS)-dependent antibacterial activity was reduced in *Escherichia coli clpP:kan* and can be fully complemented *in trans*. **(A)** Recovery of surviving *E. coli* cells at 0 h and 16 h after being co-cultured with either *A. tumefaciens* wild type C58 (wt) or Δ*tssL* at a ratio of 30:1. **(B)** The susceptibility index (SI) of *E. coli* BW25113 wild type (BW), Δ*clpP*, and Δ*clpP* complemented with *clpP* expressed on plasmid (*clpP*$^{+}$) was calculated from the recovery rate shown in **(A)**. Statistical analysis involved single-factor analysis of variance (ANOVA) and Tukey honestly significant difference (HSD). Data are mean ± SD of three independent experiments, and two groups with significant differences are indicated with different letters (a and b) ($P < 0.05$ for statistical significance).

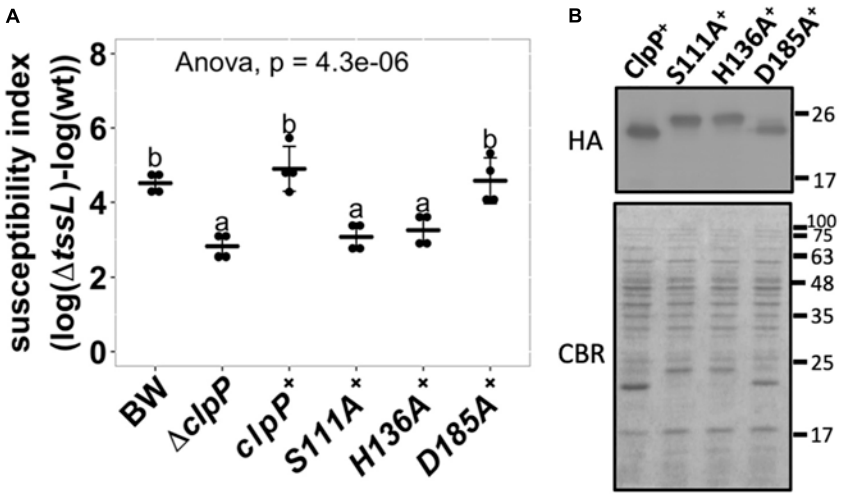

FIGURE 4 | Effects of ClpP protease catalytic variants in enhancing *Agrobacterium tumefaciens* type VI secretion system (T6SS) antibacterial activity. **(A)** The susceptibility index calculated from *A. tumefaciens* interbacterial activity assay against *Escherichia coli*. The *A. tumefaciens* C58 wild-type or Δ*tssL* were co-cultured at a ratio of 10:1 with *E. coli* BW25113 wild type (BW), Δ*clpP*, and Δ*clpP* complemented with *clpP* and its variants expressed on plasmid. The complemented *clpP* strains were either wild type (clpP^{+}) or catalytic variants $ClpP_{S111A}$ (S111A^{+}), $ClpP_{H136A}$ (H136A^{+}), and $ClpP_{D185A}$ (D185A^{+}), with C-terminus HA-tag. The susceptibility index (SI) of each *E. coli* was calculated from the logarithm recovery rate of the Δ*tssL* co-cultured group minus that of the wild-type co-cultured group. Data are mean ± SD of four biological replicates from two independent experiments. Statistical analysis involved single-factor analysis of variance (ANOVA) and Tukey honestly significant difference (HSD) with $P < 0.05$ for statistical significance. Two groups with significant differences are indicated with different letters (a and b). **(B)** The ClpP protein levels of the Δ*clpP* complemented strains used in **(A)**. The ClpP-expressing *E. coli* strains were cultured at the same condition used in interbacterial competition assay. Instead of co-culture with *A. tumefaciens*, protein samples were collected, normalized, and subjected to Western blot analysis of ClpP:HA and its variants. Representative result of three independent experiments is shown.

owing to their inability to remove the N-terminal propeptide (1–14 amino acids) as in $ClpP_{wt}$ and $ClpP_{D185A}$ (Maurizi et al., 1990; Bewley et al., 2006).

As $ClpP_{D185A}$ was able to complement the phenotype, we further investigated the ClpP protease activity of the above ClpP variants by a widely adopted ClpP protein degradation assay using GFP-ssrA as the model substrate. Loss of GFP fluorescence is used as a reporter to monitor substrate degradation by ClpXP as a function of time (Weber-Ban et al., 1999; Sriramoju et al., 2018). The results showed that over time, wild-type ClpP effectively degraded GFP-ssrA with a half-life of about 30 min (**Figure 5A**). Meanwhile, less than a 10% decrease of the GFP-ssrA signal was observed in GFP-ssrA only and wild type without ATP groups, both served as negative controls. The decreasing rates of the GFP-ssrA fluorescence of $ClpP_{S111A}$, $ClpP_{H136A}$, and $ClpP_{D185A}$ were significantly slower than those of $ClpP_{WT}$ and showed no significant difference among the three variants at the end of the test (**Figures 5A,B**). Although $ClpP_{D185A}$ showed no

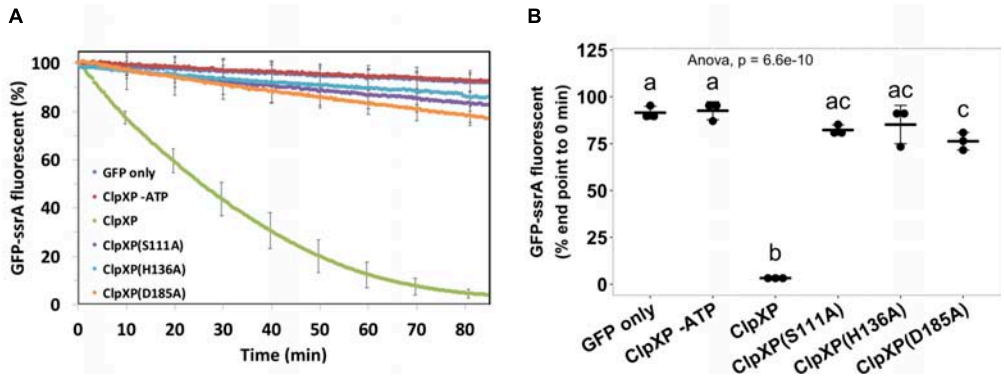

FIGURE 5 | Protease activity assay of the ClpP and its catalytic variants. The wild-type ClpP and its catalytic variants were each pre-assembled with ClpX followed by providing its substrate, the ssrA-tagged green fluorescent protein (GFP). The GFP fluorescent signals were monitored **(A)** over time, and **(B)** statistical analysis was measured at the end of the assay. Statistical analysis involved single-factor analysis of variance (ANOVA) and Tukey honestly significant difference (HSD) with $P < 0.05$ for statistical significance. Two groups with significant differences are indicated with different letters (a and b). Data are mean ± SD of three biological replicates from one representative result of at least two independent experiments.

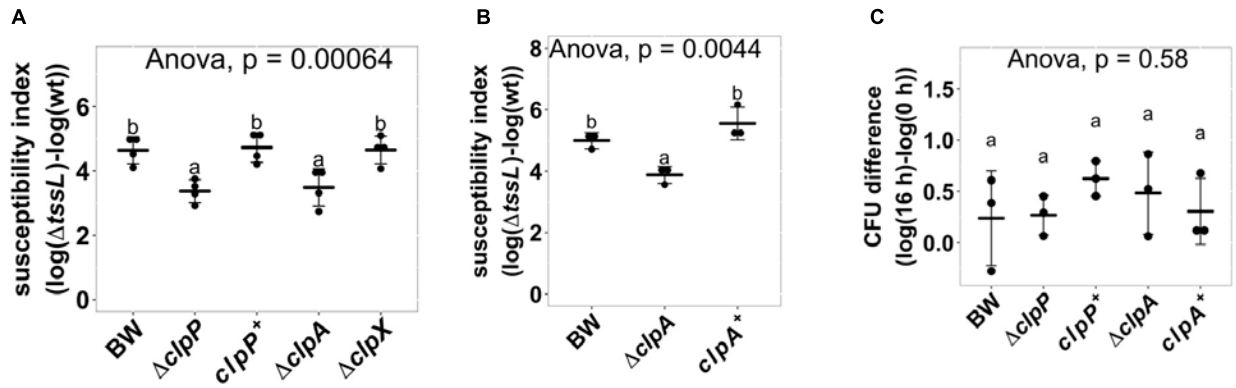

FIGURE 6 | ClpP associated AAA$^+$ ATPase ClpA but not ClpX is involved in enhancing *Agrobacterium tumefaciens* type VI secretion system (T6SS) antibacterial activity. **(A)** *A. tumefaciens* T6SS antibacterial activity against *Escherichia coli* Δ*clpP* and its complement strain, Δ*clpA* and Δ*clpX*. The *A. tumefaciens* and the *E. coli* were co-cultured at a ratio of 10:1 on *Agrobacterium* Kill (AK) agar medium for 16 h. Afterward, the recovery of *E. coli* strains was quantified, and the susceptibility index was calculated by subtracting the difference of the recovered log(cfu) of that attacked by Δ*tssL* to that by wild-type *A. tumefaciens* C58. **(B)** *A. tumefaciens* T6SS antibacterial activity assay and the susceptibility index were performed as described in **(A)** using *E. coli* wild type (BW), Δ*clpA*, and Δ*clpA* complemented with *clpA* expressed on plasmid (*clpA*$^+$). **(C)** Growth of *E. coli* when co-culturing with the Δ*tssL A. tumefaciens*. Data in **(A–C)** are mean ± SD of at least three independent experiments. Statistical analysis involved single-factor analysis of variance (ANOVA) and Tukey honestly significant difference (HSD) with $P < 0.05$ for statistical significance. Two groups with significant differences are indicated with different letters (a and b).

statistically difference in GFP-ssrA degradation compared with $ClpP_{S111A}$ and $ClpP_{H136A}$ at the final time point, it showed significantly lower GFP-ssrA signal to that of the negative control groups (**Figure 5B**).

The ClpP-Associated AAA$^+$ ATPase ClpA but Not ClpX Is Involved in Enhancing Susceptibility to *Agrobacterium tumefaciens* Type VI Secretion System Activity

ClpP is a protein protease dependent on other adapter proteins such as ClpA and ClpX for substrate recognition (Maurizi, 1991; Gottesman et al., 1998). Therefore, we next determined whether the resistant phenotype of Δ*clpP* is mediated by ClpA or ClpX through the interbacterial competition assay of the deletion mutants Δ*clpA*:kan (hereafter referred to as Δ*clpA*) and Δ*clpX*:kan (hereafter referred to as Δ*clpX*) as recipients. SI demonstrates that Δ*clpA* was less susceptible to *A. tumefaciens* T6SS killing than BW25113 wild-type ($P = 0.02$), whereas Δ*clpX* was similar to BW25113 wild type ($P = 1.00$) (**Figure 6A**). The decreased *A. tumefaciens* T6SS killing phenotype of Δ*clpA* was fully complemented *in trans* (**Figure 6B**). No difference could be detected among the growth of the BW25113 wild-type, Δ*clpA*, Δ*clpP*, and their respective complemented strains when co-cultured with Δ*tssL* ($P = 0.58$) (**Figure 6C**). Therefore, the killing outcome is caused by *Agrobacterium* T6SS-mediated interbacterial competition rather than the growth rate of the different recipient strains under the competition condition. This suggested that ClpA could be the adapter that interacts with

ClpP leading to the enhanced susceptibility to T6SS attack in BW25113 wild type. In this case, the interaction between ClpA and ClpP should be required for enhancing *A. tumefaciens* T6SS killing. The interaction between ClpA and ClpP is well studied, and it has been demonstrated that the R26A and D32A variants of ClpP lose their ability to bind to ClpA by 50 and 100%, respectively (Bewley et al., 2006). Therefore, we complemented $ClpP_{R26A}$ and $ClpP_{D32A}$ in Δ*clpP* to determine whether the two variants could restore the susceptibility. The $R26A^{+}$ was able to complement (P = 0.96, compared to $ClpP^{+}$), whereas $D32A^{+}$ failed to complement and showed no statistical difference in SI than that of Δ*clpP* ($P < 10^{-4}$) (**Figure 7**). These results suggest that the phenotype observed in Δ*clpP* and in Δ*clpA* could be associated with ClpA–ClpP interaction. Because the retained N-terminal propeptide does not prevent ClpP–ClpA binding (Maurizi et al., 1990), the inability of unprocessed $ClpP_{S111A}$ and $ClpP_{H136A}$ in enhanced susceptibility is independent of ClpP–ClpA complex formation.

DISCUSSION

This study provides evidence that the genetic factors of the recipient cells play an important role in affecting the outcome of the T6SS antibacterial activity. The high throughput interbacterial competition platform developed in this study proved to be an effective method in identifying recipient factors that affect the outcome of *A. tumefaciens* T6SS antibacterial activity. Further exploration led to the confirmation of at least six genes (*clpP*, *clpA*, *gltA*, *ydhS*, *ydaE*, and *cbpA*) encoding known or putative cytoplasmic proteins (Keseler et al., 2016), whereas CbpA resides both in the cytoplasm and in the nucleoid (Orfanoudaki and Economou, 2014). None of these gene products were localized to the inner membrane, periplasm, outer membrane, or extracellular milieu. This result implies that the process affecting the outcome of *A. tumefaciens* T6SS killing to *E. coli* occurs in the cytoplasm, presumably after the injection of the T6SS puncturing apparatus. Previous studies have mainly focused on how attacker T6SS is regulated and sensed (Filloux and Sagfors, 2015; Alteri and Mobley, 2016; Hood et al., 2017). This study provides a new insight that recipient cell genes can also affect the T6SS killing outcome and that it could take place after the injection of the T6SS apparatus into the recipient cytoplasm.

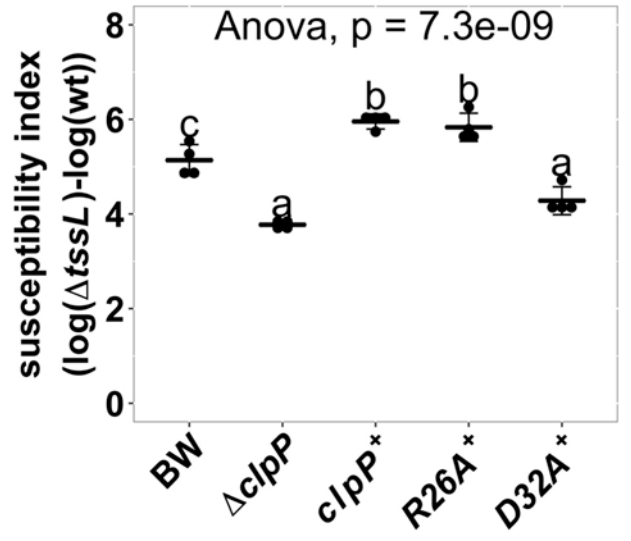

FIGURE 7 | Effects of ClpP variants impaired with ClpA-binding ability in enhancing *Agrobacterium tumefaciens* type VI secretion system (T6SS) antibacterial activity. Interbacterial competition assay between *A. tumefaciens* and *Escherichia coli* wild type, Δ*clpP*, and Δ*clpP* complement strains expressing wild-type ClpP (*clpP*$^{+}$), ClpAP complex formation mutants $ClpP_{R26A}$ ($R26A^{+}$), and $ClpP_{D32A}$ ($D32A^{+}$). The ClpAP complex forming ability is half than that of wild-type ClpP in $ClpP_{R26A}$ and is completely lost in $ClpP_{D32A}$ (Bewley et al., 2006). The T6SS killing data are mean ± SD of four biological replicates from two independent experiments. Statistical analysis involved single-factor analysis of variance (ANOVA) and Tukey honestly significant difference (HSD) with $P < 0.05$ for statistical significance. Two groups with significant differences are indicated with different letters (a and b).

Our data showed that ClpA but not ClpX, together with ClpP, contributes to the susceptibility of the recipient *E. coli* to *A. tumefaciens* T6SS killing. The *clpX* transcript level drops and fades 15 min after the onset of carbon starvation (Li et al., 2000), which is the condition used for our interbacterial competition. Thus, ClpX is probably not available to form the ClpXP complex during *Agrobacterium* T6SS attacks. The Δ*clpA* was indeed identified in the first screening but was accidentally misplaced and did not enter the second screening process. Therefore, Δ*clpA* did not appear in our final candidate list until we obtained the correct strain for confirmation. The results that the three catalytic variants $ClpP_{S111A}$, $ClpP_{H136A}$, and $ClpP_{D185A}$ did not significantly differ in their ability to degrade GFP-ssrA substrate suggested that the protease activity may not be the leading cause in enhancing *A. tumefaciens* T6SS attack. On the other hand, unlike $ClpP_{S111A}$ and $ClpP_{H136A}$, which do not exhibit significant protease activity as compared with that of the negative controls, $ClpP_{D185A}$ may possess weak protease activity, as the GFP-ssrA fluorescence level is significantly lower than that of the negative controls at the final time point. Thus, the involvement of the ClpP protease activity cannot be completely ruled out as the weak protease activity of $ClpP_{D185A}$ may be sufficient to exhibit its function in enhancing *A. tumefaciens* T6SS attack. Of note, the ClpP protease activity monitored by the *in vitro* protease activity assay using either ClpX or ClpA as a protein unfoldase showed a highly similar pattern among 24 ClpP variants (Bewley et al., 2006). As this GFP-ssrA degradation assay is an *in vitro* system and that it is difficult to monitor the ClpP protease activity of the recipient under competition condition, the role of ClpP protease remains elusive.

Our data also suggest that ClpAP complex is required in enhancing recipient susceptibility during *A. tumefaciens* T6SS killing on the basis of the results that ClpP variant that loses its ability to form a complex with ClpA did not complement the phenotype whereas those with ClpA binding ability do. This implies that the ClpA–ClpP complex, rather than ClpP alone, is the cause of the enhanced susceptibility

to T6SS attack. As ClpP allosterically activates the polypeptide translocation activity of ClpA (Miller et al., 2013), the necessity of the ClpAP complex may depend on the unfoldase activity of ClpA. The detailed mechanism on how recipient ClpAP is involved in T6SS susceptibility enhancement awaits further investigations. One promising future direction would be identifying the potential ClpA substrates and their effects on increasing susceptibility of T6SS attack.

Hijacking a highly conserved and essential molecule of the recipient cell to improve attacker fitness is not uncommon. The examples are CdiA-CT^{EC93} hijacking essential proteins BamA and AcrB, CdiA-CT^{EC536} hijacking the recipient CysK, and Ssp2 and Ssp4 hijacking recipient DsbA (Aoki et al., 2008; Diner et al., 2012; Mariano et al., 2018). The ClpP protease, on the other hand, is highly conserved in both prokaryotes and eukaryotic organelles like plastid and mitochondria (Culp and Wright, 2016; Moreno et al., 2017). The ClpP protease cooperates with different AAA$^+$ ATPases in different organisms. It works with ClpA and ClpX in Gram-negative bacteria; with ClpC and ClpE in Gram-positive bacteria; with ClpC1, ClpC2, and ClpD in the chloroplast; and with ClpX in human mitochondria. In all these cases, the ClpP protease seems to play a central role in protein homeostasis. Dysfunction of the system can lead to severe developmental defects, a reduction in the pathogenicity, or lethality (Cole et al., 2015; Nishimura and Van Wijk, 2015; Bhandari et al., 2018). The current result suggests that the ClpP protease system could be another target hijacked by the T6SS attacker to improve its competitive advantage.

To our knowledge, the involvement of the ClpAP complex in enhancing the recipient's susceptibility to *A. tumefaciens* T6SS activity has not been described in the contact-dependent competitor elimination systems in Gram-negative bacteria like T1SS, T4SS, CDI, and T6SS. It would be of interest to uncover how and what *A. tumefaciens* factors hijack this universal and highly conserved ClpP and its associated AAA$^+$ ATPase substrate recognizing partner. The current finding provides additional evidence to support that T6SS can manipulate the essential and highly conserved molecules of recipient cells to achieve better inhibition of the performance (Russell et al., 2014). Elucidating the underlying molecular mechanisms of ClpAP and other recipient factors would be the next direction to understand further how genetic factors can affect the recipient susceptibility to the T6SS attacks.

DATA AVAILABILITY STATEMENT

All datasets generated for this study are included in the article/**Supplementary Material**.

AUTHOR CONTRIBUTIONS

H-HL, MY, and E-ML conceived and designed the experiments. H-HL performed most of the experiments. MS contributed to the protease activity assay. MS and S-TH provided the materials and tools for the protease activity assay. S-TH, C-TL, and E-ML supervised the execution of the experiments. H-HL and E-ML, with contributions from MY, MS, S-TH, and C-TL wrote the manuscript. All authors read and approved the final manuscript.

FUNDING

The funding for this project was provided by the Ministry of Science and Technology of Taiwan (MOST) (Grant Nos. 104-2311-B-001-025-MY3 to E-ML; 107-2628-M-001-005-MY3 to S-TH; and 107-2811-M-001-1574 to MS) and Academia Sinica Investigator Award to E-ML (Grant No. AS-IA-107-L01).

ACKNOWLEDGMENTS

We thank National BioResource Project (NIG, Japan): *E. coli* for providing the Keio collection. We also thank Lai lab members for discussion and suggestions. We acknowledge the staffs in the Plant Cell Biology Core Laboratory and the DNA Sequencing Core Laboratory at the Institute of Plant and Microbial Biology, and Biophysics Facility at the Institute of Biological Chemistry, Academia Sinica, Taiwan, and Chia Lee for technical support.

SUPPLEMENTARY MATERIAL

The Supplementary Material for this article can be found online at: https://www.frontiersin.org/articles/10.3389/fmicb.2019.03077/full#supplementary-material

REFERENCES

Alexopoulos, J. A., Guarné, A., and Ortega, J. (2012). ClpP: a structurally dynamic protease regulated by AAA+ proteins. *J. Struct. Biol.* 179, 202–210. doi: 10.1016/j.jsb.2012.05.003

Alteri, C. J., and Mobley, H. L. T. (2016). The versatile type VI secretion system. *Microbiol. Spectr.* 4:26.

Aoki, S. K., Diner, E. J., De Roodenbeke, C. T. K., Burgess, B. R., Poole, S. J., Braaten, B. A., et al. (2010). A widespread family of polymorphic contact-dependent toxin delivery systems in bacteria. *Nature* 468, 439–442. doi: 10.1038/nature09490

Aoki, S. K., Malinverni, J. C., Jacoby, K., Thomas, B., Pamma, R., Trinh, B. N., et al. (2008). Contact-dependent growth inhibition requires the essential outer membrane protein BamA (YaeT) as the receptor and the inner membrane transport protein AcrB. *Mol. Microbiol.* 70, 323–340. doi: 10.1111/j.1365-2958.2008.06404.x

Aoki, S. K., Pamma, R., Hernday, A. D., Bickham, J. E., Braaten, B. A., and Low, D. A. (2005). Contact-dependent inhibition of growth in *Escherichia coli*. *Science* 309, 1245–1248. doi: 10.1126/science.1115109

Baba, T., Ara, T., Hasegawa, M., Takai, Y., Okumura, Y., Baba, M., et al. (2006). Construction of *Escherichia coli* K-12 in-frame, single-gene knockout mutants: the Keio collection. *Mol. Syst. Biol.* 2:2006.0008.

Basler, M., Ho, B. T., and Mekalanos, J. J. (2013). Tit-for-tat: type VI secretion system counterattack during bacterial cell-cell interactions. *Cell* 152, 884–894. doi: 10.1016/j.cell.2013.01.042

Bayer-Santos, E., Cenens, W., Matsuyama, B. Y., Di Sessa, G., Mininel, I. D. V., and Farah, C. S. (2019). The opportunistic pathogen *Stenotrophomonas maltophilia*

utilizes a type IV secretion system for interbacterial killing. *PLoS Pathog.* 15:e1007651. doi: 10.1371/journal.ppat.1007651

Bewley, M. C., Graziano, V., Griffin, K., and Flanagan, J. M. (2006). The asymmetry in the mature amino-terminus of ClpP facilitates a local symmetry match in ClpAP and ClpXP complexes. *J. Struct. Biol.* 153, 113–128. doi: 10.1016/j.jsb.2005.09.011

Bhandari, V., Wong, K. S., Zhou, J. L., Mabanglo, M. F., Batey, R. A., and Houry, W. A. (2018). The role of ClpP protease in bacterial pathogenesis and human diseases. *ACS Chem. Biol.* 13, 1413–1425. doi: 10.1021/acschembio.8b00124

Cole, A., Wang, Z., Coyaud, E., Voisin, V., Gronda, M., Jitkova, Y., et al. (2015). Inhibition of the mitochondrial protease ClpP as a therapeutic strategy for human acute myeloid leukemia. *Cancer Cell* 27, 864–876. doi: 10.1016/j.ccell.2015.05.004

Costa, T. R. D., Felisberto-Rodrigues, C., Meir, A., Prevost, M. S., Redzej, A., Trokter, M., et al. (2015). Secretion systems in Gram-negative bacteria: structural and mechanistic insights. *Nat. Rev. Microb.* 13, 343–359. doi: 10.1038/nrmicro3456

Culp, E., and Wright, G. D. (2016). Bacterial proteases, untapped antimicrobial drug targets. *J. Antibiot.* 70, 366–377. doi: 10.1038/ja.2016.138

Diner, E. J., Beck, C. M., Webb, J. S., Low, D. A., and Hayes, C. S. (2012). Identification of a target cell permissive factor required for contact-dependent growth inhibition (CDI). *Genes Dev.* 26, 515–525. doi: 10.1101/gad.182345.111

Filloux, A., and Sagfors, A. (2015). "3 - News and views on protein secretion systems," in *The Comprehensive Sourcebook of Bacterial Protein Toxins (Fourth Edition)*, eds J. Alouf, D. Ladant, and M. R. Popoff, (Boston: Academic Press), 77–108. doi: 10.1016/b978-0-12-800188-2.00003-3

García-Bayona, L., Gozzi, K., and Laub, M. T. (2019). Mechanisms of resistance to the contact-dependent bacteriocin CdzC/D in *Caulobacter crescentus*. *J. Bacteriol.* 201:e538-18. doi: 10.1128/JB.00538-18

García-Bayona, L., Guo, M. S., and Laub, M. T. (2017). Contact-dependent killing by *Caulobacter crescentus* via cell surface-associated, glycine zipper proteins. *eLife* 6:e24869. doi: 10.7554/eLife.24869

Gottesman, S., Roche, E., Zhou, Y., and Sauer, R. T. (1998). The ClpXP and ClpAP proteases degrade proteins with carboxy-terminal peptide tails added by the SsrA-tagging system. *Genes Dev.* 12, 1338–1347. doi: 10.1101/gad.12.9.1338

Graves, S., Piepho, H.-P., Selzer, L., and Dorai-Raj, S. (2015). "multcompView: visualizations of paired comparisons," in *R package version 0.1-7*.

Harrell, F. E. Jr., Dupont, C., and Others, M. (2018). *Hmisc: Harrell Miscellaneous*. Vienna: R Foundation for Statistical Computing.

Heckman, K. L., and Pease, L. R. (2007). Gene splicing and mutagenesis by PCR-driven overlap extension. *Nat. Protoc.* 2, 924–932. doi: 10.1038/nprot.2007.132

Hood, R. D., Peterson, S. B., and Mougous, J. D. (2017). From striking out to striking gold: discovering that type VI secretion targets bacteria. *Cell Host Microbe* 21, 286–289. doi: 10.1016/j.chom.2017.02.001

Johnson, P. M., Beck, C. M., Morse, R. P., Garza-Sánchez, F., Low, D. A., Hayes, C. S., et al. (2016). Unraveling the essential role of CysK in CDI toxin activation. *Proc. Natl. Acad. Sci. U.S.A.* 113, 9792–9797. doi: 10.1073/pnas.1607112113

Jones, A. M., Garza-Sánchez, F., So, J., Hayes, C. S., and Low, D. A. (2017). Activation of contact-dependent antibacterial tRNase toxins by translation elongation factors. *Proc. Natl. Acad. Sci. U.S.A.* 114, E1951–E1957. doi: 10.1073/pnas.1619273114

Kassambara, A. (2018). *ggpubr: 'ggplot2' Based Publication Ready Plots*. New York, NY: Springer.

Keseler, I. M., Mackie, A., Santos-Zavaleta, A., Billington, R., Bonavides-Martínez, C., Caspi, R., et al. (2016). The EcoCyc database: reflecting new knowledge about *Escherichia coli* K-12. *Nucleic Acids Res.* 45, D543–D550. doi: 10.1093/nar/gkw1003

LeRoux, M., De Leon, J. A., Kuwada, N. J., Russell, A. B., Pinto-Santini, D., Hood, R. D., et al. (2012). Quantitative single-cell characterization of bacterial interactions reveals type VI secretion is a double-edged sword. *Proc. Natl. Acad. Sci. U.S.A.* 109, 19804–19809. doi: 10.1073/pnas.1213963109

Li, C., Tao, Y. P., and Simon, L. D. (2000). Expression of different-size transcripts from the *clpP-clpX* operon of *Escherichia coli* during carbon deprivation. *J. Bacteriol.* 182, 6630–6637. doi: 10.1128/jb.182.23.6630-6637.2000

Lien, Y.-W., and Lai, E.-M. (2017). Type VI secretion effectors: methodologies and biology. *Front. Cell Infect. Microbiol.* 7:254. doi: 10.3389/fcimb.2017.00254

Ma, L.-S., Hachani, A., Lin, J.-S., Filloux, A., and Lai, E.-M. (2014). *Agrobacterium tumefaciens* deploys a superfamily of type VI secretion dnase effectors as weapons for interbacterial competition in planta. *Cell Host Microbe* 16, 94–104. doi: 10.1016/j.chom.2014.06.002

Ma, L.-S., Narberhaus, F., and Lai, E.-M. (2012). IcmF family protein TssM exhibits ATPase activity and energizes type VI secretion. *J. Biol. Chem.* 287, 15610–15621. doi: 10.1074/jbc.M111.301630

Mahmoud, S. A., and Chien, P. (2018). Regulated proteolysis in bacteria. *Annu. Rev. Biochem.* 87, 677–696. doi: 10.1146/annurev-biochem-062917-012848

Mariano, G., Monlezun, L., and Coulthurst, S. J. (2018). Dual role for DsbA in attacking and targeted bacterial cells during type VI secretion system-mediated competition. *Cell Rep.* 22, 774–785. doi: 10.1016/j.celrep.2017.12.075

Maurizi, M. R. (1991). ATP-promoted interaction between Clp A and Clp P in activation of Clp protease from *Escherichia coli*. *Biochem. Soc. Trans.* 19, 719–723. doi: 10.1042/bst0190719

Maurizi, M. R., Clark, W. P., Kim, S. H., and Gottesman, S. (1990). Clp P represents a unique family of serine proteases. *J. Biol. Chem.* 265, 12546–12552.

Michalska, K., Gucinski, G. C., Garza-Sánchez, F., Johnson, P. M., Stols, L. M., Eschenfeldt, W. H., et al. (2017). Structure of a novel antibacterial toxin that exploits elongation factor Tu to cleave specific transfer RNAs. *Nucleic Acids Res.* 45, 10306–10320. doi: 10.1093/nar/gkx700

Miller, J. M., Lin, J., Li, T., and Lucius, A. L. (2013). E. coli ClpA catalyzed polypeptide translocation is allosterically controlled by the protease ClpP. *J. Mol. Biol.* 425, 2795–2812. doi: 10.1016/j.jmb.2013.04.019

Moreno, J. C., Tiller, N., Diez, M., Karcher, D., Tillich, M., Schöttler, M. A., et al. (2017). Generation and characterization of a collection of knock-down lines for the chloroplast Clp protease complex in tobacco. *J. Exp. Bot.* 68, 2199–2218. doi: 10.1093/jxb/erx066

Nishimura, K., and Van Wijk, K. J. (2015). Organization, function and substrates of the essential Clp protease system in plastids. *Biochim. Biophys. Acta* 1847, 915–930. doi: 10.1016/j.bbabio.2014.11.012

Olivares, A. O., Baker, T. A., and Sauer, R. T. (2015). Mechanistic insights into bacterial AAA+ proteases and protein-remodelling machines. *Nat. Rev. Microbiol.* 14, 33–44. doi: 10.1038/nrmicro.2015.4

Orfanoudaki, G., and Economou, A. (2014). Proteome-wide subcellular topologies of *E. coli* polypeptides database (STEPdb). *Mol. Cell. Proteomics* 13, 3674–3687. doi: 10.1074/mcp.O114.041137

Quentin, D., Ahmad, S., Shanthamoorthy, P., Mougous, J. D., Whitney, J. C., and Raunser, S. (2018). Mechanism of loading and translocation of type VI secretion system effector Tse6. *Nat. Microbiol.* 3, 1142–1152. doi: 10.1038/s41564-018-0238-z

R Core Team, (2018). *R: A Language and Environment for Statistical Computing*. Vienna: R Foundation for Statistical Computing.

RStudio Team, (2015). *RStudio: Integrated Development for R*. Boston, MA: RStudio, Inc.

Russell, A. B., Peterson, S. B., and Mougous, J. D. (2014). Type VI secretion system effectors: poisons with a purpose. *Nat. Rev. Microbiol.* 12, 137–148. doi: 10.1038/nrmicro3185

Souza, D. P., Oka, G. U., Alvarez-Martinez, C. E., Bisson-Filho, A. W., Dunger, G., Hobeika, L., et al. (2015). Bacterial killing via a type IV secretion system. *Nat. Commun.* 6:6453. doi: 10.1038/ncomms7453

Sriramoju, M. K., Chen, Y., Lee, Y.-T. C., and Hsu, S.-T. D. (2018). Topologically knotted deubiquitinases exhibit unprecedented mechanostability to withstand the proteolysis by an AAA+ protease. *Sci. Rep.* 8:7076. doi: 10.1038/s41598-018-25470-0

Studier, F. W., and Moffatt, B. A. (1986). Use of bacteriophage T7 RNA polymerase to direct selective high-level expression of cloned genes. *J. Mol. Biol.* 189, 113–130. doi: 10.1016/0022-2836(86)90385-2

Vergunst, A. C., Schrammeijer, B., Den Dulk-Ras, A., De Vlaam, C. M. T., Regensburg-Tuïnk, T. J. G., and Hooykaas, P. J. (2000). VirB/D4-dependent protein translocation from *Agrobacterium* into plant cells. *Science* 290, 979–982. doi: 10.1126/science.290.5493.979

Wang, J., Hartling, J. A., and Flanagan, J. M. (1997). The structure of ClpP at 2.3 Å resolution suggests a model for ATP-dependent proteolysis. *Cell* 91, 447–456. doi: 10.1016/s0092-8674(00)80431-6

Weber-Ban, E. U., Reid, B. G., Miranker, A. D., and Horwich, A. L. (1999). Global unfolding of a substrate protein by the Hsp100 chaperone ClpA. *Nature* 401, 90–93. doi: 10.1038/43481

Whitney, J. C., Quentin, D., Sawai, S., Leroux, M., Harding, B. N., Ledvina, H. E., et al. (2015). An interbacterial NAD(P)+ glycohydrolase toxin requires

elongation factor Tu for delivery to target cells. *Cell* 163, 607–619. doi: 10.1016/j.cell.2015.09.027

Wickham, H. (2011). The split-apply-combine strategy for data analysis. *J. Stat. Softw*. 40:29.

Wickham, H. (2016). *ggplot2: Elegant Graphics for Data Analysis*. New York, NY: Springer-Verlag.

Willett, J. L. E., Gucinski, G. C., Fatherree, J. P., Low, D. A., and Hayes, C. S. (2015). Contact-dependent growth inhibition toxins exploit multiple independent cell-entry pathways. *Proc. Natl. Acad. Sci. U.S.A.* 112, 11341–11346. doi: 10.1073/pnas.1512124112

Conflict of Interest: The authors declare that the research was conducted in the absence of any commercial or financial relationships that could be construed as a potential conflict of interest.

Copyright © 2020 Lin, Yu, Sriramoju, Hsu, Liu and Lai. This is an open-access article distributed under the terms of the Creative Commons Attribution License (CC BY). The use, distribution or reproduction in other forums is permitted, provided the original author(s) and the copyright owner(s) are credited and that the original publication in this journal is cited, in accordance with accepted academic practice. No use, distribution or reproduction is permitted which does not comply with these terms.

frontiers in Microbiology

ORIGINAL RESEARCH
published: 17 April 2020
doi: 10.3389/fmicb.2020.00705

HpaR, the Repressor of Aromatic Compound Metabolism, Positively Regulates the Expression of T6SS4 to Resist Oxidative Stress in *Yersinia pseudotuberculosis*

Zhuo Wang†, Tietao Wang†, Rui Cui, Zhenxing Zhang, Keqi Chen, Mengyun Li, Yueyue Hua, Huawei Gu, Lei Xu, Yao Wang, Yantao Yang and Xihui Shen**

State Key Laboratory of Crop Stress Biology for Arid Areas, Shaanxi Key Laboratory of Agricultural and Environmental Microbiology, College of Life Sciences, Northwest A&F University, Yangling, China

OPEN ACCESS

Edited by:
Eric Cascales, Aix-Marseille Université, France

Reviewed by:
Gabriella Fiorentino, University of Naples Federico II, Italy
Sébastien Bontemps-Gallo, Institut Pasteur de Lille, France

***Correspondence:**
Yantao Yang
yyt811113@nwsuaf.edu.cn
Xihui Shen
xihuishen@nwsuaf.edu.cn

† These authors have contributed equally to this work

Specialty section:
This article was submitted to Microbial Physiology and Metabolism, a section of the journal Frontiers in Microbiology

Received: *23 December 2019*
Accepted: *26 March 2020*
Published: *17 April 2020*

Citation:
Wang Z, Wang T, Cui R, Zhang Z, Chen K, Li M, Hua Y, Gu H, Xu L, Wang Y, Yang Y and Shen X (2020) HpaR, the Repressor of Aromatic Compound Metabolism, Positively Regulates the Expression of T6SS4 to Resist Oxidative Stress in Yersinia pseudotuberculosis. Front. Microbiol. 11:705. doi: 10.3389/fmicb.2020.00705

HpaR, a MarR family transcriptional regulator, was first identified in *Escherichia coli* W for its regulation of the *hpa-meta* operon. Little else is known regarding its functionality. Here, we report that in *Yersinia pseudotuberculosis*, HpaR negatively regulates the *hpa-meta* operon similar to in *E. coli* W. To investigate additional functions of HpaR, RNA sequencing was performed for both the wild-type and the Δ*hpaR* mutant, which revealed that the type VI secretion system (T6SS) was positively regulated by HpaR. T6SS4 is important for bacteria resisting environmental stress, especially oxidative stress. We demonstrate that HpaR facilitates bacteria resist oxidative stress by upregulating the expression of T6SS4 in *Y. pseudotuberculosis*. HpaR is also involved in biofilm formation, antibiotic resistance, adhesion to eukaryotic cells, and virulence in mice. These results greatly expand our knowledge of the functionality of HpaR and reveal a new pathway that regulates T6SS4.

Keywords: HpaR, type VI secretion system, *Yersinia pseudotuberculosis*, oxidative stress, biofilm, aromatic compounds degradation

INTRODUCTION

HpaR has been characterized as a repressor of the *hpa-meta* operon (Galan et al., 2003). It has been shown that *Escherichia coli* strains B, C, and W can use 4-hydroxyphenylacetic acid (4-HPA) as a carbon source via the *hpa-meta* pathway, while *E. coli* K-12 does not have this ability (Cooper and Skinner, 1980). Studies of the *hpa-meta* cluster have focused mainly on *E. coli* W (Galan et al., 2001). The *hpa-meta* cluster of *E. coli* W is composed of 11 genes in two putative operons (Prieto et al., 1996; Galan et al., 2003). The *upper* operon consists of *hpaBC*, which encodes the two-component 4-HPA monooxygenase, which converts 4-HPA to 3,4-dihydroxyphenylacetic acid (3,4-HPA) (Prieto and Garcia, 1994; Galan et al., 2000). Transcription of the *hpaBC* operon is controlled by HpaA, which belongs to the AraC/XylS family and functions as an activator to activate the expression of *hpaBC*, except for the *meta* operon in the presence of 4-HPA or 3-HPA (Prieto and Garcia, 1997).

The *meta* operon is composed of *hpaGEDFHI*, which encodes enzymes that catalyze 3,4-HPA in the Krebs cycle (Roper et al., 1993; Prieto et al., 1996). The expression of both the *meta* operon and *hpaR* are regulated by HpaR (Galan et al., 2003). HpaR was first identified as a repressor in *E. coli* W and is identical to HpcR in *E. coli* C (Roper et al., 1993; Galan et al., 2003). The *hpa-meta* cluster has also been found in other bacteria. In *Pseudomonas putida* U, the *hpa* pathway is coupled with the *tyn* pathway to degrade tyramine and dopamine (Barbour and Bayly, 1981; Arcos et al., 2010). Together these form the 3,4-HPA catabolon, in which 3,4-HPA is the central intermediate. The *hpa-meta* pathway in *P. putida* U is composed of the genes *hpaRBCIHXFDEG2G1AY*. HpaR of *P. putida* U is similar to that in *E. coli* in that it represses the *meta* operon (Arcos et al., 2010). Interestingly, a second *hpaR* (*hpaY*) was found in *P. putida* U with similar functionality, ensuring stronger control of the *meta* operon (Arcos et al., 2010). In *Burkholderia xenovorans* LB400, the *hpa-meta* pathway is made up of *hpaG1G2EDFHI* and *hpaBC*, while *hpaA* and *hpaX* are absent and *hpaBC* is not adjacent to the *meta* operon (Mendez et al., 2011). HpaR of *B. xenovorans* LB400 also regulates the *meta* operon as a repressor (Mendez et al., 2011). However, previous research has defined HpaR as a repressor that negatively controls expression of the *meta* operon, but not *hpaBC*. According to sequence comparison and a three-dimensional model, HpaR is classified into the MarR transcriptional regulator family, which is involved in various physiological processes (Alekshun et al., 2001; Galan et al., 2003; Grove, 2013). However, whether HpaR might exert other functions in addition to acting as a repressor of the *hpa-meta* operon remains unknown.

Yersinia pseudotuberculosis is a Gram-negative enteric pathogen of animals and humans that causes a variety of diseases such as acute ileitis, mesenteric lymphadenitis, and septicemia (Brubaker, 1991; Smego et al., 1999; Fallman and Gustavsson, 2005). During infection, environmental stress and host immunity reactions can cause an increase in reactive oxygen species (ROS) levels of *Y. pseudotuberculosis* (Green et al., 2016). Elevated cellular ROS levels lead to oxidative stress, which induces oxidative damage to macromolecules such as proteins, lipids, and DNA (D'Autreaux and Toledano, 2007). Protection against the adverse effects of ROS is vital—bacteria have developed a wide range of systems including antioxidant enzymes, i.e., peroxidase, superoxide dismutase, glutaredoxin, and thioredoxin; low molecular weight antioxidants, i.e., the tripeptide glutathione (GSH) and β-carotene; and vitamins, i.e., vitamins C and E (D'Autreaux and Toledano, 2007; Si et al., 2015, 2017a; Staerck et al., 2017). Recently, we found that the type VI secretion system (T6SS) in *Y. pseudotuberculosis* was also involved in resistance to oxidative stress; it secretes a zinc-binding protein that imports zinc to mitigate ROS (Wang et al., 2015).

T6SS is a versatile transmembrane machine used by many Gram-negative bacteria to inject effector proteins into cells, either prokaryotic or eukaryotic, or the extracellular milieu (Durand et al., 2014; Russell et al., 2014; Basler, 2015). Although traditionally T6SS is recognized as a contact-dependent bacterial weapon for interspecies competition, some T6SSs from diverse species are also found to play roles in bacterial pathogenesis, biofilm formation, and stress response (Durand et al., 2014; Russell et al., 2014; Yang et al., 2018). For example, a *Vibrio anguillarum* T6SS regulated by the general stress response regulator RpoS is involved in resistance to hydrogen peroxide, ethanol, and low pH (Weber et al., 2009). Enterohemorrhagic *E. coli* (EHEC) uses its T6SS to deliver KatN, an Mn-containing catalase, into the host cytosol, resulting in reduced levels of intracellular ROS and greater survival of the pathogen (Wan et al., 2017). In *B. thailandensis*, T6SS4 exports TseZ and TseM into the extracellular medium to acquire the antioxidant metal ions Zn^{2+} and Mn^{2+}, respectively, to combat oxidative stress by reducing intracellular ROS levels (Si et al., 2017b,c). The avian pathogenic *E. coli* (APEC) strain TW-XM harbors two functional T6SSs. The first, T6SS1, plays versatile roles in adherence to host cells, biofilm formation, and bacterial competition; the second, T6SS2, is responsible only for cerebral infection (Ma et al., 2014; Navarro-Garcia et al., 2019).

Despite being reported to control expression of the *hpa-meta* operon, knowledge of HpaR in *Y. pseudotuberculosis* is lacking. Unexpectedly, in this study, we found that HpaR not only acts as a repressor of the *hpa-meta* operon in a similar manner to that of *E. coli* but also acts as an activator to upregulate the expression of T6SS4 to acquire Zn^{2+} and resist oxidative stress. HpaR is also involved in biofilm formation, antibiotic resistance, adhesion to eukaryotic cells, and virulence in mice. These results greatly expand our current knowledge of the functions of HpaR.

MATERIALS AND METHODS

Bacterial Strains and Growth Conditions

Bacterial strains and plasmids used in this study are listed in **Supplementary Table S1**. *Escherichia coli* strains were cultured at 37°C in Lysogeny Broth (LB) or LB plates. *Y. pseudotuberculosis* strains were grown in Yersinia-Lysogeny-Broth (YLB) broth (tryptone 1%, yeast extract 0.5%, NaCl 0.5%) or YLB plates at 30 or 26°C. The *Y. pseudotuberculosis strain* YPIII was the parent of all derivatives used in this study. To construct the *hpaR* in-frame deletion mutant, the wild-type *Y. pseudotuberculosis* was mated with *E. coli* S17-1λpir carrying pDM4-*hpaR* and chromosomal integration was selected by plating on YLB agar plates supplemented with nalidixic acid and chloramphenicol. The *hpaR* deletion mutant was subsequently screened on YLB agar plates with 20% sucrose and confirmed by polymerase chain reaction (PCR) and DNA sequencing. Appropriate antibiotics were included in growth medium at the following concentrations: ampicillin, 100 μg/ml; kanamycin, 50 μg/ml; nalidixic acid, 20 μg/ml; chloramphenicol, 20 μg/ml.

Plasmid Construction

Primers used in this study are listed in **Supplementary Table S2**. The *lacZ* fusion reporter vector pDM4-T6SS4*p:lacZ* was made in previous study (Zhang et al., 2013). To obtain the expression plasmid, *hpaR*-F-*Bam*HI/*hpaR*-R-*Sal*I primer pair was used

to amplify *hpaR* gene fragment from *Y. pseudotuberculosis* genomic DNA by PCR. The *hpaR* gene fragment were digested with *Bam*HI/*Sal*I and then inserted into similar digested pET28a yielding the pET28a-*hpaR*. The suicide plasmid pDM4-*hpaR* used to construct the *hpaR* mutant was prepared by overlap PCR. Briefly, *hpaR*-UF-*Xba*I/*hpaR*-UR and *hpaR*-DF/*hpaR*-DR-*Spe*I primers were used to amplify the 1000 bp upstream fragment and 1000 bp downstream fragment of *hpaR*, respectively. Then, the amplified fragments were fused together by overlap PCR with *hpaR*-UF-*Xba*I/*hpaR*-DR-*Spe*I. The fused PCR products were digested with *Xba*I/*Spe*I and cloned into similar digested pDM4 resulting pDM4-*hpaR*. In order to construct the complementary plasmid pKT100-*hpaR*, *hpaR*-F-*Bam*HI/*hpaR*-R-*Sal*I primers were used to amplify *hpaR* gene from template. The PCR product was digested with *Bam*HI/*Sal*I and inserted into similarly digested pKT100 to produce pKT100-*hpaR*, which is subsequently electroporated into Δ*hpaR* to construct the complementation strains. To construct the *hpaG1* promoter reporter vector, *hpaG1p*-F-*Sal*I/*hpaG1p*-R-*Xba*I primer pair was used to amplify the 387 bp promoter fragment from *Y. pseudotuberculosis*. The product of PCR was digested with *Sal*I/*Xba*I and cloned into similar digested pDM4-T6SS4*p:lacZ* to produce pDM4-*hpaG1p:lacZ*. To construct the T6SS4 promoter fragments with HpaR binding site mutations, overlap PCR was performed to replace the HpaR binding site with identical amount of irrelevant base pairs. T6SS4*p*M$_{HpaR}$-R and T6SS4*p*M$_{HpaR}$-F were designed to contain 22 bp overlapping DNA fragment (ATTTGTTAGATTCCGAACCGTC) used to replace the HpaR binding site. T6SS4*p*-F-*Sal*I/T6SS4*p*M$_{HpaR}$-R and T6SS4*p*M$_{HpaR}$-F/T6SS4*p*-R-*Xba*I primers used to amplify the up-fragment and down-fragment of T6SS4*p* promoter, respectively. The PCR products were ligated with T6SS4*p*-F-*Sal*I/T6SS4*p*-R-*Xba*I by overlap PCR to produce the mutant promoter fragment T6SS4*p*M$_{HpaR}$. The T6SS4*p*M$_{HpaR}$ fragment were digested with *Sal*I/*Xba*I and ligated into similarly digested pDM4-T6SS4*p:lacZ* to produce pDM4-T6SS4*p*M$_{HpaR}$*:lacZ*. The validity of all the plasmids constructed above was confirmed by DNA sequencing.

Sequence Data Analysis

Sequence alignment was performed as previously described (Shen et al., 2005; Huang et al., 2008). The sequence of *hpaRGEDFHIXABC* (Accession No. Z37980.2) of *E. coli* W were retrieved from GenBank. Sequence comparisons were carried out using BLAST program at National Center for Biotechnology Information website[1]. Multiple protein sequence alignment was made by CLUSTAL W. The sequences used in alignment have been deposited in the GenBank database [Accession No. EcC *E. coli* C (S56952.1), EcW *E. coli* W (Z37980.2), Yptb *Y. pseudotuberculosis* YPIII (ACA68739.1), PpU *P. putida* U (FJ904934.1), BxLB400 *B. xenovorans* LB400 (ABE33958.1)]. The result was exported by ESPript[2].

[1]https://www.ncbi.nlm.nih.gov/

[2]http://espript.ibcp.fr/ESPript/cgi-bin/ESPript.cgi

Construction of Chromosomal Fusion Reporter Strains and β-Galactosidase Activity Assay

The *lacZ* fusion reporter vector pDM4-T6SS4*p:lacZ*, pDM4-T6SS4*p*M$_{HpaR}$*:lacZ* and pDM4-*hpaG1p:lacZ* was transformed into *E. coli* S17-1λpir and then introduced into *Y. pseudotuberculosis* by conjugation as described (Xu et al., 2014). All constructed *lacZ* fusion reporter strains were grown in YLB broth at 26°C and *o*-nitrophenyl-β-galactoside (ONPG) as substrate for measuring β-galactosidase activities as described by Miller (1992). The β-galactosidase results shown represent the mean of one representative assay performed in triplicate, and error bars represent standard deviation. Statistical analysis was carried out with Student's *t*-test.

Protein Expression and Purification

To express and purify His$_6$- tagged HpaR, the constructed expression vector pET28a-*hpaR* were transformed into BL21(DE3). Single colony was cultured in 5 ml LB broth at 37°C overnight and diluted 100-fold into 500 ml LB. Until the OD_{600} = 0.5, the culture was shifted to 22°C, induced with 0.3 mM IPTG and further cultivated for 12 h to express the recombinant proteins. Cell pellet was collected by centrifugation, washed and resuspended in His binding buffer, and lysed by sonication. The recombinant proteins were purified with the His·Bind Ni-NTA resin (Novagen) according to the manufacturer's instructions. Eluted recombinant proteins were dialyzed against the appropriate buffer at 4°C for 4 h and then stored at −80°C until used.

Electrophoretic Mobility Shift Assay (EMSA)

EMSA was performed as previously described (Zhang et al., 2013; Wang et al., 2015). Bio-T6SS4p_{HpaR}-F/Bio-T6SS4p_{HpaR}-R primers were used to amplify the biotin 5′-end-labeled promoter probes (Bio-T6SS4p_{HpaR}) from *Y. pseudotuberculosis* genomic DNA. The unlabeled T6SS4p_{HpaR} was amplified with T6SS4p_{HpaR}-F/T6SS4p_{HpaR}-R from template, which used as a competitor. In addition, the unrelated protein BSA was used as negative control. All promoter probes were purified by EasyPure Quick Gel Extraction Kit (TransGen Biotech). According to the manufacturer's protocol (LightShift Chemiluminescent EMSA Kit; Thermo Fisher Scientific), each 20 μl EMSA reaction solution was prepared as follows: 1 × binding buffer, 50 ng poly (dI-dC), 2.5% glycerol, 0.05% Nonidet P-40, 5 mM $MgCl_2$, 3 ng Bio-T6SS4p_{HpaR} DNA, 1 ng T6SS4p_{HpaR} DNA as competitor, and different concentration of protein (0, 0.6, 0.8, 0.8 μg). Reaction solutions were incubated for 20 min at room temperature. The samples were loaded onto a 6% polyacrylamide native gel and transferred to a Biodyne B nylon membrane (Thermo Fisher Scientific). The biotin-labeled DNA bands were visualized by chemiluminescent substrate according to the manufacturer's protocol. *hpaG1p*-F/*hpaG1p*-R primers were used to amplify the *hpaG1p* probes from template. An unrelated DNA (URD) in the similar length or bovine serum albumin (BSA) was included in the binding assay system to serve as negative controls. Increasing

concentrations of purified His6-HpaR (0, 0.4, 0.8, 1.2, 1.2 μg) were incubated with 20 ng *hpaG1p* probes in EMSA buffer (20 mM Tris-HCl [pH 7.4], 4 mM $MgCl_2$, 100 mM NaCl, 1 mM dithiothreitol, 10% glycerol). After incubation for 20 min at 26°C, the sample was subjected to electrophoresis on a 6% polyacrylamide native gel. Then the DNA probe was detected using SYBR green.

Stress Survival Assay

Yersinia pseudotuberculosis strains grown in YLB broth until mid-exponential are diluted 50-fold into M9 medium (Na_2HPO_4, 6 g/L; KH_2PO_4, 3 g/L; NaCl, 0.5 g/L; NH_4Cl, 1 g/L; $MgSO_4$, 1 mM; $CaCl_2$, 0.1 mM; glucose 0.2%) with or without H_2O_2 (1.5 mM), cumene hydroperoxide (CHP, 0.5 mM), ampicillin (0.5 μg/ml), gentamicin (0.2 μg/ml) at 26°C for 1 h at 100 rpm. After treatment, the cultures were diluted 1000-fold and plated onto YLB agar plates with nalidixic acid. Colonies were counted after 24 h at 26°C. The survival percentage of *Y. pseudotuberculosis* is calculated by dividing the number of CFU of stressed cells by the number of CFU of cells without stress. All these assays were performed in triplicate at least three times.

Fluorescence Dye-Based Intracellular ROS Detection

The intracellular ROS levels were detected by the fluorescent reporter dye 5-(and-6)-chloromethyl-2′,7′-dichlorodihydro fluorescein diacetate, acetylester (CM-H_2DCFDA, Invitrogen) as previously reported (Si et al., 2017c). Briefly, 1 ml culture were collected after treatment, washed with M9 medium and resuspended in 1 ml of M9 medium containing 10 μM CM-H_2DCFDA. Samples were incubated at 26°C in the dark for 20 min. Then the cells were pelleted, washed with M9 medium and resuspended in 1 ml of PBS. Then 200 μl samples were transferred to a dark 96-well plate. Fluorescence signals were measured using a SpectraMax M2 Plate Reader (Molecular Devices) with excitation/emission wavelengths of 495/520 nm. The results shown represented the mean of one representative assay performed in triplicate, and error bars represent the standard deviation (SD).

Protein Secretion Assay

Secretion of YezP (encoded by *ypk_3459*) was detected as previously described (Wang et al., 2015). Briefly, all strains were grown in 180 ml YLB broth at 26°C on a rotary shaker (220 rpm) until OD_{600} = 1.6. A 2 ml culture was centrifuged and the cell pellet was resuspended in 100 μl SDS-loading buffer to serve as the total cell pellet sample. A total of 150 ml culture was centrifuged at low speed (5000 rpm) for 10 min to remove most cell pellets, and the supernatant was further centrifuged at high speed (8000 rpm) for 15 min to eliminate bacteria. To remove the remaining bacteria, the supernatant was filtered through a 0.22-μm filter (Millipore, Billerica, MA, United States). The supernatant was filtered three times through a nitrocellulose filter (BA85) (Whatman) to collect all secretion proteins. The filter was cut into pieces in 1.5 ml tubes and resuspended in 100 μl SDS-loading buffer for 20 min at 65°C to recover the proteins. All samples were normalized to the OD_{600} of the culture and volume used in preparation.

Western Blot Analysis

Western blot analysis was performed as described previously (Shen et al., 2009; Lin et al., 2017). Samples were resuspended in SDS-Loading buffer and separated in 15% polyacrylamide gel, then transferred onto PVDF membranes (Millipore). The membrane was blocked in 5% (w/v) BSA for 4 h at room temperature, and incubated with primary antibody at 4°C overnight. The primary antibodies were anti-VSVG (sc-365019, Santa Cruz biotechnology, United States), 1:1000 and anti-ICDH, 1:6000. The ICDH antisera were made in our previous study (Xu et al., 2010). The membrane was washed five times with TBST buffer (50 mM Tris, 150 mM NaCl, 0.05% Tween 20, pH 7.4), and incubated with 1:5,000 dilution of horseradish peroxidase conjugated secondary antibody (Shanghai Genomics) for 4 h at 4°C. Signals were detected using the ECL plus kit (GE Healthcare, Piscataway, NJ, United States) according to the manufacturer's specified protocol.

DNase I Footprinting Assay

DNase I footprinting assay was performed as described preciously (Zhao et al., 2017). Briefly, *hpaG1p* and T6SS4*p* were amplified by PCR with *hpaG1p*-FP-F/*hpaG1p*-FP-R and T6SS4*p*-FP-F/T6SS4*p*-FP-R primers, respectively. The PCR products were cloned into the pMD-18T vector (TaKaRa) as template to further amplify the fluorescent FAM labeled probes with primers M13R(FAM-labeled) and M13F(-47). The FAM-labeled probes were purified by the Wizard SV Gel and PCRClean-Up System (Promega) and quantified with NanoDrop 2000C (Thermo). For DNase I footprinting assay, 400 ng probes were incubated with various amount of His_6-HpaR in 40 μl of each sample. After binding at 30°C for 30 min, 10 μl solution containing about 0.010 unit DNase I (Promega) and 100 nmol $CaCl_2$ were added and further incubated for 1 min at 25°C. 140 μl DNase I stop solution (200 mM unbuffered sodium acetate, 30 mM EDTA and 0.15% SDS) was added into samples to stop the reaction. Samples were extracted by phenol/chloroform to remove proteins, precipitated with ethanol, washed and dissolved in 35 μl MiniQ water. The preparation of the DNA ladder, electrophoresis, and data analysis were similar to described previously (Wang et al., 2012).

RNA-seq Experiments

Yersinia pseudotuberculosis and the Δ*hpaR* mutant were used for RNA-Seq transcriptomics analysis (Wang et al., 2017). Two strains (three biological replicates) were grown in YLB medium at 26°C to OD_{600} = 1.6. Total RNA was extracted from each sample for cDNA library construction by using bacteria total RNA isolation kit (Tiangen) and analyzed with the Bioanalyzer 2100 system (Agilent Technologies). Library sequencing was completed at the Beijing Genomic Institute (BGI-Shenzhen). The result of sequencing was aligned with the reference genome of *Y. pseudotuberculosis* and RPKM (Reads per kilobase transcriptome per million mapped reads) was used to normalize the expression level of genes. The differential expressed

genes were shown as fold change calculated by $\log_2$ (RPKM of Δ*hpaR*/WT).

Quantitative Real-Time PCR

All strains were cultured at mid-exponential, harvested, washed with PBS. Total RNA was isolated from each sample using the RNAprep Pure Cell/Bacteria Kit, treated with RNase-free DNase (Tiangen) and measured the purity and concentration by gel electrophoresis and spectrophotometer (NanoDrop, Thermo Scientific). 1.5 μg of total RNA was used to synthesis the first-strand cDNA by reverse transcriptase (TransGen Biotech). Quantitative real-time PCR (qRT-PCR) was performed in CFX96 Real-Time PCR Detection System (Bio-Rad) with TransStart Green qPCR SuperMix (TransGen Biotech). The qRT-PCR primers were listed in **Supplementary Table S2** and qRT-PCR parameter was set as follows: 95°C for 30 s followed by 40 cycles of 94°C for 15 s, 52°C for 30 s. The relative abundance of 16S rRNA was used as the internal standard for standardization of results.

Determination of Intracellular Ion Content

Intracellular ion content was determined as described previously (Wang et al., 2015). Briefly, *Y. pseudotuberculosis* wild-type, Δ*hpaR* and Δ*hpaR* (*hpaR*) strains were grown in YLB medium to mid-exponential. 20 ml culture were collected, washed with PBS, resuspended in 20 ml PBS buffer containing 0.4% glucose, 1.5 mM H_2O_2 and 1 μM Zn^{2+}, and then incubated further for 20 min at 26°C. After centrifugation at low speed (4000 rpm) for 10 min, the supernatant was removed and the cell pellet weight was measured. Then the pellet was resuspended and chemically lysed on a rotating mixer at a slow setting for 20 min by using Bugbuster (Novagen, Madison, WI, United States) according to the manufacturer's instructions. The protein concentration was analyzed with NanoDrop ND-1000 spectrophotometer (NanoDrop Technologies) according to the manufacturer's instructions. The lysis solution was diluted 100-fold in 2% molecular grade nitric acid to 10 ml. These samples were analyzed by Inductively Coupled Plasma Mass Spectrometry (ICP-MS) (Varian 802-MS), and the results were corrected using the appropriate buffers for reference and dilution factors. Triplicate cultures of each strain were analyzed during a single experiment and the experiment was repeated at least three times.

Biofilm Formation Assay

Biofilm formation was measured using the test tube, performed as previously described (Guan et al., 2015). *Y. pseudotuberculosis* strains were grown in YLB broth, and then transferred into 3 ml of M9 medium containing 0.4% glucose on a rotary shaker (220 rpm) at 26°C. After 24 h, the test tube was washed gently three times with PBS and stained with 1% crystal violet for 15 min, then washed three times with PBS again to remove redundant crystal violet. The remaining crystal violet was resolved with 95% ethanol and 200 μl of samples were measured the absorbance at 595 nm by a microplate reader (BioTek Instruments, Inc.).

Cell Adhesion Assay

The adhesion ability of bacteria was measured as previously reported (Tan et al., 2017). HeLa cells were seeded into 12-well plate at a concentration of 1×10^5 cells/ml before infection. *Y. pseudotuberculosis* wild-type, Δ*hpaR* and Δ*hpaR* (pKT100-*hpaR*) strains were grown at 26°C till OD_{600} = 1.0 and then collected, washed and resuspended in DMEM. The bacterial suspensions were serial diluted and plated onto YLB agar plates to count the actual number of the bacteria. HeLa cells were infected with bacterial strains at a multiplicity of infection (MOI) of 100 and then centrifuged for 5 min at 1500 rpm to promote contact between bacteria and HeLa cells. After 2 h, HeLa cells were washed for three times using prewarmed PBS. Cell-associated bacteria were liberated by treatment with 0.1% Triton X-100 in sterile PBS for 5 min. The number of cell-associated bacteria was divided by the total number of bacteria in a well to calculate the adhesion percentage.

Mouse Infection

All mice were maintained and handled in accordance with the Regulations for the Administration of Affairs Concerning Experimental Animals approved by the State Council of People's Republic of China. The protocol was approved by the Animal Welfare and Research Ethics Committee of Northwest A&F University (protocol number: NWAFUSM2018001). All strains growing in YLB broth at 26°C until mid-exponential were harvested, washed, resuspended in sterilized PBS to a final concentration of 3×10^9 bacteria for survival assays. The 6–8 weeks old female C57BL/6 mice were orogastric infected with *Y. pseudotuberculosis* using a ball-tipped feeding needle. The survival rate of the mice was determined by monitoring the survival everyday for 24 days.

Statistical Analysis

Statistical analyses of gene expression data, LacZ activity, survival assay, ROS determination, intracellular ion content determination, and cell adhesion assay were performed using paired two-tailed Student's *t*-test. Statistical analyses were performed using GraphPad Prism software (GraphPad Software).

RESULTS

Regulation of the *hpa* Gene Cluster in *Y. pseudotuberculosis*

The 4-hydroxyphenylacetic acid (4-HPA) catabolic pathway was determined by alignment with *E. coli* W (ATCC 11105) while searching for the complete genome sequence of *Y. pseudotuberculosis* (**Figure 1A**). Analyses of the open reading frames of the gene cluster suggested that the 4-HPA metabolic cluster is composed of 11 genes in *Y. pseudotuberculosis*, similar to that of *E. coli* W (Roper et al., 1993; Prieto and Garcia, 1994). These genes include the genes of 4-HPA monooxygenase (*hpaBC*), the genes of homoprotocatechuate (HPC) *meta* cleavage enzymes (*hpaG1G2EDFHI*), the HPA transport protein gene (*hpaX*), and one regulatory gene (*hpaR*).

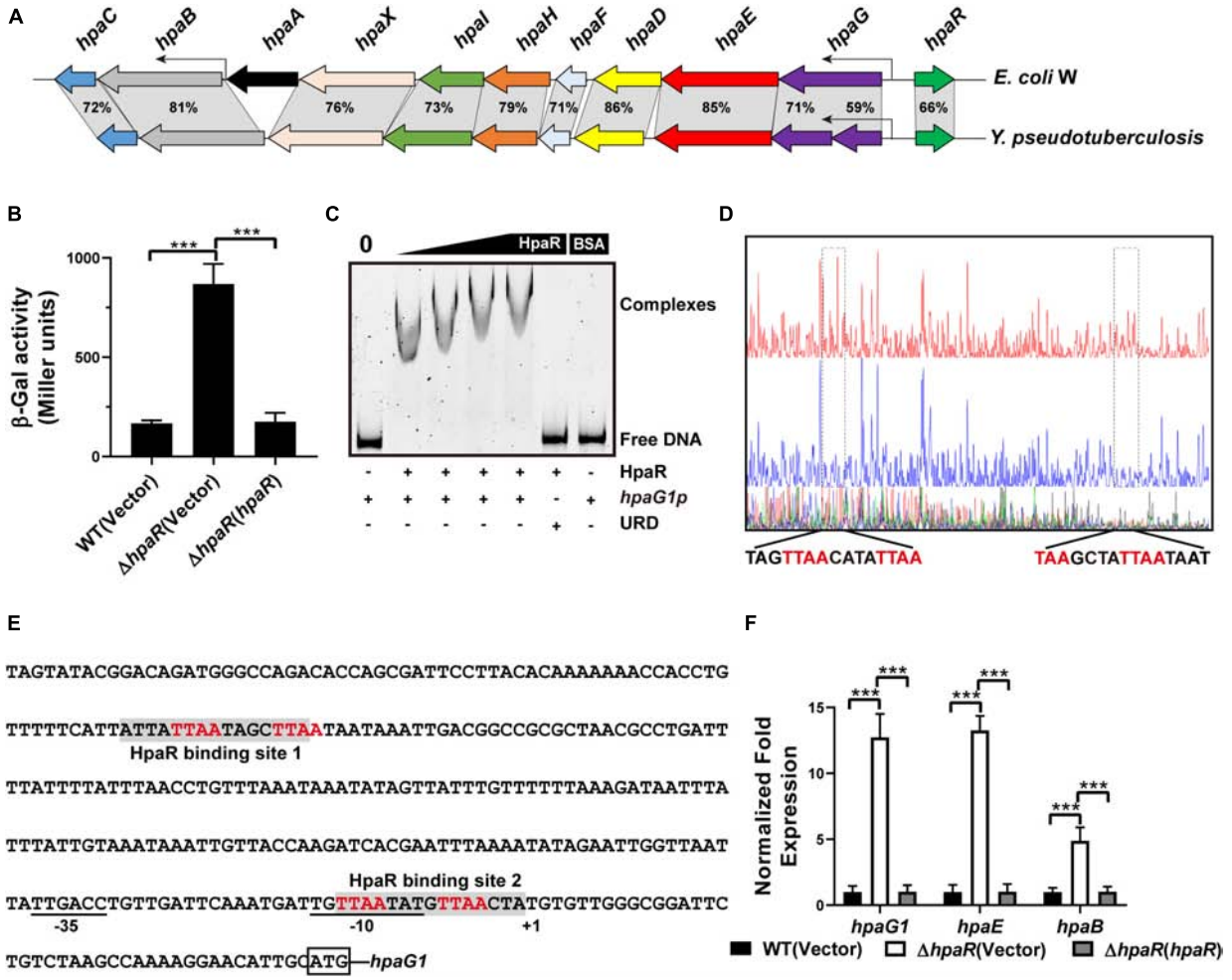

FIGURE 1 | HpaR negatively regulates *hpa-meta* operon in *Yersinia pseudotuberculosis*. **(A)** Gene organization of *hpa-meta* cluster and identities of protein sequence in *Escherichia coli* W and *Y. pseudotuberculosis*. **(B)** β-Galactosidase activity of the *hpaG1* promoter in *Y. pseudotuberculosis* Wild-type, Δ*hpaR* mutant, and its complementary strain Δ*hpaR*(*hpaR*). Data shown are the average of three independent experiments. The error bars indicate standard deviations of the average. ***$P < 0.001$. **(C)** EMSA was performed to analyze the interactions between His_6-HpaR and the *hpaG1* promoter. URD, unrelated DNA fragment. **(D)** Identification of the HpaR-binding site within the *hpaG1* promoter using the DNase I footprinting assay. Letters in red denote inverted repeat sequences. **(E)** The HpaR binding sites detected by DNase I footprinting assay were shown in the *hpaG1* promoter region by shading. Letters in red denote inverted repeat sequences. **(F)** Relative expression levels of *hpaG1*, *hpaE,* and *hpaB* were measured by quantitative RT-PCR in wild-type, Δ*hpaR* mutant, and complementary strain Δ*hpaR*(*hpaR*).

All genes (*hpaG1G2EDFHIXBC*) lay in a continuous row in the same direction as in *E. coli*. The translation products of these genes were identified as the homologs of the 4-HPA hydroxylases in *E. coli* W with high identities (**Figure 1A**). HpaBC, the HPA monooxygenase, oxidizes 4-HPA or 3-HPA to HPC. HpaD (HPC 2,3-dioxygenase), HpaE (CHMS dehydrogenase), HpaF (CHM isomerase), HpaG (OPET decarboxylase), HpaH (hydratase), and *Hpa*I (HHED aldolase) form the HPA catabolic pathway, which degrades HPC in the pyruvic acid or succinic semialdehyde pathways. The HpaR protein shares 66, 66, 48, and 34% amino acid sequence identities with identified HpaR in *E. coli* C, *E. coli* W, *P. putida* U, and *B. xenovorans* LB400, respectively (**Supplementary Figure S1**). Thus, we propose the gene cluster from *ypk_2452* to *ypk_2462* as an *hpa-meta* gene cluster in *Y. pseudotuberculosis*.

In *E. coli* W, the *meta* cleavage enzymes (HpaGEDFHI) that catabolize 4-HPA are repressed by HpaR, and the HPA monooxygenase (HpaBC) is positively regulated by HpaA (Prieto and Garcia, 1997). To verify the role of HpaR in expression of the *hpa* gene cluster in *Y. pseudotuberculosis*, a single-copy *hpaG1p:lacZ* fusion reporter was introduced into the chromosomes of wild-type, Δ*hpaR* mutant, and complemented Δ*hpaR*(*hpaR*) strains. The β-galactosidase activity of the three strains was quantitatively measured (**Figure 1B**). The deletion of *hpaR* significantly increased the activity of the *hpa* promoter, which could be fully restored by introducing a complementary plasmid expressing HpaR (**Figure 1B**). Next, we analyzed the interaction between HpaR and the putative operator with an electrophoresis mobility shift assay (EMSA). Incubation of HpaR with a probe containing the promoter of the *hpa-meta* operon

(*hpaG1p*) led to the formation of DNA–protein complexes (**Figure 1C**), which suggests direct interaction of HpaR and the *hpaG1p* promoter. DNase I footprinting analysis further revealed that the putative HpaR binding site was protected from digestion in DNA–HpaR complexes. Two HpaR-protected sites upstream of the transcriptional start site in the *hpaG1p* promoter were identified (**Figures 1D,E**). Thus, HpaR specifically recognizes an operator within the *hpa-meta* promoter, likely influencing its expression. Indeed, negative regulation of the *hpa-meta* operon by HpaR was confirmed by qRT-PCR analyses. The data indicated that the expression of *hpaG1*, *hpaE*, and *hpaB* was upregulated in Δ*hpaR*, and such an increase could be restored to wild-type levels by complementation with the expression plasmid pKT100-*hpaR* (**Figure 1F**). Overall, in *Y. pseudotuberculosis*, HpaR functions as a repressor and negatively regulates the *hpa-meta* gene cluster in a similar manner to *E. coli* W.

Genome-Wide Analysis of the Genes Regulated by HpaR

The multiple antibiotic resistance regulator (MarR) family transcriptional regulator has a variety of biological functions, including resistance to multiple antibiotics and other toxic chemicals such as organic solvents, household disinfectants, and oxidative stress agents (Alekshun and Levy, 1999; Wei et al., 2007). As a MarR family regulator, we speculate that HpaR may play other regulatory roles besides aromatic degradation. Thus, RNA sequencing (RNA-seq) was employed to detect the genes regulated by HpaR, except the *hpa-meta* gene cluster.

To identify the HpaR-dependent expression genes in *Y. pseudotuberculosis*, RNA was extracted for RNA-seq from both wild-type and Δ*hpaR* mutant strains in mid-exponential phase (SRA accession: PRJNA612340). After RNA-seq, quality control and gene expression level analysis were performed by fragments per kilobase of transcript per million mapped reads (FPKM). A total of 106 gene candidates that exhibited differential expression were found between wild-type and Δ*hpaR* mutant strains, including 57 upregulated and 49 downregulated genes (**Supplementary Table S3**). To verify the RNA-seq data, qRT-PCR analysis of 11 representative genes was conducted. The log_2-transformed values of each gene were in good agreement with the RNA-seq data (**Figure 2A**), which confirmed the credibility of the RNA-seq data. Subsequently, the functions of differentially expressed genes were identified by KEGG pathway analysis. As shown in **Figure 2B**, 17 different pathways were found in the DGE (Different Gene Expression), in which eight pathways were up-regulated and nine were down-regulated. These included degradation of aromatic compounds, metabolism, microbial metabolism in a diverse environment, purine metabolism, bacterial secretion system, and tyrosine metabolism. In the RNA-seq data, two gene clusters were found to be fully regulated by HpaR. One cluster was the *hpa-meta* operon, which was 2.3–4.56-fold upregulated in the Δ*hpaR* mutant (**Table 1**). The other was the T6SS4 gene cluster in *Y. pseudotuberculosis*. T6SS is a newly described secretion system in many Gram-negative bacteria (Bingle et al., 2008; Jani and Cotter, 2010). The RNA-seq data

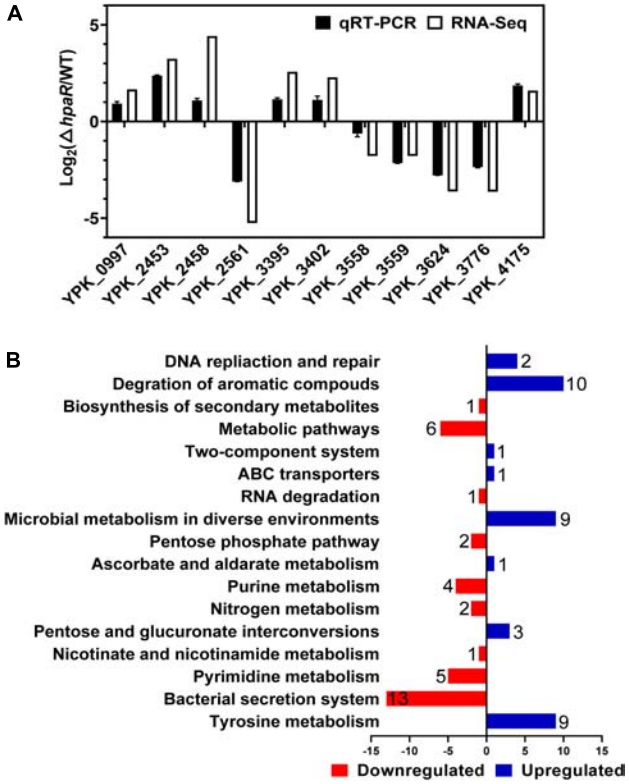

FIGURE 2 | Transcriptomics analysis of HpaR regulated genes in *Y. pseudotuberculosis*. **(A)** Validation of RNA-Seq data using qRT-PCR. Eleven representative genes were evaluated for validation of the RNA-seq data using qRT-PCR. **(B)** KEGG pathway analysis of differentially expressed genes (*hpaR* mutant VS wild-type). The red and blue bars represent up- and down-regulated genes, respectively, and the numeric labels represent the number of genes with corresponding function.

revealed that the genes in the T6SS4 operon were 0.54–0.96-fold downregulated in the Δ*hpaR* mutant (**Table 2**). Hemolysin co-regulated protein (Hcp), which forms the hexameric rings for the T6SS syringe needle, was 0.68-fold downregulated. Valine-glycine repeat protein G (VgrG) was 0.54-fold downregulated. The periplasmic domain protein IcmF was 0.62-fold downregulated. ImpA/B (VipA/VipB), which serve as tail sheath proteins in T6SS, were 0.73/0.94-fold downregulated. The same was true with other structural genes. These data suggest that the *hpa-meta* operon was negatively regulated by HpaR, consistent with the transcription of chromosomal *hpaG1p:lacZ* fusions. The data also suggest that T6SS4 is positively regulated by the transcriptional regulator HpaR.

HpaR Positively Regulates T6SS4 Expression by Directly Binding to Its Promoter

Based on the RNA-seq data, we found HpaR could positively regulate the expression of T6SS4. To further determine the role of HpaR in the expression of T6SS4, a single copy T6SS4*p:lacZ* fusion was introduced into the chromosomes of wild-type, *hpaR*

TABLE 1 | The *hpa-meta* operon genes regulated by HpaR in *Y. pseudotuberculosis*.

Locus tag	Product	Gene description	Fold change*
YPK_2452	HpaC	4-Hydroxyphenylacetate-3-monooxygenase small chain	2.31
YPK_2453	HpaB	4-Hydroxyphenylacetate-3-monooxygenase large chain	3.24
YPK_2454	HpaX	4-Hydroxyphenylacetate permease	3.37
YPK_2455	HpaI	2,4-Dihydroxyhept-2-ene-1,7-dioic acid aldolase	3.83
YPK_2456	HpaH	2-Oxo-hept-3-ene-1,7-dioate hydratase	3.91
YPK_2457	HpaF	5-Carboxymethyl-2-hydroxymuconate isomerase	4.25
YPK_2458	HpaD	3,4-Dihydroxyphenylacetate 2,3-dioxygenase	4.42
YPK_2459	HpaE	5-Carboxymethyl-2-hydroxymuconic-semialdehyde dehydrogenase	4.45
YPK_2460	HpaG2	2-Hydroxyhepta-2,4-diene-1,7-dioate isomerase	4.56
YPK_2461	HpaG1	2-Hydroxyhepta-2,4-diene-1,7-dioate isomerase	4.50

**Fold change: log_2(Δ*hpaR*/WT).*

TABLE 2 | T6SS4 genes regulated by HpaR in *Y. pseudotuberculosis*.

Locus tag	Product	Gene description	Fold change*
YPK_3550	ImpL	Type VI secretion system protein ImpL	−1.52
YPK_3551	ImpK	Type VI secretion system protein ImpK	−1.53
YPK_3552	ImpJ	Type VI secretion system protein ImpJ	−1.63
YPK_3556		Pentapeptide repeat protein	−1.74
YPK_3557		Pentapeptide repeat protein	−1.77
YPK_3558	VgrG	Type VI secretion system secreted protein VgrG	−1.78
YPK_3559	VasG	Type VI secretion system protein VasG	−1.70
YPK_3560	ImpH	Type VI secretion system protein ImpH	−1.52
YPK_3561	ImpG	Type VI secretion system protein ImpG	−1.79
YPK_3564	ImpC	Type VI secretion system protein ImpC	−1.77
YPK_3565	ImpB	Type VI secretion system protein ImpB	−1.69
YPK_3566	ImpA	Type VI secretion system protein ImpA	−1.90

**Fold change: log_2(Δ*hpaR*/WT).*

mutant, and complemented Δ*hpaR*(*hpaR*) strains and LacZ activity of the resulting strains was quantitatively measured (**Figure 3A**). Compared to the wild-type strain, the T6SS4*p:lacZ* fusion was decreased significantly in Δ*hpaR*; this decrease could be restored by the complementary plasmid (pKT100-*hpaR*). This suggests that HpaR positively regulates T6SS4 expression. To test whether the T6SS4 gene clusters were regulated by HpaR directly, the interaction between HpaR and the T6SS4 promoter was examined by EMSA. Incubation of a probe containing the T6SS4 promoter with HpaR led to the formation of DNA–protein complexes (**Figure 3C**). DNase I footprinting analysis revealed that the binding site was protected from digestion in DNA–HpaR complexes, further indicating the recognition of this DNA element by HpaR (**Figure 3D**). An HpaR-protected site (CCTCTTATTTTGGCTATTCATCCACGTCATCGTGCTA) upstream of the -35 and -10 elements was identified (**Figure 3E**).

The interactions between HpaR and the T6SS4 promoter appeared to be site-specific, as mutation of the HpaR binding site in the T6SS4 promoter prevented formation of the protein–DNA complex (**Figure 3C**) and abolished HpaR dependent T6SS4 regulation (**Figure 3B**). The positive regulation of T6SS4 by HpaR was further confirmed by qRT-PCR analysis (**Figure 3F**). The data indicated that the expression of T6SS4 components *clpV4*, *hcp4*, and *vgrG4* were reduced in Δ*hpaR*, which could be restored by plasmid (pKT100-*hpaR*). Thus, HpaR recognizes and binds to the promoter of T6SS4 specifically to activate expression.

HpaR Affects the Antioxidant Activity of *Y. pseudotuberculosis* by Regulating T6SS4

In our previous study, T6SS4 of *Y. pseudotuberculosis* was discovered to play important roles in multiple stress defenses, especially oxidative stress (Wang et al., 2015). The regulation of T6SS4 by HpaR prompted us to examine whether HpaR plays a role in oxidative stress resistance via T6SS4. To test the hypothesis that HpaR exerts antioxidant activity by regulating T6SS4, the survival rate and ROS level in cells treated with cumene hydroperoxide (CHP) or hydrogen peroxide (H_2O_2) were measured. After incubation with CHP, approximately 60% of wild-type cells survived. The survival rate of the mutant lacking *hpaR* decreased to 16%, and a 13% survival rate was observed for the double mutant Δ*hpaR*Δ*clpV4*. Expressing HpaR could fully rescue such a decrease in the Δ*hpaR*, but only increased the survival rate slightly in the double mutant Δ*hpaR*Δ*clpV4* (**Figure 4A**). The ROS level under oxidative stress was also examined using CM-H_2DCFDA fluorescent dye. The data showed that the ROS level in Δ*hpaR* and Δ*hpaR*Δ*clpV4*

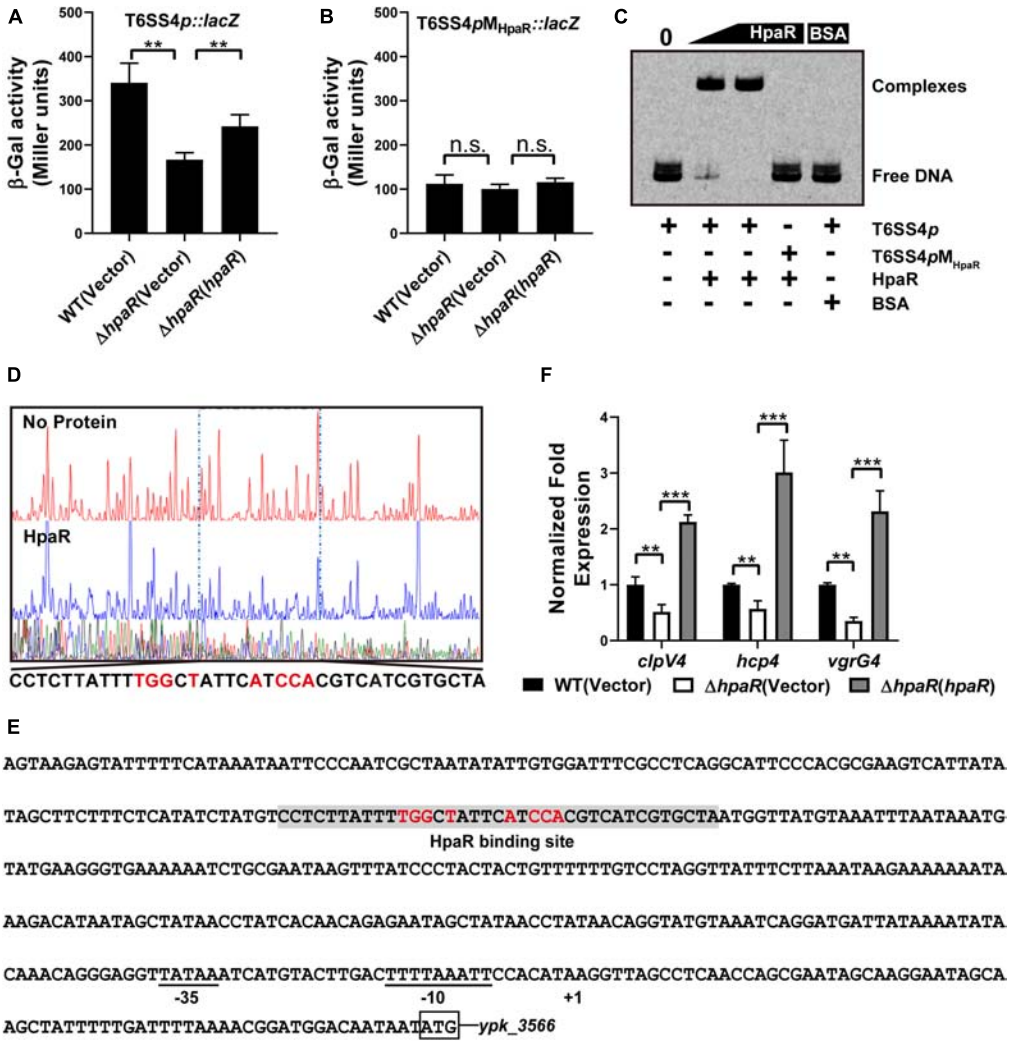

FIGURE 3 | HpaR positively regulates the T6SS4 expression in *Y. pseudotuberculosis*. β-galactosidase activity of the T6SS4 promoter **(A)** and T6SS4 promoter with mutations in the HpaR binding site **(B)** in *Y. pseudotuberculosis* Wild-type, Δ*hpaR* mutant, and its complementary strain Δ*hpaR*(*hpaR*). Data shown are the average of three independent experiments. The error bars indicate standard deviations of the average. $^{**}P < 0.01$; n.s., not significant. **(C)** EMSA was performed to analyze the interactions between His_6-HpaR and the T6SS4 promoter (T6SS4*p*) or the promoter mutant identified His_6-HpaR binding region (T6SS4*pM*$_{HpaR}$). **(D)** Identification of the HpaR-binding site within the T6SS4 promoter using the DNase I footprinting assay. Letters in red denote inverted repeat sequences. **(E)** The HpaR binding site detected by DNase I footprinting assay were shown in the T6SS4 promoter region by shading. Letters in red denote inverted repeat sequences. **(F)** Relative expression levels of *clpV4*, *hcp4,* and *vgrG4* were measured by qRT-PCR. The error bars indicate the standard deviation from three independent experiments. $^{***}P < 0.001$; $^{**}P < 0.01$.

was higher than the wild-type strain. Complementation with the plasmid pKT100-*hpaR* could reduce the ROS level in Δ*hpaR*, but not in the Δ*hpaR*Δ*clpv4* double mutant (**Figure 4B**). Similar results were obtained with H_2O_2 treatment (**Figures 4C,D**). T6SS4 could secrete the zinc-binding protein YezP for zinc import in *Y. pseudotuberculosis* (Wang et al., 2015). Thus, YezP-VSVG was expressed in relevant *Y. pseudotuberculosis* strains to test the secretion of YezP. Significant amounts of YezP-VSVG could be readily detected in culture supernatant from wild-type bacteria. The secretion of YezP decreased by 32% in the Δ*hpaR* mutant and was completely restored in a mutant complemented with HpaR (**Figure 4E**). The zinc contents in bacteria challenged with H_2O_2 were measured using inductively coupled plasma mass spectrometry (ICP-MS). The results revealed that the deletion of *hpaR* significantly lowered the intracellular Zn^{2+} level and expression of HpaR restored the defects (**Figure 4F**). These results established that HpaR benefited *Y. pseudotuberculosis* resisting oxidative stress by upregulating T6SS4.

HpaR Contributes to Biofilm Formation and Adhesion to Epithelial Cells

Similar to other Gram-negative bacteria, *Y. pseudotuberculosis* is capable of forming biofilms on abiotic surfaces. The biofilm formation ability of wild-type, Δ*hpaR* mutant, and complemented Δ*hpaR*(*hpaR*) strains were observed in a test tube

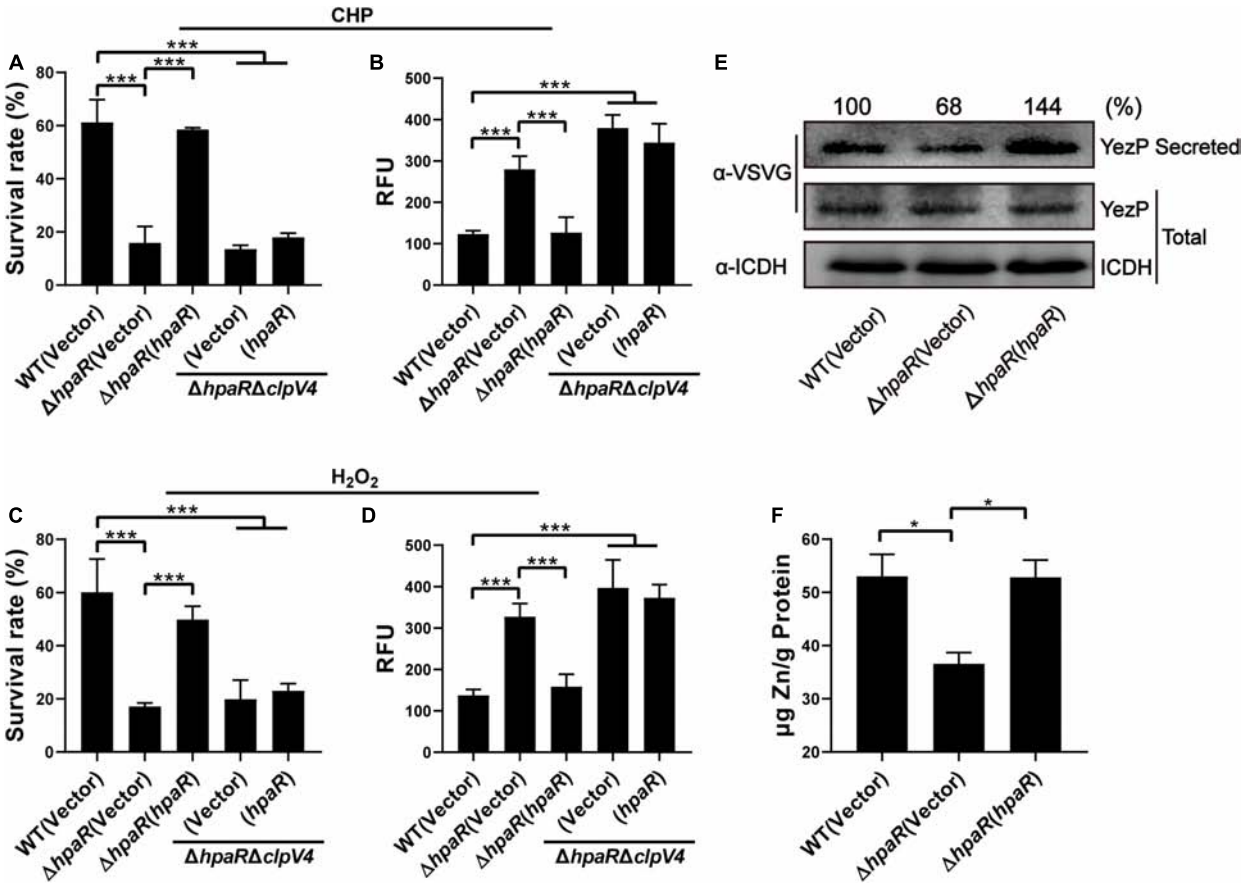

FIGURE 4 | HpaR plays a role in resisting oxidative stress via T6SS4. Survival rate of indicated *Y. pseudotuberculosis* strains were determined after treatment with CHP **(A)** or H_2O_2 **(C)** for 1 h. **(B,D)** Intracellular ROS of indicated strains were stained with H_2DCFDA dye (Invitrogen) and fluorescence signals were measured using a SpectraMax M2 Plate Reader (Molecular Devices) with excitation/emission wavelengths of 495/520. **(E)** Western blot detection of YezP secretion in *Y. pseudotuberculosis* wild-type, Δ*hpaR* mutant, and its complementary strain Δ*hpaR*(*hpaR*). Proteins in culture supernatant of relevant *Y. pseudotuberculosis* strains expressing YezP-VSVG were probed for VSVG (upper) by immunoblotting. **(F)** Mid-exponential phase of *Y. pseudotuberculosis* strains were exposed to 1.5 mM H_2O_2 for 30 min in PBS containing 1 μM $ZnCl_2$. Zn^{2+} associated with bacterial cells was measured by inductively coupled plasma mass spectrometry (ICP-MS). Data shown are the average of three independent experiments. The error bars indicate the standard deviation from three independent experiments. $^{***}P < 0.001$; $^{**}P < 0.01$; $^{*}P < 0.05$.

by staining with crystal violet (**Figure 5A**) and quantified by resolving with 95% ethanol and measuring the absorbance at 595 nm (**Figure 5B**). The Δ*hpaR* mutant showed attenuated biofilm formation when compared to wild-type and the decrease could be restored by expressing *hpaR*. Note that there's no significant difference between the growth activities of these strains (**Supplementary Figure S2**). Biofilm formation plays an important role in the pathogen lifecycle. It is imperative in chronic infection, antibiotic resistance, and adhesion to host cells. Thus, ampicillin and gentamicin, two commonly used antibiotics in clinics, were used to verify viability of the *hpaR* mutant in antibiotic resistance. The survival rates of the Δ*hpaR* strain were only 34 and 18% following gentamicin and ampicillin treatment, respectively, while approximately 72 and 51% of wild-type cells survived under the same conditions (**Figure 5C**). This suggests that the Δ*hpaR* mutant was more sensitive to antibiotics than the wild-type. Adhesion to host cells is a crucial step in the infection process and host colonization. Thus, the adherence of wild-type, *hpaR* mutant, and complemented strains to HeLa cells was evaluated. As shown in **Figure 5D**, the Δ*hpaR* strain had fewer adherences to HeLa cells than wild-type. Overall, *hpaR* may assist in the maintenance of biofilm formation activity, antibiotic resistance, and adhesion to eukaryotic cells.

Y. pseudotuberculosis Mutant Lacking *hpaR* Is Defective in Virulence in Mice

Biofilm formation is helpful for the survival and colonization of *Y. pseudotuberculosis* in hosts. In addition, oxidative burst is an important microbial-killing mechanism in phagocytes. The findings that HpaR affects the antioxidant activity, biofilm formation and the ability of adhesion to eukaryotic cells point to its role in the virulence of *Y. pseudotuberculosis.* To examine this, C57BL/6 mice were inoculated orogastrically with relevant bacterial strains. Wild-type bacteria caused more than 90% lethality within 3 weeks of inoculation. By contrast,

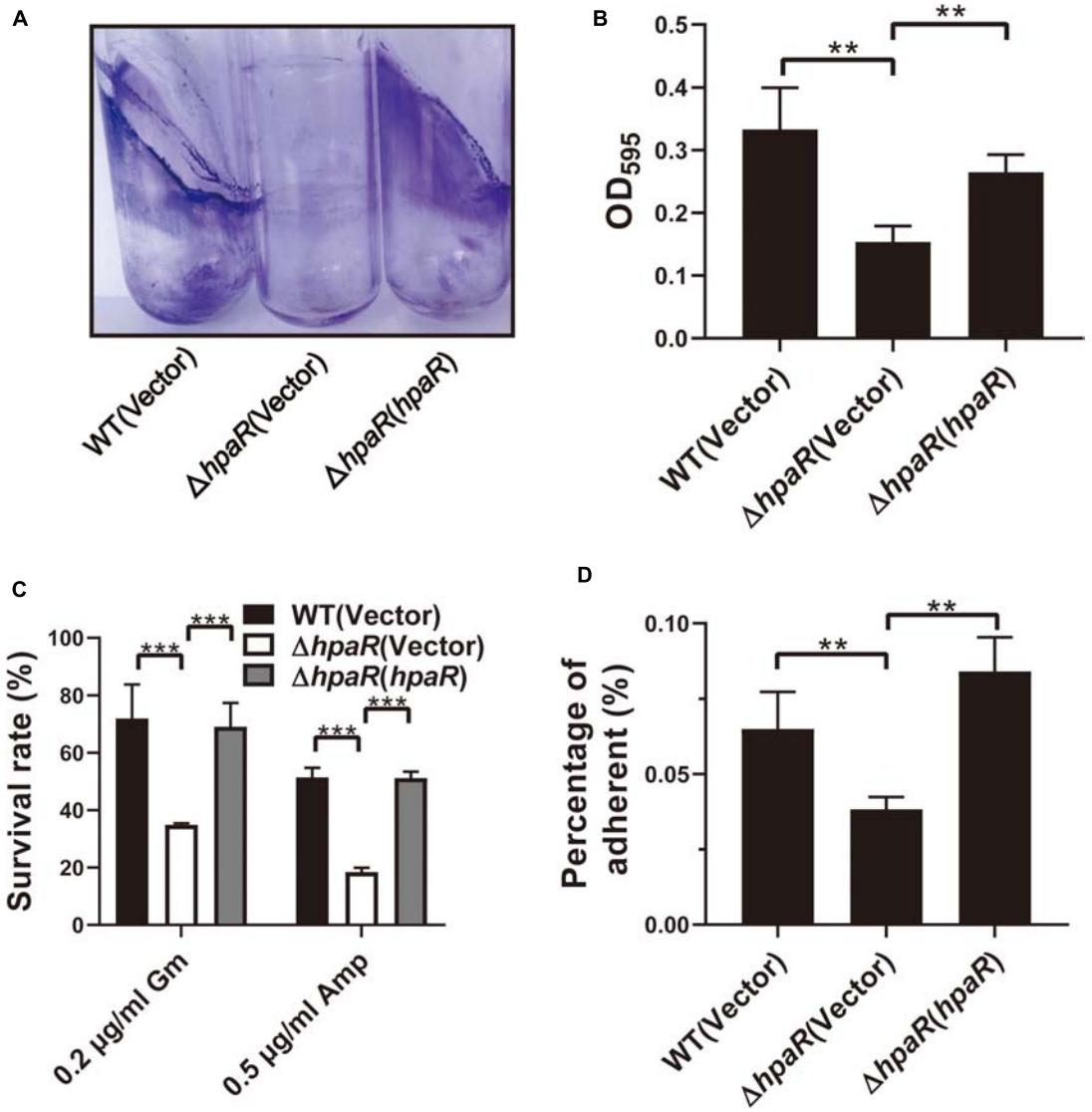

FIGURE 5 | HpaR is involved in biofilm formation, antibiotic resistance and adhesion to eukaryotic cells. **(A)** Direct observation of *Y. pseudotuberculosis* biofilm formation by Wild-type, Δ*hpaR* mutant, and its complementary strain Δ*hpaR* (*hpaR*). The results shown the biofilm biomass stained with crystal violet in glass test tubes. **(B)** Quantitative measurement of biofilm formation by resolving in 95% ethanol and measuring the absorbance at OD_{595}. **(C)** The survival rate of Wild-type, Δ*hpaR* mutant, and its complementary strain Δ*hpaR* (*hpaR*) under 0.2 μg/ml gentamicin (Gm) or 0.5 μg/ml ampicillin (Amp) treatment. **(D)** Adhesion of the strains to HeLa cells. Adherence level is expressed as the percentage of adherent bacteria relative to the inoculum count. Data shown are the average of three independent experiments; the error bars indicate the standard deviation from three independent experiments. $^{***}P < 0.001$; $^{**}P < 0.01$; $^{*}P < 0.05$; n.s., not significant.

consistent with the hypothesis, mice infected with mutants lacking *hpaR* or T6SS4 had better survival rates than the wild-type (**Figure 6**). The data indicate that *hpaR* affects the virulence of *Y. pseudotuberculosis* in the infection of mammalian hosts.

DISCUSSION

MarR family transcriptional regulators are widely distributed in bacteria and archaea (Perez-Rueda and Collado-Vides, 2001; Perez-Rueda et al., 2004). They play crucial roles in the bacterial lifecycle as they control various genes involved in antibiotic resistance, aromatic compound catabolism, oxidative stress responses, and produce of virulence factors (Alekshun and Levy, 1999; Fiorentino et al., 2007; Deochand and Grove, 2017). Some of these regulators are involved in the degradation of specific aromatic compounds (Diaz and Prieto, 2000). For example, BadR in *Rhodopseudomonas palustris* regulates anaerobic benzoate degradation in cooperation with AadR (Egland and Harwood, 1999). In *Comamonas testosteroni* BR60, CbaR controls the *cbaABC* operon for converting 3-chlorobenzoate to protocatechuate (PCA) and 5-Cl-PCA (Providenti and Wyndham, 2001). HpaR was first identified in *E. coli* W (Roper et al., 1993). As a repressor, HpaR regulates

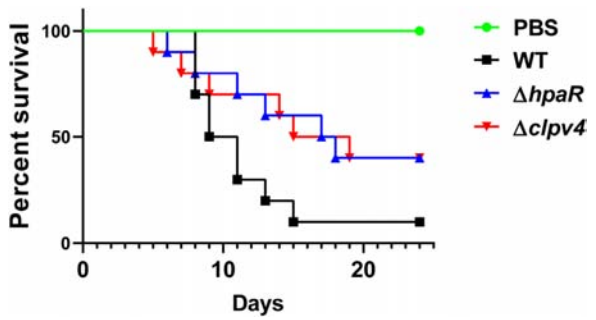

FIGURE 6 | Yptb mutants lacking *hpaR* or T6SS4 are defective in virulence against mice. Bacterial strains grown in YLB were washed twice in sterilized PBS and used for orogastric infection of 6–8 weeks old female C57BL/6 mice using a ball-tipped feeding needle. For survival assays 3×10^9 bacteria of each strain were applied to different groups of mice (n = 10/strain), and the survival rate of the mice was determined by monitoring the survival daily for 24 days.

the *hpa-meta* operon in 4-HPA catabolism (Prieto et al., 1996; Galan et al., 2003). However, whether HpaR has other functions remains unclear. Here, we report that in *Y. pseudotuberculosis*, HpaR acts as a dual-functional regulator. It not only negatively regulates the *hpa-meta* cluster but also positively controls T6SS4 expression to resist oxidative stress, which maintains cellular ROS levels.

The *hpa-meta* cluster in *E. coli* W is composed of 11 genes within two operons, *hpaBC* and *hpaGEDFHI,* which are controlled by HpaA and HpaR, respectively (Galan et al., 2001). Based on sequence alignment with *E. coli* W, we identified the *hpa-meta* cluster in *Y. pseudotuberculosis*. An HpaA homolog was not identified in *Y. pseudotuberculosis*. The *hpa-meta* cluster of one operon consisted of 11 genes, *hpaG1G2EDFHIXBC,* and one regulator, HpaR (**Figure 1A**). Using a β-galactosidase activity assay and qRT-PCR, we revealed that HpaR represses expression of the *hpaG1G2EDFHIXBC* operon in *Y. pseudotuberculosis*, similar to *E. coli* W. HpaR binding sites 1 and 2, both composed of a 15 bp region, were identified on the *hpaG1* promoter containing a palindromic sequence of 4 bp (TTAA-XXXX-TTAA) on each side separated by 4 bp similar to *E. coli* W (**Figure 1E**). Site 1 was located -189 bp relative to the transcription start site + 1 of the *hpaG1* promote. Site 2 was centered at position -8 of the *hpaG1* promoter, overlapping the -10 element, which implies that HpaR inhibits the binding of RNA polymerase on the promoter to repress transcription of the *hpa-meta* cluster.

So far HpaR was specifically recognized as a repressor of the 4-HPA catabolic pathway (Galan et al., 2003; Arcos et al., 2010; Mendez et al., 2011). Unexpectedly, in the RNA-seq based transcriptomics analysis we found that in addition to the *hpa-meta* cluster genes, genes of the T6SS4 cluster were also found to be regulated by HpaR. Based on the β-galactosidase activity assay and qRT-PCR results, we confirmed that HpaR acts as an activator rather than a repressor to regulate T6SS4 (**Figure 3A**). We also identified the HpaR binding site on the T6SS4 promoter located -241 bp relative to the transcription start site + 1 of the T6SS4 promote, containing an imperfect invert sequence TGGXT-XXXX-AXCCA on each side separated by 4 bp (**Figure 3E**). The HpaR binding site of *hpaG1* and T6SS4 promoter both contain a 4–5 bp palindromic sequence on each side separated by 4 bp but the site on T6SS4 promoter is imperfect. The binding site of T6SS4 promoter is far from the

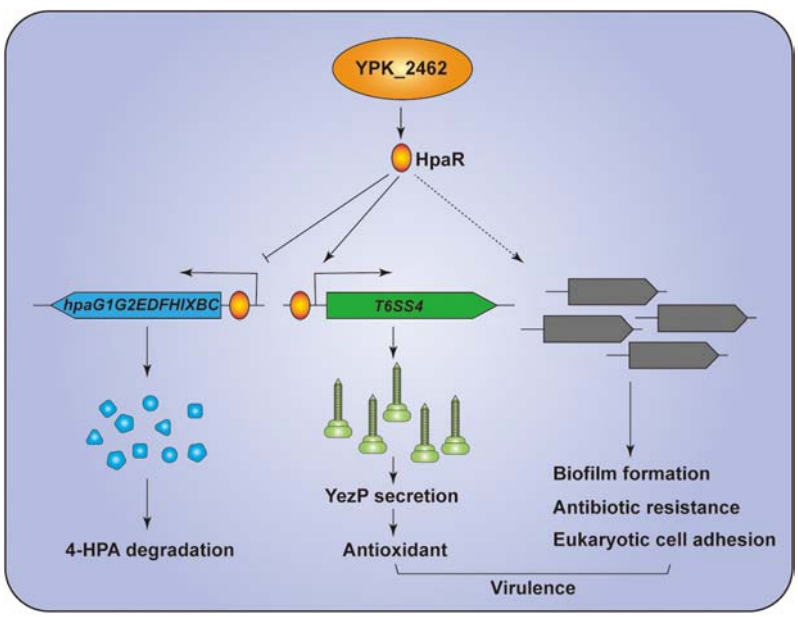

FIGURE 7 | Hypothetical model for the function of HpaR in *Y. pseudotuberculosis*. HpaR represses the 4-HPA catabolic pathway but activates the transcription of T6SS4 to maintain ROS levels in response to oxidative stress. HpaR also affects the biofilm formation, eukaryotic cell adhension, antibiotic resistance, and virulence of *Y. pseudotuberculosis*.

transcription start site. Besides, the GC content of binding site on T6SS4 promoter is higher than that on *hpaG1* promoter. We presume that HpaR may bind to the stable site upstream of the -35 and -10 elements recruiting RNA polymerase to activate the transcription of T6SS4.

T6SS has been recognized as an anti-bacterial weapon to attack target cells in a contact-dependent manner (Durand et al., 2014; Ho et al., 2014; Russell et al., 2014). However, our previous report showed that the T6SS4 in *Y. pseudotuberculosis* is related to resistance to multiple environmental stresses, including high osmolarity, low pH, and oxidative stress (Song et al., 2015; Wang et al., 2015). We therefore speculated that HpaR might protect against oxidative stress via T6SS4. And we confirmed this by observing the survival rate and determining the intracellular ROS levels of wild-type and mutant strains under oxidative stress (**Figures 4A–D**). *Y. pseudotuberculosis* could import Zn^{2+} via secretion of YezP through T6SS4 to maintain intracellular ROS levels (Wang et al., 2015). Our results showed that the levels of YezP secreted by T6SS4 and the intracellular Zn^{2+} levels of Δ*hpaR* were also decreased under H_2O_2 stress (**Figures 4E,F**), indicating that HpaR regulates the expression of T6SS4 to resist oxidative stress.

Biofilm formation was also affected by HpaR (**Figures 5A,B**). However, no other biofilm-related gene was found to be differentially expressed in the RNA-seq results. Biofilm formation is complex—it may be indirectly regulated by other mechanisms that will require further investigation. Biofilm formation is beneficial to bacterial survival in a harmful environment and is associated with adhesion to eukaryotic cells (Flemming and Wingender, 2010; Hall and Mah, 2017). Our results also showed that HpaR was involved in antibiotic resistance and adhered to HeLa cells (**Figures 5C,D**). *Y. pseudotuberculosis* is an enteric pathogen of animals and humans (Smego et al., 1999). In host cells, the oxidative burst is an important method to kill bacteria and biofilm formation is essential for bacterial infection (Flemming and Wingender, 2010; Slauch, 2011). Besides, the adhesion to host cell is also crucial for bacterial colonization. It has been shown that T6SS4 is required for *Y. pseudotuberculosis* virulence in a mouse model (Wang et al., 2015). This work revealed that HpaR also plays important roles in virulence and biofilm formation, potentially also via regulation of T6SS4.

In summary, we revealed that HpaR is a dual-functional regulator in *Y. pseudotuberculosis*. HpaR not only represses expression of genes of the 4-HPA catabolic pathway but also activates the transcription of T6SS4 to acquire Zn^{2+} to maintain ROS levels in response to oxidative stress. Biofilm formation, antibiotic resistance, eukaryotic cell adhesion, and bacterial virulence were also affected by *hpaR* (**Figure 7**). This study has greatly expanded the function of HpaR beyond the regulation of aromatic compound catabolism and revealed a new pathway to regulate T6SS4 in response to environmental stress.

DATA AVAILABILITY STATEMENT

The datasets generated for this study can be found in the RNA-seq data was deposited in SRA (SRA accession: PRJNA612340).

ETHICS STATEMENT

All mice were maintained and handled in accordance with the Regulations for the Administration of Affairs Concerning Experimental Animals approved by the State Council of People's Republic of China. The protocol was approved by the Animal Welfare and Research Ethics Committee of Northwest A&F University (protocol number: NWAFUSM2018001).

AUTHOR CONTRIBUTIONS

ZW, TW, YY, and XS conceived the study, designed the experiments, analyzed the data, and wrote the manuscript. ZW, TW, RC, ZZ, KC, ML, YH, HG, LX, and YW performed the experimental work.

FUNDING

This work was supported by the grant of National Key R&D Program of China (2018YFA0901200 to XS), the National Natural Science Foundation of China (31670053 and 31725003 to XS and, 31970114 and 31671292 to YW), the Open Project Program of the State Key Laboratory of Pathogen and Biosecurity (SKLPBS1825 to XS). LX was supported by China Postdoctoral Science Foundation (2018M631201) and Shaanxi Postdoctoral Science Foundation (2018BSHTDZZ20).

ACKNOWLEDGMENTS

We thank the Teaching and Research Core Facility at College of Life Sciences, NWAFU for their support in this work.

SUPPLEMENTARY MATERIAL

The Supplementary Material for this article can be found online at: https://www.frontiersin.org/articles/10.3389/fmicb.2020.00705/full#supplementary-material

FIGURE S1 | Protein sequence alignment of HpaR homologs by CLUSTAL W. The sequences used in alignment have been deposited in the GenBank database [Accession No. EcC *Escherichia coli* C (S56952.1), EcW *Escherichia coli* W (Z37980.2), Yptb *Yersinia pseudotuberculosis* YPIII (ACA68739.1), PpU *Pseudomonas putida* U (FJ904934.1), BxLB400 *Burkholderia xenovorans* LB400 (ABE33958.1)]. The result was exported by ESPript (http://espript.ibcp.fr/ESPript/cgi-bin/ESPript.cgi).

FIGURE S2 | Growth curves of the wild-type (WT), Δ*hpaR* mutant, and the complemented strain Δ*hpaR* (*hpaR*) under normal condition. The growth of the indicated strains in YLB medium was monitored by measuring OD_{600} at indicated time points under 26°C.

TABLE S1 | The strains and plasmids used in this study.

TABLE S2 | Primers used in this study.

TABLE S3 | Genes differentially transcribed in Δ*hpaR* mutant compared to the *Y. pseudotuberculosis* wild-type detected by RNA-seq.

REFERENCES

Alekshun, M. N., and Levy, S. B. (1999). The mar regulon: multiple resistance to antibiotics and other toxic chemicals. *Trends Microbiol.* 7, 410–413. doi: 10.1016/s0966-842x(99)01589-1589

Alekshun, M. N., Levy, S. B., Mealy, T. R., Seaton, B. A., and Head, J. F. (2001). The crystal structure of MarR, a regulator of multiple antibiotic resistance, at 2.3 A resolution. *Nat. Struct. Biol.* 8, 710–714. doi: 10.1038/90429

Arcos, M., Olivera, E. R., Arias, S., Naharro, G., and Luengo, J. M. (2010). The 3,4-dihydroxyphenylacetic acid catabolon, a catabolic unit for degradation of biogenic amines tyramine and dopamine in *Pseudomonas putida* U. *Environ. Microbiol.* 12, 1684–1704. doi: 10.1111/j.1462-2920.2010.02233.x

Barbour, M. G., and Bayly, R. C. (1981). Control of meta-cleavage degradation of 4-hydroxyphenylacetate in *Pseudomonas putida*. *J. Bacteriol.* 147, 844–850. doi: 10.1128/jb.147.3.844-850.1981

Basler, M. (2015). Type VI secretion system: secretion by a contractile nanomachine. *Philos. Trans. R. Soc. Lond. B Biol. Sci.* 370, 1679. doi: 10.1098/rstb.2015.0021

Bingle, L. E., Bailey, C. M., and Pallen, M. J. (2008). Type VI secretion: a beginner's guide. *Curr. Opin. Microbiol.* 11, 3–8. doi: 10.1016/j.mib.2008.01.006

Brubaker, R. R. (1991). Factors promoting acute and chronic diseases caused by yersiniae. *Clin. Microbiol. Rev.* 4, 309–324. doi: 10.1128/cmr.4.3.309

Cooper, R. A., and Skinner, M. A. (1980). Catabolism of 3- and 4-hydroxyphenylacetate by the 3,4-dihydroxyphenylacetate pathway in *Escherichia coli*. *J. Bacteriol.* 143, 302–306. doi: 10.1128/jb.143.1.302-306.1980

D'Autreaux, B., and Toledano, M. B. (2007). ROS as signalling molecules: mechanisms that generate specificity in ROS homeostasis. *Nat. Rev. Mol. Cell Biol.* 8, 813–824. doi: 10.1038/nrm2256

Deochand, D. K., and Grove, A. (2017). MarR family transcription factors: dynamic variations on a common scaffold. *Crit. Rev. Biochem. Mol. Biol* 52, 595–613. doi: 10.1080/10409238.2017.1344612

Diaz, E., and Prieto, M. A. (2000). Bacterial promoters triggering biodegradation of aromatic pollutants. *Curr. Opin. Biotechnol.* 11, 467–475. doi: 10.1016/s0958-1669(00)00126-129

Durand, E., Cambillau, C., Cascales, E., and Journet, L. (2014). VgrG, Tae, Tle, and beyond: the versatile arsenal of Type VI secretion effectors. *Trends Microbiol.* 22, 498–507. doi: 10.1016/j.tim.2014.06.004

Egland, P. G., and Harwood, C. S. (1999). BadR, a new MarR family member, regulates anaerobic benzoate degradation by Rhodo *Pseudomonas palustris* in concert with AadR, an Fnr family member. *J. Bacteriol.* 181, 2102–2109. doi: 10.1128/jb.181.7.2102-2109.1999

Fallman, M., and Gustavsson, A. (2005). Cellular mechanisms of bacterial internalization counteracted by Yersinia. *Int. Rev. Cytol.* 246, 135–188. doi: 10.1016/S0074-7696(05)46004-46000

Fiorentino, G., Ronca, R., Cannio, R., Rossi, M., and Bartolucci, S. (2007). MarR-like transcriptional regulator involved in detoxification of aromatic compounds in *Sulfolobus solfataricus*. *J. Bacteriol.* 189, 7351–7360. doi: 10.1128/JB.00885-887

Flemming, H. C., and Wingender, J. (2010). The biofilm matrix. *Nat. Rev. Microbiol.* 8, 623–633. doi: 10.1038/nrmicro2415

Galan, B., Diaz, E., Prieto, M. A., and Garcia, J. L. (2000). Functional analysis of the small component of the 4-hydroxyphenylacetate 3-monooxygenase of *Escherichia coli* W: a prototype of a new Flavin:NAD(P)H reductase subfamily. *J. Bacteriol.* 182, 627–636. doi: 10.1128/jb.182.3.627-636.2000

Galan, B., Kolb, A., Garcia, J. L., and Prieto, M. A. (2001). Superimposed levels of regulation of the 4-hydroxyphenylacetate catabolic pathway in *Escherichia coli*. *J. Biol. Chem.* 276, 37060–37068. doi: 10.1074/jbc.M103033200

Galan, B., Kolb, A., Sanz, J. M., Garcia, J. L., and Prieto, M. A. (2003). Molecular determinants of the hpa regulatory system of *Escherichia coli*: the HpaR repressor. *Nucleic Acids Res.* 31, 6598–6609. doi: 10.1093/nar/gkg851

Green, E. R., Clark, S., Crimmins, G. T., Mack, M., Kumamoto, C. A., and Mecsas, J. (2016). Fis is essential for yersinia pseudotuberculosis virulence and protects against reactive oxygen species produced by phagocytic cells during infection. *PLoS Pathog.* 12:e1005898. doi: 10.1371/journal.ppat.1005898

Grove, A. (2013). MarR family transcription factors. *Curr. Biol.* 23, R142–R143. doi: 10.1016/j.cub.2013.01.013

Guan, J., Xiao, X., Xu, S., Gao, F., Wang, J., Wang, T., et al. (2015). Roles of RpoS in *Yersinia pseudotuberculosis* stress survival, motility, biofilm formation and type VI secretion system expression. *J. Microbiol.* 53, 633–642. doi: 10.1007/s12275-015-0099-96

Hall, C. W., and Mah, T. F. (2017). Molecular mechanisms of biofilm-based antibiotic resistance and tolerance in pathogenic bacteria. *FEMS Microbiol. Rev.* 41, 276–301. doi: 10.1093/femsre/fux010

Ho, B. T., Dong, T. G., and Mekalanos, J. J. (2014). A view to a kill: the bacterial type VI secretion system. *Cell Host Microb.* 15, 9–21. doi: 10.1016/j.chom.2013.11.008

Huang, Y., Zhao, K. X., Shen, X. H., Jiang, C. Y., and Liu, S. J. (2008). Genetic and biochemical characterization of a 4-hydroxybenzoate hydroxylase from *Corynebacterium glutamicum*. *Appl. Microbiol. Biotechnol.* 78, 75–83. doi: 10.1007/s00253-007-1286-1280

Jani, A. J., and Cotter, P. A. (2010). Type VI secretion: not just for pathogenesis anymore. *Cell Host Microb.* 8, 2–6. doi: 10.1016/j.chom.2010.06.012

Lin, J., Zhang, W., Cheng, J., Yang, X., Zhu, K., Wang, Y., et al. (2017). A *Pseudomonas* T6SS effector recruits PQS-containing outer membrane vesicles for iron acquisition. *Nat. Commun.* 8:14888. doi: 10.1038/ncomms14888

Ma, J., Bao, Y., Sun, M., Dong, W., Pan, Z., Zhang, W., et al. (2014). Two functional type VI secretion systems in avian pathogenic *Escherichia coli* are involved in different pathogenic pathways. *Infect. Immun.* 82, 3867–3879. doi: 10.1128/IAI.01769-1714

Mendez, V., Agullo, L., Gonzalez, M., and Seeger, M. (2011). The homogentisate and homoprotocatechuate central pathways are involved in 3- and 4-hydroxyphenylacetate degradation by *Burkholderia xenovorans* LB400. *PLoS One* 6:e17583. doi: 10.1371/journal.pone.0017583

Miller, J. H. (1992). *A Short Course in Bacterial Genetics - A Laboratory Manual and Handbook for Escherichia coli and Related Bacteria*. Cold Spring Harbor, NY: Cold Spring Harbor Laboratory Press.

Navarro-Garcia, F., Ruiz-Perez, F., Cataldi, A., and Larzabal, M. (2019). Type VI secretion system in pathogenic *Escherichia coli*: structure, role in virulence, and acquisition. *Front. Microbiol.* 10:1965. doi: 10.3389/fmicb.2019.01965

Perez-Rueda, E., and Collado-Vides, J. (2001). Common history at the origin of the position-function correlation in transcriptional regulators in archaea and bacteria. *J. Mol. Evol.* 53, 172–179. doi: 10.1007/s002390010207

Perez-Rueda, E., Collado-Vides, J., and Segovia, L. (2004). Phylogenetic distribution of DNA-binding transcription factors in bacteria and archaea. *Comput. Biol. Chem.* 28, 341–350. doi: 10.1016/j.compbiolchem.2004.09.004

Prieto, M. A., Diaz, E., and Garcia, J. L. (1996). Molecular characterization of the 4-hydroxyphenylacetate catabolic pathway of *Escherichia coli* W: engineering a mobile aromatic degradative cluster. *J. Bacteriol.* 178, 111–120. doi: 10.1128/jb.178.1.111-120.1996

Prieto, M. A., and Garcia, J. L. (1994). Molecular characterization of 4-hydroxyphenylacetate 3-hydroxylase of *Escherichia coli*. A two-protein component enzyme. *J. Biol. Chem.* 269, 22823–22829.

Prieto, M. A., and Garcia, J. L. (1997). Identification of a novel positive regulator of the 4-hydroxyphenylacetate catabolic pathway of *Escherichia coli*. *Biochem. Biophys. Res. Commun.* 232, 759–765. doi: 10.1006/bbrc.1997.6368

Providenti, M. A., and Wyndham, R. C. (2001). Identification and functional characterization of CbaR, a MarR-like modulator of the cbaABC-encoded chlorobenzoate catabolism pathway. *Appl. Environ. Microbiol.* 67, 3530–3541. doi: 10.1128/AEM.67.8.3530-3541.2001

Roper, D. I., Fawcett, T., and Cooper, R. A. (1993). The *Escherichia coli* C homoprotocatechuate degradative operon: hpc gene order, direction of transcription and control of expression. *Mol. Gen. Genet.* 237, 241–250. doi: 10.1007/bf00282806

Russell, A. B., Peterson, S. B., and Mougous, J. D. (2014). Type VI secretion system effectors: poisons with a purpose. *Nat. Rev. Microbiol.* 12, 137–148. doi: 10.1038/nrmicro3185

Shen, X., Banga, S., Liu, Y., Xu, L., Gao, P., Shamovsky, I., et al. (2009). Targeting eEF1A by a *Legionella pneumophila* effector leads to inhibition of protein synthesis and induction of host stress response. *Cell Microbiol.* 11, 911–926. doi: 10.1111/j.1462-5822.2009.01301.x

Shen, X. H., Jiang, C. Y., Huang, Y., Liu, Z. P., and Liu, S. J. (2005). Functional identification of novel genes involved in the glutathione-independent gentisate pathway in *Corynebacterium glutamicum*. *Appl. Environ. Microbiol.* 71, 3442–3452. doi: 10.1128/AEM.71.7.3442-3452.2005

Si, M., Wang, T., Pan, J., Lin, J., Chen, C., Wei, Y., et al. (2017a). Graded response of the multifunctional 2-cysteine peroxiredoxin, CgPrx, to increasing levels of

hydrogen peroxide in *Corynebacterium glutamicum*. *Antioxid. Redox. Signal.* 26, 1–14. doi: 10.1089/ars.2016.6650

Si, M., Wang, Y., Zhang, B., Zhao, C., Kang, Y., Bai, H., et al. (2017b). The type VI secretion system engages a redox-regulated dual-functional heme transporter for zinc acquisition. *Cell Rep.* 20, 949–959. doi: 10.1016/j.celrep.2017.06.081

Si, M., Zhao, C., Burkinshaw, B., Zhang, B., Wei, D., Wang, Y., et al. (2017c). Manganese scavenging and oxidative stress response mediated by type VI secretion system in *Burkholderia thailandensis*. *Proc. Natl. Acad. Sci. U.S.A.* 114, E2233–E2242. doi: 10.1073/pnas.1614902114

Si, M., Zhang, L., Chaudhry, M. T., Ding, W., Xu, Y., Chen, C., et al. (2015). *Corynebacterium glutamicum* methionine sulfoxide reductase A uses both mycoredoxin and thioredoxin for regeneration and oxidative stress resistance. *Appl. Environ. Microbiol.* 81, 2781–2796. doi: 10.1128/AEM.04221-4214

Slauch, J. M. (2011). How does the oxidative burst of macrophages kill bacteria? Still an open question. *Mol. Microbiol.* 80, 580–583. doi: 10.1111/j.1365-2958.2011.07612.x

Smego, R. A., Frean, J., and Koornhof, H. J. (1999). Yersiniosis I: microbiological and clinicoepidemiological aspects of plague and non-plague Yersinia infections. *Eur. J. Clin. Microbiol. Infect. Dis.* 18, 1–15. doi: 10.1007/s100960050219

Song, Y., Xiao, X., Li, C., Wang, T., Zhao, R., Zhang, W., et al. (2015). The dual transcriptional regulator RovM regulates the expression of AR3- and T6SS4-dependent acid survival systems in response to nutritional status in *Yersinia pseudotuberculosis*. *Environ. Microbiol.* 17, 4631–4645. doi: 10.1111/1462-2920.12996

Staerck, C., Gastebois, A., Vandeputte, P., Calenda, A., Larcher, G., Gillmann, L., et al. (2017). Microbial antioxidant defense enzymes. *Microb. Pathog.* 110, 56–65. doi: 10.1016/j.micpath.2017.06.015

Tan, Y., Liu, W., Zhang, Q., Cao, S., Zhao, H., Wang, T., et al. (2017). *Yersinia pestis* YopK inhibits bacterial adhesion to host cells by binding to the extracellular matrix adaptor protein matrilin-2. *Infect. Immun.* 85:e01069-16. doi: 10.1128/IAI.01069-1016

Wan, B., Zhang, Q., Ni, J., Li, S., Wen, D., Li, J., et al. (2017). Type VI secretion system contributes to enterohemorrhagic *Escherichia coli* virulence by secreting catalase against host reactive oxygen species (ROS). *PLoS Pathog* 13:e1006246. doi: 10.1371/journal.ppat.1006246

Wang, T., Chen, K., Gao, F., Kang, Y., Chaudhry, M. T., Wang, Z., et al. (2017). ZntR positively regulates T6SS4 expression in *Yersinia pseudotuberculosis*. *J. Microbiol.* 55, 448–456. doi: 10.1007/s12275-017-6540-6542

Wang, T., Si, M., Song, Y., Zhu, W., Gao, F., Wang, Y., et al. (2015). Type VI secretion system transports Zn2+ to combat multiple stresses and host immunity. *PLoS Pathog.* 11:e1005020. doi: 10.1371/journal.ppat.1005020

Wang, Y., Cen, X. F., Zhao, G. P., and Wang, J. (2012). Characterization of a new GlnR binding box in the promoter of amtB in *Streptomyces coelicolor* inferred a PhoP/GlnR competitive binding mechanism for transcriptional regulation of amtB. *J. Bacteriol.* 194, 5237–5244. doi: 10.1128/JB.00989-912

Weber, B., Hasic, M., Chen, C., Wai, S. N., and Milton, D. L. (2009). Type VI secretion modulates quorum sensing and stress response in *Vibrio anguillarum*. *Environ. Microbiol.* 11, 3018–3028. doi: 10.1111/j.1462-2920.2009.02005.x

Wei, K., Tang, D. J., He, Y. Q., Feng, J. X., Jiang, B. L., Lu, G. T., et al. (2007). hpaR, a putative marR family transcriptional regulator, is positively controlled by HrpG and HrpX and involved in the pathogenesis, hypersensitive response, and extracellular protease production of *Xanthomonas campestris* pathovar campestris. *J. Bacteriol.* 189, 2055–2062. doi: 10.1128/JB.01331-1336

Xu, L., Shen, X., Bryan, A., Banga, S., Swanson, M. S., and Luo, Z. Q. (2010). Inhibition of host vacuolar H+-ATPase activity by a *Legionella pneumophila* effector. *PLoS Pathog.* 6:e1000822. doi: 10.1371/journal.ppat.1000822

Xu, S., Peng, Z., Cui, B., Wang, T., Song, Y., Zhang, L., et al. (2014). FliS modulates FlgM activity by acting as a non-canonical chaperone to control late flagellar gene expression, motility and biofilm formation in *Yersinia pseudotuberculosis*. *Environ. Microbiol.* 16, 1090–1104. doi: 10.1111/1462-2920.12222

Yang, X., Pan, J., Wang, Y., and Shen, X. (2018). Type VI secretion systems present new insights on pathogenic yersinia. *Front. Cell Infect. Microbiol.* 8:260. doi: 10.3389/fcimb.2018.00260

Zhang, W., Wang, Y., Song, Y., Wang, T., Xu, S., Peng, Z., et al. (2013). A type VI secretion system regulated by OmpR in *Yersinia pseudotuberculosis* functions to maintain intracellular pH homeostasis. *Environ. Microbiol.* 15, 557–569. doi: 10.1111/1462-2920.12005

Zhao, R., Song, Y., Dai, Q., Kang, Y., Pan, J., Zhu, L., et al. (2017). A starvation-induced regulator, RovM, acts as a switch for planktonic/biofilm state transition in *Yersinia pseudotuberculosis*. *Sci. Rep.* 7:639. doi: 10.1038/s41598-017-00534-539

Conflict of Interest: The authors declare that the research was conducted in the absence of any commercial or financial relationships that could be construed as a potential conflict of interest.

Copyright © 2020 Wang, Wang, Cui, Zhang, Chen, Li, Hua, Gu, Xu, Wang, Yang and Shen. This is an open-access article distributed under the terms of the Creative Commons Attribution License (CC BY). The use, distribution or reproduction in other forums is permitted, provided the original author(s) and the copyright owner(s) are credited and that the original publication in this journal is cited, in accordance with accepted academic practice. No use, distribution or reproduction is permitted which does not comply with these terms.

Advantages of publishing in Frontiers

OPEN ACCESS
Articles are free to read for greatest visibility and readership

FAST PUBLICATION
Around 90 days from submission to decision

HIGH QUALITY PEER-REVIEW
Rigorous, collaborative, and constructive peer-review

TRANSPARENT PEER-REVIEW
Editors and reviewers acknowledged by name on published articles

Frontiers
Avenue du Tribunal-Fédéral 34
1005 Lausanne | Switzerland

Visit us: www.frontiersin.org
Contact us: info@frontiersin.org | +41 21 510 17 00

REPRODUCIBILITY OF RESEARCH
Support open data and methods to enhance research reproducibility

DIGITAL PUBLISHING
Articles designed for optimal readership across devices

FOLLOW US
@frontiersin

IMPACT METRICS
Advanced article metrics track visibility across digital media

EXTENSIVE PROMOTION
Marketing and promotion of impactful research

LOOP RESEARCH NETWORK
Our network increases your article's readership